Outer Continental Shelf Environmental Assessment Program

Final Reports of Principal Investigators

Volume 50 **December 1986**

U.S. DEPARTMENT OF COMMERCE
National Oceanic and Atmospheric Administration
National Ocean Service
Office of Oceanography and Marine Assessment
Ocean Assessments Division
Alaska Office

U.S. DEPARTMENT OF THE INTERIOR
Minerals Management Service
OCS Study, MMS 86-0112

"Outer Continental Shelf Environmental Assessment Program Final Reports of Principal Investigators" ("OCSEAP Final Reports") continues the series entitled "Environmental Assessment of the Alaskan Continental Shelf Final Reports of Principal Investigators."

It is suggested that sections of this publication be cited as follows:

Hampton, M. A. and W. J. Winters. 1983. Geotechnical framework study of the northern Bering Sea, Alaska. U.S. Dep. Commer., NOAA, OCSEAP Final Rep. 50(1986):1-386

Karl, H. A. and P. R. Carlson. Seafloor hazards and related surficial geology, Navarin Basin Province, northern Bering Sea. 1983. U.S. Dep. Commer., NOAA, OCSEAP Final Rep. 50 (1986):387-636

Hampton, M. A. 1983. Geotechnical framework study of Shelikof Strait, Alaska. U.S. Dep. Commer., NOAA, OCSEAP Final Rep. 50(1986):637-760

OCSEAP Final Reports are published by the U.S. Department of Commerce, National Oceanic and Atmospheric Administration, National Ocean Service, Office of Oceanography and Marine Assessment, Ocean Assessments Division, Alaska Office, Anchorage, and primarily funded by the Minerals Management Service, U.S. Department of the Interior, through interagency agreement.

Requests for receipt of OCSEAP Final Reports on a continuing basis should be addressed to:

NOAA-OMA-OAD
Alaska Office
701 C Street
P.O. Box 56
Anchorage, AK 99513

OUTER CONTINENTAL SHELF

ENVIRONMENTAL ASSESSMENT PROGRAM

FINAL REPORTS OF PRINCIPAL INVESTIGATORS

Volume 50

December 1986

U.S. DEPARTMENT OF COMMERCE
National Oceanic and Atmospheric Administration
National Ocean Service
Office of Oceanography and Marine Assessment
Alaska Office

U.S. DEPARTMENT OF THE INTERIOR
Minerals Management Service
Alaska OCS Region
OCS Study, MMS 86-0112

Anchorage, Alaska

The facts, conclusions, and issues appearing in these reports are based on research results of the Outer Continental Shelf Environmental Assessment Program (OCSEAP), which is managed by the National Oceanic and Atmospheric Administration, U.S. Department of Commerce, and funded (wholly or in part) by the Minerals Management Service, U.S. Department of the Interior, through an Interagency Agreement.

Mention of a commercial company or product does not constitute endorsement by the National Oceanic and Atmospheric Administration. Use for publicity or advertising purposes of information from this publication concerning proprietary products or the tests of such products is not authorized.

Content of these reports has not been altered from that submitted by the Principal Investigators. In some instances, minor grammatical, spelling, and punctuation errors have been corrected to improve readability; some figures, charts, and tables have been enhanced to improve clarity in reproduction.

Outer Continental Shelf Environmental Assessment Program

Final Reports of Principal Investigators

VOLUME 50 DECEMBER 1986

CONTENTS

GEOTECHNICAL FRAMEWORK STUDY OF THE NORTHERN BERING SEA, ALASKA

by

Monty A. Hampton and William J. Winters

U.S. Geological Survey

Final Report
Outer Continental Shelf Environmental Assessment Program
Research Unit 589

1983

TABLE OF CONTENTS

LIST OF FIGURES

Appendix G Figures:

LIST OF TABLES

INTRODUCTION

Geologic studies in the northern Bering Sea (Fig. 1) have identified several features and processes that can have significant impact on offshore industrial operations (Thor and Nelson, 1980; Larsen and others, 1980). Faulting, thermogenic and biogenic gas charging, sediment liquefaction, ice gouging, current scouring, and bedform migration have been identified as potential hazards (Fig. 2). The occurrence of specific conditions depends partly on local geologic history, especially with regard to the types of sediment that have accumulated. Also important are modern environmental forces, which in the northern Bering Sea include severe storms, strong geostrophic ocean currents, and movement of seasonal ice.

This report presents the results of a two-year geotechnical framework study, designed to determine representative values of sediment mechanical (geotechnical) properties and to use these values in an assessment of soil response to engineering and natural loading. Geotechnical data have been gathered previously and applied to the analysis of particular problems in the area (Olsen and others, 1980; Clukey and others, 1980). The framework study is a quantitative supplement to the other geologic and geotechnical studies and provides engineering data that can be used from a regional perspective in preliminary evaluations for siting offshore operations.

An important aspect of this study is that geotechnical properties were measured in situ, as well as in the laboratory. The in situ tests consist of pushing a cone-tipped rod into the seabed and measuring the resistance to penetration, from which correlations to sediment properties are made. Laboratory techniques involve deformation testing of sediment core samples. An advantage of in situ testing is that it measures properties of sediment in

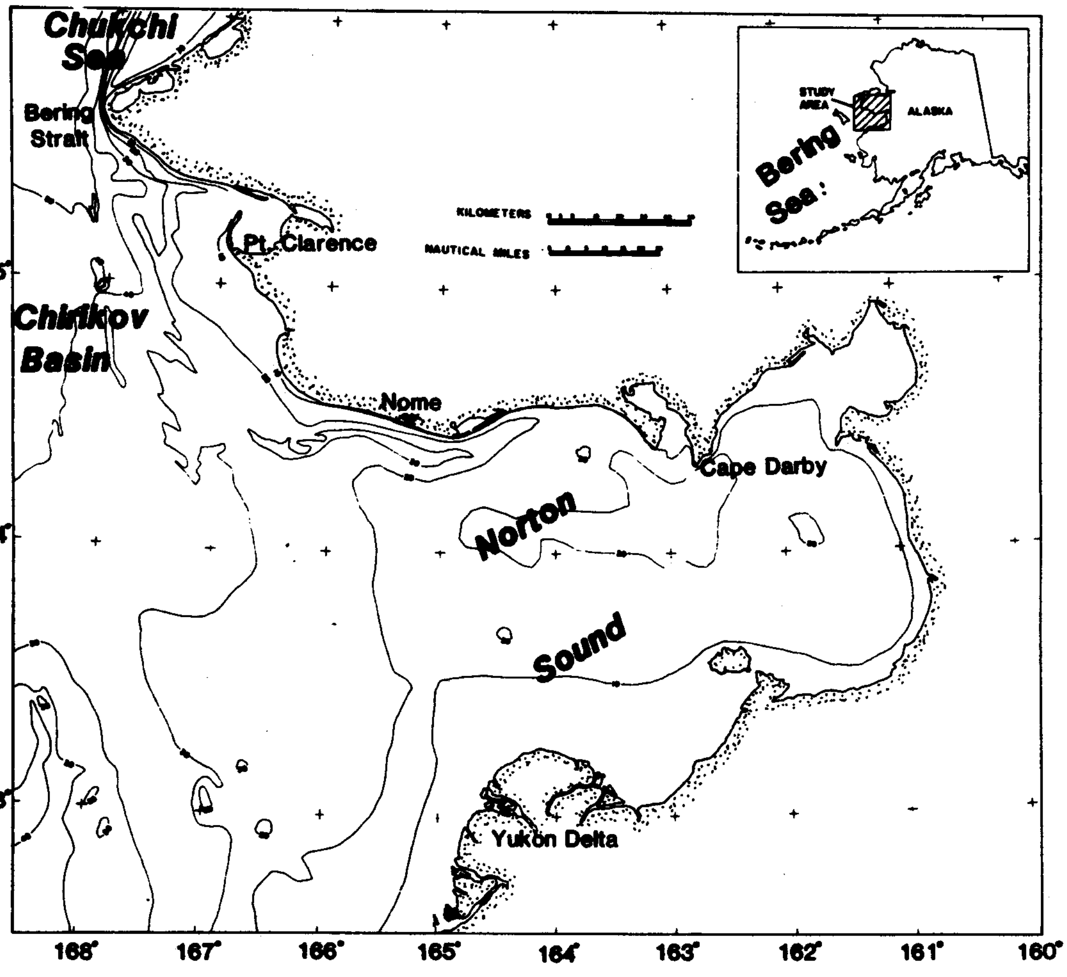

Fig. 1. Location map of the study area in the northern Bering Sea.

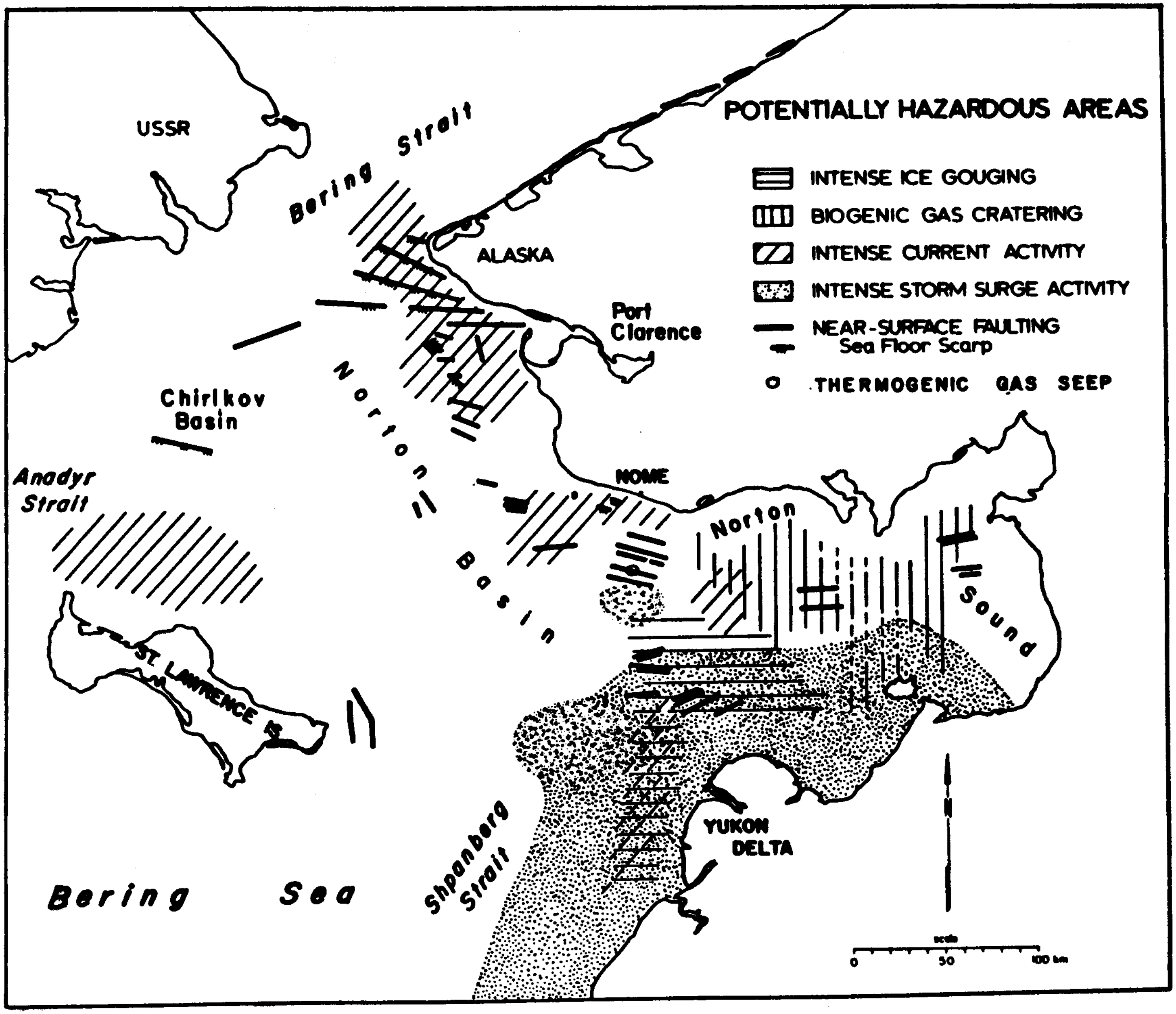

Fig. 2. Geo-hazard locations in the northern Bering Sea (from Larsen and others, 1980).

the natural, undisturbed state. Sediment cores can suffer significant disturbance before they are tested in the laboratory. This is particularly true for the silty and sandy sediment types in the northern Bering Sea that were cored using vibratory methods (Koutsoftas and others, 1976). The natural stress state is difficult to reproduce in the laboratory, and original sediment fabric can be broken down during and after coring operations. Laboratory testing of disturbed core samples can measure physical properties that are different from those of sediment in the natural state. However, present equipment allows examination of a wider range of properties with laboratory testing than with in situ testing. This study offers an excellent opportunity to compare the two methods.

GEOLOGIC SETTING.

The northern Bering Sea comprises a broad, shallow epicontinental shelf that extends about 200,000 km^2 between Alaska and Siberia (Figs. 1 and 2). Two major physiographic subdivisions are Norton Sound (water depth < 30 m) and Chirikov Basin (water depth < 60 m). The entire region was emergent during Pleistocene low stands of sea level. Glaciers encroached on western and northern portions. An extensive tundra vegetation developed on the remainder of the shelf, except where rivers carved channels that led to large submarine canyons. Shoreline transgression at the close of Pleistocene time initiated marine sedimentation, first in the deeper parts of Chirikov Basin and finally across shallow Norton Sound (Nelson, 1980a). The Yukon River migrated north to its present position from the vicinity of Cape Romanzov about 2500 years ago (Dupré and Thompson, 1979). During sealevel stillstands, coastal shoals were formed near Port Clarence and Nome (Nelson and others, 1980).

The distribution of unconsolidated sediment types therefore reflects glacial, subaerial, and marine processes (Nelson, 1980a). In Chirikov Basin the sequence is in most places less than a few meters thick and consists of coarse glacial till and outwash, limnic peaty mud, transgressive gravel to medium sand, and inner-shelf fine sand. This sediment is Pleistocene age, and individual units are patchy in their distribution. Strong northward geostrophic flow has bypassed Holocene sediment and deposited it in the southern Chukchi Sea (Nelson and Creager, 1977).

Peaty mud, with incised fluvial deposits, covers bedrock in Norton Sound. Transgressive sand has been found only in the central sound and in a trough in the northern sound. Yukon River silt with interbedded storm-sand layers is the dominant sediment type. It covers nearly all of the seafloor in Norton Sound and has accumulated up to 14 m thickness. The sediment type grades to silt and mud in the eastern sound.

METHODS

Field methods: A geotechnical cruise in the northern Bering Sea was conducted August 3-18, 1981 aboard the NOAA ship DISCOVERER. Sites were occupied that represent a broad range of geologic environments, many where special engineering problems might be encountered (Figs. 2 and 3; Table 1). In Chirikov Basin, only the shoreline shoals near Port Clarence were visited. The rest of the stations were in Norton Sound at locations of biogenic gas-charged sediment (2 stations), a thermogenic gas seep, muddy sediment, and a range of Yukon prodelta sediment types (5 stations).

Geotechnical data were obtained with in situ testing equipment and from laboratory testing of sediment cores. The in situ device is a static cone

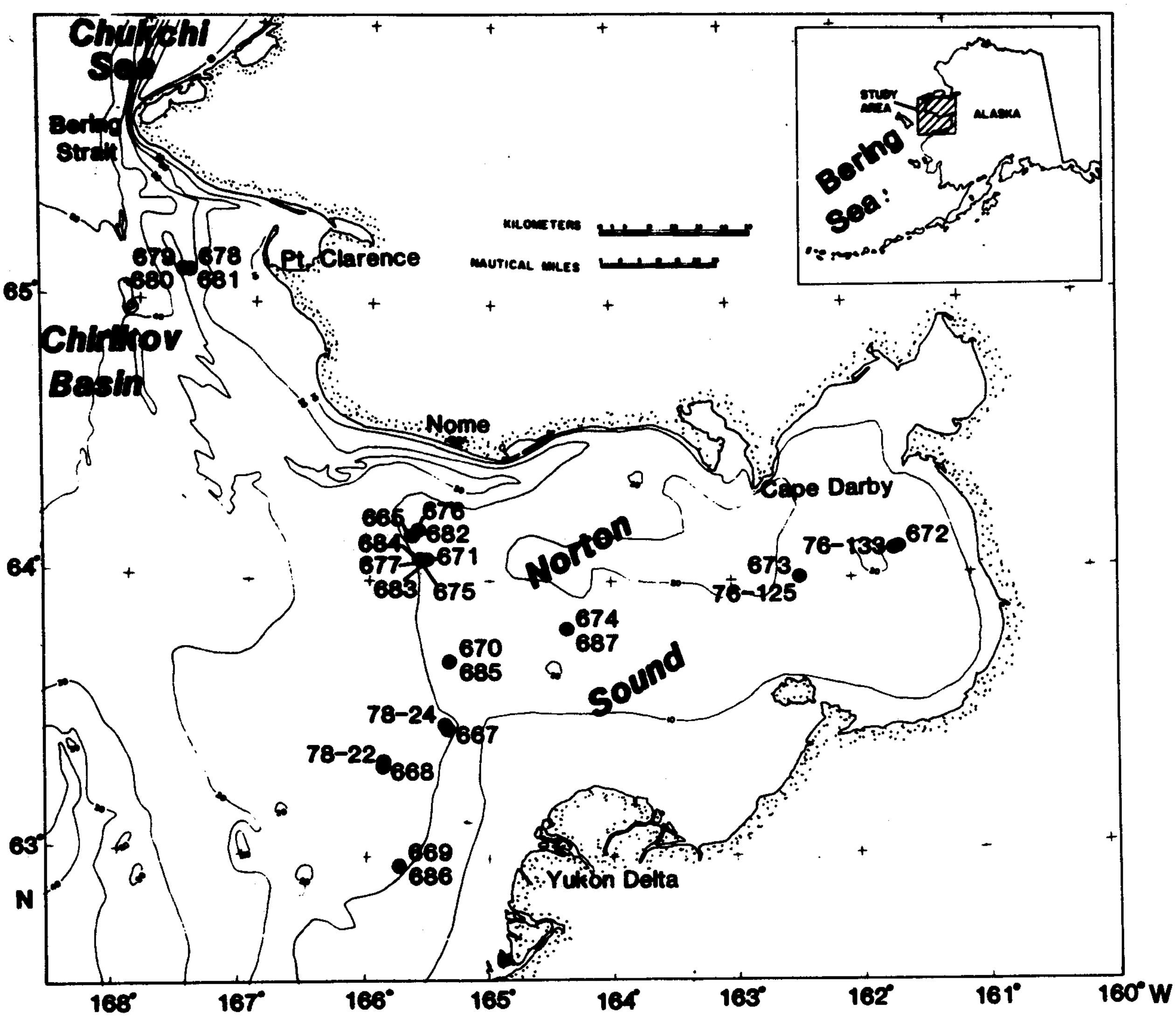

Fig. 3. Station location map.

Table 1. Stations.

A. XSP-40 penetrometer

Station	Attempt	Latitude (N)	Longitude (W)	Water depth (m)	Geologic environment	Penetration Depth (m)	Distance from first penetrometer test (m)
667	1	63°28.60'	165°19.18'	18	Yukon prodelta	2.43	-
668	1	63°20.13'	165°49.90'	23	Yukon prodelta	0.49	-
	2	63°20.13'	165°49.91'	23		0.56	13
	3	63°20.02'	165°49.95'	23		0.55	148
	4	63°20.02'	165°49.94'	23		0.61	142
669	1	62°57.87'	165°41.71'	19	Yukon prodelta	0.48	-
	2	62°57.86'	165°41.70'	19		0.46	29
670	1	63°41.77'	165°18.69'	18	Yukon prodelta	1.43	-
	3	63°41.69'	165°18.67'	18		1.33	145
	4	63°41.67'	165°18.69'	18		1.64	169
671	1	64°05.58'	165°29.25'	19	east of thermo-genic gas seep	1.34	-
671 (cont)	2	64°05.58'	165°29.24'			1.12	20
	3	64°05.64'	165°29.18'			0.78	146
	4	64°05.64'	165°29.19'			0.80	136
	5	64°05.66'	165°29.03'			1.03	384
	6	64°05.66'	165°29.01'			1.48	412
	7	64°05.66'	165°26.78'			0.94	4037
	8	64°05.65'	165°26.72'			1.02	4134
672	1	64°06.08'	161°36.19'	18	eastern Norton Sound	2.94	-
	2	64°06.08'	161°36.20'			2.71	10
673	1	64°00.46'	162°24.62'	18	biogenic gas	0.51	-
	2	64°00.46'	162°24.61'			0.42	10
	3	64°00.33'	162°24.59'			0.41	222
	4	64°00.33'	162°24.59'			0.46	222

Table 1. Stations (cont'd).

Station	Attempt	Latitude (N)	Longitude (W)	Water depth (m)	Geologic environment	Penetration Depth (m)	Distance from first penetrometer test (m)
674	1	63°49.68'	164°21.19'	18	Yukon prodelta	0.92	-
	2	63°49.68'	164°21.17'			0.82	40
675	1	64°05.31'	165°30.54'	19	thermogenic gas seep	2.20	-
	2	64°05.30'	165°30.57'			1.15	53
	3	64°05.40'	165°30.87'			1.93	558
	4	64°05.57'	165°30.79'			1.17	589
676	1	64°11.45'	165°34.36'	20	biogenic gas	3.66	-
	2	64°11.45'	165°34.33'			3.67	49
677	1	64°05.70'	165°31.71'	20	west of thermogenic gas seep	0.90	-
	2	64°05.70'	165°31.75'			0.89	69

Station	Attempt	Latitude (N)	Longitude (W)	Water depth (m)	Geologic environment	Penetration Depth (m)	Distance from first penetrometer test (m)
678	1	65°06.97'	167°33.09'	32	swale	2.12	-
	2	65°06.97'	167°33.09'			2.28	0
679	1	65°06.55'	167°37.73'	20	ridge	1.09	-
	2	65°06.54'	167°37.73'			1.48	19

Table 1B.

Station	Attempt	Latitude (N)	Longitude (W)	Water depth (m)	Geologic environment	Use of core	Core length (m)	Distance from nearest penetration test (m)
680	1	65°05.94'	167°37.38'	21	ridge	geological	2.72	1107
681	2	65°07.06'	167°32.81'	30	swale	geotechnical	5.72	465
	3	65°07.27'	167°33.34'			geological	5.49	615
682	1	64°11.41'	165°33.85'	20	biogenic gas	geotechnical	5.17	782
	2	64°11.44'	165°33.58'			geological	5.16	1219
683	1	64°05.24'	165°30.33'	20	thermogenic gas seep	geotechnical	6.10	362
	2	64°05.23'	165°30.46'			geological	4.50	180
684	1	64°05.92'	165°32.73'	20	west of thermo-genic gas seep	geotechnical	2.60	1636
	2	64°05.95'	165°32.74'			geological	2.61	1647
685	1	63°41.74'	165°18.15'	18	Yukon prodelta	geological	3.26	895
	2	63°41.76'	165°18.12'			geotechnical	4.85	944

Station	Attempt	Latitude (N)	Longitude (W)	Water depth (m)	Geologic environment	Use of core	Core length (m)	Distance from nearest penetration test (m)
686	1	62°58.03'	165°41.51'	18	Yukon prodelta	geotechnical	3.88	426
	2	62°58.16'	165°41.42'			geological	3.88	699
687	1	63°49.95'	164°21.64'	18	Yukon prodelta	geotechnical	5.50	865
	3	63°49.93'	164°21.64'			geological	5.50	850
76-125	1	64°00.04'	162°24.92'	18	biogenic gas	geological	1.55	717
76-133	1	64°05.62'	161°36.78'	18	eastern Norton Sound	geological	1.70	1206
78-22	1	63°20.86'	165°50.14'	23	Yukon prodelta	geological	2.81	1152
78-24	1	63°28.53'	165°20.13'	18	Yukon prodelta	geological	4.95	1586

penetrometer, the XSP-40, that belongs to the Naval Civil Engineering Laboratory (Fig. 4; Beard and Lee, 1982). The instrument measures resistance to penetration of a 3.56-cm diameter cone that can be driven into the seabed a maximum depth of 6 m. Frictional resistance along the side of a sleeve above the cone is also measured. The instrument is housed in a tall frame supported on four broad-based, retractable legs. Total weight is about 4.5 metric tons, which determines the maximum force that can be measured. The cone and sleeve are attached to the end of a rod that is driven by a double chain. In operation the instrument is lowered to the seafloor, and penetration at a rate of 1 m/min is actuated by an onboard switch to the 1-horsepower drive motor. Cone and sleeve resistance are plotted continuously versus penetration depth on a chart recorder; tilt angle is also monitored. A test is terminated either when the maximum penetration depth is achieved or when the tilt meters indicate that the instrument has lifted from the seafloor (i.e., the maximum reaction force has been reached). The push rod and cone are retracted from the seabed by reversing the drive motor.

Core samples were taken with a large vibracorer (Fig. 5). This device is housed on a frame similar to that of the XSP-40. Cores are retrieved in plastic liners, 8 cm inside diameter, and maximum core length is 6 m. The core barrel is driven into the seabed by a pneumatic hammer mounted at the top of the barrel. Penetration rate of the core barrel was recorded during sampling operations (Table 2). Two cores were taken at each station. Both were cut into 1-m-long sections, and the ends were capped. One core was split lengthwise onboard ship, described geologically and subsampled at regular intervals for grain size, water content, grain specific gravity and carbon content determinations. When fine-grained cohesive sediment was encountered,

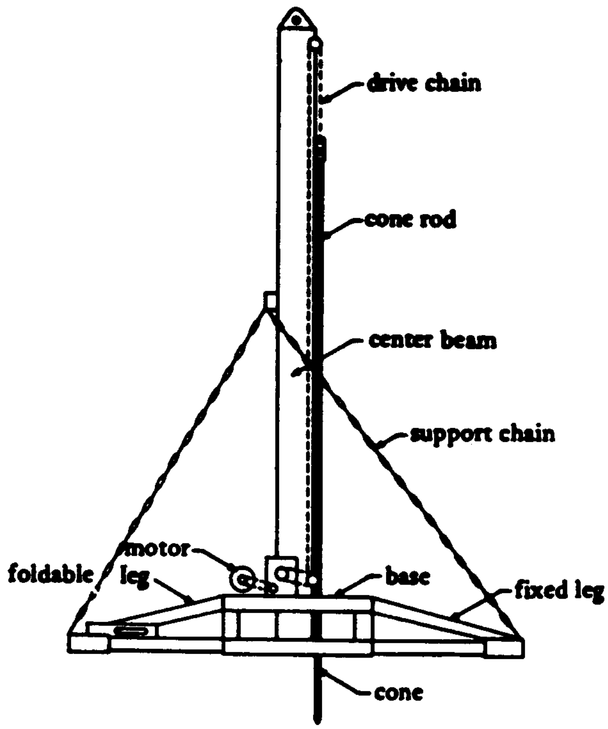

Fig. 4. XSP - 40 penetrometer (from Beard and Lee, 1982).

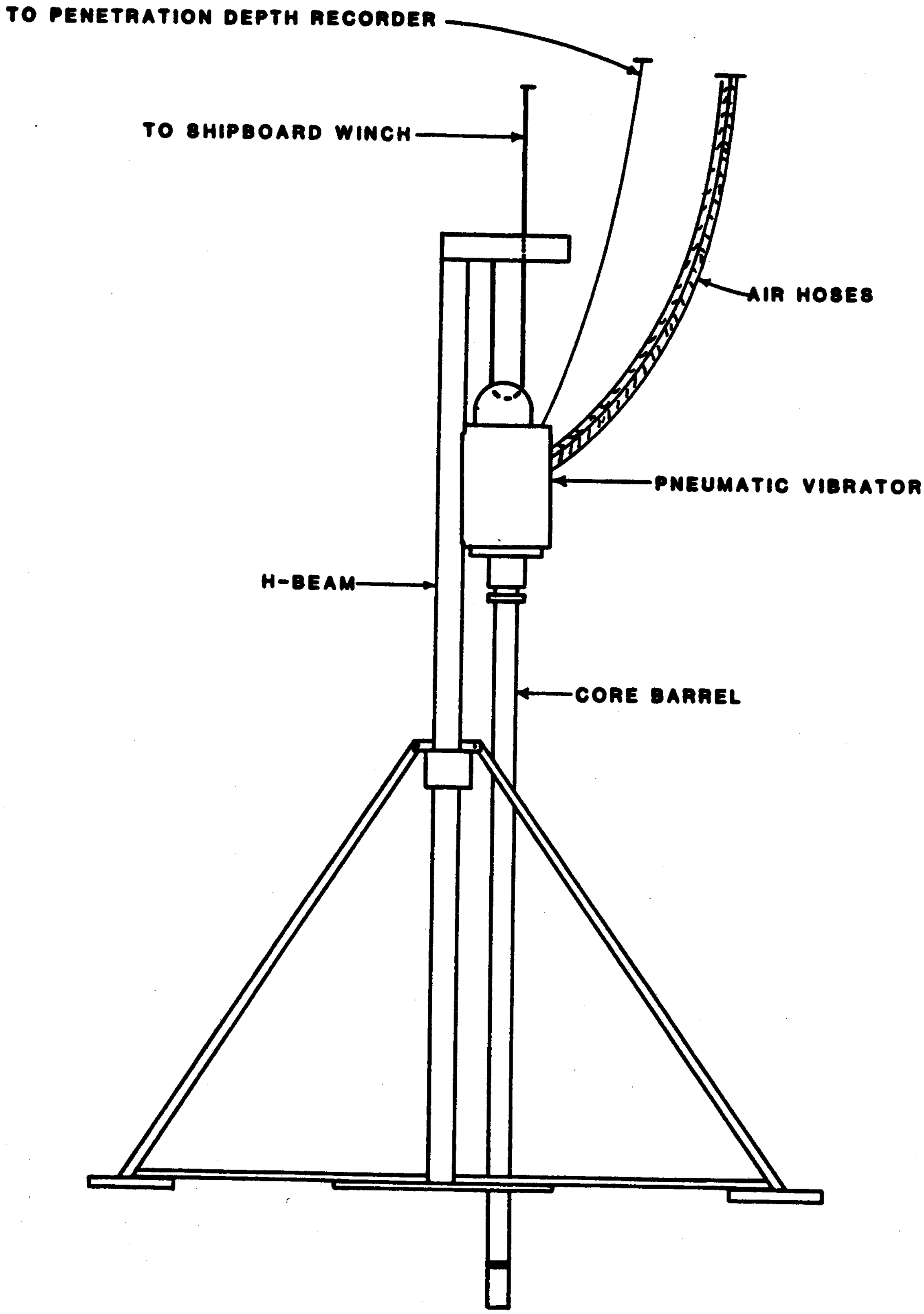

Fig. 5   Pneumatic vibracorer.

Table 2. Vibracorer penetration rates (in meters/min).

DEPTH (m) \ CORE	680A3	681A2	681A3	682A1	682A2	683A1	683A2	684A1	684A2	685A1	685A2	686A1	686A2	687A1	687A3
0.2	1.5	22.9	22.9	45.7	36.6	61.0	26.1	20.3	45.7	45.7	45.7	18.3	36.6	61.0	45.7
0.5	4.6	6.8	5.9	30.5	18.3	6.1	6.3	8.7	5.4	91.4	12.2	1.2	1.6	15.2	12.2
0.8	3.0	9.6	8.3	10.2	8.7	5.5	2.8	2.1	2.4	10.8	6.3	0.7	0.7	1.5	0.6
1.1	2.1	8.7	10.2	9.1	5.7	4.6	2.6	1.5	2.6	7.6	5.5	1.7	0.8	1.1	2.2
1.4	1.6	6.5	6.8	18.3	9.6	4.5	1.1	0.8	1.0	4.6	4.6	1.3	1.1	1.6	2.0
1.7	0.9	3.8	3.3	30.5	10.2	2.6	0.4	2.3	0.3	5.7	3.0	0.6	0.5	1.5	2.0
2.0		2.3	2.4	22.9	8.3	1.5	0.5	0.2	0.3	1.4	0.9	0.5	0.5	1.6	1.8
2.3		1.8	2.4	18.3	8.7	1.8	0.2	0.3	0.2	0.6	0.5	0.7	0.7	0.9	1.1
2.6		1.1	1.4	16.6	8.3	2.2	0.5	0.3		0.5	0.3	0.8	1.0	1.0	1.4
2.9		0.8	0.9	14.1	8.0	2.8	0.5	0.3		0.2	0.1	1.0	0.8	1.1	1.2
3.2		0.6	1.2	11.4	8.0	2.3	0.6	0.1		0.3	0.2	0.7	0.6	1.2	1.3
3.5		0.6	1.2	11.4	7.6	1.5	0.5			0.2	0.3	0.5		1.1	1.0
3.8		0.4	1.1	8.0	6.1	1.4	0.4				0.4	0.4		1.0	0.7
4.1		0.3	0.5	0.6	5.2	1.5					0.4			0.8	0.7
4.4		0.2	0.1		4.9	1.1					0.5			0.6	0.7
4.7					4.9	0.6					0.2			0.4	0.5
5.0					4.3	0.4								0.3	0.4
5.3					3.5	0.4								0.3	0.5
5.6					2.3	0.3								0.2	0.4

strength was measured with a motorized vane shear device, and subsamples were taken for determination of plasticity (Atterberg limits). The sections of the other core were wrapped in cheesecloth, covered with microcrystalline wax, and stored upright in a refrigerator. This core was used for geotechnical testing in the shorebased laboratory.

Shipboard operations at each station were as follows. A seismic-reflection line was run over each station, using 12 kHz, 3.5 kHz, and 600 joule minisparker systems. Navigation used Loran C with satellite updates. The ship was anchored at each station, the XSP-40 was deployed from an outboard storage position using the ship's deep-sea winch and large crane, and a cone penetration test (CPT) was run. More than one test was run at each station. Some successive tests were run after lifting the XSP-40 a small distance off the seafloor and setting it down again at essentially the same location. Other tests were rerun after the ship was allowed to drift a short distance, in order to study local variability of penetration resistance.

After all the penetrometer stations were occupied, the vibracorer was exchanged with the XSP-40 in the outboard storage position, and several stations were re-occupied. After anchoring, two vibracores were taken at these stations.

Vibracores had been taken in previous years for geological study at all but one of the stations we did not re-occupy, so most sites discussed in this paper have companion vibracores and cone penetration tests. Vibracores for laboratory geotechnical testing are not available for all stations, however.

The XSP-40 and the vibracorer were not both deployed at a single anchorage because the large size of the instruments made frequent interchange to the deployment position unfeasible. The XSP-40 was used first at all stations while the vibracorer was stored on deck. Then, stations were re-occupied, and cores were taken. Relocation of the stations had a positional error of from 180 to 1647 m, so the CPT and vibracores were not from exactly the same place (Table 1B).

Laboratory methods:

In the shipboard lab, vane shear tests were made with a standard motorized apparatus, using a 1.27-cm diameter by 1.27-cm long vane and a rotation rate of 90°/min. Peak undisturbed and remolded strengths were measured at regular intervals down split cores (Table 4). In the shorebased lab, Atterberg limits were determined according to standard procedures (Lambe, 1951, p. 22-28), but with water content corrected for a salt concentration of 35 ppt. Grain sizes were measured by sieve, pipette and hydrometer methods (Carver, 1971; Lambe, 1951) (Tables 3 and 4, Appendix A). A LECO model WR-12 carbon determinator with an acid digestor and an induction furnace was used to measure organic carbon and carbonate content. An air comparison pycnometer aided in the calculation of grain density (Table 4).

Consolidation tests to measure sub-failure deformation properties of sediment were run by two different methods. Seven tests were performed on standard front-loading oedometers in a stress-controlled mode (Lambe, 1951), whereas 15 tests were run in triaxial loading cells at constant rate of strain (Wissa and others, 1971).

Static strength tests were run in triaxial loading cells on cylindrical samples approximately 3.6-cm diameter and 7.6-cm long. Tests were performed under undrained conditions with pore pressure measurements (Bishop and Henkel, 1964). Most samples were consolidated isotropically prior to testing, but some were consolidated anisotropically.

Table 3. Detailed grain size summary.

CORE	DEPTH (m)	TEST	D_{60} (μm)	D_{50} (μm)	D_{10} (μm)	$C_u = \frac{D_{60}}{D_{10}}$	LEE & PITTON (1968)	KISHIDA (1969)	BOTH RANGES (1)
680A3	0.30		273	261	175	1.6	•	•	
	0.82		255	250	180	1.4	•	•	
	1.52		245	237	161	1.5	•	•	
	2.22		225	212	156	1.4	•	•	
681A2	1.46	D 100,101	40	33	4.7	8.5			
681A3	0.20		225	197	20	11.2		•	
	0.40		270	245	110	2.4		•	
	0.84		141	126	40	3.5	•	•	
	1.40		107	95	12.3	8.7		•	
	2.20		120	114	19.5	6.2		•	
	2.84		41	23.5	2.0	20.5			
682A1	0.97	TC 38,39	80	68	9.2	8.7		•	
	1.09	TE 76,77	39	26	4.2	9.3			
	1.78	TE 98,99	16	12.4	1.4	11.4			
	1.89	TC 76,77	45	34	4	11.0			
683A1	1.05		62	60	10.1	6.1			•
	4.25	TE 109,110	62	60	21	3.0			•
684A1	0.66	TC 90,91	62	56	9.4	6.6			•
685A2	0.44	TC 80,81	54	49	11.8	4.6			•
	1.05	TC 62,74	60	54	9.6	6.2			•
686A1	0.45	TC 96,97	105	84	11.5	9.1		•	
687A1	0.49	TC 94,95	34	30	4.7	7.2			

• Grain size distribution curve falls within the zone of liquefaction susceptibility (Figure 19).

(1) Part of grain size distribution curve falls within the zone designated by both Lee and Fitton (1968) and Kishida (1969).

Table 4. Index properties and vane shear strength.

CORE	DEPTH IN CORE (m)	GRAIN SIZE (%) GRAVEL	SAND	SILT	CLAY	WATER CONTENT (%)	BULK DENSITY (gm/cm^3)	GRAIN DENSITY (gm/cm^3)	ORGANIC CARBON (%)	$CaCO_3$ (%)	VANE SHEAR STRENGTH (kPa) INTACT	REMOLDED	SENSITIVITY	ATTERBERG LIMITS LIQUID LIMIT	PLASTIC LIMIT	PLASTICITY INDEX	LIQUIDITY INDEX
665G1	0.02	0.0	20.2	75.8	4.0				0.43	1.35							
	0.10	0.0	26.9	62.4	10.7	40.5	1.86	2.76	0.61	1.26						NP	
	0.20					41.1	1.78	2.56									
672G1	0.02					89.4	1.38	2.01									
	0.35					112.5	1.46	2.78			4.9 *	2.6 *	1.9				
672G3	0.02					93.3	1.53	2.80			2.6 *	0.6 *	4.6				
680A3	0.02	0.0	98.1	0.9	1.0				0.12	0.61							
	0.36	0.0	98.8	0.9	0.3	20.9	2.09	2.66	0.09	0.74						NP	
	0.60					21.1	2.17	2.64									
	0.82	0.0	97.6	1.8	0.6	16.7	2.16	2.65	0.07	0.84						NP	
	1.12					16.8	2.12	2.58									
	1.32					18.7	2.12	2.65									
	1.52	0.0	99.2	0.2	0.6	19.5	2.11	2.66	0.08	0.95						NP	
	1.82					18.9	2.11	2.64									
	2.02					19.4	1.60	1.80									
	2.22	0.0	98.4	0.4	1.2	21.1	2.06	2.61	0.08	0.98						NP	
	2.57					22.9	1.64	1.91									
681A2	0.02					24.8	2.01	2.63									
	0.76					50.2	1.71	2.56									
	1.77					21.1	2.03	2.57									
	2.75					23.2	2.10	2.78			21.8 *	3.5 *	6.2				
	3.74					23.0	2.12	2.80			61.8 *	4.2 *	14.5				
	4.74					23.4	2.14	2.88			28.1 *	3.5 *	8.0				
681A3	0.02	0.0	76.9	15.4	7.7				0.49	1.57							
	0.10					25.7	1.99	2.62									
	0.20	0.0	83.8	10.6	5.6	20.3	2.10	2.67	0.31	1.47						NP	
	0.30					24.4	1.98	2.57									
	0.40	14.9	75.6	6.4	3.1	19.1	1.77	2.66	0.39	2.41						NP	
	0.61					26.8	1.98	2.64									
	0.84	0.0	87.7	9.0	3.3	28.9	1.97	2.68	1.70	1.08						NP	
	1.00					30.2	1.96	2.71									
	1.20					16.6	2.21	2.73									
	1.40	0.0	64.3	27.1	8.6	18.9	2.16	2.74	0.56	3.64						NP	
	1.80					19.7	2.14	2.73									
	1.98					15.2	2.20	2.67									
	2.20	1.0	77.1	10.8	11.1	18.4	2.15	2.69	0.41	1.63						NP	
	2.40					17.8	2.18	2.73									
	2.60					26.0	2.02	2.71									
	2.84	0.0	26.3	51.1	22.6	35.0	1.90	2.70	1.00	4.48	34.8	7.5	4.7	33	24	9	1.22
	3.00	1.1	75.7	16.1	7.1	19.7	1.57	1.76	0.47	2.19						NP	
	3.20					20.6	2.13	2.74									
	3.37					36.3	1.99	3.01			38.0	11.2	3.4				
	3.57	0.0	15.0	57.6	27.4	41.7	1.90	2.96	0.95	2.12	38.6	9.0	4.3	50	32	18	0.54
	3.81					32.8	1.97	2.82			39.2	11.2	3.5				
	3.99					28.1	2.03	2.79			41.7	9.3	4.5				
	4.16	1.4	35.1	37.7	25.8	21.0	2.13	2.76	0.90	1.96	61.0	18.0	3.4	30	20	10	0.10
	4.35					23.0	2.08	2.73			62.8	14.9	4.2				
	4.55					25.7	2.07	2.80			34.8	9.3	3.7				
	4.75	22.6	46.3	22.0	9.1	16.8	2.24	2.79	0.60	5.01						NP	
	4.95					14.7	2.26	2.74									
	5.15					12.8	2.30	2.74									
	5.35	28.7	54.5	11.8	5.0	10.5	2.36	2.73	0.68	5.71						NP	

Table 4. Index properties and vane shear strength (cont'd).

CORE	DEPTH IN CORE (m)	GRAIN SIZE (%) GRAVEL	SAND	SILT	CLAY	WATER CONTENT (%)	BULK DENSITY (gm/cm^3)	GRAIN DENSITY (gm/cm^3)	ORGANIC CARBON (%)	$CaCO_3$ (%)	VANE SHEAR STRENGTH (kPa) INTACT	REMOLDED	SENSITIVITY	ATTERBERG LIMITS LIQUID LIMIT	PLASTIC LIMIT	PLASTICITY INDEX	LIQUIDITY INDEX
682A1	1.17					73.5	1.56	2.52			35.1	6.3	5.5				
	2.16					75.9	1.55	2.54			8.8	0.7	12.5				
	3.15					67.3	1.60	2.58			21.4	7.7	2.8				
	4.14					33.8	1.90	2.66			3.9	0.7	5.5				
682A2	0.02	0.0	22.7	67.0	10.3				0.85	1.09							
	0.19	0.0	18.7	68.7	12.6	39.9	1.87	2.78	0.74	1.29	11.6	1.8	6.4			NP	
	0.41					29.0	1.97	2.68			5.8	1.1	5.5				
	0.66					28.9	1.97	2.69			16.5	2.1	7.7				
	0.80	0.0	52.5	41.0	6.5	27.1	2.01	2.73	0.65	0.93	29.6	3.5	8.4			NP	
	1.00					69.8	1.57	2.51			23.0	4.9	4.7				
	1.05					78.2	1.52	2.42			22.8	7.1	3.2				
	1.18										27.2 *	6.3 *	4.3				
	1.40	0.0	56.3	33.1	10.6	62.7	1.62	2.56	3.81	1.27	35.6	9.9	3.6	65	43	22	0.90
	1.60					62.9	1.62	2.57			34.6	10.9	3.2				
	1.80					69.9	1.58	2.53			34.0	11.4	3.0				
	2.00	0.0	3.0	63.2	27.8	61.5	1.64	2.59	4.71	0.99	27.9	9.0	3.1	68	42	26	0.75
	2.20	0.0	17.4	52.8	29.8	63.4	1.62	2.56	4.02	1.28	19.2	6.9	2.8	73	43	30	0.68
	2.40					89.6	1.48	2.48			23.0	9.3	2.5				
	2.60					89.6	1.48	2.47			24.5	8.2	3.0				
	2.80	0.0	4.3	51.7	44.0	95.4	1.27	1.66	5.22	1.32	22.8	8.5	2.7	97	58	39	0.96
	3.00					77.2	1.49	2.29			23.1	9.1	2.6				
	3.26	0.0	21.8	42.9	29.3	62.9	1.63	2.59	4.12	0.69	28.1	9.5	3.0	73	43	30	0.66
	3.40					83.7	1.53	2.62			23.0	9.0	2.6				
	3.65					69.4	1.59	2.59			35.3	10.5	3.4				
	3.80	0.0	4.4	58.2	37.4	75.2	1.55	2.53	6.47	0.73	41.4	14.6	2.8	101	49	52	0.50
	4.00										35.1	14.7	2.4				
	4.24	0.0	57.5	31.7	10.8	49.3	1.71	2.54	3.37	0.87	20.9	9.3	2.2			NP	
	4.40										16.9	6.6	2.6				
	4.60	TR	69.3	25.1	5.6	36.1	1.88	2.68	1.90	0.58	14.8	5.8	2.5			NP	
	4.80					37.9	1.84	2.64									
	5.00	0.0	83.7	14.3	0.0	23.1	2.05	2.67	0.32	0.54						NP	
683A1	0.85					20.5	2.13	2.74									
	2.91					27.6	1.99	2.69									
	3.90					26.6	1.98	2.63									
	4.90					27.2	2.03	2.77									
683A2	0.02	0.0	36.0	57.4	6.6				0.45	0.66							
	0.10	0.0	54.4	40.0	5.6	27.1	2.02	2.73	0.51	0.49						NP	
	0.30					26.7	1.98	2.64									
	0.50					21.8	2.08	2.69									
	0.74	0.2	72.0	23.8	4.0	19.6	2.16	2.75	0.25	0.76						NP	
	0.88					20.1	2.08	2.62									
	1.14	0.0	38.4	46.1	15.5	51.0	1.73	2.66	0.45	0.48						NP	
	1.34					25.0	1.99	2.61									
	1.52					23.7	2.22	3.06									
	1.70	0.0	61.8	35.3	2.9	25.4	2.02	2.68	0.35	0.60						NP	
	1.90	0.0	75.7	22.3	2.0	23.7	2.03	2.65	0.21	0.47						NP	
	2.10	0.0	85.7	12.6	1.7	24.2	2.02	2.64	0.08	0.76						NP	
	2.30					23.6	2.05	2.69									
	2.50	3.9	86.1	8.8	1.2	22.9	2.05	2.66	0.23	0.41						NP	
	2.70					27.5	2.01	2.74									
	2.90					27.2	2.17	3.12									
	3.10	0.0	34.6	62.5	2.9	27.1	1.99	2.68	0.27	0.31						NP	
	3.30					25.1	2.04	2.71									
	3.50					26.4	2.00	2.66									
	3.67					27.6	1.98	2.67									
	3.87	0.0	39.0	57.8	3.2	27.6	1.96	2.62	0.22	0.65						NP	
	4.07					27.4	1.98	2.65									
	4.27	0.0	42.0	54.6	3.4	26.3	1.99	2.65	0.28	0.43						NP	
684A1	1.55					19.4	2.14	2.72									
	2.55					27.5	1.99	2.68			2.0 *	0.7 *	2.7				

Table 4. Index properties and vane shear strength (cont'd).

CORE	DEPTH IN CORE (m)	GRAIN SIZE (%) GRAVEL	SAND	SILT	CLAY	WATER CONTENT (%)	BULK DENSITY (gm/cm^3)	GRAIN DENSITY (gm/cm^3)	ORGANIC CARBON (%)	$CaCO_3$ (%)	VANE SHEAR STRENGTH (kPa) IMPACT	REMOLDED	SENSITIVITY	ATTERBERG LIMITS LIQUID LIMIT	PLASTIC LIMIT	PLASTICITY INDEX	LIQUIDITY INDEX
684A2	0.02	0.0	15.2	70.2	14.6				0.92	1.57							
	0.27	0.0	25.5	61.9	12.6	55.2	1.70	2.68	0.86	1.03						NP	
	0.57					26.2	2.03	2.74									
	0.71					23.3	2.08	2.74									
	0.91	0.0	76.3	17.5	6.2	22.9	2.07	2.71	0.39	0.84						NP	
	1.31					21.9	2.08	2.68									
	1.71	0.0	72.3	24.1	3.6	24.6	2.05	2.73	0.30	1.05						NP	
	1.91					24.8	2.03	2.69									
	2.11	0.0	62.8	20.5	2.7	25.5	1.97	2.57	0.31	0.60						NP	
	2.51	0.0	65.8	36.1	3.1	24.1	2.01	2.62	0.26	0.89						NP	
685A1	0.02	0.0	38.6	47.3	14.1	41.3	1.84	2.75	0.95	1.64						NP	
	0.26	0.0	45.3	47.3	7.4	37.1	1.87	2.69	0.72	1.23	5.7	1.4	4.1			NP	
	0.40					60.5	1.37	1.72			4.9	1.8	2.7				
	0.60	0.0	46.7	45.1	8.2	32.1	1.93	2.70	0.98	1.12	14.0	4.7	3.0			NP	
	0.80					61.0	1.45	1.93			16.5	6.5	2.5				
	1.00					28.1	1.99	2.71									
	1.20	0.0	61.5	32.9	5.6	26.9	1.74	2.14	0.42	0.88						NP	
	1.29					30.6	1.64	2.01									
	1.40					31.2	1.68	2.10									
	1.60	0.0	51.5	41.9	6.6	23.2	2.09	2.76	0.42	1.40						NP	
	1.80					22.8	2.10	2.75									
	2.00					23.1	2.10	2.76									
	2.20	0.0	61.5	32.4	6.1	21.9	2.11	2.75	0.45	0.99						NP	
	2.28					27.4	2.02	2.76									
	2.40					23.1	1.80	2.18									
	2.60	0.0	50.8	42.7	6.5	23.9	2.08	2.76	0.44	1.38						NP	
	2.80					22.8	2.10	2.76									
	3.00	0.0	43.3	50.9	5.8	23.4	2.08	2.73	0.44	1.17						NP	
	3.20					23.0	2.08	2.73									
685A2	0.85					31.8	1.95	2.73									
	1.85					23.7	2.09	2.77									
	2.85					22.2	2.10	2.73									
	3.85					25.7	2.04	2.74									
686A1	1.35					57.4	1.34	1.63			50.9 *	13.2 *	3.9				
	2.36					29.8	1.98	2.74			131.2 *	37.7 *	3.5				
686A2	0.02	0.0	74.0	19.8	6.2				0.55	0.88							
	0.20	0.0	64.6	24.9	10.5	27.5	1.88	2.44	0.57	1.68						NP	
	0.40					20.9	2.10	2.68									
	0.60					21.8	2.09	2.71									
	0.80	0.0	60.3	33.4	6.3	22.2	2.09	2.71	0.41	1.54						NP	
	1.00					27.3	2.00	2.71									
	1.20	0.0	69.6	26.1	0.3	35.4	1.88	2.68	1.09	1.34						NP	
	1.40					28.5	1.97	2.67									
	1.60	0.0	30.7	58.2	11.1	29.4	1.97	2.71	1.42	1.87						NP	
	1.80					28.5	1.99	2.73									
	2.02	0.0	49.9	47.2	2.9	26.4	2.02	2.71	0.35	1.46						NP	
	2.20					30.3	1.95	2.68									
	2.40	3.1	56.5	40.4		40.3	1.78	2.76	3.58	4.17				68	48	20	0.02
	2.60					29.3	1.97	2.71									
	2.76	0.0	9.4	70.6	20.0	32.9	1.93	2.73	1.63	2.72						NP	
687A1	1.91					30.8	1.97	2.80			99.5 *	32.4 *	3.1				
	2.91					38.8	1.83	2.71			50.3 *	16.8 *	3.0				
	3.91					27.8	1.94	2.62			92.3 *	16.8 *	5.5				

Table 4. Index properties and vane shear strength (cont'd).

CORE	DEPTH IN CORE (m)	GRAIN SIZE (%) GRAVEL	SAND	SILT	CLAY	WATER CONTENT (%)	BULK DENSITY (gm/cm^3)	GRAIN DENSITY (gm/cm^3)	ORGANIC CARBON (%)	$CaCO_3$ (%)	VANE SHEAR STRENGTH (kPa) INTACT	REMOLDED	SENSI-TIVITY	ATTERBERG LIMITS LIQUID LIMIT	PLASTIC LIMIT	PLASTICITY INDEX	LIQUIDITY INDEX
687A3	0.02	0.0	25.4	61.6	13.0				0.86	1.41							
	0.40										18.9						
	0.45					55.9	1.67	2.68									
	0.60										60.5	12.6	4.8				
	0.70	0.0	12.1	82.3	9.6	26.6	2.01	2.69	0.66	1.20						NP	
	0.80										102.1	63.0	1.6				
	1.00										39.1	36.6	1.1				
	1.10					32.0	1.90	2.62									
	1.20										124.8	89.5	1.4				
	1.30	0.0	10.0	80.6	9.4	26.9	2.00	2.68	0.78	1.61						NP	
	1.40										151.3	93.3	1.6				
	1.60										155.1	34.0	4.6				
	1.70					33.7	1.91	2.69									
	1.80										132.4	18.9	7.0				
	1.90					37.5	1.86	2.69									
	2.00										116.0	65.6	1.8				
	2.10					25.5	2.00	2.65									
	2.20										156.3	88.3	1.8				
	2.30					30.8	1.97	2.75									
	2.40										131.1	100.9	1.3				
	2.55					33.1	1.94	2.75									
	2.60										45.4	16.4	2.8				
	2.75	0.0	1.5	87.6	10.9	31.5	1.93	2.68	0.68	1.55							
	2.80										107.2	30.3	3.5				
	2.95					29.9	1.97	2.72									
	3.00										104.6	22.7	4.6				
	3.15	0.0	4.6	82.1	13.3	36.9	1.87	2.68	0.89	1.80				53	35	18	0.11
	3.20										83.2	42.9	1.9				
	3.35					35.6	1.89	2.70									
	3.40										63.0	26.5	2.4				
687A3 (cont)	3.60					27.0	2.04	2.78									
	3.65										84.5	25.2	3.4				
	3.80	0.0	11.9	77.2	10.9	28.3	1.98	2.70	0.84	1.32						NP	
	3.85										131.1	40.3	3.2				
	4.00					26.0	2.02	2.71									
	4.05										138.7	34.0	4.1				
	4.20	0.0	9.6	83.7	6.7	27.9	1.97	2.65	0.76	1.83						NP	
	4.25										100.9	5.0	20.0				
	4.62										191.6	65.6	2.9				
	4.66					25.1	2.19	3.12									
	4.70										175.3	83.2	2.1				
	4.85	0.0	14.4	74.3	11.3				0.68	1.93						NP	
	4.90										148.8	66.8	2.2				
	5.05					28.4	2.08	2.79									
	5.10										114.7	36.6	3.1				
	5.20	0.0	2.2	73.1	24.7	47.2	1.78	2.80	1.51	1.67						NP	
	5.35										76.9	27.7	2.8				
	5.45					40.7	1.86	2.86									

NOTE: NP = Non-plastic

* = Vane inserted parallel to core axis

Cyclically loaded triaxial tests were also run, with the axial stress on samples varied sinusoidally at 0.1 H_z. Both compression and tension were applied at a predetermined percentage of the confining (consolidation) stress.

A total of 23 static and 38 cyclically loaded triaxial tests were conducted according to the scheme presented in Table 5. Some test specimens were consolidated to the in situ level before axial loading to failure was initiated. Others were consolidated to at least four times the maximum past stress for plastic sediment, in order to minimize the effects of disturbance (Ladd and Foott, 1974). Consolidation was isotropic in most tests but anisotropic in some. A condition of overconsolidation was induced in some test samples, whereby a high consolidation stress state was followed by rebounding to a lower consolidation stress before axial loads were applied. The ratio of the higher consolidation stress to the lower, rebounded stress defines the overconsolidation ratio (OCR).

Derived test parameters: The in situ penetration tests and laboratory tests described above are standard civil engineering procedures for evaluating the behavior of soil. Typical applications are the design of foundations, excavations, and artificial fills. The parameters that are derived from geotechnical test data can be used in geologic analyses as well, to determine the triggering forces for submarine sediment slides, for example.

Three sediment properties commonly deduced from cone penetration records are 1) stratigraphic variation 2) sediment type, and 3) relative density. Stratigraphic variation is a qualitative evaluation based on the shape of the cone pressure versus depth curve (Fig. 6, Appendix B). A smooth curve indicates uniform stratigraphy, whereas abrupt changes in slope reflect

Table 5. Triaxial test types.

STATIC TESTS	DESCRIPTION	NUMBER OF TESTS PERFORMED
T-2	Isotropically consolidated to the in situ vertical stress with undrained shear.	1
T-3	Isotropic normally consolidated (OCR=1) undrained shear.	11
T-4	Isotropic overconsolidated (OCR ~ 6) undrained shear.	8
T-7	Anisotropic normally consolidated (OCR = 1) undrained shear.	1
T-8	Isotropic overconsolidated (OCR ~ 3) undrained shear.	2
CYCLIC TESTS		
T-5	Isotropic normally consolidated (OCR = 1) undrained shear with a high cyclic shear stress ratio ($\tau_{cyc\ ave\ max}/\sigma_c$).	13
T-6	Isotropic normally consolidated (OCR = 1) undrained shear with a low cyclic shear stress ratio.	15
T-9	Isotropic overconsolidated (OCR ~ 6) undrained shear with a high cyclic shear stress ratio.	3
T-10	Isotropic overconsolidated (OCR ~ 6) undrained shear with a low cyclic shear stress ratio.	3
T-11	Isotropically consolidated to the in situ vertical stress with undrained shear and a high cyclic shear stress ratio.	1
T-12	Isotropically consolidated to the in situ vertical stress with undrained shear and a low cyclic shear stress ratio.	1
T-13	Isotropically consolidated to the in situ vertical stress. Cyclic shear stresses were increased and drainage was allowed between burst cycles to simulate storm wave events and densification due to pore pressure dissipation.	1
T-14	Anisotropically consolidated to the in situ vertical stress. Cyclic shear stresses were increased and drainage was allowed between burst cycles to simulate storm wave events and densification due to pore pressure dissipation.	1

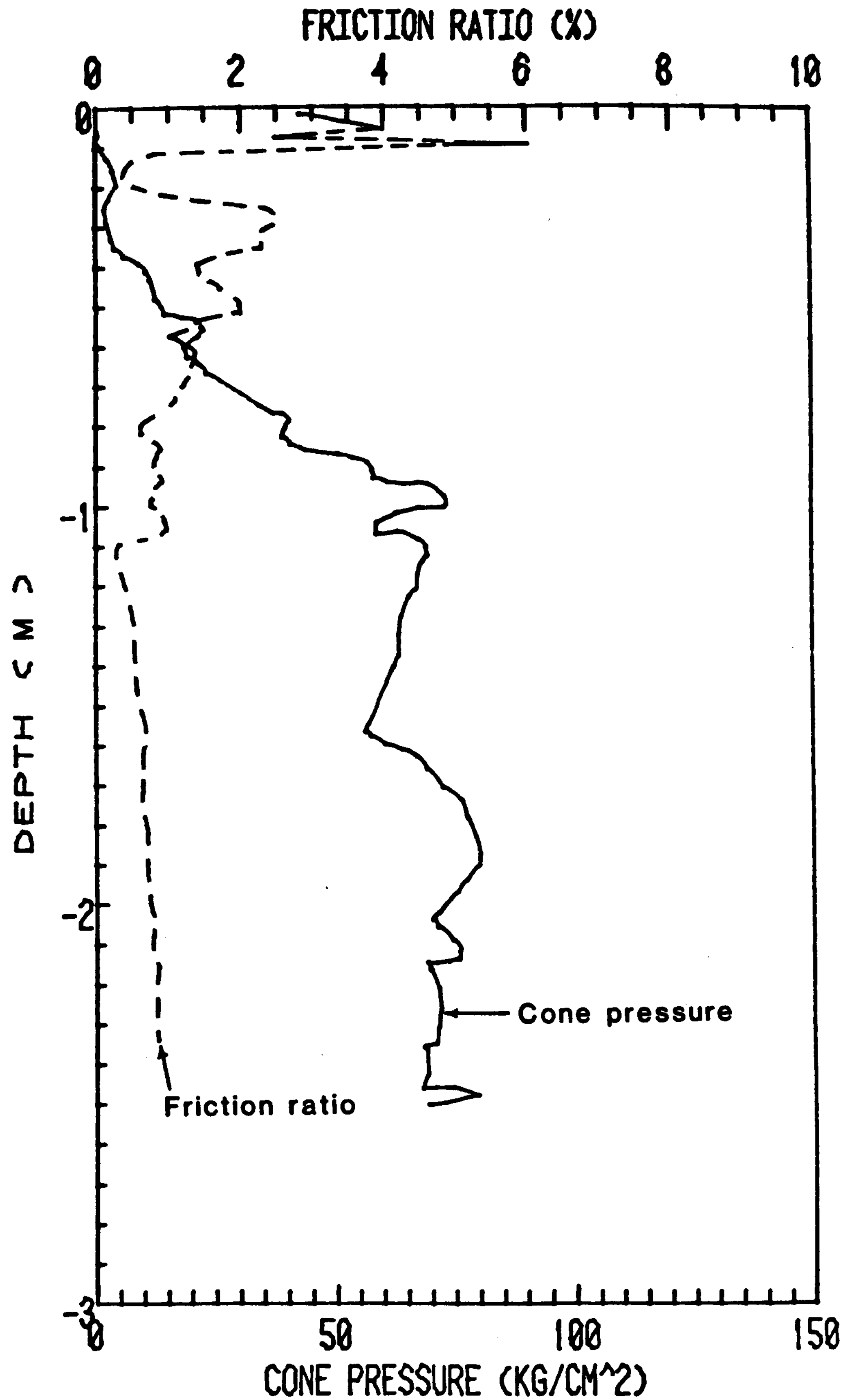

Fig. 6 Typical cone penetration test record illustrating cone pressure and friction ratio vs subbottom depth.

stratigraphic interfaces between different sediment types. Of particular importance to engineering applications are major increases in slope of the curve, possibly beyond vertical, which identify soft strata beneath more firm material (Fig. 6).

Several attempts have been made to estimate sediment type from penetrometer data (Begemann, 1965; Schmertmann, 1978a; Martin and Douglas, 1981). The common technique is to delineate distinct fields of sediment types on plots of friction ratio (sleeve friction stress/cone pressure, expressed as a percent) versus cone pressure (Fig. 7). Successful correlations have been made, but they are somewhat limited to the local area from which the data were collected. Substantial engineering information about soil behavior can be deduced from a general knowledge of sediment type, and once a correlation has been established within an area, the expense and effort of collecting core samples can be reduced or eliminated.

Relative density refers to the magnitude of the natural density state relative to maximum and minimum density states. A relative density of 100% means that a sediment exists naturally in its densest possible state, and a relative density of 0% indicates the least dense state. Schmertmann (1978b) derived an empirical correlation between cone pressure, vertical effective stress (a measure of the buoyant weight of the sediment column at a particular depth below the surface), and relative density:

$$D_r = 0.34 \ln [(q_c/(12.31\, \sigma'_{vo}{}^{10.71})] \times 100$$

where D_r = relative density in percent

q_c = cone pressure in kg/cm^2

σ'_{vo} = effective vertical (overburden) stress

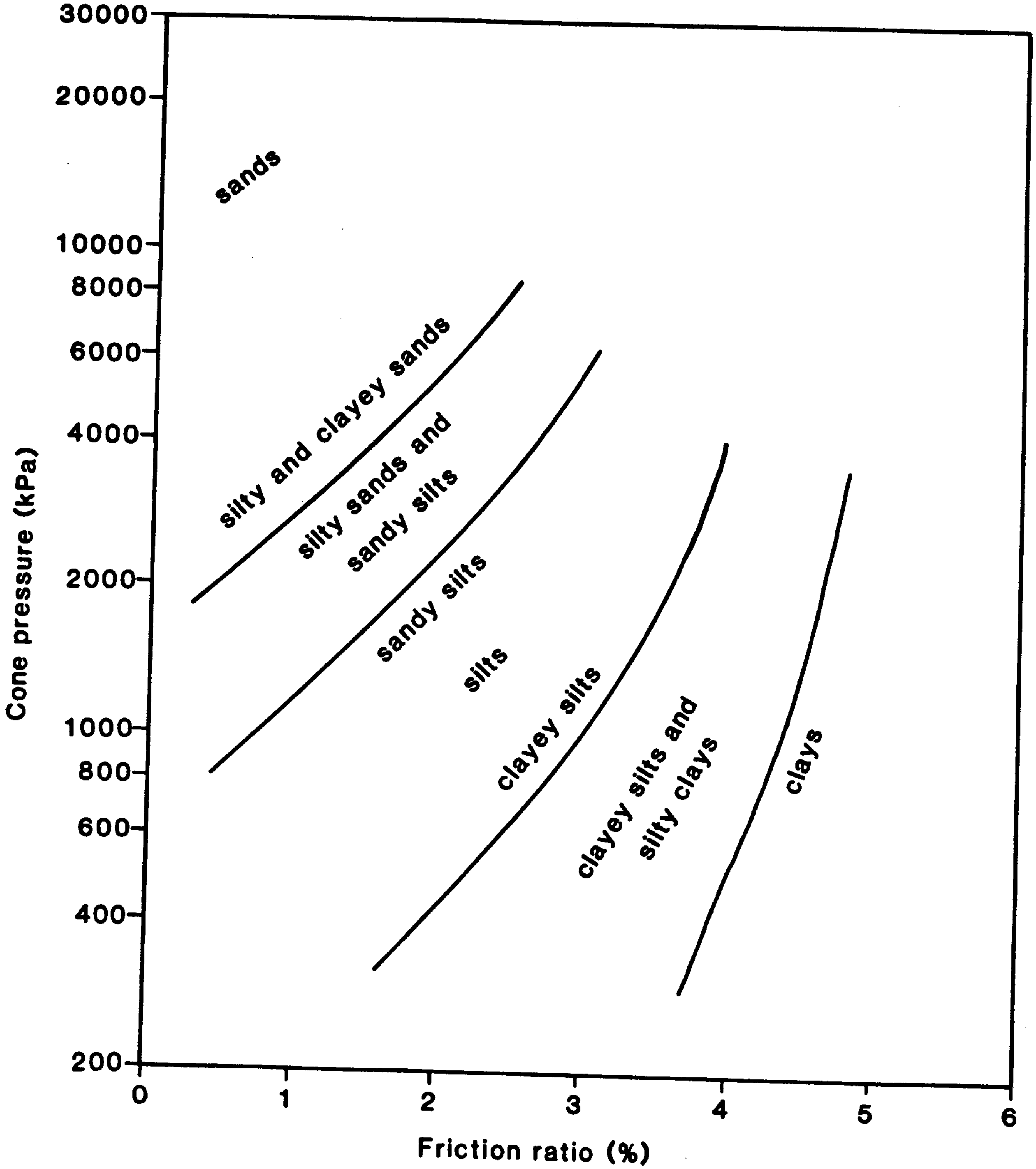

Fig. 7 Sediment type plotted as a function of CPT cone pressure vs friction ratio.

This correlation was derived from laboratory testing of normally consolidated sand, and its application to field situations may be imprecise (Appendix C).

As discussed by Schmertmann (1978a), measurements of cone pressure are influenced by the proximity of an interface between materials of different physical properties. In particular, as the cone enters the seabed, it must penetrate up to about 8 cone diameters (28 cm in our case) before the failure surface around the cone tip is fully developed and cone pressure readings truly reflect sediment physical properties. A similar argument applies to friction sleeve readings, and also to interfaces between sediment strata. As applied to the present study, the cone-pressure and friction-ratio curves (Appendix B) have only qualitative significance at depths less that about 0.28 m in the seabed; stratigraphic variation can be detected from irregularities in the shape of the curve, but measurement of relative density and identification of sediment type are inaccurate.

Laboratory consolidation tests are used to predict the amount and rate of consolidation of sediment in response to sustained loads, as well as to deduce the stress history of the sediment. Test results are plotted as void ratio (e = volume of voids/volume of solids) versus the logarithm of effective vertical stress (σ'_v) (Table 6, Appendix D). The curve typically has a straight line segment, termed the "virgin compression curve", in the range of high consolidation pressures. The slope of this line is the compression index (C_c), which indicates the amount of consolidation for a tenfold increase in load. The maximum past pressure (σ'_{vm}) is the greatest effective overburden stress that the sediment has ever been exposed to and is determined from the e-log σ_v' curve by a simple graphical construction (Casagrande, 1936). The ratio of σ'_{vm} to the effective overburden stress at the time of

Table 6. Consolidation test results.

CORE	DEPTH (m)	TEST No.	σ'_{vo} (kPa)	σ'_{vm} (kPa)	C_c	C_r	c_v(ave)x10^{-2} (cm^2/sec)	OCR	w (%)	e_o	$\frac{C_c}{1 + e_o}$
681A2	2.13	OE36	24	500	0.11	0.002	2.0	21	21.6	0.520	0.07
	5.53	OE38	66	410	0.07	0.003	0.6	6	13.9	0.382	0.05
682A1	1.47	OE34	8	64	0.53	0.065	0.3	8	65.3	1.886	0.18
	2.91	OE35	16	70	0.69	0.072	0.3	4	75.1	1.991	0.23
	4.61	CE19	28	190	0.06	-	-	7	33.6	0.967	0.03
683A1	1.50	CE34	13	20	0.04	-	-	2	28.6	0.809	0.02
	2.55	CE35	22	660	0.09	-	-	30	30.0	0.967	0.05
	4.47	CE43	38	280	0.08	-	-	7	25.6	0.636	0.05
684A1	0.37	CE37	4	250	0.08	-	-	61	28.5	0.724	0.05
	1.07	CE47	11	200	0.12	-	-	18	21.0	0.625	0.07
	2.37	CE49	24	170	0.07	-	-	7	23.5	0.605	0.04
685A2	0.77	OE39	5	105	0.25	0.018	0.9	20	40.0	1.165	0.12
	1.53	CE20	12	190	0.10	-	-	16	27.0	0.671	0.06
	1.81	CE21	19	260	0.03	-	-	14	21.7	0.551	0.02
686A1	0.28	CE39	3	300	0.09	-	-	100	26.7	0.678	0.05
	0.77	CE41	8	425	0.08	-	-	53	29.0	0.740	0.05
	1.83	CE40	18	1100	0.05	-	-	61	24.3	0.600	0.03
	2.86	CE42	28	280	0.24	-	-	10	37.3	1.044	0.12
687A1	0.67	OE42	6	490	0.11	0.007	1.9	77	29.0	0.748	0.06
	1.07	CE48	10	300	0.22	-	-	30	33.4	0.881	0.12
	2.20	OE43	21	320	0.14	0.010	1.1	15	31.0	0.774	0.08
	3.63	CE44	33	470	0.14	-	-	14	29.0	0.854	0.08

sampling (σ'_{vo}) is the overconsolidation ratio (OCR), which describes the stress history, for example in terms of the amount of unloading that may have occurred by erosion. The rate of consolidation is determined for each load increment of an oedometer test, and is denoted by the coefficient of consolidation (c_v).

Sediment properties derived from static triaxial strength tests can be used to predict failure conditions of sedimentary deposits. The primary measured property is undrained shear strength ($S_u = q_{max}$) (Table 7, Fig. 8, Appendix E). It is the maximum sustainable shear stress within a sample that experiences no pore water drainage after consolidation to a predetermined stress level (σ'_c). S_u acts along a plane inclined at 45° to the axial load. The arcsine of S_u divided by the effective normal stress across this plane is the effective friction angle ($\dot{\phi}'$), whose magnitude is an indication of the strength of the sediment under slow (drained) loading conditions. In comparison, the ratio S_u/σ'_c gives an indication of the strength during rapid (undrained) loading conditions. The difference between drained and undrained strength behavior depends on the pore water pressure generated in response to the tendency for volume change when the sediment is axially loaded. If a sediment has a high tendency for volume change, the difference in strength between rapid and slow loading can be substantial.

Cyclically loaded triaxial strength tests are performed in order to study the strength properties of sedimentary deposits under the repeated application of loads, such as by earthquakes or waves. Tests are run at a predetermined cyclic stress level ($\tau_{cyc\ ave\ max}/\sigma'_c$), which is the average maximum cyclically applied shear stress ($\tau_{cyc\ ave\ max}$) divided by the consolidation stress (σ'_c) (Table 8, Figs. 9-11, Appendix F). Pore water pressure and

Table 7. Static triaxial test results.

CORE	DEPTH (m)	TEST NO. (TE)	TEST TYPE	w (%)	w SHEARED (%)	σ'_c (kPa)	A_f	INDUCED OCR	STRAIN AT FAILURE (%)	q AT FAILURE (kPa)	p' AT FAILURE (kPa)	$\frac{q_{max}}{\sigma'_c}$ (1)	ϕ' (degrees) (2)
681A2	1.36	107	T-8	34.7	30.6	151.0	0.07	2.0	11.9	186.0	312.3	1.23	<37.3
	1.36	108	T-4	32.1	28.7	40.7	-0.19	7.4	17.3	149.0	247.2	3.66	<40.4
682A1	1.12	76	T-3	29.7	25.5	236.7	0.25	1.0	13.1	183.9	327.7	0.78	35.2
	1.12	77	T-7	40.4	32.3	242.3	0.19	1.0	10.2	124.5	197.5	0.51	39.2
	1.26	85	T-4	71.2	54.0	44.1	0.03	5.5	17.4	82.9	121.4	1.88	<43.4
	1.26	86	T-8	69.3	50.9	77.9	0.18	3.0	19.2	89.5	135.3	1.15	<41.4
	1.78	98	T-3	78.4	52.5	201.3	0.81	1.0	17.6	93.2	144.3	0.46	40.2
	1.78	99	T-4	77.8	59.0	27.3	0.04	8.3	14.6	63.6	85.5	2.33	<48.9
683A1	4.26	109	T-3	25.5	25.5	289.7	-0.13	1.0	9.9	882.4	1409.2	3.05	38.8
	4.26	110	T-4	26.0	25.0	47.4	-0.30	6.3	8.6	634.3	1064.5	13.38	<37.8
684A1	0.95	105	T-3	21.4	21.4	293.0	-0.17	1.0	7.2	969.8	1591.1	3.31	38.0
	0.95	106	T-4	21.0	21.0	48.1	-0.35	6.2	8.5	675.3	1116.4	14.04	<37.7
685A2	0.55	103	T-3	29.9	26.6	303.8	0.01	1.0	10.7	423.4	719.0	1.39	38.1
	0.55	104	T-4	29.8	26.9	38.3	-0.32	7.5	14.6	281.3	499.7	7.34	<37.8
	1.35	119	T-2	30.2	29.3	20.9	-0.212	(?)	11.65	77.54	131.33	3.71	<42.1
	1.35	120	T-3	29.8	26.7	292.0	0.159	1.0	17.62	266.20	473.60	0.91	36.8
	2.36	94	T-3	23.6	23.6	101.5	-0.20	1.0	9.2	427.6	703.3	4.21	38.8
	2.46	95	T-3	23.5	21.9	343.2	-0.16	1.0	8.4	1189.5	1916.5	3.47	39.0
686A1	1.75	100	T-3	-	25.6	304.2	0.01	1.0	9.4	419.9	716.7	1.38	42.0
	1.75	101	T-4	-	24.9	47.7	-0.26	6.2	8.8	372.9	616.1	7.82	<38.2
687A1	0.60	102	T-4	27.9	27.7	45.1	-0.28	6.5	9.6	409.7	686.3	9.08	<39.9
	1.15	96	T-3	34.3	32.3	299.6	0.26	1.0	20.0	248.5	419.0	0.83	38.3
	1.15	97	T-3	33.9	32.9	94.4	0.03	1.0	12.9	147.6	232.4	1.56	42.1

(1) $q_{max}/\sigma'_c = S_u/\sigma'_c$ may be influenced by overconsolidation in some cores (even at high consolidation stresses).

(2) ϕ' = arcsine (q/p') for (q/p') with the highest σ'_1/σ'_3 ratio; ϕ' is valid only for T-3 and T-7 tests at high consolidation stresses.

Table 8. Cyclic triaxial test results.

CORE	DEPTH (m)	TEST NO. (TC)	TEST TYPE	w (%)	w SHEARED (%)	σ'_c (kPa)	INDUCED OCR	τ_{max}/σ'_c (%)	τ_{min}/σ'_c (%)	CYCLES TO 5% STRAIN	CYCLES TO 10% STRAIN	CYCLES TO 20% STRAIN	COMMENTS
681A2	1.46	100	T-5	31.4	26.1	294.5	1.0	47.9	-39.2	4 C	15 C	35 C	M.B.
	1.46	101	T-6	26.7	21.6	298.4	1.0	36.3	-34.0	9 T	28 T	47 T	
	1.56	127	T-6	25.3	21.4	300.4	1.0	22.4	-18.7	571C	722C	765C	
	1.56	128	T-5	24.4	20.7	55.3	1.0	66.7	-60.9	196C	272C	460C	CSR
682A1	0.80	44	T-6	29.8	24.1	241.8	1.0	27.2	-23.5	91 C	130 C	214 C	
	0.80	45	T-6	30.5	25.5	239.4	1.0	18.1	-8.8	216 C	320 C	413 C	
	0.90	40	T-6	24.3	21.6	240.4	1.0	39.5	-36.1	3 T	5 T	5 T	NECKING
	0.90	41	T-6	26.8	26.1	241.8	1.0	38.2	-44.6	4 T	12 T	15 T	
	1.00	38	T-5	24.0	-	238.4	1.0	53.4	-55.0	1 T	3 T	-	M.B.
	1.00	39	T-6	24.0	-	237.3	1.0	35.5	-52.1	2 T	7 T	17 T	M.B.
	1.38	78	T-10	69.5	52.6	37.8	6.3	98.1	-82.3	105 T	193 C	242 C	
	1.38	79	T-9	69.6	53.0	39.8	6.0	151.5	-131.2	4 C	10 C	20 C	
	1.90	76	T-6	76.9	49.1	238.0	1.0	28.3	-22.4	339 C	390 C	440 C	CSR
	1.90	77	T-5	69.1	44.8	239.1	1.0	47.3	-45.5	4 T	7 T	12 T	
684A1	0.66	90	T-6	23.6	21.0	296.6	1.0	54.1	-36.5	11 T	60 T	62 T	
	0.66	91	T-5	26.0	21.4	297.2	1.0	94.8	-79.6	1 T	4 T	13 T	
685A2	0.33	111	T-5	39.9	31.3	292.6	1.0	47.6	-41.8	2 T	5 T	6 T	
	0.33	112	T-6	39.8	29.8	298.0	1.0	26.4	-22.8	107 C	152 C	163 T	
	0.44	80	T-6	37.0	27.5	289.8	1.0	19.5	-16.1	427 T	591 C	653 T	
	0.44	81	T-5	47.2	35.9	297.4	1.0	46.7	-39.5	2 T	4 T	5 T	
	0.65	82	T-10	31.0	26.0	46.7	6.4	108.8	-96.4	13 T	61 T	122 T	
	0.65	83	T-9	31.1	26.3	49.7	6.0	171.0	-161.2	2 T	10 T	18 T	
	0.95	D113	T-12	31.5	28.8	16.4	1.0	112.0	112.0	192 T	885 T	980 T	(1)
	0.95	D120	T-11	28.6	25.9	17.0/8.7	1.0	171.0	-122.0	-	35 C	150 C	(2)
	1.05	62	T-5	28.6	25.8	17.4	1.0	81.6	-86.2	180 C	389 C	800 C	CSR
	1.05	74	T-6	26.1	25.3	20.8	1.0	32.7	-29.8	1200	1600	1800	CSR
	2.06	50	T-5	23.0	21.8	301.0	1.0	51.4	-40.0	40 T	-	-	M.B.
	2.06	51	T-5	26.4	25.4	294.1	1.0	66.2	-50.1	14 T	-	-	M.B.
686A1	0.20	88	T-9	25.2	21.3	53.4	5.7	101.5	-100.2	13 T	48 T	53 T	
	0.20	89	T-10	27.4	21.8	50.0	6.0	68.2	-63.6	113 C	211 C	356 C	
	0.35	84	T-6	20.6	-	296.7	1.0	54.4	-44.5	22 T	-	-	M.B.
	0.35	85	T-5	21.3	-	298.9	1.0	76.8	-65.7	4 T	-	-	M.B.
	0.45	96	T-6	22.2	20.6	295.5	1.0	61.6	-51.9	96 C	-	-	M.B.
	0.45	97	T-5	-	-	298.1	1.0	103.0	-57.5	2 T	-	-	M.B.
	0.56	109	T-6	-	-	293.6	1.0	54.2	-46.2	420 T	423 T	426 T	M.B.
	0.56	110	T-5	-	-	297.1	1.0	93.1	-76.9	11 T	25 T	40 T	M.B.
687A1	0.49	95	T-5	33.6	29.4	298.7	1.0	64.3	-57.8	2 T	5 T	6 T	
	0.49	94	T-6	40.6	34.0	296.7	1.0	26.7	-22.5	330 C	402 T	414 T	

C = Compressive strain;

T = Tensile strain;

M.B. = Membrane broke during cycling;

CSR = Changed stress ratio (results are questionable);

(1) Isotropic consolidation, drainage between bursts, τ/σ'_c = 6; 12; 25; 56; 112%

(2) Anisotropic consolidation, drainage between bursts, τ/σ'_c = 37, 4; 49, 0; 73, -24; 98, -49; 122, -73; 171, -122%

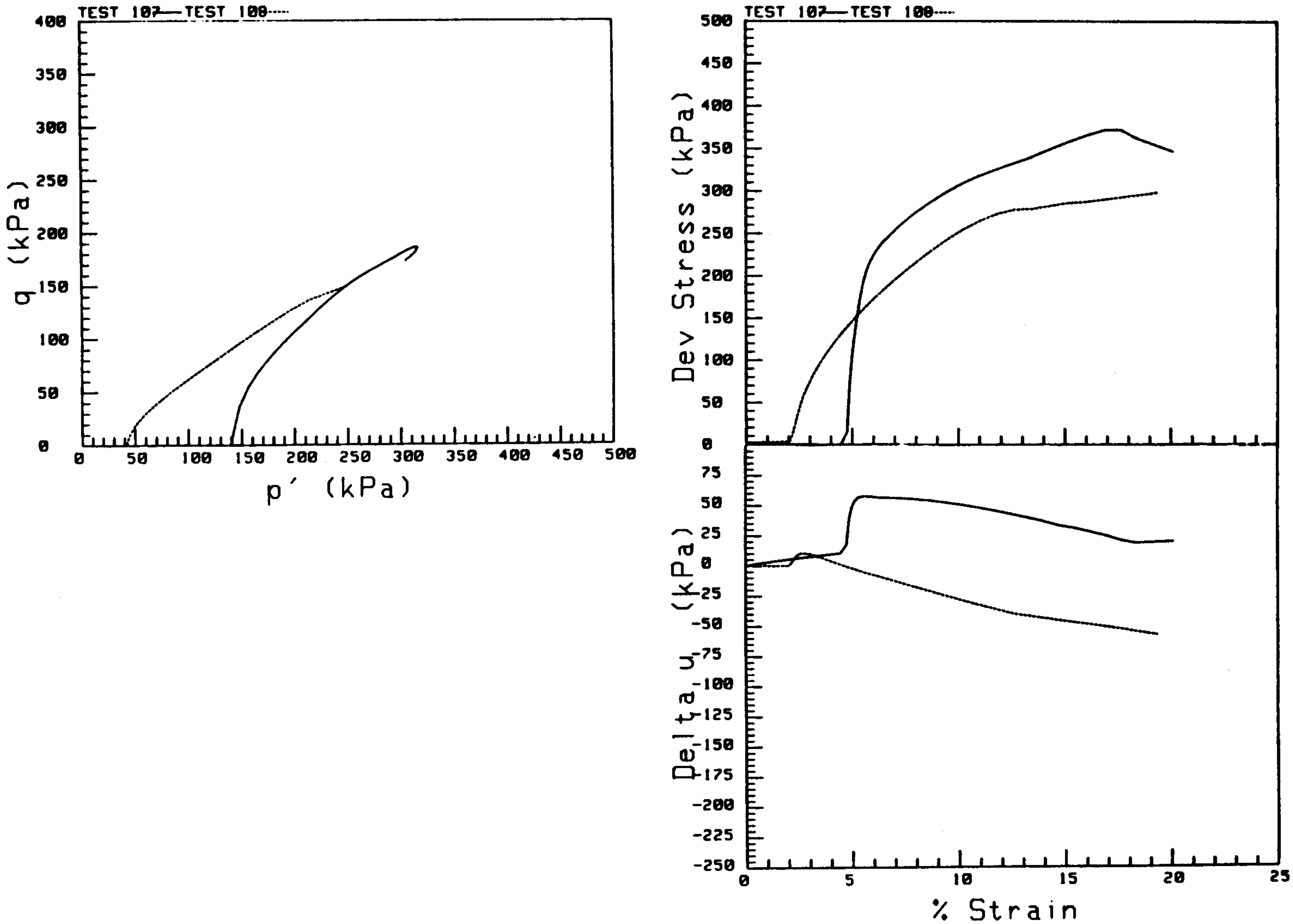

Fig. 8a. Multiple static triaxial test results (core 681 A2).

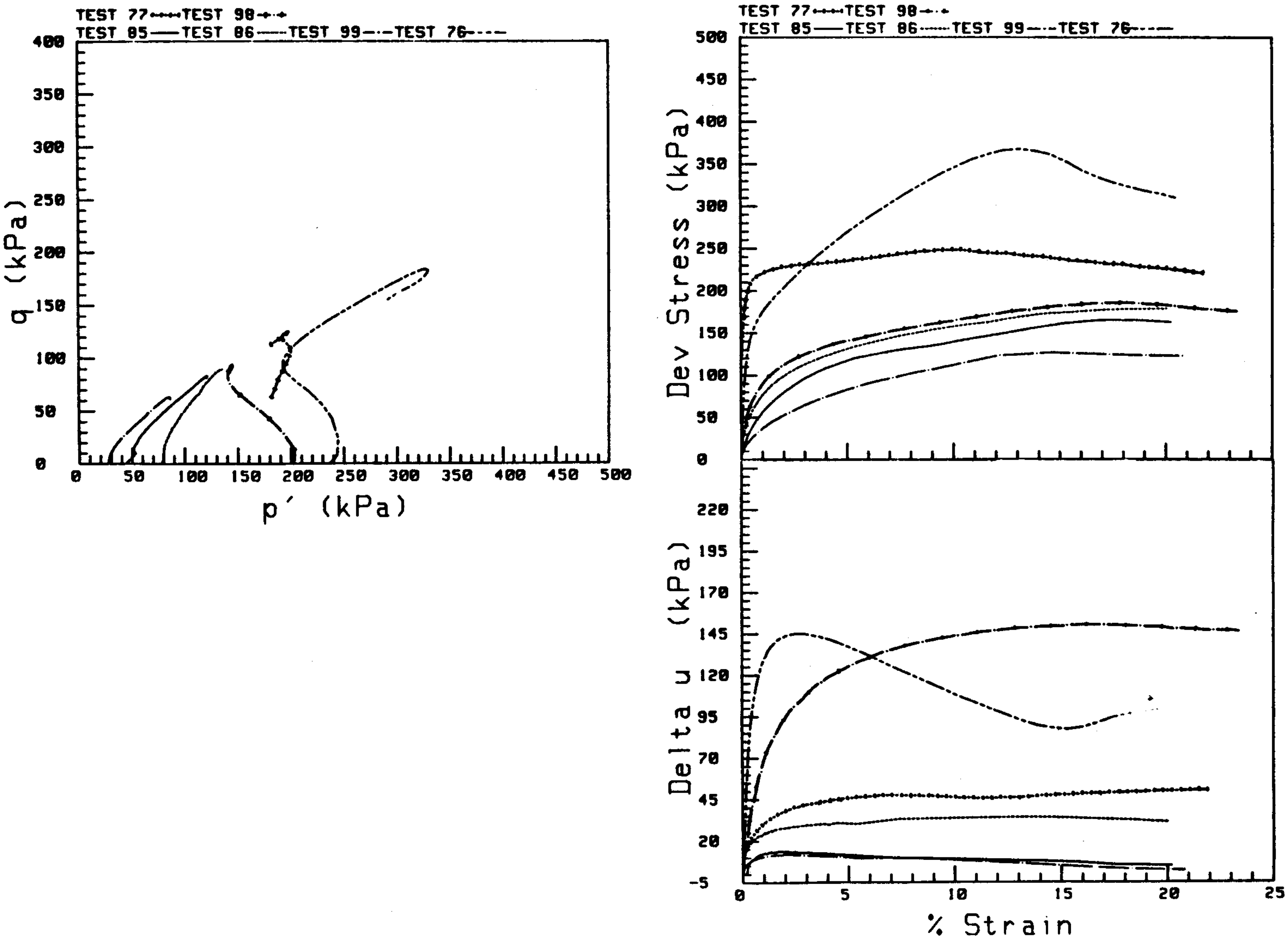

Fig. 8b. Multiple static triaxial test results (core 682 Al).

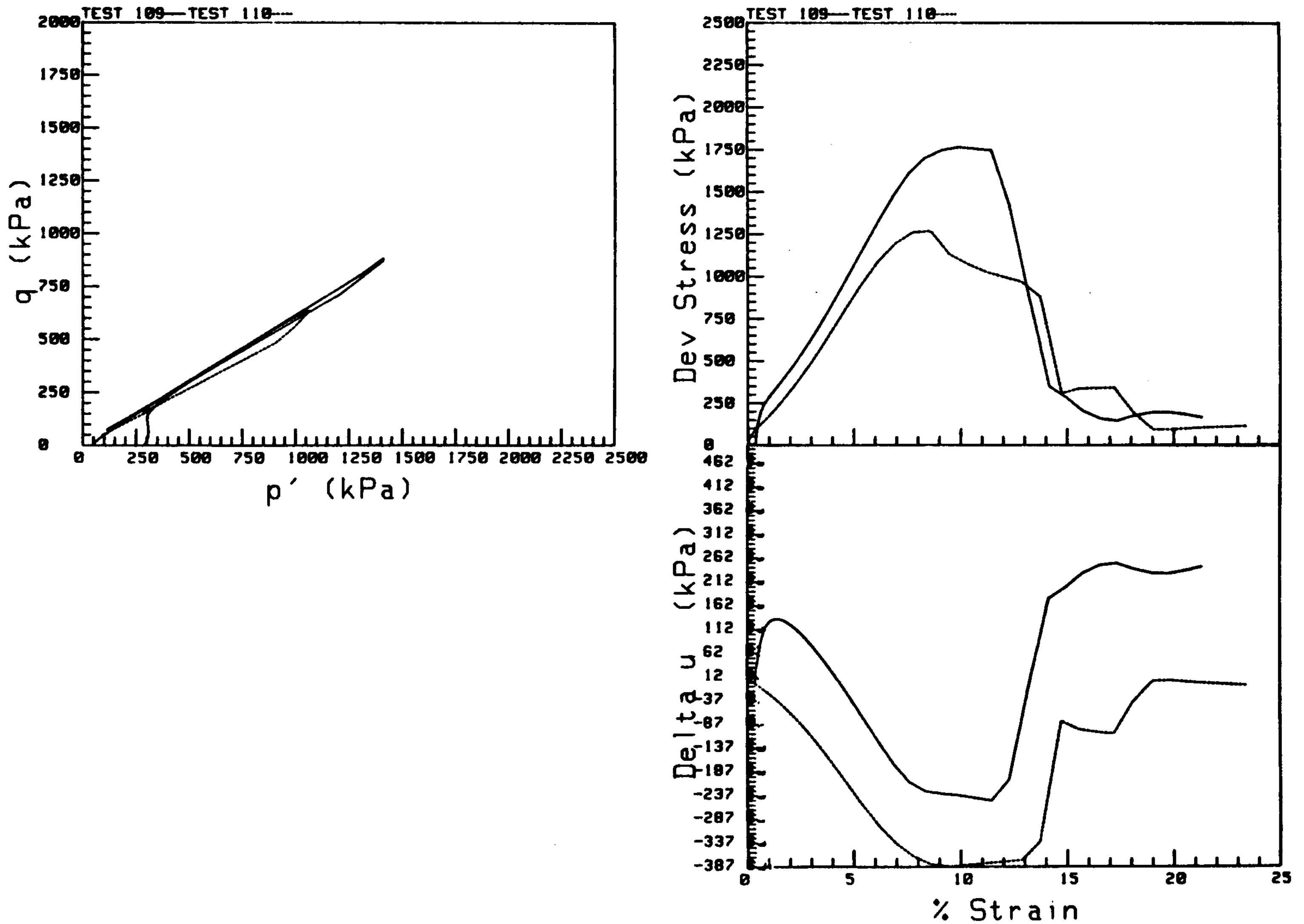

Fig. 8c. Multiple static triaxial test results (core 683 Al).

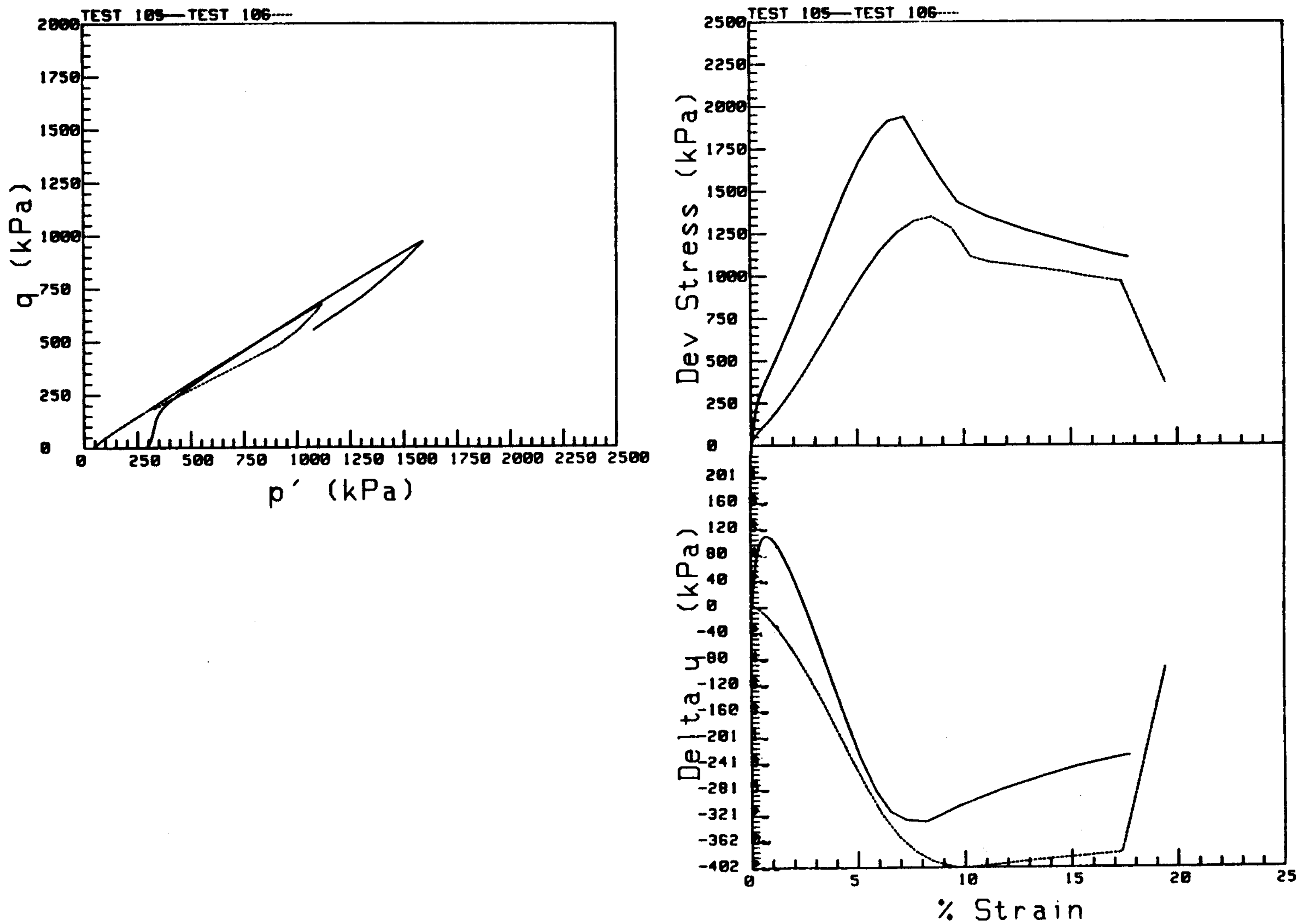

Fig. 8d. Multiple static triaxial test results (core 684 A1).

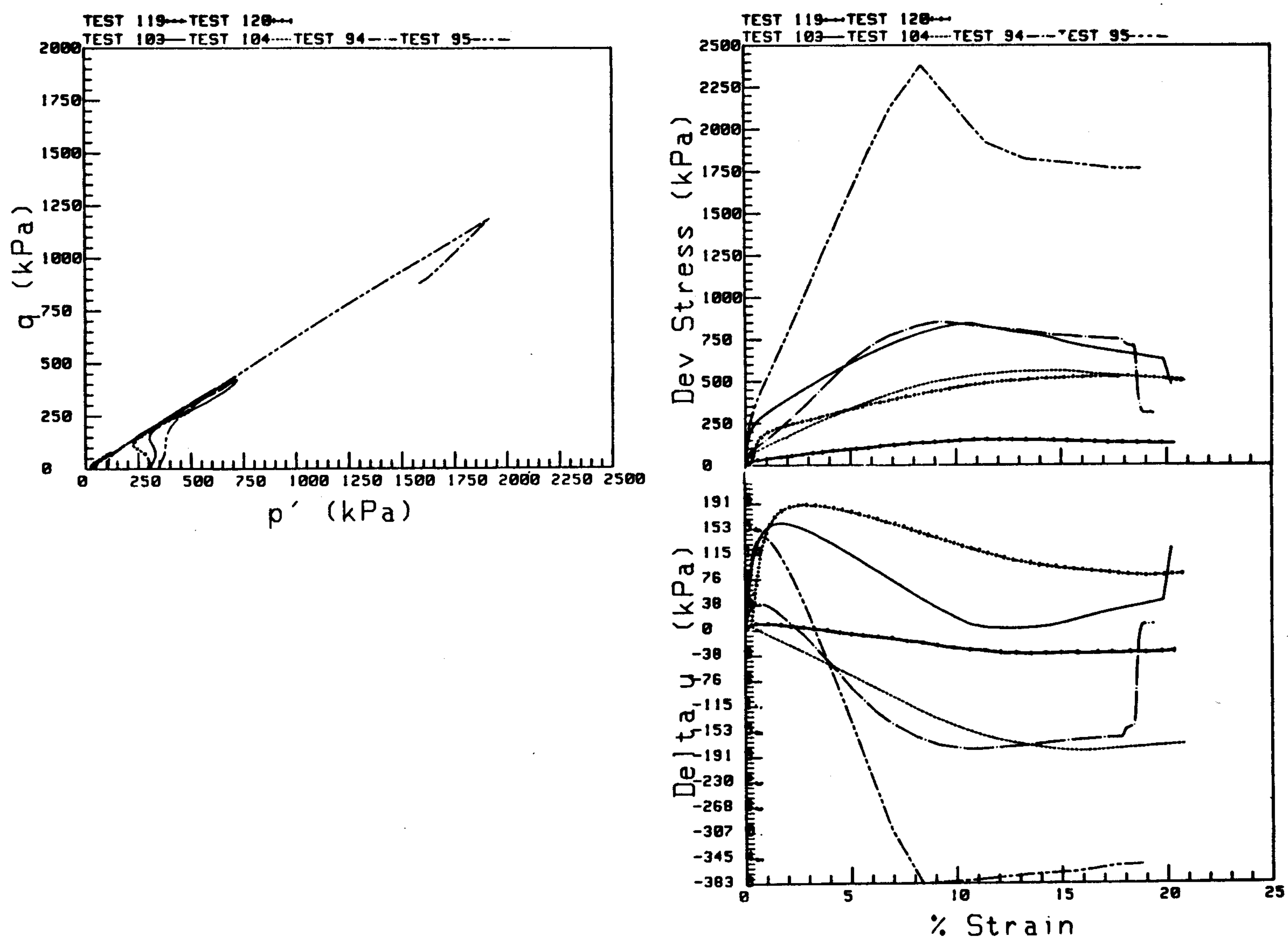

Fig. 8e. Multiple static triaxial test results (core 685 A2).

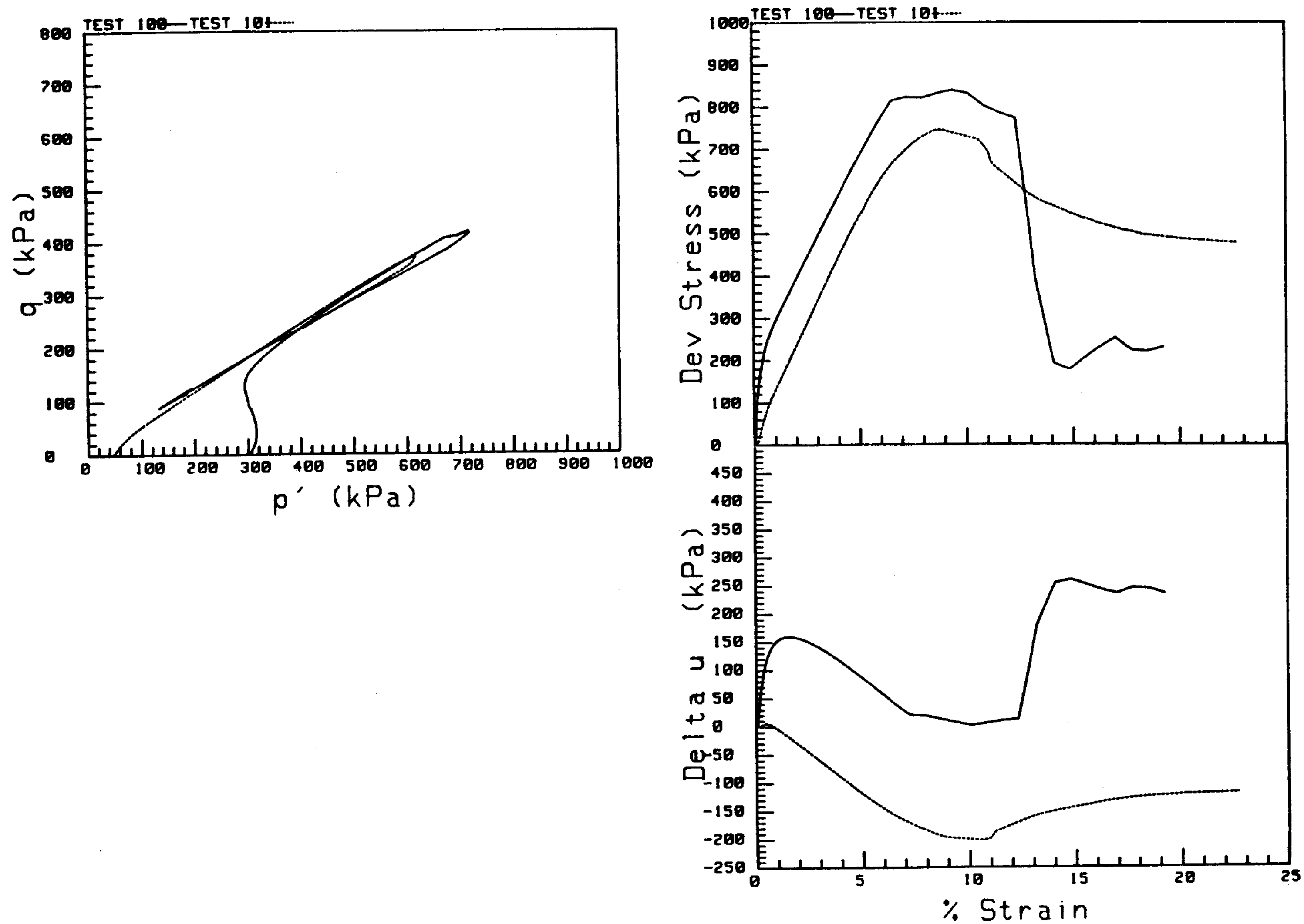

Fig. 8f. Multiple static triaxial test results (core 686 A1).

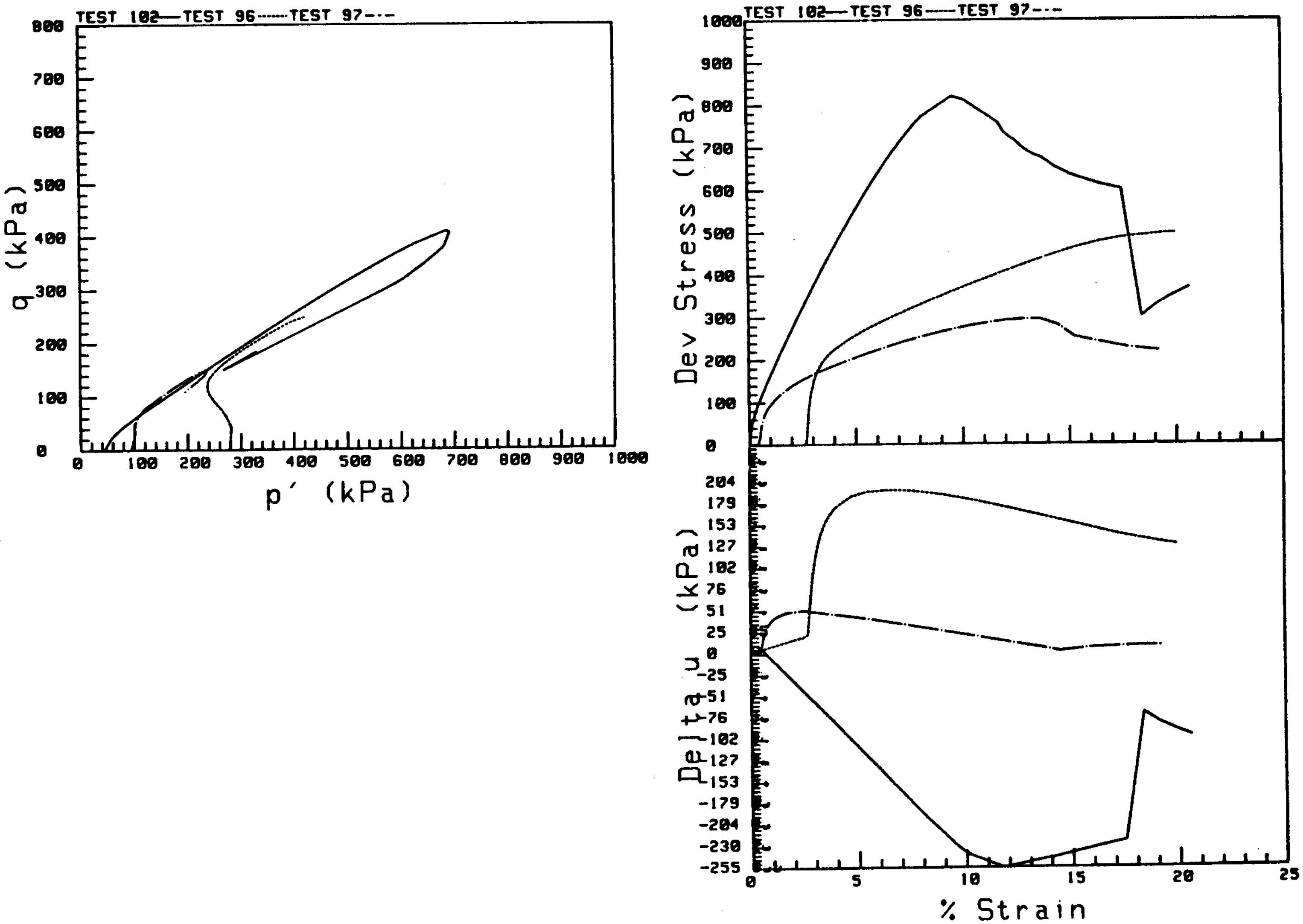

Fig. 8g. Multiple static triaxial test results (core 687 Al).

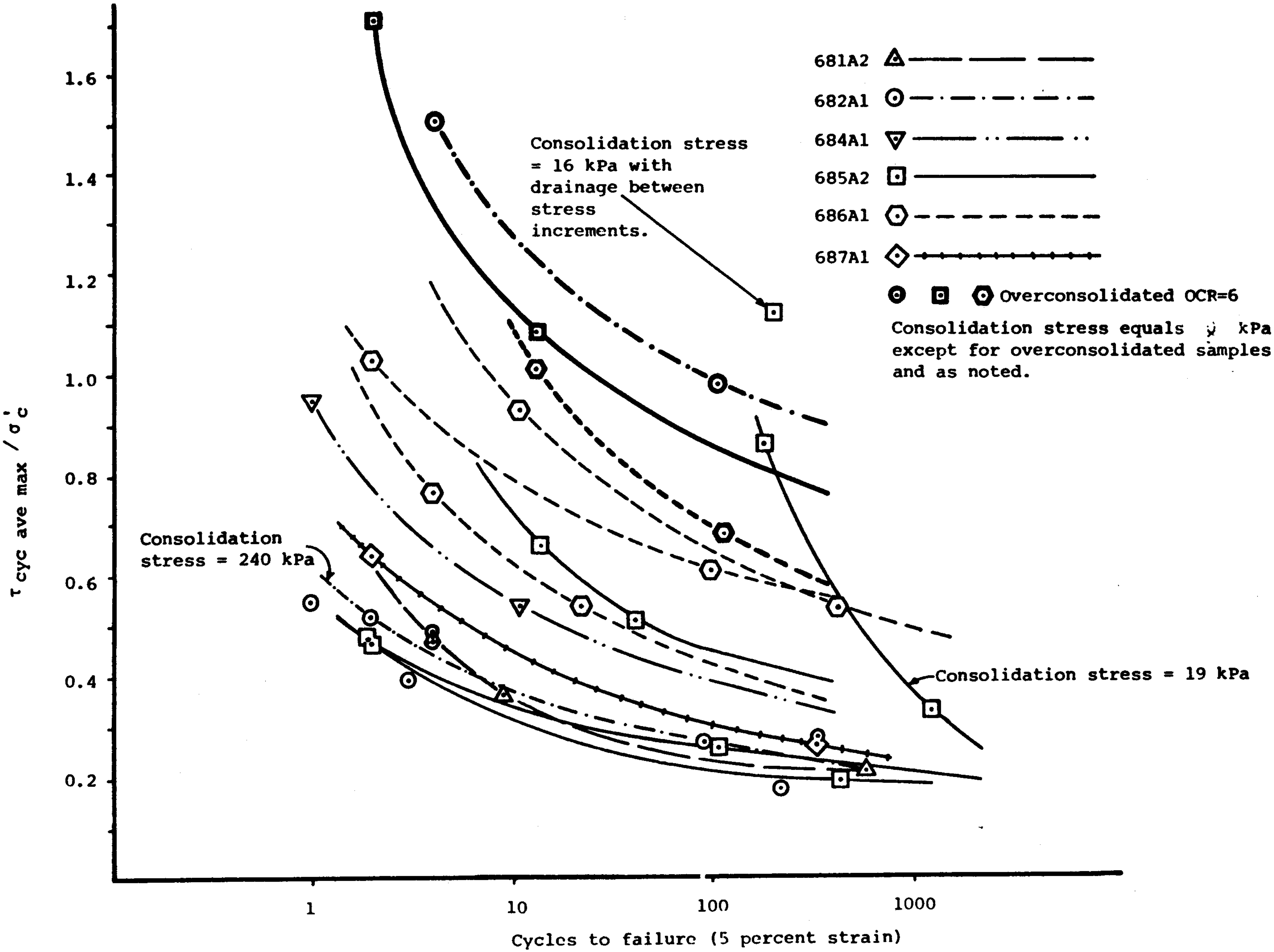

Fig. 9. Cyclic stress ratio vs number of cycles to reach 5% strain in cyclic triaxial tests.

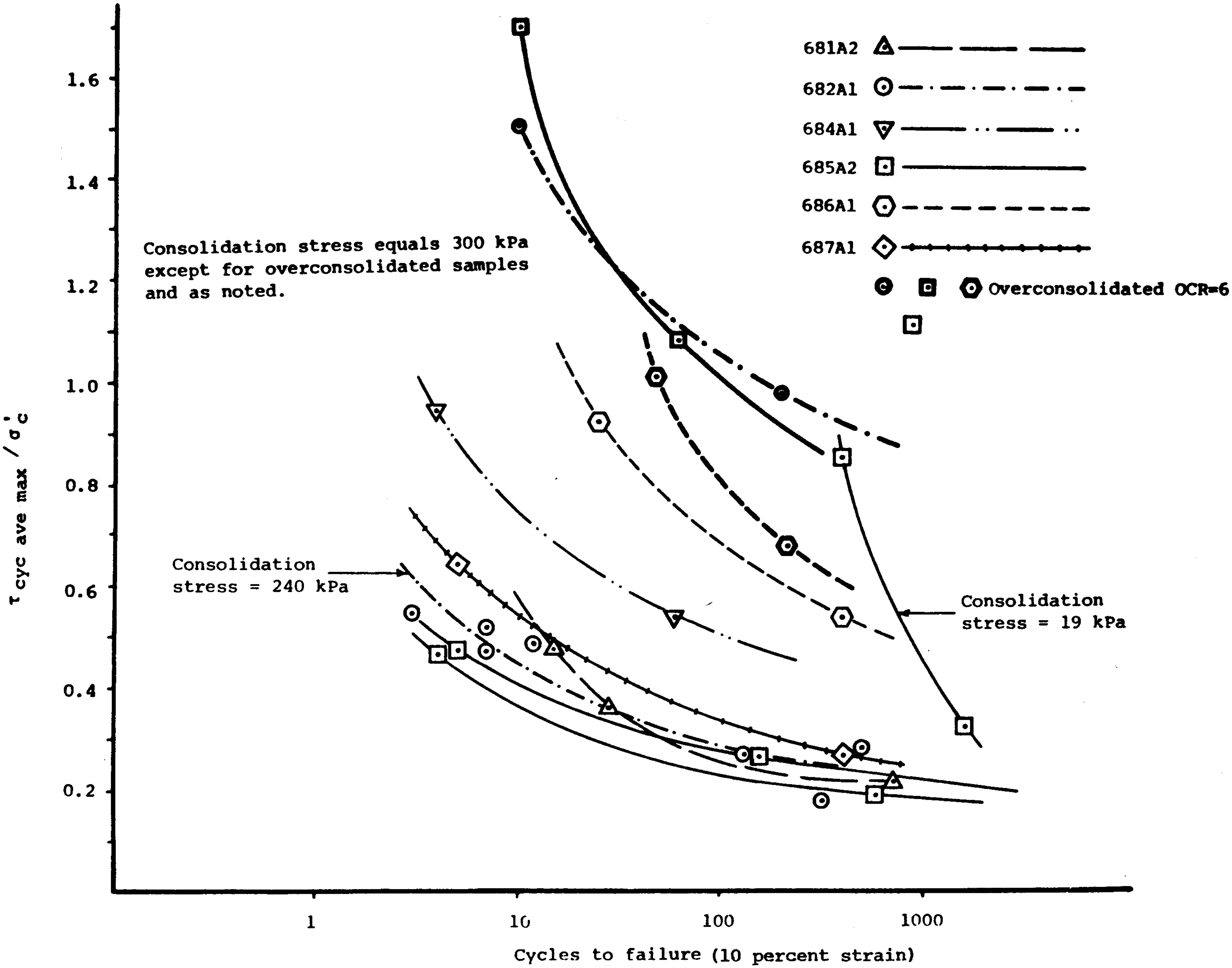

Fig. 10. Cyclic stress ratio vs number of cycles to reach 10% strain in cyclic triaxial tests.

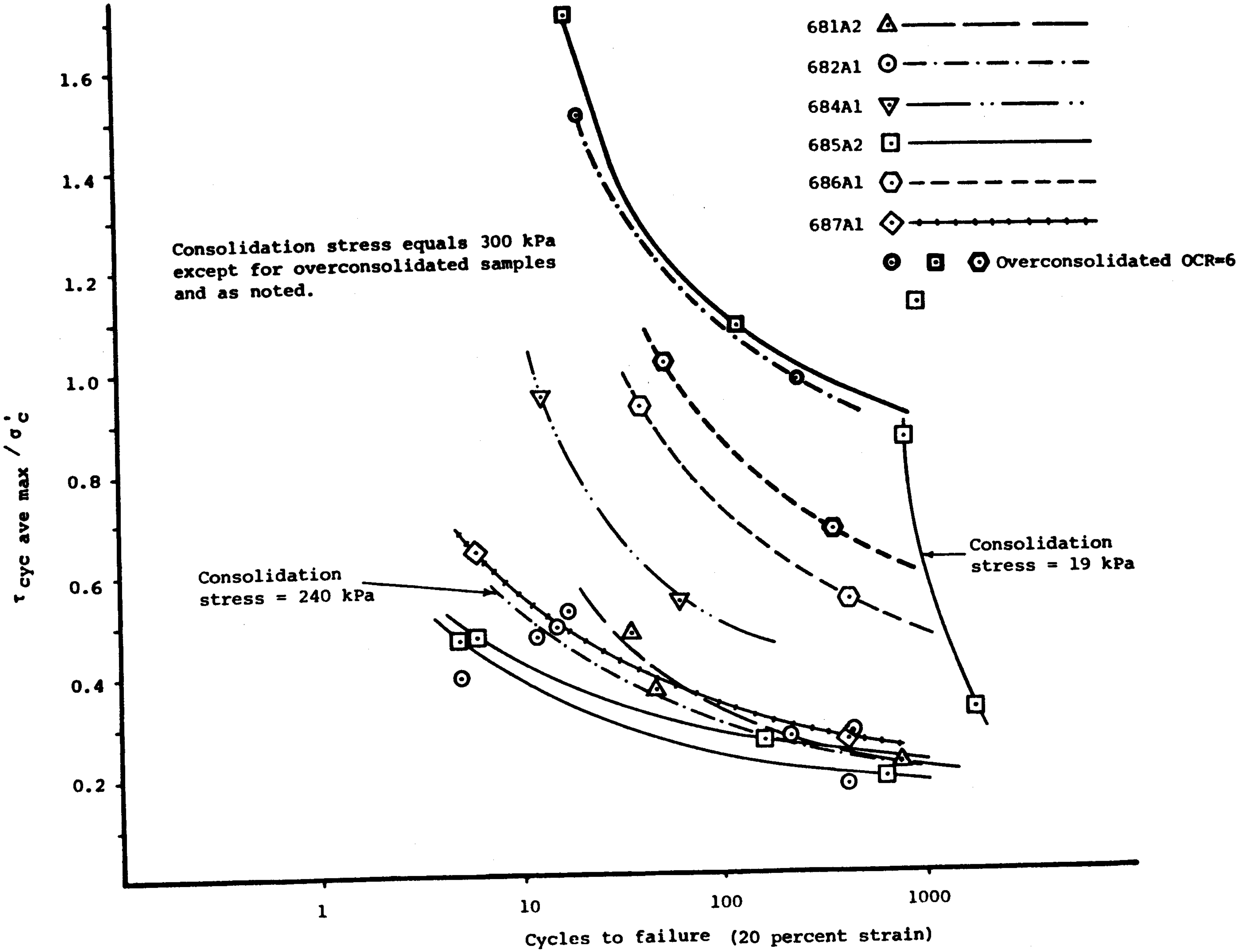

Fig. 11. Cyclic stress ratio vs number of cycles to reach 20% strain in cyclic triaxial tests.

strain accumulate with repeated application of $\tau_{cyc\ ave\ max}$. At some point, the pore water pressure approaches the confining stress, strain increases at a faster rate, and the sediment fails. In our tests, failure was chosen when 5% strain was reached.

RESULTS

Yukon prodelta: The Yukon River delta protrudes into Norton Sound from the south coast (Fig. 1). The prodelta - the outer, low-gradient, submerged area - extends over 100 km offshore and marks the distal zone of deltaic sedimentation. Sediment from the Yukon River is deposited mostly from suspension on the prodelta and is reworked by large storm waves and strong geostrophic currents (Dupré and Thompson, 1979; Nelson 1980b). Much of the fine-grained fraction from the Yukon River is eventually transported north to the Chukchi Sea (Nelson and Creager, 1977; Cacchione and Drake, 1979). The material left behind on the prodelta is predominantly silt and very fine sand (McManus and others, 1977). Graded storm-sand layers (mean grain size = 0.250 mm, bedding thickness 10-20 cm) make up 50-100% of the deposits near shore; in distal areas 60-75 km from the source, they are finer (mean size = 0.125 mm), thinner (1-2 cm), and make up 35% of the section (Nelson, 1980b).

We occupied five penetrometer stations on the prodelta (667, 668, 669, 670, 674) and collected vibracores near three of these (685 near 670, 686 near 669, and 687 near 674) (Fig. 1, Table 1). Cores were collected near the two other sites on previous cruises (78-22 near 668, 78-24 near 667) (Fig. 1, Table 1).

Sediment cores on the prodelta are mixtures of non-plastic sand and silt, with clay content commonly less than 10% (Table 4, Figs. 12-16). The cores

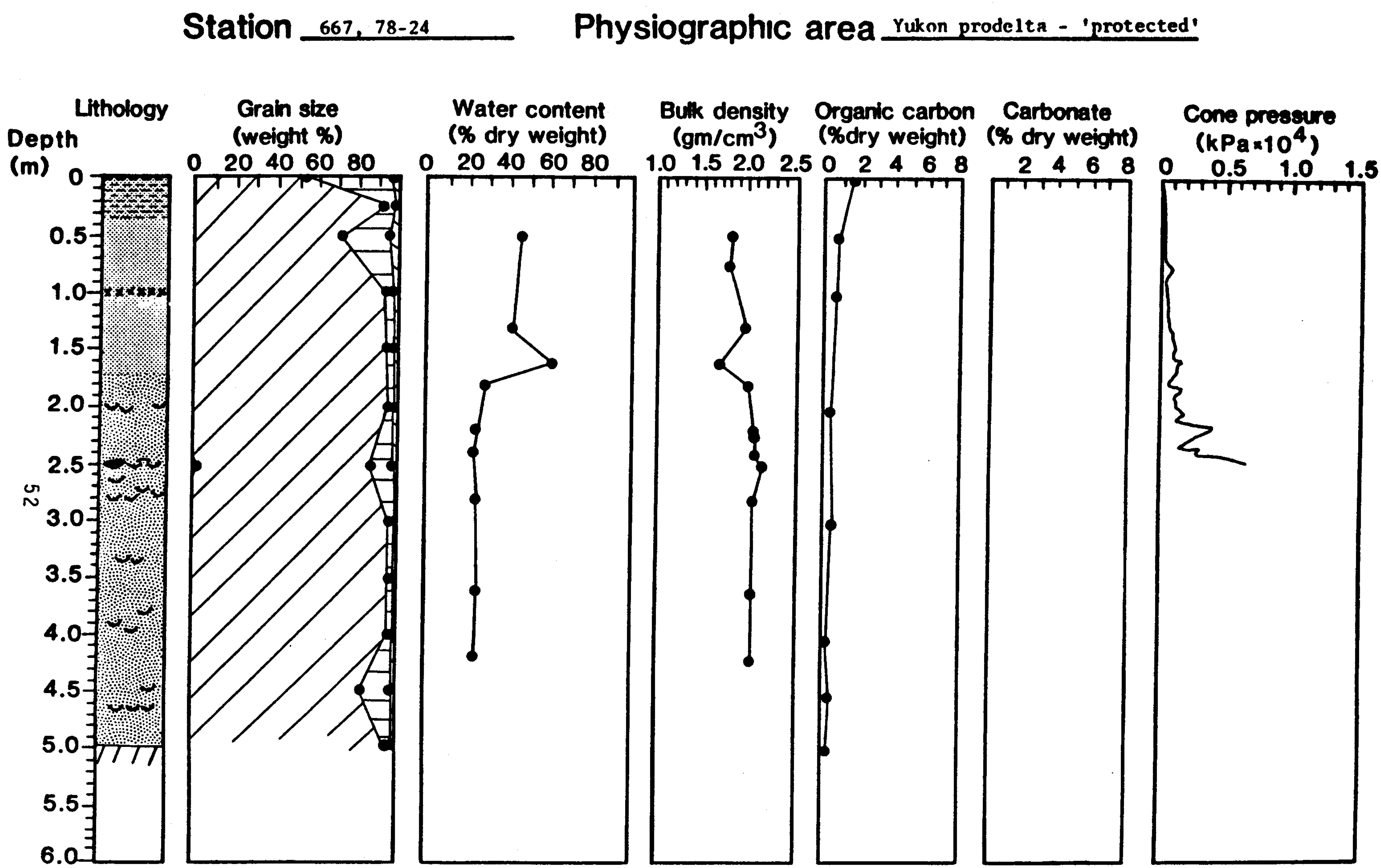

Fig. 12. Lithology, index properties and cone pressure vs subbottom depth for stations 667 and 78-24 (Yukon prodelta - "protected").

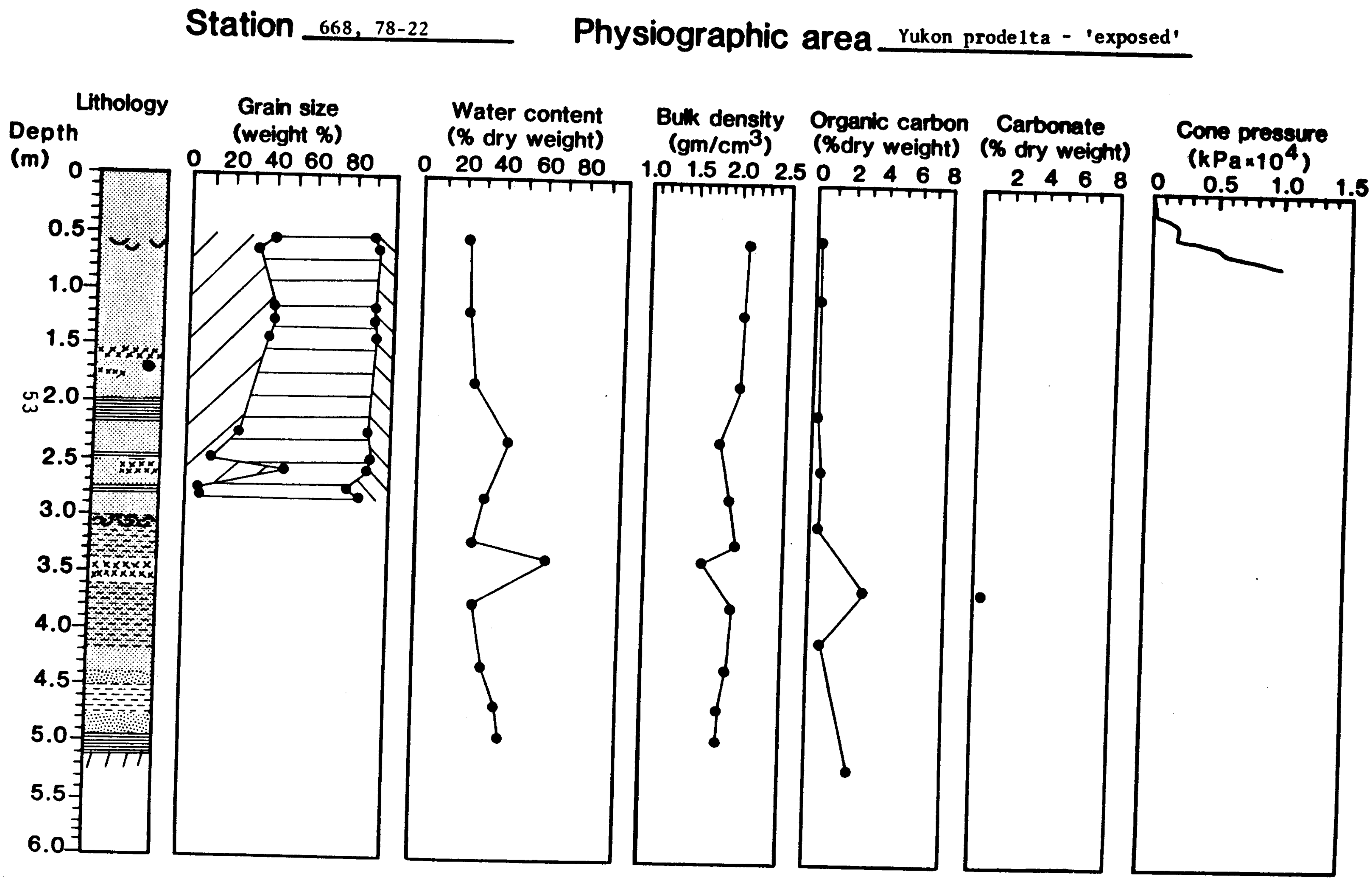

53

Fig. 13. Lithology, index properties and cone pressure vs subbottom depth for stations 668 and 78-22 (Yukon prodelta - "exposed").

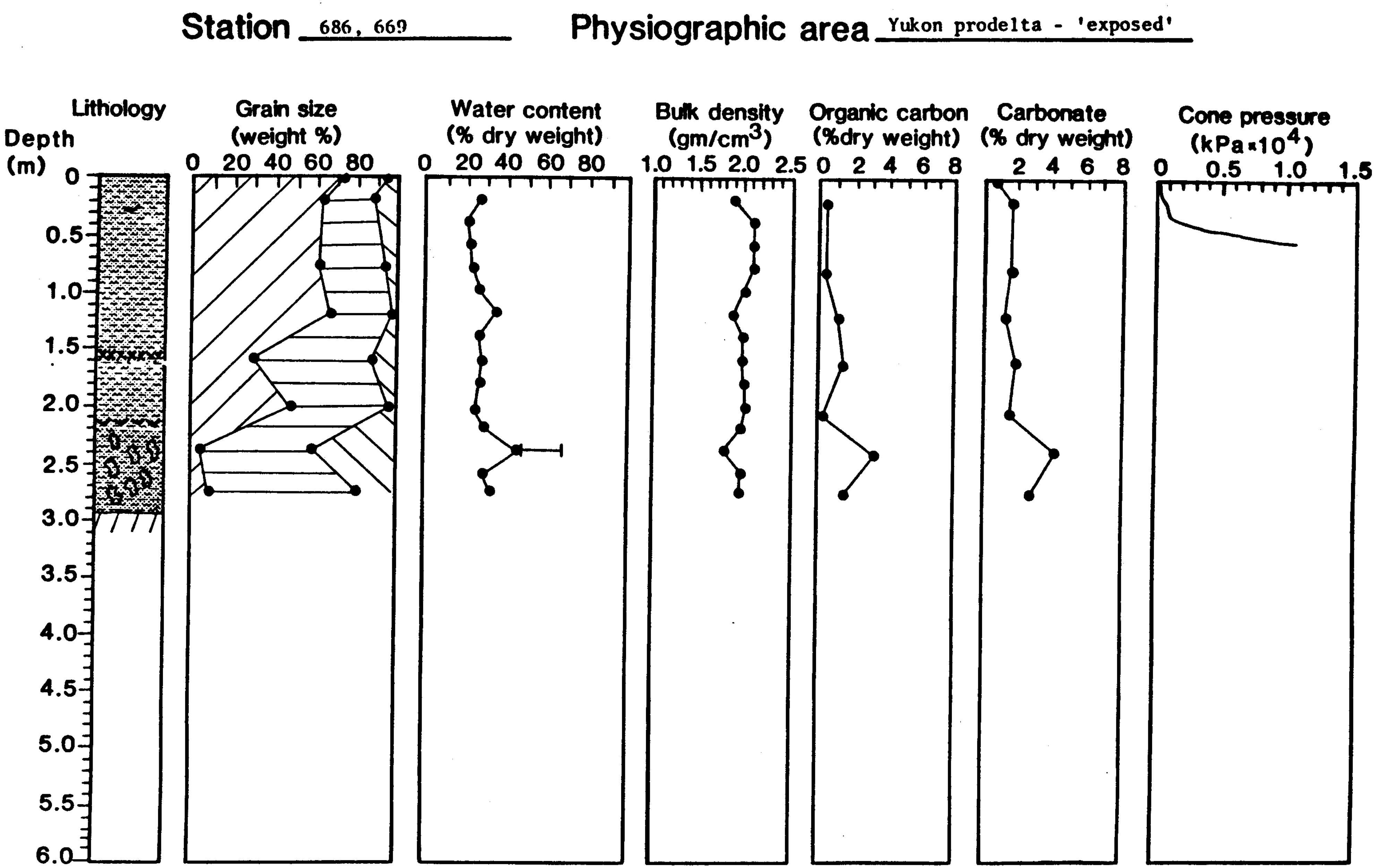

Fig. 14. Lithology, index properties and cone pressure vs subbottom depth for stations 686 and 669 (Yukon prodelta - "exposed").

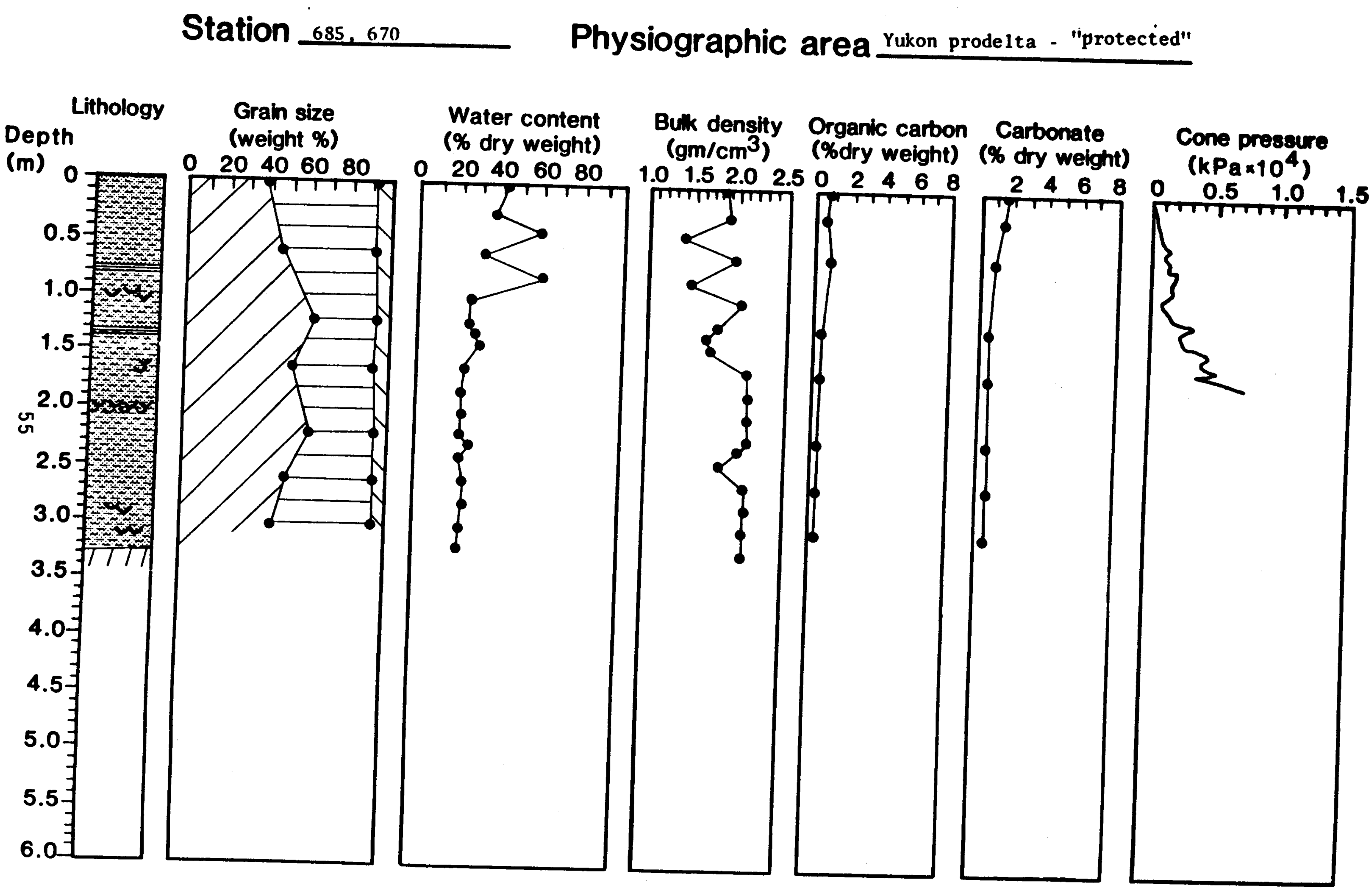

Fig. 15. Lithology, index properties and cone pressure vs subbottom depth for stations 685 and 670 (Yukon prodelta - "protected").

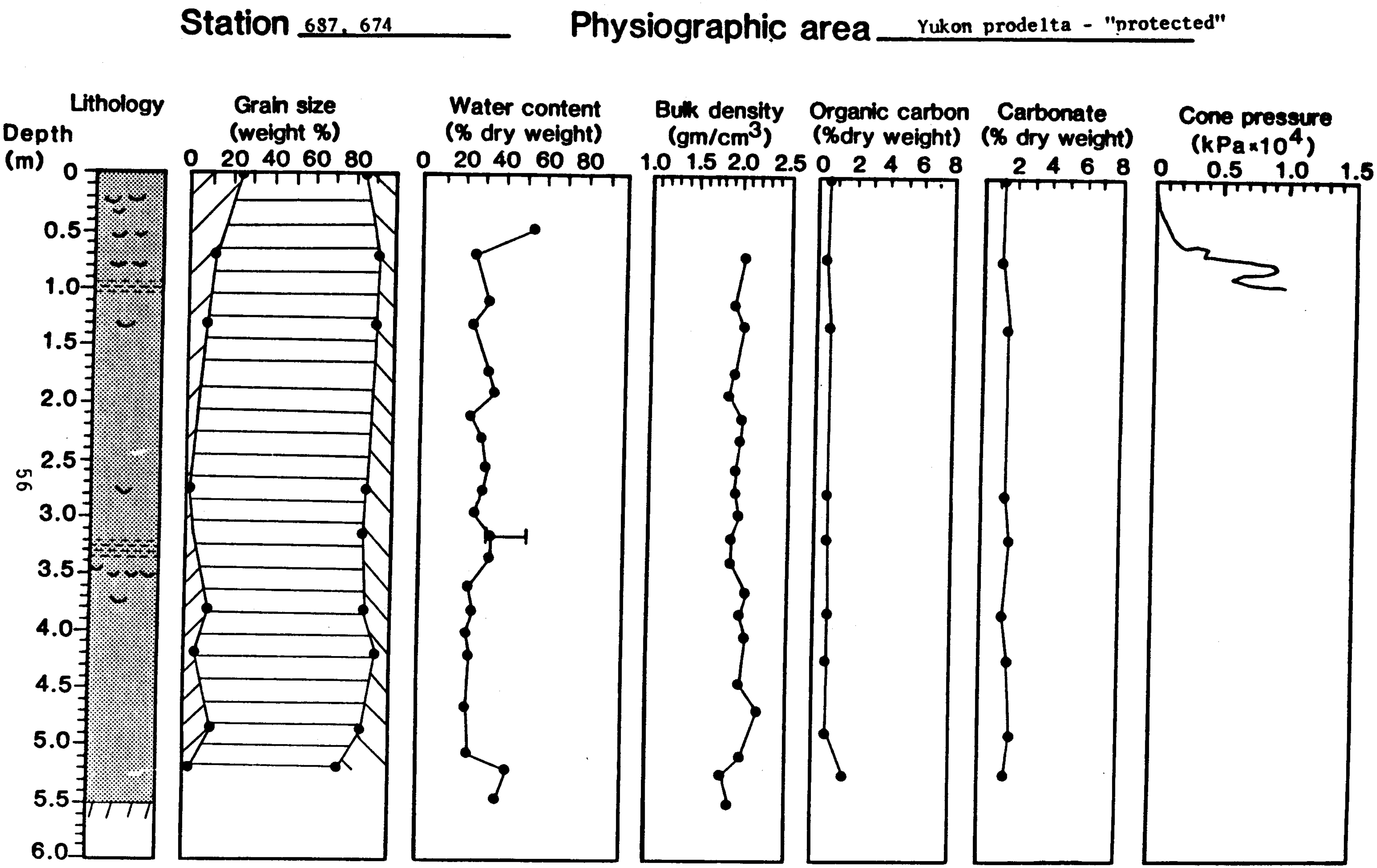

Fig. 16. Lithology, index properties and cone pressure vs subbottom depth for stations 687 and 674 (Yukon prodelta - "protected").

have similar textures and compositions, and these change relatively little with depth, except at station 686 there is a general downward fining of grain size. Thin shell layers occur sparsely. Burrow mottles and a carbon-rich layer appear in core 686. The Alpine vibracorer penetrated at a slower rate and to a shallower depth west of the delta (station 686) than to the northeast (stations 685 and 687) (Table 2).

Maximum XSP-40 penetration depth is shallow for the two stations west of the delta (668, 669), greater at the next two stations to the northeast (667, 670) and intermediate at the farthest northeast station (674) (Figs. 12-16). Replicate tests are similar at each site (Appendix B). Cone pressure increases abruptly and relatively smoothly at the first two stations, whereas it is more gradual and somewhat erratic at the others. The cores show only minor stratigraphic variation with depth, which is consistent with the shape of the penetrometer curves.

Plots of friction ratio versus cone pressure for stations on the prodelta where penetration exceeded 0.28 m (stations 669, 670, and 674) are inconsistent in terms of the sediment types they imply when compared to samples recovered in cores. Silt-rich muddy sediment, with major amounts of sand at stations 669 and 670 and minor amount of sand at station 674, constitutes the core samples. The penetrometer data indicate a wider range of sediment types: clay and mud at station 669, silt and sandy silt at station 670 (the closest correlation between cores and penetrometer data), and silt to sand at station 674 (Fig. 17). As clearly pointed out by Martin and Douglas (1981), a sediment classification scheme developed from penetrometer data is area-dependent and refers to sediment behavior types; that is, sediment types classified according to physical properties and not necessarily according to

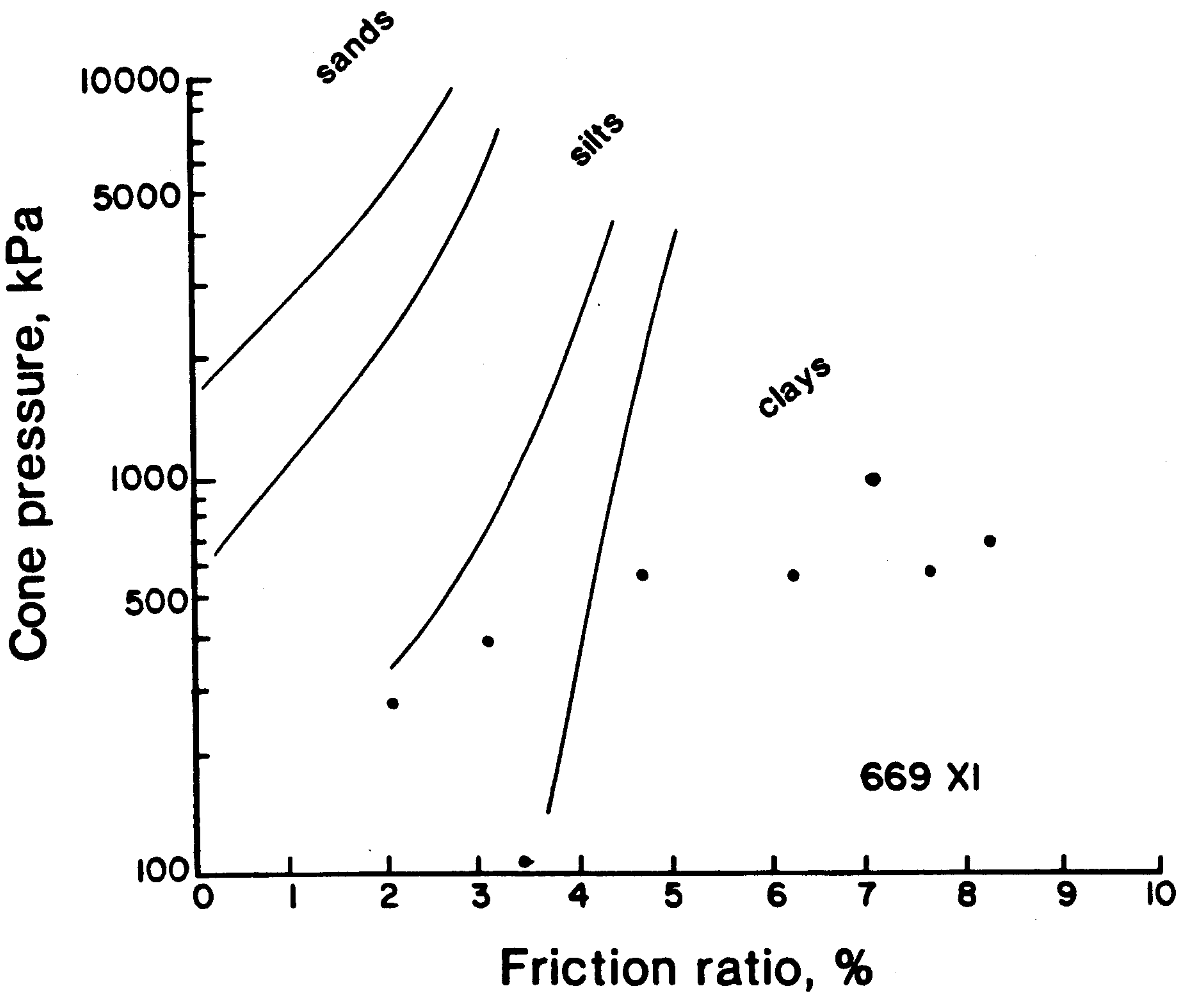

Fig. 17a. Sediment type determined from cone penetration test 669X1 (Yukon prodelta - "exposed" - near station 686).

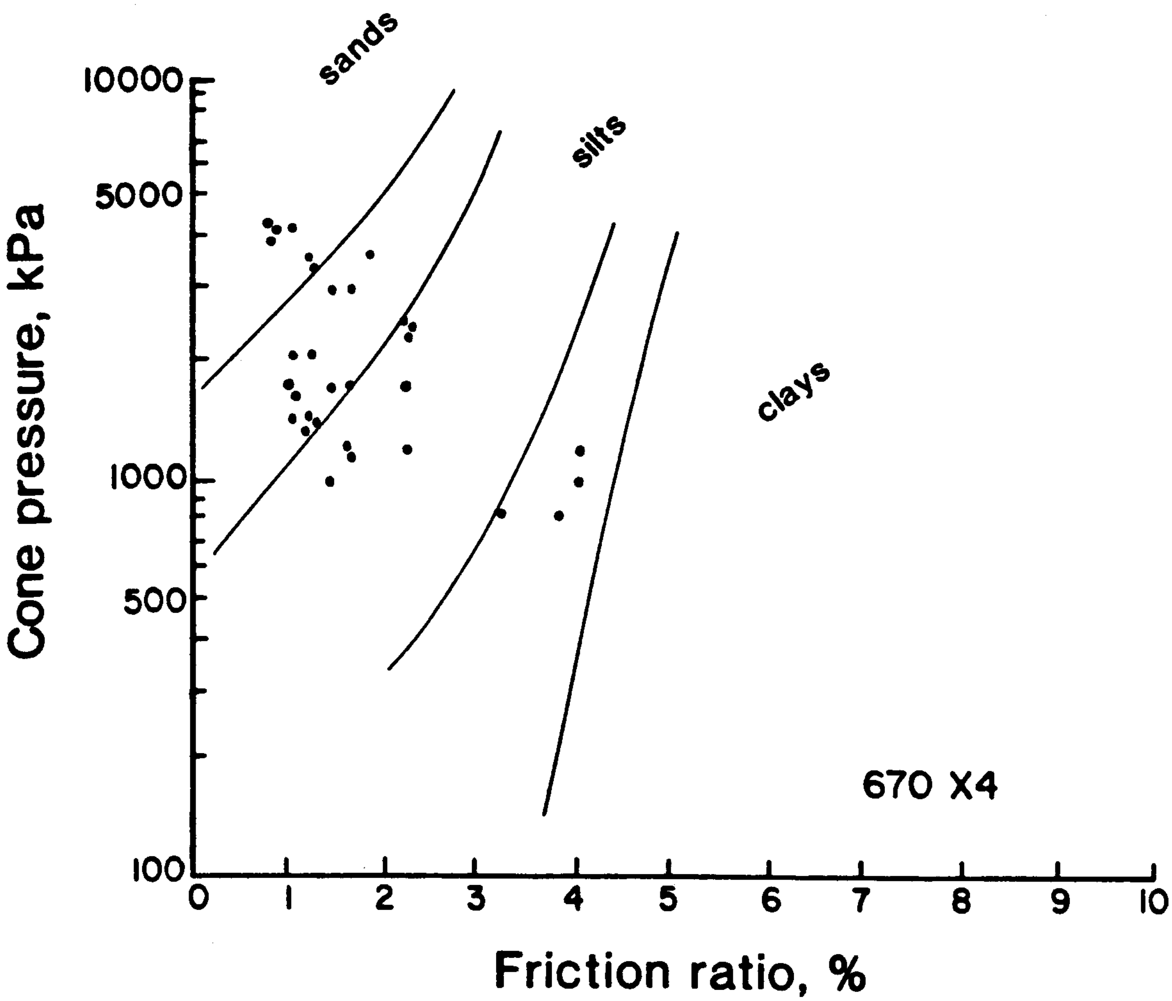

Fig. 17b. Sediment type determined from cone penetration test 670X4 (Yukon prodelta - "protected" - near station 685).

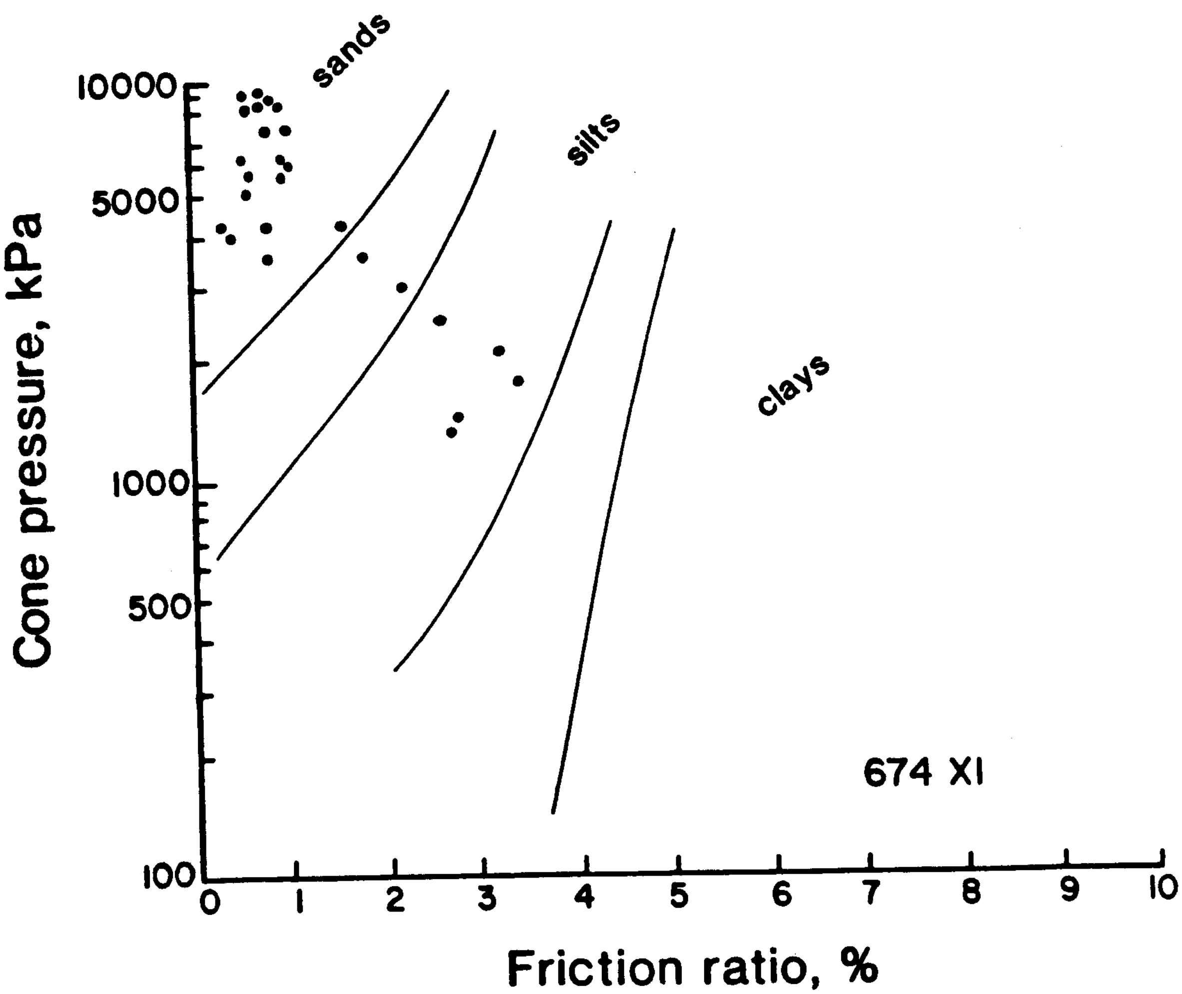

Fig. 17c. Sediment type determined from cone penetration test 674X1 (Yukon prodelta - "protected" - near station 687).

texture. Perhaps the variation in sediment behavior types on the prodelta reflects more than grain size. Organic carbon is one compositional variable that would be an obvious suspect, but values are uniformly low at all 3 stations.

Relative density is high at the two southwest stations (668 and 669); typical values in excess of 100% were calculated with Schmertmann's equation (Appendix C). These numbers are unrealistic, of course, because the upper limit of relative density is 100%. The calculations probably indicate that the sediment is overconsolidated; that is, its state of consolidation is greater than would be produced by the existing overburden stress (Beard and Lee, 1982). Schmertmann's equation assumes normal consolidation. Although the calculations give unrealistically high values for relative density, they at least imply a dense sediment state shallow in the seabed at these sites. In contrast, the two stations farther to the northeast (667, 670) have comparatively low calculated relative densities, whereas intermediate values were calculated for station 674.

Laboratory test results show that low values of compression index (C_c = 0.03 - 0.25) are present west and north of the delta (stations 685, 686 and 687), and they vary erratically down-core (Table 6). The results agree relatively well with material from other study areas (Fig. 18) (Lambe and Whitman, 1969, p. 321). Sediment in the western prodelta appears the most overconsolidated (station 686), station 685 in the north is the least overconsolidated, and sediment in the northeast (station 687) is in between, however OCR values typically decrease with subbottom depth at all locations (Table 6).

Triaxial tests demonstrate that sediment at the various sites behaves differently under static loading (Table 7). West of the delta (station 686) the material has the highest friction angle ($\phi' = 42°$) and a high S_u/σ'_c ratio (1.38), whereas to the northeast (station 687) a low friction angle (38.3°) and S_u/σ'_c ratio (0.83) are present. North of the delta (station 685) sediment down-core responded differently to testing (tests 95, 103 and 120 in Fig. 8e), ϕ' varied from 36.8° to 38.1° and the S_u/σ'_c ratio from 0.91 to 1.39. Contractive behavior occurred in all areas at high consolidation stresses (the S- shaped curves in the q versus p' plots in Figs. 8e - 8g), whereas dilatant behavior developed at lower stresses ($\sigma'_c < 100$ kPa). Dilatant undrained behavior produces stronger sediment than contractive behavior would at the same consolidation stress. Some tests at each station produced peaked stress-strain curves that are indicative of sensitive behavior (Figs. 8e - 8g).

Liquefaction, caused by repeated loading of waves or earthquakes, transforms sediment from a solid into a liquefied state as a consequence of increased pore pressure and reduced effective stress (Committee on Soil Dynamics of the Geotechnical Engineering Division, 1978). Liquefaction does not imply that ground failure will occur; however, many sediment movements have been attributed to the process. North and west of the delta (stations 685 and 686) the sediment type is within the limits for observed liquefaction, whereas in the northeast (station 687) the one detailed grain size distribution was close to but not fully in the range (Table 3, Fig. 19 and Appendix A). Susceptibility to liquefaction in cyclic triaxial tests is indicated by a low cyclic shear stress ratio ($\tau_{cyc\ ave\ max}/\sigma'_c$) (Table 8, Fig. 9). Cyclic test results of sediment from the northern prodelta (station 685)

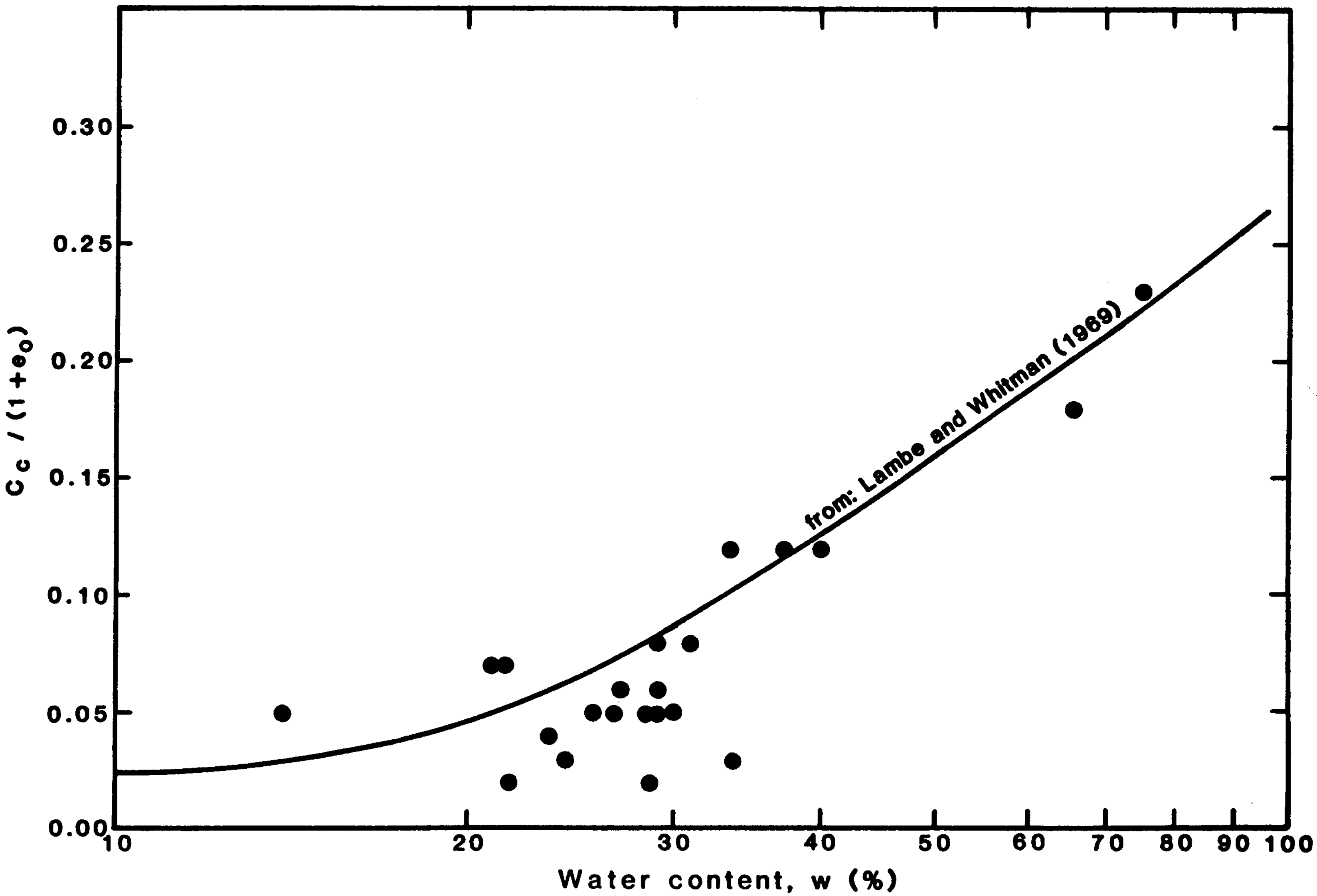

Fig. 18. Compression index (C_c) determined from consolidation tests related to the initial void ratio (e_o) vs water content (w).

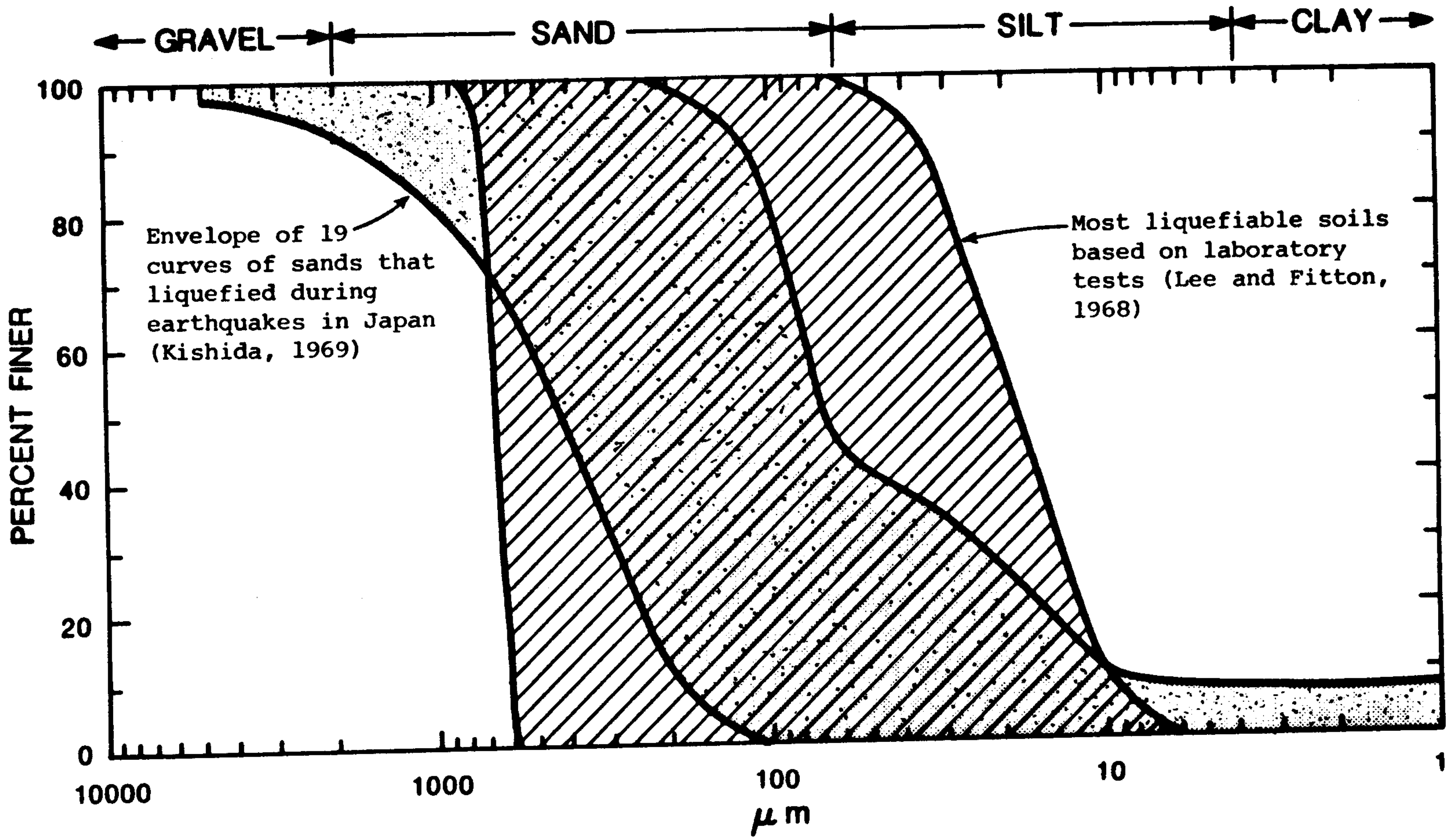

Fig. 19. Zones of grain size distributions of liquefiable soil (from Finn, 1972).

plotted lowest on Figure 9, followed by material from the northeast (station 687), and west (station 686). A plot of laboratory cyclic triaxial stress ratio versus in situ cone penetration test (CPT) relative density for nearby sediment illustrates that loose sediment is more likely to liquefy (because it builds up pore pressure more readily) than dense material (Fig. 20).

Analyses, incorporating laboratory cyclic triaxial test and CPT results, determined the minimum seafloor earthquake acceleration (a_{max}) and the smallest sustained storm wave height (H) necessary to cause liquefaction at particular stations (Table 9, Appendix G). Liquefaction potential varies markedly on the prodelta. Sediment at the northern station (685) requires an a_{max} from 0.09 g to 0.14 g and a wave height from 9 to over 13 meters, depending on the analysis, to induce liquefaction. At the northeast station (687) a_{max} ranges from 0.11 g to 0.27 g and wave heights over 13 meters are required to cause instability. The range in earthquake acceleration is 0.15 g to 0.35 g, at station 686 in the western prodelta, with waves over 13 meters necessary to cause liquefaction (Table 9).

Thermogenic gas seep: Thermogenically derived gas is actively seeping from the seafloor in Norton Sound about 40 km south of Nome (Fig. 2). Anomalously high concentration of hydrocarbon gas in the water column originally pointed to the existence of the seep (Holmes and Cline, 1979). Subsequent seismic-reflection profiling identified an area of about 50 km^2 where reflector pull-downs and terminations (acoustic anomalies) occur in the sediment column (Holmes and Cline, 1979). Bubbles escaping from the seafloor have been observed with underwater television and high frequency seismic-reflection profilers over this area (Nelson and others, 1978).

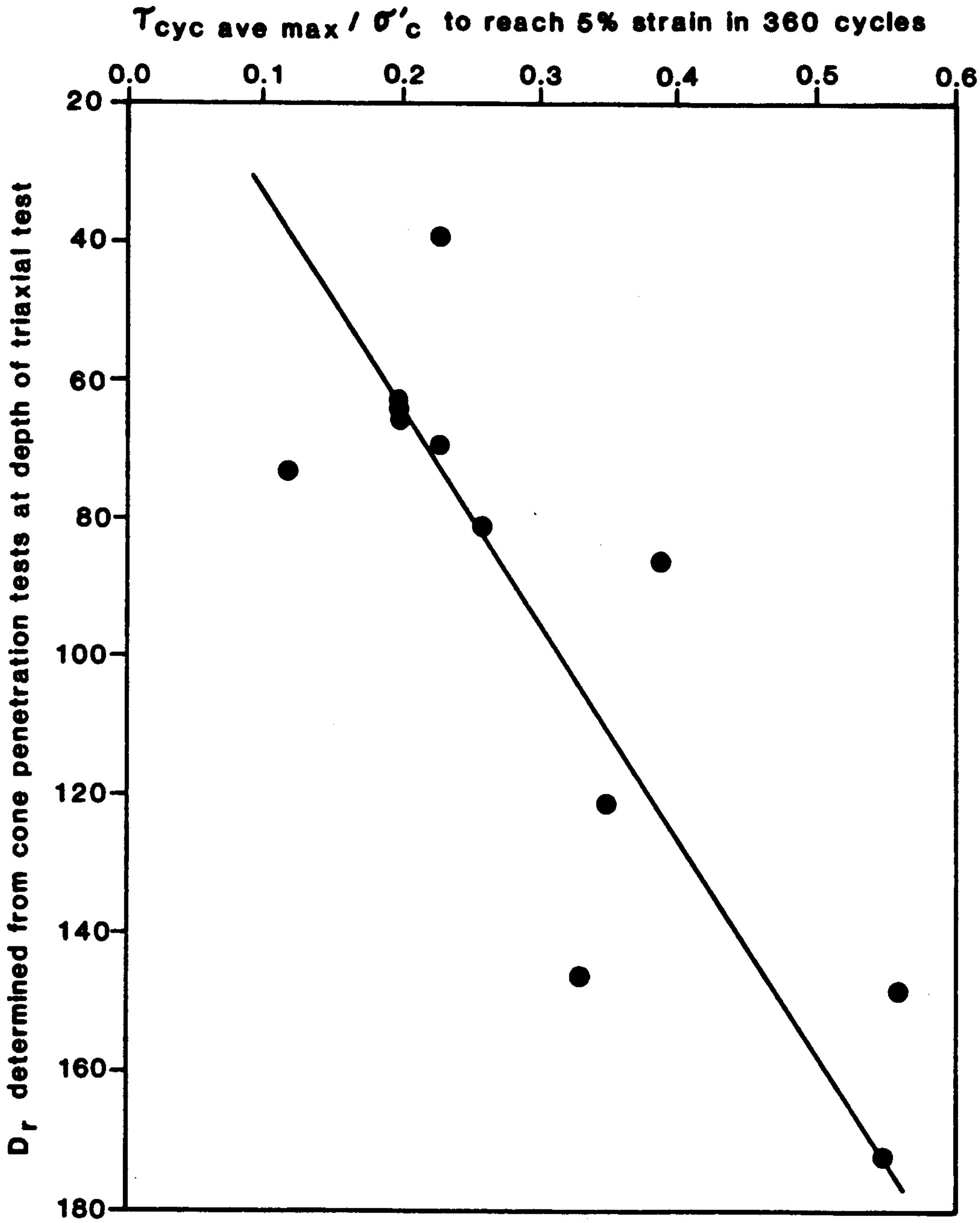

Fig. 20. Cyclic stress ratio determined from cyclic triaxial tests vs the relative density of nearby sediment determined from cone penetration tests.

Table 9. Liquefaction susceptibility based on laboratory cyclic triaxial and cone penetration tests.

AREA/STATION	ANALYSIS 1				ANALYSIS 2				ANALYSIS 3	ANALYSIS 3a (2)	ANALYSIS 4
	M = 5.25		M = 6.75		M = 5.25		M = 6.75		OCR = 1	OCR = 6	
	a_{max} (g)	D (1) (km)	a_{max} (g)	D (1) (km)	a_{max} (g)	D (1) (km)	a_{max} (g)	D (1) (km)	H (m)	H (m)	H (m)
PRODELTA											
674-687	0.27	9	0.21	33	0.14	19	0.11	63	>13	-	11
670-685	0.14	19	0.11	63	0.11	24	0.09	76	9	>13	8
667	-	-	-	-	-	-	-	-	-	-	-
668	-	-	-	-	0.21	12	0.16	44	-	-	>13
669-686	0.35	6	0.26	26	0.19	13	0.15	47	>13	>13	>13
E. THERMO. GAS											
671	-	-	-	-	0.10	26	0.07	94	-	-	8
THERMO. GAS											
675-683	-	-	-	-	0.12	22	0.09	76	-	-	9
W. THERMO. GAS											
677-684	0.32	7	0.26	26	0.26	9	0.20	35	>13	-	>13
BIOGENIC GAS											
676-682	0.22	11	0.18	39	0.10	26	0.07	94	9	>13	6
E. NORTON SOUND											
673	-	-	-	-	0.14	19	0.11	63	-	-	-
E. NORTON SOUND											
672	-	-	-	-	0.07	36	0.06	107	-	-	-
RIDGE											
679-680	-	-	-	-	0.13	20	0.10	69	-	-	>13
SWALE											
678-681	0.37	5	0.25	27	0.13	20	0.10	69	>13	-	>13

Analysis 1 determined the minimum ground surface earthquake acceleration (a_{max}) required to cause liquefaction in deep subbottom sediment based on laboratory cyclic triaxial test data.

Analysis 2 determined the minimum ground surface earthquake acceleration (a_{max}) required to cause liquefaction in shallow subbottom sediment based on cone penetration test data.

Analysis 3 determined the smallest sustained storm wave height (H) required to cause liquefaction in normally consolidated sediment based on laboratory cyclic triaxial test data.

Analysis 3a determined the smallest sustained storm wave height (H) required to cause liquefaction in overconsolidated (OCR = 6) sediment based on laboratory cyclic triaxial test data.

Analysis 4 determined the smallest sustained storm wave height (H) (valid only as a comparison of relative liquefaction susceptibility between stations) required to cause liquefaction based on cone penetration test data. This analysis compared the stress ratio caused by storm waves to the stress ratio required to cause liquefaction induced by a M = 5.25 earthquake. The values of wave height (H) do not represent actual conditions, but are presented solely for comparing liquefaction susceptibility between stations.

(1) Distance to fault (D) necessary to cause the specified ground surface acceleration was determined from Woodward-Clyde Consultants (1978).

(2) Because the northern Bering Sea sediment is typically overconsolidated near the seafloor, this analysis is probably more appropriate than Analysis 3.

Geochemical analyses of sediment cores show that the gas is composed of about 98% CO_2 (Kvenvolden and others, 1979). The remainder is hydrocarbons with high relative abundance of homologues heavier than methane, which indicates that the gas is derived from a deep, thermogenic source (Nelson and others, 1978; Kvenvolden and others, 1979). The gas has accumulated in a zone a few hundred meters thick; and the top of the zone is 50 to 200 m beneath the seafloor. Gas is believed to percolate upward from this zone along faults (Holmes and Cline, 1979).

We ran a network of seismic lines that allowed us to map the extent of the seep (Fig. 21). It covers approximately 4 km^2 and is elongate in a northwest direction, parallel to the trend of major faults (Johnson and Holmes, 1978). We deployed the penetrometer four times within the seep area, at station 675 (Fig. 3, Table 1). Between successive deployments the ship was allowed to drift so that some areal coverage of the seep was achieved. One vibracore station was occupied within the seep area. For comparison, two penetrometer stations were occupied outside, but near, the seep, as was one vibracore station.

The vibracore within the seep area is a silty sand with minor biogenic mottling (Fig. 22). At intervals down the core are zones of voids that apparently mark levels of bubble-phase gas. Some, but not all, grain-size measurements from these zones show more silt (less sand) than at other levels, but no other distinctive features are evident.

Confirmation that this core was gas-charged was obtained after it was cut into meter-long sections. End caps on the sections bulged markedly, which indicates that active degassing was occurring.

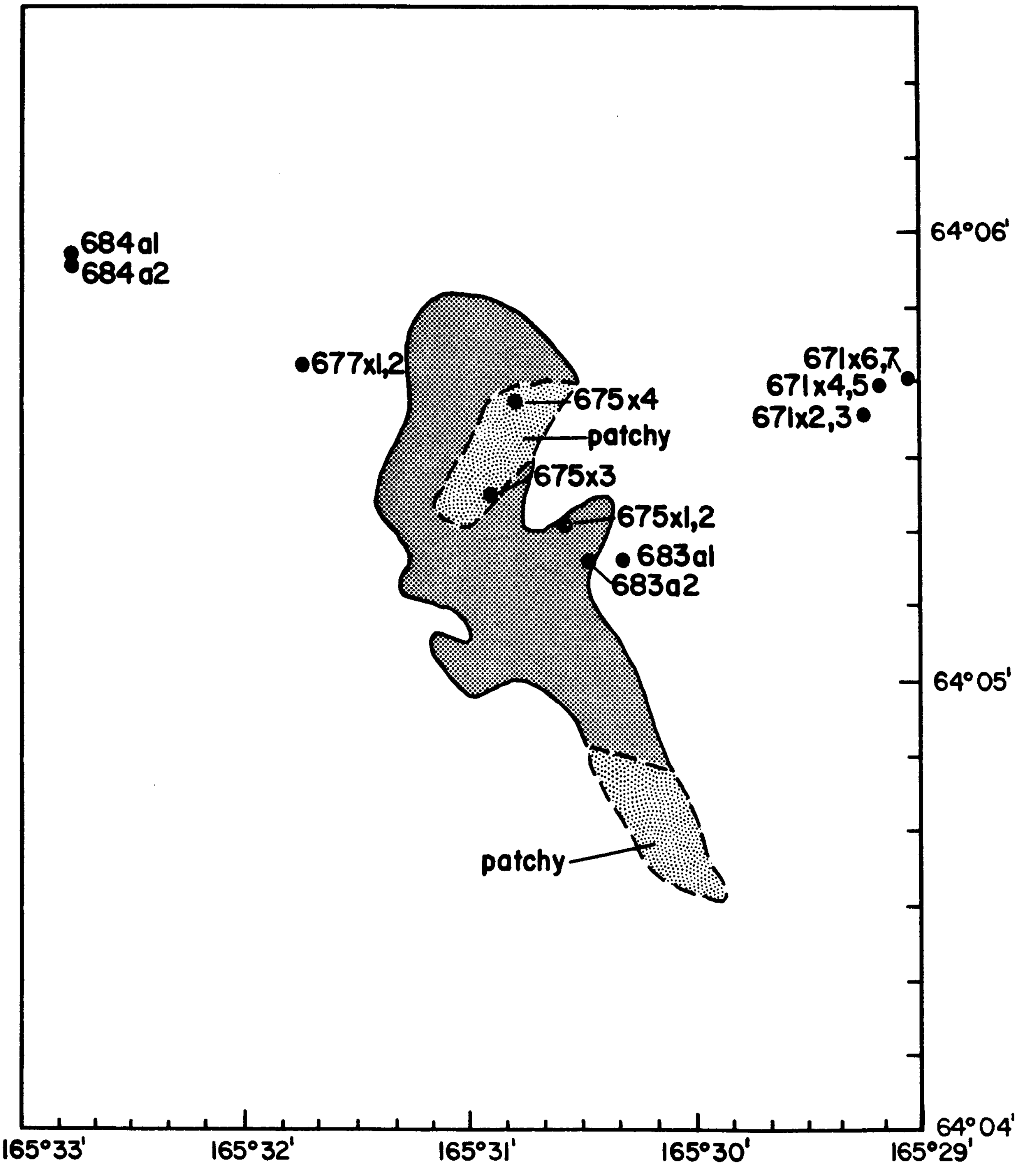

Fig. 21. Map of thermogenic gas seep.

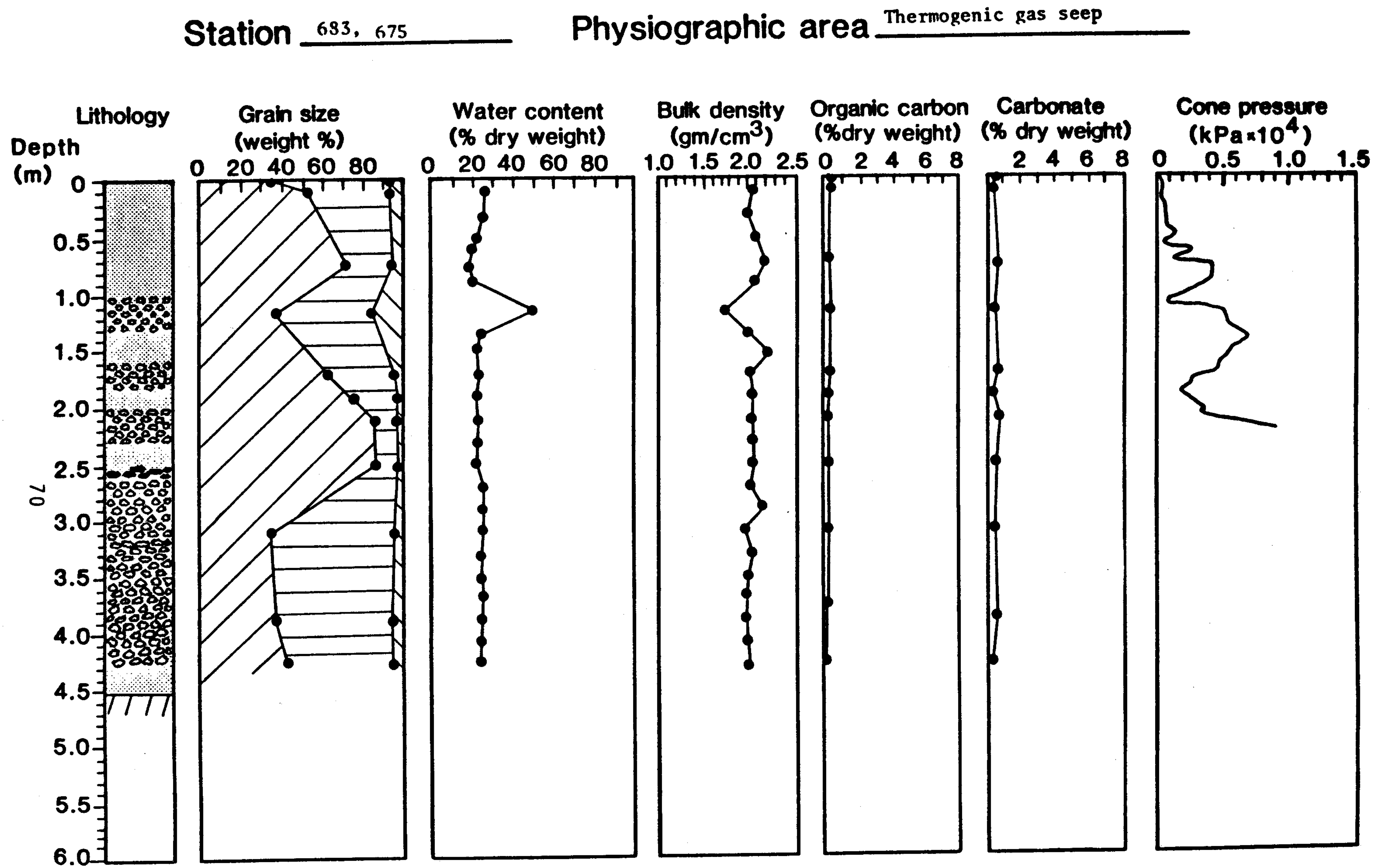

Fig. 22. Lithology, index properties and cone pressure vs subbottom depth for stations 683 and 675 (thermogenic gas seep).

The penetrometer records from within the seep area all show erratic variation of cone pressure (Fig. 22, Appendix B). But, a tangent to the maximum values shows a fairly uniform increase in cone pressure with depth, and narrow intervals of low resistance are superimposed upon this general trend.

The vibracore outside the seep area has similar lithology to the one from within (silty sand), except for the top few centimeters (mud to sandy mud) (Fig. 22). Other physical and compositional properties also are similar, except that the zones of voids do not occur in the core from outside the seep. The vibracorer penetrated to a shallower depth and usually at a slower rate outside the seep (Table 2). The penetrometer record west of the seep (station 677) shows shallow total penetration with a fairly uniform increase in cone pressure and high relative density (Fig. 23, Appendices B and C). The penetrometer records east of the seep, at station 671, are more erratic (Appendix B). Most show a general increase in cone pressure with intervals of minor decrease.

The erratic nature of the cone pressure versus depth curves within the seep area probably reflects the presence of bubble-phase gas, distributed nonuniformly with depth. The narrow intervals of low cone pressure could correspond to the zones of voids in the sediment core. The reason for vertical variation in gas content is uncertain; there is some indication that gas concentration occurs at locations of finer grain size (Fig. 22). Pressurized cores taken from the Mississippi Delta show analogous vertical variations in gas content (Denk and others, 1981).

Evidence for areal nonuniformity in gas distribution also exists. Fathometer records across the seep show variations in cloudiness of the water

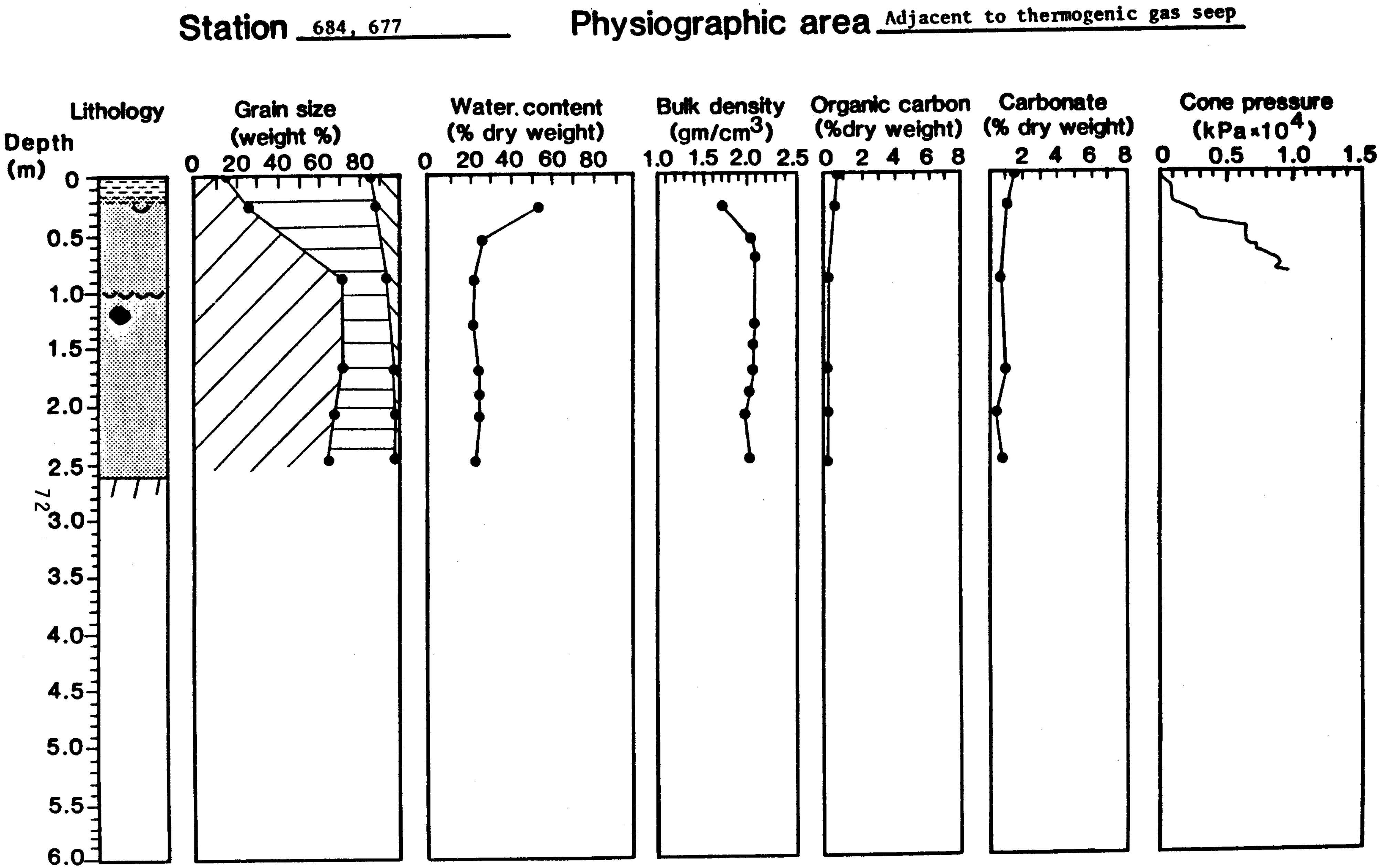

Fig. 23. Lithology, index properties and cone pressure vs subbottom depth for stations 684 and 677 (adjacent to thermogenic gas seep).

column that extend down to the seafloor (Fig. 24). This may indicate that gas is seeping strongly from some local areas (piping) and weakly or not at all from others. In some sectors, the variation is so strong as to warrant mapping the gas seepage as "patchy" (Fig. 21).

Olsen and others (1980) report low gas concentrations in two of three cores taken from the seep area. This also implies areal variation in gas-charging.

To the west of the seep, conditions are similar to those on the western prodelta (Fig. 23). The sediment apparently is not gas-charged and has uniformly high penetration resistance and calulated relative densities, at least to the shallow depths we were able to test (Table 2, Appendix C). Seismic-reflection records do not show anomalous acoustic returns that would indicate gas-charging, and the vibracore contained no zones of voids nor did it show any signs of degassing.

Intervals of low cone pressure in penetrometer records east of the mapped seep perhaps are indicative of gas-charging, but further study is necessary for confirmation. This station was originally planned to be within the mapped seep area, but strong winds and currents caused the ship to drag anchor, and we drifted away from the seep by the time conditions settled. Therefore, we have no seismic-reflection records over this site, and time did not permit collection of a sediment core. The low cone pressure intervals are not as pronounced as at station 675, which remains an unresolved question pertaining to records at this site.

Sediment type as inferred from friction-ratio plots are shown for station 675 (within the gas seep) and station 677 (west of the gas seep) in Figures 25 and 26, respectively. Most data points center around the silt-sand category,

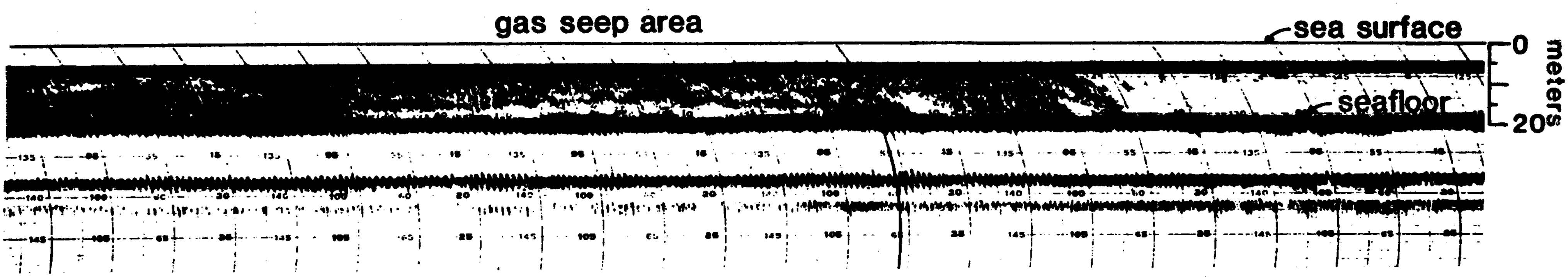

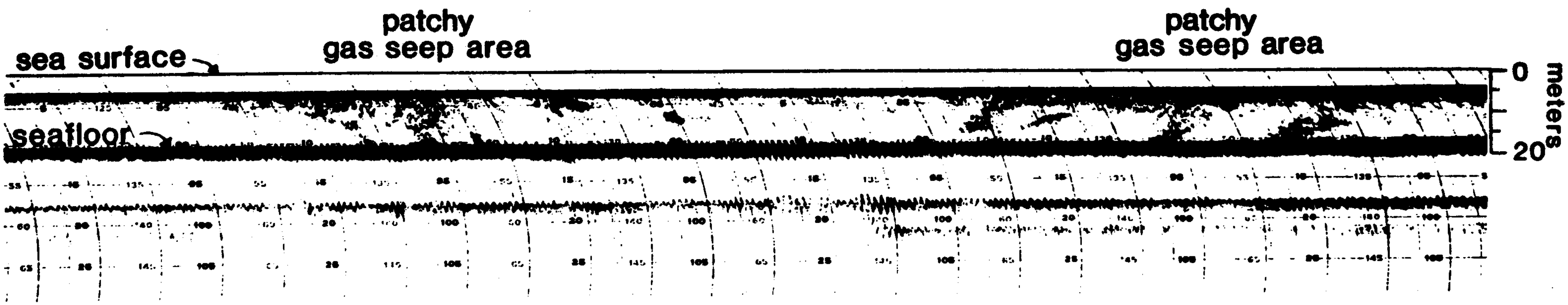

Fig. 24. Fathometer record of thermogenic gas seep.

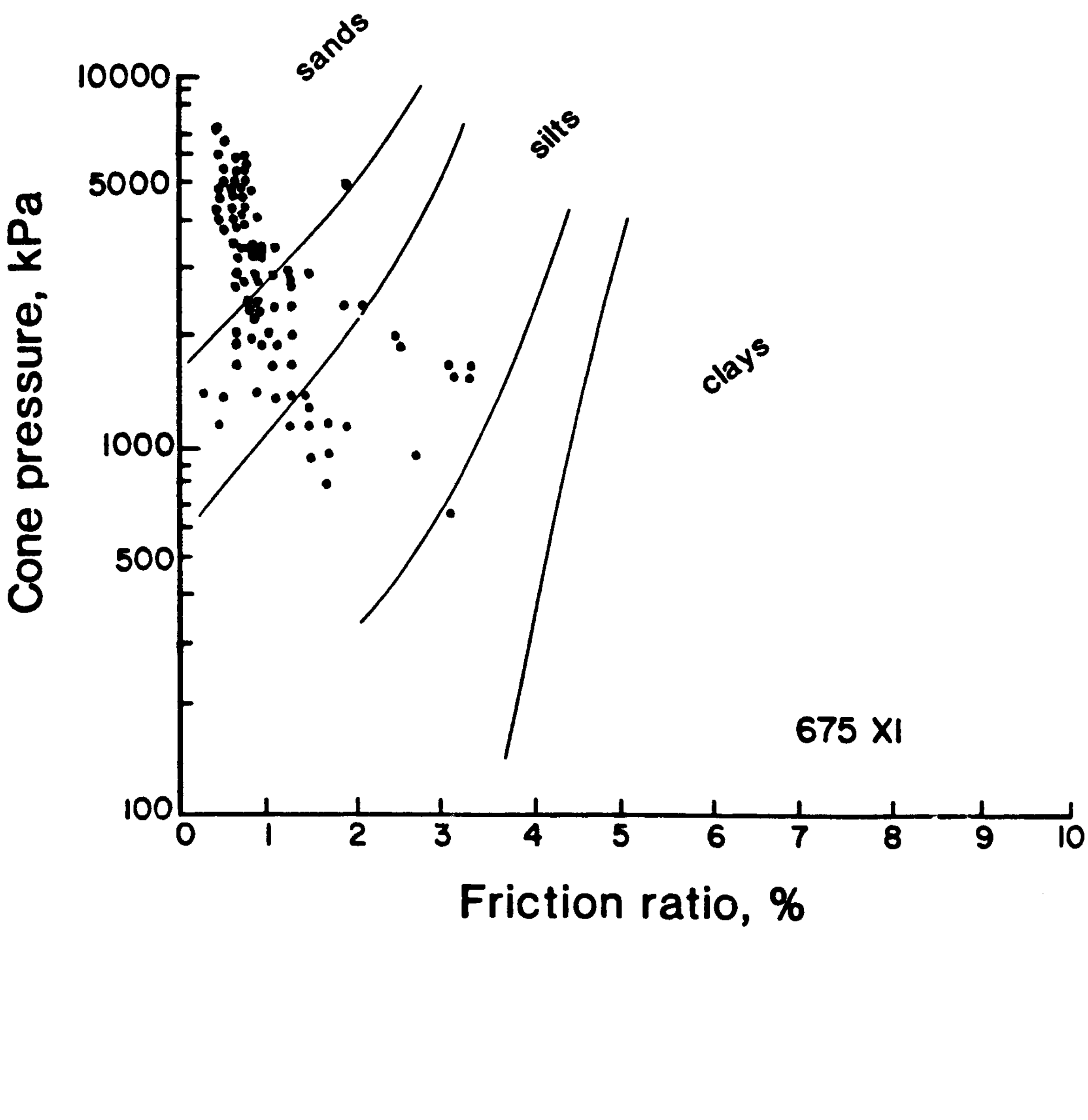

Fig. 25. Sediment type determined from cone penetration test 675X1 (thermogenic gas seep - near station 683).

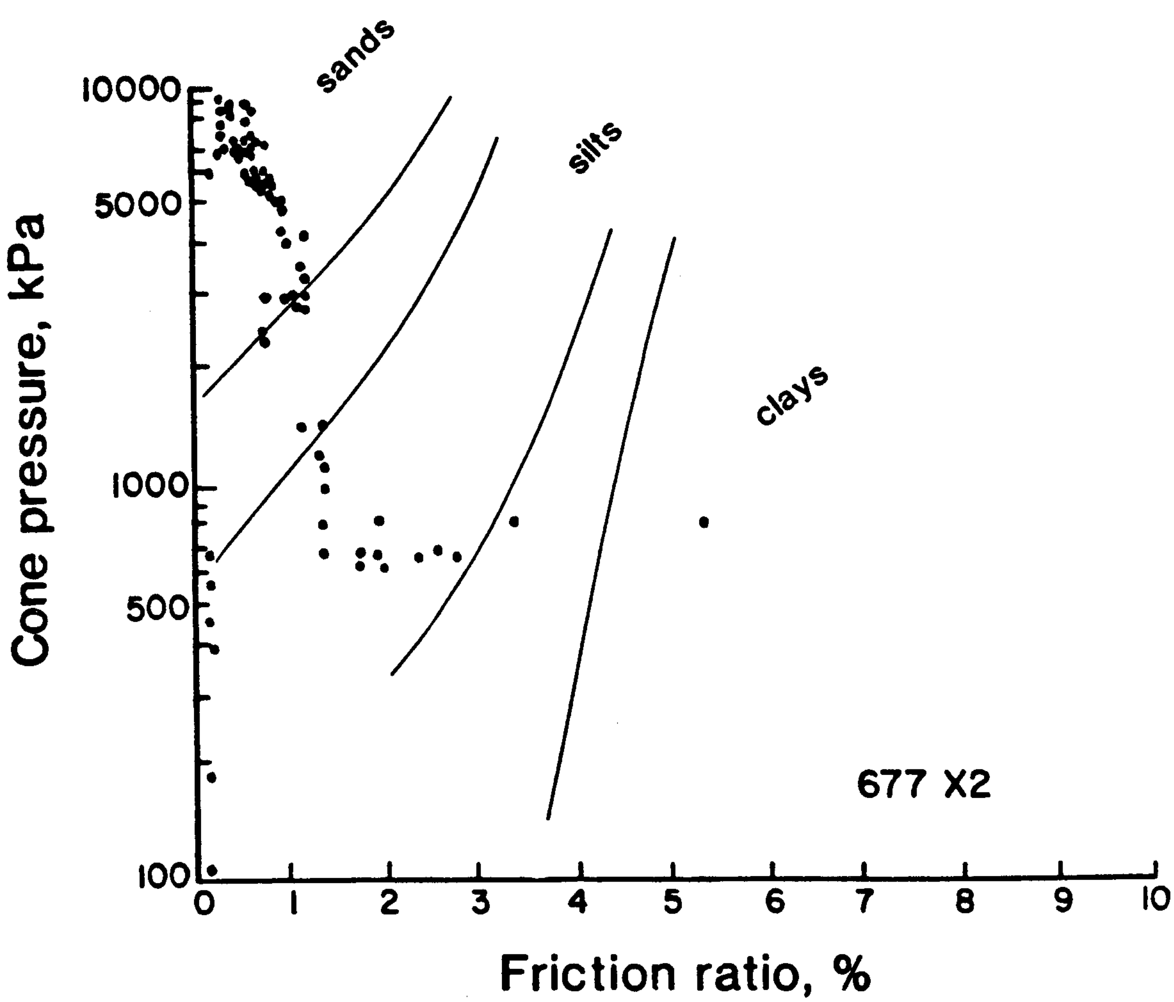

Fig. 26. Sediment type determined from cone penetration test 677X2 (west of thermogenic gas seep-near station 684).

but with much scatter. The cores appear to be more uniform and contain less fine material than indicated by the penetrometer data.

Compression index (C_c) ranges from 0.04 to 0.09 inside (station 683), and from 0.07 to 0.12 outside (station 684) the gas seep (Table 6). Evidently, from the low values, consolidation tests were not performed in stratigraphic intervals that had been expanded due to gas-charging within the seep. Overconsolidation ratios decrease with subbottom depth outside the gas seep, whereas an anomalously low value (OCR = 2) was determined within gas-seep sediment. The C_c value for that test appears to be low in relation to other test data (Table 6, Fig. 18). Whether gas charging, and resultant de-gassing, affected the consolidation behavior is unclear. The other test values plot closer to Lambe and Whitman's curve (Fig. 18).

Behavior under static loading is similar for sediment inside and west of the gas seep, perhaps indicating that the gas is not uniformly distributed within the area, i.e., the triaxial tests performed on sediment from the gas-seep area were located in a non-gas-charged stratum. Friction angles are: 38.8° inside (station 683), 38.0° outside (station 684) the gas-prone region. Ratios of S_u/σ'_c are also similar: 3.05 inside and 3.31 outside (Table 7). Remarkably analogous shear behavior was recorded, including peaked stress-strain curves (Figs. 8c and 8d). Contractive behavior at high consolidation stresses was less pronounced at stations 683 and 684 than from prodelta material (stations 685, 686 and 687). That behavior, coupled with the high S_u/σ'_c values, indicates that overconsolidation effects may have influenced the test results.

Detailed grain size distributions indicate that similar liquefiable sediment types exist within and outside the seep (Table 3, Fig. 19, Appendix

A). De-gassed sections of core could not be trimmed for cyclic testing, however sediment west of the thermogenic gas seep (station 684) showed cyclic triaxial behavior approximately midway between the other station's results (Table 8, Fig. 9). Liquefaction analyses show that an earthquake acceleration between 0.20 g and 0.32 g or wave heights greater than 13 meters are necessary to cause instability at station 684, whereas the analysis based on CPT data indicates a higher liquefaction potential within (station 675) and east (station 671) of the seep (a_{max} = 0.07 - 0.12 g) (Table 9).

Areas of biogenic gas:

Seismic-reflection profiles that exhibit anomalous acoustic returns from the sediment column have been collected over most of Norton Sound and eastern Chirikov Basin, and it has been estimated that over 7000 km^2 of seafloor is underlain by gas-charged sediment (Holmes and Thor, 1982). We occupied two sites (Fig. 3, Table 1) where cores that contain high concentrations of biogenically derived gas have previously been collected and where acoustic anomalies exist (Kvenvolden and others, 1980). The biogenic gas is believed to originate at shallow depths in the seabed as a byproduct of microbial breakdown of peat deposits. It is composed mostly of methane.

One biogenic gas site is about 10 km north of the thermogenic gas seep (Fig. 3). A vibracore at station 682 consists of interbedded sandy silt, silty sand, and mud (silt-clay) (Appendix A, Fig. 27). The conspicuous interval with high organic carbon content, high water content, and low bulk density from about 1 to 4.5m is a peat layer. Plant fragments and a distinctive brownish tint typify this interval in split core sections. The core smelled of hydrogen sulfide but did not show signs of degassing.

Station 682, 676 **Physiographic area** Biogenic gas, south of Nome

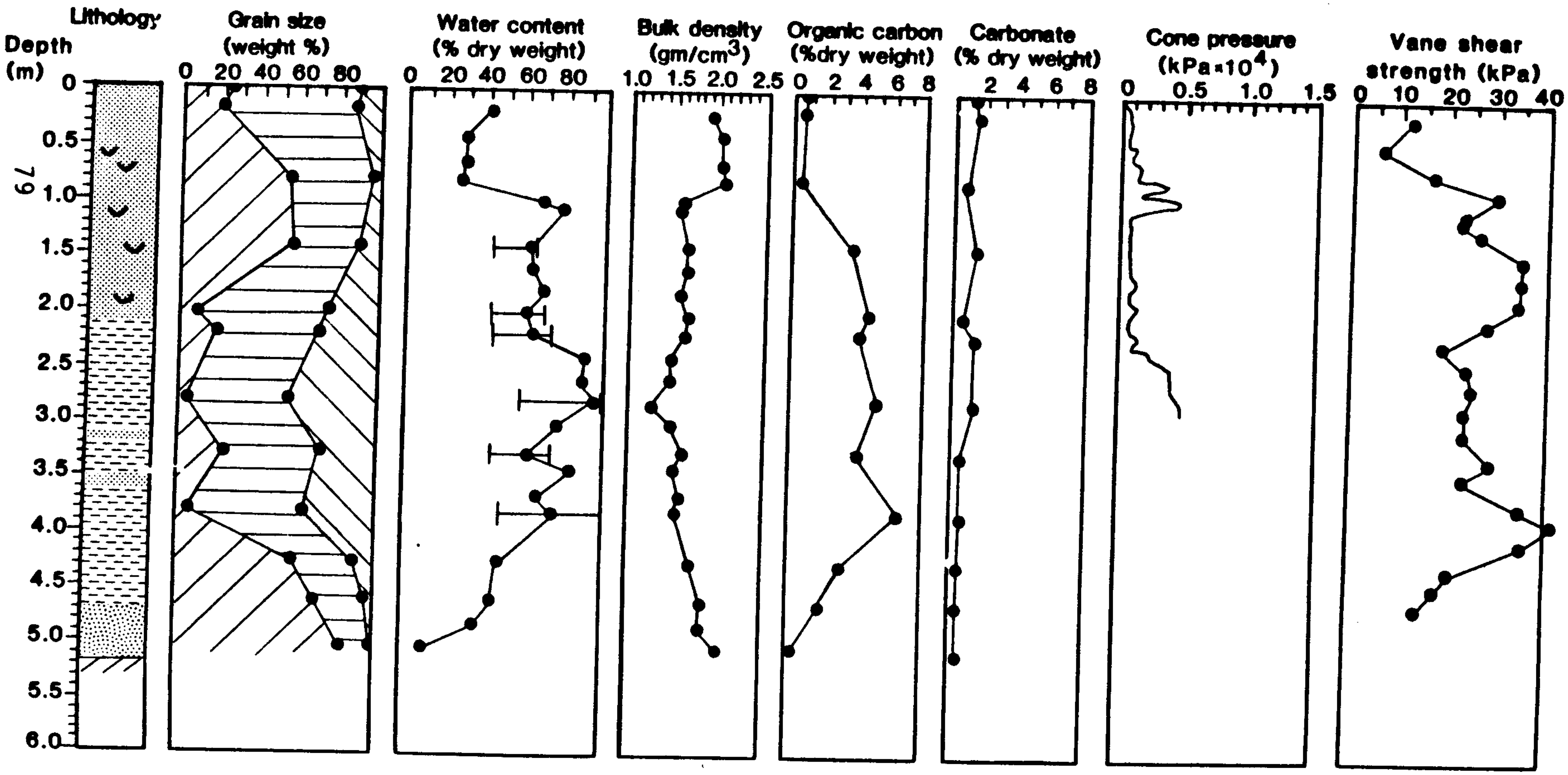

Fig. 27. Lithology, index properties and cone pressure vs subbottom depth for stations 682 and 676 (biogenic gas seep, south of Nome).

The vibracorer penetrated deeply and with the most rapid penetration rate (Table 2). The XSP-40 deployments at this site (station 676) achieved the deepest penetration of all tests (Fig. 27, Appendix B). The records show variable cone pressure with depth, but the tangent to maximum pressures trends nearly vertical (constant value). Calculated relative densities typically are low (Appendix C).

The implication of the penetrometer tests is that the sediment is weak; it does not become stronger with depth as most sedimentary deposits do. Vane shear measurements of this cohesive material support this conclusion (Fig. 27). The cause of this behavior is probably a consequence of the relatively high levels of water or organic carbon. It cannot be directly attributed to bubble-phase gas, because no evidence for its presence was detected in this core. However, high levels of methane-rich gas were measured in a vibracore previously collected 3 km from our core (Kvenvolden and others, 1980). It has concentrations of organic carbon in excess of 2% in a peat layer over 1-m thick beginning at about 1-m depth. Low penetration resistance (deduced from vibracore penetration rate) was encountered to a depth of about 3 m (Olsen and others, 1980). Although the data are scant, the low penetration resistance seems to correlate better with high water and organic carbon contents than with high biogenic gas levels.

The other biogenic gas site is in eastern Norton Sound, about 35 km south of Cape Darby (Fig. 3, Table 1). A penetrometer station (673) was occupied approximately 0.7 km from where a 155-cm-long vibracore (76-125) was previously taken (Fig. 28). The vibracore grades from silty sand to sandy silt and has physical and chemical properties that show similarity to other Yukon River-derived deposits in Norton Sound. In particular, the organic carbon

Station 673, 76-125 Physiographic area Biogenic gas seep, south of Cape Darby

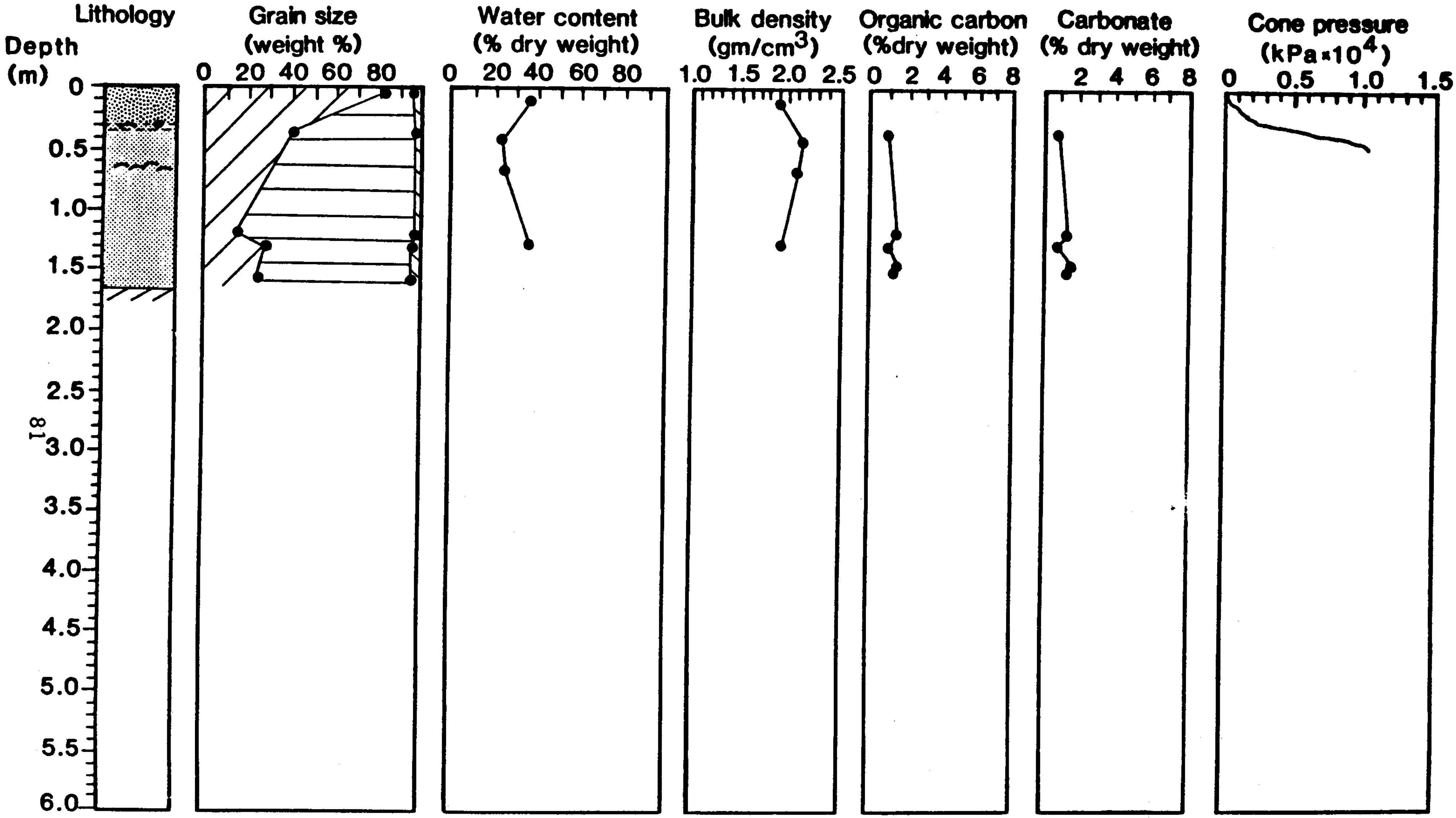

Fig. 28. Lithology, index properties and cone pressure vs subbottom depth for stations 673 and 76-125 (biogenic gas seep, south of Cape Darby).

level is less than 2% and water content is 20-40%. However, high levels of biogenic gas were measured (Kvenvolden and others, 1980). Olsen and others (1980) report an abrupt increase of vibracore penetration resistance with depth at this station. Our penetrometer records show a similar trend (Fig. 28, Appendix B); total penetration depth is small, cone pressure increases sharply, and calculated relative density is high (Appendix C).

The vibracore penetration-rate data at both biogenic-gas sites suggest the same conclusion: gas, if it is present, does not significantly decrease penetration resistance. Perhaps the in situ gas pressure is not high enough at these sites to significantly decrease the effective stress between grains (as it apparently is at the thermogenic gas site), although bubble-phase gas may well exist at the penetrometer stations.

The penetrometer data at station 676 south of Nome indicate a range of sediment behavior types mostly from sandy silt to silty clay, which is roughly the textural range recovered in the core at nearby staion 682 (Fig. 29). This correspondence might be coincidental, to judge from plots of other penetrometer data that have similarly large ranges of sediment behavior types where cores indicate a relatively uniform sediment type.

The sediment within the peat zone (station 682) is by far the most compressible of all the tested material (C_c = 0.53-0.69) (Table 6). The C_c values plot in the high compressibility range in good agreement with results of soils from western United States and Colombia (Fig. 18). The one test performed below the organic layer shows a low compressibility (C_c = 0.06) that is consistent with other northern Bering Sea sediment (Table 6), but with a lower $C_c/(1 + e_o)$ ratio than most of the other tests (Fig. 18). Overconsolidation ratios are somewhat lower (OCR = 4 - 8) than in other regions (Table 6).

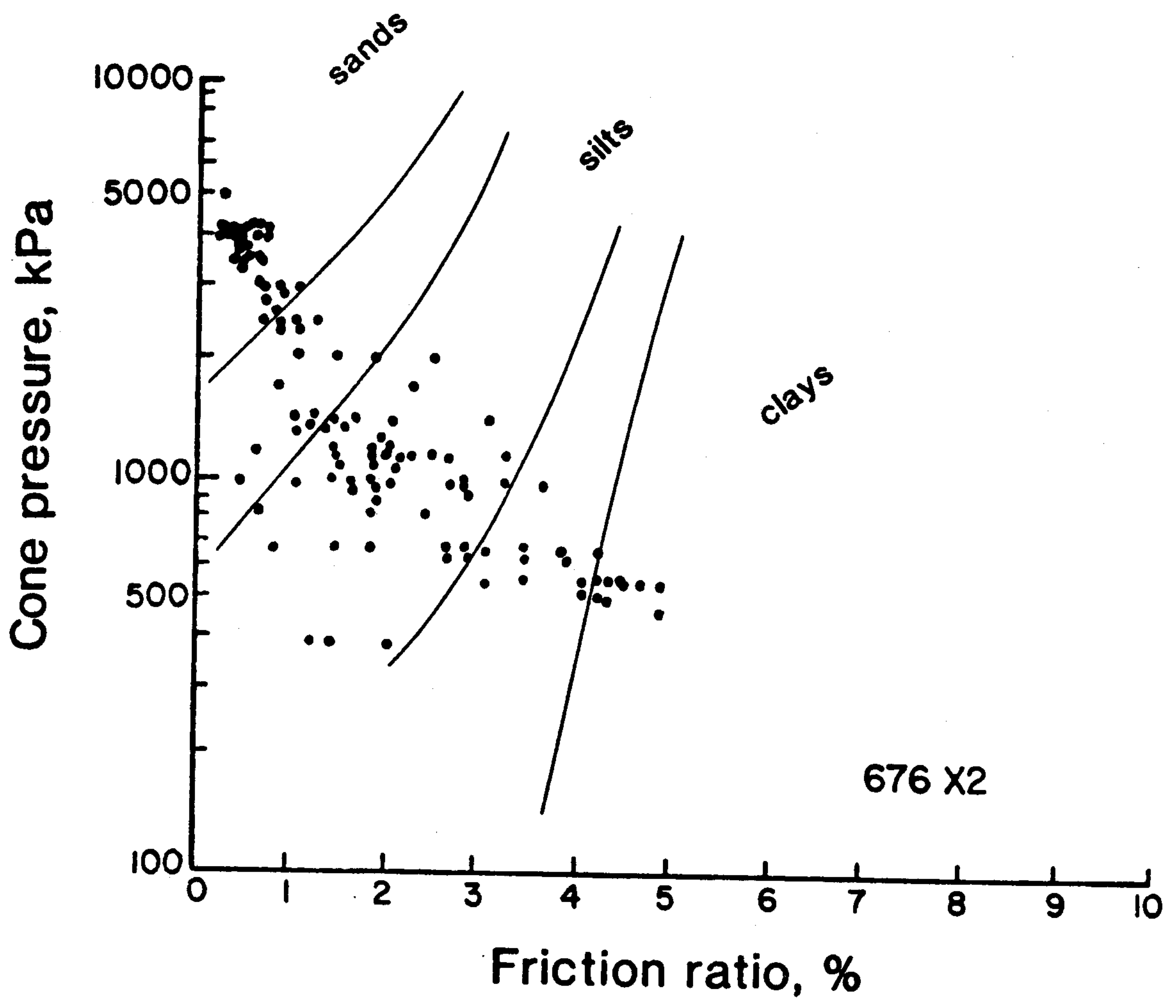

Fig. 29. Sediment type determined from cone penetration test 676X2 (biogenic gas seep, south of Nome - near station 682).

The sediment above the organic zone in core 682 has a higher strenth ratio (S_u/σ'_c = 0.78 versus 0.46), but a lower friction angle (ϕ = 35.2° versus 40.2°) than the peat (Table 7). Similar static loading behavior is exhibited by both the organic and non-organic sediment in this core. Contractive behavior occurs at high consolidation stresses; however, the slightly contractive response at low confining stresses, is atypical for northern Bering Sea material. Sensitive (peaked) stress-strain behavior is also less pronounced than at other Norton Sound sites.

The peaty sediment is slightly finer grained than other liquefiable sediment (Table 3, Fig. 19, Appendix A), but repeated loading reduces its strength, nevertheless. Cyclic stress ratios for the organic material plot in the low range in relation to the other stations (Table 8, Fig. 9). The minimum earthquake acceleration necessary to induce liquefaction is 0.07 g to 0.22 g, and waves 9 meters high would liquefy normally consolidated sediment; however, waves 13 meters high would not liquefy overconsolidated material (Table 9). Earthquake accelerations (a_{max} = 0.11-0.14g), based on CPT data, necessary to cause liquefaction at the eastern Norton Sound biogenic gas site (station 673) are within the range for station 682.

Eastern Norton Sound:

Eastern Norton Sound is protected from high wave energy that is imparted to the seafloor farther west, and a relatively tranquil sedimentary environment exists (Howard and Nelson, 1980). A vibracore collected in 1976 (station 76-133, Fig. 3) contains silty sediment with minor amounts of sand and clay (Fig. 30). Relative to other sediment cores in Norton Sound, water contents are high, and bulk densities are low. The few measurements of

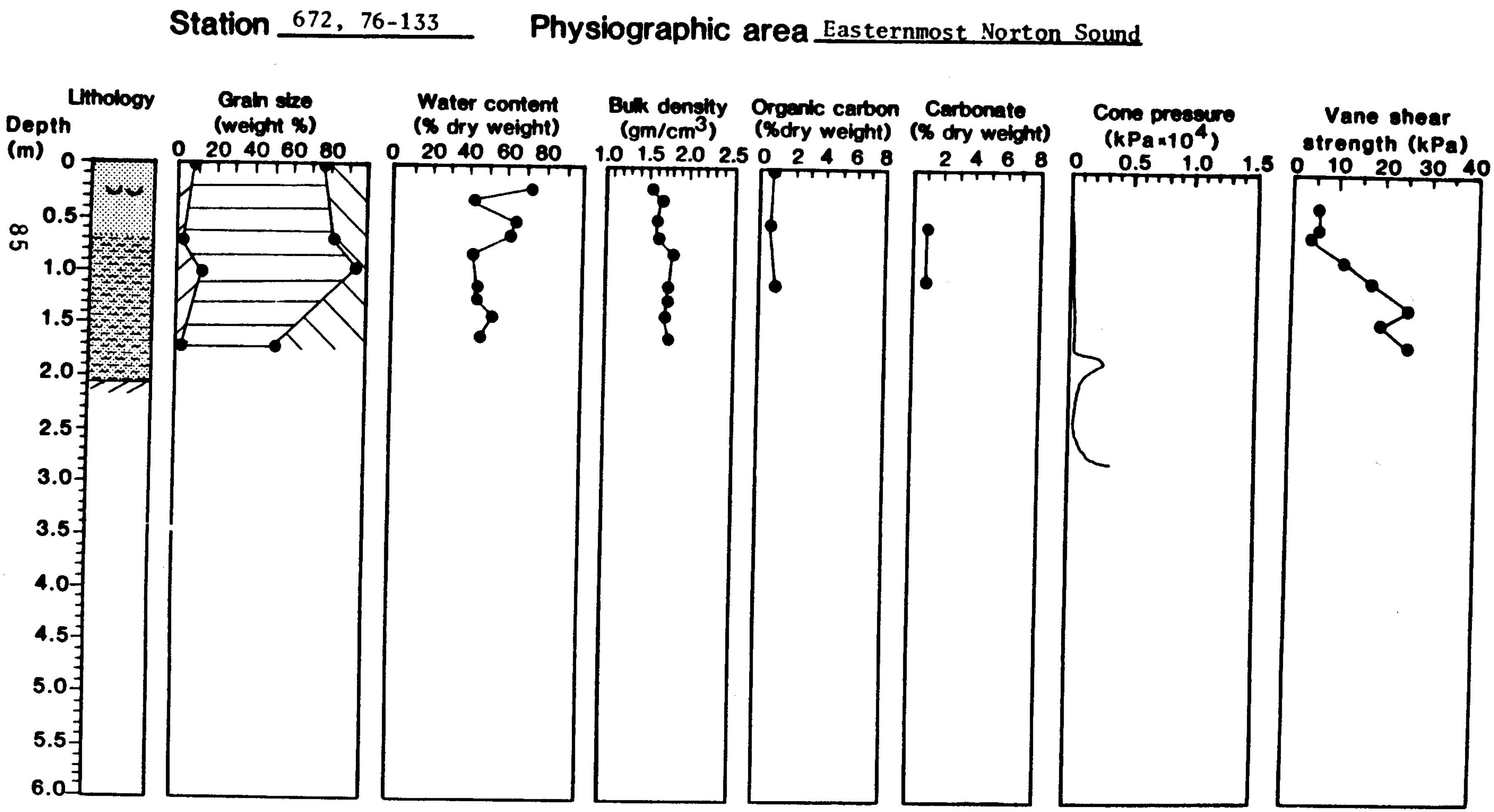

Fig. 30. Lithology, index properties and cone pressure vs subbottom depth for stations 672 and 76-133 (easternmost Norton Sound).

organic carbon show low levels. Several other cores in the eastern sound have similar features (Howard and Nelson, 1980).

Our penetrometer test near the vibracore station experienced low cone pressure throughout most of its extent, evidently reflecting the high water content (Fig. 30, Appendix B). The values of cone pressure and relative density are similar to the low values at the biogenic gas site south of Nome, where water contents and organic carbon levels are high (Fig. 27, Appendix B).

Penetrometer data predict sediment behavior types that correlate well with the core sample. Most data points fall in the silt and silty clay categories (Fig. 31).

Ridge and swale topography

Ridge and swale topography exists near Port Clarence in Chirikov Basin (Fig. 32). The ridges are in 10-40m water depth and are 15-30 km long, 3-7 km wide, and 10-15m high. They are believed to be ancient shoreline shoals, analogous to present-day subaerial Port Clarence spit, deposited upon truncated Tertiary bedrock during the Holocene transgression (Nelson and others, 1980). Strong currents have prevented burial of these features by Holocene deposits, and sediment on the ridges is being reworked into a series of migrating sand waves (Field and others, 1981).

Vibracores from a ridge and an ajacent swale exhibit strikingly different compositions (Figs. 33 and 34). The core from the ridge is well sorted sand with scattered shells. Muddy sand occurs at the top of the swale core, with some peat layers and lenses. Below this, the sediment is varied but generally contains more mud, except for the lowest 50 cm, and gravel (to cobble size) appears in increasing quantity. Water and organic carbon contents are in the

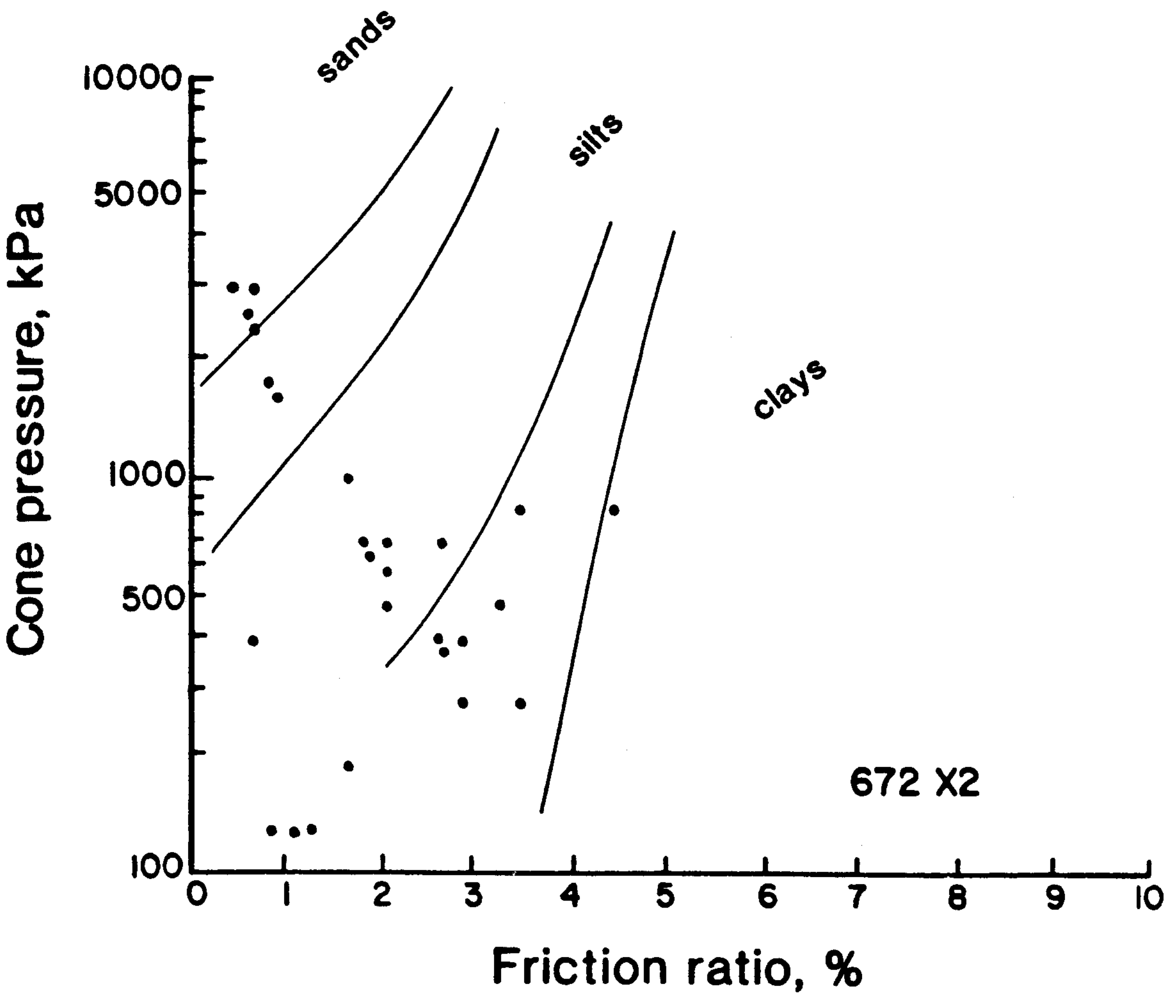

Fig. 31. Sediment type determined from cone penetration test 672X2 (easternmost Norton Sound).

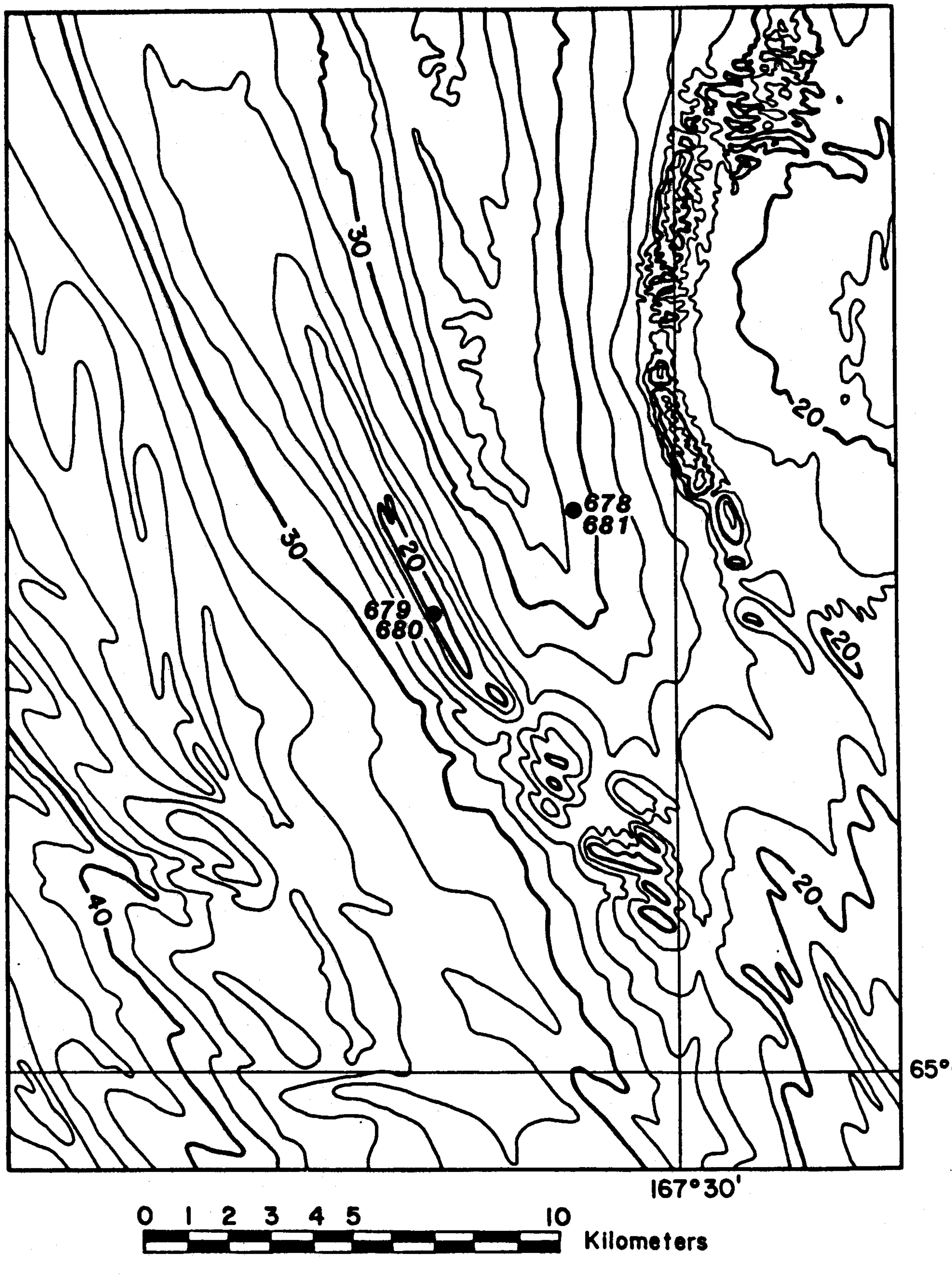

Fig. 32. Bathymetric map of ridge and swale area.

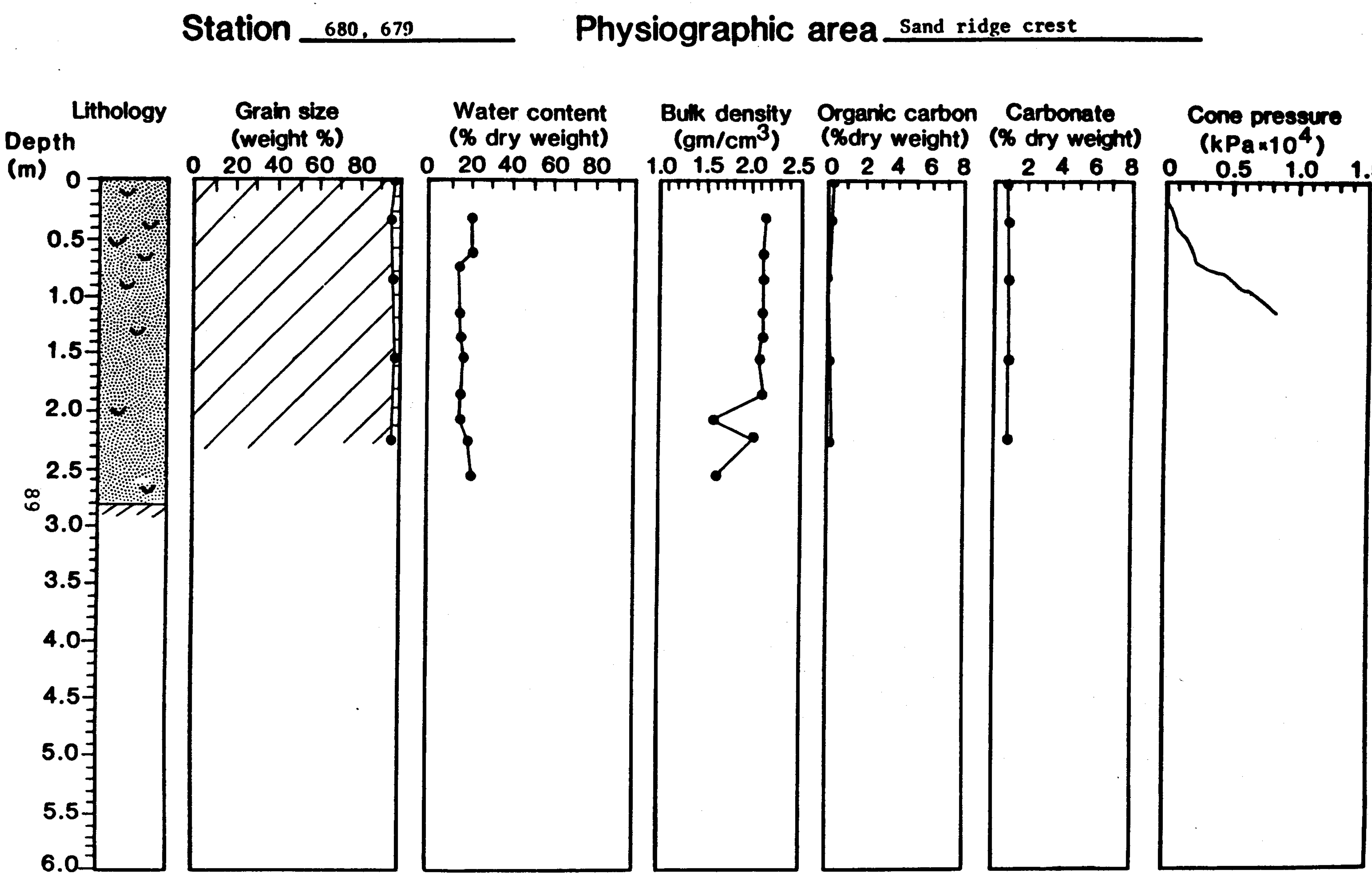

Fig. 33. Lithology, index properties and cone pressure vs subbottom depth for stations 680 and 679 (sand ridge crest).

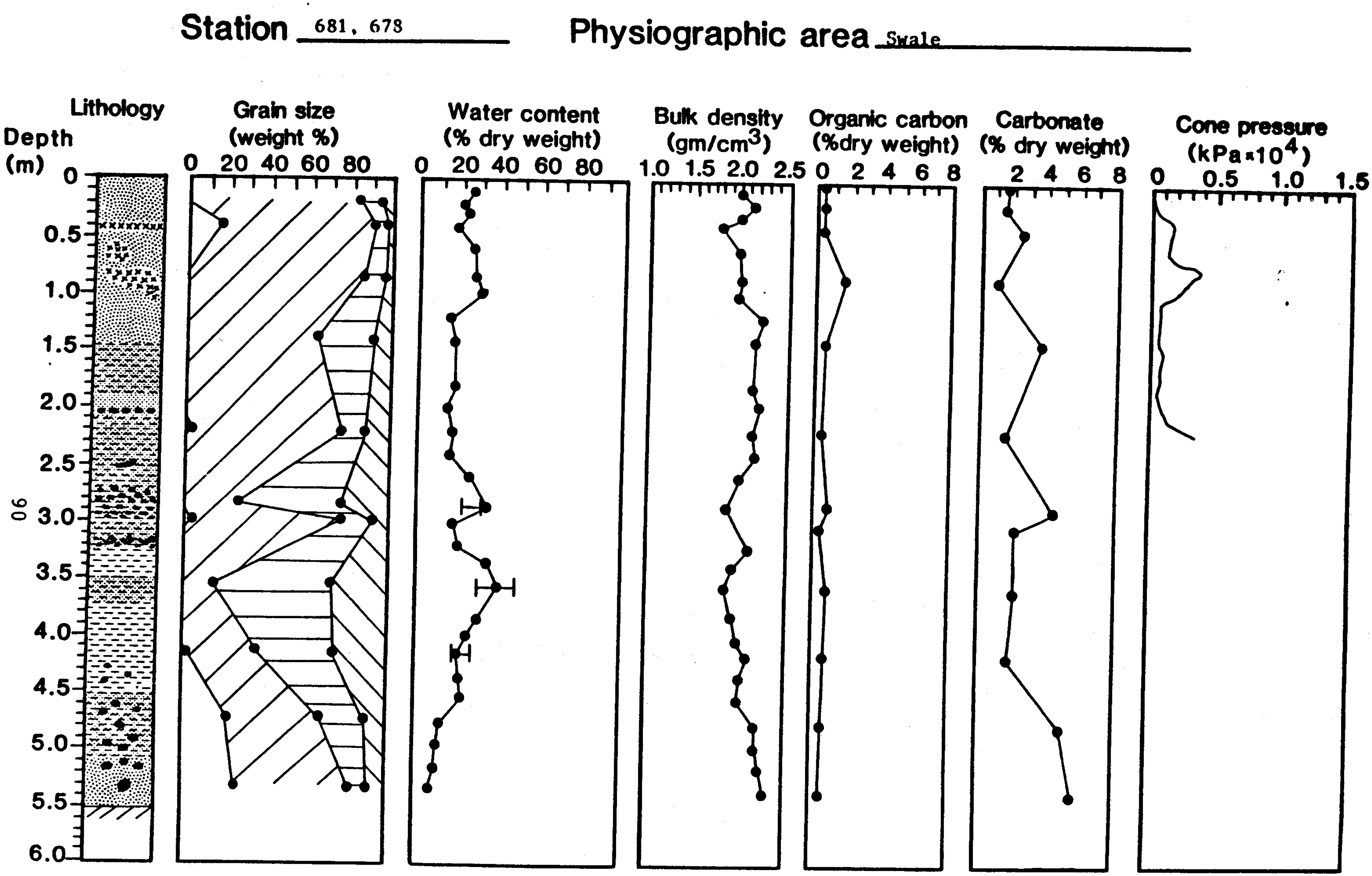

Fig. 34. Lithology, index properties and cone pressure vs subbottom depth for stations 681 and 678 (swale).

normal range for Norton Sound sediment (Table 4). Shallow depth with a relatively slow penetration rate was achieved by the vibracorer on the ridge (station 680), whereas the penetration rate and depth were much greater in the trough (station 681) (Table 2).

The penetrometer records from the ridge and swale are also distinctly different. The test on the ridge shows a uniform increase of cone resistance, and shallow penetration (Fig. 33, Appendix B), similar to the silt and sand deposits elsewhere except that the calculated relative densities are less (Appendix C). The test in the swale achieved greater penetration depth and recorded a relatively low gradient and substantial variation of cone pressure with depth (Fig. 34, Appendix B).

The data at these sites demonstrate a large variation in sediment type and physical properties over a small distance. The sediment on the ridge is relatively dense. The sediment in the swale is relatively weak, which evidently reflects its greater percentage of silt and clay. Interestingly, water and organic carbon contents are not as high as at other locations where penetration resistance is low (Figs. 27 and 30). Sediment in the swale beneath the level of the penetrometer test probably becomes stronger due to the decrease in silt and clay and the appearance of gravel.

The penetrometer tests at station 679 on the ridge yield consistently low friction ratios, which implies sandy material as was recovered in the core sample (Fig. 35). The two tests in the trough at station 678 show different results. The test with less scatter indicates silty to sandy material. This correlates fairly well with the cone (Fig. 36).

The consolidation characteristics (C_c = 0.07-0.11, OCR = 21-6) of the sediment in the trough (station 681) are typical of northern Bering Sea

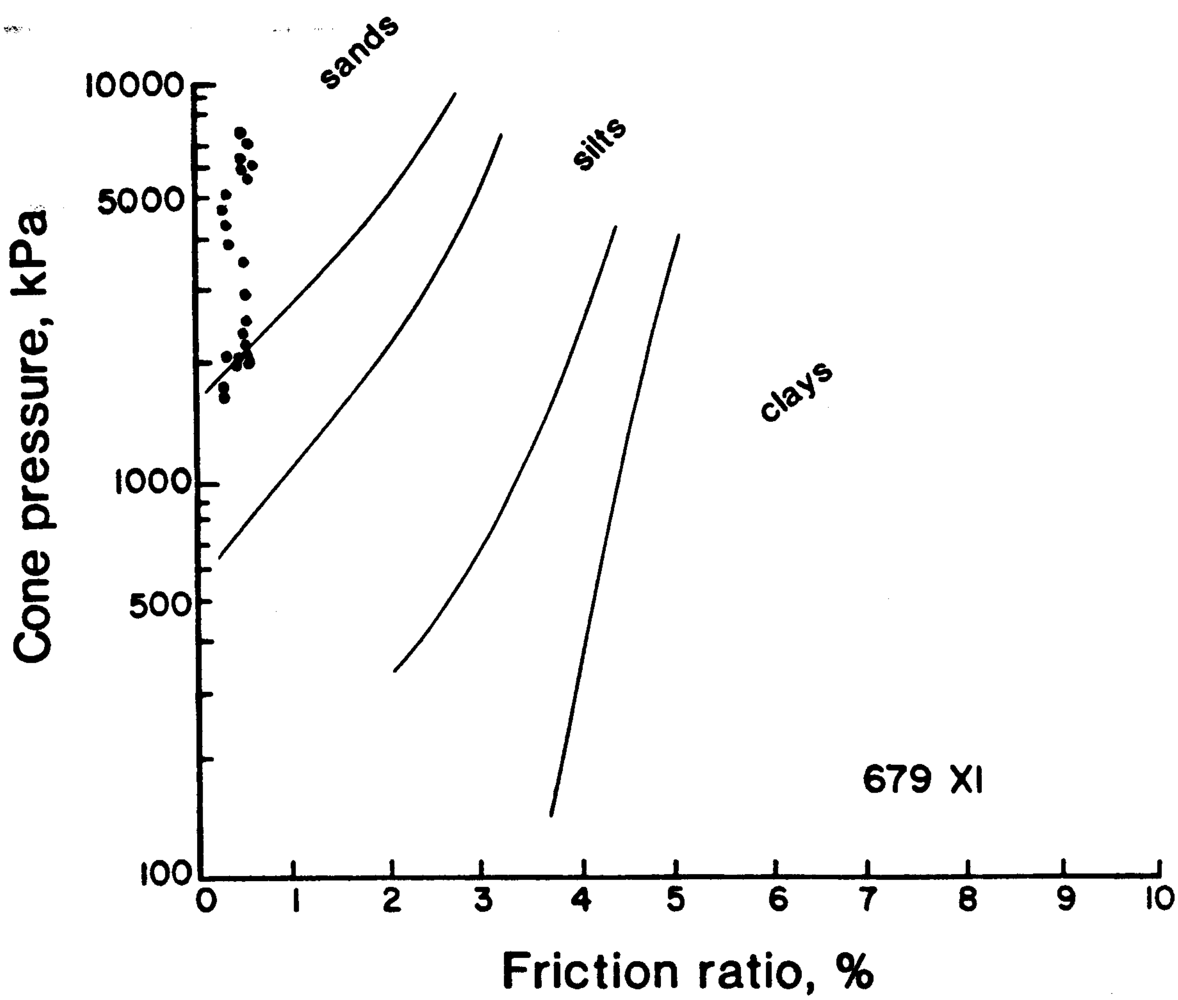

Fig. 35. Sediment type determined from cone penetration test 679X1 (sand ridge crest - near station 680).

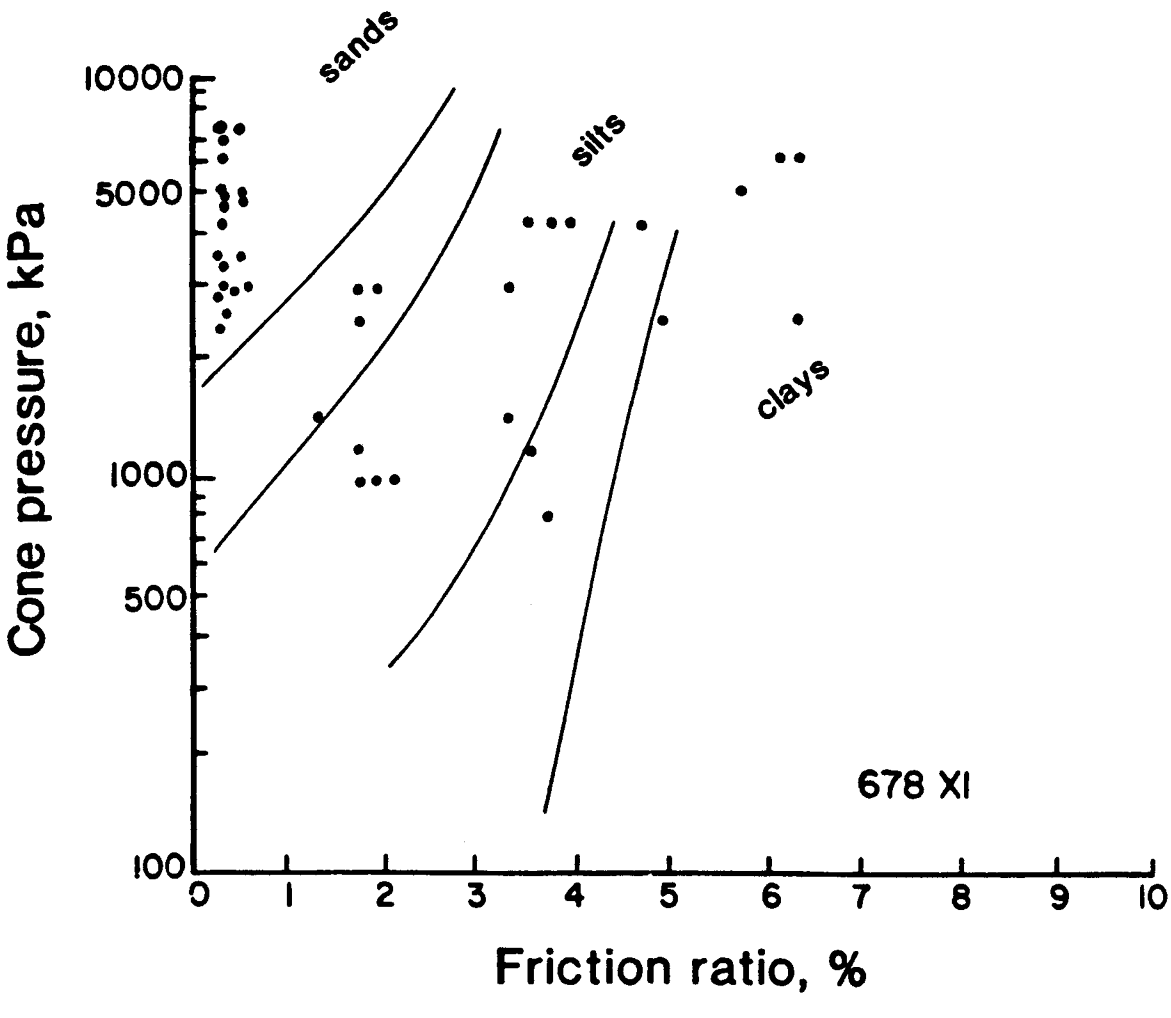

Fig. 36. Sediment type determined from cone penetration test 678X1 (swale - near station 681).

material (Table 6, Fig. 18). Static loading behavior is also similar to other tests; the strength ratio S_u/σ'_c is 1.23 and the friction angle is 37.3° for slightly overconsolidated sediment (OCR = 2). Dilatant properties exist at low confining stresses, and analogous to the sediment at the biogenic gas area (station 682), peaked stress-strain behavior is limited (Fig. 8a).

The grain size distributions of sediment within the ridge and swale areas are similar to material that has previously undergone liquefaction (Table 3, Fig. 19, Appendix A). Cyclic triaxial tests on trough sediment (station 681) show low resistance to liquefaction (Table 8, Fig. 9). Analyses indicate that a 0.10 g to 0.37 g earthquake acceleration will liquefy trough sediment (Table 9). Earthquake accelerations (a_{max} = 0.10-0.13 g) based on CPT data suggest that some sediment on the ridge (station 679) has the same liquefaction susceptibility as trough material (station 678). Sustained wave heights greater than 13 m are required to liquefy both ridge and swale sediment (Table 9).

DISCUSSION

The northern Bering Sea encompasses a diverse suite of geologic environments that contain sedimentary deposits with distinct physical properties. The aim of this geotechnical framework study is to characterize the deformational behavior of sediment in each environment and to explain the behavior in terms of geology.

Two types of geotechnical testing were employed. Each has its own advantages and limitations with regard to accurately defining the deformational behavior of northern Bering Sea sediment. Cone penetrometer tests were used to measure sediment properties in situ, in a nearly undisturbed state. However, most sediment in the northern Bering Sea is highly resistant to penetration, and tests were possible only to shallow depths beneath the seafloor. Moreover, the penetrometer can only be used to infer a few physical properties, and no sediment sample is recovered. Laboratory testing of sediment cores, on the other hand, enables inferences to be made about a wide range of static and dynamic loading parameters. But, sediment samples are disturbed during coring operations, which can only be partly compensated for with special laboratory techniques.

Yukon prodelta: The variation in sediment physical properties on the Yukon prodelta might be related to the degree of exposure to large storm waves that approach dominantly from the southwest. Exposure to wave-induced stresses should decrease around the prodelta to the northeast because of topographic shielding and frictional dissipation. The penetration resistance appears to roughly correlate with the level of wave-energy exposure. This correlation could be the result of sediment liquefaction during exposure to major storm waves (see Clukey and others, 1980) followed by reconsolidation to a greater density state during quiet periods. It could also result from preloading by soft Yukon River silt during quiet periods and removal of this soft surface material during passage of major storms (Nelson, 1980b; Cacchione and Drake, 1979). At station 686, the sediment is incompressible and has a high friction angle (ϕ'), stress ratio (S_u/σ_c'), and penetration resistance, all of which indicate high strength and relative density. In fact, relative densities well in excess of 100% were calculated at that site, indicating a state of overconsolidation at shallow subbottom depths and consequent strong, dilatant behavior.

The western prodelta sediment has a low wave-induced liquefaction suseptibility (Table 9), despite having one of the highest concentrations of wave energy in the northern Bering Sea. The material probably is reworked and densified often enough that a substantial thickness of loose, liquefiable sediment cannot accumulate.

Relative density and strength decrease between station 686 and station 685 to the northeast. Of the 5 stations on the prodelta, the sediment at station 685 is the loosest, weakest, and least consolidated. Although it is the most suseptible to liquefaction, failure due to storm-wave loading seems unlikely because of its shielded location. Infrequent, large storm waves from the north could cause failure if the sediment was normally consolidated and if pore pressure was not dissipated (Table 9), but these conditions are unlikely.

Station 687 north on the prodelta is denser than at station 685 to the southeast, in spite of being more shielded from storm waves. Forces caused by intense ice-gouging on the northern prodelta may act to locally densify and strengthen the sediment (Thor and Nelson, 1980).

It is worthwhile to note that the wave and ice forces that have acted to stabilize sediment on the prodelta can be significant agents of erosion and also can have significant impact directly on engineering structures. Therefore, they are potential hazards.

The effects of earthquakes on prodelta sediment stability must be considered. Seismic activity in western Alaska, particularly on the Seward Peninsula, is moderate (Biswas and Gedney, 1979), but earthquakes above magnitude 4.0 with epicenters under Norton Sound are unlikely (Biswas, University of Alaska, pers. communication, 1982). Therefore, liquefaction in response to earthquakes in southwest Norton Sound is unlikely.

Thermogenic gas seep: The occurrence of thermogenic gas 40 km south of Nome is vertically and areally discontinuous, as shown by the uneven distribution of gas bubbles in sediment cores and seismic-reflection profiles. Laboratory tests on lithologically similar cores collected within and west of the seep show high sensitivity, low compressibility, and a state of overconsolidation for both. Only sections that were undisturbed by gas bubbles were tested in the core from within the seep. Penetrometer tests suggest that the bubble-rich intervals are weak and relatively suseptible to liquefaction. Exposure to storm waves does not appear severe enough to induce liquefaction, however a M6.75 earthquake located in the vicinity of Nome could cause liquefaction within and east of the seep (Table 9). The occurrence of that event is improbable. Analysis of penetrometer data suggests that liquefaction is unlikely at the station west (684) of the seep.

Areas of biogenic gas: Two stations were occupied within extensive areas of biogenic gas-charged sediment in Norton Sound. Station 682, approximately 10 km north of the thermogenic gas seep has a 3.5-m thick peat layer with high percentages of water and organic carbon. The peat is weak and is the most compressible material sampled in the northern Bering Sea. The low strength correlates better with high water and organic carbon contents than with gas content. Possibly, the gas pressure is not high enough to significantly decrease the effective stress within the sediment. Sensitivity and degree of overconsolidation are less at this site compared to others, indicating that although the sediment is weak, the strength will not rapidly decrease after shear.

Liquefaction analysis indicates that an M6.75 earthquake located in the south-western Seward Peninsula could cause sediment failure, but as previously mentioned a seismic event of that magnitude is unlikely.

Physical properties of sediment at the other biogenic-gas station (673) are somewhat different from those at station 682. Penetrometer records indicate high sediment density, for which there is no obvious explanation in terms of exposure to environmental forces. Liquefaction analysis predicts that susceptibility is less than at station 682, but a M6.75 earthquake located approximately 63 km from the site could induce failure.

More testing within areas of biogenic gas is necessary to determine the variability of gas-changing, as well as the range of physical properties and deformational behavior.

Eastern Norton Sound: Although local variations exist, the silty sediment core in eastern Norton Sound has high water content, perhaps because of an open sedimentary fabric produced in this relatively tranquil environment. An earthquake of magnitude 6.75 at an approximate distance of 107 km theoretically could cause liquefaction at station 672 (Table 9). Because an M6.5 earthquake occurred in 1950, approximately 30 km inland from the northeastern coast of Norton Sound, sediment in the vicinity of station 672 appears to be more suseptible to liquefaction than at any other station.

Ridge and swale topography: Large variation in physical properties over small lateral distance characterize sediment at stations on a ridge and in a swale near Port Clarence. The ridge material is a dense, uniform sand, whereas the swale sediment is a less-dense, muddy sand with gravel at depth.

Laboratory tests imply that static engineering behavior of sediment in the swale is similar to the loose prodelta sediment at station 685, except that sensitivity is not as pronounced. As at most other stations, earthquake-induced liquefaction is improbable. Although unlikely, the ridge material is more prone to liquefy from wave action, because at the shallower water depth energy is more readily imparted to it, than the trough.

CONCLUSIONS

Sediment cover in the northern Bering Sea is thin, typically less than 10 m, and physical properties of the widespread silt and sand indicate generally favorable engineering behavior. Local conditions such as high gas concentration pose special concerns in some areas.

Environmental forces from waves, currents, and ice can be severe, and they can have direct impact on engineering structures or they can erode sediment that is meant to serve as a base for foundations. Expectable levels of environmental forces do not appear to be high enough to cause large scale failure of sediment, however.

ACKNOWLEDGEMENTS

This study was jointly funded by the U.S. Geological Survey and the Bureau of Land Management through interagency agreement with the National Oceanic and Atmospheric Administration, under which a multi-year program responding to needs of petroleum development of the Alaskan continental shelf is managed by the Outer Continental Shelf Environmental Assessment Program (OCSEAP) office.

REFERENCES

Arctic Environmental Information and Data Center, 1977, Climatic Atlas of the Outer Continental Shelf Waters and Coastal Regions of Alaska, Vol. II: Bering Sea. Anchorage, University of Alaska, 443p.

Beard, R.M., and Lee, H.J., 1982, A 40-foot static core penetrometer. Proceedings 14th Offshore Technology Conference, p. 69-818.

Begemann, H.K., 1965, The friction jacket core as an aid in determining the soil profile. Proceedings 6th International Conference on Soil Mechanics and Foundation Engineering, v. 1, p. 17-20.

Bishop, A.W., and Henkel, D.J., 1964, The Measurement of Soil Properties in the Triaxial Test. London, Edward Arnold, Ltd (Publishers), 227p.

Biswas, H.N., and Gedney, L., 1979, Seismotectonic studies of northern and western Alaska. In: Outer Continental Shelf Environmental Assessment Program, Environmental Assessment of the Alaskan Continental Shelf Annual Reports of Principal Investigators For the Year Ending March 1979, vol. X. Hazards Data Management, Boulder, p. 155-208.

Cacchione, D.A., and Drake, D.E., 1979, Sediment transport in Norton Sound, Alaska: Regional patterns and GEOPROBE system measurements. U.S. Geological Survey Open-File Report 79-1555, 88 p.

Carver, R.E., 1971, Procedures in Sedimentary Petrology. New York, John Wiley and Sons, Inc., 653p.

Casagrande, A., 1936, The determination of the pre-consolidation load and its practical significance. Proceedings First International Conference on Soil Mechanics and Foundation Engineering, V. III, Cambridge, Massachusetts, p. 60-64.

Clukey, E.C., Cacchione, D.A., and Nelson, C.H., 1980, Liquefaction potential of the Yukon prodelta, Bering Sea. Proceedings 12th Offshore Technology Conference, p. 315-325.

Committee on Soil Dynamics of the Geotechnical Engineering Division, 1978, Definition of terms related to liquefaction. Journal Geotechnical Engineering Division, ASCE, September, p. 1197-1200.

Denk, E.W., Dunlap, W.A., Bryant, W.R., Milberger, L.J., Whellan, T.J., III, 1981, A pressurized core barrel for sampling gas-charged marine sediments. Proceedings 13th Offshore Technology Conference, p. 43-52.

Dupré, W.R., and Thompson, R., 1979, The Yukon Delta: A model for deltaic sediment in an ice-dominated environment. Proceedings 11th Offshore Technology Conference, p. 657-664.

Field, M.E., Nelson, C.H., Cacchione, D.A., and Drake, D.E., 1981, Sand waves on an epicontinental shelf: northern Bering Sea. Marine Geology, v. 42, p. 233-258.

Finn, W.D., 1972, Soil dynamics liquefaction of sands. Proceedings International Conference on Microzonation for Safer Construction Research and Application, v. 1, Seattle, p, 87-111.

Holmes, M.L., and Cline, J.D., 1979, Geologic setting and source depth of the Norton Basin gas seep. Jour. Petroleum Technology, October, p. 1241-1248.

Holmes, M.L., and Thor, D.R., 1982, Distribution of gas-charged sediment in Norton Sound and Chirikov Basin. Geologie en Mijnbouw, v. 61, p. 79-90.

Howard, J.D., and Nelson, C.H., 1980, Sedimentary structures on a delta-influenced shallow shelf, Norton Sound, Alaska. In: Larsen, M.C., Nelson, C.H., and Thor, D.R. (eds.), Geological, Geochemical, and Geotechnical Observations on the Bering Shelf, Alaska. U.S. Geological Survey Open-File Report 80-979, 19 p.

Johnson, J.L., and Holmes, M.L., 1978, Report on surface and subsurface faulting in Norton Sound and northeastern Chirikov Basin, Alaska. In: Larsen, M.C., Nelson, C.H., and Thor, D.R. (eds.), Geological, Geochemical, and Geotechnical Observations on the Bering Shelf, Alaska U.S. Geological Survey Open-File Report 80-979, 25 p.

Kishida, H., 1969, A note on the liquefaction of hydraulic fill during the Tokachi-Oki earthquake. Second Seminar on Soil Behavior and Ground Response During Earthquakes, University of California, Berkeley, Aug.

Koutsoftas, D.C., Fischer, J.A., Dette, J.T., and Singh, H., 1976, Evaluation of the vibracorer as a tool for underwater geotechnical explorations. Proceedings 8th Offshore Technology Conference, p. 107-121.

Kvenvolden, K.A., Nelson, C.H., Thor, D.R., Larsen, M.C., Redden, G.D., Rapp, J.B., and Des Marais, D.J., 1979, Biogenic and thermogenic gas in gas-charged sediment of Norton Sound, Alaska. Proceedings 11th Offshore Technology Conference, p. 479-486.

Kvenvolden, K.A., Redden, G.D., Thor, D.R., and Nelson, C.H., 1980, Hydrocarbon gases in near-surface sediment of northern Bering Sea (Norton Sound and Chirikov Basin). In: Larsen, M.C., Nelson, C.H., and Thor, D.R. (eds.), Geological, Geochemical, and Geotechnical Observations on the Bering Shelf, Alaska. U.S. Geological Survey Open-File Report 80-979, 28 p.

Ladd, C.C., and Foott, R., 1974, New design procedure for stability of soft clays. Journal Geotechnical Engineering Division, ASCE, July, p. 763-786.

Lambe, T.W., 1951, Soil Testing for Engineers. New York, John Wiley and Sons, Inc., 165 p.

Lambe, T.W., and Whitman, R.V., 1969, Soil Mechanics. New York, John Wiley and Sons, Inc., 553 p.

Larsen, M.C., Nelson, C.H., and Thor, D.R. (eds.) 1980, Geological, geochemical, and geothechnical observations on the Bering Shelf, Alaska. U.S. Geological Survey Open-File Report 80-979, 492 p.

Lee, K.L., and Fitton, J.A., 1968, [1969], Factors affecting the cyclic loading strength of soil. In: Vibration Effects of Earthquakes on Soils and Foundations, ASTM Special Technical Pub. 450, p. 71-95.

Martin, F.R., and Douglas, B.J., 1981, Evaluation of the core penetrometer for liquefaction hazard assessment. U.S. Geological Survey Open-File Report 81-284, 185 p.

Mayne, P.W., and Kulhawy, F.H., 1982, K_o-OCR relationships in soil. Journal Geotechnical Engineering Division, ASCE, June, p. 851-872.

McCormick, J.M., and Thiruvathukal, J.V., 1976, Elements of Oceanography. Philadelphia, W.B. Saunders Company, 346 p.

McManus, D.A., Kolle', V., Hopkins, D.M., and Nelson, C.H., 1977, Distribution of bottom sediments on the continental shelf, northern Bering Sea, in U.S.G.S. Professional Paper, 759-C.

Nelson, C.H., 1980a, Late Pleistocen-Holocene transgressive sedimentation in deltaic and non-deltaic areas of the Bering continental shelf. In: Larsen, M.C., Nelson, C.H., and Thor, D.R. (eds.), Geological, Geochemical, and Geotechnical Observations on the Bering Shelf, Alaska. U.S. Geological Survey Open-File Report 80-979, 30 p.

Nelson, C.H., 1980b, Graded storm sand layers offshore from the Yukon delta, Alaska. In: Larsen, M.C., Nelson, C.H., and Thor, D.R. (eds.), Geological, Geochemical, and Geotechnical Observations on the Bering Shelf, Alaska. U.S. Geological Survey Open-File Report 80-979, 21 p.

Nelson, C.H., and Creager, J.S., 1977, Displacement of Yukon-derived sediment from Bering Sea to Chukchi Sea during the Holocene. Geology, v. 5, p. 141-146.

Nelson, C.H., Duprè, W.R., Field, M.E., and Howard, J.D., 1980, Linear sand bodies in the Bering Sea epicontinental shelf. In: Larsen, M.C., Nelson, C.H., and Thor, D.R. (eds.), Geological, Geochemical, and Geotechnical Observations on the Bering Shelf, Alaska. U.S. Geological Survey Open-File Report 80-979, 28 p.

Nelson, C.H., Kvenvolden, C.H., and Clukey, E.C., 1978, Thermogenic gases in near-surface sediments of Norton Sound, Alaska. Proceedings 10th Offshore Technology Conference, p. 2623-2633.

Olsen, H.W., Clukey, E.C., and Nelson, C.H., 1980, Geotechnical characteristics of bottom sediments in the northern Bering Sea. In: Larsen, M.C., Nelson, C.H., and Thor, D.R. (eds.), Geological, Geochemical, and Geotechnical Observations on the Bering Shelf, Alaska. U.S. Geological Survey Open-File Report 80-979, 32 p.
Shelf, Alaska. U.S. Geological Survey Open-File Report 80-979, 21 p.

Olsen, H.W., Clukey, E.C., and Nelson, C.H., 1980, Geotechnical characteristics of bottom sediments in the northern Bering Sea. In: Larsen, M.C., Nelson, C.H., and Thor, D.R. (eds.), Geological, Geochemical, and Geotechnical Observations on the Bering Shelf, Alaska. U.S. Geological Survey Open-File Report 80-979, 32 p.

Peck, Ralph B., Hanson, Walter E., Thornburn, Thomas H., Foundation Engineering, John Wiley & Sons, New York, 2974, p. 312.

Schmertmann, J.H., 1976, Predicting the Q_c/N ratio. Final report D-636, Engineering and industrial experiment station, Dept. of Civil Engineering, University of Florida, Gainesville, October. (Cited in: Martin, G.R., and Douglas, B.J., 1981).

Schmertmann, J.H., 1978a, Guidelines for core penetration test performance and design. U.S. Department of Transportation, FWHA-TS-78-209, 145 p.

Schmertmann, J.H., 1978b, Study of feasibility of using Wissa-type piezometer probe to identify liquefaction potential of saturated fine sands. U.S. Army Waterways Experiment Station Technical Report S-78-2, 73 p.

Seed, H.B., 1979, Soil liquefaction and cyclic mobility evaluation for level ground during earthquakes. Journal Geotechnical Engineering Division, ASCE, February, p. 201-255.

Seed, H.B., and Idriss, I.M., Evaluation of liquefaction potential using field performance data. Journal Geotechnical Engineering Division, ASCE, in press.

Seed, H.B., and Idriss, I.M., 1971, Simplified procedure for evaluating soil liquefaction potential. Journal Geotechnical Engineering Division, ASCE, September, p. 1249-1273.

Seed, H.B., and Rahman, M.S., 1978, Wave-induced pore pressure in relation to ocean floor stability of cohesionless soils. Marine Geotechnology, Vol. 3, No. 2, p. 123-150.

Thor, D.R., and Nelson, C.H., 1980, A summary of interacting, surficial geologic processes and potential geologic hazards in the Norton Basin, northern Bering Sea. Jour. Petroleum Technology, March, p.355-362.

Wiegel, R.L., 1964, Oceanographical Engineering. Prentice-Hall, Inc., Englewood Cliffs, NJ. (Cited in: Seed, H.B., and Rahman, M.S., 1978)

Wissa, A.E., Christian, J.T., Davis, E.H., and Heiberg, S., 1971, Consolidation at constant rate of strain. Journal Soil Mechanics and Foundations Division, ASCE, October, p. 1393-1413.

Woodward-Clyde Consultants, 1978, Offshore Alaska Seismic Exposure Study, v. 2, Attenuation, Prepared for the Alaska Subarctic Offshore Committee, San Francisco, 256p.

NOMENCLATURE

A_f	-	The coefficient of pore pressure response at failure during a triaxial test (change in pore pressure at failure/change) in deviator stress).
AVG MAX q	-	The average single amplitude cyclic compressive stress applied to a cyclic triaxial test sample.
AVG MIN q	-	The average single amplitude cyclic tensile stress applied to a cyclic triaxial test sample.
a_{max}	-	The maximum earthquake induced acceleration at the ground surface.
C_c	-	The compression index, defined as the slope of the linear part of a consolidation curve plotted on a graph of void ratio vs. log of effective stress.
CE	-	The prefix for a constant rate of strain (CRS) consolidation test number.
C_N	-	A factor applied to the blow count to correct for influence of overburden pressure (reference value is 1 ton/sq ft).
C_u	-	Uniformity coefficient = D_{60}/D_{10}.
cm	-	Centimeter.
c_m	-	A coefficient that relates unidirectional cyclic shear test results to multidirectional shaking in situ.
c_r	-	A coefficient that modifies the cyclic triaxial stress ratio to a corresponding cyclic simple shear stress ratio that is more representative of field conditions.
C_r	-	Rebound index, determined from a consolidation test.

c_v	- The coefficient of consolidation, a sediment property that reflects the rate at which consolidation will occur.
$C_{v\ ave}$	- The average of all coefficients of consolidation except rebound values determined from an oedometer test.
D	- Prefix for a cyclic triaxial test number.
D	- Maximum distance to an earthquake fault from which a particular ground acceleration would occur.
D_L	- Subbottom depth to which liquefaction may occur due to a particular sustained average storm wave.
D_r	- Relative density, natural density state relative to maximum and minimum density states.
D_{60}	- Diameter at which 60% of the soil is finer.
D_{50}	- Diameter at which 50% of the soil is finer.
D_{10}	- Diameter at which 10% of the soil is finer.
d	- Still water depth.
Damping	- A dynamic sediment property calculated from a cyclic triaxial test. It represents the amount of energy lost per cycle as a percentage of the energy introduced.
DELU	- Same as Delta u.
Delta u	- The change in excess porewater pressure from the beginning of a shear test.
Dev Stress	- The deviator stress or difference between the major and minor principal effective stresses ($\sigma'_1 - \sigma'_3$).
E	- The modulus of elasticity.
e	- The void ratio.

e_o - Initial void ratio in a consolidation test, in situ void ratio.

g - Acceleration due to gravity (9.8 m/sec^2).

H - Sustained average storm wave height.

h - Subbottom depth at which a shear stress is determined.

K_o - Coefficient of earth pressure at rest in situ, horizontal effective stress/vertical effective stress.

km - Kilometer.

kPa - KiloPascal, kN/m^2.

L - Sustained average storm wave length.

M - Earthquake magnitude.

m - Meter.

mm - Millimeter.

N - Blow count, the number of blows required to drive a sampling spoon 1 ft during a standard penetration test.

N_c - Blow count corrected to an overburden pressure of 1 ton/sq ft.

NP - Non-plastic.

OCR - Overconsolidation ratio ($\sigma'_{vm}/\sigma'_{vo}$).

OE - Prefix for oedometer test numbers.

p' - The average normal effective stress acting on a sample at some point in a triaxial shear test $\frac{\sigma_1' + \sigma_3'}{2}$.

q - The peak shear stress acting on a sample at some point in a triaxial shear test $\frac{\sigma'_1 - \sigma'_3}{2}$.

q_c	-	Cone pressure, determined during a cone penetration test.
q_{max}	-	Maximum value of q reached during a static triaxial test, equal to S_u.
r_d	-	Stress coefficient to reduce horizontal shear stresses, induced by an earthquake, from a rigid to a deformable body.
SIG 1_c'	-	The major (or vertical) principal stress applied to a triaxial test sample prior to shear.
SIG 3_c'	-	The minor (or horizontal) principal stress applied to a triaxial test sample prior to shear.
STATIC q_f	-	Strength of a static triaxial test sample, however in Appendix E it typically refers to the test consolidation stress.
S_u	-	Undrained shear strength, determined from a static triaxial test.
T	-	Sustained average storm wave period.
TC	-	Prefix for a cyclic triaxial test number.
TE	-	Prefix for a static triaxial test number.
TR	-	Trace.
w	-	Water content expressed as a percent of dry weight.
w sheared	-	Water content of a sheared triaxial test sample.
Z	-	Subbottom depth at which a shear stress is determined.
°	-	Symbol for angular degrees.
%	-	Percent.
γ	-	The total unit weight of a sediment.
γ'	-	The buoyant (submerged) unit weight of a sediment.

γ_w - The unit weight of saltwater (10.05 kN/m^3).

μm - Micrometer.

σ'_1 - The major (or vertical) principal effective stress applied at any point in a triaxial test.

σ'_3 - The minor (or horizontal) principal effective stress applied at any point in a triaxial test.

σ'_c - The consolidation stress exerted on a triaxial test sample.

$\sigma'_v = \sigma'_{vo}$ - The in situ vertical effective stress exerted by the weight of overburden.

σ'_{vm} - The maximum vertical effective stress that a sediment has ever experienced.

ϕ' - The friction angle of a sediment expressed in terms of effective stresses.

τ_{ave} - Average horizontal shear stress at a subbottom depth induced by an earthquake.

τ_c - Horizontal shear stress at a subbottom depth caused by storm waves.

$\tau_{cyc\ ave\ max}$ - The maximum average single amplitude cyclic stress applied to a cyclic triaxial test sample.

τ_h - Horizontal shear stress at a subbottom depth induced by an earthquake.

τ_{max} - Same as AVG MAX q.

τ_{min} - Same as AVG MIN q.

LITHOLOGIC SYMBOLS.

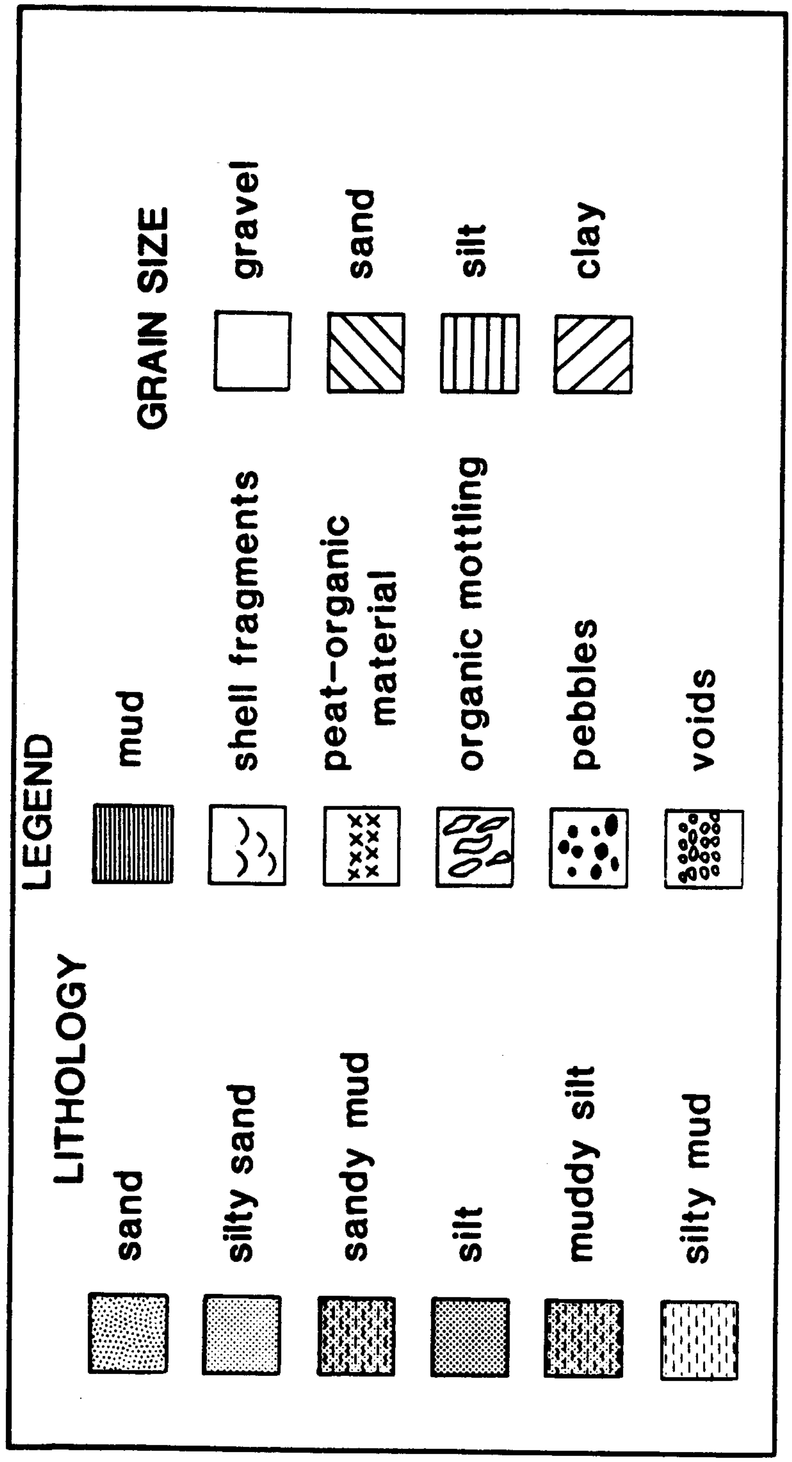

APPENDIX A:

GRAIN-SIZE DISTRIBUTION CURVES

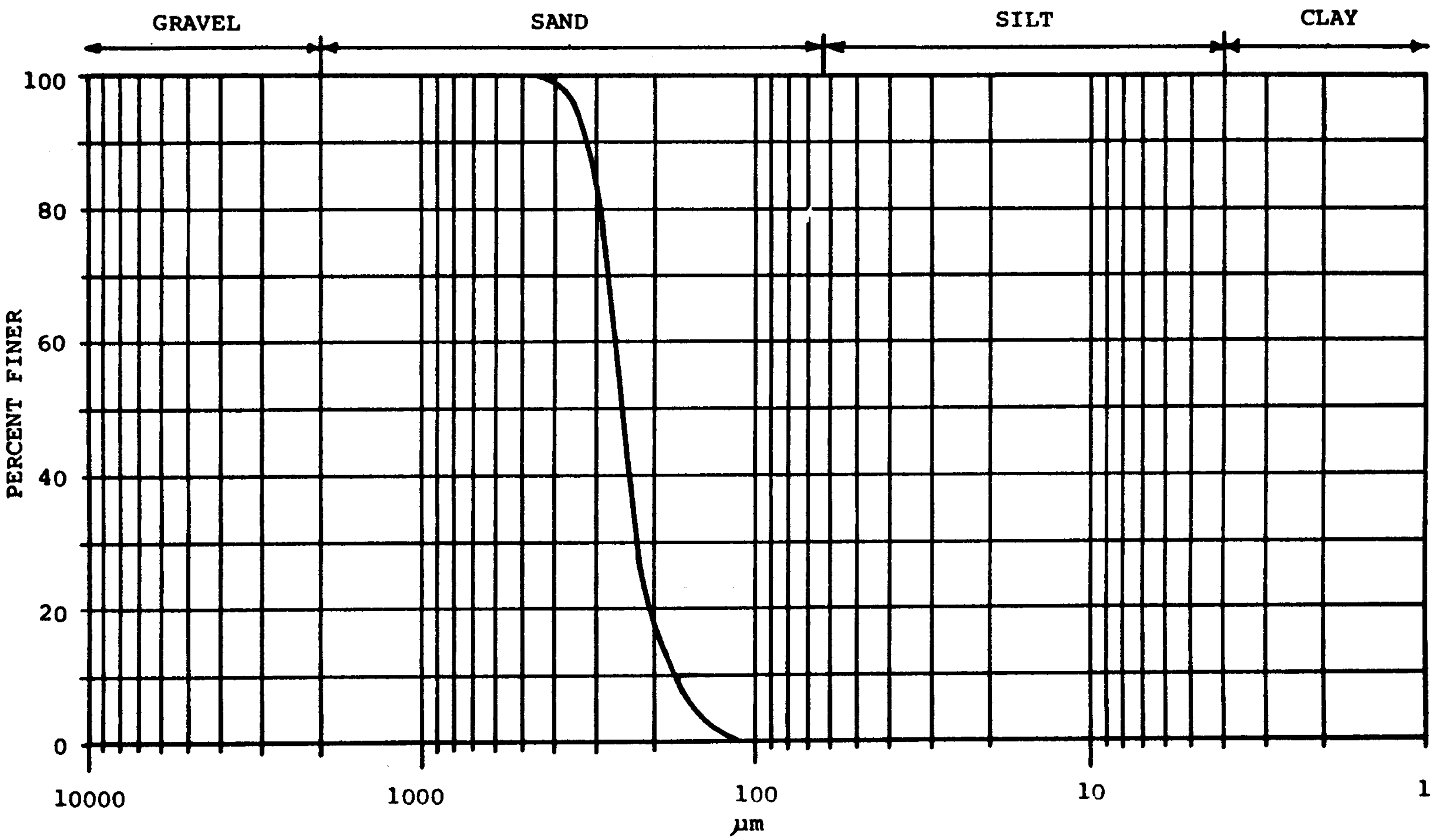

Core: 680A3, Depth: 0.30 m

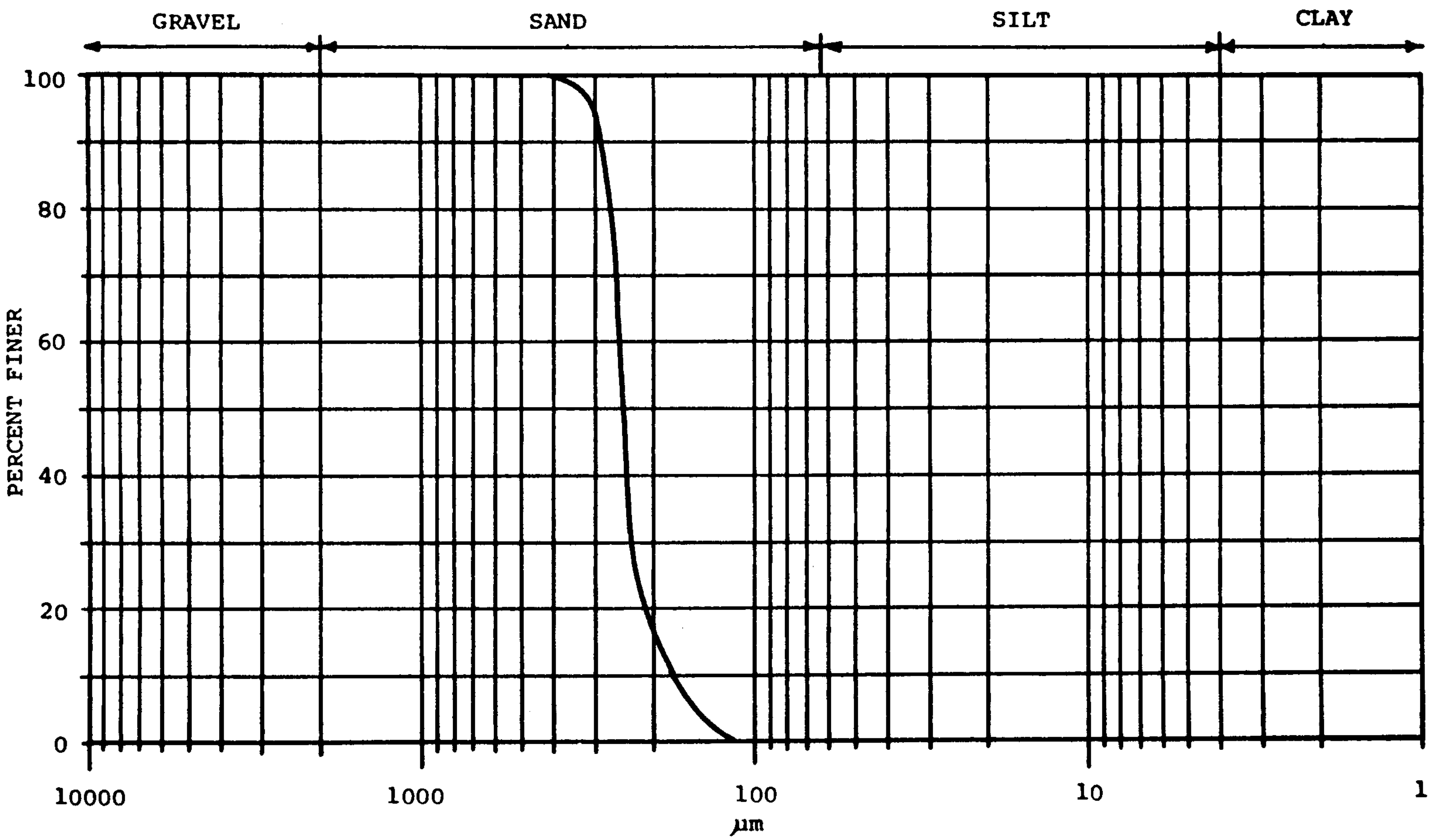

Core: 680A3, Depth: 0.82 m

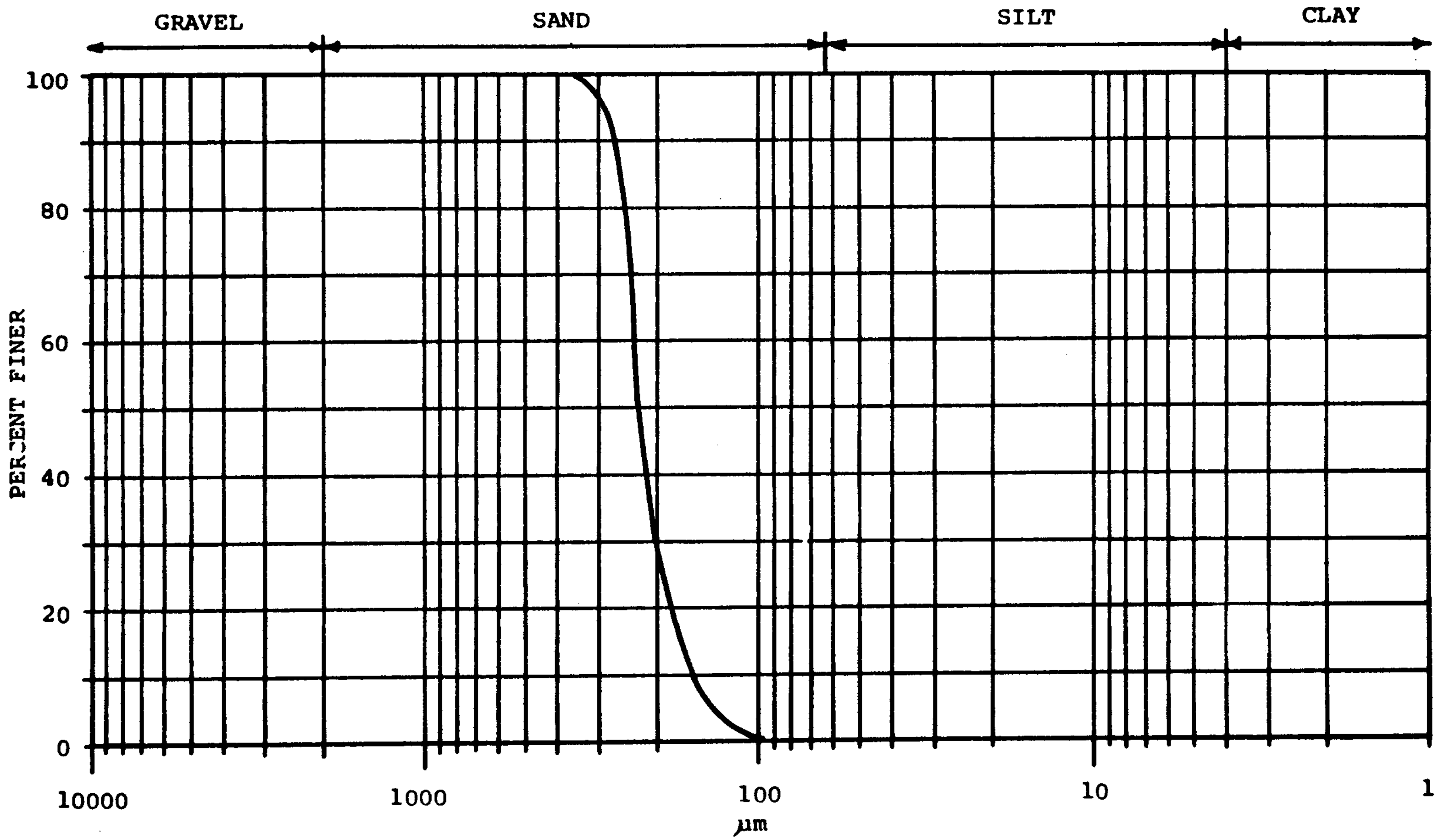

Core: 680A3, Depth: 1.52 m

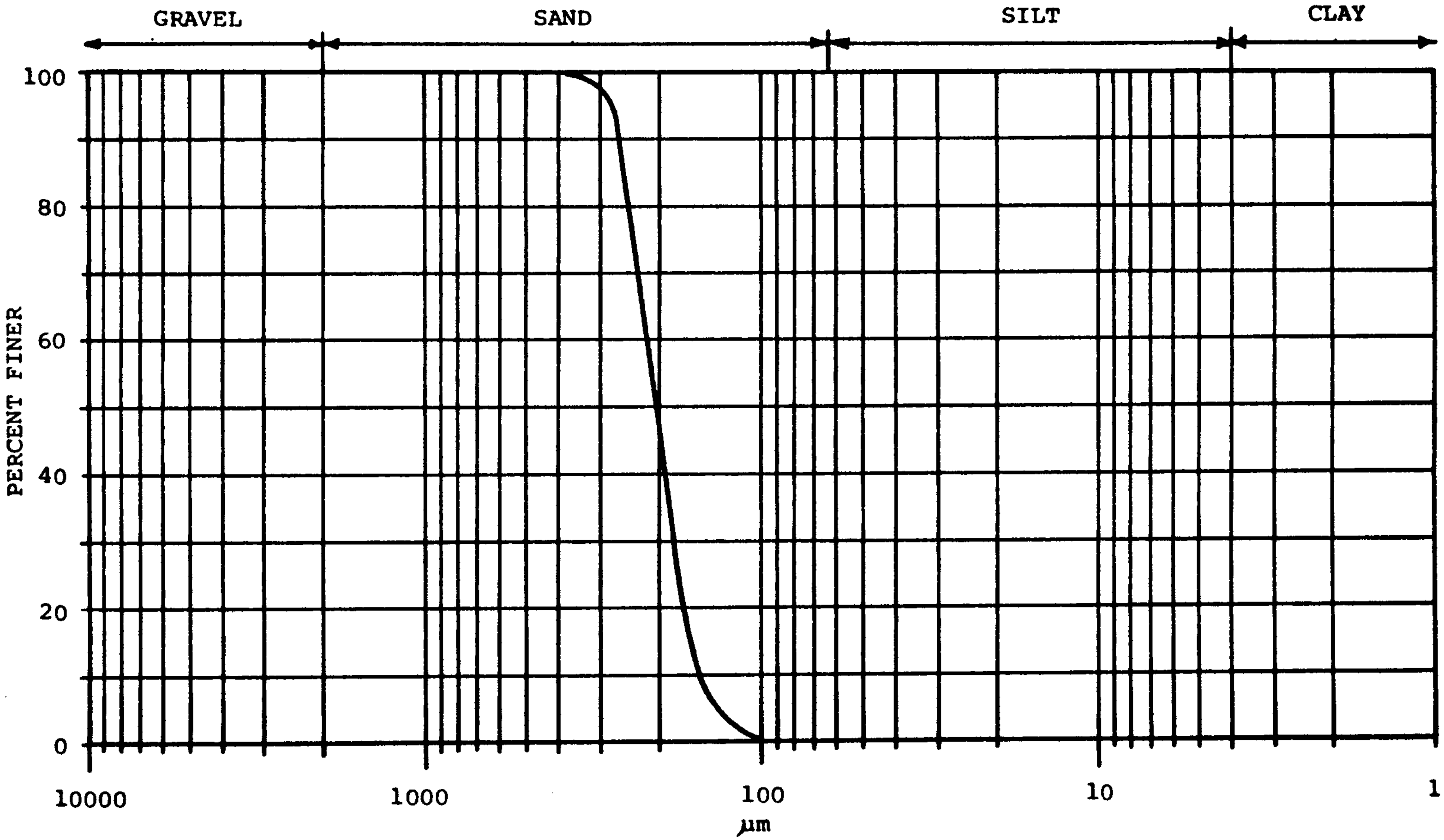

Core: 680A3, Depth: 2.22 m

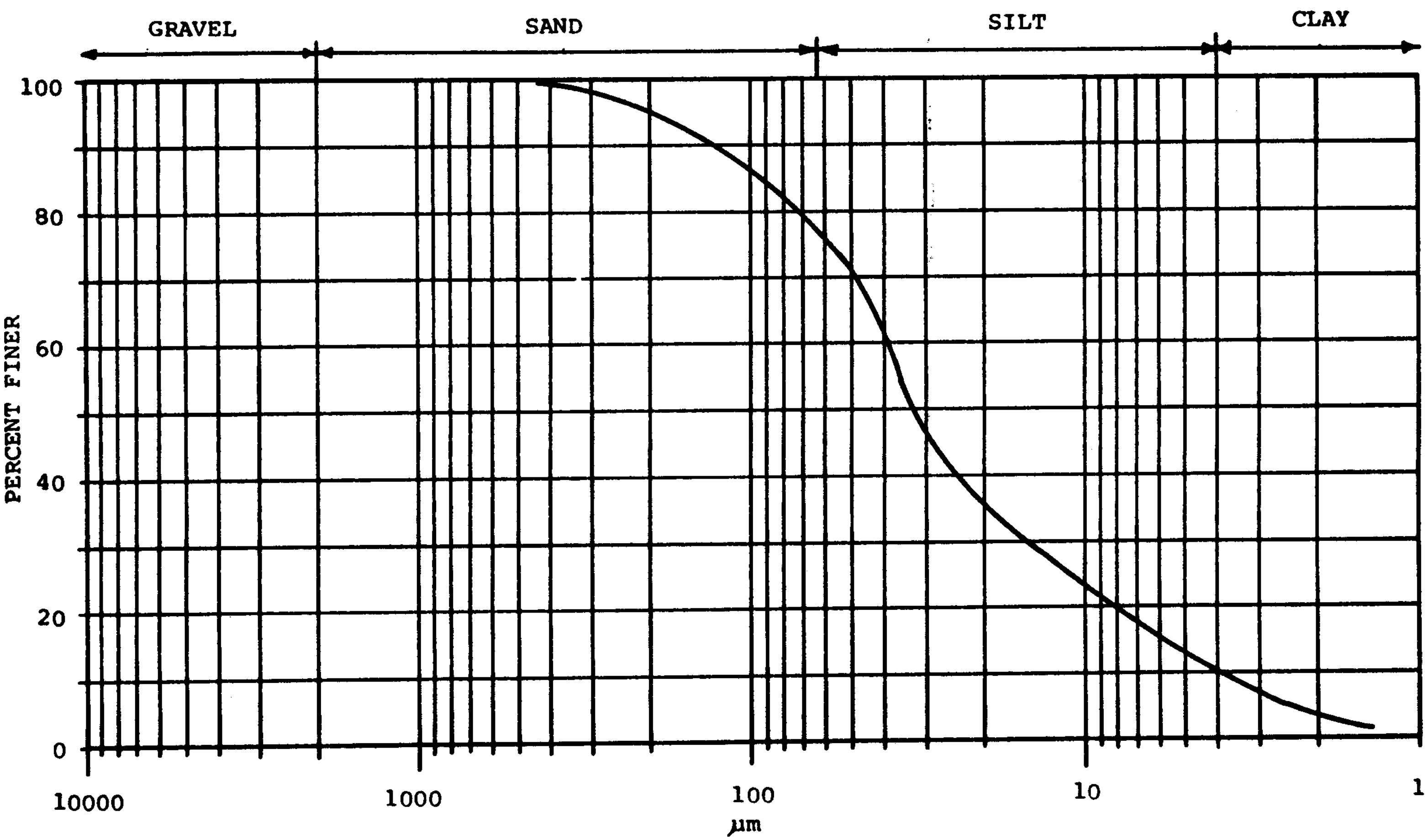

Core: 681A2, Depth: 1.46 m, Sampled from tests D 100, D 101

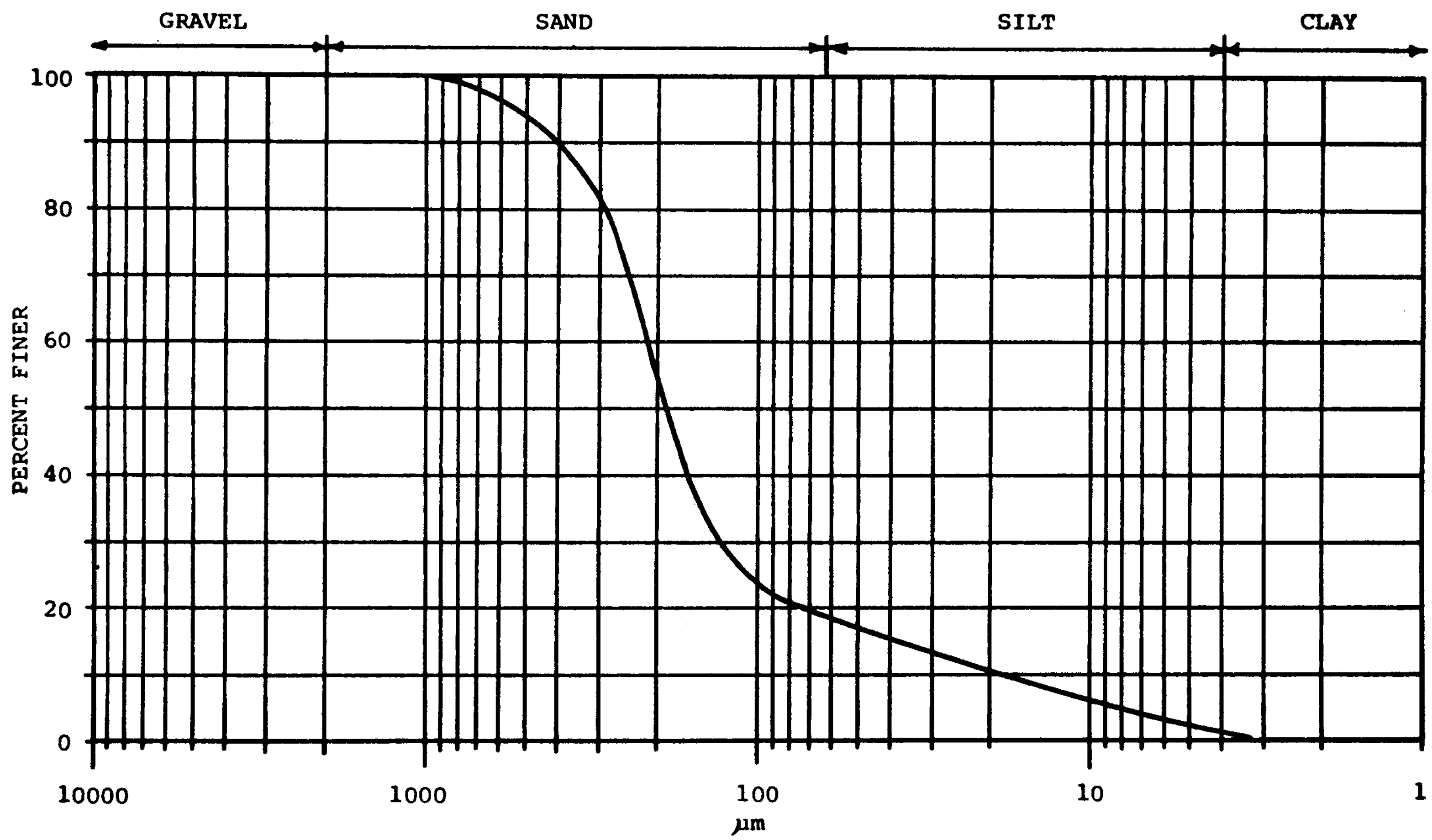

Core: 681A3, Depth: 0.20 m

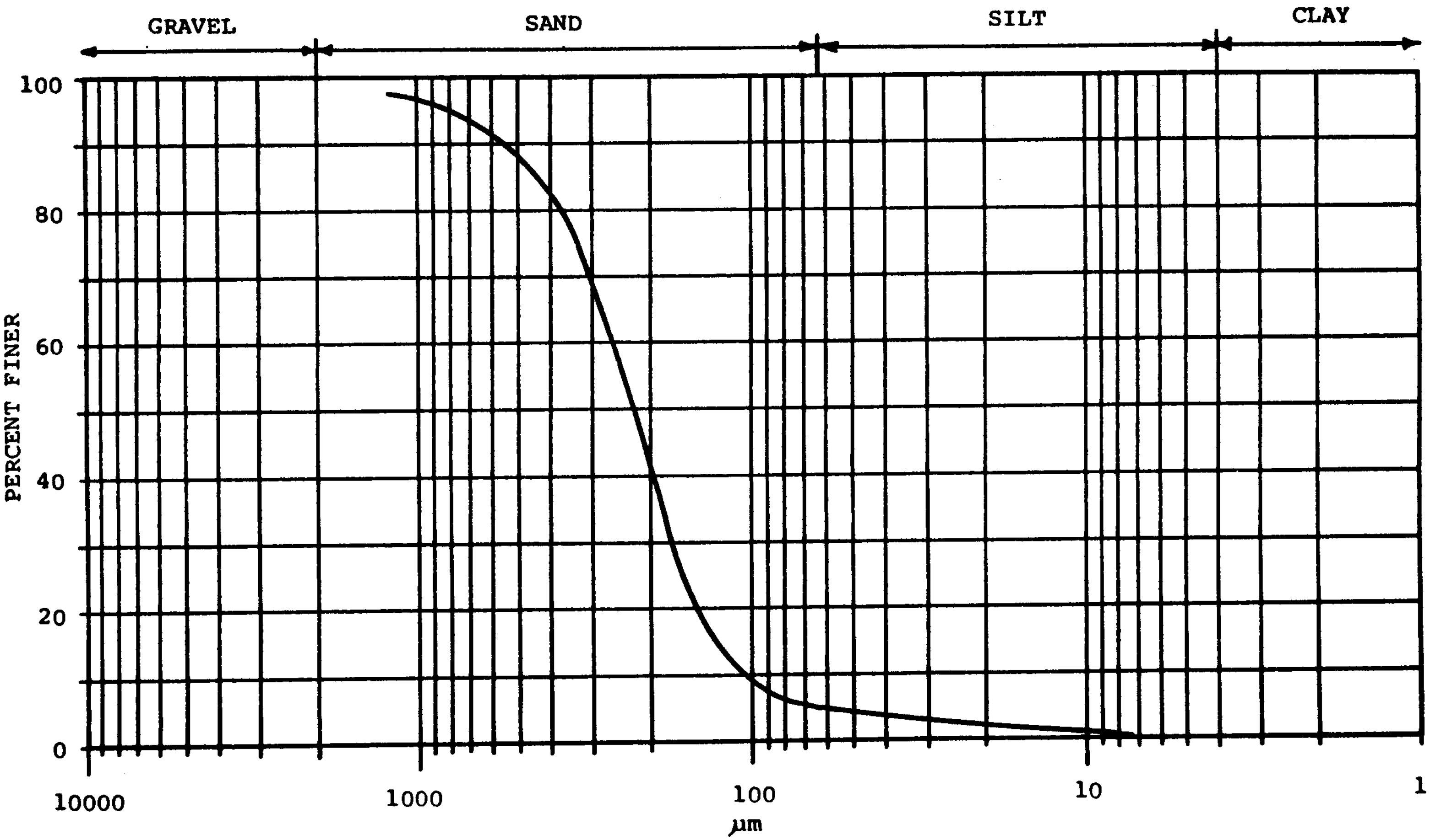

Core: 681A3, Depth: 0.40 m

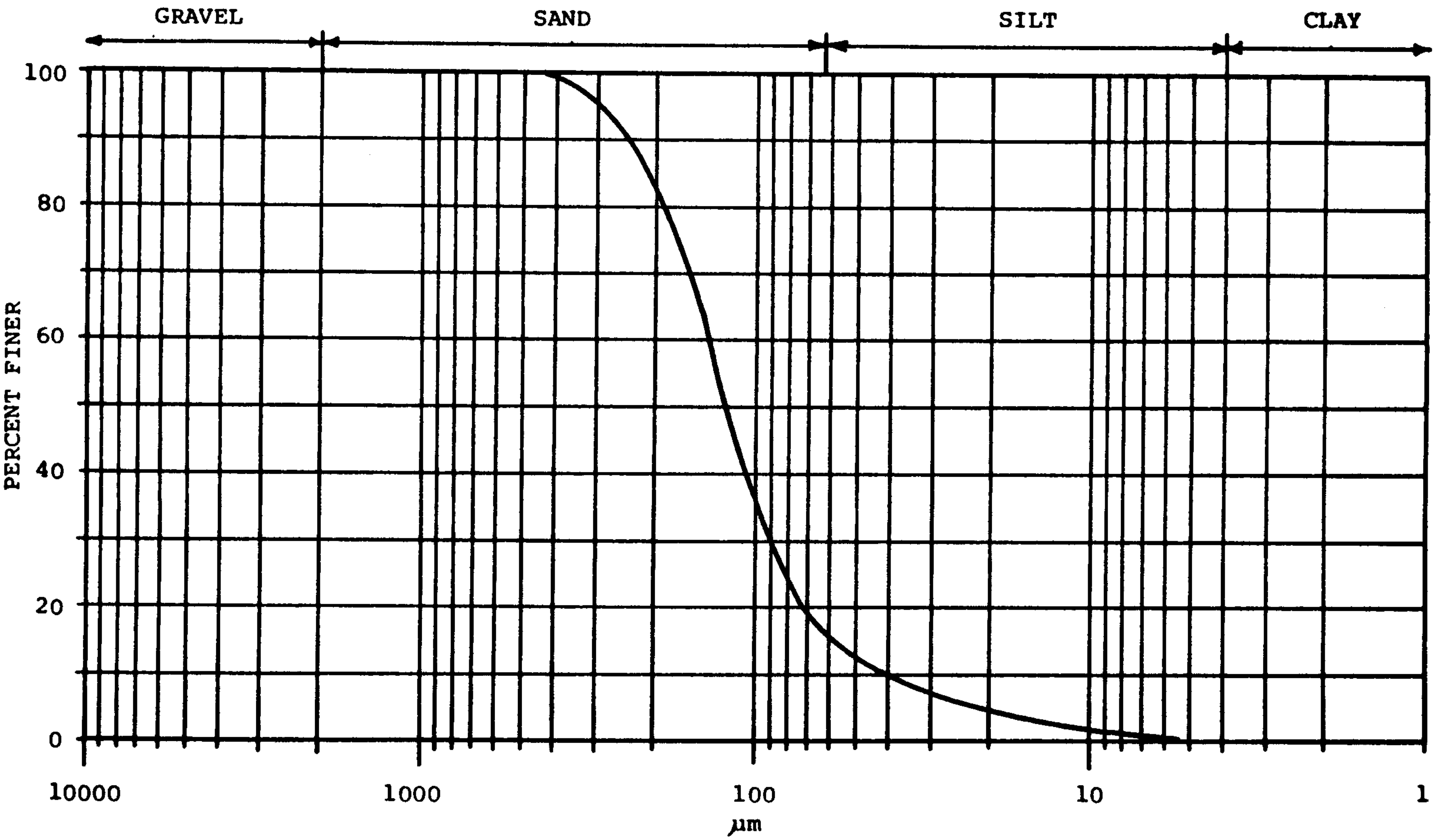

Core: 681A3, Depth: 0.84 m

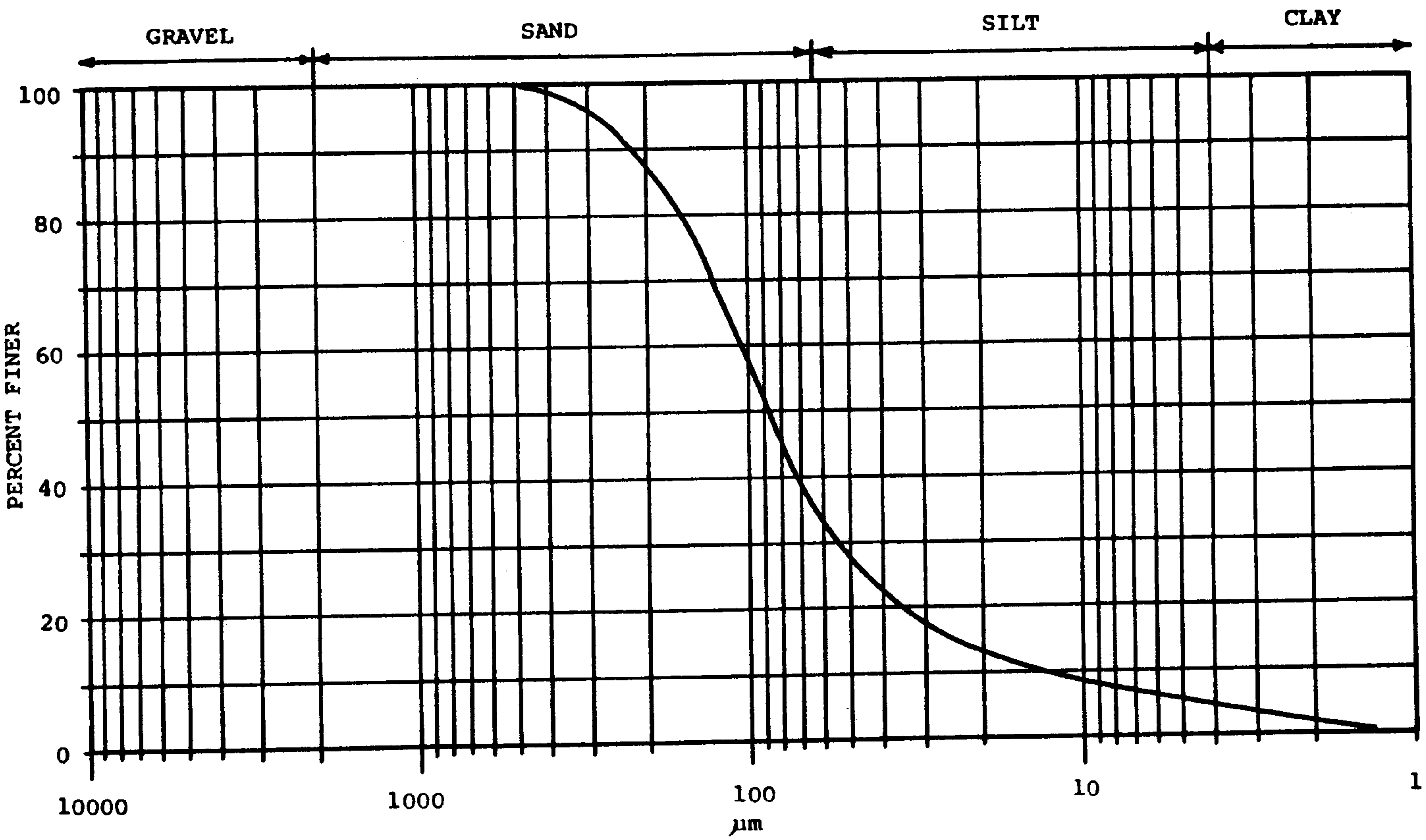

Core: 681A3, Depth: 1.40 m

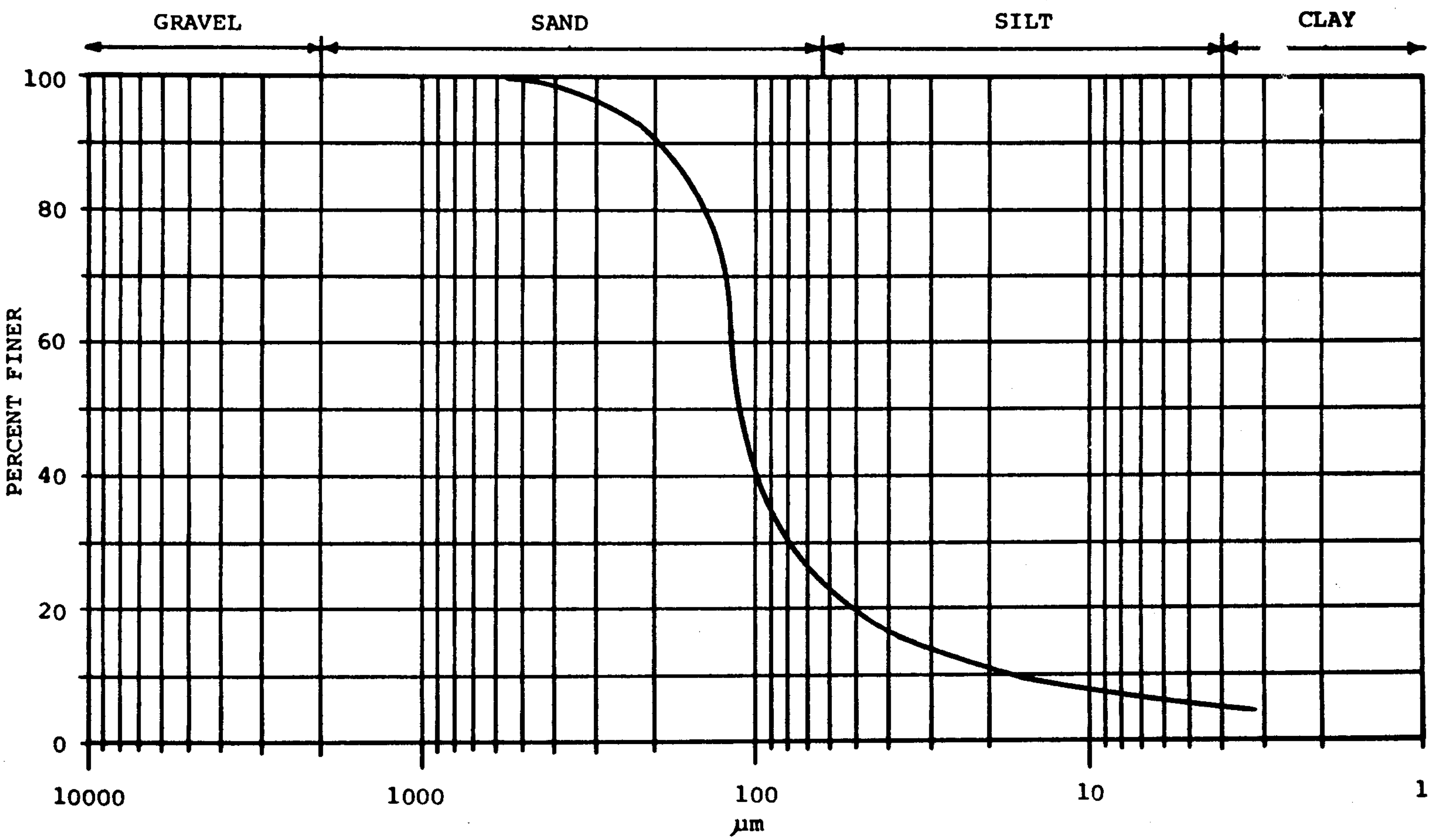

Core: 681A3, Depth: 2.20 m

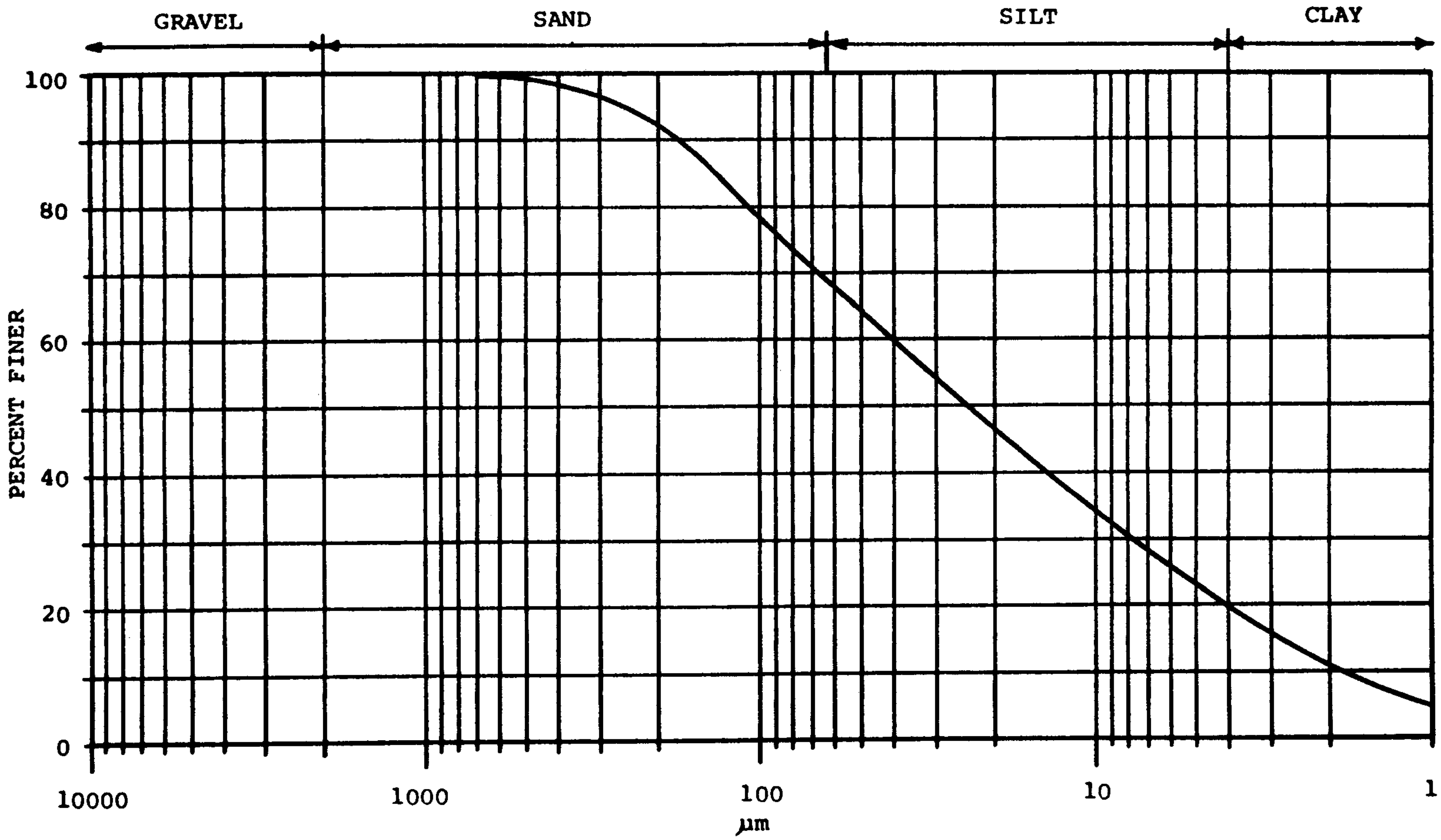

Core: 681A3, Depth: 2.84 m

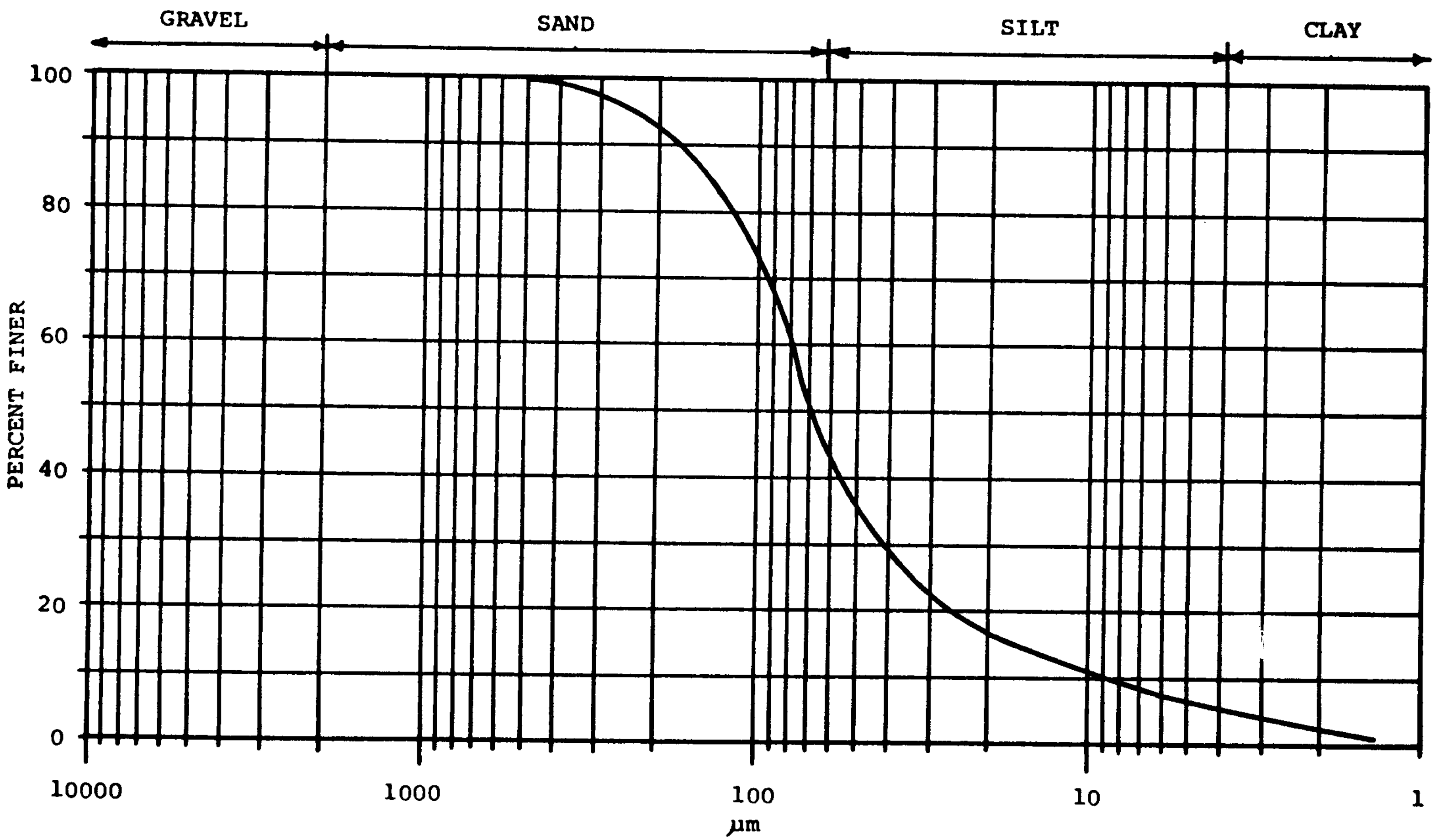

Core: 682A1, Depth: 0.97 m, Sampled from tests TC 38, TC 39

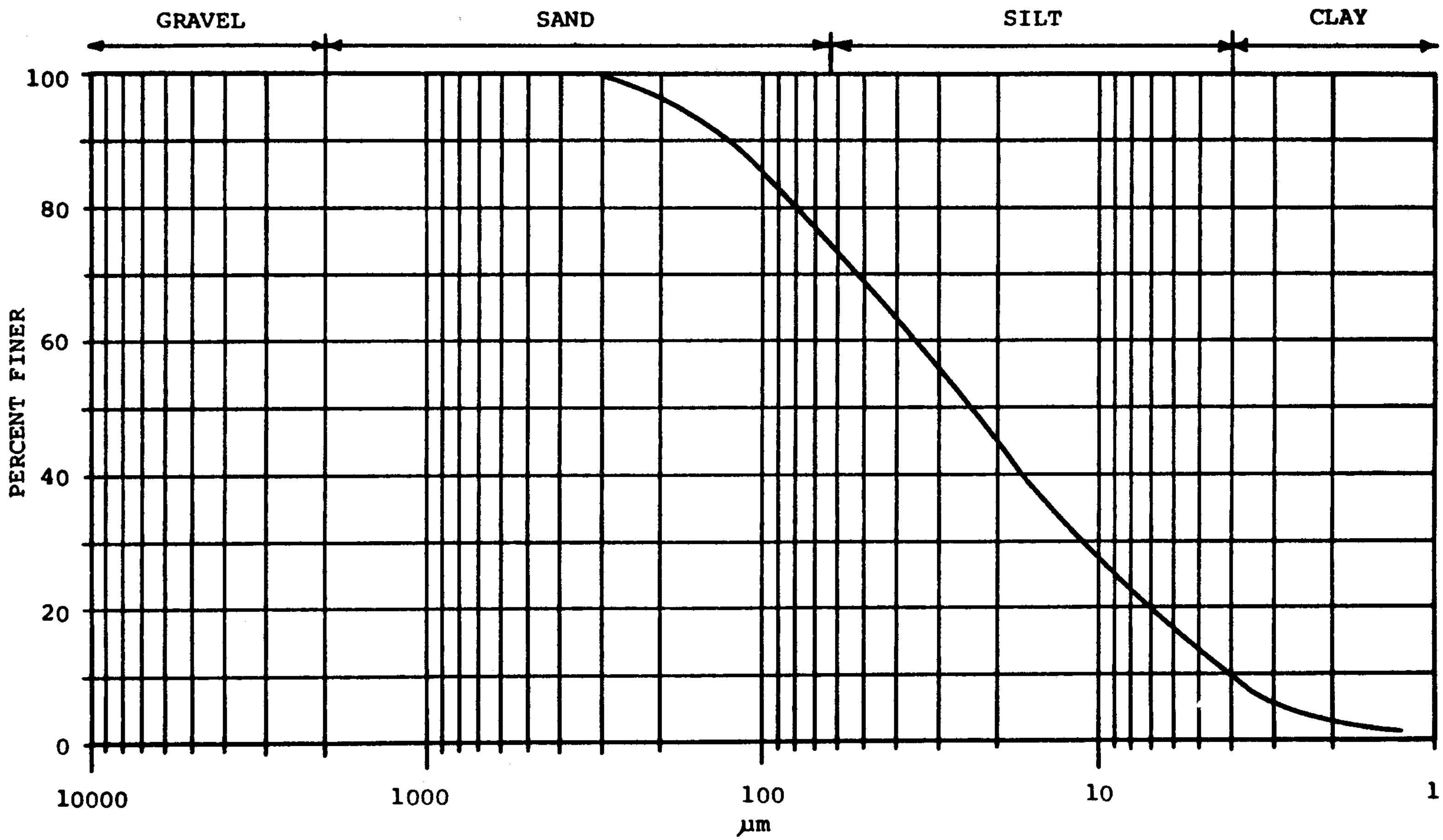

Core: 682A1, Depth: 1.09 m, Sampled from tests TE 76, TE 77

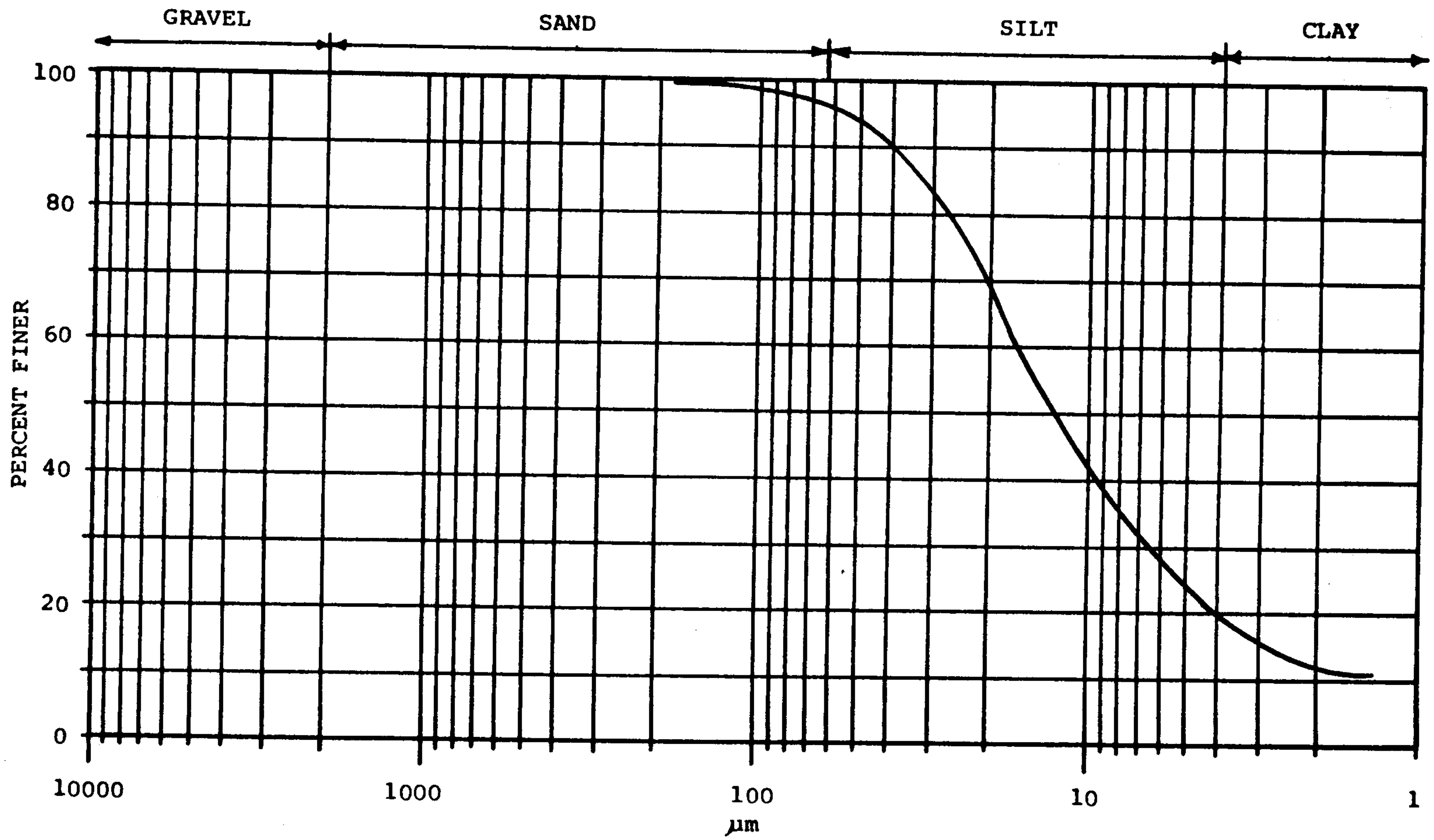

Core: 682A1, Depth: 1.78 m, Sampled from tests TE 98, TE99

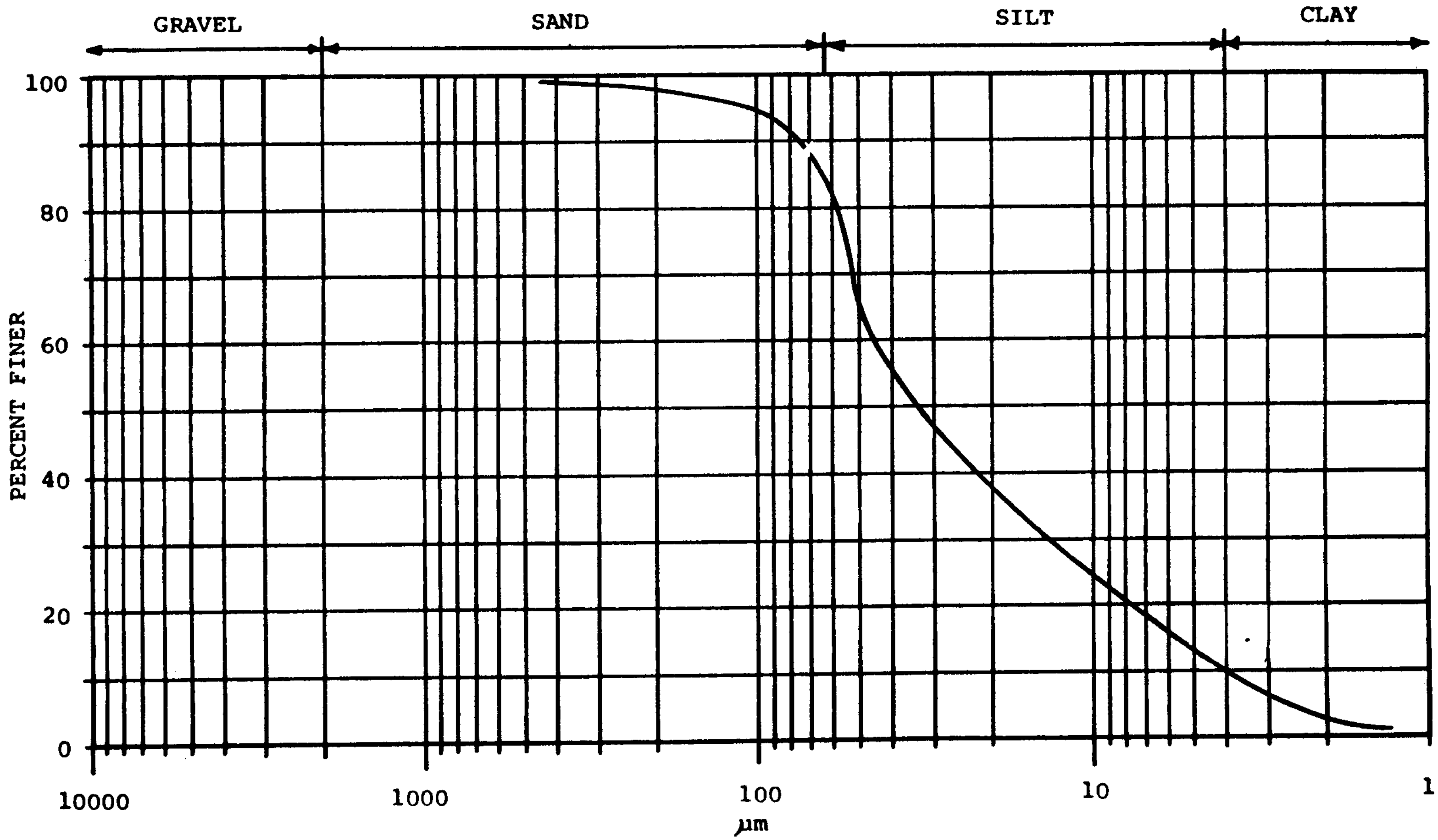

Core: 682A1, Depth: 1.89 m, Sampled from tests TC 76, TC 77

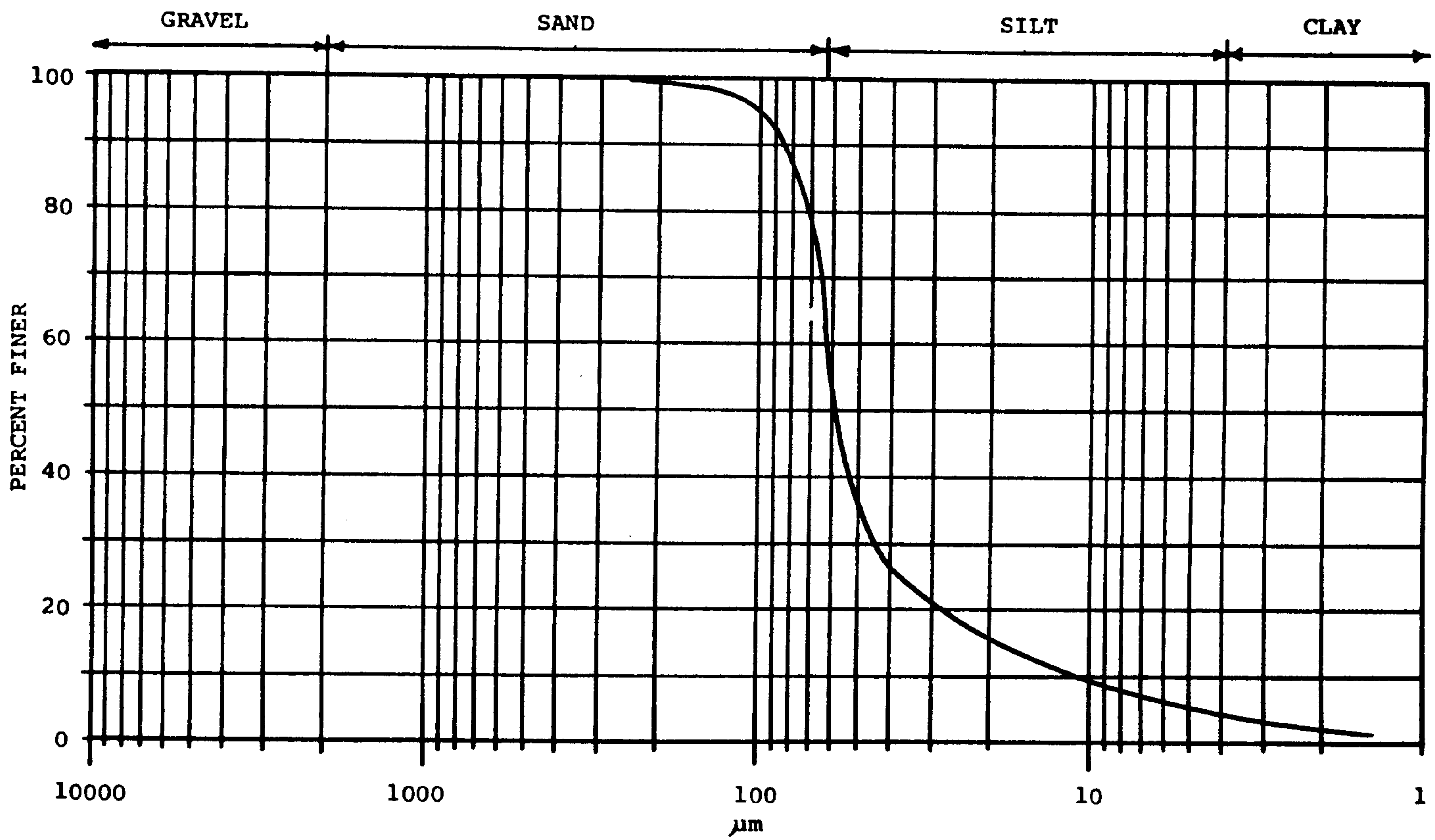

Core: 683A1, Depth: 1.05 m

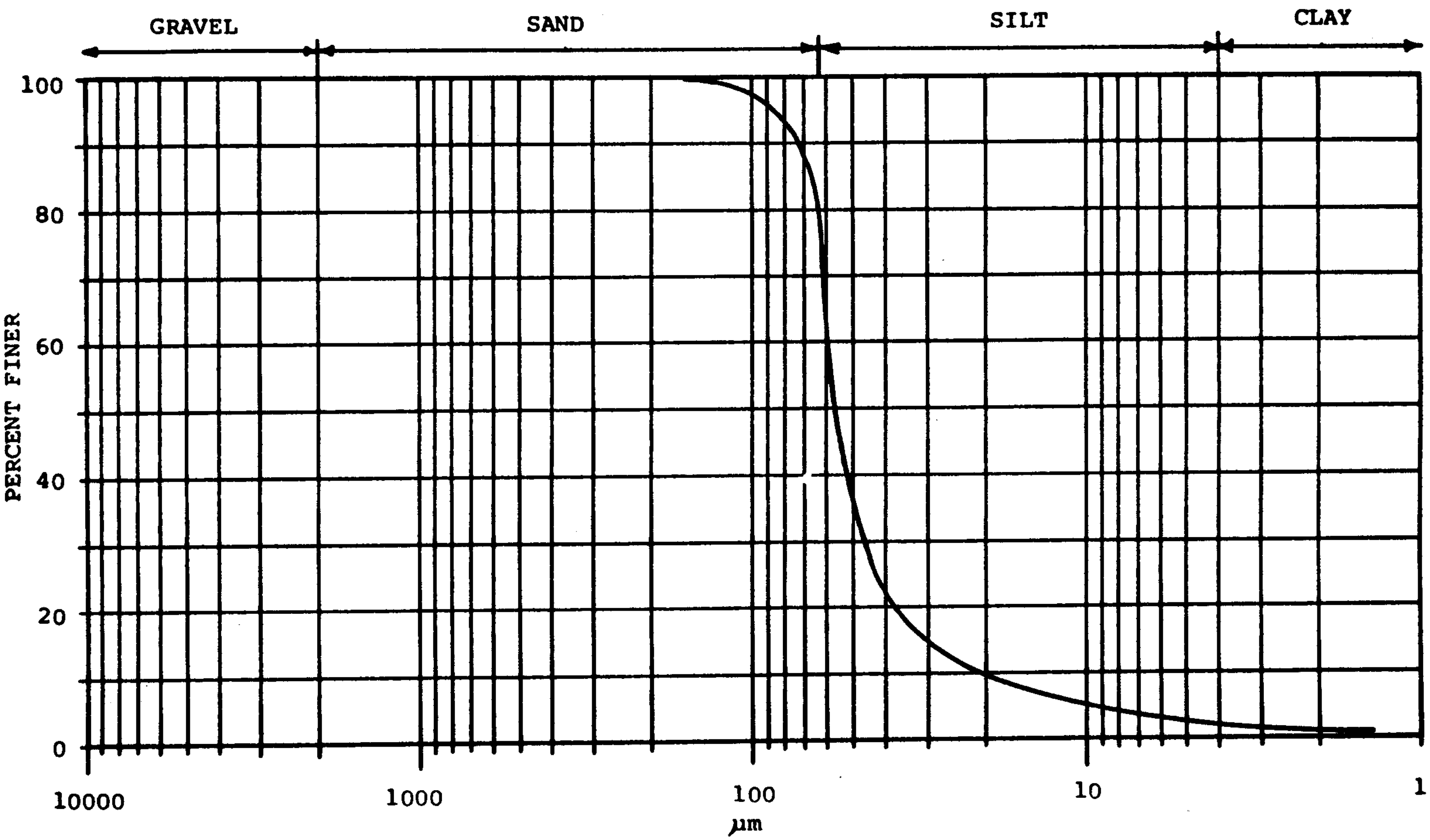

Core: 683Al, Depth: 4.25 m, Sampled from tests TE 109, TE110

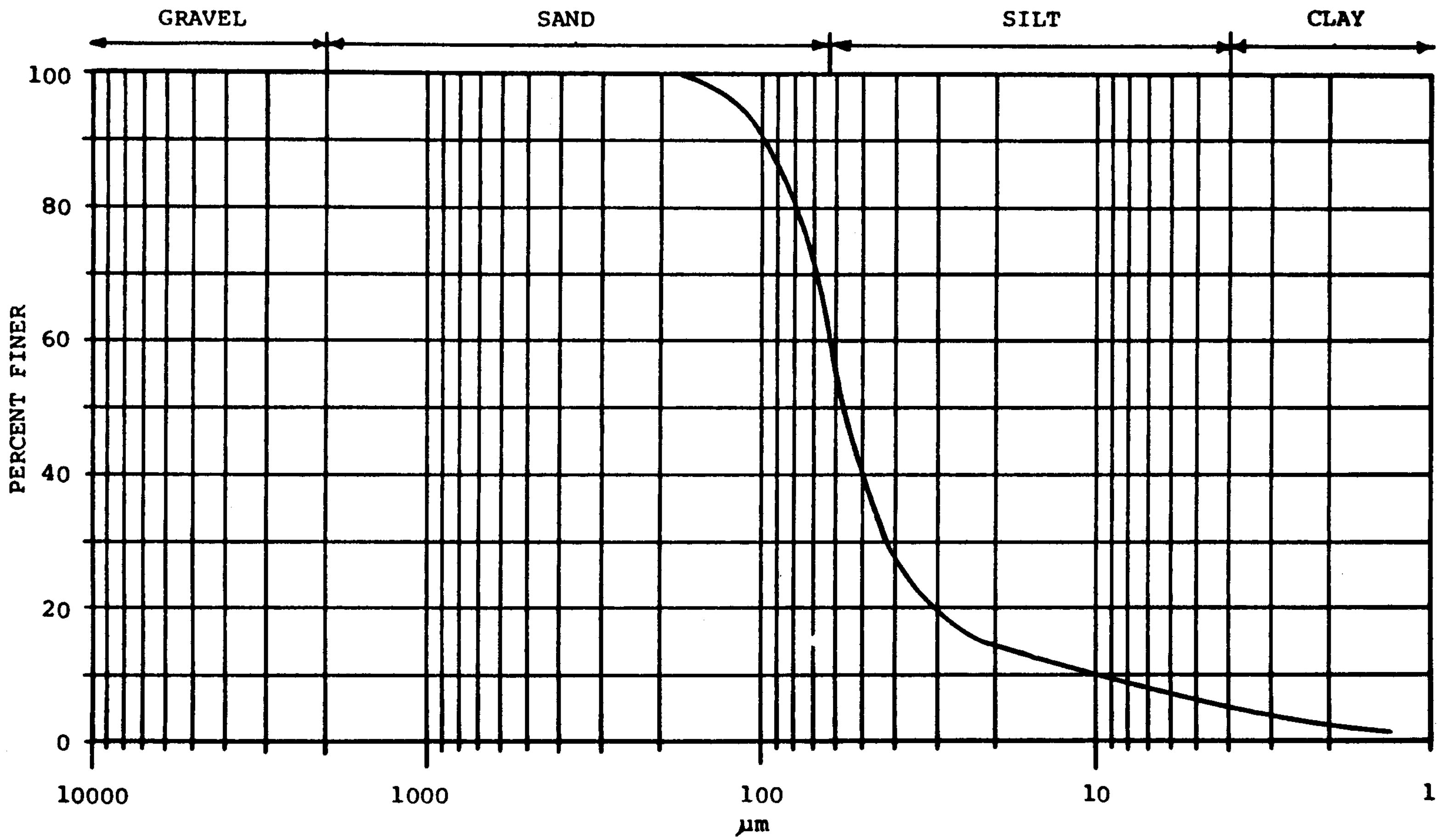

Core: 684A1, Depth: 0.66 m, Sampled from tests TC 90, TC 91

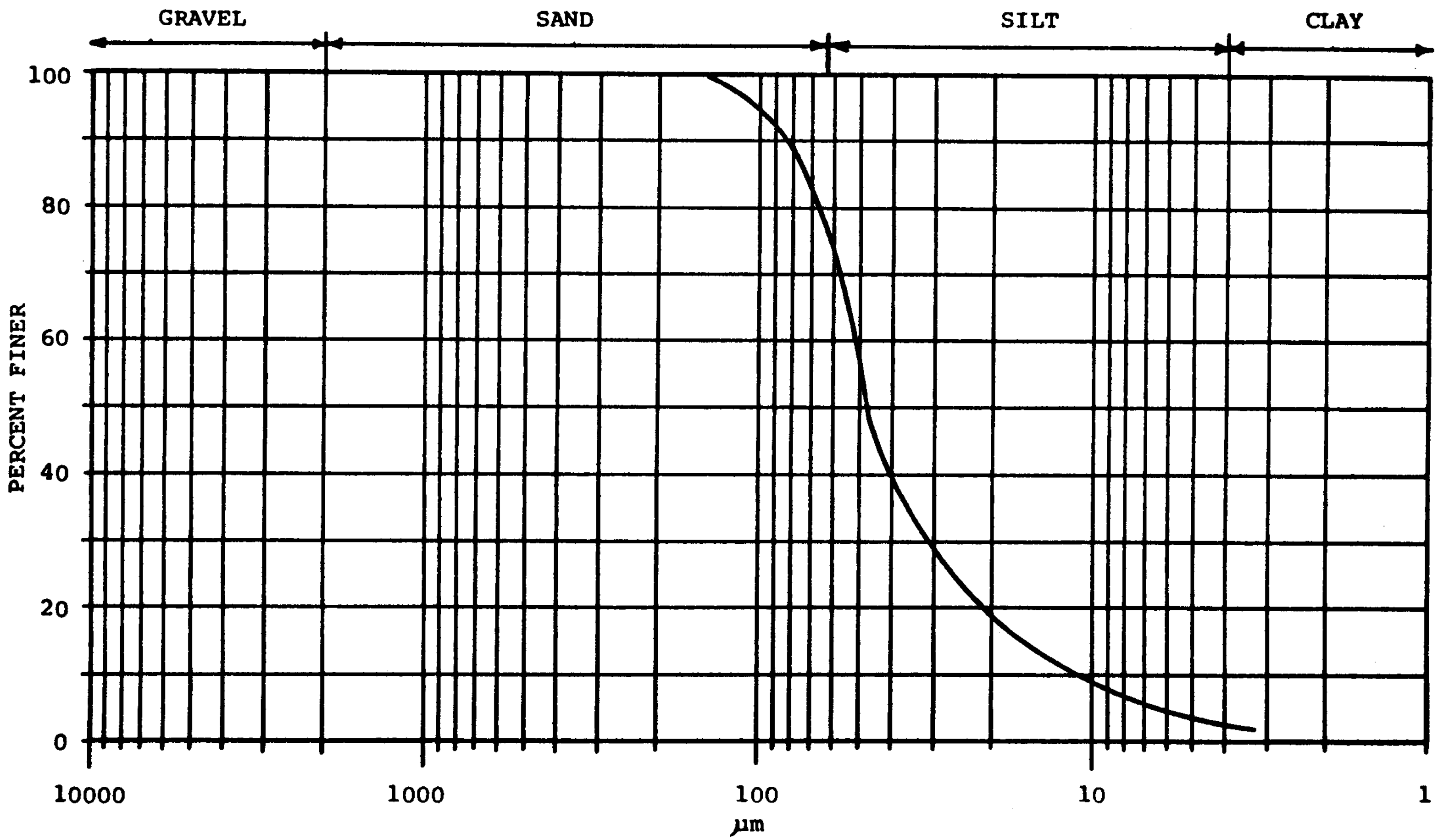

Core: 685A2, Depth: 0.44 m, Sampled from tests TC 80, TC 81

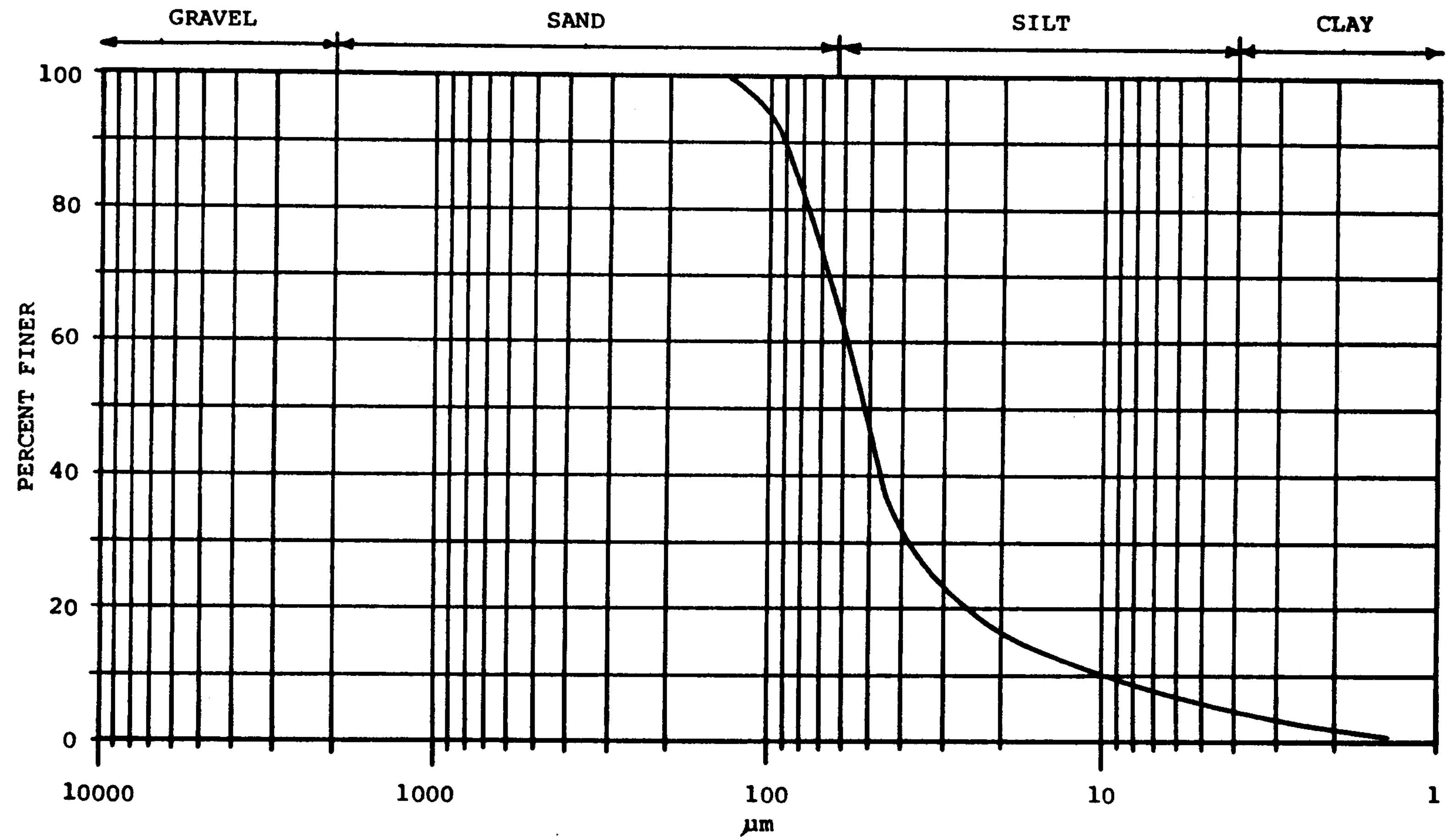

Core: 685A2, Depth: 1.05 m, Sampled from tests TC 62, TC 74

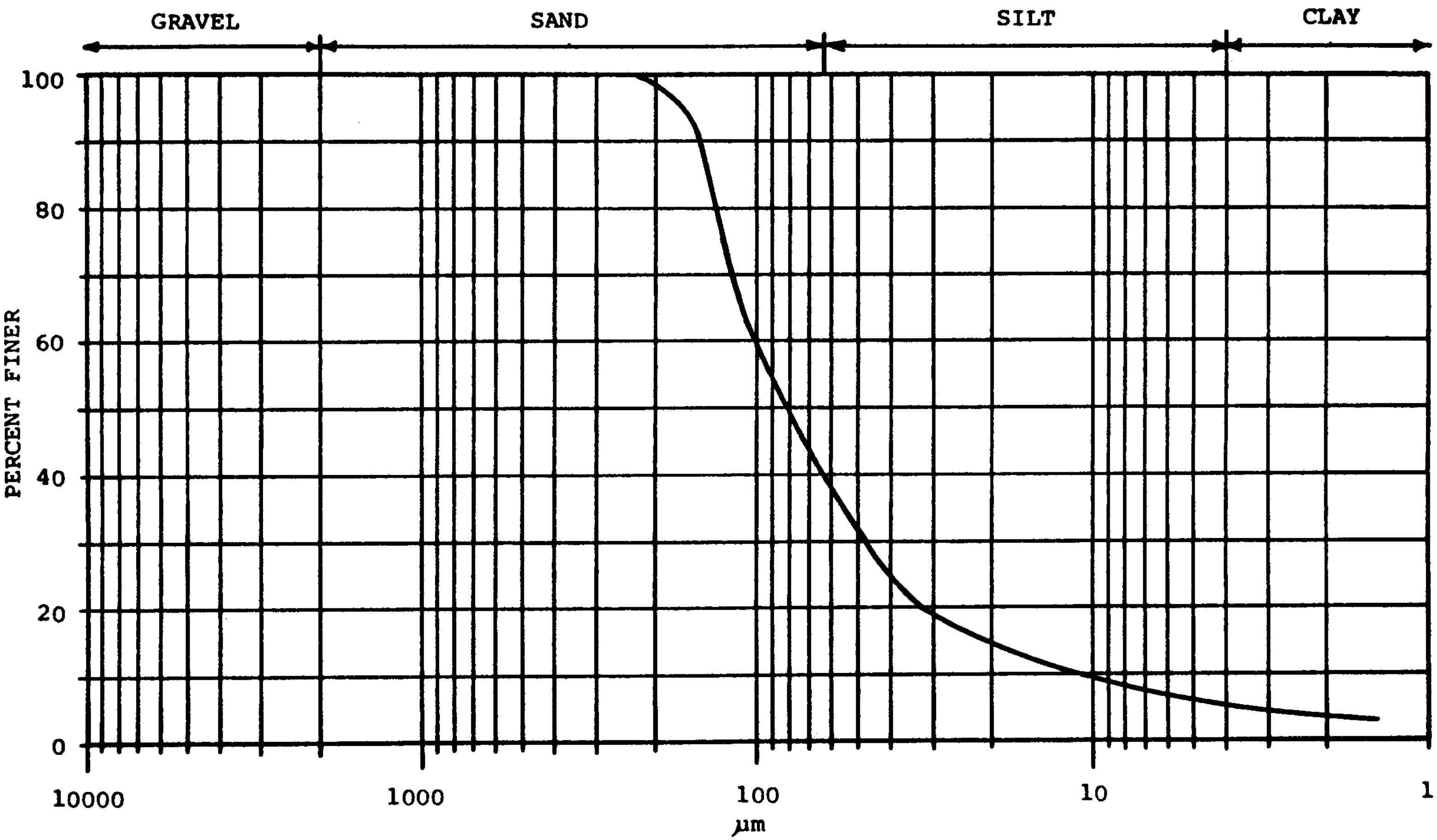

Core: 686A1, Depth: 0.45 m, Sampled from tests TC 96, TC 97

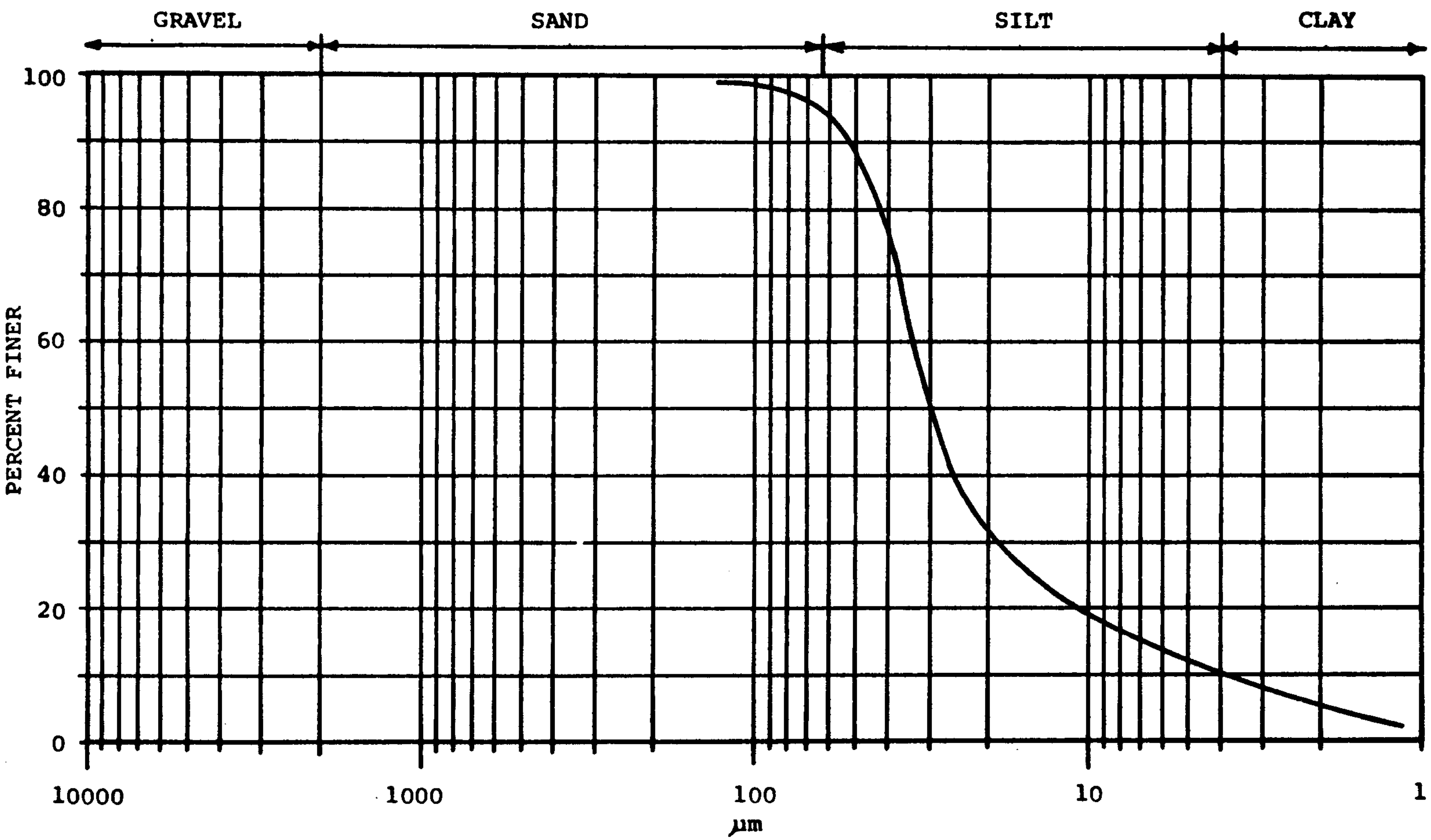

Core: 687A1, Depth: 0.49 m, Sampled from tests TC 94, TC 95

APPENDIX B:

CONE-PENETRATION TEST PLOTS

In the following diagrams, the first three numbers in the title identify the ocean station from which the data were gathered. The fourth number reflects the number of attempts made to get the data.

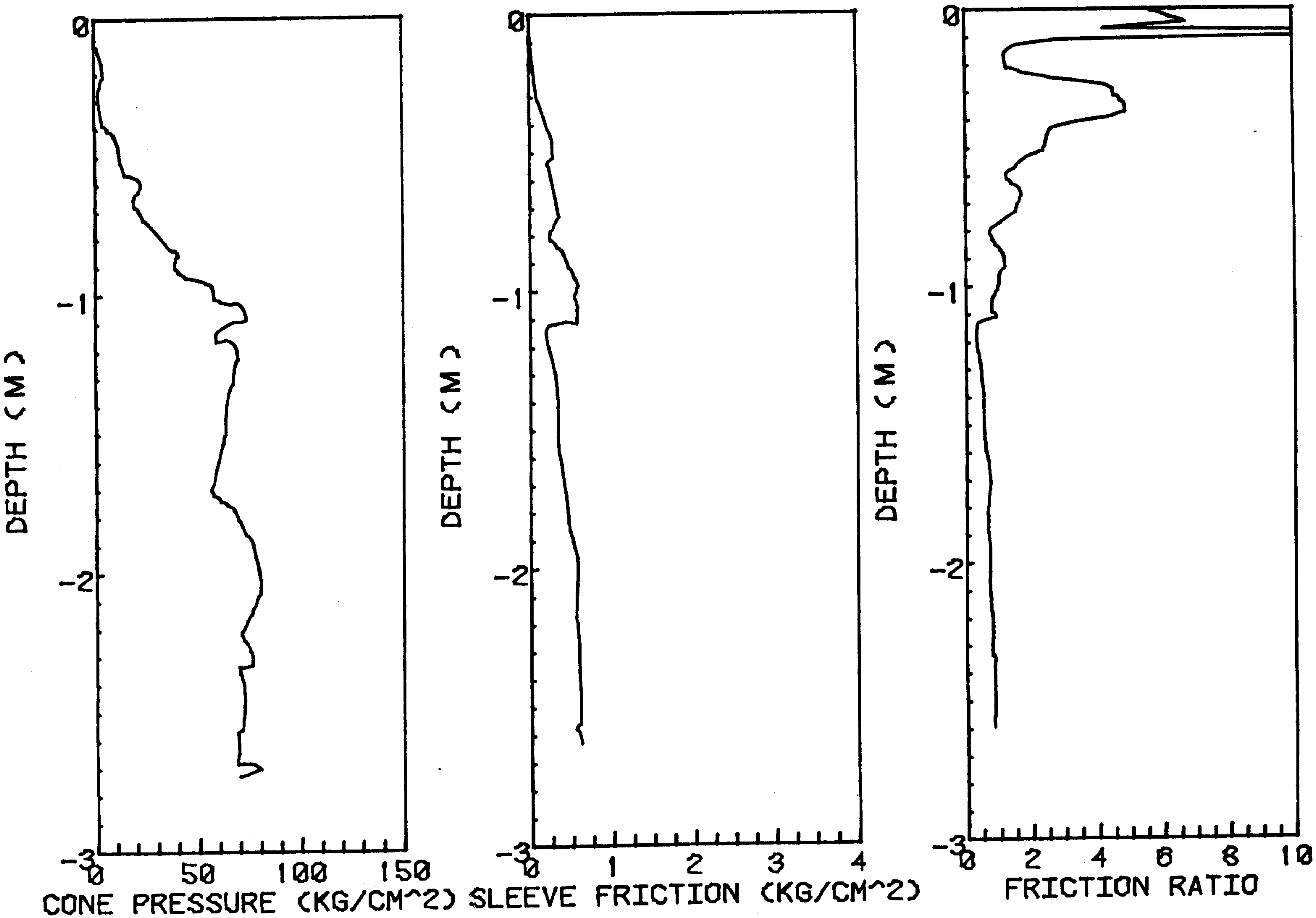

665X1. NON-GAS ZONE S. OF NOME. ALASKA.

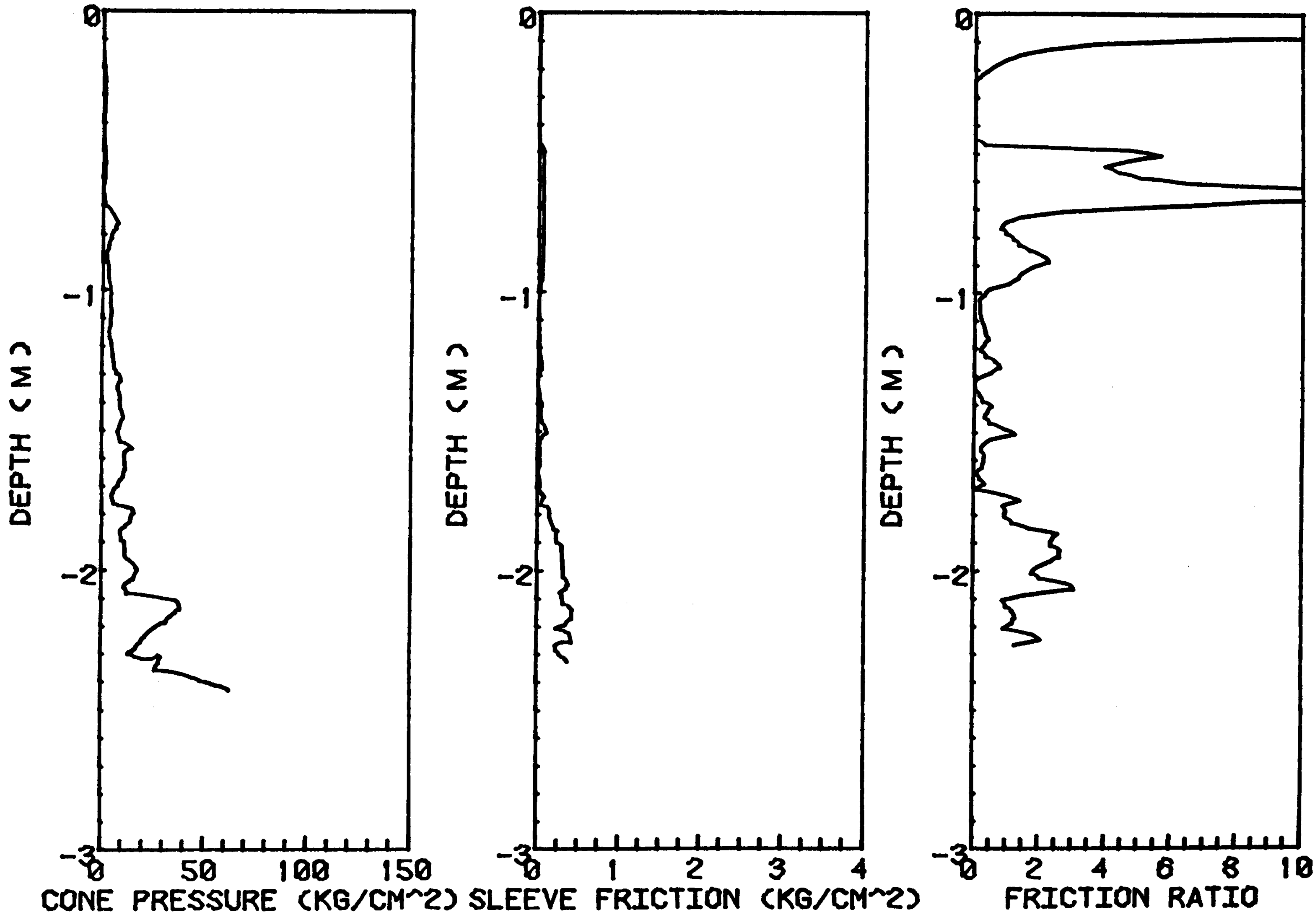

667X1. N. S. YUKON DELTA - PROTECTED. ALASKA.

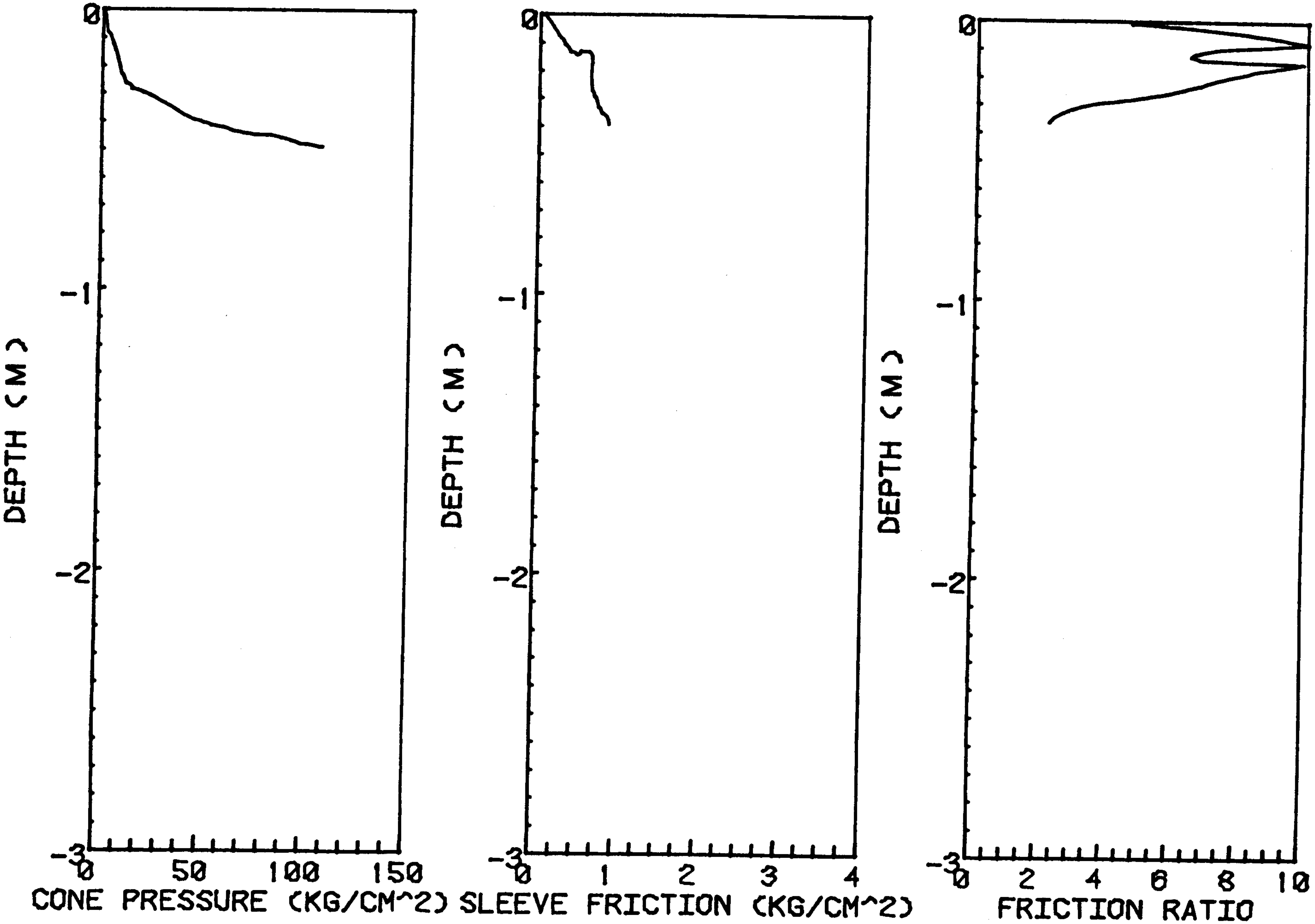

668X1. W. YUKON DELTA - PROTECTED. ALASKA.

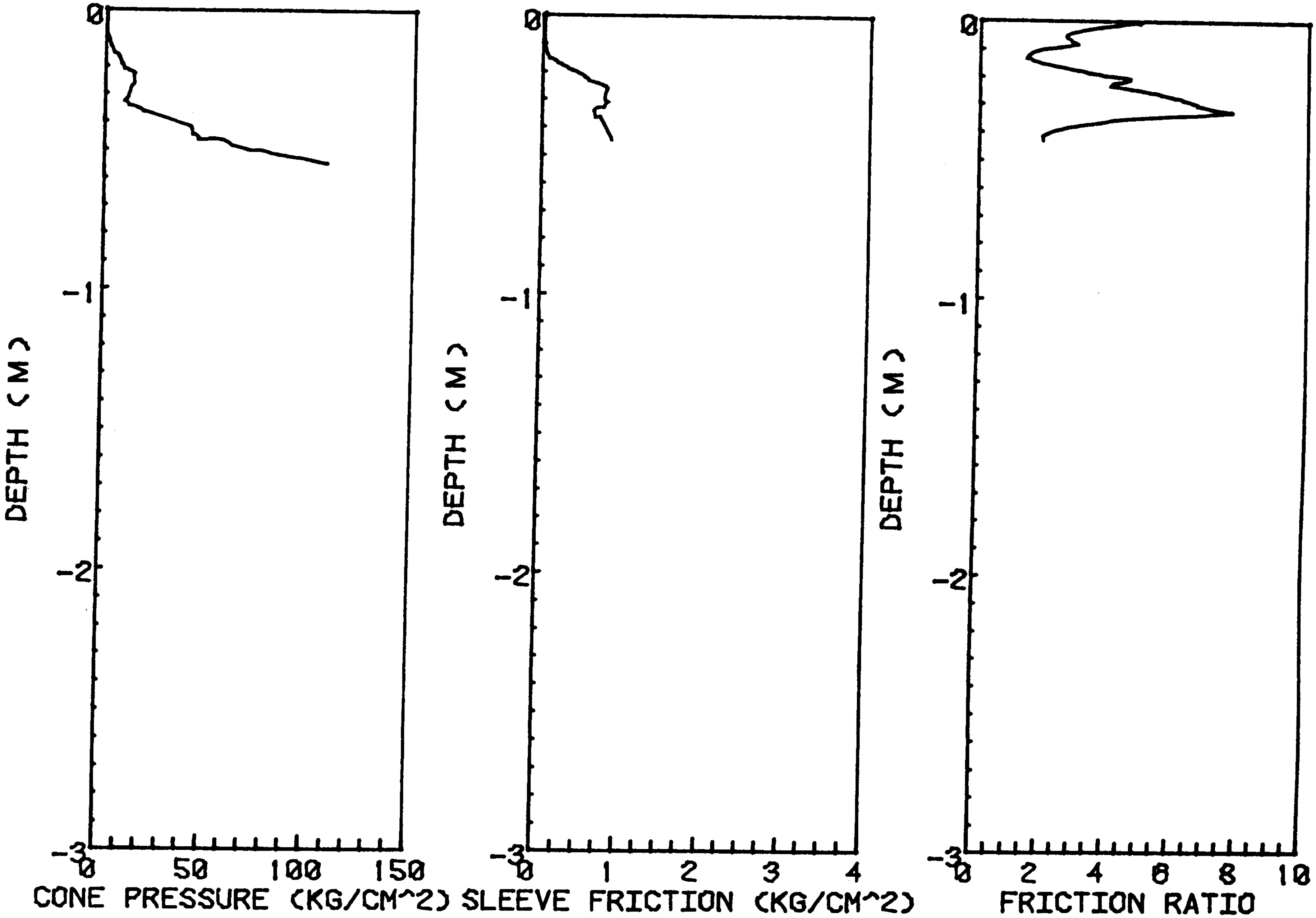

A668X2. W. YUKON DELTA - EXPOSED. ALASKA.

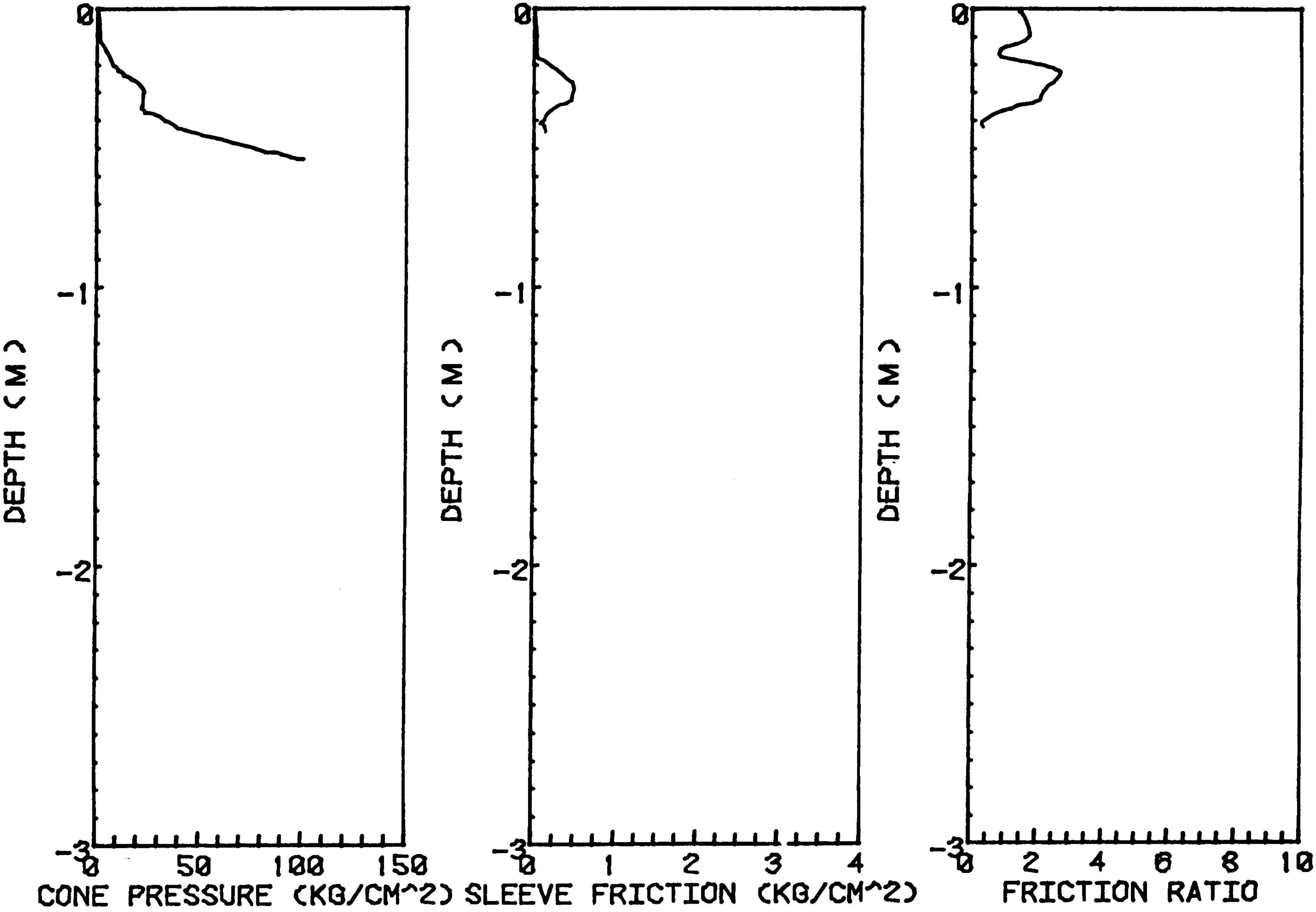

668X3. W. OF YUKON DELTA - EXPOSED. ALASKA.

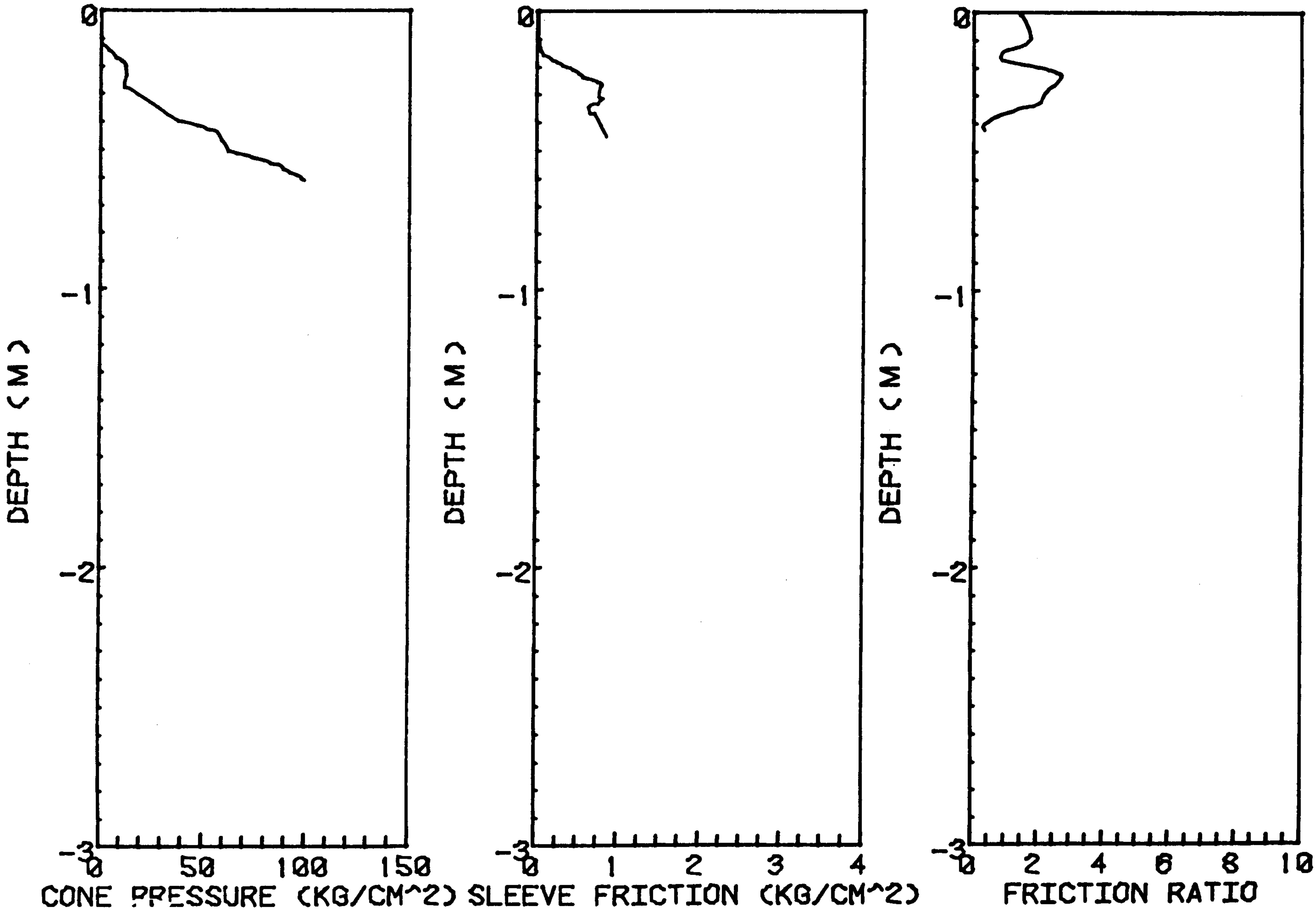

668X4. W. OF YUKON DELTA - EXPOSED. ALASKA.

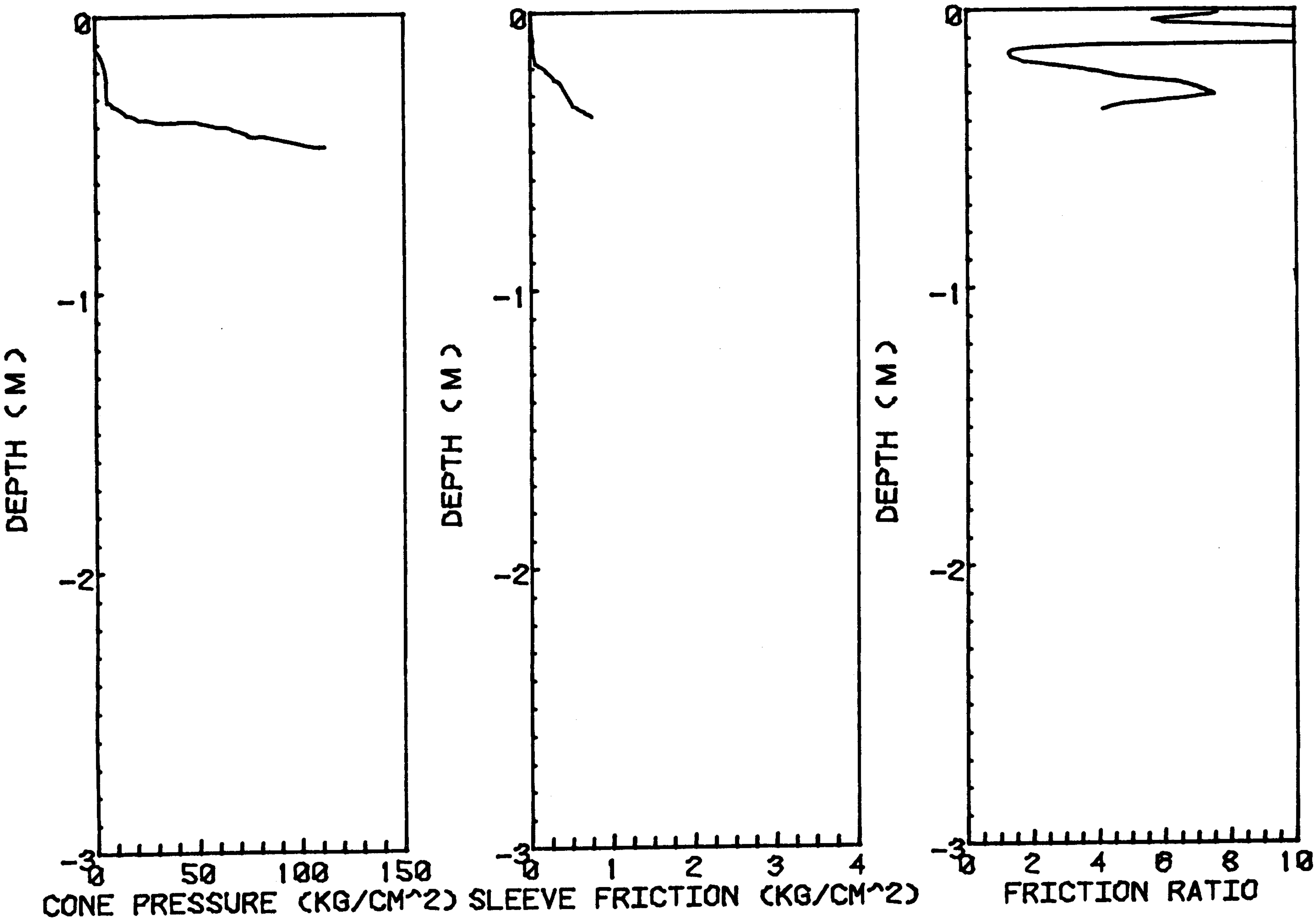

669X1 . W. OF YUKON DELTA - EXPOSED. ALASKA.

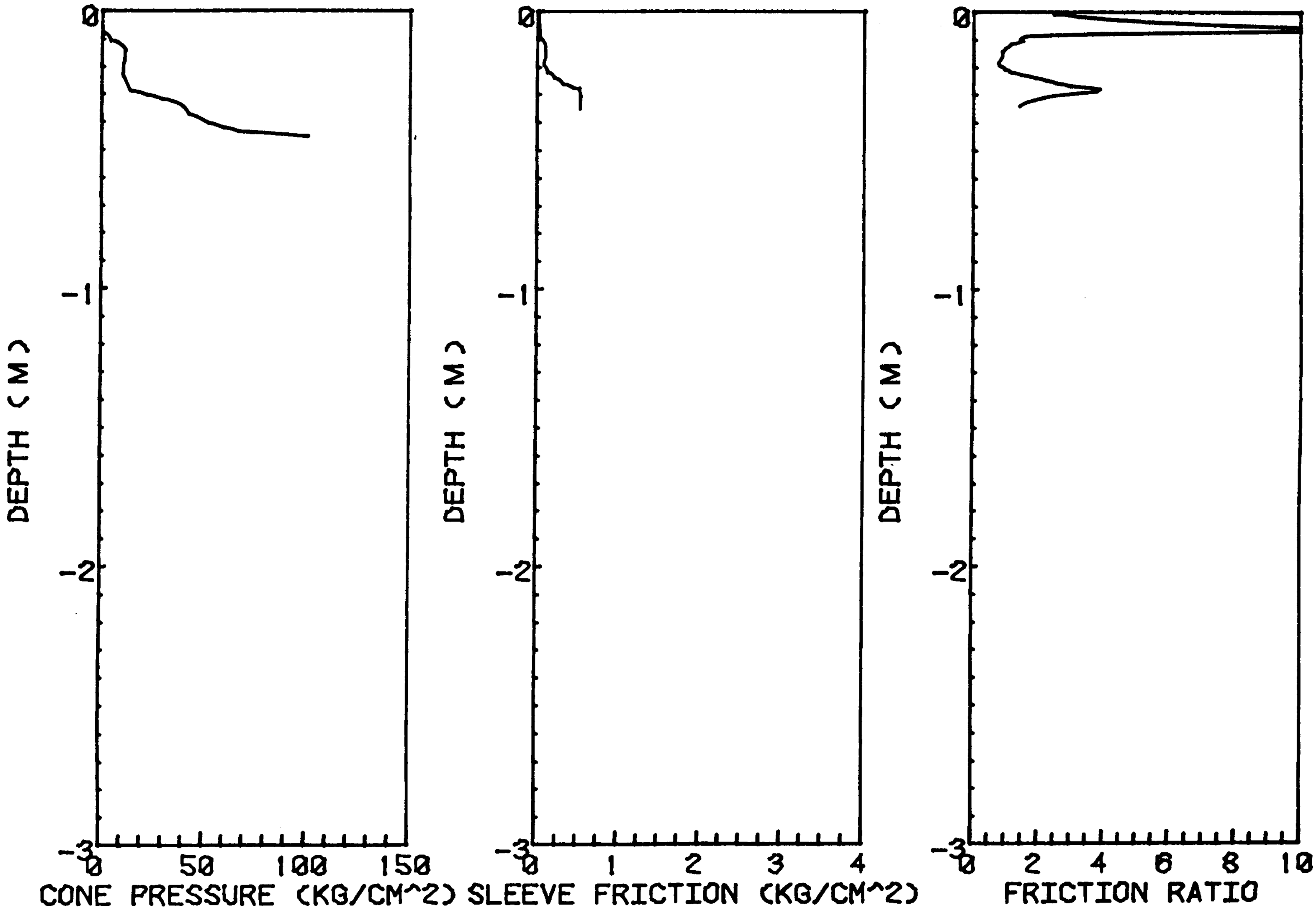

669X2. W. YUKON DELTA - EXPOSED. ALASKA.

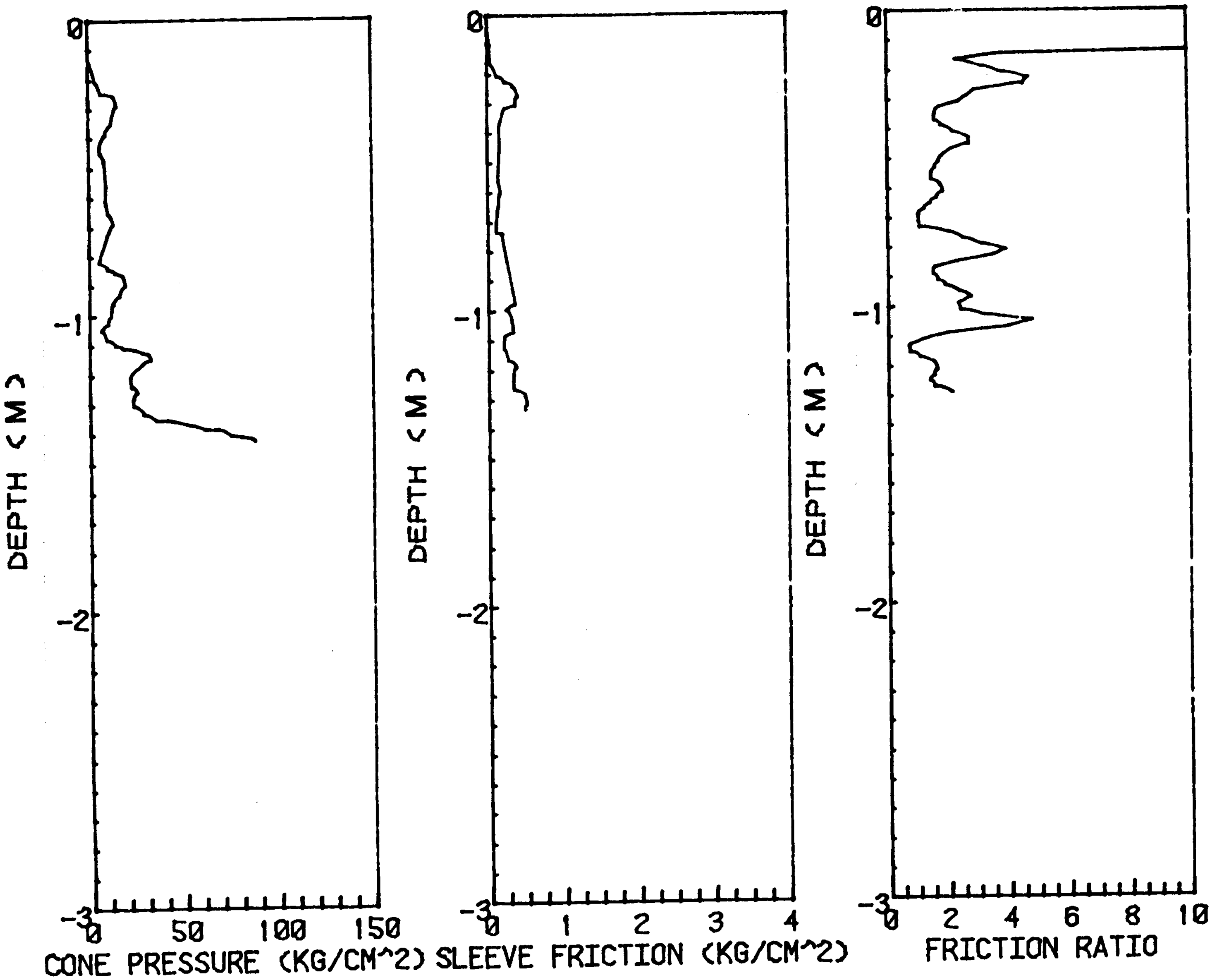

670X1. N. N. W. YUKON DELTA - PROTECTED. ALASKA.

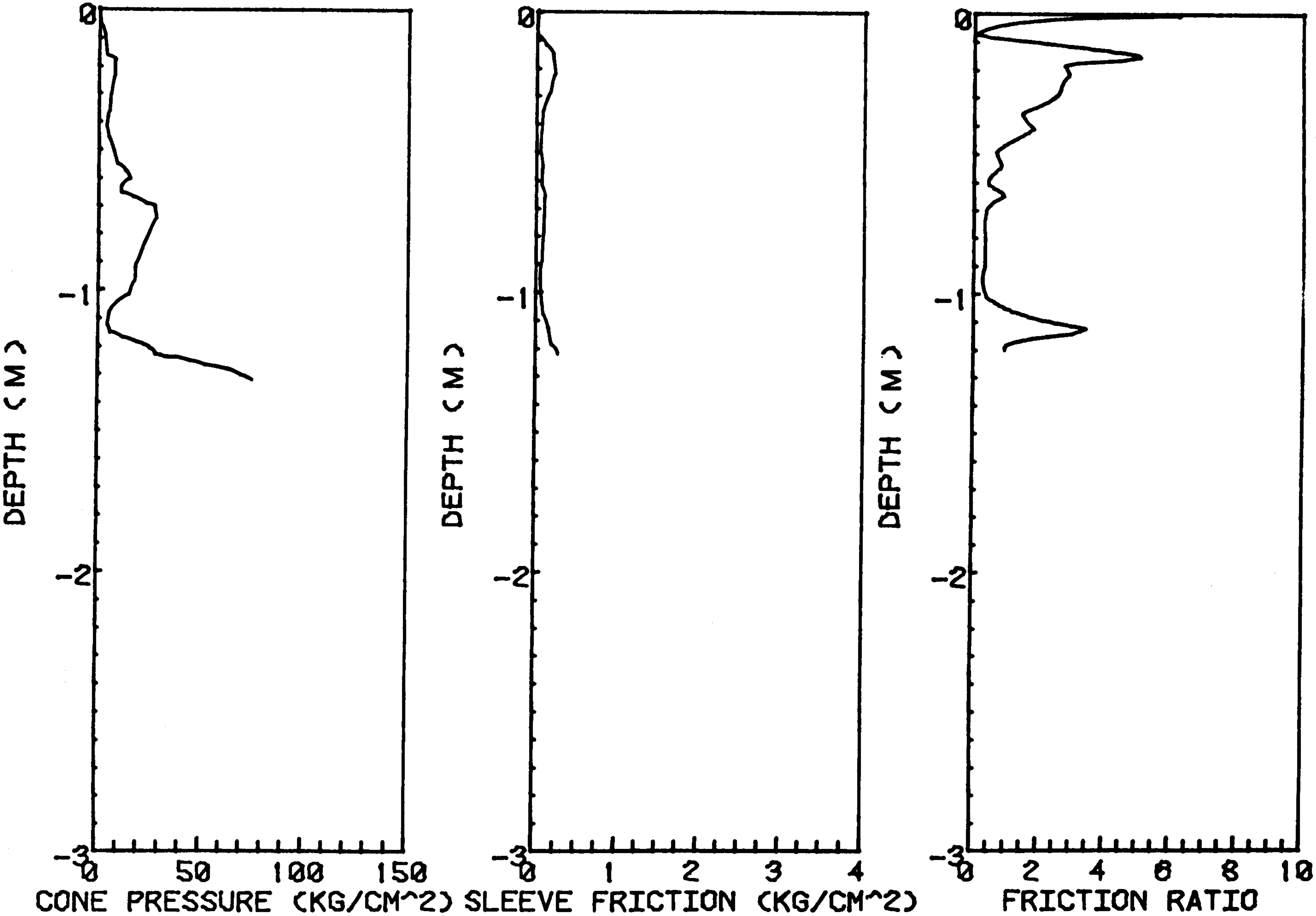

670X3. N. N. W. YUKON DELTA - PROTECTED. ALASKA.

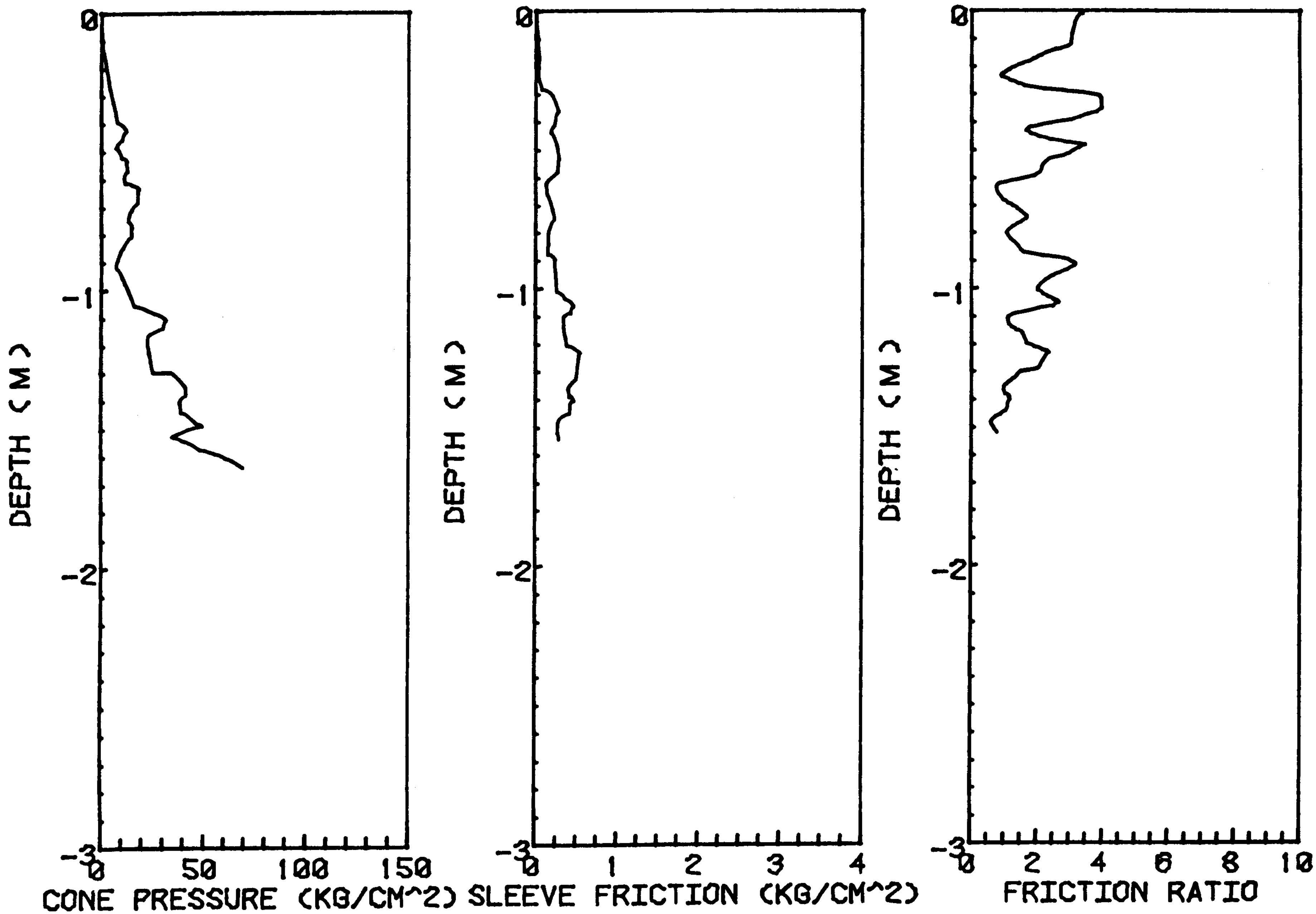

670X4. N. N. W. YUKON DELTA - PROTECTED. ALASKA.

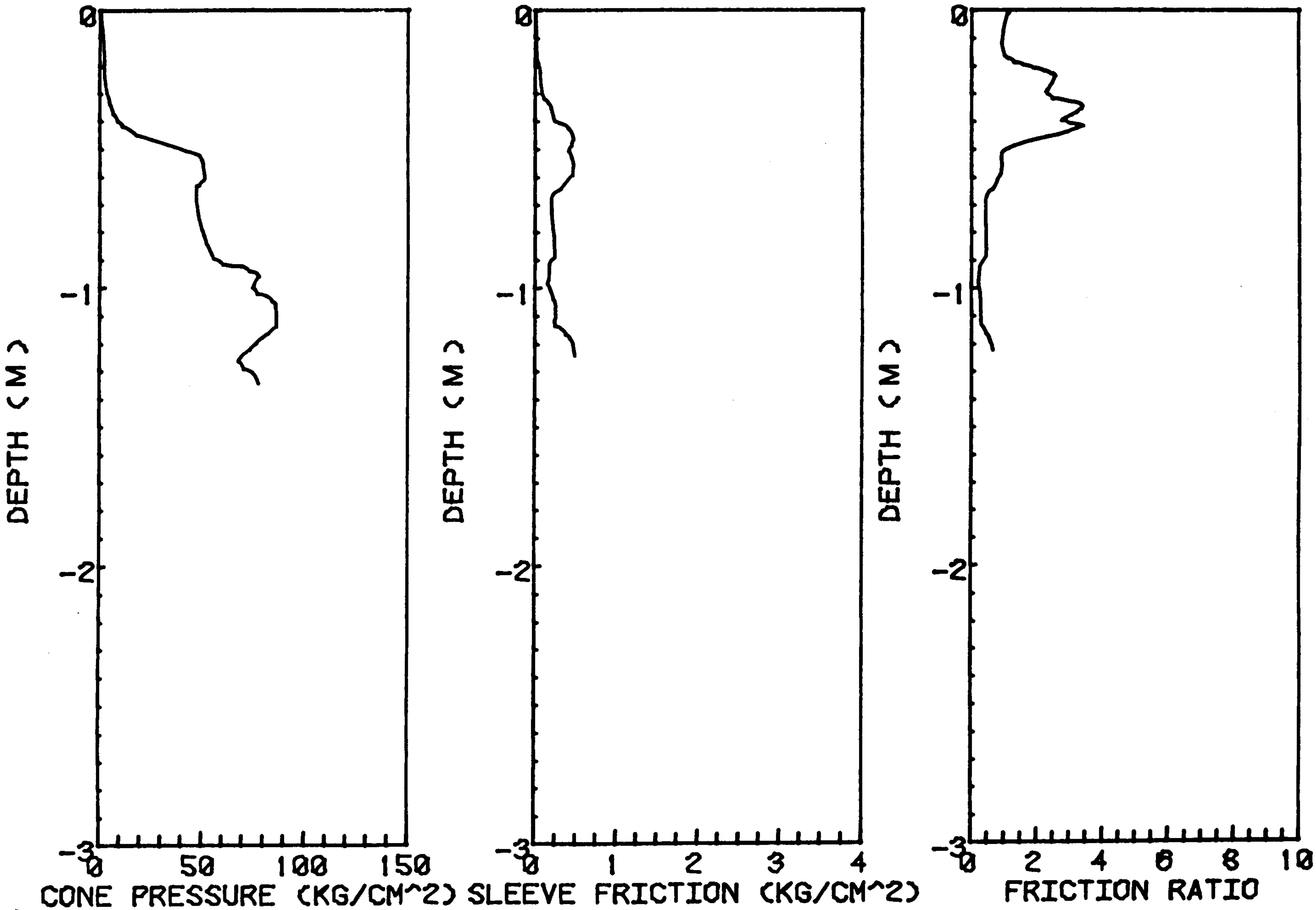

871X1. E. OF THERMOGENIC GAS ZONE. ALASKA.

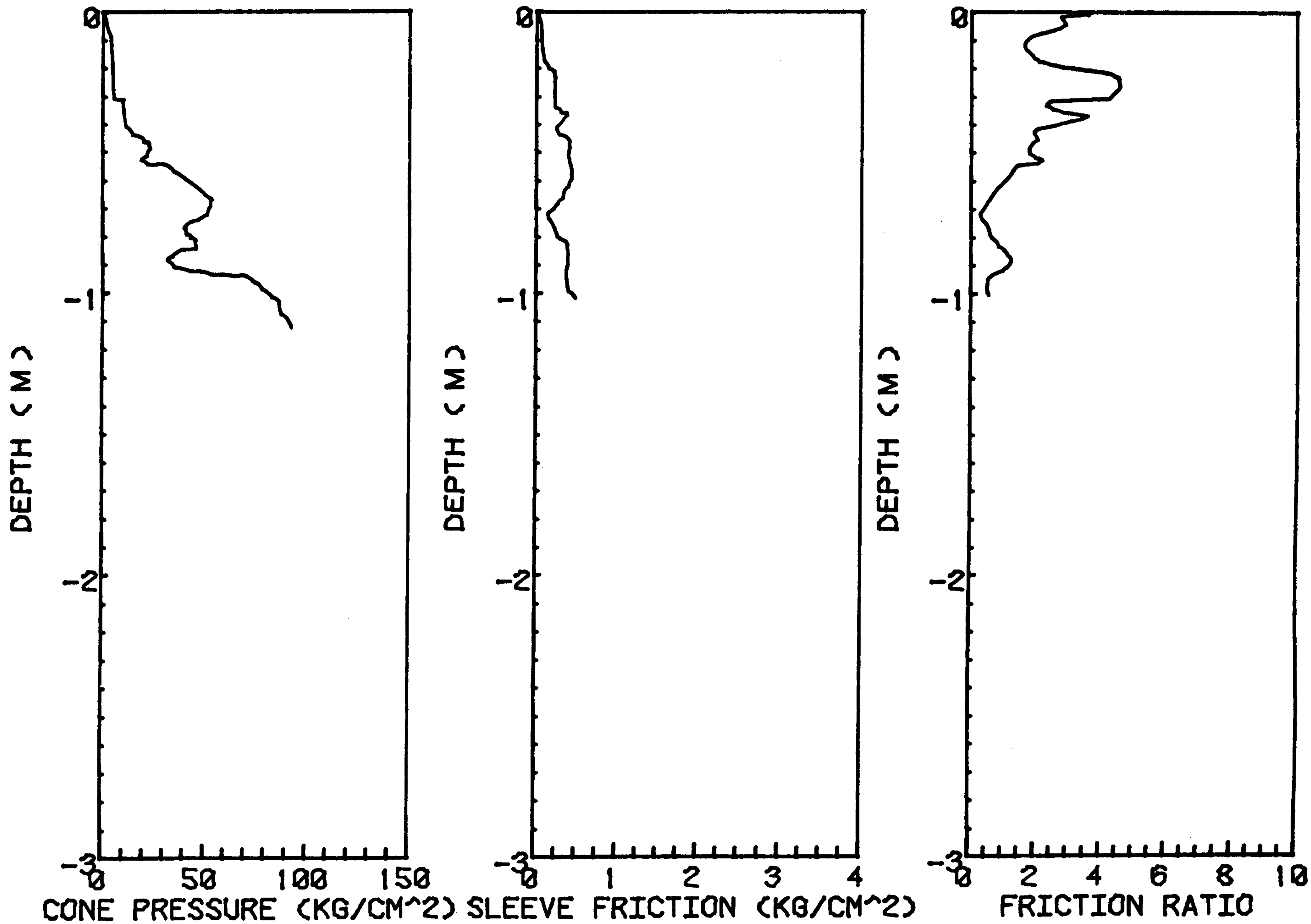

671X2. E. OF THERMOGENIC GAS ZONE. ALASKA.

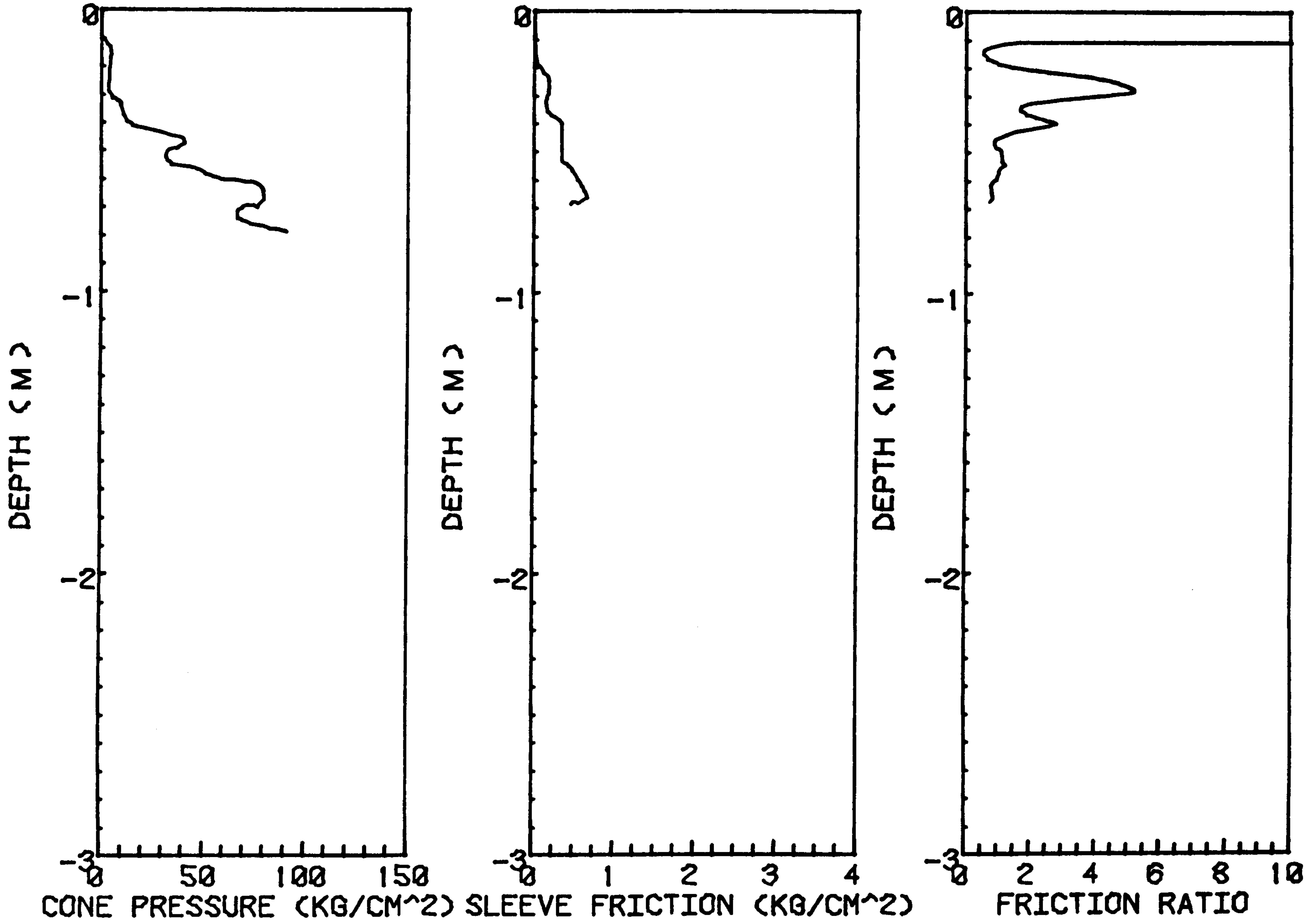

671X3. E. OF THERMOGENIC GAS ZONE. ALASKA.

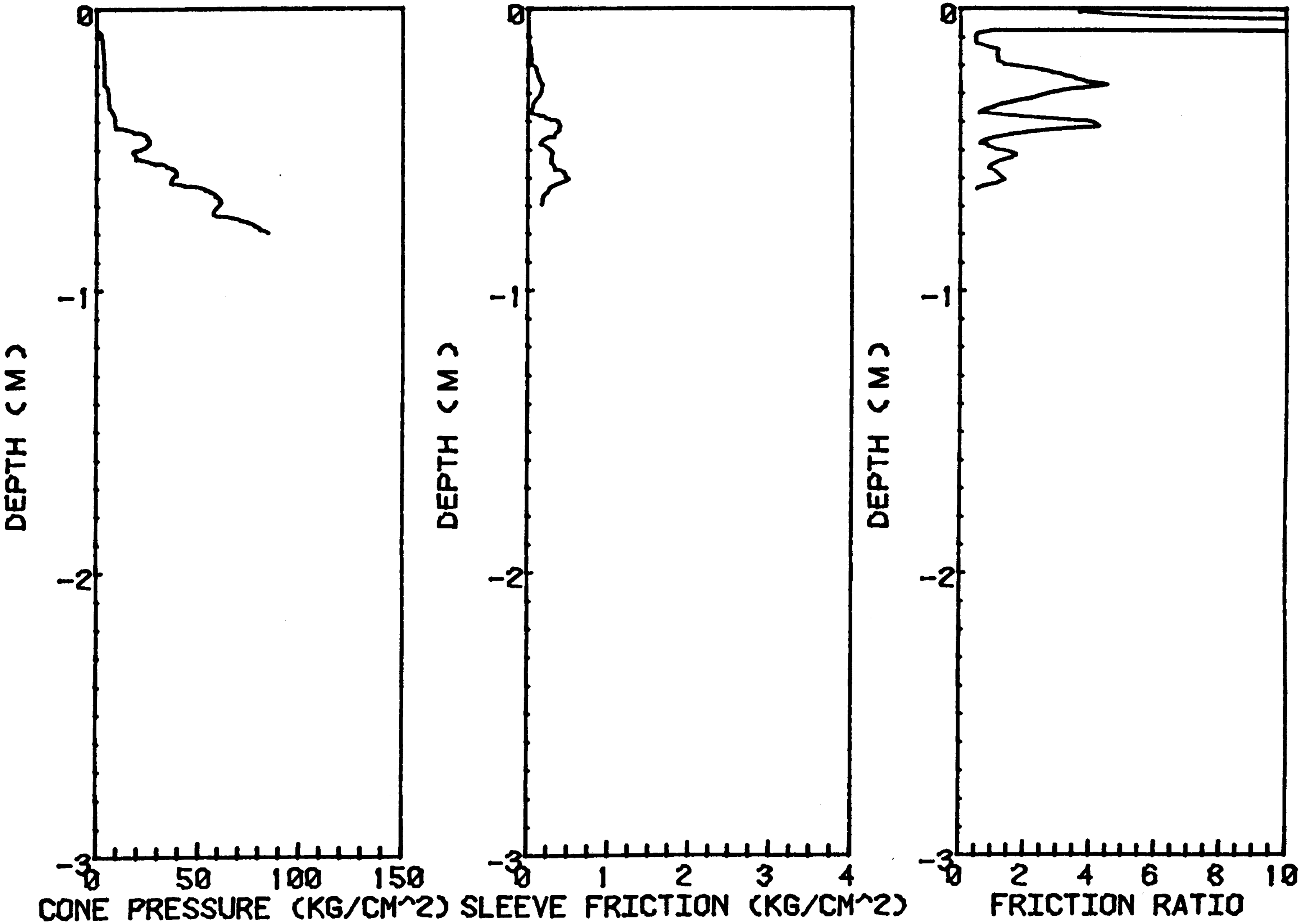

671X4. E OF THERMOGENIC GAS ZONE. ALASKA.

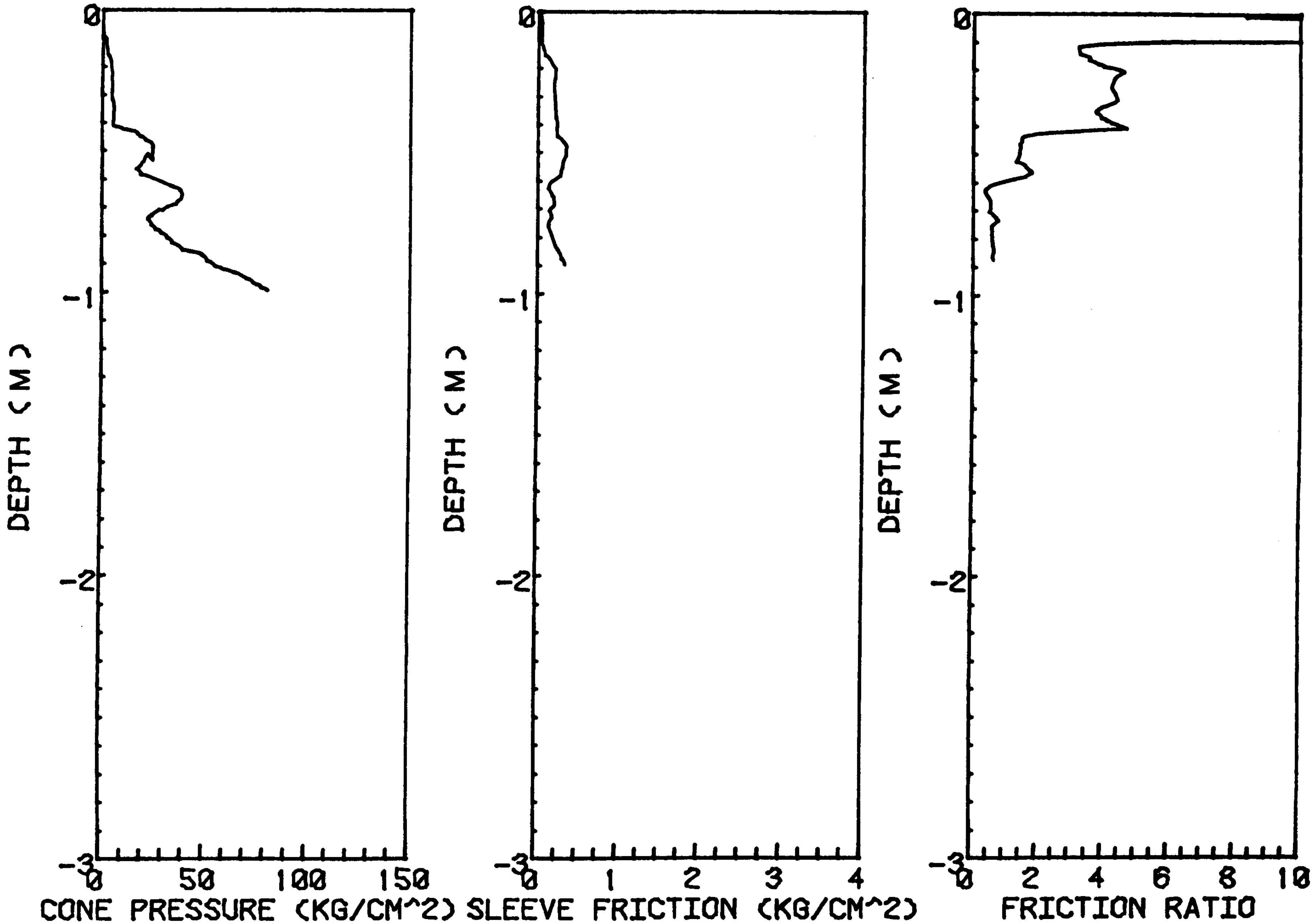

671X5. E. OF THERMOGENIC GAS ZONE. ALASKA.

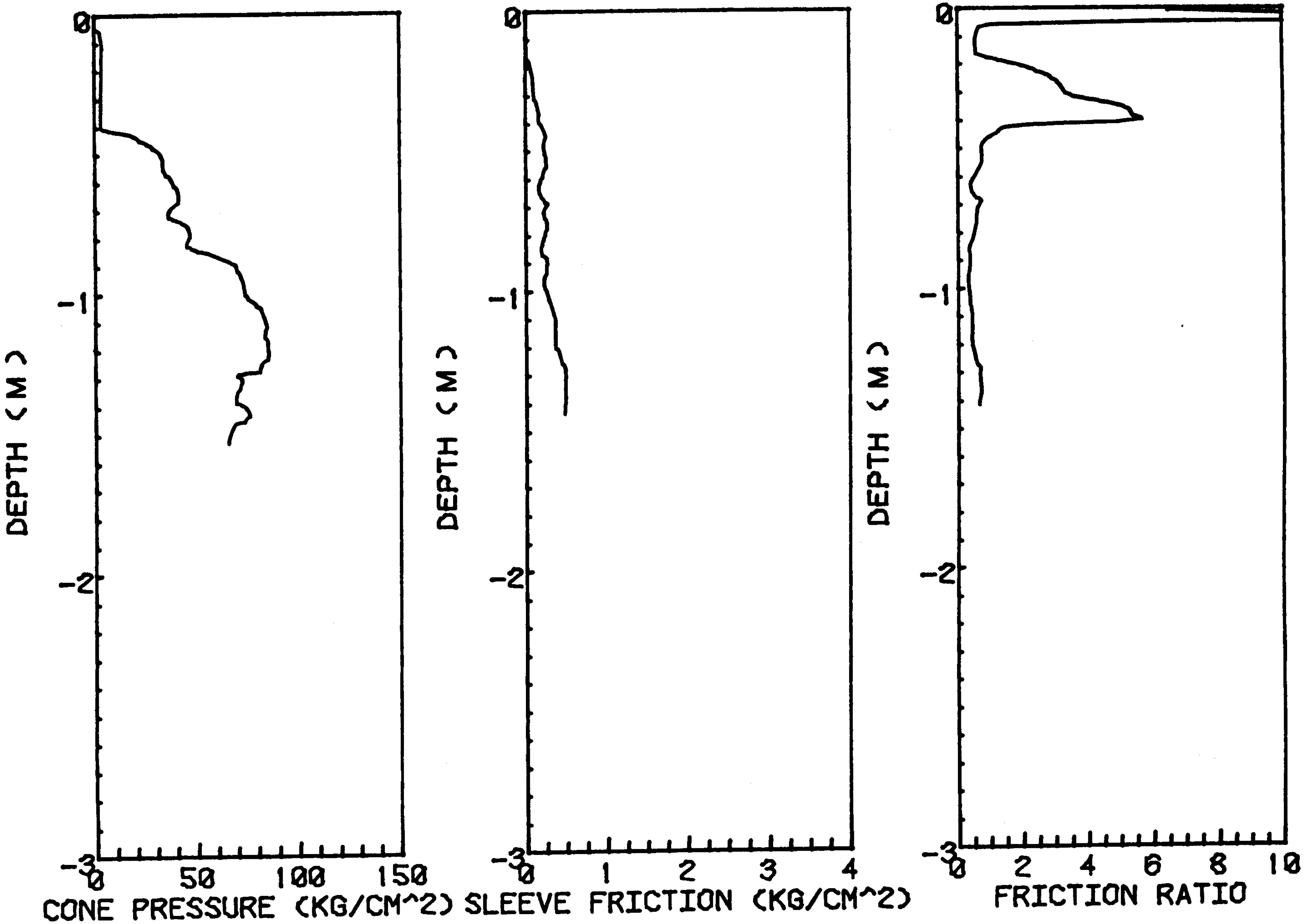

671X6. E. OF THERMOGENIC GAS ZONE. ALASKA.

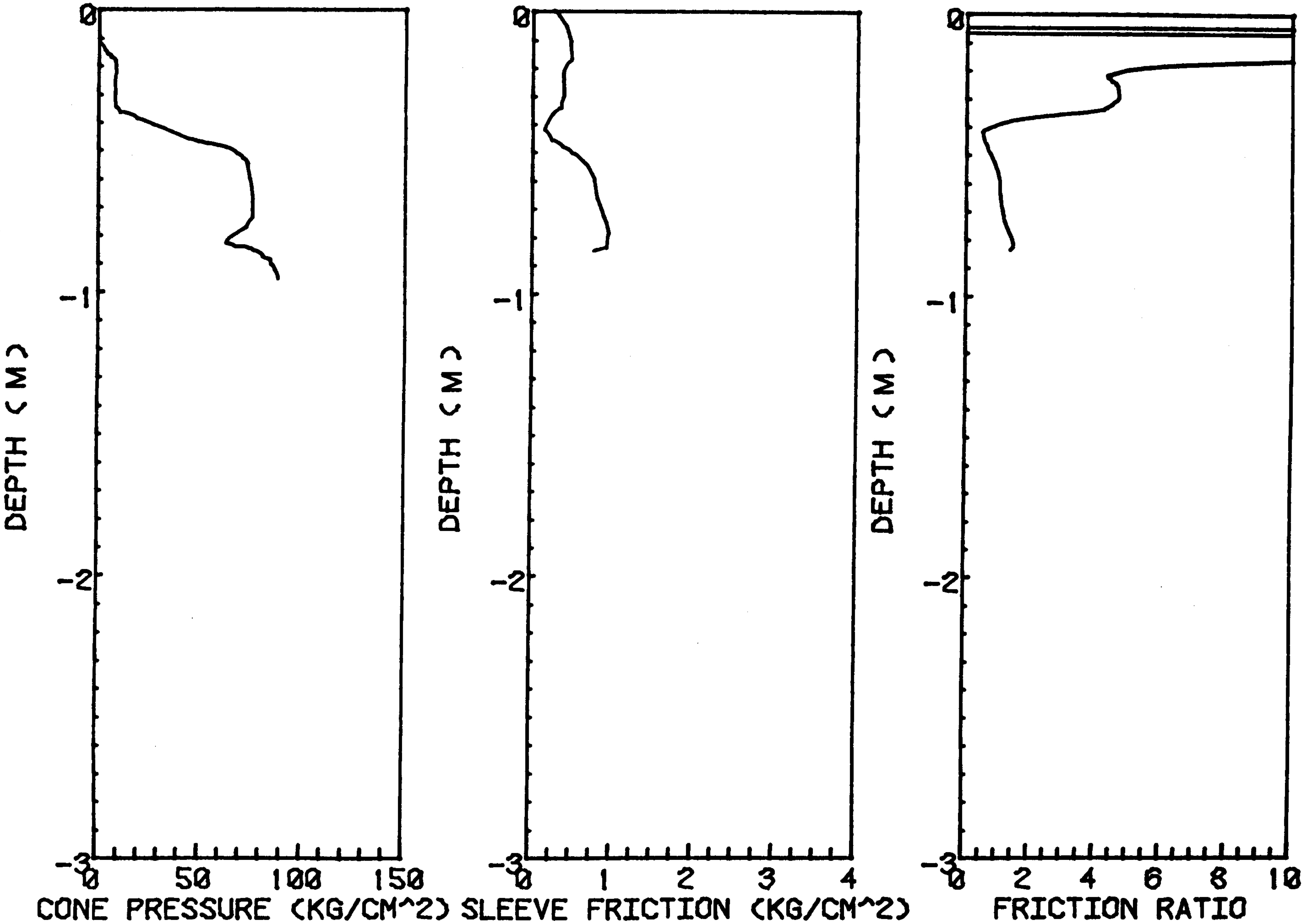

671X7. E. OF THERMOGENIC GAS ZONE. ALASKA.

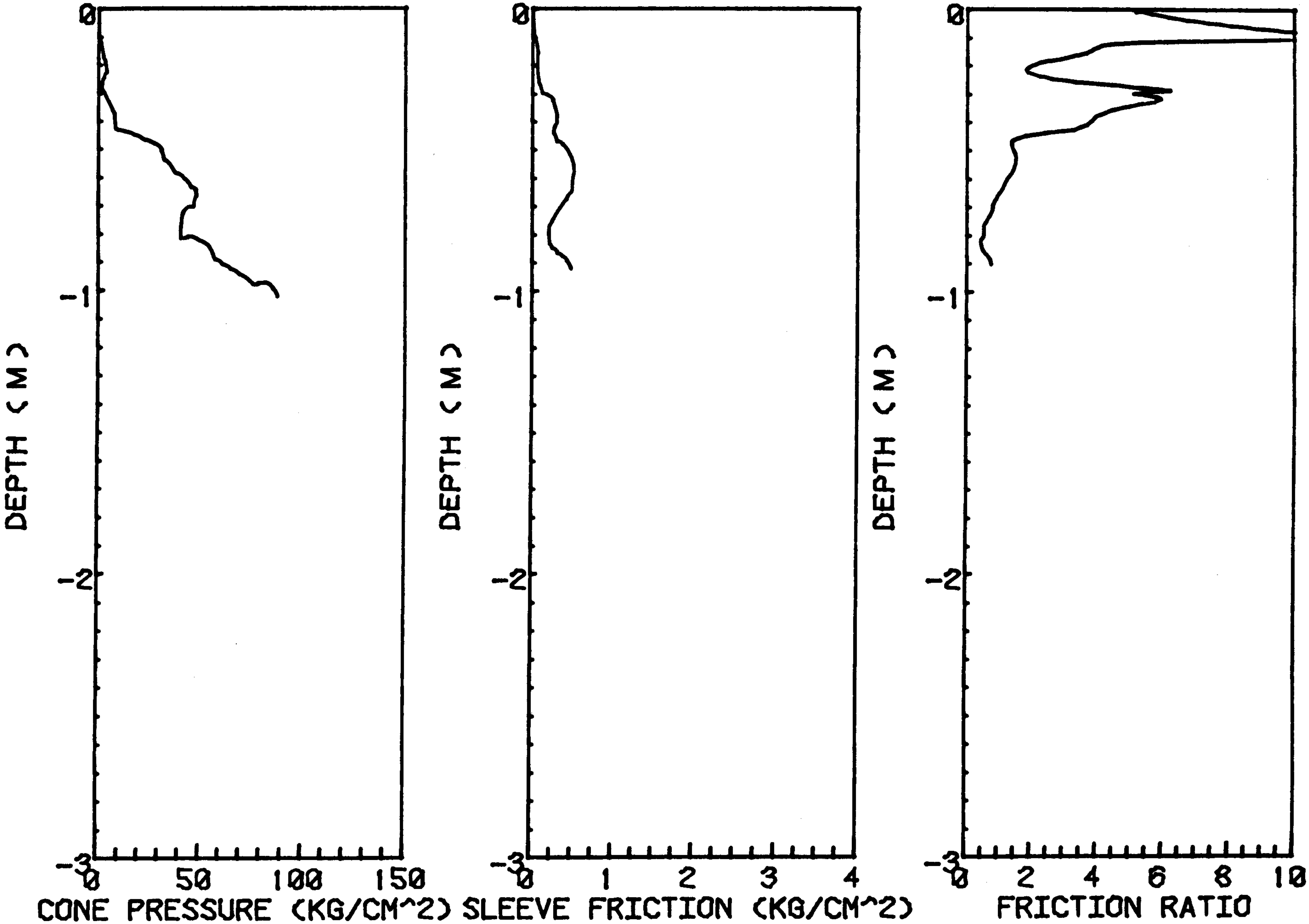

671X8. E. OF THERMOGENIC GAS ZONE. ALASKA.

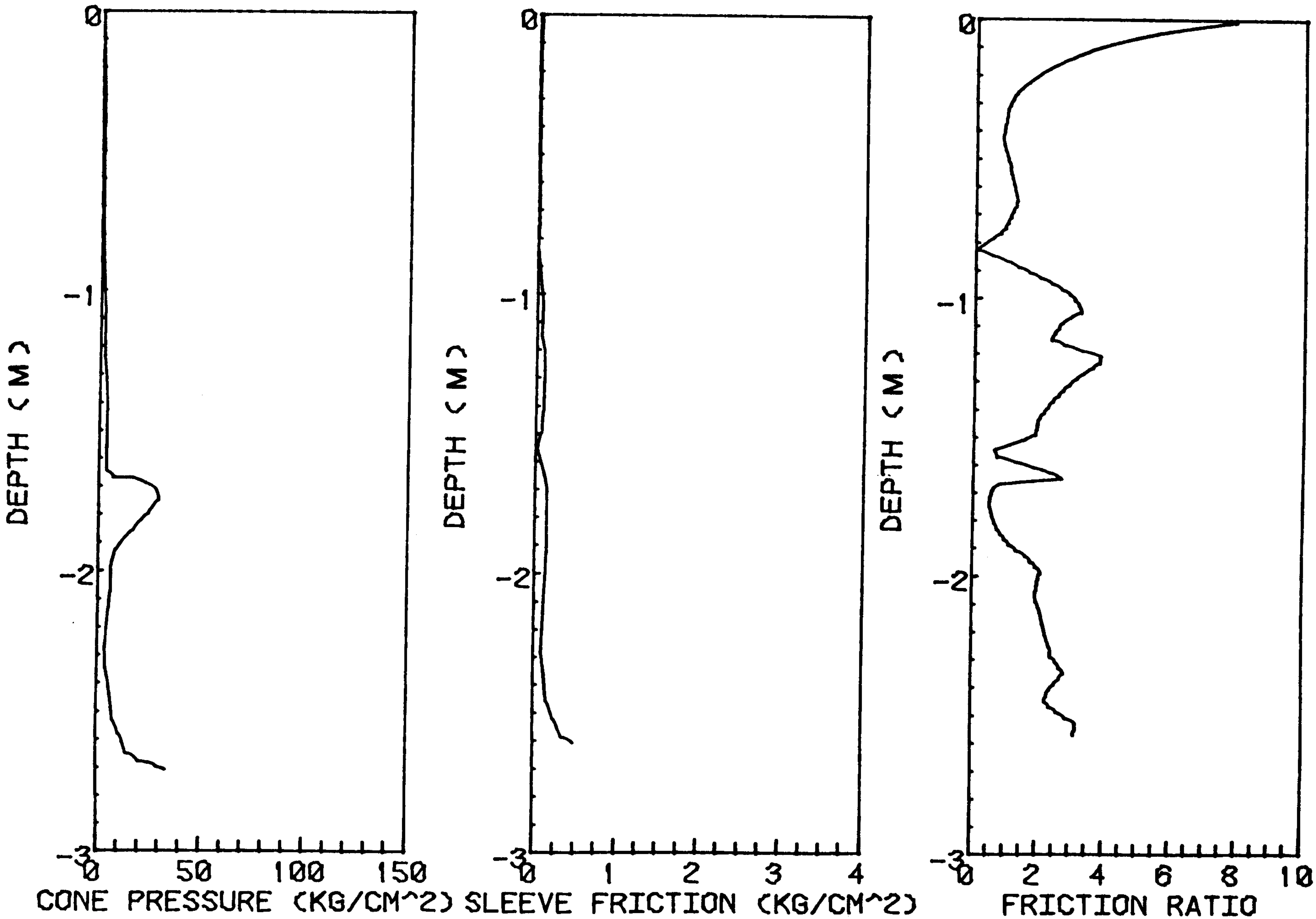

672X2. CENTRAL FAR E. NORTON SOUND. ALASKA.

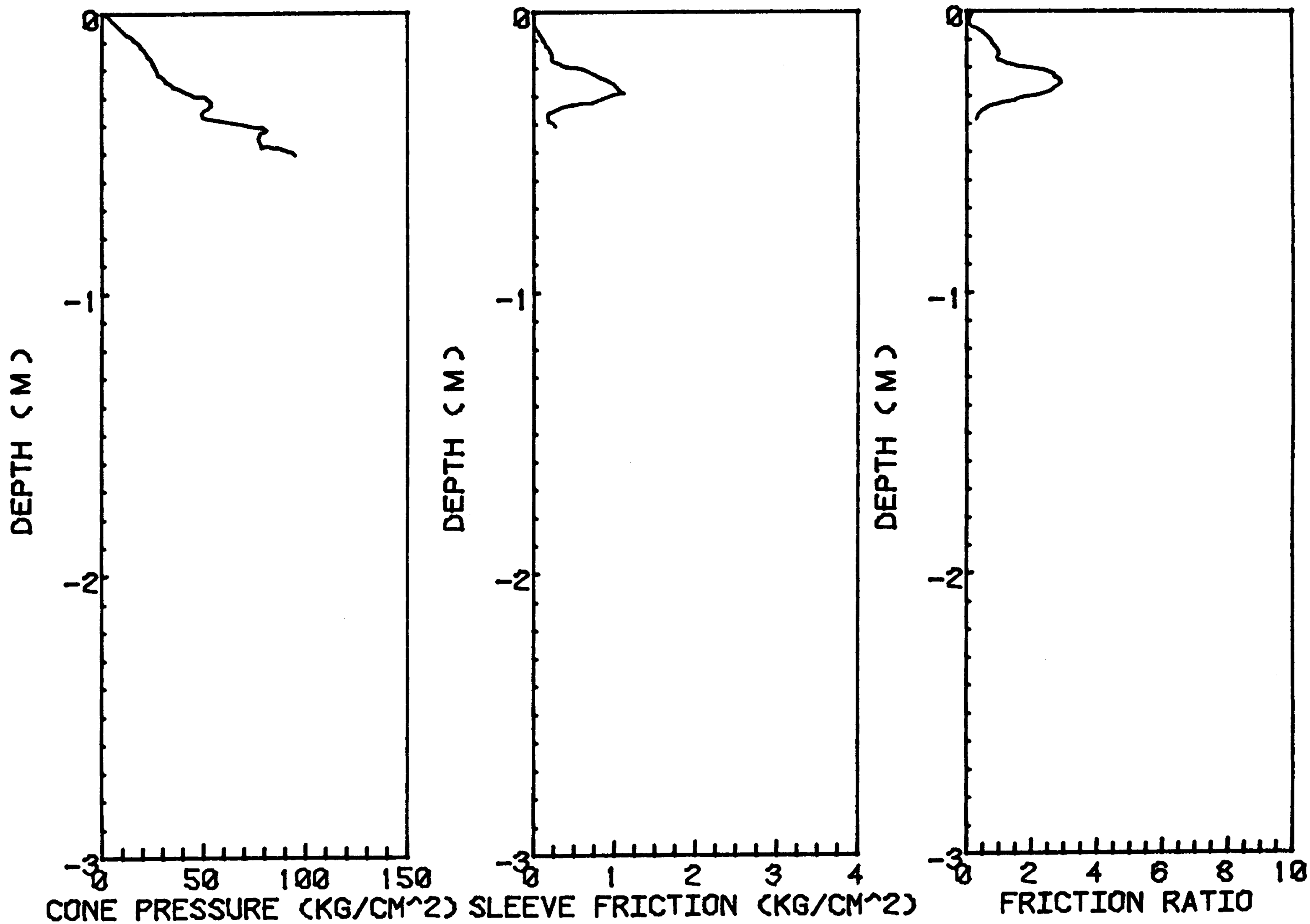

673X1. CENTRAL E. NORTON SOUND. ALASKA.

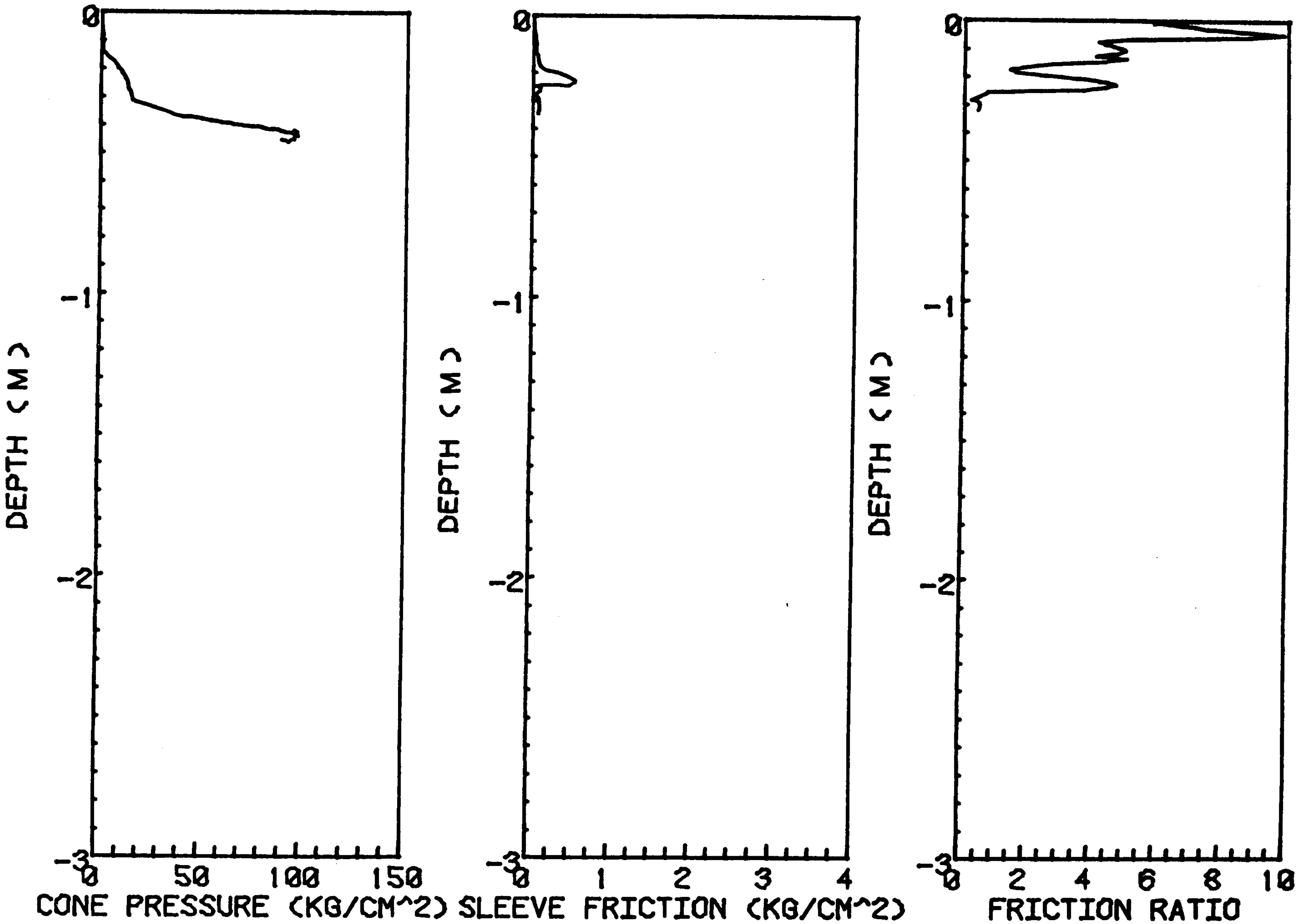

673X2. CENTRAL E. NORTON SOUND. ALASKA.

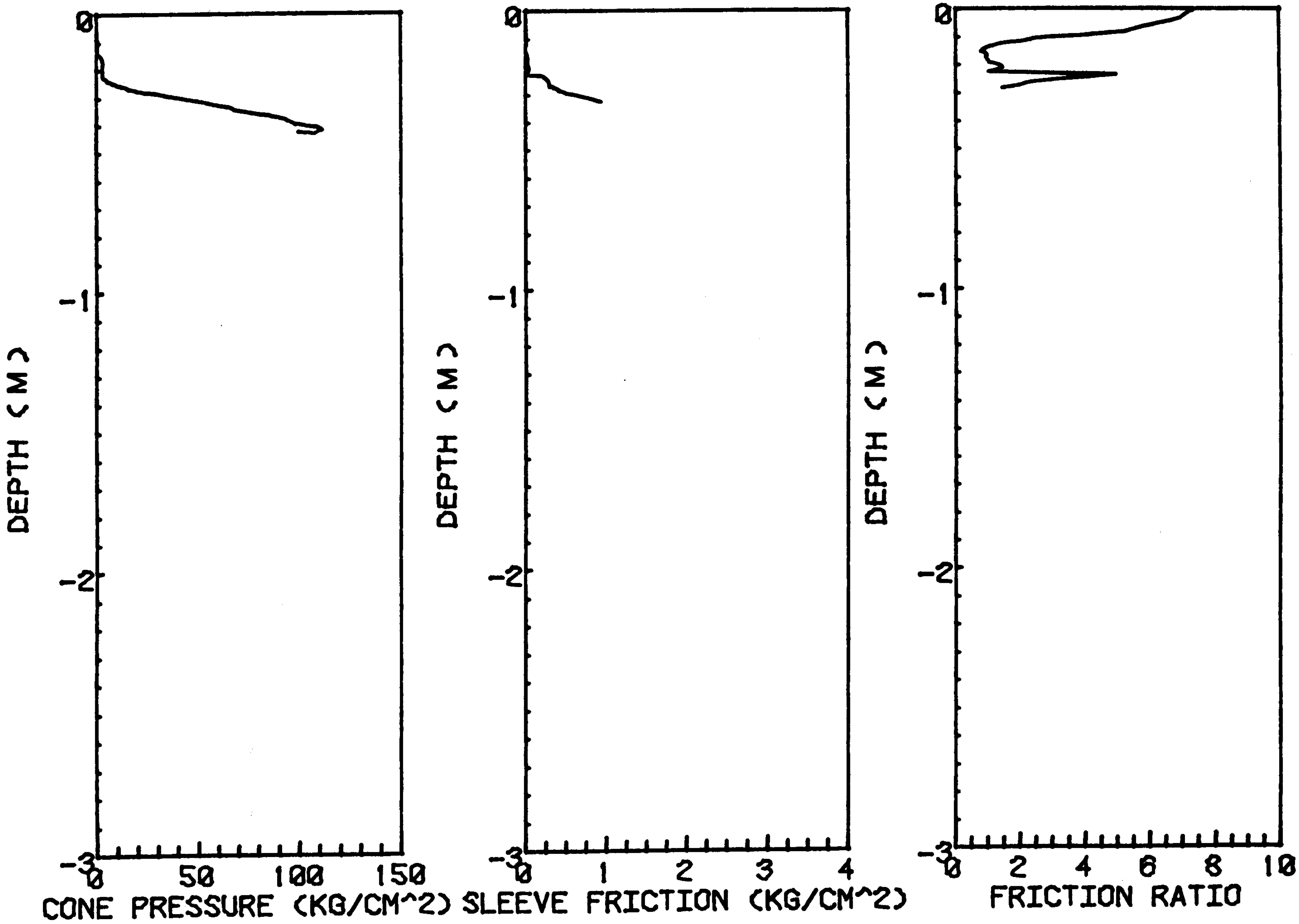

673X3. CENTRAL E. NORTON SOUND. ALASKA.

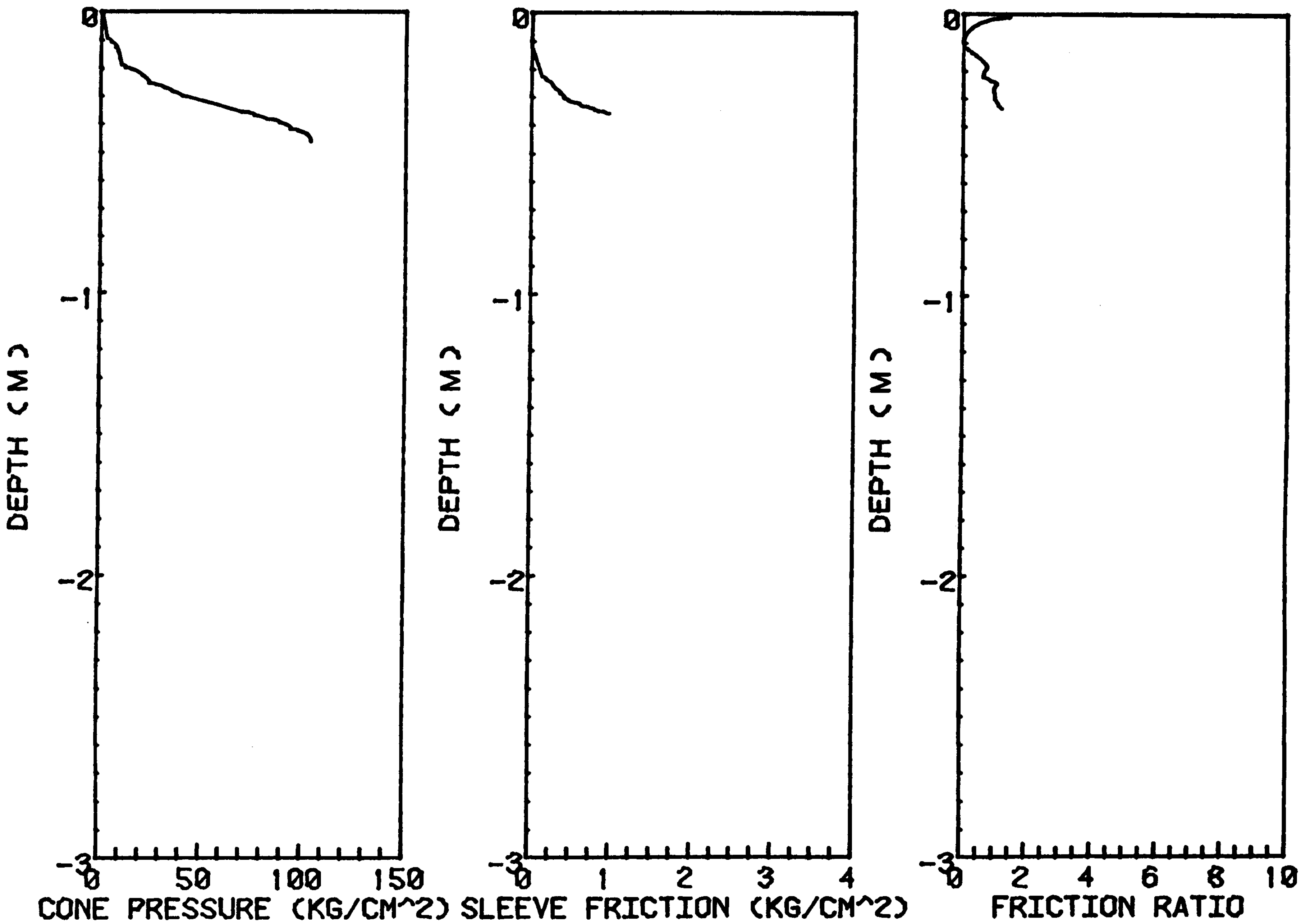

673X4. CENTRAL E. NORTON SOUND. ALASKA.

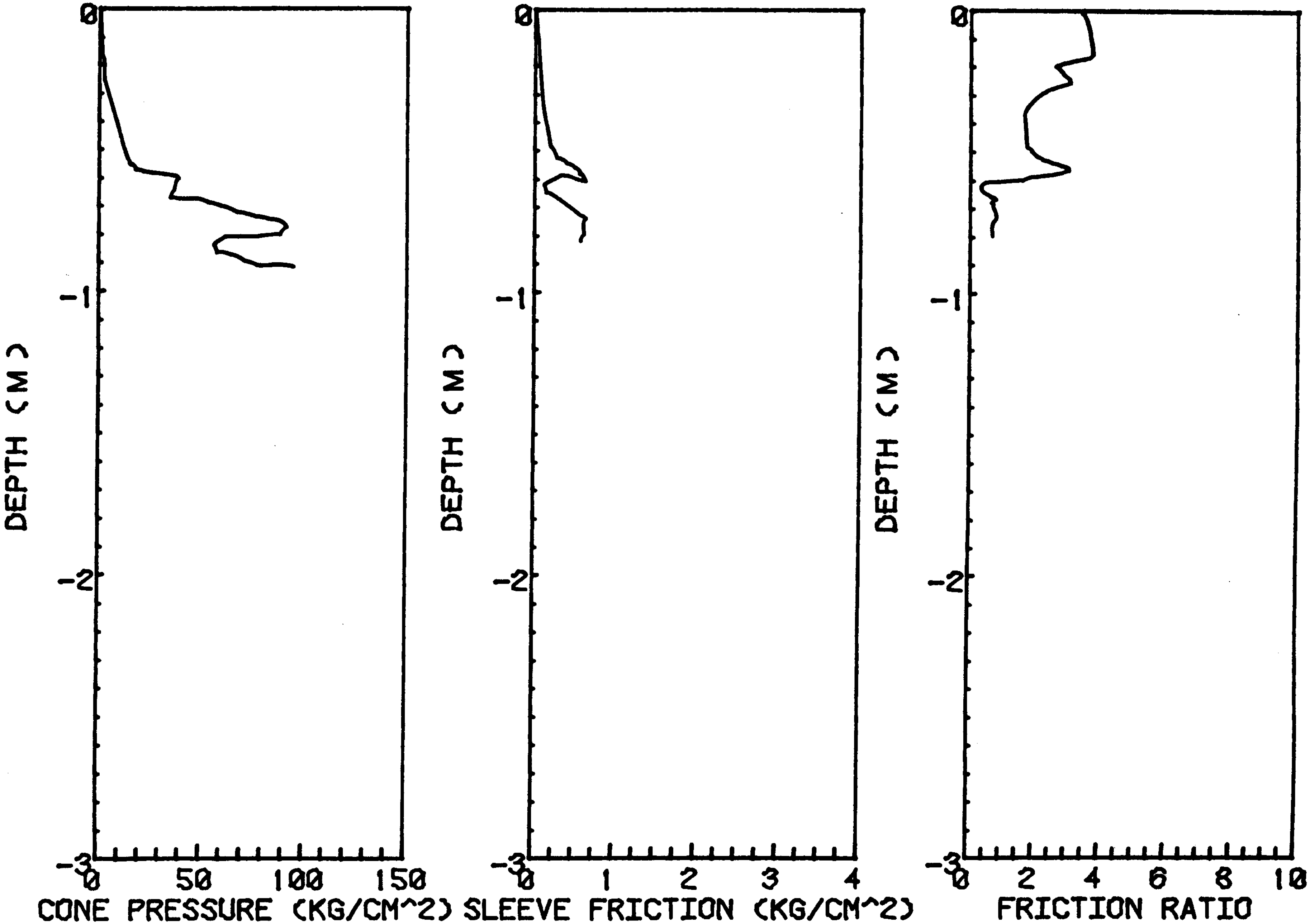

674X1. N. YUKON DELTA ICE GOUGE AREA. ALASKA.

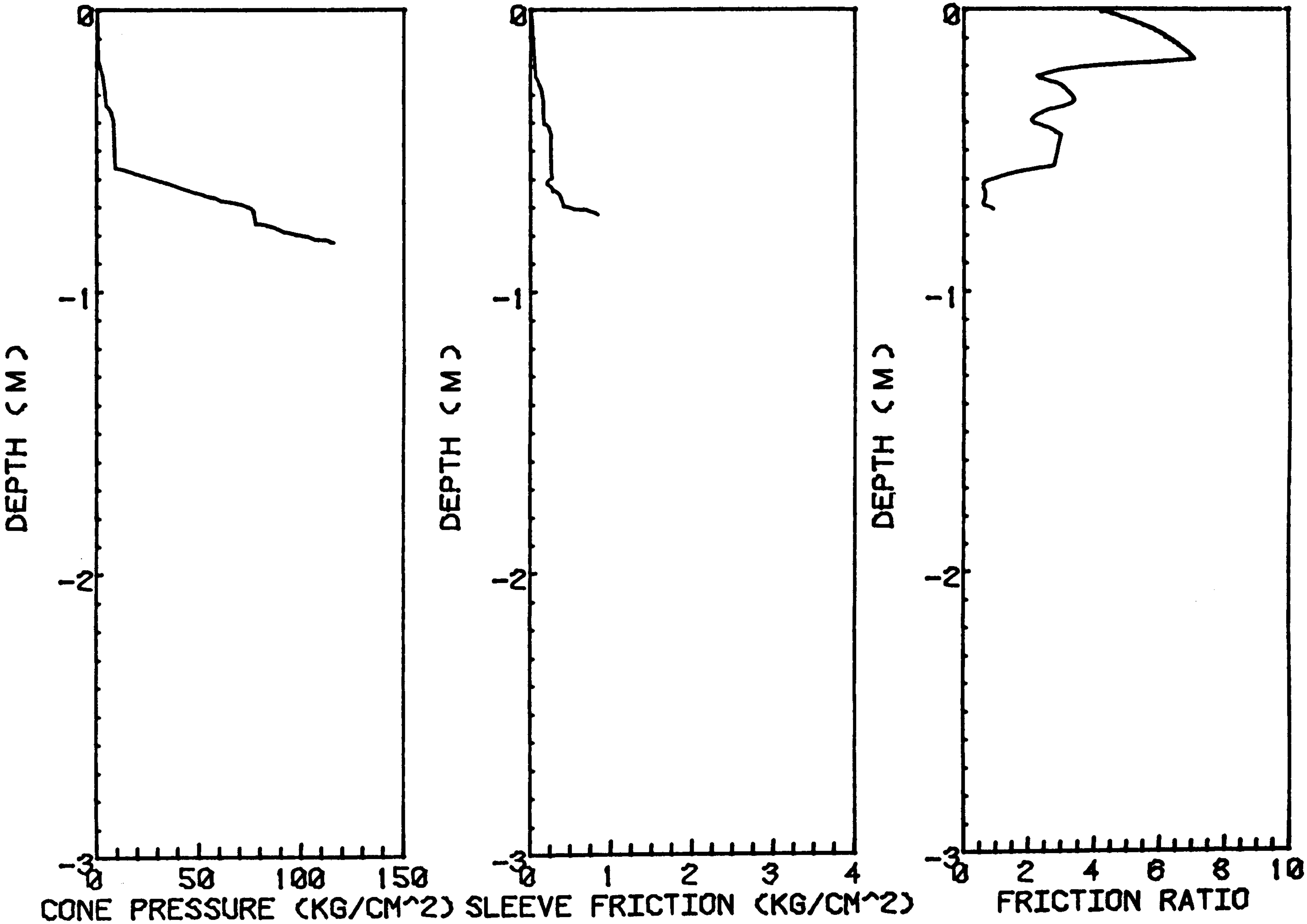

674X2. N. YUKON DELTA ICE GOUGE AREA. ALASKA.

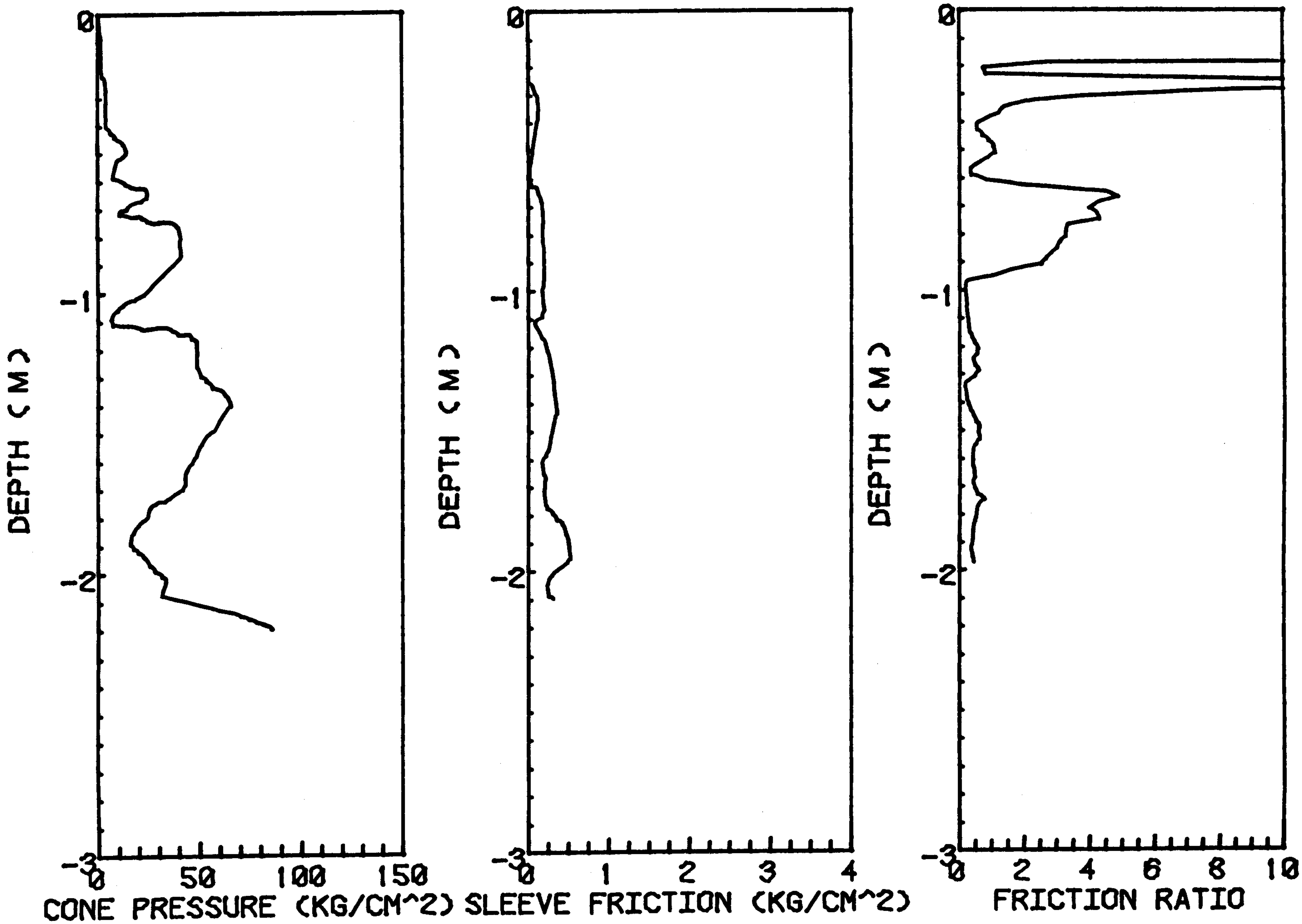

675X1. THERMOGENIC GAS ZONE. ALASKA.

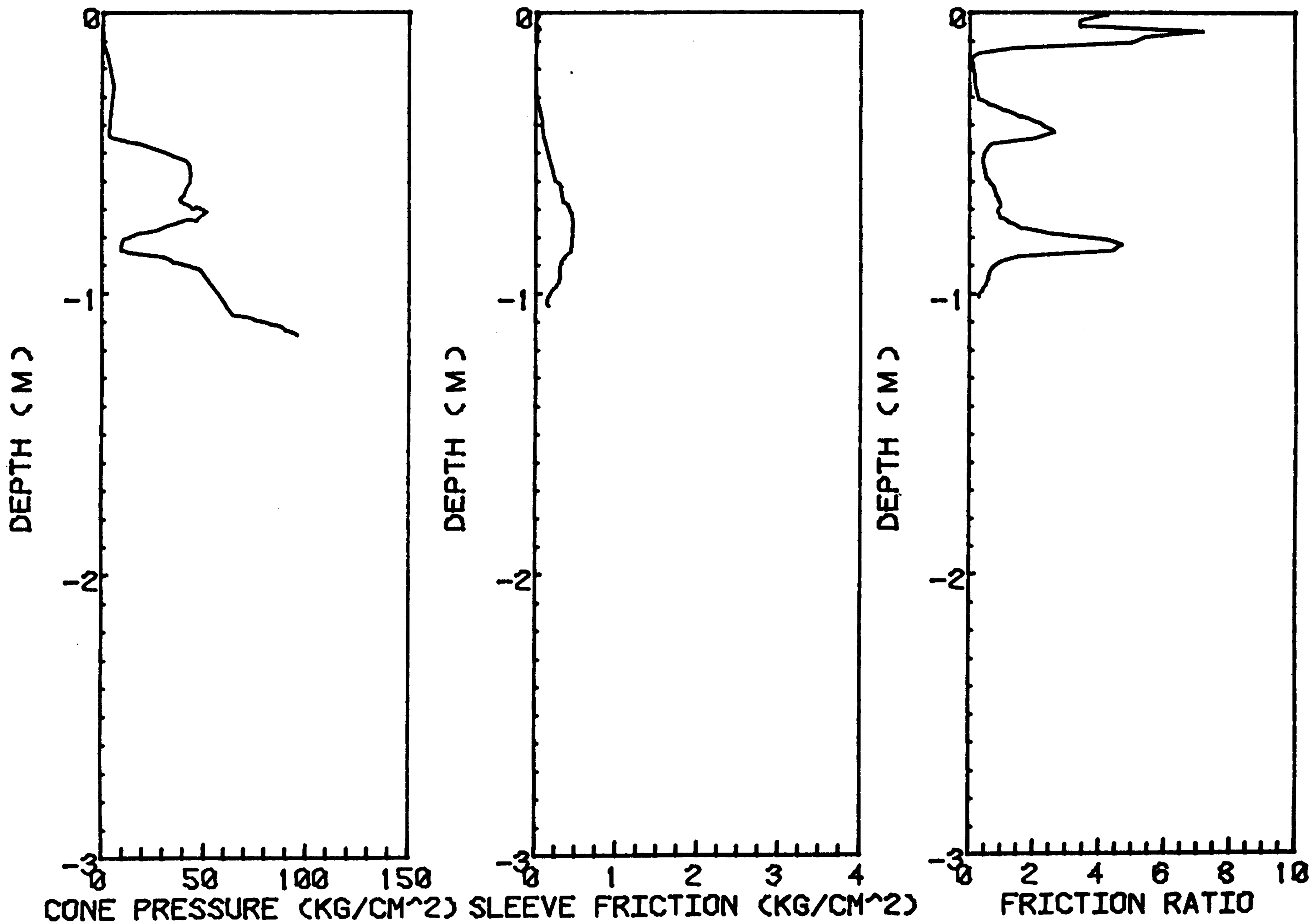

675X2. THERMOGENIC GAS ZONE. ALASKA.

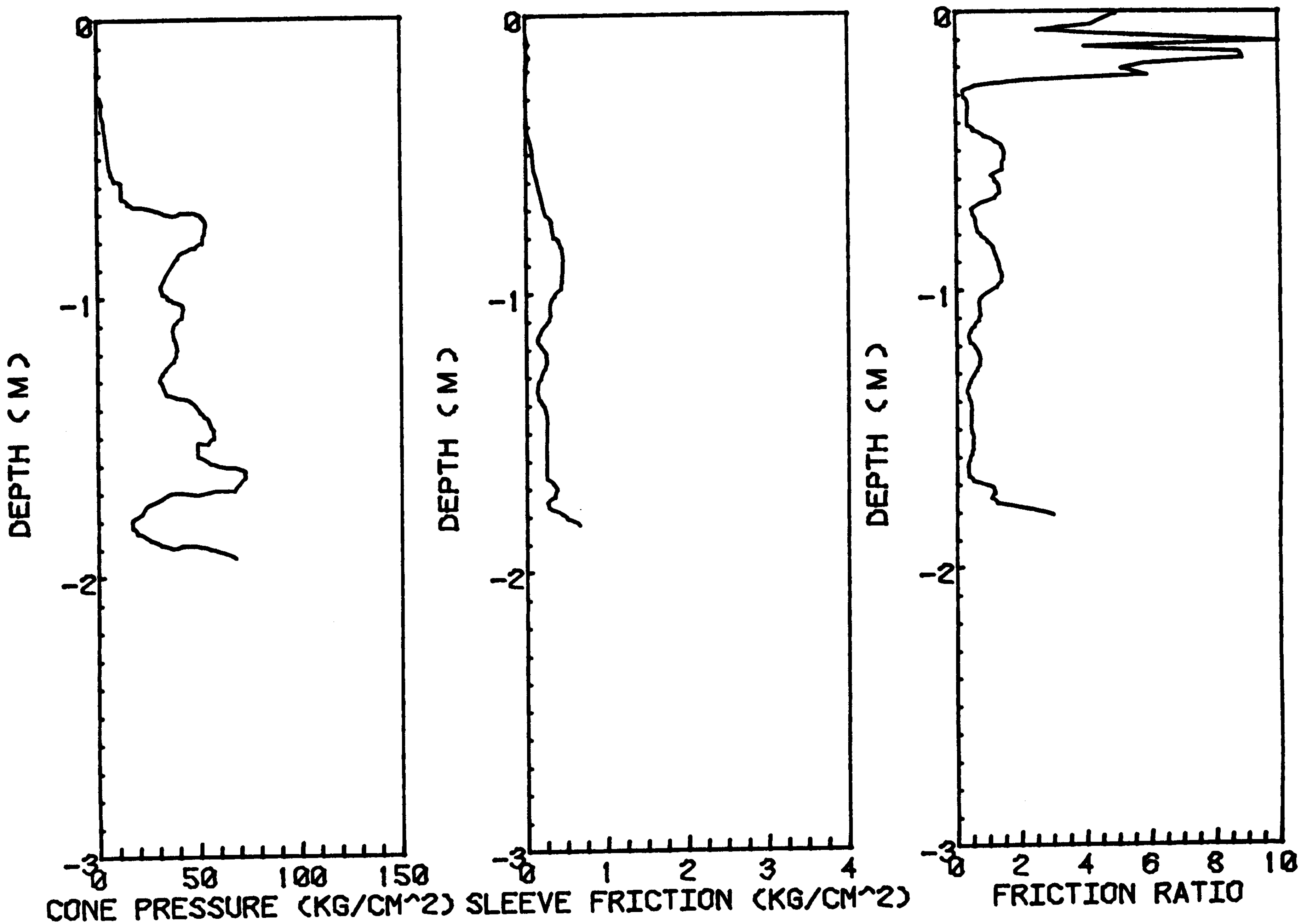

675X3. THERMOGENIC GAS ZONE. ALASKA.

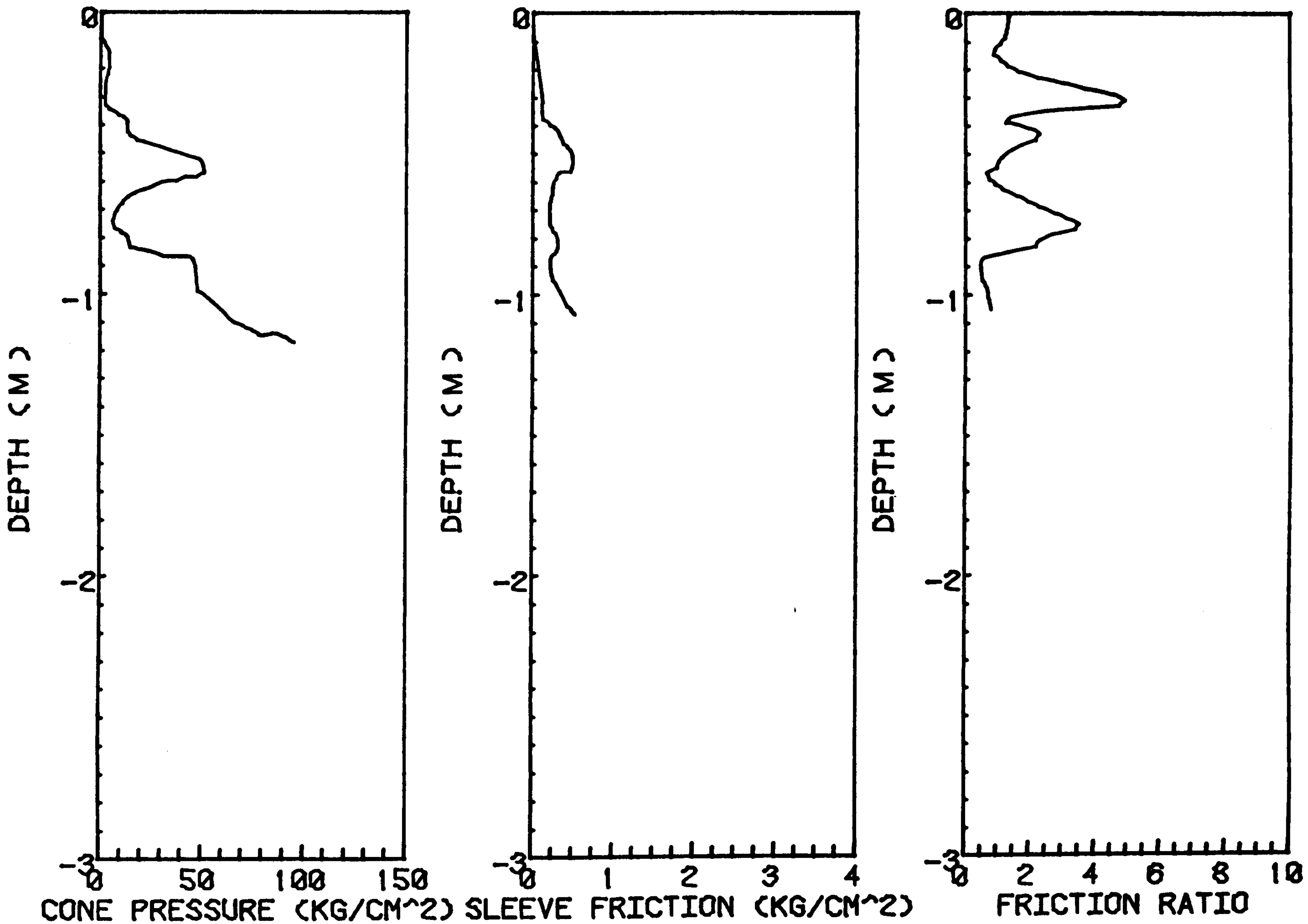

675X4. THERMOGENIC GAS ZONE. ALASKA.

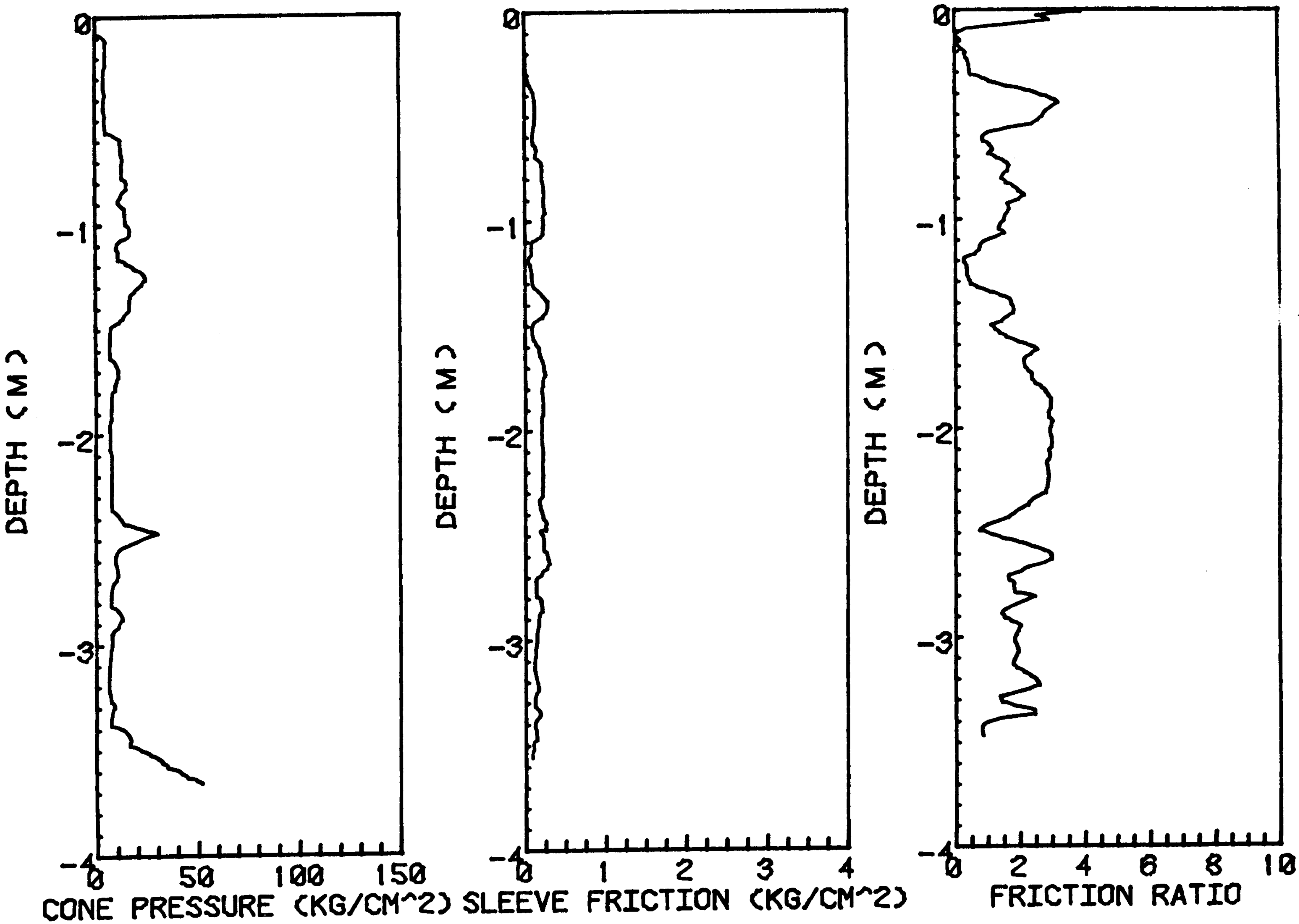

676X1. BIOGENIC GAS ZONE. ALASKA.

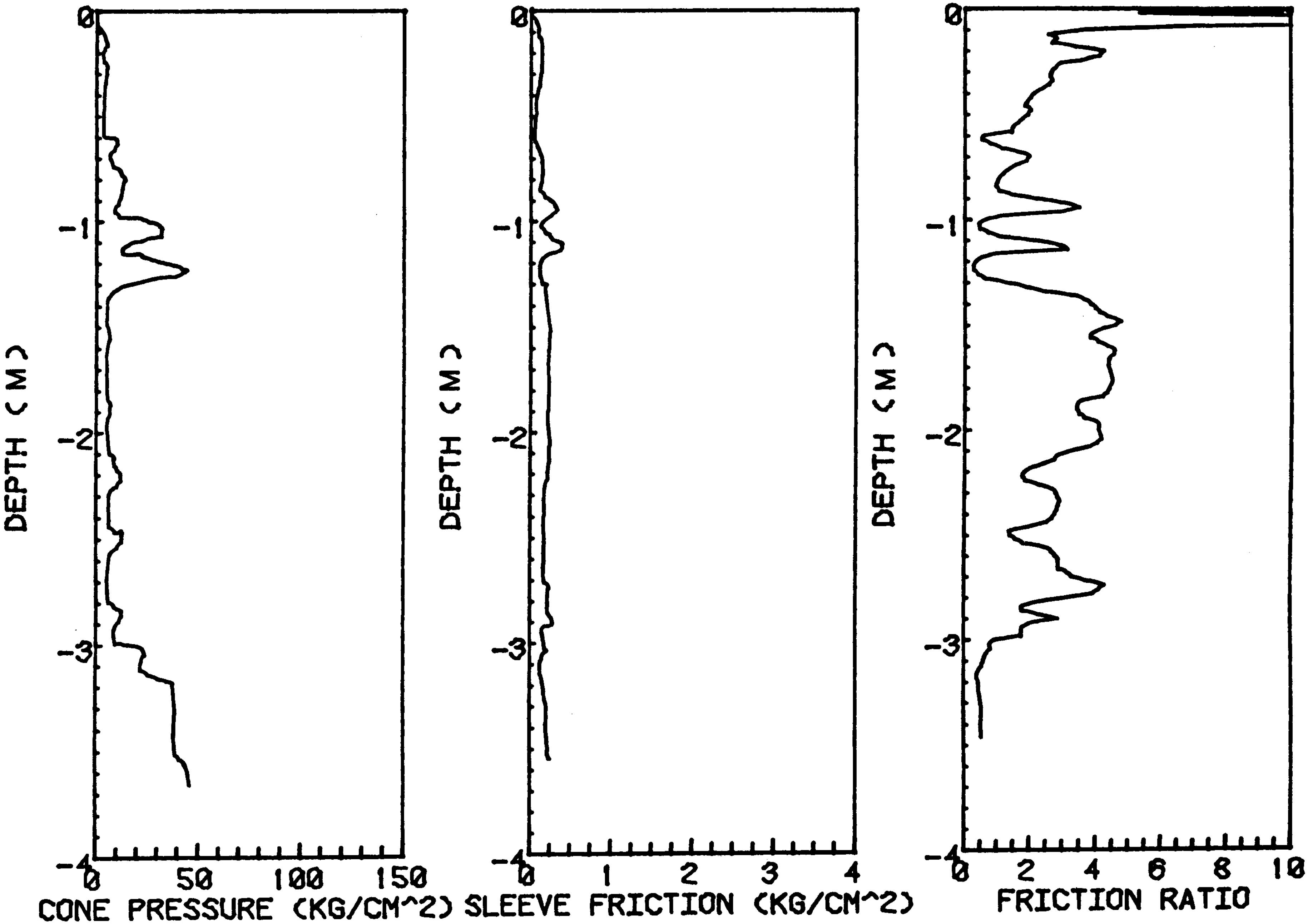

676X2. BIOGENIC GAS ZONE. ALASKA.

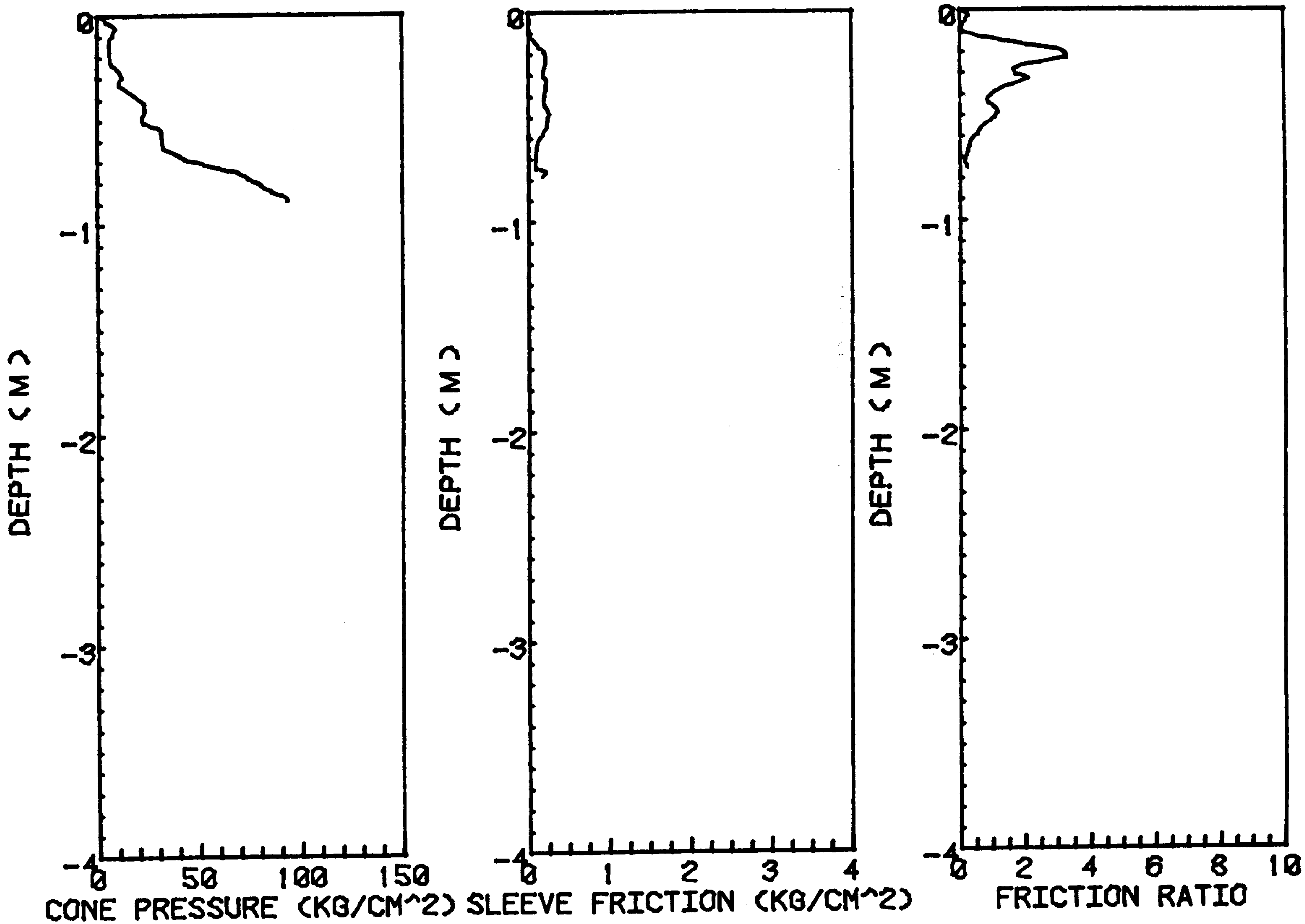

677X1. W. OF THERMOGENIC GAS ZONE. ALASKA.

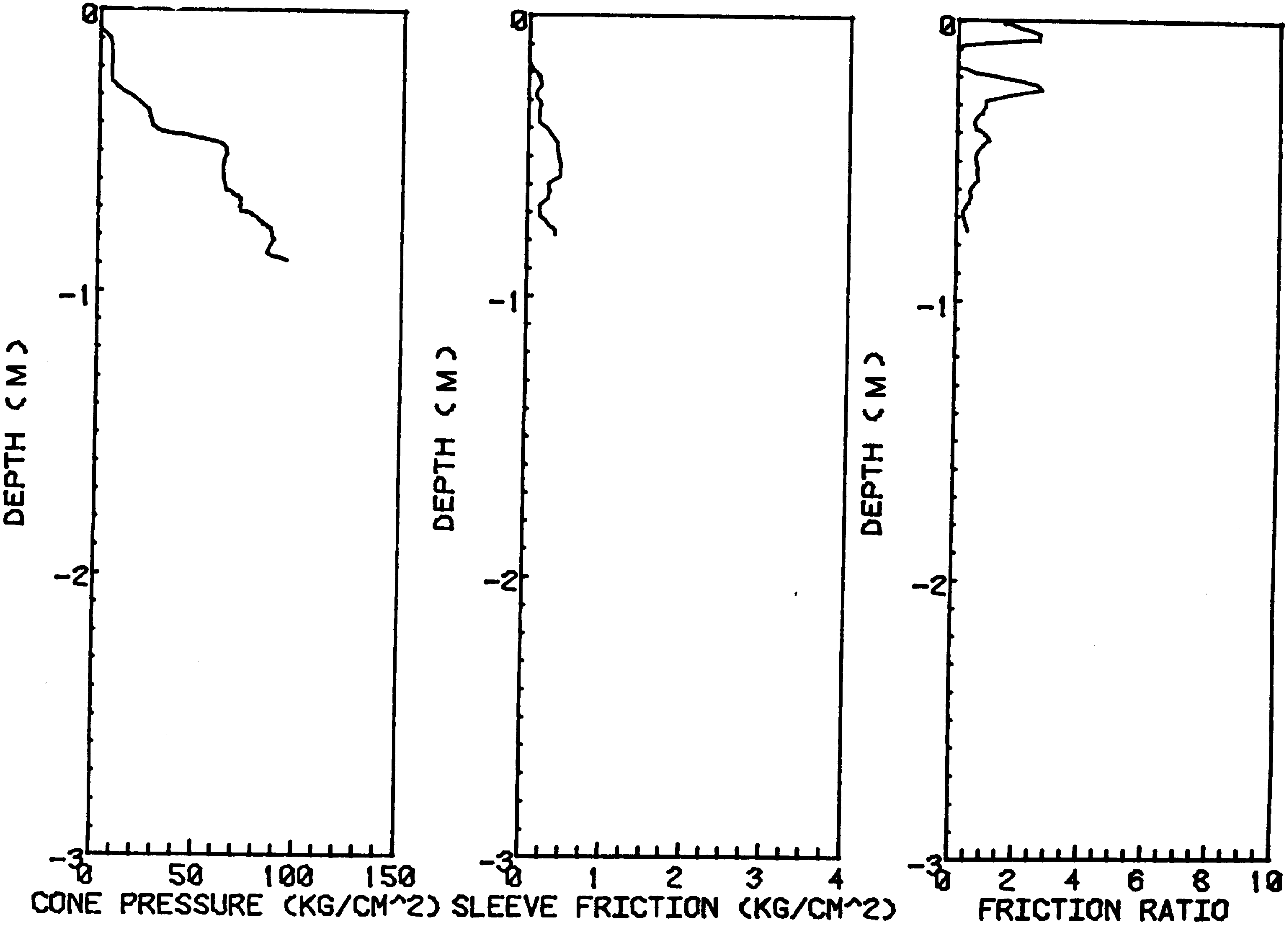

677X2. W. OF THERMOGENIC GAS ZONE. ALASKA.

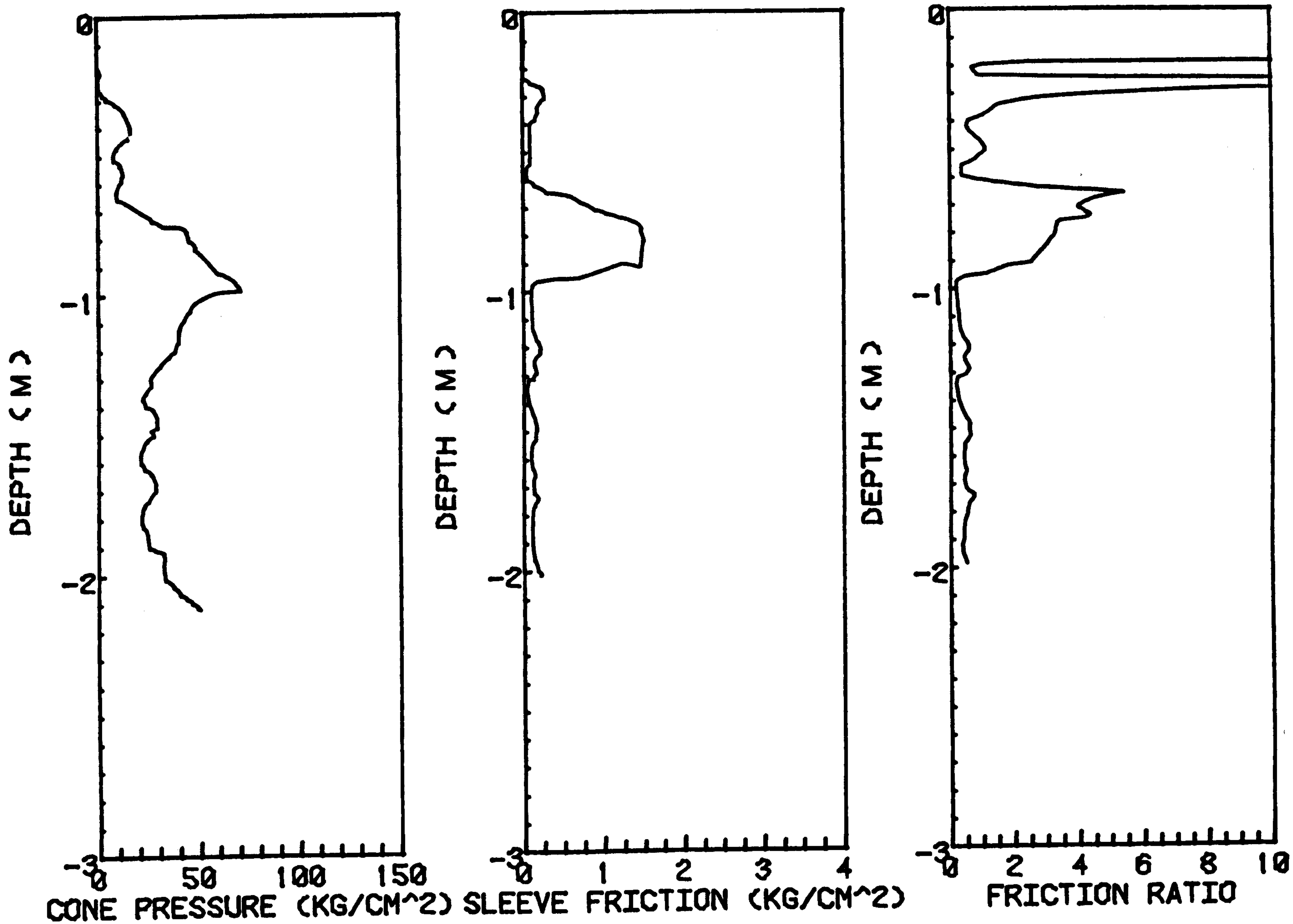

678X1. CHIRIKOV BASIN SAND RIDGE AREA - TROUGH. ALASKA.

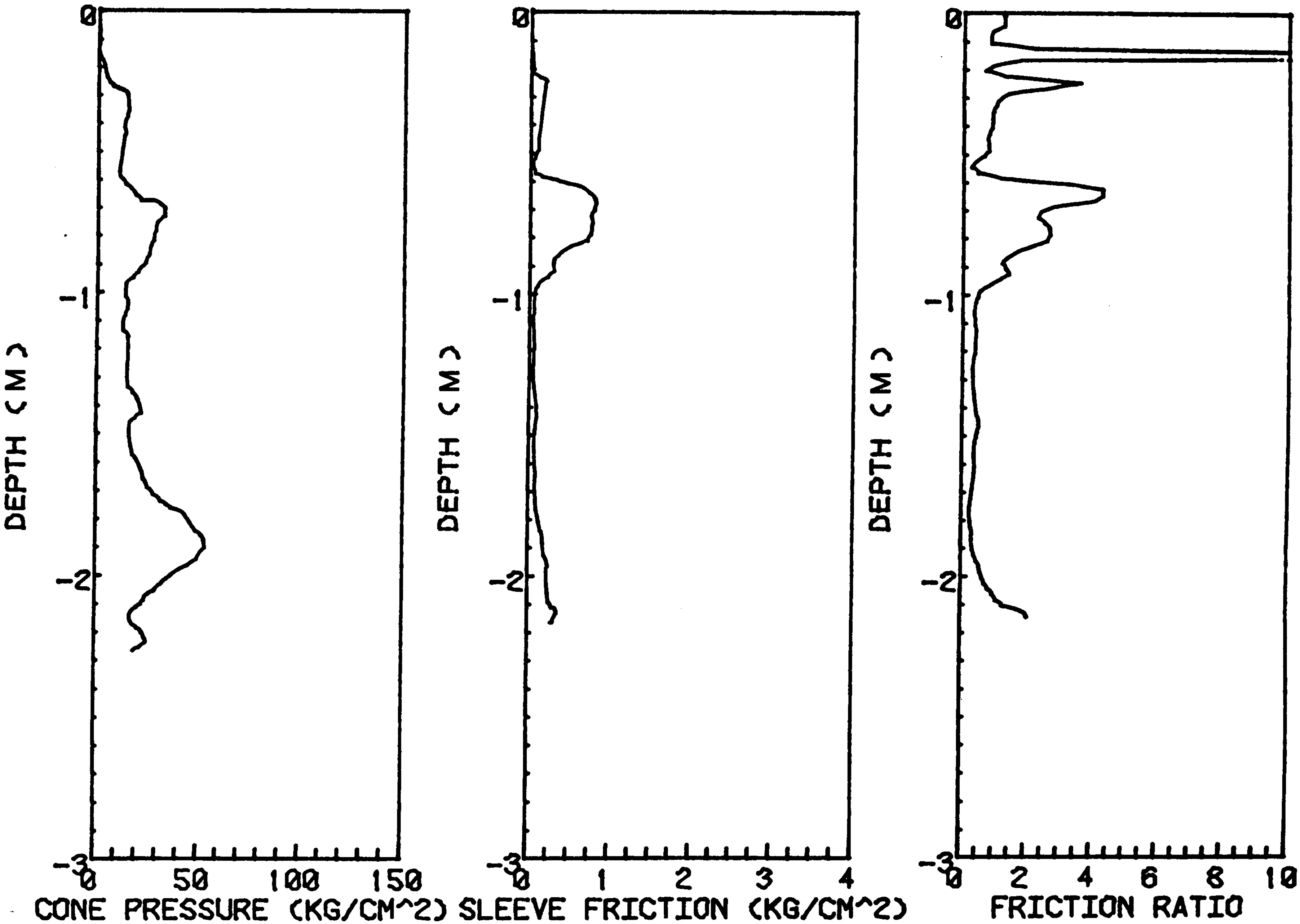

678X2. CHIRIKOV BASIN SAND RIDGE AREA - TROUGH. ALASKA.

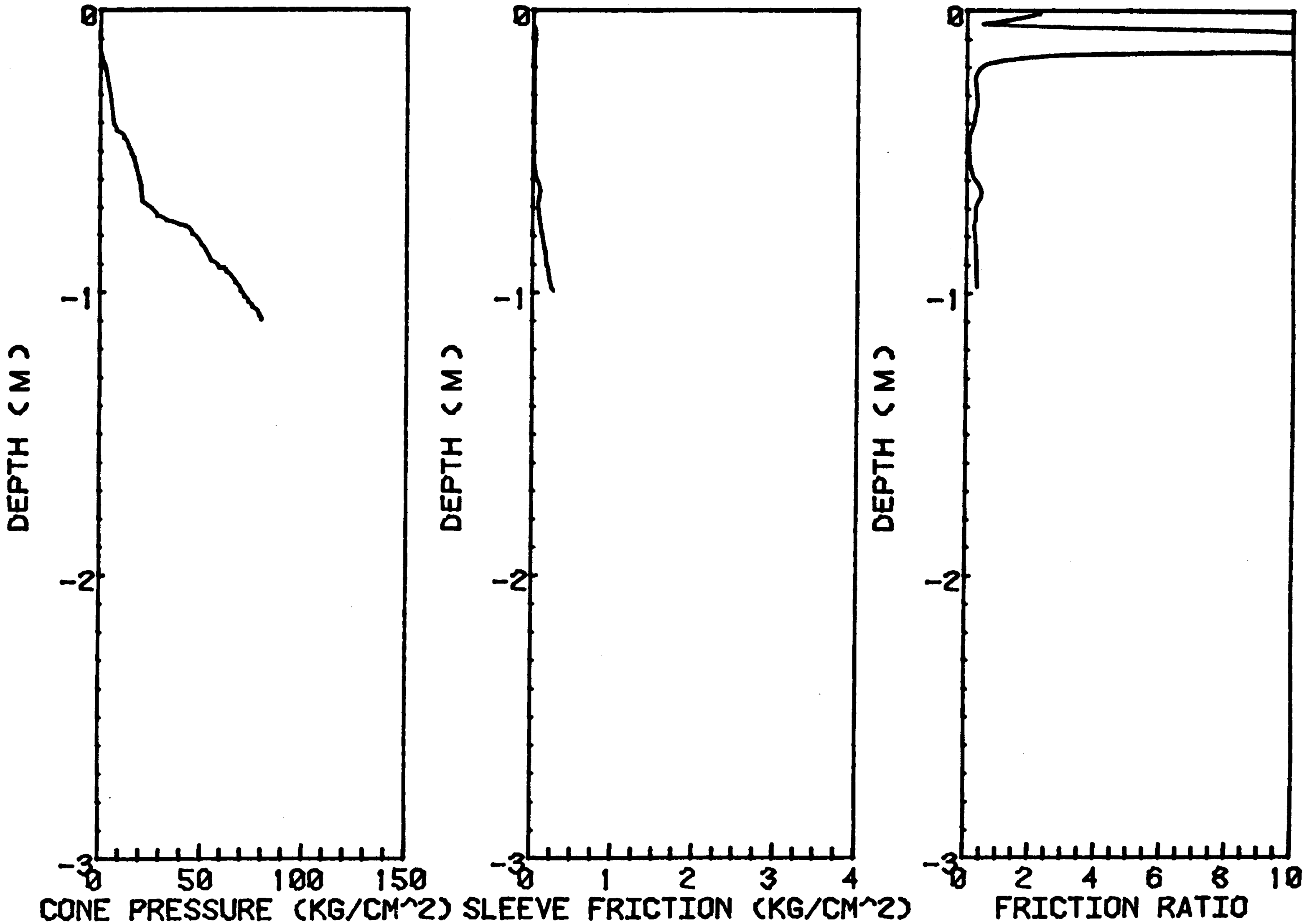

679X1. CHIRIKOV BASIN SAND RIDGE AREA - CREST. ALASKA.

APPENDIX C:

RELATIVE DENSITY PLOTS

In the following diagrams, the first three numbers on the right side of the y-axis identify the ocean station from which the data were gathered. The fourth number reflects the number of attempts made to get the data.

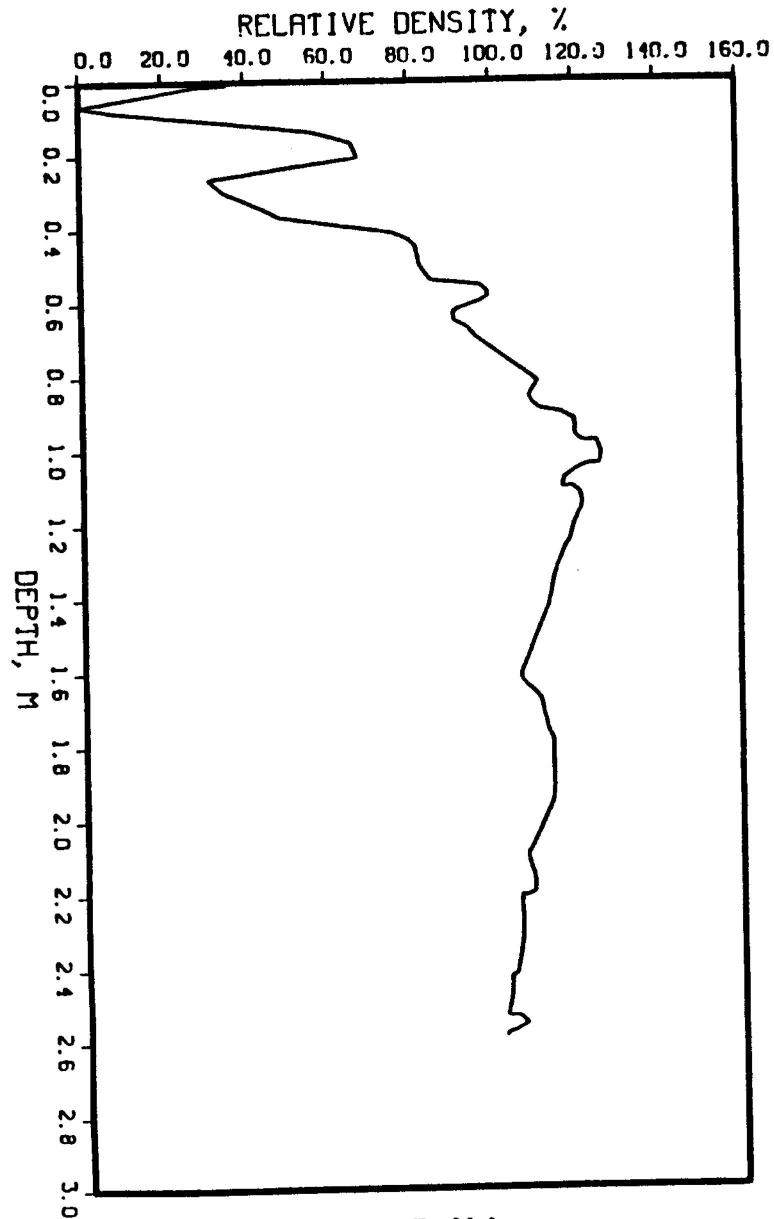
RELATIVE DENSITY, %
0.0 20.0 40.0 60.0 80.0 100.0 120.0 140.0 160.0
DEPTH, M
0.0 0.2 0.4 0.6 0.8 1.0 1.2 1.4 1.6 1.8 2.0 2.2 2.4 2.6 2.8 3.0

665 X1

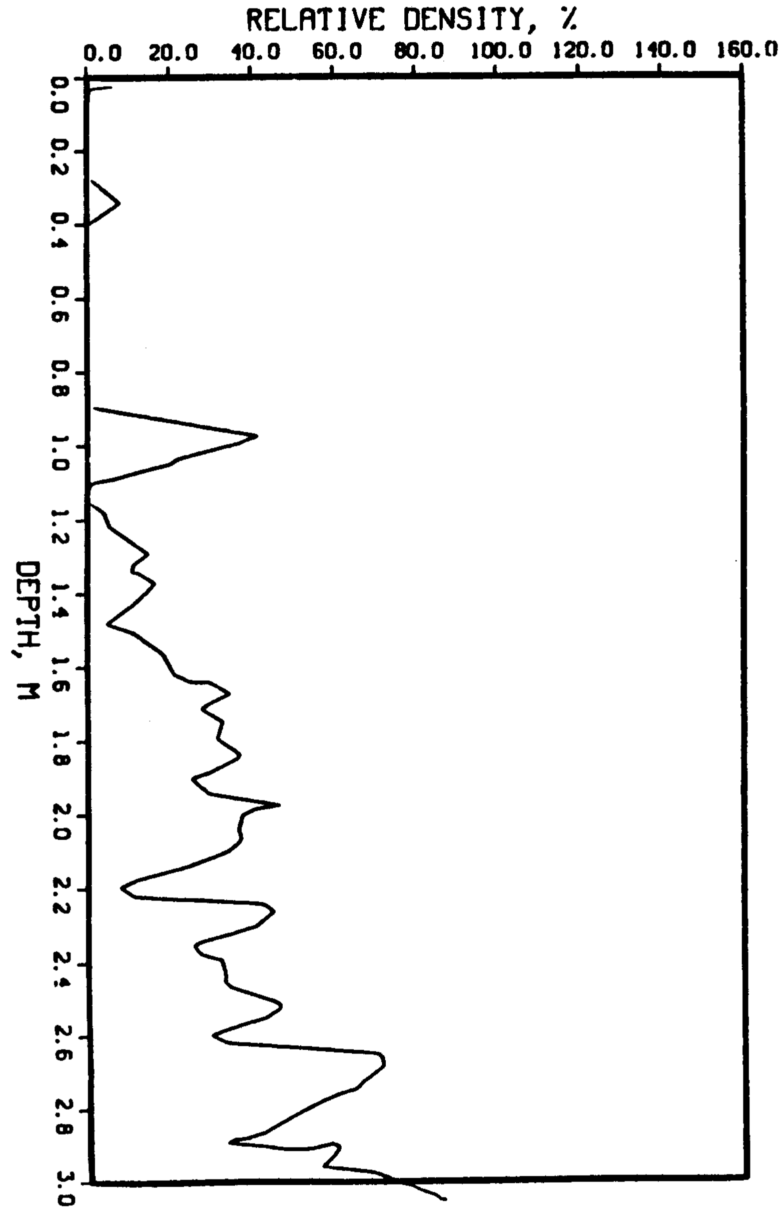
RELATIVE DENSITY, %
0.0
20.0
40.0
60.0
80.0
100.0
120.0
140.0
160.0
DEPTH, M
0.0
0.2
0.4
0.6
0.8
1.0
1.2
1.4
1.6
1.8
2.0
2.2
2.4
2.6
2.8
3.0

667 X1

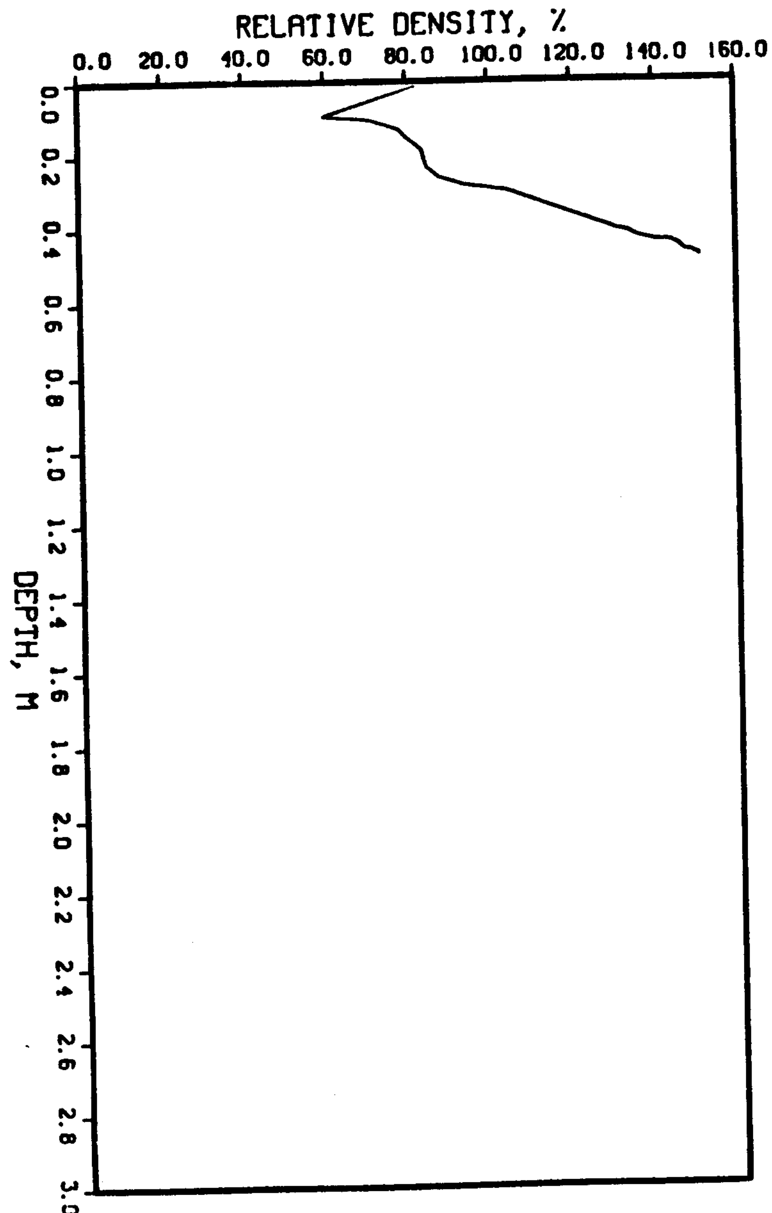
RELATIVE DENSITY, %
0.0
20.0
40.0
60.0
80.0
100.0
120.0
140.0
160.0
DEPTH, M
0.0
0.2
0.4
0.6
0.8
1.0
1.2
1.4
1.6
1.8
2.0
2.2
2.4
2.6
2.8
3.0

668 X1

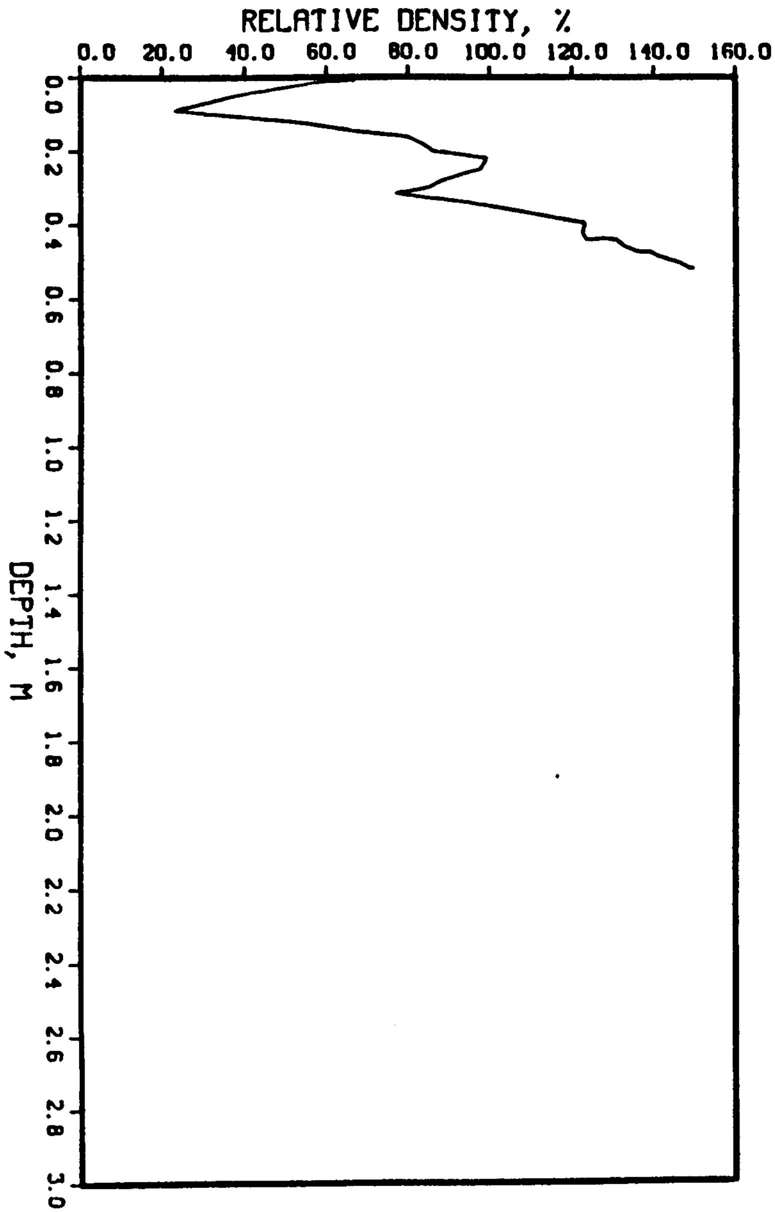
RELATIVE DENSITY, %
0.0
20.0
40.0
60.0
80.0
100.0
120.0
140.0
160.0
DEPTH, M
0.0
0.2
0.4
0.6
0.8
1.0
1.2
1.4
1.6
1.8
2.0
2.2
2.4
2.6
2.8
3.0

668 X2

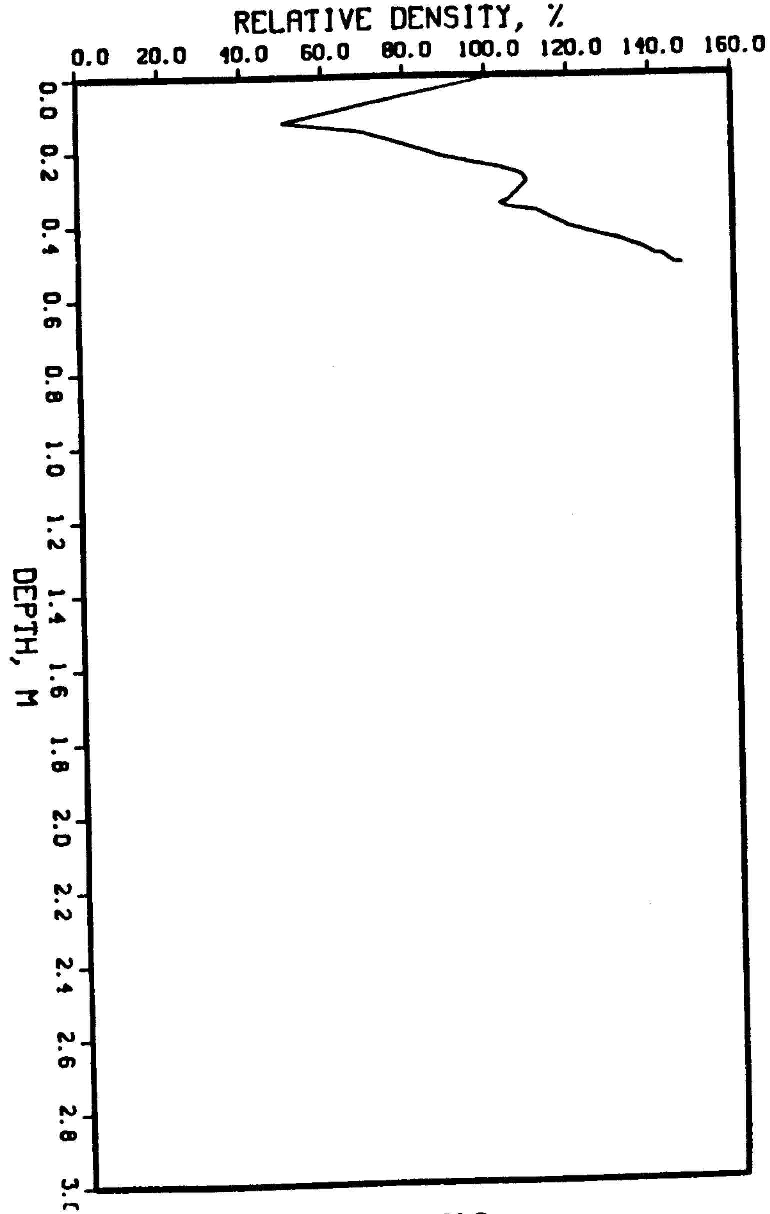

RELATIVE DENSITY, %
0.0 20.0 40.0 60.0 80.0 100.0 120.0 140.0 160.0
DEPTH, M
0.0 0.2 0.4 0.6 0.8 1.0 1.2 1.4 1.6 1.8 2.0 2.2 2.4 2.6 2.8 3.0

668 X3

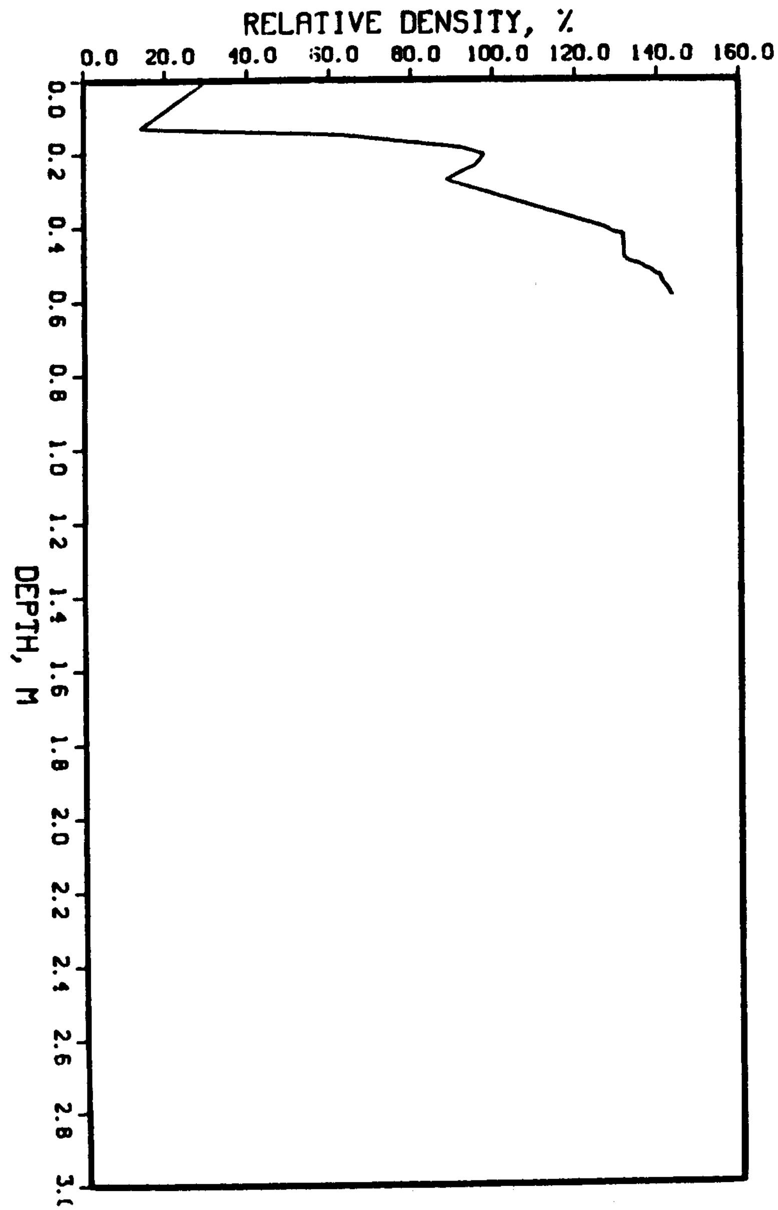
RELATIVE DENSITY, %
0.0 20.0 40.0 60.0 80.0 100.0 120.0 140.0 160.0
DEPTH, M
0.0 0.2 0.4 0.6 0.8 1.0 1.2 1.4 1.6 1.8 2.0 2.2 2.4 2.6 2.8

668 X4

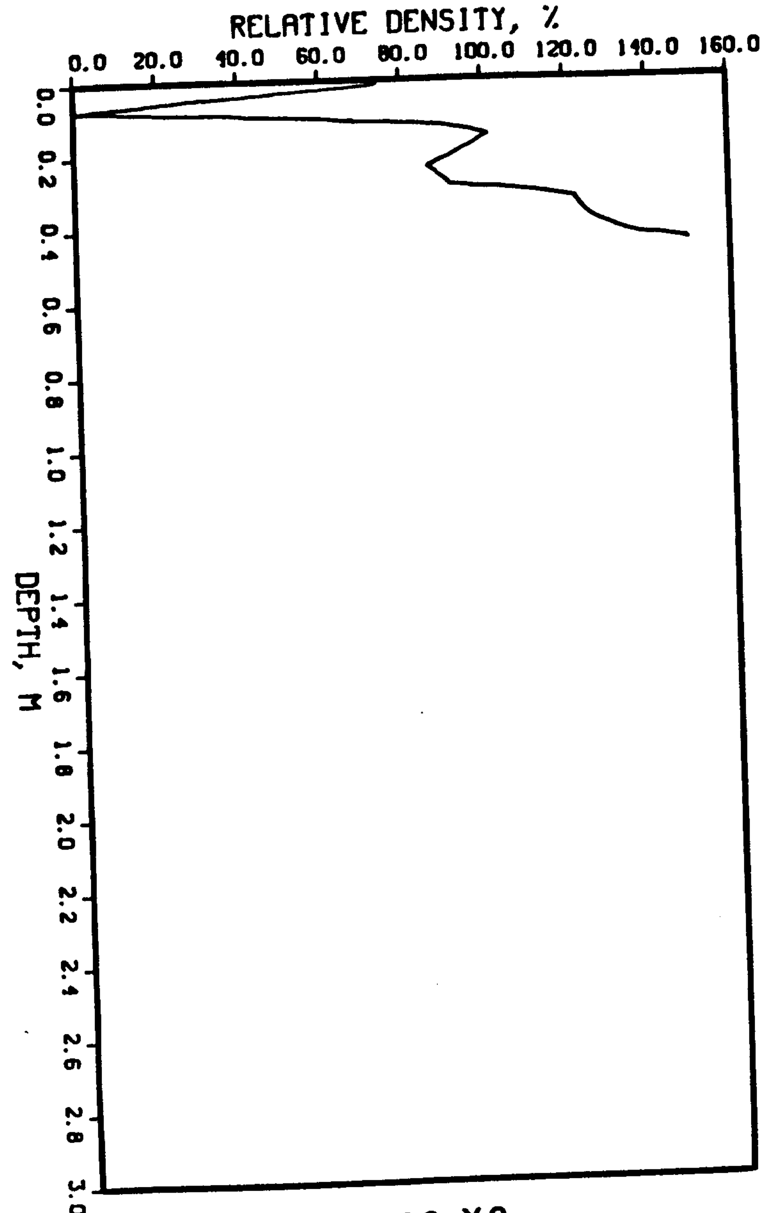
RELATIVE DENSITY, %
0.0 20.0 40.0 60.0 80.0 100.0 120.0 140.0 160.0
DEPTH, M
0.0 0.2 0.4 0.6 0.8 1.0 1.2 1.4 1.6 1.8 2.0 2.2 2.4 2.6 2.8 3.0

669 X2

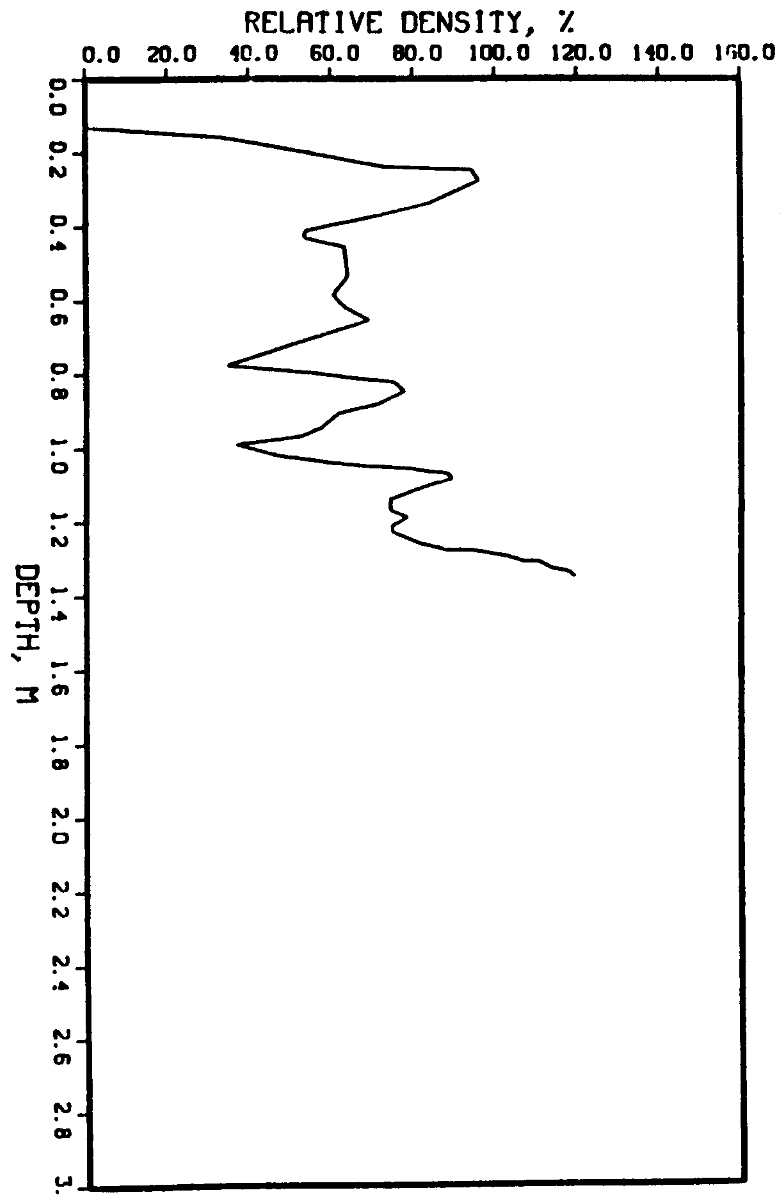
RELATIVE DENSITY, %
0.0 20.0 40.0 60.0 80.0 100.0 120.0 140.0 160.0
DEPTH, M
0.0 0.2 0.4 0.6 0.8 1.0 1.2 1.4 1.6 1.8 2.0 2.2 2.4 2.6 2.8

670 X1

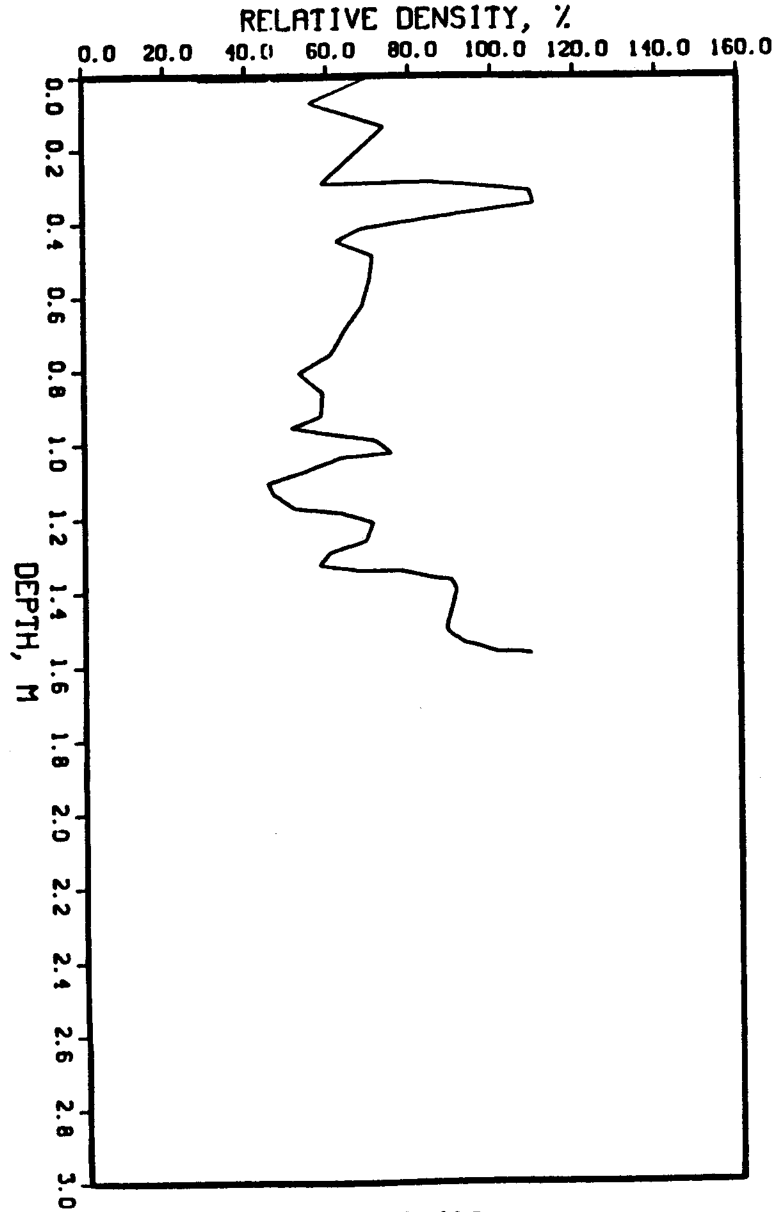
RELATIVE DENSITY, %
0.0
20.0
40.0
60.0
80.0
100.0
120.0
140.0
160.0
DEPTH, M
0.0
0.2
0.4
0.6
0.8
1.0
1.2
1.4
1.6
1.8
2.0
2.2
2.4
2.6
2.8
3.0

670 X2

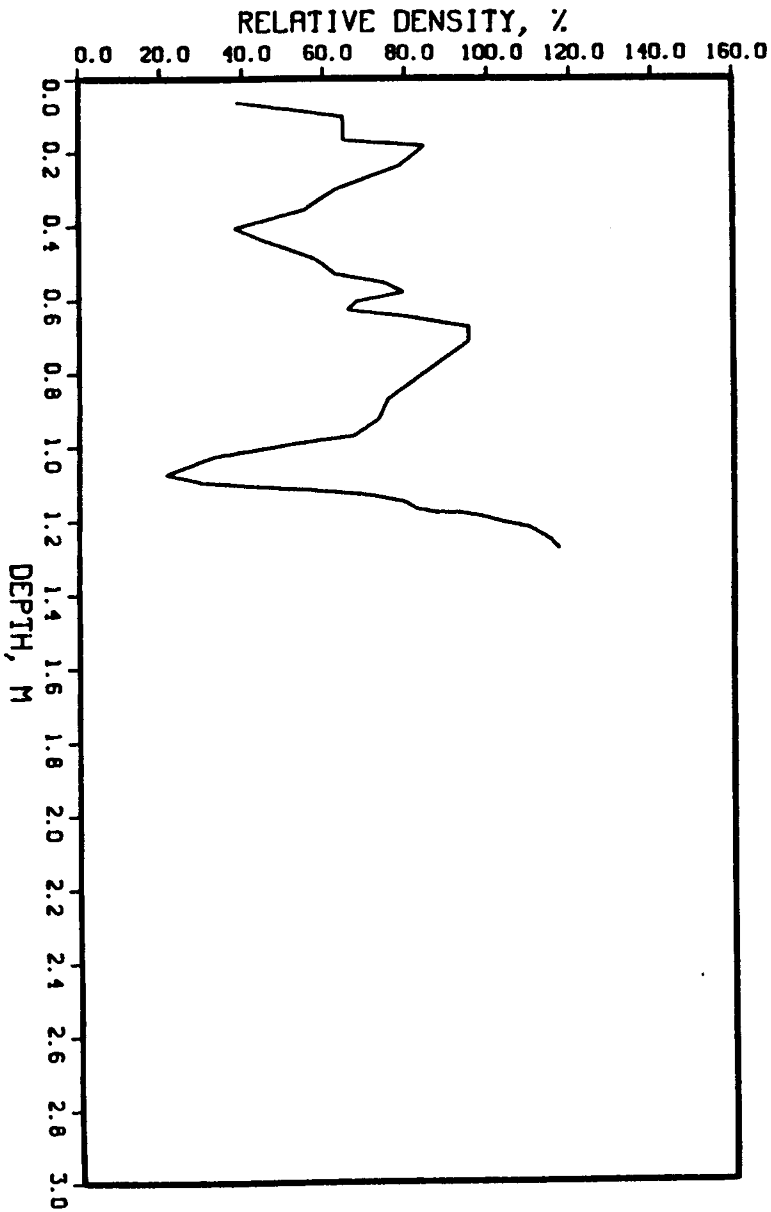
RELATIVE DENSITY, %
0.0 20.0 40.0 60.0 80.0 100.0 120.0 140.0 160.0
DEPTH, M
0.0 0.2 0.4 0.6 0.8 1.0 1.2 1.4 1.6 1.8 2.0 2.2 2.4 2.6 2.8 3.0

670 X3

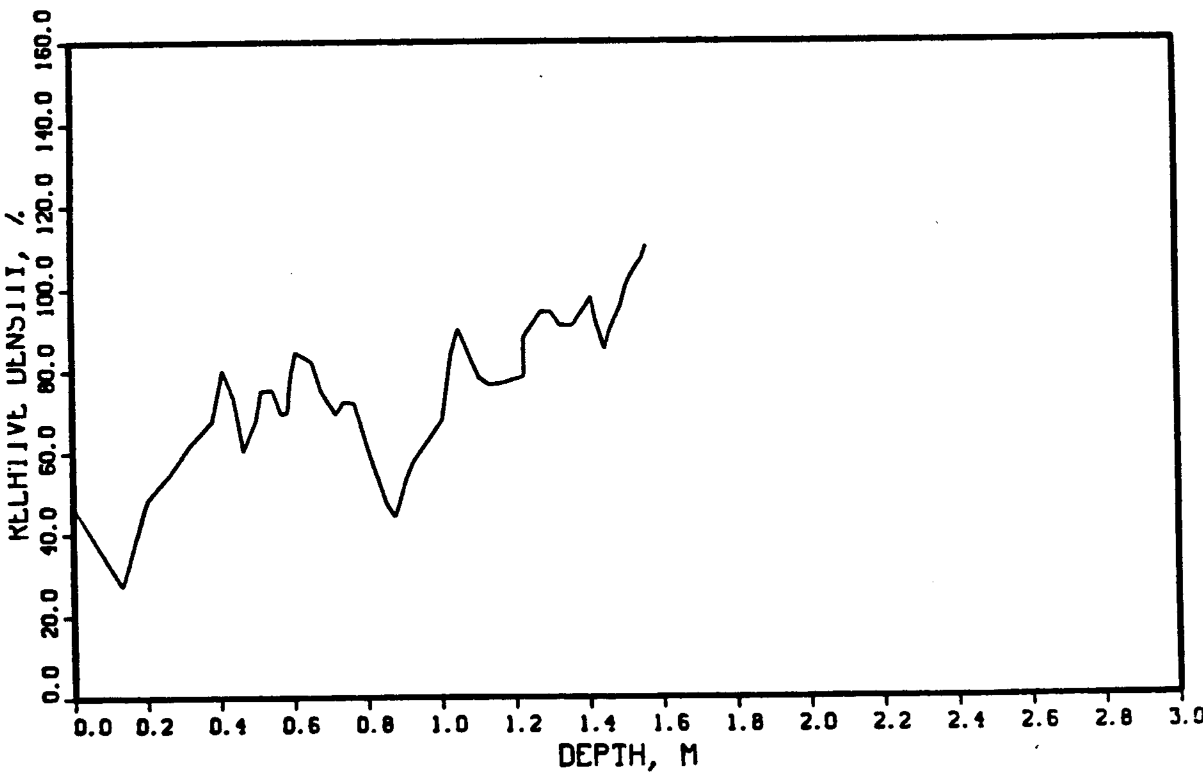
RELATIVE DENSITY, %
0.0 20.0 40.0 60.0 80.0 100.0 120.0 140.0 160.0
DEPTH, M
0.0 0.2 0.4 0.6 0.8 1.0 1.2 1.4 1.6 1.8 2.0 2.2 2.4 2.6 2.8 3.0

670 X4

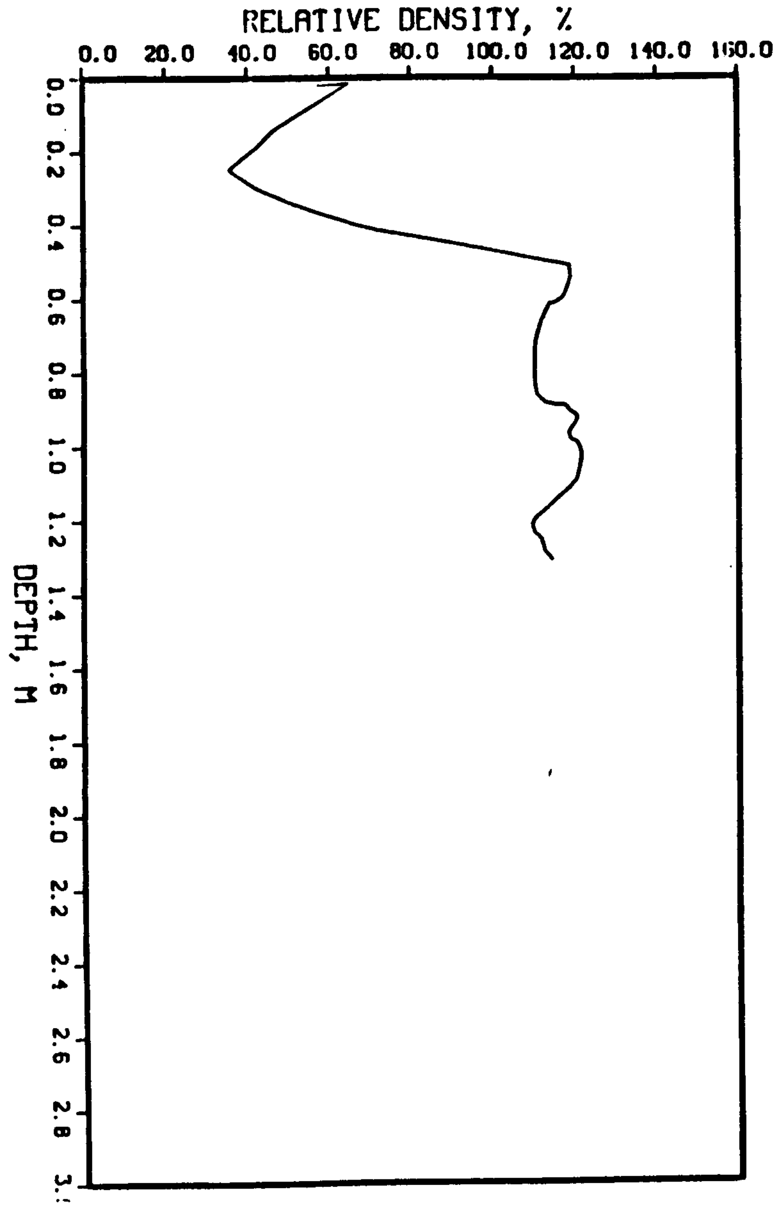
RELATIVE DENSITY, %
0.0 20.0 40.0 60.0 80.0 100.0 120.0 140.0 160.0
DEPTH, M
0.0 0.2 0.4 0.6 0.8 1.0 1.2 1.4 1.6 1.8 2.0 2.2 2.4 2.6 2.8

671 X1

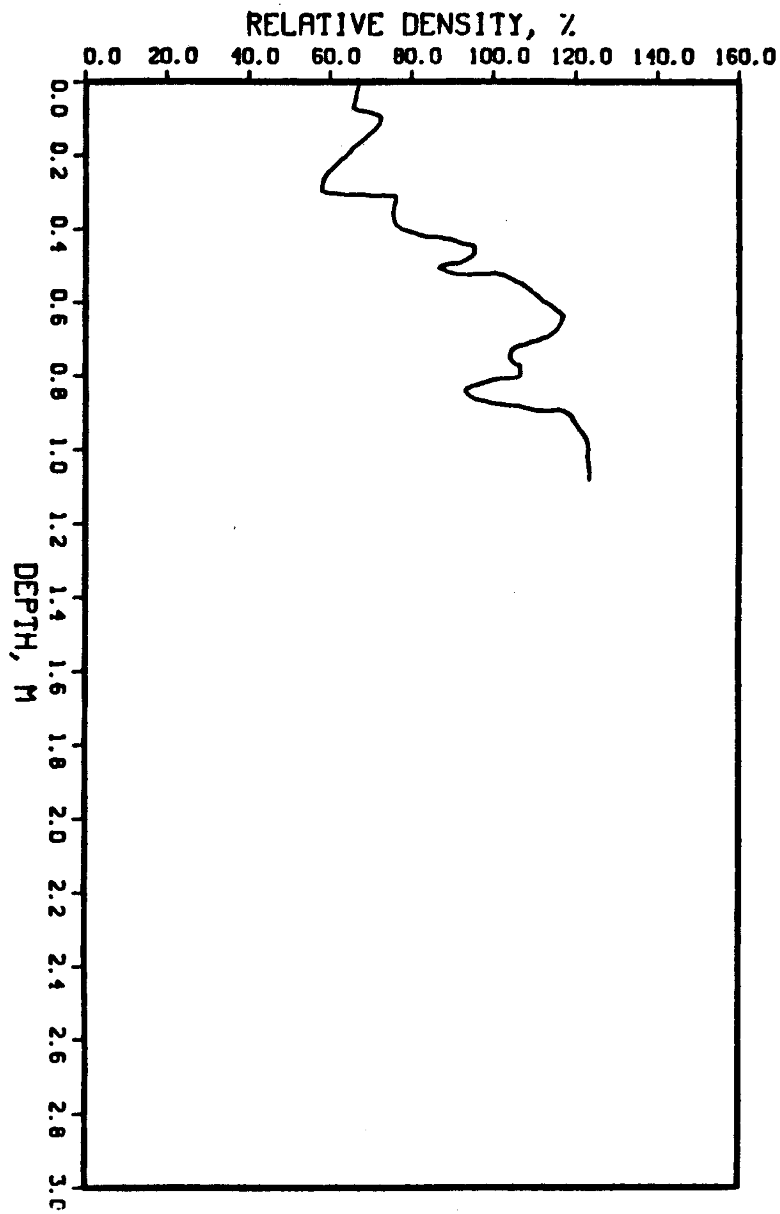
RELATIVE DENSITY, %
0.0
20.0
40.0
60.0
80.0
100.0
120.0
140.0
160.0
DEPTH, M
0.0
0.2
0.4
0.6
0.8
1.0
1.2
1.4
1.6
1.8
2.0
2.2
2.4
2.6
2.8
3.0

671X2

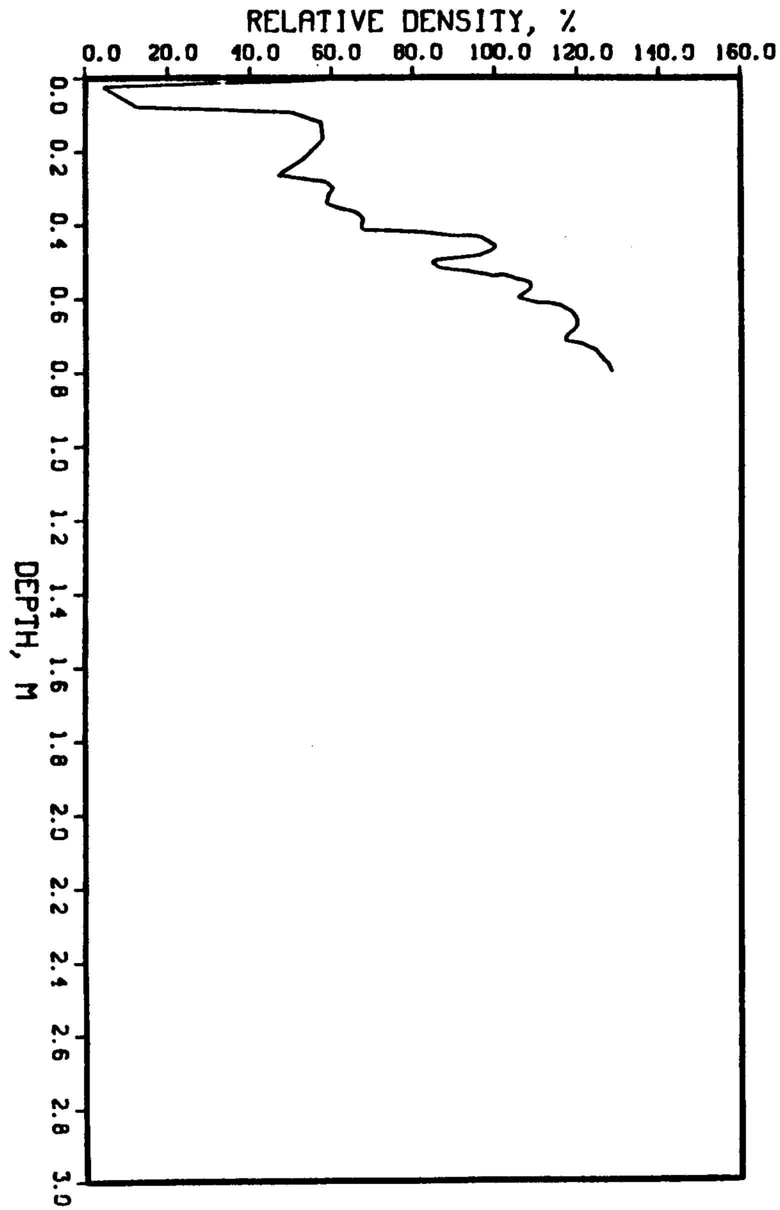
RELATIVE DENSITY, %
0.0 20.0 40.0 60.0 80.0 100.0 120.0 140.0 160.0
DEPTH, M
0.0 0.2 0.4 0.6 0.8 1.0 1.2 1.4 1.6 1.8 2.0 2.2 2.4 2.6 2.8 3.0

671 X4

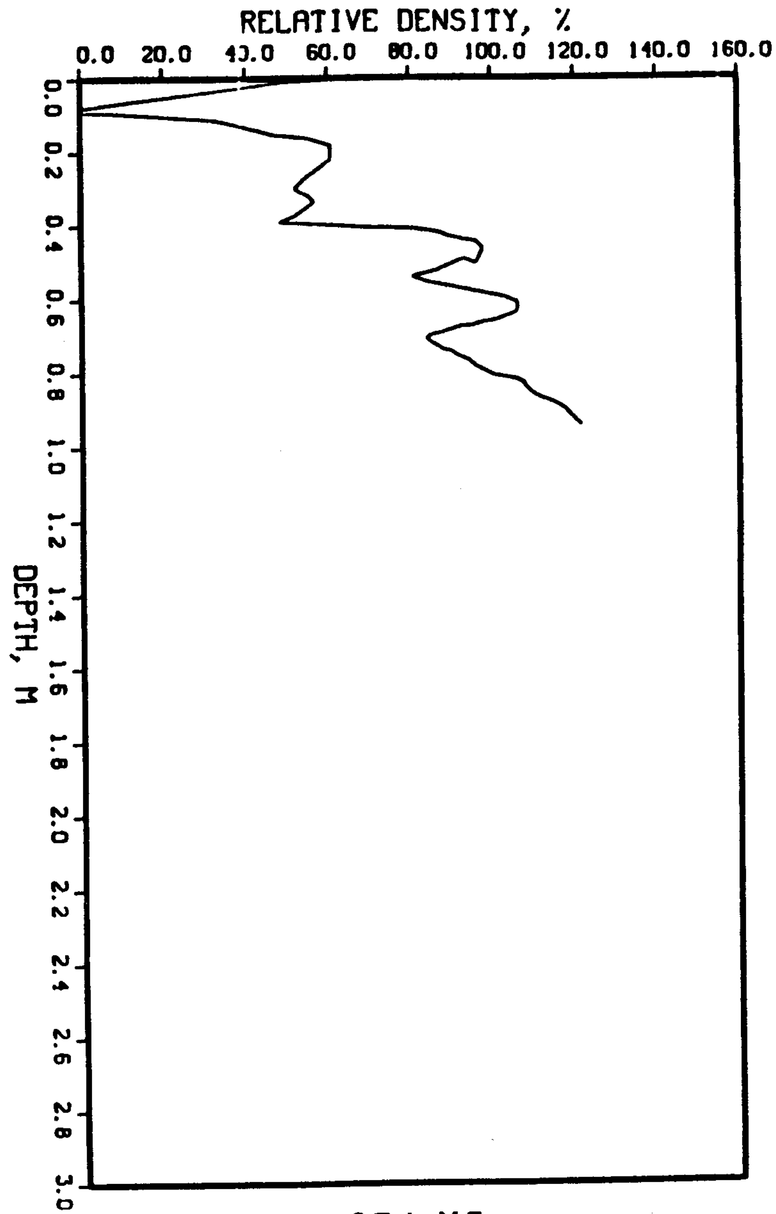
RELATIVE DENSITY, %
0.0
20.0
40.0
60.0
80.0
100.0
120.0
140.0
160.0
DEPTH, M
0.0
0.2
0.4
0.6
0.8
1.0
1.2
1.4
1.6
1.8
2.0
2.2
2.4
2.6
2.8
3.0

671 X5

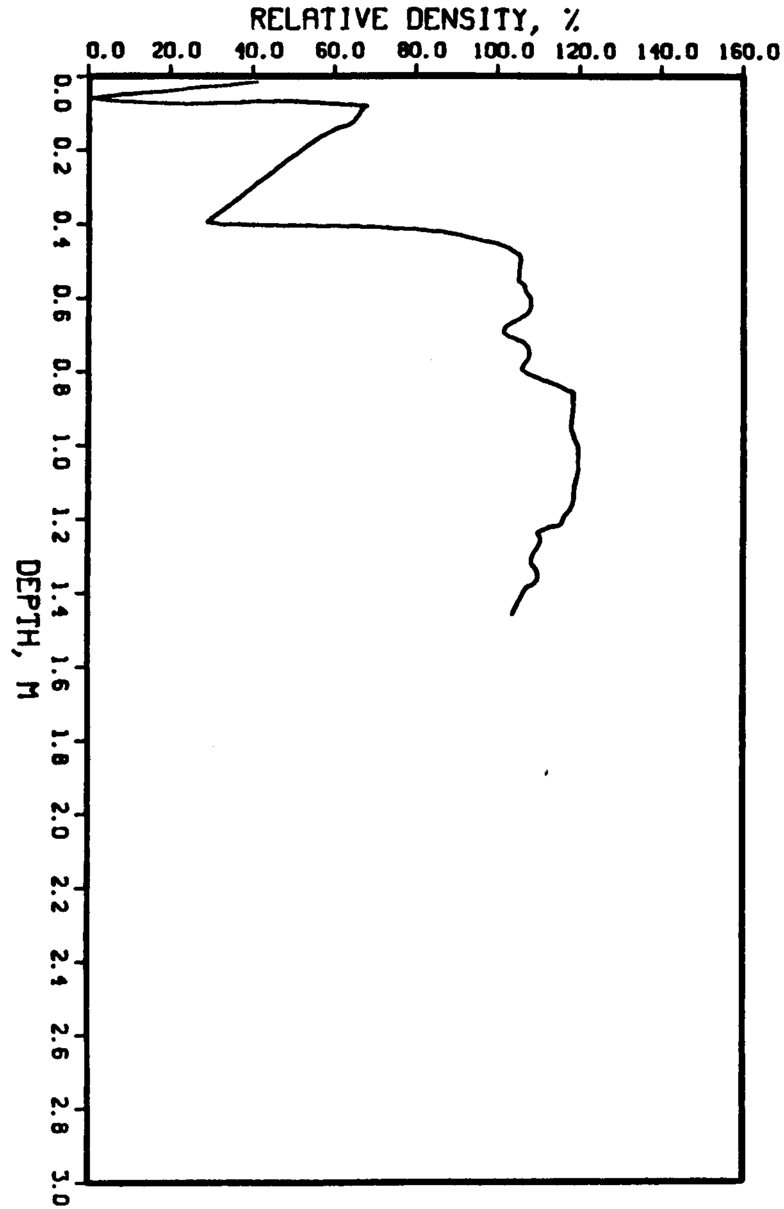
RELATIVE DENSITY, %
0.0 20.0 40.0 60.0 80.0 100.0 120.0 140.0 160.0
DEPTH, M
0.0 0.2 0.4 0.6 0.8 1.0 1.2 1.4 1.6 1.8 2.0 2.2 2.4 2.6 2.8 3.0

671 X6

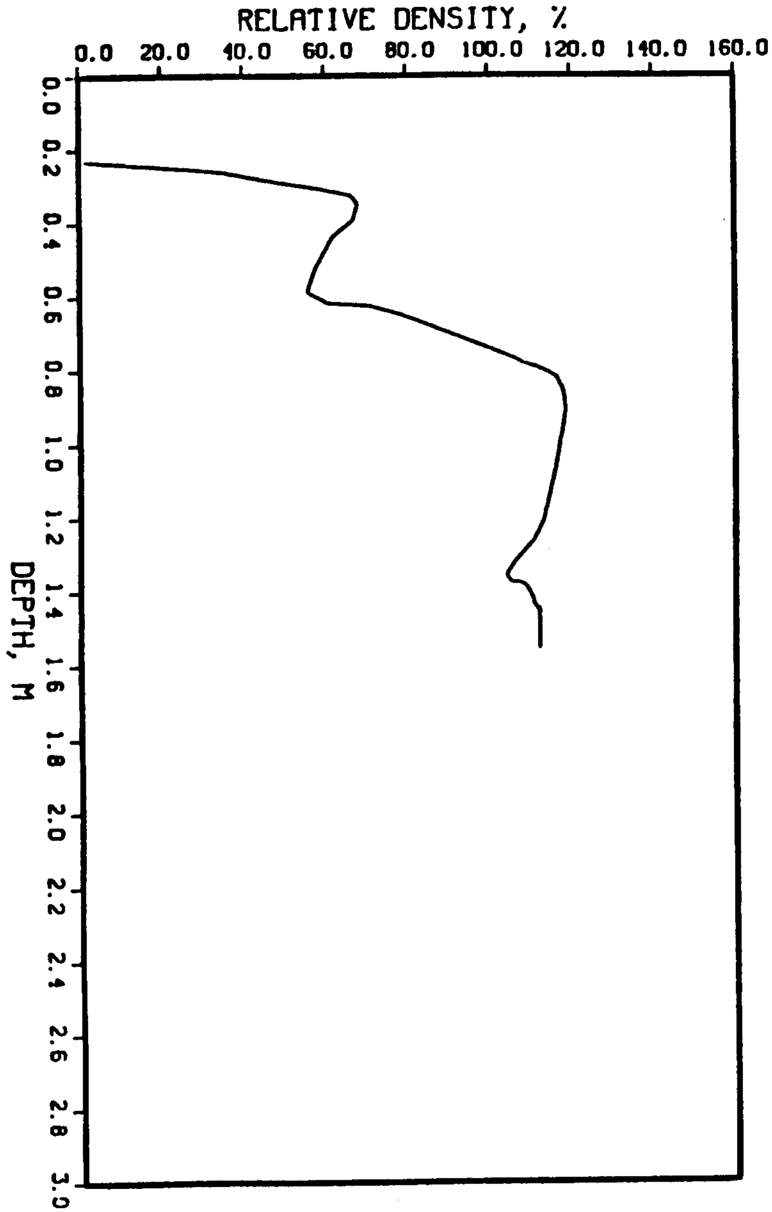
RELATIVE DENSITY, %
0.0
20.0
40.0
60.0
80.0
100.0
120.0
140.0
160.0
DEPTH, M
0.0
0.2
0.4
0.6
0.8
1.0
1.2
1.4
1.6
1.8
2.0
2.2
2.4
2.6
2.8
3.0

671 X7

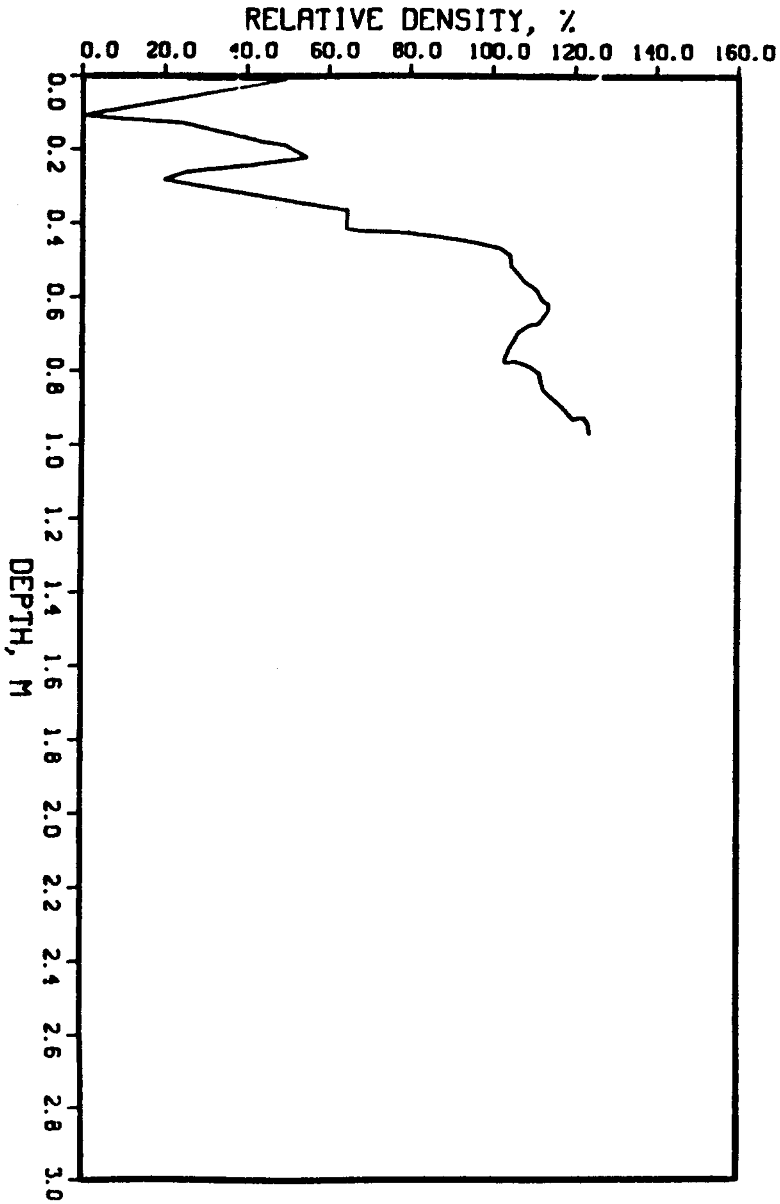
RELATIVE DENSITY, %
0.0
20.0
40.0
60.0
80.0
100.0
120.0
140.0
160.0
DEPTH, M
0.0
0.2
0.4
0.6
0.8
1.0
1.2
1.4
1.6
1.8
2.0
2.2
2.4
2.6
2.8
3.0

671 X8

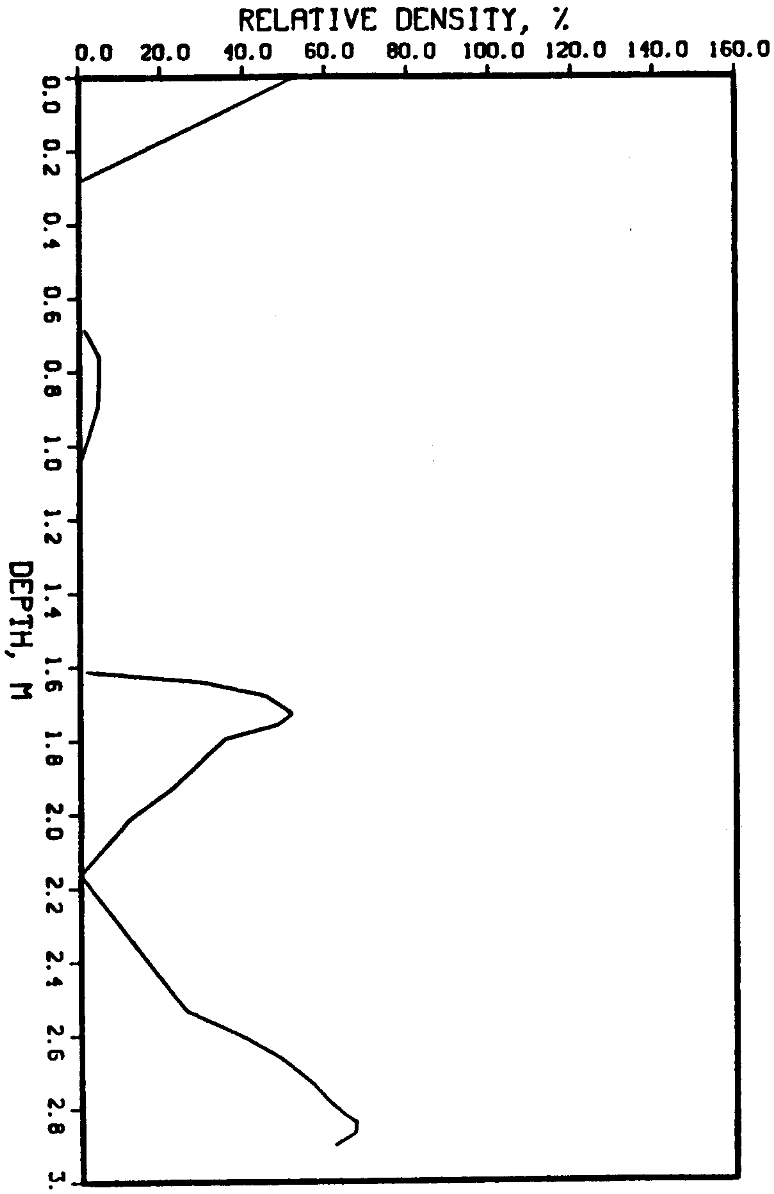
RELATIVE DENSITY, %
0.0 20.0 40.0 60.0 80.0 100.0 120.0 140.0 160.0
DEPTH, M
0.0 0.2 0.4 0.6 0.8 1.0 1.2 1.4 1.6 1.8 2.0 2.2 2.4 2.6 2.8 3.

672 X1

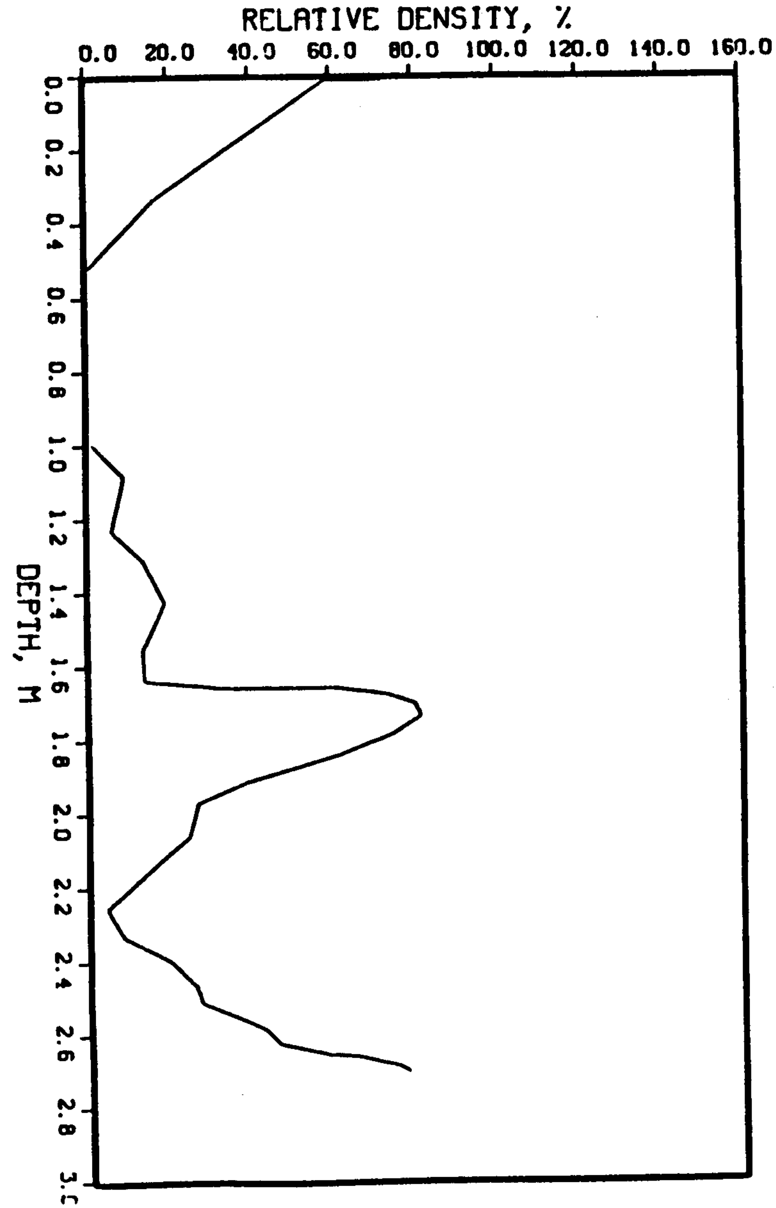
RELATIVE DENSITY, %
0.0 20.0 40.0 60.0 80.0 100.0 120.0 140.0 160.0
DEPTH, M
0.0 0.2 0.4 0.6 0.8 1.0 1.2 1.4 1.6 1.8 2.0 2.2 2.4 2.6 2.8 3.0

672 X2

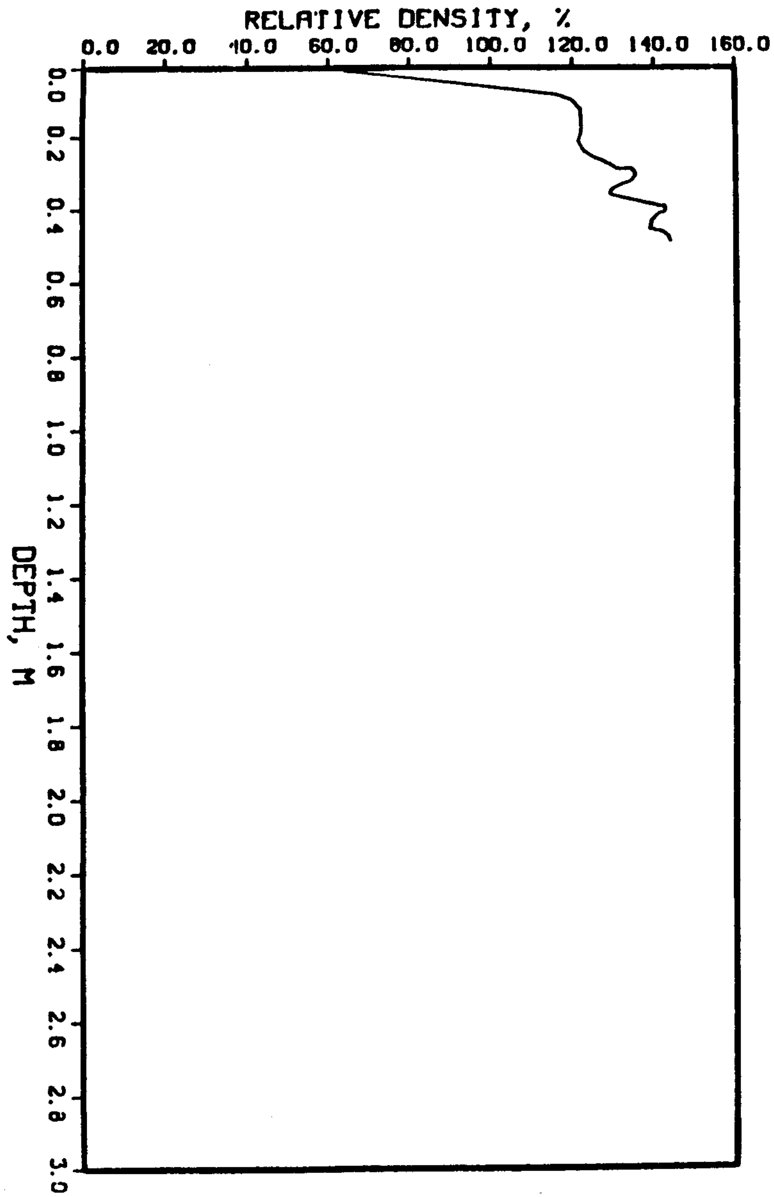
RELATIVE DENSITY, %
0.0 20.0 40.0 60.0 80.0 100.0 120.0 140.0 160.0
DEPTH, M
0.0 0.2 0.4 0.6 0.8 1.0 1.2 1.4 1.6 1.8 2.0 2.2 2.4 2.6 2.8 3.0

673 X1

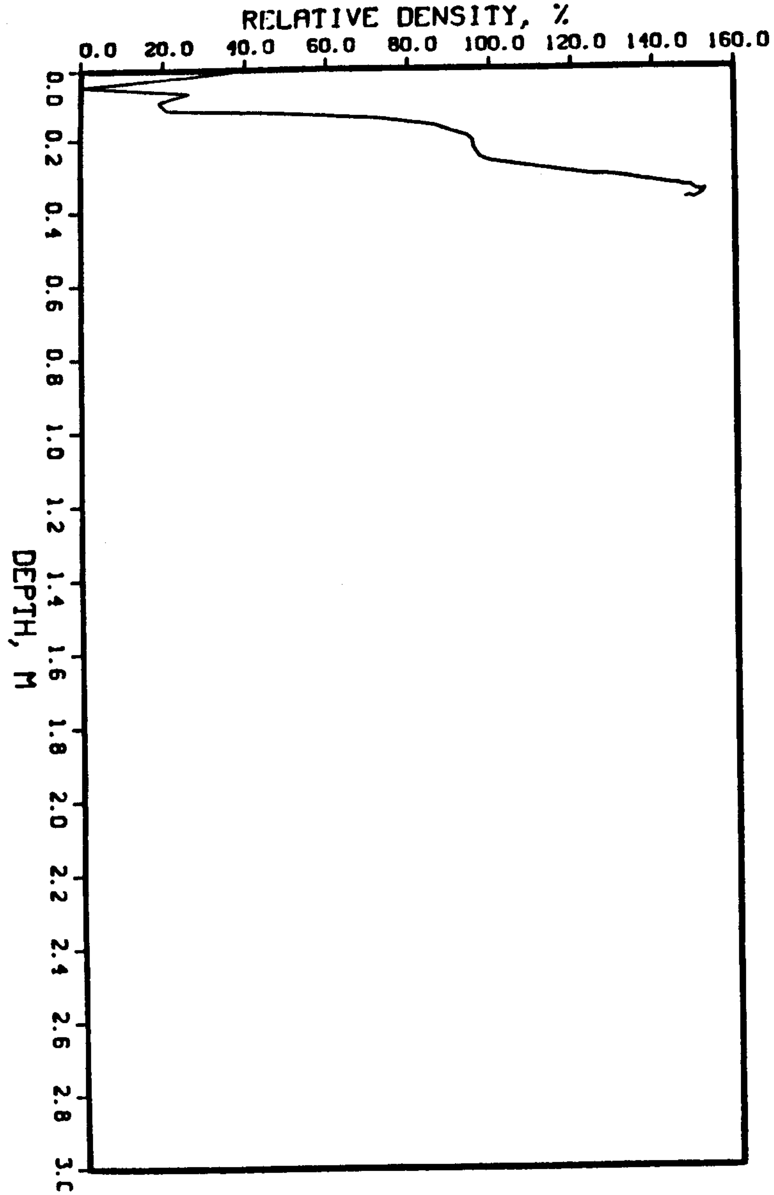
RELATIVE DENSITY, %
0.0 20.0 40.0 60.0 80.0 100.0 120.0 140.0 160.0
DEPTH, M
0.0 0.2 0.4 0.6 0.8 1.0 1.2 1.4 1.6 1.8 2.0 2.2 2.4 2.6 2.8 3.0

673 X2

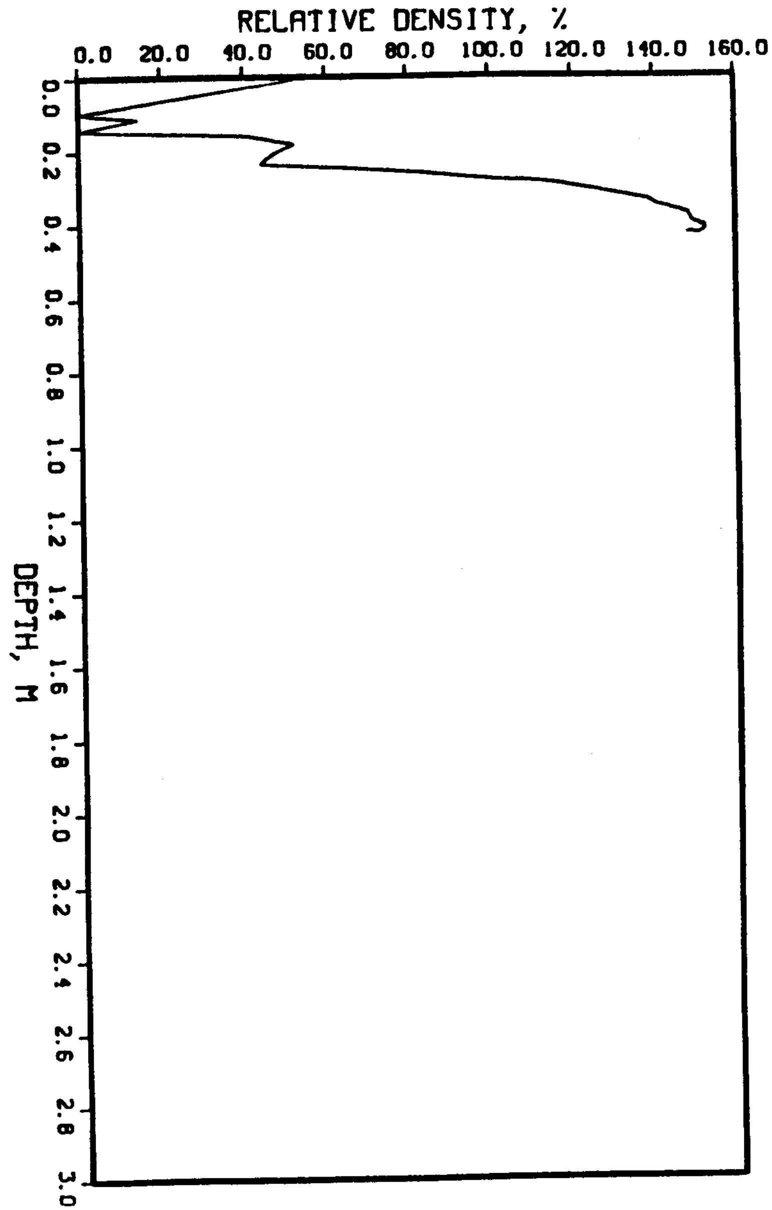
RELATIVE DENSITY, %
0.0
20.0
40.0
60.0
80.0
100.0
120.0
140.0
160.0
DEPTH, M
0.0
0.2
0.4
0.6
0.8
1.0
1.2
1.4
1.6
1.8
2.0
2.2
2.4
2.6
2.8
3.0

673 X3

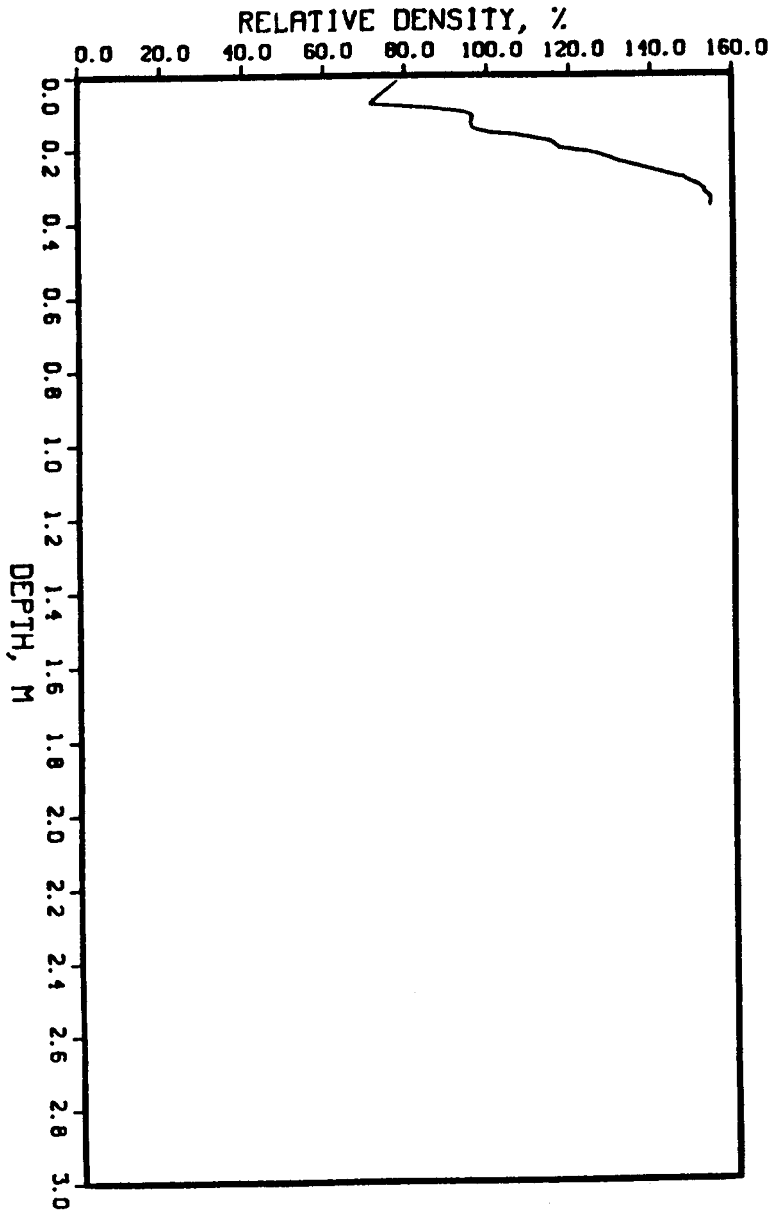
RELATIVE DENSITY, %
0.0 20.0 40.0 60.0 80.0 100.0 120.0 140.0 160.0
DEPTH, M
0.0 0.2 0.4 0.6 0.8 1.0 1.2 1.4 1.6 1.8 2.0 2.2 2.4 2.6 2.8 3.0

673 X4

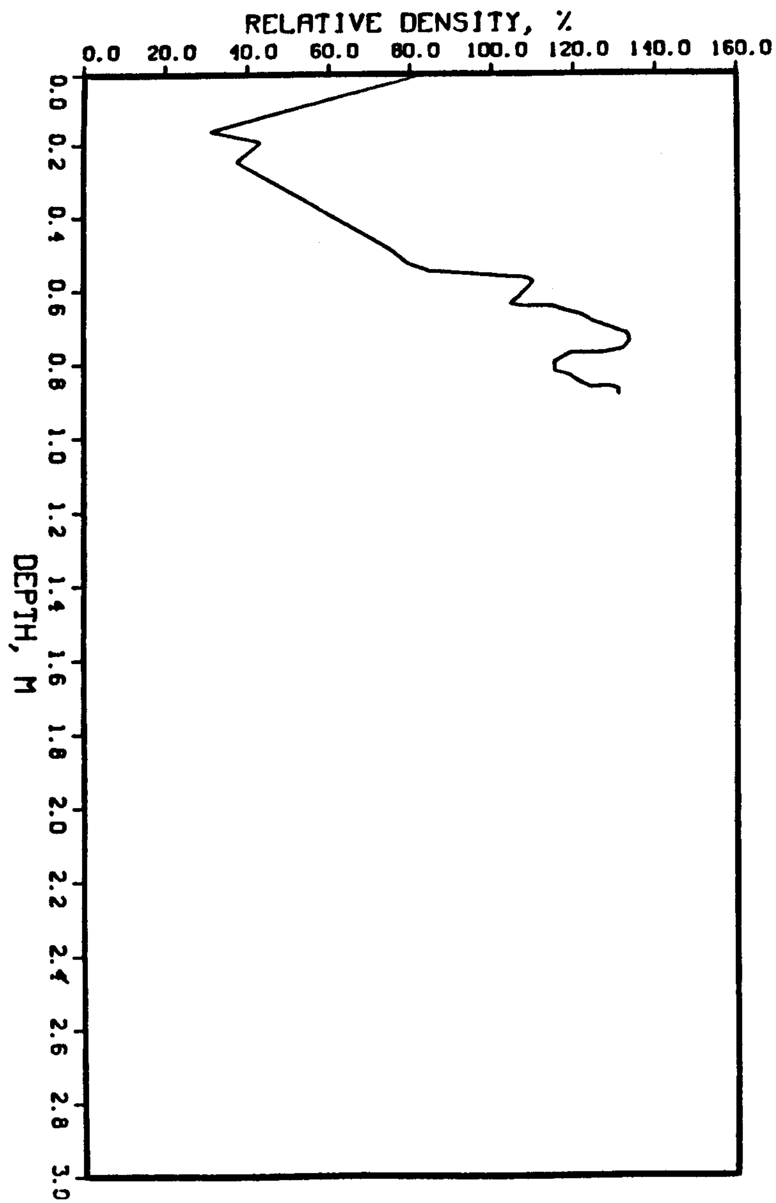
RELATIVE DENSITY, %
0.0 20.0 40.0 60.0 80.0 100.0 120.0 140.0 160.0
DEPTH, M
0.0 0.2 0.4 0.6 0.8 1.0 1.2 1.4 1.6 1.8 2.0 2.2 2.4 2.6 2.8 3.0

674 X1

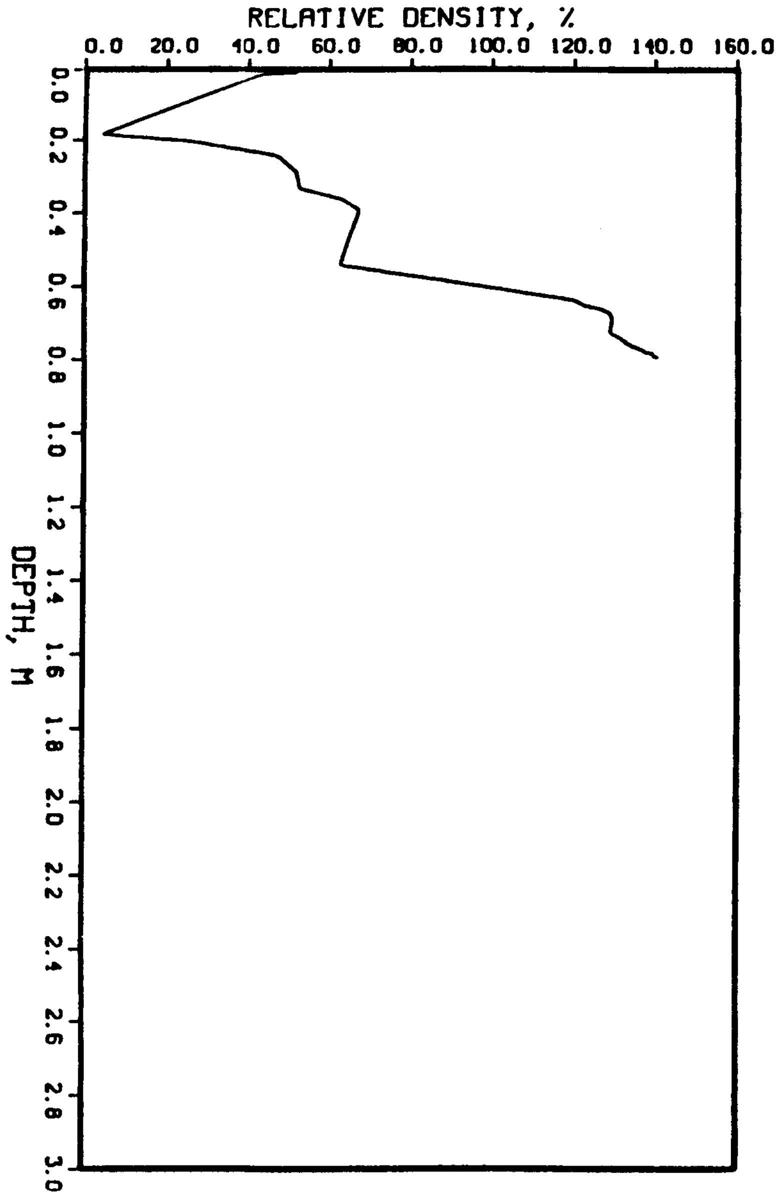
RELATIVE DENSITY, %
0.0 20.0 40.0 60.0 80.0 100.0 120.0 140.0 160.0
DEPTH, M
0.0 0.2 0.4 0.6 0.8 1.0 1.2 1.4 1.6 1.8 2.0 2.2 2.4 2.6 2.8 3.0

674 X2

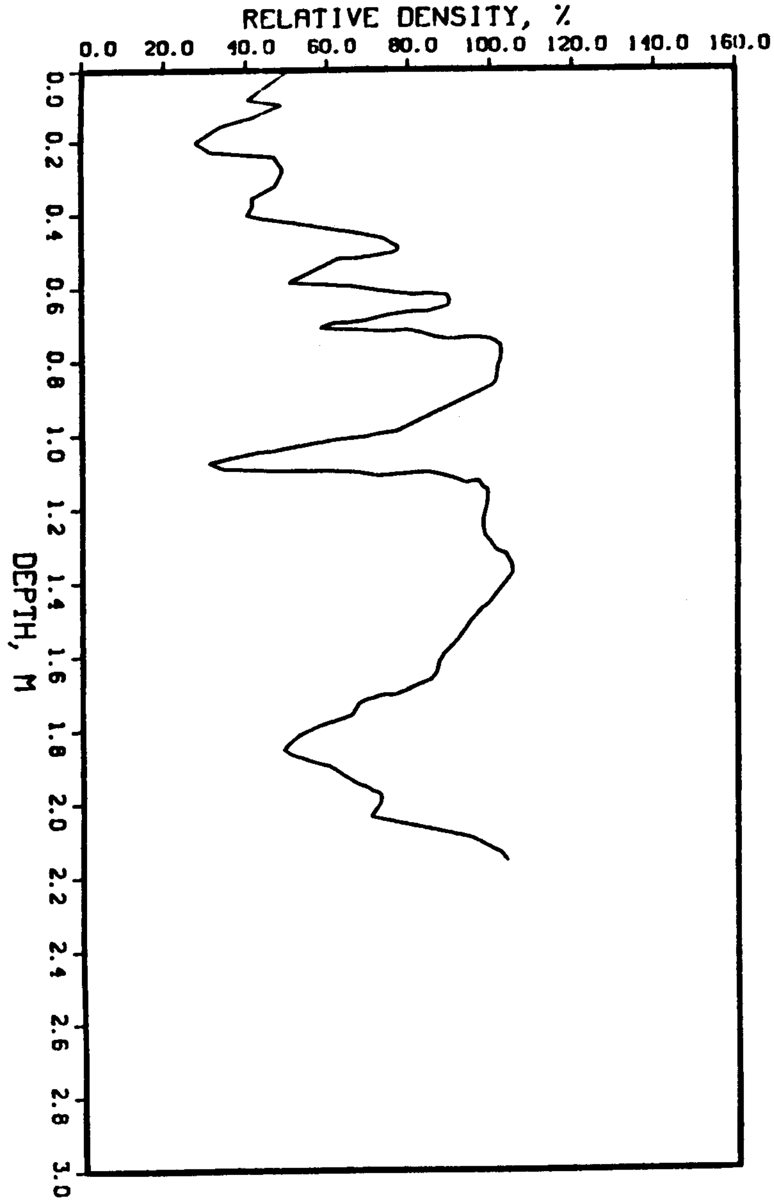
RELATIVE DENSITY, %
0.0 20.0 40.0 60.0 80.0 100.0 120.0 140.0 160.0
DEPTH, M
0.0 0.2 0.4 0.6 0.8 1.0 1.2 1.4 1.6 1.8 2.0 2.2 2.4 2.6 2.8 3.0

675 X1

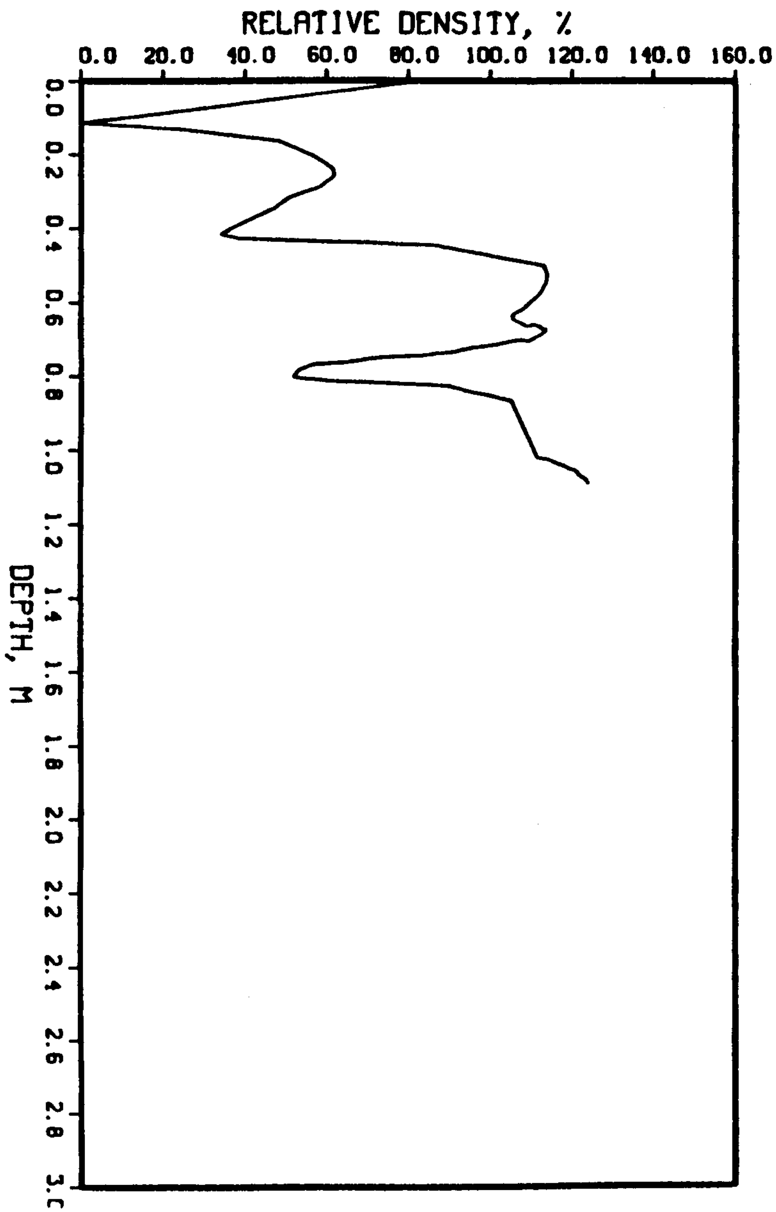
RELATIVE DENSITY, %
0.0 20.0 40.0 60.0 80.0 100.0 120.0 140.0 160.0
DEPTH, M
0.0 0.2 0.4 0.6 0.8 1.0 1.2 1.4 1.6 1.8 2.0 2.2 2.4 2.6 2.8 3.0

675 X2

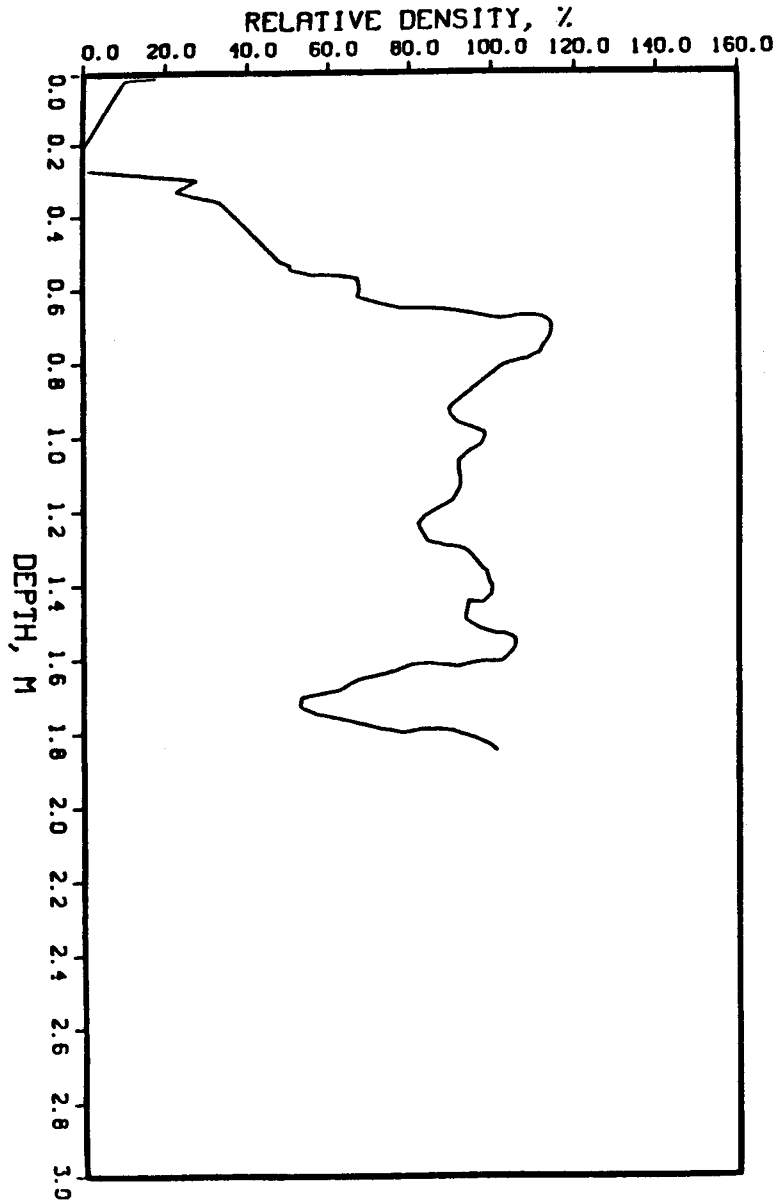
RELATIVE DENSITY, %
0.0 20.0 40.0 60.0 80.0 100.0 120.0 140.0 160.0
DEPTH, M
0.0 0.2 0.4 0.6 0.8 1.0 1.2 1.4 1.6 1.8 2.0 2.2 2.4 2.6 2.8 3.0

675 X3

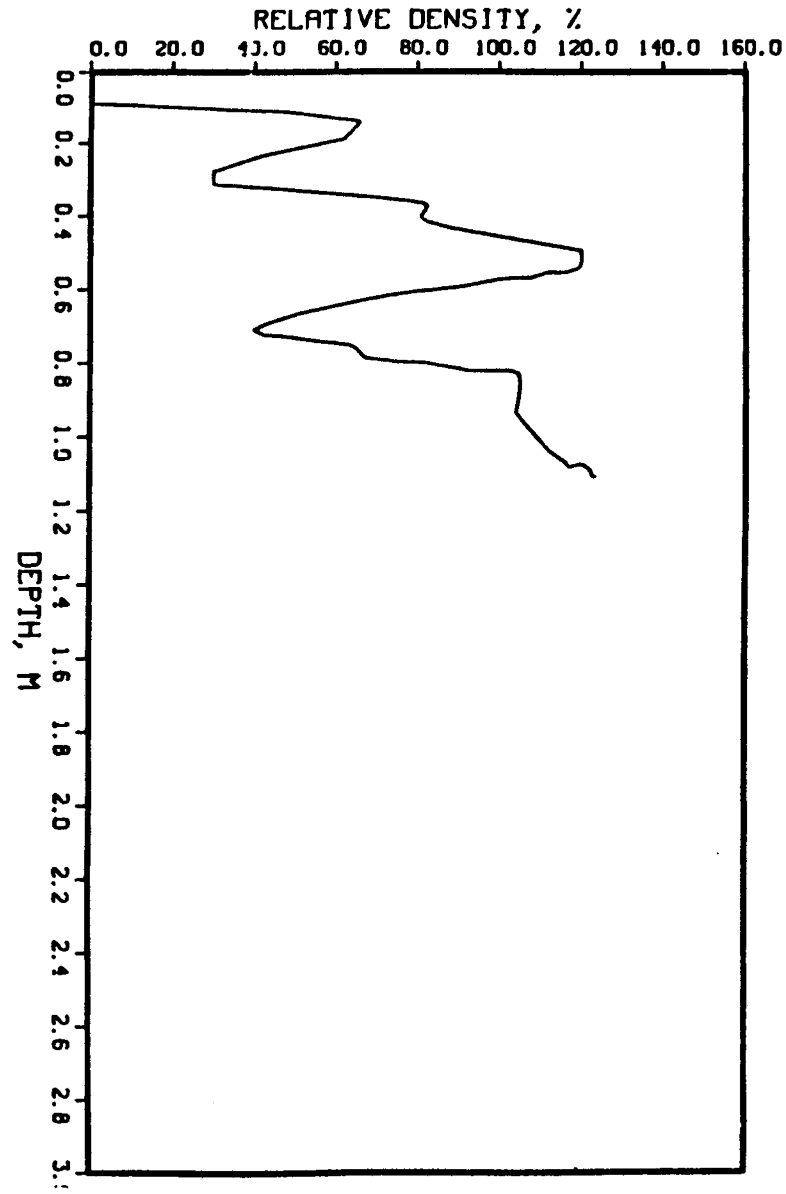
RELATIVE DENSITY, %
0.0 20.0 40.0 60.0 80.0 100.0 120.0 140.0 160.0
DEPTH, M
0.0 0.2 0.4 0.6 0.8 1.0 1.2 1.4 1.6 1.8 2.0 2.2 2.4 2.6 2.8

675 X4

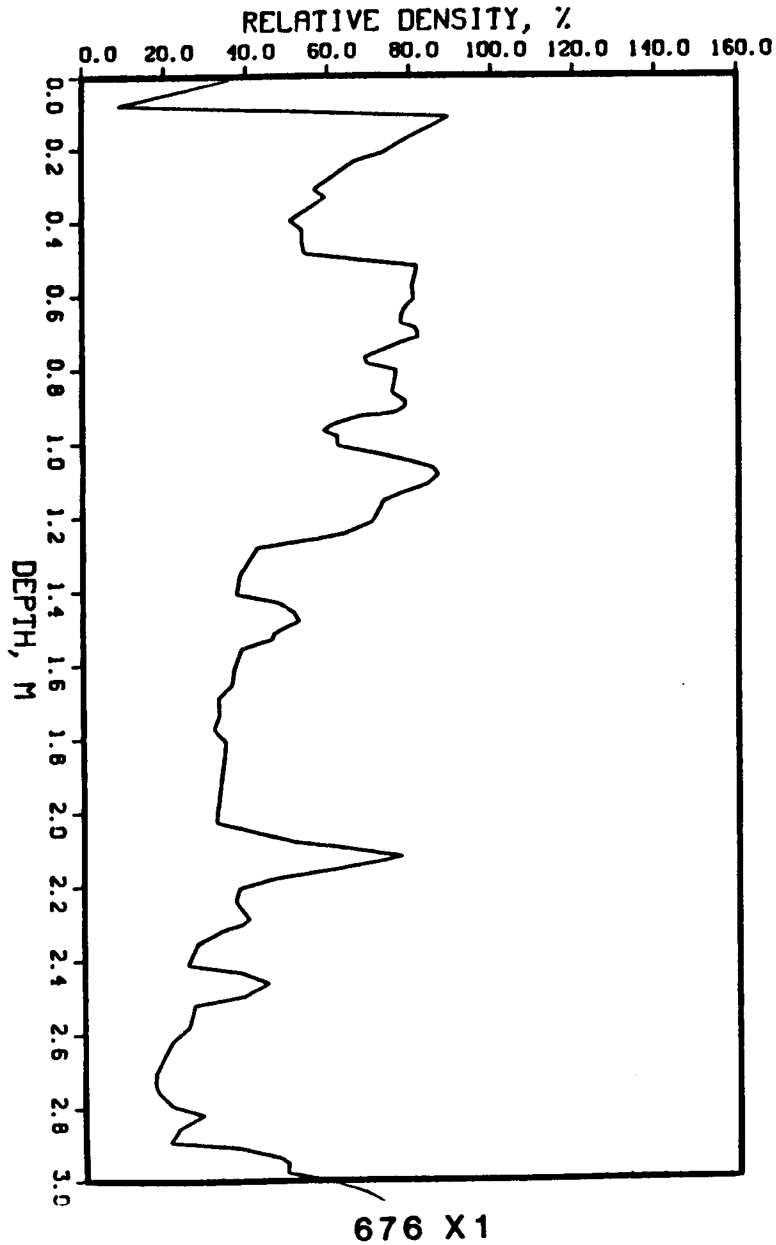
RELATIVE DENSITY, %
0.0 20.0 40.0 60.0 80.0 100.0 120.0 140.0 160.0
DEPTH, M
0.0 0.2 0.4 0.6 0.8 1.0 1.2 1.4 1.6 1.8 2.0 2.2 2.4 2.6 2.8 3.0
676 X1

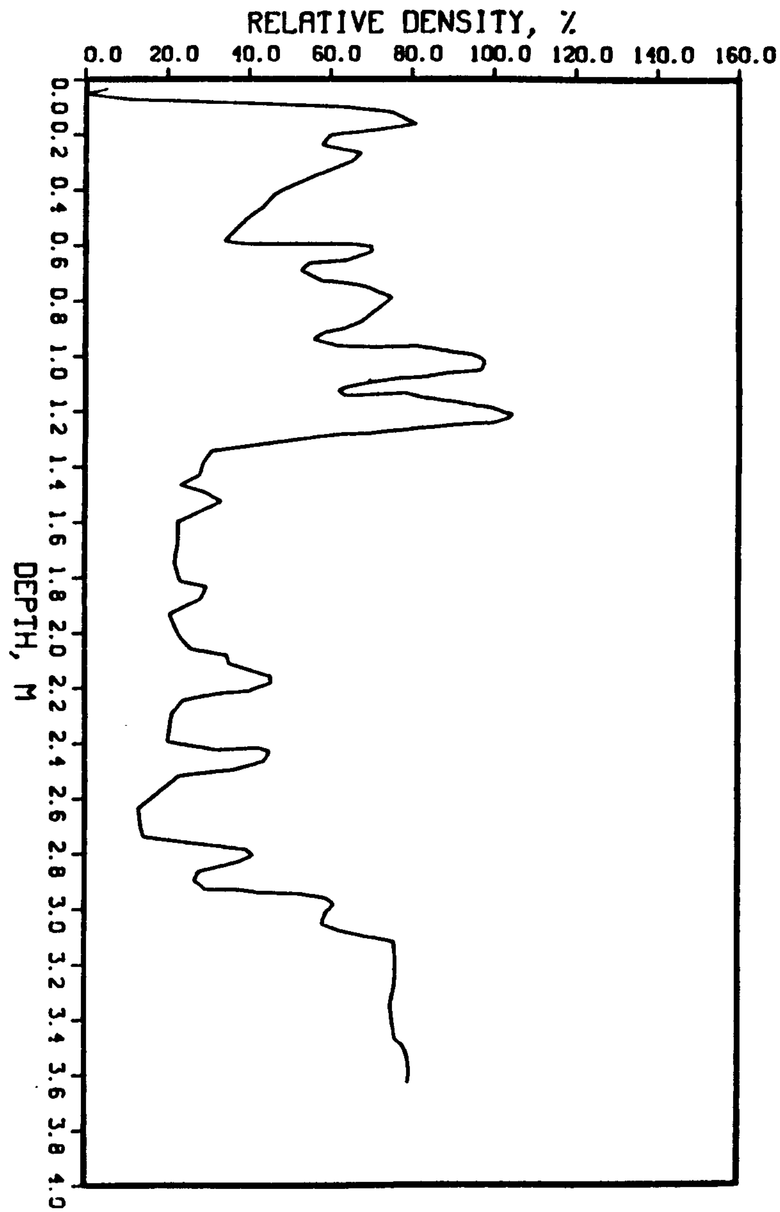
RELATIVE DENSITY, %
0.0 20.0 40.0 60.0 80.0 100.0 120.0 140.0 160.0
DEPTH, M
0.0 0.2 0.4 0.6 0.8 1.0 1.2 1.4 1.6 1.8 2.0 2.2 2.4 2.6 2.8 3.0 3.2 3.4 3.6 3.8 4.0

676 X2

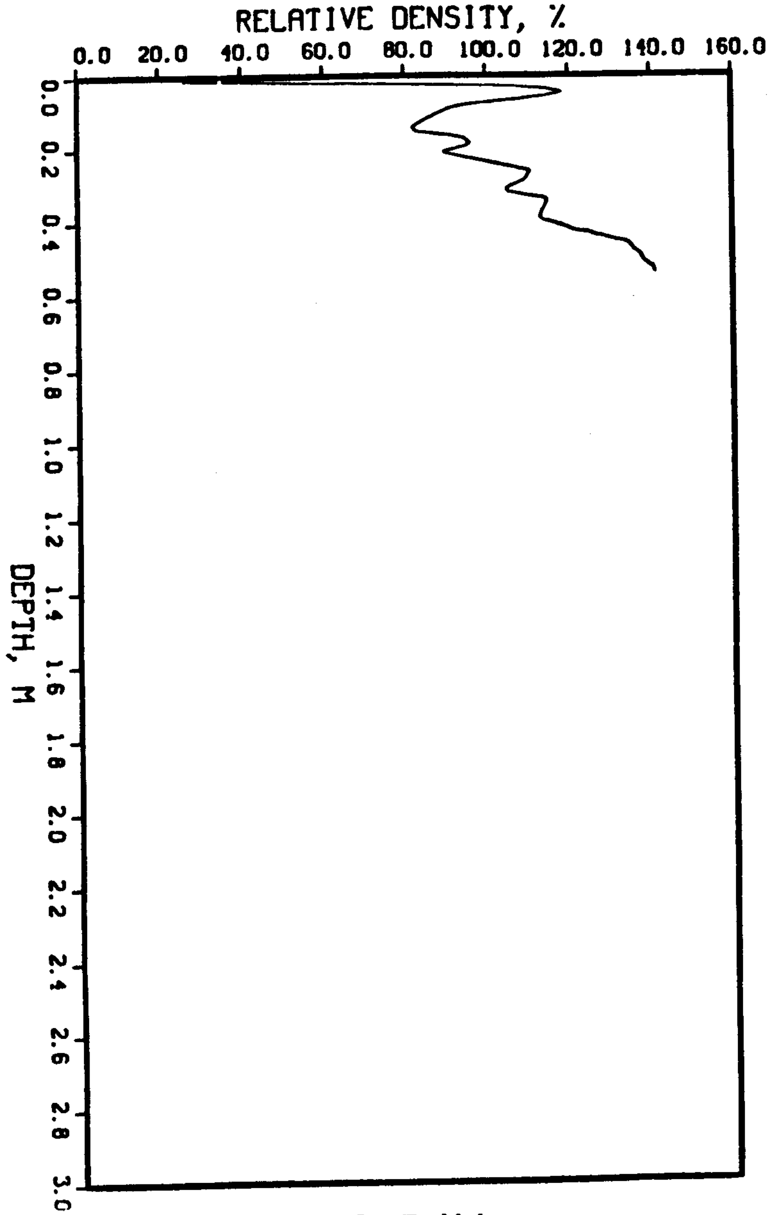
RELATIVE DENSITY, %
0.0
20.0
40.0
60.0
80.0
100.0
120.0
140.0
160.0
DEPTH, M
0.0
0.2
0.4
0.6
0.8
1.0
1.2
1.4
1.6
1.8
2.0
2.2
2.4
2.6
2.8
3.0

677 X1

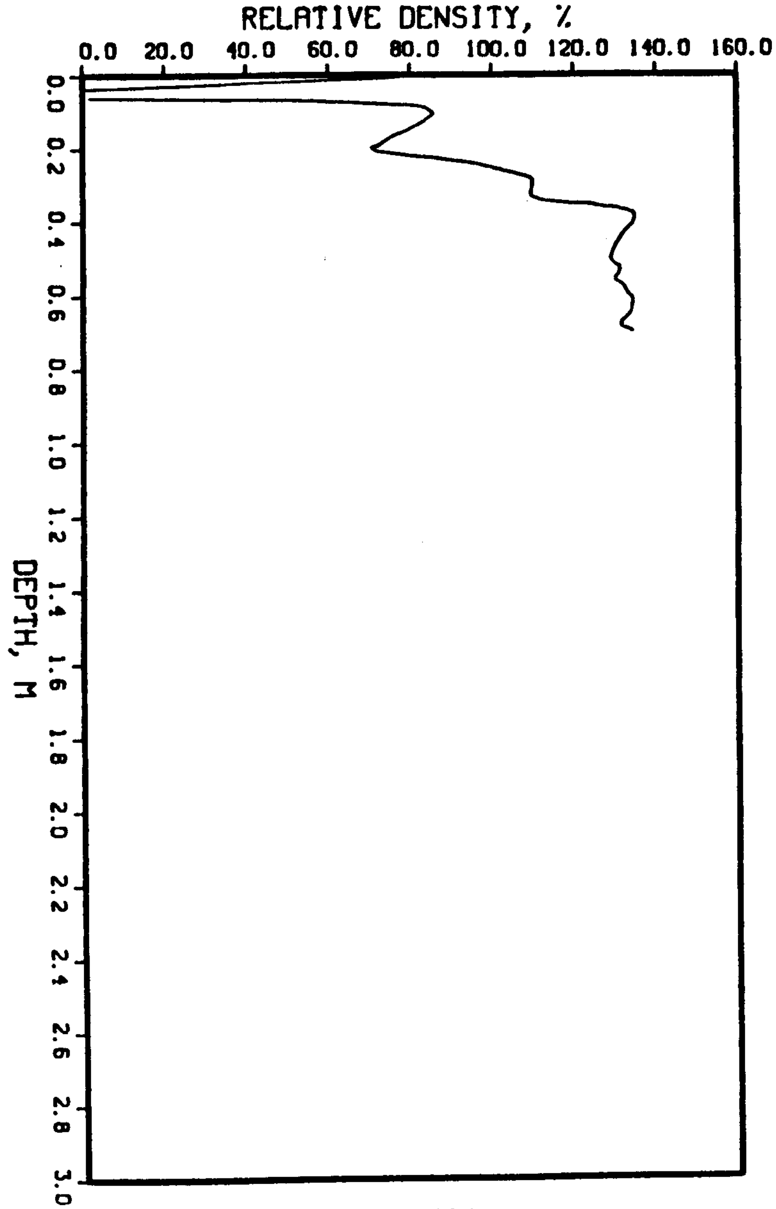
RELATIVE DENSITY, %
0.0 20.0 40.0 60.0 80.0 100.0 120.0 140.0 160.0
DEPTH, M
0.0 0.2 0.4 0.6 0.8 1.0 1.2 1.4 1.6 1.8 2.0 2.2 2.4 2.6 2.8 3.0

677 X2

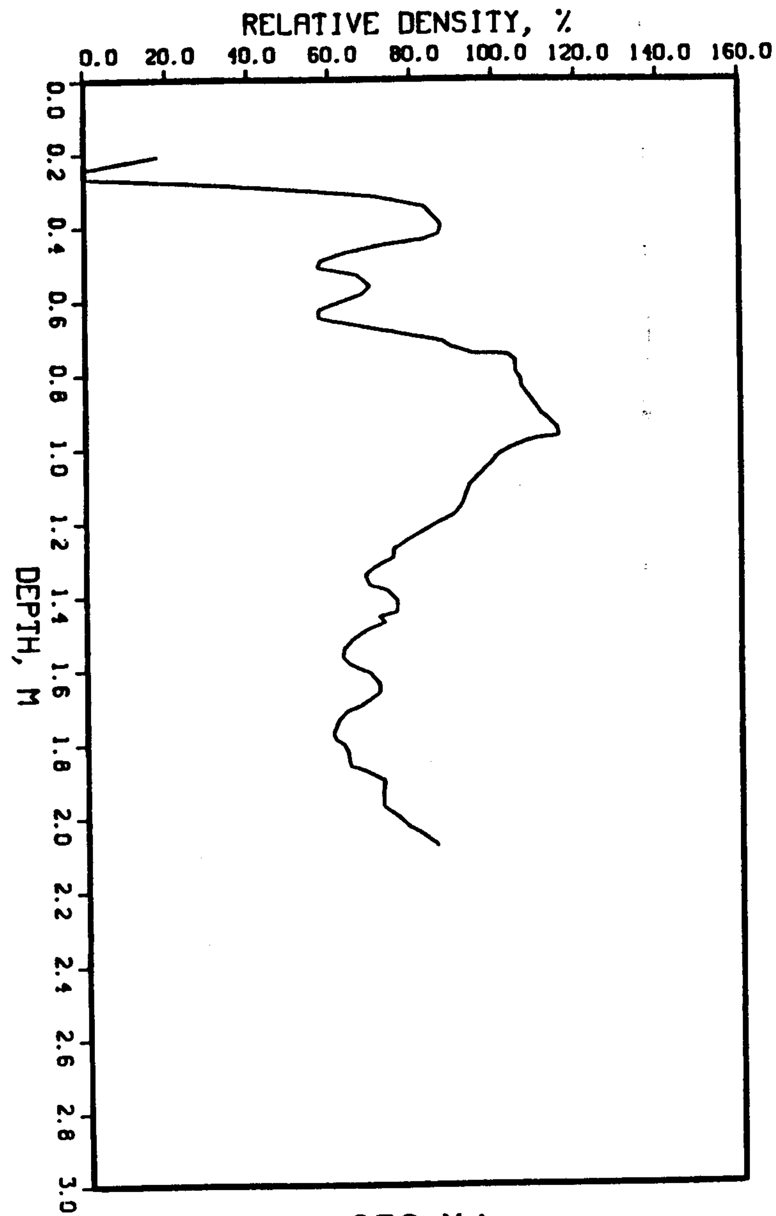
RELATIVE DENSITY, %
0.0
20.0
40.0
60.0
80.0
100.0
120.0
140.0
160.0
DEPTH, M
0.0
0.2
0.4
0.6
0.8
1.0
1.2
1.4
1.6
1.8
2.0
2.2
2.4
2.6
2.8
3.0

678 X1

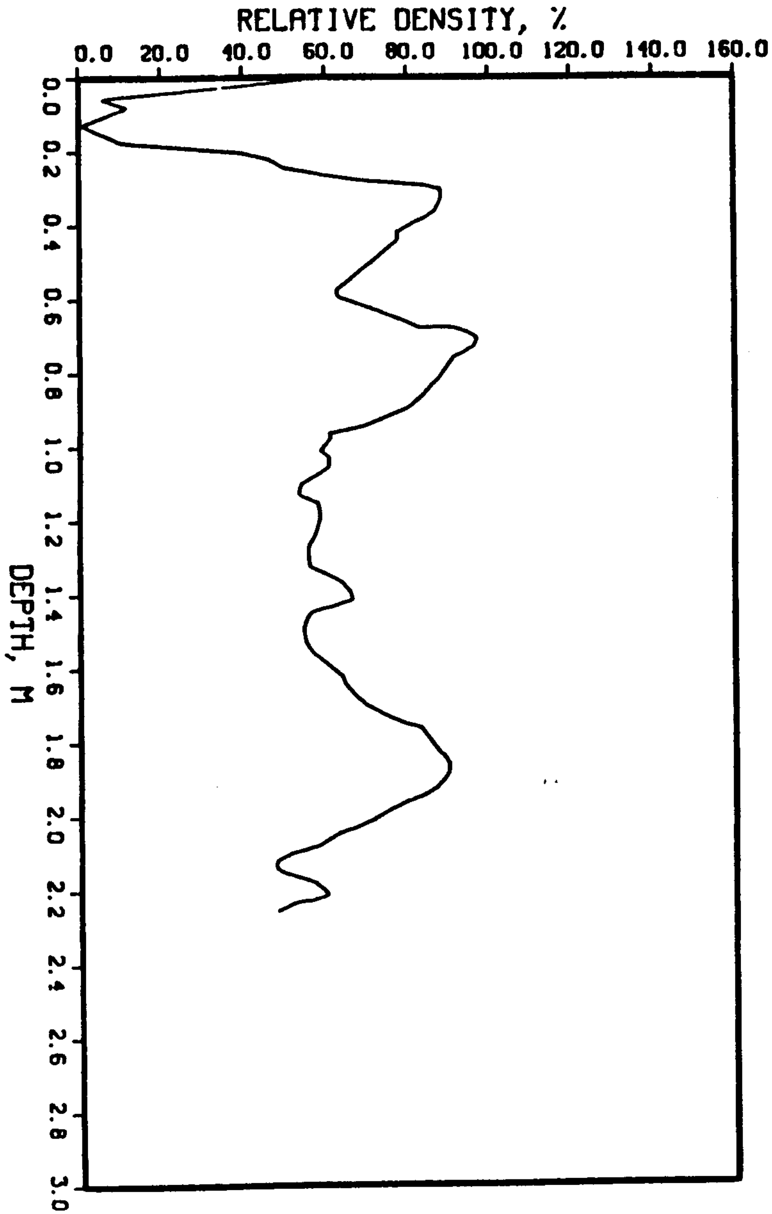
RELATIVE DENSITY, %
0.0 20.0 40.0 60.0 80.0 100.0 120.0 140.0 160.0
DEPTH, M
0.0 0.2 0.4 0.6 0.8 1.0 1.2 1.4 1.6 1.8 2.0 2.2 2.4 2.6 2.8 3.0

678 X2

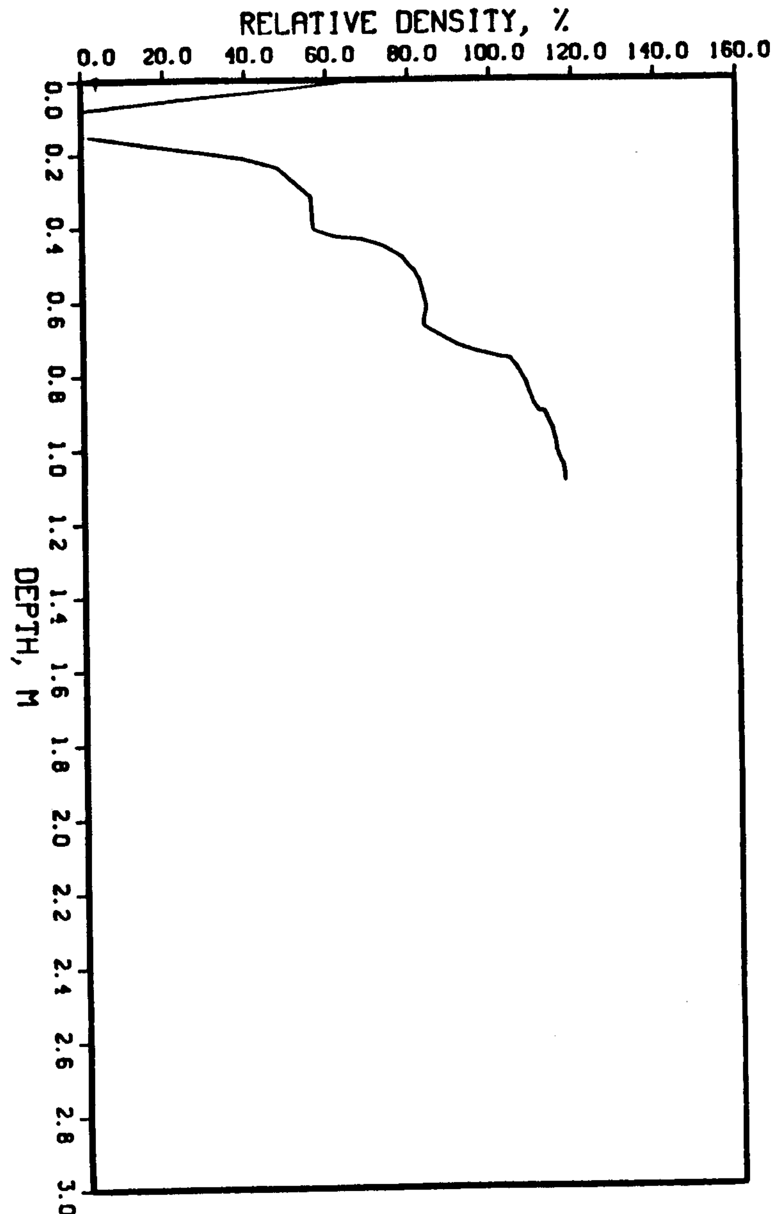
RELATIVE DENSITY, %
0.0 20.0 40.0 60.0 80.0 100.0 120.0 140.0 160.0
DEPTH, M
0.0 0.2 0.4 0.6 0.8 1.0 1.2 1.4 1.6 1.8 2.0 2.2 2.4 2.6 2.8 3.0

679 X1


0.0 20.0 40.0 60.0 80.0 100.0 120.0 140.0 160.0
DEPTH, M
0.0 0.2 0.4 0.6 0.8 1.0 1.2 1.4 1.6 1.8 2.0 2.2 2.4 2.6 2.8 3.0

679 X2

APPENDIX D:

CONSOLIDATION TEST PLOTS

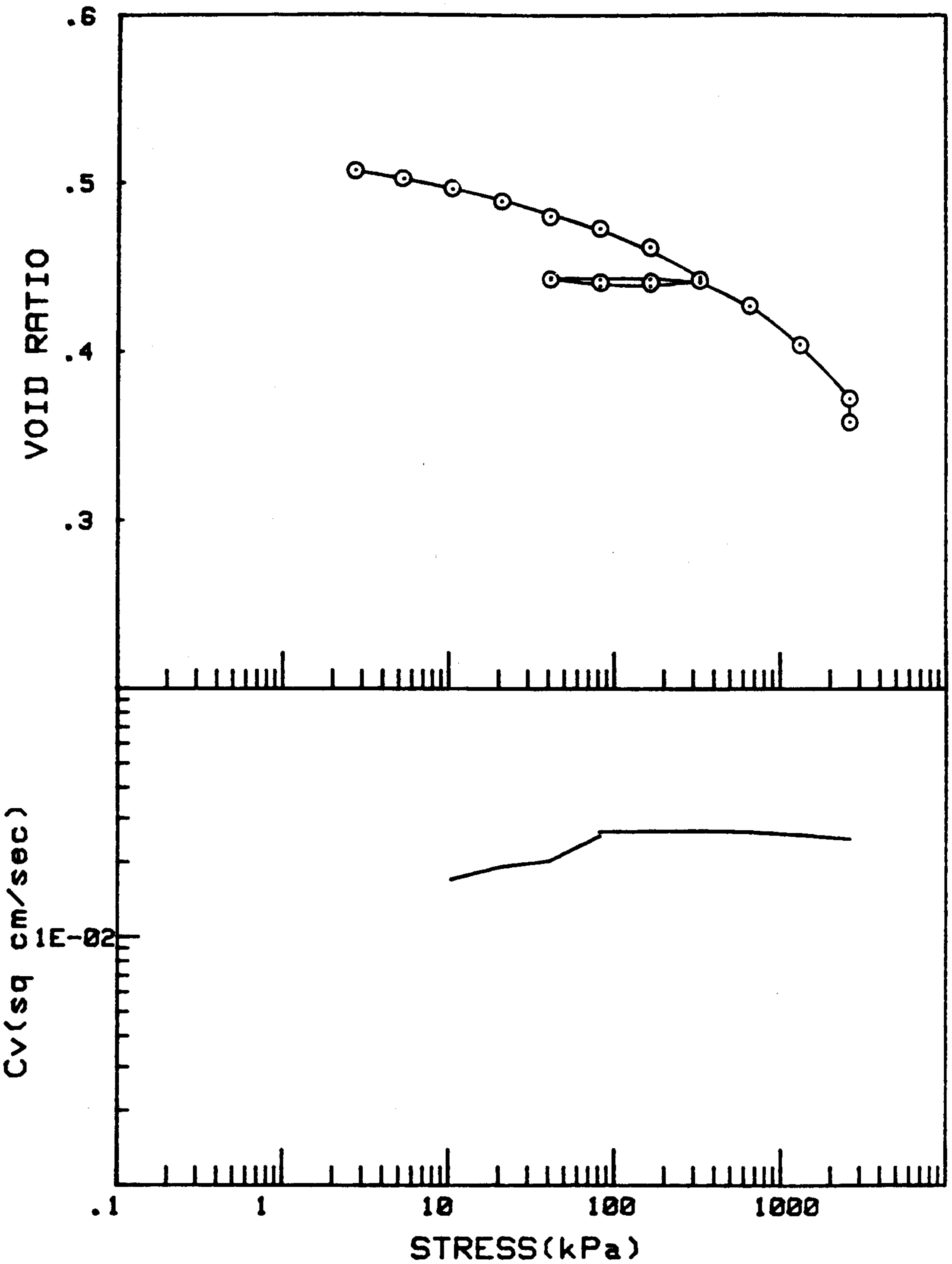

CRUISE DC4-81-NS		INCREMENT (cm)	212-214
CORE NO.	681A2	TEST NO.	OE36

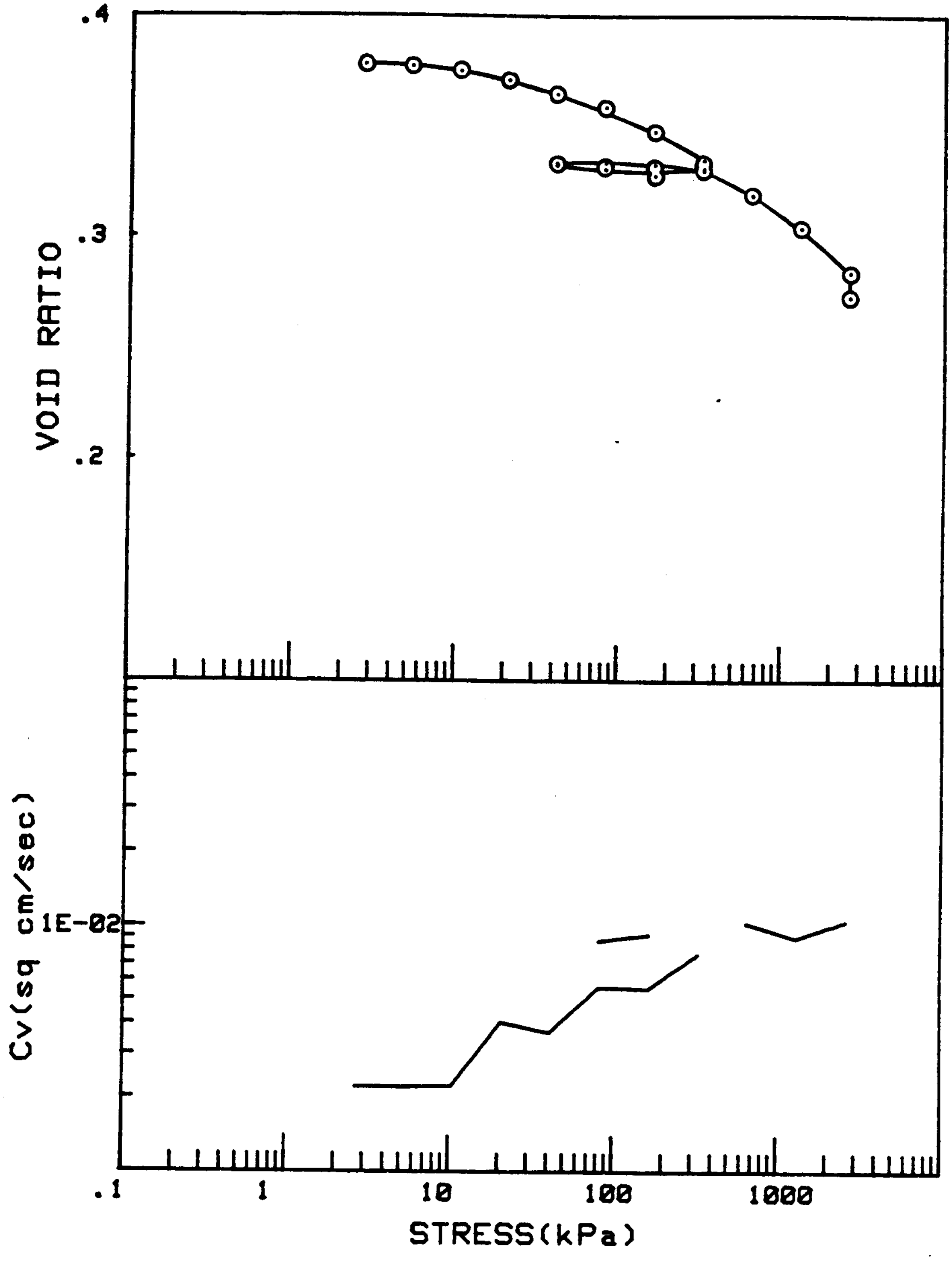

CRUISE DC4-81-NS		INCREMENT (cm)	552-554
CORE NO.	681A2	TEST NO.	OE38

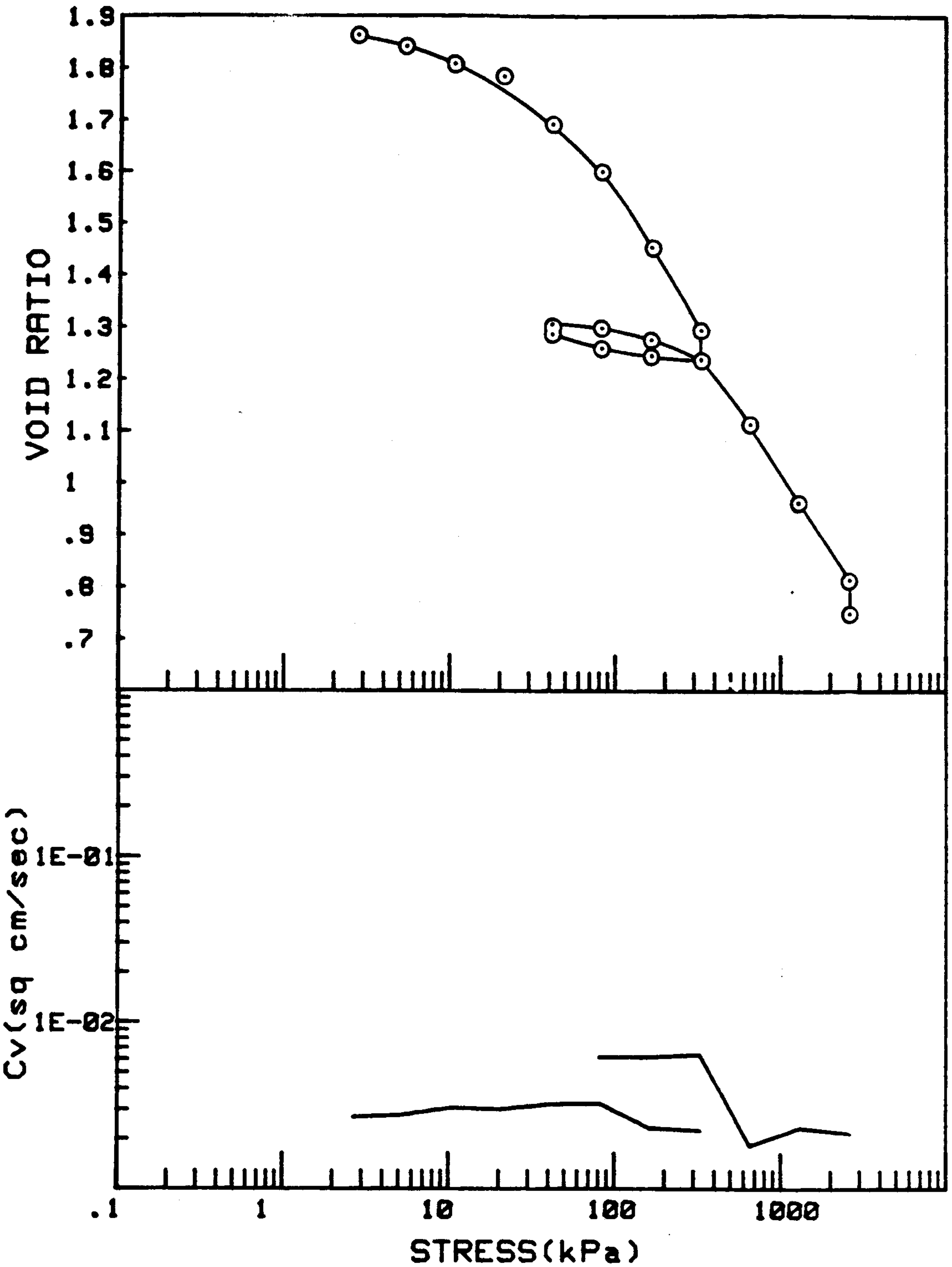

CRUISE DC4-81-NS		INCREMENT (cm)	146-148
CORE NO.	682A1	TEST NO.	OE34

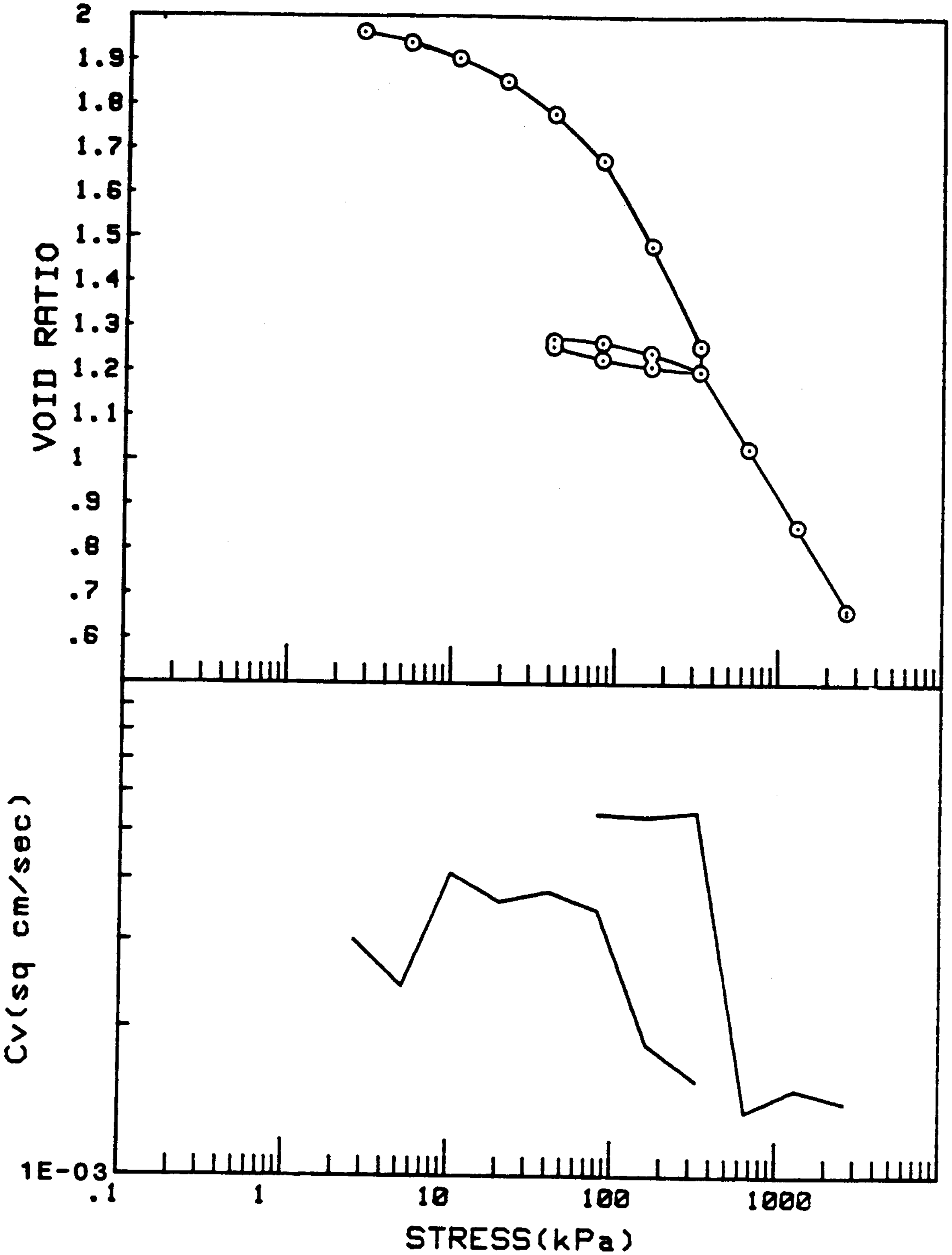

CRUISE DC4-81-NS	INCREMENT (cm)	290-292
CORE NO. 682A1	TEST NO.	OE35

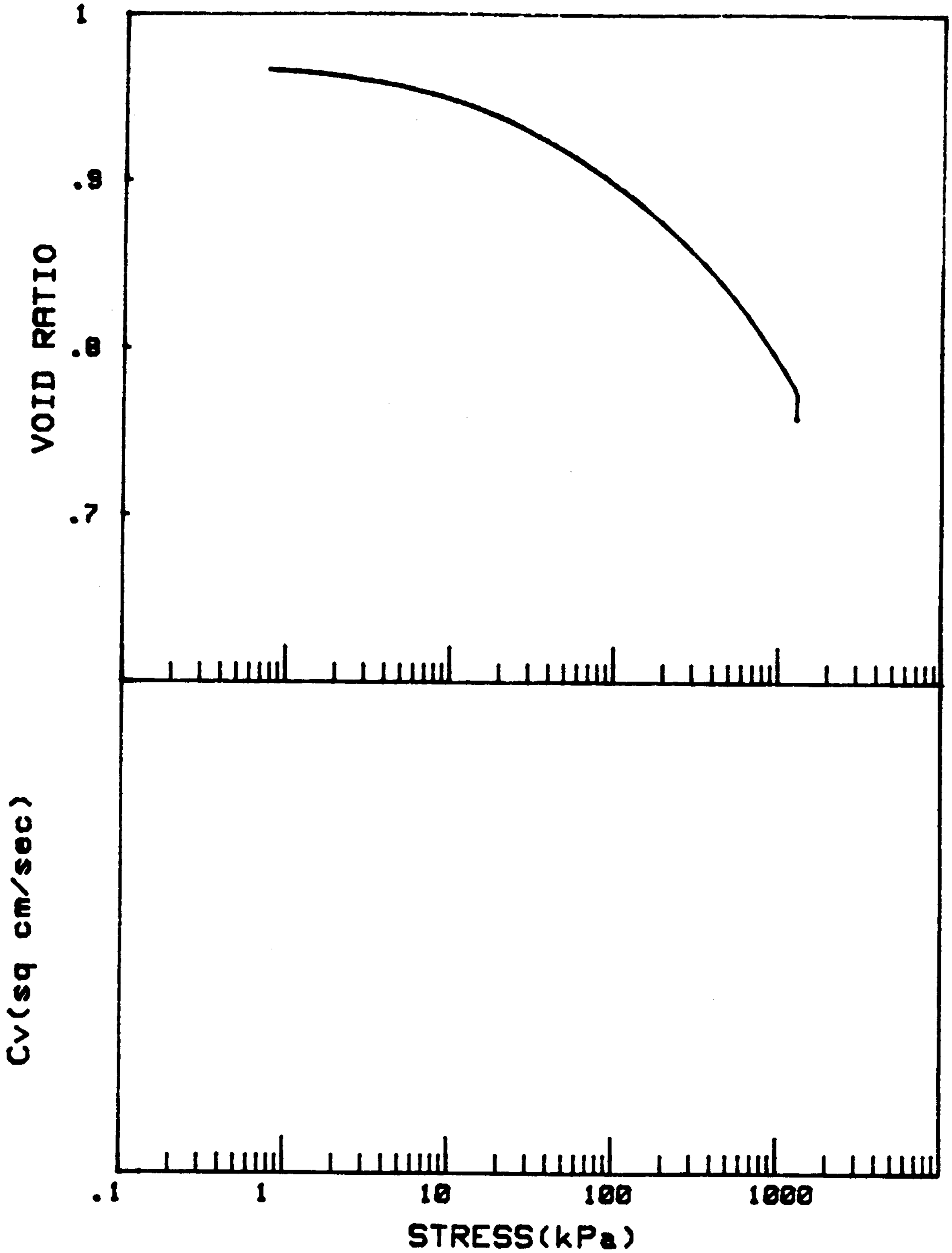

CRUISE DC4-81-NS		INCREMENT (cm)	458-464
CORE NO.	682A1	TEST NO.	CE19

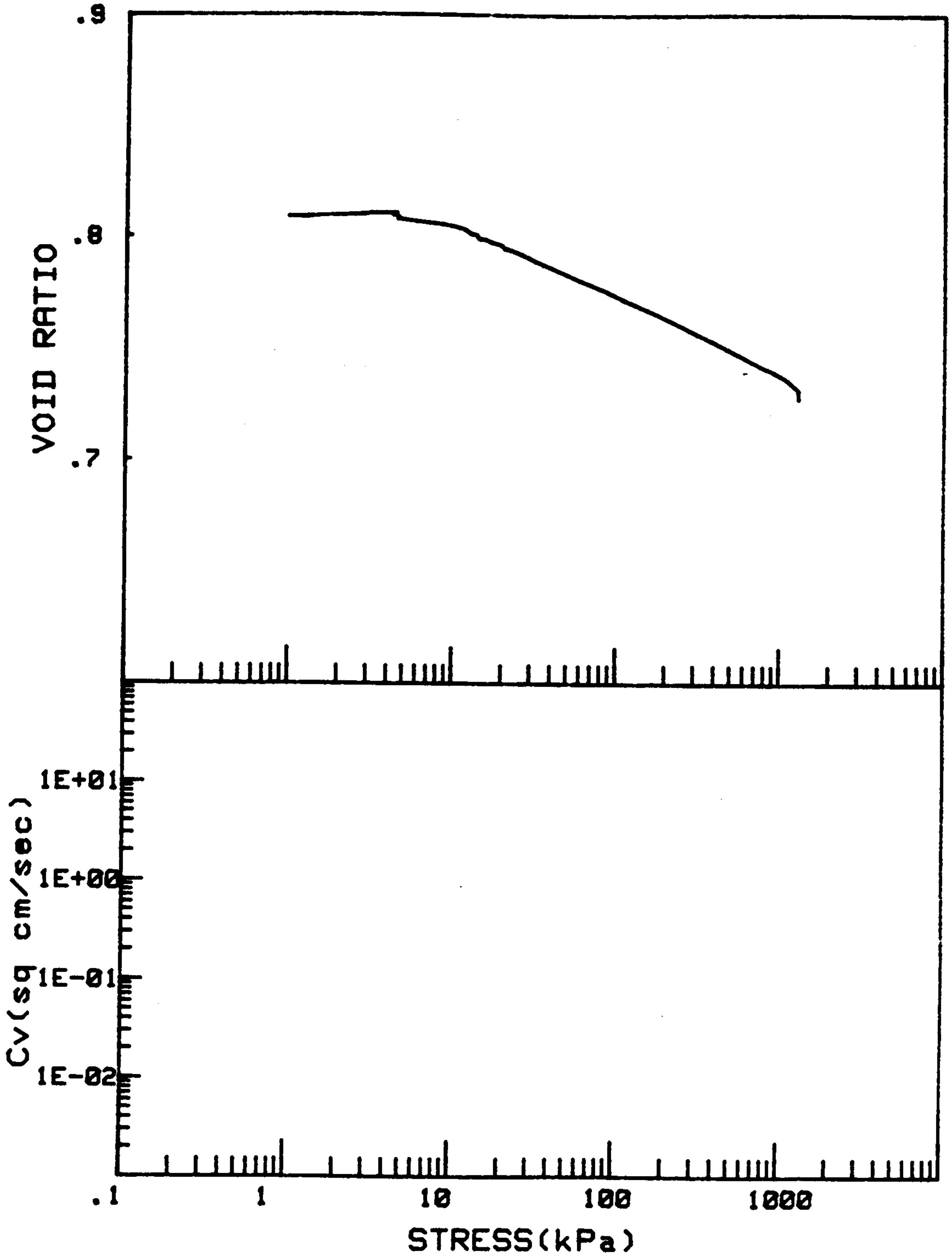

CRUISE DC4-81-NS		INCREMENT (cm)	147-152
CORE NO.	683A1	TEST NO.	CE34

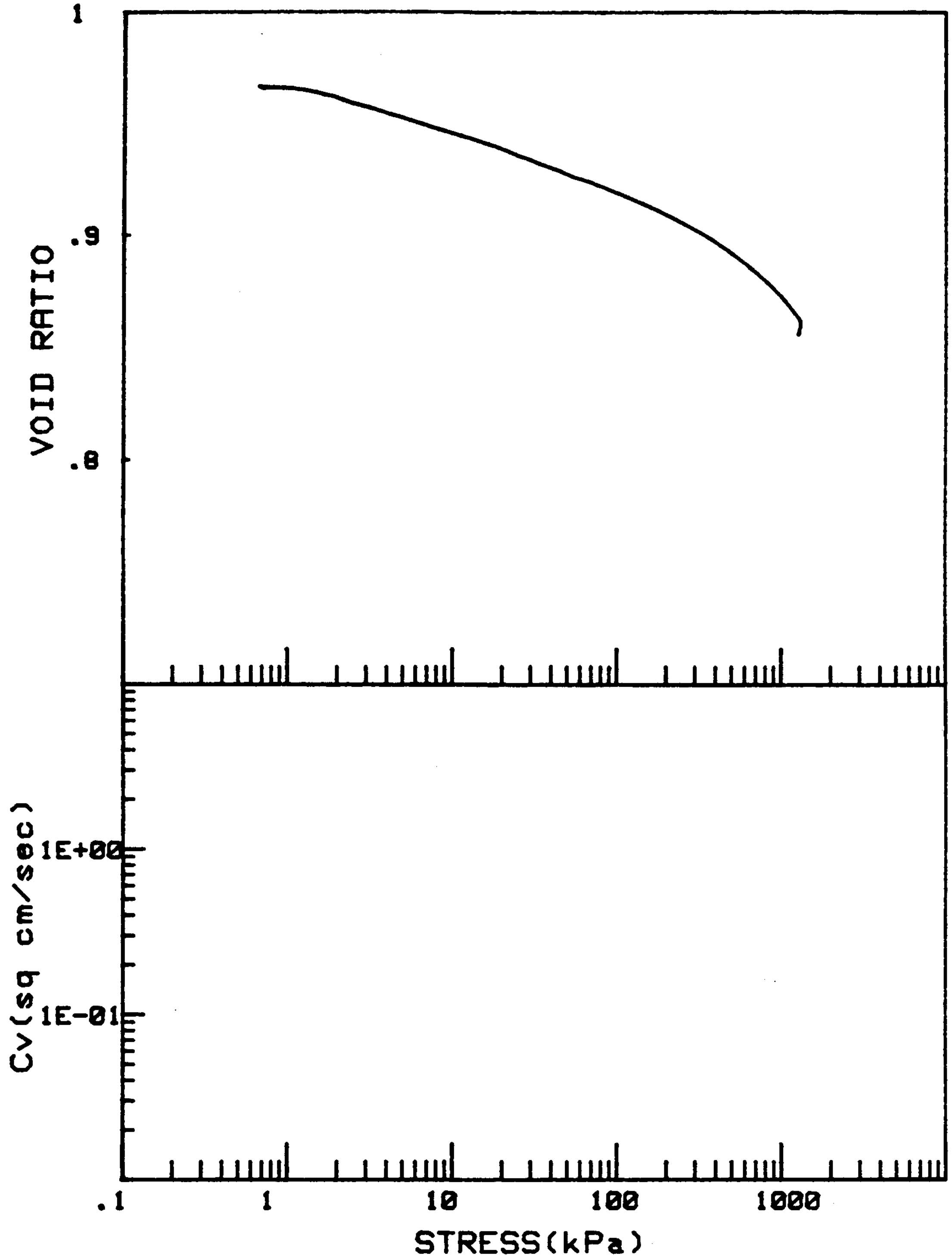

CRUISE DC4-81-NS		INCREMENT (cm)	252-257
CORE NO.	683A1	TEST NO.	CE35

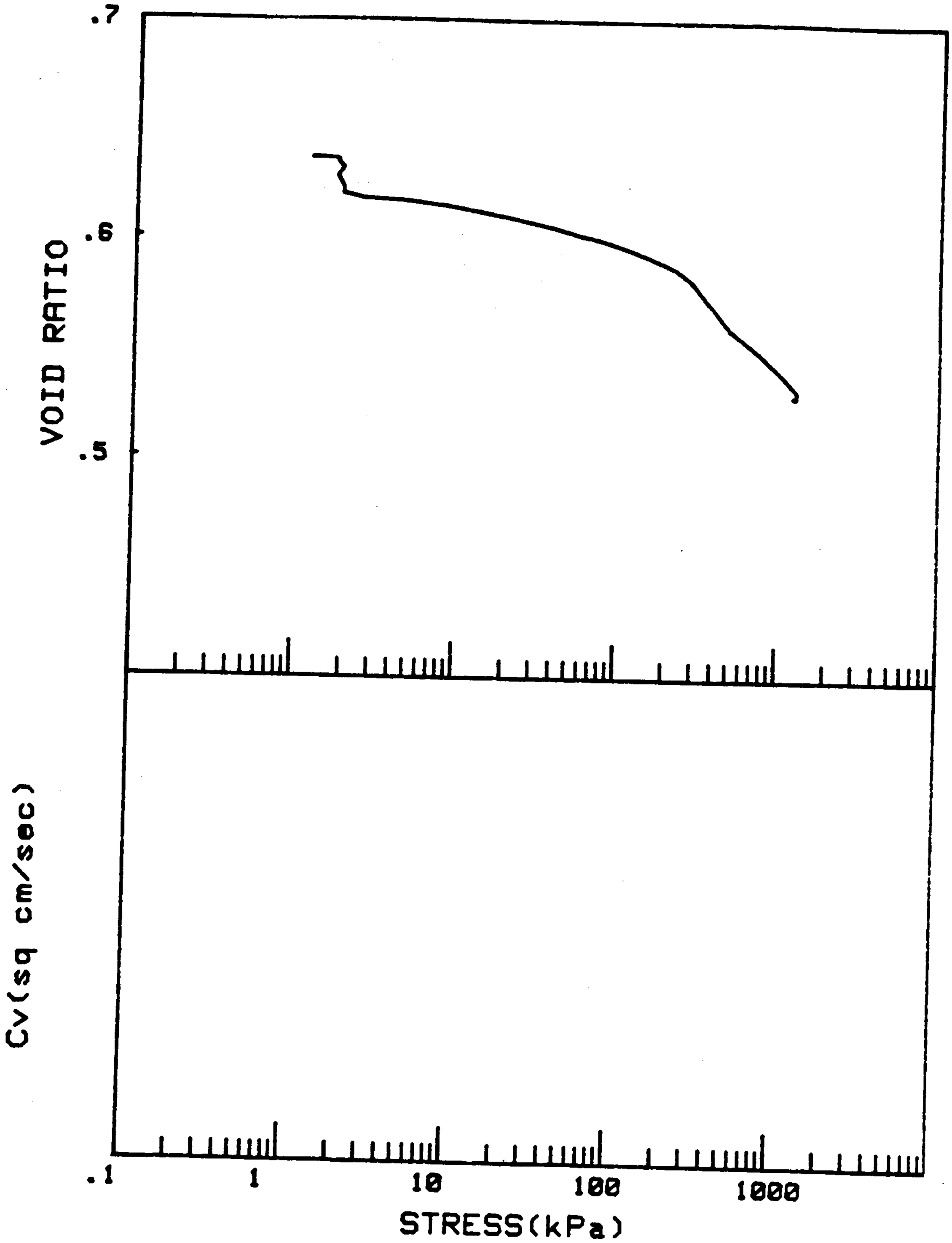

CRUISE DC4-81-NS		INCREMENT (cm)	446-448
CORE NO.	683A1	TEST NO.	CE43

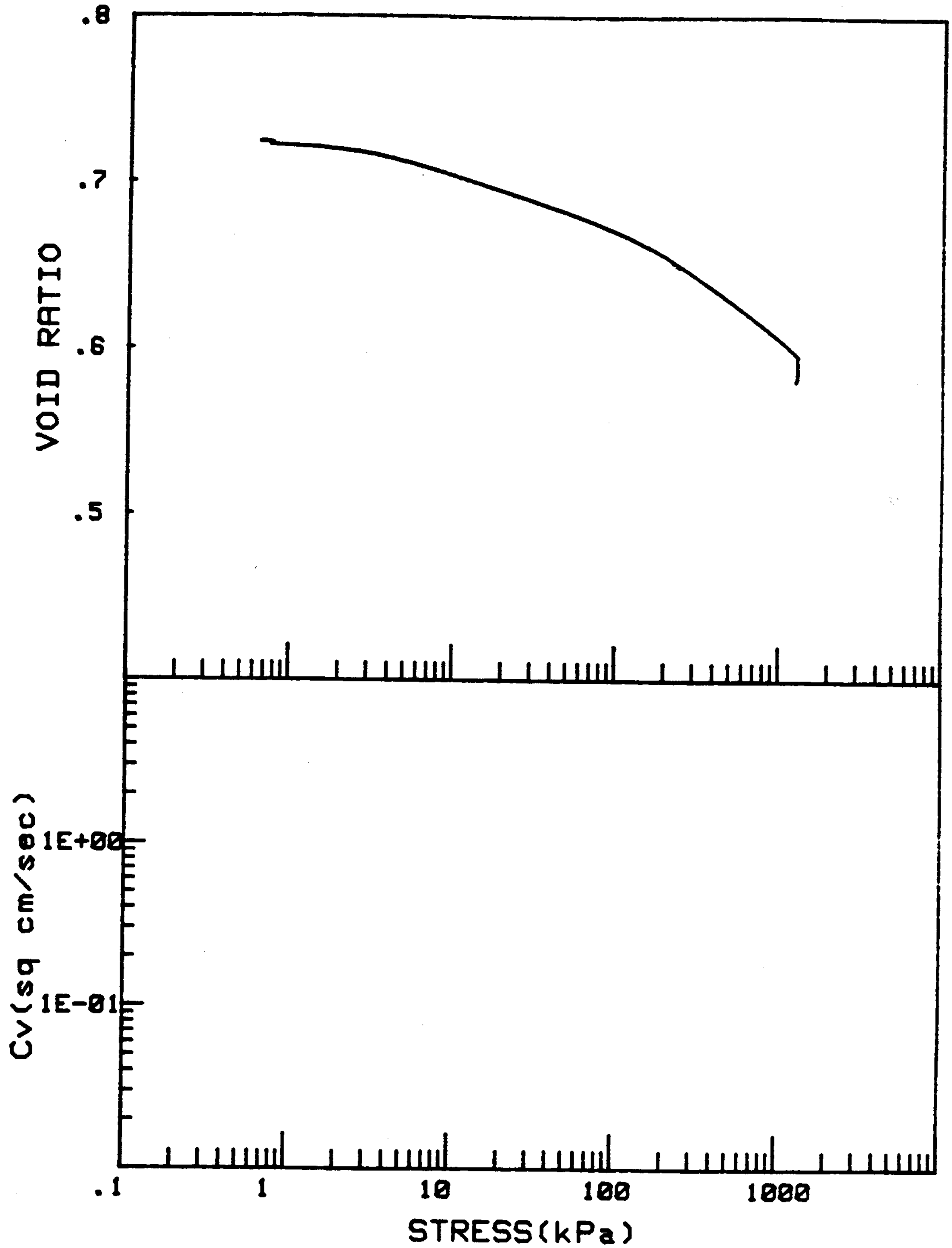

CRUISE DC4-81-NS	INCREMENT (cm)	35-40
CORE NO. 684A1	TEST NO.	CE37

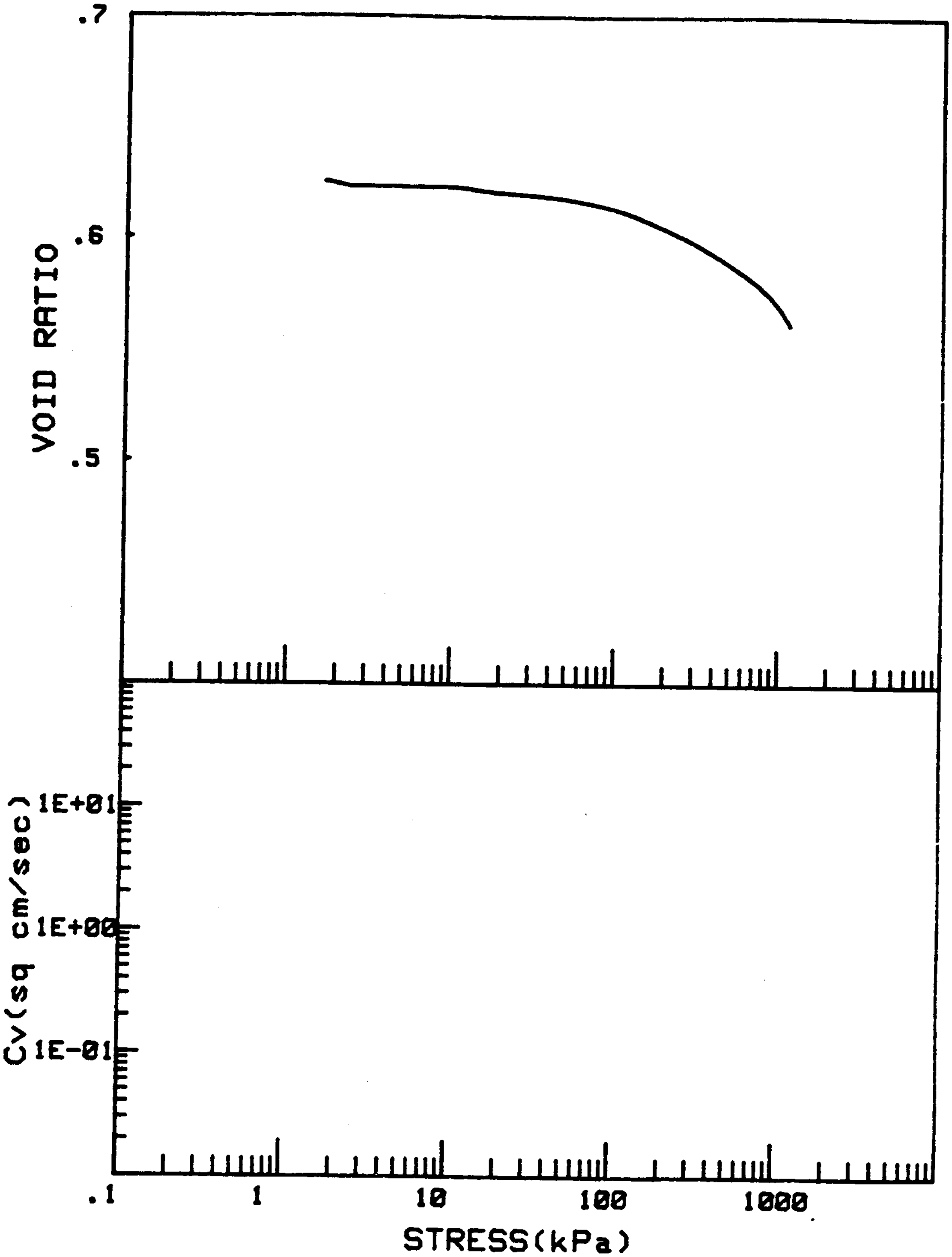

CRUISE DC4-81-NS		INCREMENT (cm)	106-108
CORE NO.	684A1	TEST NO.	CE47

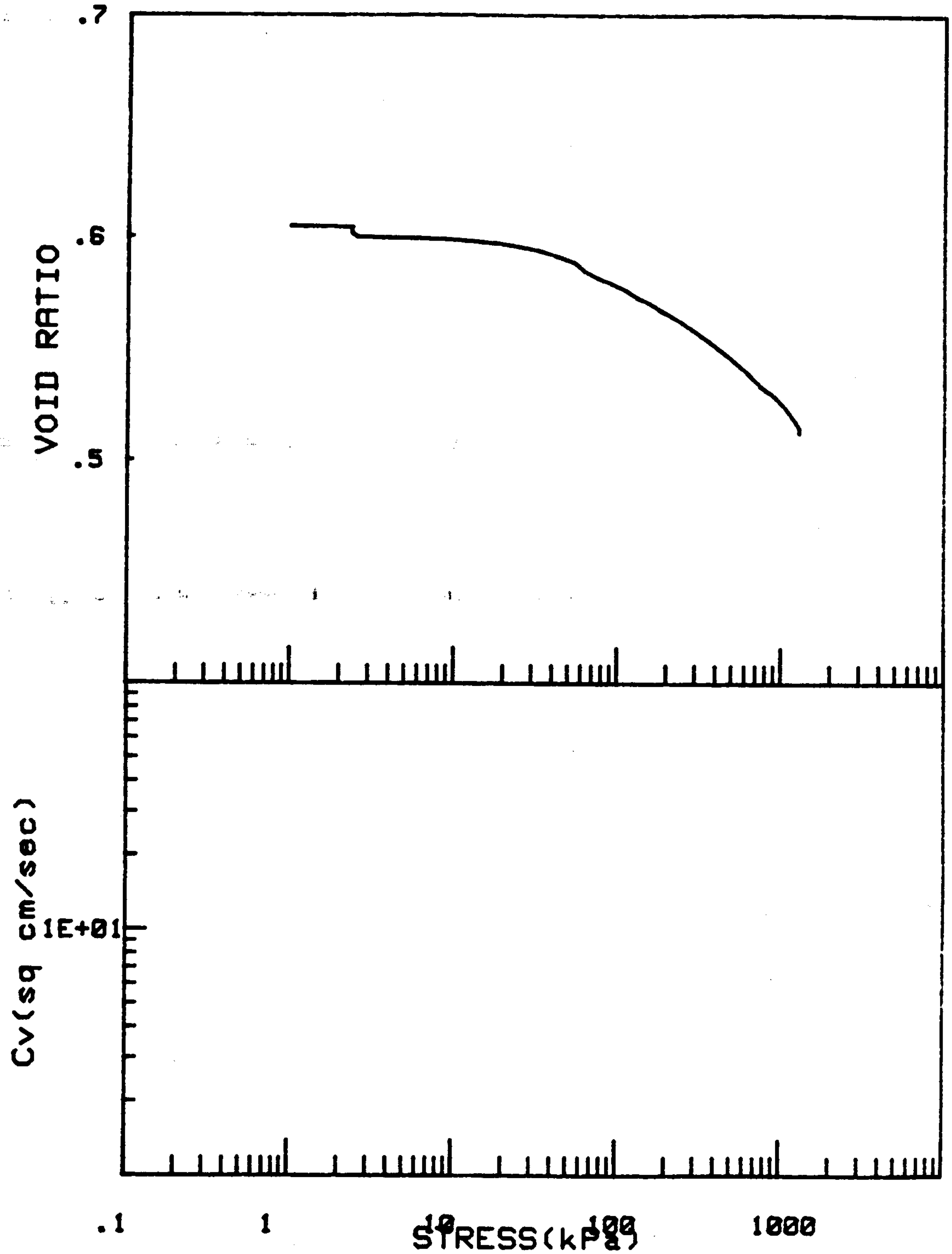

CRUISE	DC4-81-NS	INCREMENT (cm)	236-238
CORE NO.	684A1	TEST NO.	CE49

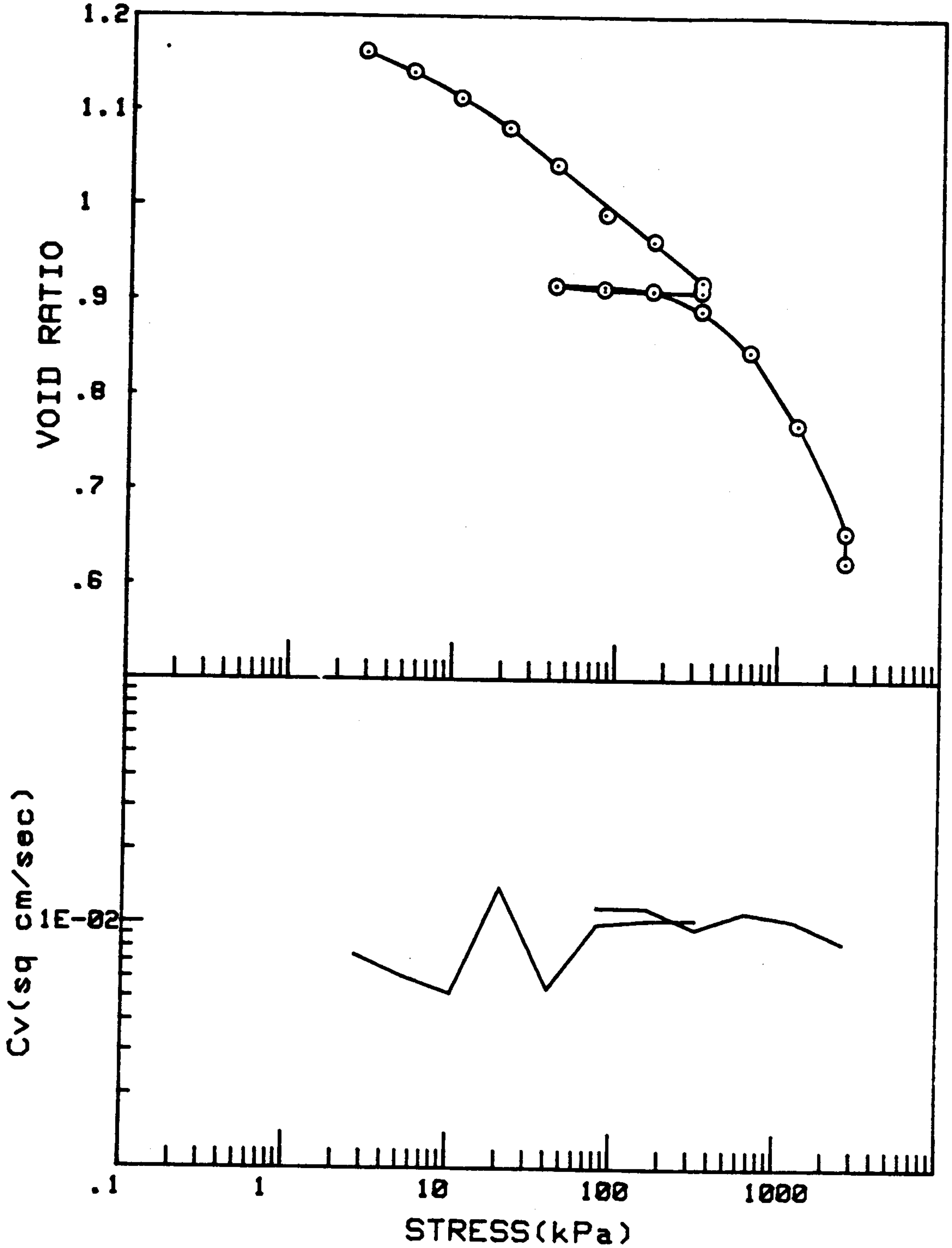

CRUISE DC4-81-NS		INCREMENT (cm)	76-78
CORE NO.	685A2	TEST NO.	OE39

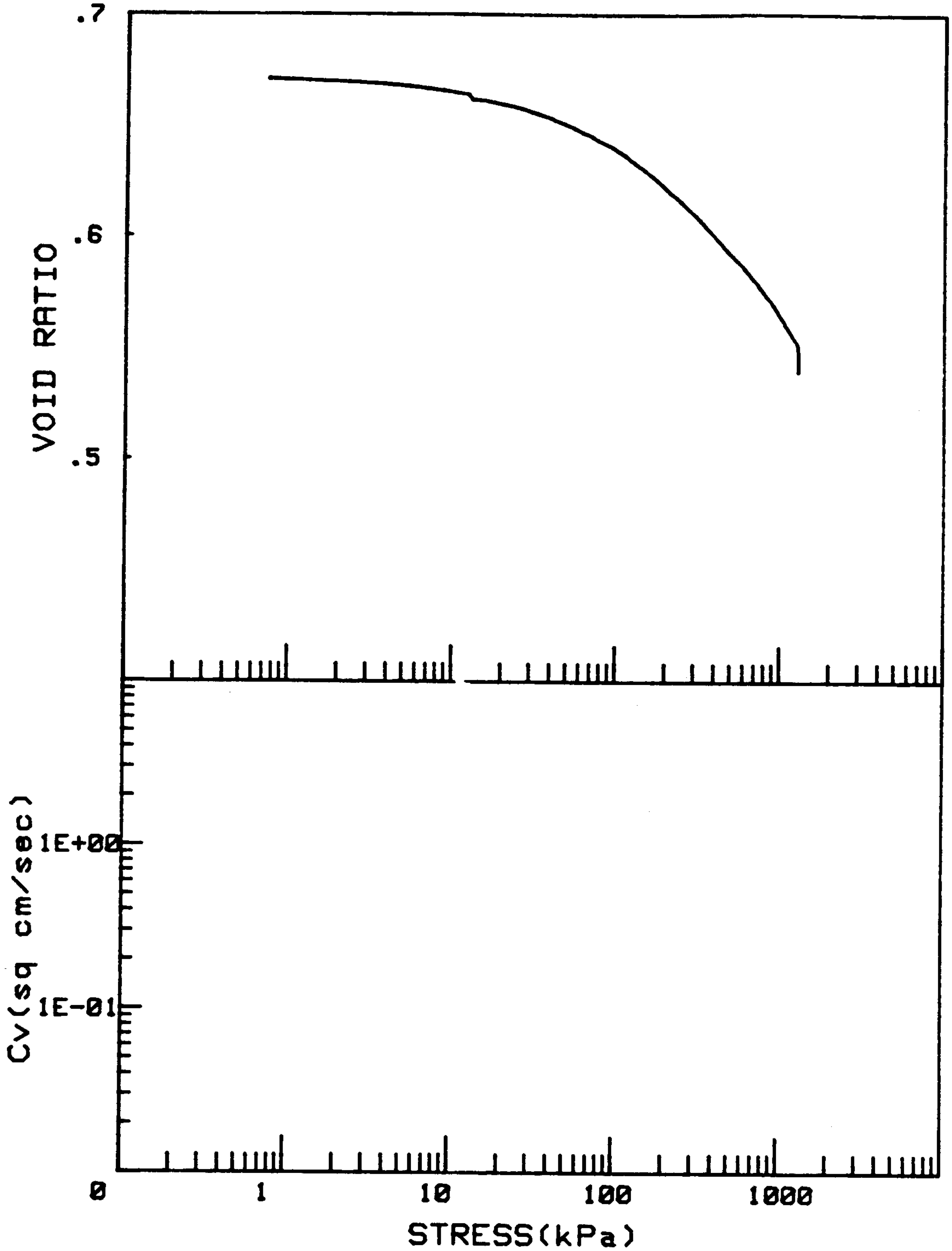

CRUISE DC4-81-NS		INCREMENT (cm)	150-156
CORE NO.	685A2	TEST NO.	CE20

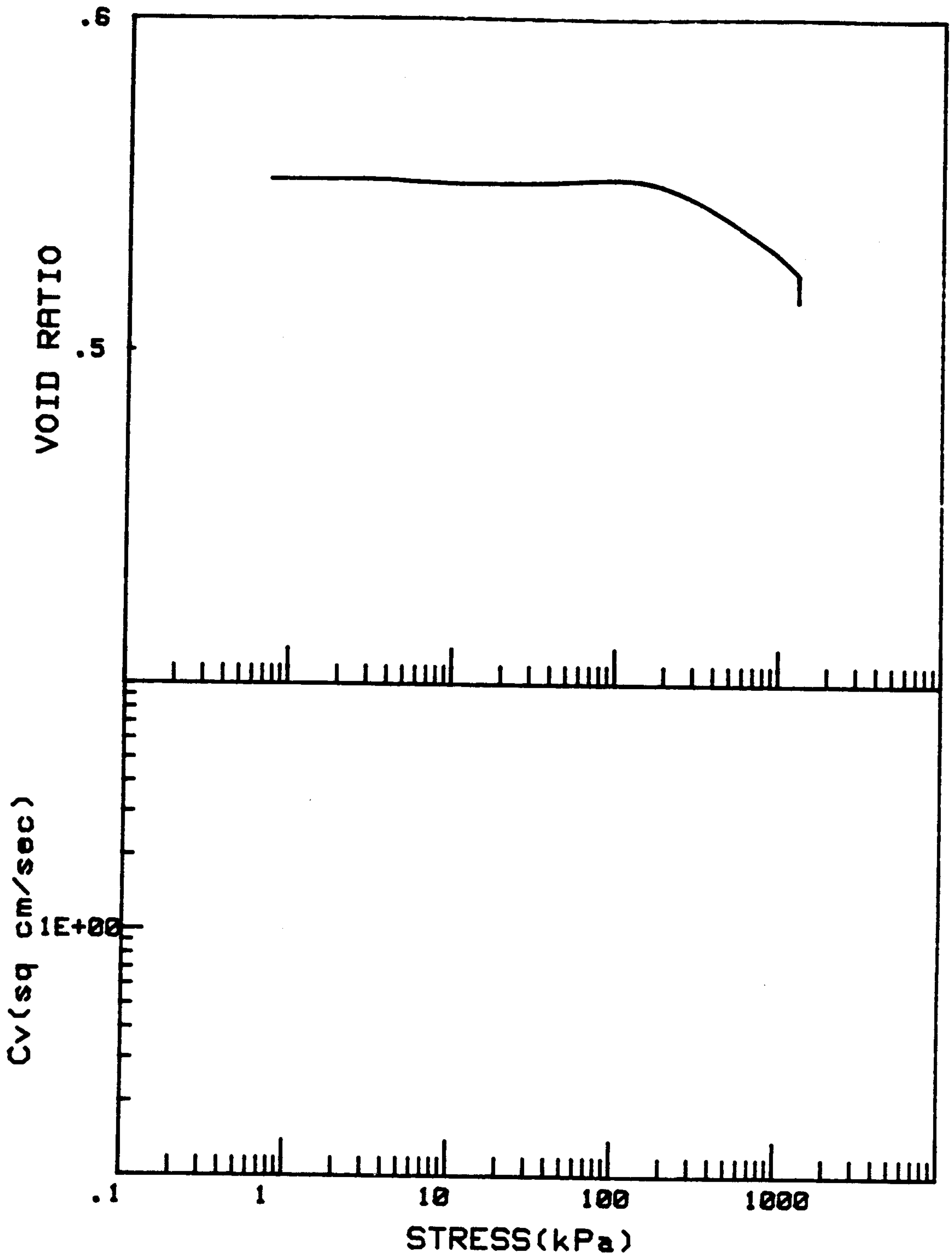

CRUISE DC4-81-NS		INCREMENT (cm)	180-182
CORE NO.	685A2	TEST NO.	CE21

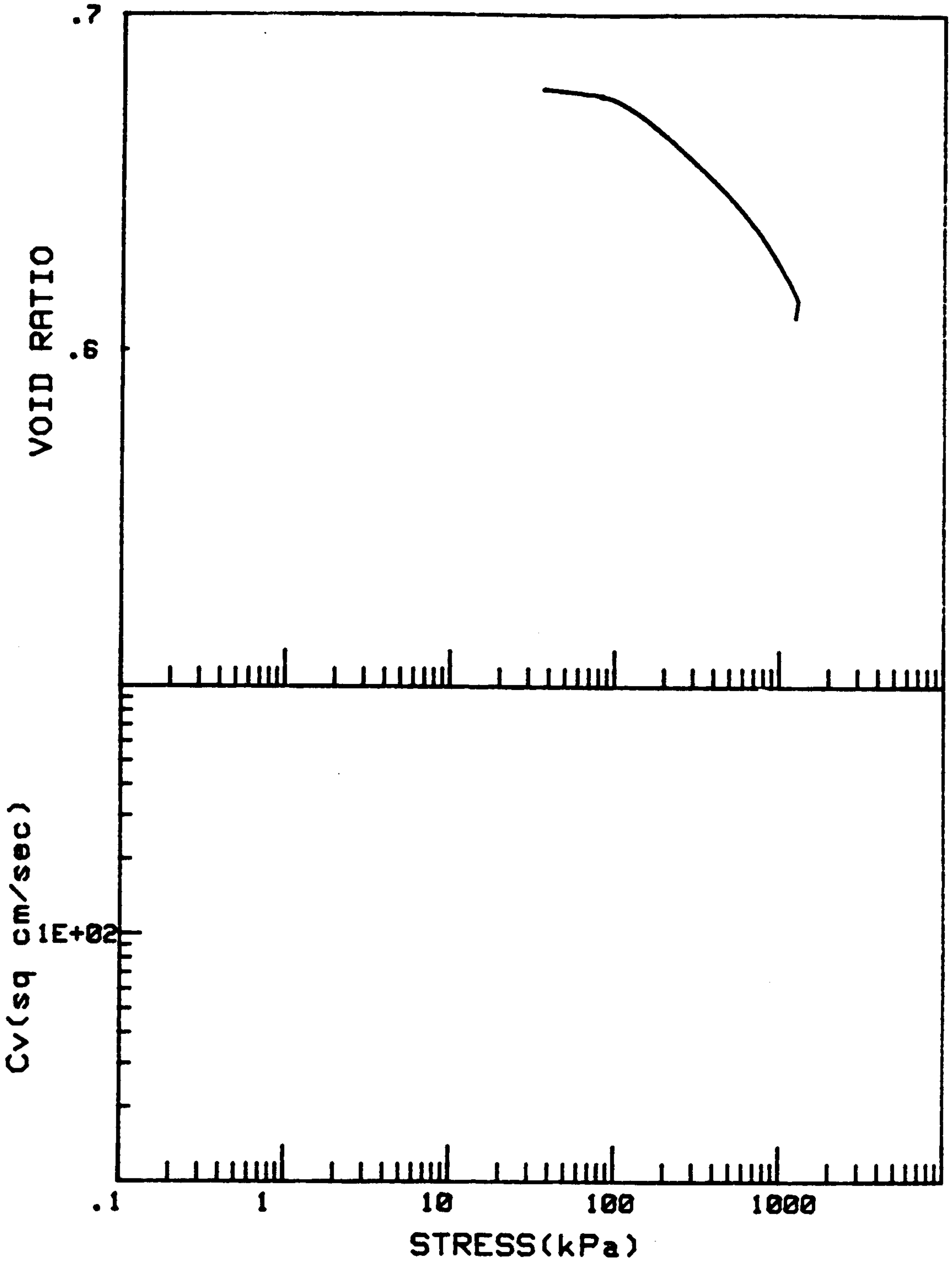

CRUISE DC4-81-NS		INCREMENT (cm)	25-30
CORE NO.	686A1	TEST NO.	CE39

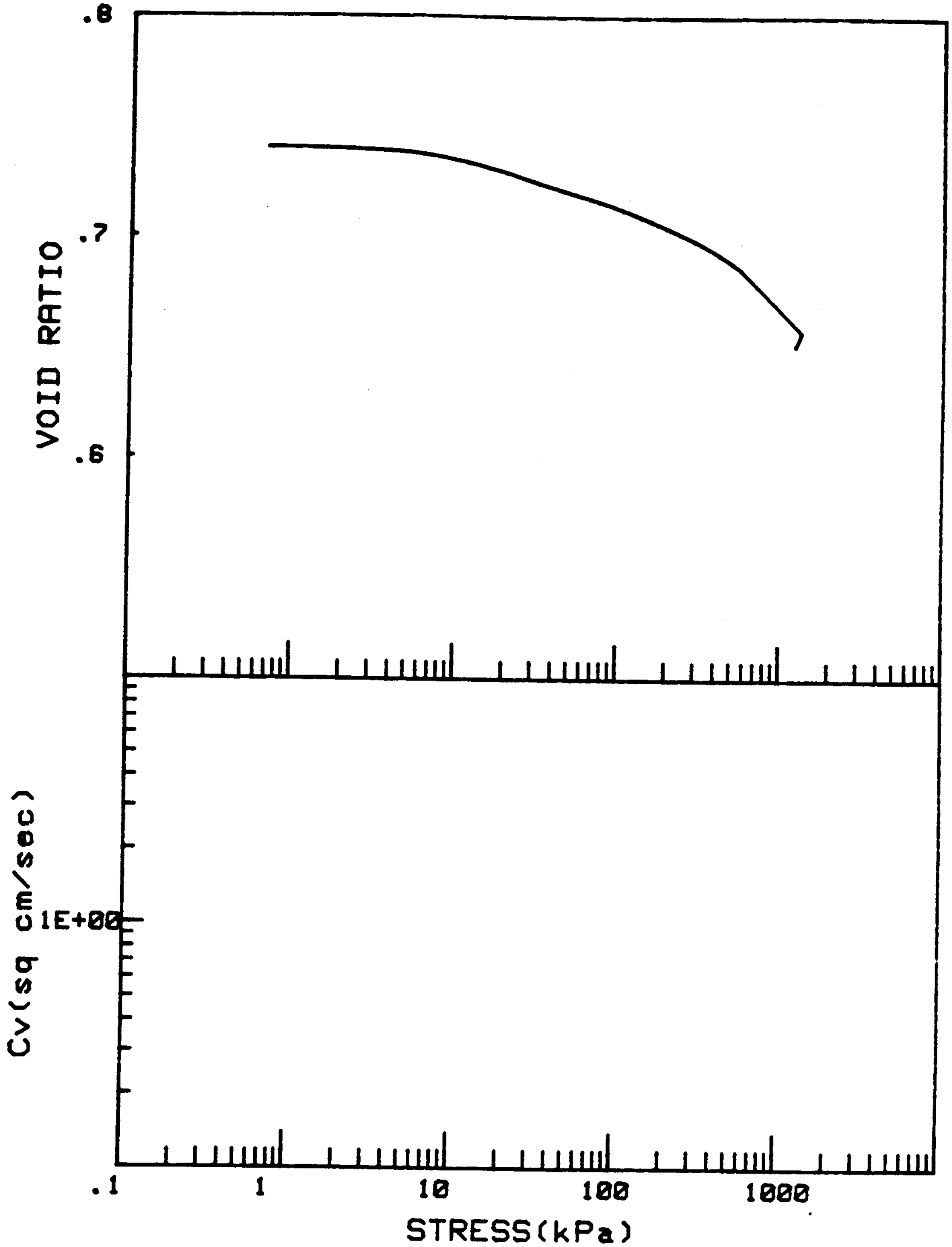

CRUISE DC4-81-NS		INCREMENT (cm)	75-80
CORE NO.	686A1	TEST NO.	CE41

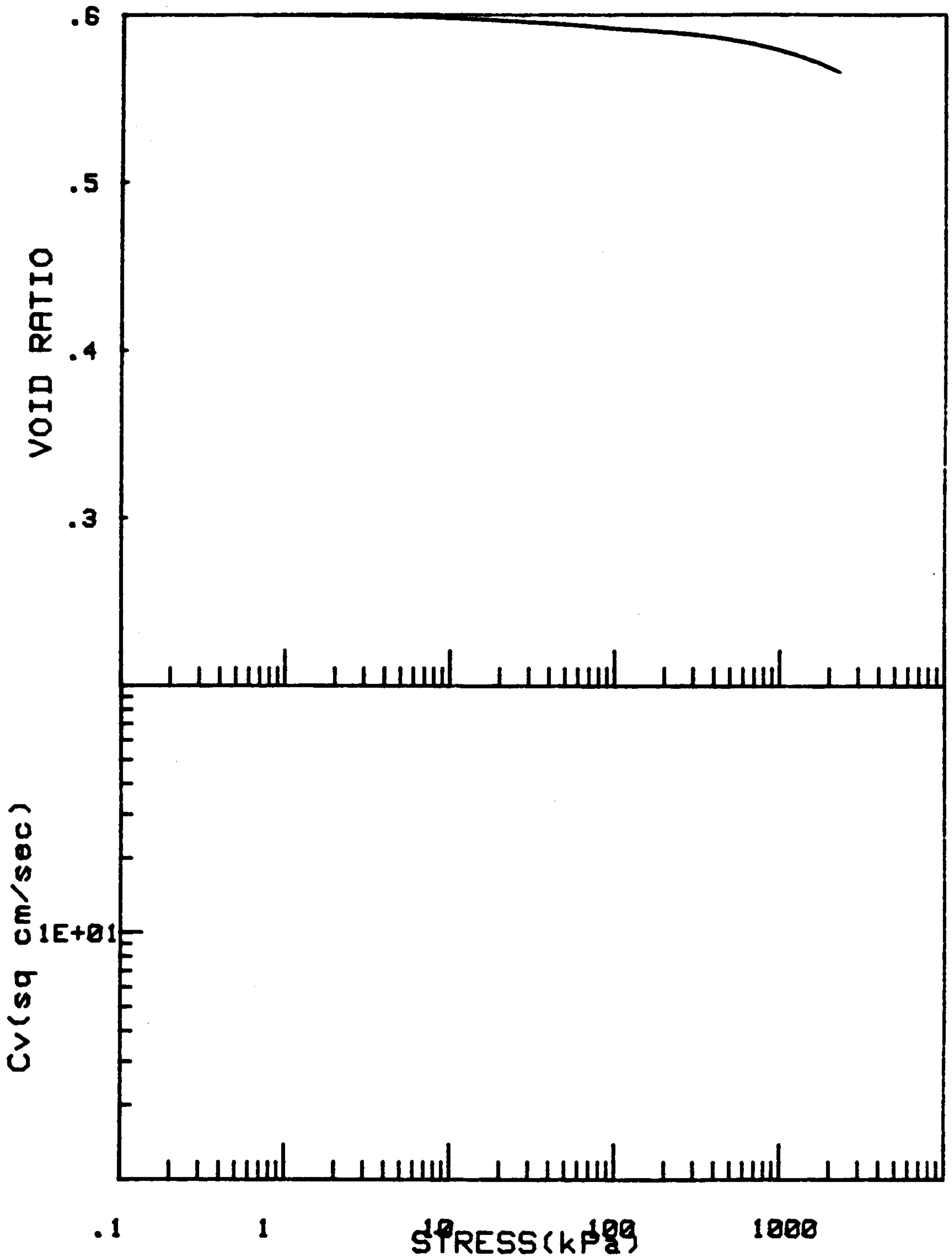

CRUISE DC4-81-NS		INCREMENT (cm)	180-185
CORE NO.	686A1	TEST NO.	CE40

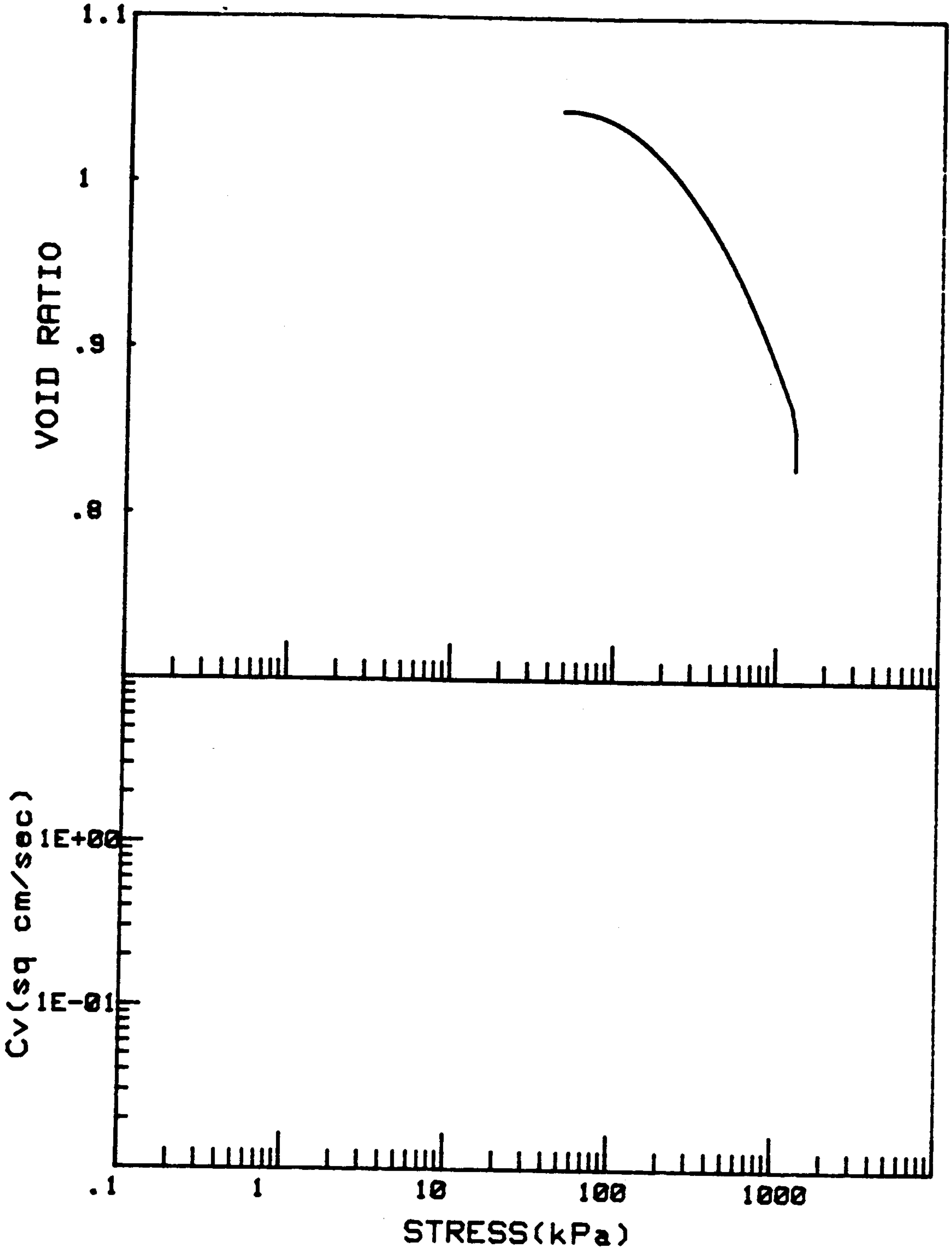

CRUISE DC4-81-NS	INCREMENT (cm)	284-289
CORE NO. 686A1	TEST NO.	CE42

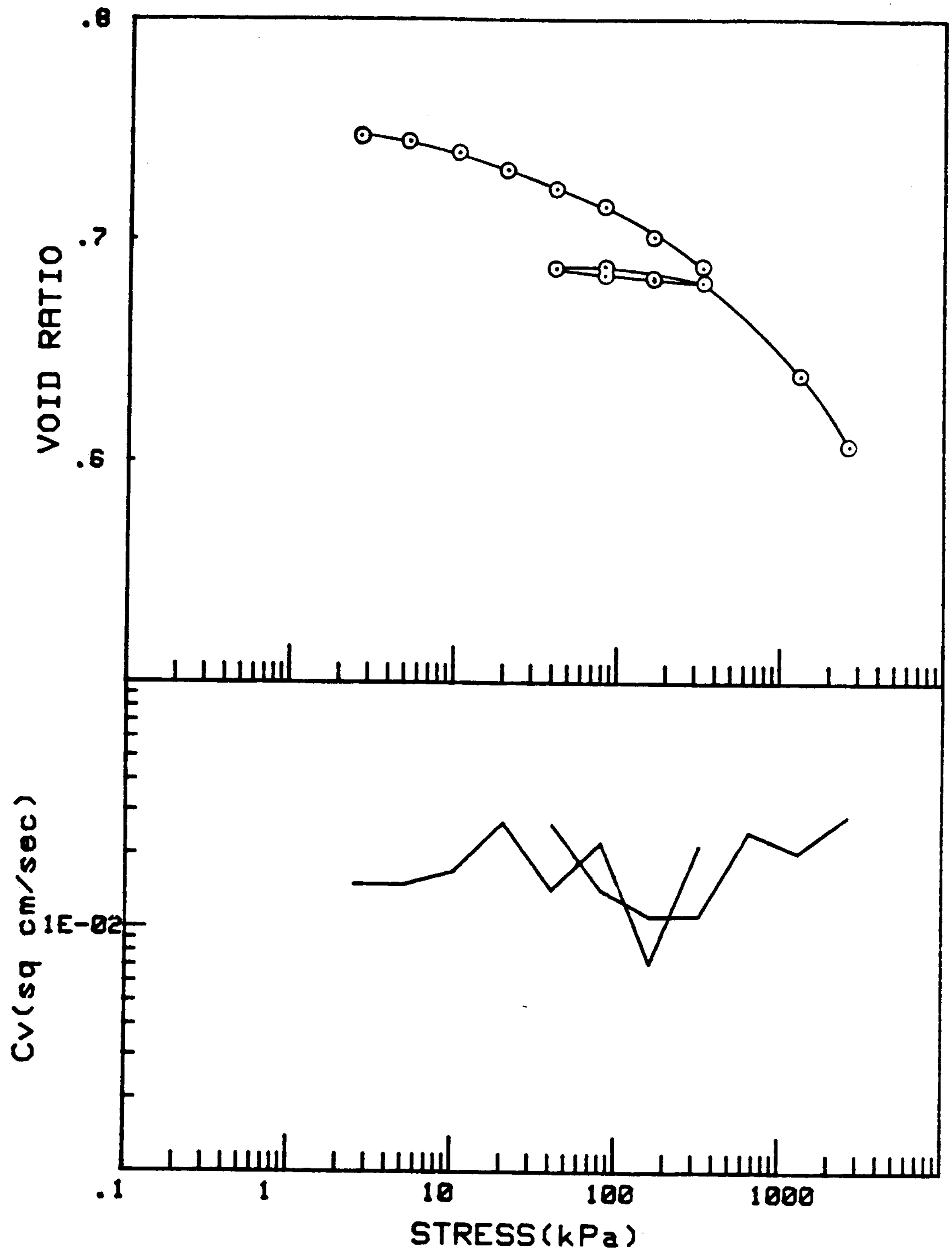

CRUISE DC4-81-NS		INCREMENT (cm)	65-70
CORE NO.	687A1	TEST NO.	OE42

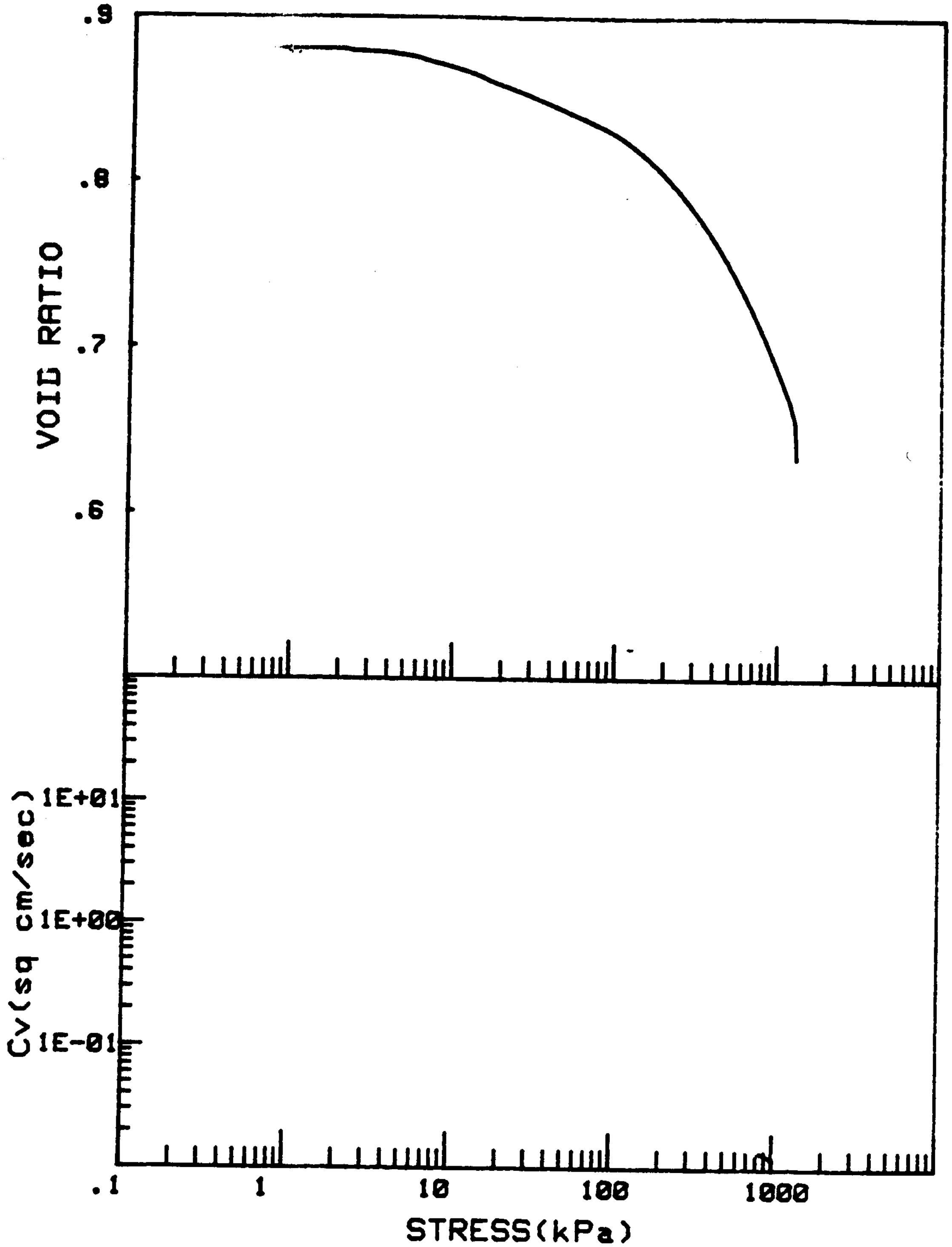

CRUISE DC4-81-NS		INCREMENT (cm)	106-108
CORE NO.	687A1	TEST NO.	CE48

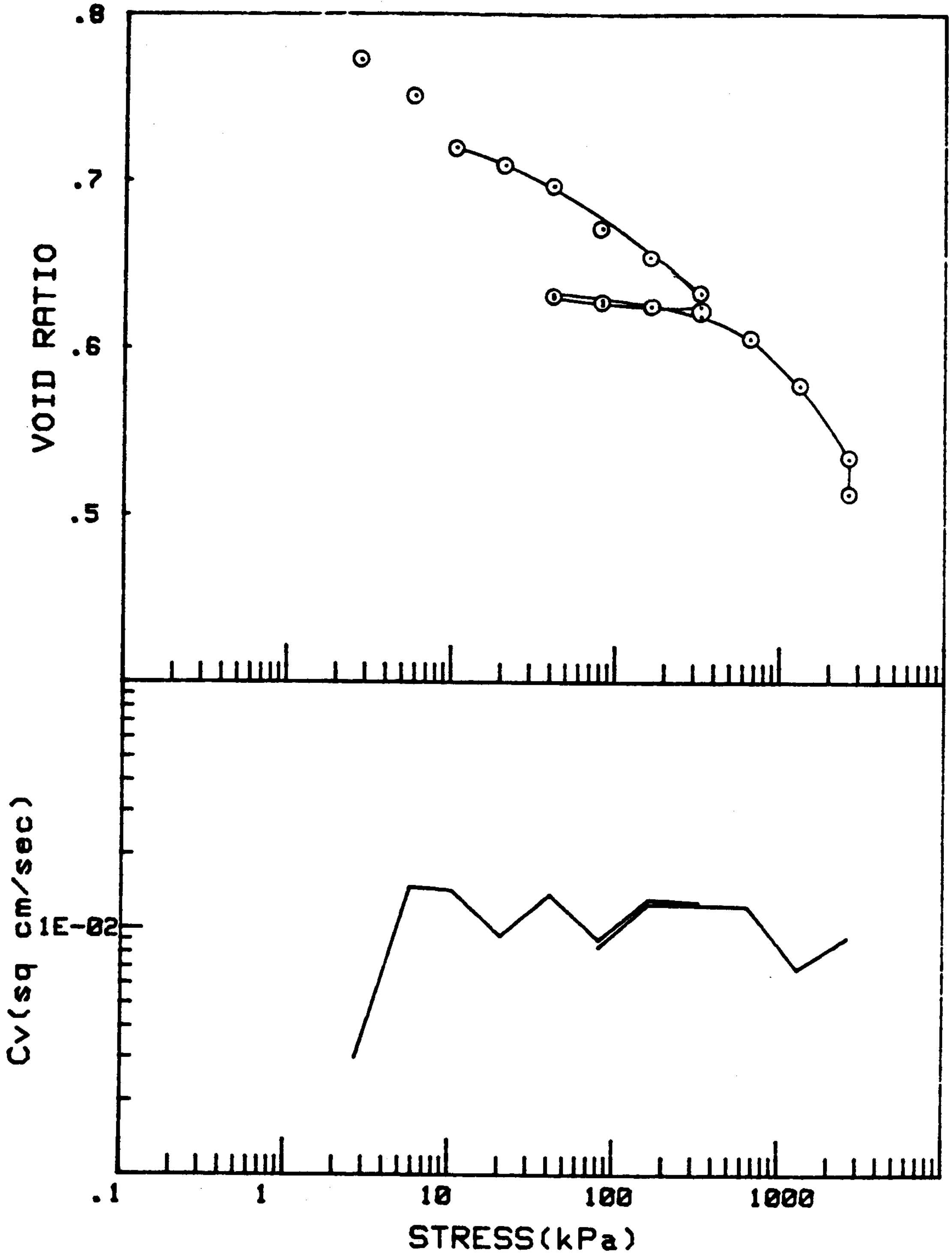

CRUISE DC4-81-NS		INCREMENT (cm)	216-222
CORE NO.	687A1	TEST NO.	OE43

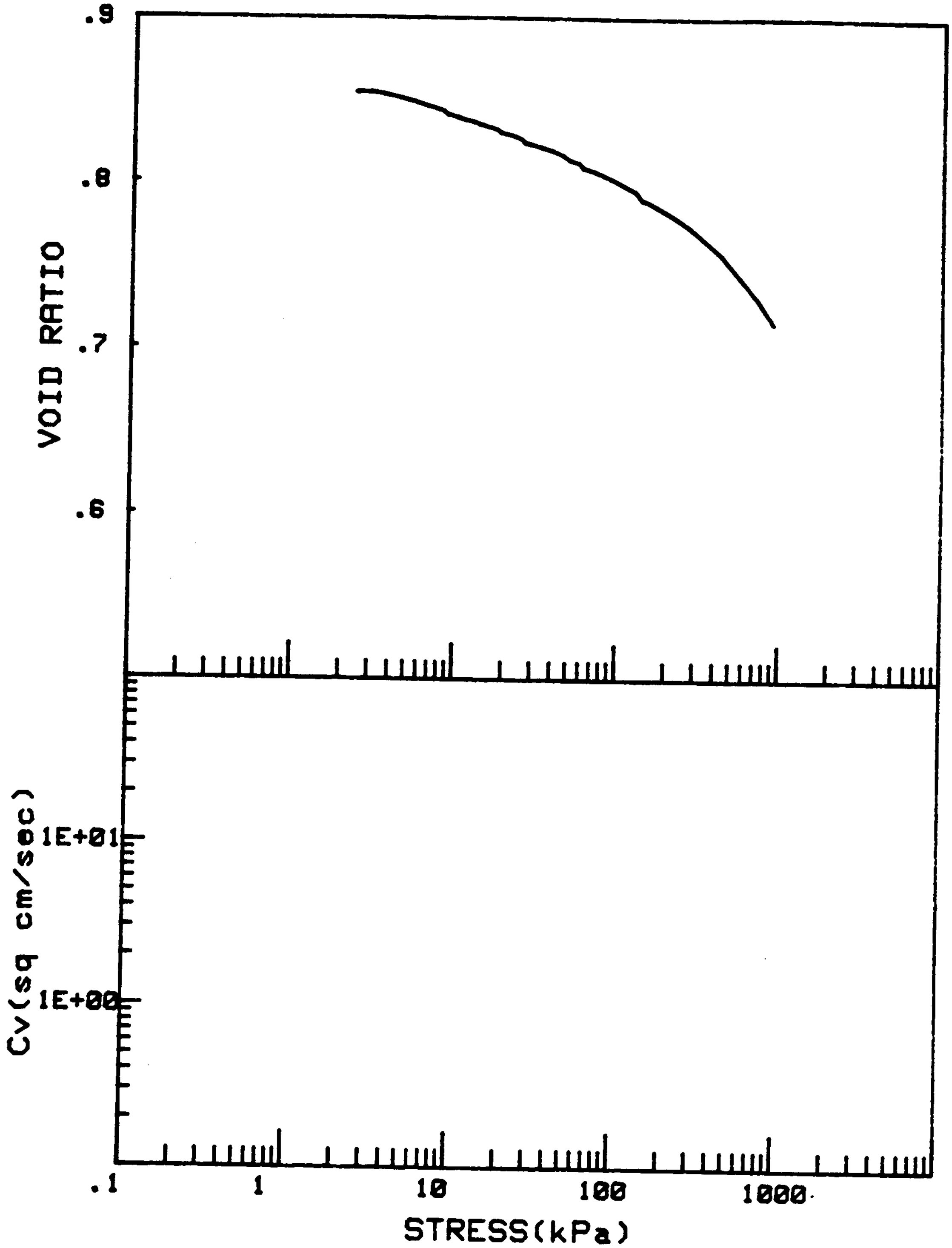

CRUISE DC4-81-NS		INCREMENT (cm)	362-364
CORE NO.	687A1	TEST NO.	CE44

APPENDIX E:

STATIC TRIAXIAL TEST PLOTS

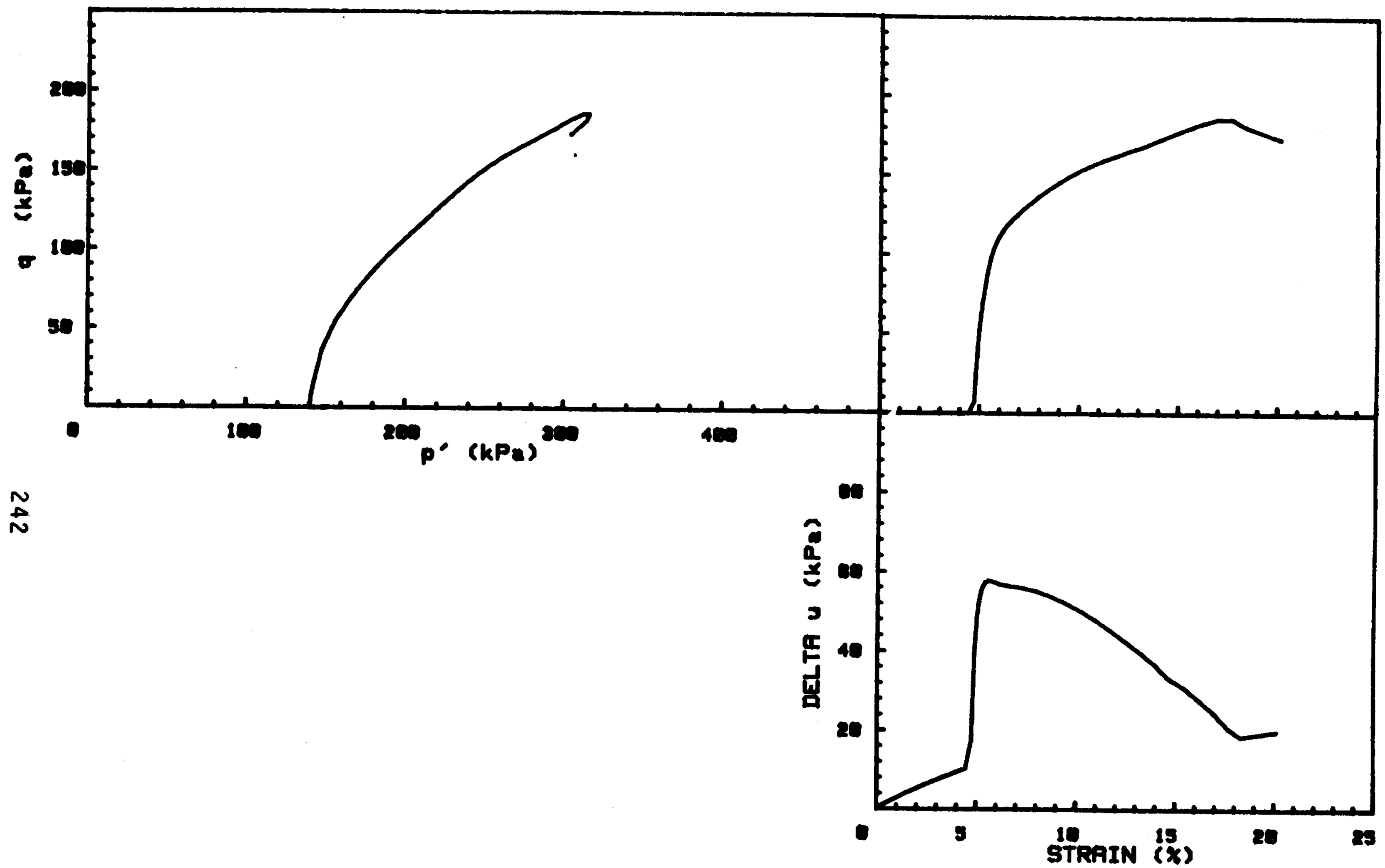

CRUISE DC4-81-NS		INCREMENT (cm)	131-140
CORE NO.	681A2	TEST NO.	TE107

SIG1c′(kPa) 151.0
SIG3c′(kPa) 151.0
INDUCED OCR 1.0

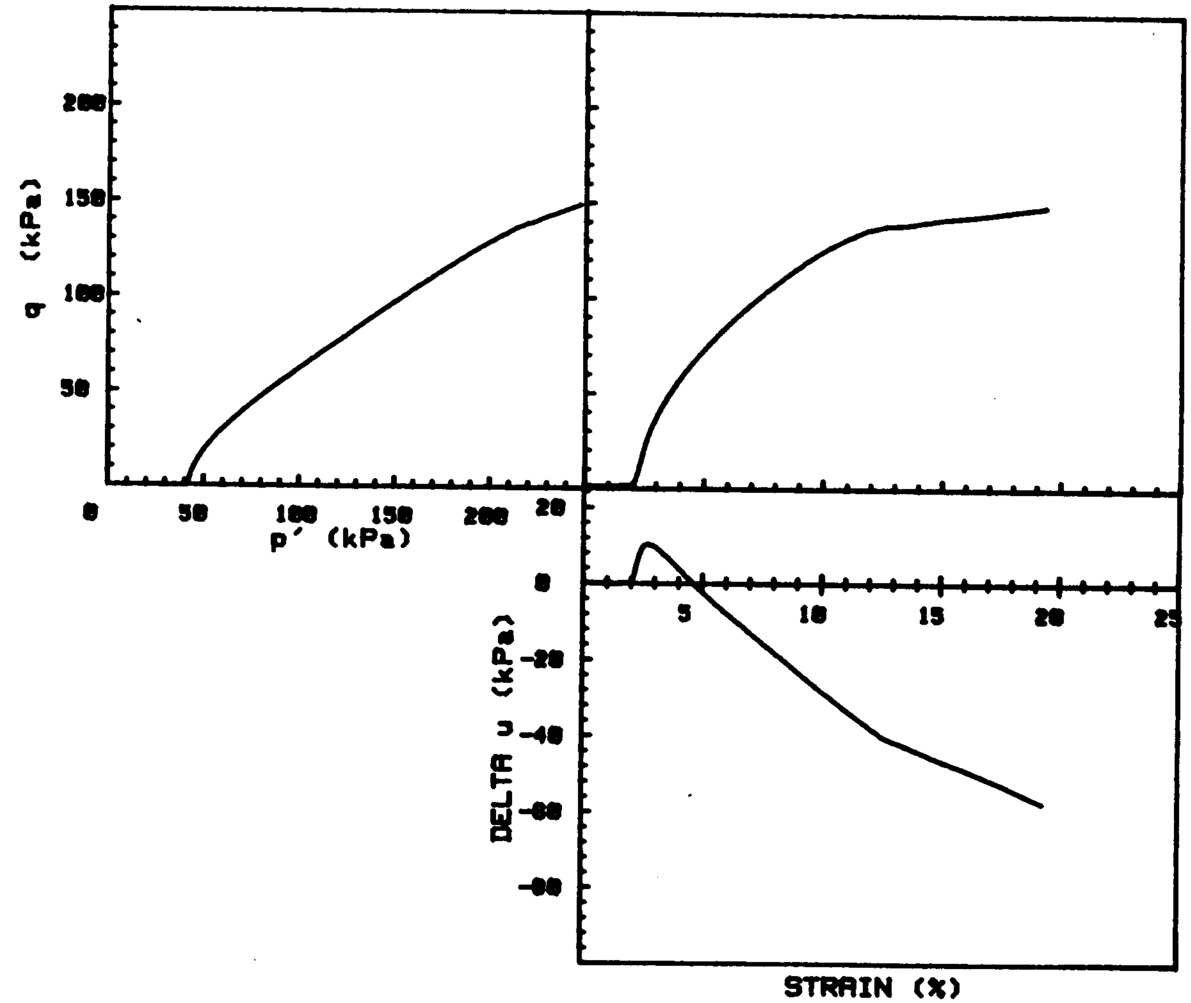

CRUISE	DC4-81-NS	INCREMENT (cm)	131-140
CORE NO.	681A2	TEST NO.	TE108

SIG1c′(kPa) 40.7
SIG3c′(kPa) 40.7
INDUCED OCR 6.0

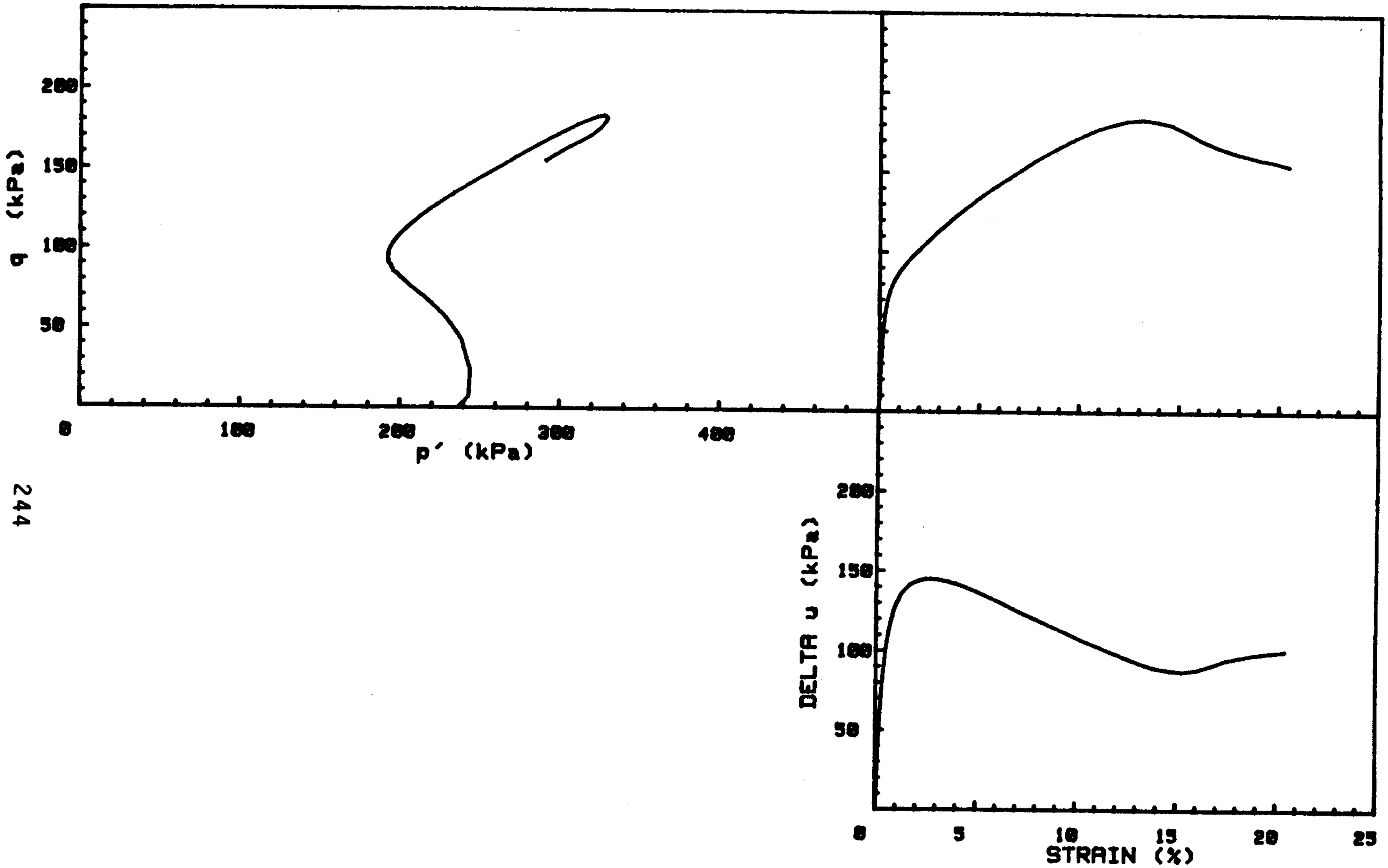

CRUISE DC4-81-NS		INCREMENT (cm)	107-116
CORE NO.	602A1	TEST NO.	TE76
SIG1c′(kPa)	236.7		
SIG3c′(kPa)	236.7		
INDUCED OCR	1.0		

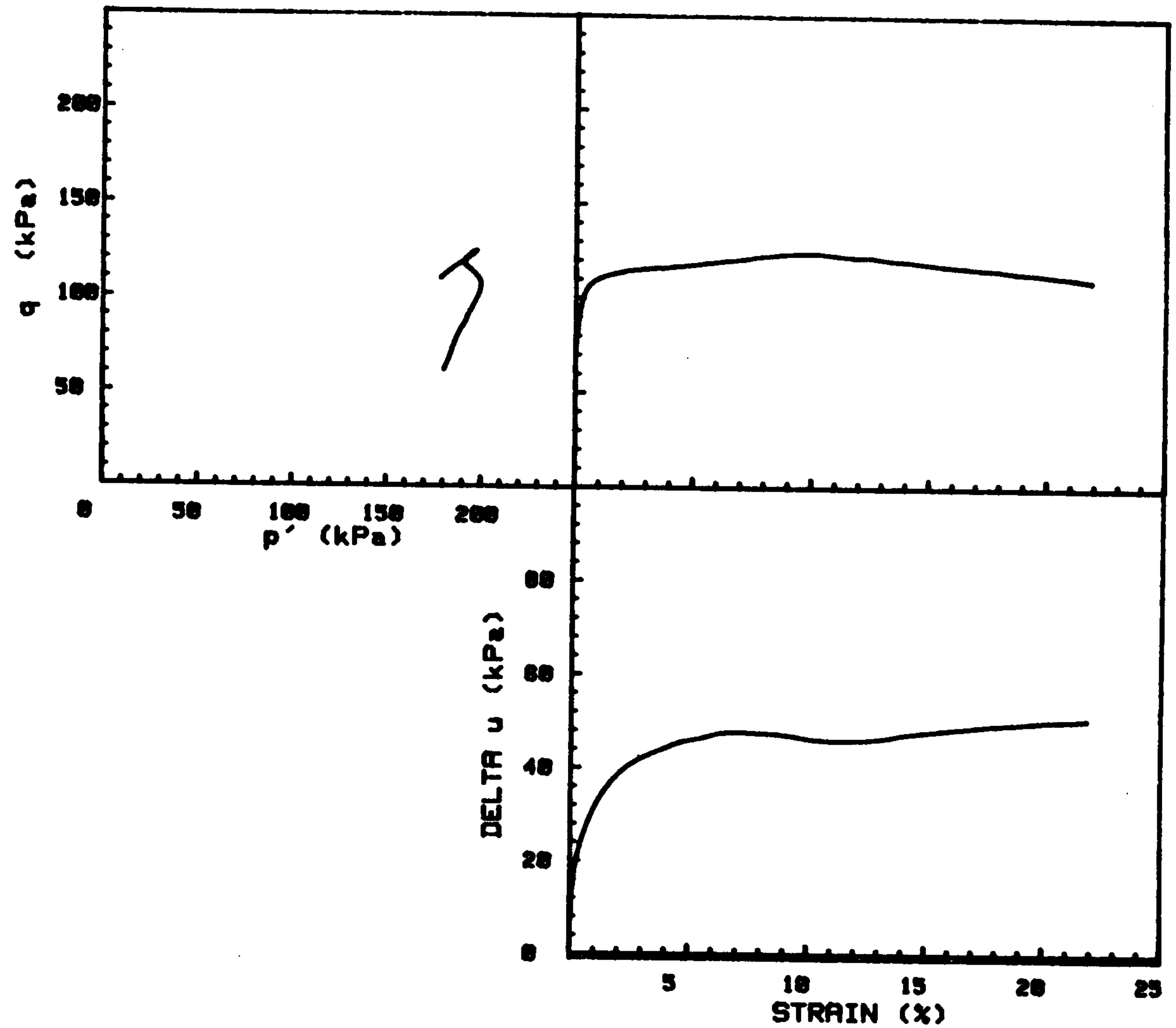

CRUISE DC4-81-NS		INCREMENT (cm)	106-117
CORE NO.	682A1	TEST NO.	TE77
SIG1c´(kPa)	242.3		
SIG3c´(kPa)	119.2		
INDUCED OCR	1.0		

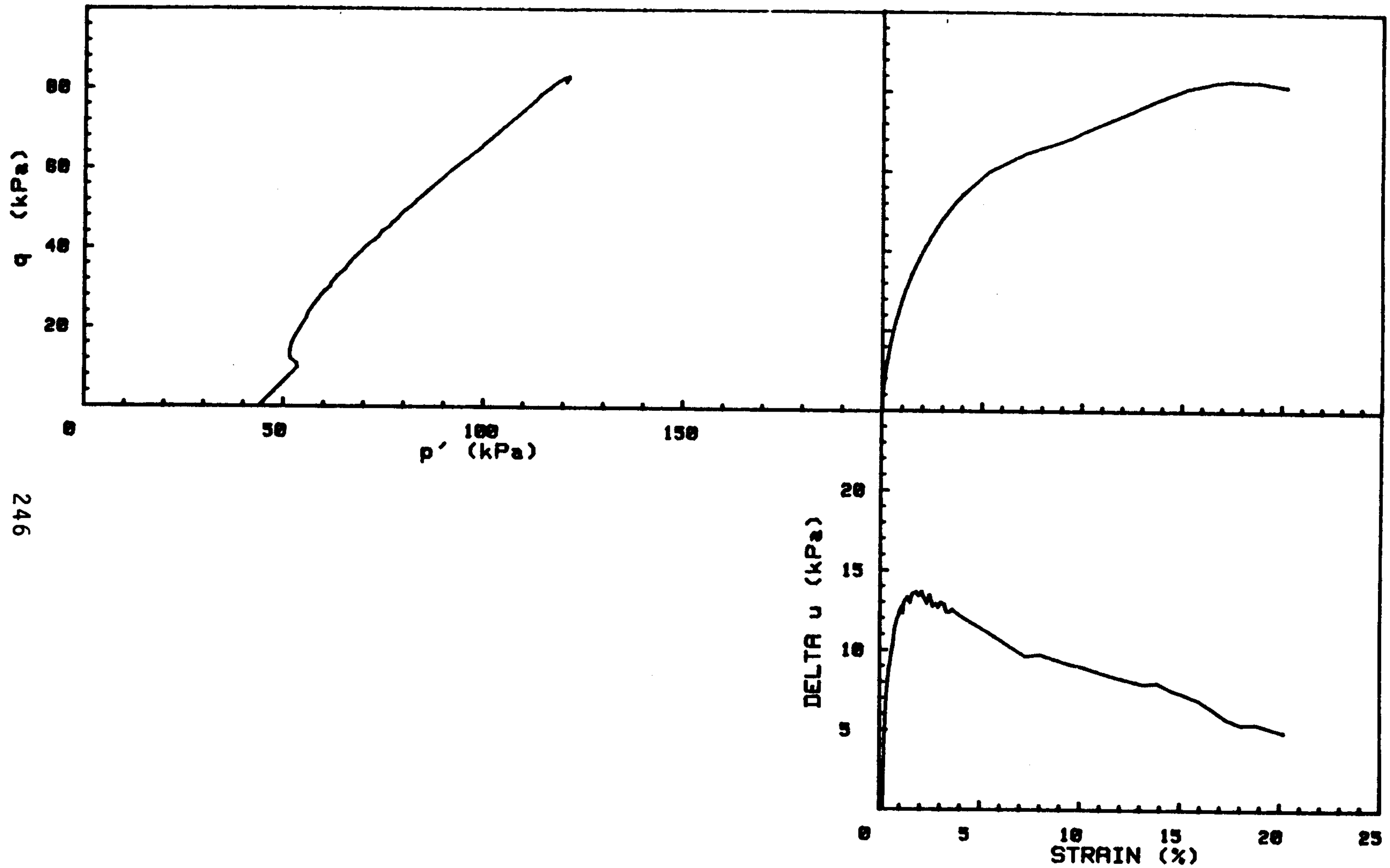

CRUISE DC4-81-NS		INCREMENT (cm)	121-132
CORE NO.	682A1	TEST NO.	TE85
SIG1c′(kPa)	44.1		
SIG3c′(kPa)	44.1		
INDUCED OCR	6.0		

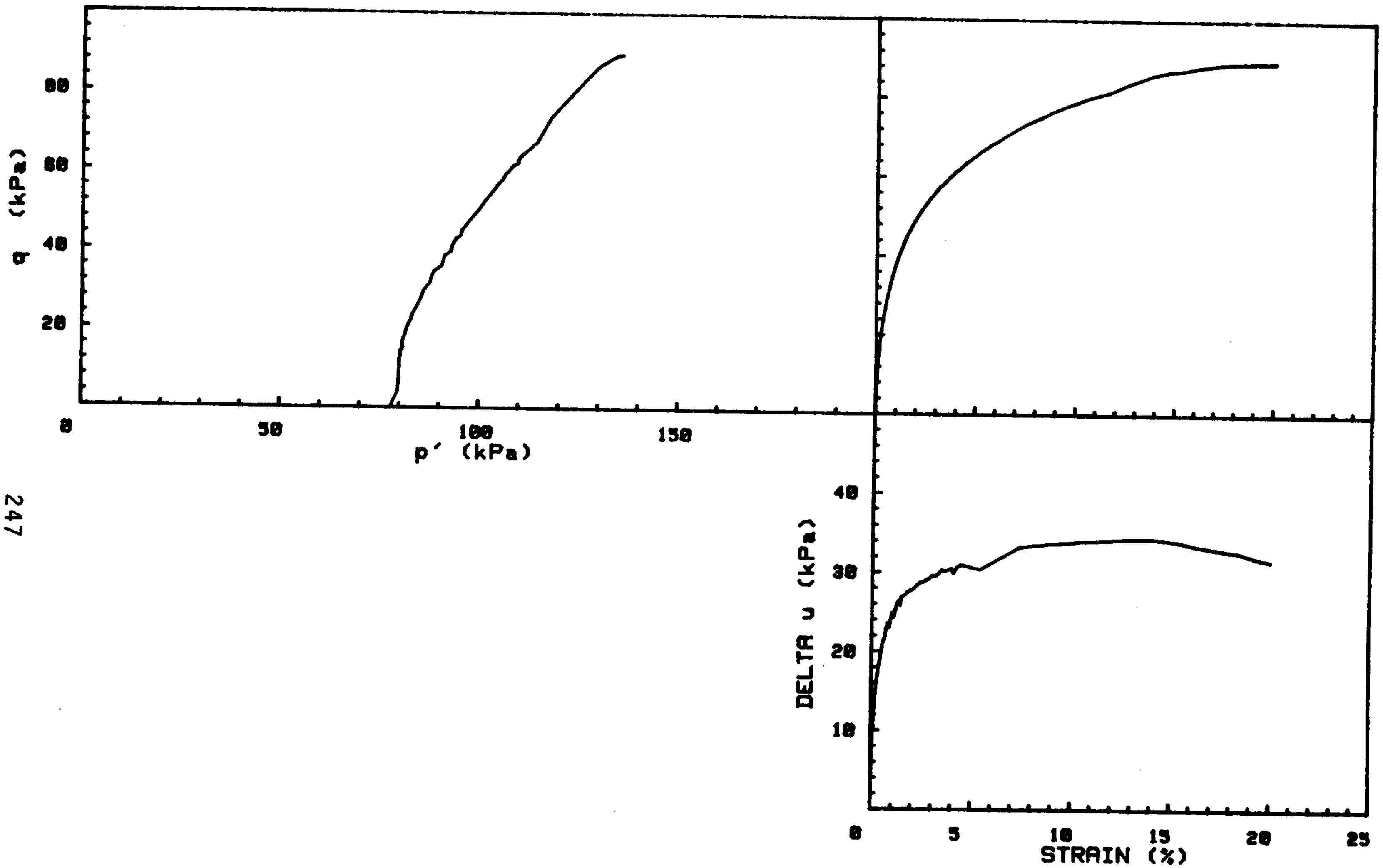

CRUISE DC4-81-NS		INCREMENT (cm)	121-132
CORE NO.	682A1	TEST NO.	TE86

SIG1c′(kPa) 77.9
SIG3c′(kPa) 77.9
INDUCED OCR 3.0

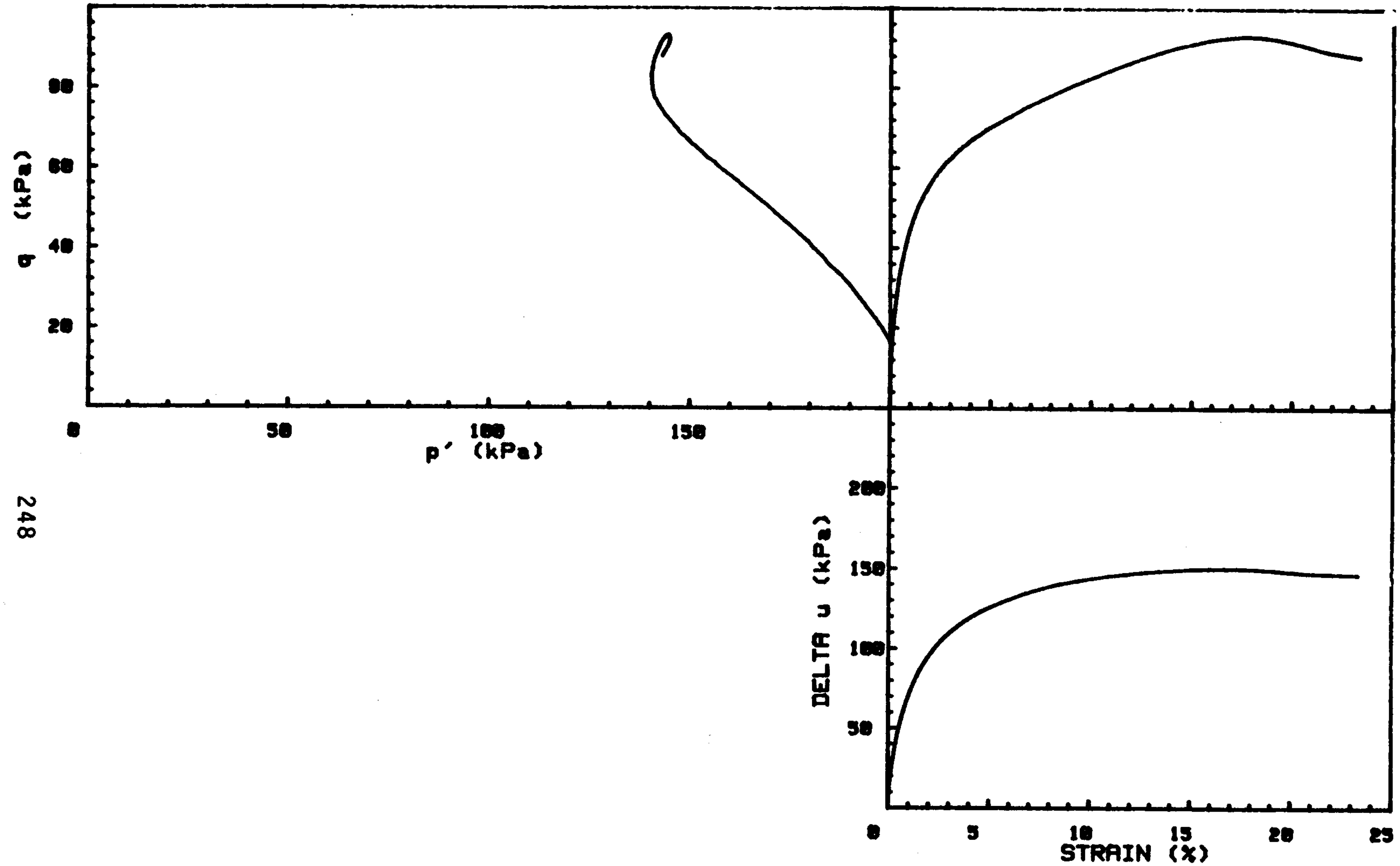

CRUISE	DC4-81-NS	INCREMENT (cm)	174-183
CORE NO.	682A1	TEST NO.	TE98

SIG1c′(kPa) 201.3
SIG3c′(kPa) 201.3
INDUCED OCR 1.0

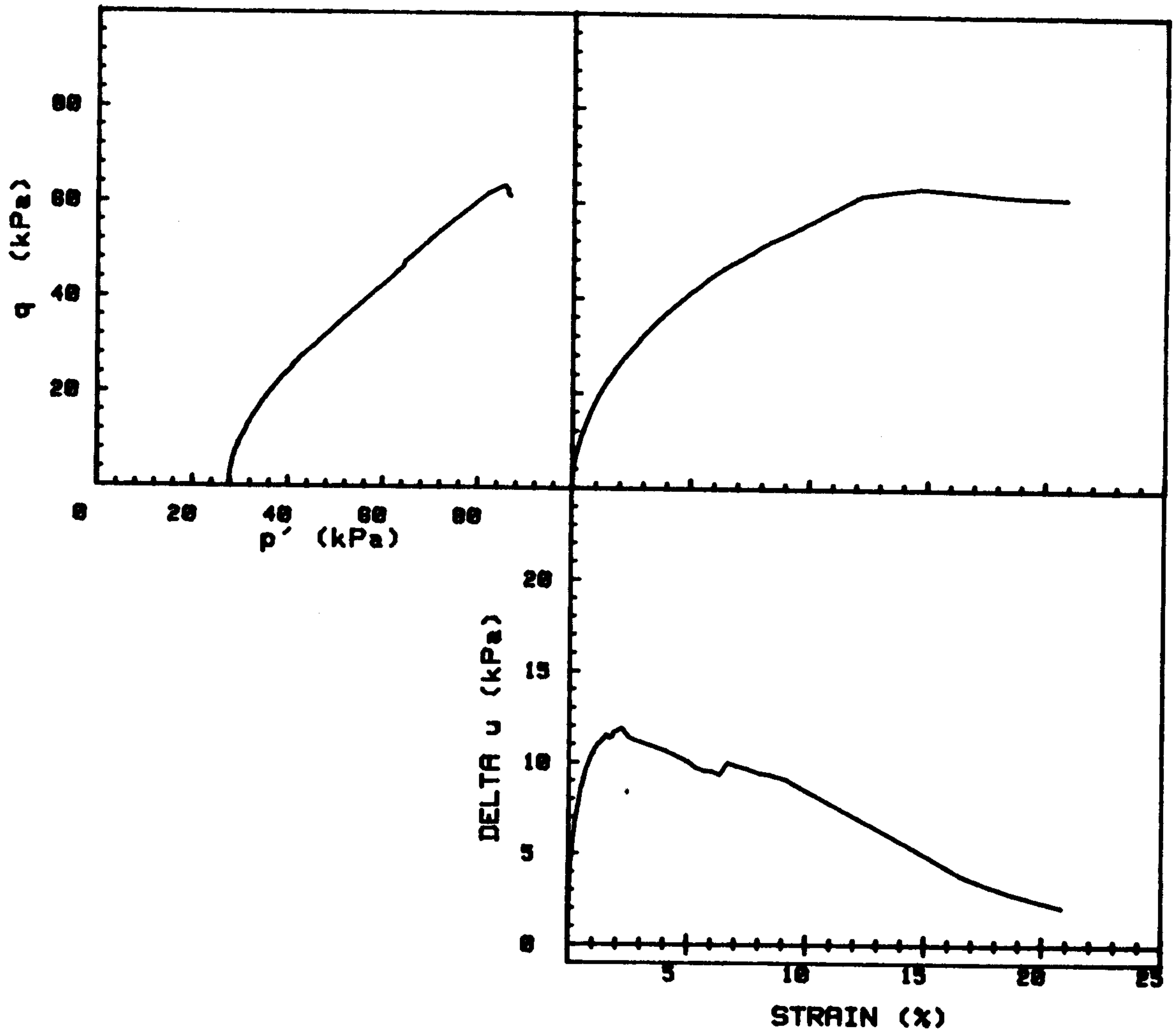

CRUISE	DC4-81-NS	INCREMENT (cm)	175-183
CORE NO.	682A1	TEST NO.	TE99
SIG1c′(kPa)	27.3		
SIG3c′(kPa)	27.3		
INDUCED OCR	6.0		

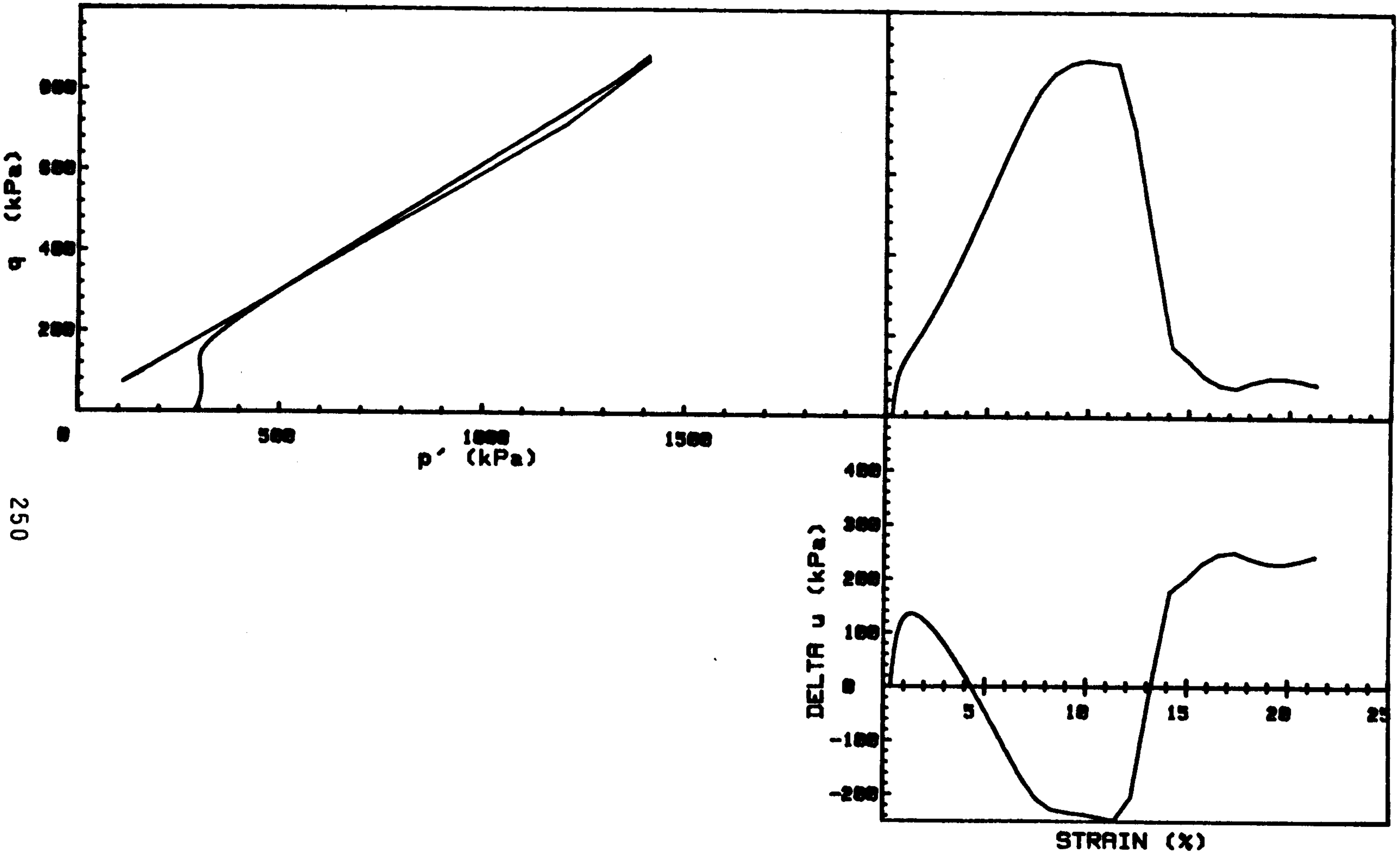

250

CRUISE	DC4-81-NS	INCREMENT (cm)	421-430
CORE NO.	683A1	TEST NO.	TE109

SIG1c'(kPa) 289.7
SIG3c'(kPa) 289.7
INDUCED OCR 1.0

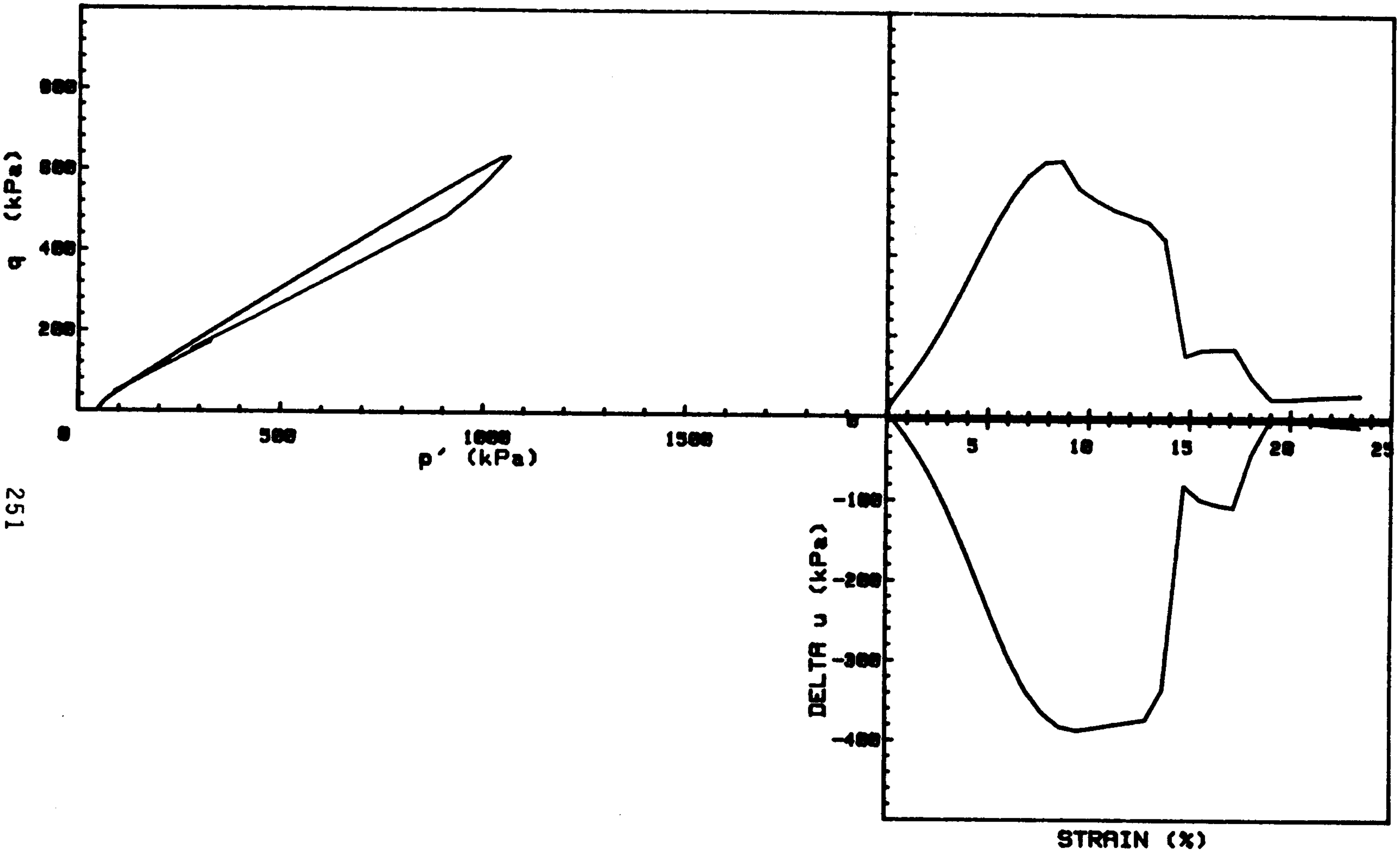

CRUISE DC4-81-NS		INCREMENT (cm)	421-430
CORE NO.	603A1	TEST NO.	TE110
SIG1c′(kPa)	47.4		
SIG3c′(kPa)	47.4		
INDUCED OCR	6.0		

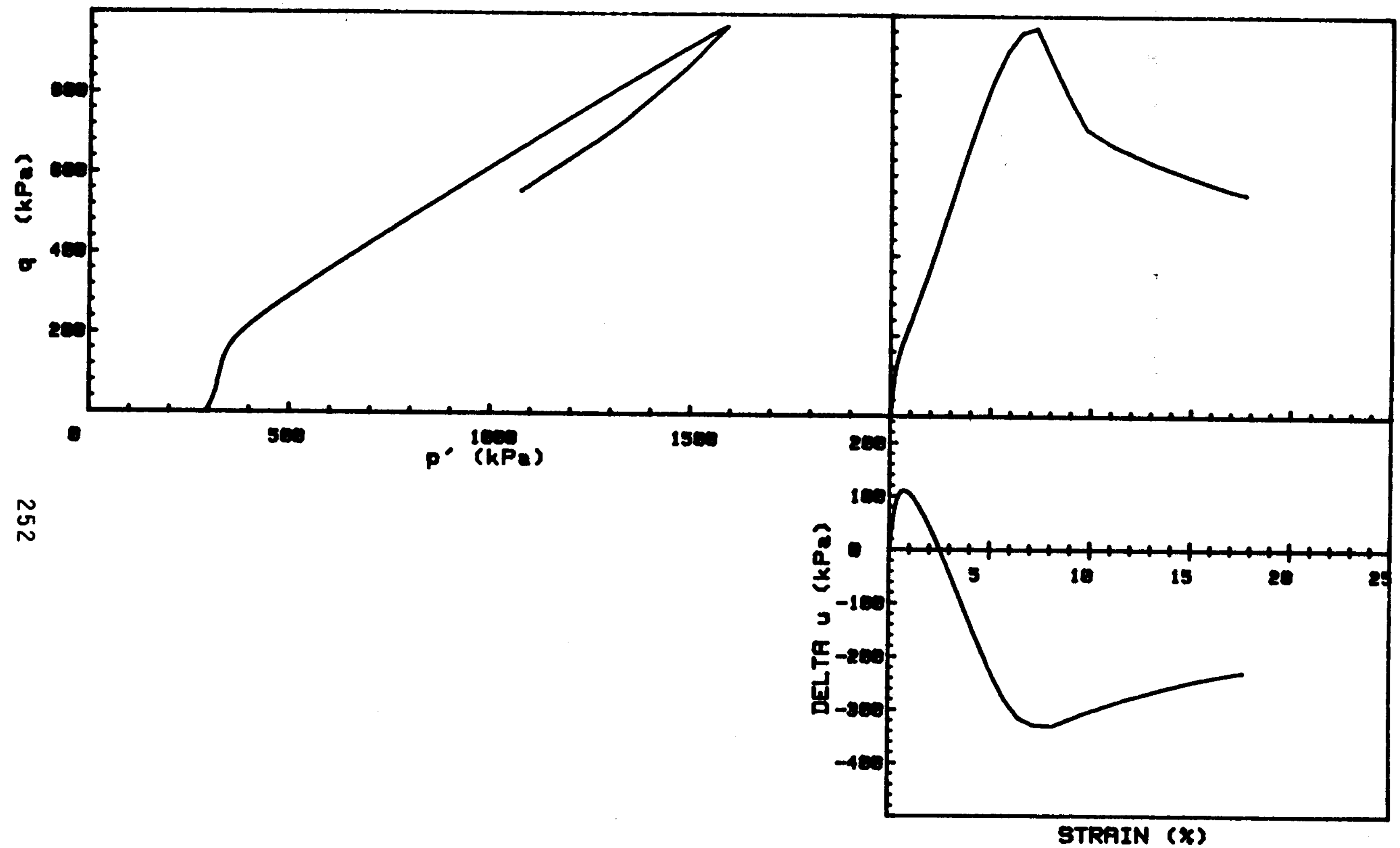

CRUISE DC4-81-NS		INCREMENT (cm)	90-99
CORE NO.	684A1	TEST NO.	TE105
SIG1c′(kPa)	293.0		
SIG3c′(kPa)	293.0		
INDUCED OCR	1.0		

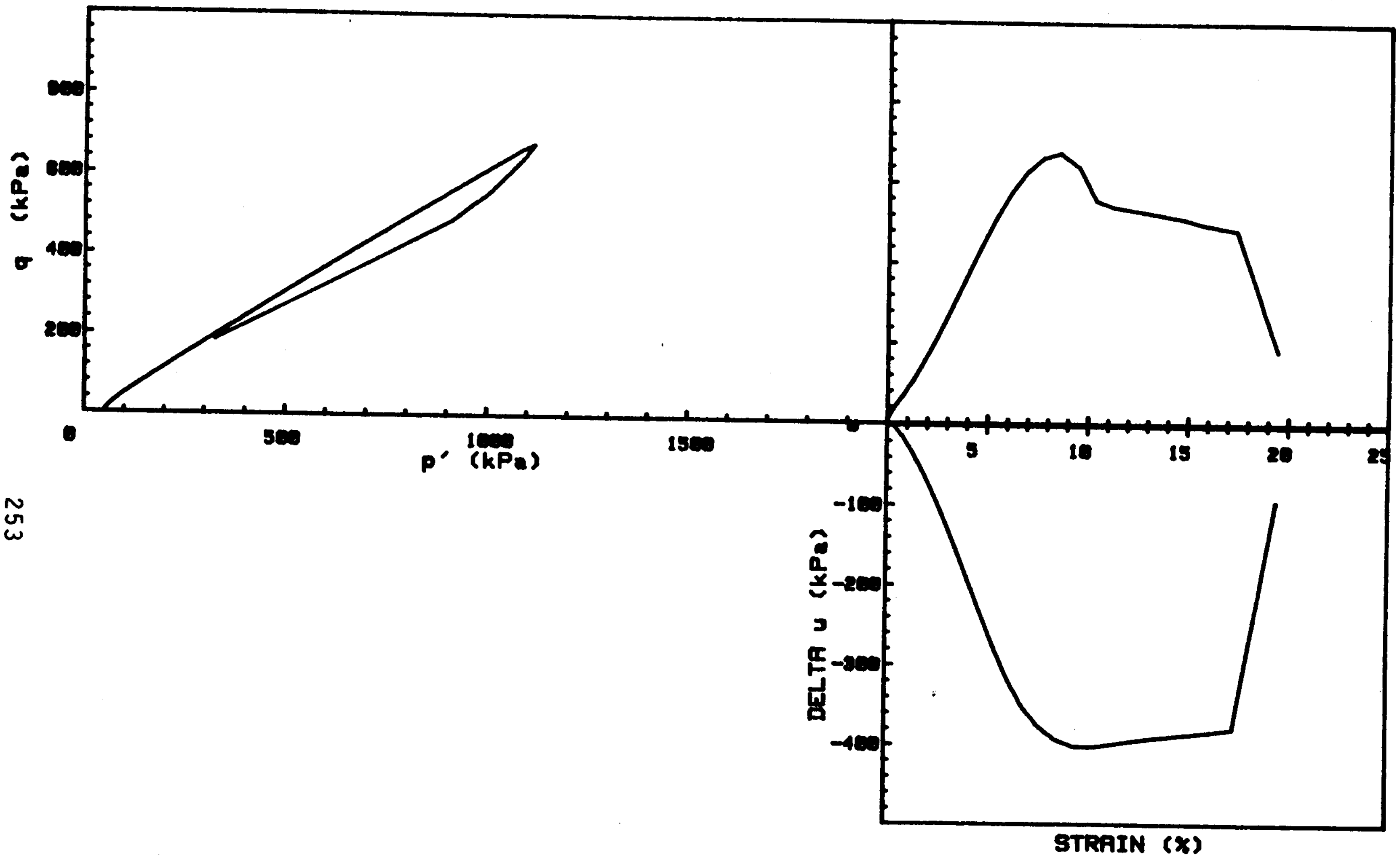

CRUISE DC4-81-NS		INCREMENT (cm)	90-99
CORE NO.	684A1	TEST NO.	TE106

SIG1c′(kPa) 48.1
SIG3c′(kPa) 48.1
INDUCED OCR 6.0

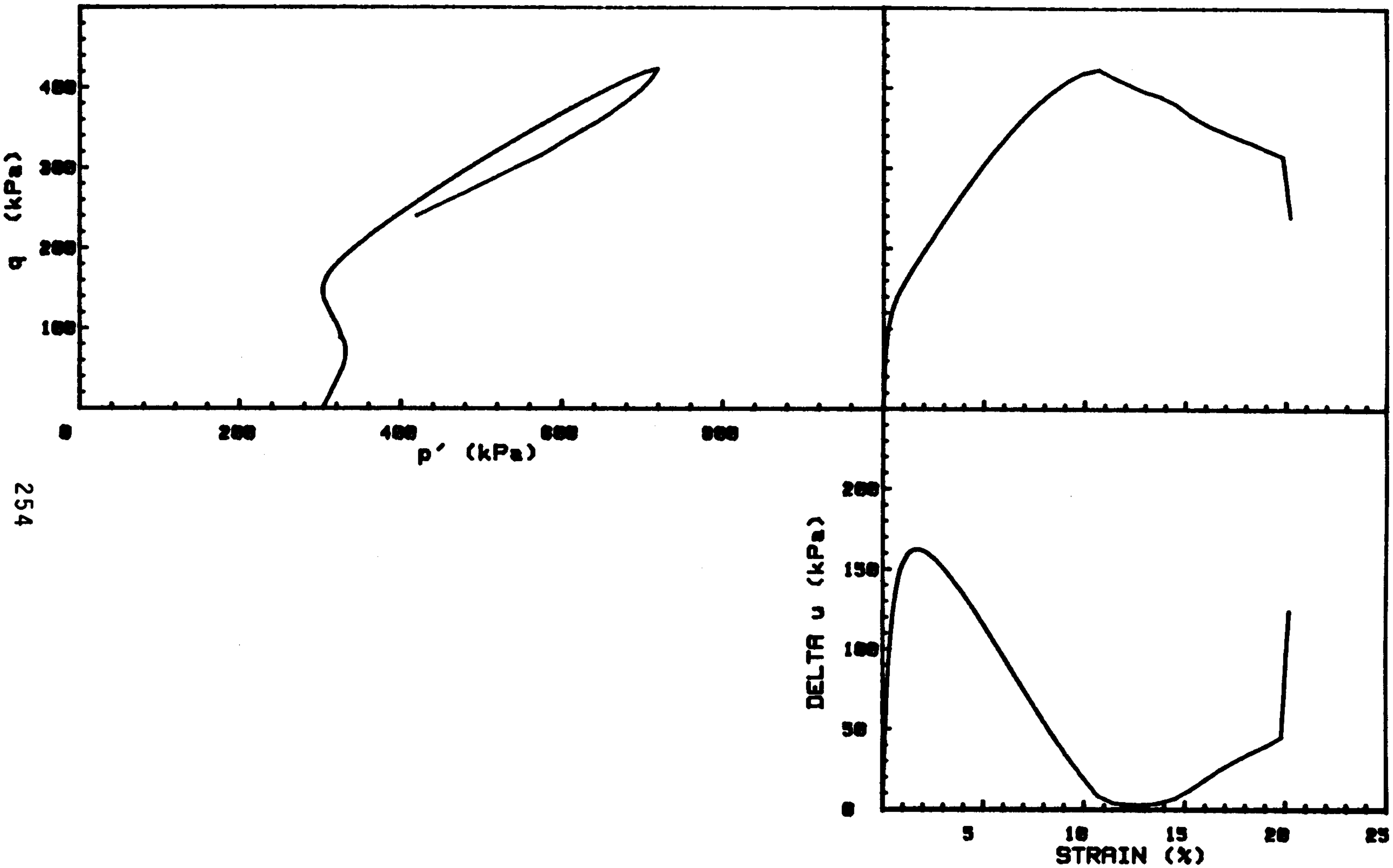

CRUISE	DC4-81-NS	INCREMENT (cm)	50-59
CORE NO.	685A1	TEST NO.	TE103

SIG1c′(kPa) 303.8
SIG3c′(kPa) 303.8
INDUCED OCR 1.0

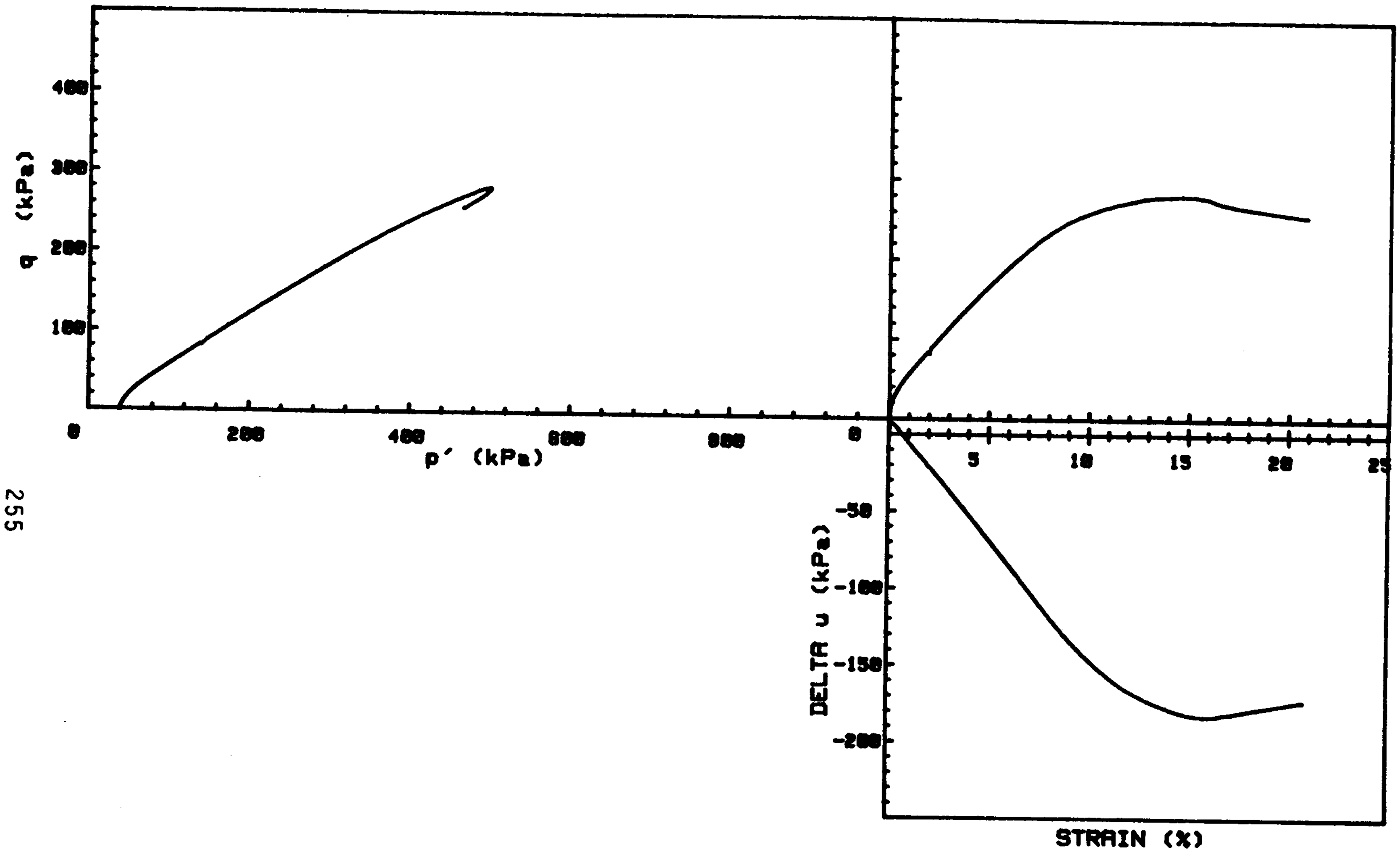

CRUISE DC4-81-NS		INCREMENT (cm)	50-59
CORE NO.	685A2	TEST NO.	TE104
SIG1c′(kPa)	38.3		
SIG3c′(kPa)	38.3		
INDUCED OCR	6.0		

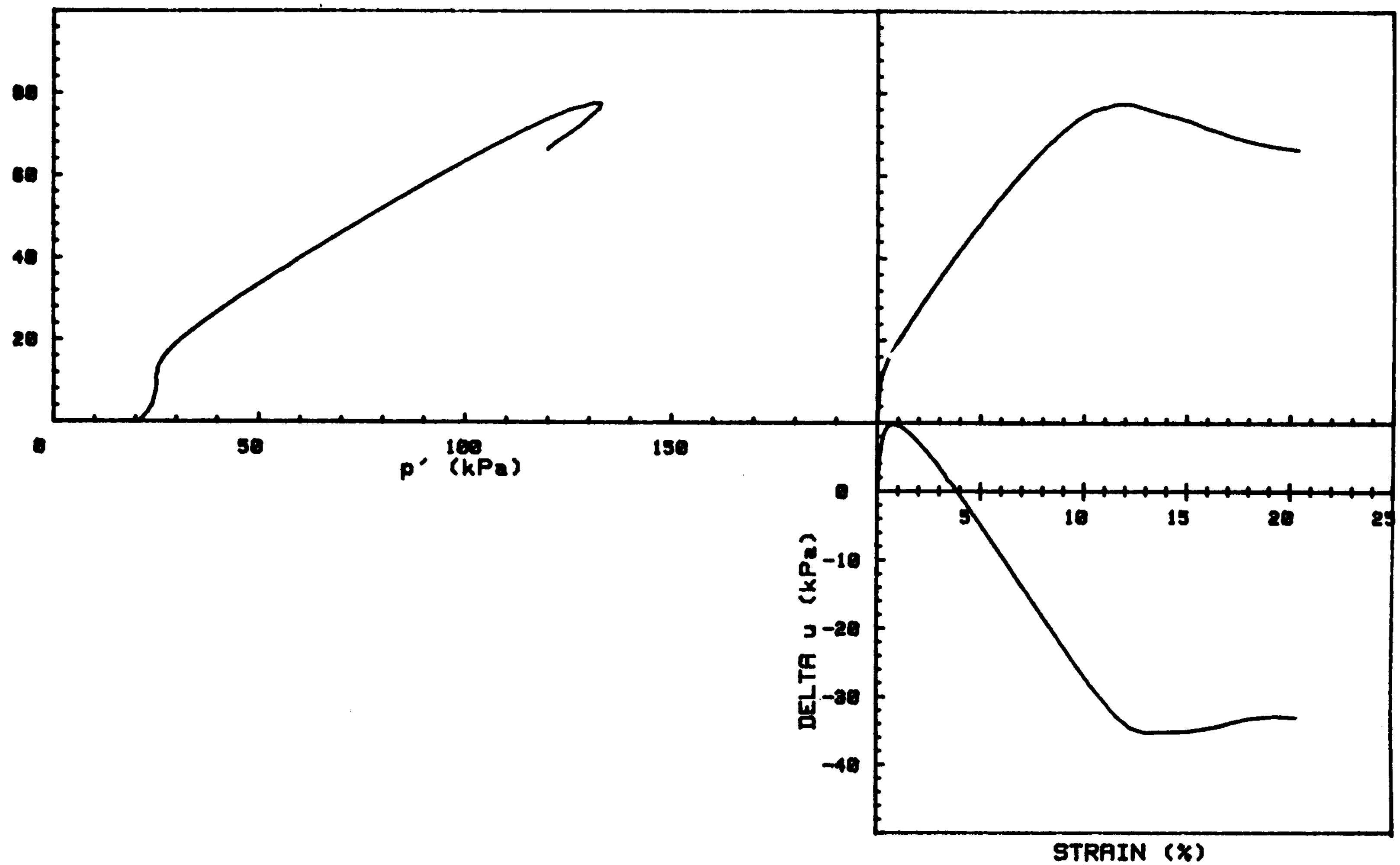

CRUISE DC4-81-NS		INCREMENT (cm)	131-140
CORE NO.	685A2	TEST NO.	TE119
SIG1c′(kPa)	20.9		
SIG3c′(kPa)	20.9		
INDUCED OCR	1.0		

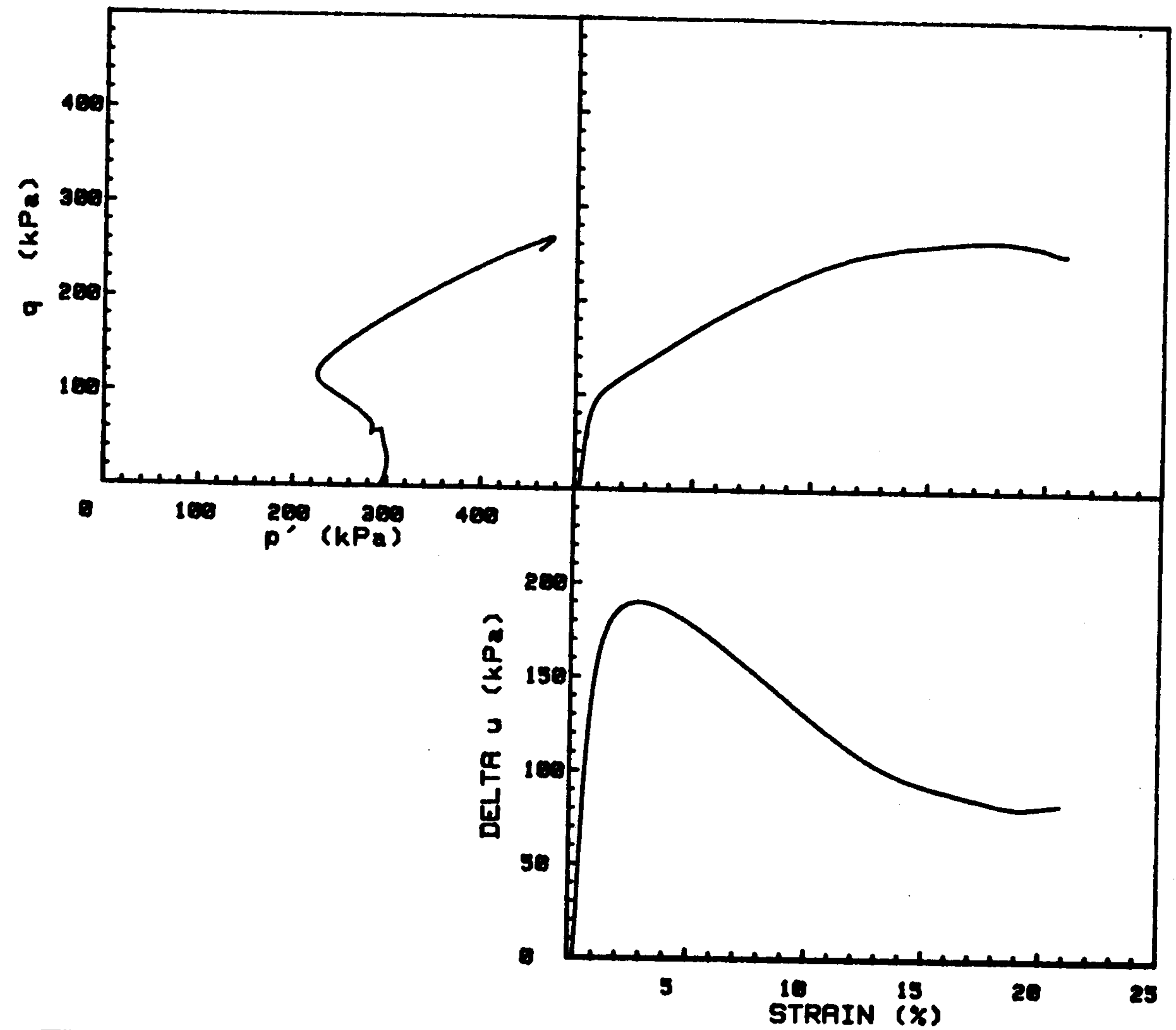

CRUISE	DC4-81-NS	INCREMENT (cm)	131-140
CORE NO.	685A2	TEST NO.	TE120
SIG1c´(kPa)	292.0		
SIG3c´(kPa)	292.0		
INDUCED OCR	1.0		

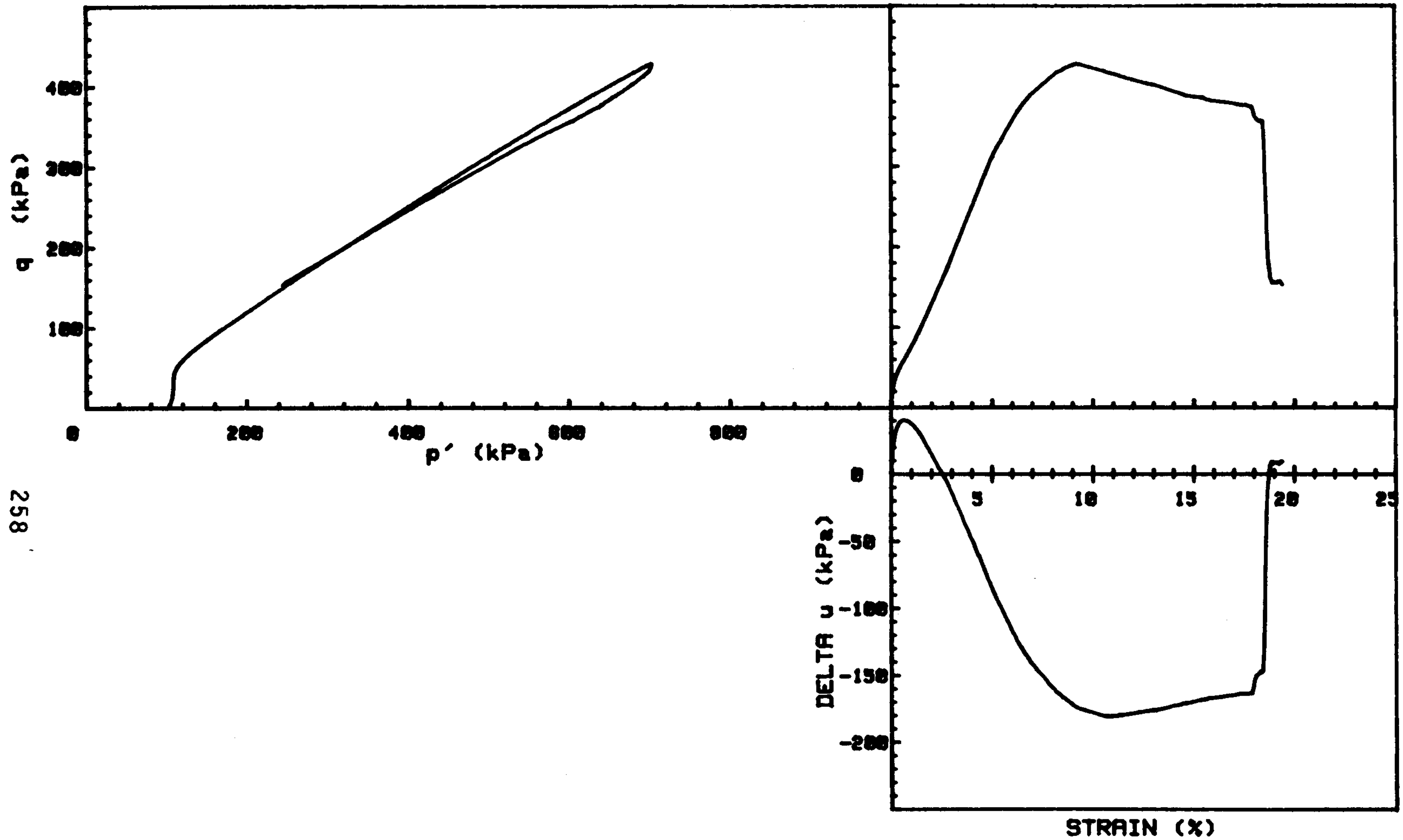

CRUISE DC4-81-NS		INCREMENT (cm)	231-240
CORE NO.	685A2	TEST NO.	TE94
SIG1c′(kPa)	101.5		
SIG3c′(kPa)	101.5		
INDUCED OCR	1.0		

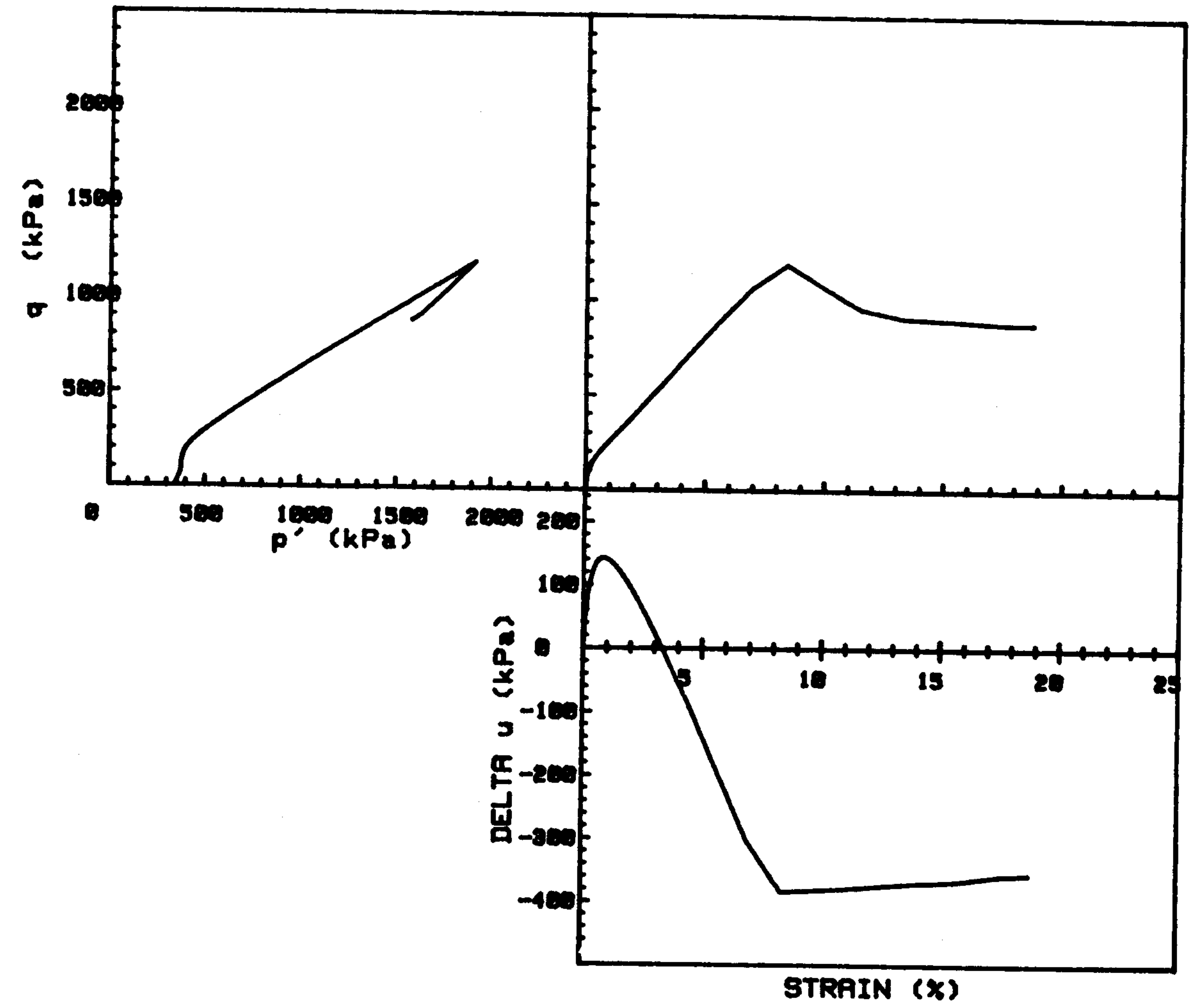

CRUISE DC4-81-NS		INCREMENT (cm)	242-251
CORE NO.	685A2	TEST NO.	TE95
SIG1c′(kPa)	343.2		
SIG3c′(kPa)	343.2		
INDUCED OCR	1.0		

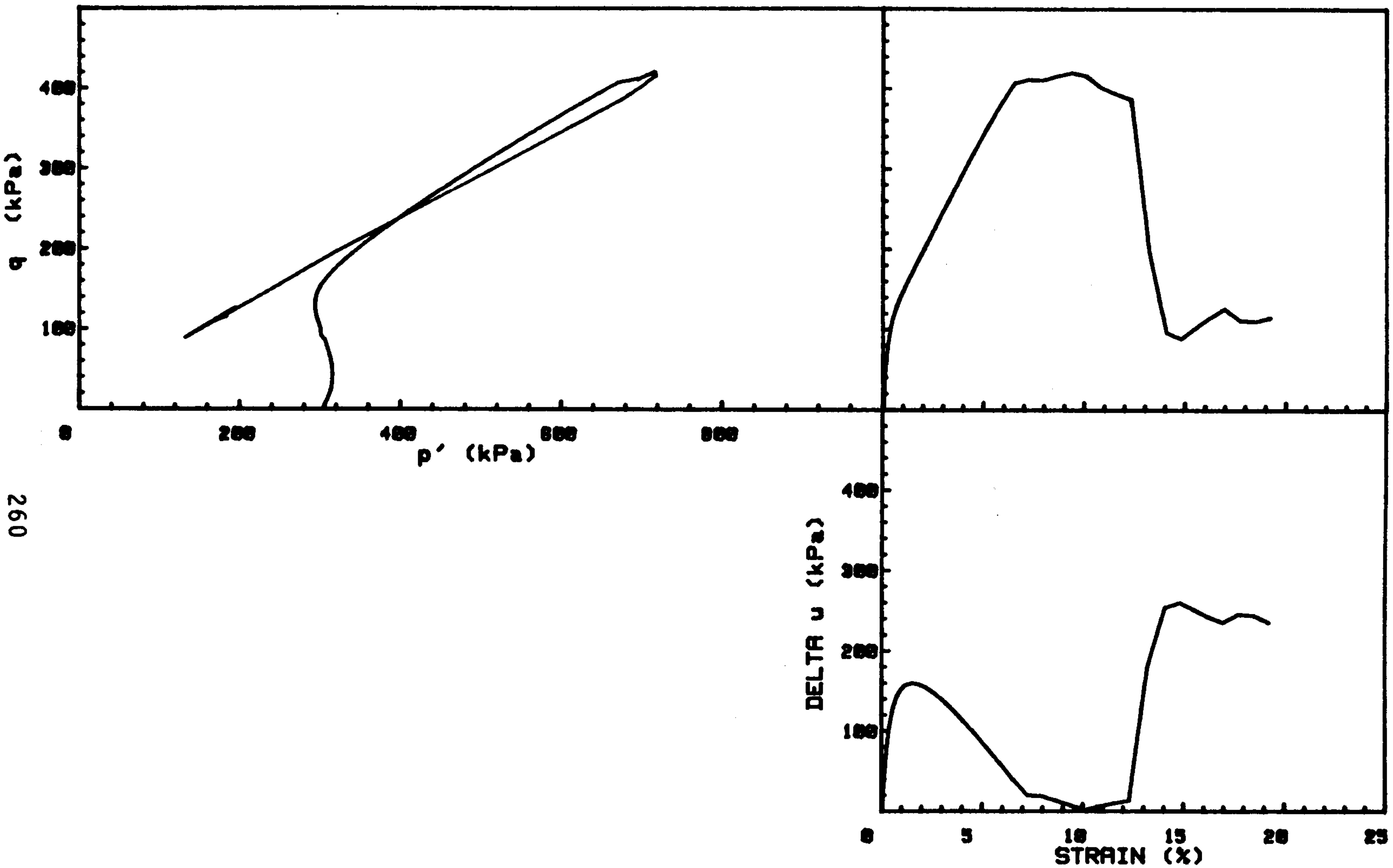

CRUISE	DC4-81-NS	INCREMENT (cm)	170-179
CORE NO.	686A1	TEST NO.	TE100

SIG1c′(kPa) 304.2
SIG3c′(kPa) 304.2
INDUCED OCR 1.0

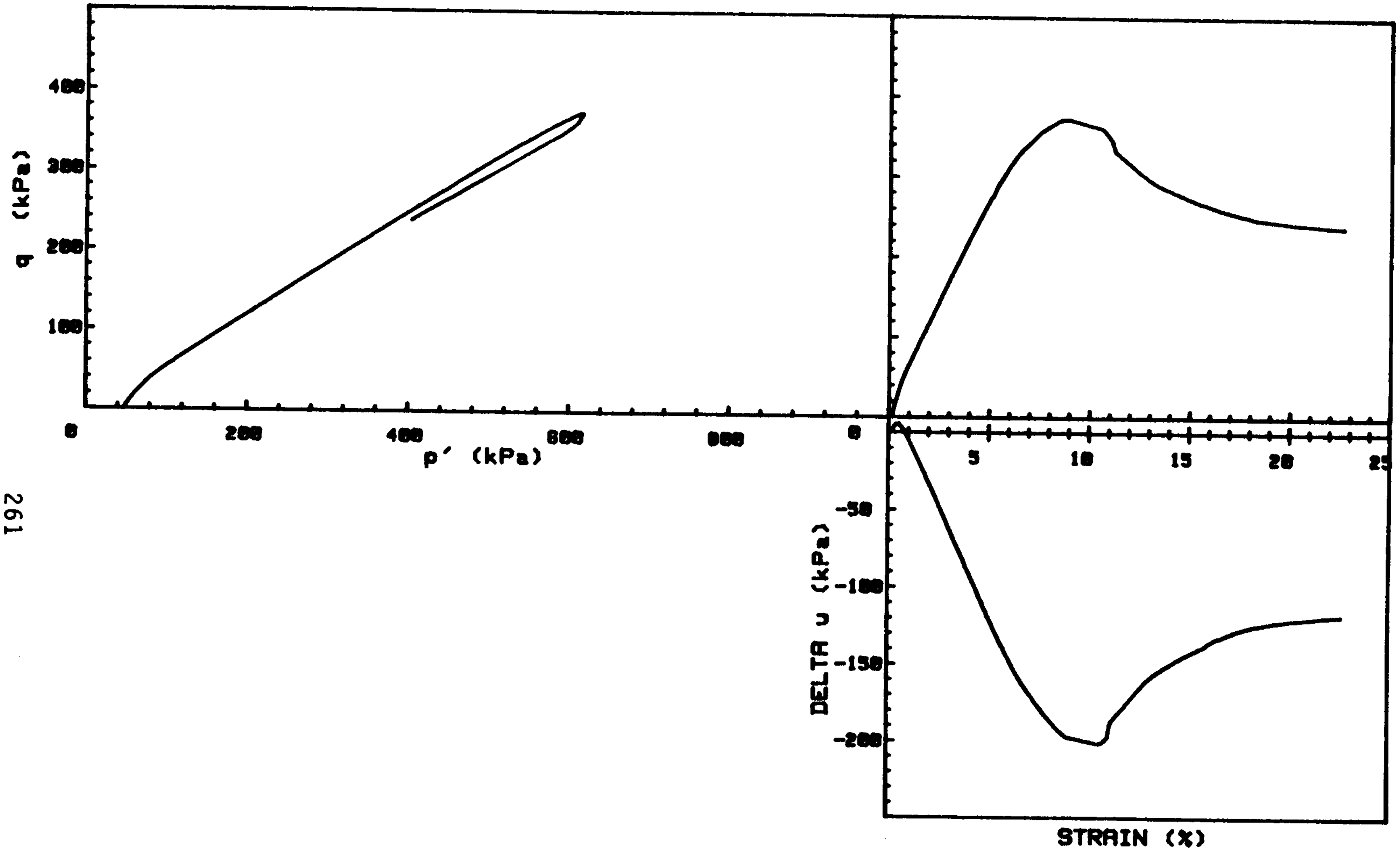

CRUISE DC4-81-NS		INCREMENT (cm)	170-179
CORE NO.	686A1	TEST NO.	TE101
SIG1c′(kPa)	47.7		
SIG3c′(kPa)	47.7		
INDUCED OCR	6.0		

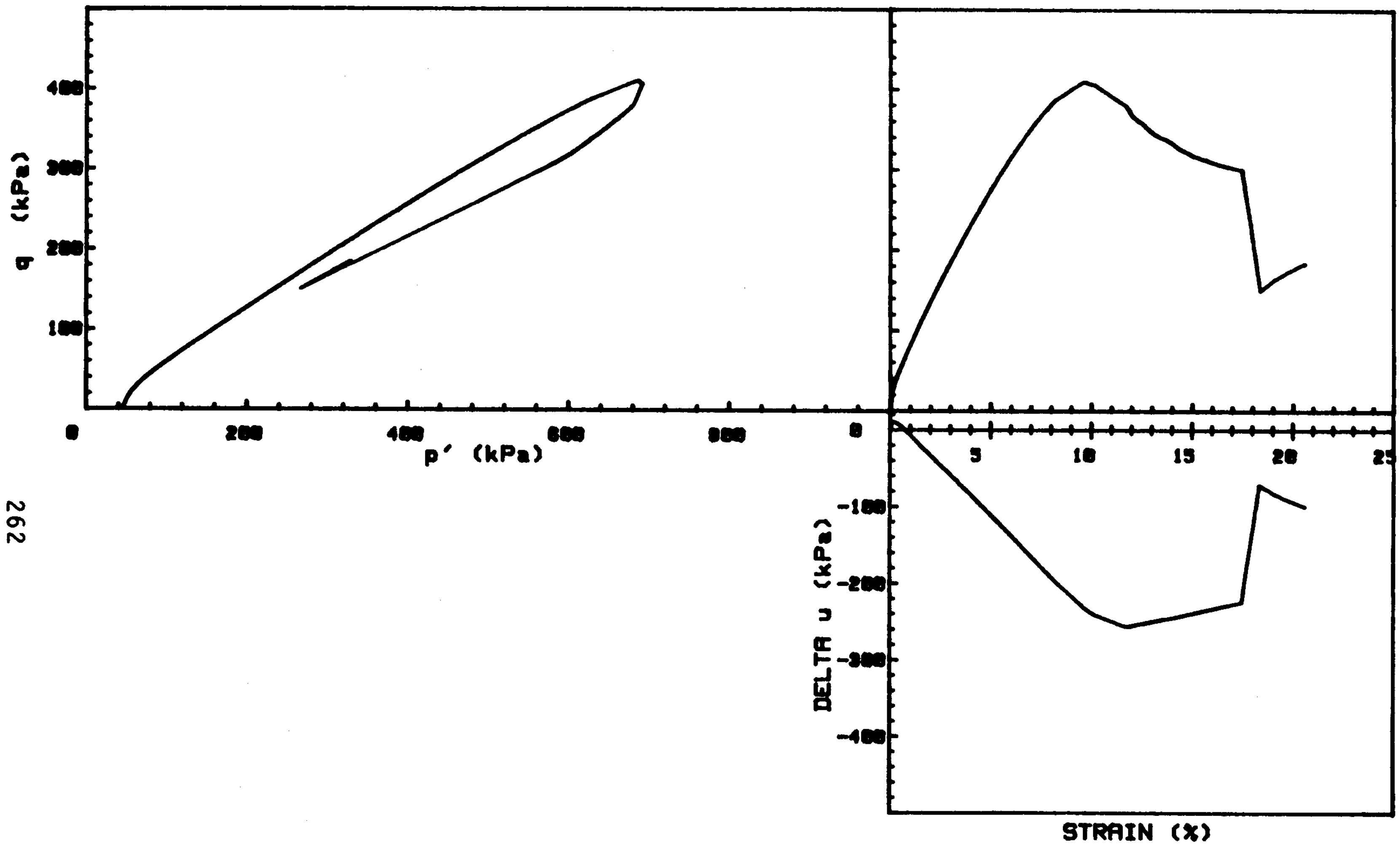

CRUISE DC4-81-NS		INCREMENT (cm)	55-64
CORE NO.	687A1	TEST NO.	TE102
SIG1c'(kPa)	45.1		
SIG3c'(kPa)	45.1		
INDUCED OCR	6.0		

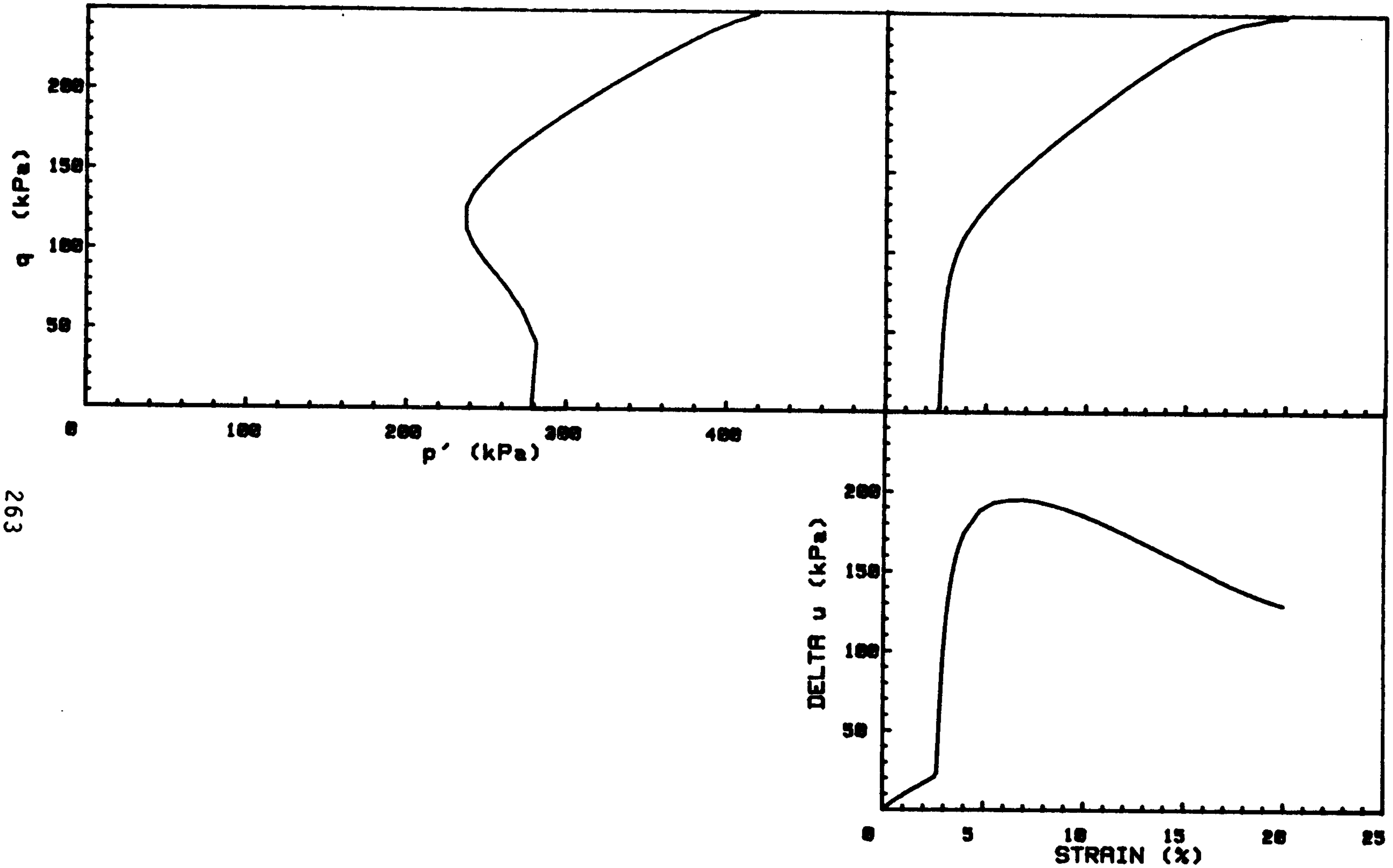

CRUISE DC4-81-NS		INCREMENT (cm)	111-120
CORE NO.	687A1	TEST NO.	TE96

SIG1c′(kPa) 299.6
SIG3c′(kPa) 299.6
INDUCED OCR 1.0

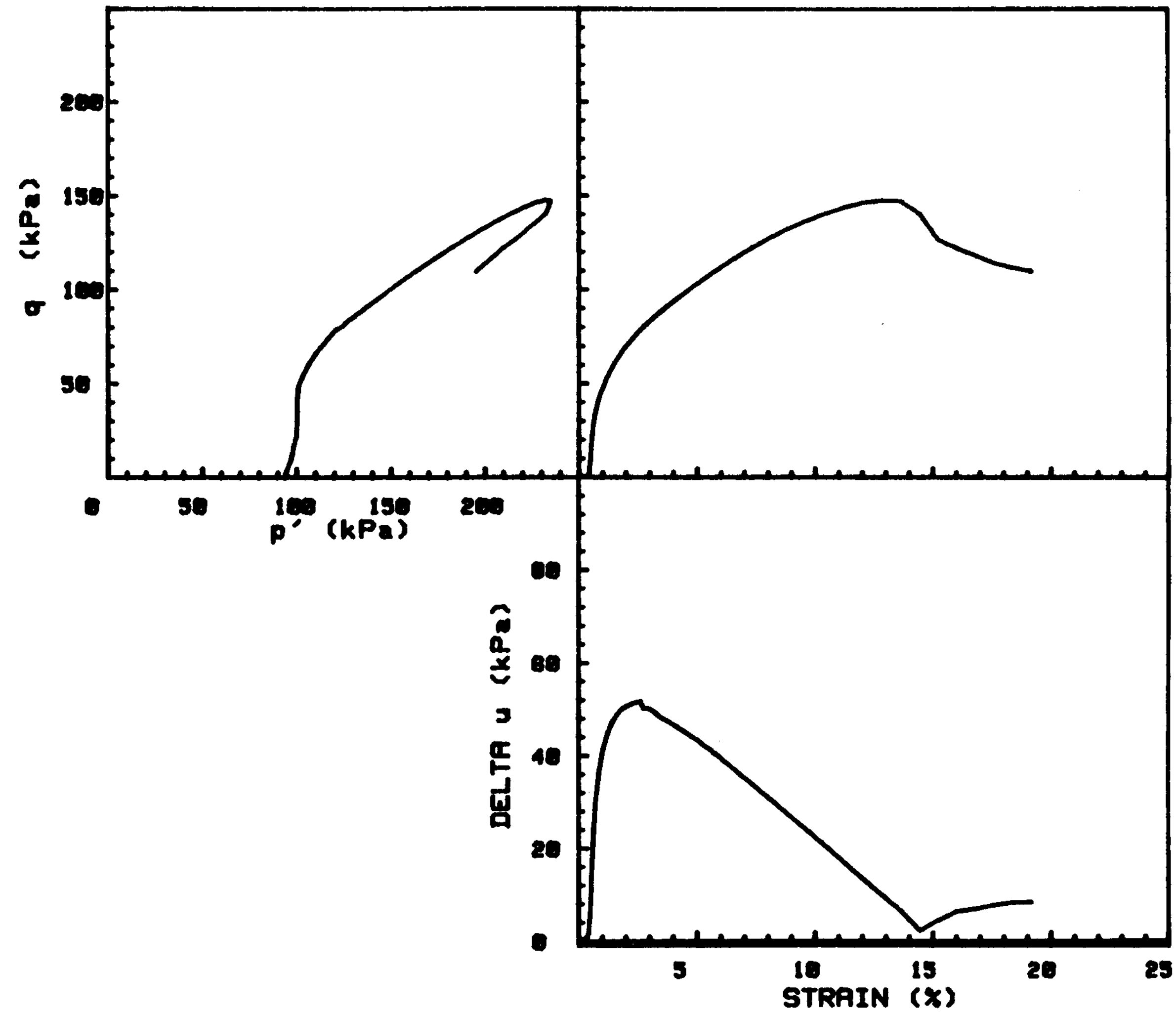

CRUISE	DC4-81-NS	INCREMENT (cm)	111-120
CORE NO.	687A1	TEST NO.	TE97

SIG1c′(kPa) 94.4
SIG3c′(kPa) 94.4
INDUCED OCR 1.0

APPENDIX F:

CYCLIC TRIAXIAL TEST PLOTS

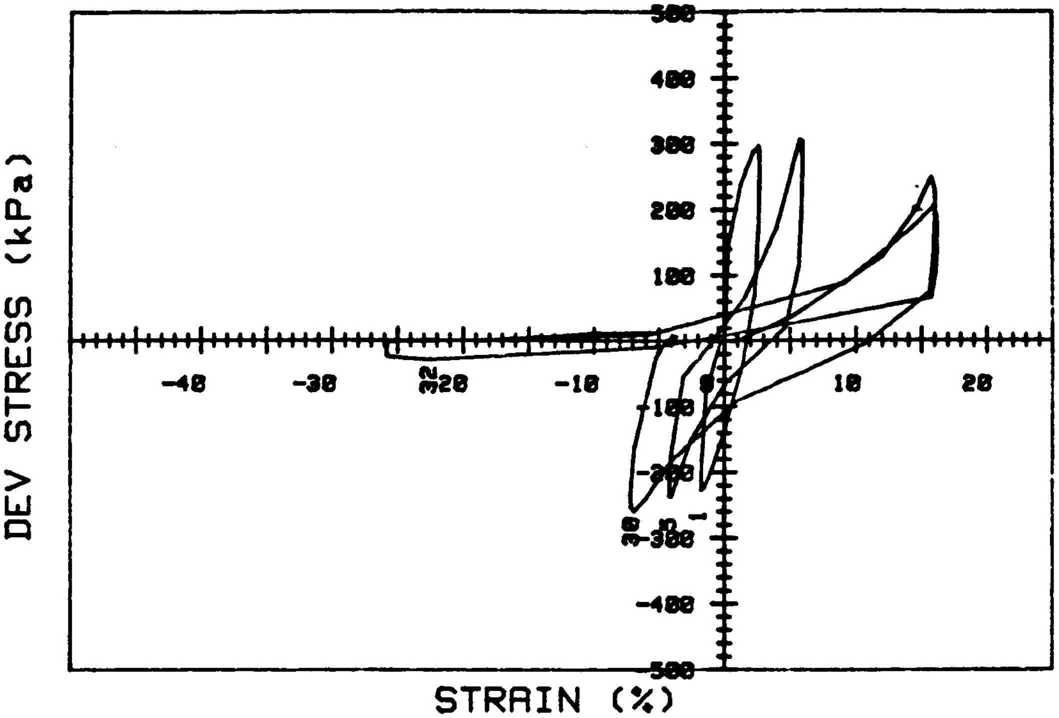

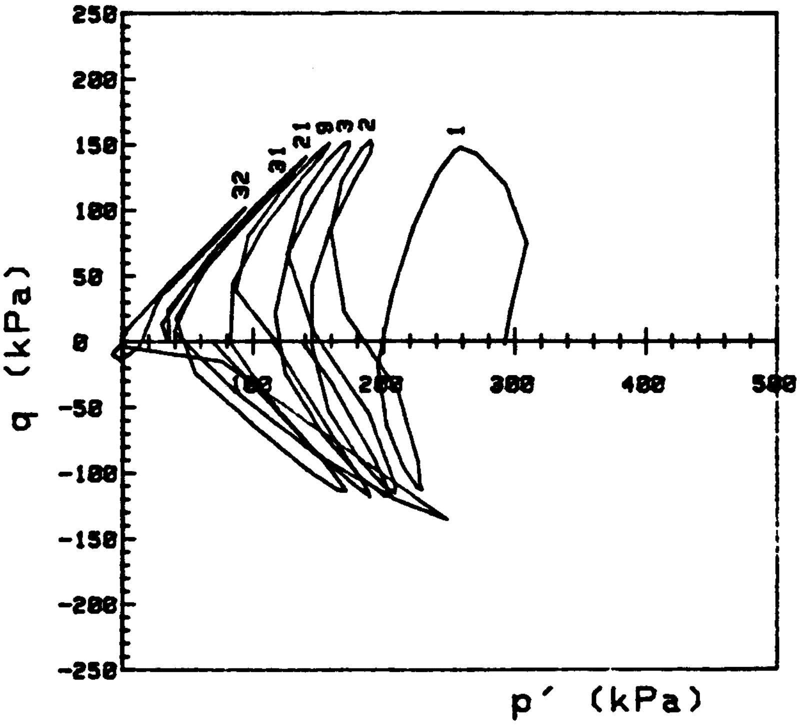

CRUISE DC4-81-NS		INCREMENT (cm)		142-150	
CORE NO.	681A2	TEST NO.		D100	
SIG1c′(kPa)	294.5	STATIC qf (kPa)		300.0	
SIG3c′(kPa)	294.5	AVG MAX q (kPa)		141.0 (47.0%)	
INDUCED OCR	1.0	AVG MIN q (kPa)		-115.5 (38.5%)	

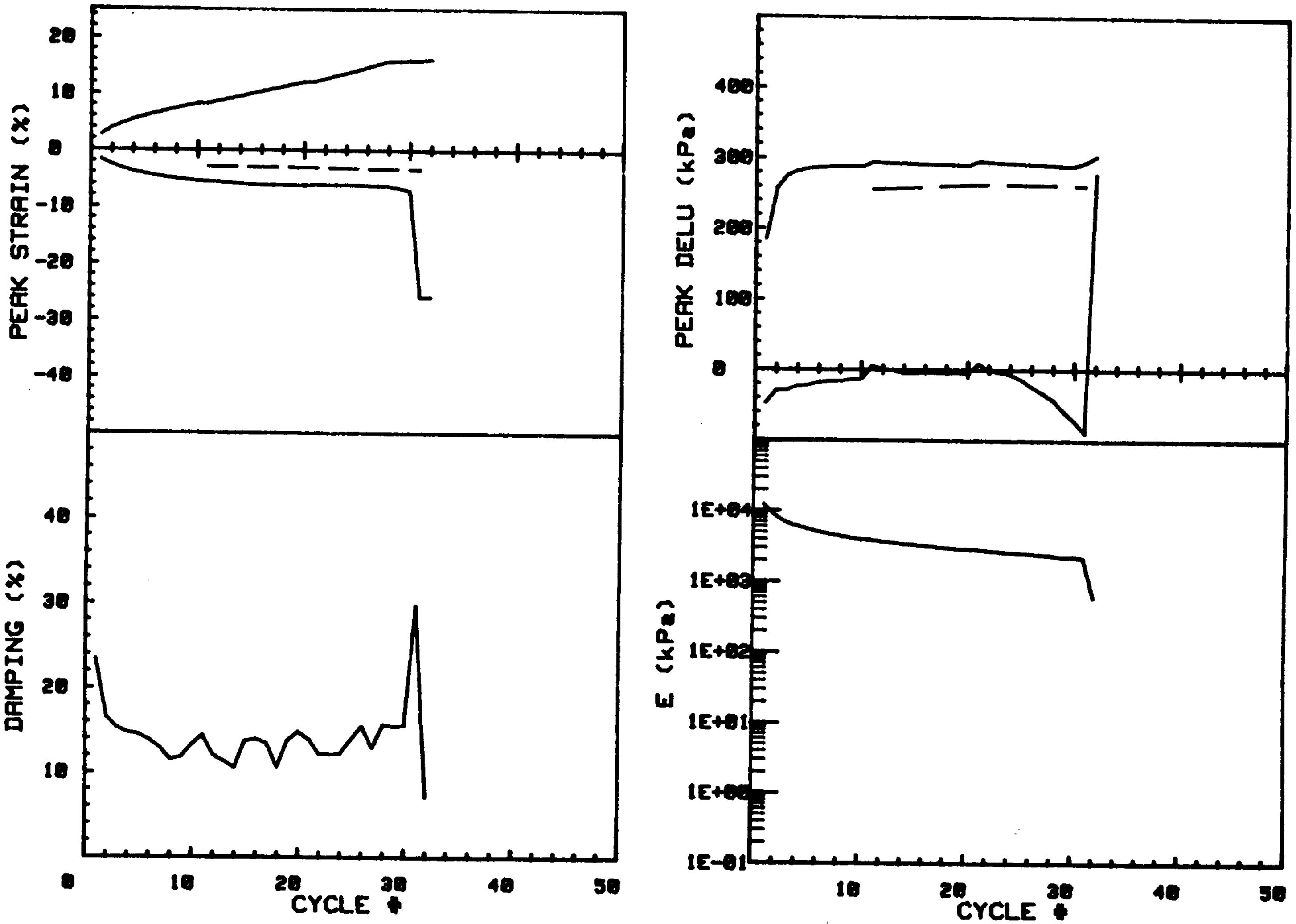

CRUISE DC4-81-NS		INCREMENT (cm)	142-150
CORE NO.	681A2	TEST NO.	D100
SIG1c'(kPa)	294.5	STATIC qf (kPa)	300.0
SIG3c'(kPa)	294.5	AVG MAX q (kPa)	141.0 (47.0%)
INDUCED OCR	1.0	AVG MIN q (kPa)	-115.5 (38.5%)

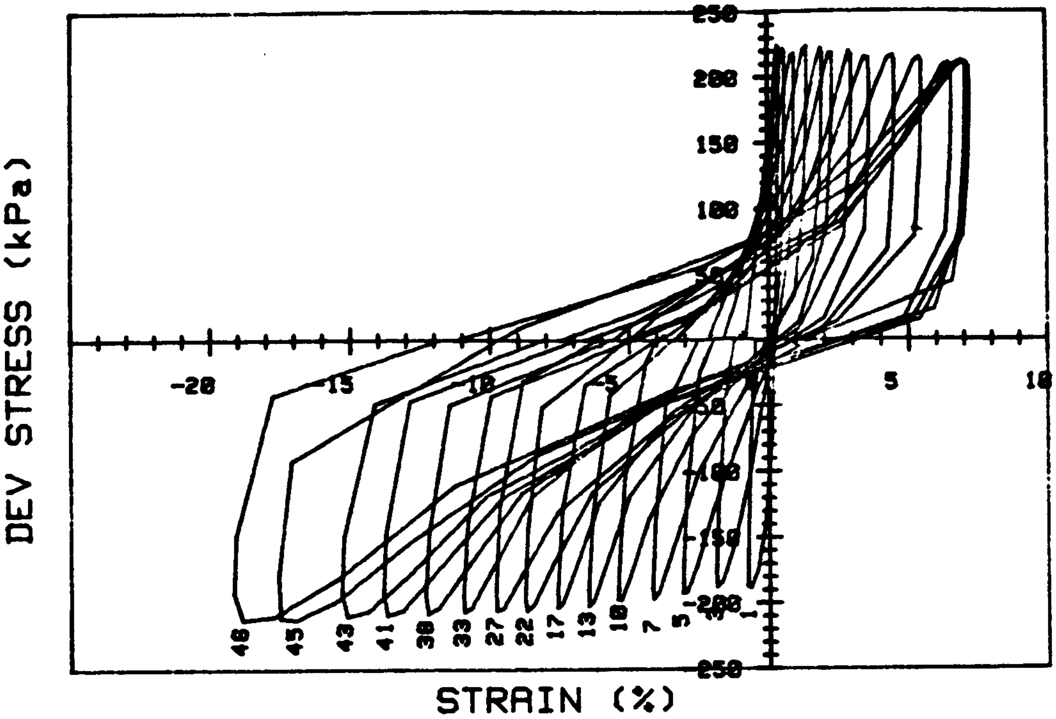

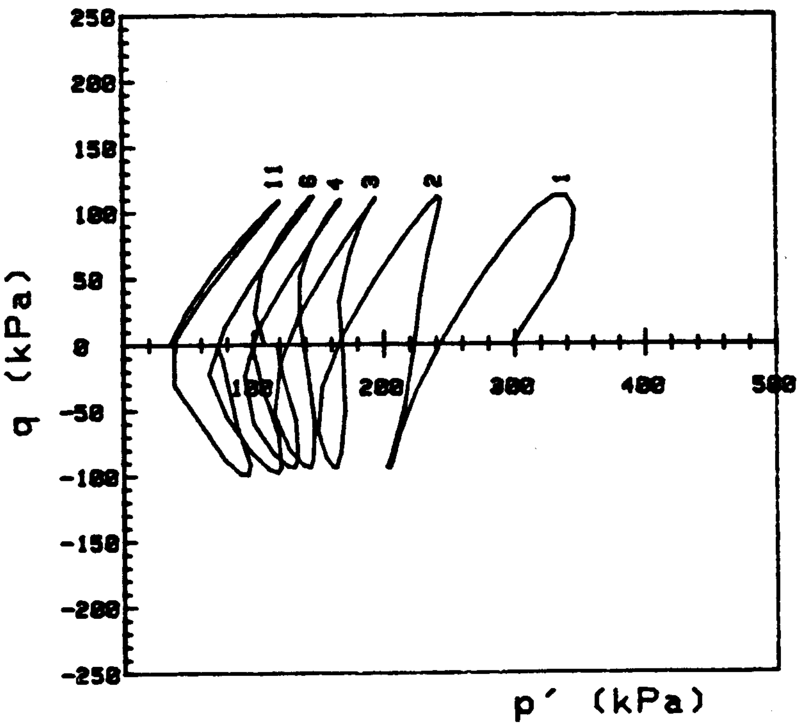

CRUISE DC4-81-NS		INCREMENT (cm)	142-149
CORE NO.	681A2	TEST NO.	D101
SIG1c′(kPa)	298.4	STATIC qf (kPa)	300.0
SIG3c′(kPa)	298.4	AVG MAX q (kPa)	108.2 (36.1%)
INDUCED OCR	1.0	AVG MIN q (kPa)	-101.5 (33.8%)

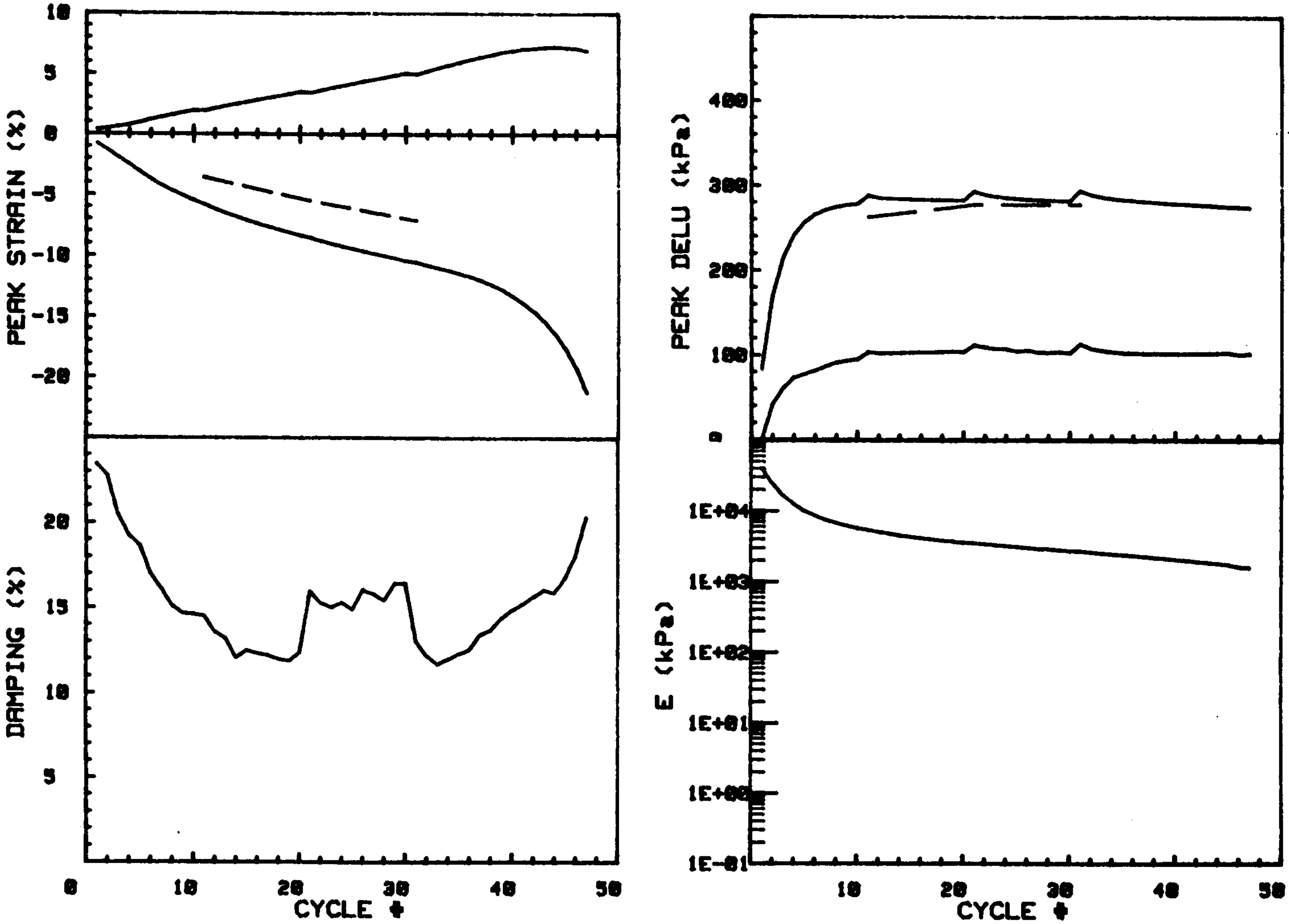

CRUISE DC4-81-NS		INCREMENT (cm)	142-149
CORE NO.	681A2	TEST NO.	D101
SIG1c'(kPa)	298.4	STATIC qf (kPa)	300.0
SIG3c'(kPa)	298.4	AVG MAX q (kPa)	108.2 (36.1%)
INDUCED OCR	1.0	AVG MIN q (kPa)	-101.5 (33.8%)

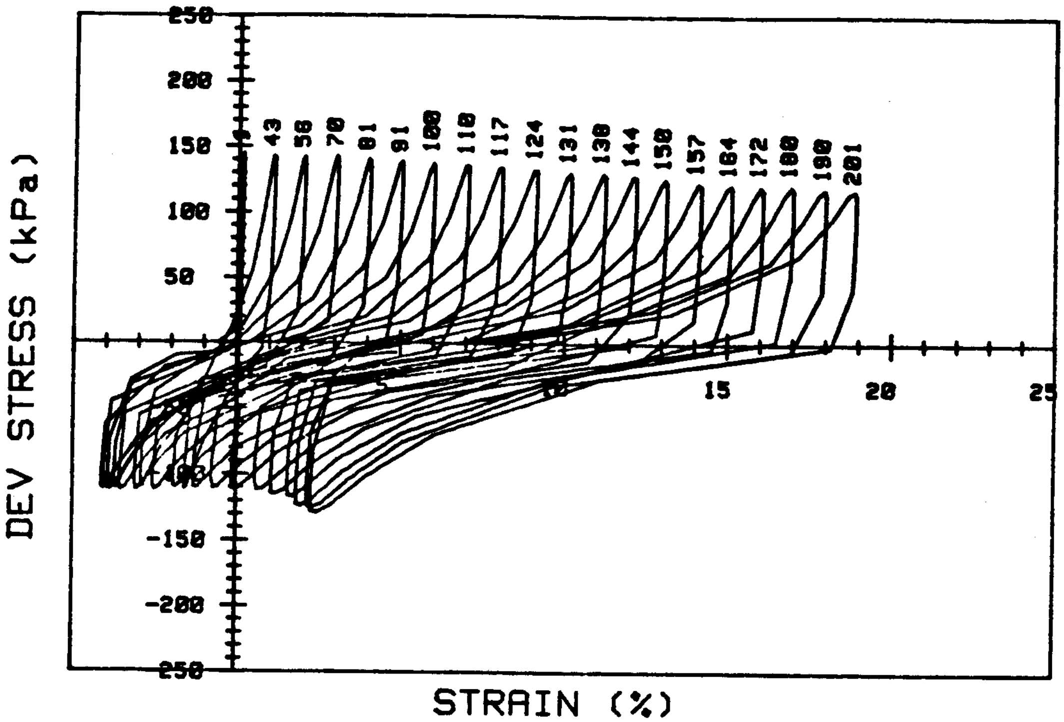

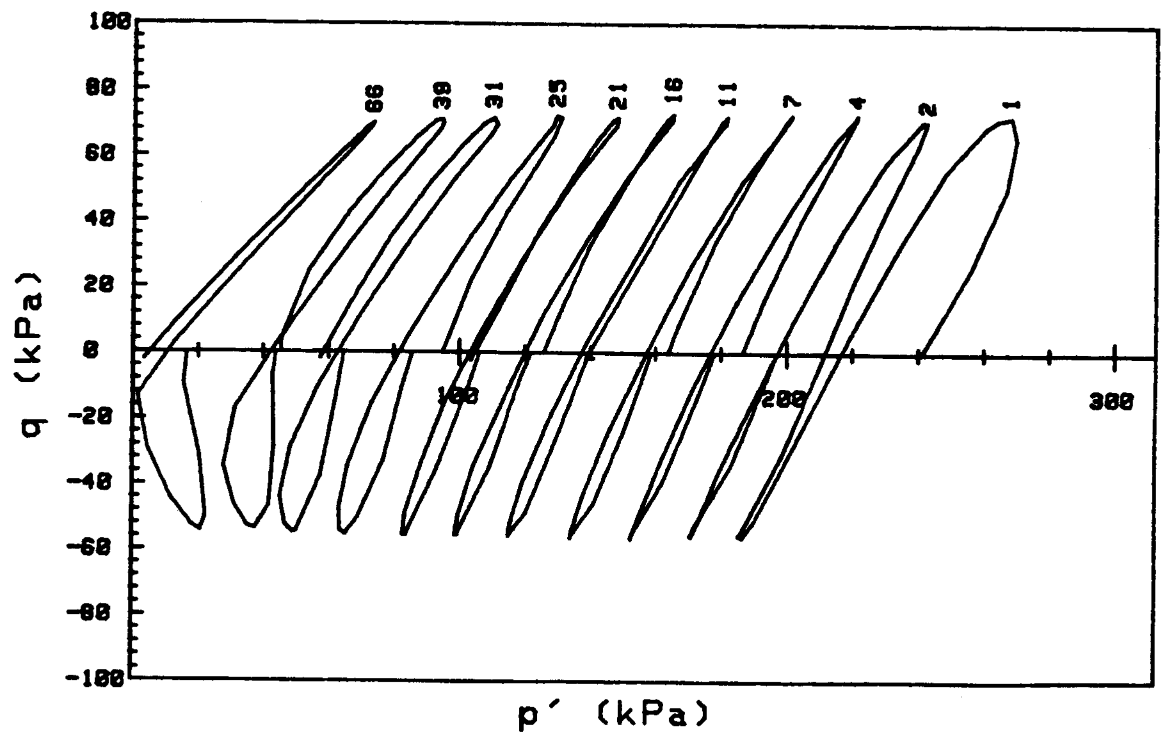

CRUISE DC4-81-NS		INCREMENT (cm)	76-83
CORE NO.	682A1	TEST NO.	TC44
SIG1c′(kPa)	241.8	STATIC qf (kPa)	184.0
SIG3c′(kPa)	241.8	AVG MAX q (kPa)	65.8 (35.8%)
INDUCED OCR	1.0	AVG MIN q (kPa)	-56.9 (30.9%)

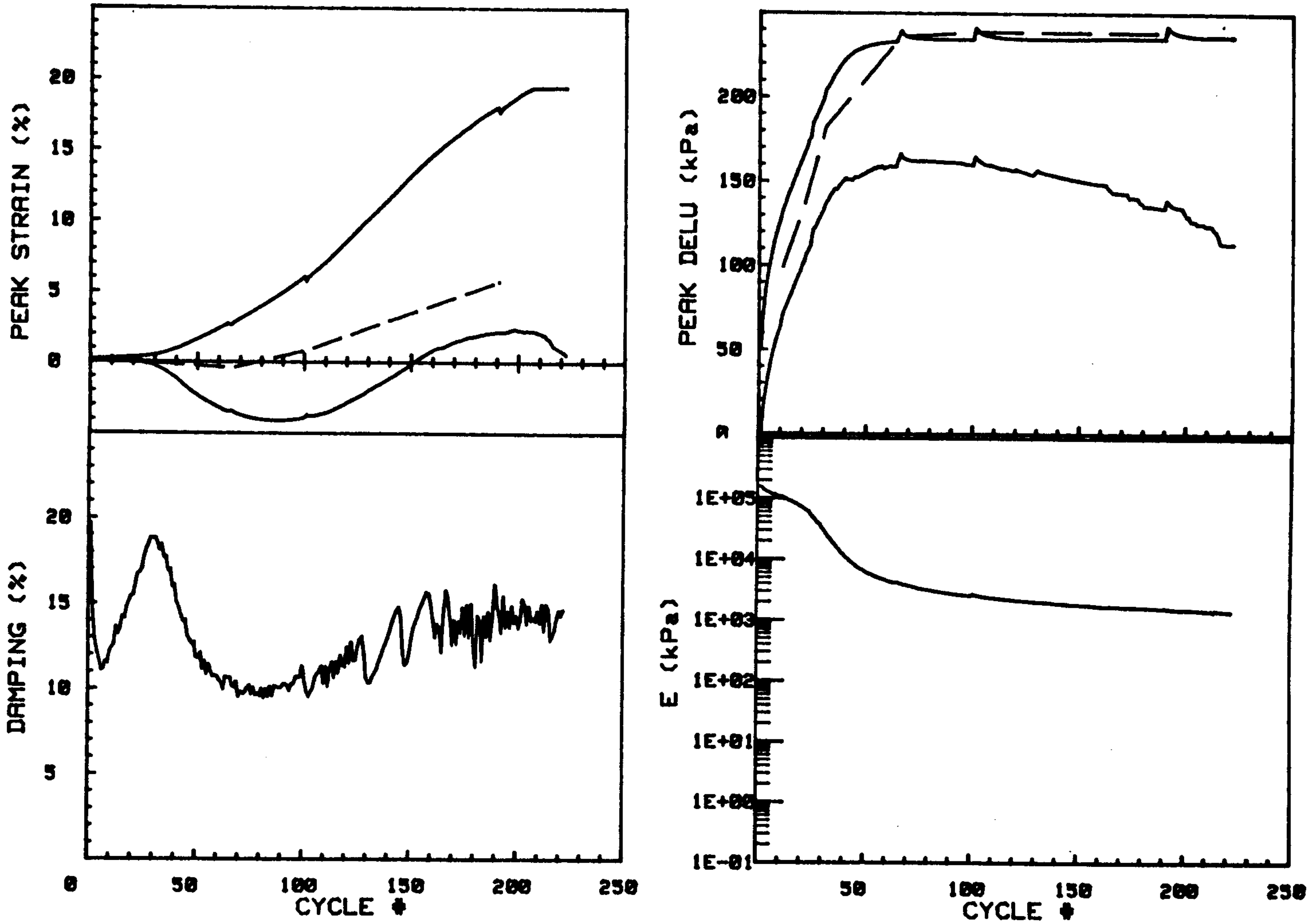

CRUISE DC4-81-NS		INCREMENT (cm)	76-83
CORE NO.	682A1	TEST NO.	TC44
SIG1c'(kPa)	241.8	STATIC qf (kPa)	184.0
SIG3c'(kPa)	241.8	AVG MAX q (kPa)	65.8 (35.8%)
INDUCED OCR	1.0	AVG MIN q (kPa)	-56.9 (30.9%)

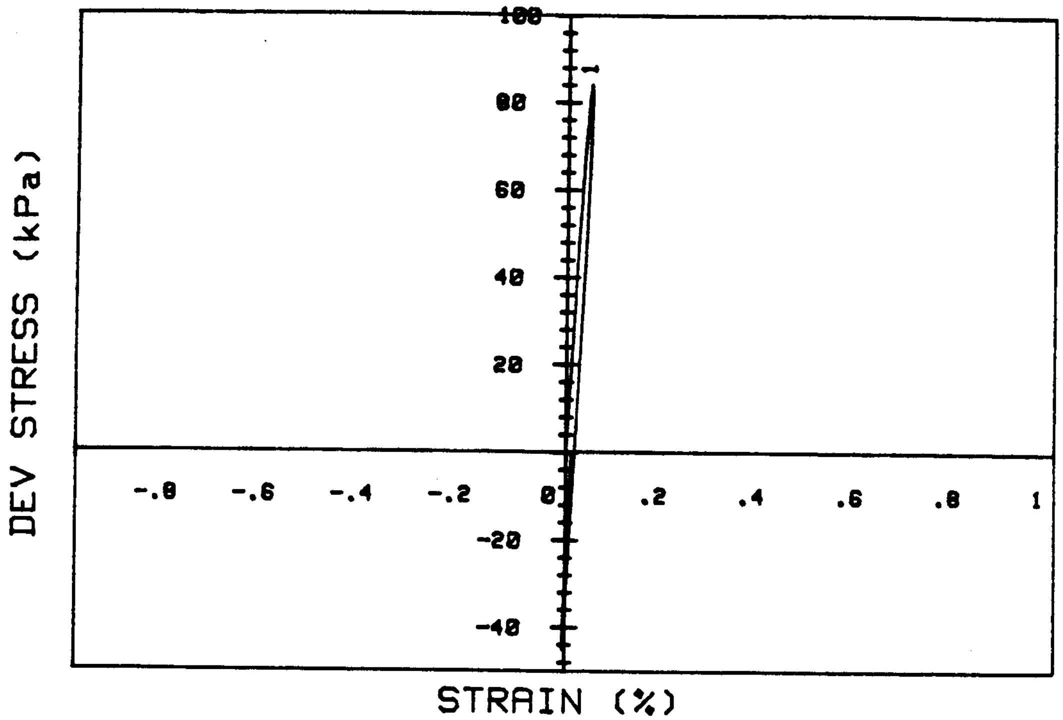

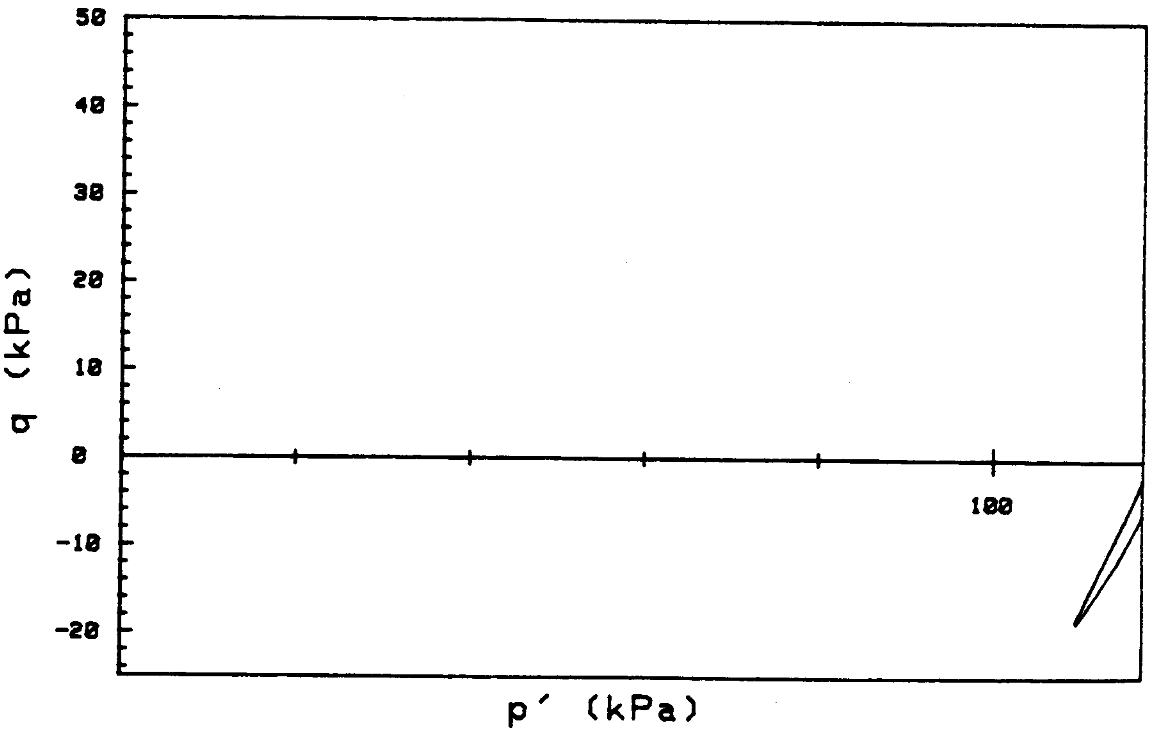

CRUISE DC4-81-NS		INCREMENT (cm)	76-84
CORE NO.	682A1	TEST NO.	TC45
SIG1c′(kPa)	239.4	STATIC qf (kPa)	183.9
SIG3c′(kPa)	239.4	AVG MAX q (kPa)	41.6 (22.6%)
INDUCED OCR	1.0	AVG MIN q (kPa)	-19.4 (10.5%)

Cycles 1-470

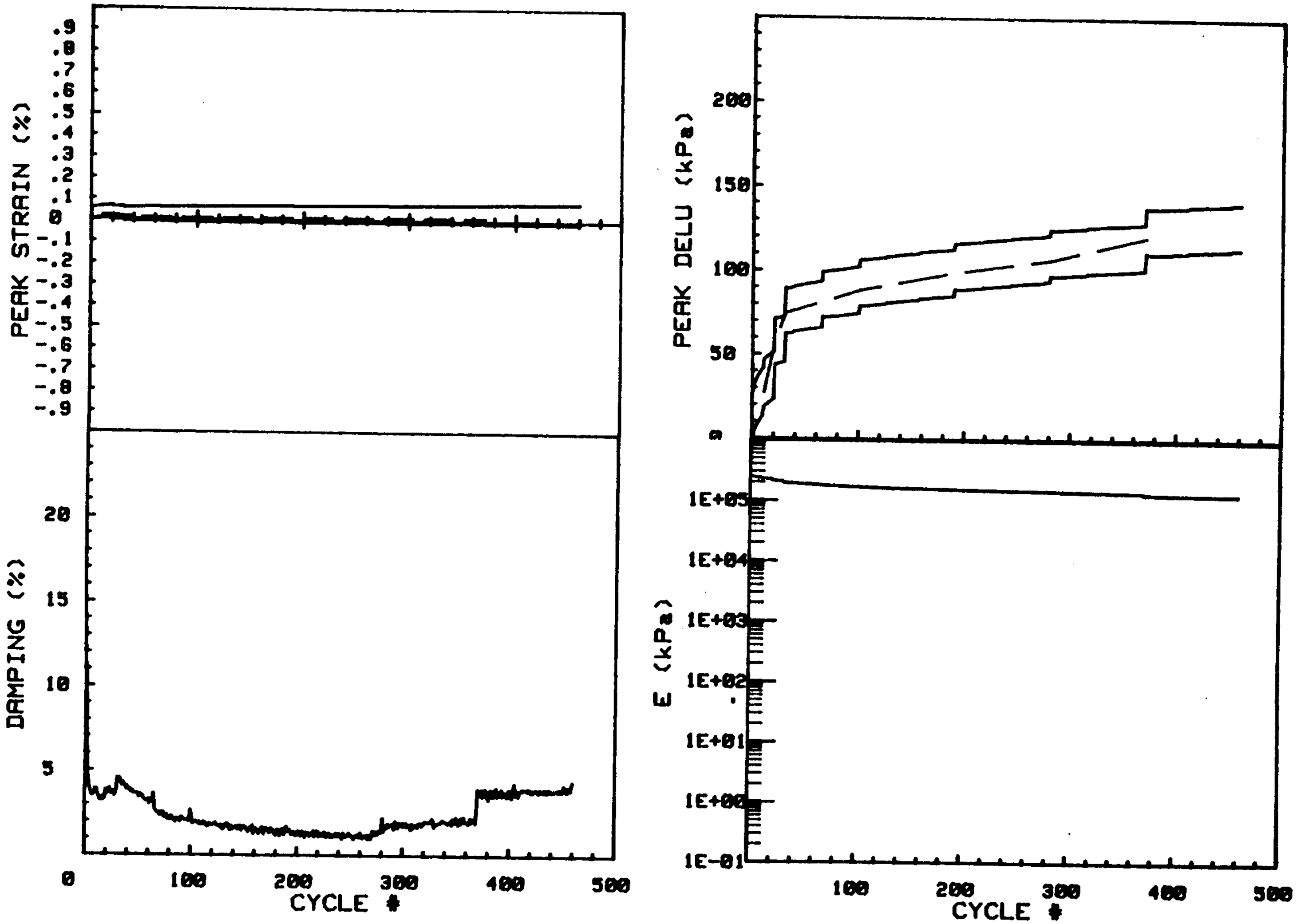

CRUISE DC4-81-NS		INCREMENT (cm)	76-84
CORE NO.	682A1	TEST NO.	TC45
SIG1c'(kPa)	239.4	STATIC qf (kPa)	183.9
SIG3c'(kPa)	239.4	AVG MAX q (kPa)	41.6 (22.6%)
INDUCED OCR	1.0	AVG MIN q (kPa)	-19.4 (10.5%)

Cycles 1-470

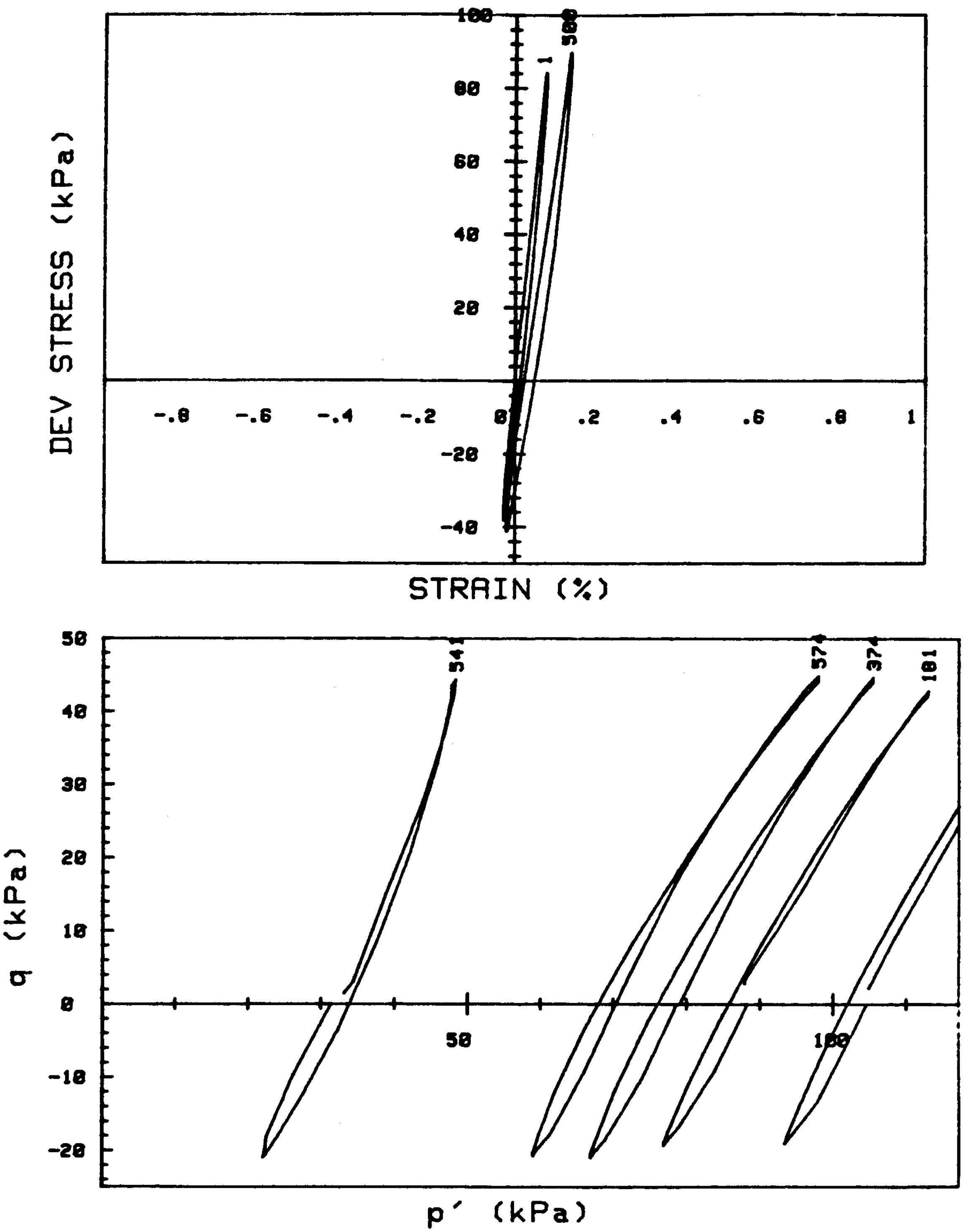

CRUISE DC4-81-NS		INCREMENT (cm)	76-84
CORE NO.	682A1	TEST NO.	TC45
SIG1c′(kPa)	102.7	STATIC qf (kPa)	183.9
SIG3c′(kPa)	102.7	AVG MAX q (kPa)	43.9 (23.9%)
INDUCED OCR	1.0	AVG MIN q (kPa)	-20.3 (11.0%)

Cycles 741 - 1370

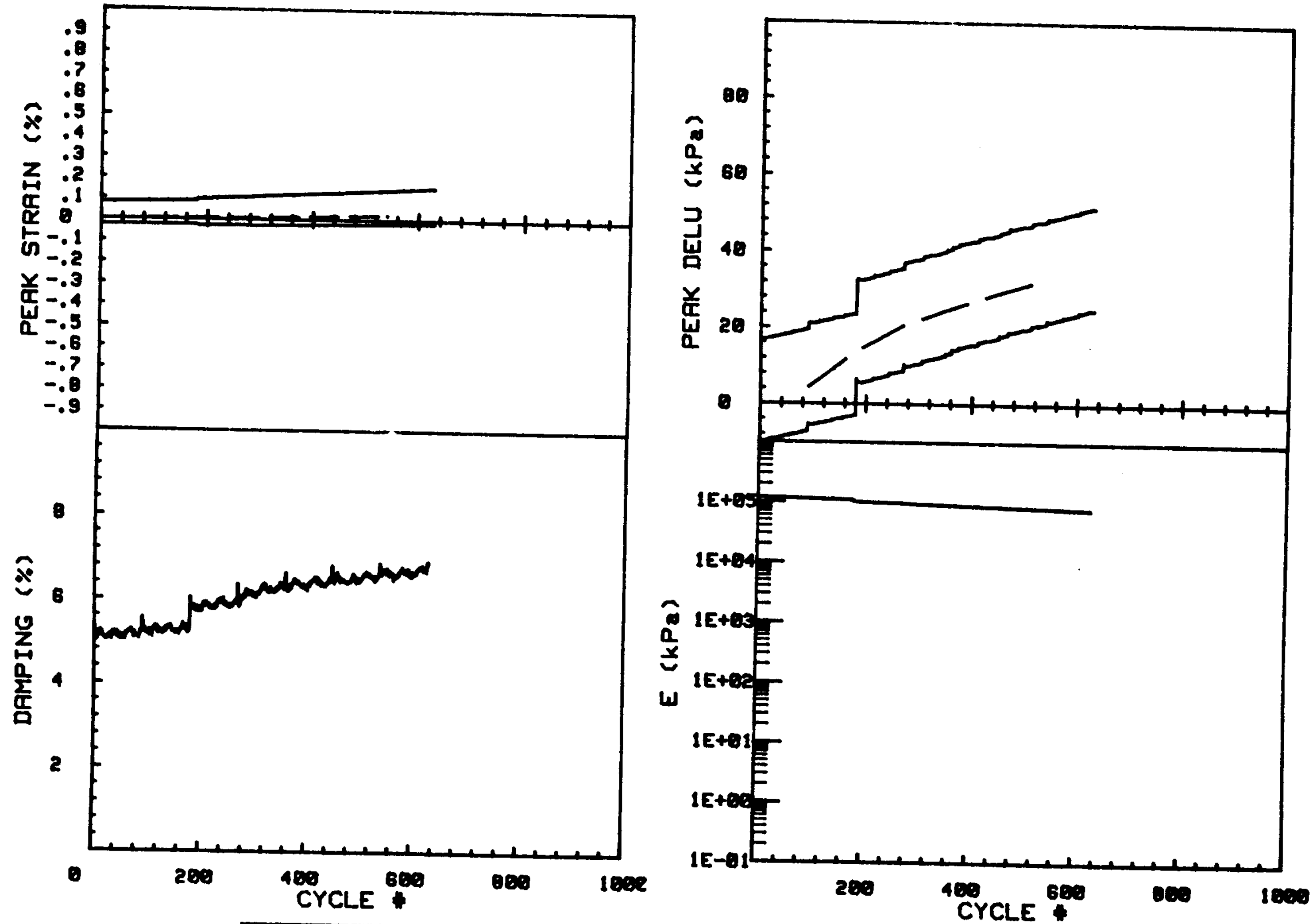

CRUISE DC4-81-NS		INCREMENT (cm)	76-84
CORE NO.	682A1	TEST NO.	TC45
SIG1c′(kPa)	102.7	STATIC qf (kPa)	183.9
SIG3c′(kPa)	102.7	AVG MAX q (kPa)	43.9 (23.9%)
INDUCED OCR	1.0	AVG MIN q (kPa)	-20.3 (11.0%)

Cycles 741 - 1370

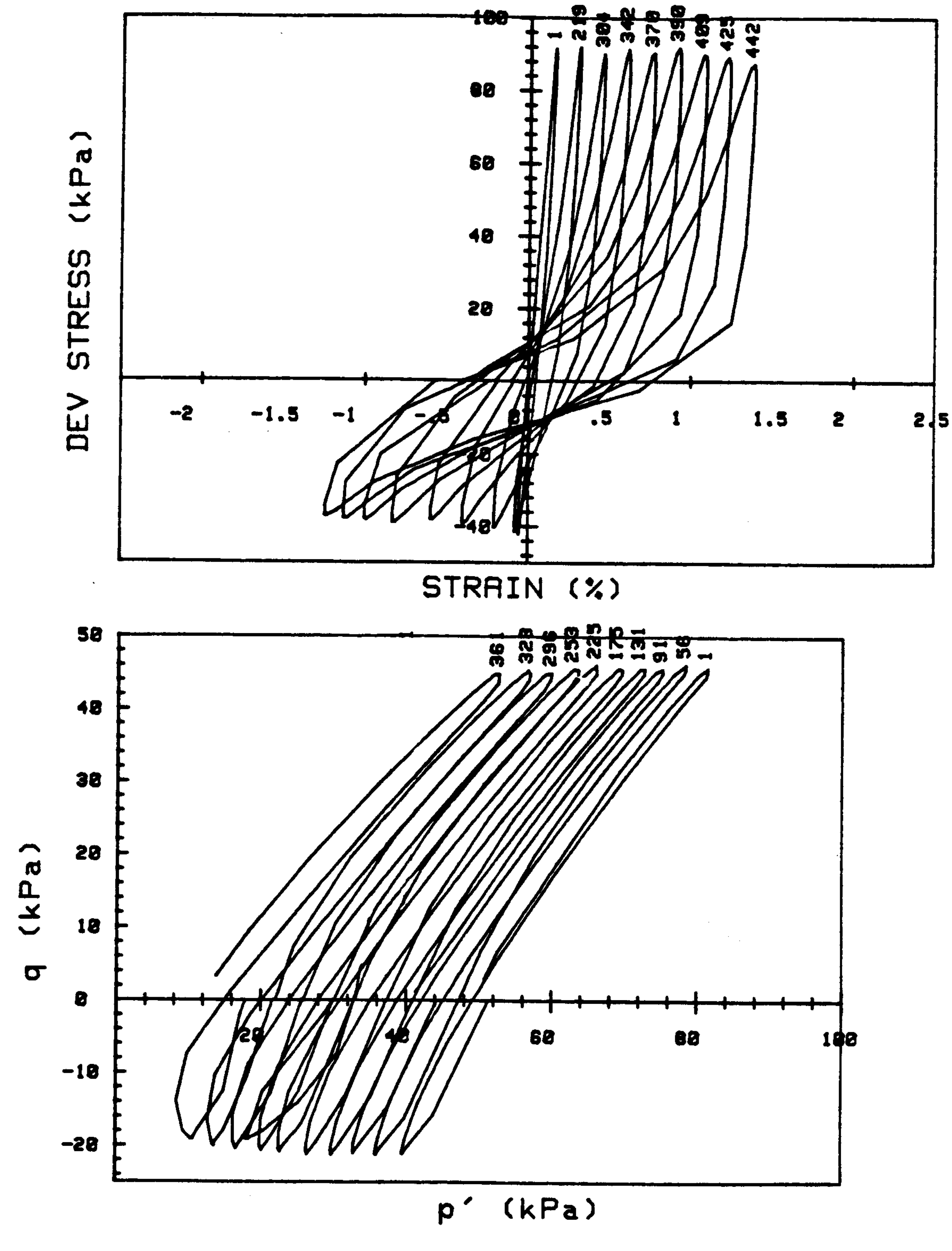

CRUISE DC4-81-NS		INCREMENT (cm)	76-84
CORE NO.	682A1	TEST NO.	TC45
SIG1c´(kPa)	47.8	STATIC qf (kPa)	183.9
SIG3c´(kPa)	47.8	AVG MAX q (kPa)	45.5 (24.7%)
INDUCED OCR	1.0	AVG MIN q (kPa)	-20.4 (11.1%)

Cycles 1461 - 1910

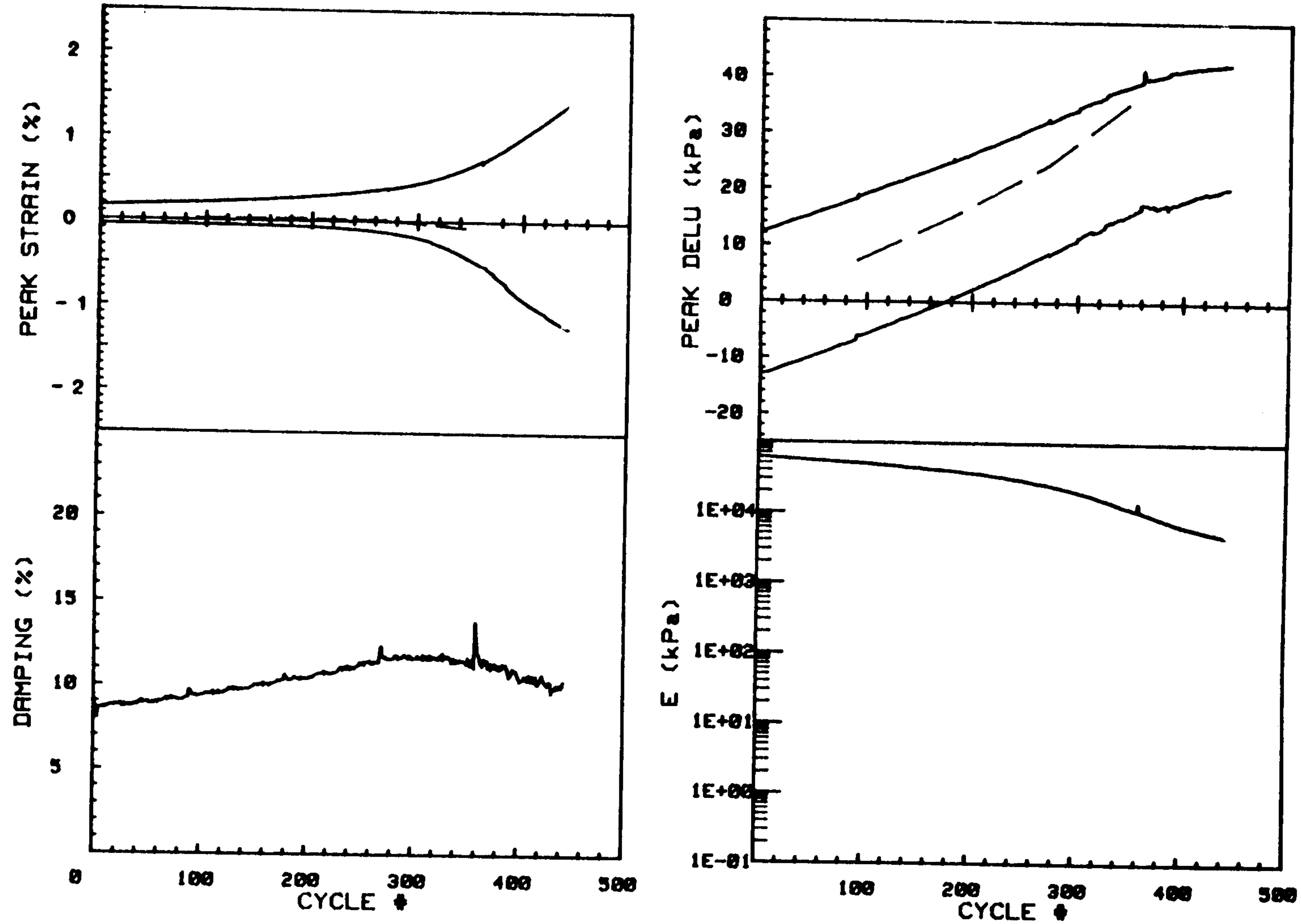

CRUISE DC4-81-NS		INCREMENT (cm)	76-84
CORE NO.	682A1	TEST NO.	TC45
SIG1c′(kPa)	47.8	STATIC qf (kPa)	183.9
SIG3c′(kPa)	47.8	AVG MAX q (kPa)	45.5 (24.7%)
INDUCED OCR	1.0	AVG MIN q (kPa)	-20.4 (11.1%)

Cycles 1461 - 1910

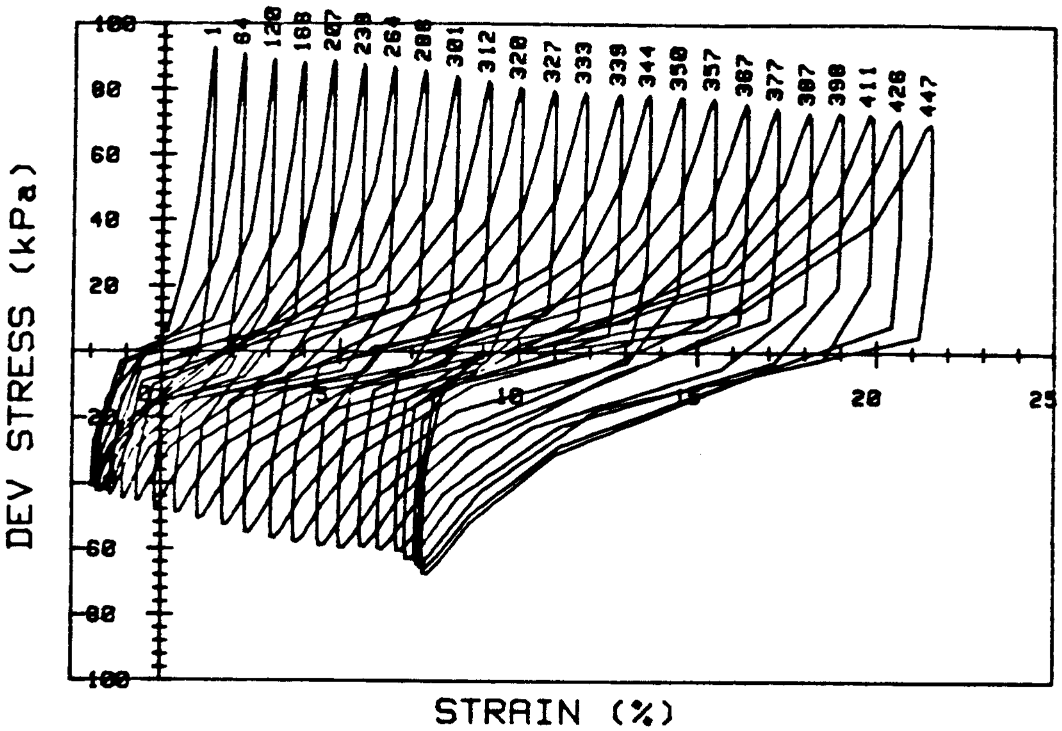

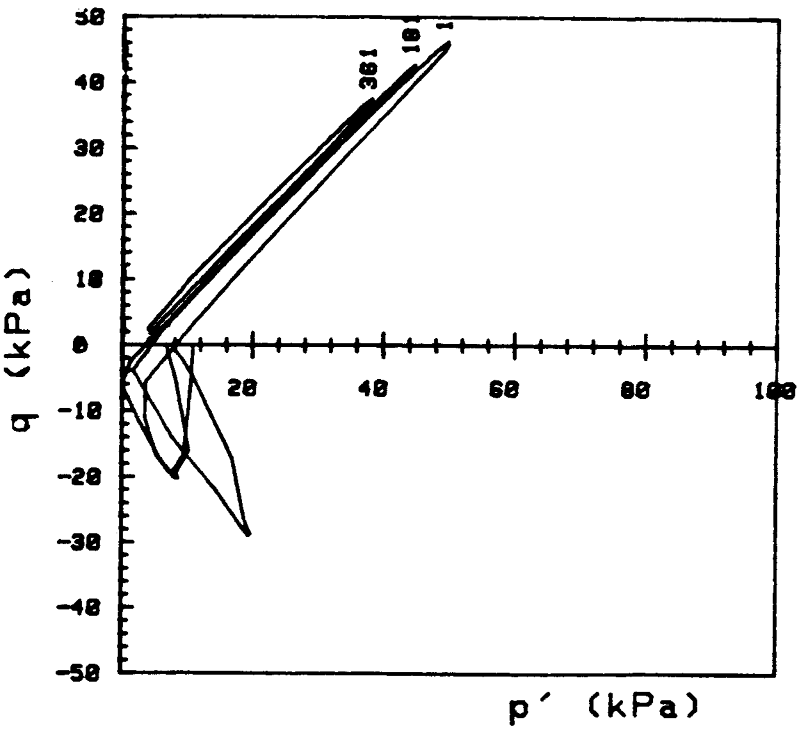

CRUISE DC4-81-NS		INCREMENT (cm)	76-84
CORE NO.	682A1	TEST NO.	TC45
SIG1c′(kPa)	4.2	STATIC qf (kPa)	183.9
SIG3c′(kPa)	4.2	AVG MAX q (kPa)	42.0 (22.8%)
INDUCED OCR	1.0	AVG MIN q (kPa)	-23.8 (12.9%)

Cycles 1911 - 2360

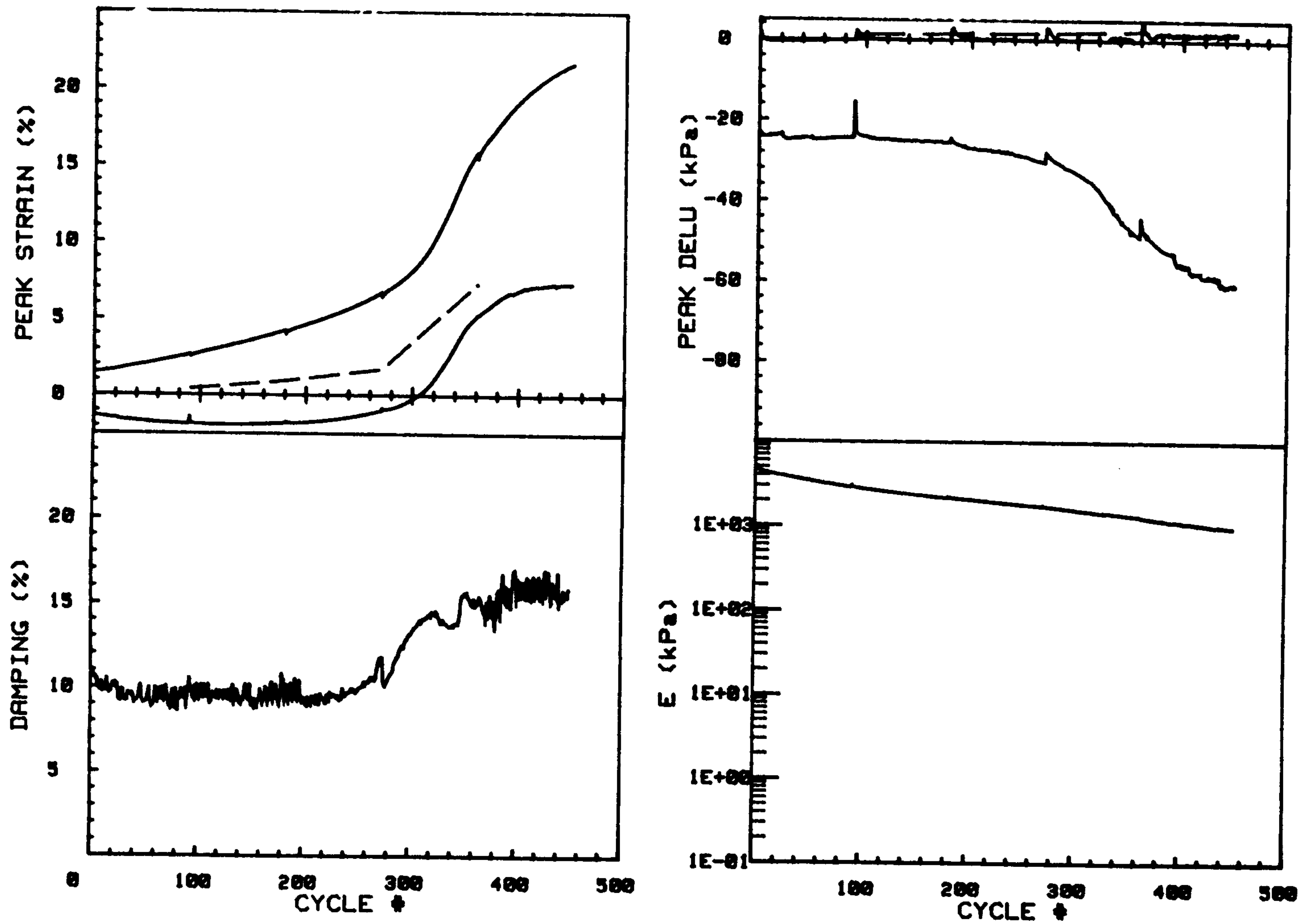

CRUISE DC4-81-NS		INCREMENT (cm)	76-84
CORE NO.	682A1	TEST NO.	TC45
SIG1c'(kPa)	4.2	STATIC qf (kPa)	183.9
SIG3c'(kPa)	4.2	AVG MAX q (kPa)	42.0 (22.8%)
INDUCED OCR	1.0	AVG MIN q (kPa)	-23.8 (12.9%)

Cycles 1911 - 2360

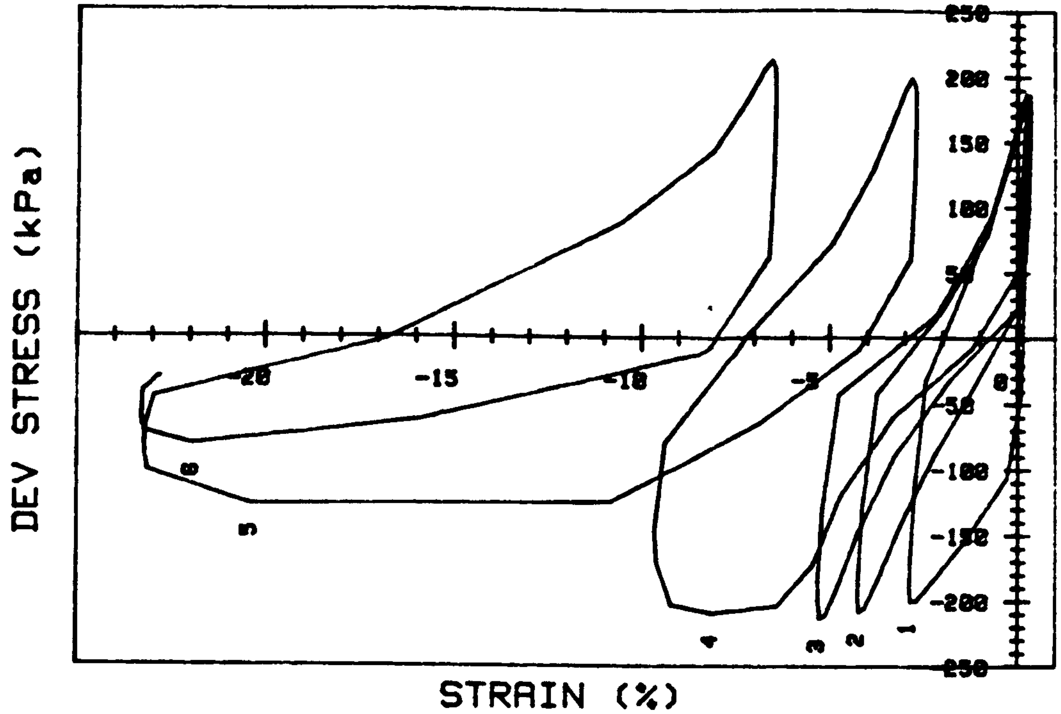

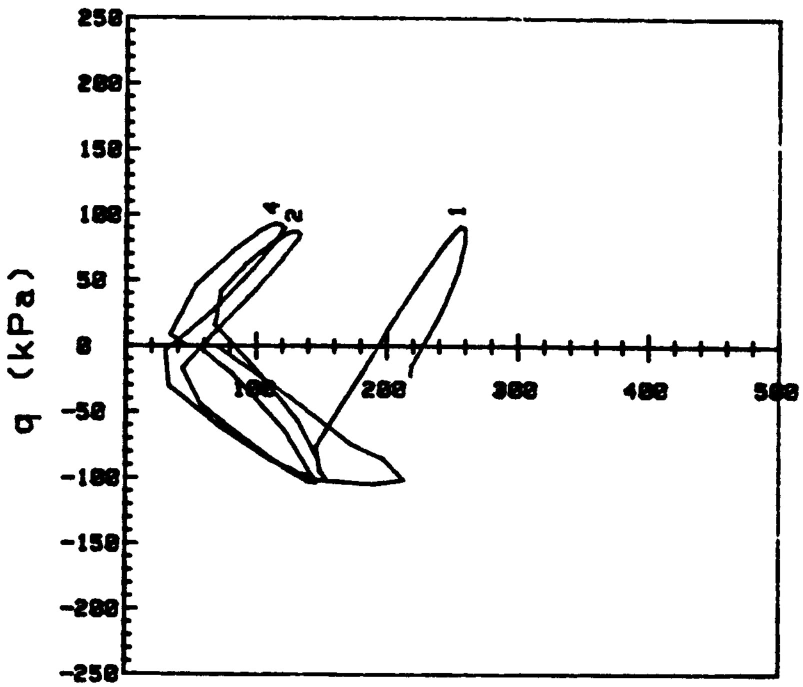

CRUISE DC4-81-NS		INCREMENT (cm)	86-93
CORE NO.	682A1	TEST NO.	TC40
SIG1c'(kPa)	240.4	STATIC qf (kPa)	183.9
SIG3c'(kPa)	240.4	AVG MAX q (kPa)	94.9 (51.6%)
INDUCED OCR	1.0	AVG MIN q (kPa)	-86.7 (47.1%)

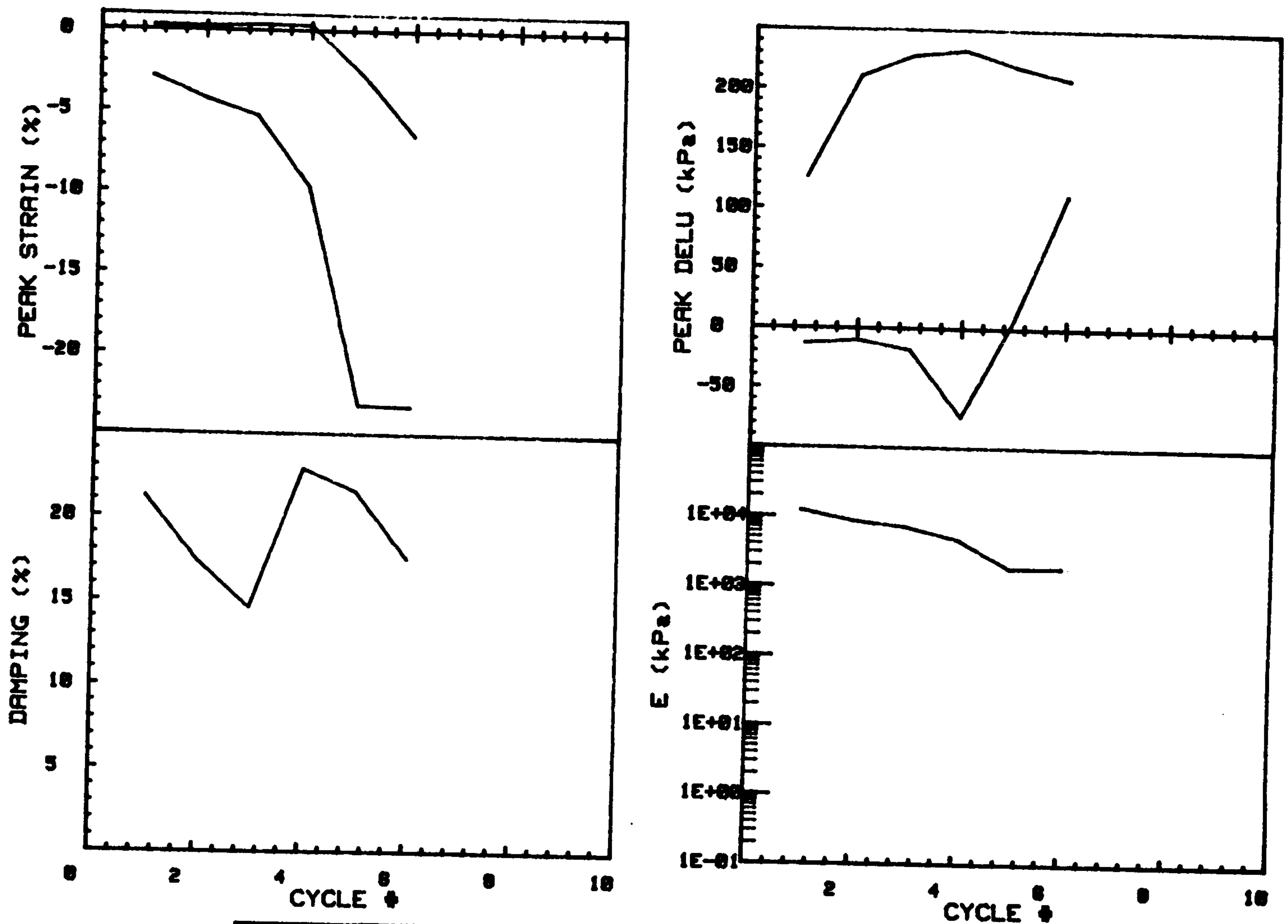

CRUISE DC4-81-NS		INCREMENT (cm)	86-93
CORE NO.	682A1	TEST NO.	TC40
SIG1c'(kPa)	240.4	STATIC qf (kPa)	183.9
SIG3c'(kPa)	240.4	AVG MAX q (kPa)	94.9 (51.6%)
INDUCED OCR	1.0	AVG MIN q (kPa)	-86.7 (47.1%)

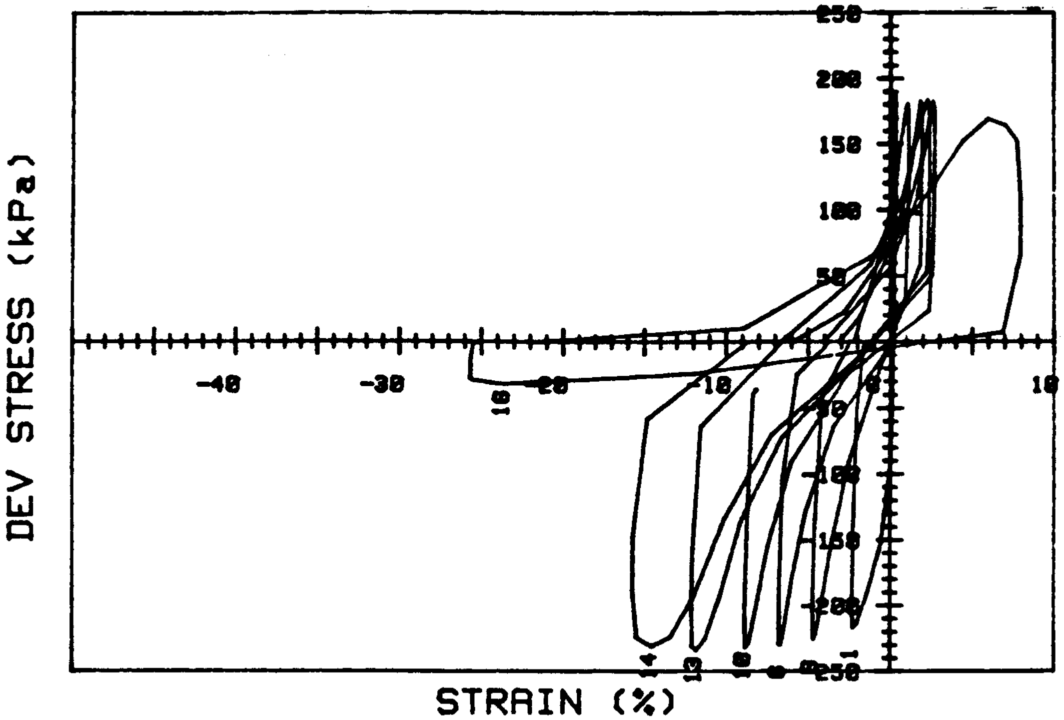

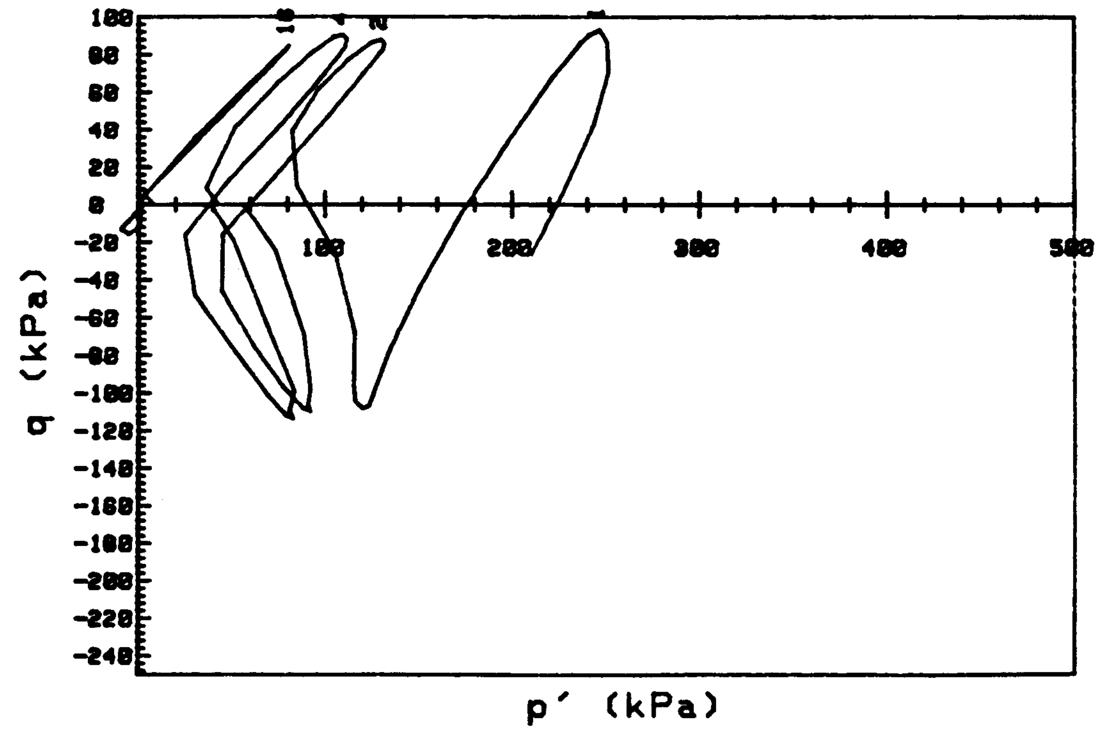

CRUISE DC4-81-NS		INCREMENT (cm)	86-93
CORE NO.	682A1	TEST NO.	TC41
SIG1c′(kPa)	236.8	STATIC qf (kPa)	183.9
SIG3c′(kPa)	236.8	AVG MAX q (kPa)	90.4 (49.2%)
INDUCED OCR	1.0	AVG MIN q (kPa)	-105.7 (57.5%)

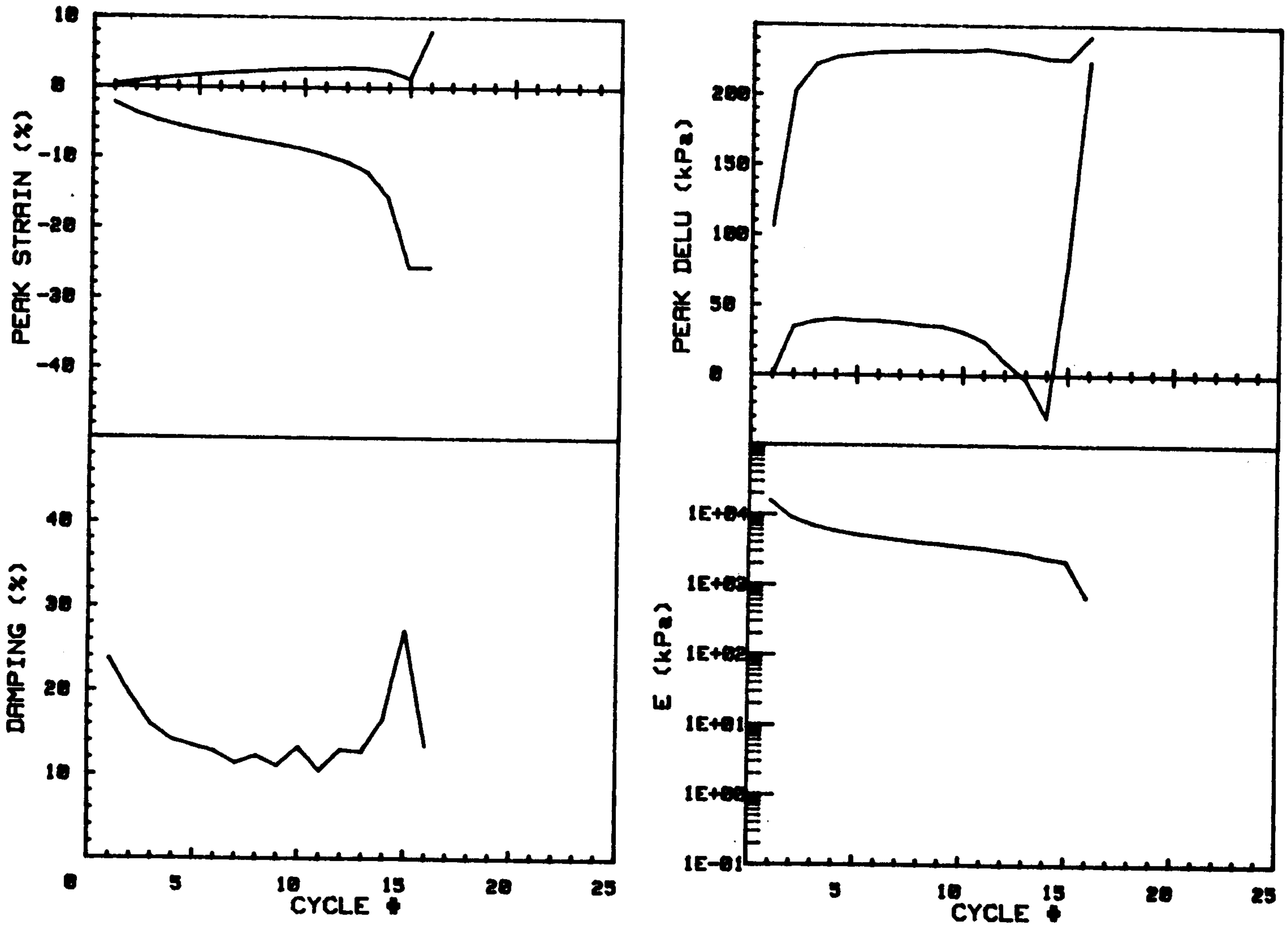

CRUISE DC4-81-NS		INCREMENT (cm)	86-93
CORE NO.	682A1	TEST NO.	TC41
SIG1c'(kPa)	236.8	STATIC qf (kPa)	183.9
SIG3c'(kPa)	236.8	AVG MAX q (kPa)	90.4 (49.2%)
INDUCED OCR	1.0	AVG MIN q (kPa)	-105.7 (57.5%)

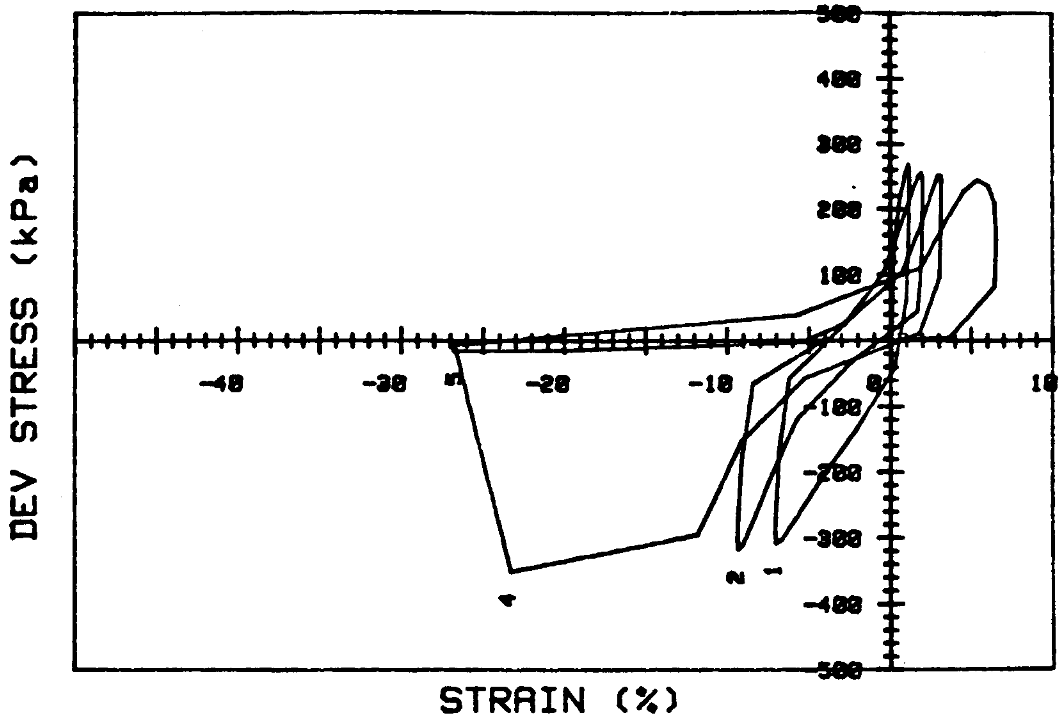

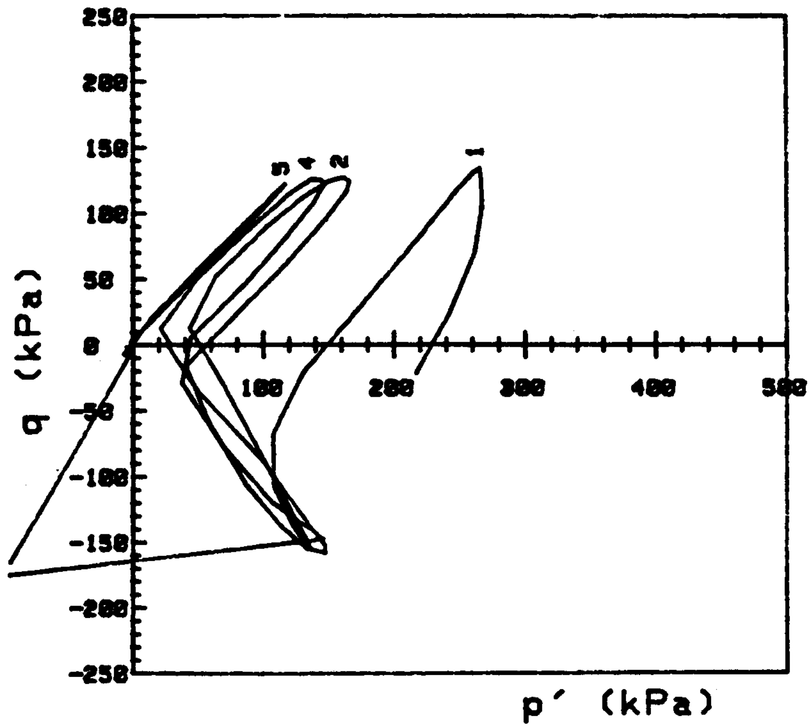

CRUISE DC4-81-NS		INCREMENT (cm)	95-106
CORE NO.	682A1	TEST NO.	TC38
SIG1c′(kPa)	238.4	STATIC qf (kPa)	183.9
SIG3c′(kPa)	238.4	AVG MAX q (kPa)	127.3 (69.2%)
INDUCED OCR	1.0	AVG MIN q (kPa)	-131.1 (71.3%)

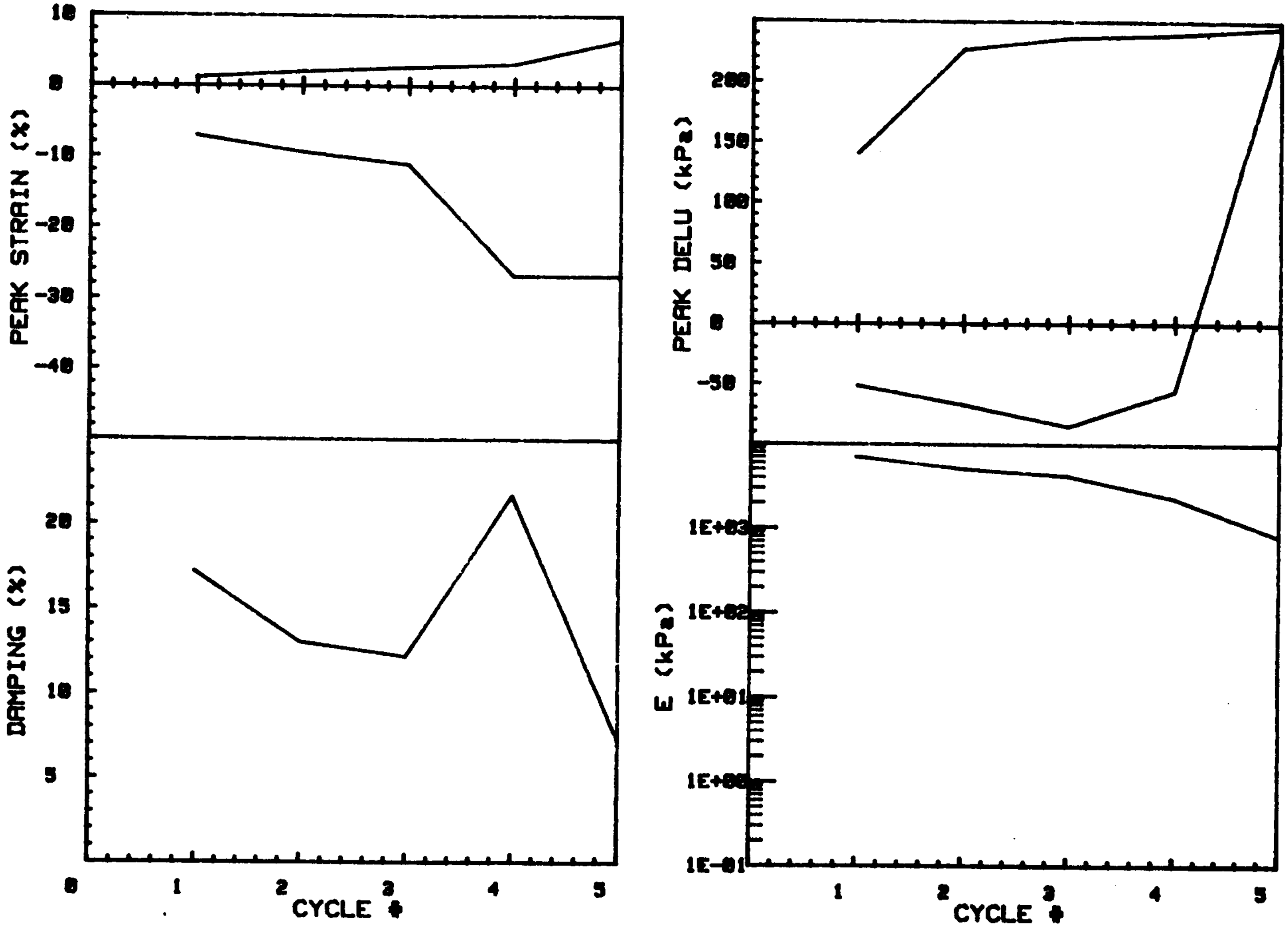

CRUISE DC4-81-NS		INCREMENT (cm)	95-106
CORE NO.	682A1	TEST NO.	TC38
SIG1c′(kPa)	230.4	STATIC qf (kPa)	183.9
SIG3c′(kPa)	230.4	AVG MAX q (kPa)	127.3 (69.2%)
INDUCED OCR	1.0	AVG MIN q (kPa)	-131.1 (71.3%)

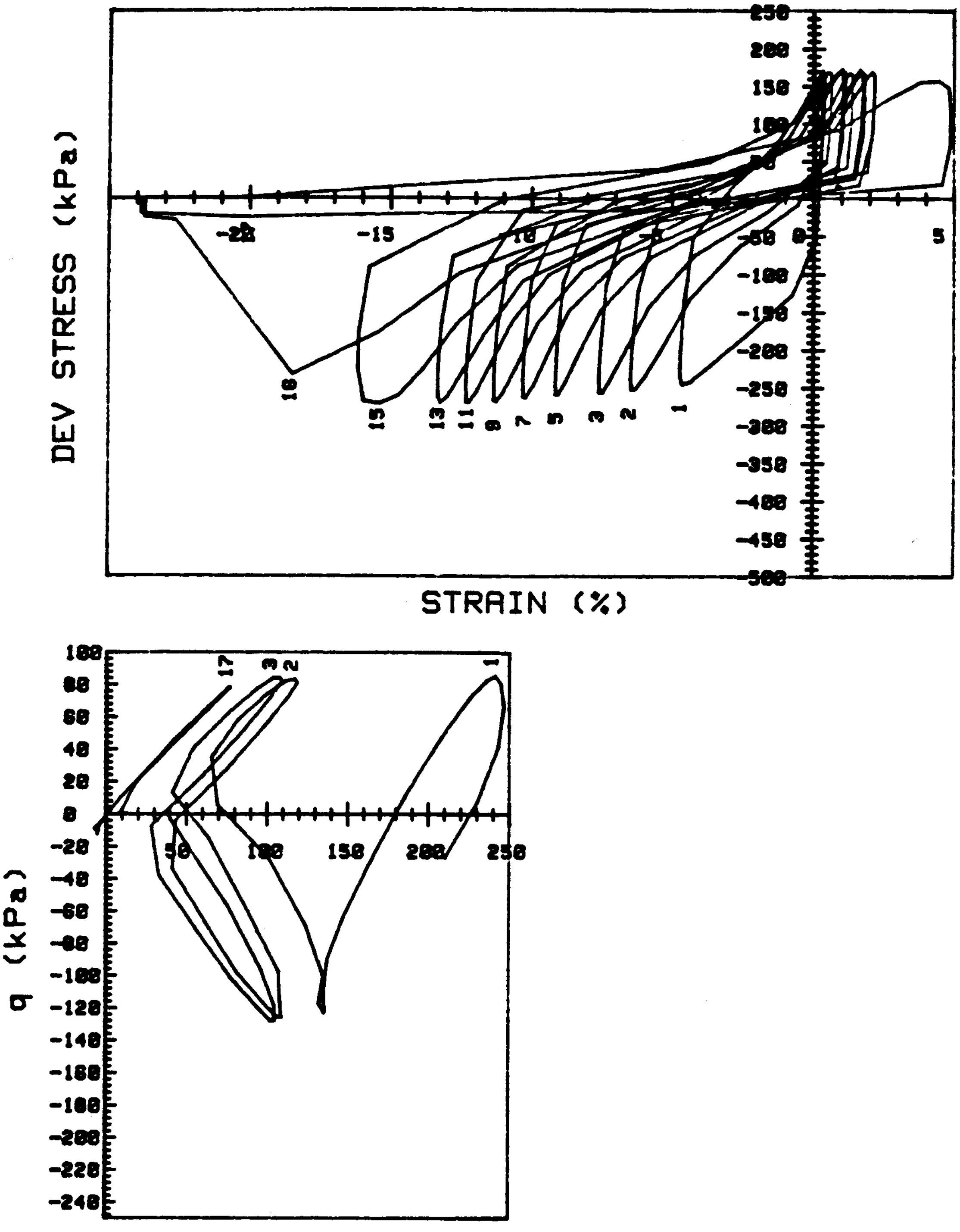

CRUISE DC4-81-NS		INCREMENT (cm)	95-106
CORE NO.	682A1	TEST NO.	TC39
SIG1c′(kPa)	237.3	STATIC qf (kPa)	183.9
SIG3c′(kPa)	237.3	AVG MAX q (kPa)	84.2 (45.8%)
INDUCED OCR	1.0	AVG MIN q (kPa)	-123.6 (67.2%)

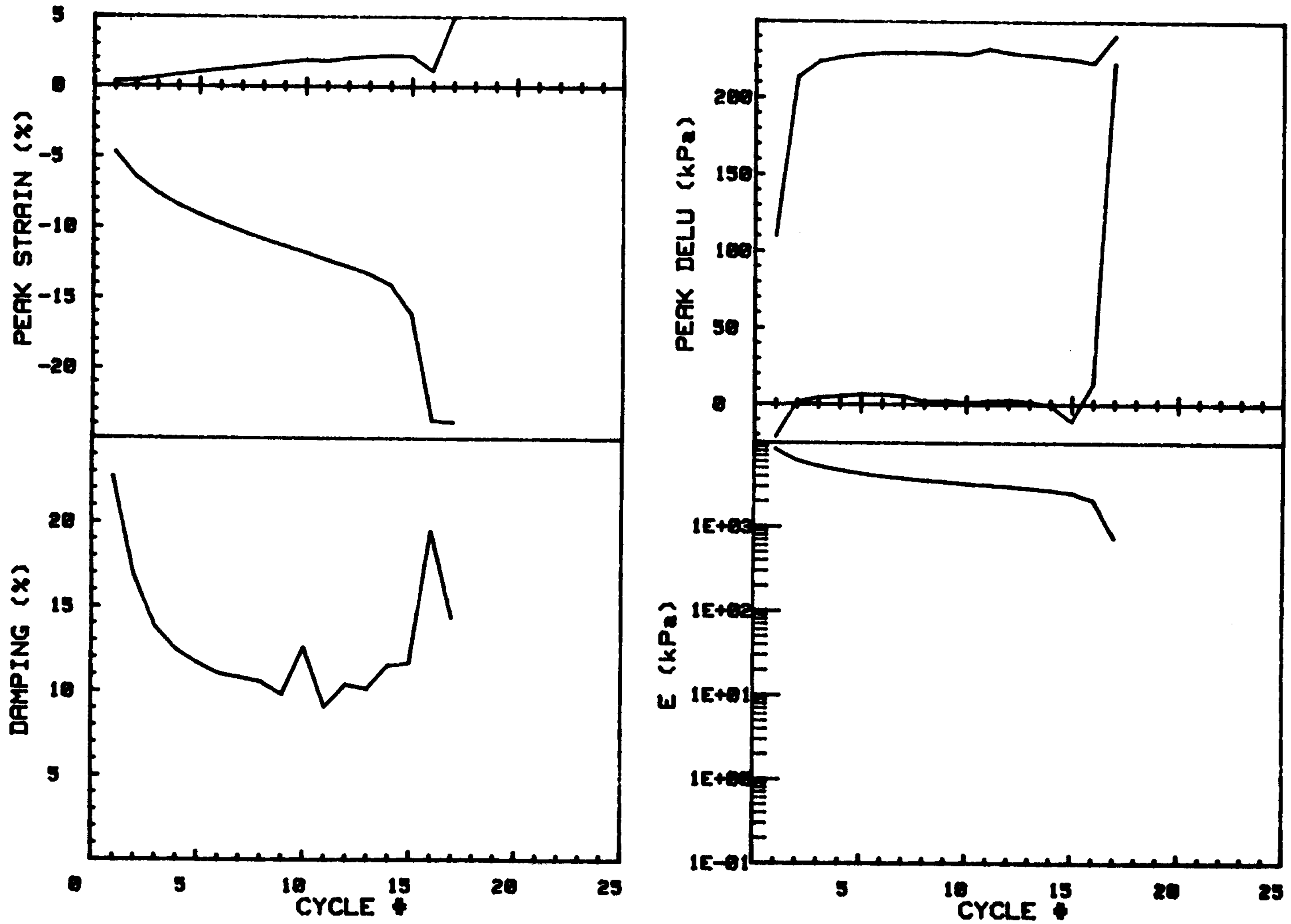

CRUISE DC4-81-NS		INCREMENT (cm)	95-106
CORE NO.	682A1	TEST NO.	TC39
SIG1c'(kPa)	237.3	STATIC qf (kPa)	183.9
SIG3c'(kPa)	237.3	AVG MAX q (kPa)	84.2 (45.8%)
INDUCED OCR	1.0	AVG MIN q (kPa)	-123.6 (67.2%)

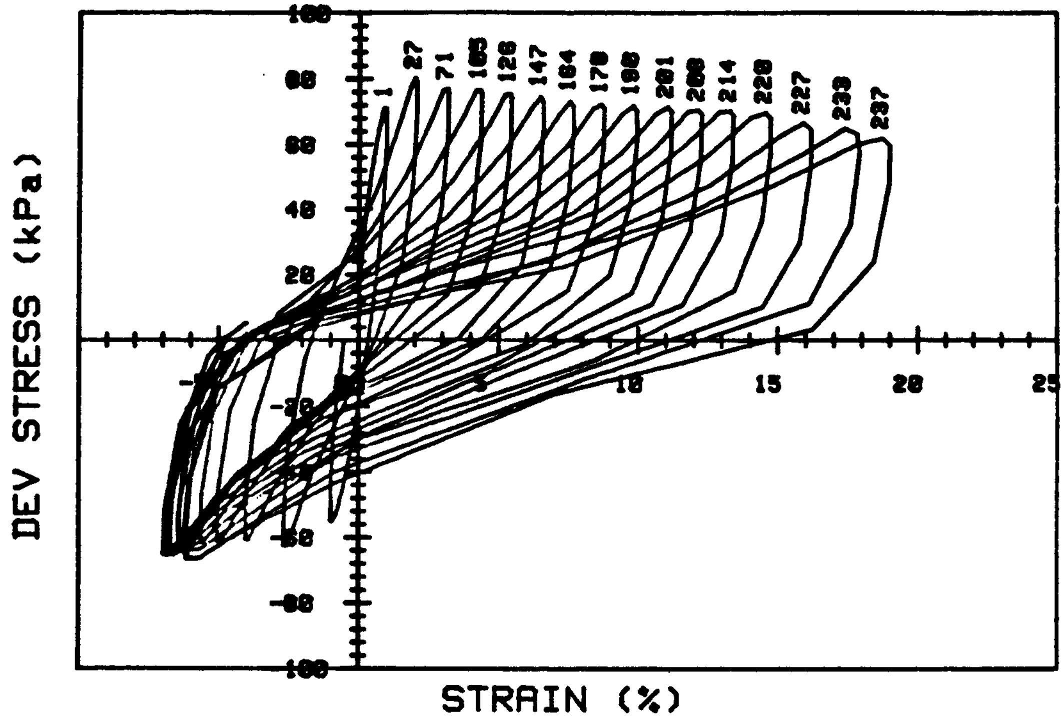

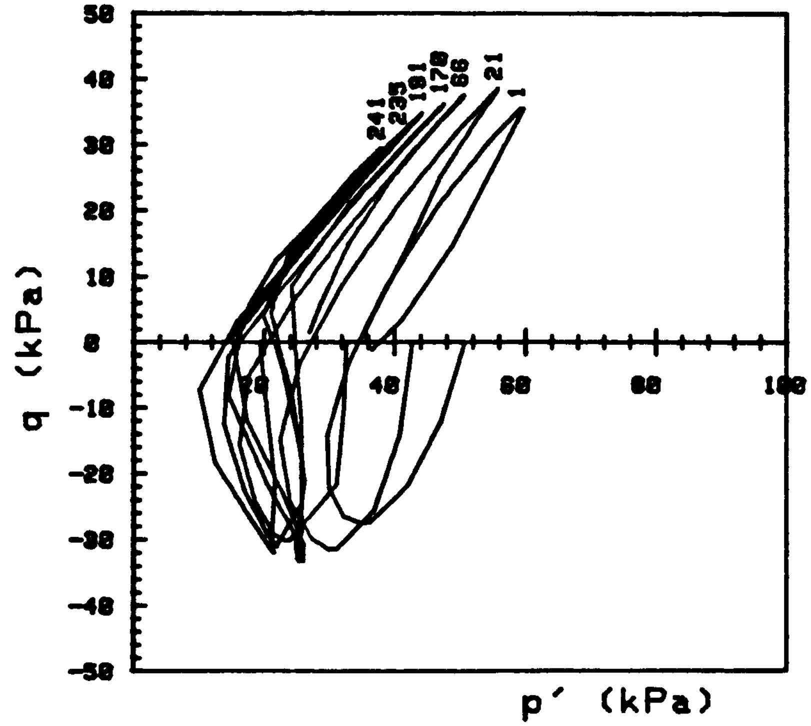

CRUISE DC4-81-NS		INCREMENT (cm)	134-142
CORE NO.	682A1	TEST NO.	TC78
SIG1c′(kPa)	37.8	STATIC qf (kPa)	82.9
SIG3c′(kPa)	37.8	AVG MAX q (kPa)	37.1 (44.8%)
INDUCED OCR	6.3	AVG MIN q (kPa)	-31.1 (37.5%)

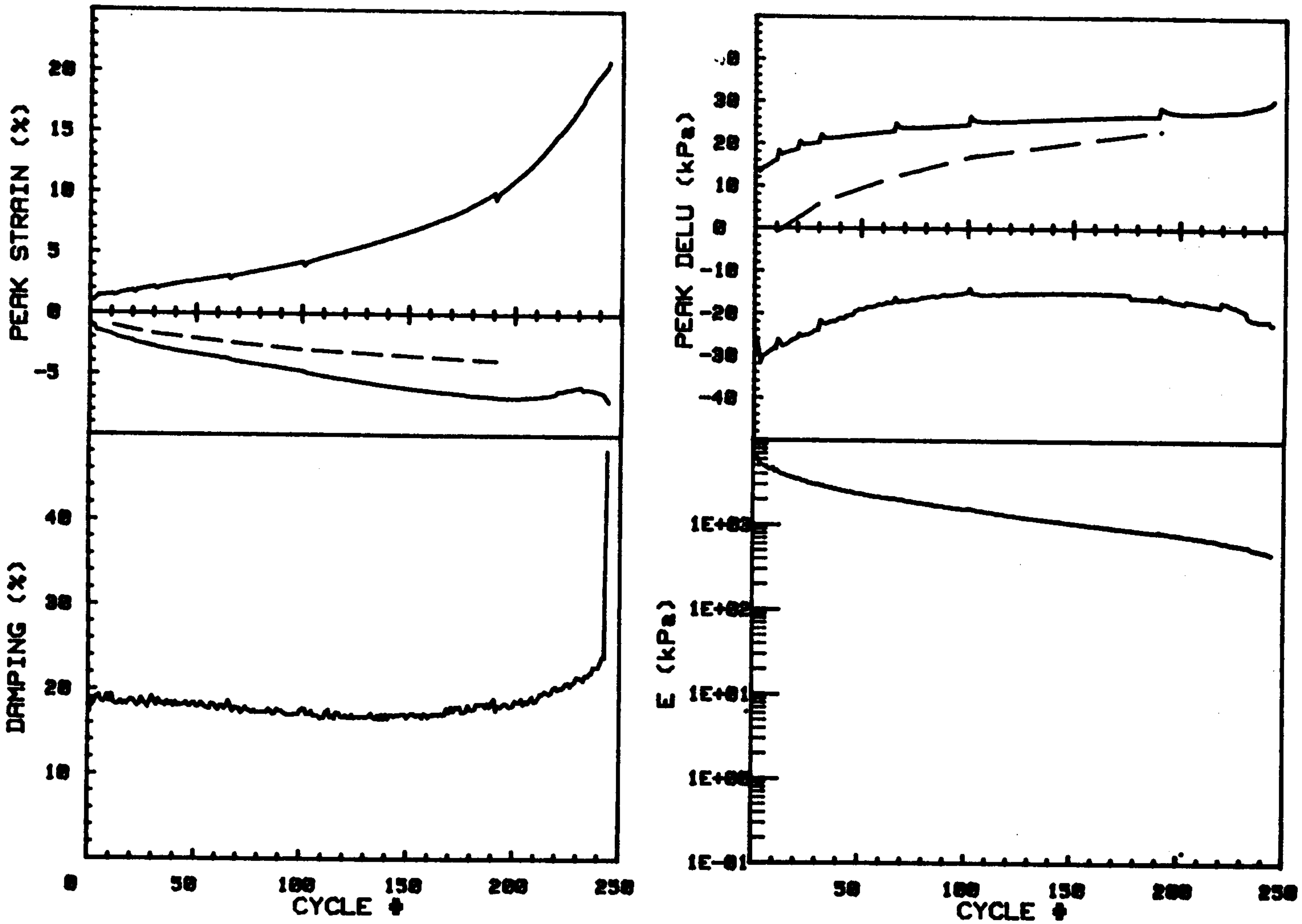

CRUISE DC4-81-NS		INCREMENT (cm)	134-142
CORE NO.	682A1	TEST NO.	TC78
SIG1c'(kPa)	37.8	STATIC qf (kPa)	82.9
SIG3c'(kPa)	37.8	AVG MAX q (kPa)	37.1 (44.8%)
INDUCED OCR	6.3	AVG MIN q (kPa)	-31.1 (37.5%)

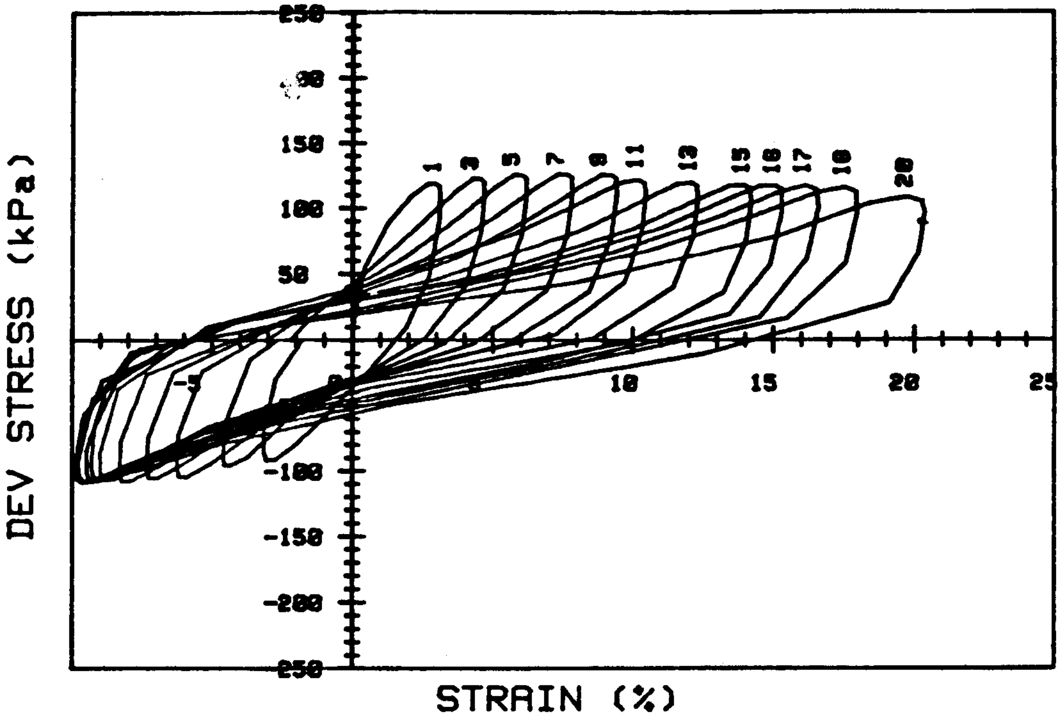

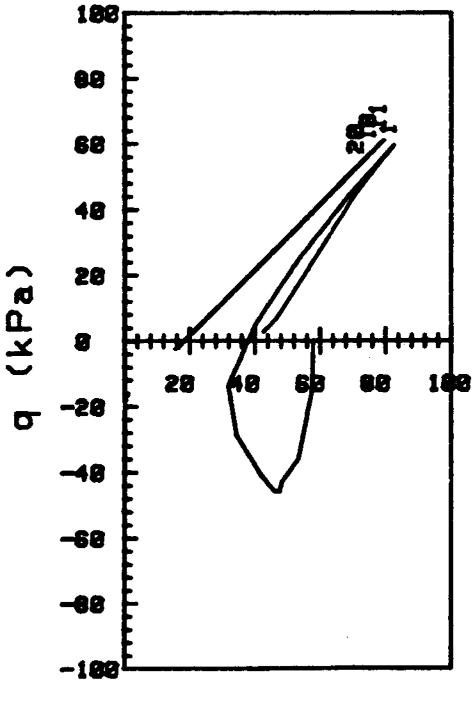

CRUISE DC4-81-NS		INCREMENT (cm)	134-142
CORE NO.	682A1	TEST NO.	TC79
SIG1c′(kPa)	39.8	STATIC qf (kPa)	82.9
SIG3c′(kPa)	39.8	AVG MAX q (kPa)	60.3 (72.7%)
INDUCED OCR	6.0	AVG MIN q (kPa)	-52.2 (63.0%)

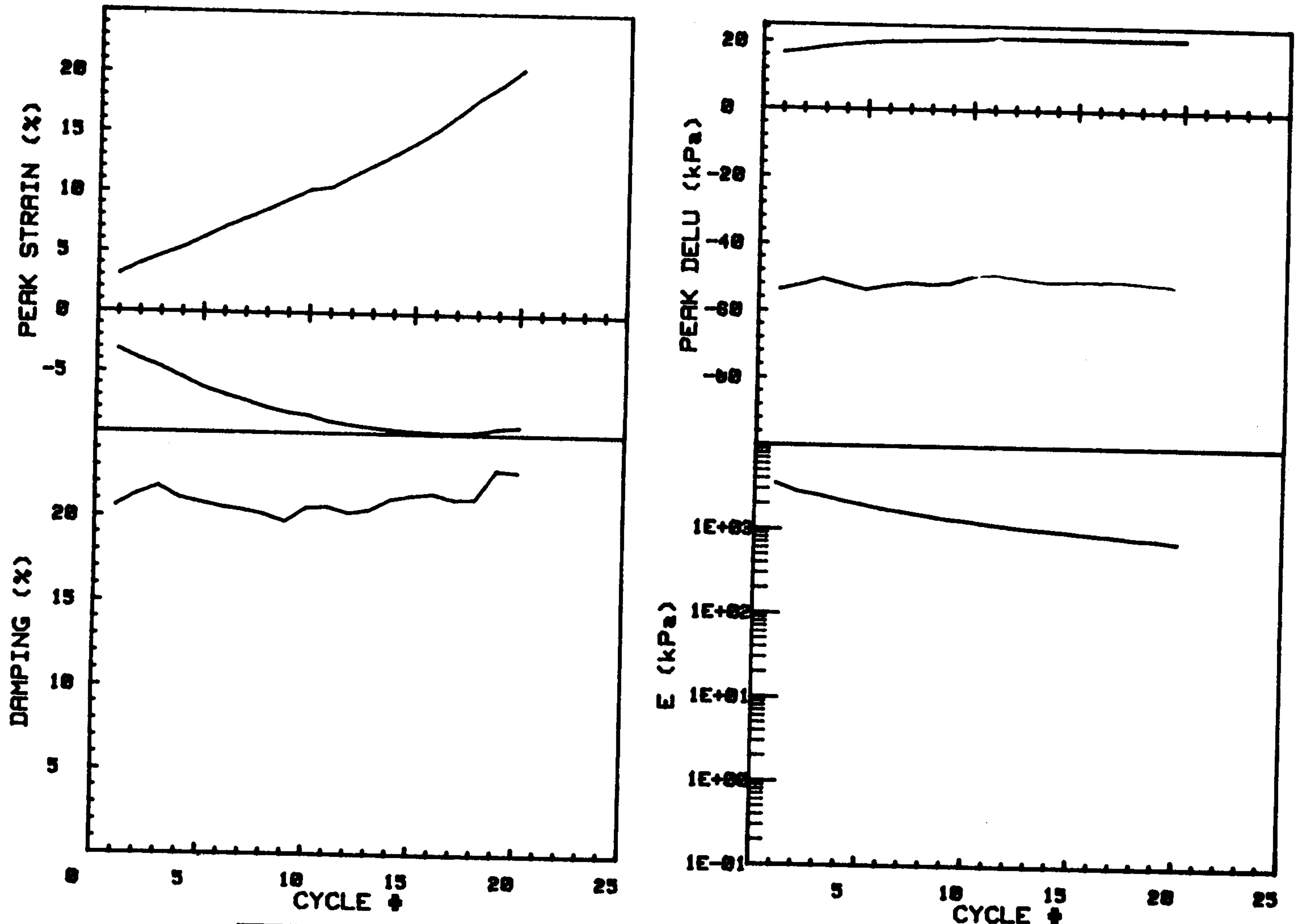

CRUISE DC4-81-NS		INCREMENT (cm)	134-142
CORE NO.	682A1	TEST NO.	TC79
SIG1c'(kPa)	39.8	STATIC qf (kPa)	82.9
SIG3c'(kPa)	39.8	AVG MAX q (kPa)	60.3 (72.7%)
INDUCED OCR	6.0	AVG MIN q (kPa)	-52.2 (63.0%)

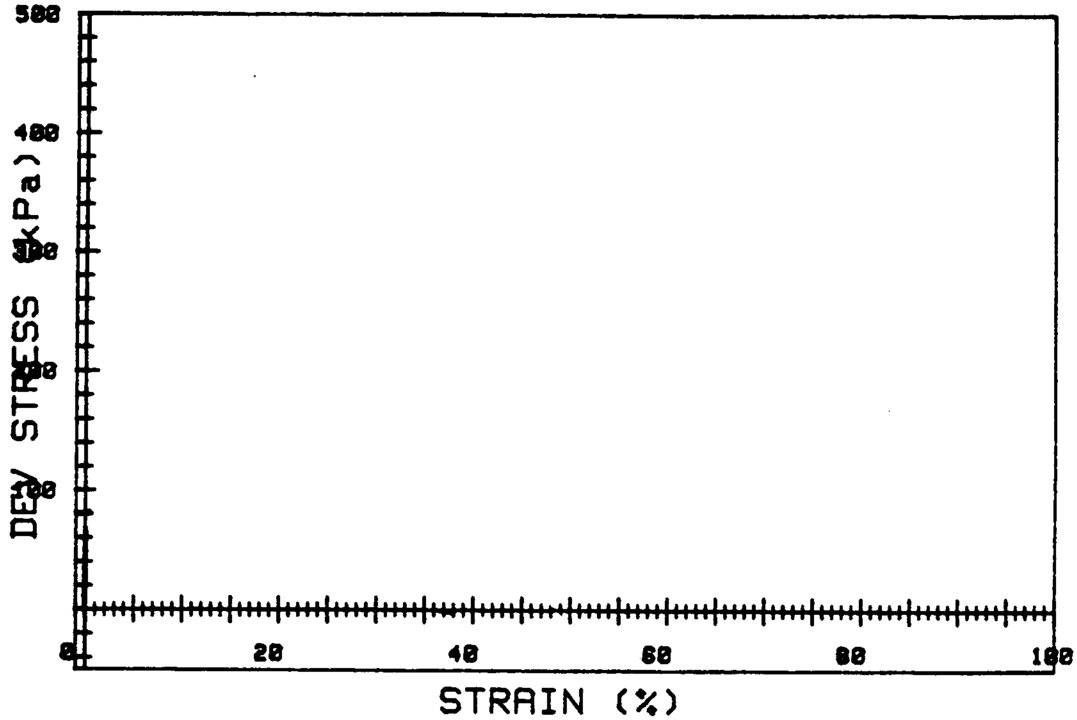

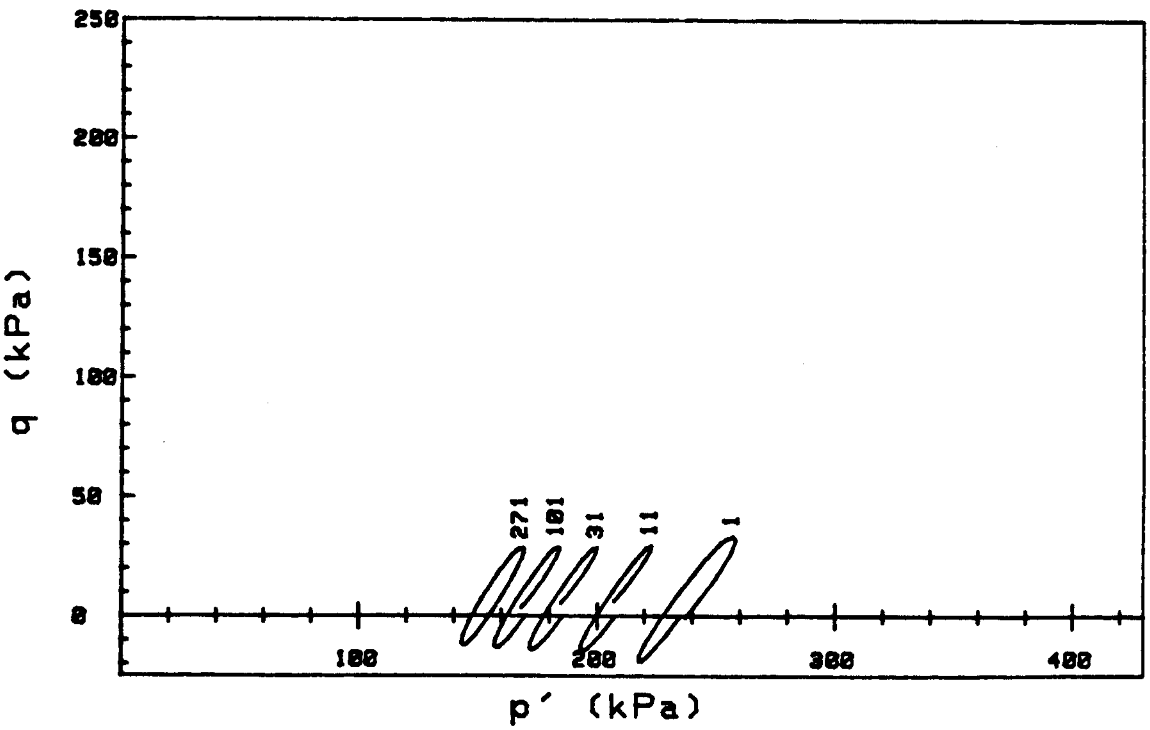

CRUISE DC4-81-NS		INCREMENT (cm)	186-193
CORE NO.	682A1	TEST NO.	TC76
SIG1c′(kPa)	238.0	STATIC qf (kPa)	93.2
SIG3c′(kPa)	233.0	AVG MAX q (kPa)	29.3 (31.4%)
INDUCED OCR	1.9	AVG MIN q (kPa)	-12.4 (13.3%)

Cycles 1 - 500

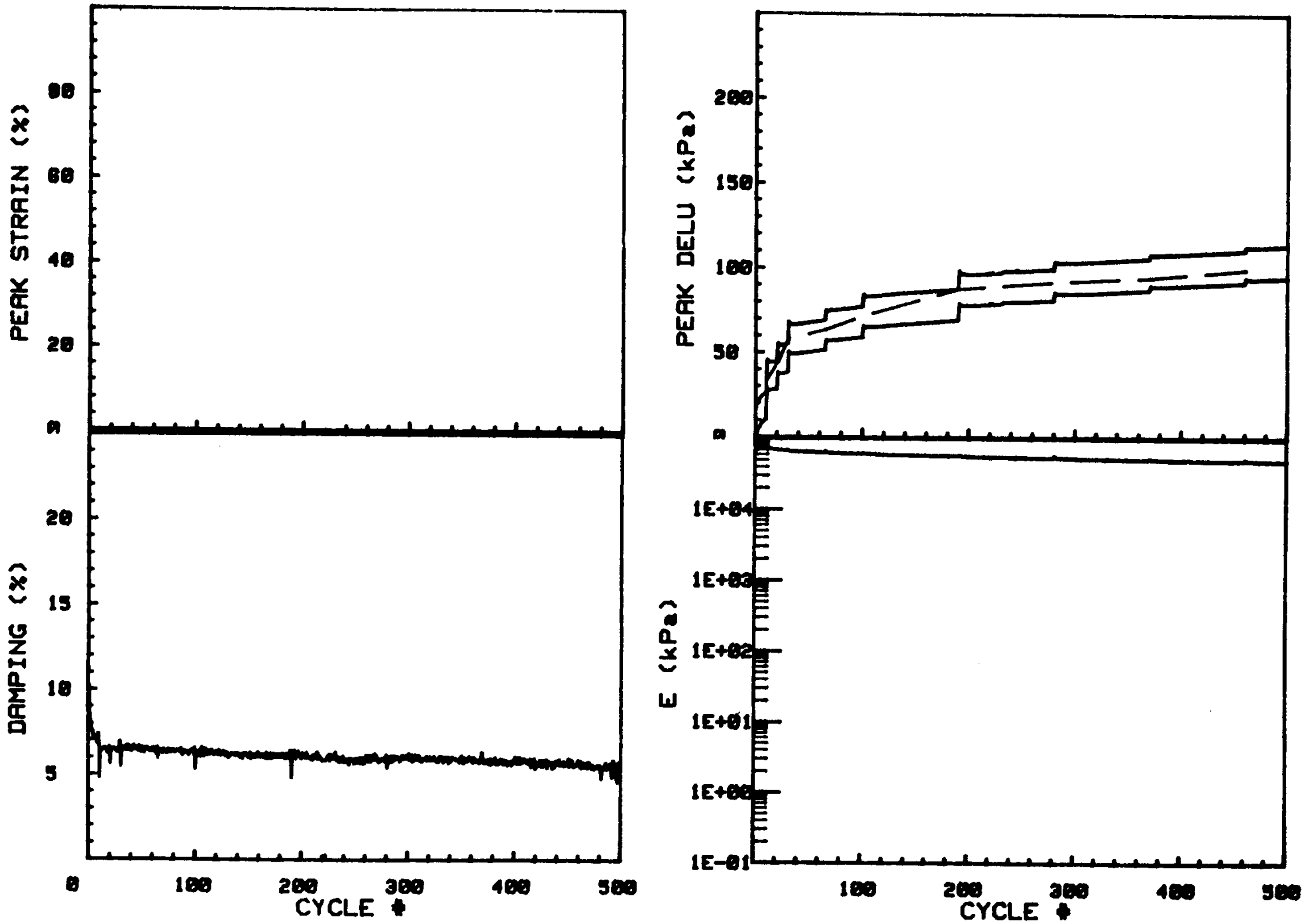

CRUISE DC4-81-NS		INCREMENT (cm)	186-193
CORE NO.	682A1	TEST NO.	TC76
SIG1c′(kPa)	238.0	STATIC qf (kPa)	93.2
SIG3c′(kPa)	238.0	AVG MAX q (kPa)	29.3 (31.4%)
INDUCED OCR	1.0	AVG MIN q (kPa)	-12.4 (13.3%)

Cycles 1 - 500

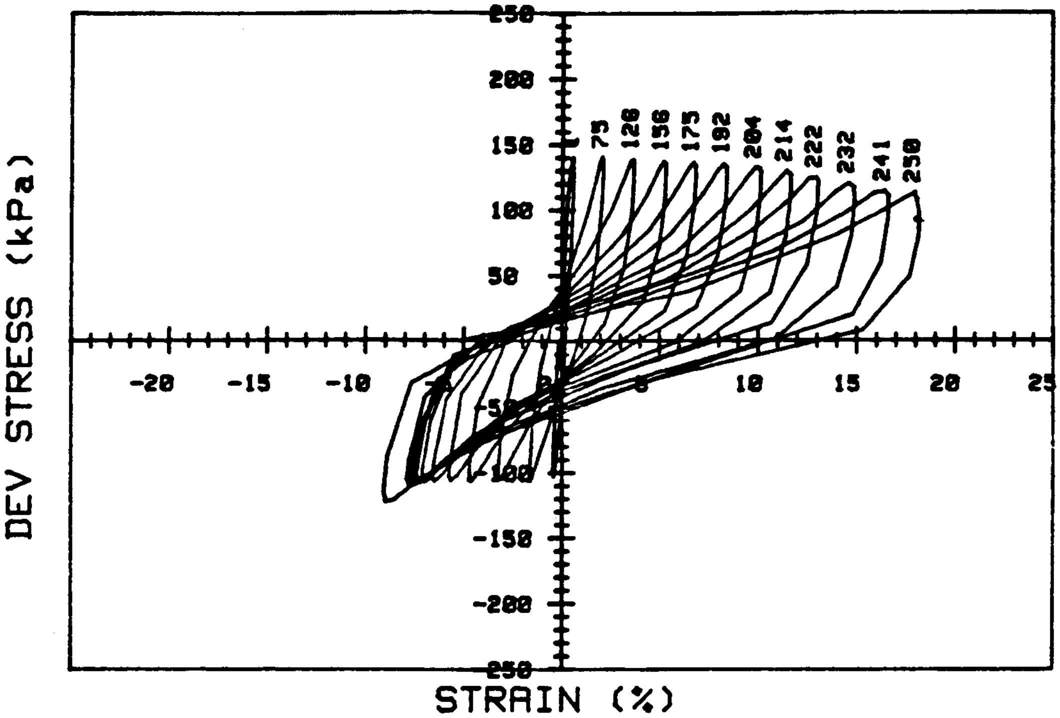

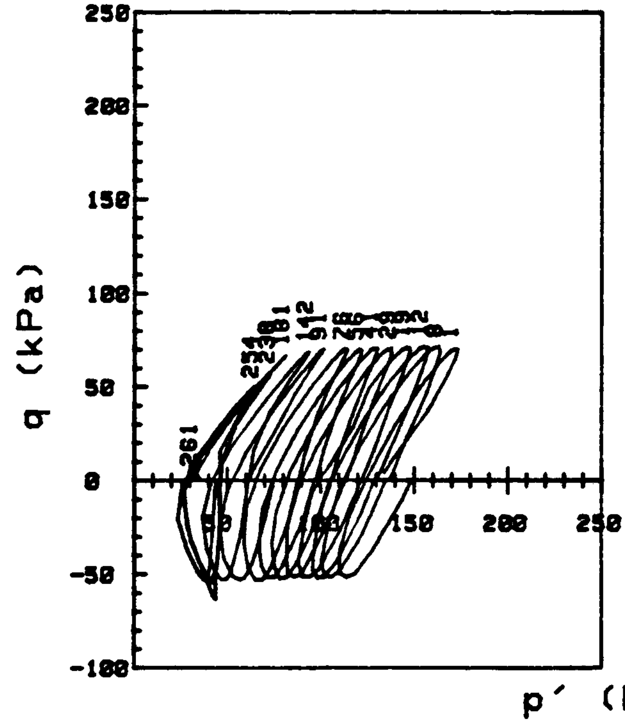

CRUISE DC4-81-NS		INCREMENT (cm)	186-193
CORE NO.	682A1	TEST NO.	TC76
SIG1c´(kPa)	130.4	STATIC qf (kPa)	93.2
SIG3c´(kPa)	130.4	AVG MAX q (kPa)	67.3 (72.2%)
INDUCED OCR	1.0	AVG MIN q (kPa)	-53.2 (57.1%)

Cycles 501 - 761

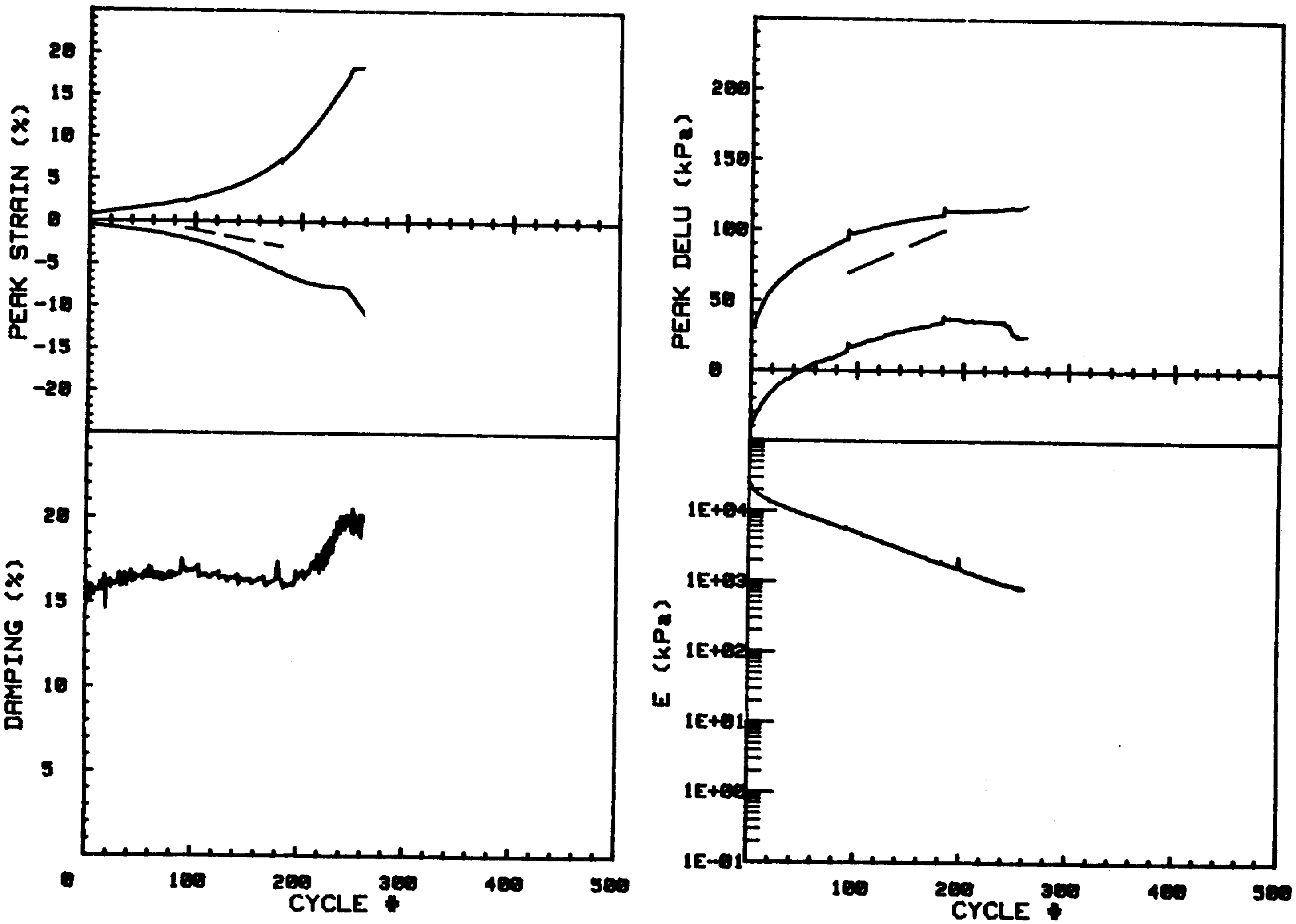

CRUISE DC4-81-NS		INCREMENT (cm)	186-193
CORE NO.	682A1	TEST NO.	TC76
SIG1c'(kPa)	130.4	STATIC qf (kPa)	93.2
SIG3c'(kPa)	130.4	AVG MAX q (kPa)	67.3 (72.2%)
INDUCED OCR	1.0	AVG MIN q (kPa)	-53.2 (57.1%)

Cycles 501 - 761

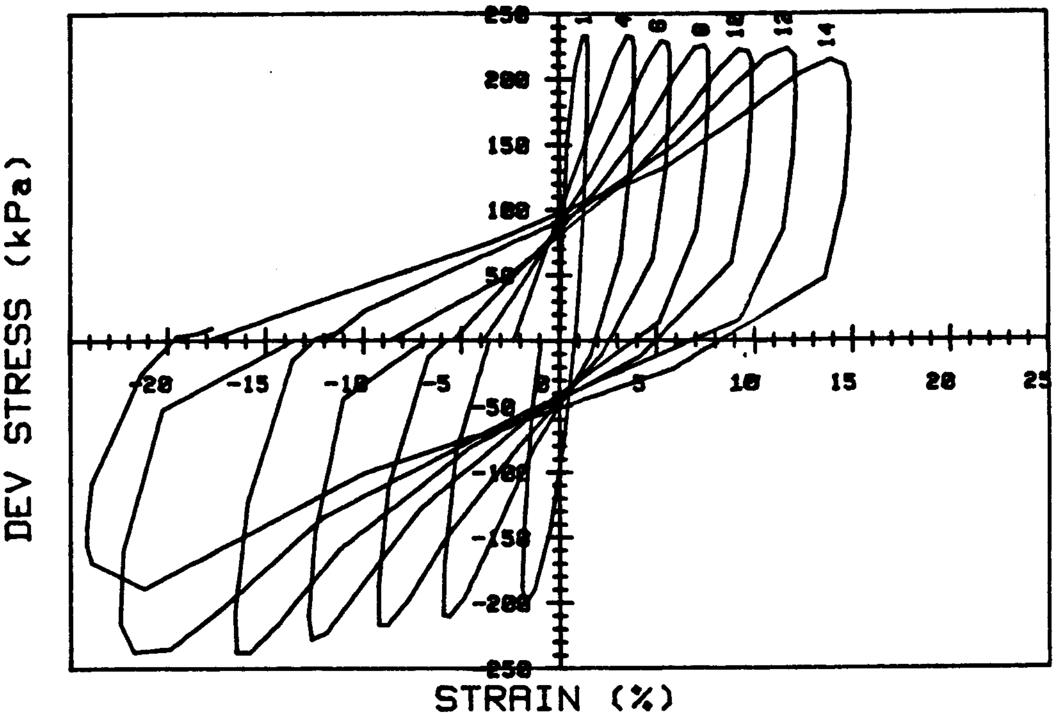

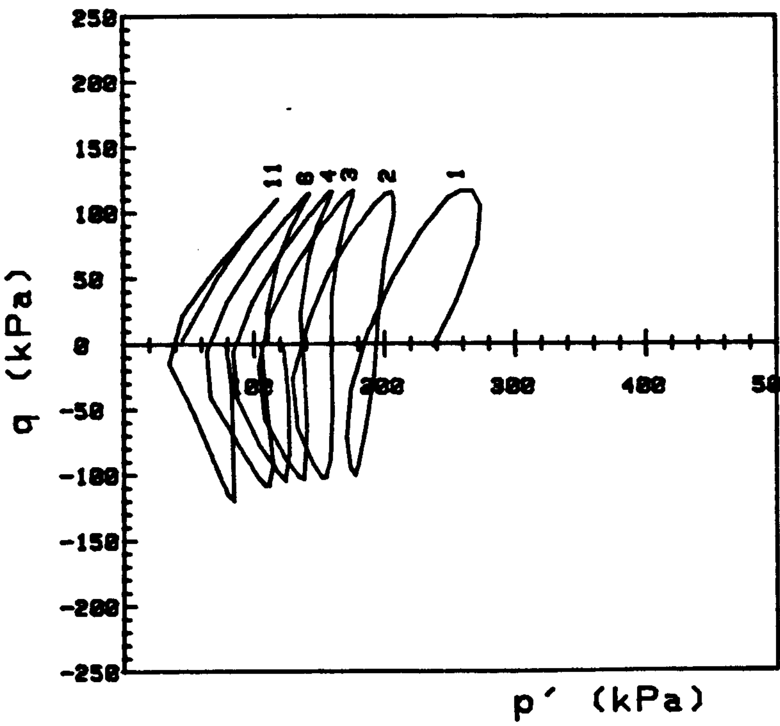

CRUISE	DC4-81-NS	INCREMENT (cm)		186-194	
CORE NO.	682A1	TEST NO.		TC77	
SIG1c′(kPa)	239.1	STATIC qf	(kPa)	93.2	
SIG3c′(kPa)	239.1	AVG MAX q	(kPa)	113.0	(121.2%)
INDUCED OCR	1.0	AVG MIN q	(kPa)	-108.9	(116.8%

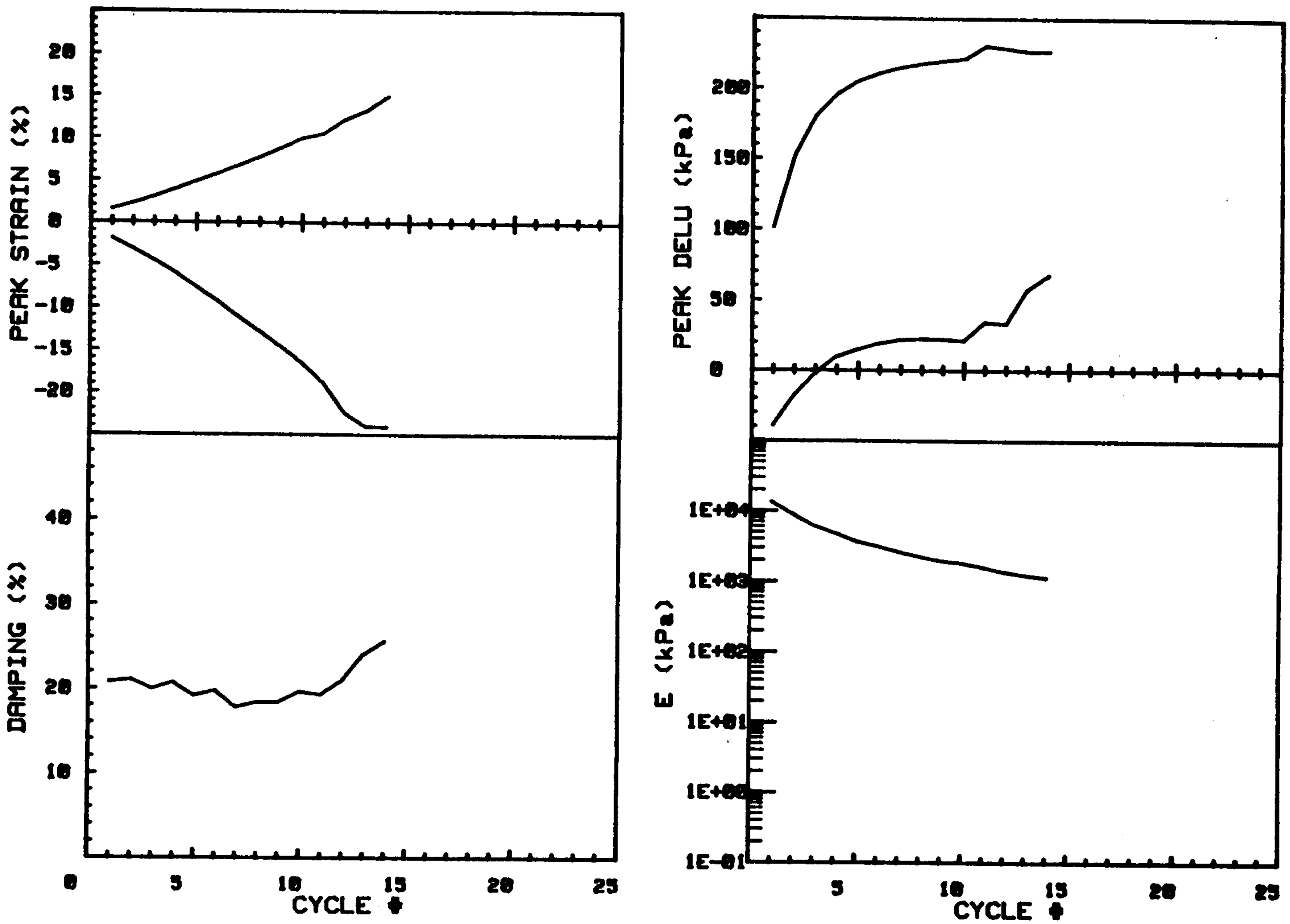

CRUISE DC4-81-NS		INCREMENT (cm)	186-194
CORE NO.	682A1	TEST NO.	TC77
SIG1c'(kPa)	239.1	STATIC qf (kPa)	93.2
SIG3c'(kPa)	239.1	AVG MAX q (kPa)	113.0 (121.2%)
INDUCED OCR	1.0	AVG MIN q (kPa)	-108.9 (116.8%

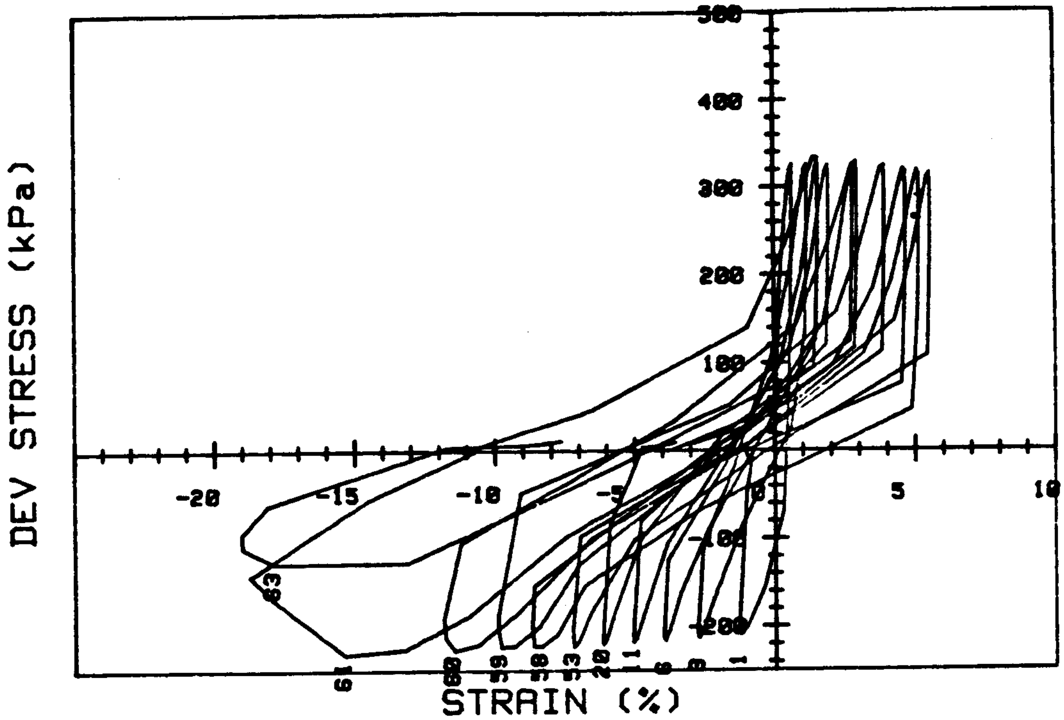

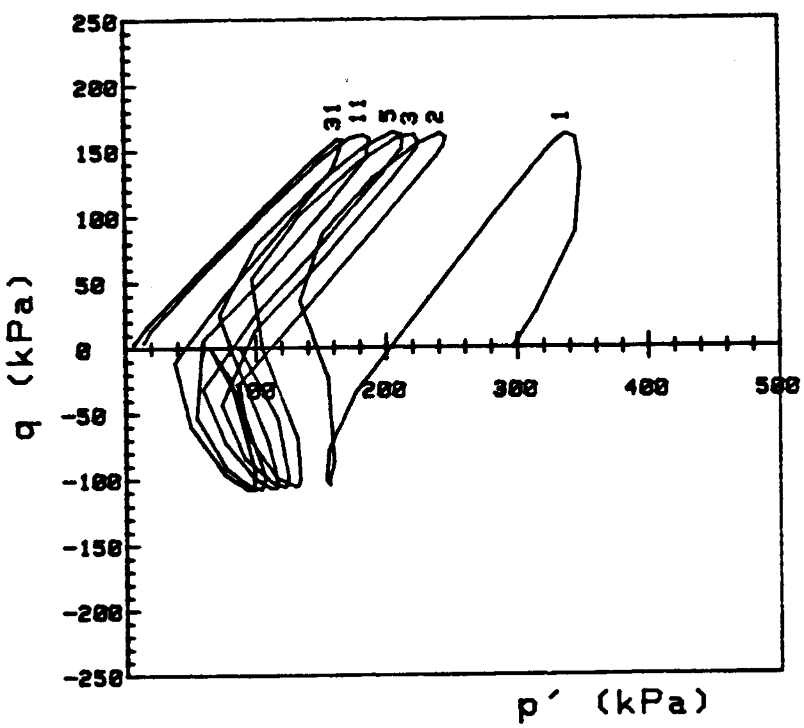

CRUISE DC4-81-NS		INCREMENT (cm)	62-70
CORE NO.	684A1	TEST NO.	TC90
SIG1c′(kPa)	296.6	STATIC qf (kPa)	300.0
SIG3c′(kPa)	296.6	AVG MAX q (kPa)	160.4 (53.5%)
INDUCED OCR	1.0	AVG MIN q (kPa)	-108.2 (36.1%)

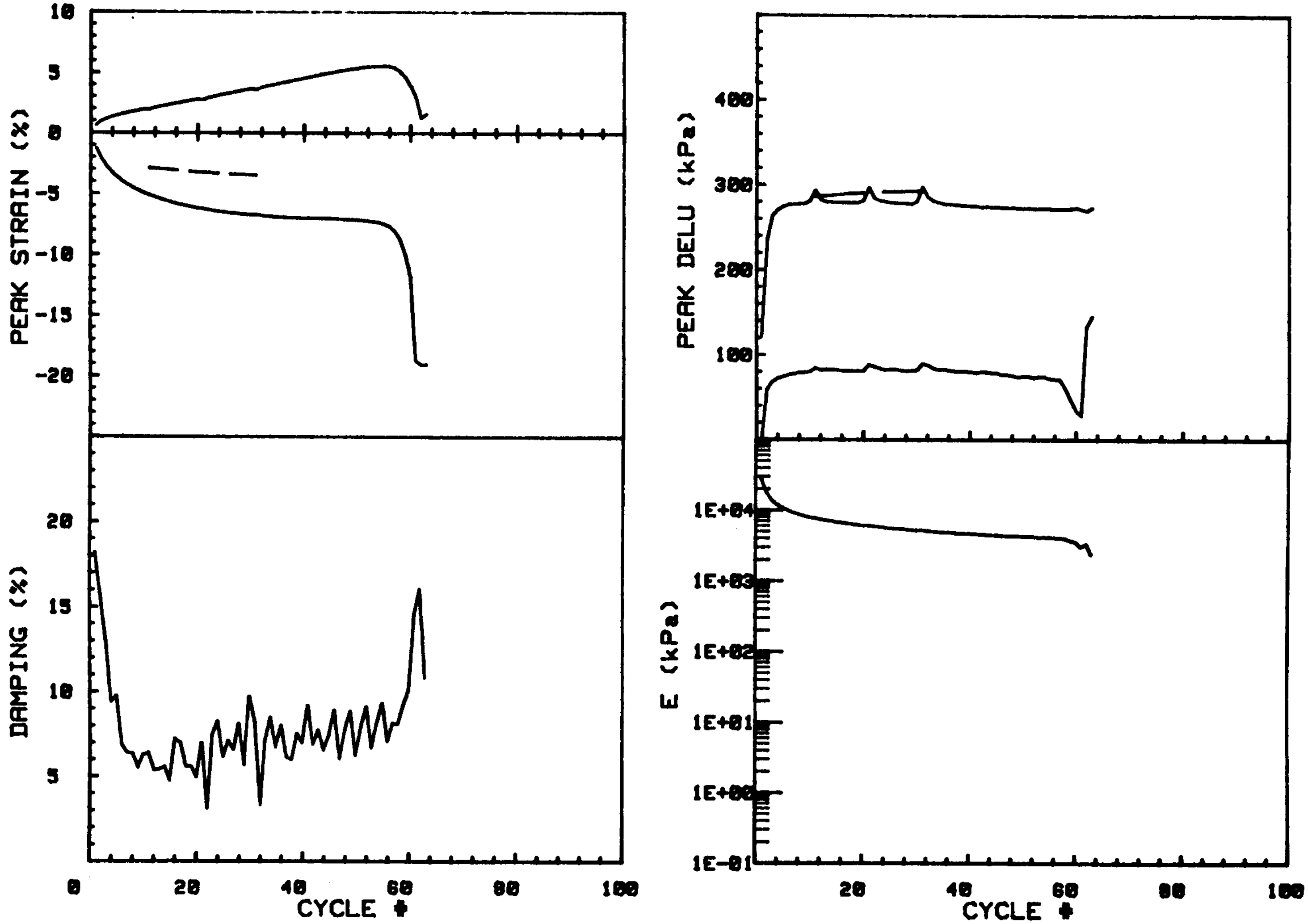

CRUISE DC4-81-NS		INCREMENT (cm)	62-70
CORE NO.	684A1	TEST NO.	TC90
SIG1c'(kPa)	296.6	STATIC qf (kPa)	300.0
SIG3c'(kPa)	296.6	AVG MAX q (kPa)	160.4 (53.5%)
INDUCED OCR	1.0	AVG MIN q (kPa)	-108.2 (36.1%)

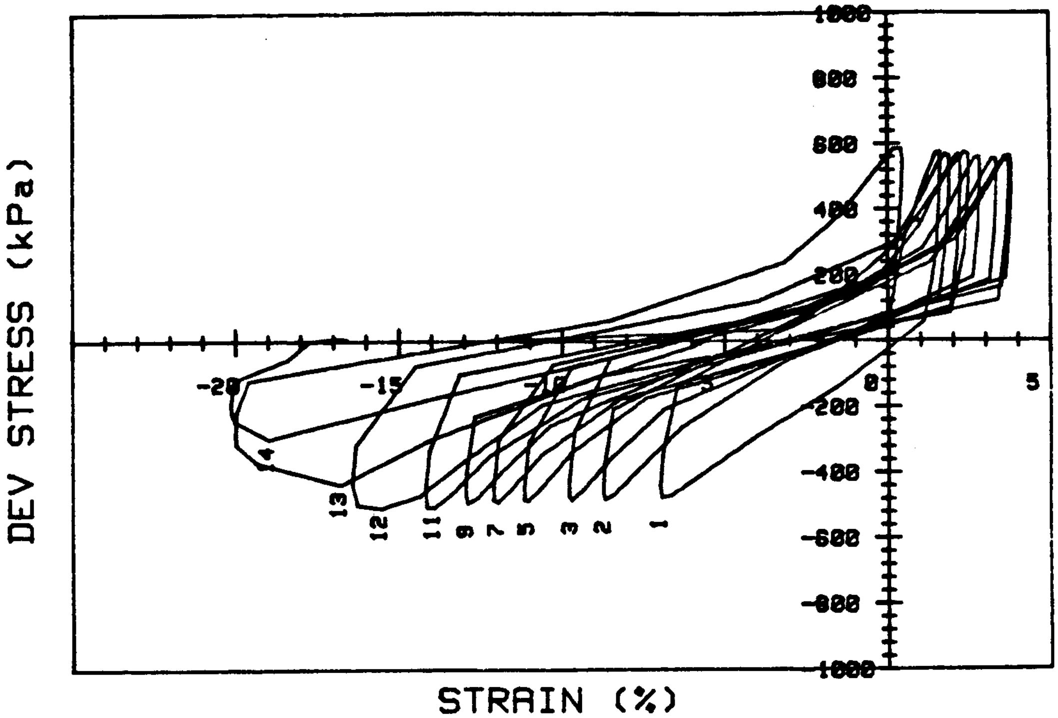

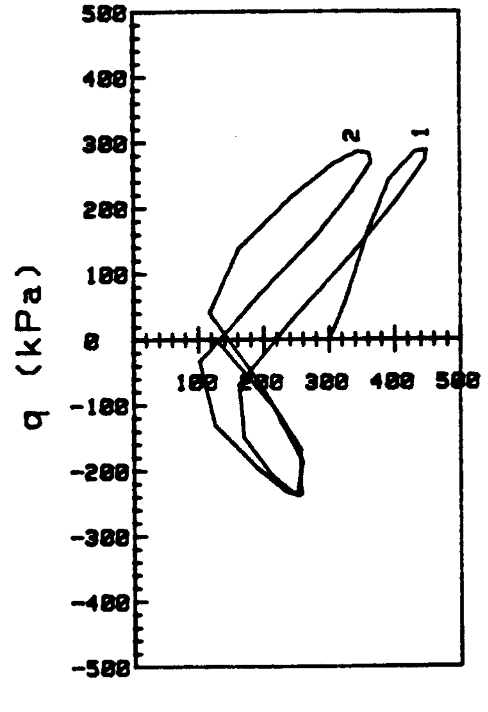

CRUISE DC4-81-NS		INCREMENT (cm)	62-70
CORE NO.	684A1	TEST NO.	TC91
SIG1c′(kPa)	297.2	STATIC qf (kPa)	300.0
SIG3c′(kPa)	297.2	AVG MAX q (kPa)	281.8 (93.9%)
INDUCED OCR	1.0	AVG MIN q (kPa)	-236.5 (78.8%)

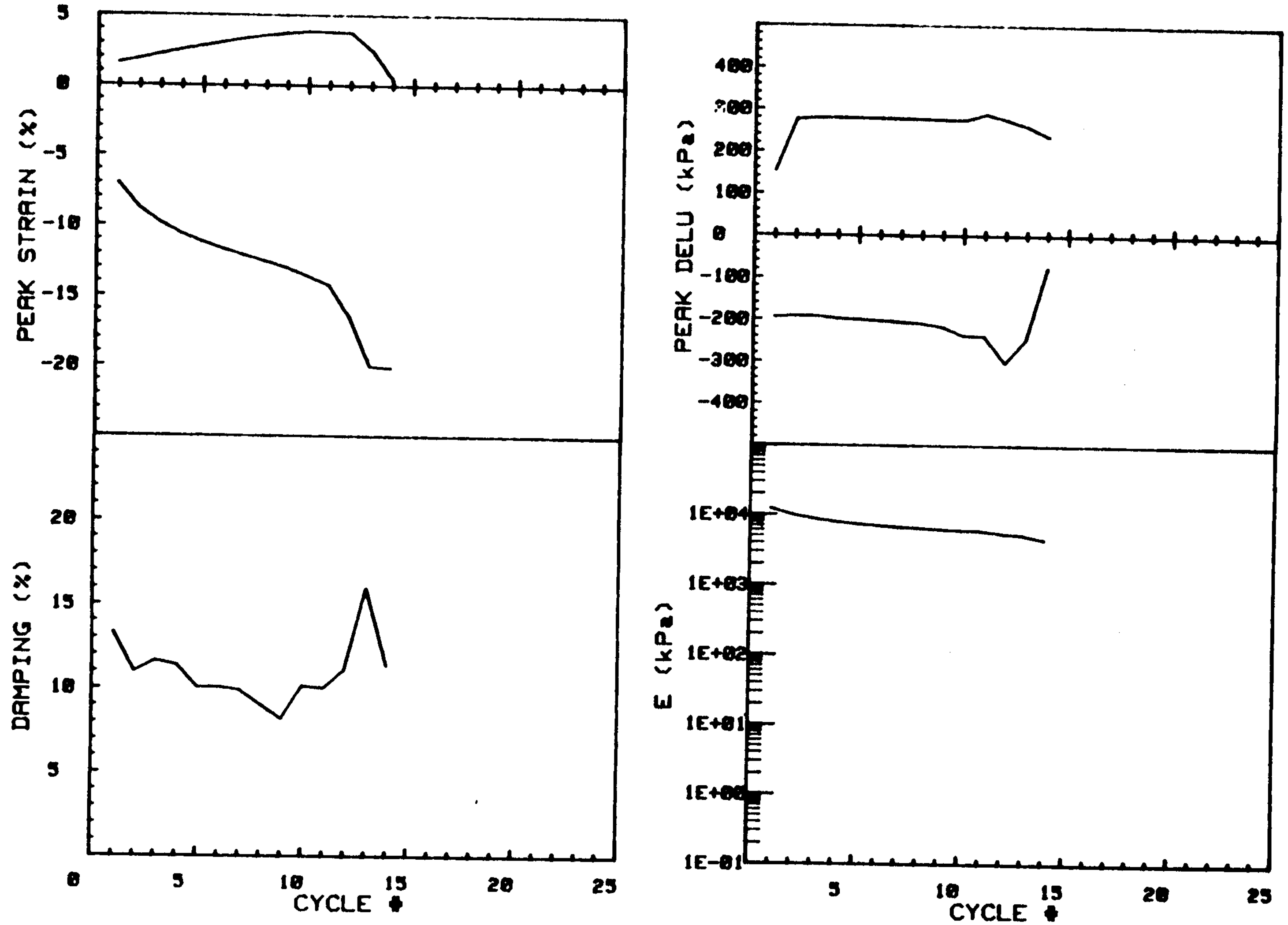

CRUISE DC4-81-NS		INCREMENT (cm)	62-70
CORE NO.	684A1	TEST NO.	TC91
SIG1c′(kPa)	297.2	STATIC qf (kPa)	300.0
SIG3c′(kPa)	297.2	AVG MAX q (kPa)	281.8 (93.9%)
INDUCED OCR	1.0	AVG MIN q (kPa)	-236.5 (78.8%)

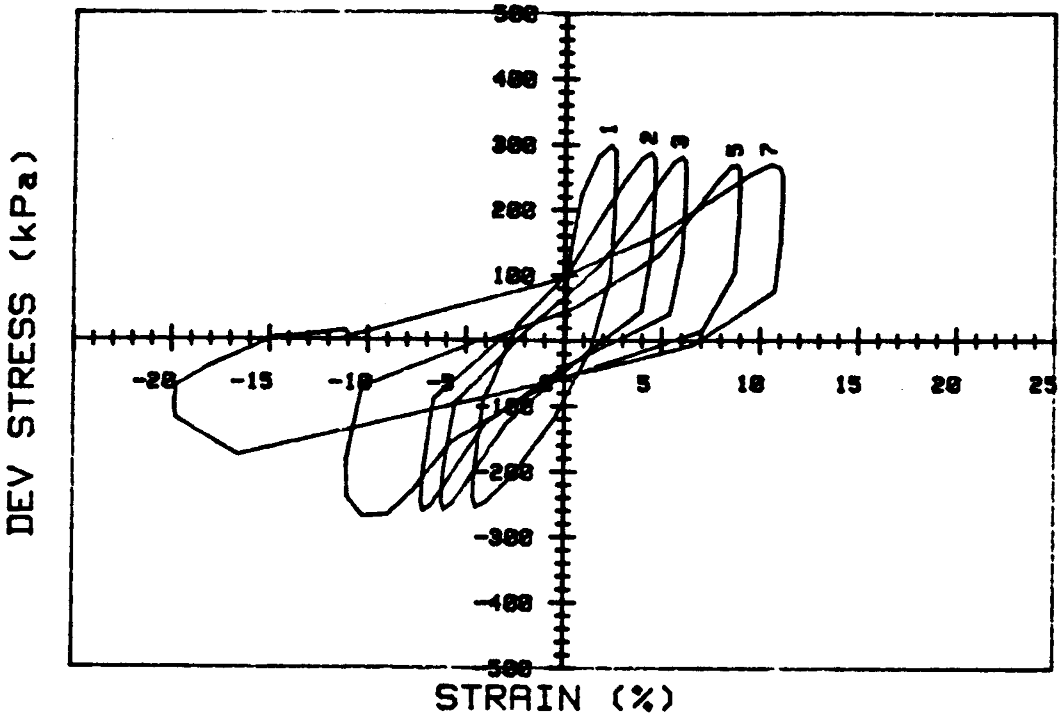

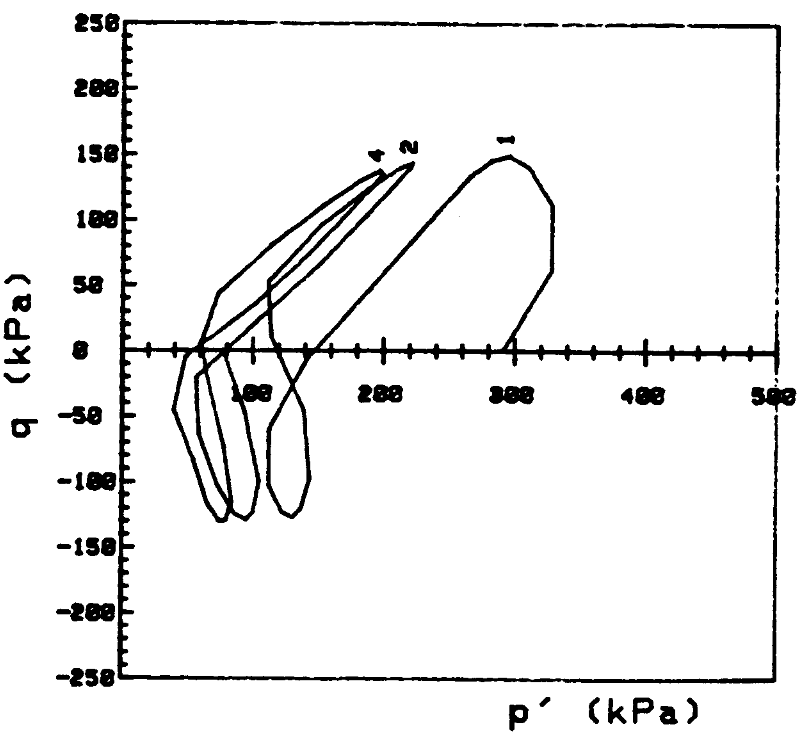

CRUISE DC4-81-NS		INCREMENT (cm)		30-37	
CORE NO.	685A2	TEST NO.		D111	
SIG1c′(kPa)	292.6	STATIC qf	(kPa)	300.0	
SIG3c′(kPa)	292.6	AVG MAX q	(kPa)	139.3	(46.4%)
INDUCED OCR	1.0	AVG MIN q	(kPa)	-122.4	(40.8%)

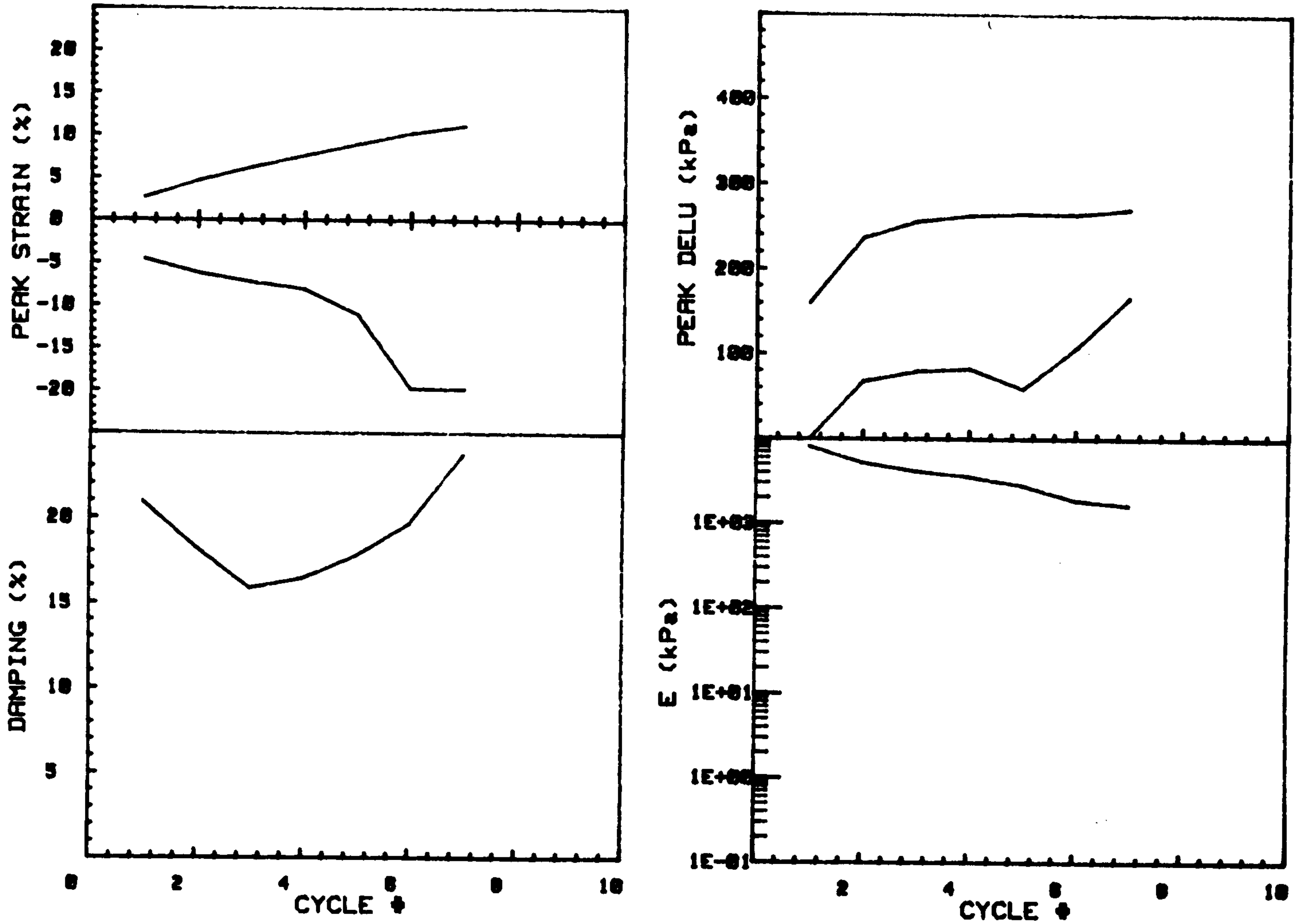

CRUISE DC4-81-NS		INCREMENT (cm)	30-37
CORE NO.	685A2	TEST NO.	D111
SIG1c'(kPa)	292.6	STATIC qf (kPa)	300.0
SIG3c'(kPa)	292.6	AVG MAX q (kPa)	139.3 (46.4%)
INDUCED OCR	1.0	AVG MIN q (kPa)	-122.4 (40.8%)

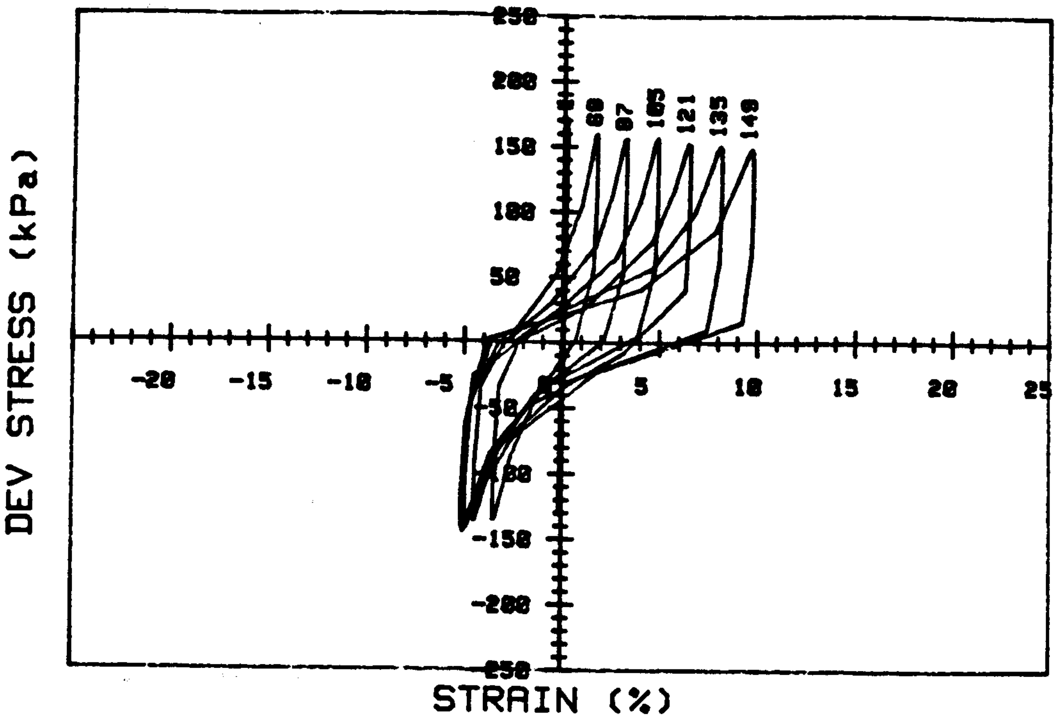

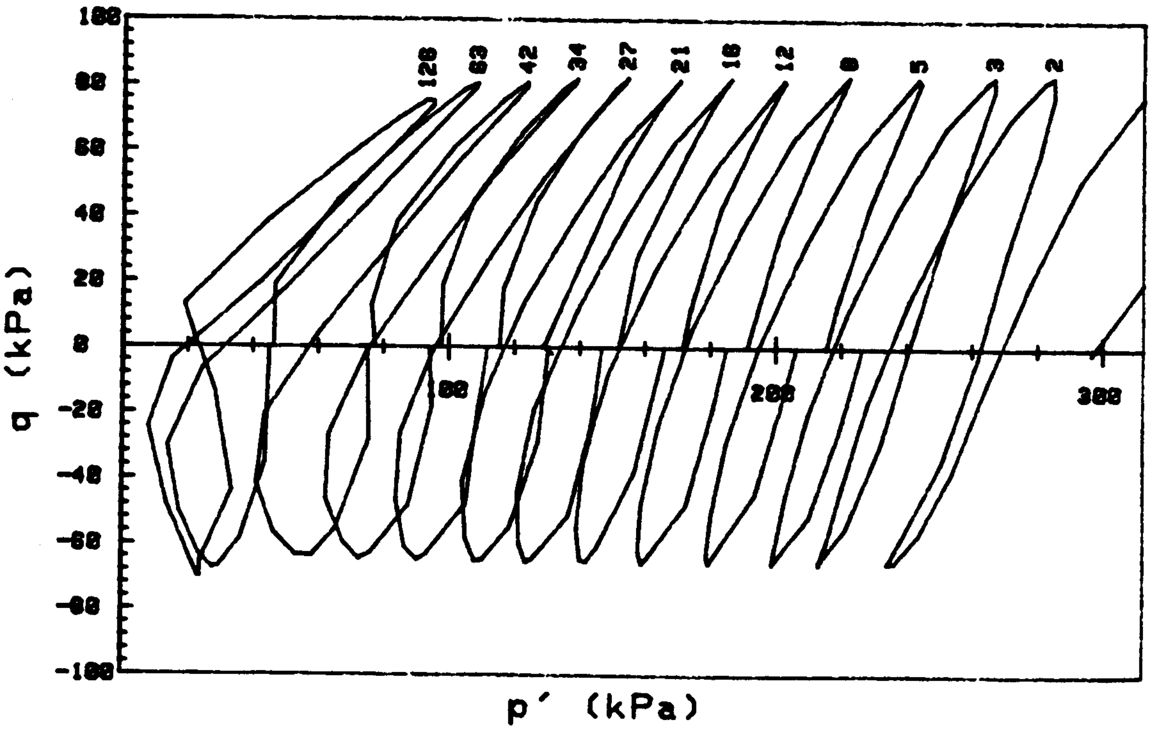

CRUISE DC4-81-NS		INCREMENT (cm)	30-37
CORE NO.	685A2	TEST NO.	D112
SIG1c′(kPa)	298.0	STATIC qf (kPa)	300.0
SIG3c′(kPa)	298.0	AVG MAX q (kPa)	78.6 (26.2%)
INDUCED OCR	1.0	AVG MIN q (kPa)	-68.0 (22.7%)

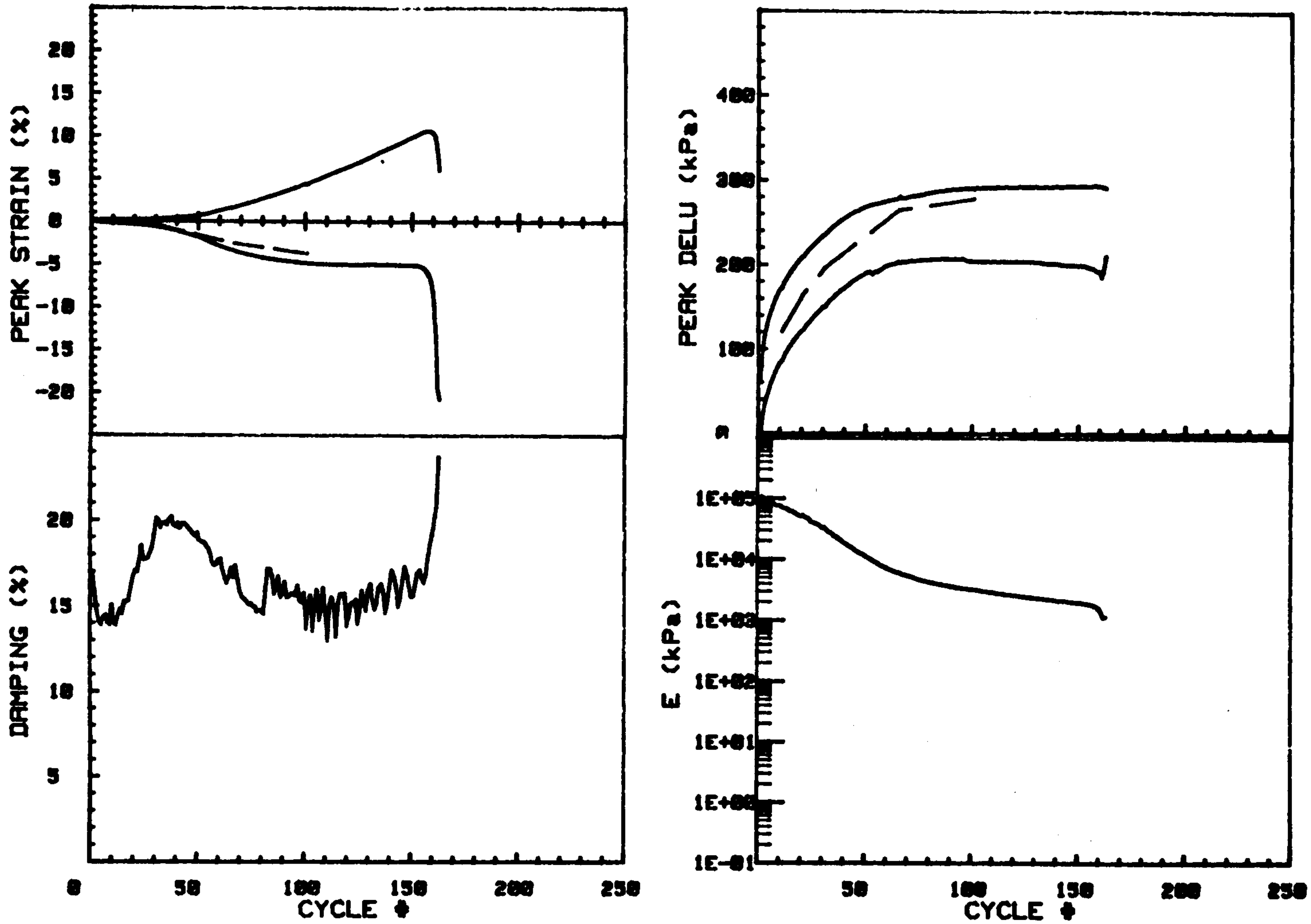

CRUISE	DC4-81-NS	INCREMENT (cm)	30-37
CORE NO.	605A2	TEST NO.	D112
SIG1c'(kPa)	298.0	STATIC qf (kPa)	300.0
SIG3c'(kPa)	298.0	AVG MAX q (kPa)	78.6 (26.2%)
INDUCED OCR	1.0	AVG MIN q (kPa)	-68.0 (22.7%)

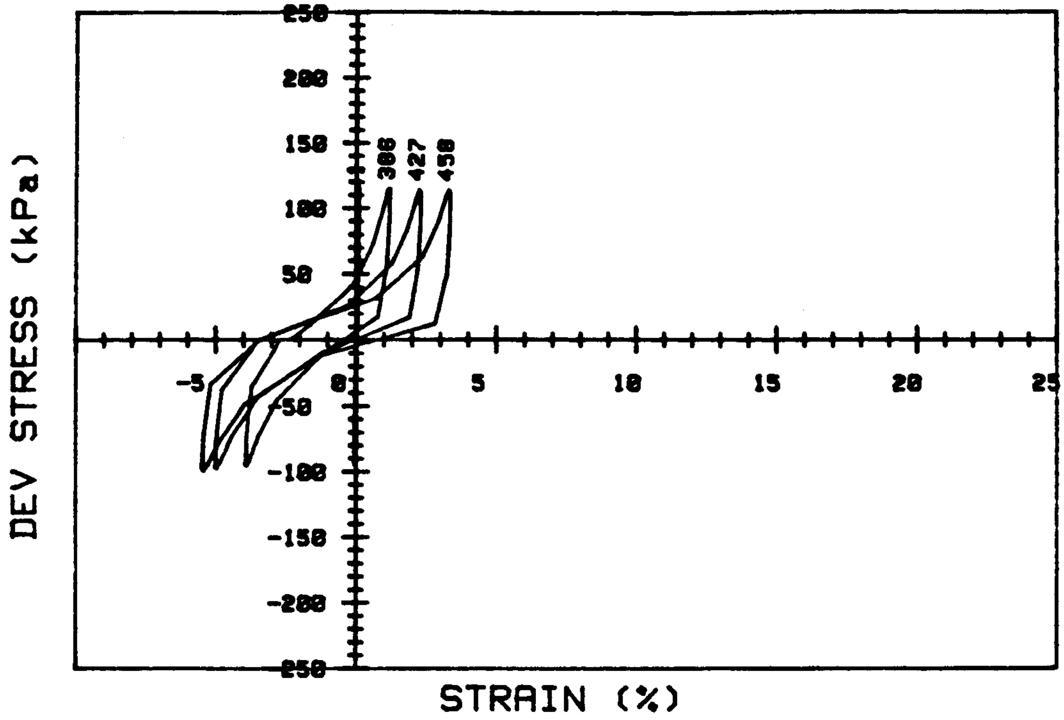

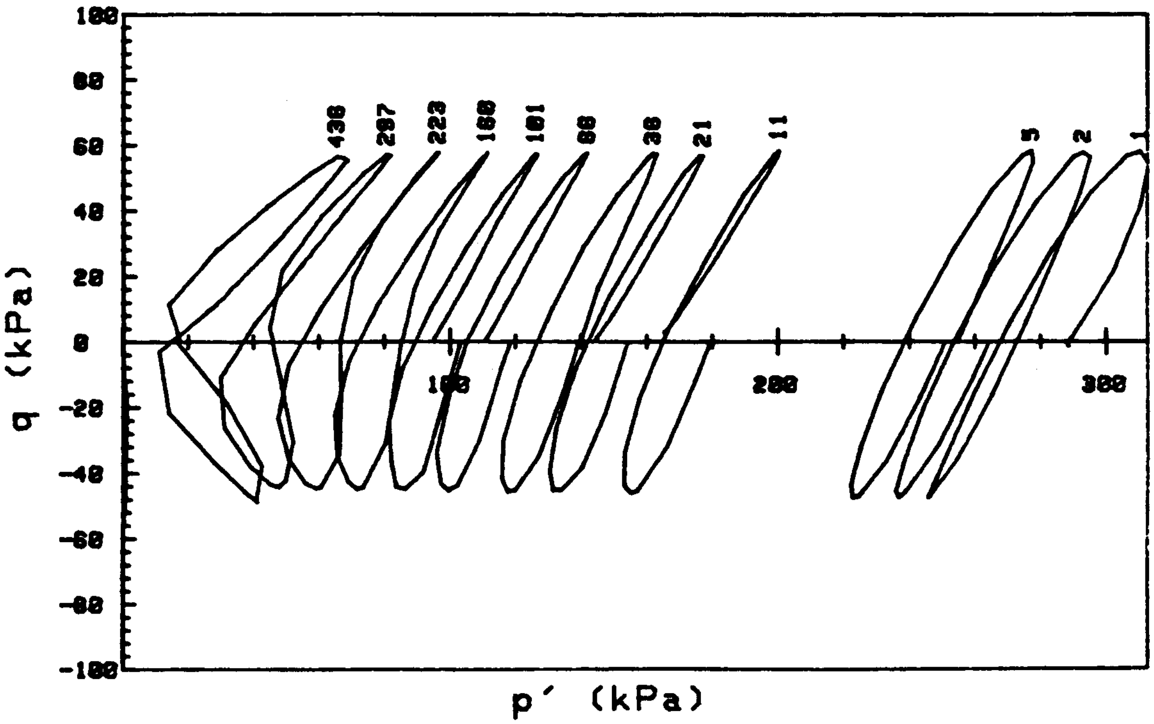

CRUISE DC4-81-NS		INCREMENT (cm)	40-48
CORE NO.	685A2	TEST NO.	TC80
SIG1c′(kPa)	289.8	STATIC qf (kPa)	300.0
SIG3c′(kPa)	289.8	AVG MAX q (kPa)	56.5 (18.8%)
INDUCED OCR	1.0	AVG MIN q (kPa)	-46.8 (15.6%)

Cycles 1 - 640

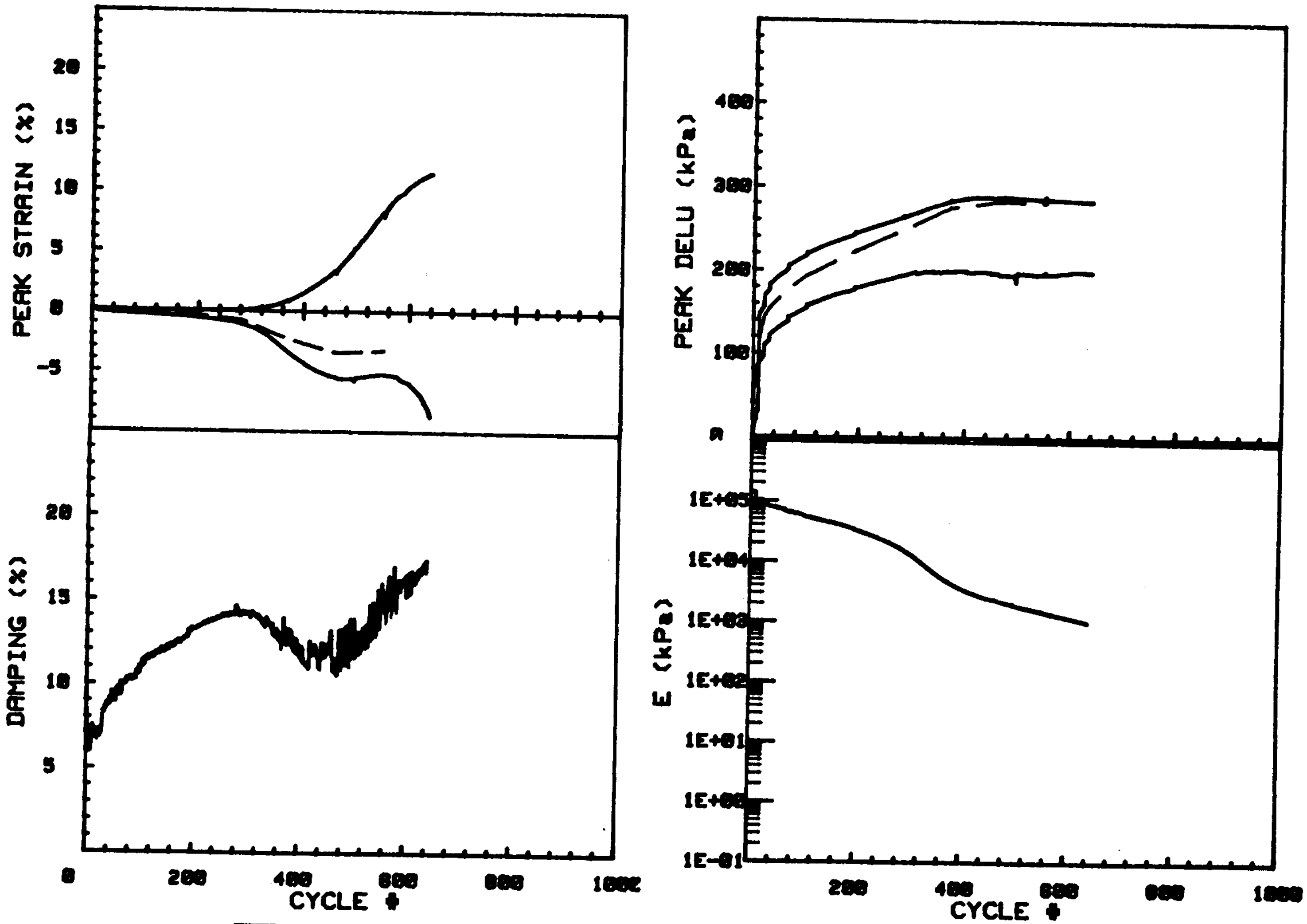

CRUISE DC4-81-NS		INCREMENT (cm)	40-48
CORE NO.	685A2	TEST NO.	TC80
SIG1c'(kPa)	289.8	STATIC qf (kPa)	300.0
SIG3c'(kPa)	289.8	AVG MAX q (kPa)	56.5 (18.8%)
INDUCED OCR	1.0	AVG MIN q (kPa)	-46.8 (15.6%)

Cycles 1 - 640

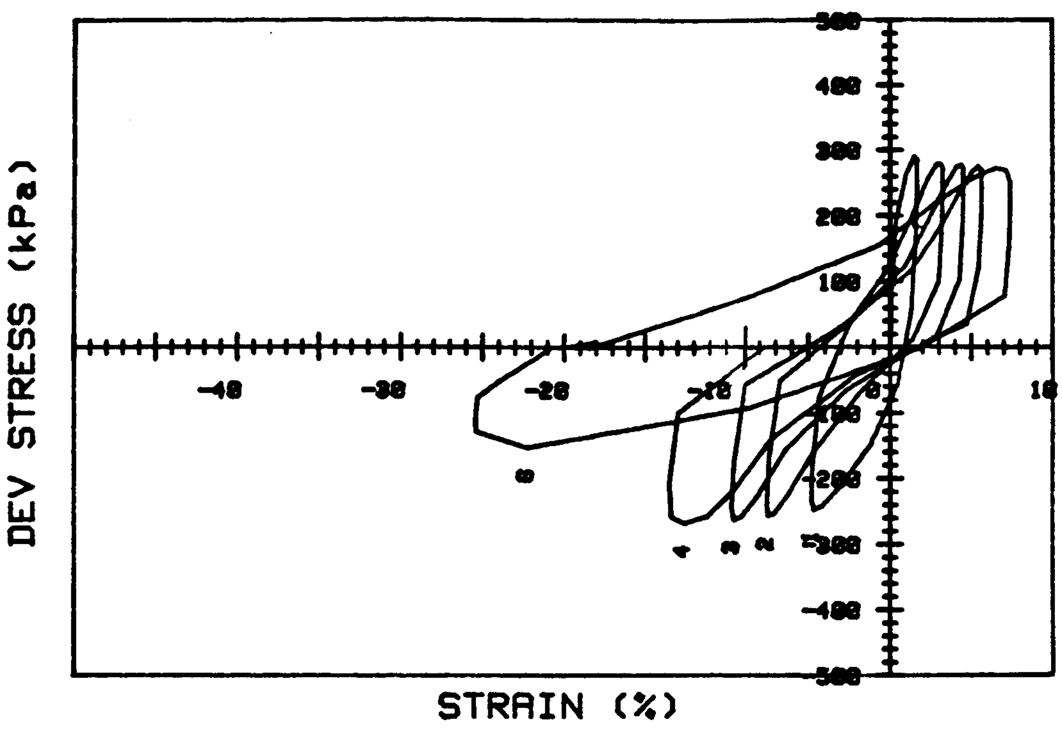

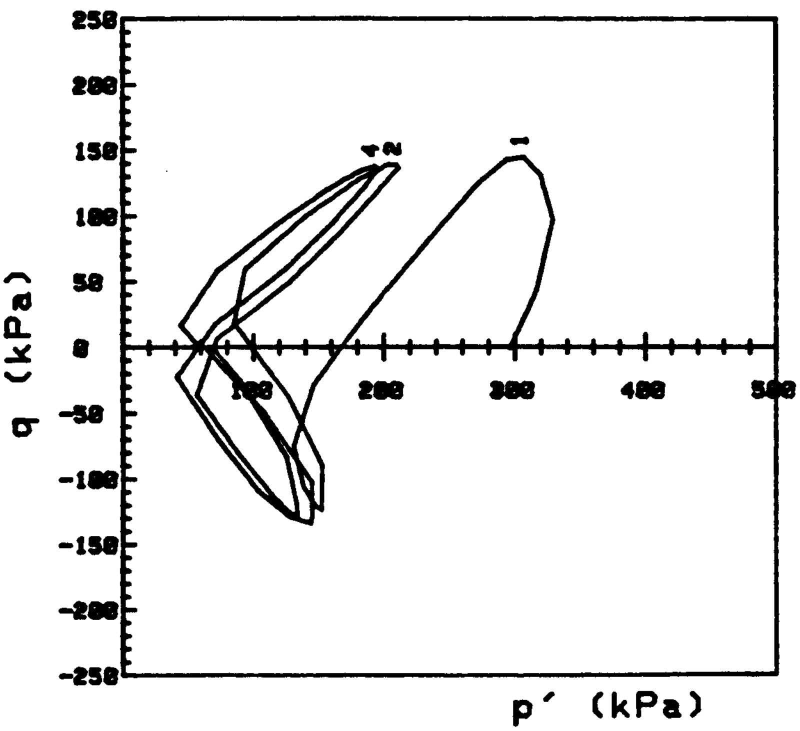

CRUISE DC4-81-NS		INCREMENT (cm)	40-48
CORE NO.	685A2	TEST NO.	TC81
SIG1c′(kPa)	297.4	STATIC qf (kPa)	300.0
SIG3c′(kPa)	297.4	AVG MAX q (kPa)	139.0 (46.3%)
INDUCED OCR	1.0	AVG MIN q (kPa)	-117.4 (39.1%)

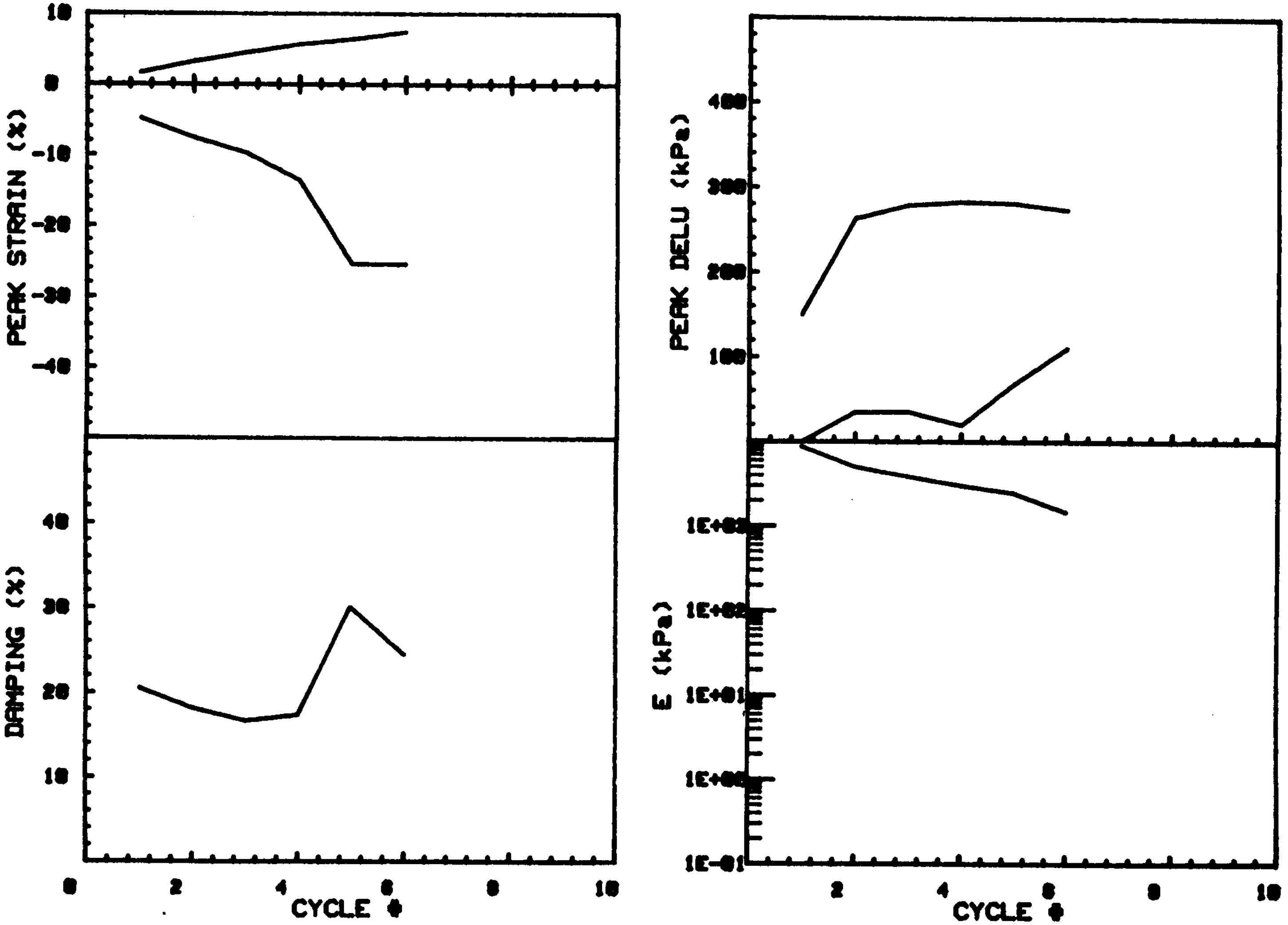

CRUISE DC4-81-NS		INCREMENT (cm)	40-48
CORE NO.	685A2	TEST NO.	TC81
SIG1c'(kPa)	297.4	STATIC qf (kPa)	300.0
SIG3c'(kPa)	297.4	AVG MAX q (kPa)	139.0 (46.3%)
INDUCED OCR	1.0	AVG MIN q (kPa)	-117.4 (39.1%)

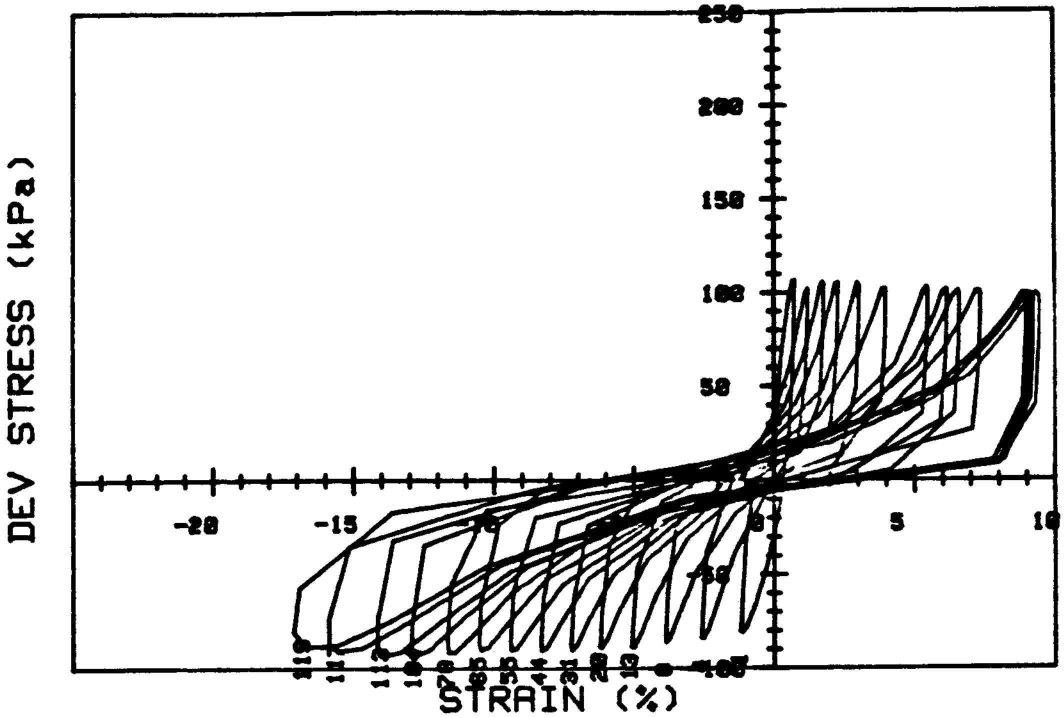

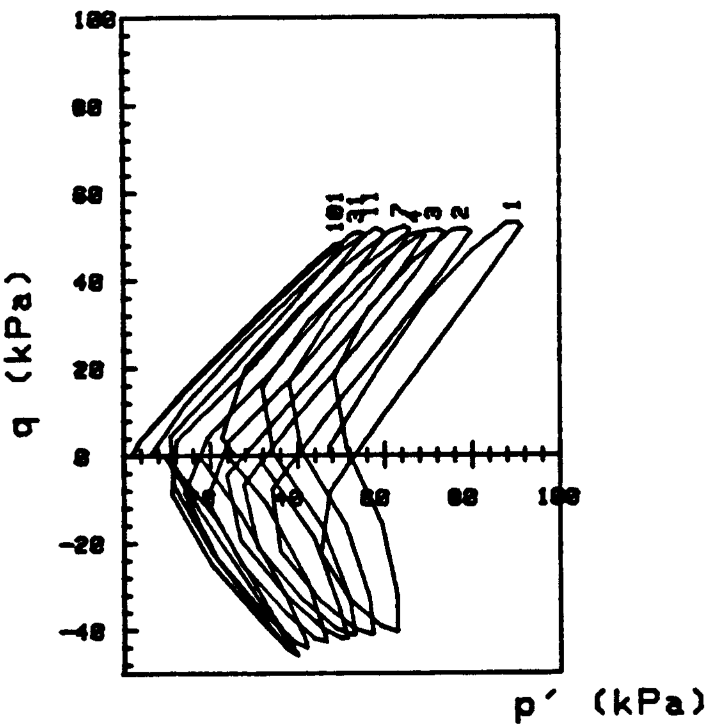

CRUISE DC4-81-NS		INCREMENT (cm)	61-69
CORE NO.	685A2	TEST NO.	TC82
SIG1c′(kPa)	46.7	STATIC qf (kPa)	50.0
SIG3c′(kPa)	46.7	AVG MAX q (kPa)	50.8 (101.6%)
INDUCED OCR	6.0	AVG MIN q (kPa)	-45.0 (90.0%)

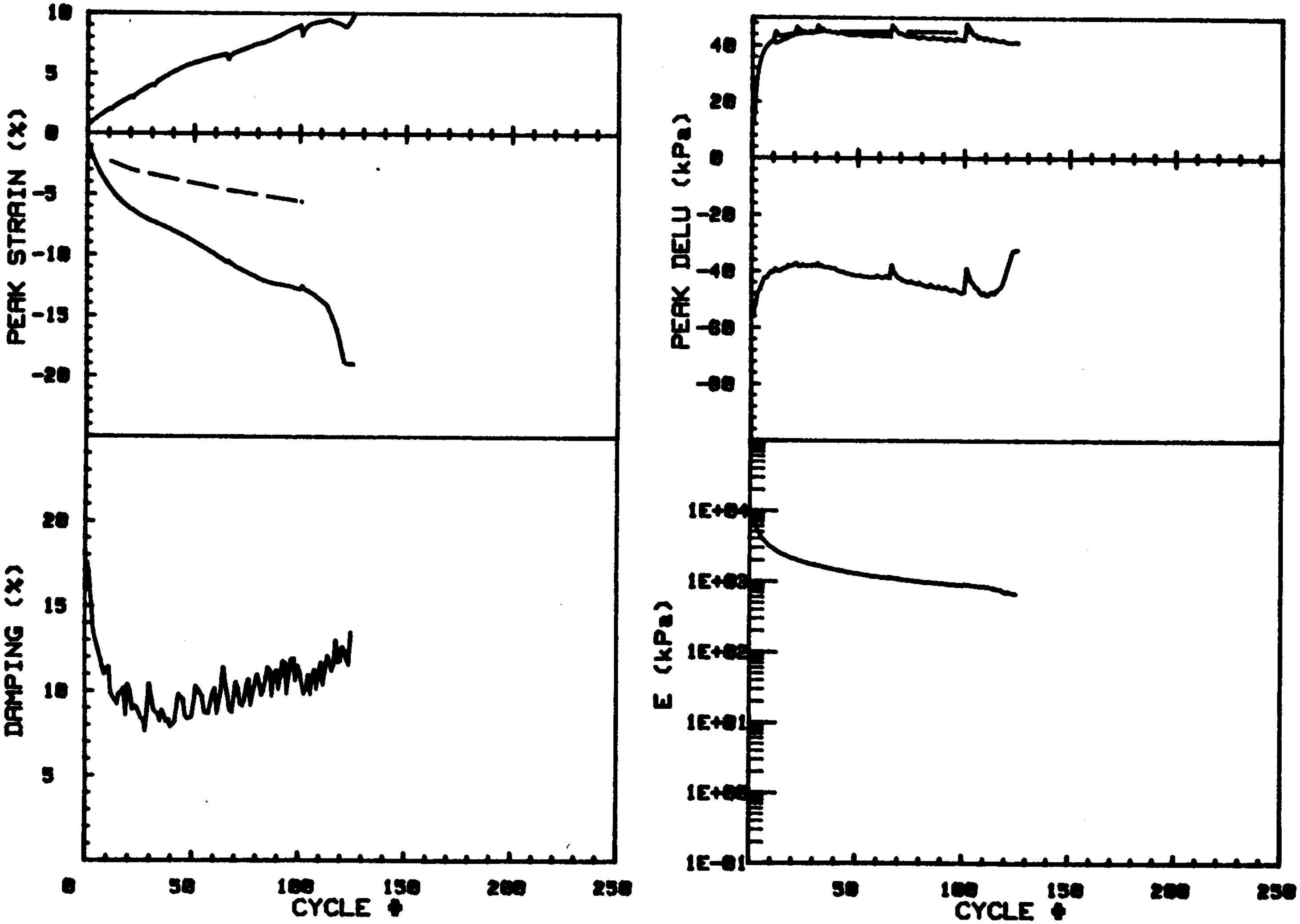

CRUISE DC4-81-NS		INCREMENT (cm)	61-69
CORE NO.	685A2	TEST NO.	TC82
SIG1c′(kPa)	46.7	STATIC qf (kPa)	50.0
SIG3c′(kPa)	46.7	AVG MAX q (kPa)	50.8 (101.6%)
INDUCED OCR	6.0	AVG MIN q (kPa)	-45.0 (90.0%)

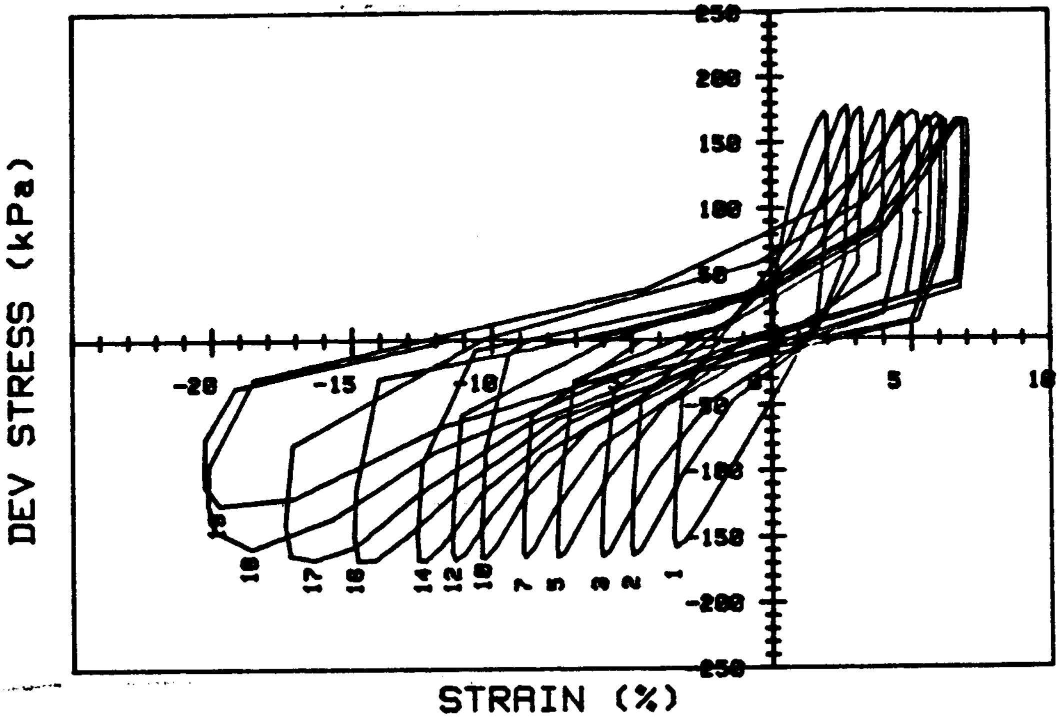

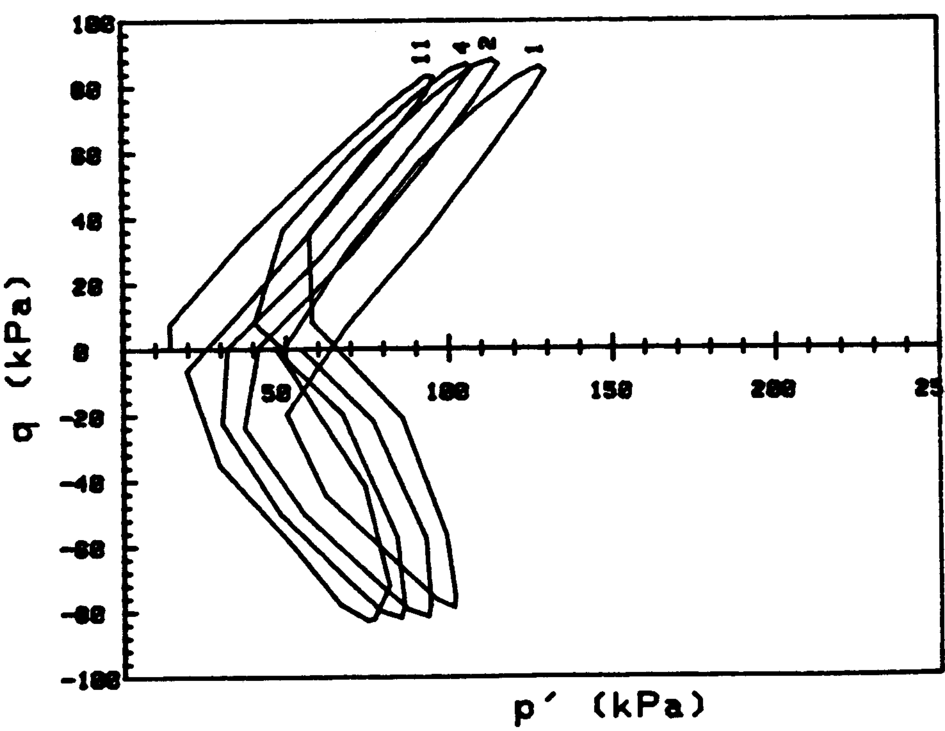

CRUISE DC4-81-NS		INCREMENT (cm)	61-69
CORE NO.	685A2	TEST NO.	TC83
SIG1c′(kPa)	49.7	STATIC qf (kPa)	50.0
SIG3c′(kPa)	49.7	AVG MAX q (kPa)	85.0 (170.0%)
INDUCED OCR	6.0	AVG MIN q (kPa)	-80.1 (160.2%)

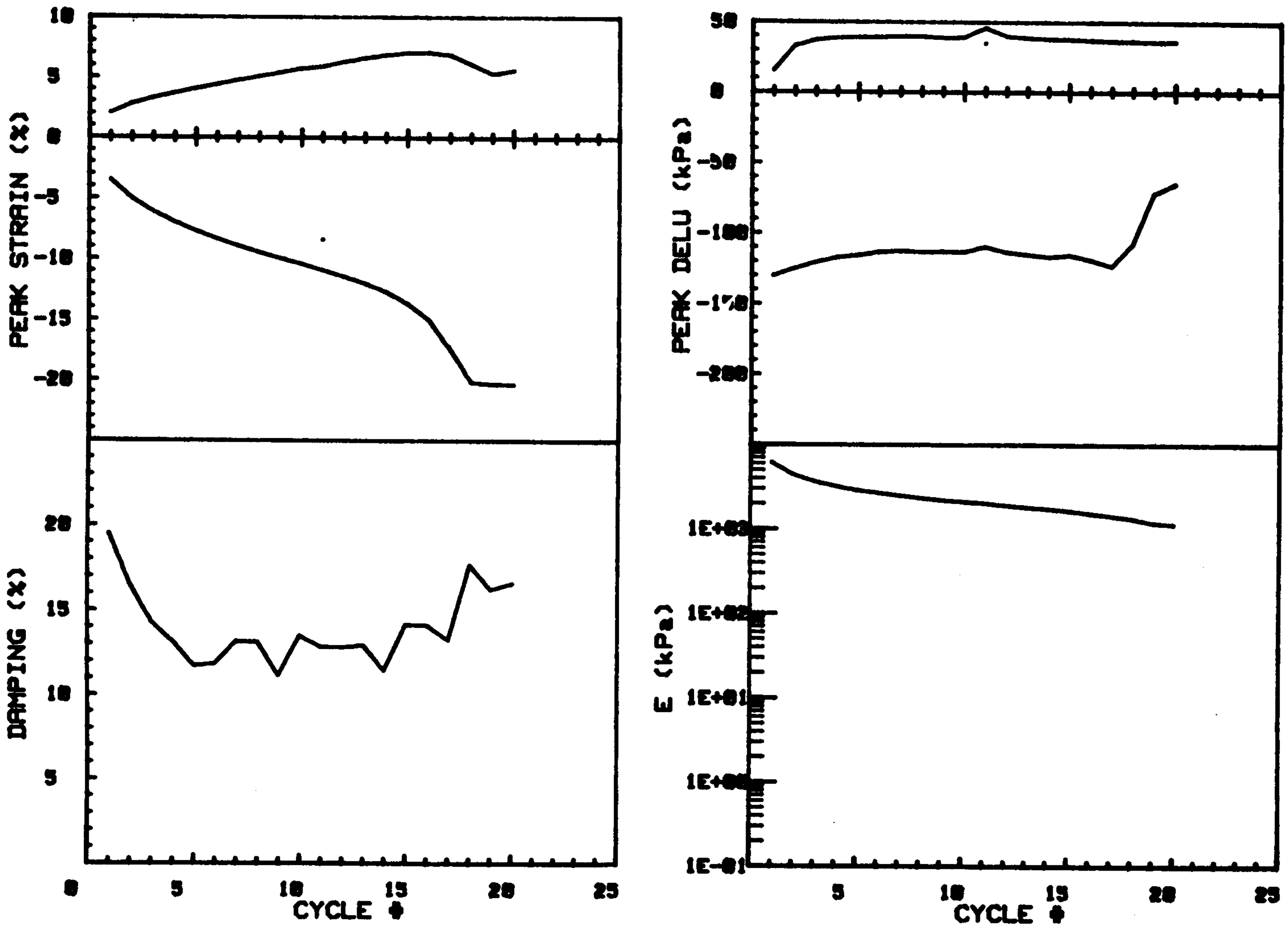

CRUISE	DC4-81-NS	INCREMENT (cm)	61-69
CORE NO.	685A2	TEST NO.	TC83
SIG1c′(kPa)	49.7	STATIC qf (kPa)	50.0
SIG3c′(kPa)	49.7	AVG MAX q (kPa)	85.0 (170.0%)
INDUCED OCR	6.0	AVG MIN q (kPa)	-80.1 (160.2%)

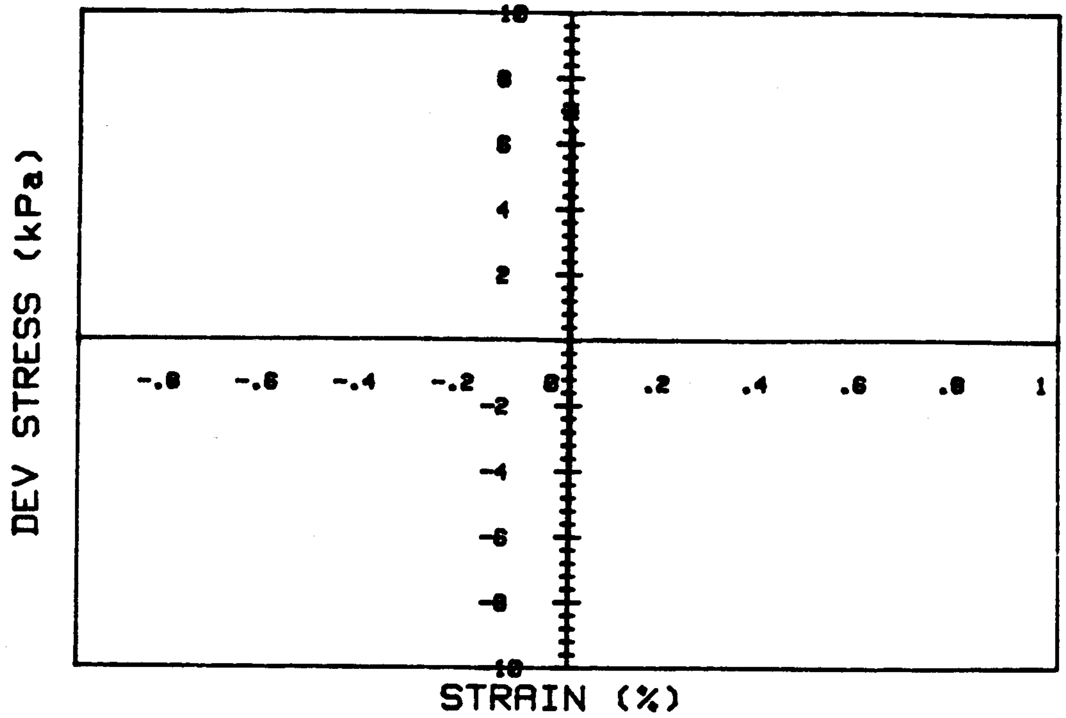

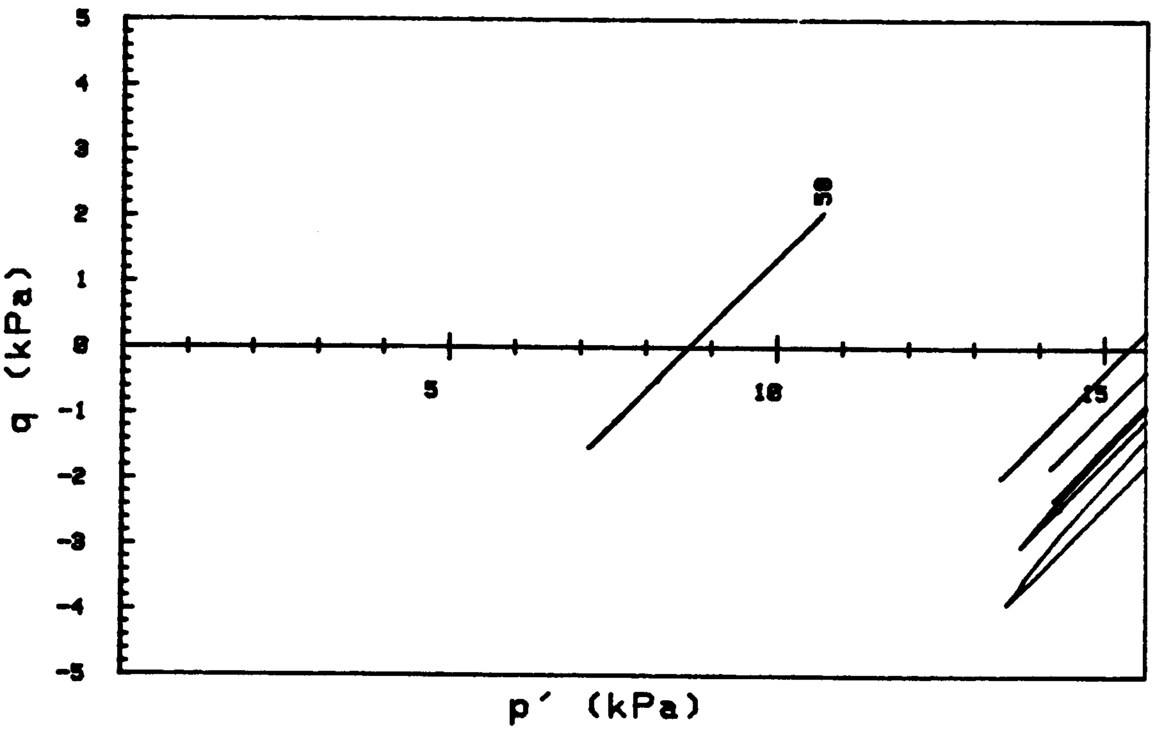

CRUISE DC4-81-NS		INCREMENT (cm)	101-109
CORE NO.	685A2	TEST NO.	TC62
SIG1c′(kPa)	17.4	STATIC qf (kPa)	18.0
SIG3c′(kPa)	17.4	AVG MAX q (kPa)	1.5 (8.3%)
INDUCED OCR	1.0	AVG MIN q (kPa)	-2.1 (11.7%)

Cycles 1 - 500

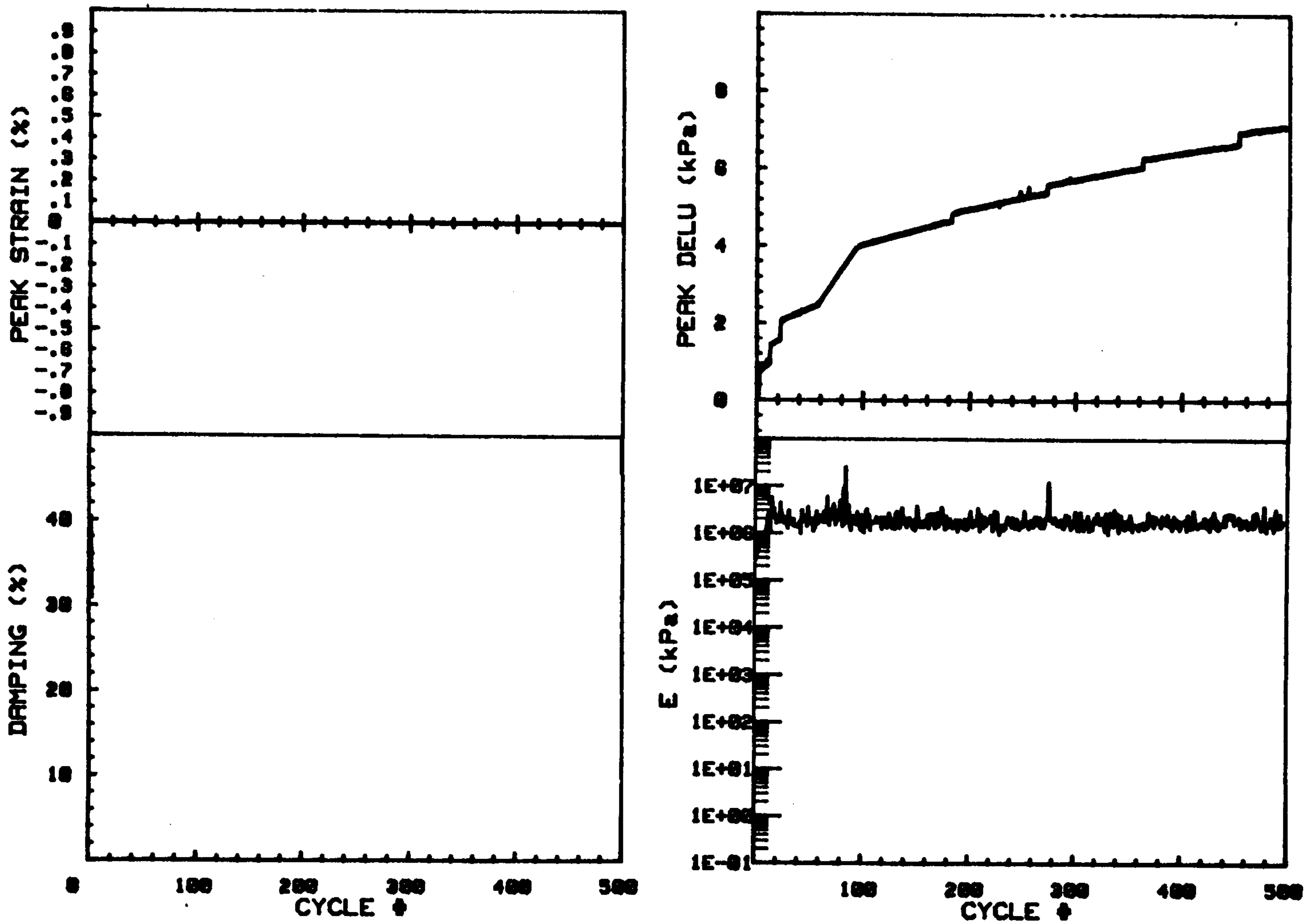

CRUISE DC4-81-NS		INCREMENT (cm)	101-109
CORE NO.	685A2	TEST NO.	TC62
SIG1c'(kPa)	17.4	STATIC qf (kPa)	18.0
SIG3c'(kPa)	17.4	AVG MAX q (kPa)	1.5 (8.3%)
INDUCED OCR	1.0	AVG MIN q (kPa)	-2.1 (11.7%)

Cycles 1 - 500

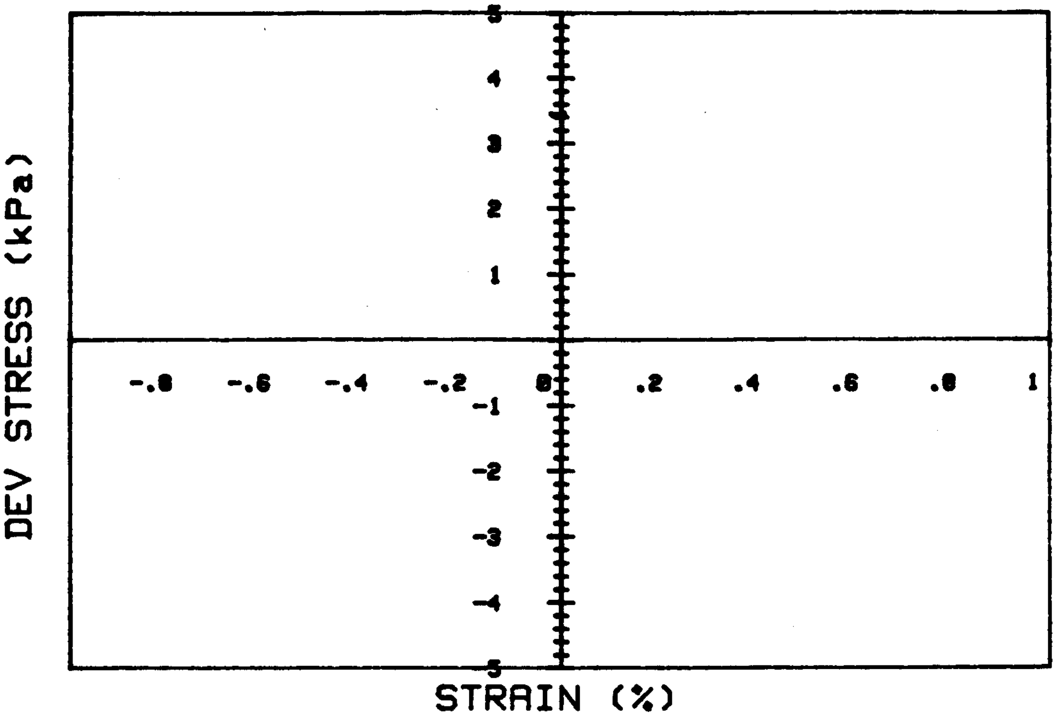

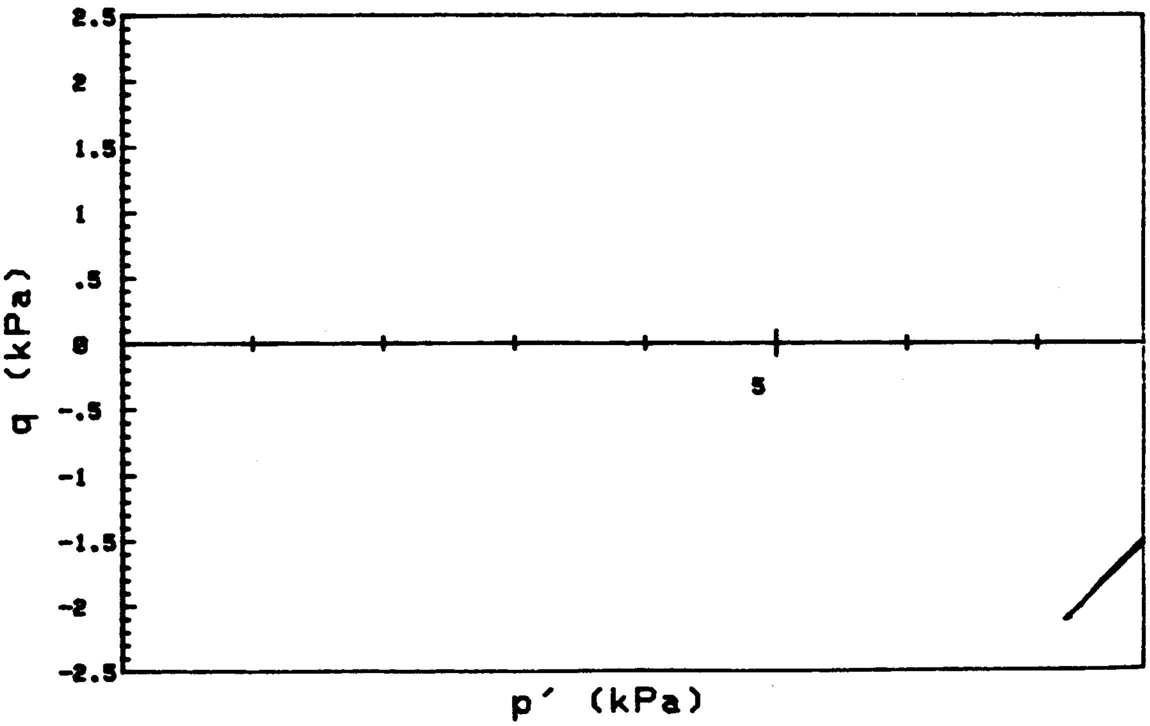

CRUISE DC4-81-NS		INCREMENT (cm)	101-109
CORE NO.	685A2	TEST NO.	TC62
SIG1c′(kPa)	10.2	STATIC qf (kPa)	18.0
SIG3c′(kPa)	10.2	AVG MAX q (kPa)	1.6 (8.9%)
INDUCED OCR	1.0	AVG MIN q (kPa)	-2.0 (11.1%)

Cycles 501 - 860

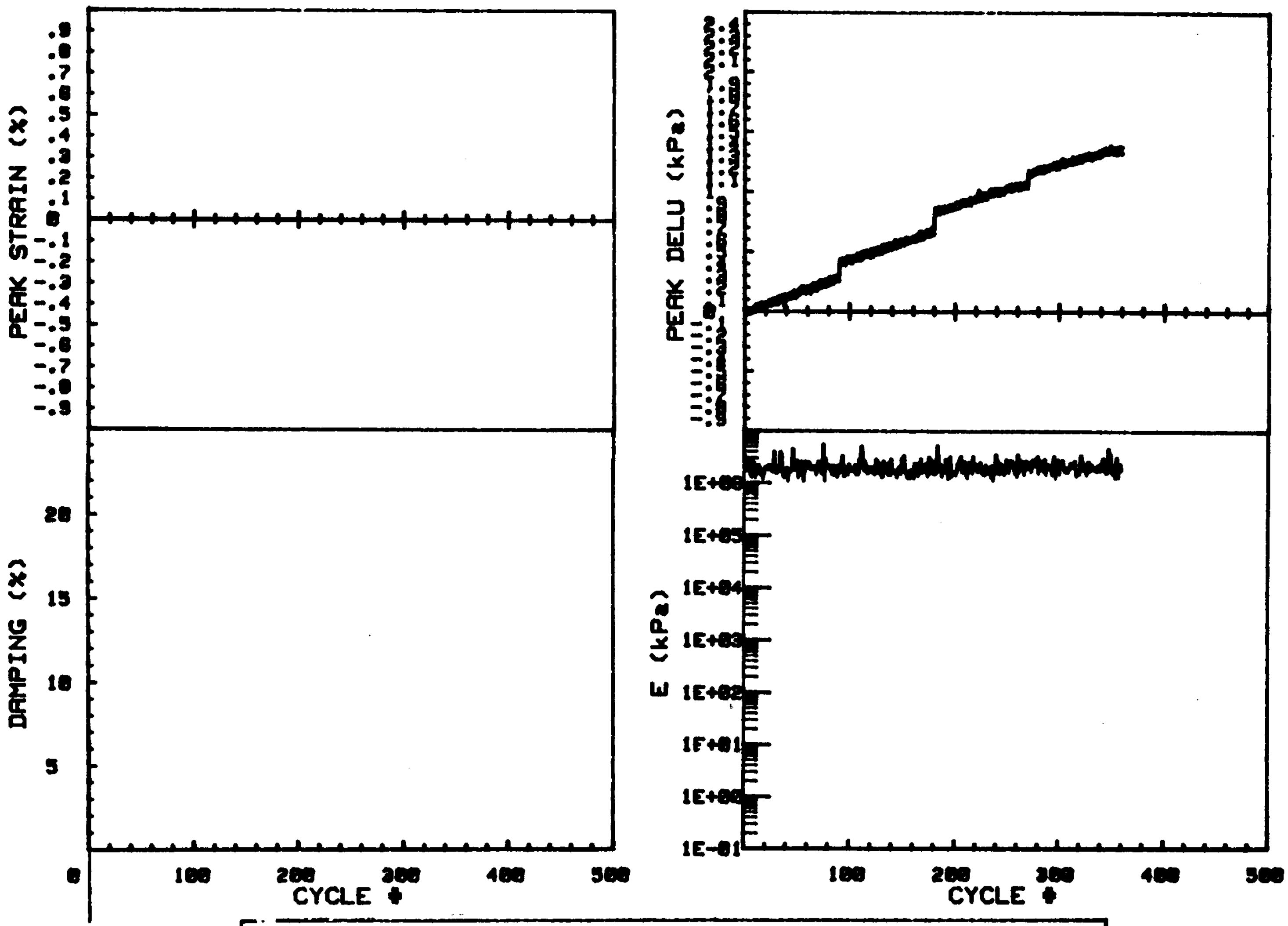

CRUISE DC4-81-NS		INCREMENT (cm)	101-109
CORE NO.	685A2	TEST NO.	TC62
SIG1c'(kPa)	10.2	STATIC qf (kPa)	18.0
SIG3c'(kPa)	10.2	AVG MAX q (kPa)	1.6 (8.9%)
INDUCED OCR	1.0	AVG MIN q (kPa)	-2.0 (11.1%)

Cycles 501 - 860

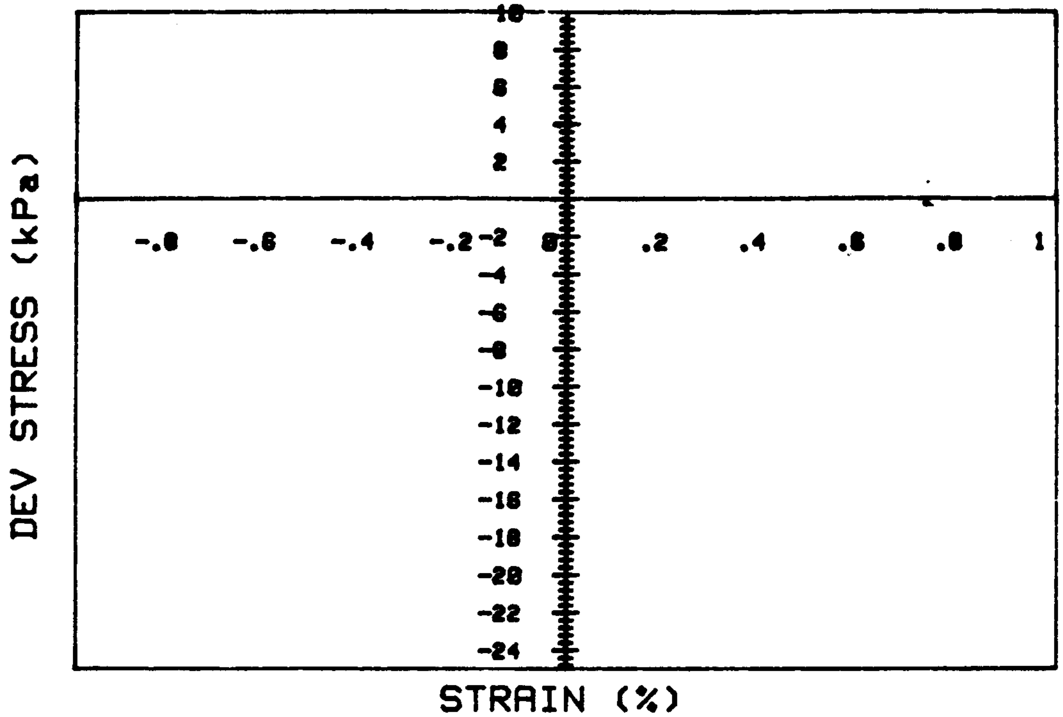

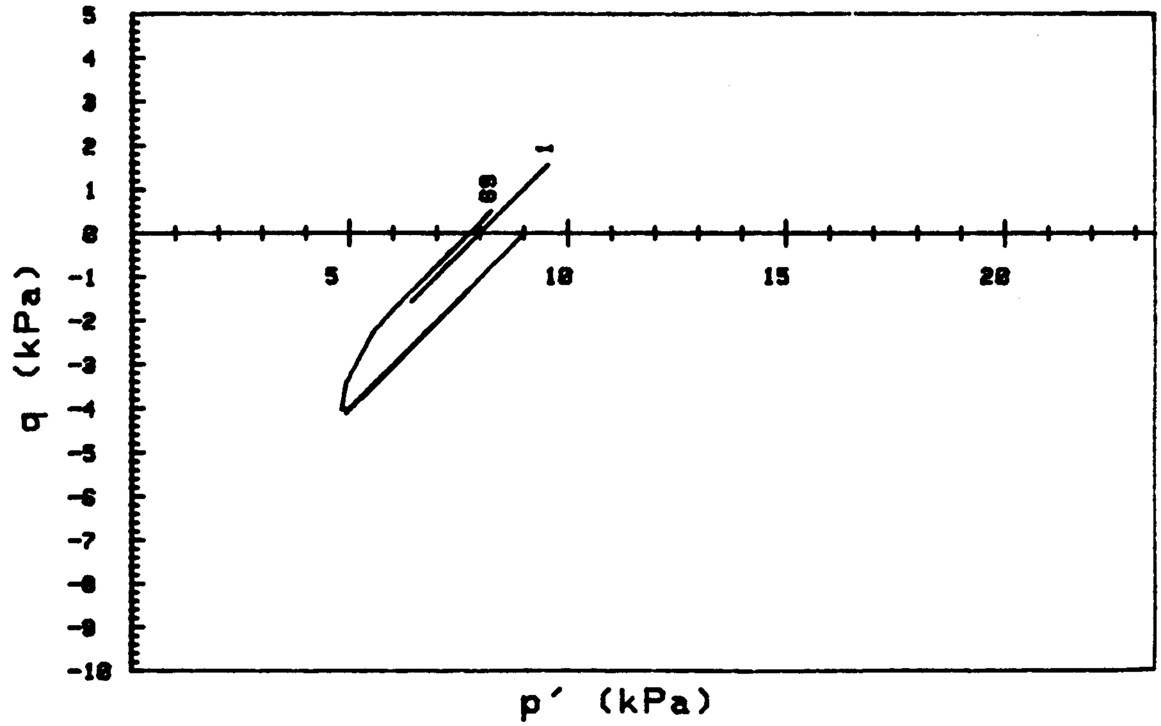

CRUISE DC4-81-NS		INCREMENT (cm)	101-109
CORE NO.	685A2	TEST NO.	TC62
SIG1c′(kPa)	8.0	STATIC qf (kPa)	18.0
SIG3c′(kPa)	8.0	AVG MAX q (kPa)	1.7 (9.4%)
INDUCED OCR	1.0	AVG MIN q (kPa)	-1.7 (9.4%)

Cycles 1147 - 1600

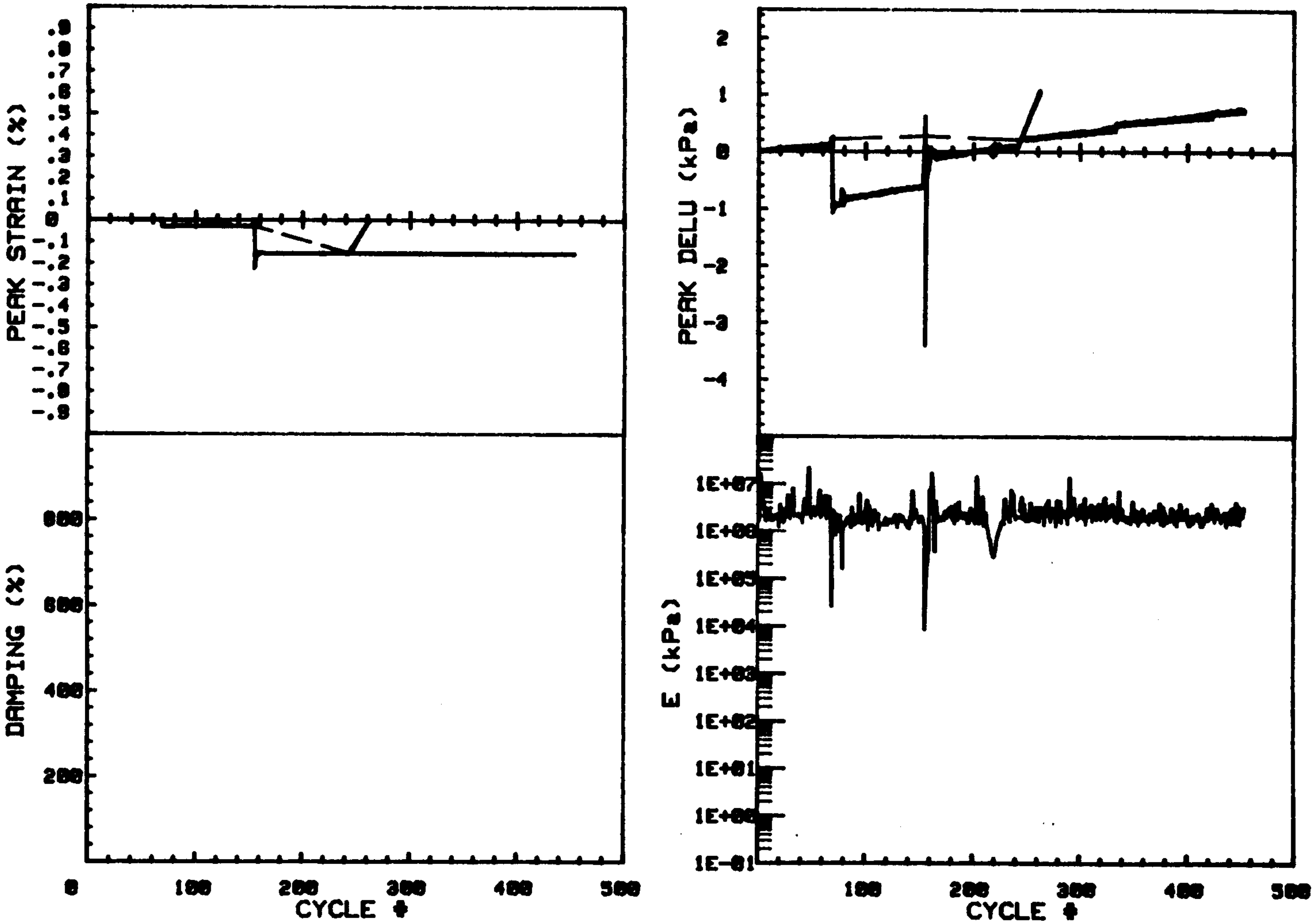

CRUISE	DC4-81-NS	INCREMENT (cm)	101-109
CORE NO.	685A2	TEST NO.	TC62
SIG1c′(kPa)	8.0	STATIC qf (kPa)	18.0
SIG3c′(kPa)	8.0	AVG MAX q (kPa)	1.7 (9.4%)
INDUCED OCR	1.0	AVG MIN q (kPa)	-1.7 (9.4%)

Cycles 1147 - 1600

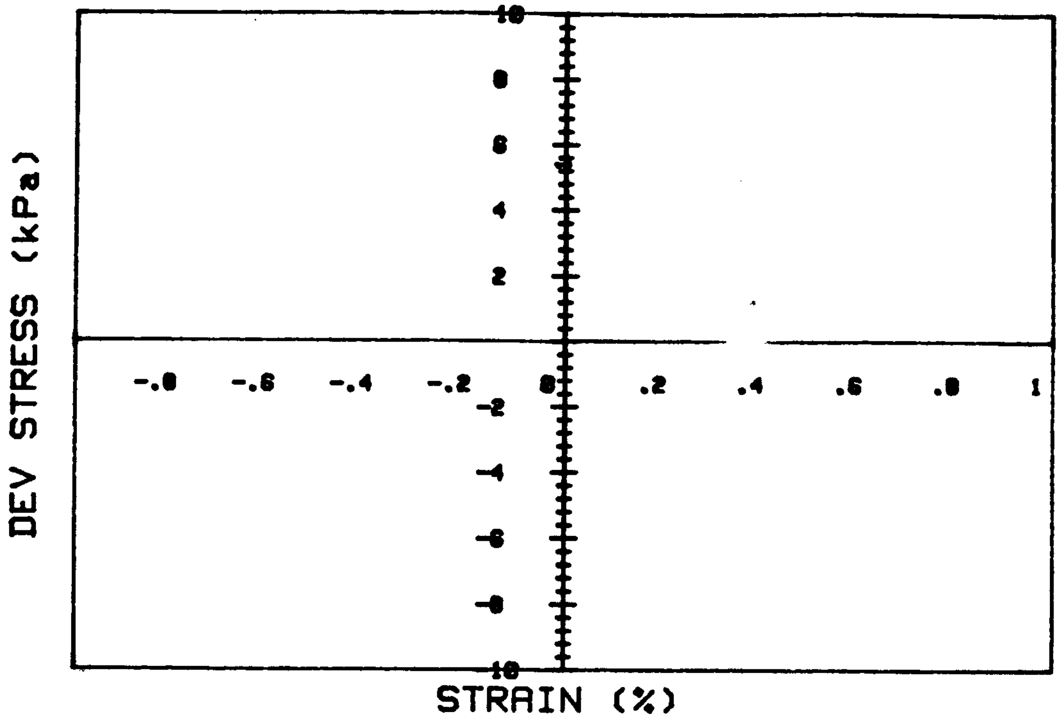

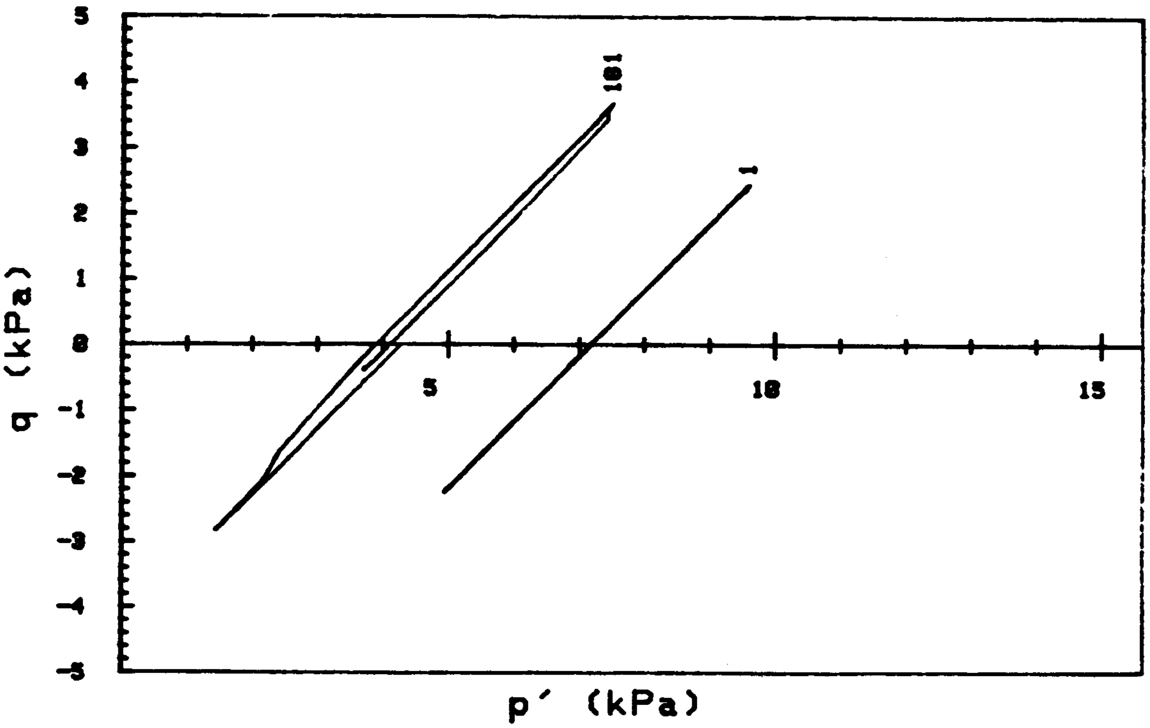

CRUISE DC4-81-NS		INCREMENT (cm)	101-109
CORE NO.	685A2	TEST NO.	TC62
SIG1c′(kPa)	7.2	STATIC qf (kPa)	18.0
SIG3c′(kPa)	7.2	AVG MAX q (kPa)	3.9 (21.7%)
INDUCED OCR	1.0	AVG MIN q (kPa)	-3.5 (19.4%)

Cycles 1601 - 2000

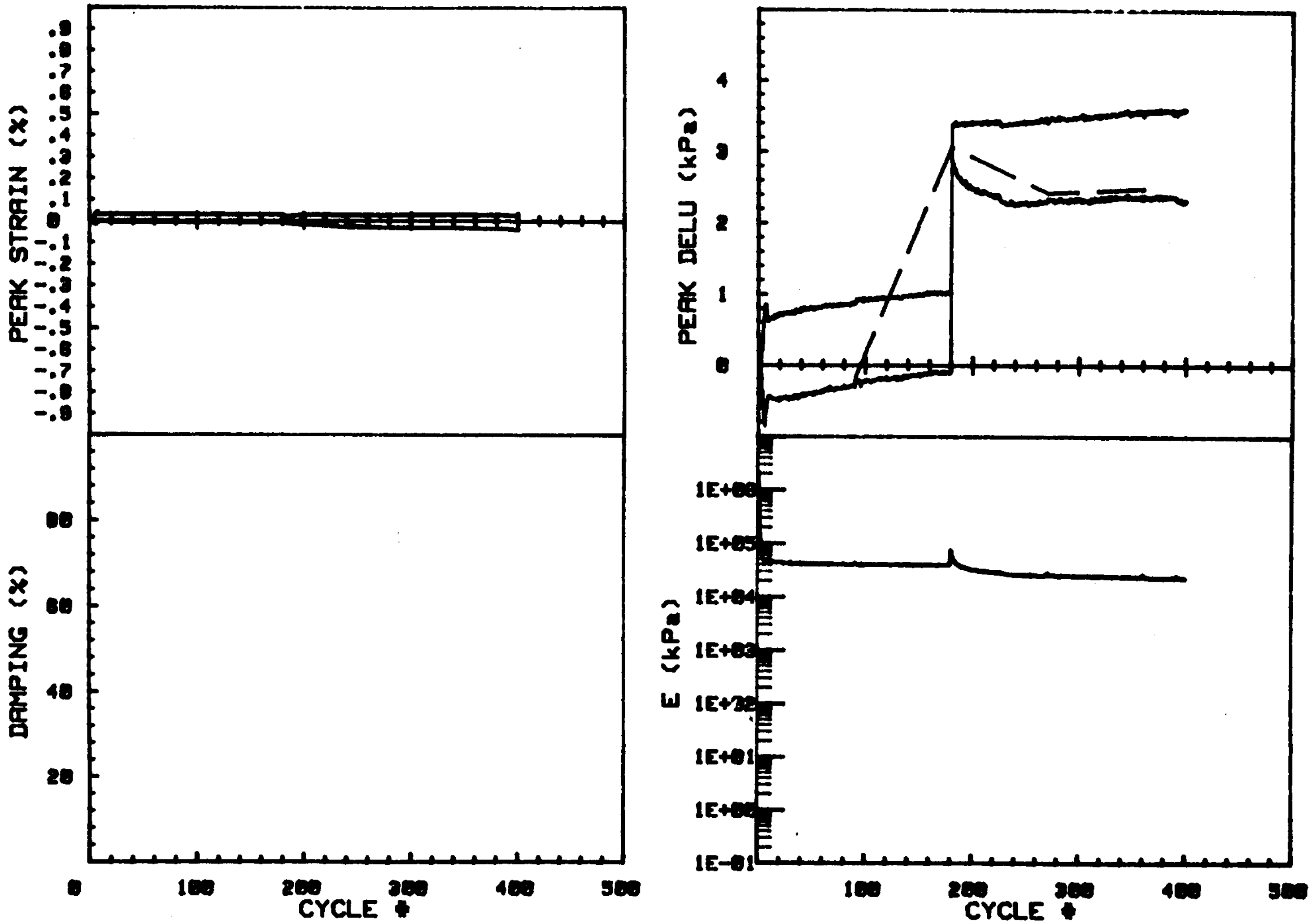

CRUISE DC4-81-NS		INCREMENT (cm)	101-109
CORE NO.	685A2	TEST NO.	TC62
SIG1c'(kPa)	7.2	STATIC qf (kPa)	18.0
SIG3c'(kPa)	7.2	AVG MAX q (kPa)	3.9 (21.7%)
INDUCED OCR	1.0	AVG MIN q (kPa)	-3.5 (19.4%)

Cycles 1601 - 2000

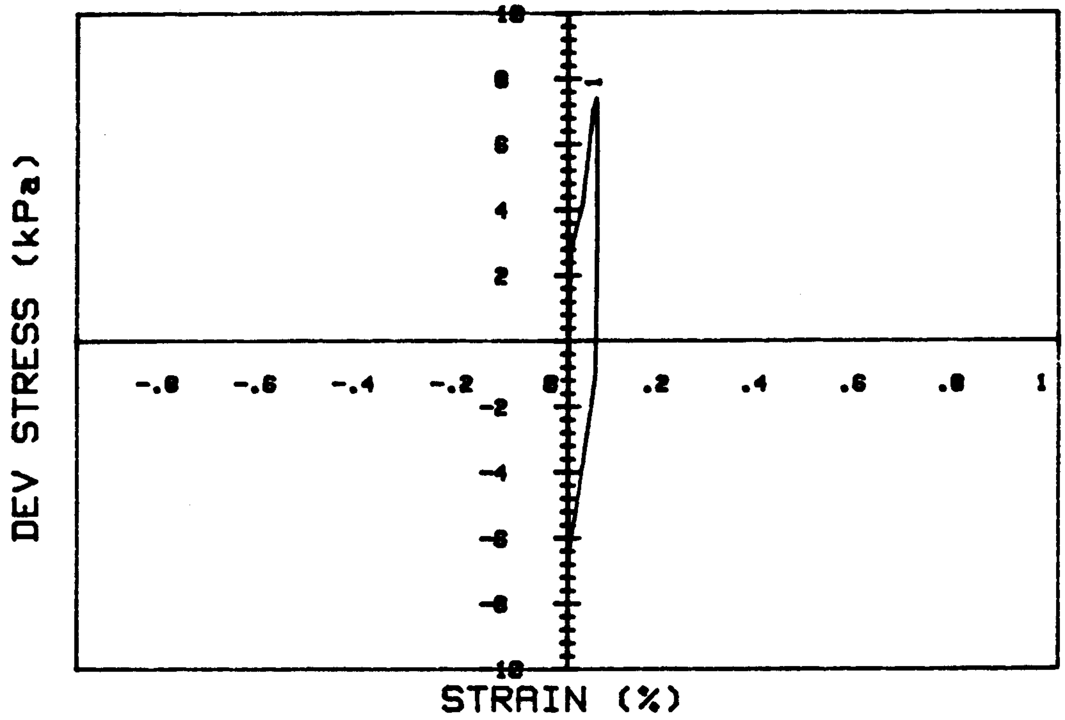

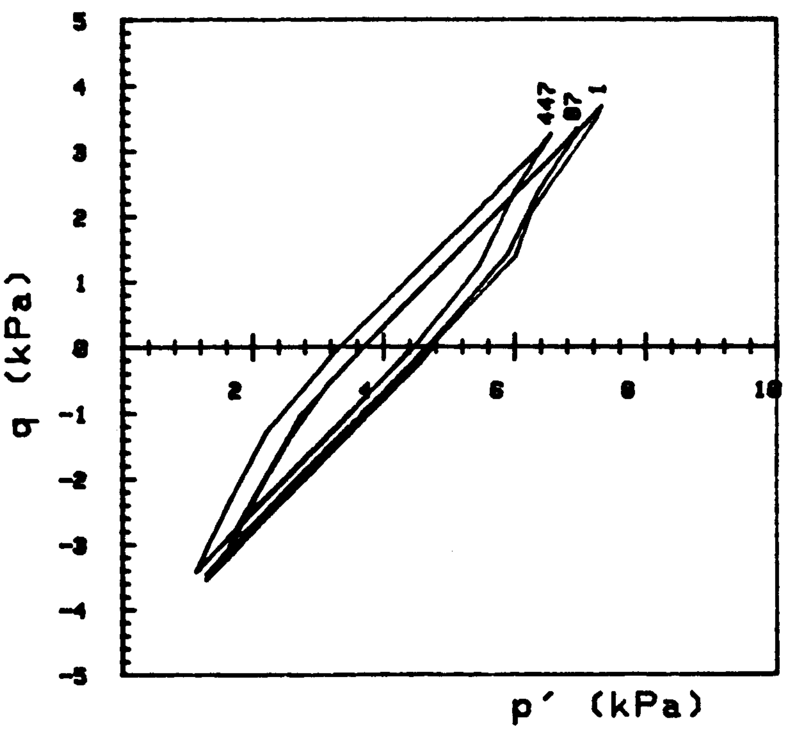

CRUISE	DC4-81-NS	INCREMENT (cm)		101-109	
CORE NO.	685A2	TEST NO.		TC62	
SIG1c′(kPa)	4.7	STATIC qf	(kPa)	10.0	
SIG3c′(kPa)	4.7	AVG MAX q	(kPa)	3.6	(20.0%)
INDUCED OCR	1.0	AVG MIN q	(kPa)	-3.5	(19.4%)

Cycles 2001 - 2500

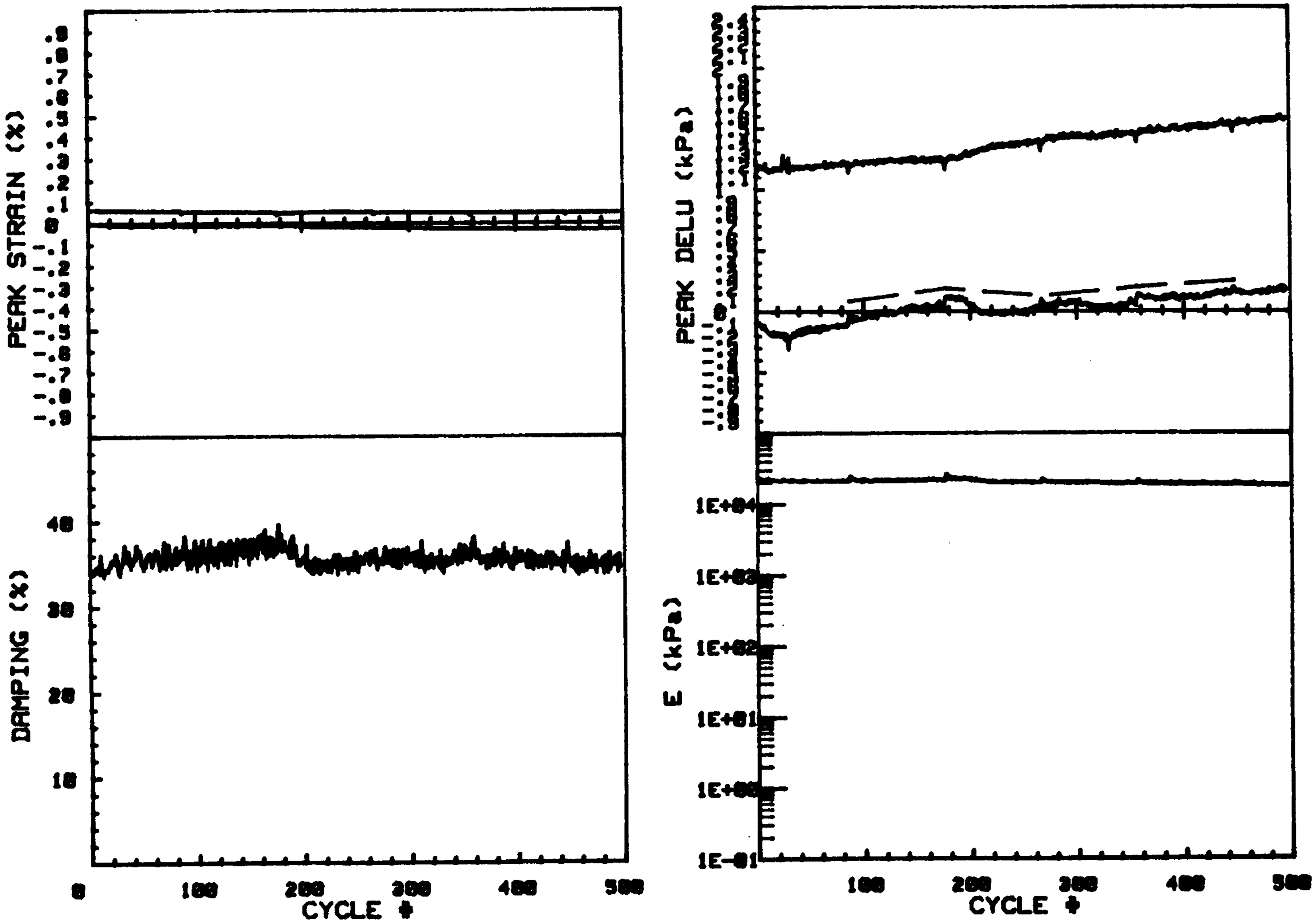

CRUISE DC4-81-NS		INCREMENT (cm)	101-109
CORE NO.	685A2	TEST NO.	TC62
SIG1c'(kPa)	4.7	STATIC qf (kPa)	18.0
SIG3c'(kPa)	4.7	AVG MAX q (kPa)	3.6 (20.0%)
INDUCED OCR	1.0	AVG MIN q (kPa)	-3.5 (19.4%)

Cycles 2001 - 2500

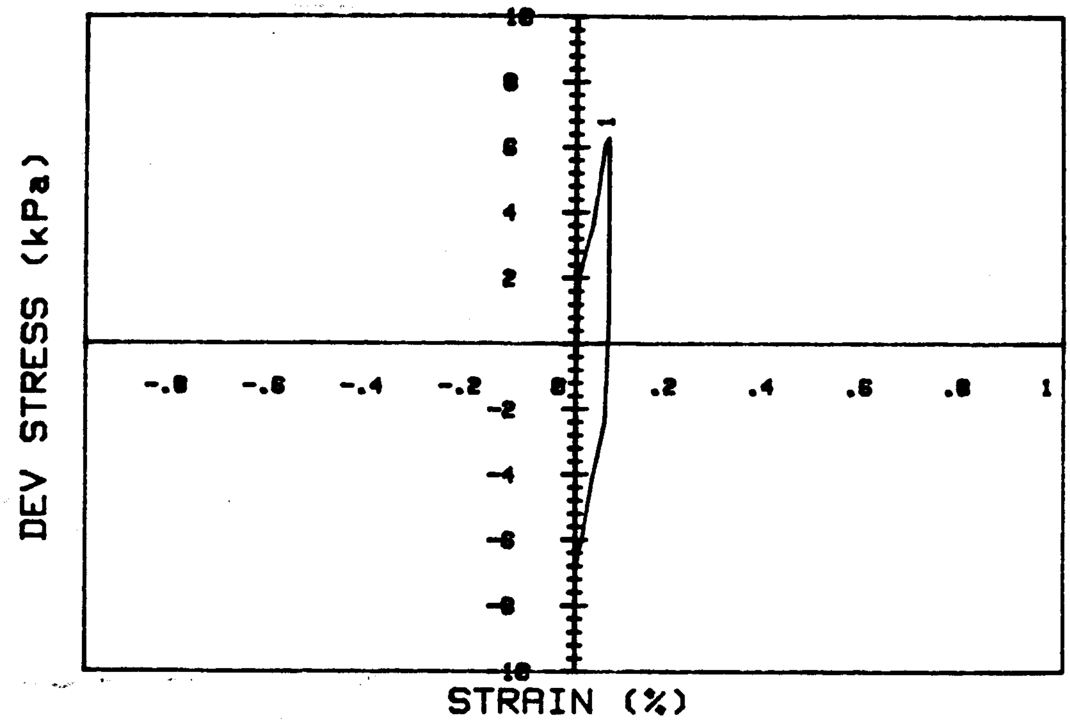

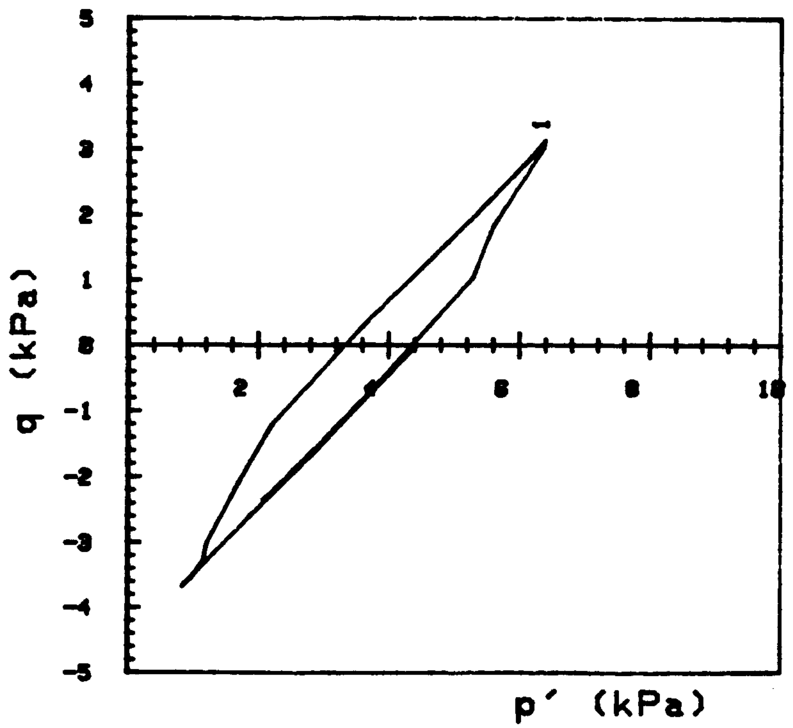

CRUISE DC4-81-NS		INCREMENT (cm)	101-109
CORE NO.	685A2	TEST NO.	TC62
SIG1c′(kPa)	4.4	STATIC qf (kPa)	10.0
SIG3c′(kPa)	4.4	AVG MAX q (kPa)	3.7 (20.6%)
INDUCED OCR	1.0	AVG MIN q (kPa)	-3.6 (20.0%)

Cycles 2501 - 3000

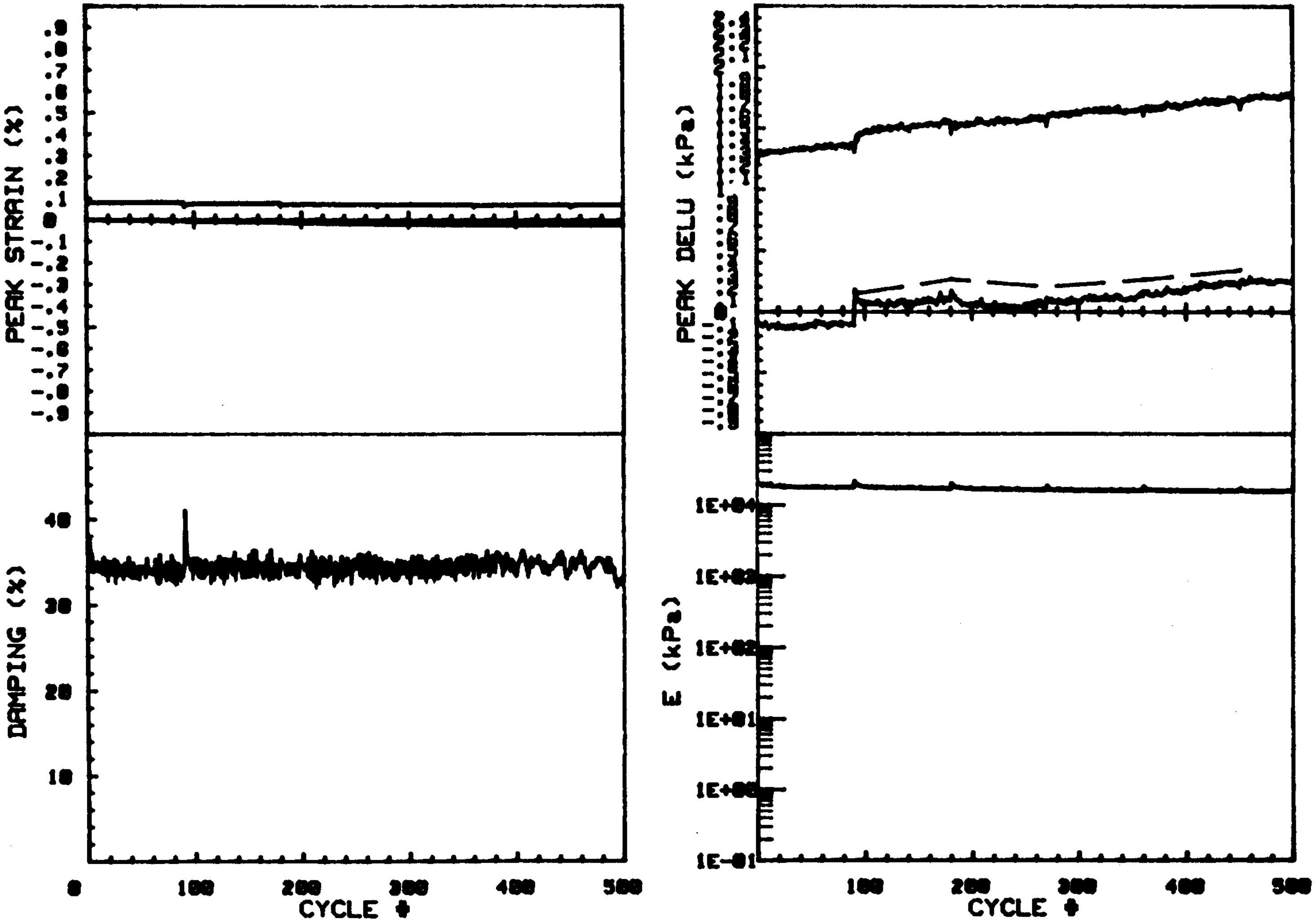

CRUISE DC4-81-NS		INCREMENT (cm)	101-109
CORE NO.	685A2	TEST NO.	TC62
SIG1c'(kPa)	4.4	STATIC qf (kPa)	18.0
SIG3c'(kPa)	4.4	AVG MAX q (kPa)	3.7 (20.6%)
INDUCED OCR	1.0	AVG MIN q (kPa)	-3.6 (20.0%)

Cycles 2501 - 3000

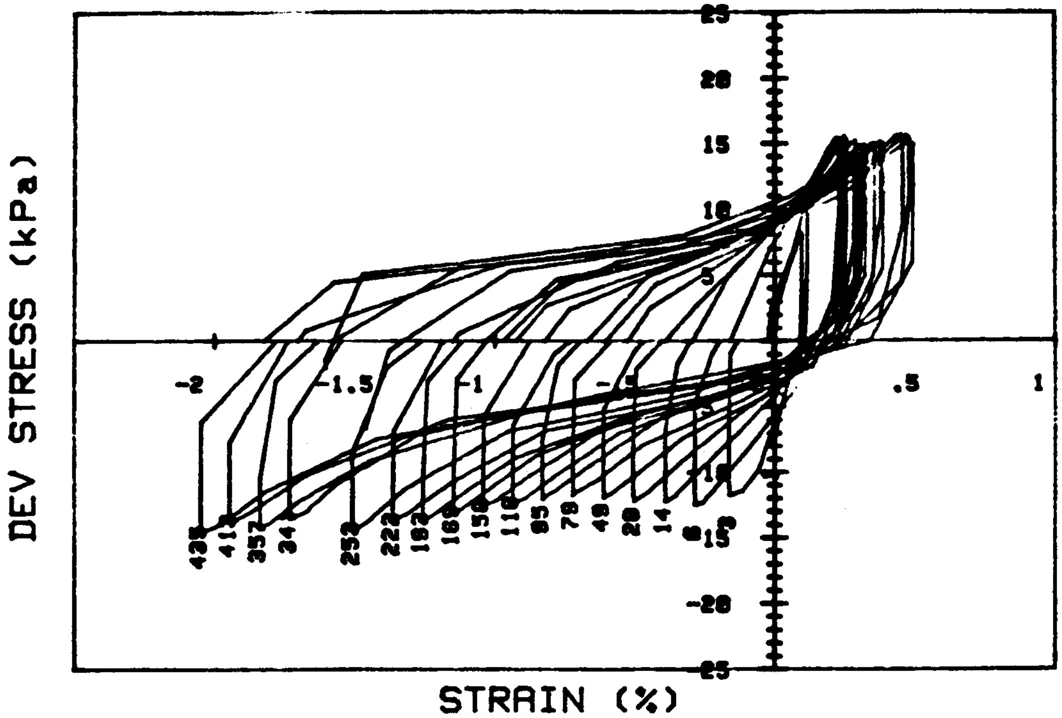

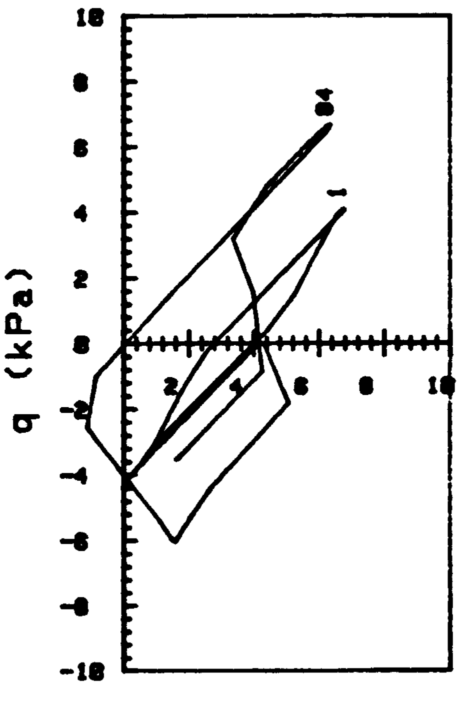

CRUISE DC4-81-NS		INCREMENT (cm)	101-109
CORE NO.	685A2	TEST NO.	TC62
SIG1c′(kPa)	4.0	STATIC qf (kPa)	18.0
SIG3c′(kPa)	4.0	AVG MAX q (kPa)	7.5 (41.7%)
INDUCED OCR	1.0	AVG MIN q (kPa)	-6.6 (36.7%)

Cycles 3001 - 3500

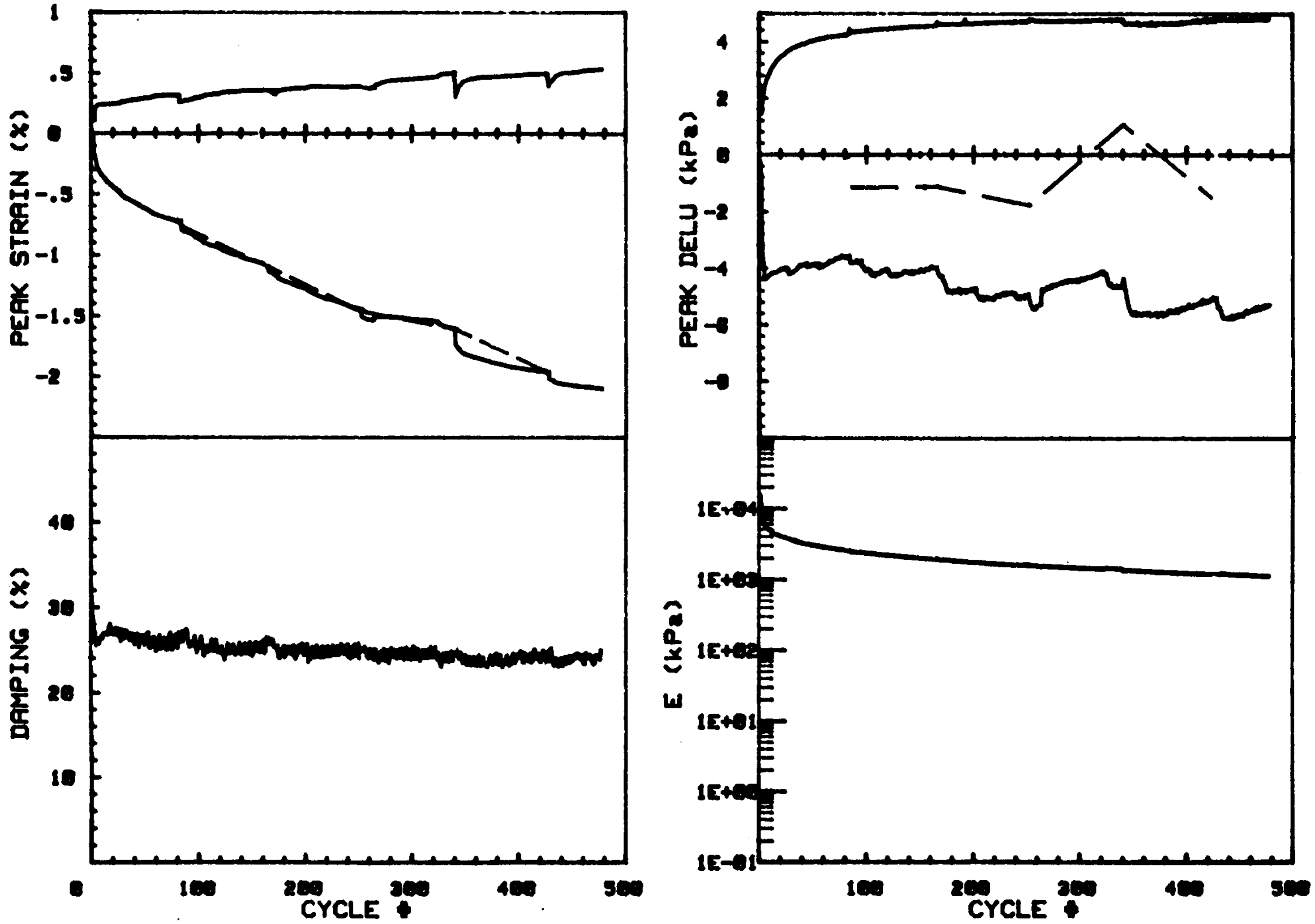

CRUISE DC4-81-NS		INCREMENT (cm)	101-109
CORE NO.	685A2	TEST NO.	TC62
SIG1c'(kPa)	4.0	STATIC qf (kPa)	18.0
SIG3c'(kPa)	4.0	AVG MAX q (kPa)	7.5 (41.7%)
INDUCED OCR	1.0	AVG MIN q (kPa)	-6.6 (36.7%)

Cycles 3001 - 3500

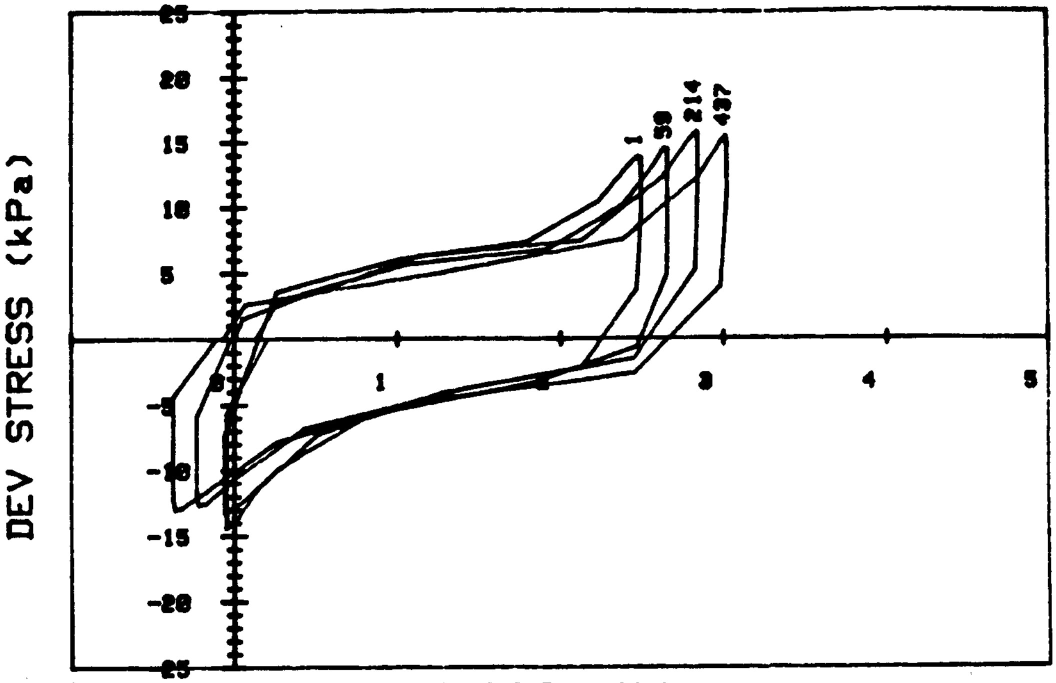

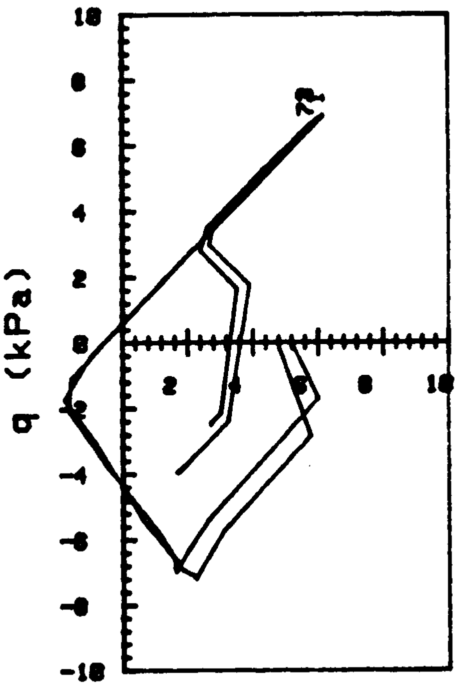

CRUISE DC4-81-NS		INCREMENT (cm)	101-109	
CORE NO.	685A2	TEST NO.	TC62	
SIG1c′(kPa)	5.7	STATIC qf (kPa)	18.0	
SIG3c′(kPa)	5.7	AVG MAX q (kPa)	7.6 (42.2%)	
INDUCED OCR	1.0	AVG MIN q (kPa)	-6.6 (36.7%)	

Cycles 3501 - 4000

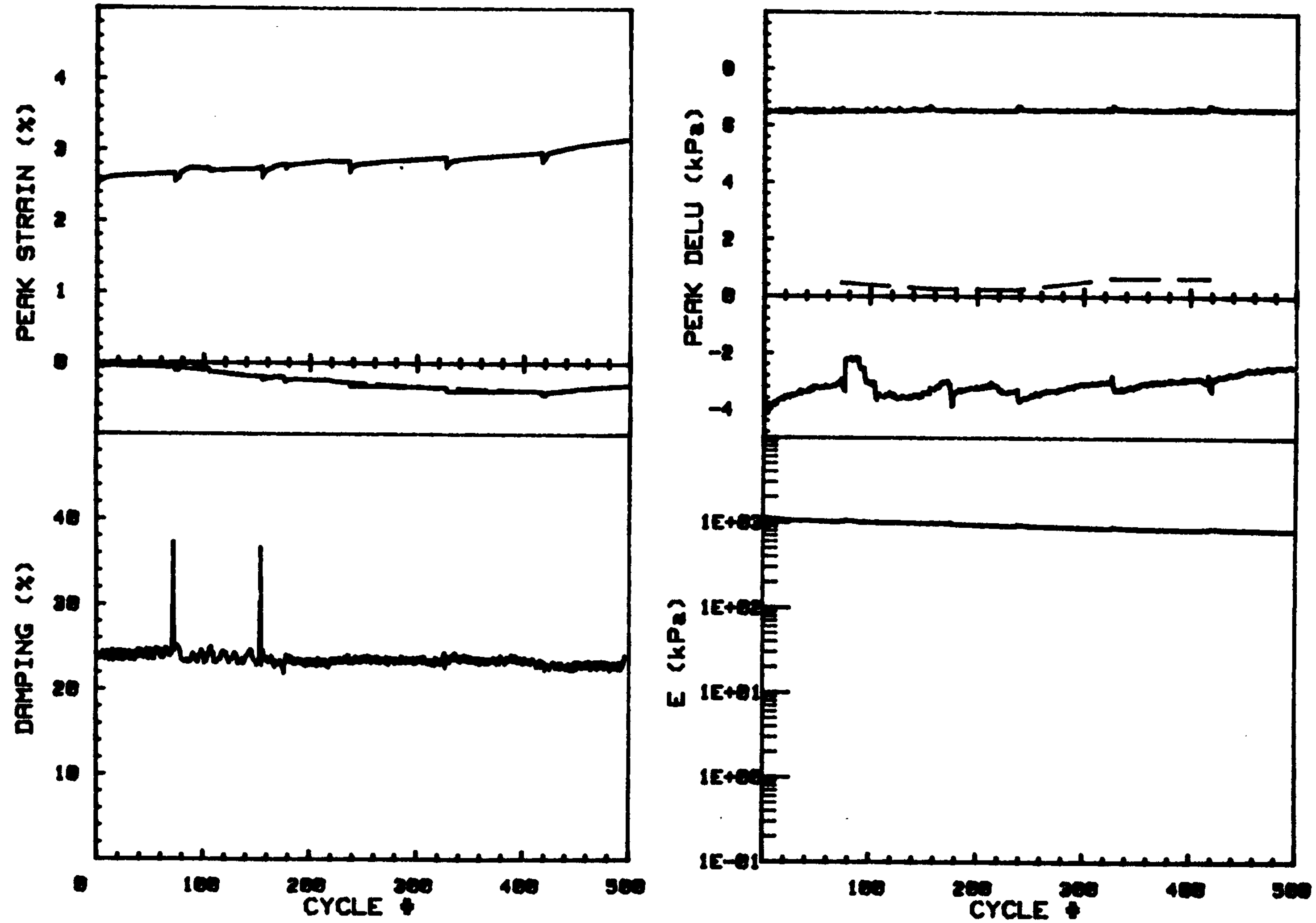

CRUISE DC4-81-NS		INCREMENT (cm)	101-109
CORE NO.	685A2	TEST NO.	TC62
SIG1c'(kPa)	5.7	STATIC qf (kPa)	18.0
SIG3c'(kPa)	5.7	AVG MAX q (kPa)	7.6 (42.2%)
INDUCED OCR	1.0	AVG MIN q (kPa)	-6.6 (36.7%)

Cycles 3501 - 4000

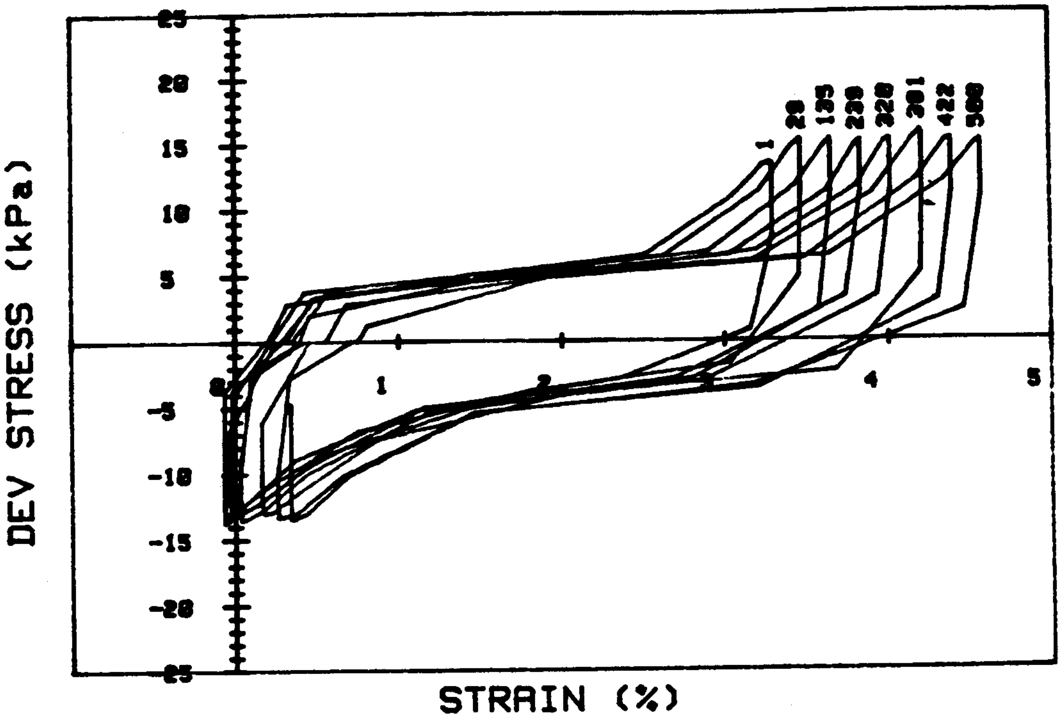

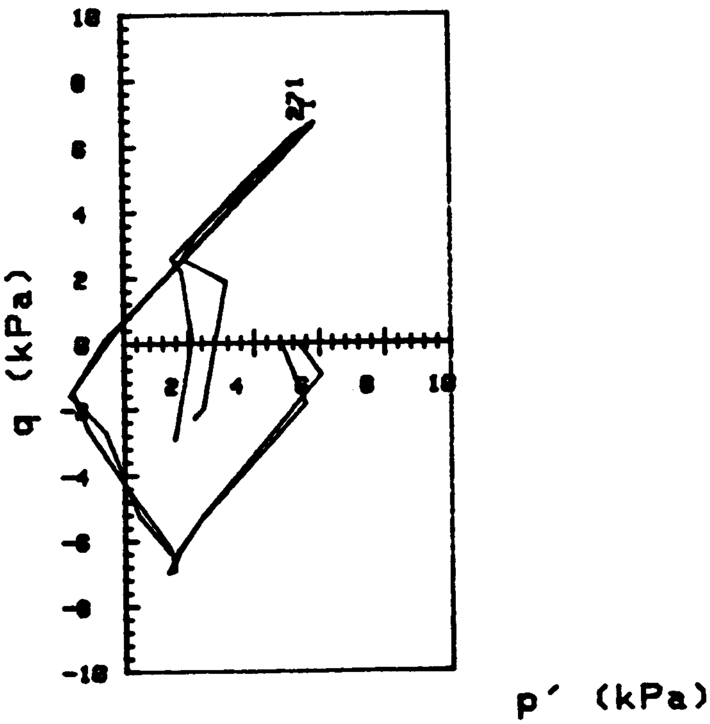

CRUISE DC4-81-NS		INCREMENT (cm)	101-109
CORE NO.	685A2	TEST NO.	TC62
SIG1c′(kPa)	4.4	STATIC qf (kPa)	18.0
SIG3c′(kPa)	4.4	AVG MAX q (kPa)	7.6 (42.2%)
INDUCED OCR	1.0	AVG MIN q (kPa)	-6.6 (36.7%)

Cycles 4001 - 4500

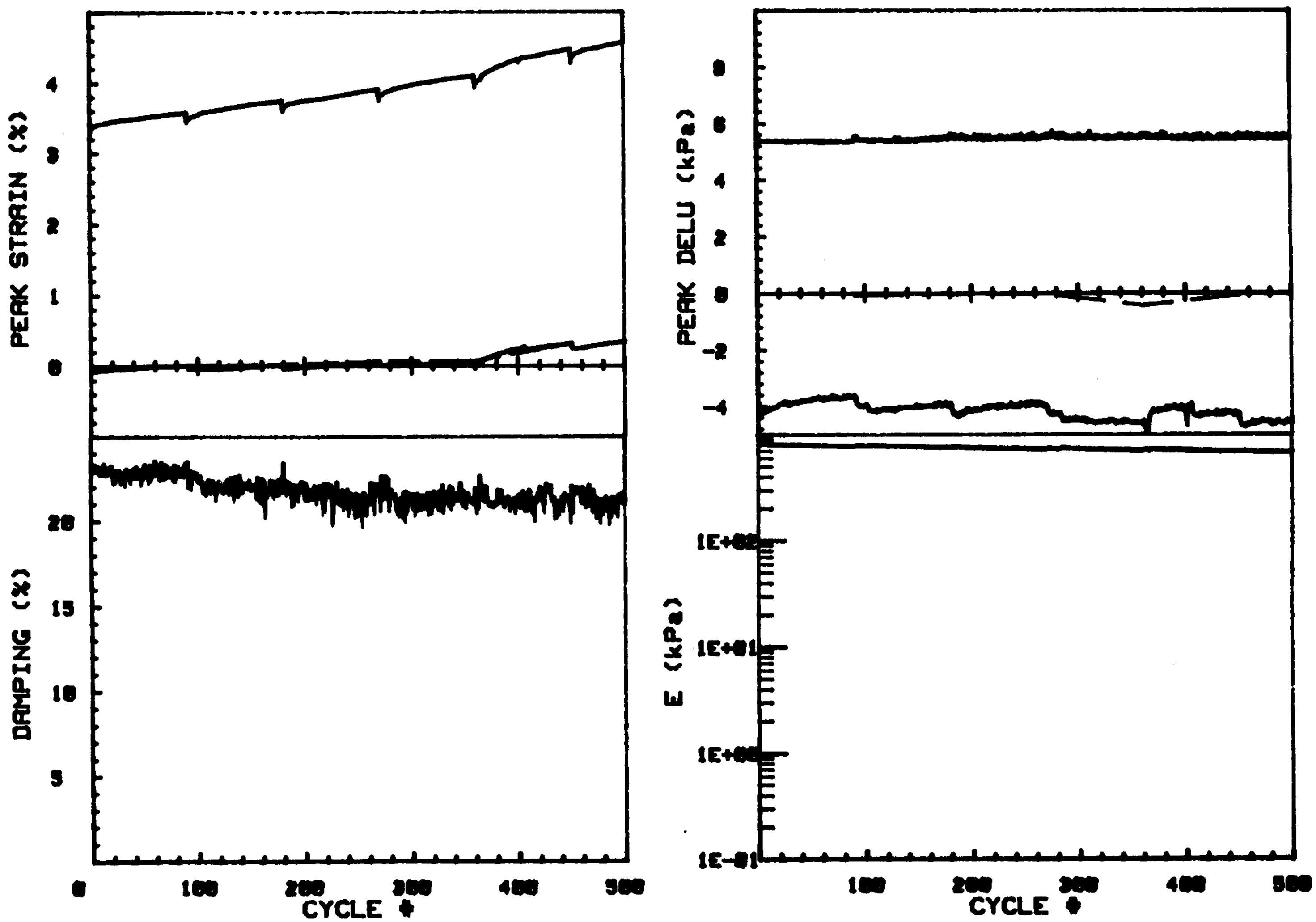

CRUISE DC4-81-NS		INCREMENT (cm)	101-109
CORE NO.	685A2	TEST NO.	TC62
SIG1c'(kPa)	4.4	STATIC qf (kPa)	18.0
SIG3c'(kPa)	4.4	AVG MAX q (kPa)	7.6 (42.2%)
INDUCED OCR	1.0	AVG MIN q (kPa)	-6.6 (36.7%)

Cycles 4001 - 4500

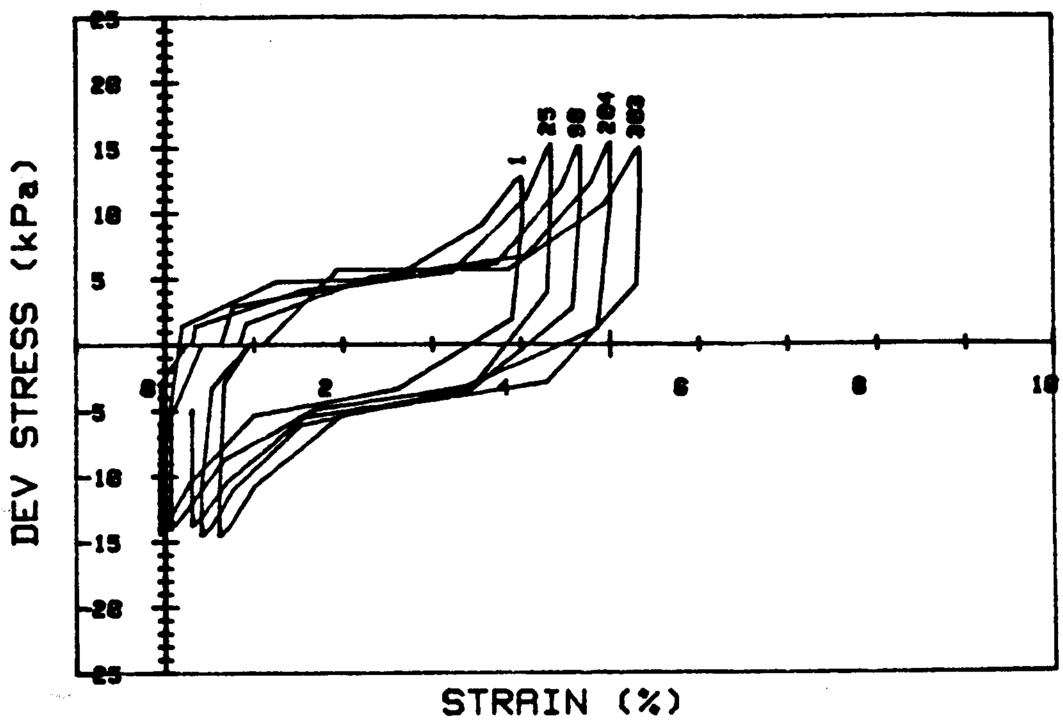

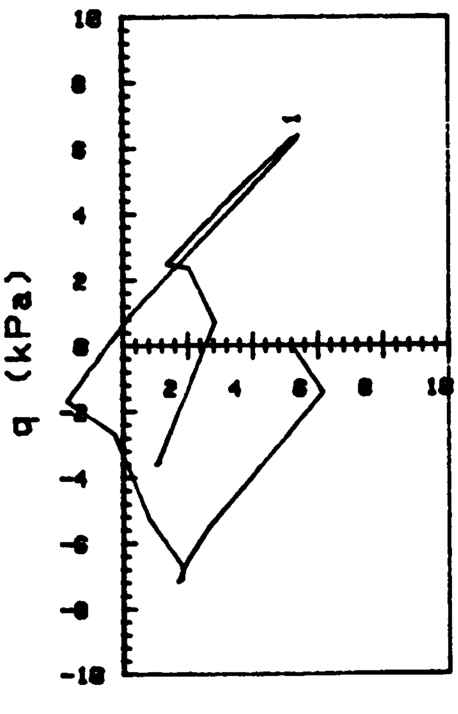

CRUISE DC4-81-NS		INCREMENT (cm)	101-109
CORE NO.	605A2	TEST NO.	TC62
SIG1c'(kPa)	4.7	STATIC qf (kPa)	18.0
SIG3c'(kPa)	4.7	AVG MAX q (kPa)	7.6 (42.2%)
INDUCED OCR	1.0	AVG MIN q (kPa)	-7.1 (39.4%)

Cycles 4501 - 4860

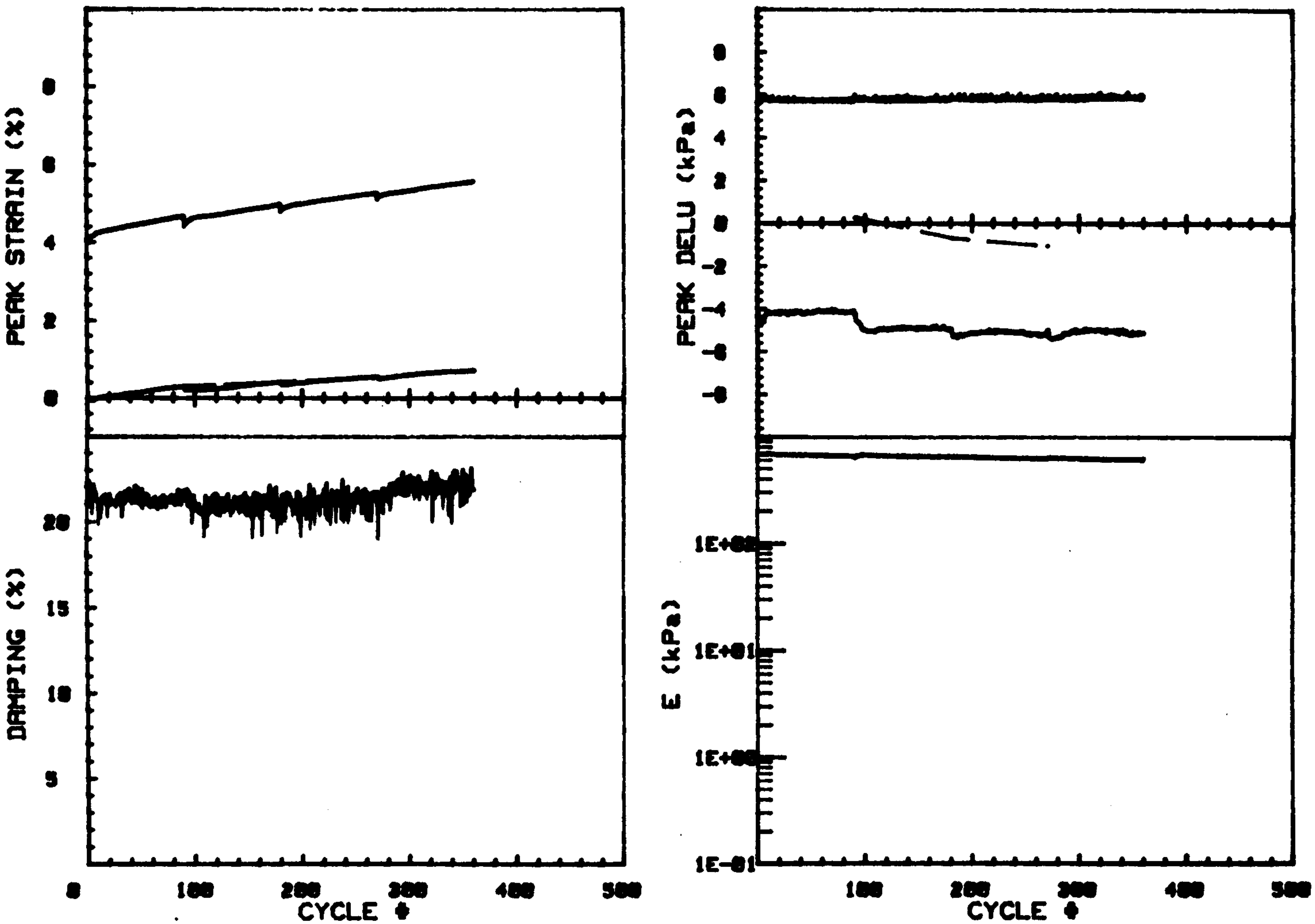

CRUISE	DC4-81-NS	INCREMENT (cm)	101-109
CORE NO.	685A2	TEST NO.	TC62
SIG1c'(kPa)	4.7	STATIC qf (kPa)	18.0
SIG3c'(kPa)	4.7	AVG MAX q (kPa)	7.6 (42.2%)
INDUCED OCR	1.0	AVG MIN q (kPa)	-7.1 (39.4%)

Cycles 4501 - 4860

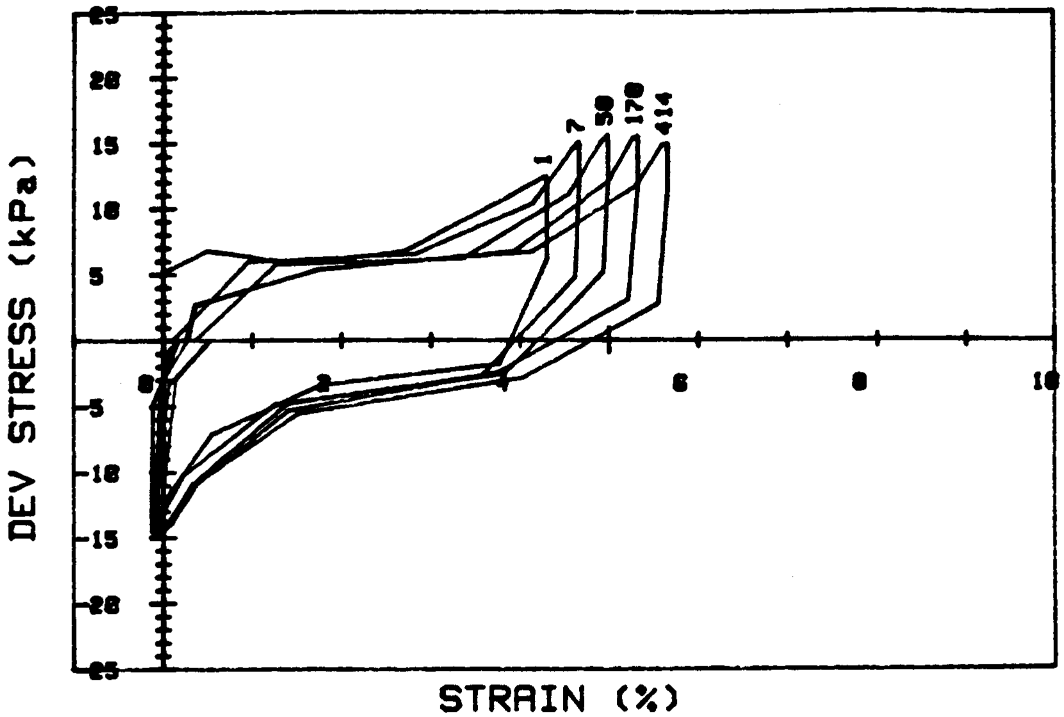

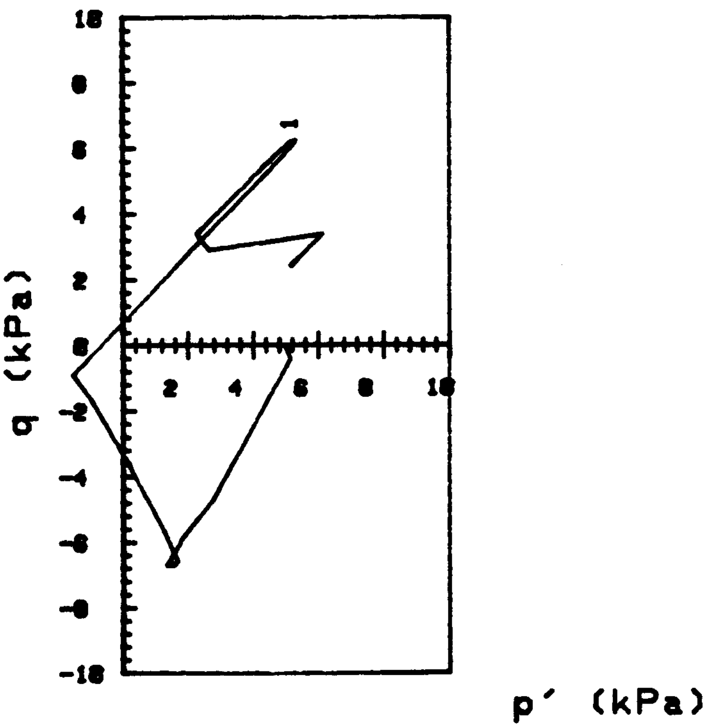

CRUISE DC4-81-NS		INCREMENT (cm)	101-109
CORE NO.	685A2	TEST NO.	TC62
SIG1c′(kPa)	2.7	STATIC qf (kPa)	18.0
SIG3c′(kPa)	2.7	AVG MAX q (kPa)	7.7 (42.8%)
INDUCED OCR	1.0	AVG MIN q (kPa)	-7.1 (39.4%)

Cycles 4861 - 5300

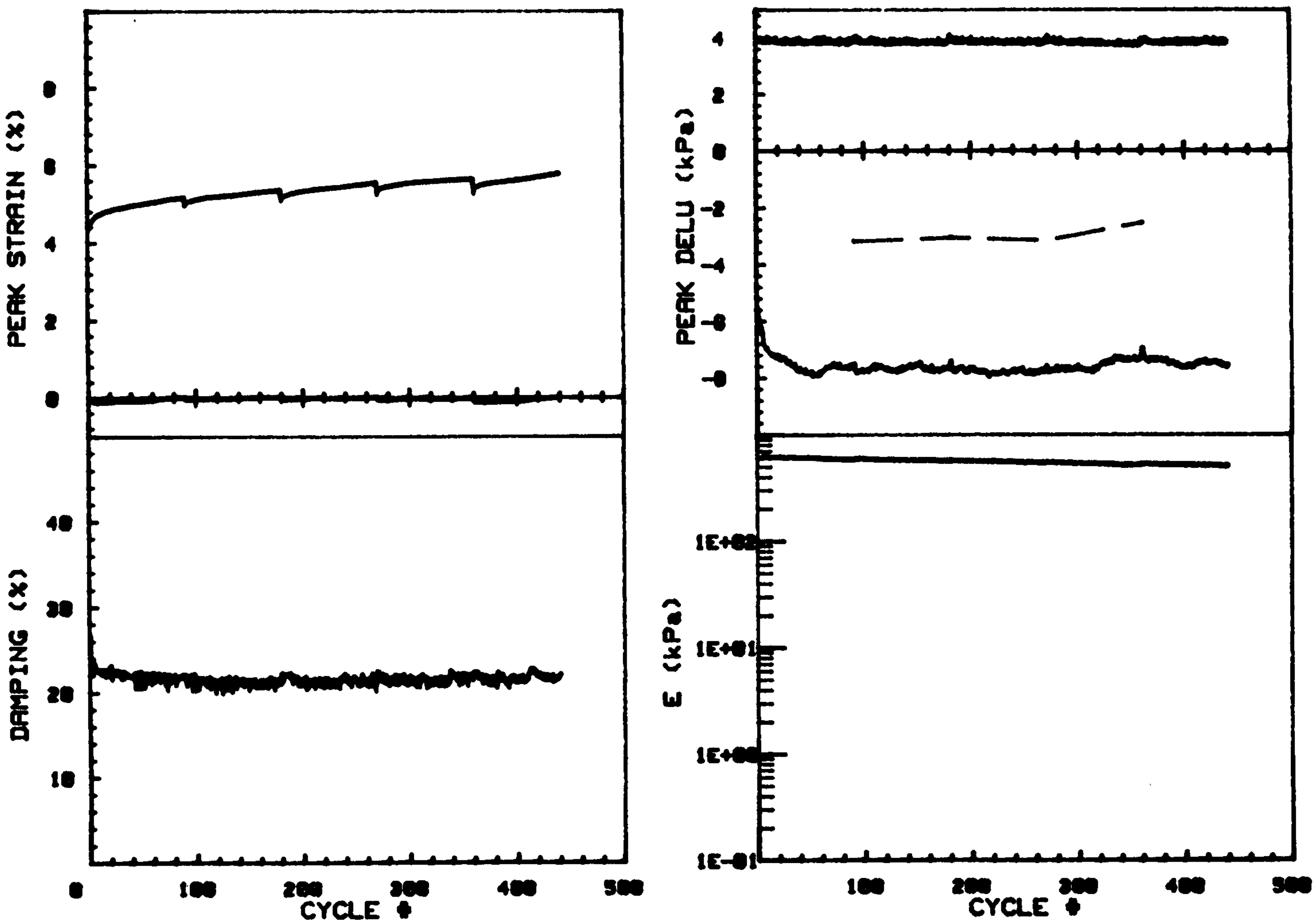

CRUISE	DC4-81-NS	INCREMENT (cm)	101-109
CORE NO.	685A2	TEST NO.	TC62
SIG1c'(kPa)	2.7	STATIC qf (kPa)	18.0
SIG3c'(kPa)	2.7	AVG MAX q (kPa)	7.7 (42.8%)
INDUCED OCR	1.0	AVG MIN q (kPa)	-7.1 (39.4%)

Cycles 4861 - 5300

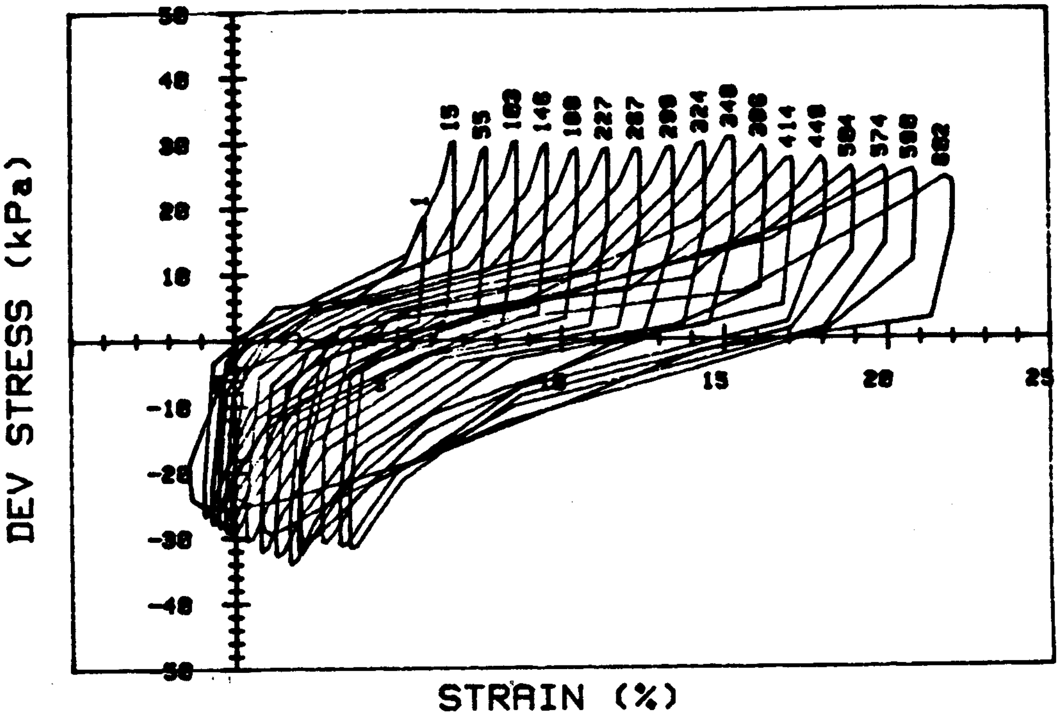

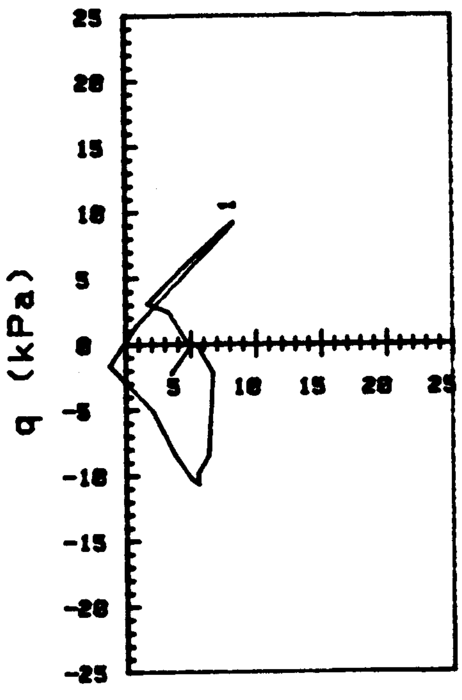

CRUISE DC4-81-NS		INCREMENT (cm)	101-109
CORE NO.	685A2	TEST NO.	TC62
SIG1c′(kPa)	5.7	STATIC qf (kPa)	18.0
SIG3c′(kPa)	5.7	AVG MAX q (kPa)	14.2 (78.9%)
INDUCED OCR	1.0	AVG MIN q (kPa)	-15.0 (83.3%)

Cycles 5301 - 5910

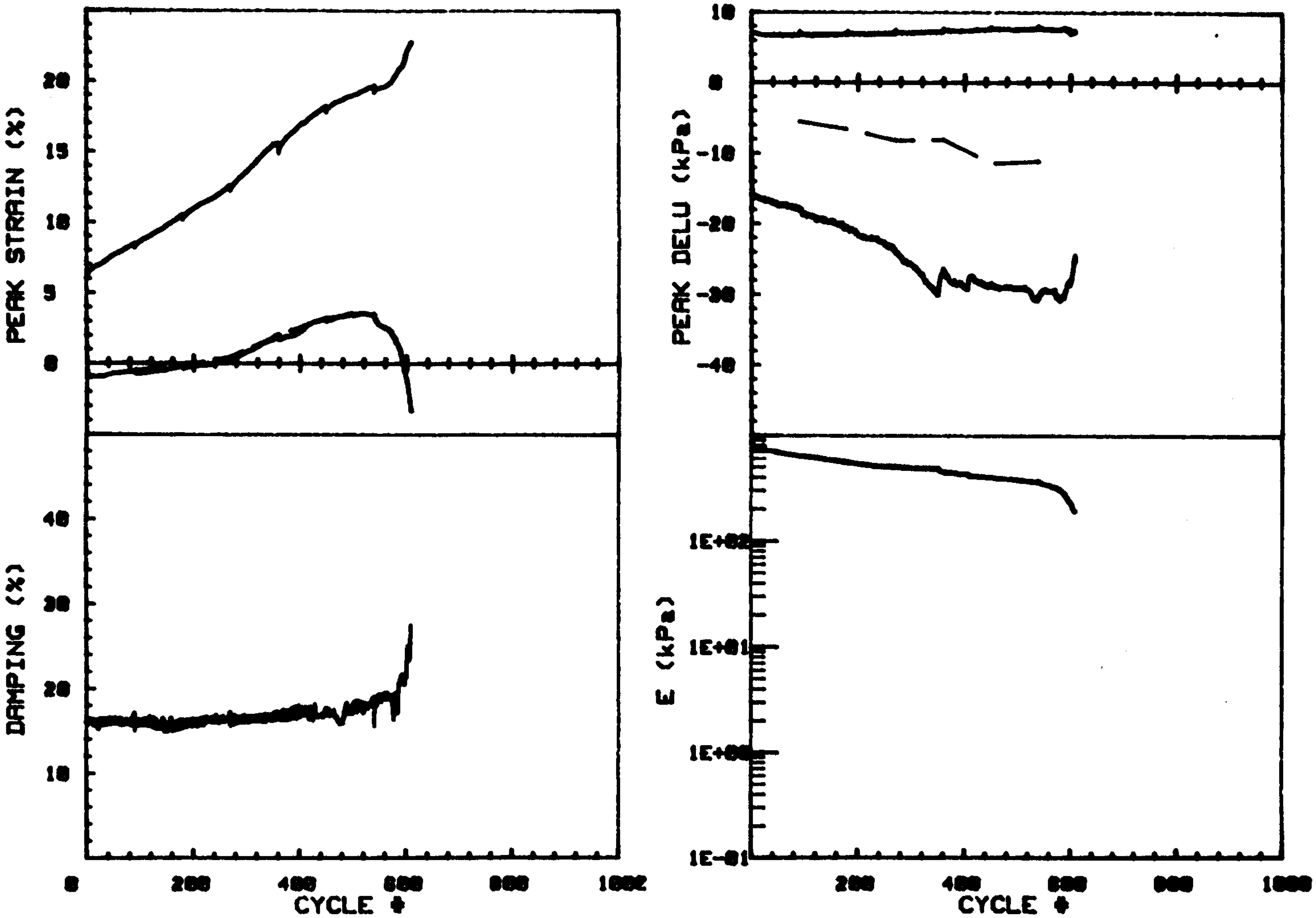

CRUISE DC4-81-NS		INCREMENT (cm)	101-109
CORE NO.	685A2	TEST NO.	TC62
SIG1c'(kPa)	5.7	STATIC qf (kPa)	18.0
SIG3c'(kPa)	5.7	AVG MAX q (kPa)	14.2 (78.9%)
INDUCED OCR	1.0	AVG MIN q (kPa)	-15.0 (83.3%)

Cycles 5301 - 5910

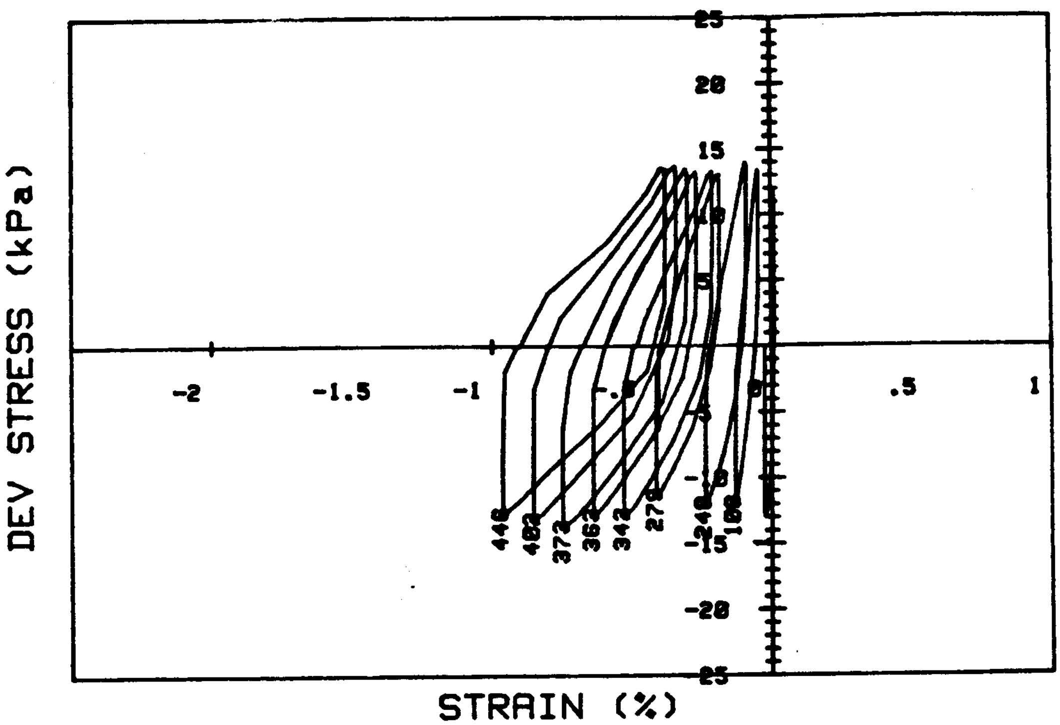

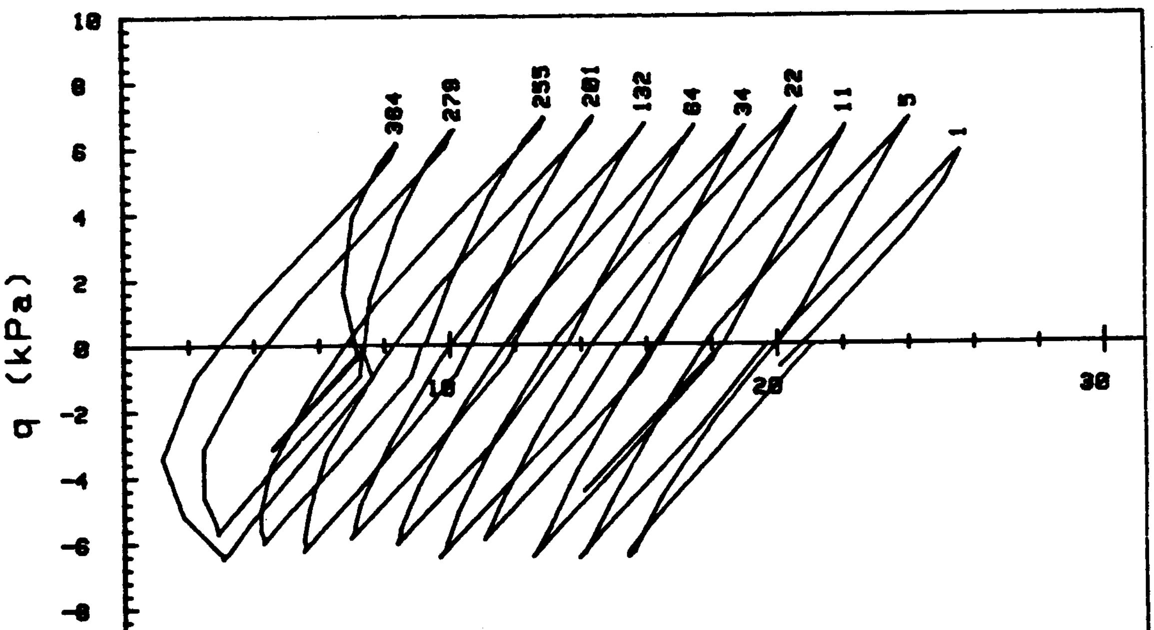

CRUISE DC4-81-NS		INCREMENT (cm)	101-109
CORE NO.	685A2	TEST NO.	TC74
SIG1c′(kPa)	20.8	STATIC qf (kPa)	20.8
SIG3c′(kPa)	20.8	AVG MAX q (kPa)	6.8 (32.7%)
INDUCED OCR	1.0	AVG MIN q (kPa)	-6.2 (29.8%)

Cycles 1 - 820

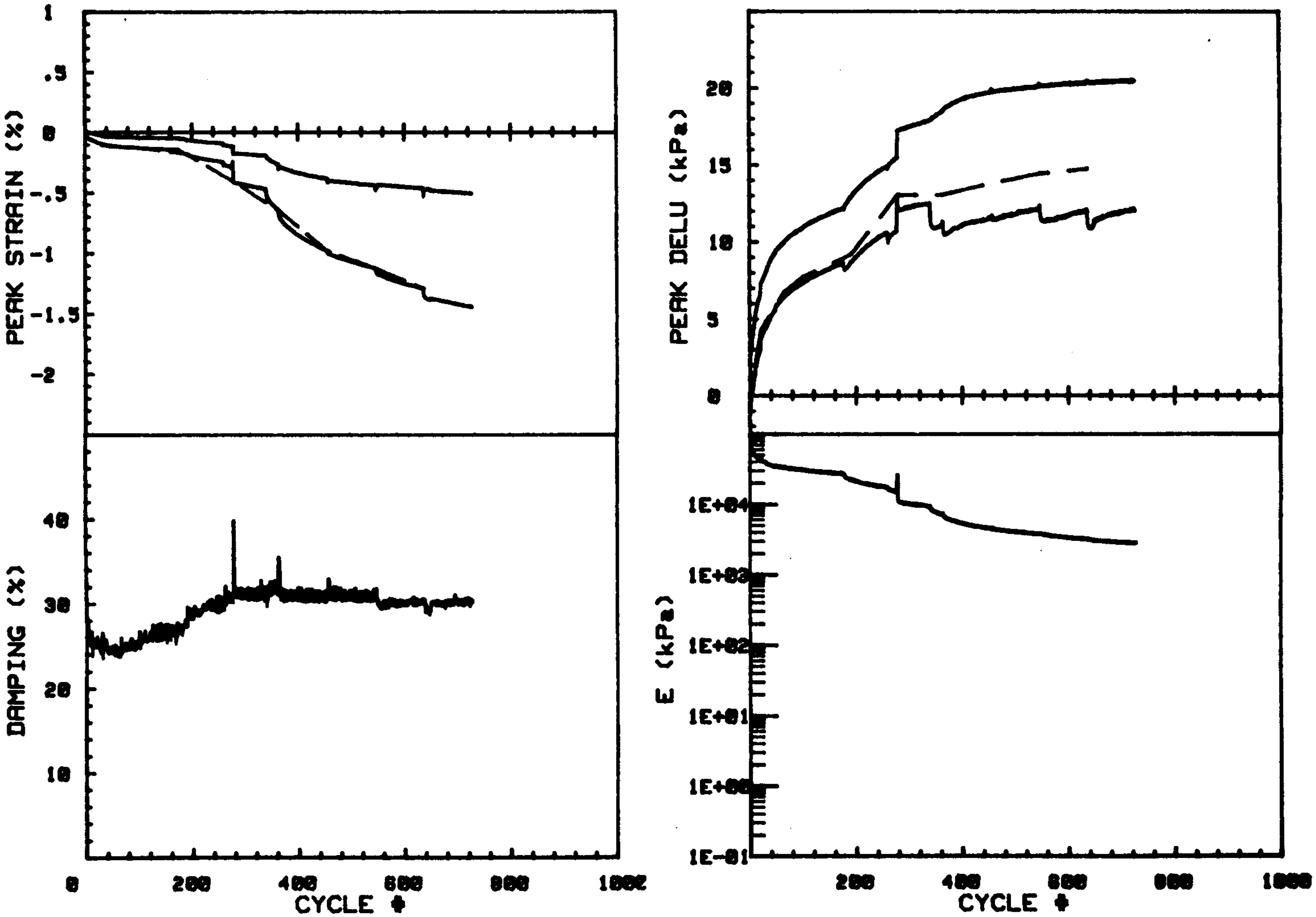

CRUISE DC4-81-NS		INCREMENT (cm)	101-109
CORE NO.	685A2	TEST NO.	TC74
SIG1c'(kPa)	20.8	STATIC qf (kPa)	20.8
SIG3c'(kPa)	20.8	AVG MAX q (kPa)	6.8 (32.7%)
INDUCED OCR	1.0	AVG MIN q (kPa)	-6.2 (29.8%)

Cycles 1 - 820

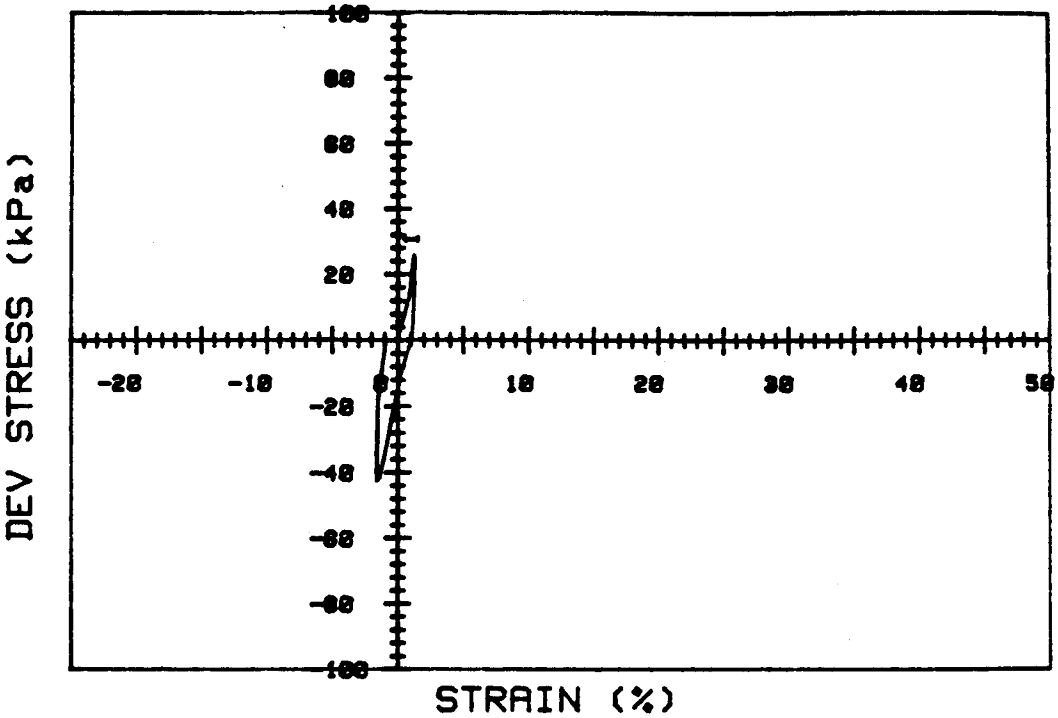

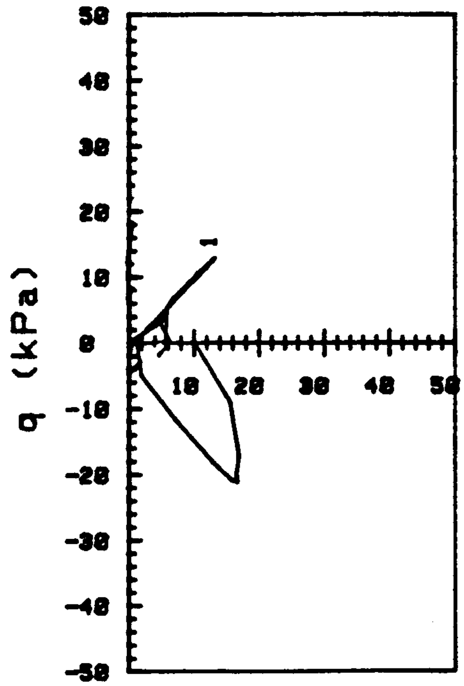

CRUISE DC4-81-NS		INCREMENT (cm)	101-109
CORE NO.	685A2	TEST NO.	TC74
SIG1c′(kPa)	6.4	STATIC qf (kPa)	20.8
SIG3c′(kPa)	6.4	AVG MAX q (kPa)	29.9 (143.8%)
INDUCED OCR	1.0	AVG MIN q (kPa)	-26.6 (127.9%)

Cycles 821 - 850

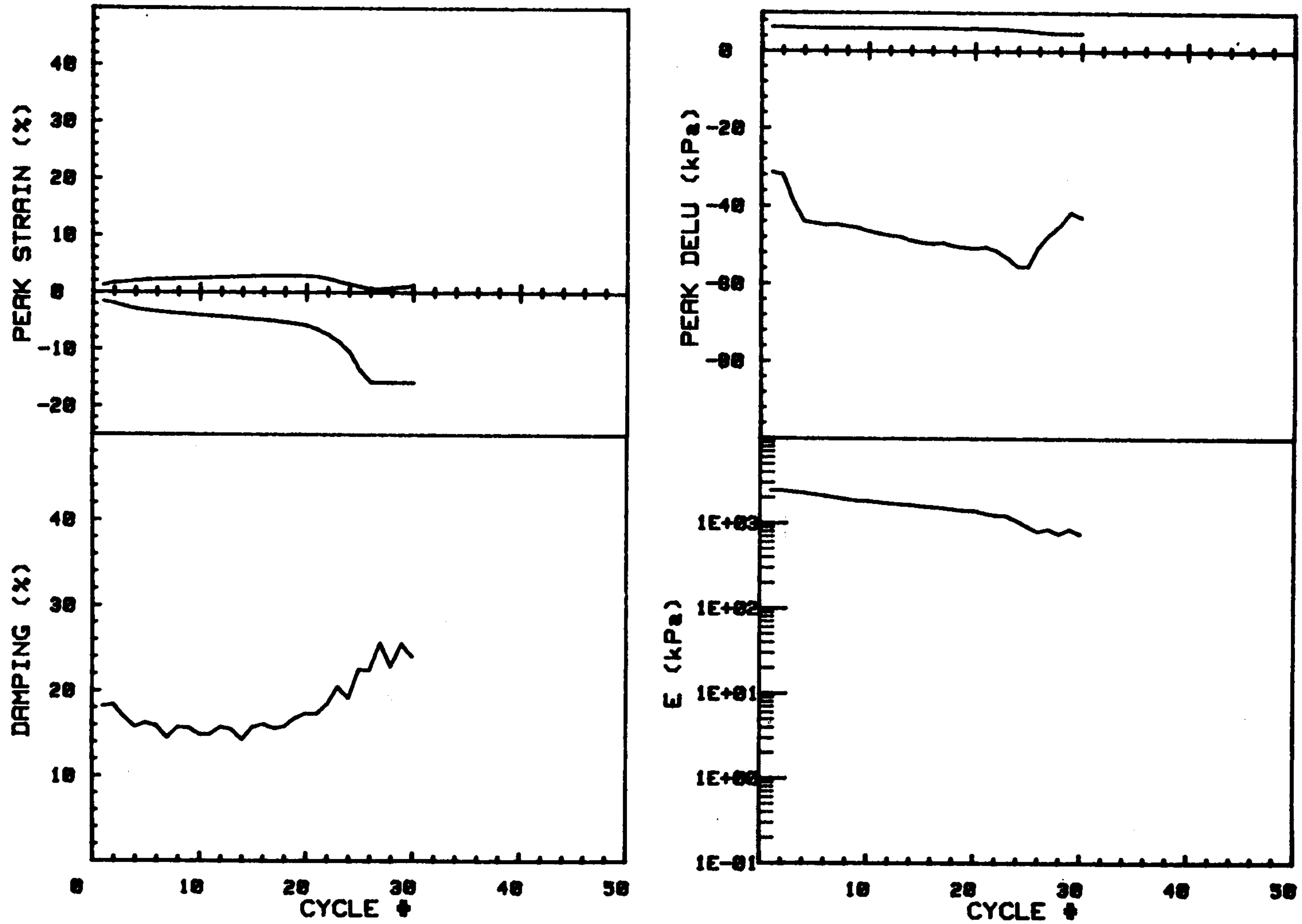

CRUISE	DC4-81-NS	INCREMENT (cm)	101-109
CORE NO.	685A2	TEST NO.	TC74
SIG1c'(kPa)	6.4	STATIC qf (kPa)	20.8
SIG3c'(kPa)	6.4	AVG MAX q (kPa)	29.9 (143.8%)
INDUCED OCR	1.0	AVG MIN q (kPa)	-26.6 (127.9%)

Cycles 821 - 850

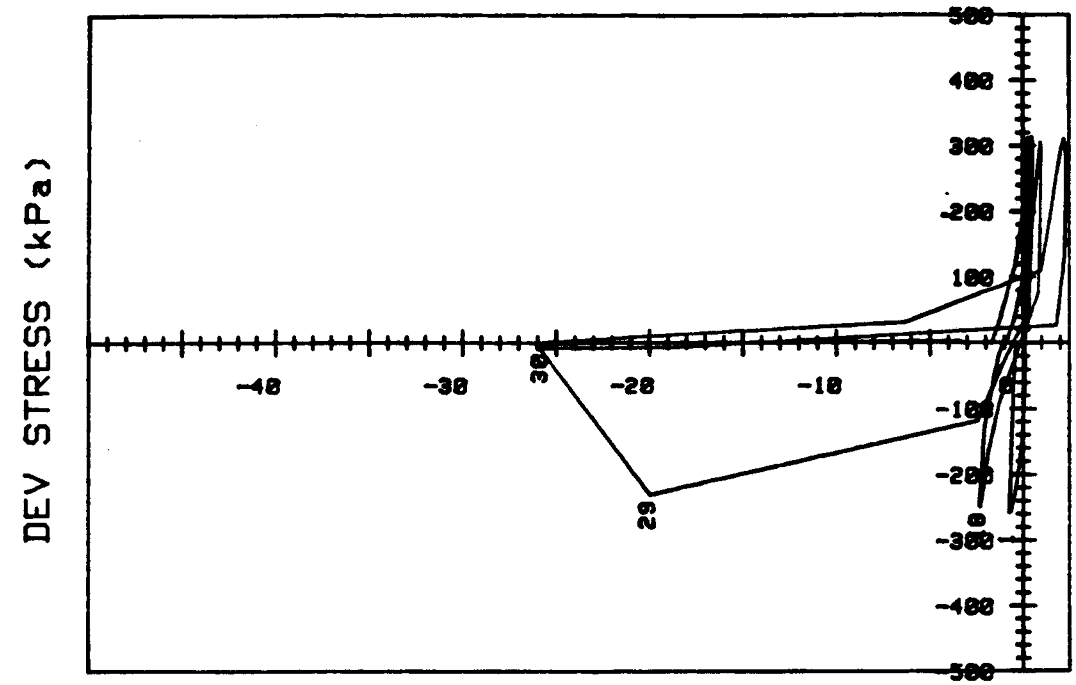

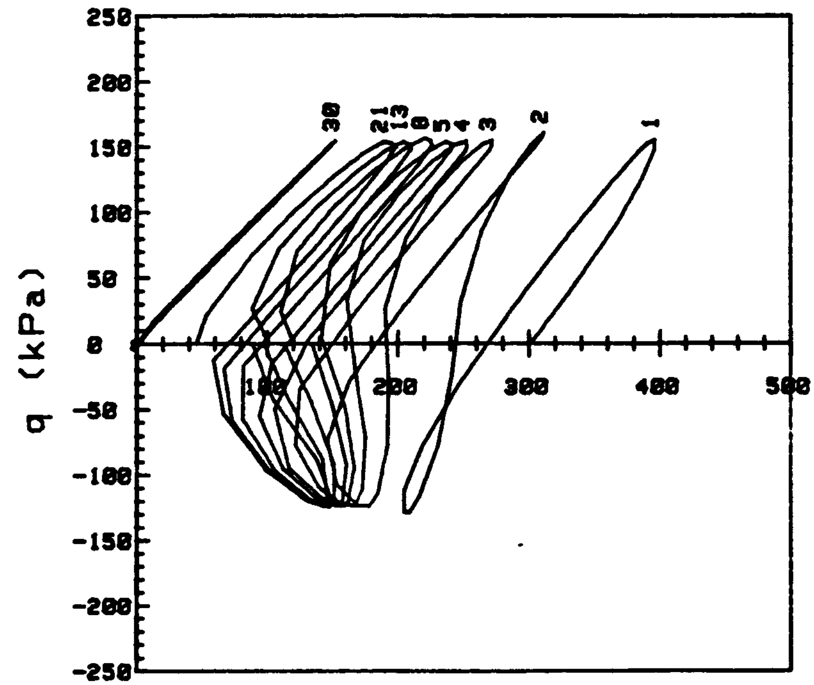

CRUISE DC4-81-NS		INCREMENT (cm)	200-210
CORE NO.	685A2	TEST NO.	TC50
SIG1c′(kPa)	301.0	STATIC qf (kPa)	300.0
SIG3c′(kPa)	301.0	AVG MAX q (kPa)	154.6 (51.5%)
INDUCED OCR	1.0	AVG MIN q (kPa)	-120.4 (40.1%)

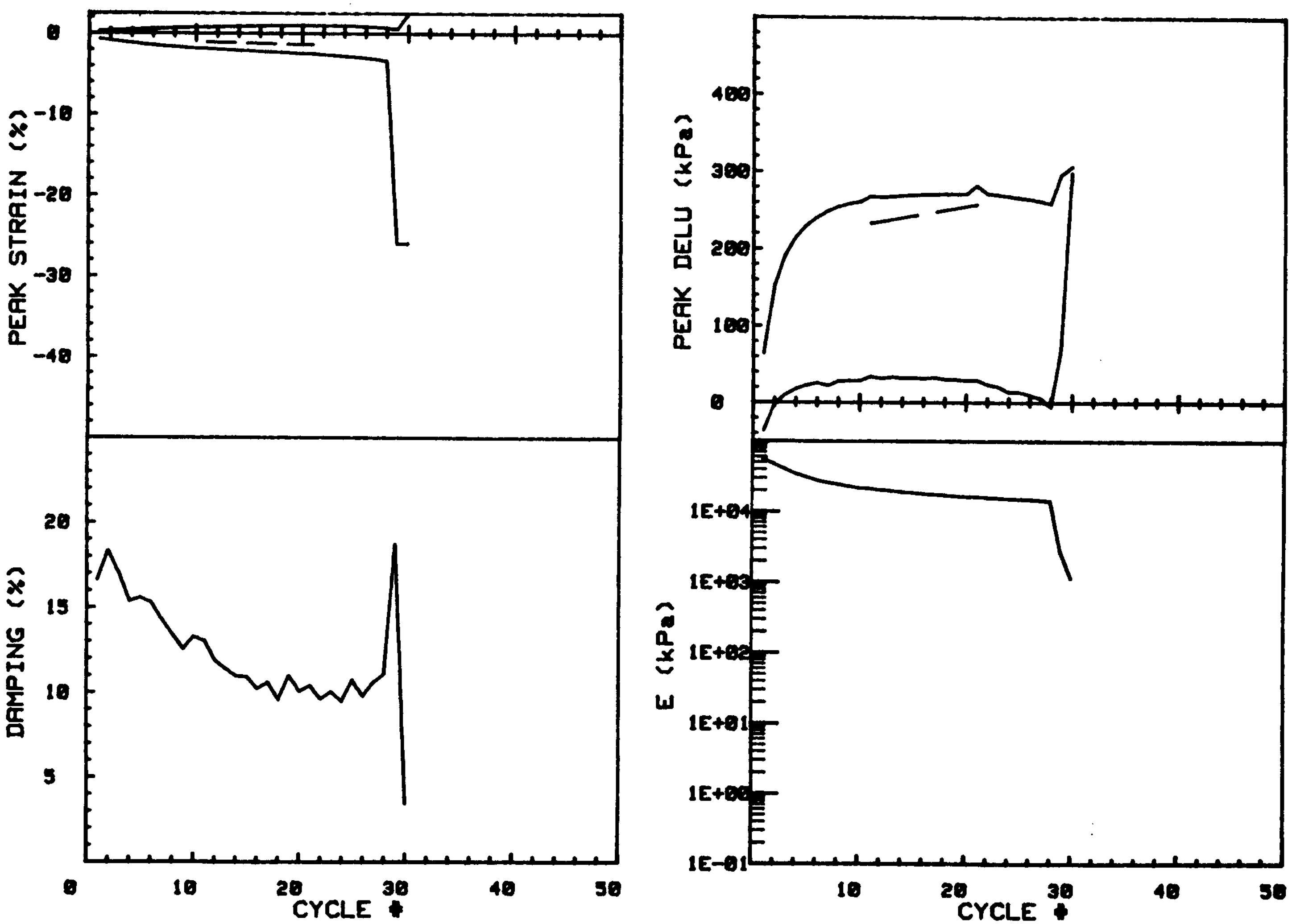

CRUISE DC4-81-NS		INCREMENT (cm)	200-210
CORE NO.	685A2	TEST NO.	TC50
SIG1c'(kPa)	301.0	STATIC qf (kPa)	300.0
SIG3c'(kPa)	301.0	AVG MAX q (kPa)	154.6 (51.5%)
INDUCED OCR	1.0	AVG MIN q (kPa)	-120.4 (40.1%)

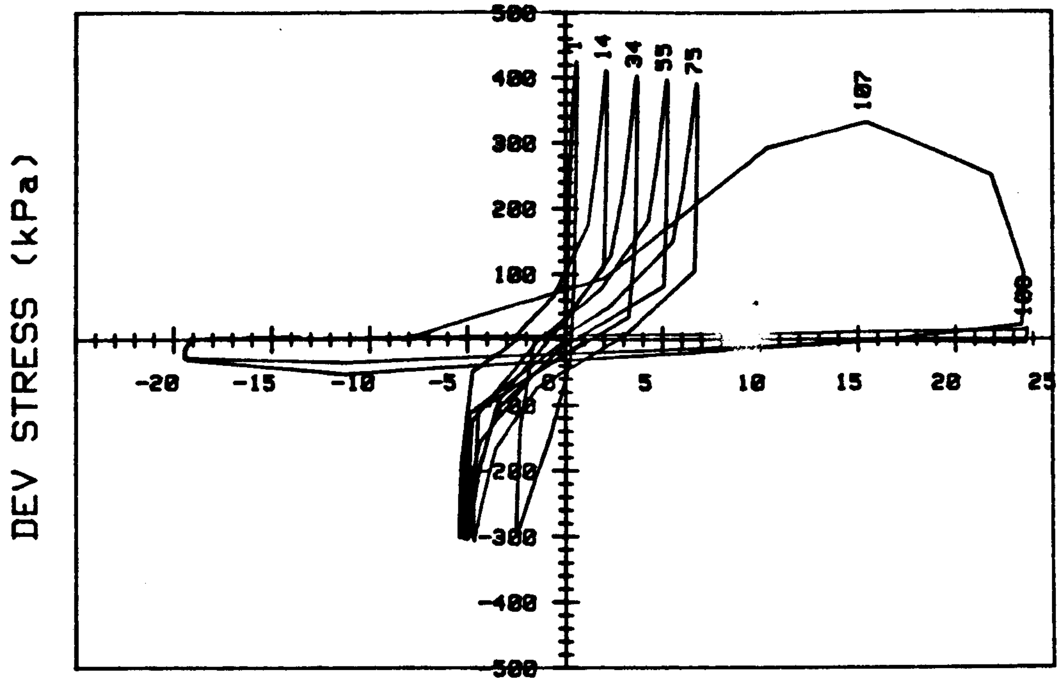

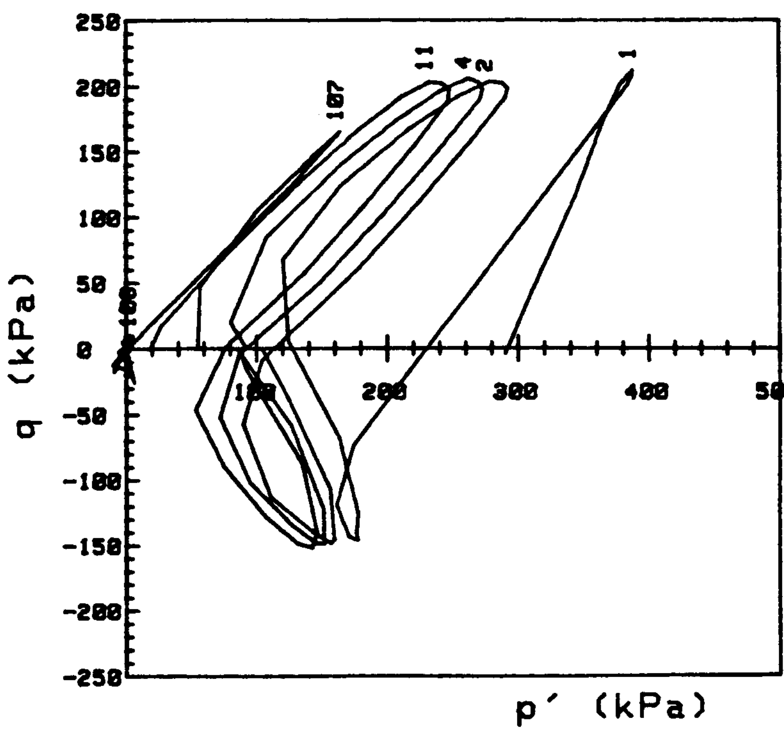

CRUISE DC4-81-NS		INCREMENT (cm)	200-210
CORE NO.	685A2	TEST NO.	TC51
SIG1c′(kPa)	294.1	STATIC qf (kPa)	300.0
SIG3c′(kPa)	294.1	AVG MAX q (kPa)	.94.7 (64.9%)
INDUCED OCR	1.0	AVG MIN q (kPa)	-147.4 (49.1%)

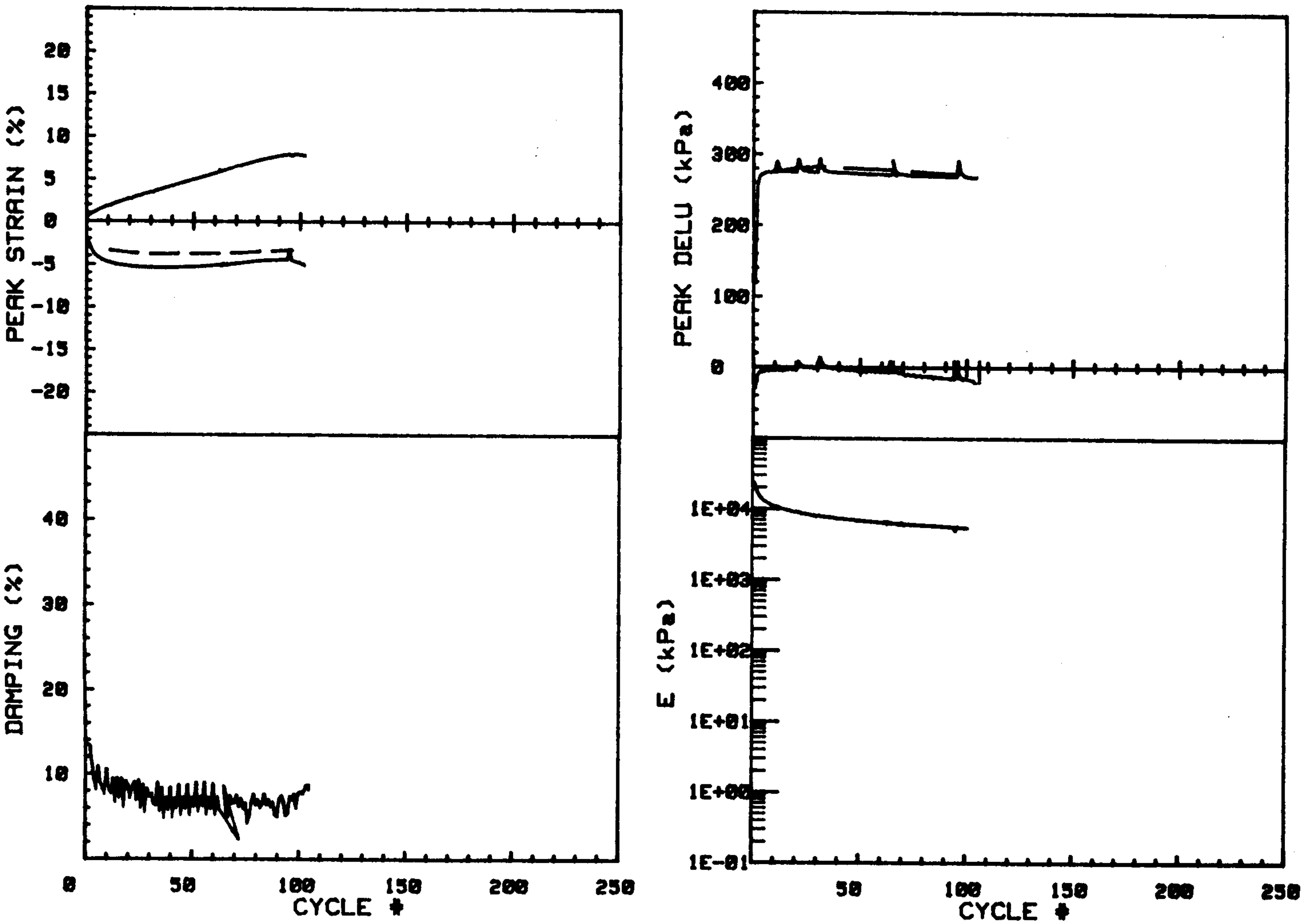

CRUISE DC4-81-NS		INCREMENT (cm)	200-210
CORE NO.	685A2	TEST NO.	TC51
SIG1c'(kPa)	294.1	STATIC qf (kPa)	300.0
SIG3c'(kPa)	294.1	AVG MAX q (kPa)	194.7 (64.9%)
INDUCED OCR	1.0	AVG MIN q (kPa)	-147.4 (49.1%)

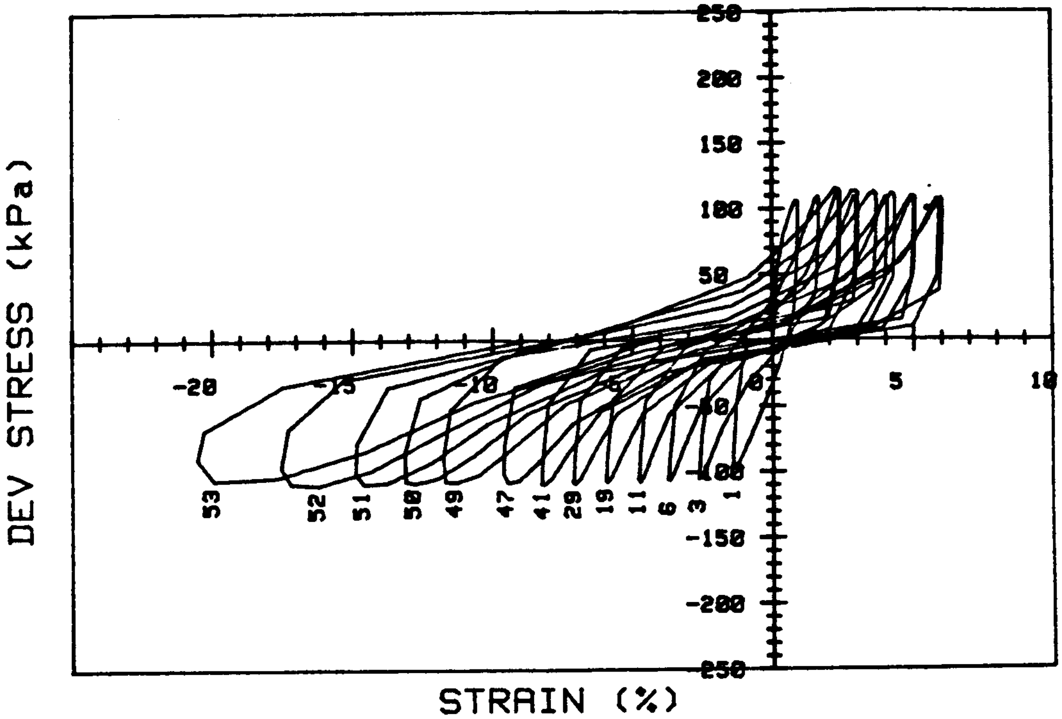

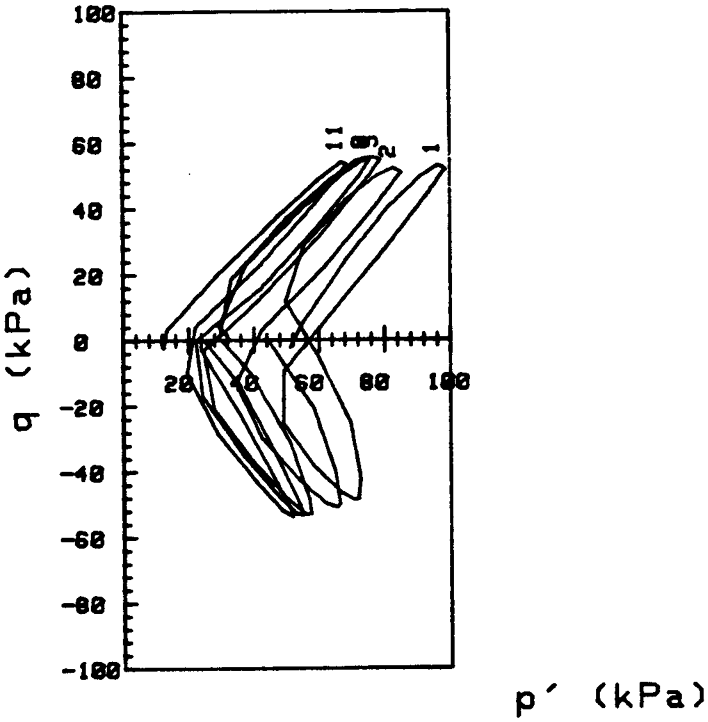

CRUISE DC4-81-NS		INCREMENT (cm)	16-24
CORE NO.	686A1	TEST NO.	TC88
SIG1c′(kPa)	53.4	STATIC qf (kPa)	50.0
SIG3c′(kPa)	53.4	AVG MAX q (kPa)	54.2 (108.4%)
INDUCED OCR	6.0	AVG MIN q (kPa)	-53.5 (107.0%)

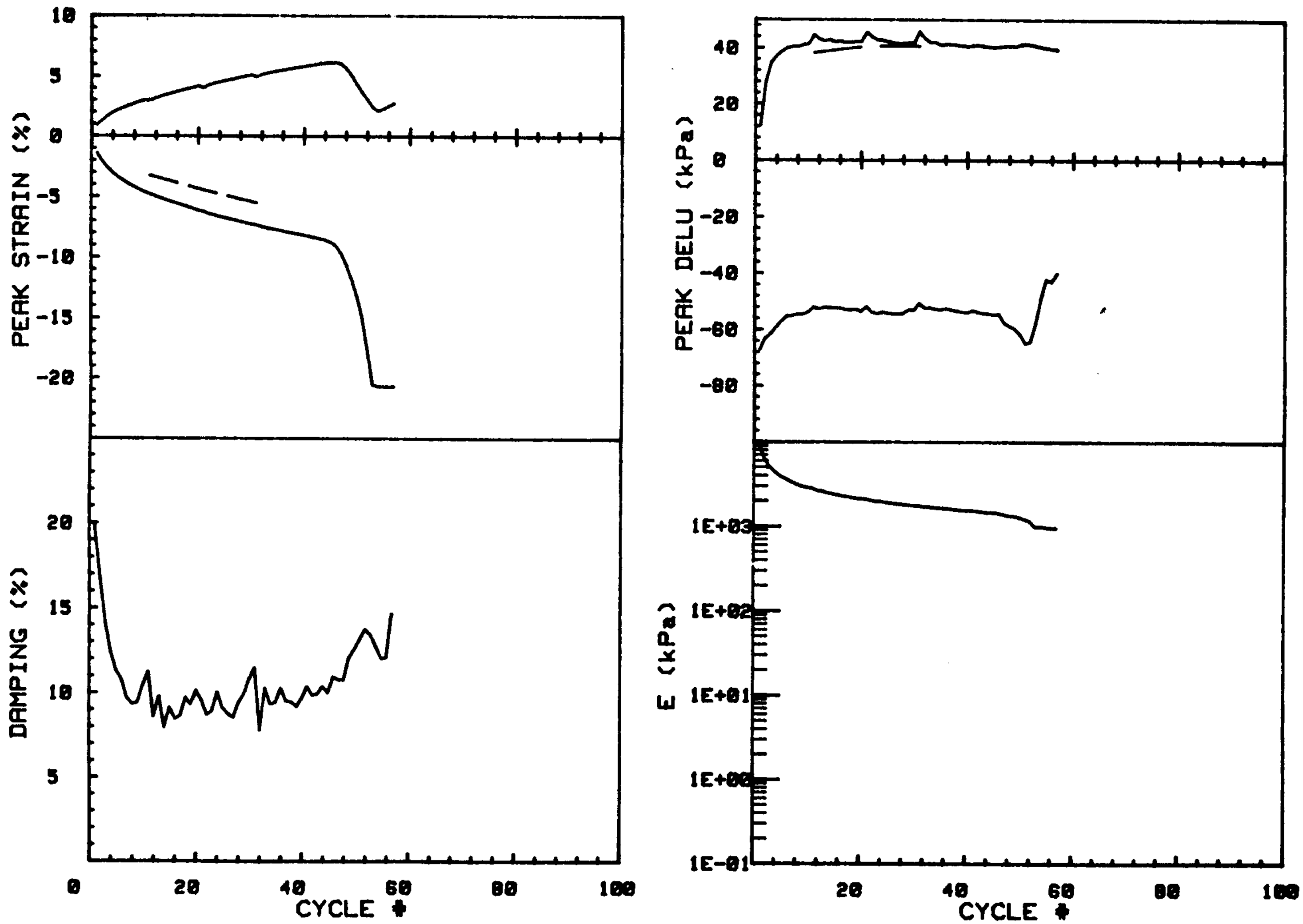

CRUISE DC4-81-NS		INCREMENT (cm)	16-24
CORE NO.	686A1	TEST NO.	TC88
SIG1c′(kPa)	53.4	STATIC qf (kPa)	50.0
SIG3c′(kPa)	53.4	AVG MAX q (kPa)	54.2 (108.4%)
INDUCED OCR	6.0	AVG MIN q (kPa)	-53.5 (107.0%)

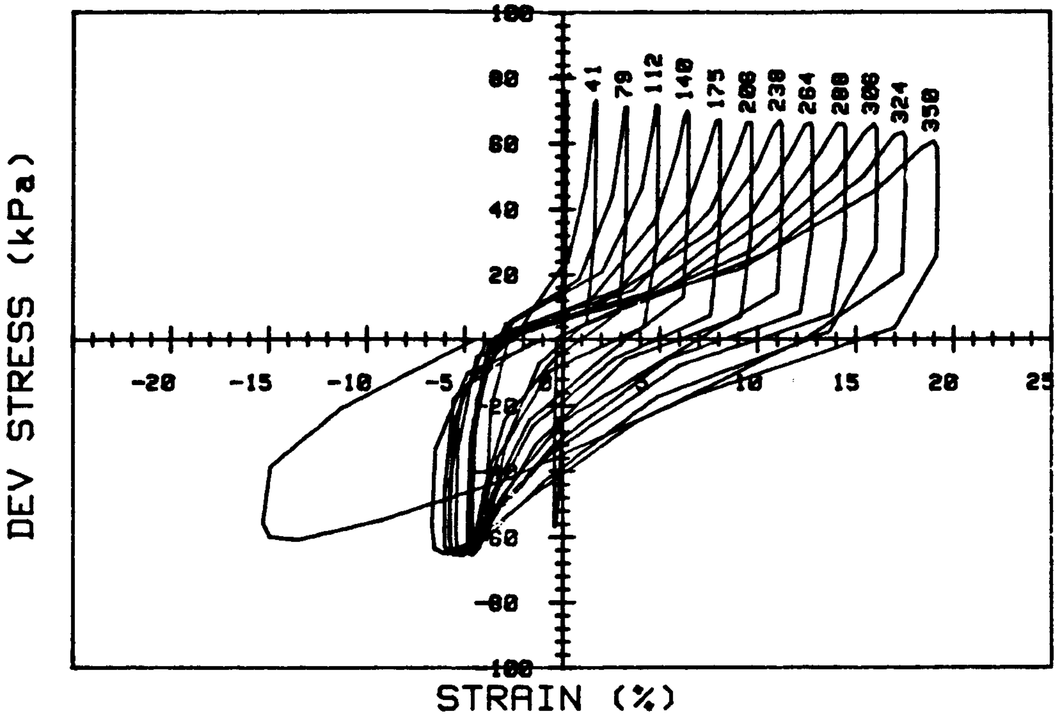

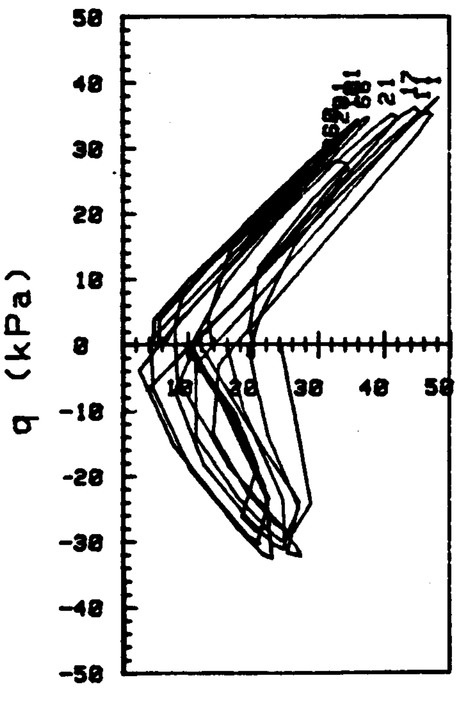

CRUISE DC4-81-NS		INCREMENT (cm)	16-24
CORE NO.	686A1	TEST NO.	TC89
SIG1c′(kPa)	50.0	STATIC qf (kPa)	50.0
SIG3c′(kPa)	50.0	AVG MAX q (kPa)	34.1 (68.2%)
INDUCED OCR	6.0	AVG MIN q (kPa)	-31.8 (63.6%)

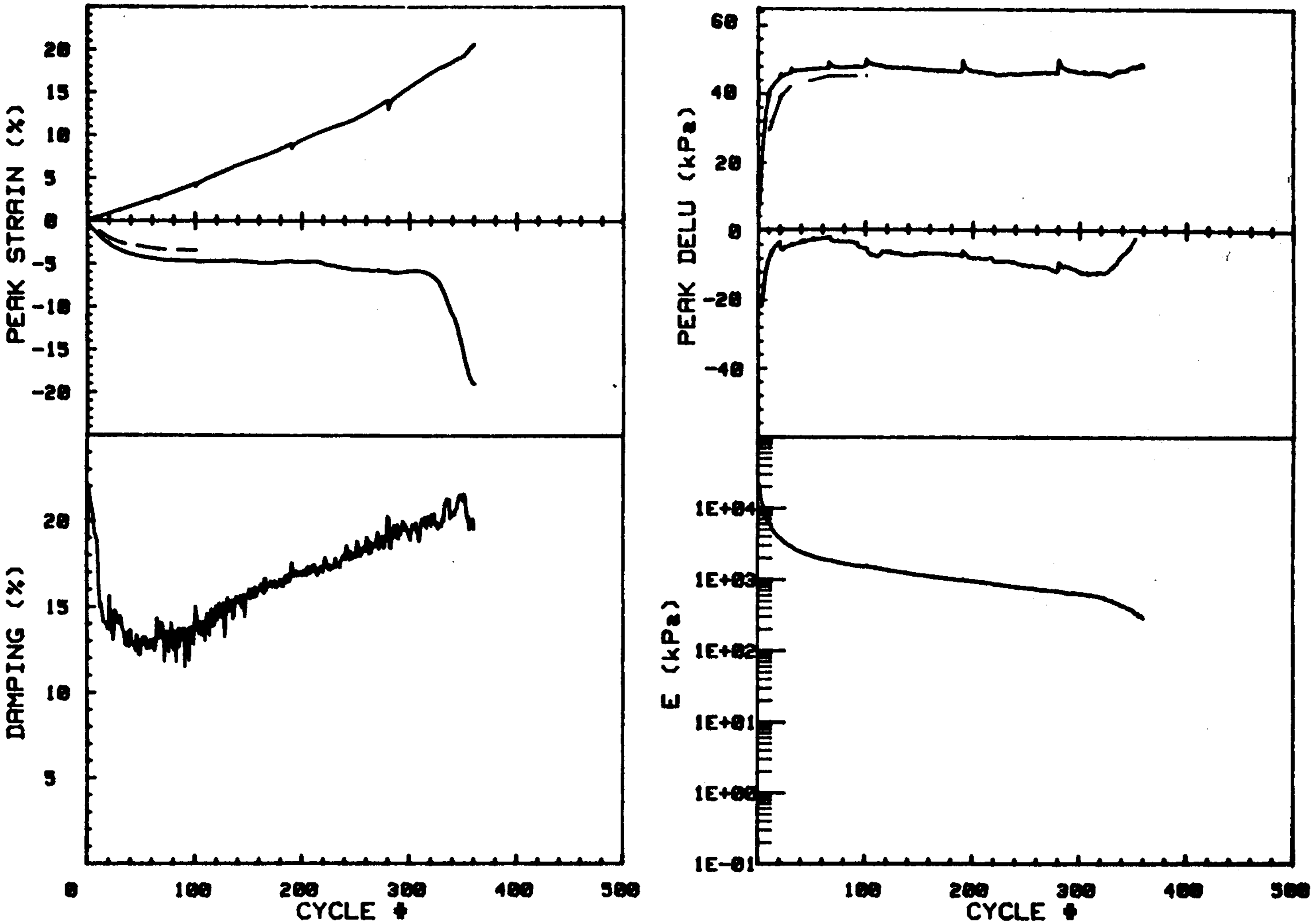

CRUISE DC4-81-NS		INCREMENT (cm)	16-24
CORE NO.	686A1	TEST NO.	TC89
SIG1c′(kPa)	50.0	STATIC qf (kPa)	50.0
SIG3c′(kPa)	50.0	AVG MAX q (kPa)	34.1 (68.2%)
INDUCED OCR	6.0	AVG MIN q (kPa)	-31.8 (63.6%)

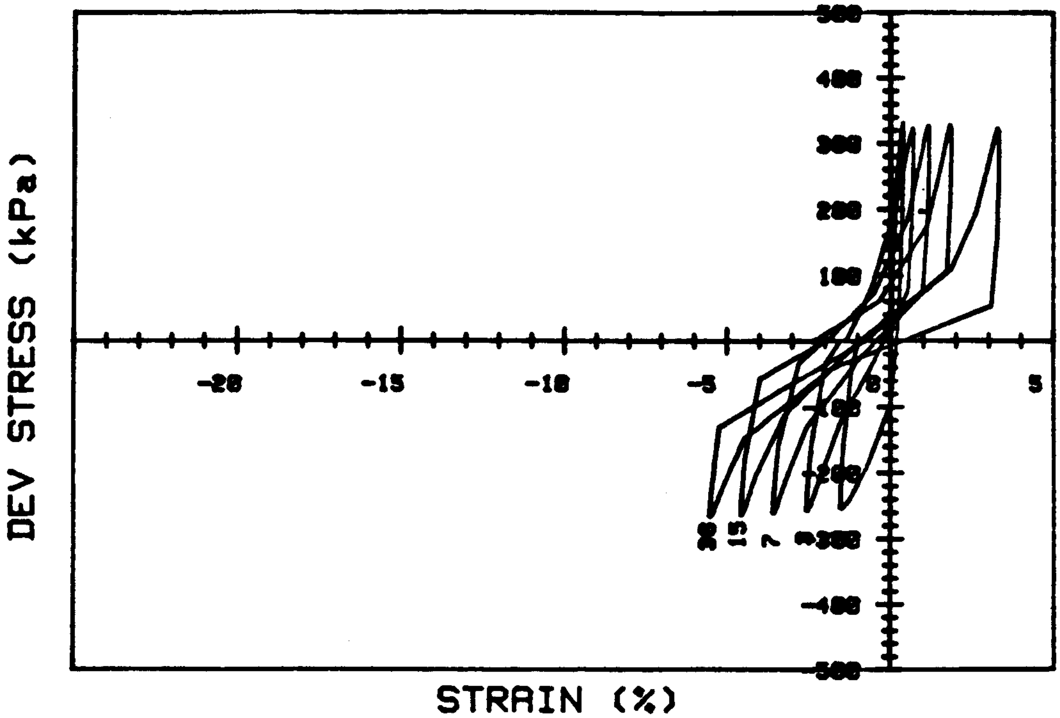

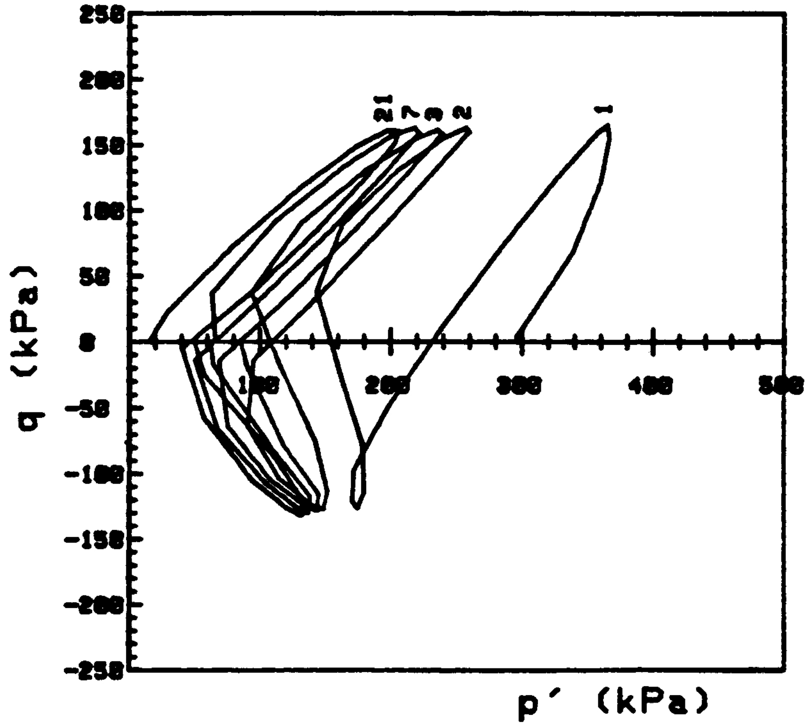

CRUISE DC4-81-NS		INCREMENT (cm)	31-39
CORE NO.	686A1	TEST NO.	TC84
SIG1c′(kPa)	296.7	STATIC qf (kPa)	300.0
SIG3c′(kPa)	296.7	AVG MAX q (kPa)	161.4 (53.8%)
INDUCED OCR	1.0	AVG MIN q (kPa)	-132.0 (44.0%)

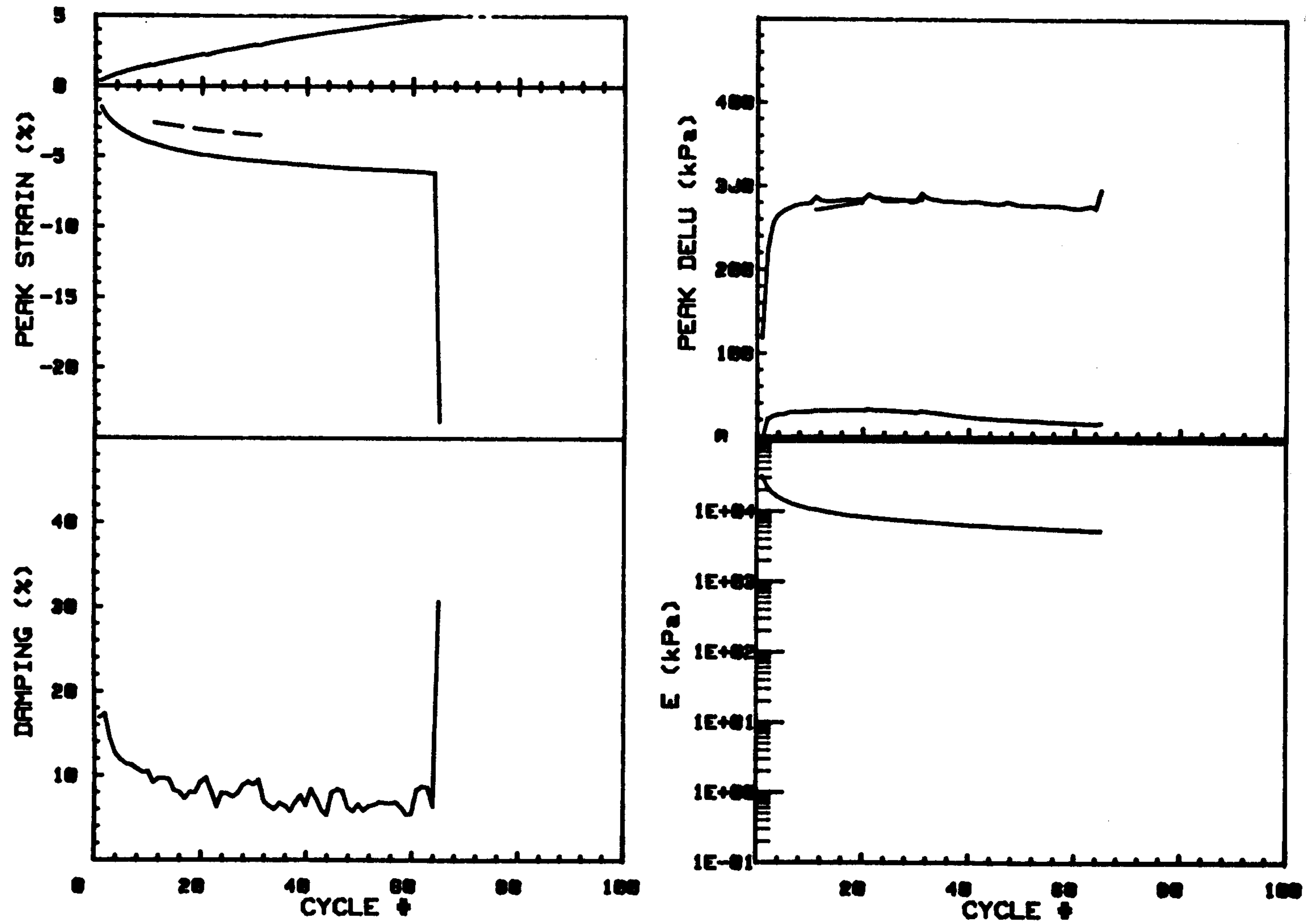

CRUISE DC4-81-NS		INCREMENT (cm)	31-39
CORE NO.	686A1	TEST NO.	TC84
SIG1c'(kPa)	296.7	STATIC qf (kPa)	300.0
SIG3c'(kPa)	296.7	AVG MAX q (kPa)	161.4 (53.8%)
INDUCED OCR	1.0	AVG MIN q (kPa)	-132.0 (44.0%)

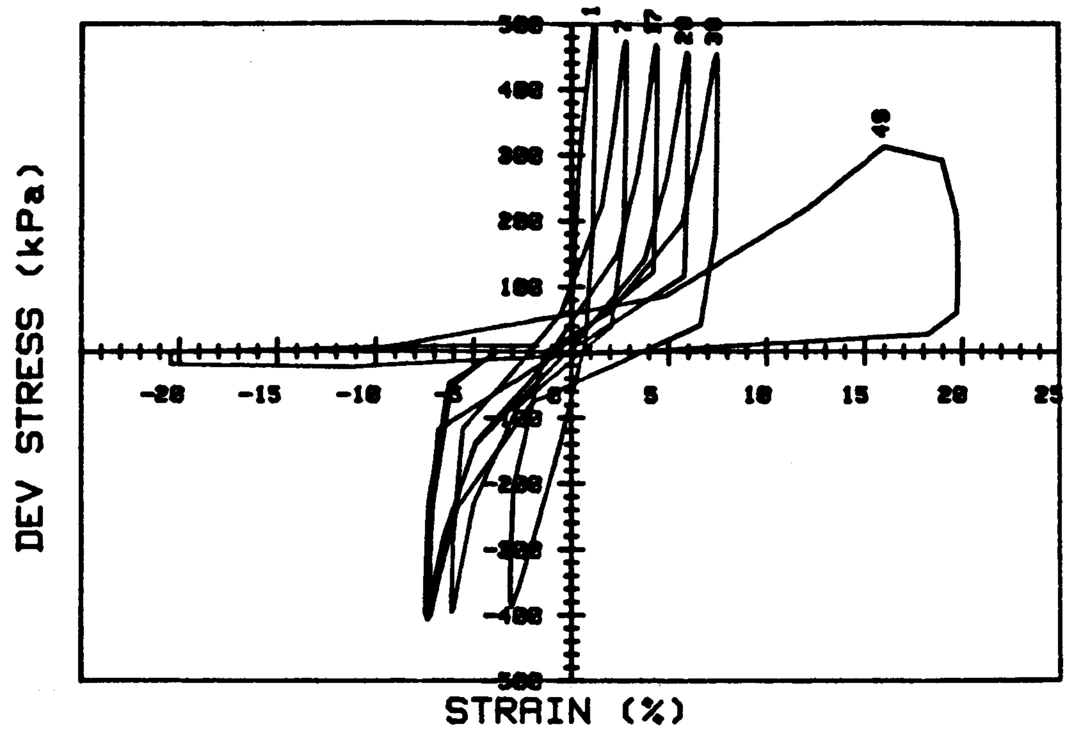

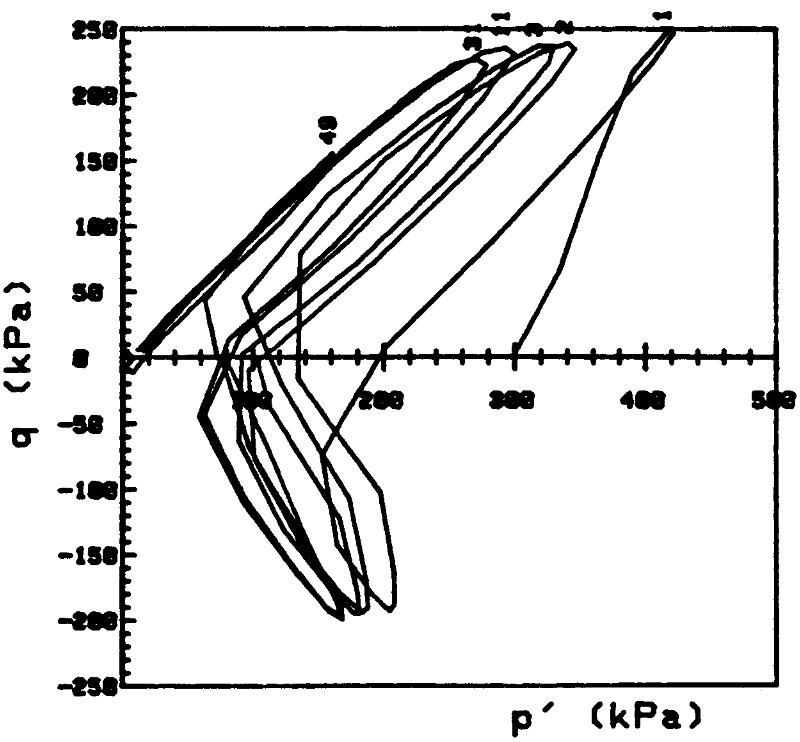

CRUISE DC4-81-NS		INCREMENT (cm)	31-39
CORE NO.	686A1	TEST NO.	TC85
SIG'c′(kPa)	298.9	STATIC qf (kPa)	300.0
SIG3c′(kPa)	298.9	AVG MAX q (kPa)	229.6 (76.5%)
INDUCED OCR	1.0	AVG MIN q (kPa)	-196.4 (65.5%)

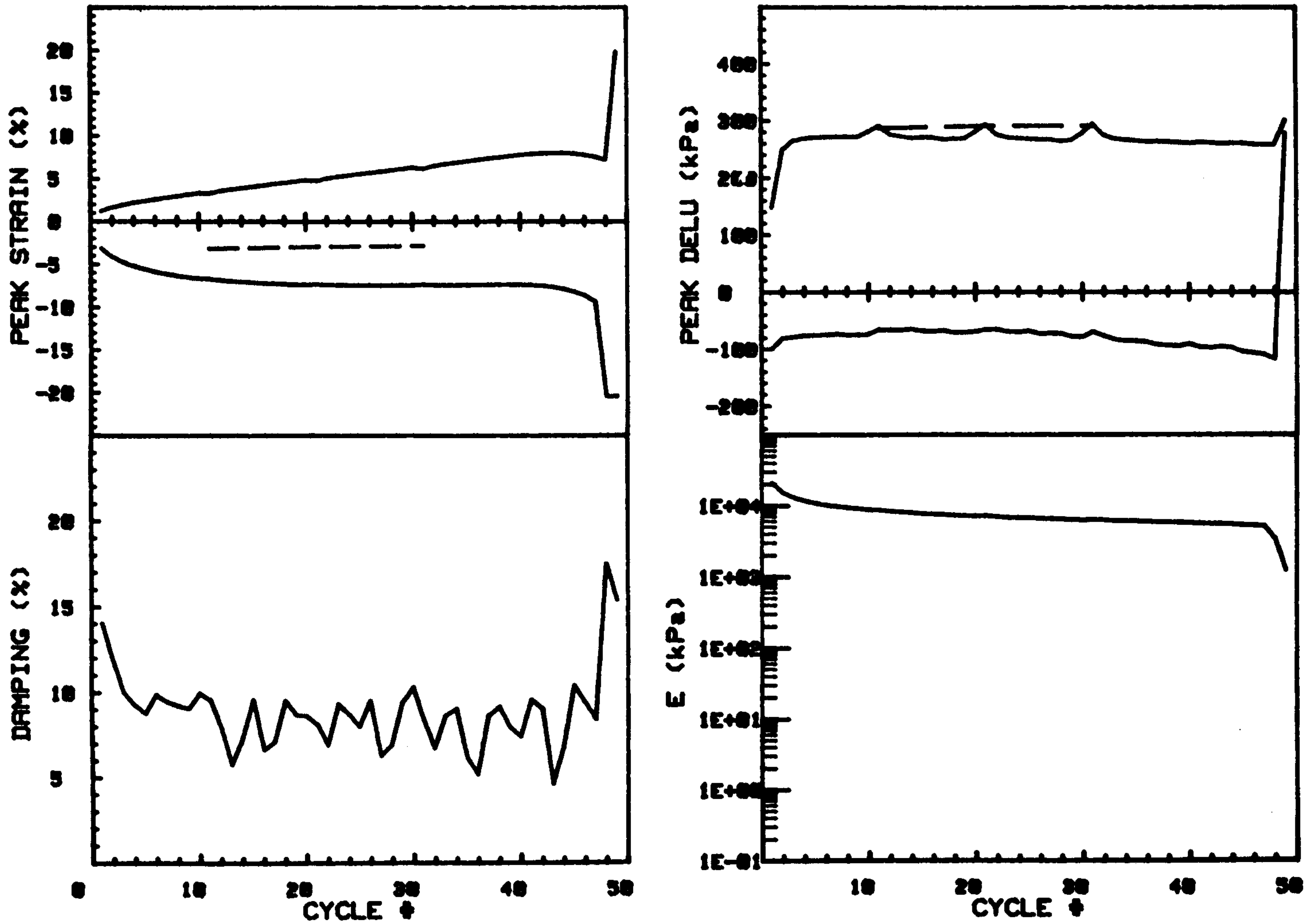

CRUISE DC4-81-NS		INCREMENT (cm)	31-39
CORE NO.	686A1	TEST NO.	TC85
SIG1o'(kPa)	298.9	STATIC qf (kPa)	300.0
SIG3o'(kPa)	298.9	AVG MAX q (kPa)	229.6 (76.5%)
INDUCED OCR	1.0	AVG MIN q (kPa)	-196.4 (65.5%)

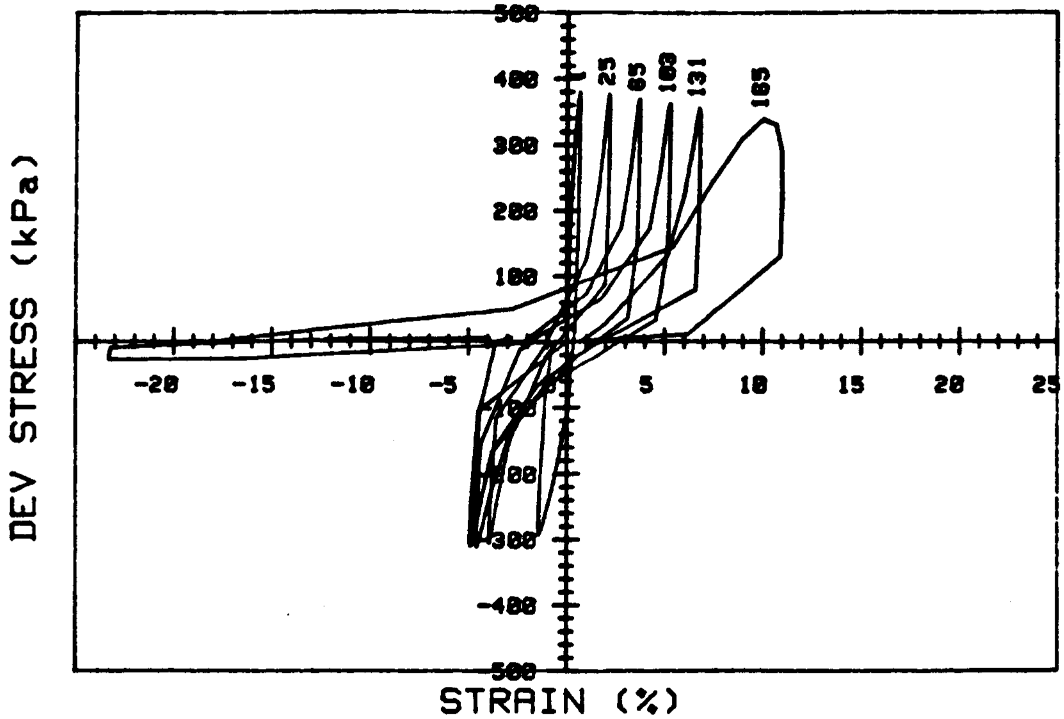

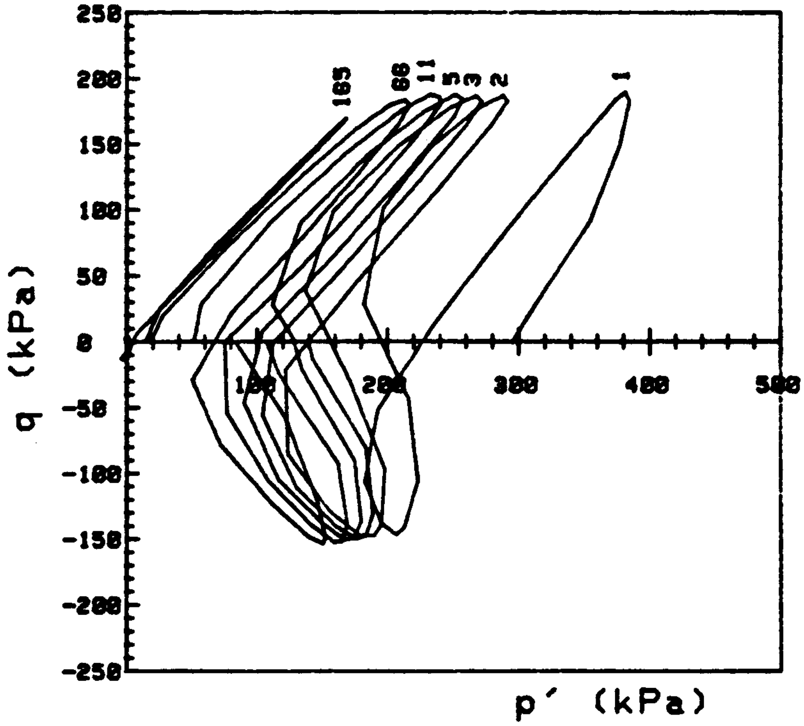

CRUISE DC4-81-NS		INCREMENT (cm)	41-49
CORE NO.	686A1	TEST NO.	TC96
SIG1c′(kPa)	295.5	STATIC qf (kPa)	300.0
SIG3c′(kPa)	295.5	AVG MAX q (kPa)	182.1 (60.7%)
INDUCED OCR	1.0	AVG MIN q (kPa)	-153.5 (51.2%)

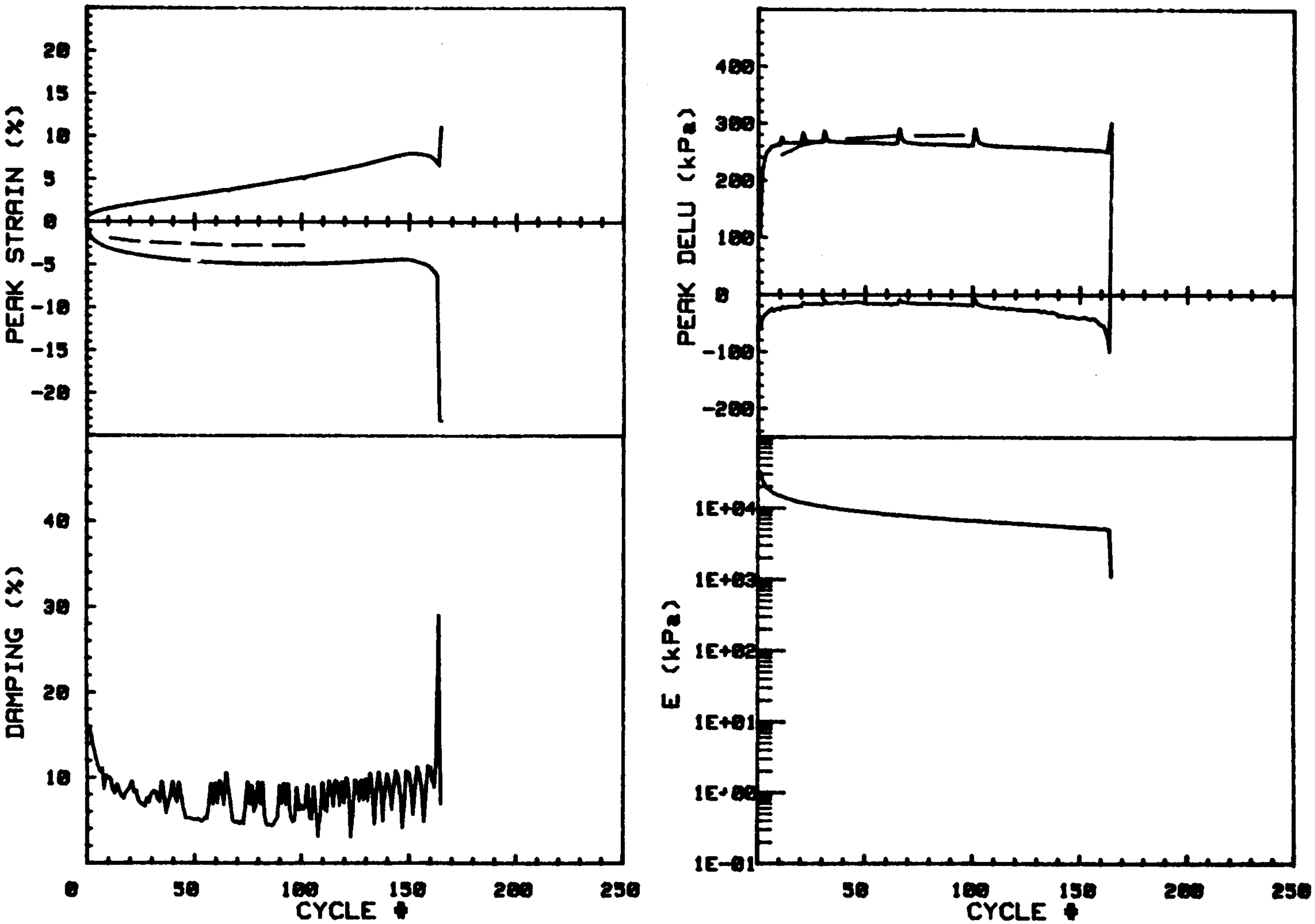

CRUISE	DC4-81-NS	INCREMENT (cm)	41-49
CORE NO.	686A1	TEST NO.	TC96
SIG1c'(kPa)	295.5	STATIC qf (kPa)	300.0
SIG3c'(kPa)	295.5	AVG MAX q (kPa)	182.1 (60.7%)
INDUCED OCR	1.0	AVG MIN q (kPa)	-153.5 (51.2%)

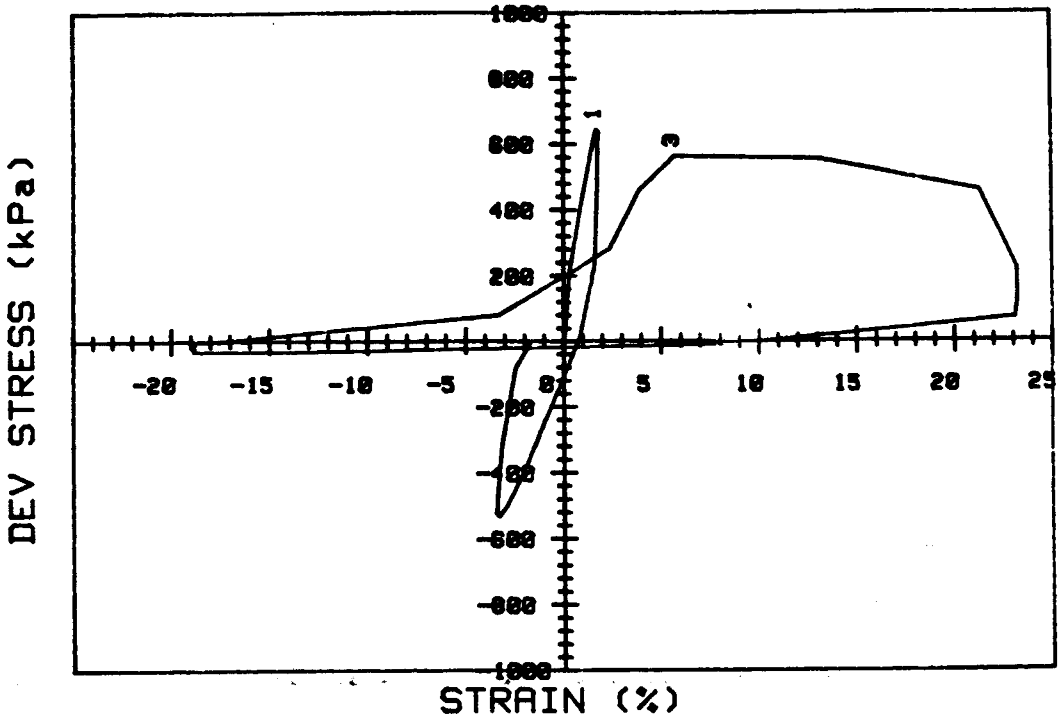

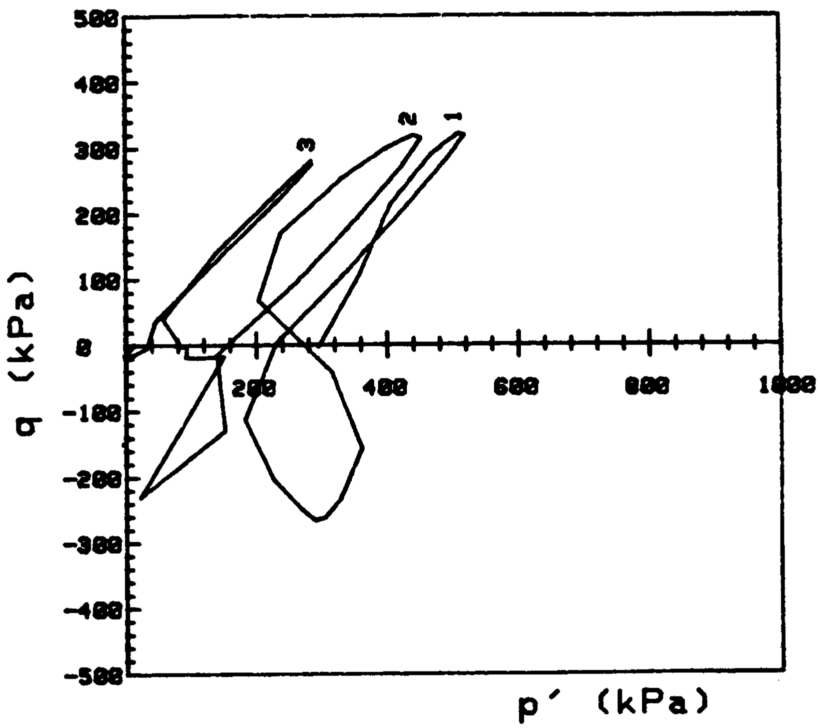

CRUISE DC4-81-NS		INCREMENT (cm)	41-49
CORE NO.	686A1	TEST NO.	TC97
SIG1c′(kPa)	298.1	STATIC qf (kPa)	300.0
SIG3c′(kPa)	298.1	AVG MAX q (kPa)	307.0 (102.3%)
INDUCED OCR	1.0	AVG MIN q (kPa)	-171.4 (57.1%)

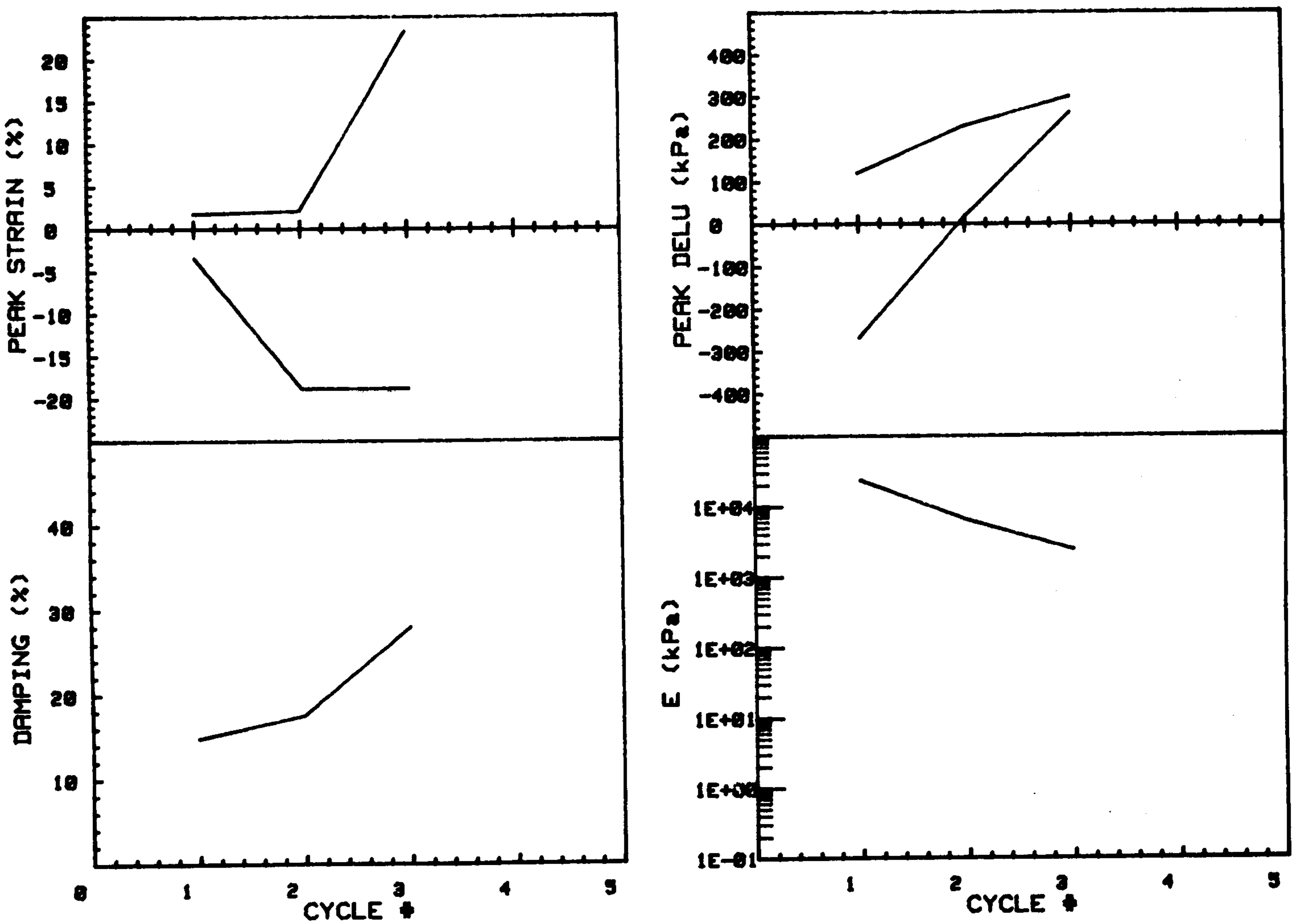

CRUISE DC4-81-NS		INCREMENT (cm)	41-49
CORE NO.	686A1	TEST NO.	TC97
SIG1c'(kPa)	298.1	STATIC qf (kPa)	300.0
SIG3c'(kPa)	298.1	AVG MAX q (kPa)	307.0 (102.3%)
INDUCED OCR	1.0	AVG MIN q (kPa)	-171.4 (57.1%)

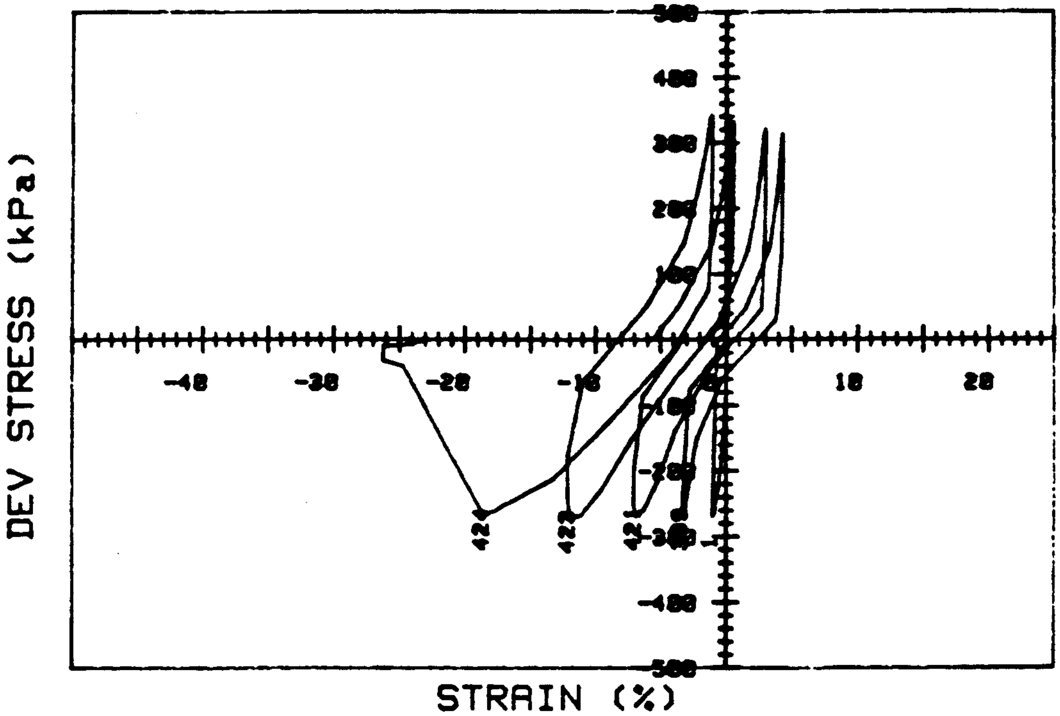

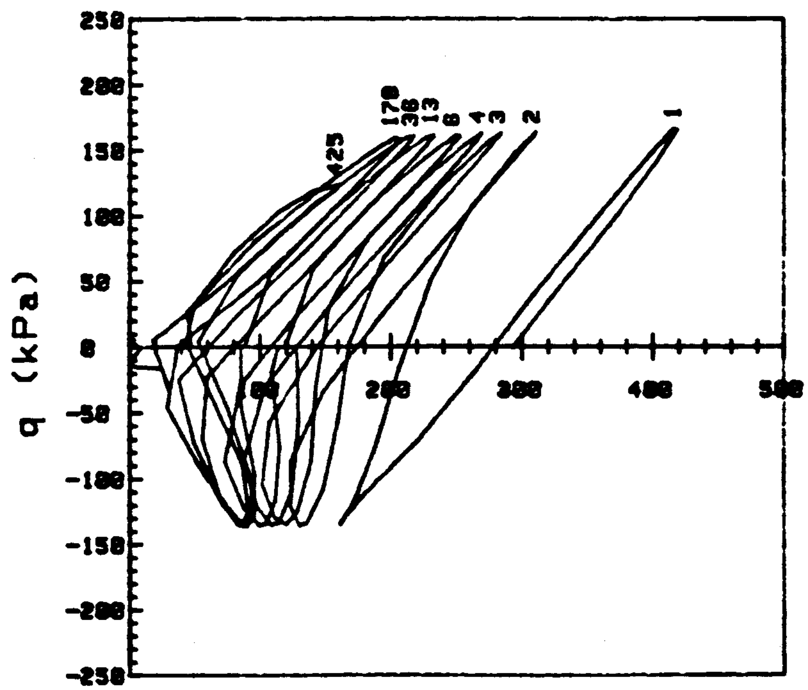

CRUISE DC4-81-NS		INCREMENT (cm)	52-59
CORE NO.	686A1	TEST NO.	D109
SIG1c′(kPa)	293.6	STATIC qf (kPa)	300.0
SIG3c′(kPa)	293.6	AVG MAX q (kPa)	159.1 (53.0%)
INDUCED OCR	1.0	AVG MIN q (kPa)	-135.6 (45.2%)

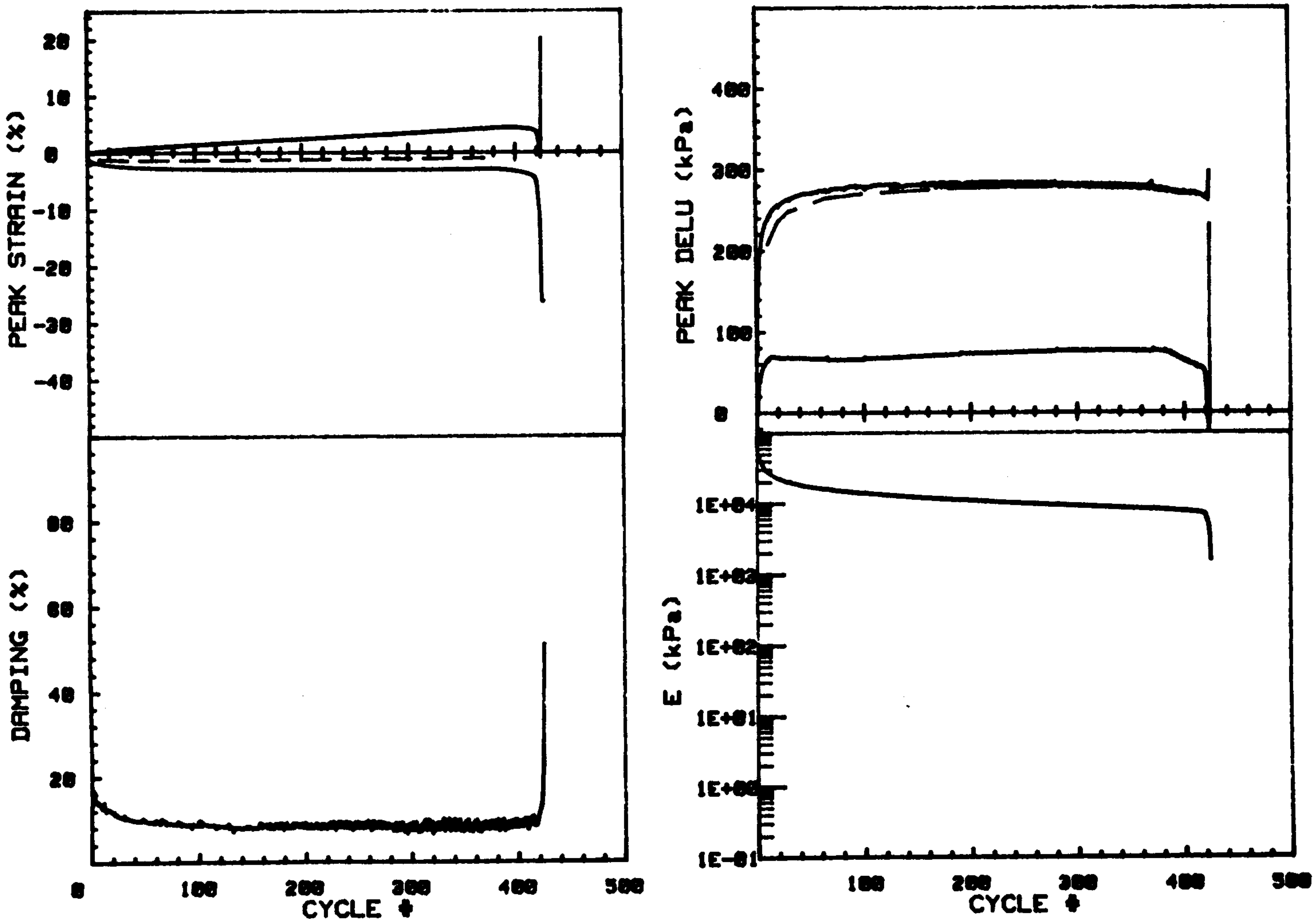

CRUISE DC4-81-NS		INCREMENT (cm)	52-59
CORE NO.	686A1	TEST NO.	D109
SIG1c′(kPa)	293.6	STATIC qf (kPa)	300.0
SIG3c′(kPa)	293.6	AVG MAX q (kPa)	159.1 (53.0%)
INDUCED OCR	1.0	AVG MIN q (kPa)	-135.6 (45.2%)

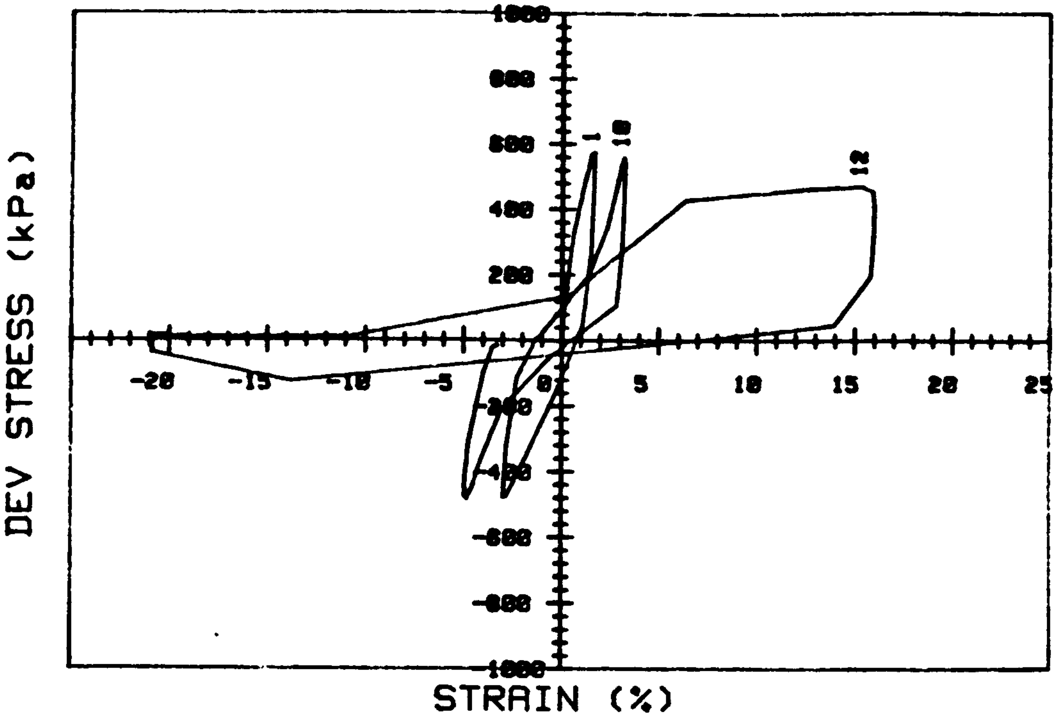

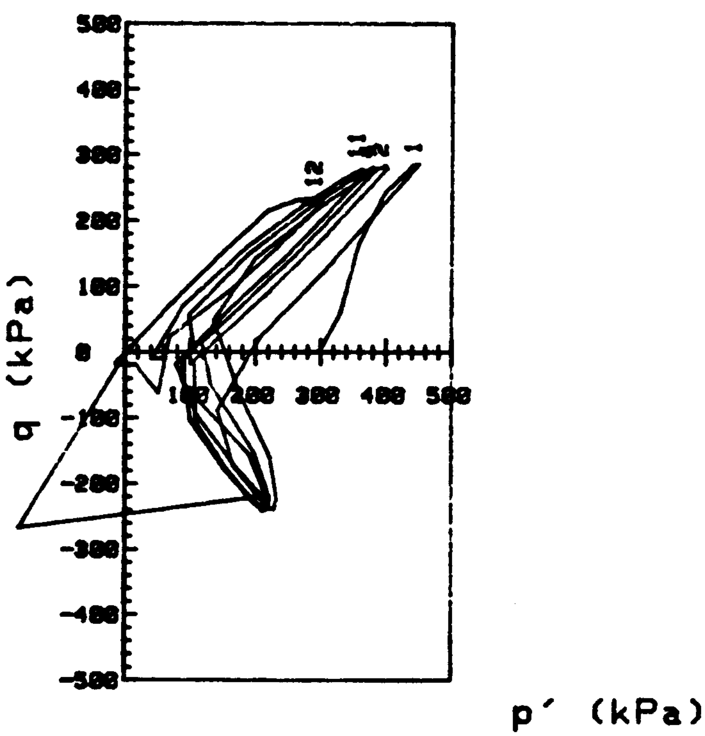

CRUISE DC4-81-NS		INCREMENT (cm)	52-59
CORE NO.	686A1	TEST NO.	D110
SIG1c′(kPa)	297.1	STATIC qf (kPa)	300.0
SIG3c′(kPa)	297.1	AVG MAX q (kPa)	276.6 (92.2%)
INDUCED OCR	1.0	AVG MIN q (kPa)	-228.5 (76.2%)

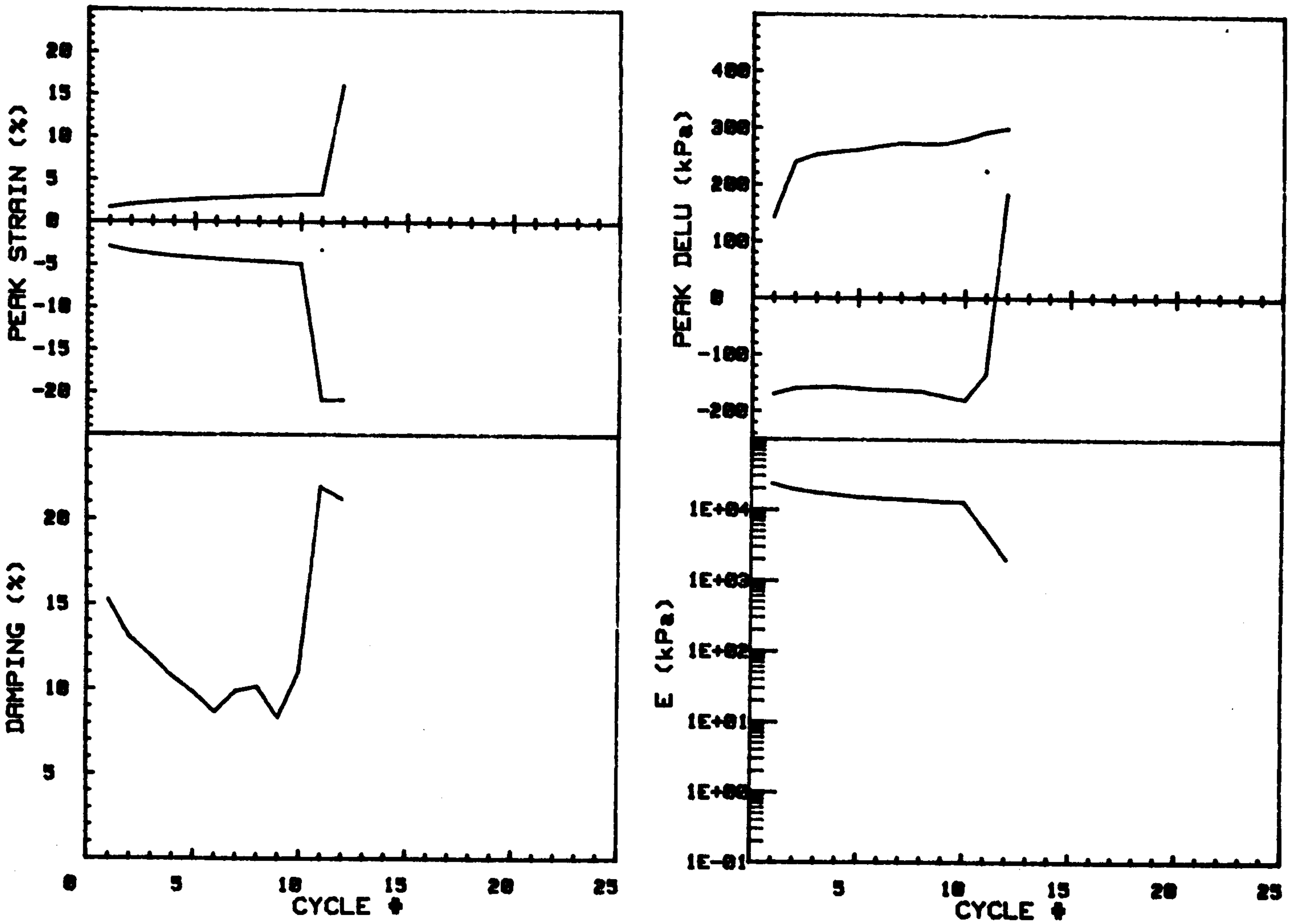

CRUISE	DC4-81-NS	INCREMENT (cm)	52-59
CORE NO.	686A1	TEST NO.	D110
SIG1c'(kPa)	297.1	STATIC qf (kPa)	300.0
SIG3c'(kPa)	297.1	AVG MAX q (kPa)	276.6 (92.2%)
INDUCED OCR	1.0	AVG MIN q (kPa)	-228.5 (76.2%)

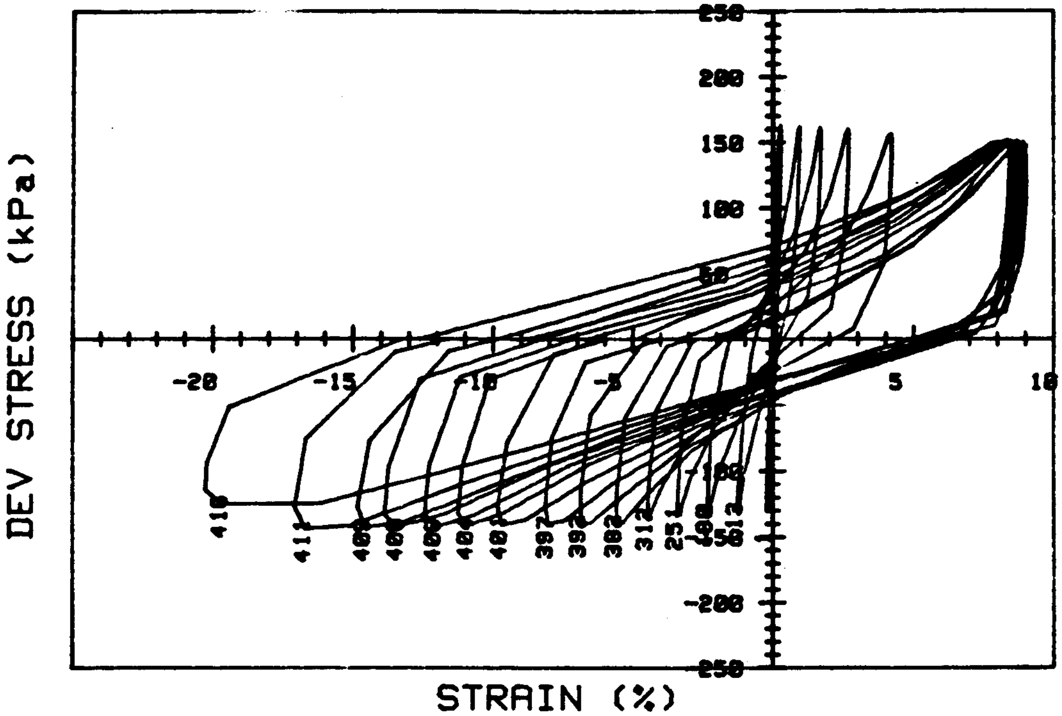

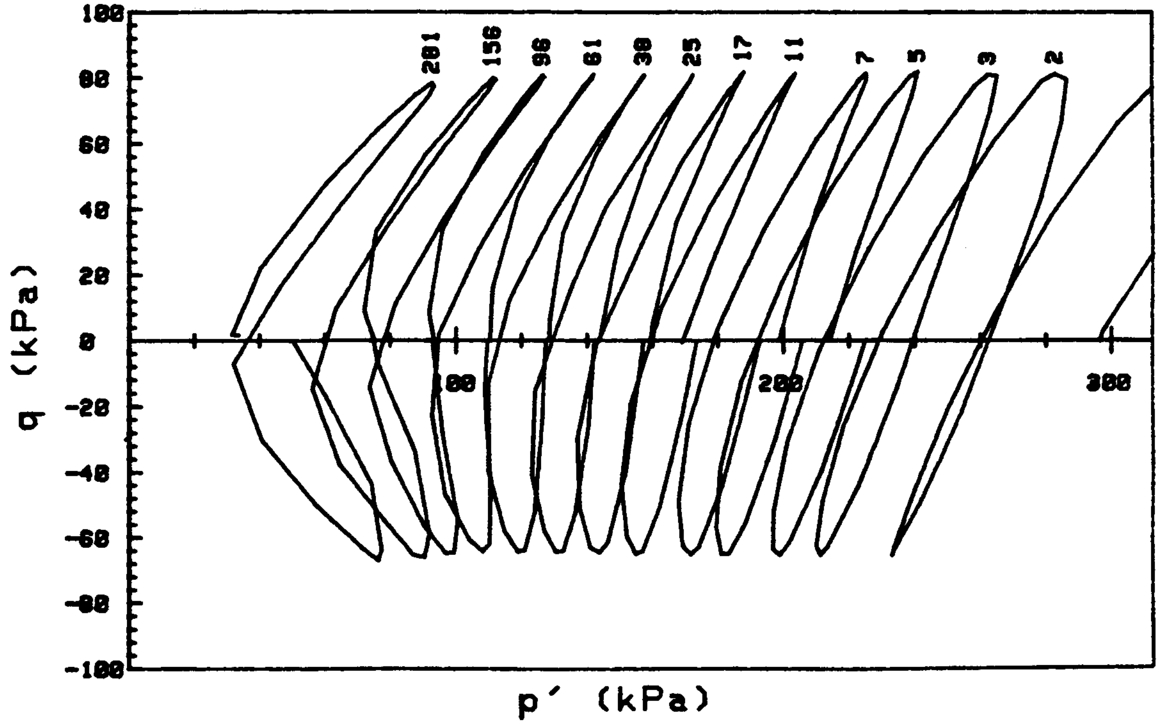

CRUISE DC4-81-NS		INCREMENT (cm)	45-53
CORE NO.	687A1	TEST NO.	TC94
SIG1c′(kPa)	296.7	STATIC qf (kPa)	300.0
SIG3c′(kPa)	296.7	AVG MAX q (kPa)	79.2 (26.4%)
INDUCED OCR	1.0	AVG MIN q (kPa)	-66.8 (22.3%)

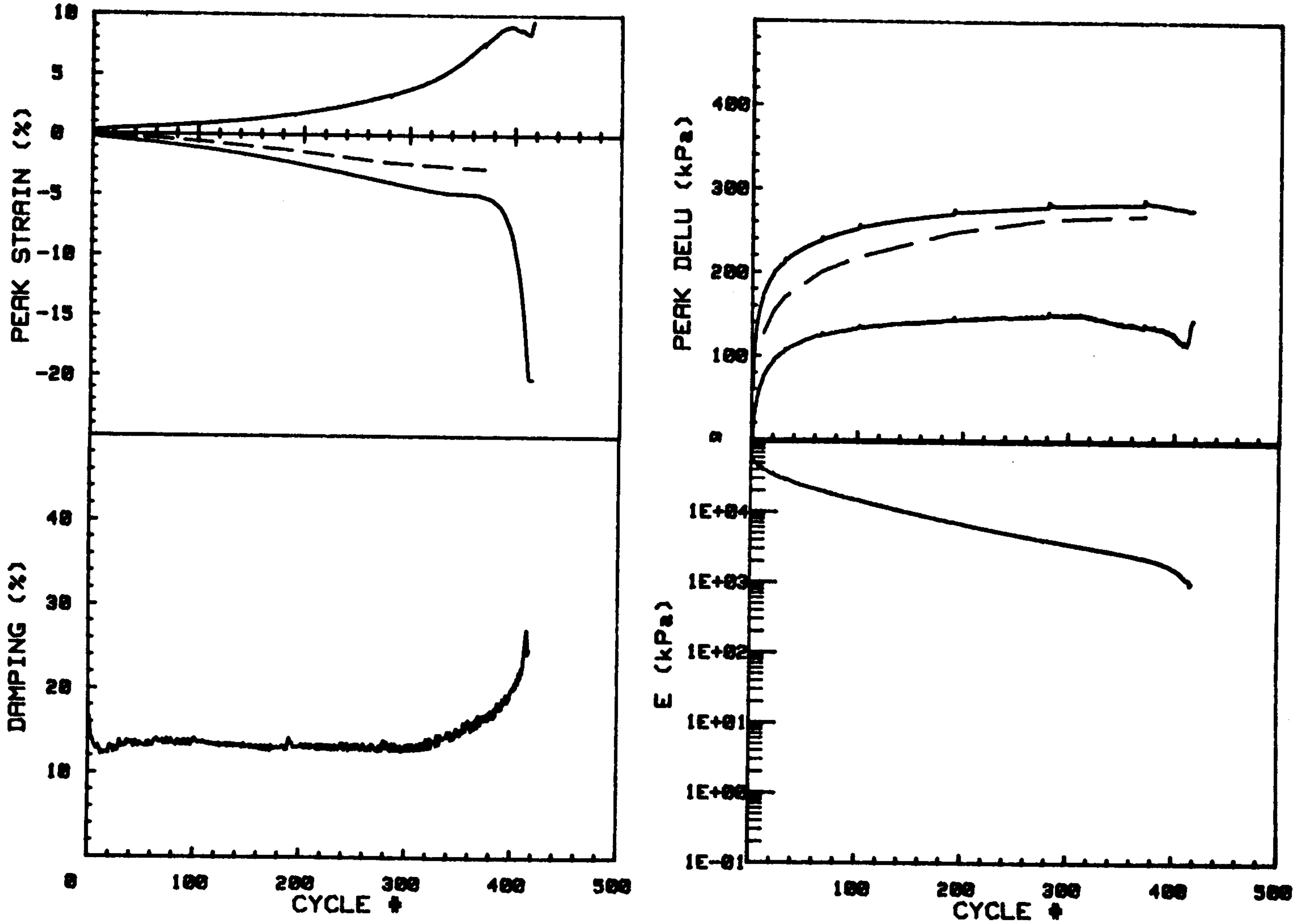

CRUISE DC4-81-NS		INCREMENT (cm)	45-53
CORE NO.	687A1	TEST NO.	TC94
SIG1c′(kPa)	296.7	STATIC qf (kPa)	300.0
SIG3c′(kPa)	296.7	AVG MAX q (kPa)	79.2 (26.4%)
INDUCED OCR	1.0	AVG MIN q (kPa)	-66.8 (22.3%)

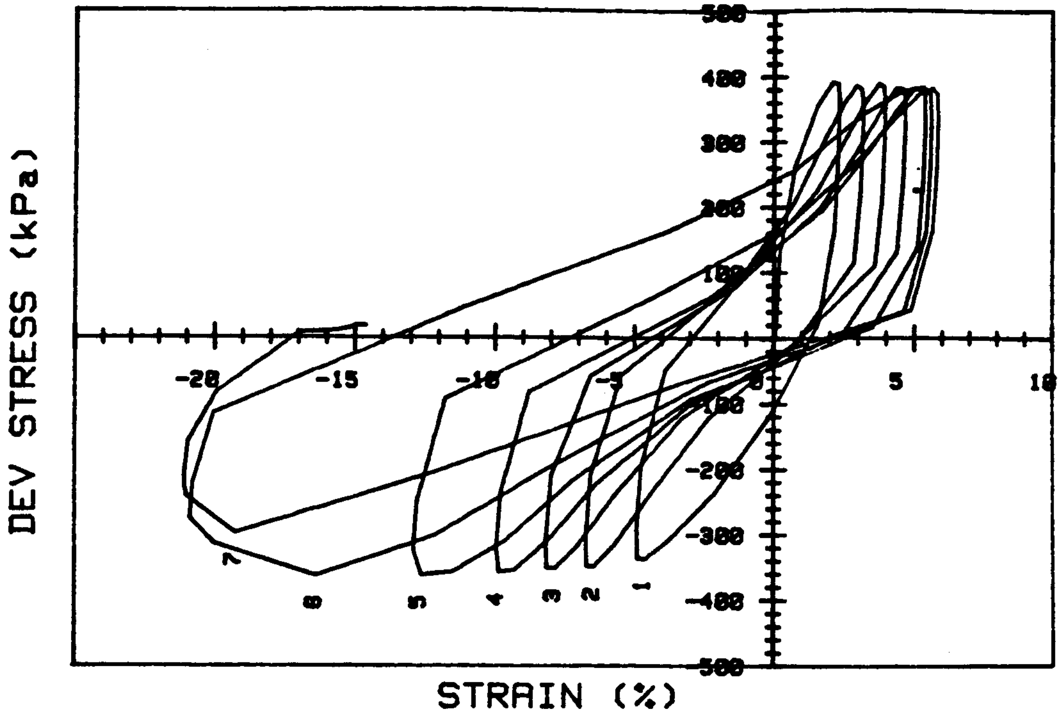

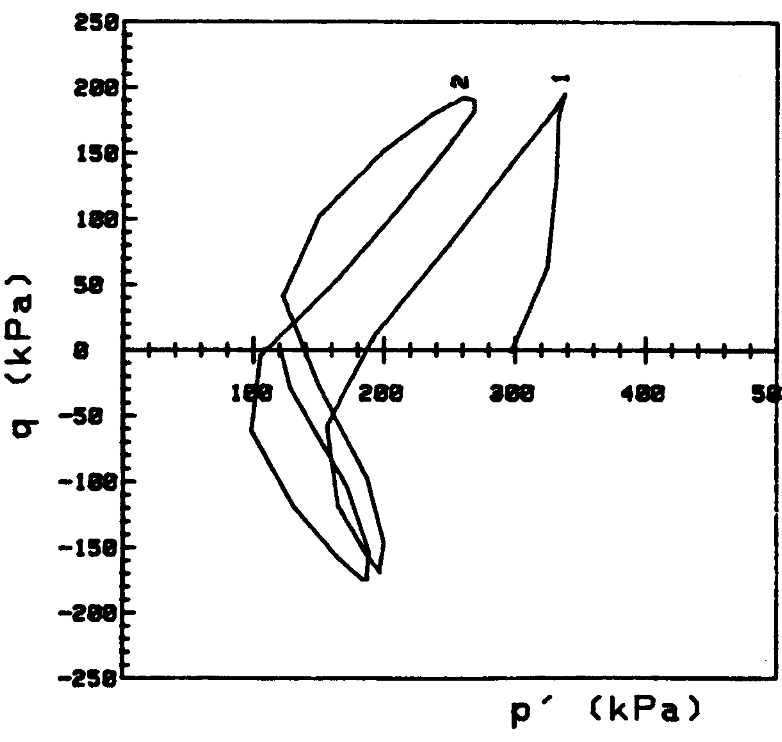

CRUISE	DC4-81-NS	INCREMENT (cm)		45-53	
CORE NO.	687A1	TEST NO.		TC95	
SIG1c′(kPa)	298.7	STATIC qf	(kPa)	300.0	
SIG3c′(kPa)	298.7	AVG MAX q	(kPa)	192.1	(64.0%)
INDUCED OCR	1.0	AVG MIN q	(kPa)	-172.7	(57.6%)

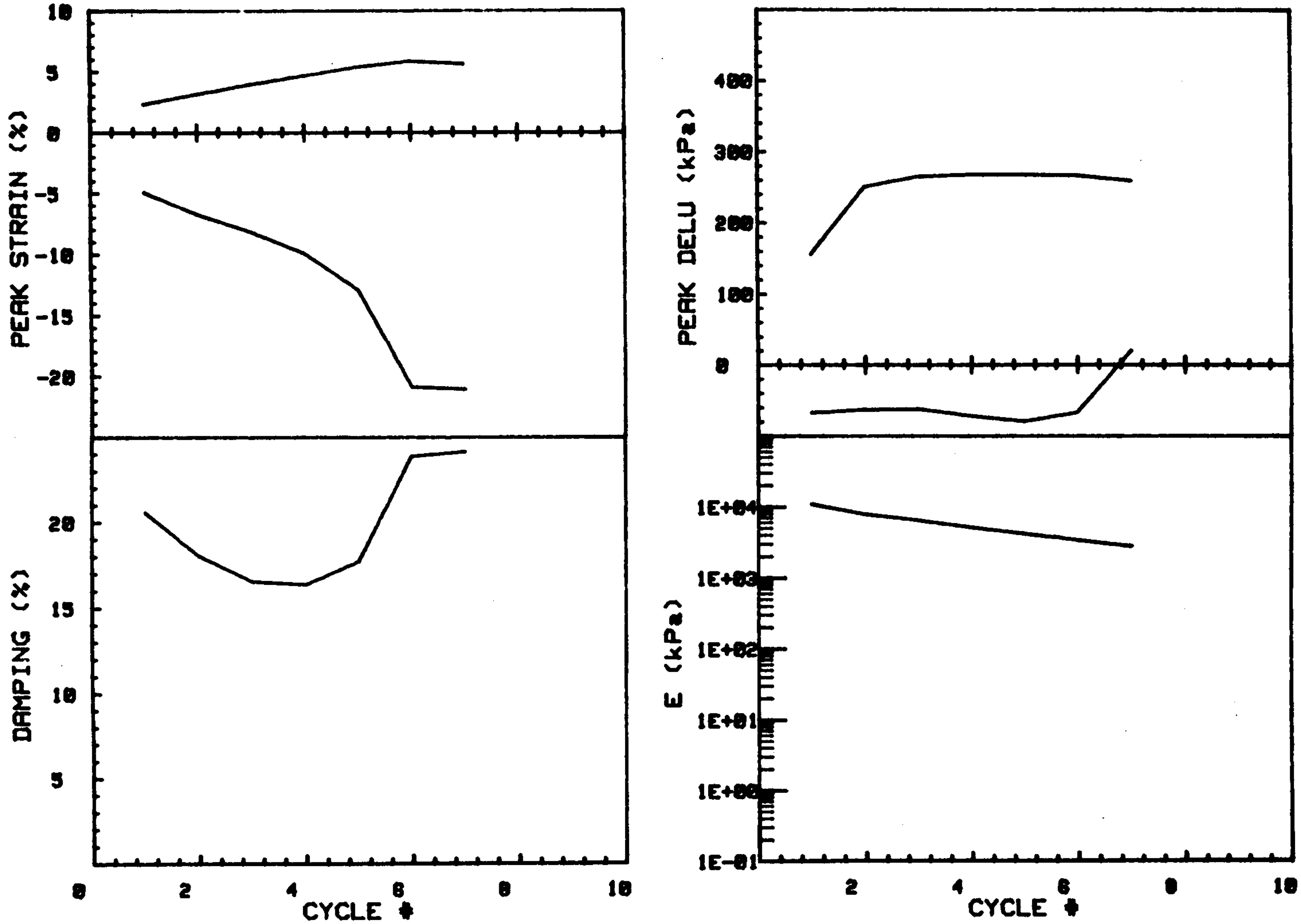

CRUISE DC4-81-NS		INCREMENT (cm)	45-53
CORE NO.	687A1	TEST NO.	TC95
SIG1c'(kPa)	298.7	STATIC qf (kPa)	300.0
SIG3c'(kPa)	298.7	AVG MAX q (kPa)	192.1 (64.0%)
INDUCED OCR	1.0	AVG MIN q (kPa)	-172.7 (57.6%)

APPENDIX G:

LIQUEFACTION SUSCEPTIBILITY ANALYSES

Appendix G

Four liquefaction analyses, based primarily on the techniques of Seed and Idriss (1971) and Seed and Rahman (1978), were performed using cone penetration test (CPT) and cyclic triaxial test data. Because sediment types in Norton Sound are different than previously studied material, some modification of the following procedures may be necessary when more information is known about the liquefaction behavior of sandy silt. The results of the analyses are presented in Table 9. A description of the procedures follow.

Analysis 1: Earthquake accelerations that will liquefy sediment at various depths were calculated using cyclic triaxial test data.

The maximum shear stresses in a soil body are primarily caused by an upward propagation of shear waves from bedrock. The average shear stress (τ_{ave}) in a deformable body is equal to (Seed and Idriss, 1971):

$$\tau_{ave} = 0.65 \ \gamma \ h \ \frac{a_{max}}{g} \ r_d \qquad (1)$$

where: τ_{ave} = average horizontal shear stress;

γ = total unit weight of the soil estimated from consolidation tests;

h = subbottom depth of stress determination;

g = acceleration due to gravity;

a_{max} = maximum ground surface acceleration;

r_d = stress coefficient to reduce stresses from a rigid to a deformable body, determined from Fig. G1.

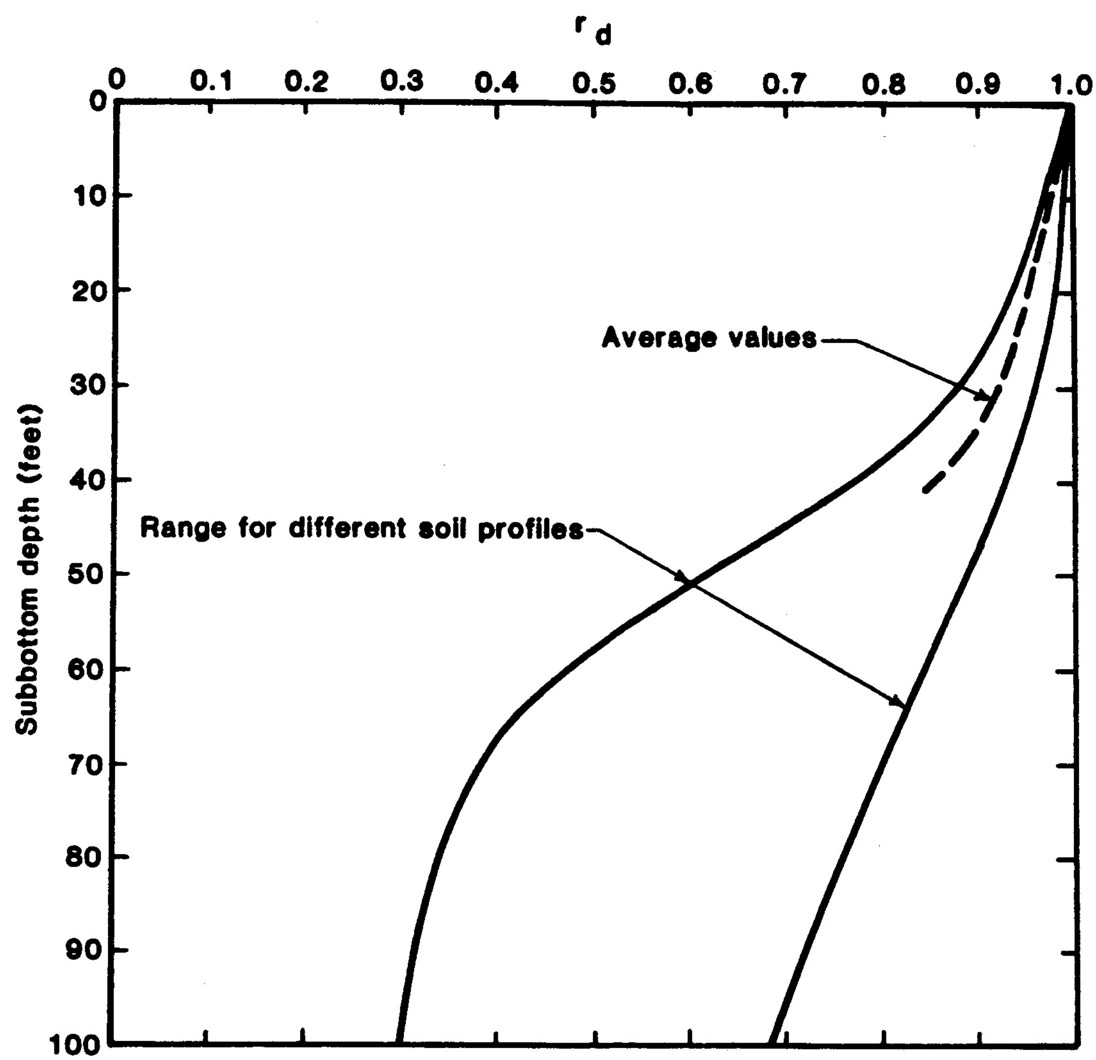

Fig. G1. Range of r_d values vs subbottom depth for different soil profiles (from Seed and Idriss, 1971).

Cyclic triaxial tests were performed to evaluate the cyclic stress ratio ($\tau_{cyc\ ave\ max}/\sigma'_c$) necessary to cause a certain strain to occur at a particular number of loading cycles. A magnitude 5.25 earthquake may be represented by approximately 3 significant cycles at 0.65 τ_{max}, a magnitude 6.0 event contains approximately 5 cycles, and a 6.75 gnitude has approximately 10 representative cycles (Seed and Idriss, in press). Useful data can be obtained from carefully conducted cyclic triaxial tests performed to 5 percent strain for dense samples (Seed, 1979) (Fig. 9). Cyclic triaxial test results typically are adjusted to agree with field stress applications. The following equation transforms cyclic triaxial stress ratios into representative field data (Seed, 1979):

$$\left(\frac{\tau_h}{\sigma'_{vo}}\right)_{field} \approx c_m \quad c_r \left(\frac{\tau_{cyc\ ave\ max}}{\sigma'_c}\right)_{triaxial} \qquad (2)$$

where: $\left(\tau_h/\sigma'_{vo}\right)_{field}$ = the horizontal shear stress caused by an earthquake normalized to its vertical in situ confining stress;

c_m = a coefficient that relates unidirectional cyclic shear tests to multidirectional shaking in the field, typically equals 0.9;

c_r = a coefficient that modifies the cyclic triaxial stress ratio to a corresponding cyclic simple shear stress ratio that is more representative of field conditions, the coefficient is dependent upon the coefficient of earth pressure at rest in the field, K_o;

$\left(\tau_{cyc\ ave\ max}/\sigma'_c\right)_{triaxial}$ =the stress ratio required to reach 5 percent strain in 3, 5 and 10 cycles as determined from cyclic triaxial tests (Fig. 9).

The triaxial to simple shear reduction coefficient, c_r, is dependent upon K_o; $c_r \approx 0.63$ for $K_o \approx 0.4$ and $c_r \approx 1.0$ for $K_o \approx 1.0$. Other values of c_r were linearly interpolated between the end values (Seed, 1979). The coefficient of earth pressure at rest was calculated from (Mayne and Kulhawy, 1982):

$$K_o = (1 - \sin \phi')\ OCR^{\sin \phi'} \quad (3)$$

where: K_o = the coefficient of earth pressure at rest;

ϕ' = the effective friction angle determined from static triaxial tests (Table 7);

OCR = overconsolidation ratio at depth of interest, estimated from Fig. G2.

Equating τ_{ave} in equation 1 with τ_h in equation 2, the maximum ground surface acceleration from an earthquake necessary to cause liquefaction at various depths was determined (Table G1):

$$a_{max} = \frac{g\ c_m\ c_r\ \sigma'_{vo}}{0.65\ \gamma\ h\ r_d} \left(\frac{\tau_{cyc\ ave\ max}}{\sigma'_c}\right)_{triaxial} \quad (4)$$

The above analysis assumed that cyclic properties at depth were the same as measured properties of shallow subbottom sediment. Deep site specific investigations are required to determine if weaker stratas exist.

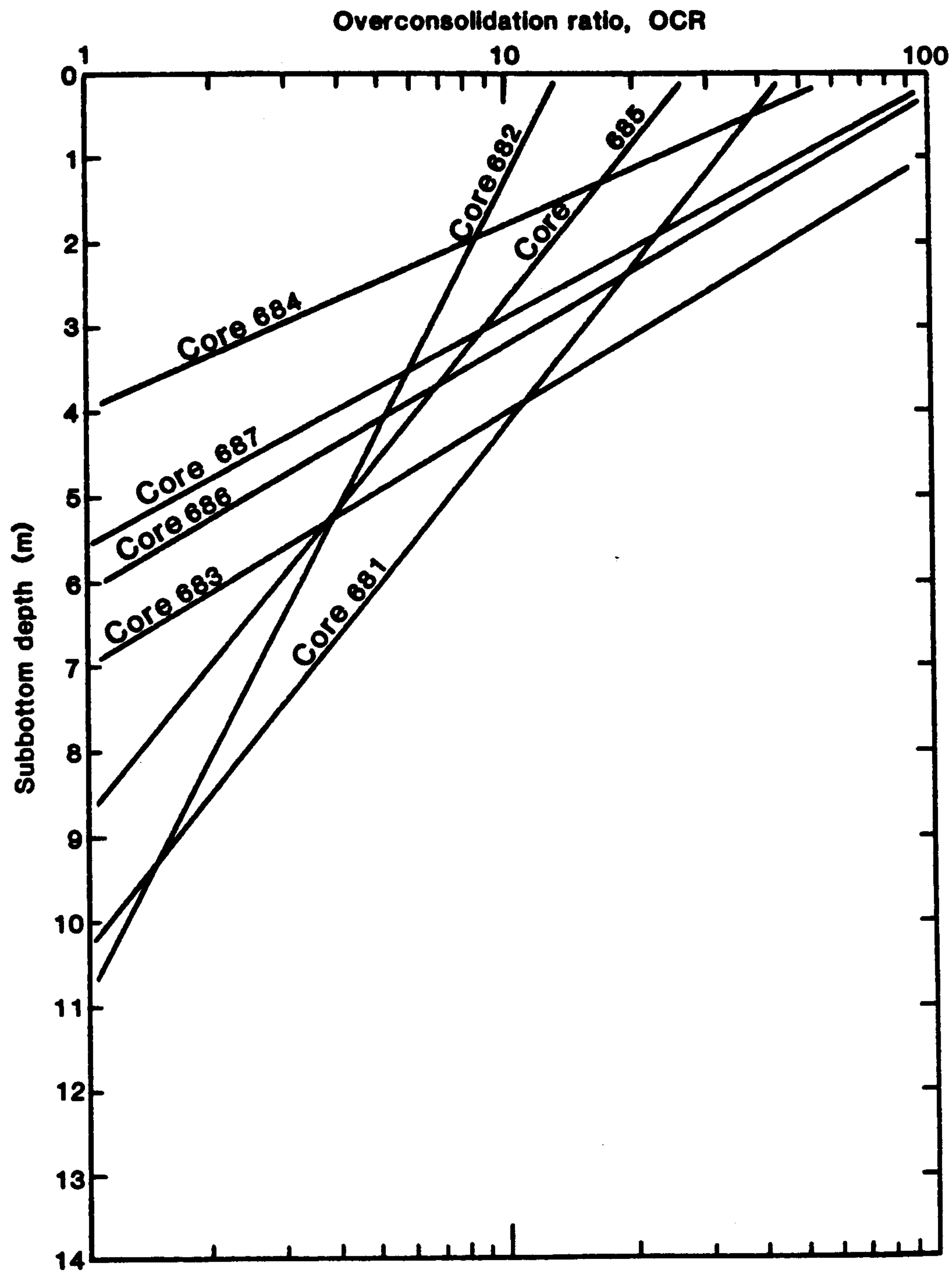

Fig. G2. Overconsolidation ratio determined from consolidation tests versus subbottom depth.

Table G1. Ground surface earthquake accelerations (a_{max}) necessary to induce liquefaction at different subbottom depths (h) based on laboratory cyclic triaxial test data (determined from equation 4).

CORE	h (m)	γ (kN/m^3)	r_d	σ'_{vo} (kN/m^2)	c_m	ϕ degrees	OCR	K_o(1)	c_r	$\frac{\tau_{cyc\ ave\ max}}{\sigma'_c}$ (triaxial) M = 5.25; 3 cycles	a_{max} (g)	$\frac{\tau_{cyc\ ave\ max}}{\sigma'_c}$ (triaxial) M= 6.0; 5 cycles	a_{max} (g)	$\frac{\tau_{cyc\ ave\ max}}{\sigma'_c}$ (triaxial) M=6.75; 10 cycles	a_{max} (g)
681A2	1	20.4	0.99	10.4	0.9	37	32	1.00(3.21)	1.00	0.52	0.37	0.44	0.31	0.35	0.25
	2	20.5	0.98	20.9			22	1.00(2.56)	1.00		0.37		0.32		0.25
	6	20.8	0.95	64.5			5	1.00(1.05)	1.00		0.39		0.33		0.26
682A1	1	16.0	0.99	6.0	0.9	35	11	1.00(1.69)	1.00	0.47	0.25	0.42	0.22	0.37	0.19
	2	16.1	0.98	12.1		40	8	1.00(1.36)	1.00		0.25		0.22		0.20
	6	16.6	0.95	39.3			3	0.72	0.83		0.22		0.20		0.18
684A1	1	20.7	0.99	10.7	0.9	38	23	1.00(2.65)	1.00	0.69	0.50	0.62	0.45	0.55	0.40
	2	20.7	0.98	21.3			8	1.00(1.38)	1.00		0.50		0.45		0.40
	6	20.8	0.95	64.5			1	0.38	0.62		0.32		0.29		0.26
685A2	1	18.0	0.99	8.0	0.9	37	19	1.00(2.34)	1.00	0.41	0.25	0.36	0.22	0.31	0.19
	2	18.1	0.98	16.1			13	1.00(1.86)	1.00		0.26		0.23		0.19
	6	18.5	0.95	50.7			3	0.77	0.86		0.23		0.21		0.18
	10	18.8	0.91	67.5			1	0.40	0.63		0.14		0.12		0.11
686A1	1	20.3	0.99	10.3	0.9	42	56	1.00(4.89)	1.00	0.82	0.58	0.72	0.51	0.62	0.44
	2	20.3	0.98	20.5			26	1.00(2.93)	1.00		0.58		0.51		0.44
	6	20.3	0.95	61.5			1	0.33	0.58		0.35		0.31		0.26
	10	20.4	0.91	103.5			1	0.33	0.58		0.37		0.32		0.28
687A1	1	19.7	0.99	9.7	0.9	38	49	1.00(4.22)	1.00	0.58	0.40	0.52	0.36	0.45	0.31
	2	19.7	0.98	19.3			21	1.00(2.50)	1.00		0.40		0.36		0.31
	6	19.9	0.95	60.7			1	0.38	0.62		0.27		0.24		0.21
	10	20.0	0.91	99.5			1	0.38	0.62		0.27		0.24		0.21

(1) Maximum K_o value allowed in analysis =1.0, higher values were assumed to have been caused by disturbance effects.

Analysis 2: Earthquake accelerations that will liquefy sediment at a shallow subbottom depth were calculated using standard correlations based on CPT data.

This analysis also is based on the simplified procedure for evaluating soil liquefaction potential of Seed and Idriss (1971) with some modification. That evaluation relies on empirical correlations between the standard penetration test (SPT) and areas of observed liquefaction caused by earthquakes. The standard penetration test is performed by dropping a weight onto drill rods and measuring the number of blows (N) required to drive a split sampling spoon 0.305 m. Representative blow counts (N) were determined from the in situ cone penetration test data obtained in Norton Sound using the relations in Fig. G3 (Schmertmann, 1976, cited in Martin and Douglas 1981). The blow counts (N) were corrected for shallow subbottom depth by multiplying by 0.75 and by C_N obtained from Fig. G4. The blow count was also increased by 7.5 to account for silt content (Seed and Idriss, in press). The equation to determine the corrected blow count, N_c, for any shallow (<3m) subbottom depth is:

$$N_c = (0.75 \quad C_N \quad N) \quad + 7.5 \qquad (5)$$

The stress ratio (τ_{cyc}/σ'_{vo}) necessary to cause liquefaction for a particular magnitude earthquake as a function of N_c is shown in Fig. G5. If the stress ratio is known, the maximum acceleration at the seafloor (a_{max}) can be calculated from equation 1 with both sides normalized by σ'_{vo}. The minimum a_{max} for each penetration is listed in Table G2.

Analysis 3: Wave heights that will liquefy shallow subbottom sediment were calculated using cyclic triaxial test data.

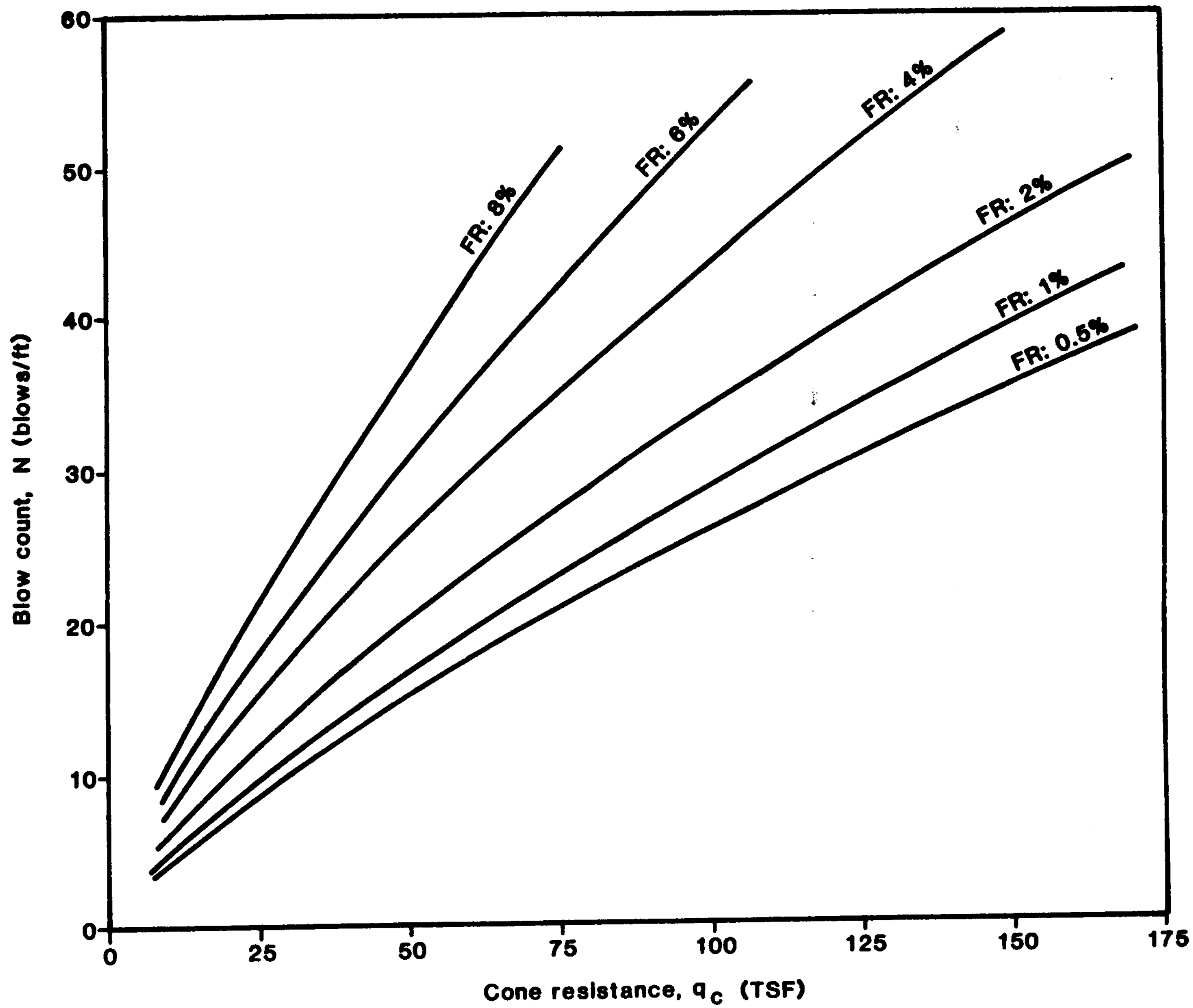

Fig. G3. Correlation of cone resistance (q_c) and friction ratio (FR) obtained from cone penetration tests with standard penetration test blow count (N) (Schmertmann, 1976, cited in Martin and Douglas, 1981).

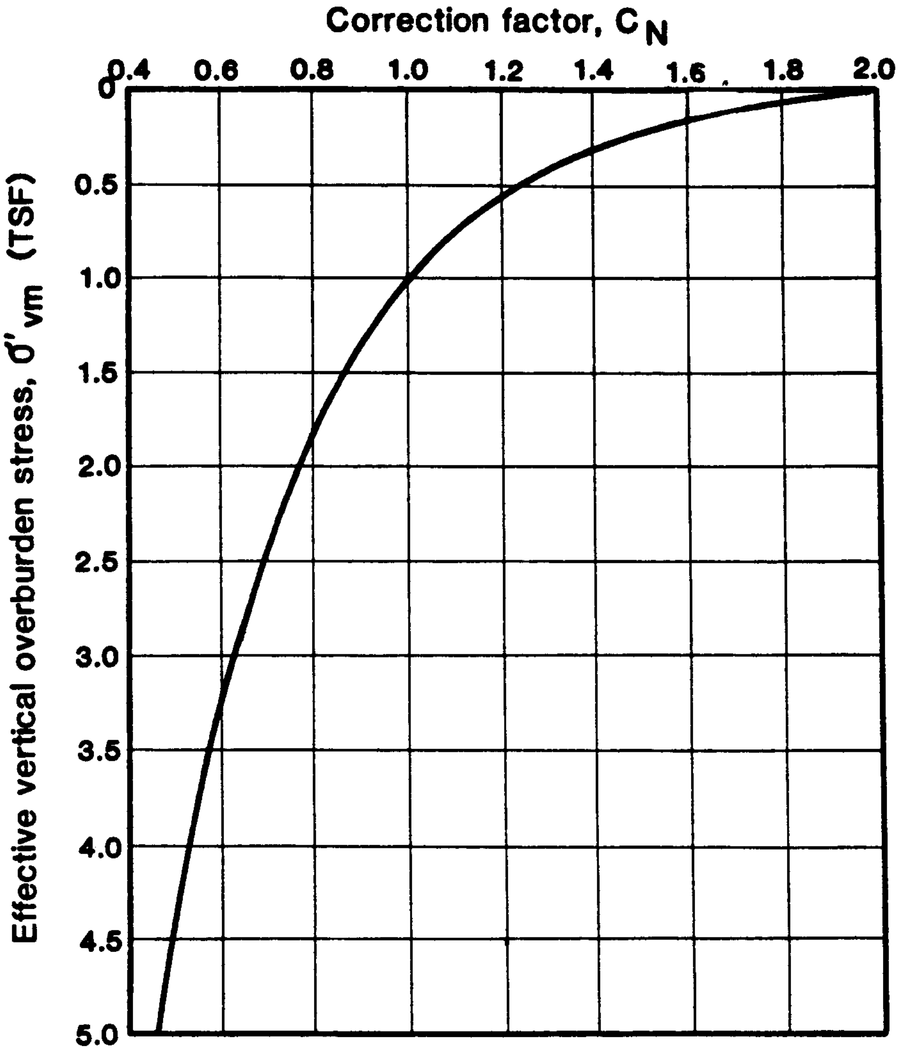

Fig. G4. Chart for correction of N-values in sand for influence of overburden pressure (reference value of effective overburden pressure is 1 ton/sq ft) (from Peck and others, 1974).

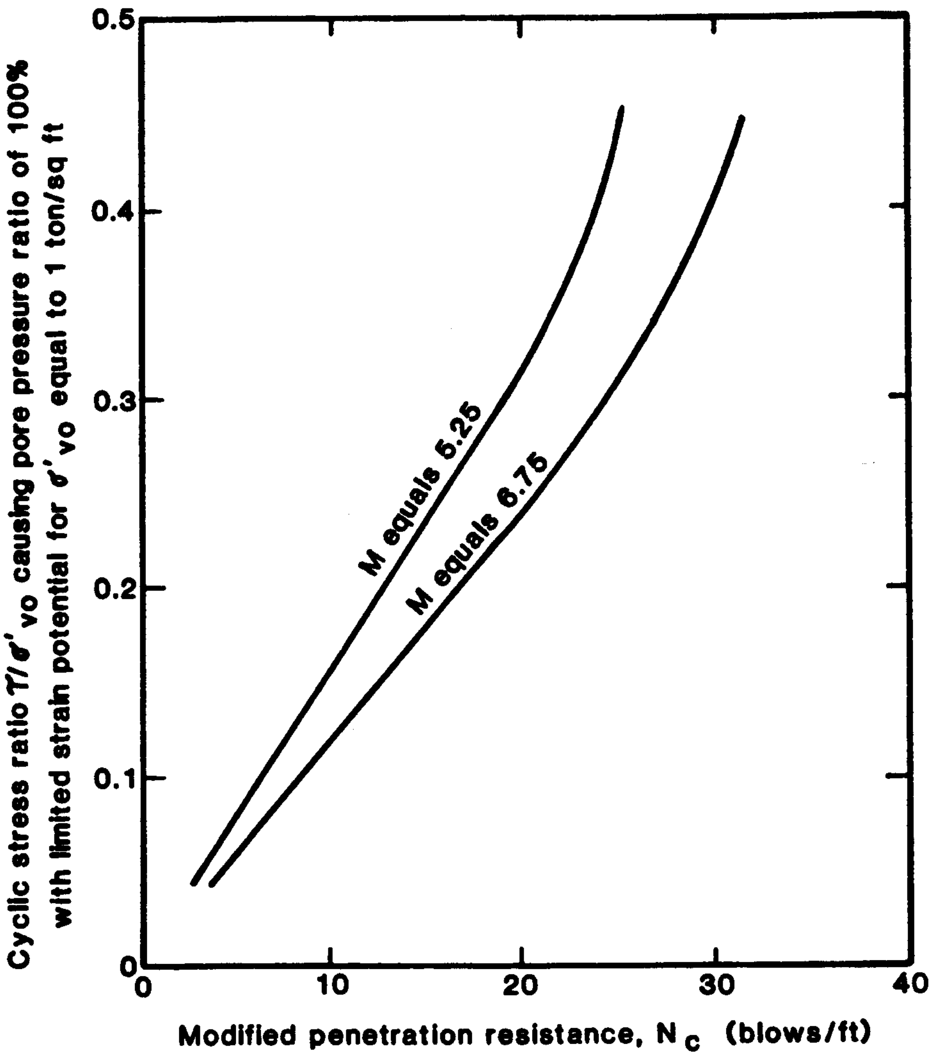

Fig. G5. Liquefaction resistance (τ/σ'_{vo}) versus modified penetration resistance (N_c) for different earthquake magnitudes (from Seed and Idriss, in press).

Table G2. Lowest stress ratios (τ/σ'_{vo}) and ground surface accelerations (a_{max}) necessary to induce liquefaction based on cone penetration test data.

CONE PENETRATION TEST		DEPTH >0.25 m	LOWEST τ/σ'_{vo} M = 5.25	LOWEST a_{max}(g) M = 5.25	LOWEST a_{max}(g) M = 6.75
674	X1	0.25	0.19	0.14	0.11
	X2	0.26	0.23	0.17	0.13
670	X1	0.80	0.20	0.14	0.10
	X2	0.45	0.21	0.14	0.11
	X3	0.49	0.17	0.11	0.09
	X4	0.27	0.22	0.15	0.12
668	X2	0.33	0.30	0.23	0.18
	X3	0.35	0.30	0.23	0.18
	X4	0.39	0.27	0.21	0.16
669	X1	0.27	0.25	0.19	0.15
	X2	0.30	0.26	0.20	0.15
671	X1	0.30	0.20	0.16	0.12
	X2	0.25	0.19	0.15	0.11
	X3	0.29	0.12	0.10	0.07
	X4	0.27	0.14	0.11	0.08
	X5	0.40	0.13	0.10	0.08
	X6	0.31	0.13	0.10	0.08
	X7	0.35	0.12	0.10	0.07
	X8	0.39	0.16	0.13	0.10
675	X1	1.05	0.18	0.15	0.11
	X2	0.56	0.16	0.13	0.10
	X3	0.28	0.15	0.12	0.09
	X4	0.28	0.18	0.14	0.11
677	X1	0.29	0.32	0.26	0.20
	X2	0.25	0.32	0.26	0.20
676	X2	0.60	0.16	0.10	0.07
673	X1	0.35	0.47	0.36	0.28
	X2	0.25	0.32	0.24	0.19
	X3	0.25	0.18	0.14	0.11
	X4	0.28	0.62	0.47	0.37
672	X1	0.28	0.14	0.08	0.06
	X2	0.52	0.13	0.07	0.06
679	X1	0.32	0.16	0.13	0.10
678	X2	0.25	0.16	0.13	0.10

Storm waves traveling over sediment in shallow water depths generate shear stresses similar to those induced by earthquakes. Liquefaction may occur if the resultant pore pressures increase sufficiently. The analysis consisted of two main parts: the stresses imparted to the seafloor were determined for design storms, and the cyclic characteristics of the sediment were measured in cyclic triaxial tests.

The shear stress ratio $\frac{\tau_c}{\sigma'_{vo}}$ at any subbottom depth induced by ocean waves was determined from (Seed and Rahman, 1978):

$$\frac{\tau_c}{\sigma'_{vo}} = \frac{\pi \gamma_w}{\gamma'} \quad \frac{H}{L} \left(\exp \frac{-2 \pi z}{L} \right) \left(\frac{1}{\cosh \frac{2 \pi d}{L}} \right) \qquad (6)$$

where: τ_c = horizontal cyclic shear stress at a particular subbottom depth;

σ'_{vo} = vertical effective stress at a particular subbottom depth;

γ_w = unit weight of salt water;

γ' = average buoyant unit weight of sediment above a particular subbottom depth;

H = sustained storm wave height;

L = wave length, determined from Fig. G6, assuming a wave period of 10 seconds (Clukey and others, 1980);

z = subbottom depth;

d = still water depth.

The average wave height was determined by multiplying the significant wave height for different return periods by 0.63 (McCormick and Thiruvathukal, 1976, p. 119) (Table G3). The shear stress ratios for different sustained wave heights at sites in the nothern Bering Sea are presented in Table G4.

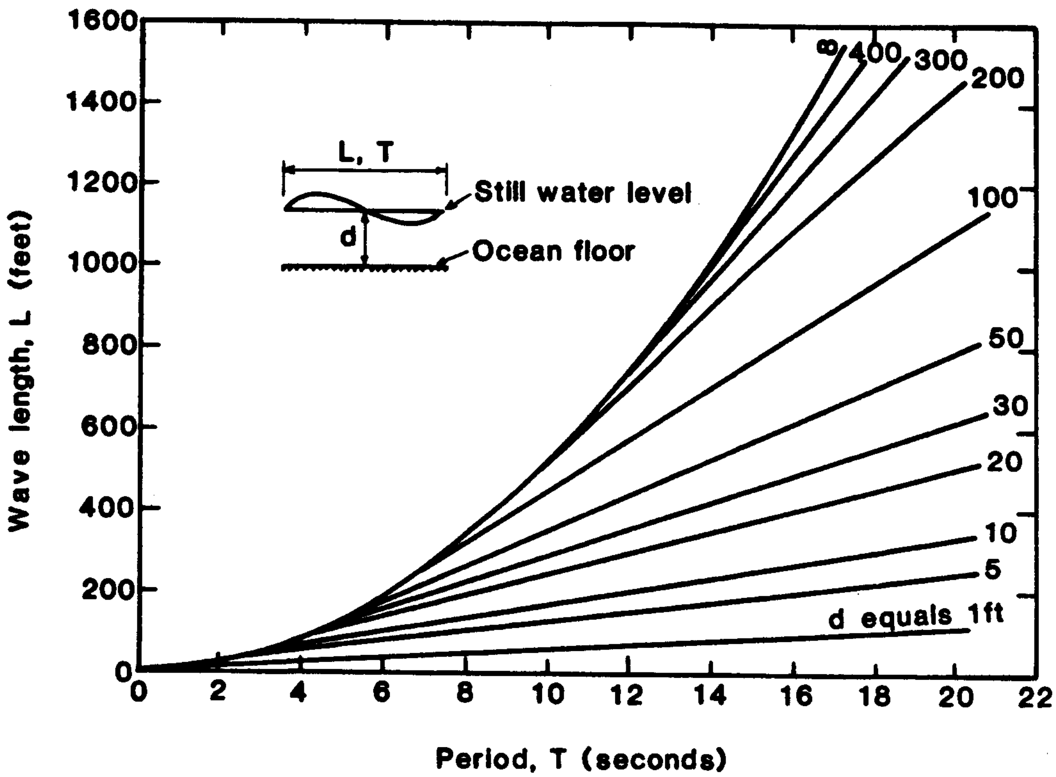

Fig. G6. Relationship between wave period, wavelength, and water depth (Wiegel, 1964, cited in Seed and Rahman, 1978).

Table G3. Estimated wind speeds and wave heights in the northern Bering Sea for different return periods (Arctic Environmental Information and Data Center, 1977).

RETURN PERIOD (YEARS)	MAXIMUM SUSTAINED WIND SPEED (KNOTS)	MAXIMUM SIGNIFICANT WAVE HEIGHT (m)	EXTREME WAVE HEIGHT (m)	AVERAGE (1) WAVE HEIGHT (m)
5	78	13.5	24.5	8.5
10	84	15.5	28.0	9.8
25	94	18.5	33.0	11.7
50	102	20.5	36.0	12.9
100	110	23.0	42.5	14.5 (2)

(1) Average wave height = 0.63 x significant wave height (McCormick and Thiruvathukal, 1976).

(2) Waves 14 m high will break in some Norton Sound areas, therefore 13 m high waves were assumed as a maximum value in the analysis. Actually, maximum sustained wave heights in the northern Bering Sea may be less than 13m because the relatively shallow water depths on the wide continental shelf dissipate wave energy.

Table G4. Storm wave induced cyclic stress ratios (τ_c/σ'_{vo}) at different subbottom depths (z) (determined from equation 6).

STATION/ CORE	z (m)	γ_w/γ' (kN/m³)	d (m)	T (sec)	L (m)	τ_c/σ'_{vo} H = 6m	τ_c/σ'_{vo} H = 7m	τ_c/σ'_{vo} H = 8m	τ_c/σ'_{vo} H = 9m	τ_c/σ'_{vo} H = 10m	τ_c/σ'_{vo} H = 11m	τ_c/σ'_{vo} H = 12m	τ_c/σ'_{vo} H = 13 m
679	0.25	0.94	20	10	122	0.09	0.11	0.12	0.14	0.15	0.17	0.18	0.20
	0.5	0.94				0.09	0.10	0.12	0.13	0.15	0.16	0.18	0.19
	1.0	0.94				0.09	0.10	0.12	0.13	0.15	0.16	0.17	0.19
	1.5	0.94				0.09	0.10	0.11	0.13	0.14	0.16	0.17	0.18
	2.0	0.94				0.08	0.10	0.11	0.12	0.14	0.15	0.17	0.18
	2.5	0.94				0.08	0.09	0.11	0.12	0.13	0.15	0.16	0.18
	3.0	0.94				0.08	0.09	0.11	0.12	0.13	0.14	0.16	0.17
	4.0	0.93				0.07	0.09	0.10	0.11	0.12	0.14	0.15	0.16
	5.0	0.93				0.07	0.08	0.09	0.11	0.12	0.13	0.14	0.15
681A2	0.25	0.97	30	10	140	0.06	0.07	0.08	0.09	0.10	0.12	0.13	0.14
	0.5	0.97				0.06	0.07	0.08	0.09	0.10	0.11	0.12	0.13
	1.0	0.97				0.06	0.07	0.08	0.09	0.10	0.11	0.12	0.13
	1.5	0.96				0.06	0.07	0.08	0.09	0.10	0.11	0.12	0.13
	2.0	0.96				0.06	0.07	0.08	0.09	0.10	0.11	0.12	0.12
	2.5	0.96				0.06	0.07	0.08	0.08	0.09	0.10	0.11	0.12
	3.0	0.95				0.06	0.06	0.07	0.08	0.09	0.10	0.11	0.12
	4.0	0.94				0.05	0.06	0.07	0.08	0.09	0.09	0.10	0.11
	5.0	0.93				0.05	0.06	0.07	0.07	0.08	0.09	0.10	0.11
682A1	0.25	1.69	20	10	122	0.16	0.19	0.22	0.24	0.27	0.30	0.33	0.35
	0.5	1.69				0.16	0.19	0.21	0.24	0.27	0.30	0.32	0.35
	1.0	1.68				0.16	0.18	0.21	0.23	0.26	0.29	0.31	0.34
	1.5	1.67				0.15	0.18	0.20	0.23	0.25	0.28	0.30	0.33
	2.0	1.66				0.15	0.17	0.20	0.22	0.24	0.27	0.29	0.32
	2.5	1.63				0.14	0.16	0.19	0.21	0.23	0.26	0.28	0.30
	3.0	1.60				0.13	0.16	0.18	0.20	0.22	0.25	0.27	0.29
	4.0	1.58				0.13	0.15	0.17	0.19	0.21	0.23	0.25	0.27
	5.0	1.55				0.12	0.14	0.16	0.18	0.20	0.21	0.23	0.25
683A1	0.25	1.01	20	10	122	0.10	0.11	0.13	0.15	0.16	0.18	0.20	0.21
	0.5	1.01				0.10	0.11	0.13	0.14	0.16	0.18	0.19	0.21
	1.0	1.01				0.09	0.11	0.13	0.14	0.16	0.17	0.19	0.20
	1.5	1.01				0.09	0.11	0.12	0.14	0.15	0.17	0.18	0.20
	2.0	1.01				0.09	0.10	0.12	0.13	0.15	0.16	0.18	0.19
	2.5	1.01				0.09	0.10	0.12	0.13	0.14	0.16	0.17	0.19
	3.0	1.01				0.08	0.10	0.11	0.13	0.14	0.16	0.17	0.18
	4.0	1.01				0.08	0.09	0.11	0.12	0.13	0.15	0.16	0.17
	5.0	1.01				0.08	0.09	0.10	0.11	0.13	0.14	0.15	0.17
684A1	0.25	0.94	20	10	122	0.09	0.11	0.12	0.14	0.15	0.17	0.18	0.20
	0.5	0.94				0.09	0.10	0.12	0.13	0.15	0.16	0.18	0.19
	1.0	0.94				0.09	0.10	0.12	0.13	0.15	0.16	0.17	0.19
	1.5	0.94				0.09	0.10	0.11	0.13	0.14	0.16	0.17	0.18
	2.0	0.94				0.08	0.10	0.11	0.12	0.14	0.15	0.17	0.18
	2.5	0.94				0.08	0.09	0.11	0.12	0.13	0.15	0.16	0.18
	3.0	0.94				0.08	0.09	0.11	0.12	0.13	0.14	0.16	0.17
	4.0	0.93				0.07	0.09	0.10	0.11	0.12	0.14	0.15	0.16
	5.0	0.93				0.07	0.08	0.09	0.11	0.12	0.13	0.14	0.15
685A2	0.25	1.26	18	10	120	0.13	0.15	0.18	0.20	0.22	0.24	0.26	0.29
	0.5	1.26				0.13	0.15	0.17	0.20	0.22	0.24	0.26	0.28
	1.0	1.26				0.13	0.15	0.17	0.19	0.21	0.23	0.25	0.28
	1.5	1.25				0.12	0.14	0.16	0.18	0.20	0.23	0.25	0.27
	2.0	1.25				0.12	0.14	0.16	0.18	0.20	0.22	0.24	0.27
	2.5	1.24				0.12	0.13	0.15	0.17	0.19	0.21	0.23	0.25
	3.0	1.23				0.11	0.13	0.15	0.17	0.19	0.20	0.22	0.24
	4.0	1.21				0.10	0.12	0.14	0.16	0.17	0.19	0.21	0.23
	5.0	1.20				0.10	0.11	0.13	0.15	0.16	0.18	0.20	0.21
686A1	0.25	0.98	18	10	120	0.10	0.12	0.14	0.15	0.17	0.19	0.21	0.22
	0.5	0.98				0.10	0.12	0.14	0.15	0.17	0.19	0.20	0.22
	1.0	0.98				0.10	0.12	0.13	0.15	0.16	0.18	0.20	0.21
	1.5	0.98				0.10	0.11	0.13	0.14	0.16	0.18	0.19	0.21
	2.0	0.98				0.09	0.11	0.13	0.14	0.16	0.17	0.19	0.20
	2.5	0.98				0.09	0.11	0.12	0.14	0.15	0.17	0.18	0.20
	3.0	0.98				0.09	0.10	0.12	0.13	0.15	0.16	0.18	0.19
	4.0	0.98				0.08	0.10	0.11	0.13	0.14	0.15	0.17	0.18
	5.0	0.98				0.08	0.09	0.11	0.12	0.13	0.15	0.16	0.17
687A1	0.25	1.04	18	10	120	0.11	0.13	0.15	0.16	0.18	0.20	0.22	0.24
	0.5	1.04				0.11	0.13	0.14	0.16	0.18	0.20	0.22	0.23
	1.0	1.04				0.10	0.12	0.14	0.16	0.17	0.19	0.21	0.23
	1.5	1.04				0.10	0.12	0.14	0.15	0.17	0.19	0.20	0.22
	2.0	1.04				0.10	0.12	0.13	0.15	0.17	0.18	0.20	0.22
	2.5	1.04				0.10	0.11	0.13	0.15	0.16	0.18	0.19	0.21
	3.0	1.04				0.09	0.11	0.13	0.14	0.16	0.17	0.19	0.20
	4.0	1.03				0.09	0.10	0.12	0.13	0.15	0.16	0.18	0.19
	5.0	1.03				0.08	0.10	0.11	0.13	0.14	0.15	0.17	0.18

The laboratory stress ratios necessary to cause 5 percent strain after 360 cycles (a storm duration of one hour with a wave period of 10 seconds, Clukey and others, 1980) (Fig. 9) were corrected using equation 2 to simulate field conditions (Table G5). A comparison of the stresses induced by storm waves (Table G4) with the corrected cyclic sediment resistance (Table G5) revealed the sustained wave height necessary to cause liquefaction to a particular subbottom depth (Table G6). The above analysis does not account for drainage during storm events; this is a very conservative assumption.

Analysis 4: Cone penetration data was modified using an earthquake associated procedure to yield values that are related to wave heights necessary to cause liquefaction.

The final analysis consists of portions of analyses 2 and 3. The smallest shear stress ratio (τ/σ'_{vo}) (Table G2) for each CPT determined from Fig. G5 (assuming M=5.25) was compared to the cyclic shear stress ratio (τ_c/σ'_{vo}) induced by storm waves (Table G4). The minimum wave heights necessary to equalize the stress ratios are presented in Table 9. Although the values show relative susceptibility to liquefaction between stations, they do not represent actual wave heights.

Table G5. Resistance to liquefaction at different subbottom depths expressed as a field stress ratio (τ_h/σ'_{vo}) (determined from cyclic triaxial test data ($\tau_{cyc\ ave\ max}/\sigma'_c$) corrected for laboratory conditions using equation 2).

CORE	DEPTH (m)	c_m	ϕ' degrees	OCR	K_o (1)	C_r	$\tau_{cyc\ ave\ max}/\sigma'_c$ (2) (triaxial)	τ_h/σ'_{vo} (field)	$\tau_{cyc\ ave\ max}/\sigma'_c$ (2) (triaxial) OCR = 6	τ_h/σ'_{vo} (field)
681A2	0.25	1.0	37	42	1.0(3.78)	1.0	0.22	0.22		
	0.5			39	1.0(3.61)	1.0		0.22		
	1.0			32	1.0(3.21)	1.0		0.22		
	1.5			27	1.0(2.89)	1.0		0.22		
	2.0			22	1.0(2.56)	1.0		0.22		
	2.5			17	1.0(2.19)	1.0		0.22		
	3.0			15	1.0(2.03)	1.0		0.22		
	4.0			11	1.0(1.69)	1.0		0.22		
	5.0			8	1.0(1.39)	1.0		0.22		
682A1	0.25	1.0	35	13	1.0(1.86)	1.0	0.23	0.23	0.91	0.91
	0.5			12	1.0(1.77)	1.0		0.23		0.91
	1.0			11	1.0(1.69)	1.0		0.23		0.91
	1.5			9	1.0(1.50)	1.0		0.23		0.91
	2.0		40	8	1.0(1.36)	1.0		0.23		0.91
	2.5			7	1.0(1.25)	1.0		0.23		0.91
	3.0			7	1.0(1.25)	1.0		0.23		0.91
	4.0			5	1.0(1.01)	1.0		0.23		0.91
	5.0			4	0.87	0.92		0.21		0.84
684A1	0.25	1.0	38	50	1.0(4.27)	1.0	0.33	0.33		
	0.5			39	1.0(3.67)	1.0		0.33		
	1.0			23	1.0(2.65)	1.0		0.33		
	1.5			14	1.0(1.95)	1.0		0.33		
	2.0			8	1.0(1.38)	1.0		0.33		
	2.5			5	1.0(1.04)	1.0		0.33		
	3.0			3	0.76	0.85		0.28		
	4.0			1	0.38	0.61		0.20		
	5.0			1	0.38	0.61		0.20		
685A2	0.25	1.0	37	25	1.0(2.76)	1.0	0.20	0.20	0.77	0.77
	0.5			23	1.0(2.63)	1.0		0.20		0.77
	1.0			19	1.0(2.34)	1.0		0.20		0.77
	1.5			16	1.0(2.11)	1.0		0.20		0.77
	2.0			13	1.0(1.86)	1.0		0.20		0.77
	2.5			11	1.0(1.69)	1.0		0.20		0.77
	3.0			9	1.0(1.49)	1.0		0.20		0.77
	4.0			6	1.0(1.17)	1.0		0.20		0.77
	5.0			4	0.92	0.95		0.19		0.73
686A1	0.25	1.0	42	>100	1.0(7.21)	1.0	0.35	0.35	0.57	0.57
	0.5			90	1.0(6.72)	1.0		0.35		0.57
	1.0			56	1.0(4.89)	1.0		0.35		0.57
	1.5			38	1.0(3.77)	1.0		0.35		0.57
	2.0			26	1.0(2.93)	1.0		0.35		0.57
	2.5			17	1.0(2.20)	1.0		0.35		0.57
	3.0			12	1.0(1.74)	1.0		0.35		0.57
	4.0			5	0.97	0.98		0.34		0.56
	5.0			2	0.53	0.71		0.25		0.40
687A1	0.25	1.0	38	94	1.0(6.30)	1.0	0.26	0.26		
	0.5			75	1.0(5.48)	1.0		0.26		
	1.0			49	1.0(4.22)	1.0		0.26		
	1.5			32	1.0(3.25)	1.0		0.26		
	2.0			21	1.0(2.50)	1.0		0.26		
	2.5			14	1.0(1.95)	1.0		0.26		
	3.0			9	1.0(1.49)	1.0		0.26		
	4.0			4	0.90	0.94		0.24		
	5.0			2	0.59	0.74		0.19		

(1) Maximum allowed K_o = 1.0.

(2) Stress ratio required to induce 5% strain in cyclic triaxial test samples after 360 loading cycles (storm wave period = 10 sec for 1 hour duration).

Table G6. Sustained storm wave heights (H) necessary to induce liquefaction in sediment from different stations (determined from a comparison of wave induced stresses in Table G4 with the corrected cyclic sediment resistance in Table G5).

CORE	H	D_L	H	D_L	H	D_L	H	D_L	H (1) OCR = 6
681A2	>13	0							
682A1	9	1.5	10	2.5	11	5.0	12	>5.0	>13
684A1	>13	0							
685A2	9	0.5	10	2.0	11	3.0	12	>5.0	>13
686A1	>13	0							>13
687A1	>13	0							

H = Wave height necessary to cause liquefaction.

D_L = Subbottom depth to which liquefaction may occur.

(1) = Wave heights necessary to liquefy sediment based on overconsolidated triaxial test samples.

SEAFLOOR HAZARDS AND RELATED SURFICIAL GEOLOGY, NAVARIN BASIN PROVINCE, NORTHERN BERING SEA

by

Herman A. Karl and Paul R. Carlson

U.S. Geological Survey

Final Report
Outer Continental Shelf Environmental Assessment Program
Research Unit 588

January 1983

TABLE OF CONTENTS

LIST OF FIGURES

Appendix Figures:

Figure G1. Sketch map of study area in northern Bering Sea, showing locations of high-resolution seismic-reflection lines, sample stations, and areas of seafloor features.

Figure G2. Seafloor morphologic features in head of Navarinsky Canyon, showing locations of illustrated profiles. Bathymetry after Fischer and others, 1982. Contour interval, 200 m.

Figure G3. Seismic-reflection profiles in head of Navarinsky Canyon. (a) Line drawing of seismic-reflection profiles (20-40-in^3 airguns), showing relative positions of profiles in Figures G3b, G3c, and G4a. (b) Minisparker profile (1,000 J), showing sand waves. (c) Minisparker profile (1,000 J), showing pull-aparts (arrows). Vertical exaggeration (V.E.) ~7.5x. See Figure G2 for locations.

Figure G4. High-resolution profiles, showing slide zone in Navarinsky Canyon. (a) 3.5 kHz profile; V.E. ~10x. (b) Uniboom profile (1200 J); V.E. ~7.5x. See Figure G2 for locations.

Figure H1. Map of study area showing seismic survey tracklines and distribution of sand waves (stippled areas). Dashed lines are 1980 tracklines and solid lines are 1981 tracklines; 1981 data were collected during preparation of this manuscript; for clarity tracklines have not been shown within sand wave fields. The deeper sand wave area in Pervenets Canyon was defined almost entirely by buried bed forms.

Fgure H2. Example of Navarinsky Canyon field sand waves; A: Minisparker record. B: Interpretive drawing; solid lines define sets of sand waves; dashed lines define angle of climb; heavy vertical dashed line is a recorder time mark.

Figure H3. Paleogeographic reconstruction of the depositional setting of the sand waves (stippled areas). Heavy solid line follows the present shelf edge and indicates the position of the Pleistocene shoreline assuming an arbitrary amount of tectonic and isostatic influence that caused local sea level to be 150 m below present sea level. Dashed line follows the present 130 m isobath. The area between these lines is that part of the shelf that would be submerged under 20 m of water assuming no local complications and only that sea level was lower eustatically by 130 m. Presence of steams is speculative.

LIST OF TABLES

OVERVIEW

I. Summary of Objectives, Conclusions and Implications with Respect to OCS Oil and Gas Development.

The principal objective of this study is to provide interpretive maps and reports of seafloor hazards in the Navarin Basin province preparatory for OCS lease sale 83 presently scheduled for December, 1984. Several geologic processes that are active in Navarin Basin province are potentially hazardous to commercial development. Preliminary conclusions and implications pertaining to OCS development follow:

1. Navarin Basin province appears to be an area of low seismicity and no faults mapped to date rupture the seafloor. However, several faults indicate movement in the last 12,000 years and, thus, are potentially active.

2. Submarine landslides are common in the heads of submarine canyons and on the upper continental slope and must be considered in the design of any seafloor structures.

3. Fields of large sediment waves have been discovered near the heads of the three large canyons. These sediment waves if active could be hazardous to seafloor structures.

4. Gas-charged sediment, present throughout a large part of the province, has reduced strength and bearing capacity as compared to strength of gas-free sediment.

5. Intense storms produce exceptionally large waves which are not only capable of eroding bottom sediment, but are also dangerous to surface structures and vessels.

6. Sea-ice commonly covers much of the Navarin Basin province for several months of the year and could pose a problem to exploration, development, or production of oil and gas during years of heavy concentrations.

II. Introduction

A. General Nature and Scope of Study

Navarin Basin province is an OCS (Outer Continental Shelf) lease sale area that is scheduled for leasing in 1984. This basin potentially contains vast accumulations of oil and gas and with the escalating energy problems will be the subject of extensive exploration activity. Preliminary to the sale, an environmental impact statement must be released by BLM. Our study in Navarin Basin will provide information about the seafloor geologic hazards that need to be considered during the exploration for and developement of petroleum on the outer continental shelf. No previous geohazards investigations had been conducted in the Navarin Basin province. Thus, we began in the summer of 1980, to collect reconnaissance geophysical and geological data. This report includes preliminary findings from the 1980 and 1981 field seasons.

B. Specific Objectives

The specific objectives of this final report are to synthesize the results of the 1980 and 1981 field seasons and to update the maps and interpretations presented in the 1980 annual report. These objectives are accomplished by including chapters on various specific topics newly written for this report by experts and by appending reports and papers written and published in the interval of time that occurred after the release of the 1980 annual report and before preparation of this final report.

C. Relevance to Problems of Petroleum Development

The Navarin Basin province encompasses an area of 45,000 km^2 and contains three sedimentary basins filled with thick sequences of Cenozoic strata. Interpretation of the stratigraphy and structure of these basins suggests areas which could trap accumulations of economically exploitable hydrocarbon deposits. The province, which includes the outer continental shelf and upper slope, is deeply dissected by large submarine canyons. The steep gradients within the canyons and along the upper continental slope result in potential instability problems in a large part of the province. Zones of gas-charged sediment that also may cause problems of seafloor instability are present over much of the outer continental shelf in the Navarin province. All areas of unstable seafloor must be carefully considered during the design and the installation of exploration and development platforms. Preliminary data from this potential petroleum province have revealed the existence of large bedforms near the heads of the large submarine canyons. The potential impact of these bedforms as well as the occurrences of gas-charged sediment and sediment slides must be considered during development phases when planning pipelines and holding tanks.

III. Current State of Knowledge

Prior to the summer of 1980, no geohazards data had been collected in the Navarin Basin province. Several marine geology and geophysics cruises to the Bering Sea had, however, collected data adjacent to and even within part of the province. The thick sedimentary sequence that makes up Navarin Basin was first discovered on a 1970 cruise of the R/V BARTLETT (Scholl and others, 1975, 1976). Marlow and others (1976) named this 10-15 km thick sedimentary sequence of Mesozoic and Cenozoic age deposits. However, detailed mapping of the "acoustic basement" was not completed until seismic-reflection surveys of 1976, 1977, and 1980 provided multi-channel coverage necessary to allow delineation of the northwest-trending basins (Marlow and others, 1981).

The Russians published the first generalized maps of sediment distribution in the study area (Lisitsyn, 1966). Without access to the original data, we only have been able to extract a few data points along the northern border of the Navarin province which we are using to supplement our sediment distribution maps. Of much greater use are data from the University of Washington cores and grab samples, some of which were collected in the eastern part of the Navarin Basin (Knebel, 1972). Other studies that will provide comparative sedimentologic data have been conducted in adjacent parts of the Bering Sea (Anadyr Basin: Kummer and Creager, 1971; Bristol Bay:

Sharma and others, 1977; Kvenvolden and others, 1979; Drake and others, 1980; St. George Basin, Gardner and others, 1980; Vallier and others, 1980).

Although oceanographic data have been gathered from the Bering Sea for at least 100 years (Dall, N. H., 1881 to Cacchione and others, 1982) and by scientists from numerous countries (e.g. USSR-Natarov, 1963; Japan-Takenouti and Ohtani, 1974; U.S.A.-Hughes and others, 1974), very little is known about the details of circulation and other oceanographic parameters within the Navarin Basin province. These other studies have involved water mass characteristics (Sayles and others, 1979) or large scale circulation (Hughes and others, 1974) of the entire Bering Sea or the deep Aleutian Basin or have concentrated on movement and characteristics of the water in and through the major outlets, the Bering Strait (Coachman and others, 1975) or the passes in the Aleutian Chain (Favorite, 1974).

Sea-ice is often present throughout most of the Navarin Basin province for about five months of the year, January through May. Whereas the average monthly limit of sea-ice in the Bering Sea has been determined (Webster, 1979), little is known about the movement and deformation of the sea-ice field (Tabata, 1974). The increasing availability of satellite imagery (Muench, 1974; Ahlnas and Wendler, 1980) together with winter field work (Drake and others, 1979; Paquette and Bourke, 1980) will provide needed detailed information helping to delineate the sea-ice fields in the Navarin Basin province.

IV. Study Area

The Navarin Basin province is located on the outer continental shelf and upper slope in the northwestern Bering Sea (Fig. 1). This promising petroleum region, scheduled for lease sale in 1984, is bounded on the northwest by the U.S.-USSR Convention Line of 1867, on the southwest by the base of the continental slope and extends to within 100 km of St. Matthew Island to the northeast and St. Paul Island to the southeast, an area of about 45,000 km^2. This province consists of a very flat continental shelf (average gradient 0.02°) and a rugged continental slope (gradient ranges from 3° to 8°) that has been deeply dissected by five large submarine canyons. Bathymetric maps of the Bering Sea constructed by Pratt and Walton (1974) and Schumacher (1976), include very limited bathymetric data from the Navarin area. We have made a more detailed bathymetric map (Fig. 2) of the study area by combining the bathymetric data obtained on the DISCOVERER cruises of 1980 and 1981 and the R/V S.P. LEE cruise of 1982 with data from several U.S. Geological Survey cruises during the past decade (Scholl, Buffington, and Marlow, 1976; Marlow and Cooper, 1979). The map and a discussion of the morphology of the Navarin continental margin are included in the appended results section (Fischer and others, 1982).

V. Sources, Methods and Rationale of Data Collection

The principal sources of data for this study have been the seismic reflection profiles and sediment samples collected on the 1980 and 1981 R/V DISCOVERER cruises (Carlson and Karl, 1981, 1982; Karl and Carlson, 1982). Some additional data were collected in 1980 from the USCG POLAR STAR and in

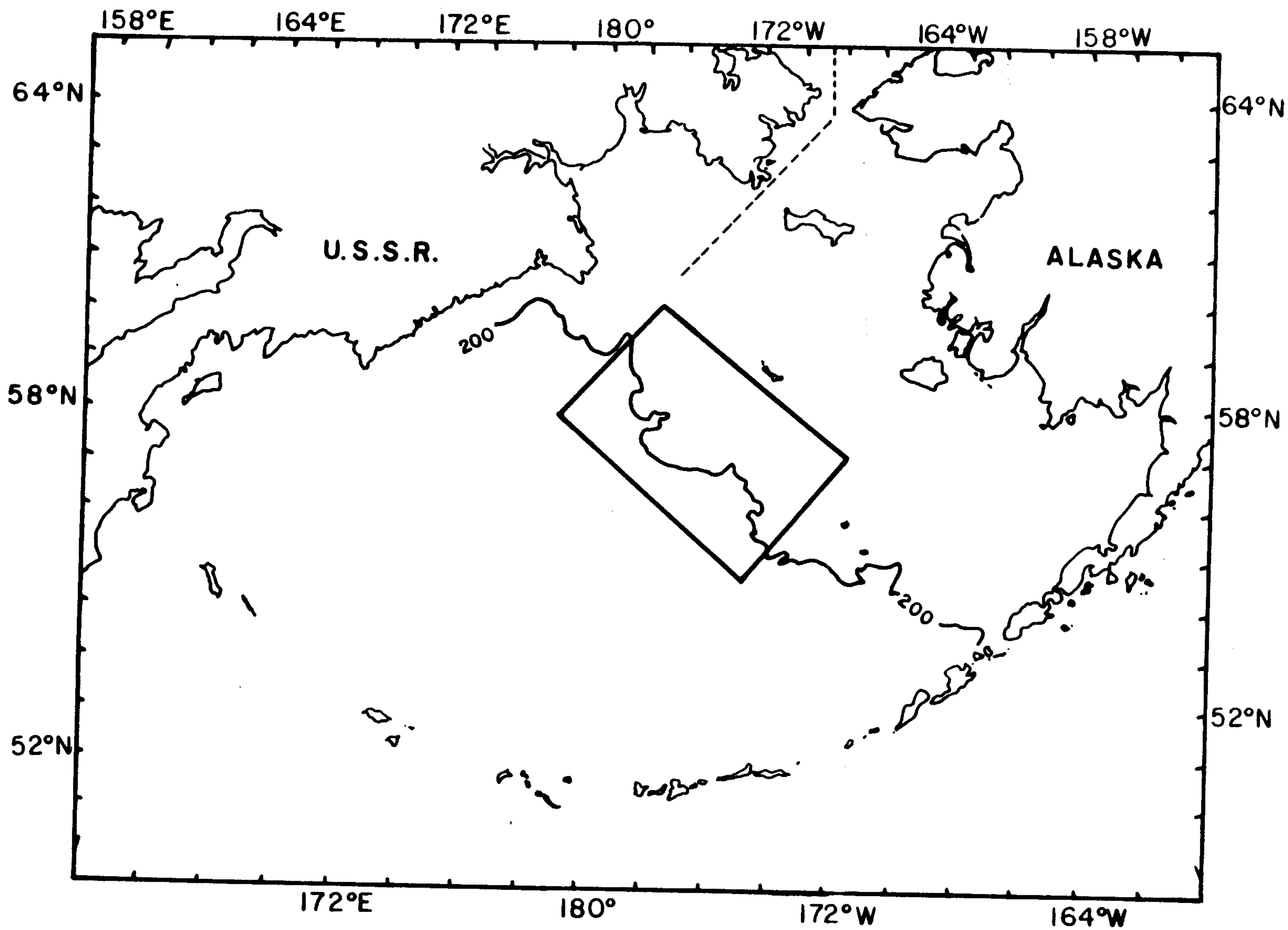

Figure 1. Location map of Navarin Basin province.

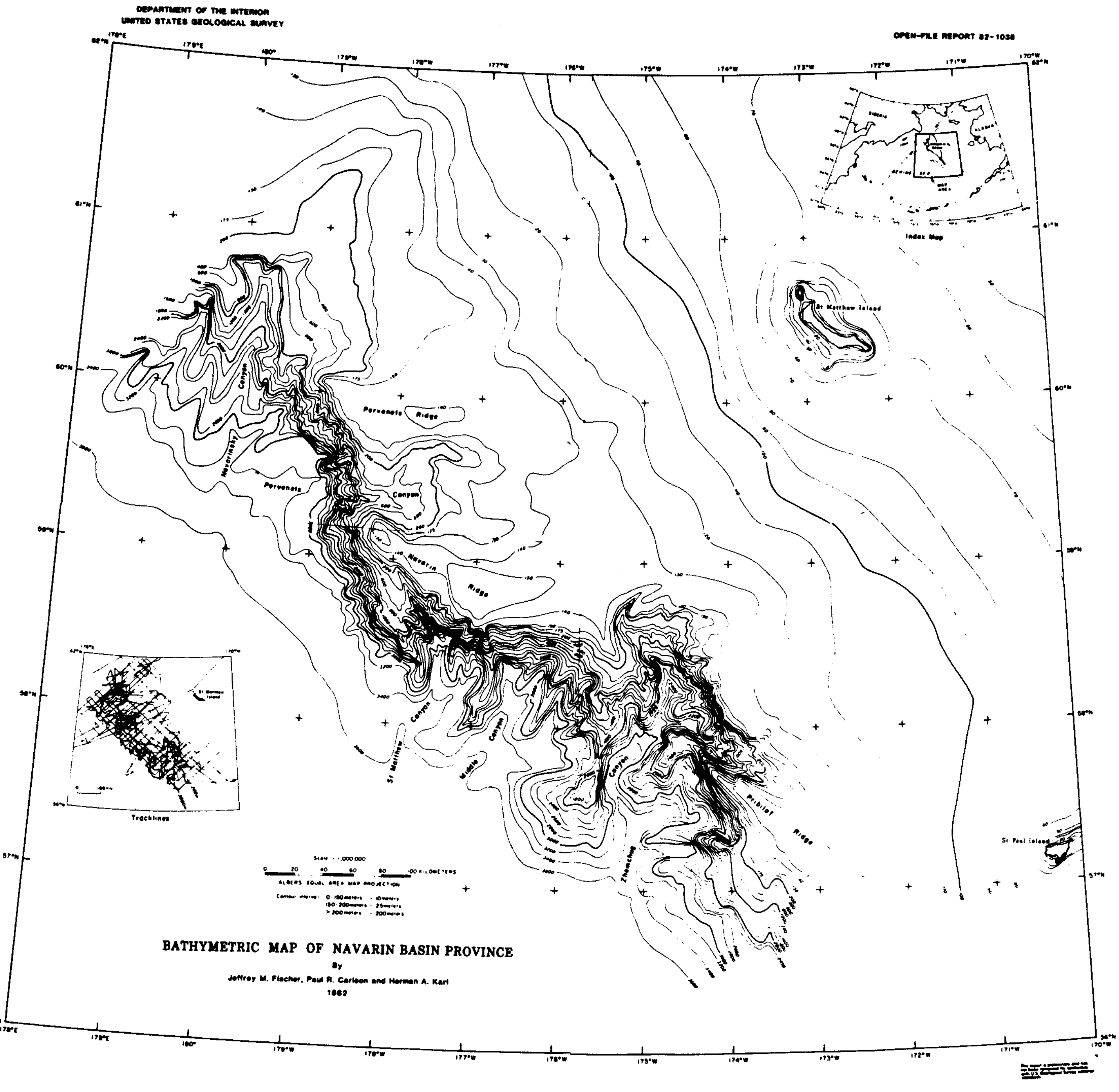

Figure 2. Bathymetric map of Navarin Basin province.

1980 and 1982 from the R/V S.P. LEE. We are also incorporating into our data base seismic reflection records that were collected over the past fifteen years by the U.S.G.S. for resource evaluation (Marlow and others, 1981). Other sources of data include studies by the University of Washington and the University of Alaska, Russian and Japanese scientists (e.g., Knebel, 1972; Sharma, 1979; Lisitsyn, 1966; Takenouti and Ohtani, 1974).

We acknowledge the assistance provided by the officers and crew of the NOAA ship DISCOVERER during the two cruises which comprise the principal source of data for this report. During DISCOVERER cruises DC 4/5-80-BS/NB (July 2 - August 17, 1980) the scientific party collected 6700 line km of seismic reflection profiles, 104 gravity cores, 10 grab samples, and 1 dredge sample (Figs. 3, 5); 8050 line km of seismic reflection profiles, 88 gravity cores, 10 grab samples, 6 box cores, and 5 vibracores were collected during DISCOVERER cruise DC 2/3-81-BS/NB (Figs. 4, 5). NOAA officers and survey technicians provided navigational control using LORAN C and satellite fixes.

Following is a list of the U.S.G.S. scientific party on each cruise.

DC 4/5-80-BS/NB:

Paul Carlson	Co-Chief scientist
Herman Karl	Co-Chief scientist
Brian Edwards	Engineering Geologist
Jeff Fischer	Physical Science Technician
George Ford	" " "
Sarah Griscom	" " "
Ken Johnson	" " "
Beth Lamb	Data coordinator
Grant Lichtman	Physical Science Technician
Paula Quinterno	Micropaleontologist
Jeff Rupert	Mechanical Technician
John Saladin	Electronics Technician
Rick Vail	Electronics Technician
Tim Vogel	Geochemist
Pat Wiberg	Physical Science Technician
Bob Wilson	Mechanical Technician
Mark Yeats	Physical Science Technician

DC 2/3-81-BS/NB:

Paul Carlson	Chief Scientist, DC 2
Herman Karl	Chief Scientist, DC 3
Jack Baldauf	Micropaleontologist
Neal Barnes	Geologist
Mike Bennett	Engineering Geologist
Dave Blunt	Geochemist
Drew Comer	Geologist (MMS)
Merid Dates	Physical Science Technician
John Eriksen	Mechanical Technician
Jeff Fischer	Physical Science Technician
Dan Hurlburt	Mechanical Technician
Ken Johnson	Physical Science Technician
Jim Joyce	Physical Science Technician

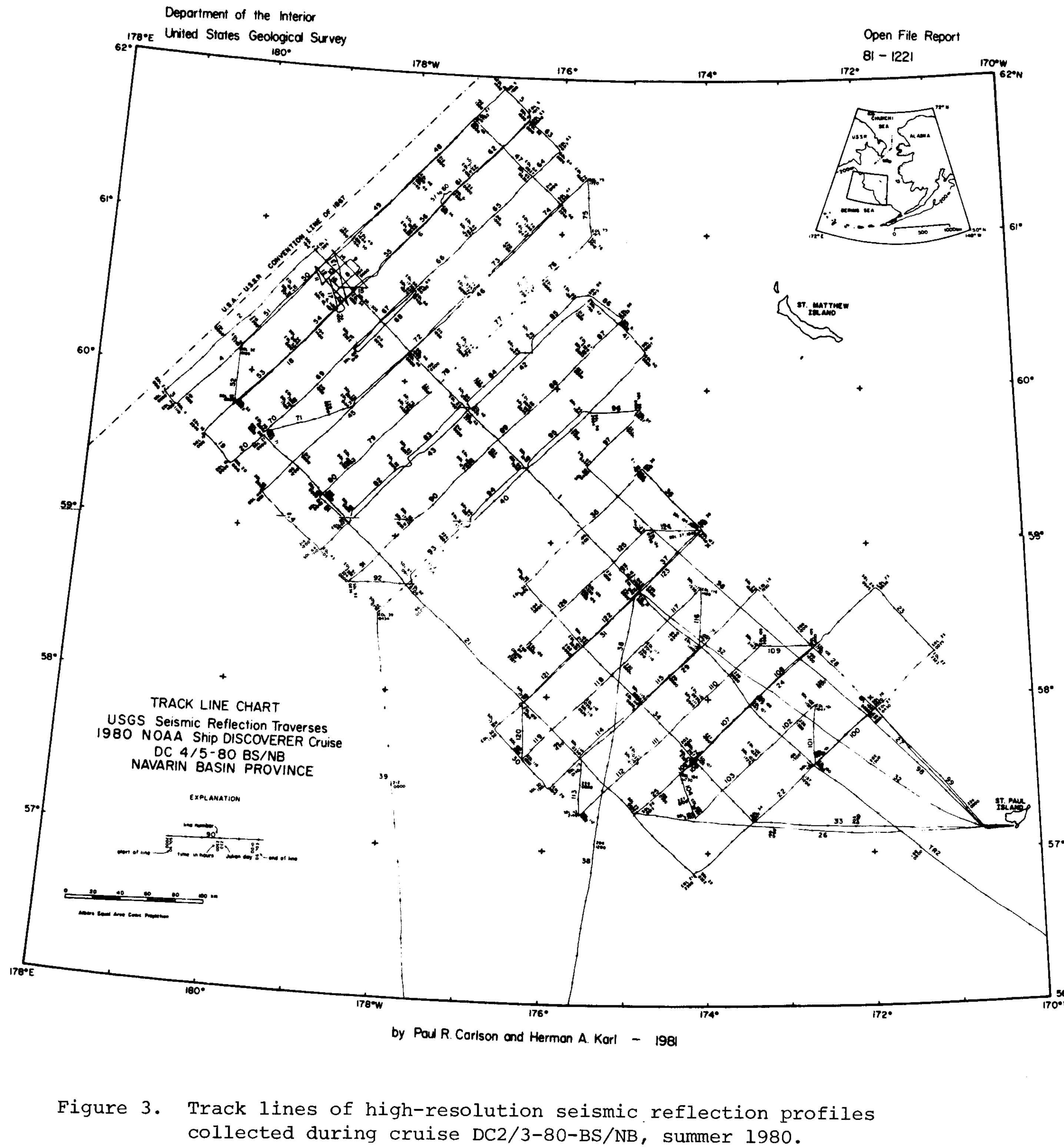

Figure 3. Track lines of high-resolution seismic reflection profiles collected during cruise DC2/3-80-BS/NB, summer 1980.

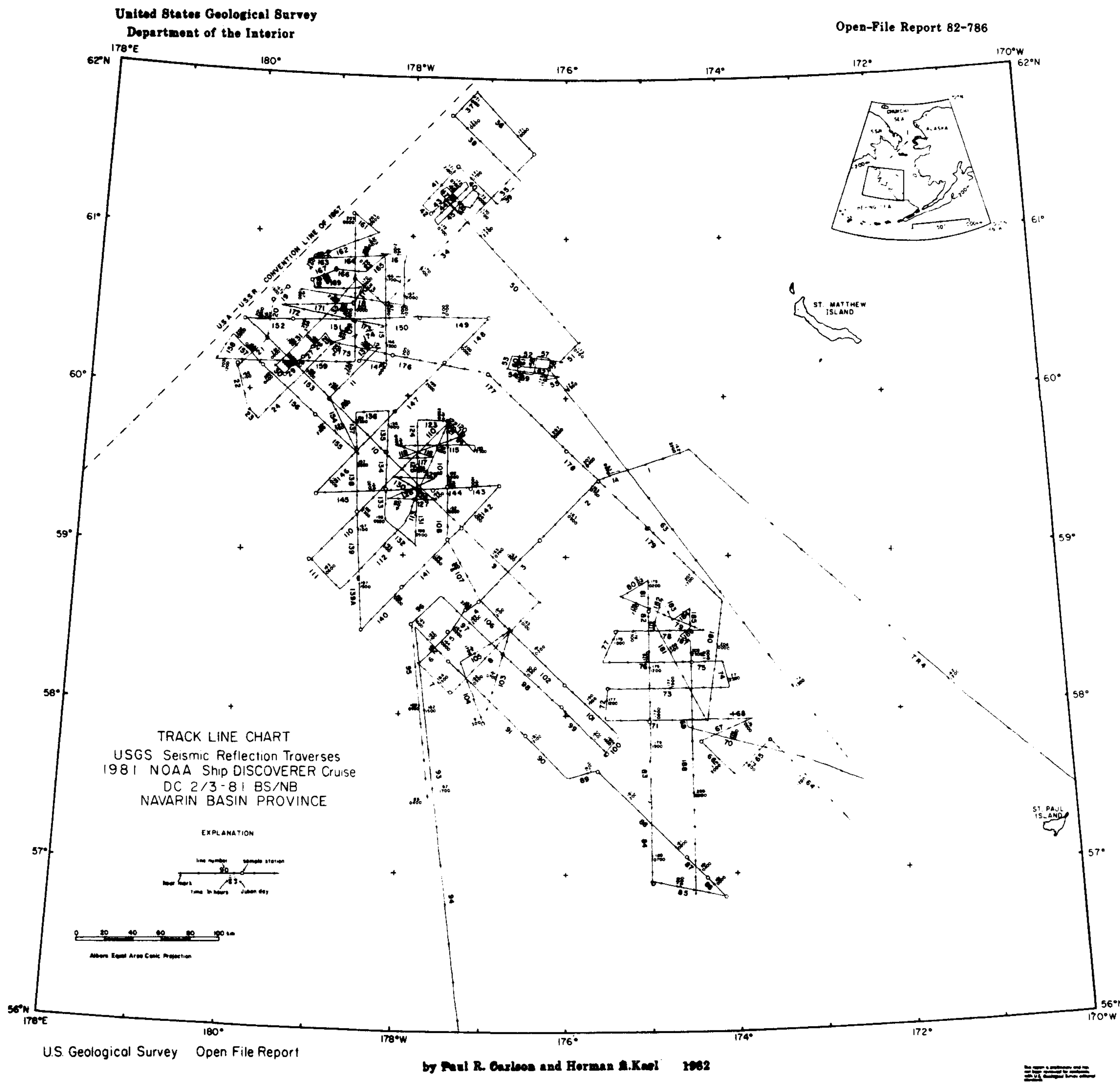

Figure 4. Track lines of high-resolution seismic reflection profiles collected during cruise DC4/5-81-BS/NB, summer, 1981.

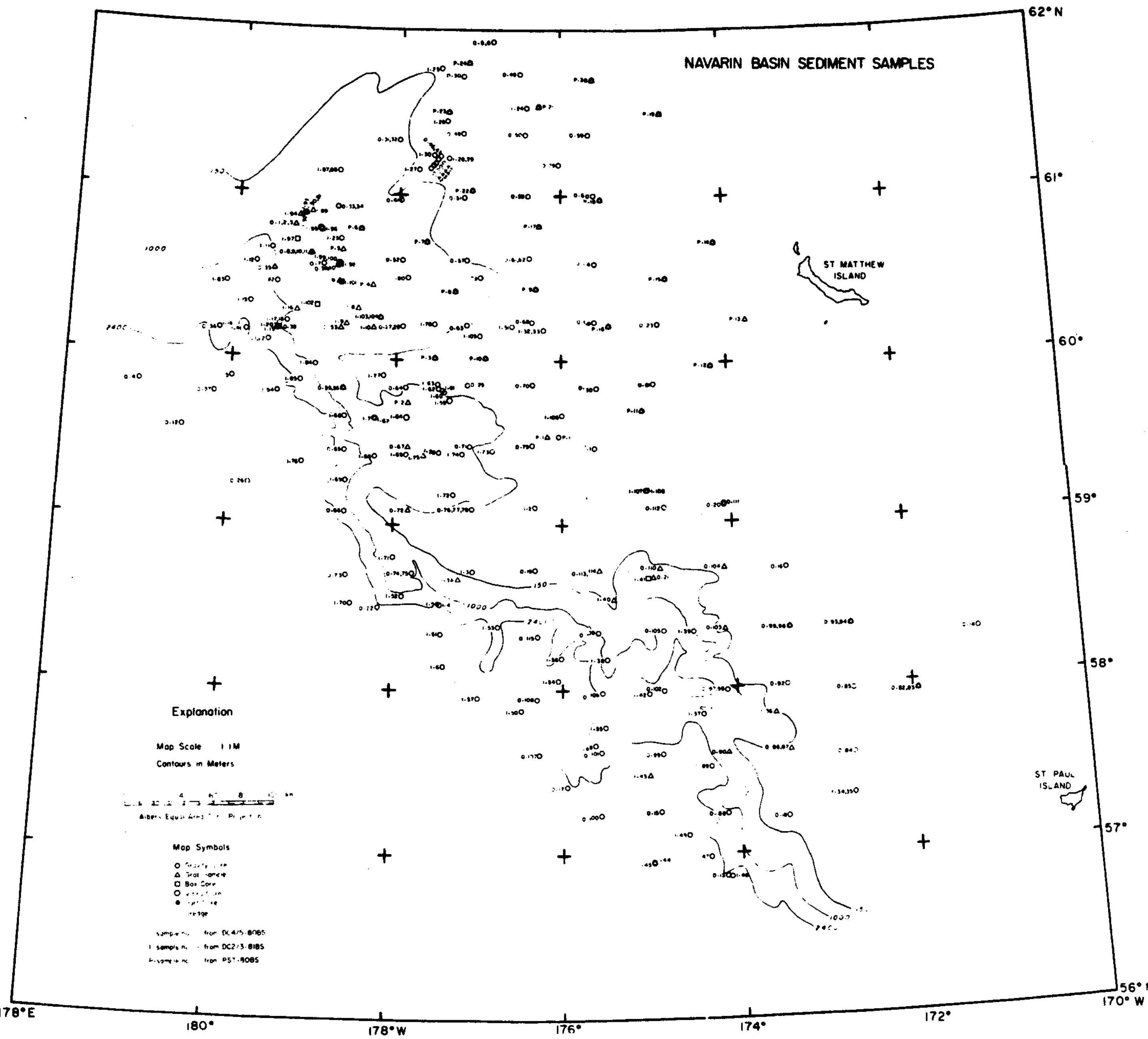

Figure 5. Locations of sediment samples.

Larry Kooker	Electronics Technician
Beth Lamb	Physical Science Technician
Larry Lawver	Geophysicist (LDGO)
Sue McGeary	Geophysicist
Jim Nicholson	Electronic Technician
Robert Patrick	Electronic Technician
Paula Quinterno	Micropaleontologist
Robin Ross	Physical Science Technician
John Saladin	Electronics Technician
Dennis Thurston	Geologist (MMS)
Tim Vogel	Geochemist
Hal Williams	Mechanical Technician
Mark Yeats	Physical Science Technician

We acknowledge also the assistance of the officers and crew of the USCG POLAR STAR and USGS R/V S.P. LEE and the scientific personnel on these supplemental cruises: Brian Edwards, Jeff Fischer, Richard Garlow, Marge Golan-Bac, Rick Herrera, Gordie Hess, Dan Hurlburt, Larry Kooker, Chris Larkin, Carol Madison, Bob Mallonee, Kevin O'Toole, Paula Quinterno, Jim Vaughn.

Sampling Methods:

State of the art high-resolution geophysical equipment (air gun, mini--sparker, 3.5 kHz), bottom samplers (gravity corer, grab, dredge) near-bottom suspended sediment samplers, and navigation (Satellite and Loran C) were used to collect data on the two cruises. Spacing between track lines was approximately 30 km., with more closely spaced lines in selected areas. Geologic samples were collected at the intersections of tracklines and at locations deemed to be geologically important by the chief scientists.

The geophysical systems used on the Navarin Basin cruises were as follows:

System	Resolution
1. Air gun (up to 80 in^3)	5 - 10 m
2. Minisparker (800 J)	1 - 3 m
3. 3.5 kHz	1 m

The bottom samplers used were: gravity corer, box corer, vibracorer, dredge, and grab samplers.

Analytical Methods:

The geophysical records are analyzed by standard methods, whereby slumps and shallow faults are identified by discontinuity of reflectors and by characteristic geometry, and seismic stratigraphic units are correlated by their continuity and seismic-reflection signature. The sediment cores are being studied megascopically and microscopically in order to classify sedimentary units and to gather data for deciphering dispersal patterns. Cores have been x-radiographed for study of internal structures that provide inferences as to depositional mechanics and post-depositional disturbance.

Grain size and mineralogy will be used to determine provenance and sediment pathways.

The types of analytical systems used in the Sedimentological Laboratory are described below:

A. General

(1) PDP-11/34 computer serving as controller for several analytical devices. Used to store analyzed data and interface with the main USGS computer.
(2) X-radiography unit for analyzing sedimentary structures in core samples.
(3) Suspended sediment concentrations are determined by gravimetric analysis of material collected on filters.

B. Particle Size Analysis

(1) Rapid sediment analyzer (height: 2.3 m; diameter: 20 cm) to measure grain-size distribution in the range of 2000 to 64 microns; fall velocities measured by a semi-conductor strain-gauge element.
(2) Coulter Counter for analysis of fine-grained sediments in the size range 2 to 64 microns.
(3) Hydrophotometer for analysis of fine-grained sediments in the size range 2 to 64 microns by measuring changes in light transmission.
(4) Pipette analysis of fine-grained sediments in the size range 2 to 64 microns by measuring rate of particle setting.

C. Mineral and Chemical Analysis

(1) LECO Carbon Analyzer - automatic analysis of total and organic carbon concentrations in sediments.
(2) Carbonate Determiner attached to LECO unit for measuring the amount of calcium carbonate in marine sediments.
(3) Scanning Electron Microscope (a Mini-SEM) having a capability for magnifications up to 40,000 X for viewing, identifying and photographing particulate matter.

In addition to routine geologic analysis, core samples will be subject to several routine laboratory tests to determine geotechnical index properties. Most routine tests will be conducted on subsamples from the core surface and at intervals downcore. Laboratory procedures will follow American Society for Testing and Materials (ASTM) standards where available.

Test	ASTM
Water content	D2216
Specific gravity of solids	D 854
Bulk unit weight	--
Atterberg limits	D423, 424
Vane shear strength	--

Specialized tests, such as one-dimensional consolidation (ASTM D 2435) and triaxial compression are being conducted on replicate cores taken at a few selected stations in an endeavor to characterize different sedimentary facies. Core sections taken for these and other laboratory tests were sealed in wax, refrigerated and stored in an upright position until analyzed.

VI. - VIII. Results, Discussion, and Conclusions

We have chosen to incorporate these three parts as a series of chapters to this final report. Each chapter, written by different authors, is an independent report on a specific topic complete within itself. Owing to time constraints on report submittal it was necessary for the authors to reduce and interpret great amounts of data relatively quickly, therefore we must stress the preliminary nature of these reports. The reports are organized into the following chapters:

1. Reports pertaining to Navarin Basin province published as of January 1983
2. Geologic hazards
3. Textural variations of surficial bottom sediment
4. Rates of sediment accumulation
5. Rocks and semi-consolidated sediment from the Navarin continental margin
6. Isopach map of Unit A, youngest sedimentary sequence in Navarin Basin
7. Summary of geotechnical characteristics
8. Hydrocarbon gases in sediments - results from 1981 field season
9. Benthic foraminifers
10. Diatom analysis of surface samples recovered from Pervenets Canyon
11. Aspartic acid geochronology of mollusks
12. Appended reports and large format maps

IX. Needs for Further Study

We have had approximately 3 months total shiptime in Navarin basin province in 1980 and 1981. During that time we have completed what is essentially a reconnaissance grid of seismic track lines and bottom sample stations over the 45,000 km^2 study area. In 1981, we not only increased systematic reconnaissance coverage but also, in anticipation of no further cruises, concentrated track lines and samples in those areas that contained potential geologic hazards as determined from 1980 results.

Further investigations will require that closely spaced seismic profile lines and bottom samples be located in specific sites chosen for exploratory drilling. Additionally, more closely spaced track lines are needed on a regional basis in order to map out the trace of near-surface faults and to decipher possible relationships between fault trends and zones of gas-charged sediment.

Another area of fruitful research involves the deployment of current measuring instruments to determine whether bottom currents of sufficient strength exist which may be potential hazards to pipelines and platforms. Investigations of this type also are necessary to understand the origin of the sand waves which are found in the heads of the large submarine canyons.

At least 2-3 years of additional data gathering are needed to refine our interpretations of the geology of Navarin basin province, although we feel that sufficient data has been collected for an adequate preliminary assessment of the potential geologic hazards in lease sale area 83.

References

Ahlnas, K. and Wendler, G., 1980, Meteorological parameters affecting the location of the ice edge in the Bering Sea: Transactions Am. Geophys. Union, EOS, v. 61, p. 1006.

Cacchione, D. A., Drake, D. E., and Wiberg, P., 1982, Velocity and bottom-stress measurements in the bottom boundary layer, outer Norton Sound, Alaska: in Nelson, C. H. and Nio, S. D., eds., The northeastern Bering shelf: new perspectives of epicontinental shelf processes and depositional products: Geologie en Mijnbouw, v. 61, p. 71-78.

Carlson, P. R. and Karl, H. A., 1981, High-resolution seismic reflection profiles: Navarin Basin province, northern Bering Sea, 1980: U.S. Geological Survey Open-File Report 82-1221, 4 p., 1 map, scale 1:1,000,000.

Carlson, P. R. and Karl, H. A., 1982, High-resolution seismic reflection profiles: Navarin Basin province, northern Bering Sea, 1981: U.S. Geological Survey Open-File Report 82-786, 5 p., 1 map, scale 1:1,000,000.

Coachman, L. K., Aagaard, K., and Tripp, R. B., 1975, Bering Strait, The regional physical oceanography: Seattle, Univ. of Washington Press, 186 p.

Dall, N. H., 1881, Hydrologie des Bering-Meeres und der benachbarten Gewasser: Pet. Geog. Mitt., v. 27, p. 361-380.

Drake, D. E., Cacchione, D. A., Muench, R. D., and Nelson, C. H., 1980, Sediment transport in Norton Sound, Alaska: Marine Geology, v. 36, p. 97-126.

Drake, D. E., Totman, C. E., and Wiberg, P. L., 1979, Sediment transport during the winter on the Yukon prodelta Norton Sound, Alaska: Journal of Sedimentology Petrology, v. 49, p. 1171-1180.

Favorite, F., 1974, Flow into the Bering Sea through Aleutian island passes: in Hood, D. W., and Kelley, E. J., ed., Oceanography of the Bering Sea. Inst. Mar. Sci., Univ. Alaska Occas. Publ. 2, p. 3-37.

Fischer, J. M., Carlson, P. R., and Karl, H. A., 1982, Bathymetric map of Navarin Basin province, northern Bering Sea: U.S. Geological Survey Open-File Report 82-1038, 11 p., 1 map, scale 1:1,000,000.

Gardner, J. V., Dean, W. E., and Vallier, T. L., 1980, Sedimentology and geochemistry of the surface sediments, outer continental shelf, southern Bering Sea: Marine Geology, v. 35, p. 299-329.

Hughes, F. W., Coachman, L. K., and Aagaard, K., 1974, Circulation, transport and water exchange in the western Bering Sea: in Hood, D. W. and Kelley, E. J., ed., Oceanography of the Bering Sea. Univ. Alaska Inst. Marine Science, Occas. Publ. 2, p. 59-98.

Karl, H. A. and Carlson, P. R., 1982, Location and description of sediment samples: Navarin Basin province, Bering Sea, 1980-81: U.S. Geological Survey Open-File Report 82-958, 5 p., 2 maps, scale 1:1,000,000.

Knebel, H. J., 1972, Holocene sedimentary framework of the east-central Bering Sea continental shelf: Ph.D. thesis, Univ. Washington, Seattle, 186 p.

Kummer, J. T., and Creager, J. S., 1971, Marine geology and Cenozoic history of the Gulf of Anadyr: Marine Geology, v. 10, p. 257-280.

Kvenvolden, K. A., Nelson, C. H., Thor, D. R., Larsen, M. C., Redden, G. D., Rapp, J. V., and Des Marias, D. J., 1979, Biogenic and thermogenic gas in gas-charged sediment of Norton Sound, Alaska: Offshore Technology Conference, Houston, Texas, Proceedings, v. 1, p. 479-486.

Lisitsyn, A. P., 1966, Protessy Sovremennogo Osodko' obrazovaniya v Beringovom More: Akad. Nauk SSR Inst. Okeal., Moskva, 574 p. (Recent sedimentation in the Bering Sea: Israel Program for Sci. Translations, 1969, Jerusalem; U.S. Dept. of Commerce, Clearinghouse for Federal Sci. Tech. Info., Springfield, VA, 614 p.).

Marlow, M. S., and Cooper, A. K., 1979, Multichannel seismic reflection profiles collected in 1977 in the northern Bering Sea: U.S. Geological Survey open-file report 79-1147.

Marlow, M. S., Carlson, P. R., Cooper, A. K., Karl, H. A., McLean, H., McMullin, R., and Lynch, M. B., 1981, Resource report for proposed OCS sale number 83 Navarin Basin, Alaska: U.S. Geological Survey open-file report 81-252, 82 p.

Marlow, M. S., Scholl, D. W., Cooper, A. K., and Buffington, E. C., 1976, Structure and Evolution of Bering Sea shelf south of St. Lawrence Island, Bulletin of the American Association of Petroleum Geologists, v. 60, no. 1, p. 161-183.

McManus, D. A., Kolla, Venkatarathnam, Hopkins, D. M., and Nelson, C. H., 1977, Distribution of bottom sediments on the continental shelf, northern Bering Sea: U.S. Geological Survey Prof. Paper 759-C, 31 p.

Muench, R. D., 1974, Satellite observations of Bering Sea ice: in Hood, D. W., and Takenouti, Y., eds., Bering Sea oceanography: an update: Univ. Alaska, Inst. Marine Science, Report No. 75-2, p. 191-192.

Nelson, C. H., Hopkins, D. M., and Scholl, D. W., 1974, Tectonic setting and Cenozoic sedimentary history of the Bering Sea, in Herman, Yvonne, ed., Marine geology and oceanography of the Arctic seas: New York, Springer-Verlag, p. 119-140.

Paquette, R. G., and Bourke, R. H., 1980, Winter conditions in the Bering Sea: Transactions Am. Geophys. Union, EOS, v. 61, p. 1006.

Pratt, R. and Walton, F., 1974, Bathymetric map of the Bering Shelf: Geological Society of America, Boulder, Colorado.

Sayles, M. A., Aagaard, K., and Coachman, L. K., 1979, Oceanographic atlas of the Bering Sea Basin: Seattle, Univ. of Washington Press, 155 p.

Scholl, D. W., Buffington, E. C., and Marlow, M. S., 1975, Plate tectonics and the structural evolution of the Aleutian Bering Sea region, in Forbes, R. B., ed., Contributions to the geology of the Bering Sea Basin and adjacent regions: Geol. Soc. of America Spec. Paper 151, p. 1-32.

Scholl, D. W., Buffington, E. C., Marlow, M. S., 1976, Aleutian-Bering Sea region seismic reflection profiles: U.S. Geol. Survey Open-File Rept. 76-748.

Schumacher, G. M., 1976, Bathymetric map of the Aleutian Trench and Bering Sea, U.S. Geological Survey open-file map 76-821, scale 1:2,500,000.

Sharma, G. D., 1979, The Alaska shelf, hydrographic, sedimentary, and geochemical environment: Springer-Verlag, New York, 498 p.

Sharma, G. D., Naidu, A. S., and Hood, D. W., 1972, Bristol Bay: model contemporary graded shelf: Am. Assoc. Petroleum Geologists, v. 56, p. 2000-2012.

Tabata, T., 1974, Movement and deformation of drift ice as observed with sea ice radar: in Hood, D. W. and Kelley, E. J., eds., Oceanography of the Bering Sea, Univ. Alaska, Inst. Marine Science, Occas. Publ. 2, p. 373-382.

Takenouti, A. Y. and Ohtani, K., 1974, Currents and water masses in the Bering Sea: a review of Japanese work: in Hood, D. W. and Kelley, E. J., eds., Oceanography of the Bering Sea, Univ. Alaska, Inst. Marine Science, Occas. Publ. 2, p. 39-57.

Vallier, T. L., Underwood, M. B., Gardner, J. V., and Barron, J. A., 1980, Neogene sedimentation on the outer continental margin, southern Bering Sea: Marine Geology, v. 36, p. 269-287.

Webster, B. D., 1979, Ice edge probabilities for the eastern Bering Sea: NOAA Technical Memorandum NWS AR-26, 20 p.

CHAPTER 1: REPORTS PERTAINING TO NAVARIN BASIN PROVINCE PUBLISHED AS OF JANUARY 1983

Baldauf, J. G., 1982, Identification of the Holocene-Pleistocene boundary in the Bering Sea by diatoms: Boreas, v. 11, p. 113-118.

Carlson, P. R. and Karl, H. A., 1981, Geologic hazards in Navarin Basin province, northwestern Bering Sea: U.S. Geological Survey Open-File Report 81-1217, 149 p.

Carlson, P. R., and Karl, H. A., 1981, High-resolution seismic reflection profiles: Navarin Basin province, northern Bering Sea, 1980: U.S. Geological Survey Open-File Report 81-1221, 4 p., 1 map, scale 1:1,000,000.

Carlson, P. R., and Karl, H. A., 1982, High-resolution seismic reflection profiles: Navarin Basin province, northern Bering Sea, 1981: U.S. Geological Survey Open-File Report 82-786, 5 p., 1 map, scale 1:1,000,000.

Carlson, P. R., Fischer, J. M., and Karl, H. A., 1983, Two newly discovered submarine canyons on Alaskan continental margin of Bering Sea: U.S. Geological Surey Open-File Report 83-24, 36 p., 1 map, scale 1:250,000.

Carlson, P. R., Karl, H. A., Fischer, J. M., and Edwards, B. D., 1982, Geologic hazards in Navarin Basin province, northern Bering Sea: 14th Offshore Technology Conference, Houston, Tex., Proceedings, v. 1, p. 73-87.

Carlson, P. R., Karl, H. A., Johnson, K. A., and Fischer, J. M., 1981, Morphology, sedimentology, and genesis of three large submarine canyons adjacent to Navarin Basin, Bering Sea: American Assoc. Petroleum Geol. Bull., v. 65, p. 909.

Carlson, P. R., Karl, H. A., Johnson, K. A., and Fischer, J. M., 1982, Submarine canyons flanking Navarin Basin, Bering Sea: U.S. Geological Survey Circular (Accomplishments in Alaska), 844, p. 139-141.

Carlson, P. R., Karl, H. A., and Quinterno, Paula, 1982, Sedimentologic processes in world's largest submarine canyons, Bering Sea, Alaska: Geol. Soc. of America, Abstracts with Programs, v. 14, no. 7, p. 459-460.

Fischer, J. M., Carlson, P. R., and Karl, H. A., 1982, Bathymetric map of Navarin Basin province, northern Bering Sea: U.S. Geological Survey Open-File Report 82-1038, 11 p., 1 map, scale 1:1,000,000.

Karl, H. A., Cacchione, D. A., and Carlson, P. R., 1982, Large sand waves in canyon heads, Bering Sea: products of internal waves or density currents: 11th International Sedimentologic Congress, Hamilton, Ontario, Canada, p. 73.

Karl, H. A., and Carlson, P. R., 1981, Large sediment waves at the shelf edge, northern Bering Sea: Geological Society of America, Abstracts with Programs, v. 13, p. 483.

Karl, H. A., and Carlson, P. R., 1982, Location and description of sediment samples: Navarin Basin province, Bering Sea, 1980-81: U.S. Geological Survey Open-File Report 82-958, 5 p., 2 maps, scale 1:1,000,000.

Karl, H. A., and Carlson, P. R., in press, Large sand waves in submarine canyon heads, Bering Sea: preliminary hypothesis of their depositional history: Geo Marine Letters, 17 ms.p.

Karl, H. A., Carlson, P. R., and Cacchione, D. A., 1981, Factors influencing sediment transport at the shelf break: Am. Assoc. Petroleum Geol. Bull., v. 65, p. 943.

Karl, H. A., Carlson, P. R., and Cacchione, D. A., 1983, Factors that influence sediment transport at the shelf break: In: Stanley, D. J., and Moore, G., (editors). Shelf-slope boundary: Critical interface on continental margins: Society Economic Paleontologists and Mineralogists Special Publication No. 33, p. 219-231.

Karl, H. A., Carlson, P. R., and Lamb, B., 1982, Sediment waves in the head of Navarinsky, Pervenets, and Zhemchug submarine canyons, northwestern Bering Sea: U.S. Geological Survey Circular (Accomplishments in Alaska) 844, p. 141-143.

Marlow, M. S., Carlson, P., Cooper, A. K., Karl, H., McLean, H., McMullin, R., and Lynch, M. B., 1981, Hydrocarbon resource report for proposed OCS lease sale 83, Navarin Basin, Alaska: U.S. Geological Survey Open-File Report 81-252, 75 p.

Quinterno, Paula, Blueford, J. R., and Baldauf, J. G., 1981, Micropalentologic analysis of Navarin Basin, Bering Sea, Alaska: American Assoc. Petroleum Geol. Bull., v. 65, p. 975.

Vogel, T. M., Kvenvolden, K. A., Carlson, P. R., and Karl, H. A., 1981, Geochemical prospecting for hydrocarbons in the Navarin Basin province: American Assoc. Petroleum Geol. Bull., v. 65, p. 1004.

CHAPTER 2: GEOLOGIC HAZARDS

by

H. A. Karl and P. R. Carlson

Based on data collected during the 1980 and 1981 DISCOVERER cruises (Carlson and Karl, 1981; 1982; Karl and Carlson, 1982) and the results of an Environmental Hazards Workshop that was part of the Navarin Synthesis meeting convened by NOAA/OCSEAP and held in Anchorage on 25-27 October, 1982, we have identified 10 elements and processes that are potential hazards to commercial development of the Navarin basin province. These are:

- Sea ice
- Superstructure icing
- Waves
- Fog
- Sediment mass movement
- Seismicity
- Faulting
- Gas-charged sediment
- Large bedforms
- Unstable sediment

Sea ice, superstructure icing, waves, and fog obviously are not seafloor geologic hazards, and, therefore, we do not discuss these at length. These environmental hazards are considered by other OCSEAP investigators- oceanographers and meteorologists- and specific treatments of these hazards are found in their reports. In this report we only mention briefly the effects of these four hazards on commercial development. Superstructure icing and fog are operational hazards and must be dealt with on a day-to-day basis. The wave climate in the Navarin area can be severe; however, industry is currently operating in areas that have a more severe wave climate, for example, the North Sea. Sea ice is a problem for part of the year in Navarin, however, it is less of a problem than in the Beaufort Sea which is presently being developed for oil and gas. Water depth and distance from land, however, are factors which may complicate development of Navarin basin. Consequently, structures that are now successful in the North Sea and the Beaufort Sea may require additional engineering before use in Navarin basin.

The six elements and processes that are seafloor geologic hazards have been described in depth in several reports and papers written and published since the 1980 annual report, Geologic Hazards in Navarin basin, was issued; these articles are reproduced as appendices to this report. Figure 6 shows the distribution of geohazards mapped during the 1980 and 1981 field seasons; maps of geotechnical indices are presented in Chapter 7 of this report.

Mass movement of sediment is ubiquitous on the slope in water depths greater than about 200 m and in the heads of the submarine canyons (Fig. 6; appendices F and G). Sediment mass movement is the process most likely to pose a hazard to the siting of drilling structures, production platforms, and pipelines. We are not able to assess the recency or the frequency of mass

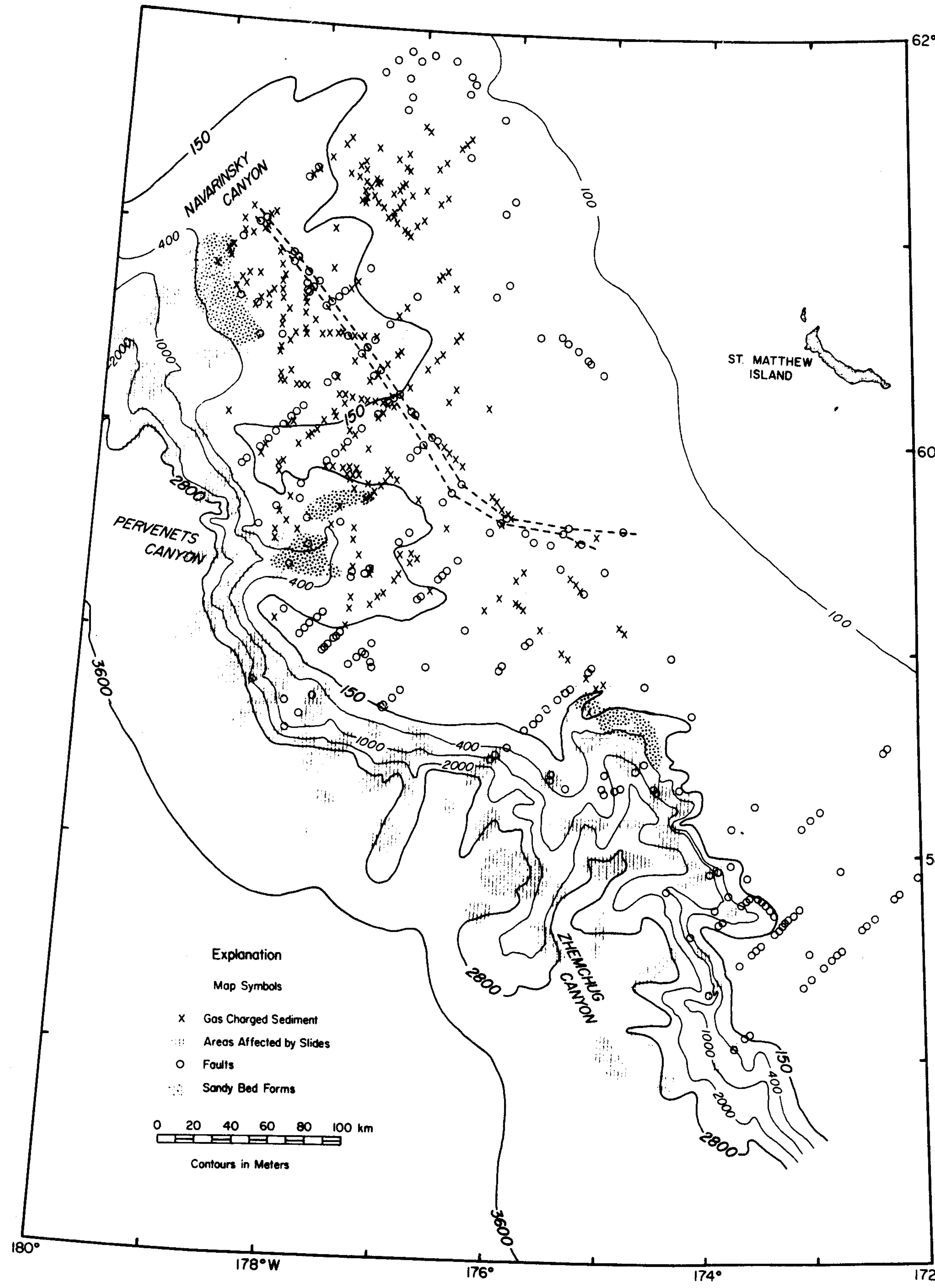

Figure 6. Map of seafloor geologic hazards in Navarin Basin province.

failures in Navarin basin province. Industry has built structures in areas prone to the mass failure of sediment deposits, the Mississippi delta, for example; however, the scale of the slump and slide blocks and the water depth in Navarin basin province may pose additional engineering problems.

Only six earthquakes, each less than magnitude 6, have been reported from Navarin Basin Province (Meyers, 1979). This data base spans less than the last 100 years. Even though earthquakes have occurred infrequently during the historic past in Navarin basin province, the numerous examples of sediment mass movement, for want of a better triggering mechanism, suggest that frequent earthquakes of significant magnitude have occurred in the geologic past (see appendix G). Seismicity, must be considered in design criteria. However, as a potential hazard it is certainly less likely a problem than in an area like southern California - a region which has undergone extensive petroleum development.

None of the faults mapped to date show any offset of the Holocene seafloor. Although the ages of these faults are unknown, ^{14}C dates of sediment in the Navarin basin province indicate accumulation rates of the upper 6 m of sediment to range from about 10 to 25 cm/10^3 yr (Askren, 1972; Knebel, 1972; Carlson and Karl, Chap. 4, this report). Therefore, faults that reach within 2-3 m of the seafloor may cut sediment as young as Holocene and are considered to be active. Faulting must be considered a potential hazard, but, like seismicity, the probability of fault-related damage to platforms and pipelines is certainly less than that in an area like southern California.

Gas-charged sediment can have a lower shear strength and bearing capacity than does equivalent gas-free sediment (Nelson and others, 1978; Whelan and others, 1976). An increase in the concentration of free or bubble-phase gas results in an increase of pore pressure and a concomitant decrease in shear strength until failure can occur. Such increases in bubble-phase gas can result from drilling into gas-charged sediment or disruption of the sediment by cyclic loading, and this may lead to failure of pipelines or platforms (U.S. Geological Survey, 1977). Examples of gas-charged sediment identified on high-resolution seismic-reflection profiles are shown in Carlson and others (1982; appendix F) and the hydrocarbon analysis of Navarin cores is discussed in Chapter 8 of this report. The potential hazard of gas-charged sediment will have to be assessed by the surveying of specific sites chosen for development.

Large bedforms are found in the heads of the submarine canyons incising the Navarin continental margin (Fig. 6; appendix H). The bedforms occur on a substrate of silty, very fine sand and have wavelengths of about 600 m and heights that vary between 5-15 m. We do not know if the sand waves are active. If the sand waves are active, they, as well as the processes responsible for them, could represent hazards.

A regional study of geotechnical properties of Navarin basin sediments are discussed in Chapter 7. It will be necessary to do geotechnical analyses on cores collected at specific sites chosen for development in order to determine design criteria for structures with foundations on the seafloor.

References

Askren, D. R., 1972, Holocene stratigraphic framework southern Bering Sea continental shelf: MS thesis, Univ. of Washington, 104 p.

Carlson, P. R. and Karl, H. A., 1981, High-resolution seismic reflection profiles: Navarin basin province, northern Bering Sea, 1980: U.S. Geological Survey Open-File Report 81-1221, 4 p., 1 map, scale 1:1,000,000.

Carlson, P. R. and Karl, H. A., 1982, High-resolutin seismic reflection profiles: Navarin basin province, northern Bering Sea, 1981: U.S. Geological Survey Open-File Report 82-786, 5 p., 1 map, scale 1:1,000,000.

Carlson, P. R., Karl, H. A., Fischer, J. M., and Edwards, B. D., 1982, Geologic hazards in Navarin basin province, northern Bering Sea: Proceedings Offshore Tech. Conf., v. 1, p. 73-87.

Karl, H. A. and Carlson, P. R., 1982, Location and description of sediment samples: Navarin basin province, Bering Sea, 1980-81: U.S. Geological Survey Open-File Report 82-958, 5 p., 2 maps, scale 1:1,000,000.

Knebel, H. J., 1972, Holocene sedimentary framework of the east-central Bering Sea continental shelf: Ph.D. Thesis, Univ. Washington, Seattle, 186 p.

Meyers, H., 1979, A historical summary of earthquake epicenters in and near Alaska: NOAA Tech. Memorandum EDS NGSDC-1, 80 P.

Nelson, H., Kvenvolden, K. A., and Clukey, E. C., 1978, Thermogenic gases in near-surface sediments of Norton Sound, Alaska: In, Proceedings of the 1978 Offshore Technology Society, p. 2623-2633.

U.S. Geological Survey, 1977, An investigation of Pennzoil's blow-out and loss of platform: U.S. Geological Survey unpublished administrative report, 22 p.

Whelan, T., Coleman, J. M., Robert, H. H., and Sukayda, J. N., 1976. The occurrence of methane is recent deltaic sediments and its effect on soil stability: Bull. of the International Association of Engineering Geology, no. 14, p. 55-64.

CHAPTER 3: TEXTURAL VARIATION OF SURFICIAL BOTTOM SEDIMENT

by

H. A. Karl and P. R. Carlson

INTRODUCTION

A total of 278 sediment sampling stations were occupied during the 1980 POLAR STAR cruise and the 1980 and 1981 DISCOVERER cruises (Karl and Carlson, 1982, Appendix C, Fig. 5). The distribution of sediment types derived from visual descriptions of surface samples reveals that (1) silts and sandy silts generally characterize the shelf and slope, (2) zones of coarser sediment (coarse silt and sand) occur at the shelf edge, on the upper slope and in the heads of submarine canyons, (3) surficial sediment on the shelf tends to be coarser in the southeastern part of the area than elsewhere on the shelf, and (4) muds typify the lower slope and rise (see appendix C for plot of visual descriptions).

METHODS

Subsamples taken from the gravity cores and grab samples were soaked in H_2O_2 solution or acetone solution to remove oxidizable organic matter. the samples were then wet sieved on a 63 micron screen to separate mud (<63 microns) and sand (>63 microns). If gravel (>2 mm) was present, it was separated from sand by dry sieving. The fine fraction (<63 microns) was analyzed by standard pipette method and the sand-size material analyzed by standard rapid settling tube (RSA) method. Statistical parameters were calculated as moment measures.

RESULTS

Table 1 contains the results of detailed sediment analyses of eight cores and grab samples selected as typical examples of each textural environment listed above (Fig. 7). All the samples are poorly sorted (Table 1, Fig. 8). Mean grain-size of the rise and slope samples is in the very fine silt class. The distribution of sediment sizes in the rise and slope samples is very similar; the samples that happen to have been chosen are both weakly bimodal and differ only in that the dominant mode shifts from clay (10.5 phi) on the rise to fine silt (6.5 phi) on the lower slope (Fig. 9). Samples from the shelf edge are considerably coarser than samples from the slope and rise with mean grain-sizes of 0.02 mm and 0.07 mm. The finer of the shelf-edge samples overlaps mean grain diameters typical of the shelf (Fig. 8). Sediment in both shelf-edge samples is concentrated in the coarser silt and finer sand classes with modes in the coarse silt (4.5 phi) and fine sand (3.5 phi) classes (Fig. 9). Grain-size distribution of the sample (80-G85) from the southeastern part of the shelf resembles shelf-edge distributions in that sediment tends to be concentrated in the finer sand and coarser silt classes with a strong mode in the coarse silt (4.5 phi) class (Fig. 9). Sample 80-G23 from the northwestern part of the shelf differs from sample 80-G85 in that sediment particles are more uniformly distributed over the very fine sand

Table 1. Results of grain-size analysis on selected samples

Environment	Shelf		Shelf Edge		Slope	Rise	Canyon Head	
Sample number	80-G23	80-G85	81-VV40	81-G63	81-G13	81-G70	81-VV75	81-VV89
Sample type	gravity core	gravity core	Van Veen	gravity	gravity	gravity	Van Veen	Van Veen
Depth of subsample (cm)	10-12	10-12	sur.	23-33	10-15	40-50	sur.	sur.
% Gravel	0.00	0.00	0.00	0.00	0.00	0.00	0.00	19.05
% Sand	10.38	20.82	74.20	21.34	5.11	3.68	94.12	76.43
% Silt	59.99	67.23	22.11	61.66	57.57	51.97	4.68	3.84
% Clay	29.62	11.94	3.68	16.99	37.30	44.33	1.19	0.66
Mean grain size (ϕ)	6.65	5.34	3.77	5.59	7.31	7.65	2.93	2.05
Mean grain size (mm)	0.010	0.025	0.07	0.02	0.006	0.005	0.13	0.24
Std. deviation (ϕ)	2.26	1.90	1.46	2.17	2.07	2.11	0.96	1.92
Skewness (ϕ)	0.27	1.12	2.23	0.94	0.03	-0.18	2.15	-0.50
Kartosis (ϕ)	-1.01	0.70	5.63	-0.19	-0.98	-1.07	15.73	1.10

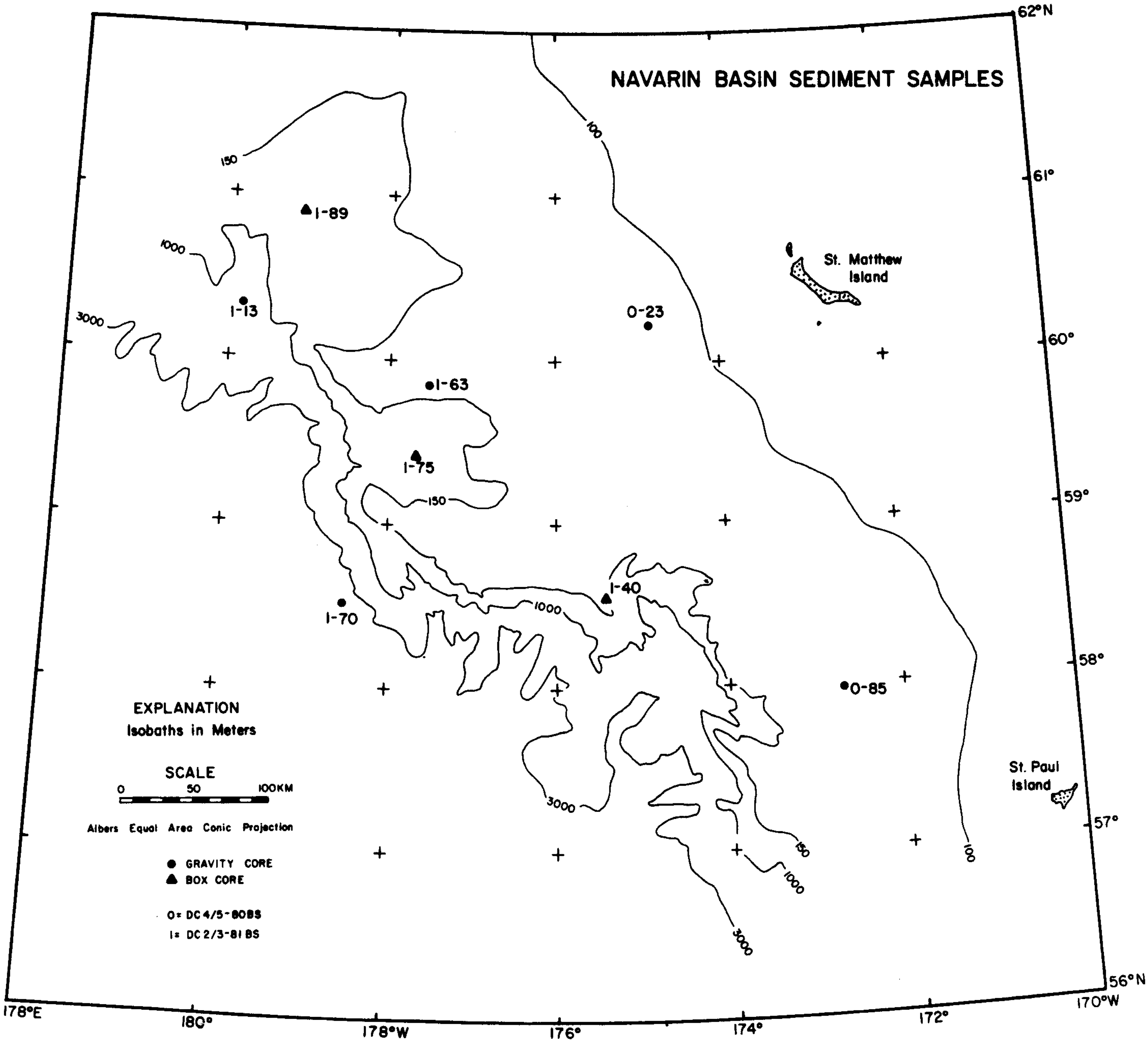

Figure 7. Location of sediment samples selected as typical examples of textural environments characterizing Navarin Basin province. (The solid triangle identifies Van Veen samples).

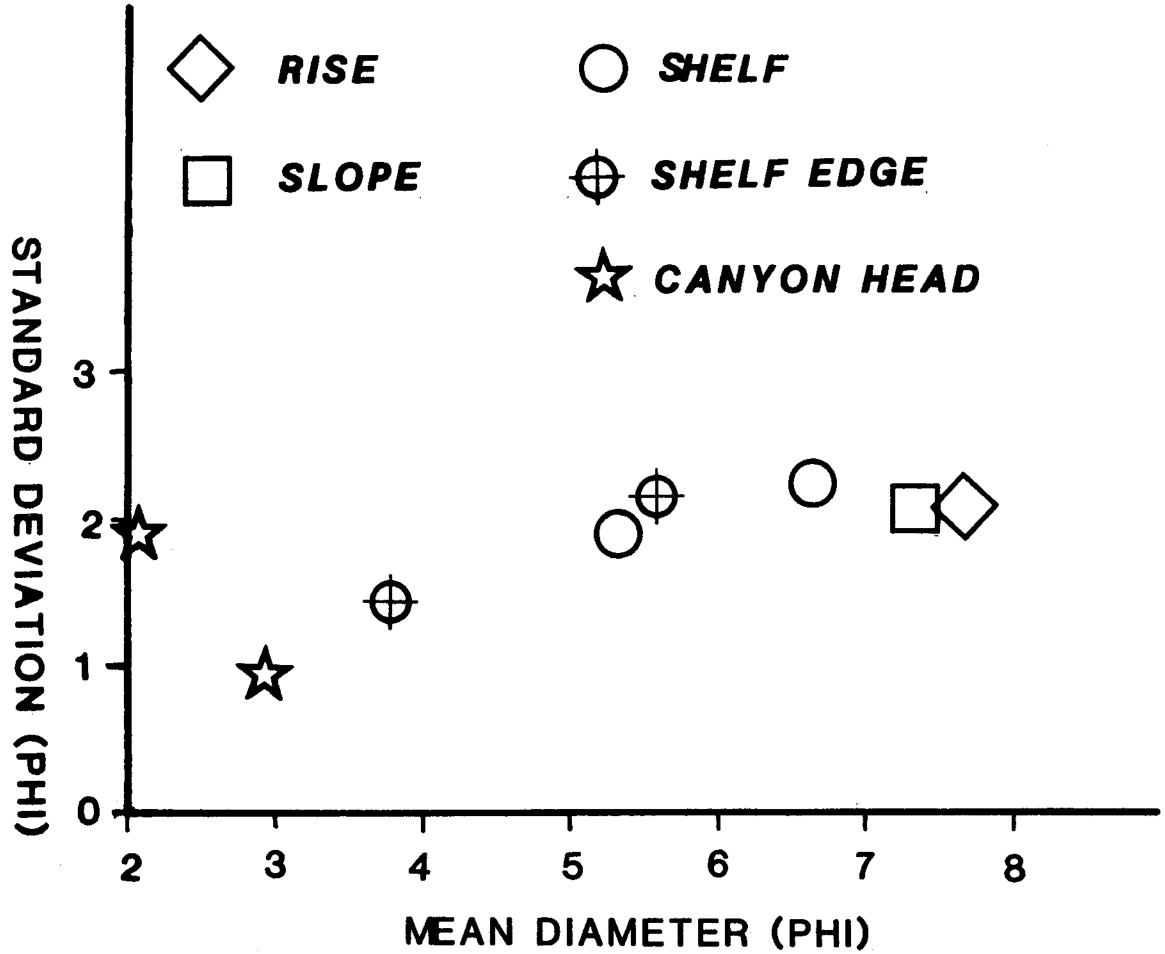

Figure 8. Plot of mean diameter vs. standard deviation.

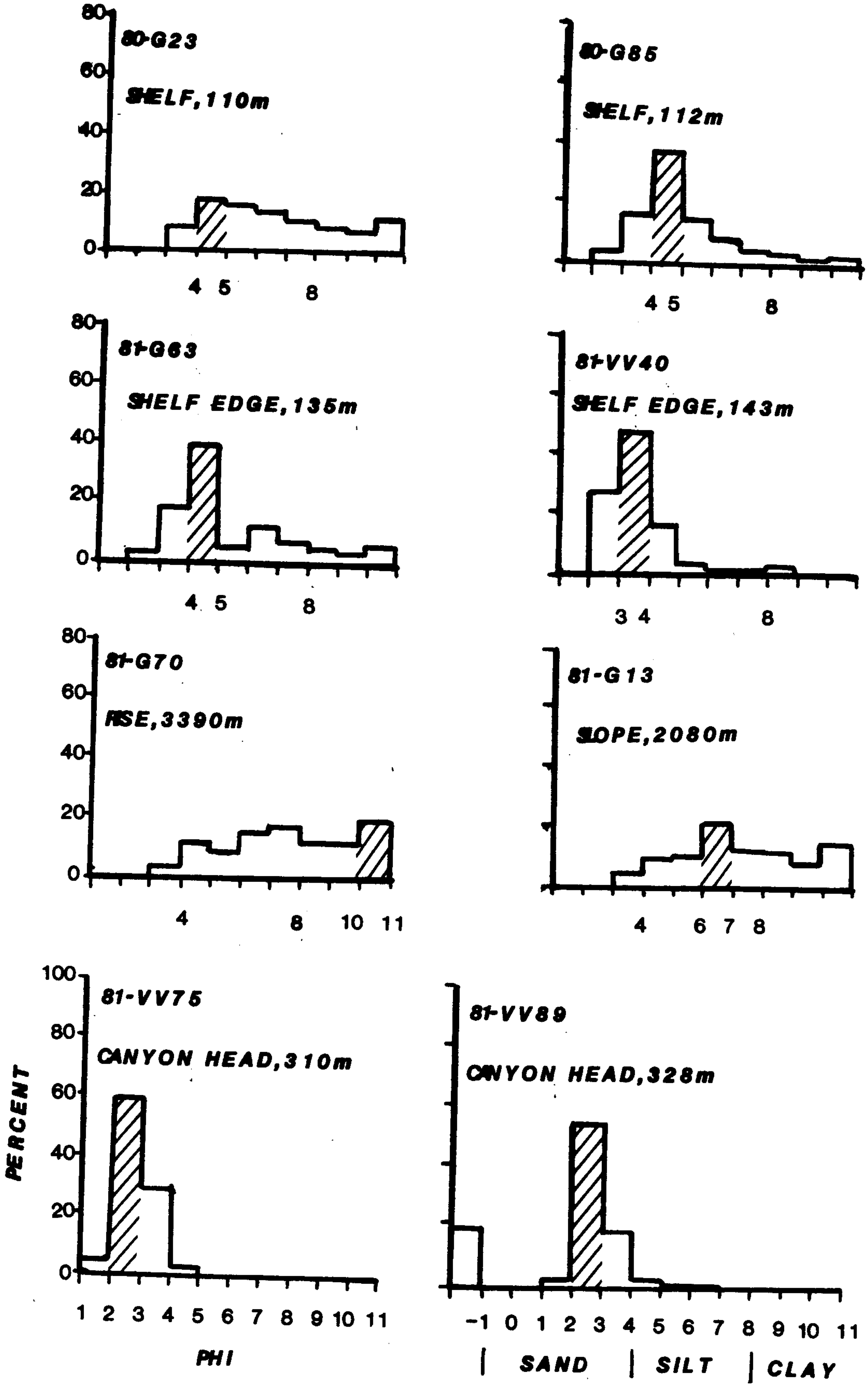

Figure 9. Histograms of selected samples. Modes identified by hachuring; dominant mode is hatchured in biomodal samples.

through clay classes with a weak mode in the coarse silt class (Fig. 9). The coarsest mean grain-sizes occur in the heads of the submarine canyons. In the samples considered here, sediment particles are concentrated in the sand classes with a very strong mode in the fine sand (2.5 phi) class (Fig. 9).

DISCUSSION

Except for the samples from the rise and slope, the factors responsible for these grain-size distributions and regional textural variations are not obvious. The predominance of fine silt and clay size material in the rise and slope samples is typical of deep water environments. Depositional conditions in these environments during the low stands of sea level in the Pleistocene probably would not have been appreciably different than present-day conditions. This, however, is not true of the shelf and canyon heads. The zones of coarser sediment at the shelf edge and in the canyon heads could be due in part to lower sea levels when shorelines were at or near these areas. In which case coarser sediment was either supplied to the shelf edge and canyon heads by streams, for example, or energy levels were sufficiently high to winnow out the fines from sediment being deposited. Alternatively, the coarser sediment in these environments relative to the shelf and slope might reflect modern processes that supply sufficient energy to winnow sediment at the shelf edge and in the canyon heads. The Bering Slope Current, which flows northward parallel to the slope, and internal waves, which may be focused in and adjacent to the heads of the submarine canyons, are potential mechanisms to supply energy to winnow sediments. The finer shelf sediments in the northwestern section of the shelf relative to the southeastern part may indicate that relict sediment from lower sea levels is being diluted with finer material following flooding of the shelf; present sediment sources are over 400 km distant. These hypothesis are conjectures, however, as not enough textural data are available at present to allow us to choose between these interpretations.

REFERENCES

Karl, H. A., and Carlson, P. R., 1982, Location and description of sediment samples: Navarin basin province, Bering Sea, 1980-81: U.S. Geological Survey Open-File Report 82-958, 5 p.

CHAPTER 4: RATES OF SEDIMENT ACCUMULATION

by

Paul R. Carlson and Herman A. Karl

INTRODUCTION

The Navarin basin province is located on the outer part of the flat, wide Bering continental shelf, a great distance (>300 km) from modern sources of detrital sediment. However, during low stands of sea level the ancestral Anadyr and Yukon Rivers must have transported vast quantities of sediment across the shelf to about the present-day 130 m isobath where the suspended and bottom sediments were entrained in the coastal currents that were sweeping through what is the present site of the Navarin basin. In order to understand the development of the Navarin continental margin, rates of accumulation of the sediment on the margin must be determined. This chapter presents some preliminary estimates of sediment accumulation rates based upon C-14 measurements of gravity core sub-samples from the Navarin shelf, slope, and rise.

DATA COLLECTION AND ANALYSIS

Gravity cores (8 cm diameter) subsampled for radiocarbon dating were collected on two cruises of the NOAA ship DISCOVERER in 1980 and 1981 (Karl and Carlson, 1982). A total of 22 cores were selected for dating (Table 2; Fig. 10). The cores collected on both the 1980 and 1981 cruises were split longitudinally and described while at sea. After each cruise, preliminary studies of core descriptions (including X-radiographs), microfaunal contents, organic carbon measurements, and interpretations of high-resolution seismic reflection records were utilized to select the cores for radiocarbon dating. The working half of each selected core was carefully sub-sampled to avoid the "smear-affect" along the core-liner. Sufficient sediment was collected to provide the analyst with about one gram of carbon from the "whole-core" samples. The intervals sampled from each core are listed in Table 2. Analyses were performed by the USGS radiocarbon dating lab in Menlo Park, California, for the 1980 cores and by Geochron Labs* in Cambridge, Massachusetts for the 1981 cores.

Calculations of preliminary rates of sediment accumulation (Table 3) are based on the assumption of a constant rate of sediment deposition to a depth in the core of the mid-point of the sampled interval.

*Any use of trade names in this publication is for descriptive purposes only and does not constitute endorsement by the U.S. Geological Survey.

Table 2. C-14 dates of Navarin samples

Core No.*	Depth in core (cm)	C-14 date (yrs BP)	Water depth (m)
0- 12	211-230	16,670 ± 100	3164
0- 13	188-228	5,580 ± 45	2692
0- 13	245-270	34,520 ± 490	"
0- 26	188-222	10,880 ± 80	3373
0- 26	235-260	33,990 ± 610	"
0- 26	322-333	33,300 ± 1800	"
0- 33	65- 90	28,980 ± 2200	210
0- 33	210-240	28,200 ± 3000	"
0- 42	170-183	13,650 ± 100	141
0- 44	125-145	14,900 ± 110	138
0- 66	65- 84	19,370 ± 160	1336
0- 66	325-335	37,500 ± 1200	"
0- 66	380-385	>32,000	"
0-115	170-200	9,505 ± 300	2870
0-115	237-262	19,990 ± 1400	"
1- 02	100-130	11,755 ± 395	143
1- 03	0- 30	7,375 ± 270	133
1- 15	65- 90	5,330 ± 180	2750
1- 15	250-275	15,975 ± 850	"
1- 31	160-190	8,815 ± 355	137
1- 32	160-190	7,500 ± 305	130
1- 44	65- 90	4,460 ± 190	3400
1- 44	220-245	10,925 ± 365	"
1- 58	25- 50	9,215 ± 310	179
1- 58	60- 88	>37,000	"
1- 58	240-265	>27,000	"
1- 65	25- 50	10,485 ± 355	436
1- 65	160-185	>32,000	"
1- 66	65- 90	>37,000	580
1- 67	65- 90	17,725 ± 680	167
1- 88	65- 90	>29,000	205
1- 88	350-375	>37,000	"
1-105	160-190	8,385 ± 310	144
1-106	160-190	8,700 ± 355	135
1-107	65- 90	8,900 ± 290	116

* 0 = DC 4/5-80   1 = DC 2/3-81

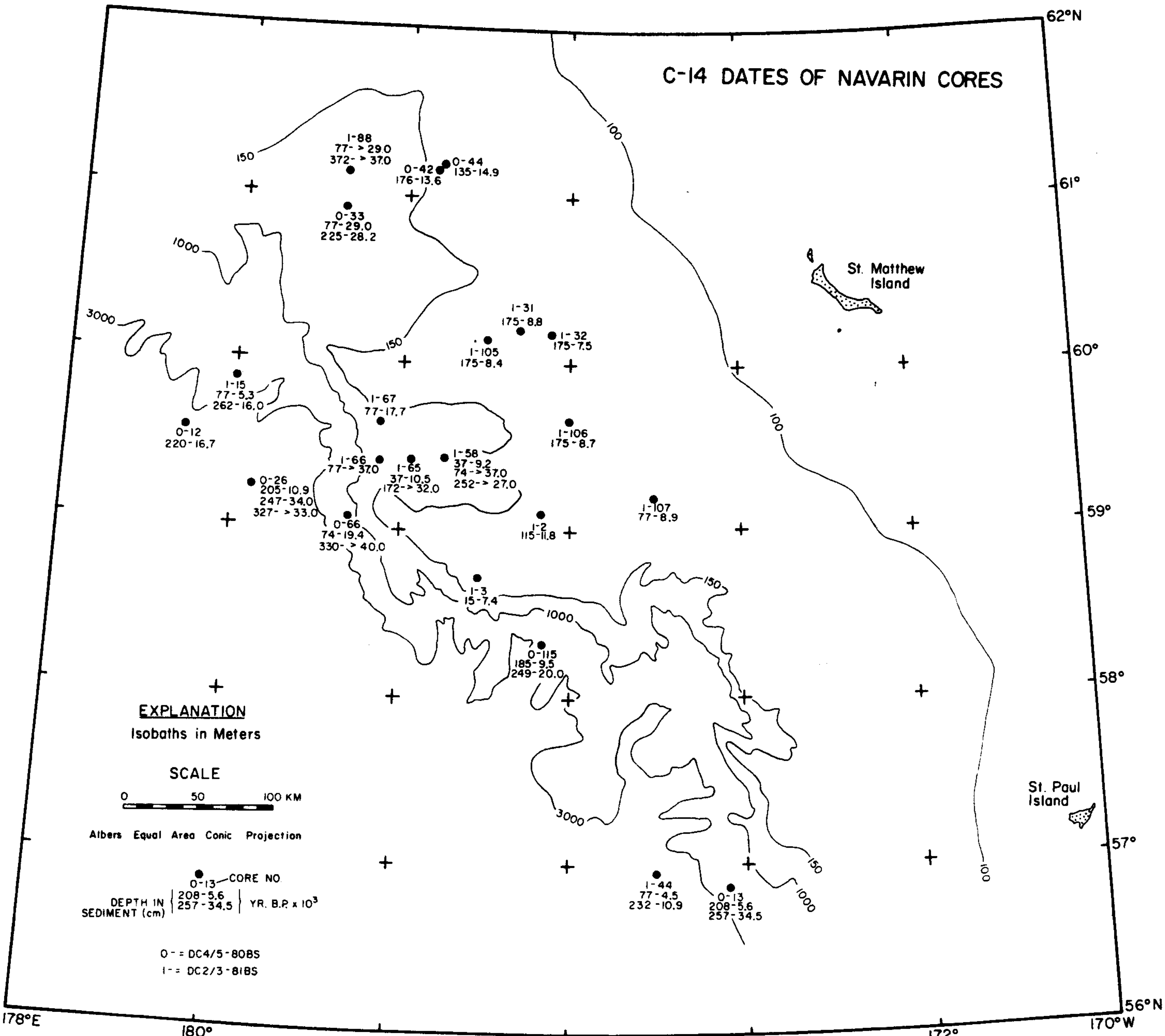

Figure 10. Location map of cores subsampled for C-14 dating.

Table 3. C-14 dates and rates of sediment accumulation listed by water depth.

	Core No.*	Water Depth (m)	C-14 Date (yrs BP)	Depth in core (cm)	Rate of Accumulation (cm/1000 yrs)
Shelf	1-107	116	8,900	77	8.8
	1- 32	130	7,500	175	23.3
	1- 03	133	7,375	15	2.0
	1-106	135	8,700	175	20.1
	0- 44	138	14,900	135	9.1
	1- 31	137	8,815	175	19.9
	0- 42	141	13,650	176	12.8
	1- 02	143	11,755	115	9.8
	1-105	144	8,385	175	20.9
Slope (upper)	1- 67	167	17,725	77	4.4
	1- 58	179	9,215	37	4.1
	"	"	>37,000	74	<2.0
	"	"	>27,000	252	<9.4
	1- 88	205	>29,000	77	<2.7
	"	"	>37,000	363	<9.8
	0- 33	210	28,980	77	2.7
	"	"	28,200	225	8.0
	1- 65	436	10,485	37	3.6
	"	"	>32,000	172	5.4
	1- 66	580	>37,000	77	<2.1
Slope (lower)	0- 66	1,336	19,370	74	3.9
	"	"	>37,500	330	8.8
	"	"	>32,000	382	11.9
	0- 13	2,692	5,580	208	37.1
	"	"	34,520	257	7.5
	1- 15	2,750	5,330	77	14.6
	"	"	15,975	262	16.5
	0-115	2,870	9,505	185	19.5
	"	"	19,990	249	12.5
Rise	0- 12	3,164	16,670	220	13.3
	0- 26	3,373	10,880	215	19.8
	"	"	33,990	247	7.3
	"	"	33,300	327	9.9
	1- 44	3,400	4,460	77	17.5
	"	"	10,925	232	21.3

*O = DC 4/5-80; 1 = DC 2/3-81

DISCUSSION

If we compare the rate of sediment accumulation with water depth (Table 3), some trends emerge for the various physiographic subdivisions of the Navarin continental margin. The average rate for all the shelf subsamples (<150 m water depth) analysed is 14.1 cm/10^3 yrs. However, a plot of these values (Fig. 11) shows that the samples make up two groups. A cluster of four cores located between the heads of Navarinsky and Pervenets canyons have an average rate of sediment accumulation of 21 cm/10^3 yrs, whereas shelf sediment north and south of the cluster averages 8.5 cm/10^3 yrs, including a low value of 2 cm/10^3 yrs from a core taken less than 10 kilometers from the shelf-slope break. The four cores that have an average rate of 21 cm/10^3 yrs plot near the center of greatest sediment thickness in Navarin basin (Chapter 6, this volume). Previous sedimentologic studies in the region illustrate the variable nature of the rates of sediment accumulation on the Bering shelf. Knebel (1972) reported rates ranging from 2.5 to 40 cm/10^3 yrs for cores collected northeast of Navarin basin. Askren (1972) reported rates ranging from 11 to 67 cm/10^3 yrs for cores collected along the southeastern edge of Navarin basin.

Accumulation rates of sediment cored on the upper slope range from 2 to nearly 10 cm/10^3 yrs, with an average value of 5 cm/10^3 yrs (Table 3). Eight of eleven of these subsamples yielded dates greater than 25,000 yrs BP, half of which came from sediment less than one meter deep in the core, suggesting either a very slow rate of deposition or erosion of some of the surficial sediment.

Cores from the lower slope range in accumulation rates from about 4 to 37 cm/10^3 yrs with an average of 15 cm/10^3 yrs (Table 3). Age dates from the upper meter of these cores, except 0-66 which was obtained from mid-slope depths, are less than 10,000 yrs B.P. indicating a much more rapid rate of deposition than on the upper slope. An explanation for the large difference in rates between upper and lower slope may be the widespread mass movement that has been noted on the Navarin continental slope (Carlson, Karl, Fischer, and Edwards, 1982), resulting in removal of sediment from the upper slope and deposition on the lower slope and rise.

Continental rise sediment apparently has accumulated at rates ranging from about 7 to 21 cm/10^3 yrs, with an average rate of nearly 15 cm/10^3 yrs (Table 3). Some of the cores from lower slope and rise depths that are associated with the large submarine canyon systems contain coarse, graded layers attributed to turbidity current deposition (Carlson, Karl, and Quinterno, 1982). Deposition recorded by these cores that contain coarse layers interbedded with hemiplagic muds must be episodic, which very likely accounts for the variability in core 0-26 for example (Table 3).

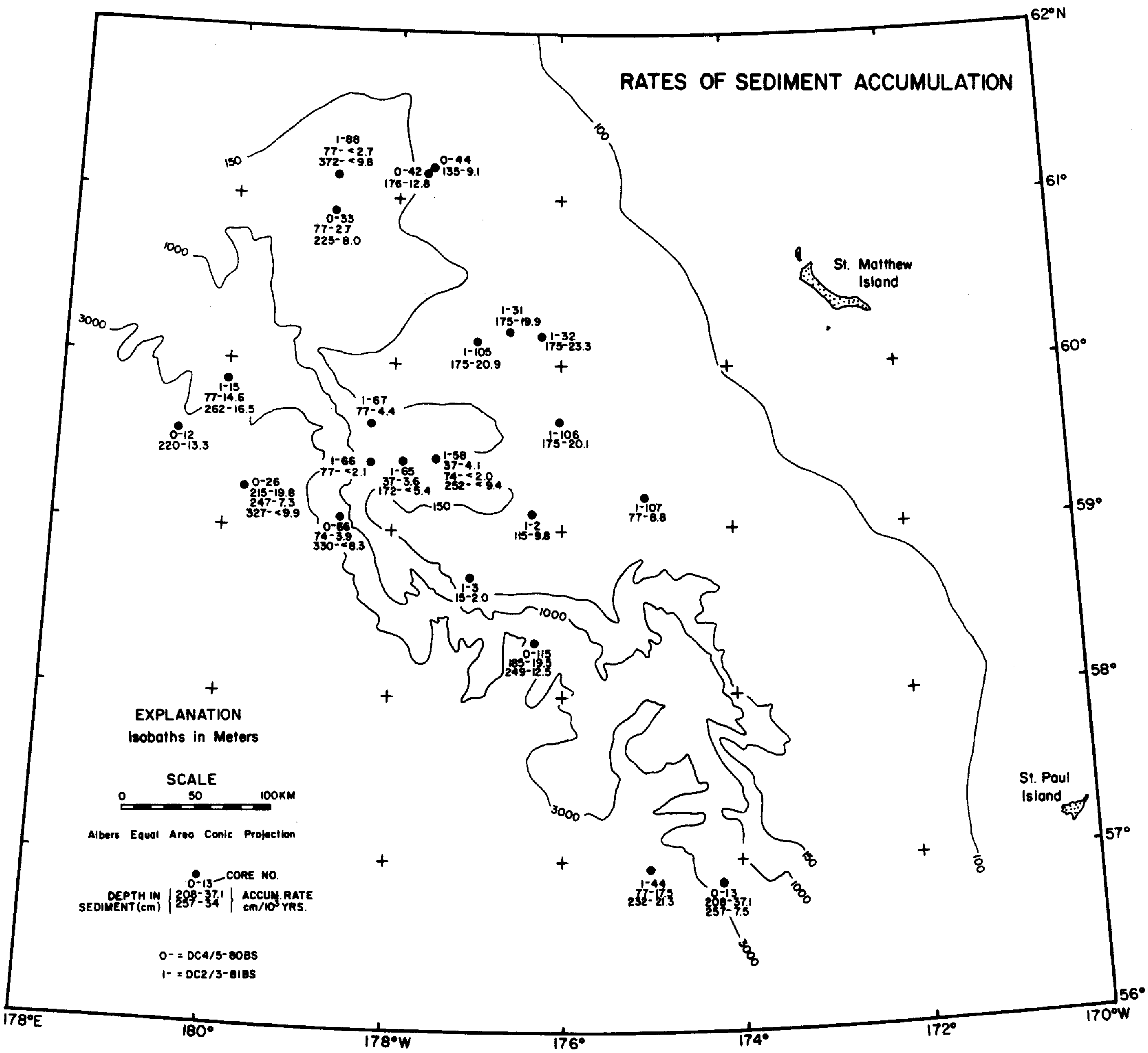

Figure 11. Map of dated cores showing calculated preliminary accumulation rates of sediment.

REFERENCES

Askren, D. R., 1972, Holocene stratigraphic framework - southern Bering Sea continental shelf: M.S. Thesis, Washington, Univ., Seattle, 104 p.

Carlson, P. R., Fischer, J. M., Karl, H. A., and Larkin, C., 1983, Isopach map of unit A, youngest sedimentary sequence in Navarin basin, Bering Sea, in Karl, H. A. and Carlson, P. R. eds., Surface and Near-surface Geology, Navarin Basin Province: Results of the 1980-81 Field Seasons: U.S. Geological Survey Open-File Report 83- , in press.

Carlson, P. R., Karl, H. A., and Quinterno, P., 1982, Sedimentologic processes in world's largest submarine canyons, Bering Sea, Alaska: Geological Society of America, Abstracts with Programs, v. 14, no. 7, p. 459-460.

Carlson, P. R., Karl, H. A., Fischer, J. M., and Edwards, B. D., 1982, Geologic hazards in Navarin Basin province, northern Bering Sea: 14th Offshore Technology Conference, Houston, Texas, Proceedings v. 1, p. 73-87.

Karl, H. A. and Carlson, P. R., 1982, Location and description of sediment samples: Navarin basin province, Bering Sea, 1980-81: U.S. Geological Survey Open-File Report 82-958, 5 p., 2 map sheets, scale 1:1,000,000.

Knebel, H. J., 1972, Holocene sedimentary framework of the east-central Bering Sea continental shelf: Ph.D. Thesis, Washington, Univ., Seattle, 186 p.

CHAPTER 5: PRE-QUATERNARY ROCKS AND SEMI-CONSOLIDATED SEDIMENT FROM THE NAVARIN CONTINENTAL MARGIN

by

Paul R. Carlson, Jack G. Baldauf, and Christopher Larkin

INTRODUCTION

The purpose of this chapter is to describe pre-Quaternary rocks and semi-consolidated sediment that have been collected from the outer shelf and slope of the Navarin basin province (see appendix D, Fischer and others, 1982, for a bathymetric map of the area). This chapter also compares these samples to rocks dredged from other parts of the Bering continental margin.

Although many of the samples we collected in 1980 and 1981 on cruises of the NOAA ship DISCOVERER (Karl and Carlson, 1982) are limited to the unconsolidated Holocene sediment blanket that covers most of the Navarin province, a few of the gravity cores penetrated through thin spots in the Holocene sediment cover into the underlying Pleistocene unit (Baldauf, 1982; Quinterno, 1981). Also, two gravity cores recovered semi-consolidated Tertiary-age strata that was cropping out on the continental slope. In addition to these cores, we also collected one chain-bag dredge of pre-Quaternary rocks from a steep scarp on the south side of Zhemchug Canyon. The locations of these three samples (1 dredge and 2 cores) are shown in figure 12.

Pre-Quaternary rocks also have been dredged from the Navarin margin from the USGS RV S.P. LEE (Marlow and others, 1979; Jones and others, 1981; see Fig. 12). Additional dredge samples were collected along the Bering margin south of Navarin basin from the RV THOMAS G. THOMPSON (Hopkins and others, 1969) and from the USGS RV SEA SOUNDER (Vallier and others, 1980).

RESULTS

Preliminary analyses of samples we collected in the Navarin province in 1980 and 1981 show that two cores and a single dredge haul recovered pre-Quaternary age material.

Core 80-106 (DC 4/5-80-106). Core 106 was taken from the lower continental slope at a water depth of 1785 m on the north side of a ridge separating Middle and Zhemchug Canyons (Fig. 12). This gravity core recovered 55 cm of very stiff olive gray (5Y 3/2) clayey silt with shale chips scattered throughout the lower 15 cm of the recovered interval. Diatoms from this semi-lithified core were assigned to the *Denticulopsis seminae* var. *fossilis* - *D. kamtschatica* zone of Barron (1980) which is the age equivalent of early late-Pliocene. An organic carbon analysis of a subsample (10-12 cm depth) from this core produced a value of 0.36 percent.

Core 81-46 (DC 2/3-81-46). Gravity core 46 was collected from the base of the continental slope south of Zhemchug Canyon in water 2530 m deep (Fig. 12). The 70 cm long core contained the most distinctive color change of

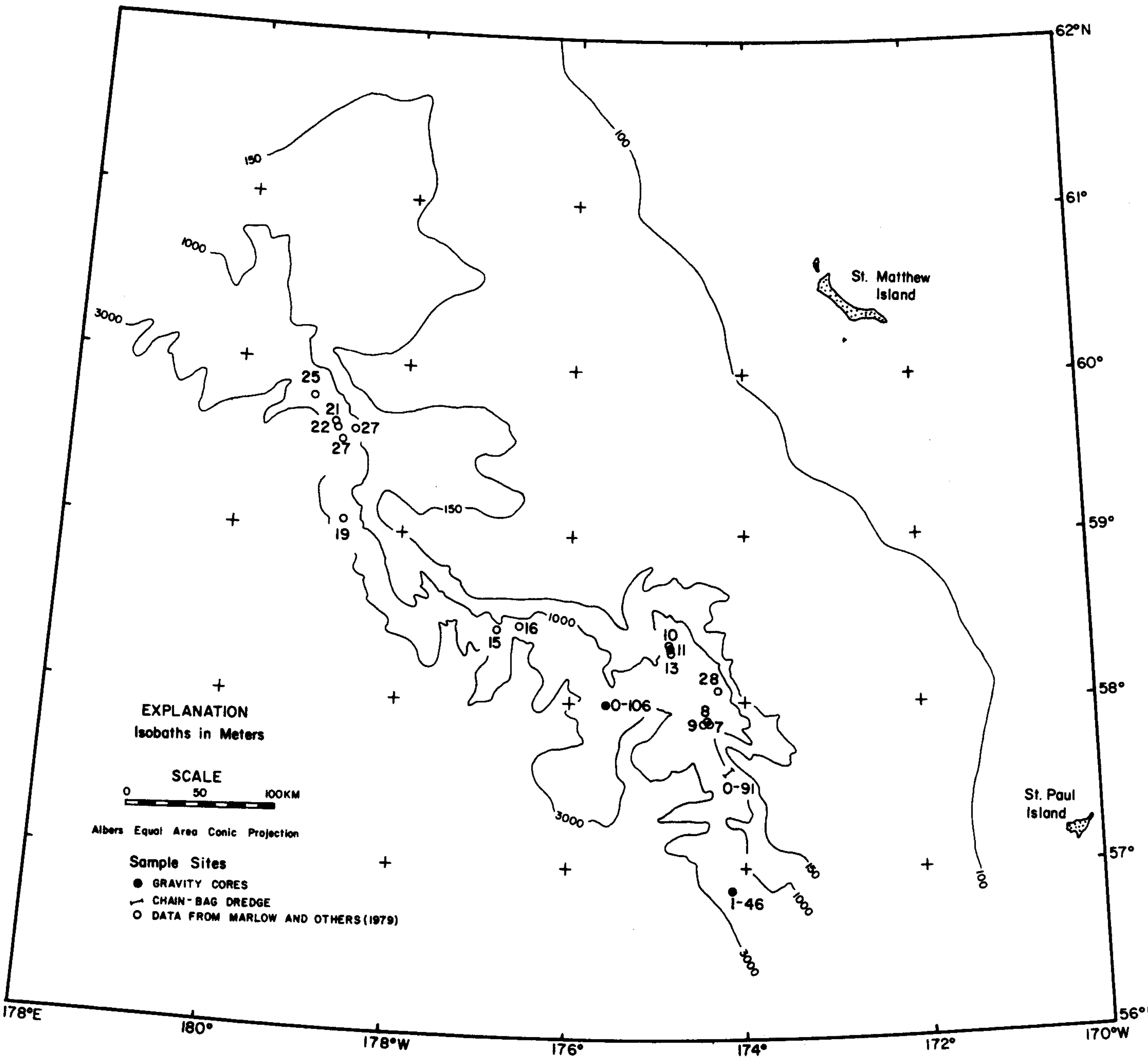

Figure 12. Locations of dredge hauls and gravity cores, Navarin margin.

any of the cores we collected. The upper 28 cm consisted of light olive brown (5Y 5/6) mud. At about 27-30 cm, there was an abrupt color change to a dark olive green gray (5GY 4/1) mud. There was no apparent textural change. Organic carbon contents of these two different colored muds was very similar, 0.41% at 11-15 cm and 0.48% at 45-49 cm. Clay mineral content in the two muds was quite different, however, with the upper unit containing 61% smectite, 18% illite, and 21% kaolinite plus chlorite compared to 46% smectite, 24% illite, and 30% kaolinite plus chlorite in the lower unit. Diatoms from both color units in this core are late Pliocene in age.

Dredge-1 (DC 4/5-80-91). A steep scarp on the wall of Pribilof Ridge, south of the main axis of Zhemchug Canyon (Fig. 12), was sampled by chain bag dredge in water depths between 2200 and 268 m. The excessive depth range of the dredge haul was due to a faulty tensiometer on the deep-sea winch, resulting in uncertainty of when the dredge was in contact with the seafloor. The dredge recovered a rather wide variety of rocks including one piece of ultra-basic rock (Pyroxenite), several small pieces of basalt, a large (40X28 cm) angular boulder of greenstone (probably metamorphosed basalt), several pieces of highly indurated conglomerate, an angular piece of black argillite, a small fragment of limestone, a small piece of calcareous siltstone, a small piece of calcareous sandstone, and many pieces of diatomaceous mudstone.

The cobble-size piece of limestone was found to be barren of calcareous nannofossils and of pollen and spores, thus not datable. The diatoms in the numerous pieces of mudstone provided age information ranging from early to late Miocene and the calcareous sandstone contained reworked mid-late Miocene diatoms.

Organic carbon contents of the mudstones range from 0.24% to 0.77% and average 0.56%. Carbonate carbon contents of the mudstones were all 0.01% or less. The calcareous siltstone has an organic carbon content of 0.79% and an inorganic carbon value of 3.63%. The limestone fragment consists of 0.72% organic and 7.28% inorganic carbon. The sandstone had the lowest organic carbon content of all samples measured (0.12%), but yielded an inorganic carbon value of 2.74%. Our carbon values agree quite closely with those reported by Vallier and others (1980), for rocks south of Navarin that yielded average organic carbon values of 0.52% and with Jones and others (1981) for mudstones from the northern half of the Bering margin, especially the Navarin margin, that have average organic carbon values of 0.55%. The inorganic carbon content of those mudstones averaged 0.08%. Jones and others (1981) also reported values from volcanic sandstones and tuffs that averaged 0.28% organic and 0.70% carbonate carbon, and from muddy and tuffaceous limestones that averaged 0.64% organic and 7.36% carbonate carbon. By way of comparison with the Tertiary mudstone samples dredged from the Bering margin, average organic carbon values of 93 Quaternary-age muds and sandy muds from cores we collected throughout the Navarin basin province was 0.83%, with the values ranging from 0.26% to 1.56%; inorganic carbon values also were higher than those of the Tertiary mudstones, averaging 0.13%, and ranging from 0.03% to 0.57% (Fischer, 1981).

A point count of 400 grains in a thin section of the mid-late Miocene sandstone (DC4/5-80-91) yielded a composition of quartz 37%, feldspar 17%, rock fragments 40% (61% of r.f. are volcanic), glauconite 3%, heavy minerals 2%, and others 1% including diatoms, and forams. The grains are sub-angular to sub-rounded, poorly-sorted, and range in size from fine sand to granules; the intergranular cement consists of microcrystalline calcite and makes up about 30% of the sample. According to Folk (1974), this sandstone would be classified as a submature calcareous volcanic arenite.

REFERENCES

Baldauf, J. G., 1982, Identification of the Holocene-Pleistocene boundary in the Bering Sea by diatoms: Boreas, v. 11, p. 113-118.

Barron, J. A., 1980, Lower Miocene to Quaternary diatom biostratigraphy of Leg 57, off northeastern Japan, Deep Sea Drilling Project, In, Honza, E. and others, Initial Reports of the Deep Sea Drilling Project, p. 641-685: Washington, D. C. (U.S. Government Printing Office).

Fischer, J. M., 1981, Carbon contents of Navarin basin sediments, In, Carlson, P. R. and Karl, H. A. (eds.), Seafloor Geologic Hazards, Sedimentology, and Bathymetry: Navarin Basin Province, Northwestern Bering Sea: U.S. Geological Survey Open-File Report 81-1217, p. 44-57.

Fischer, J. M., Carlson, P. R., and Karl, H. A., 1982, Bathymetric map of Navarin continental margin, Bering Sea: U.S. Geological Survey Open-File Report 82-1038, 11 p., 1 map sheet 1:1,000,000.

Folk, R. L., 1974, Petrology of sedimentary rocks: Hemphill Publishing Co., Austin, Tex. 182 p.

Hopkins, D., Scholl, D. W., Addicott, W. O., Pierce, R. L., Smith, P. B., Wolfe, J., Gershenovich, D., Kotenev, B., Lohrman, J. E., Lipps, J. H., and Obradovich, J., 1969, Cretaceous, Tertiary, and early Pleistocene rocks from the continental margin in the Bering Sea: Geological Society of America, Bull. 80, p. 1471-1486.

Jones, D. M., Kingston, M. J., Marlow, M. S., Cooper, A. K., Barron, J. A., Wingate, F. H., and Arnal, R. E., 1981, Age, mineralogy, physical properties, and geochemistry of dredge samples from the Bering Sea continental margin: U.S. Geological Survey Open-File Report 81-1297, 68 p.

Karl, H. A. and Carlson, P. R., 1982, Location and description of sediment samples: Navarin Basin province, Bering Sea, 1980-81: U.S. Geological Survey Open-File Report 82-958, 5 p., 2 maps, scale 1:1,000,000.

Marlow, M. S., Cooper, A. K., Scholl, D. W., Vallier, T. L., and McLean, H., 1979, Description of dredge samples from the Bering Sea continental margin: U.S. Geological Survey Open-File Report 79-1139.

Quinterno, P. J., 1981, Preliminary report on benthic foraminifers from Navarin basin province, Bering Sea, Alaska, In, Carlson, P. R. and Karl, H. A., (eds.), Seafloor Geologic Hazards, Sedimentology, and Bathymetry: Navarin Basin Province, Northwestern Bering Sea: U.S. Geological Survey Open-File Report 81-1217, p. 114-129.

Vallier, T. L., Underwood, M. B., Gardner, J. V., and Barron, J. A., 1980, Neogene sedimentation on the outer continental shelf margin, southern Bering Sea: Marine Geology, v. 36, p. 269-287.

CHAPTER 6: ISOPACH MAP OF UNIT A, YOUNGEST SEDIMENTARY SEQUENCE IN NAVARIN BASIN

by

Paul R. Carlson, Jeffrey M. Fischer,
Herman A. Karl, and Christopher Larkin

INTRODUCTION

Navarin Basin as defined by Marlow and others (1976) consists of a thick (>12 km) section of Mesozoic and Cenozoic sedimentary material that covers an area of 49,700 km^2 on the northwestern portion of the Bering continental shelf (Fig. 13). The main part of the basin, as delineated by the 2 km isopleth, is oriented northwest-southeast, parallel to the shelf-slope break.

The principal map in this chapter shows the thickness of only the uppermost unit, herein referred to as unit A, of the Navarin basin sedimentary sequence (Fig. 14). Figure 13 provides a comparison of the area covered by the isopached Unit A and the entirety of Navarin basin as mapped by Marlow and others (1979).

DATA COLLECTION AND REDUCTION

The high-resolution seismic-reflection data used in the development of the unit A isopach map were collected on cruises of the NOAA ship DISCOVERER in 1980 (DC 4/5-80) and 1981 (DC 2/3-81) (Carlson and Karl, 1981; 1982). Navigational control was by Loran C updated by satellite "fixes." Thicknesses of sediment seen on 3.5 kHz and minisparker records were measured on a digitizing table at five minute intervals. The Unit A was defined by a relatively flat-lying strong, persistent reflector that marked the base of the uppermost sedimentary unit (Fig. 15). This reflector could be traced with confidence throughout the mapped portion of the basin. The edges of the isopached area mark either an area where the reflector crops out at the seafloor (at least appears to do so within the limits of resolution of the high-resolution profiles) or the reflector cannot be traced further due to one of three factors (1) poor quality records, (2) disappearance or loss of strength of the reflector, or (3) insufficient track line coverage.

DISCUSSION

Unit A, the uppermost seismic-stratigraphic unit in the Navarin basin sequence, has been mapped over an area of 100,000 km^2 on the outer shelf in the northern Bering Sea (Fig. 14). This unit consists of unconsolidated sediment that ranges in type from clayey silt to muddy sand (Karl and Carlson, 1982) of Quaternary age (Baldauf, 1981). The average thickness of this unconsolidated unit is about 20 m. Unit A attains a maximum thickness of 45 m within a narrow (5-10 km wide) elongate trough located near the southeastern edge of Navarinsky Canyon, and just east of the deepest part of Navarin Basin (Fig. 13). This trough is part of a broader (40 km wide), shallower (30 m thick) depression filled with unit A sediment, that parallels

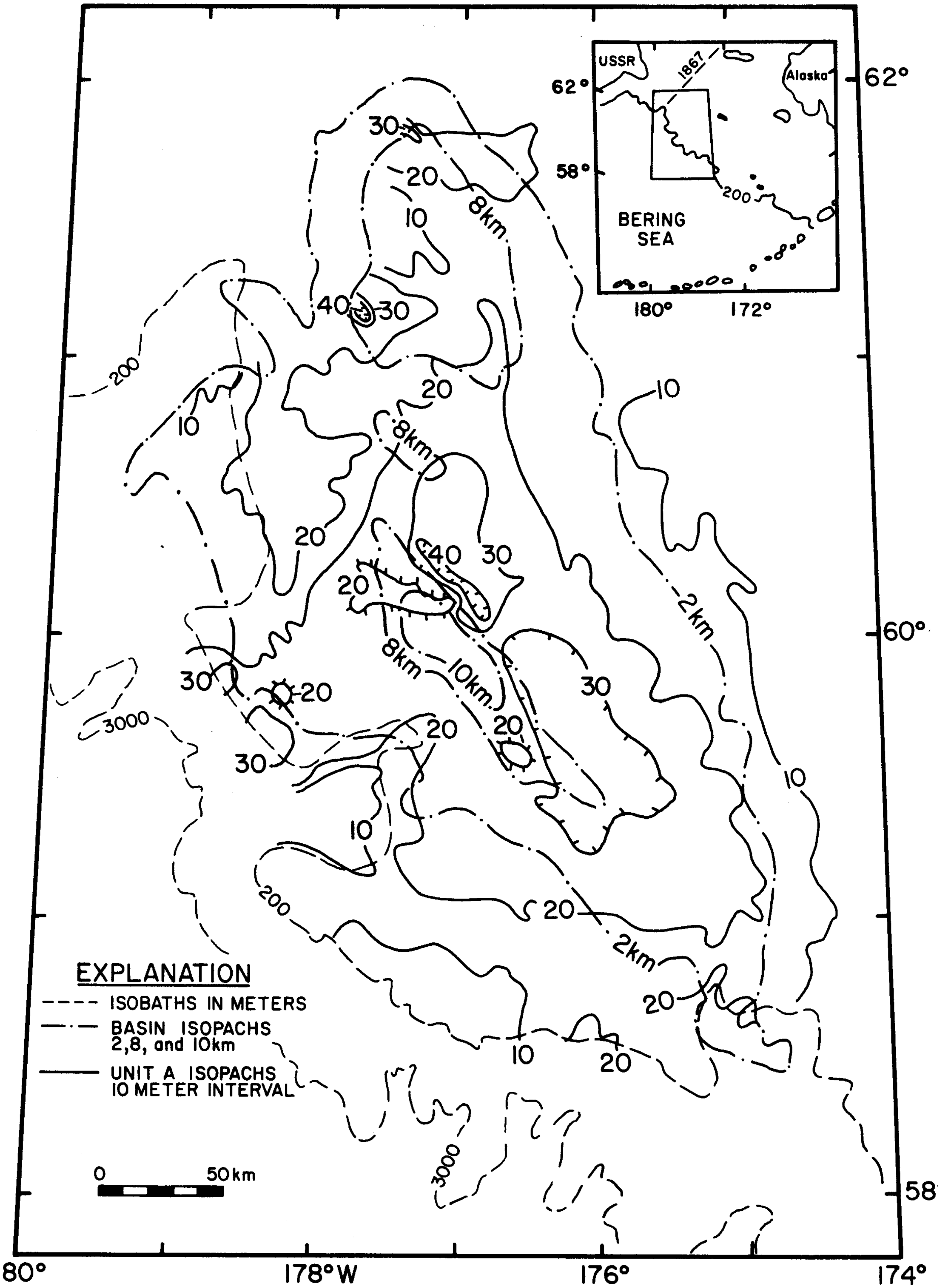

Figure 13. Isopach map of unit A superimposed on selected isopachs of strata above acoustic basement. Navarin Basin isopach above basement after Marlow and others (1979).

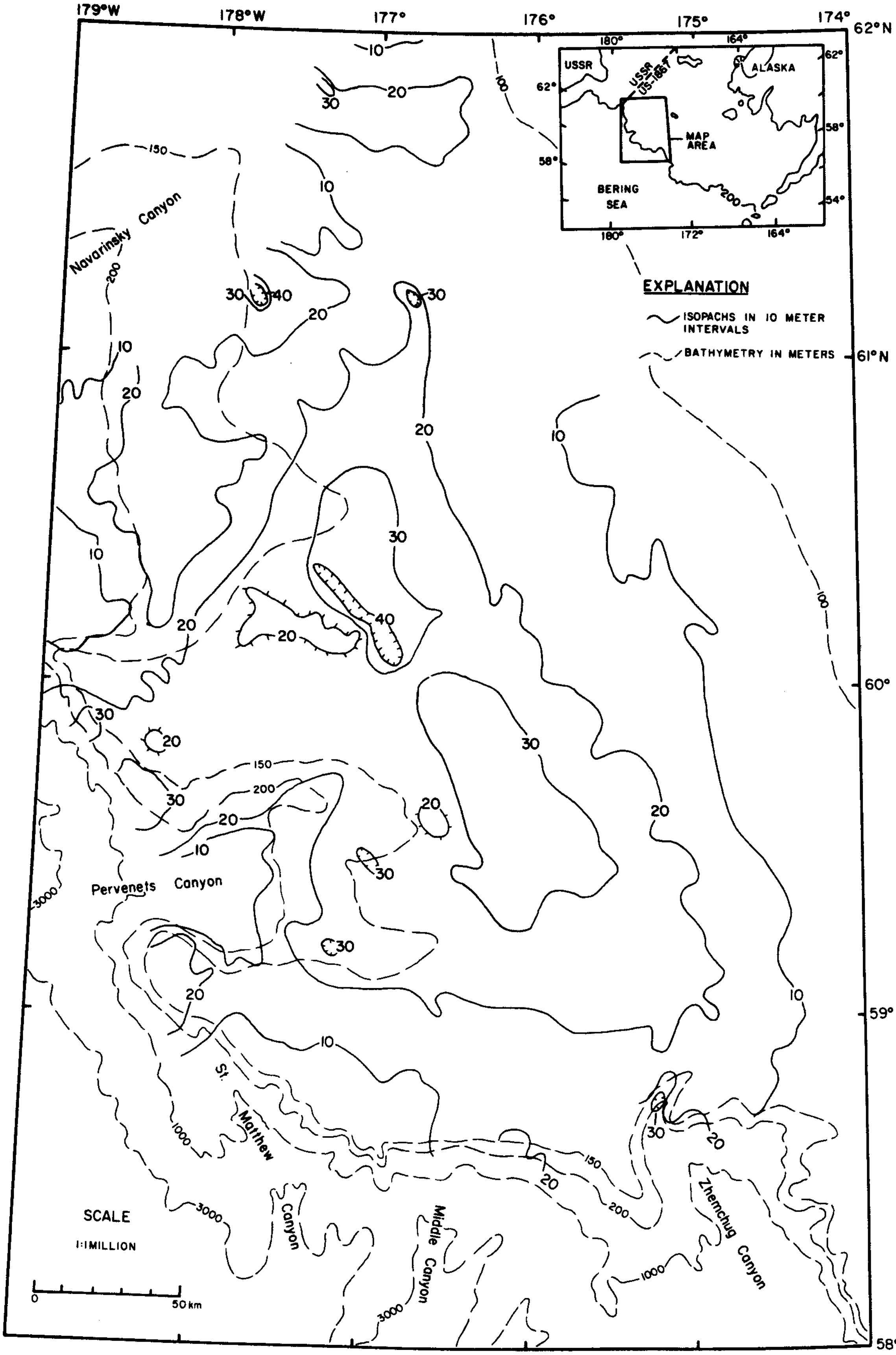

Figure 14. Isopach map of unit A, youngest stratigraphic sequence in Navarin Basin.

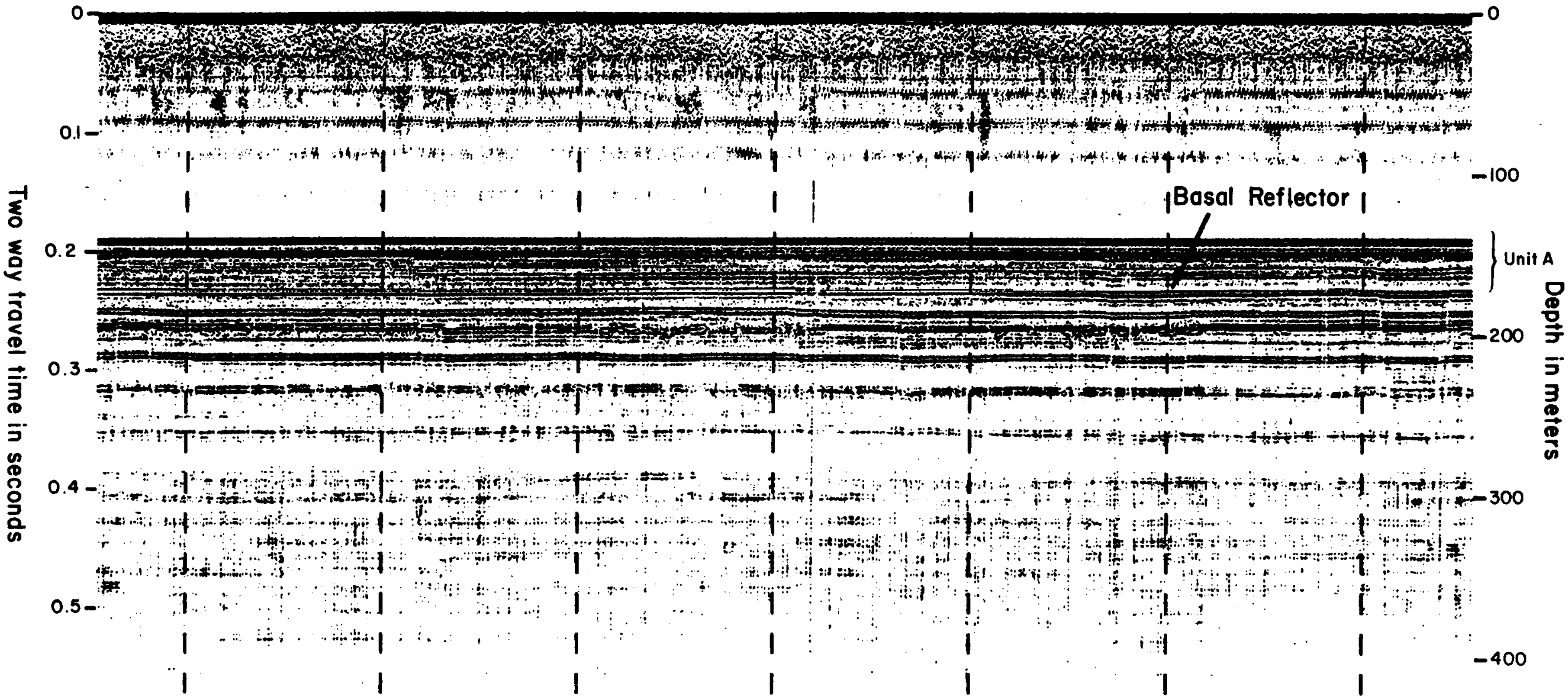

Figure 15. Minisparker profile (1000 J) showing seismic reflector (marked by arrow) that marks the base of isopached unit A. Vertical exaggeration ~8.5x.

the shelf break in present water depths of 130-150 m. The isopached unit pinches out to the northwest near the head of Navarinsky Canyon and also near the head of Pervenets Canyon. We have collected gravity cores near both canyons across the area of the outcropping reflector and are attempting to date this unit. At this time, we can only estimate that Unit A is less than 30,000 yrs B.P. based on C-14 dates and faunal data obtained from cores collected near the "pinchouts" (see Chapter 4).

REFERENCES CITED

Baldauf, J. G., 1981, Diatom analysis of late Quaternary sediments from Navarin Basin province, Bering Sea, Alaska, in Carlson, P. R. and Karl, H. A., eds., Seafloor geologic hazards, sedimentology, and bathymetry: Navarin Basin province, northwestern Bering Sea: U. S. Geological Survey Open-File Report 81-1217, p. 100-113.

Carlson, P. R. and Karl, H. A., 1981, High-resolution seismic reflection profiles: Navarin Basin province, northern Bering Sea, 1980: U.S. Geological Survey Open-File Report 81-1221, 4 p., 1 map, scale 1:1,000,000.

Carlson, P. R. and Karl, H. A., 1982, High-resolution seismic reflection profiles collected in 1981 in Navarin Basin province, Bering Sea: U.S. Geological Survey Open-File Report 82-786, 5 p., 1 map, scale 1:1,000,000.

Karl, H. A. and Carlson, P. R., 1982, Location and description of sediment samples: Navarin Basin province, Bering Sea, 1980-81: U.S. Geological Survey Open-File Report 82-958, 5 p., 2 map sheets, scale 1:1,000,000.

Marlow, M. S., Scholl, D. W., Cooper, A. K., and Buffington, E. C., 1976, Structure and evolution of Bering Sea shelf south of St. Lawrence Island: American Association of Petroleum Geologists Bulletin, v. 60, p. 161-183.

Marlow, M. S., Cooper, A. K., Parker, A. W., and Childs, J. R., 1979, Isopach map of strata above acoustic basement in the Bering Sea: U.S. Geological Survey Miscellaneous Field Studies Map MF-1164. 1 map sheet, scale 1:2,500,000.

CHAPTER 7: SUMMARY OF GEOTECHNICAL CHARACTERISTICS

by

Brian D. Edwards and Homa J. Lee

INTRODUCTION

Geotechnical properties were determined on recovered cores as a means of assessing sedimentary processes of engineering importance. One such property, the estimated in-place shearing strength, is a critical sediment geotechnical property used in the evaluation of geologic hazards. Also determined were index properties and consolidation (i.e., relative degree of compaction) characteristics of the sediment. Index properties (e.g., undrained vane shear strength, water content, and grain-size distribution) were measured to classify the sediment and to correlate with advanced strength test results. Consolidation properties were measured to correlate with relative shearing strength (Ladd and Foott, 1974) and to determine the effects of past geologic events (e.g., erosion of overburden).

Figure 16 shows major physiographic features in the Navarin Basin province. Of the 212 gravity cores and grab samples collected from the R/V DISCOVERER in 1980 and 1981 (Fig. 16), 149 were analyzed for geotechnical information. The majority of these cores were analysed only for simple index properties (vane shear strength and water content). Seven cores from the 1980 R/V DISCOVERER cruise were taken as replicate cores at selected coring sites (Fig. 17). Each replicate core was analysed for the index properties listed above in addition to grain specific gravity, Atterberg limits, one-dimensional consolidation characteristics, and static and cyclic triaxial shear strength.

After collection, each core was cut into multiple sections onboard ship using a rotary knife blade cutter. Core sections, excluding those of replicate cores, were split longitudinally using a specially designed cutting system and a wire saw. Although sample disturbance is aggravated by such longitudinal splitting, this procedure allows more frequent downcore testing while maintaining sample integrity for other analyses (e.g., X-ray radiography, photography, and textural analysis). Testing for undrained vane shear strength and water content subsampling was conducted onboard ship.

The replicate cores collected for more advanced geotechnical testing were sectioned as described above, but were not split longitudinally. Vane shear tests were conducted and water content subsamples were taken at the top of each unsplit core section. End caps were sealed on both ends of each core section. The core sections were then wrapped in cheesecloth, sealed with a non-shrinking, microcrystalline wax, labelled, and stored vertically under refrigeration. The replicate cores were shipped by refrigerated air transport from Kodiak, Alaska, to refrigerated storage facilities at the U.S. Geological Survey laboratory in Palo Alto, California. These cores were subsequently shipped by refrigerated freight to Ertec Western, Inc., a commercial geotechnical testing laboratory in Long Beach, California, for advanced geotechnical analyses.

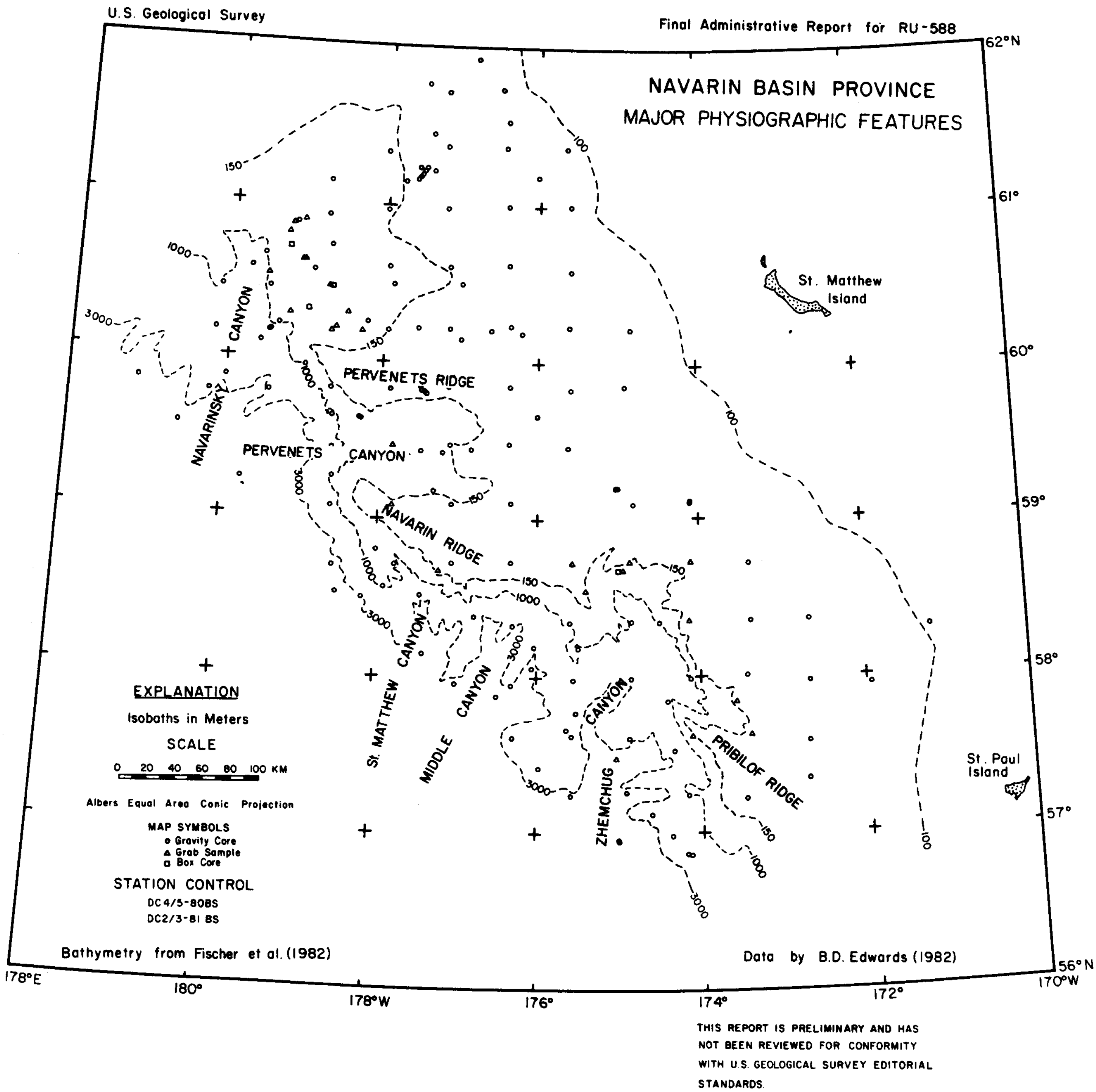

Figure 16. Major physiographic features of Navarin Basin province (after Fischer et al., 1982), and core locations for 1980 and 1981 R/V DISCOVERER cruises.

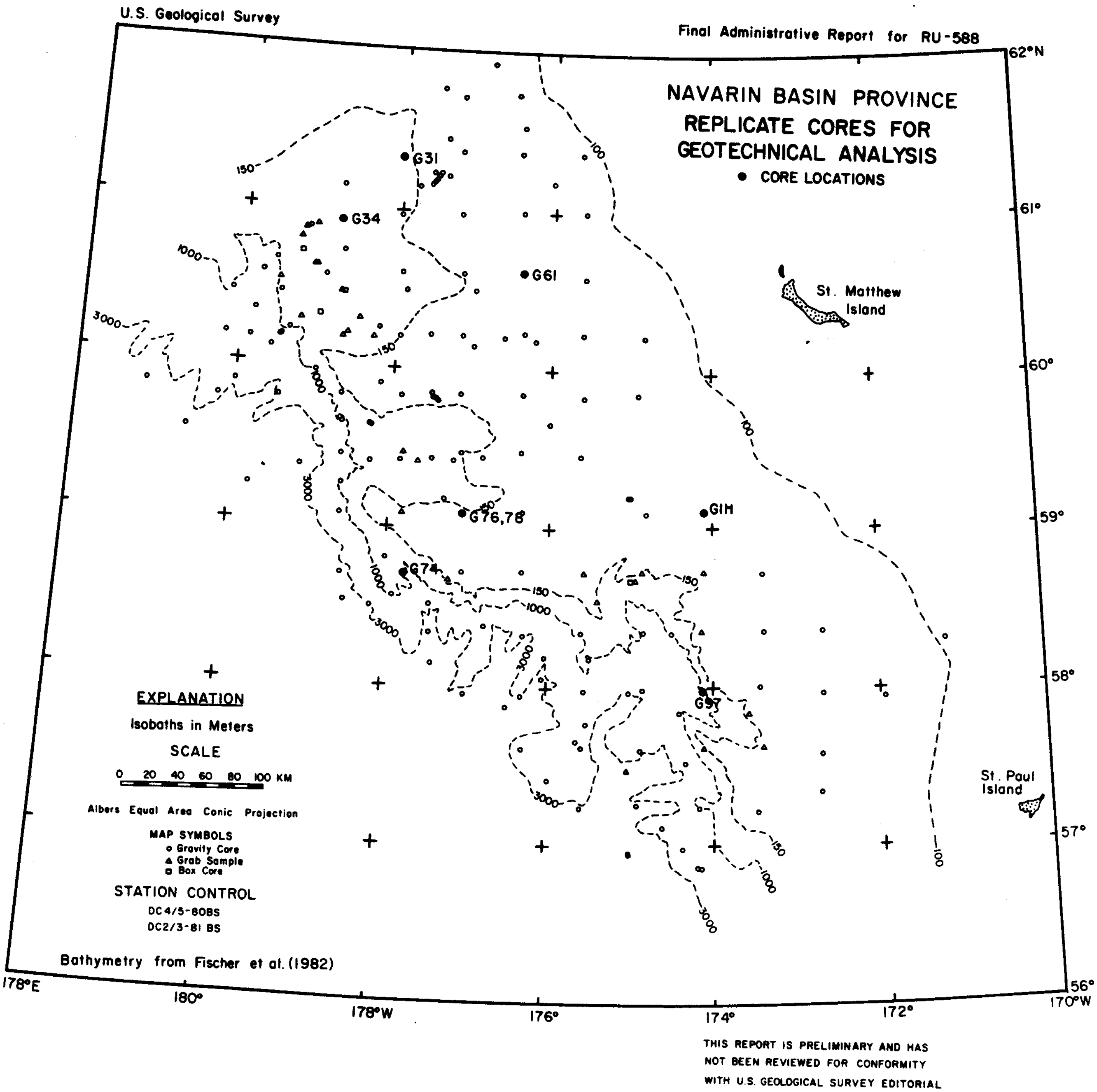

Figure 17. Location map of replicate cores collected for advanced geotechnical testing of Navarin Basin province sediment, 1980 R/V <u>Discoverer</u> cruise.

TESTING PROGRAM

Index Property Tests

Undrained Vane Shear Strength

Methods. Strength measurements were made using a motorized Wykeham-Farrance miniature vane shear device. Tests were made with a four-bladed 1/2 inch vane which was inserted into the cores so the top of the vane was buried by an amount equivalent to blade height. Torque was applied to the vane by either a torque cell that rotates the vane directly, or by a calibrated spring. Rotation rate of the torque cell and the top of the calibrated spring was a constant 90° per minute. When the spring system was used, torsion was measured and correlated directly with torque applied at the vane. Because of the spring's flexibility, rotation rate at the vane changed throughout the test. Tests were made on the ends of each core section and at 20 cm intervals on longitudinally split core sections.

Undrained vane shearing strength (S_v), as determined with the Wykeham-Ferrance device, was calculated from peak torque by assuming that the sediment builds a peak shearing resistance everywhere, and at the same time, along a right-circular cylinder inscribed around the vane. This term (S_v) is commonly equated with the undrained shear strength of the sediment (S_u); tests were made in the triaxial testing program to assess the validity of this method.

Findings. Figure 18 presents a comparison of vane shear strength as determined on split and unsplit sections with the torque cell and calibrated spring. The method of torque measurement (spring vs torque cell) and the core state (split vs unsplit) appeared to have little impact on the general trend of the shear strength versus depth variation.

The Navarin Basin province can be divided into 3 morphologic zones: (1) the shelf, typically shallower than the 150 m isobath; (2) the shelf edge and uppermost slope (about 150 to 200 m); and (3) the continental slope and continental rise (about 200 m to 3600 m). The shelf edge and uppermost slope is typically a zone of sand and muddy sand (Karl and others, 1981). Because vane shear strengths of cohesionless sediments such as those at the shelf edge have little value due to pore water drainage during sampling and testing, the zone of cohesionless sediment has been identified and excluded from the data base for undrained vane shear strength.

The areal distribution of vane shear strength at subbottom depth intervals of 1 m is shown in Figures 19-23. Data control is shown by the large, solid circles. At a subbottom depth of 1 m on the shelf, undrained vane shear strengths range from 2 kPa to 22 kPa. A zone of relatively weak sediment (<10 kPa) occupies the shelf about 150 km west of St. Matthew Island. West of this zone, adjacent to Pervenets Ridge, is a zone of relatively high (>15 kPa) shear strength. To the southeast, near the head of Zhemchug Canyon, is another zone of relatively high (>10 kPa) shear strength.

The few cores that recovered more than 2 m of sediment on the shelf were all less than 3 m long and were concentrated in the northern part of the area

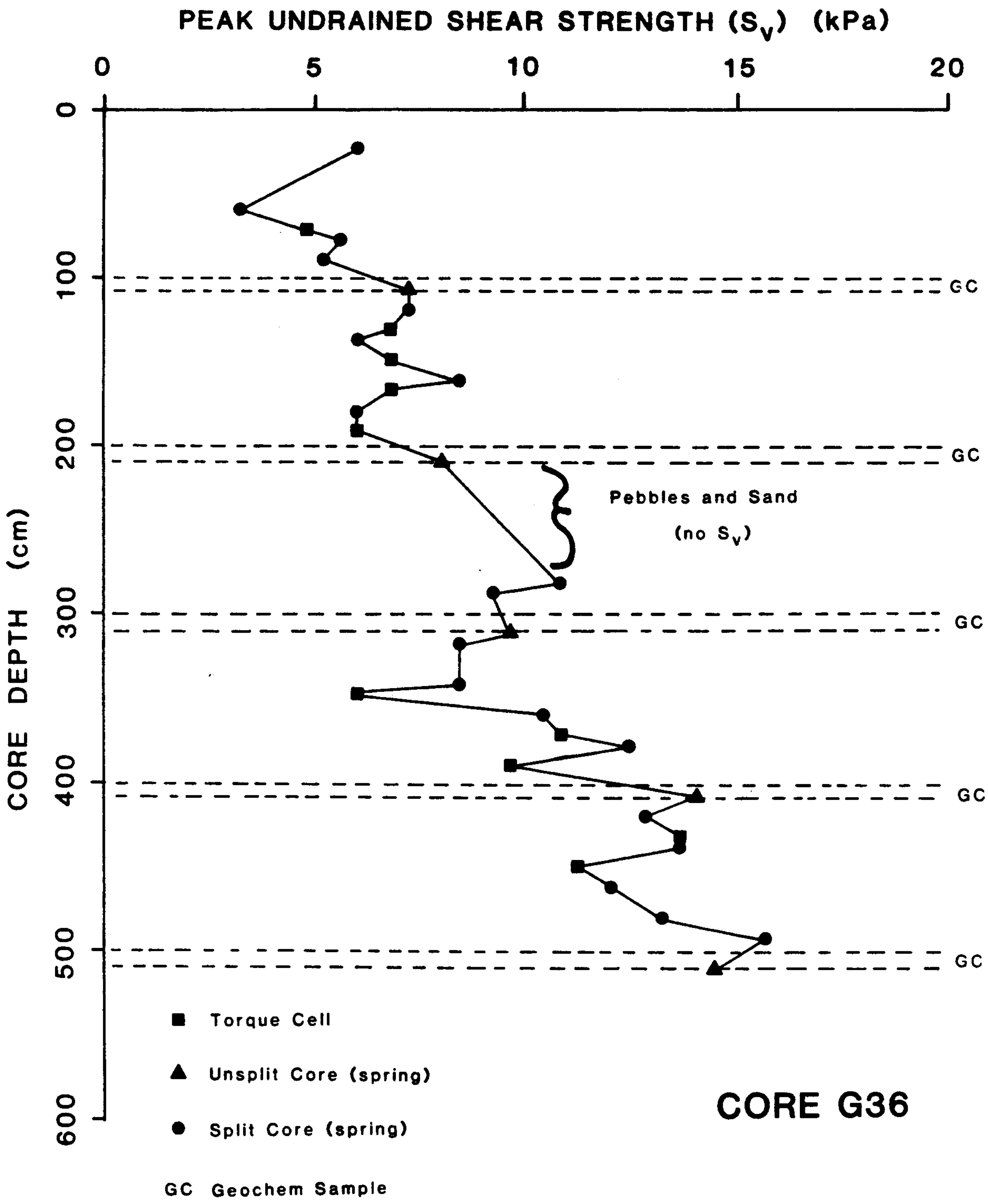

Figure 18. Comparison of S_v values as determined by calibrated spring and torque cell measurements. Anisotropic effects on S_v as shown by split and unsplit cores are small. GC indicates sample removed for geochemical analysis. Core G36, 1980 R/V Discoverer cruise.

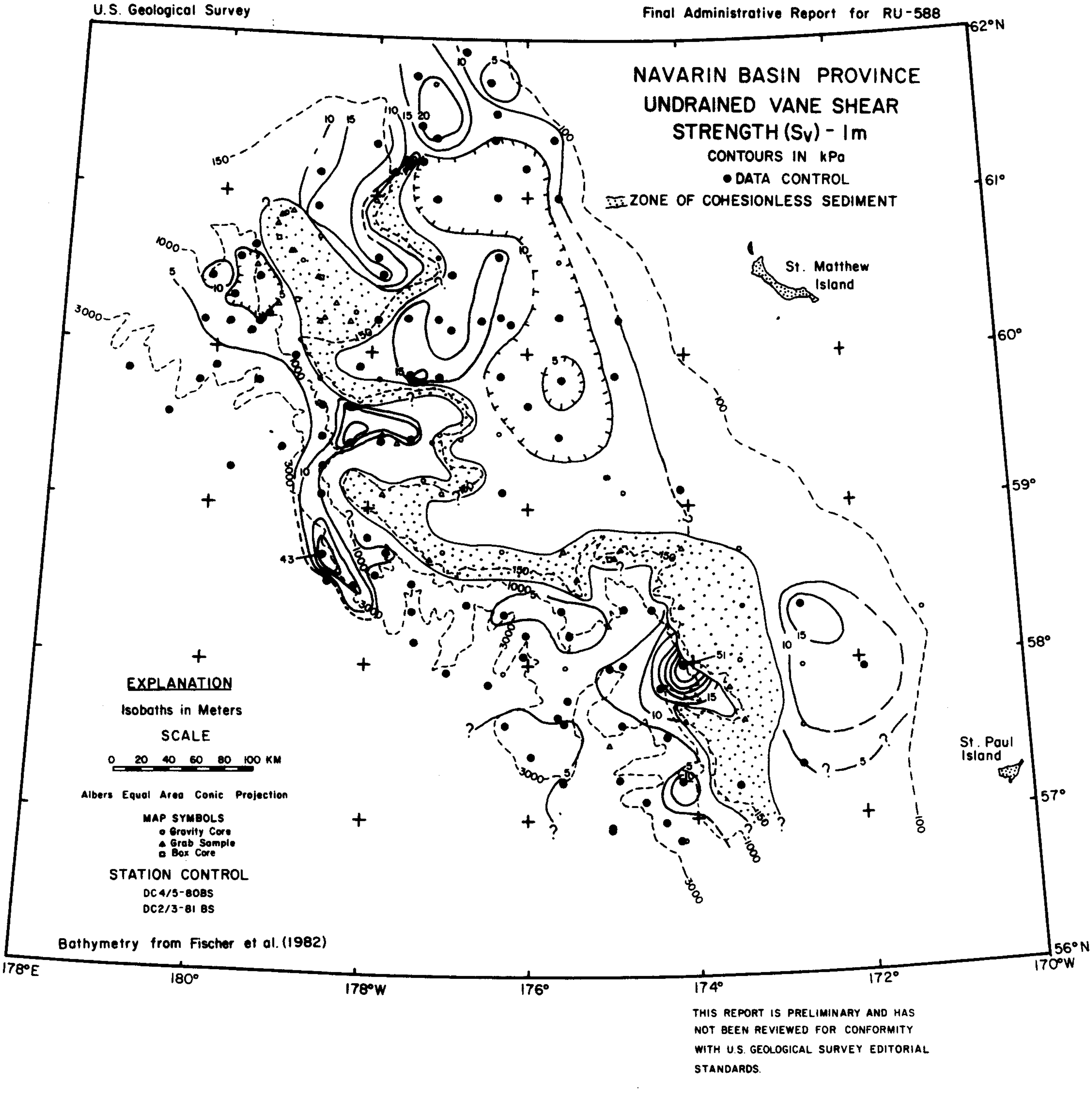

Figure 19. Areal distribution of peak undrained vane shear strength S_v at a subbottom depth of 1 m. Contour interval 5 kPa.

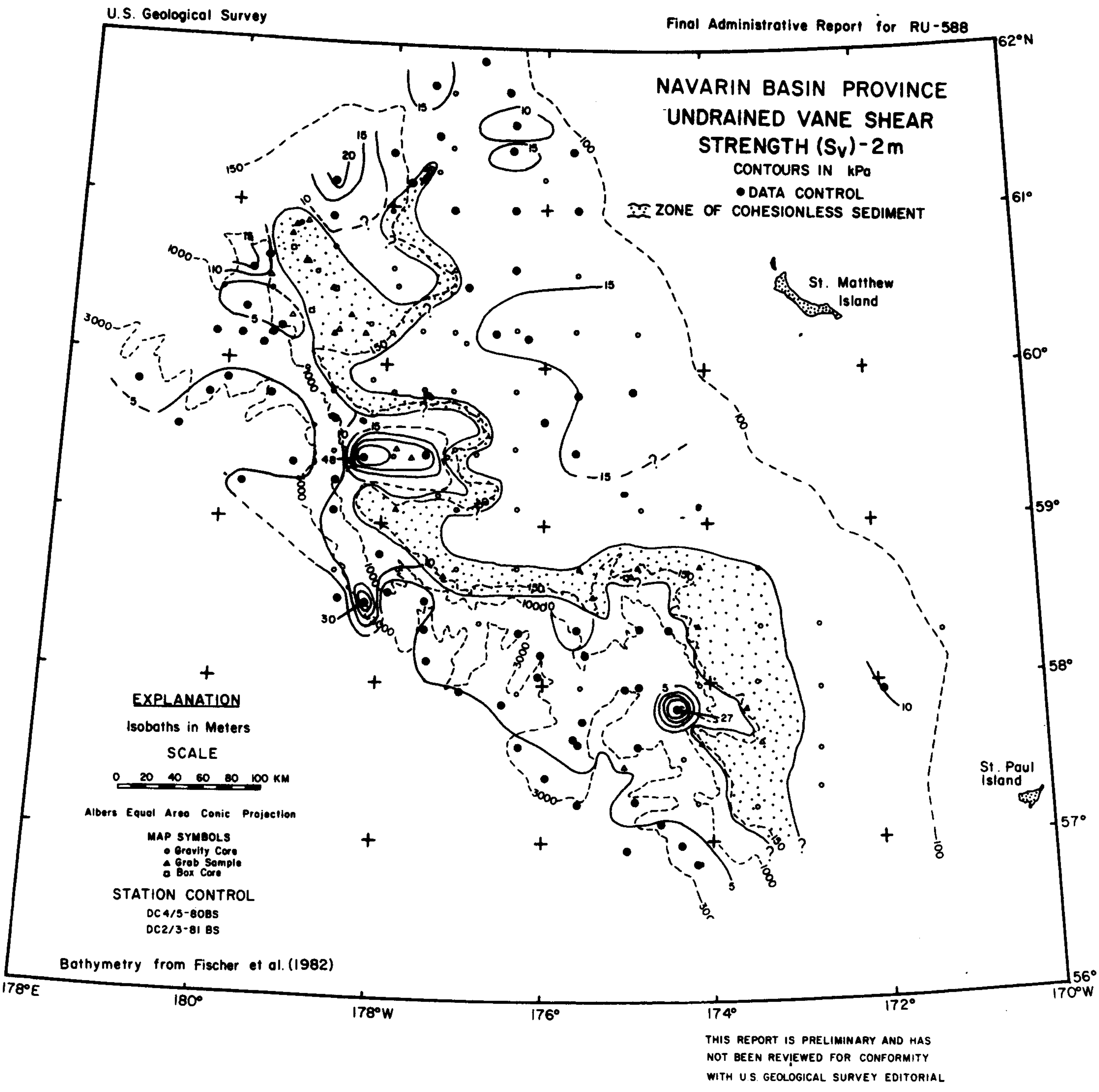

Figure 20. Areal distribution of peak undrained vane shear strength S_v at a subbottom depth of 2 m. Contour interval 5 kPa.

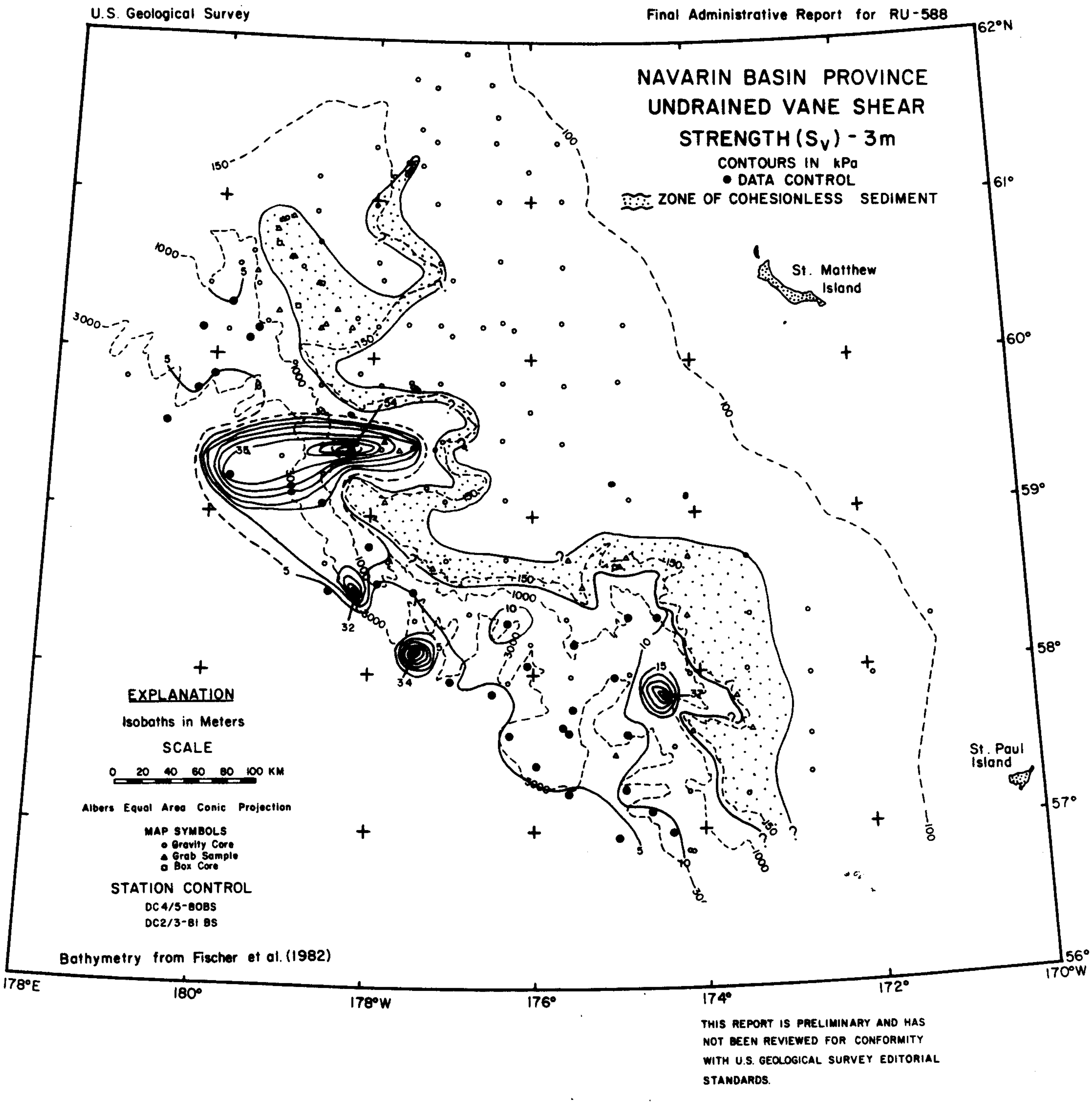

Figure 21. Areal distribution of peak undrained vane shear strength S_v at a subbottom depth of 3 m. Contour interval 5 kPa.

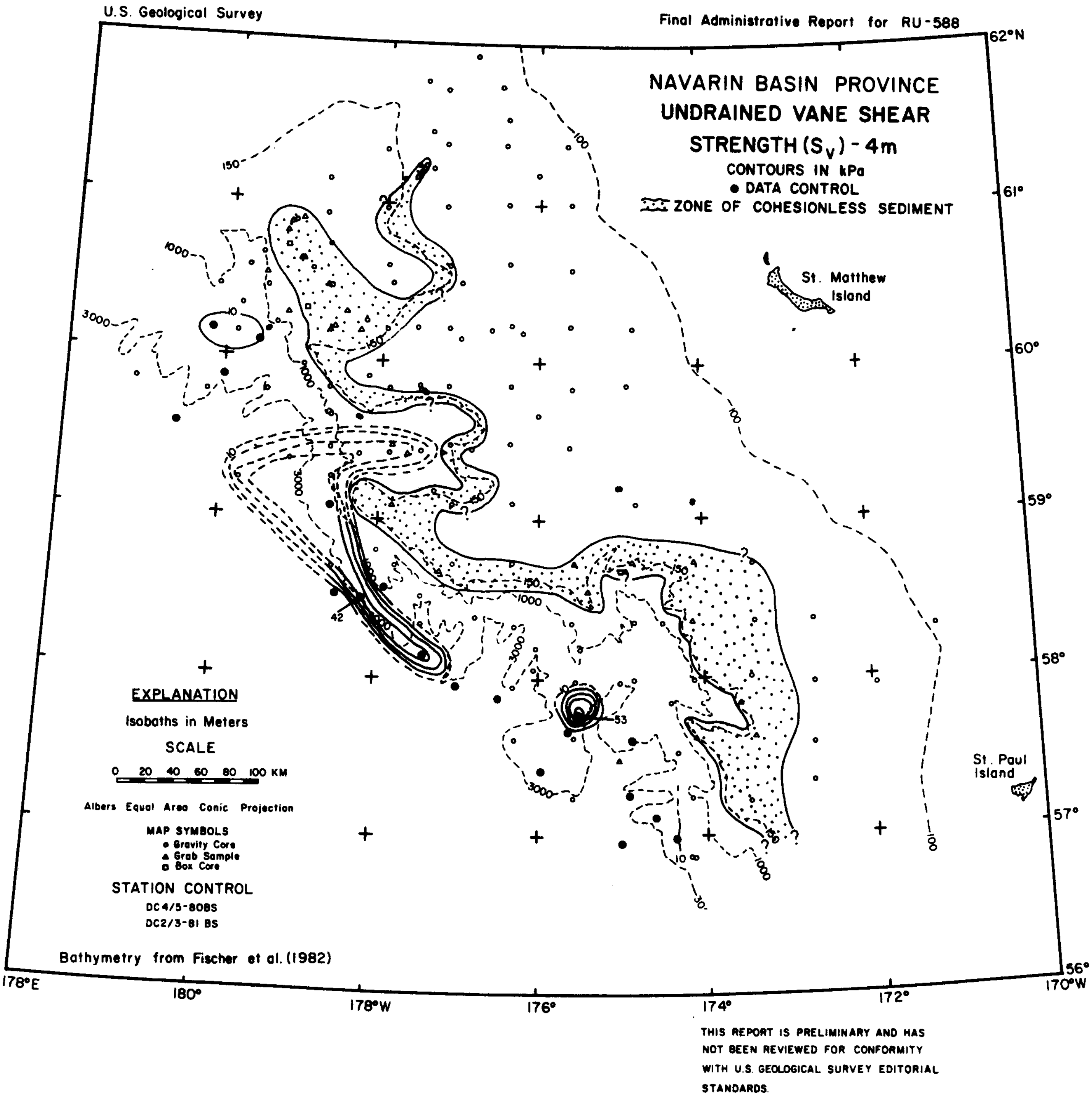

Figure 22. Areal distribution of peak undrained vane shear strength S_v at a subbottom depth of 4 m. Contour interval 10 kPa.

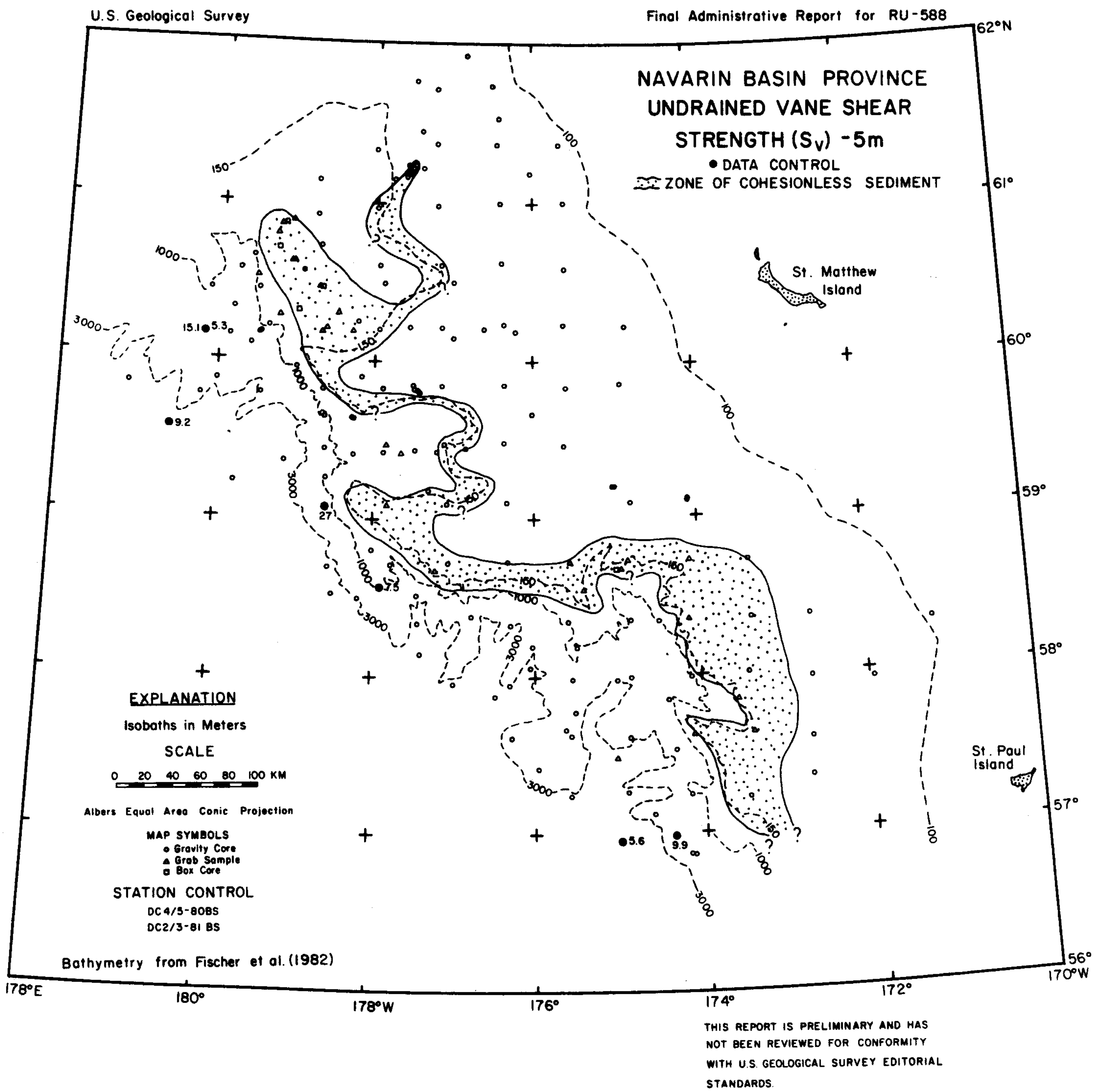

Figure 23. Areal distribution of peak undrained vane shear strength S_v at a subbottom depth of 5 m. Data values (in kPa) written beside appropriate core location.

(Figs. 20 and 21). At a subbottom depth of 2 m, shelf sediment shear strengths ranged from 7 kPa to 19 kPa. Distinct trends were not definable.

For slope cores, shear strengths ranged from 2 kPa to 51 kPa at a subbottom depth of 1 m (Fig. 19). Shear strengths were relatively high (>10 kPa) at the heads of canyons (e.g., Navarinsky Canyon). Most of the lower slope sediment, below 1500 m, had shear strengths less than 5 kPa. Three sites, one in Pervenets Canyon, one below Navarin Ridge, and a third at the headwall of Zhemchug Canyon, had high shear strengths (ranging from 38 to 51 kPa). Evidence from one-dimenional consolidation tests conducted on a replicate core from the headwall of Zhemchug Canyon (core G97) shows that sediment to be overconsolidated and likely represents older sediments exposed due to slumping or erosion. At greater subbottom depth these isolated sites of high shear strength become zones of anomalously strong sediment (cf., Figs. 19 through 23) and likely represent older (possibly Pleistocene?) sediment exposed by slumping or erosion. Few (7) cores achieved penetrations of 5 m or more. These cores were all located on the slope or rise; shear strengths at 5 m subbottom depth ranged from 5 kPa to 27 kPa (Fig. 23).

Water Content

Methods. Water content (computed as percent dry weight of sediment) and bulk density subsamples were obtained from the location of the vane test immediately following strength testing. These samples were taken with a small tube sampler and stored in sealed sample bottles for subsequent analyses at the shorebased laboratory.

Water contents were determined following ASTM D2216-80. The data were salt corrected using an assumed salinity of 32.5 parts per thousand and the relationship:

$$W_c = \frac{1.0325W}{1-0.0325W} \quad \ldots\ldots\ldots\ldots\ldots\ldots\ldots \quad (1)$$

where W_c = corrected water content
W = water content with no salt correction

Findings. Maps presenting water content are shown at subbottom depth intervals of 1 m in Figures 24 through 28. Shelf sediments at 1 m have water contents ranging from 20% to 137% with the highest values being associated with the zone of weak sediment 150 km west of St. Matthew Island. The lowest measured water contents at 1 m subbottom depth are associated with the Navarin Ridge. Shelf sediment water contents at 2 m show an unremarkable distribution that ranges from 43% to 107%.

At a 1 m subbottom depth, slope sediment water contents increase to the south and with increasing water depth (Fig. 24). With increasing subbottom depth, water contents decrease across the entire area, but, at each horizon, the trend of increasing values to the south and with increasing water depth continues.

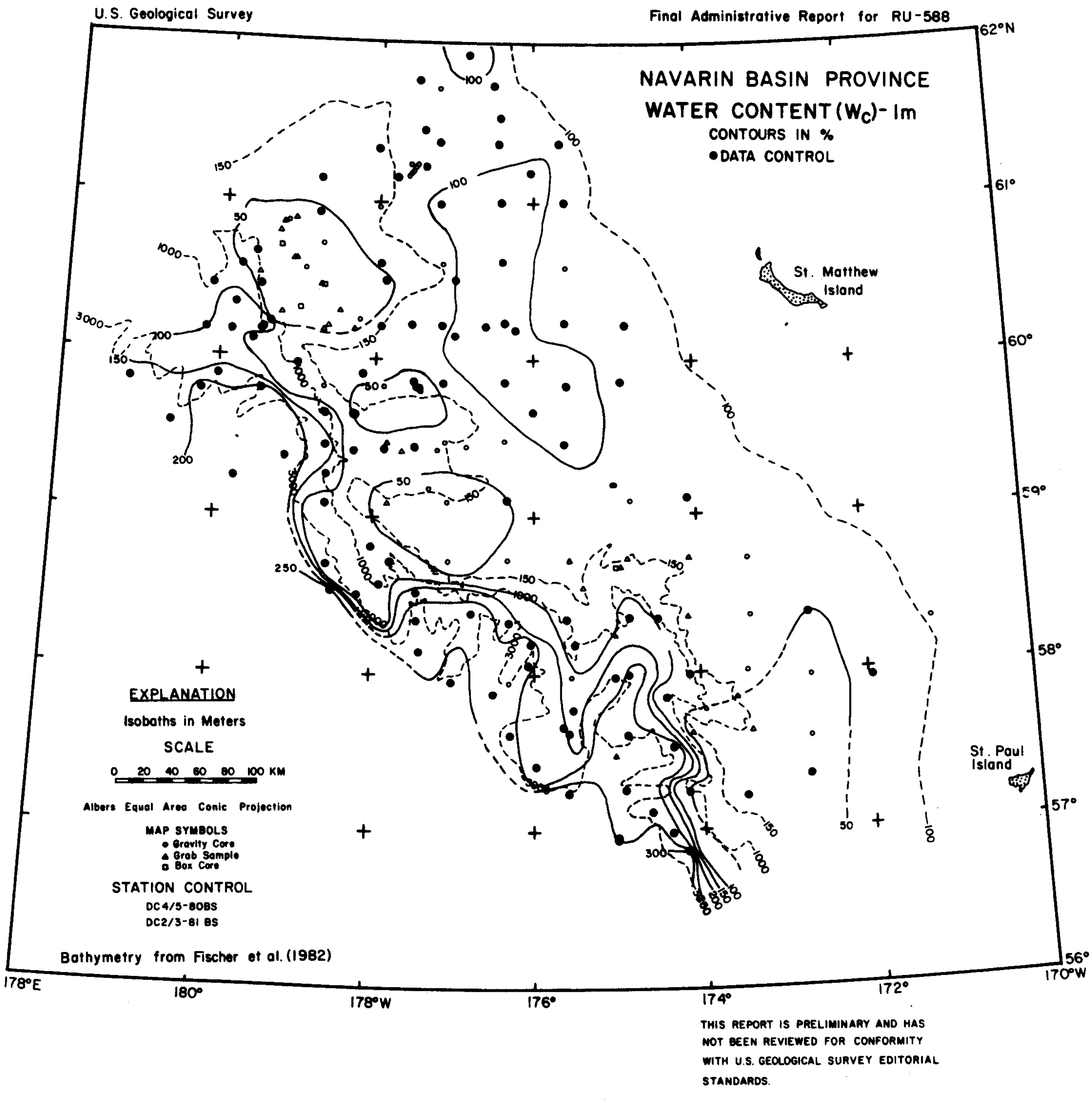

Figure 24. Areal distribution of salt corrected water content (W_c) at a subbottom depth of 1 m. Contour interval 50% by dry weight.

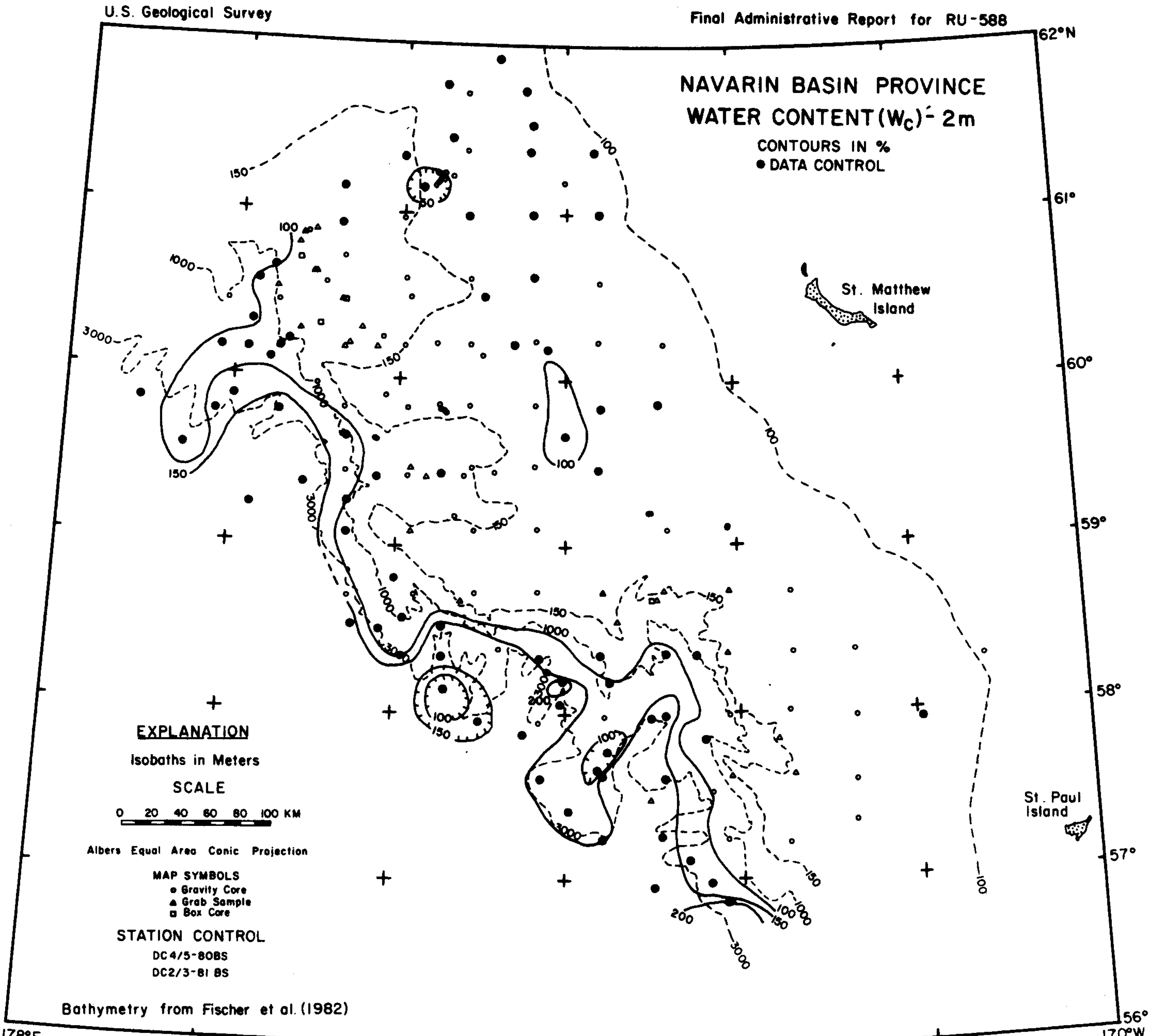

THIS REPORT IS PRELIMINARY AND HAS NOT BEEN REVIEWED FOR CONFORMITY WITH U.S. GEOLOGICAL SURVEY EDITORIAL STANDARDS.

Figure 25. Areal distribution of salt corrected water content (W_c) at a subbottom depth of 2 m. Contour interval 50% by dry weight.

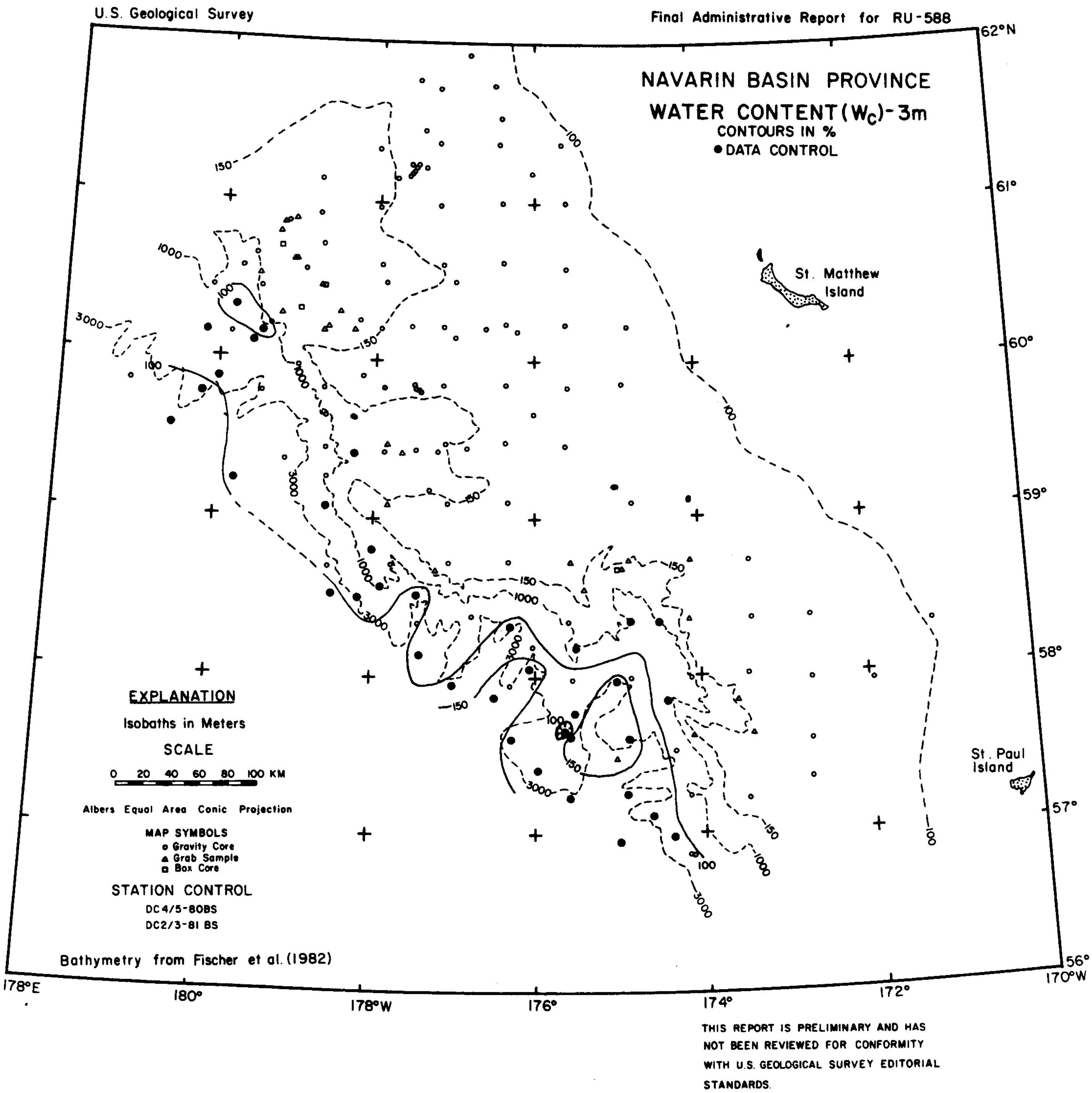

Figure 26. Areal distribution of salt corrected water content (W_c) at a subbottom depth of 3 m. Contour interval 50% by dry weight.

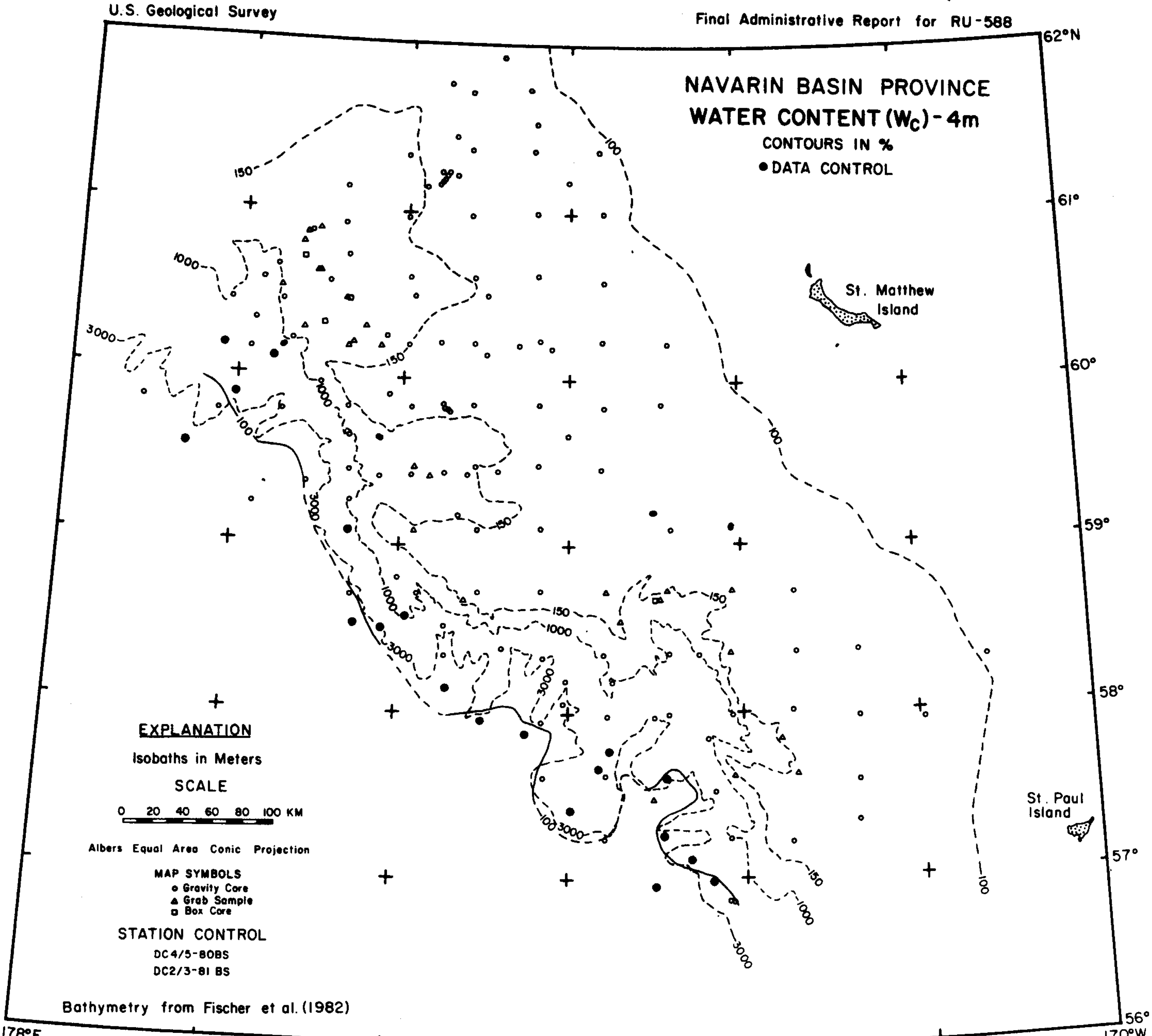

THIS REPORT IS PRELIMINARY AND HAS NOT BEEN REVIEWED FOR CONFORMITY WITH U.S. GEOLOGICAL SURVEY EDITORIAL STANDARDS.

Figure 27. Areal distribution of salt corrected water content (W_c) at a subbottom depth of 4 m. Contour interval 50% by dry weight.

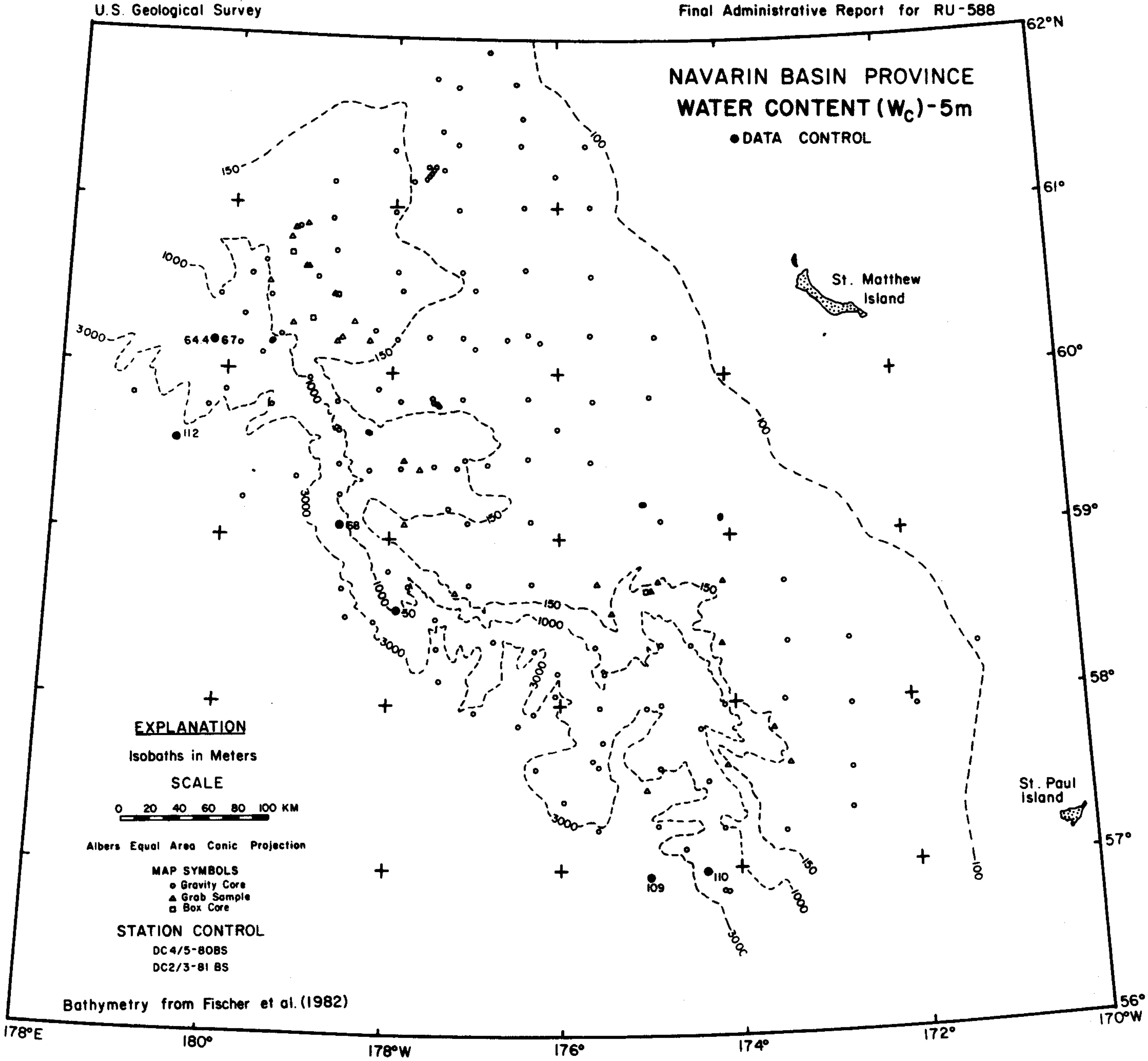

THIS REPORT IS PRELIMINARY AND HAS NOT BEEN REVIEWED FOR CONFORMITY WITH U.S. GEOLOGICAL SURVEY EDITORIAL STANDARDS.

Figure 28. Areal distribution of salt corrected water content (W_C) at a subbottom depth of 5 m. Data values in % written beside appropriate core locations.

Bulk densities were computed directly from the water content data following standard formulas and assuming 100% saturation (e.g., Lambe and Whitman, 1969). In-place effective overburden stress (σ'_v) was computed as:

$$\sigma'_v = \sum_{o}^{z} \gamma'_c \Delta z \qquad (2)$$

where
γ'_c = sediment submerged bulk density; $\gamma'_c = \gamma_c - \gamma_{sw}$
γ_c = sediment bulk density
γ_{sw} = density of seawater
z = subbottom depth in cm

Detailed downcore computations were made for most cores; values of σ'_v from the replicate cores agreed closely (±2 kPa) with this data set. For the short (less than 4 m) cores used in this study, effective overburden stress increased almost linearly with depth. Figure 29 shows linear regression fits for each of the replicate cores; correlation coefficients were better than r=0.999 in all cases. This data set was combined with the one-dimensional consolidation data to estimate overconsolidation ratios (OCR's) for the near-surface sediment of Navarin Basin.

Grain Specific Gravity

Twenty-one grain specific gravity tests were performed in accordance with ASTM D854-58. Most of the sample specimens were taken from trimmings of the triaxial test samples. Salt corrections were not applied in the computations. Values of grain specific gravity ranged from 2.55 to 2.77, with an average value of 2.64. The smaller values are lower than most continental shelf sediment grain specific gravity values and likely indicate the presence of diatoms.

Atterberg Limits

Methods. Atterberg Limits tests were performed on 50 samples following the procedures of ASTM D423-66, ASTM D424-59, and ASTM D2217-66. A salt correction assuming a salinity of 32.5 parts per thousand was applied in the computation.

Findings. The plasticity index (PI) ranged from 3 to 38 and the liquid limit (LL) ranged from 27 to 83. On a plot of liquid limit versus plasticity index (plasticity chart, Fig. 30), Navarin Basin province sediment varies dramatically. Within the Unified Soil Classification System (e.g., Mitchell, 1976), descriptive names are assigned to different parts of the plasticity chart based on empirical observations. According to this system, Navarin Basin shelf sediments (cores G61, G111) are inorganic silts of medium to high compressibility and are more highly compressible (core G61) in the northern part of the province near Navarinsky Canyon. Sediment from Navarinsky Canyon, (cores G31 and G34) however, is typically inorganic clay of low to medium plasticity combined with some inorganic silts of medium compressibility. Farther south, near the head of St. Matthew Canyon (core G74), the sediment behaves as a highly compressible inorganic silt or organic clay exhibiting a

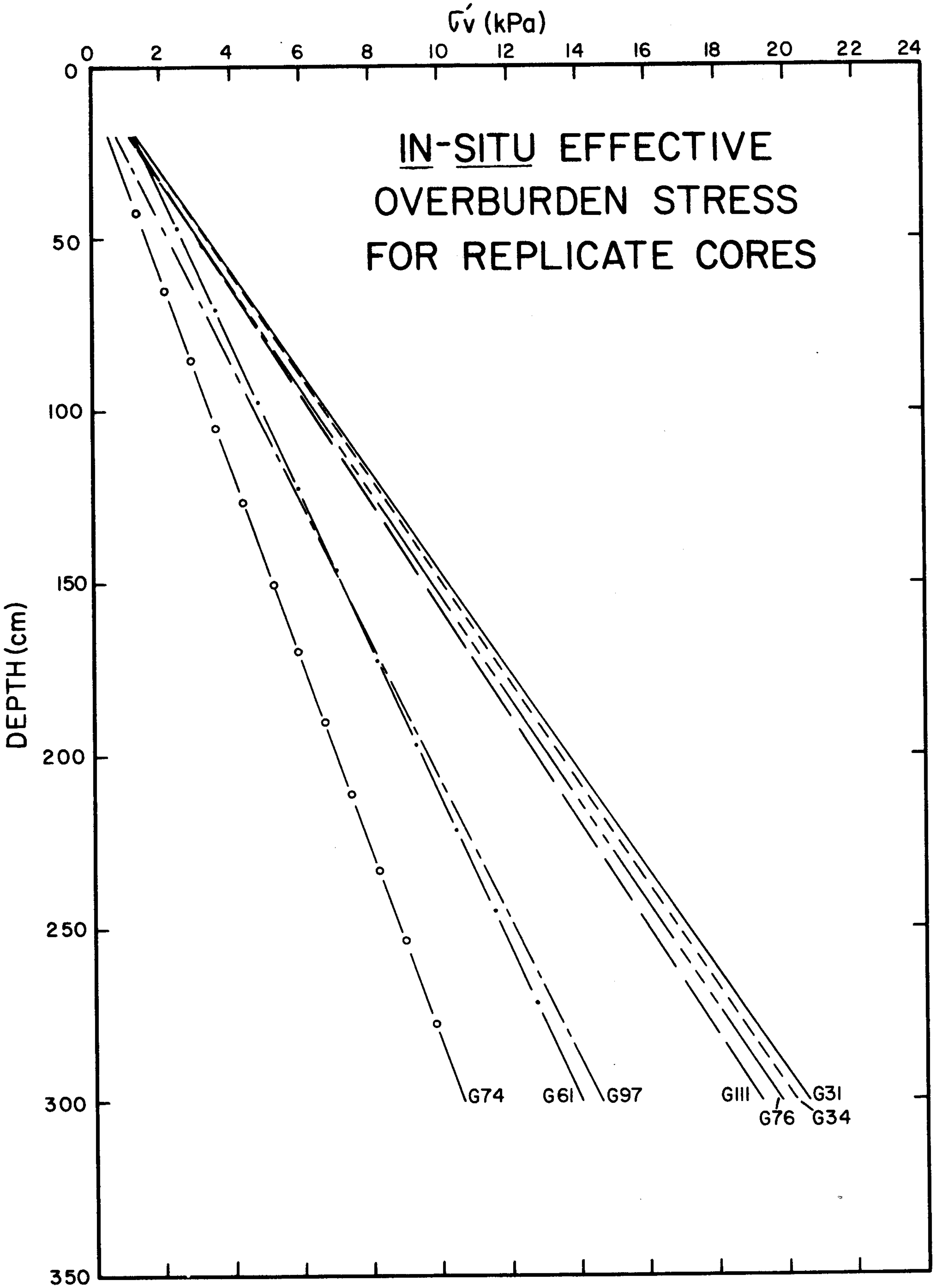

Figure 29. Linear regression best fit lines of the increase of in place effective overburden pressure (σ'_v) with subbottom depth for replicate cores. Data from 1980 Discoverer cruise.

wide range of liquid limit and plasticity index values. This behavior likely reflects significant variations in diatom content. Slope sediment near the head of Zhemchug Canyon (core G97) behaves as a highly compressible inorganic silt.

Grain-Size Distribution

Procedures and results from grain-size analyses are summarized in Chapter 3, this report.

Advanced Geotechnical Tests

Consolidation Tests

Methods. One dimensional consolidation tests were performed in general accordance with ASTM D2435-70 on 15 specimens trimmed to a sample size of 6.35 cm in diameter by 2.54 cm in length. An initial or seating stress of 2.4 kPa and a pressure increment ratio of one were used in all tests. After reaching equilibirium under a vertical stress of 383 kPa, the sample was unloaded to 48 kPa and then reloaded until a vertical stress of 1532 kPa was reached. The specimens were unloaded in one step and removed from the consolidometers. Deformation versus time readings were recorded for each loading increment.

Maximum past overburden stress (σ'_{vm}) was determined by the Casagrande procedure (Casagrande, 1936); values are summarized in Table 4. These maximum past stresses were used to determine consolidation pressures for triaxial tests and to estimate the amount of overburden removal due to slumping or erosion in some areas.

A useful consolidation state parameter is the excess past overburden stress (σ'_e). The σ'_e parameter is determined from the one-dimensional consolidation tests used to determine σ'_{vm} and the in-situ effective overburden stress (σ'_v) and is computed as:

$$\sigma'_e = \sigma'_{vm} - \sigma'_v \quad \ldots\ldots\ldots\ldots\ldots\ldots\ldots\ldots \quad (3)$$

A more commonly reported variable is the overconsolidation ratio (OCR) which is the ratio of σ'_{vm} to σ'_v. For normally consolidated sediment, $\sigma'_{vm} = \sigma'_v$ and thus OCR=1 and σ'_e=0.

Findings. All of the Navarin Basin sediment tested was overconsolidated ($\sigma'_e > 0$) as shown in Figure 31 and Table 4. A characteristic of the Navarin replicate cores is very high OCR's at shallow (<30 cm) subbottom depths (e.g.,see core G 78, 10-15 cm of Table 4). Such large OCR's are accentuated by the extreme contrast between σ'_{vm} and σ'_v that characterizes the uppermost part of the cores. Such high levels of overconsolidation are unlikely, however, given the low surface strengths, lack of obvious depositional hiatuses, and uniform increase in vane shear strength with depth which all suggest normal consolidation. The σ'_e parameter is a useful compliment to OCR because σ'_e is not enlarged at very low (e.g., <1 kPa) values of σ'_v.

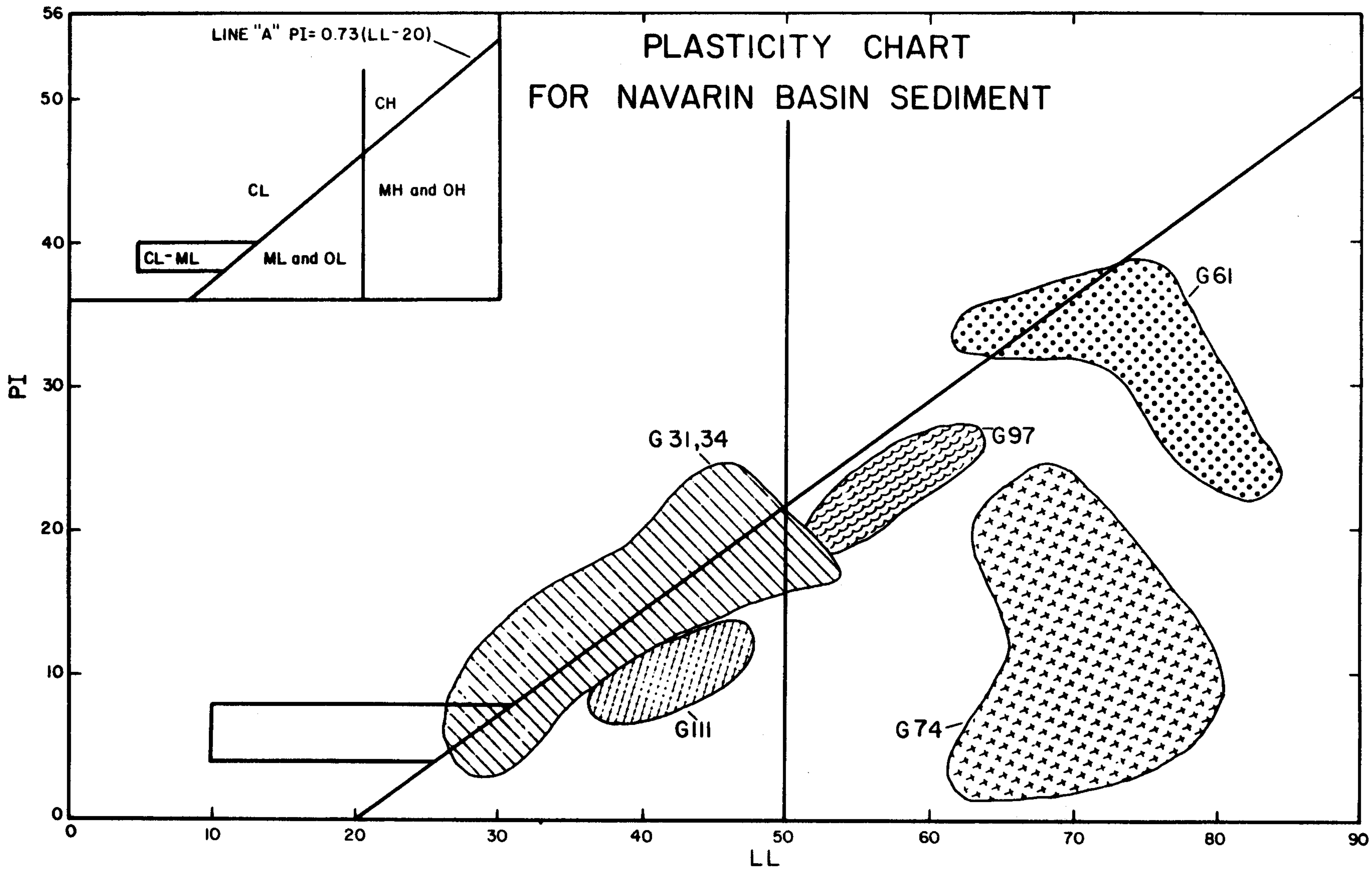

Figure 30. Plasticity chart for Navarin Basin province replicate cores. Data from 1980 R/V *Discoverer* cruise.

EXCESS PAST EFFECTIVE STRESS (σ'_e)

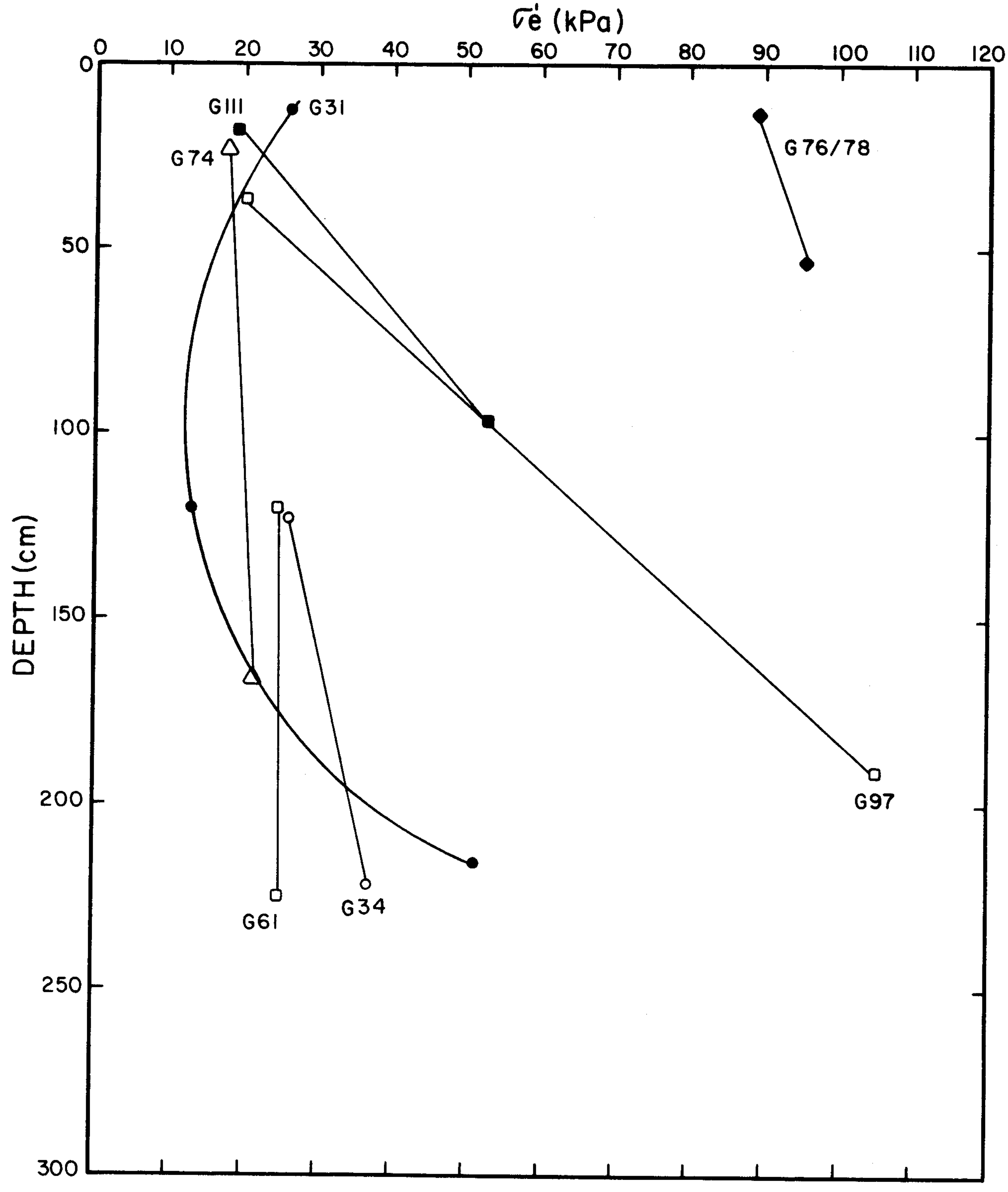

Figure 31. Plot of excess past effective stress σ'_e versus depth for Navarin Basin province replicate cores. Data from 1980 R/V <u>Discoverer</u> cruise.

Table 4. Summary of Consolidation test results

Core	Z cm	σ'_{vm} (kPa)	σ'_{v} (kPa)	σ'_{e} (kPa)	OCR
G 31	10-13	30	0.7	29	43
	119-122	20	8	12	2.5
	214-217	65	15	50	4.3
G 34	121-124	35	8	27	4.4
	220-223	52	15	37	3.5
G 61	119-121	30	6	24	5
	223-226	35	11	24	3.2
G 74	22-25	19	0.7	18	27
	164-168	30	6	24	5
G 78	10-15	90	0.8	89	112
G 76	50-55	100	3.3	96	30
G 97	35-40	22	2	20	11
	187-192	116	10	106	11.6
G 111	15-20	20	1.1	19	18
	95-100	60	6	54	10

Excluding the uppermost 30 cm, cores G31, G34, G61, and G74 are lightly to moderately overconsolidated (OCR 2-5). Core G76, taken from the shelf near Navarin Ridge, is heavily overconsolidated throughout (OCR~30). Core G97, recovered from the headwall of Zhemchug Canyon, is overconsolidated throughout (OCR~11) but a dramatic increase in σ'_e is seen at the base of the core (Fig. 31). The observed level of excess overburden pressure at the base of the core likely results from the removal of about 15 m of sediment. Core G111, collected from the shelf about 60 km north of the head of Zhemchug Canyon, exhibits overconsolidation throughout (OCR~10). The cause of the observed overconsolidation is uncertain for the shelf cores. Sediment on the shelf can be subjected to a number of loads capable of inducing this overconsolidation state (e.g., erosion of overlying material, cyclic loading, cementation, ice loading, and subaerial exposure at low sea level stands). At present, we have insufficient data to evaluate these mechanisms.

Strength Evaluation

Approach

The quality and usefulness of the strength data are limited by both the short core length (typically less than 5 m) and sediment disturbance during the coring process. Many features of geotechnical interest (e.g., basal shear surfaces of sediment failure zones) occur much deeper (50 m or more) than conventional coring devices can penetrate. Thus, the sediment involved at that horizon may not have the same properties as the sampled sediment. Further, the engineering properties of the sampled sediment can be modified by the coring process. That is, disturbance by thick-walled coring devices can alter the properties of the sampled sediment from the properties of the in place sediment. Both limitations (short corer penetration and sample disturbance) can reduce the validity of a geotechnical study.

As an approach to overcoming these limitations, we used the normalized soil parameter (NSP) method (Ladd and Foott, 1974; Mayne, 1980). The NSP method is based on empirical results that show certain engineering properties of a wide range of cohesive soils to be constant if normalized by appropriate consolidation stresses. The resulting data can be applied to a wide range of in place stress conditions. The most frequently used NSP is S_u/σ'_v. The S_u/σ'_v ratio is often a constant for a given value of OCR and can be used to construct strength profiles when overburden stresses are known. Thus, the overburden stresses and consolidation state of the sediment in question must be evaluated. By knowing the variation of OCR with depth in the sediment column, the strength profile can be predicted using the NSP derived equation (Mayne, 1980):

$$S_u/\sigma'_v = (OCR)^{\Lambda_o} S_{nc} \quad (4)$$

where S_u = undrained shearing strength

σ'_v = effective overburden stress

OCR = overconsolidation ratio

Λ_o = Normalized strength parameter that is a constant for a given sediment

S_{nc} = ratio of static undrained shearing strength to isotropic consolidation stress for normally consolidated conditions

As described in the preceeding section on consolidation, OCR is evaluated from the determination of σ'_{vm} and σ'_v. The parameter Λ_o is simply the slope of the linear relationship between S_u/σ'_v (overconsolidated)/S_{nc} and the appropriate OCR on a log-log scale. The parameter S_{nc} is the value of S_u/σ'_v for normally consolidated sediment.

One advantage of the NSP approach is the determination of parameters that are independent of consolidation stress and depth in the sediment column. These normalized parameters can therefore be used as site properties that can be mapped. A second advantage of the approach is that the normalized parameters can circumvent the effect of coring disturbance by conducting all of the strength tests at consolidation stresses much greater than those experienced in place (Ladd and Foott, 1974). That is, both a relatively undisturbed sample and a disturbed sample produce approximately equivalent normalized soil parameters if each is consolidated (in the triaxial cell) to a high stress level before testing for shear. Once the normalized strength parameters have been determined at high stress levels, the data can be applied to any stress level including the low stress state that the sample experienced in place.

Methods. A triaxial testing program was designed to evaluate the strength characteristics, including strength degradation due to cyclic loading, of the Navarin Basin sediment. A total of 36 static, consolidated, undrained triaxial compression tests were performed in general accordance with procedures described by Bishop and Henkel (1962). Sample specimens were selected using X-ray radiograph interpretations of each core section. After hand trimming to a final size of 15 cm (length) by 6.35 cm (diameter), each specimen was enclosed in a thin latex membrane, placed in the triaxial cell, and flushed under low-gradient back pressure with fresh distilled water. Tests requiring OCR's greater than 1.0 were first consolidated to the specified consolidation stresses multiplied by the required OCR, and then rebounded to the final consolidation stresses under drained conditions. Failure was defined as 20% axial strain.

Eighteen additional triaxial tests were performed to evaluate the behavior of Navarin Basin sediment under cyclic loading. Specimens were prepared, consolidated, and back-pressured according to the same procedures described for the 36 static triaxial tests.

Cyclic loads, beginning with compression, were applied in bursts with a sinusoidal, 1 Hz waveform for all isotropically consolidated samples. A series of cyclic loads consisted of three bursts of 10 cycles followed by two bursts of 35 cycles and two bursts of 100 cycles. Each burst was separated by about one hour to allow pore water pressure equilization. The cyclic loads were approximately 75 and 50 percent of the static deviator stress at failure.

All cyclic tests were terminated when either a single amplitude axial strain of 15 percent or a pore water pressure ratio of 80% was reached. In some cases, if samples did not fail within the first series of cyclic loads, a second series of cyclic loads with an amplitude of 100% of static strength was applied. If the samples did not fail after the second series, a monotonic load was applied until failure was reached.

The testing program (Table 5, Fig. 32) was divided into Special (S) and Routine (R) cores; the main distinction being that additional tests were performed on the Special cores. For the static suite, tests R1 and R2 were designed to measure the sample strength directly. Tests R3 and R4 were designed to estimate S_u for normally consolidated sediment (S_{nc}) at stress levels well above the maximum past stress (σ'_{vm}). Values of 2.5 σ'_{vm} and 4.0 σ'_{vm} were used to evaluate the NSP approach. Tests S8 and R5 were designed to determine S_u at elevated OCR's as a means of evaluating Λ_o.

For the cyclic suite, tests R6 and R7 were designed to evaluate the degree of strength degredation due to cyclic loading from earthquake or wave (surface or internal) sources. Stress levels were designed to assess failure in the vicinity of 10 cycles. Tests S9 - S11 were designed to assess the effect of induced OCR on cyclic strength degredation.

Findings. The triaxial test results are summarized in Table 6. A plot defining the normalized strength parameter Λ_o is presented in Figure 33.

Three approaches were used as estimates of S_u: (1)undrained vane shear tests, S_v, (2)direct triaxial cell tests at isotropic consolidation stresses of 1.0 kPa (R1) and σ'_v (R2), and (3)the NSP estimate following equation 4. In most cases the three methods gave similar estimates of S_u at the overburden stresses experienced in the upper 3 m of the sediment column. For example, Figure 34 shows a comparison of the S_u estimates from cores G31 and G32, collected from the head of Navarinsky Canyon. Note the close approximation of the three methods. Figure 35 presents similar data for cores G97 and G98 collected from the headwall of Zhemchug Canyon. In this case vane shear estimates for core G98 depart dramaticaly from vane and triaxial cell estimates from core G97. This difference probably results from slumping or erosion at the head of Zhemchug Canyon. As previously described, consolidation tests show that about 15 m of sediment has been removed from the site of core G97. The two cores were not collected from precisely the same location. Both sampled the overconsolidated layer but differing amounts of subsequent sedimentation overlie the slip surface. Although at a different scale, these data support the conclusion of slumping in the canyon head that is based on geophysical evidence (Carlson et al., 1982).

Undrained shear strengths were reduced to 51% to 80% of static strength (A_D) during 10 cycles of dynamic loading (Table 6). Core G31 showed an increase in strength during cyclic loading that possibly was erroneous due to procedural difficulties with that test.

Table 5. Triaxial test specifications for Routine (R) and Special (S) cores(†)

Test or Number	Static Cyclic	Consolidation Stress	Induced OCR	Cyclic Deviator Stress
R-1	static	1 kPa	1.0	N/A*
R-2	static	$\sigma'v$	1.0	N/A
R-3	static	$2.5\sigma'vm$	1.0	N/A
R-4	static	$4.0\sigma'vm$	1.0	N/A
R-5	static	$2/3\sigma'vm$	6.0	N/A
R-6	cyclic	$4.0\sigma'vm$	1.0	75%Su
R-7	cyclic	$4.0\sigma'vm$	1.0	50%Su
S-8	static	$4.0\sigma'vm$	3.0	N/A
S-9	cyclic	$2/3\sigma'vm$	6.0	75%Su
S-10	cyclic	$2/3\sigma'vm$	6.0	50%Su
S-11	cyclic	$4.0\sigma'vm$	3.0	75%Su

† refer to Figure 32 for location of tests in each core.
* N/A indicates value is not applicable.

Table 6. Summary of triaxial test results - NSP estimate of undrained sharing strength.

Core	Depth in Core (cm)	Initial OCR	Λ_o*	S_{nc}*	σ'_v (kPa)	S_u(NSP) (kPa)	OCR=1 A_D %	OCR=6 A_D %
G 31	10-13	43	0.87	0.36	0.7	6.6	162	-
	119-122	2.5			8	6.4		
	214-217	4.3			15	19.2		
G 34	121-124	4.4	0.94	0.33	8	10.6	80	75
	220-223	3.5			15	16.1		
G 61	119-121	5.0	0.84	0.48	6	11.1	75	-
	223-226	3.2			11	14.0		
G 74	22-25	27.0	0.74	0.57	0.7	4.6	63	-
	164-168	5.0			6	11.2		
G 78	10-15	112	0.77	0.69	0.8	20.9	51	-
G 76	50-55	30			3.3	31.2		
G 97	35-40	11.0	0.87	0.51	2	8.2	71	-
	187-192	11.6			10	43.0		
G 111	15-20	18	0.85	0.60	1.1	7.7	75	-
	95-100	10			6	25.5		

*Values apply to entire core

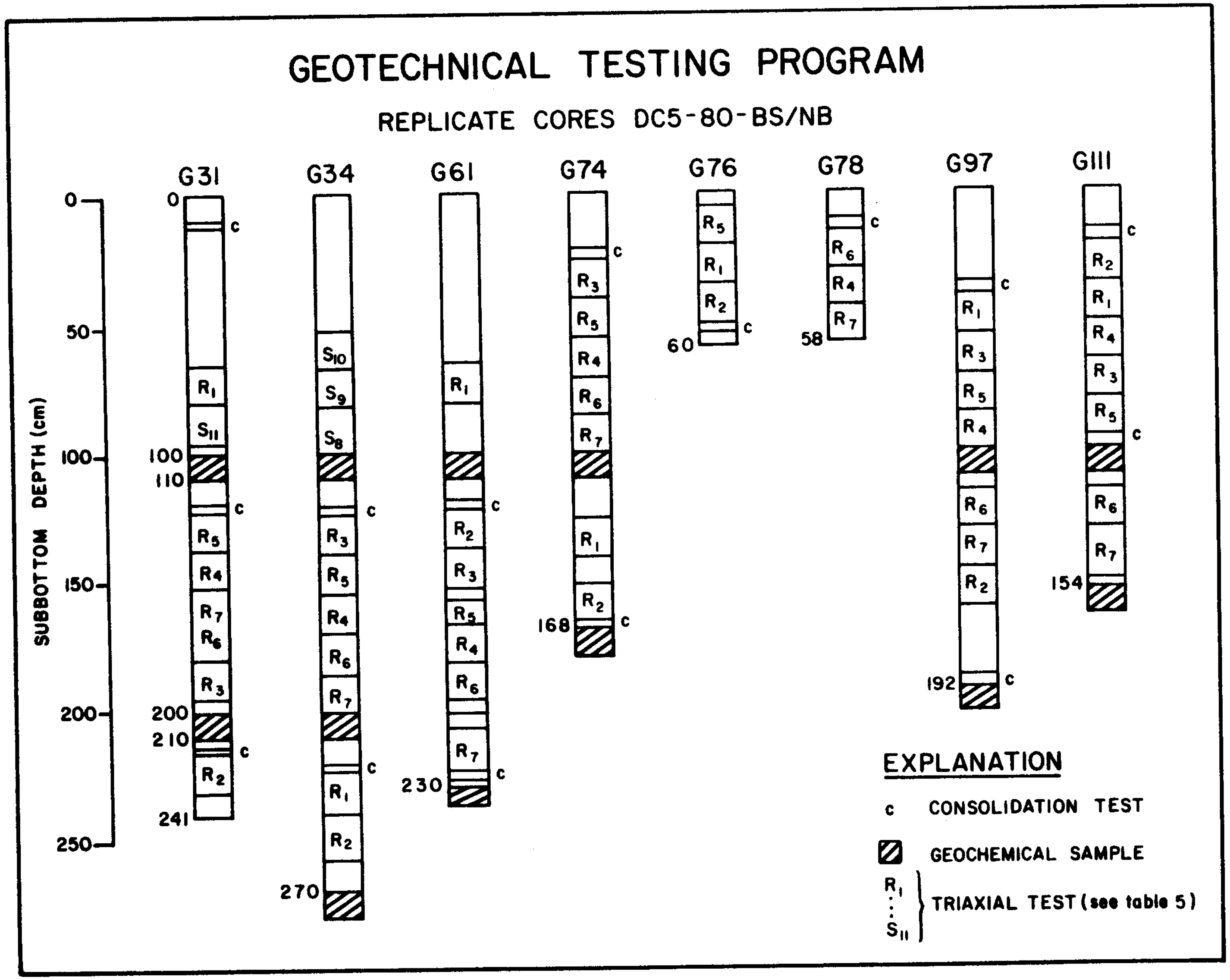

Figure 32. Location of tests for Navarin Basin province geotechnical testing program on replicate cores. Refer to Table 5 for summary of triaxial test specifications.

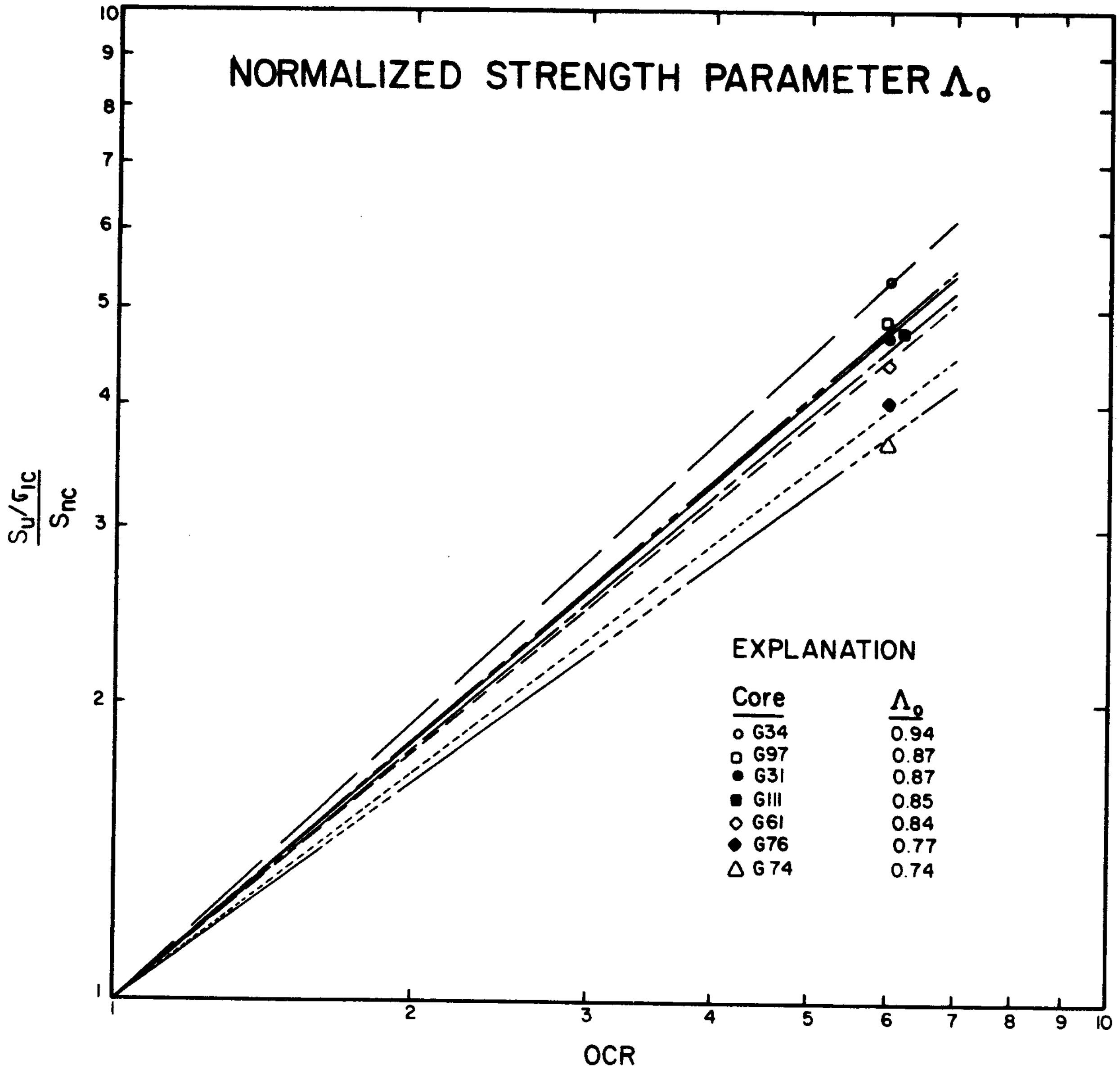

Figure 33. Plot of the normalized strength parameter Λ_o as defined by a log-log plot of S_u/σ'_v(overconsolidated)/S_{nc} versus OCR for replicate cores collected on the 1980 R/V DISCOVERER cruise. See text for explanation.

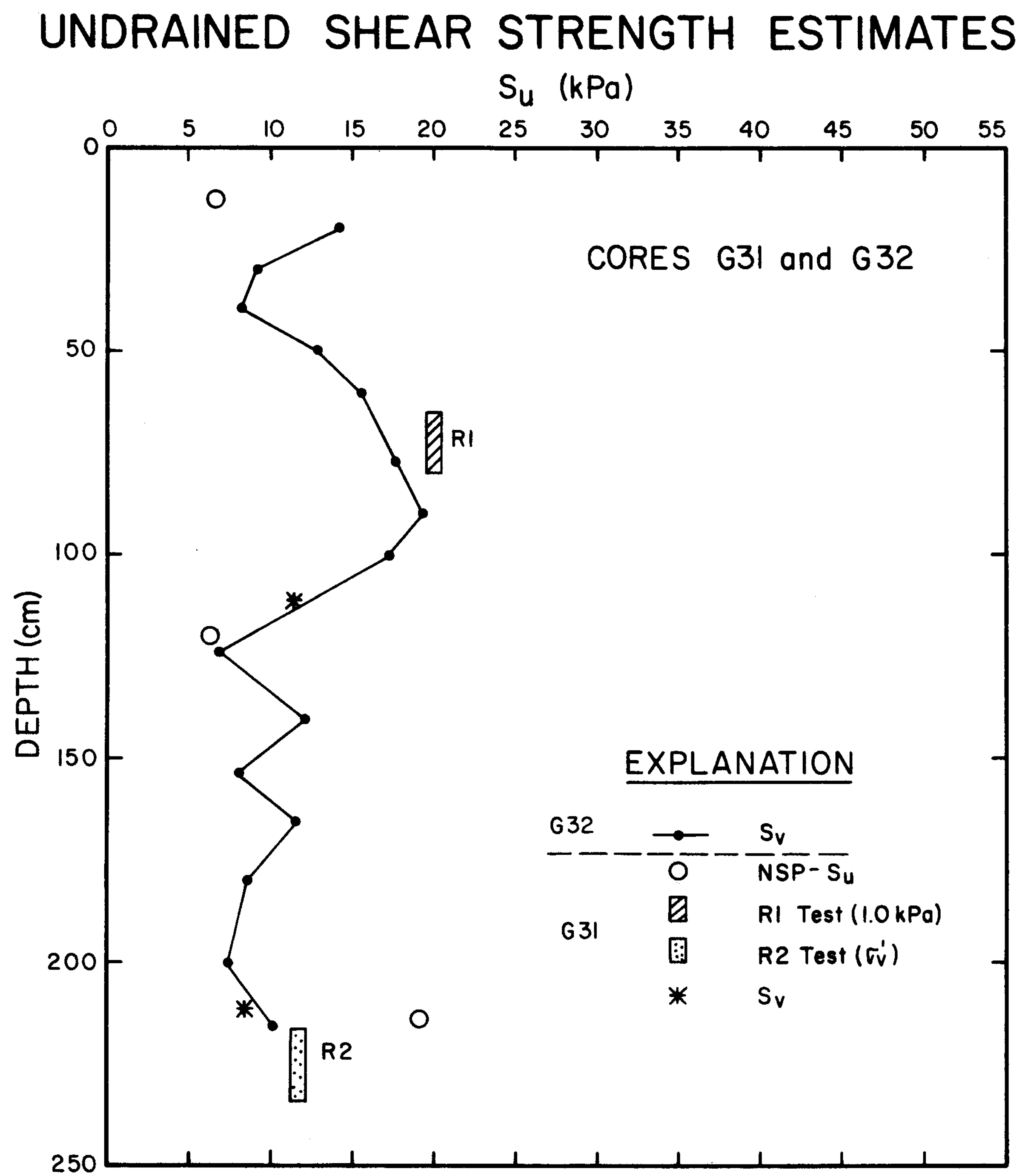

Figure 34. Example of multiple estimates of undrained shear strength (S_u) for paired cores G31 and G32, 1980 R/V DISCOVERER cruise.

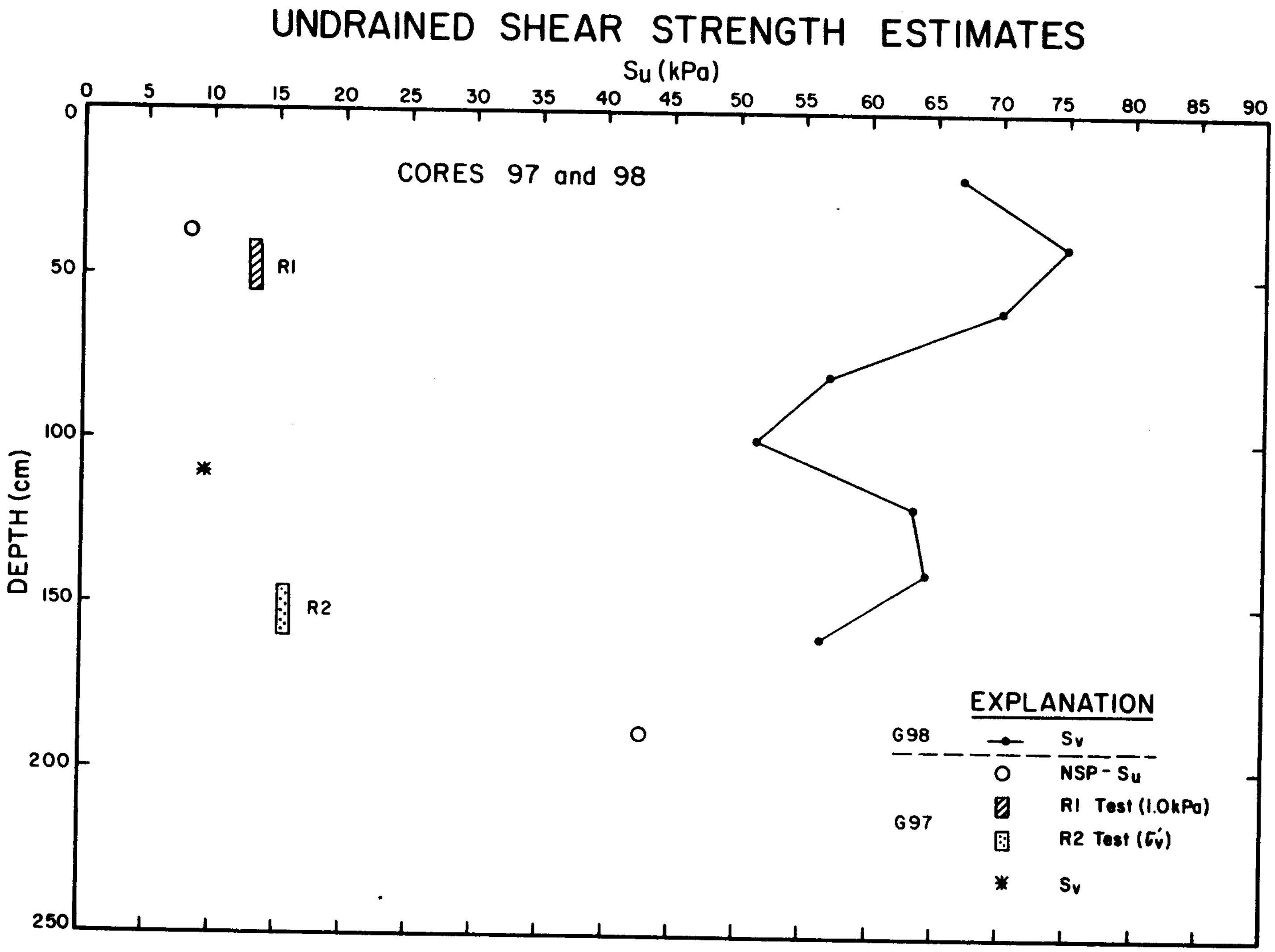

Figure 35. Example of multiple estimates of undrained shear strength (S_u) for paired cores G97 and G98, 1980 R/V DISCOVERER cruise. Disparity between G97 and G98 strength estimates is due to the removal of approximately 15 m of sediment. See text for explanation.

Stability Applications

The normalized cyclic strength (10 cycles to failure) for normal consolidation is the cyclic degradation factor, A_D, times S_{nc}. Using values from Table 6, the normalized 10-cycle cyclic strength varies between 0.26 and 0.58, with a representative shelf value of 0.36. During a major storm the number of significant cycles might range from 100 to perhaps as many as 1000. From Lee and Focht (1976) such an increase in cycle number might further degrade the strength by 50%, assuming no drainage. Therefore, the representative normalized, storm-wave-degraded, cyclic strength for the shelf would be 0.18. For an assumed peak wave height of 22 m and a wave length of 400 m, the procedures of Seed and Rahman (1978) yield a peak normalized wave-induced shearing stress of 0.18 at a water depth of 57 m. At greater water depths, such as the entire Navarin Basin province, the level of shearing stress would be less and would be insufficient to cause failure in the cohesive sediments.

In sandy areas the level of strength degradation resulting from cyclic loading is probably higher. Seed and Idriss (in press) show that liquefaction during earthquakes has occurred at normalized shear stress levels of about 0.1. If storm waves produce a further 50% strength degradation beyond the influence of earthquakes, the critical normalized shearing stress for a sand subjected to wave loading might be as low as 0.05. Such a shearing stress level could be generated in water depths to 146 m for the storm waves assumed above. Some of the cohesionless sediment in the Navarin Basin province exists at this and shallower water depths and might be susceptible to liquefaction during major storm waves. Such an occurrence is fairly unlikely, however, because partial drainage from the pervious sediment would limit pore water pressure buildup.

SUMMARY OF FINDINGS

(1) A zone of cohesionless sediment exists at the shelf break.

(2) Undrained vane shear strengths on the shelf are lowest on the central shelf about 150 km west of St. Matthew Island.

(3) Undrained vane shear strengths are highly variable across the continental slope, possibly due to slumping, erosion, or changes in the depositional regime. In general, strengths increase downcore, and decrease to the south and with increasing water depth.

(4) Water contents on the shelf are highest in the zone of weak shelf sediment.

(5) Water contents in the slope province decrease with subbottom depth, and increase to the south and with increasing water depth.

(6) Grain specific gravities ranged from 2.55 to 2.77 with an average value of 2.64. The variability likely results from changes in diatom content.

(7) Where plastic behavior is exhibited, Atterberg Limits and the Unified Soil Classification System show the shelf sediment to be mostly inorganic silts of medium to high compressibility. Slope sediments are typically highly compressible inorganic silts or organic clays.

(8) Navarin Basin sediment is typically overconsolidated, but not heavily except for a few locations. OCR values on the shelf are commonly greater than 10. Elsewhere in the province, values are OCR ~ 2-5. About 15 m of sediment has been removed from the headwalls of Zhemchug Canyon (core G97).

(9) Undrained vane shear determinations provide estimates of undrained shear strength in the upper 3 m of the sediment column that agree with triaxial strength determinations corrected for coring disturbance. Cyclic loading reduces static strength by 20 to 50%.

(10) Navarin Basin province shelf cohesionless sediment may be susceptible to liquefaction by severe storm loading. The cohesive sediment is probably not susceptible to storm-wave-induced failure.

NOMENCLATURE

A_D = cyclic degradation factor applied to S_u as a result of cyclic loading

LL = liquid limit from Atterberg Limit determinations

NSP = Normalized Soil Parameter method of shear strength determination

OCR = overconsolidation ratio; defined as OCR = σ'_{vm}/σ'_v

PI = plasticity index of Atterberg Limits; defined as PI = LL-PL

PL = plastic limit of Atterberg Limit determinations

S_{nc} = ratio of static undrained shearing strength to isotropic consolidation stress for normally consolidated conditions

S_u = static undrained shear strength

S_v = undrained peak vane shear strength

W = sediment water content by dry weight

W_c = sediment water content corrected for salt content

z = subbottom depth in cm

γ_c = sediment bulk density

γ'_c = sediment bulk density corrected for the density of seawater; $\gamma'_c = \gamma_c - \gamma_{sw}$

γ_{sw} = density of seawater

σ'_e = excess past overburden stress; defined as $\sigma'_e = \sigma'_{vm} - \sigma'_v$

σ'_v = in place effective overburden stress

σ'_{vm} = maximum past overburden stress

Λ_o = normalized strength parameter that is a constant for a given sediment

REFERENCES

ASTM, 1982, Annual Book of ASTM Standards, Part 19, Natural Building Stones, Soil and Rock; Philadelphia, 710p.

Bishop, A.W., and D.J. Henkel, 1962, The Measurement of Soil Properties in Triaxial Test, Second Edition, Edward Arnold, Ltd., London, 228 p.

Carlson, P.R., H.A. Karl, J.M. Fischer, and B.D. Edwards, 1982, Geologic hazards in Navarin Basin Province, Northern Bering Sea: OTC Paper 4172 14th Ann. Offshore Technology Conf., Houston, TX, May 3-6, p. 73-78.

Casagrande, Arthur, 1936, The determination of the preconsolidation load and its practical significance: Proc. First Int'l Conf. Soil Mech. Found. Eng., Cambridge, MA, p. 60.

Fischer, J.M., P.R. Carlson, and H.A. Karl, 1982, Bathymetric map of Navarin Basin province, northern Bering Sea: U.S. Geological Survey Open-File Report 82-1038, 11p.

Karl, H.A., P.R. Carlson, Jeff Fischer, Ken Johnson, and Beth Lamb, 1981, Textural variations and composition of bottom sediment: <u>in</u> P.R. Carlson and H.A. Karl, Seafloor geologic hazards, sedimentology, and bathymetry: Navarin Basin province, northwestern Bering Sea: U.S. Geological Survey Open-File Report 81-1217, 149p.

Ladd, C.C., and Roger Foott, 1974, New design procedure for stability of soft clays: Am. Soc. Civil Eng., Jour. Geotech. Eng. Div., v. 100, no. GT7, p 763-786.

Lamb, T.W., and R.V. Whitman, 1969, Soil Mechanics, John Wiley & Sons, Inc., New York, 553p.

Lee, K.L., and J.A. Focht, Jr., 1976, Strength of the clay subjected to cyclic loading: Marine Geotchnology, v. 1, p. 165-185.

Mayne, P.W., 1980, Cam-clay predictions of undrained strength: Am. Soc. Civil Eng., Jour. Geotech. Eng. Div., v. 106, no. GT11, p. 1219-1242.

Mitchell, I.K., 1976, Fundamentals of Soil Behavior, John Wiley and Sons, Inc., New York, 422 p.

Seed, H.B., and I.M. Idriss, in press, Evaluation of liquefaction potential of sand deposits based on observations of performance in previous earthquakes: Am. Soc. Civil Eng., Jour. Geotech., Eng. Div.

Seed, H.B., and M.S. Rahman, 1978, Wave-induced pore pressure in relation to ocean floor stability of cohesionless soil: Marine Geotechnology, v. 3, p. 123-150.

CHAPTER 8: HYDROCARBON GASES IN SEDIMENTS -- RESULTS FROM 1981 FIELD SEASON

by

Margaret Golan-Bac and Keith A. Kvenvolden

This study examines the distribution and origin of the hydrocarbon gases methane (C_1), ethane (C_2), ethene ($C_{2=}$), propane (C_3), propene ($C_{3=}$), isobutane (i-C_4), and normal butane (n-C_4) in surficial sediments from the shelf, slope, and rise areas of the Navarin Basin province in the Bering Sea. The report covers results obtained on samples collected in 1981. Results for samples collected in 1980 have been reported previously (Vogel and Kvenvolden, 1981).

METHODS

Conventional gravity cores were taken from the shelf, slope, and rise areas of the Navarin Basin province. The 8 cm internal diameter core liner was cut into 10 cm sections at approximately 1 meter intervals (usually 90-100, 190-200, 290-300 cm, etc.). The sediment section was immediately extruded into one liter unlined paint cans which had two septa-covered holes on the side near the top. Each can was filled with helium-purged salt water and 100 ml of water was removed before the can was closed with a double-friction-seal lid. This resulting 100 ml headspace was then purged with helium through the septa, and the cans were immediately inverted and frozen. In the shore-based laboratory, the cans of sediment were brought to room temperature and shaken for 10 minutes by a mechanical shaker to equilibrate the hydrocarbon gases that are released from the sediment and are partitioned into the helium headspace. A sample of gas in this headspace was withdrawn through a septa with a gas-tight syringe. One milliliter of this sample was analyzed by gas chromatography using both flame ionization and thermal conductivity detectors. Concentrations of gases were determined by comparison of the integrated area of each hydrocarbon with the integrated area of a quantitative hydrocarbon standard. These values were then corrected for the different solubilities of the hydrocarbon gases in the interstitial water of the sediment sample by use of partition coefficients (0.8 for methane; 0.7 for ethane, propane, and butanes; 0.6 for ethene and propene).

The method of extraction yields semi-quantitative results; however, because all the samples were processed in the same manner, the results can be compared. The concentrations reported in Table 7 are rounded with respect to limitations of the analytical techniques. The detection limit is approximately 0.1 μl of methane/liter of wet sediment and 1 nl of gas/liter of wet sediment for the other hydrocarbon gases. Error determined from analytical variation and repeat analysis is less than 20%.

RESULTS

Core locations, concentrations of hydrocarbon gas, and other relevant information for Navarin Basin province are listed in Table 7. This table is

Table 7. Hydrocarbon Gas (C_1-nC_4) Concentrations and Ratios from Sediment Samples from the Navarin Basin Province (1981)

Core No. and Interval (cm)	Water Depth (m)	Station No.	C_1 ul/l wet sediment	C_2	$C_{2:1}$	C_3	$C_{3:1}$	i-C_4	n-C_4	$\frac{C_1}{C_2+C_3}$	$\frac{C_2}{C_{2:1}}$	Location Latitude	Location Longitude
				nl/l wet sediment									
Shelf Sediment													
G1 90-100	135	1	50	78	44	26	28	n.d.	n.d.	480	1.8	59°28.9'	175°35.7'
202-212			140	690	42	47	250	n.d.	n.d.	190	16		
G2 90-100	143	1	47	270	150	170	68	12	33	110	1.8	59°05.6'	176°20.1'
G24 90-100	104	22	8.1	47	58	34	95	3	n.d.	99	0.82	61°31.6'	176°25.5'
190-200			13	100	100	73	130	6	14	73	1.0		
G25 90-100	123	23	79	190	67	39	86	8	4	340	2.8	61°46.2'	177°30.2'
190-200			210	470	33	82	210	36	6	380	14.0		
G26 90-100	122	24	7.8	43	57	31	81	11	n.d.	110	0.76	61°27.1'	177°25.2'
190-200			18	66	81	44	200	6	5	160	0.82		
G27 90-100	145	25	11	33	51	28	65	5	4	180	0.64	61°09.0'	177°47.0'
190-200			19	27	15	9	12	n.d.	n.d.	530	1.8		
G28 90-100	128	26	29	42	66	31	83	4	3	400	0.64	61°13.5'	177°23.4'
G29 90-100	128	26	4.8	26	60	27	93	n.d.	5	90	0.44	61°13.5'	177°23.6'
G31 90-100	137	28	120	270	94	54	97	8	6	380	2.9	60°12.1'	176°35.5'
190-200			37	34	44	22	85	4	n.d.	660	0.76		
G32 90-100	130	29	34	120	210	100	130	21	22	160	0.54	60°11.0'	176°13.1'
190-200			62	70	61	30	20	4	n.d.	610	1.1		
G33 90-100	130	29	47	43	86	26	89	3	n.d.	670	0.50	60°11.1'	176°13.1'
190-200			160	340	91	80	81	8	13	380	3.7		
G34 90-100	115	30	3.9	42	72	34	120	4	6	51	0.59	57°20.1'	172°42.7'
G35 90-100	115	30	7.5	34	39	24	67	4	n.d.	130	0.88	57°20.0'	172°42.7'
G60 90-100	140	56	23	270	40	34	34	5	6	77	6.7	59°48.3'	177°24.6'
190-200			11	390	55	62	71	15	n.d.	25	7.1		
G61 90-100	141	57	36	230	30	28	98	n.d.	n.d.	140	7.4	59°48.3'	177°26.0'
G62 90-100	139	58	33	250	38	36	63	4	n.d.	120	6.4	59°49.6'	177°29.8'
189-199			92	1300	56	52	120	6	n.d.	66	24		
G63 90-100	135	59	28	180	17	23	65	18	2	140	11	59°51.2'	177°29.5'
G73 90-100	146	69	28	200	31	20	88	3	n.d.	130	6.5	59°27.1'	176°29.4'
G77 90-100	145	73	33	470	270	330	120	25	62	41	1.8	59°54.1'	178°09.1'
G78 90-100	139	74	18	420	430	360	190	66	26	23	0.96	60°13.1'	177°33.1'
G79 90-100	141	75	56	31	51	15	25	n.d.	n.d.	1200	0.6	60°30.1'	176°59.2'
190-200			120	370	130	130	75	13	28	240	2.7		
G105 90-100	144	95	29	31	20	15	35	n.d.	n.d.	630	1.6	60°09.0'	176°59.3'
191-201			140	180	38	31	34	5	n.d.	670	4.8		
G106 90-100	135	96	57	40	38	18	36	n.d.	n.d.	970	1.1	59°40.0'	175°59.3'
190-200			180	540	27	26	57	5	n.d.	320	20		

n.d. = not detectable

Table 7. (Continued)

Core No. and Interval (cm)	Water Depth (m)	Station No.	C_1 ul/l wet sediment	C_2	$C_{2:1}$	C_3	$C_{3:1}$	$i\text{-}C_4$	$n\text{-}C_4$	$\frac{C_1}{C_2+C_3}$	$\frac{C_2}{C_{2:1}}$	Location Latitude	Longitude
				nl/l wet sediment									
Slope Sediment													
G4 90-100	2816	5	8.2	n.d.	n.d.	23	34	n.d.	n.d.	360	-	58°31.3'	177°26.0'
190-200			11	67	82	49	36	4	10	96	0.82		
290-300			17	76	46	40	32	n.d.	8	150	1.6		
G7 95-105	173	7	53	420	140	110	55	16	21	99	3.0	59°38.3'	178°15.3'
G11 90-100	980	11	180	230	24	52	3400	170	170	630	9.8	60°39.2'	179°34.6'
190-200			84000	950	110	3400	*	150	180	19000	8.7		
G12 90-100	1683	12	9.6	59	63	32	36	6	4	110	0.94	60°34.3'	179°45.1'
190-200			17	150	41	410	25	180	46	30	3.6		
262-272			25	300	22	610	37	260	46	28	13		
G13 90-100	2080	13	5.8	38	36	34	29	n.d.	n.d.	81	1.0	60°19.3'	179°49.1'
190-200			460	360	14	59	770	46	n.d.	1100	27		
290-300			49000	450	150	700	*	32	36	43000	3.1		
G14 90-100	1826	14	37	160	75	140	39	9	26	120	2.1	60°09.6'	179°50.1'
190-200			230	300	19	610	120	65	49	260	16		
290-300			780	430	22	690	130	84	59	700	20		
390-400			12000	410	39	2700	*	34	26	3900	10		
552-562			44000	270	420	1700	*	55	28	22000	0.63		
G15 90-100	2744	15	25	42	73	24	50	5	3	370	0.58	59°52.4'	179°59.5'
190-200			57	33	74	19	31	4	n.d.	1100	0.44		
290-300			150	640	40	49	33	5	n.d.	220	16		
390-400			1400	1300	22	240	63	20	n.d.	900	61		
G17 90-100	900	17	1.2	26	50	18	29	1	n.d.	28	0.51	60°12.6'	179°21.5'
190-200			4.5	57	45	28	45	4	n.d.	54	1.2		
283-293			6.4	49	30	21	43	6	n.d.	92	1.6		
G18 90-100	884	17	2.8	37	36	18	23	3	n.d.	50	1.0	60°13.1'	179°21.5'
190-200			11	37	35	13	52	3	n.d.	230	1.1		
G19 90-100	1018	18	16	100	41	39	55	3	3	110	2.4	60°10.2'	179°27.9'
190-200			13	270	190	130	70	9	17	34	1.4		
290-300			170	1000	22	210	70	24	2	140	47		
370-380			290	990	39	240	110	52	9	230	26		

n.d. = not detectable
- = not reported
* = concentration not reported due to methane interference

Table 7. (Continued)

Core No. and Interval (cm)		Water Depth (m)	Station No.	C_1 ul/l wet sediment	C_2	$C_{2:1}$	C_3	$C_{3:1}$	$i\text{-}C_4$	$n\text{-}C_4$	$\frac{C_1}{C_2+C_3}$	$\frac{C_2}{C_{2:1}}$	Location Latitude	Longitude
					nl/l wet sediment									
Slope Sediment (continued)														
G20	90-100	1005	18	15	270	180	85	80	8	14	41	1.5	60°10.6'	179°26.9'
	190-200			27	510	200	130	83	12	17	43	2.6		
	290-300			47	710	93	150	48	12	19	55	7.6		
	364-374			52	780	180	270	97	30	36	50	4.3		
G21	90-100	1630	19	5.7	61	59	36	51	6	n.d.	58	1.0	60°06.1'	179°34.5'
	190-200			8.8	100	170	54	61	7	3	56	0.60		
G22	90-100	1670	19	5.7	150	200	120	75	12	20	21	0.76	60°06.1'	179°34.5'
	190-200			5.8	140	120	100	52	9	17	24	1.1		
	290-300			7.0	52	44	28	27	5	n.d.	89	1.2		
	390-400			8.5	65	36	26	36	3	n.d.	93	1.8		
G37	190-200	1100	32	5.7	97	52	32	68	7	n.d.	45	1.8	57°49.6'	174°23.5'
	290-300			8.9	160	130	46	120	9	10	42	1.2		
G38	90-100	1080	33	1.3	37	41	32	53	3	n.d.	18	0.91	58°10.1'	175°29.2'
	190-200			7.8	81	36	29	85	3	n.d.	71	2.3		
	290-300			130	1600	70	43	130	10	4	77	23		
G39	90-100	915	34	13	56	66	39	65	7	6	140	0.84	58°20.1'	174°29.1'
	190-200			32	60	56	32	84	8	4	350	1.1		
	290-300			39	250	36	35	31	4	n.d.	140	6.9		
G44	90-100	2530	39	5.4	20	54	16	86	3	n.d.	150	0.37	56°51.4'	174°08.5'
	190-200			13	26	52	17	61	n.d.	n.d.	310	0.50		
	290-300			14	54	63	39	63	4	n.d.	150	0.86		
	390-400			19	45	56	29	52	3	n.d.	260	0.80		
	490-500			17	41	86	26	67	3	n.d.	250	0.47		
G47	90-100	2760	41	2.7	36	87	23	81	3	n.d.	45	0.41	56°58.2'	174°21.2'
	190-200			7.5	150	240	120	130	19	20	27	0.64		
	290-300			6.8	39	59	21	86	3	n.d.	110	0.67		
	390-400			7.0	67	100	42	110	7	9	64	0.65		
	490-500			6.2	41	56	28	68	4	n.d.	91	0.73		
G49	90-100	1770	43	4.8	30	47	26	71	n.d.	n.d.	85	0.64	57°38.5'	175°38.0'
	190-200			7.8	45	75	28	57	n.d.	3	110	0.61		
	290-300			10	31	92	18	57	n.d.	n.d.	210	0.34		
	390-400			14	57	51	23	92	4	n.d.	180	1.1		
	490-500			16	63	71	32	80	4	n.d.	170	0.89		

n.d. = not detectable

Table 7. (Continued)

Core No. and Interval (cm)		Water Depth (m)	Station No.	C_1 ul/l wet sediment	C_2	$C_{2:1}$	C_3	$C_{3:1}$	$i\text{-}C_4$	$n\text{-}C_4$	$\frac{C_1}{C_2+C_3}$	$\frac{C_2}{C_{2:1}}$	Location Latitude	Location Longitude
					nl/l wet sediment									
Slope Sediment (continued)														
G52	90-100	1070	46	4.3	48	31	22	21	4	n.d.	61	1.5	58°33.6'	177°53.2'
	190-200			4.3	22	20	13	17	n.d.	n.d.	120	1.1		
	290-300			5.6	22	22	11	19	3	n.d.	170	1.0		
	390-400			5.1	15	28	13	12	n.d.	n.d.	180	0.53		
	490-500			5.3	26	17	16	25	n.d.	n.d.	130	1.6		
	570-580			5.3	30	23	14	30	3	n.d.	120	1.3		
G53	90-100	2676	47	3.0	53	72	45	32	3	9	31	0.74	58°23.2'	176°25.1'
G55	90-100	2320	49	5.2	27	12	13	10	n.d.	n.d.	130	2.3	57°45.7'	175°30.4'
	190-200			18	36	14	13	23	n.d.	n.d.	360	2.5		
	290-300			25	55	23	16	21	n.d.	n.d.	350	2.5		
	390-400			34	210	22	26	28	3	n.d.	140	9.5		
G58	90-100	179	53	11	44	39	41	22	n.d.	n.d.	130	1.1	59°26.1'	177°28.4'
	190-200			19	1400	250	350	110	25	61	11	5.5		
G65	90-100	436	61	6.3	35	24	22	23	3	n.d.	110	1.5	59°25.4'	177°51.2'
	190-200			7.3	34	28	24	56	5	n.d.	130	1.2		
G66	90-100	580	62	56	62	31	500	54	200	24	100	2.0	59°24.7'	178°14.5'
	190-200			110	4800	83	790	77	260	31	20	58		
	290-300			200	7300	17	970	110	320	26	24	440		
G67	90-100	167	63	74	540	71	80	66	8	11	120	7.6	59°38.7'	178°14.2'
G68	90-100	1048	64	19	130	23	20	75	n.d.	n.d.	130	5.7	59°38.6'	178°37.2'
	190-200			63	440	13	26	130	n.d.	n.d.	130	34		
G69	90-100	1230	65	1.6	76	62	57	98	n.d.	n.d.	12	1.2	59°15.8'	178°34.4'
	190-200			8.8	57	32	32	100	3	n.d.	99	1.8		
G71	90-100	520	67	18	180	38	22	130	7	n.d.	89	4.7	58°48.0'	178°00.0'
	190-200			71	1400	37	45	58	10	n.d.	47	39		
	290-300			170	93	16	120	57	10	n.d.	790	6.0		
G74	85-95	152	70	30	190	17	18	140	n.d.	n.d.	150	11	59°25.5'	177°11.9'
G80	90-100	152	76	16	180	180	150	73	9	31	48	1.0	60°29.4'	177°53.3'
G82	90-100	860	78	5.6	61	37	23	33	5	n.d.	66	1.6	60°27.2'	179°29.1'
G83	90-100	1120	79	2.4	38	48	27	49	n.d.	4	37	0.8	60°26.2'	179°53.4'
G84	90-100	780	80	23	74	33	31	68	4	n.d.	220	2.2	59°57.9'	178°59.2'
G85	90-100	1745	81	6.4	28	41	21	52	4	n.d.	130	0.68	59°51.9'	179°09.7'
	190-200			10	49	41	34	51	5	n.d.	130	1.2		
G86	90-100	2195	82	64	90	150	74	80	5	18	390	0.59	60°09.2'	179°51.4'
	190-200			320	930	38	120	170	21	7	310	24		
	280-290			34000	1900	54	1700	*	54	n.d.	9400	35		
G88	90-100	205	83	4.8	120	32	52	31	8	8	28	3.6	61°08.1'	178°46.1'
	190-200			9.2	290	86	120	47	n.d.	14	23	3.3		

n.d. = not detectable
* = concentration not reported due to methane interference

Table 7. (Continued)

Core No. and Interval (cm)		Water Depth (m)	Station No.	C_1 ul/l wet sediment	C_2	$C_{2:1}$	C_3	$C_{3:1}$	$i\text{-}C_4$	$n\text{-}C_4$	$\frac{C_1}{C_2+C_3}$	$\frac{C_2}{C_{2:1}}$	Location Latitude	Longitude
					nl/l wet sediment									
Rise Sediment														
G6	90-100	3395	6	4.1	39	140	49	58	5	11	47	0.29	58°08.3'	177°23.5'
	190-200			8.5	41	58	27	34	5	n.d.	120	0.71		
	290-300			3.5	120	310	95	120	8	19	16	0.39		
	390-400			7	29	23	8	33	n.d.	n.d.	190	1.3		
G42	90-100	3150	37	8.4	20	34	19	50	1	n.d.	210	0.59	57°57.8'	175°00.0'
	190-200			17	43	66	32	77	3.	n.d.	220	0.65		
	290-300			21	48	48	22	69	2	n.d.	300	0.99		
G48	90-100	2910	42	7.7	24	39	22	81	n.d.	n.d.	170	0.62	57°06.6'	174°35.5'
	190-200			13	45	88	26	59	3	n.d.	190	0.50		
	290-300			15	23	52	16	77	3	n.d.	380	0.44		
	390-400			20	37	100	24	65	5	n.d.	320	0.37		
G50	90-100	3430	44	4.4	21	55	22	89	3	n.d.	100	0.39	57°52.2'	176°28.5'
	190-200			6.3	36	69	28	74	2	n.d.	98	0.52		
	290-300			7.9	47	62	30	75	3	n.d.	100	0.77		
	390-400			12	26	43	17	97	n.d.	n.d.	290	0.60		
	490-500			19	100	91	54	29	5	73	120	1.1		
G51	90-100	3220	45	4.3	18	26	13	28	n.d.	n.d.	140	0.71	58°20.4'	177°25.1'
	190-200			7.5	20	24	16	24	n.d.	n.d.	210	0.83		
G54	90-100	3220	48	10	60	32	24	19	n.d.	n.d.	120	1.9	58°08.4'	176°02.9'
	190-200			18	29	28	15	32	n.d.	n.d.	420	1.0		
	290-300			16	30	25	16	28	n.d.	n.d.	350	1.2		
G56	90-100	2925	50	6.0	19	34	14	70	n.d.	n.d.	180	0.55	58°11.6'	176°00.1'
	190-200			16	27	44	16	96	4	n.d.	360	0.60		
G57	90-100	3395	51	3.9	14	25	10	25	n.d.	n.d.	160	0.58	57°57.3'	176°58.8'
	190-200			6.9	24	32	16	54	4	n.d.	170	0.77		
	290-300			13	240	270	200	110	15	39	30	0.90		
	390-400			12	190	320	170	130	15	39	33	0.59		
	470-480			26	520	18	71	22	7	n.d.	44	29		
G70	90-100	3390	66	6.5	13	22	41	22	n.d.	n.d.	300	0.61	58°31.6'	178°28.0'
	190-200			8	18	25	16	62	n.d.	n.d.	230	0.72		
	290-300			12	51	38	25	89	4	n.d.	160	1.3		
	390-400			8.7	15	20	16	46	n.d.	n.d.	280	0.76		
G76	90-100	3210	72	4.4	36	74	39	42	n.d.	5	59	0.49	59°21.5'	179°06.6'
	190-200			11	130	170	110	79	8	19	45	0.72		

n.d. = not detectable

divided into three sections, namely, cores taken from the outer shelf (water depths from 100 to 150 m), the slope (water depths from 150 to 2800 m), and the rise (water depths from 2800 to approximately 3600 m). These three areas are delineated by the 150 m and 2800 m contour lines, and in Figure 36 samples are identified by their core number.

Information relative to the ranges of concentrations of hydrocarbon gases found in sediments of the shelf, slope, and rise are summarized in Table 8. Methane is the most abundant hydrocarbon gas in all the sediment samples analyzed and is typically present in concentrations that are 2 to 3 orders of magnitude greater than the concentrations of the other low molecular weight hydrocarbons (LMWH).

Areal distributions of maximum concentrations of C_1, C_2+C_3 and $n\text{-}C_4+i\text{-}C_4$ are shown in Figures 37, 38 and 39, respectively. These maximum concentrations generally reflect results of analyses of the deepest samples obtained at a given core location, because the deepest samples usually have the highest concentrations of gas (Table 7). In five cores (11, 13, 14, 15 and 86), all located on the slope, the maximum concentrations of C_1 exceed 1000 $\mu l/l$ and range from 1400 to 84000 $\mu l/l$. In each of these cores C_1 concentrations increase 2 to 4 orders of magnitude with depth (Table 7).

Concentrations of C_2 exceed 1000 nl/l in samples from seven cores of slope sediment (15, 19, 38, 58, 66, 71 and 86) and from one core of shelf sediment (62). In these cores, C_2 concentrations increase 1 to 2 orders of magnitude with depth (Table 7). Concentrations of C_3 are usually less than concentrations of C_2, but the distributions of these gases tend to be parallel. Figure 38 shows locations of eleven cores where the maximum concentrations of $C_2 + C_3$ exceed 1000 nl/l. These cores include numbers 11,13 and 14 in addition to the eight cores listed above.

Butane ($n\text{-}C_4$ and $i\text{-}C_4$) is generally the least abundant LMWH in shelf, slope and rise sediment. Wherever detected, $i\text{-}C_4$ is generally more abundant than n-C4; in samples $n\text{-}C_4$ could not be measured. The highest concentrations of $n\text{-}C_4+i\text{-}C_4$ are found in slope sediment. Core 66 had the highest amount of $i\text{-}C_4$ (320 nl/l) and core 11 had the most $n\text{-}C_4$ (100 nl/l).

The alkenes ($C_{2=}$ and $C_{3=}$) are present in most sediment samples in amounts less than C_2 but generally greater than C_3. Concentrations of $C_{2=}$ and $C_{3=}$ show no discernible trends with depth. In those samples where C_1 concentrations exceeded about 12000 $\mu l/l$, $C_{3=}$ could not be measured because of interference resulting from our method of analysis.

Biogenic Methane

The most abundant gas in sediments of Navarin Basin province is C_1, and in five cores (11, 13, 14, 15, 86), all located in Navarinsky Canyon, maximum concentrations exceed 1000 $\mu l/l$ (Table 7 and Figure 37). During the 1980 season, the only core (G-37) analyzed with concentrations of C_1 exceeding 1000 $\mu l/l$ (1900 $\mu l/l$) was from the rise near the mouth of Navarinsky Canyon (Vogel and Kvenvolden, 1981). Concentrations for four of the five cores (11, 13, 14, and 86) taken during 1981 approach or exceed the saturation of the

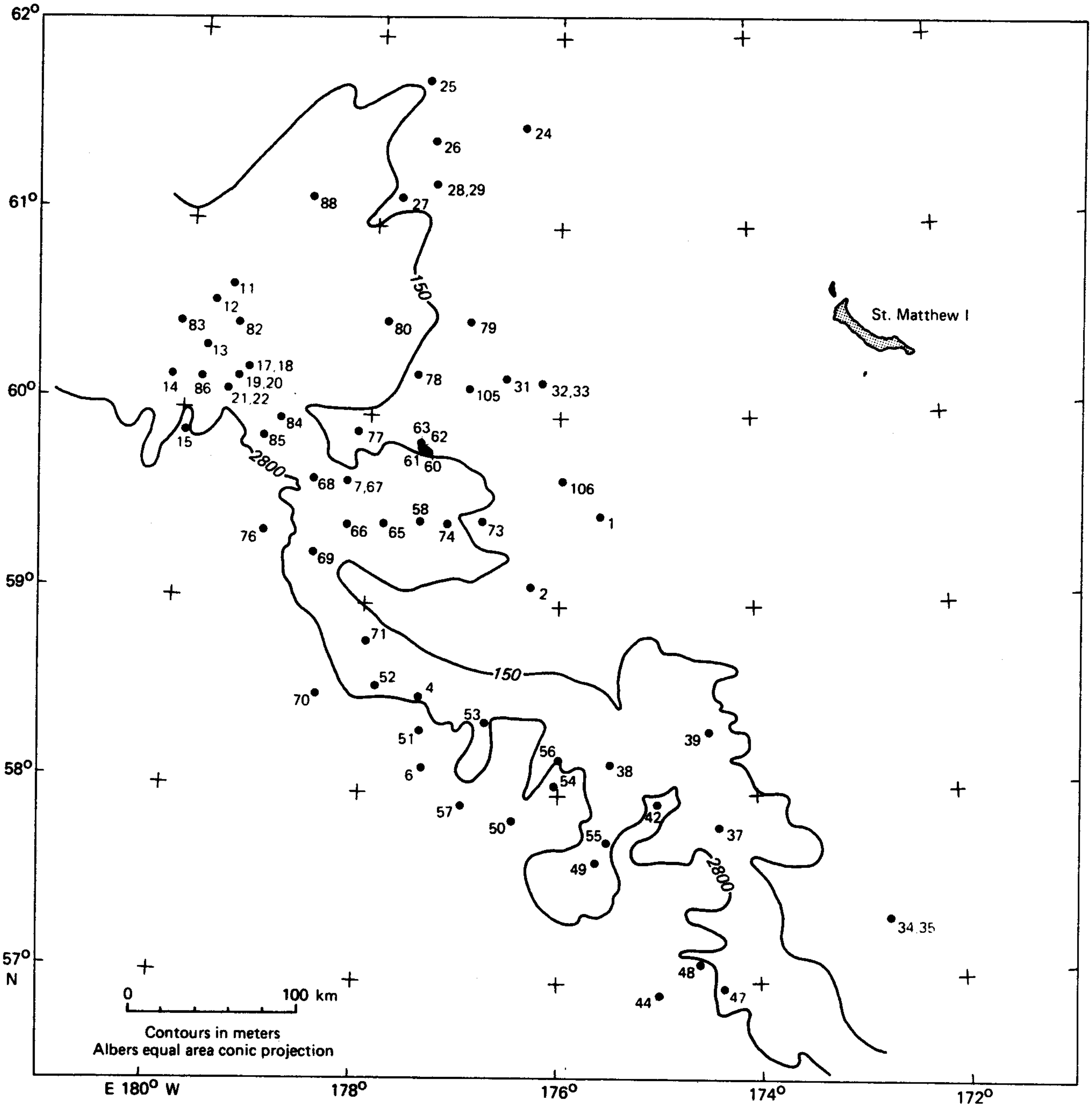

Figure 36. Location of hydrocarbon gas sampling sites in the Navarin Basin province. Sites are designated with core numbers.

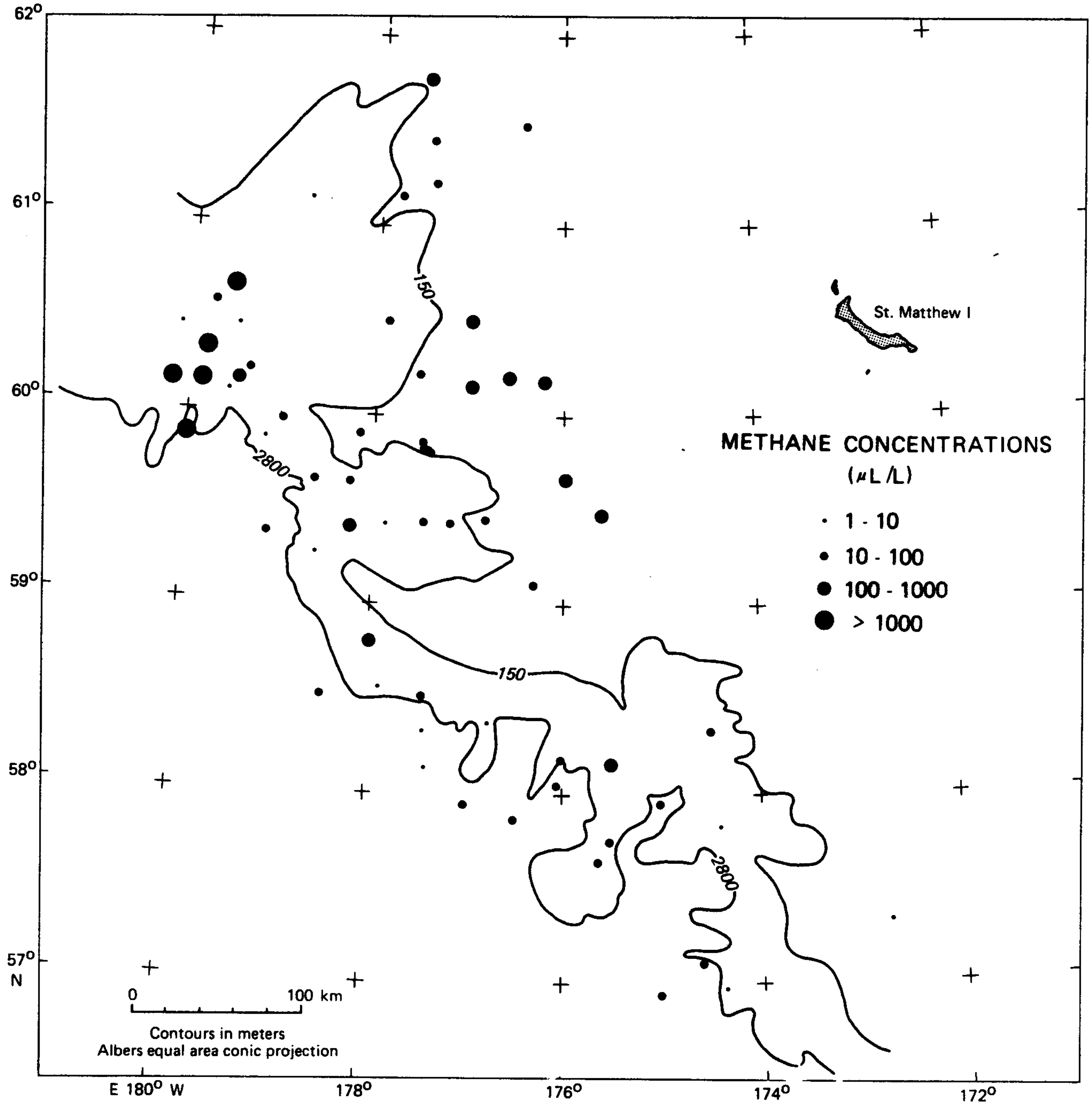

Figure 37. Distribution of maximum concentrations of methane in μl/l of wet sediment.

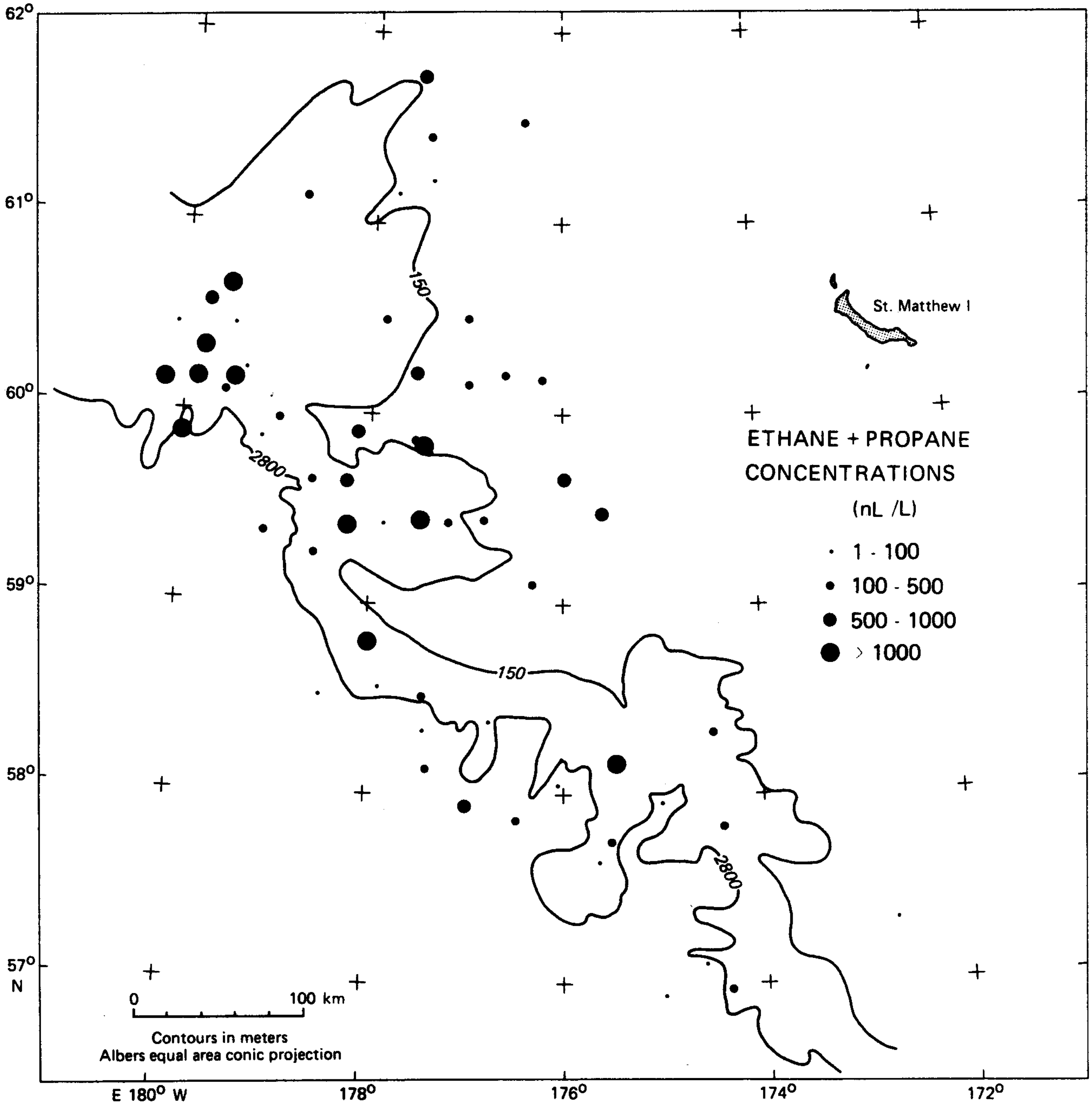

Figure 38. Distribution of maximum concentrations of ethane plus propane in nl/l of wet sediment.

interstitial water at atmospheric pressure and temperature (about 40 ml of C_1 per liter of seawater according to Yamamoto et al., 1976). Because C_1 solubility increases with increasing pressure, the measured concentrations only represent minimum values; some quantity of gas likely escaped during the sampling procedure. In fact, core descriptions for three of the five cores include remarks about cracks attributed to escape of gas. The possibility that C_1 is present at concentrations exceeding its solubility in the interstitial water at depth may lead to high pore-water pressures and hence, sediment instability; seismic evidence indicates slumping of the sediments in the Navarinsky Canyon region (Carlson et al, 1982) which may be due in part to the high concentrations of gas present. C_1 concentration profiles with depth for these five cores are shown in Figure 40A. The rapid increase in amount of C_1 with depth can be attributed to the presence of C_1-producing bacteria operating under anoxic conditions. A zone of low C_1 concentration probably exists between the sediment-water interface and about 100 cm depth where the first measurements were made. This zone is generally referred to as the zone of sulfate reduction, where the low C_1 concentrations have been attributed to bioturbation and oxidation by molecular oxygen (Reeburgh, 1969), sulfate inhibition of methanogenesis (Martens and Berner, 1974), and to anaerobic C_1 oxidation by sulfate-reducing bacteria (Barnes and Goldberg, 1976; Reeburgh and Heggie, 1977). Below the zone of sulfate reduction is the zone of C_1 production where high concentration of C_1 occurs. Here the C_1 is being generated by the anaerobic microbial decomposition of the organic-rich mud which ranges from 0.7 to 1.43% organic carbon (Fischer, 1981). Those samples having high C_1 concentrations (greater than 1000 μl/l) also have large $C_1/(C_2+C_3)$ values ranging from 900 to 43,000 (Table 7). These ratios indicate a biogenic source for C_1 according to criteria defined by Bernard et al. (1977).

At most stations in Navarin Basin the C_1 concentrations are less than 1000 μl/l (Table 7 and Fig. 37). For these stations $C_1/(C_2+C_3)$ values are usually low. In fact, for many samples the ratio is less than 50, which is the upper limit of the range of values assigned by Bernard et al. (1978) to gas from thermogenic sources. However, as pointed out by Kvenvolden and Redden (1980), use of this ratio for assigning source is equivocal where gas concentrations are low. In the case of Navarin Basin, we believe that most of the C_1 and other hydrocarbon gases present are from biogenic sources and not from thermogenic sources. The low $C_1/(C_2+C_3)$ ratios are attributed to preferential loss of C_1 during sampling from sediments in which the original concentrations of C_1 are much lower than 1000 μl/l.

Other Biogenic Hydrocarbons

Other LMWH besides C_1 may be biologically produced, as suggested by Emery and Hoggan (1958) and Bernard et al. (1978). The relationship of C_1 to these other hydrocarbon gases may provide a clue to their origin. At the eleven sites with C_2+C_3 concentrations greater than 1000 nl/l (11, 13, 14, 15, 19, 38, 58, 62, 66, 71, and 86), five sites (11, 13, 14, 15, and 86) show a strong correlation between increasing C_1 concentrations and increasing C_2+C_3 concentrations with depth (Figure 41). This correlation suggests that the microbiological processes that produced C_1 may be operating in parallel with the process responsible for C_2 and C_3. Samples at all five sites also have anomalously high butane values (Table 7, Figs. 39 and 42) which suggest butane may also result from microbiological processes.

The production of alkenes is controlled by biological processes and has been produced by microbes in the laboratory (Davis and Squires, 1954), by marine organisms (Hunt, 1974), and by bacteria in soils (Primrose and Dilworth, 1976). In the Navarin Basin province, alkene concentrations vary with depth but generally remain at about the same level of concentration throughout the area.

Thermogenic Hydrocarbons

Two ratios ($C_1/(C_2+C_3)$ and $C_2/C_{2=}$) were used by Kvenvolden et al. (1981) to attempt to distinguish biogenic and thermogenic hydrocarbon gases in sediments. Extrapolating from the work of Bernard et al. (1976) and from Cline and Holmes (1977) they proposed that samples containing gases with $C_1/(C_2+C_3)$ values less than 50 and with $C_2/C_{2=}$ values greater than 1 may have thermogenic sources.

Of the thirteen sites (12, 19, 20, 22, 38, 57, 58, 60, 62, 66, 71, 77, and 88) where $C_1/(C_2+C_3)$ ratios are low and $C_2/C_{2=}$ ratios are high (Table 7), core 66 is of particular interest. The $C_1/(C_2+C_3)$ values in core 66 are 20 and 24 at 200 and 300 cm depth. These values are comparable to the ratios of possible thermogenic gas in cores from St. George Basin (Kvenvolden and Redden, 1980) and core 36 from the 1980 work in Navarin Basin (Vogel and Kvenvolden, 1981). The $C_2/C_{2=}$ ratio of 440 in Core 66 is the highest in the sampling area and in fact, is two orders of magnitude greater than most of the other ratios in the region. The value of the ratio is one order of magnitude greater than the highest value (50) at a minor anomaly observed on the Bering Shelf of St. George Basin (Kvenvolden and Redden, 1980; Kvenvolden et al., 1981). The value of the $C_2/C_{2=}$ ratio in core 66 is almost a factor of three greater than the highest value (160) obtained from the 1980 Navarin Basin study from core 36 (Vogel and Kvenvolden, 1981).

Figure 42 summarizes the cores with anomalous concentrations of C_1, C_2, and/or C_3 and with $C_1/(C_2+C_3)$ and $C_2/C_{2=}$ values indicating a possible thermogenic origin. Of the thirteen cores mentioned above, where the $C_1/(C_2+C_3)$ values are less than 50 and the $C_2/C_{2=}$ values are greater than 1, the majority are not of special interest for various reasons. For example, concentrations from core 12 did not increase particularly rapidly with depth. Core 38 has mostly background concentration levels, with only one anomalous concentration (ethane) at the 300-cm depth, the deepest sample analyzed in the core. Core 77 was only sampled at the 90-100 cm depth interval and also had high concentrations of alkenes. Core 88 has background concentrations and cores 22, 57, and 71 have erratic concentration versus depth profiles. Cores 19 and 20 are at almost the same coring location and have mostly high amounts of ethane. A longer core is needed here to determine if these high values continue to increase with depth. Cores 60 and 62 on the shelf and core 58 on the slope are of some interest, but due to the short cores obtained from these locations, it is difficult to predict and interpret the concentration gradient with depth.

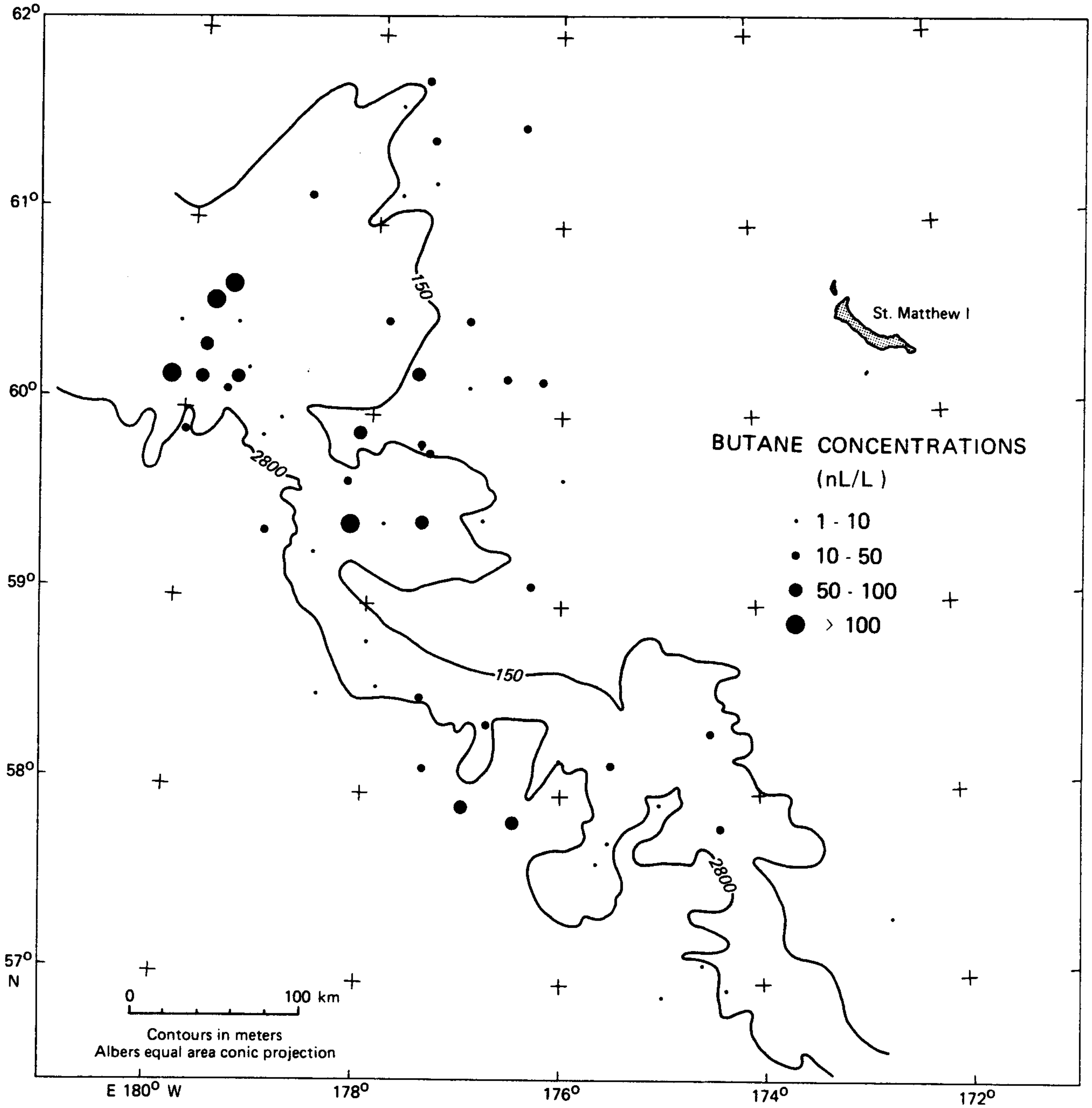

Figure 39. Distribution of maximum concentrations of butane in nl/l of wet sediment.

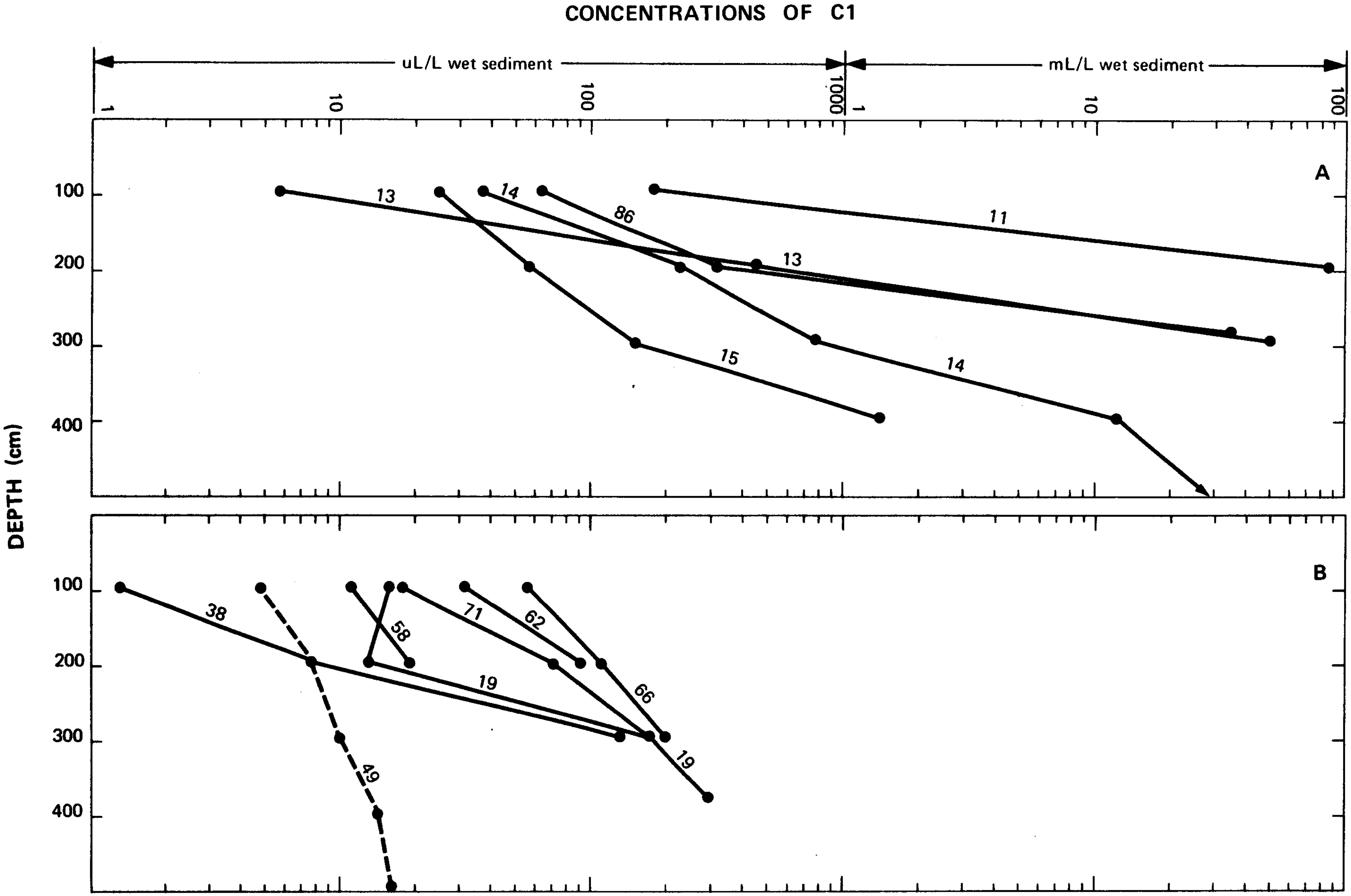

Figure 40. Graph of concentrations of C_1 in µl/l and ml/l wet sediment vs. depth in centimeters for sediment samples from the eleven sites in the Navarin Basin Province where C_2+C_3 concentrations reach or exceed 1 µl/l wet sediment at some depth interval. Figure A groups those profiles whose C_1 concentrations exceed 1 ml/l wet sediment at some depth interval while Figure B groups the remaining cores. The dashed line in Figure B is the profile of a core which represents background concentration levels.

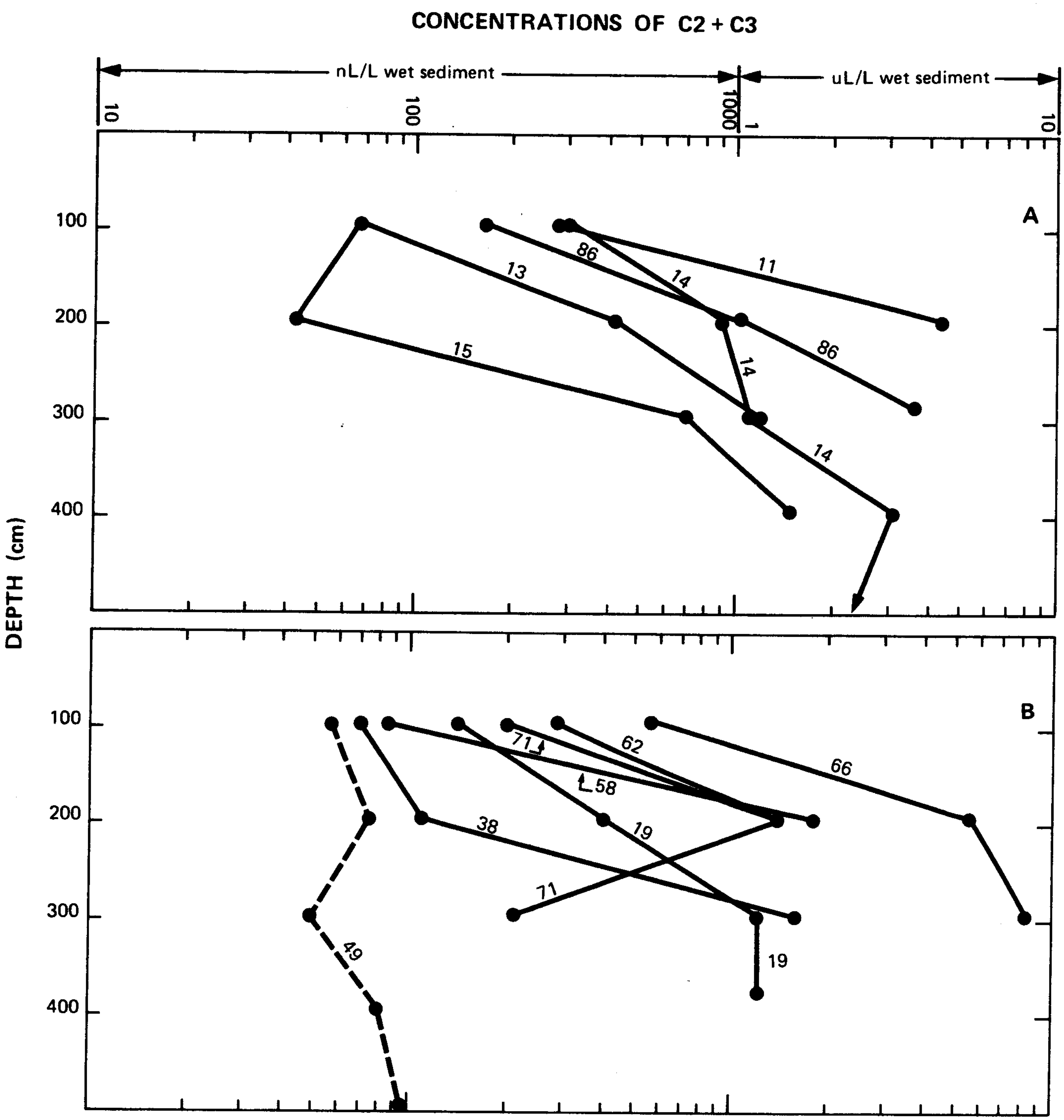

Figure 41. Graph of concentrations of C_2+C_3 in nl/l and µl/l wet sediment vs. depth in centimeters for sediment samples from the eleven sites in the Navarin Basin Province where C_2+C_3 concentrations reach or exceed 1 µl/l wet sediment at some depth interval. Figure A groups those profiles whose C_1 concentrations exceed 1 ml/l wet sediment at some depth interval while Figure B is the profile of a core which represents background concentration levels.

Anomalous* Parameters				Core #		
C1	C2	C3	R	Shelf	Slope	Basin
	●			61,73,79	7,67	
		●		32		6,76
			●		22,88	
●	●			1,25,31,33, 105,106		
●		●			13,14	
	●	●		2,78		
	●		●	60		
		●	●		12	
●	●	●			11,15,86	
●	●		●	62	38,71	
	●	●	●	77	20,58	57
●	●	●	●		19,66	

* Concentrations of C1 (methane), C2 (ethane), C3 (propane) that are above background for the region indicated and R (ratios) that indicate a thermogenic origin (C1/(C2+C3) values that are low and C2/C2= values that are high).

Figure 42. Tally of anomalous parameters for cores in the regions indicated.

RELATIONSHIP TO GEOPHYSICAL ACOUSTIC ANOMALIES

Geophysical evidence shows that extensive areas in the northern shelf areas of the Navarin Basin province may contain gas-charged sediment (Carlson and others, 1982). Geochemical data from the same areas on the shelf show that gas is present in cores collected where seismic anomalies suggest gas-charged sediment. However, the amount of gas observed is not large enough to be responsible for the seismic anomalies. Actually, the anomalies occur at depths below which sediment samples could be recovered (i.e. greater than about 15 m). Thus, a correlation between our geochemical data and the occurrence of geophysical anomalies attributed to gas-charging of sediment cannot be firmly established.

CONCLUSIONS

Hydrocarbon gases are common in the upper five meters of sediment in the Navarin Basin province. Locations with highest concentrations of gases are found in the slope sediment, followed by sediment of the shelf and rise, respectively. C_1 is the most abundant hydrocarbon gas in all three regions and is generally present in concentrations that are two to three orders of magnitude greater than the higher molecular weight hydrocarbon gases. In four cores, all from the slope, the concentration of C_1 ranged from 12,000 to 84,000 μl/l and is probably being generated from the microbial decomposition of organics in the anoxic mud found in Navarinsky Canyon. Ratios of $C_1/(C_2+C_3)$ are very large for these samples, ranging from 900 to 43,000, indicating mainly a biogenic source. These concentrations may be near or exceed the solubility of C_1 in interstitial water at depth and thus the gas may affect the stability of the sediment.

C_2+C_3 concentrations are greater than 1000 nl/l in eleven cores taken at nine locations on the slope and two on the shelf. In seven of these cores, the trends of increasing C_2+C_3 concentration strongly correlate with increasing concentration of C_1 down the core. Therefore, the microbiological processes that account for the C_1 concentrations may be related to the processes producing the high C_2+C_3 concentrations in these cores.

Low concentrations of $i\text{-}C_4$ and $n\text{-}C_4$ are present but are not detectable in many samples. The highest $i\text{-}C_4+n\text{-}C_4$ concentrations are found in the slope sediment. Anomalously high $i\text{-}C_4+n\text{-}C_4$ concentrations were found in all five cores that had concentrations of C_2+C_3 >1000 nl/l and C_1 >1000 μl/l.

The alkenes are generally present in all the samples and are likely the result of biological activity in the sediment. Concentrations are generally low and average about 50 nl/l in the sediment of the shelf and slope and are slightly higher in the rise sediment, averaging about 70 nl/l. Concentrations of the alkenes do not show distinctive trends with depth.

One core in the Navarin Basin province is of particular interest with respect to geochemical prospecting. Core 66 has a mixture of gases that suggest a thermogenic source. The $C_1/(C_2+C_3)$ ratios are 20 and 24 at the 200 and 300 cm depths, respectively, and the $C_2/C_{2=}$ ratios are 58 and 440. C_2+C_3 has the highest concentration (>8000 nl/l) of any measured in the 1981 study

Table 8. Hydrocarbon Gas (C_1-nC_4) Concentration and Ratio Ranges from Sediment Samples from the Navarin Basin Province (1981). Methane (C_1) concentrations are in µl/l; the other hydrocarbon concentrations are in nl/l.

	Shelf	Slope	Rise
C_1	4 - 200	1 - 84000	4 - 26
C_2	27 - 1300	n.d.- 7300	13 - 520
C_3	10 - 360	11 - 3400	8 - 200
$C_{2=}$	15 - 430	n.d.- 420	18 - 320
$C_{3=}$	12 - 250	n.d.- 3400	19 - 130
i-C_4	n.d.- 66	n.d.- 320	n.d.- 15
n-C_4	n.d.- 62	n.d.- 180	n.d.- 73
C_1/C_2+C_3	23 - 1200	11 - 43000	16 - 420
$C_2/C_{2=}$	0.44- 24	0.44- 440	0.29- 29

n.d. - not detectable

area. C_4's are also present in anomalously high concentrations: for example, the amount of the i-C_4 (320 nl/l) is the highest measured in the study area.

ACKNOWLEDGMENT

We thank T. M. Vogel and D. J. Blunt for collecting the samples and helping with some preliminary analyses.

References

Barnes, R. O., and Goldberg, E. D., 1976, Methane production and consumption in anoxic marine sediments: Geology, v. 4, p. 297-300.

Bernard, B. B., Brooks, J. M., and Sackett, W. M., 1976, Natural gas seepage in the Gulf of Mexico: Earth and Planet. Sci. Lett., 31, p. 48-54.

Bernard, B. B., Brooks, J. M., and Sackett, W. M., 1977, A geochemical model for characterization of hydrocarbon gas sources in marine sediments: Proc. 9th Offshore Tech. Conf., 1, p. 435-438.

Bernard, B. B., Brooks, J. M., and Sackett, W. M., 1978, Light hydrocarbons in recent continental shelf and slope sediments: Jour. Geophys. Res., 83, p. 4053-4061.

Carlson, P. C., Karl, H. A., Fischer, J. M., and Edwards, B. D., 1982, Geological hazards in Navarin Basin Province, Northern Bering Sea: Proc. 14th Offshore Tech. Conf., OTC 4172, p. 73-87.

Cline, J. D., and Holmes, M. L., 1977, Submarine seepage of natural gas in Norton Sound, Alaska: Science, no. 198, p. 1149-1153.

Davis, J. B., and Squires, R. M., 1954, Detection of microbially produced gaseous hydrocarbons other than methane: Science, no. 119, p. 381-382.

Emery, K. O., and Hoggan, D., 1958, Gases in marine sediments: Am. Assoc. Petrol. Geol. Bull., no. 42, p. 2174-2188.

Fischer, J. M.,1981, Carbon contents of Navarin Basin sediments: In Carlson, P. R., and Karl, H. A., (eds.), Seafloor Geologic Hazards, Sedimentology, and Bathymetry: Navarin Basin Province, Northwestern Bering Sea: U.S. Geological Survey Open-File Report 81-1217, p. 44-57.

Hunt, J. M., 1974, Hydrocarbon geochemistry of Black Sea: In The Black Sea - Geology, Chemistry, and Biology, Am. Assoc. Pet. Geol. Mem., no. 20, p. 499-504.

Kvenvolden, K. A., and Redden, G. D., 1980, Hydrocarbon gas in sediment from the shelf, slope,. and basin of the Bering Sea: Geochim. Cosmochim. Acta, vol. 44, p. 1145-1150.

Kvenvolden, K. A., Vogel, T. M., and Gardner, J. V., 1981, Geochemical prospecting for hydrocarbons in the outer continental shelf, southern Bering Sea, Alaska: Jour. Geochem. Expl., 14, p. 209-219.

Martens, C. S., and Berner, R. A., 1974, Methane production in the interstitial waters of sulfate-depleted marine sediments: Science, 185, p. 1167-1169.

Primrose, S. B., and Dilworth, M. J., 1976, Ethylene production by bacteria: Jour. General Microbiology, no. 93, p. 177-181.

Reeburgh, W. S., 1969, Observations of gases in Chesapeake Bay sediments: Limnol. Oceanog., no. 14, p. 368-375.

Reeburgh, W. S., and Heggie, D. T., 1977, Microbial methane consumption reactions and their effect on methane distributions in fresh water and marine environments: Limnol. Oceanogr., no. 22, p. 1-9.

Vogel, T. M., and Kvenvolden, K. A., 1981, Hydrocarbon gases in Navarin Basin province sediments: In Carlson, P. R., and Karl, H. A., (eds.), Seafloor Geologic Hazards, Sedimentology, and Bathymetry: Navarin Basin Province, Northwestern Bering Sea: U.S. Geological Survey Open-File Report 81-1217, p. 80-99.

Yamamoto, S., Alcauskas, J. B., and Crozier, T. E., 1976, Solubility of methane in distilled water and seawater: Jour. Chem. and Eng. Data, vol. 21, no. 1, p. 78-80.

CHAPTER 9. BENTHIC FORAMINIFERS

by

Paula Quinterno

INTRODUCTION

Samples collected by the U.S. Geological Survey from the Navarin Basin province were analyzed for benthic foraminifers. This study is a continuation of previous work (Quinterno, 1981) and includes samples collected during both 1980 and 1981 (Fig. 43).

Other studies of benthic foraminifers in the Bering Sea have been in areas to the north and west (Saidova, 1967; Lisitsyn, 1966) and in shallow waters to the east and northeast of the study area (Anderson, 1963; Knebel and others, 1974).

The purpose of this study is to determine the distribution of benthic foraminifers in the surface sediments and to record faunal changes with depth in the cores.

METHODS

Samples were processed by washing the sediment over a 62 micron-mesh sieve to remove silt and clay. In samples with much sediment, foraminifers were concentrated by floating in carbon tetrachloride. A microsplitter was used to obtain a representative split of approximately 300 benthic foraminifers. The actual number of benthic foraminifers in the splits ranged from 3 to 2,860.

Foraminifers were mounted on cardboard slides, identified, and the relative frequency percentage of each species calculated.

SURFACE DISTRIBUTION

Samples from the approximate upper 2 cm of forty-two gravity cores or grab samples were examined for benthic foraminifers; the relative frequency percentages of the species present are listed in Table 9. Table 10 is the key to abbreviations for species. In order to recognize faunal trends that might be related to water depth, stations were arranged from left to right in order of increasing water depth and the relative frequency percentages of the most abundant species were plotted (Fig. 44). To simplify plotting and to make Figure 44 more legible, the species abundances for samples having similar water depths were averaged and the average plotted. Although percentages fluctuate with depth, some general trends are apparent.

The peak abundances of *Reophax arctica* (35 and 37%) are at depths of 91 and 99 m. At depths greater than 150 m, the abundance decreases to 5% or less (Fig. 44). Anderson (1963) reports *R. arctica* in the Bering Sea as dominant

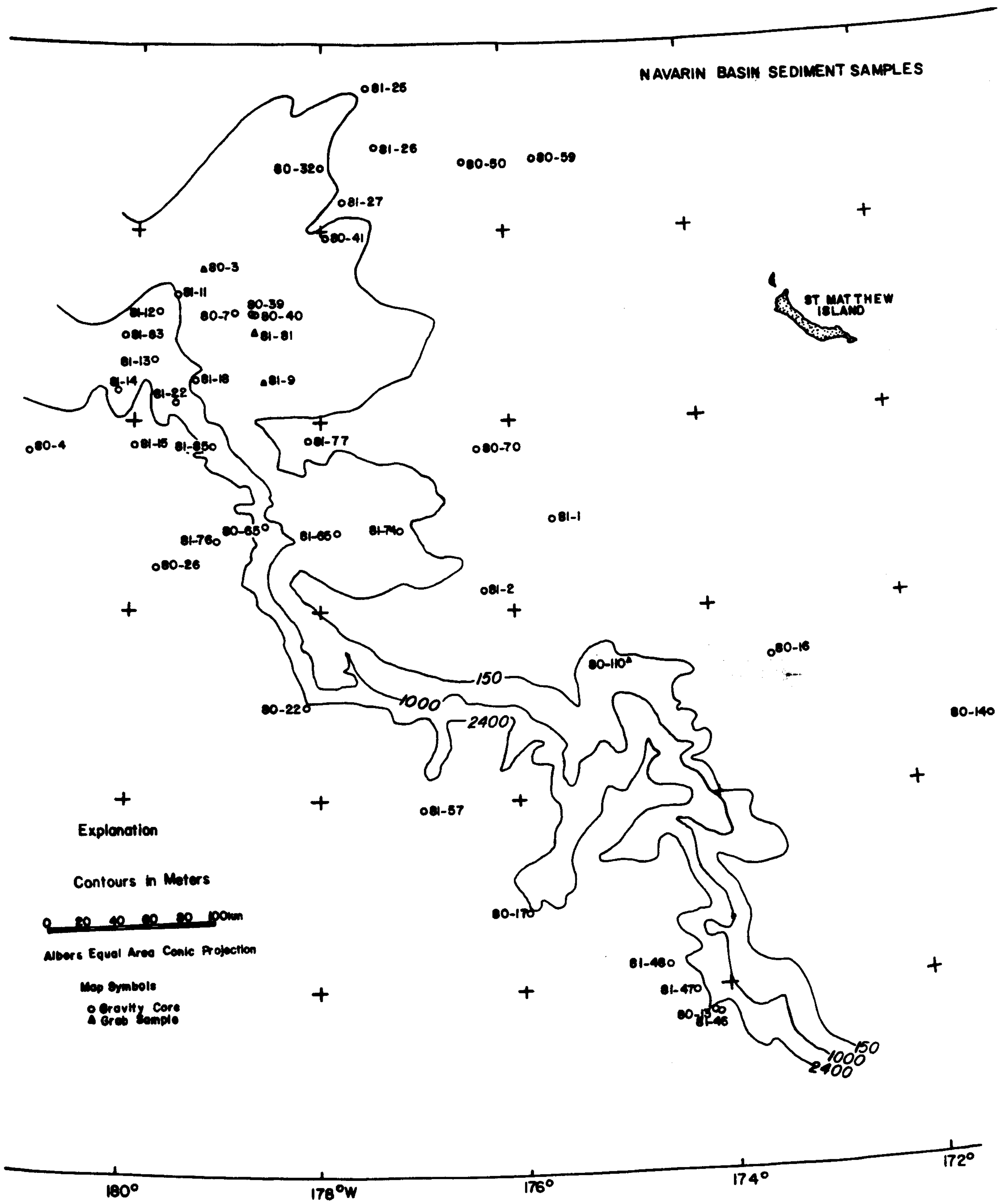

Figure 43. Sample locations.

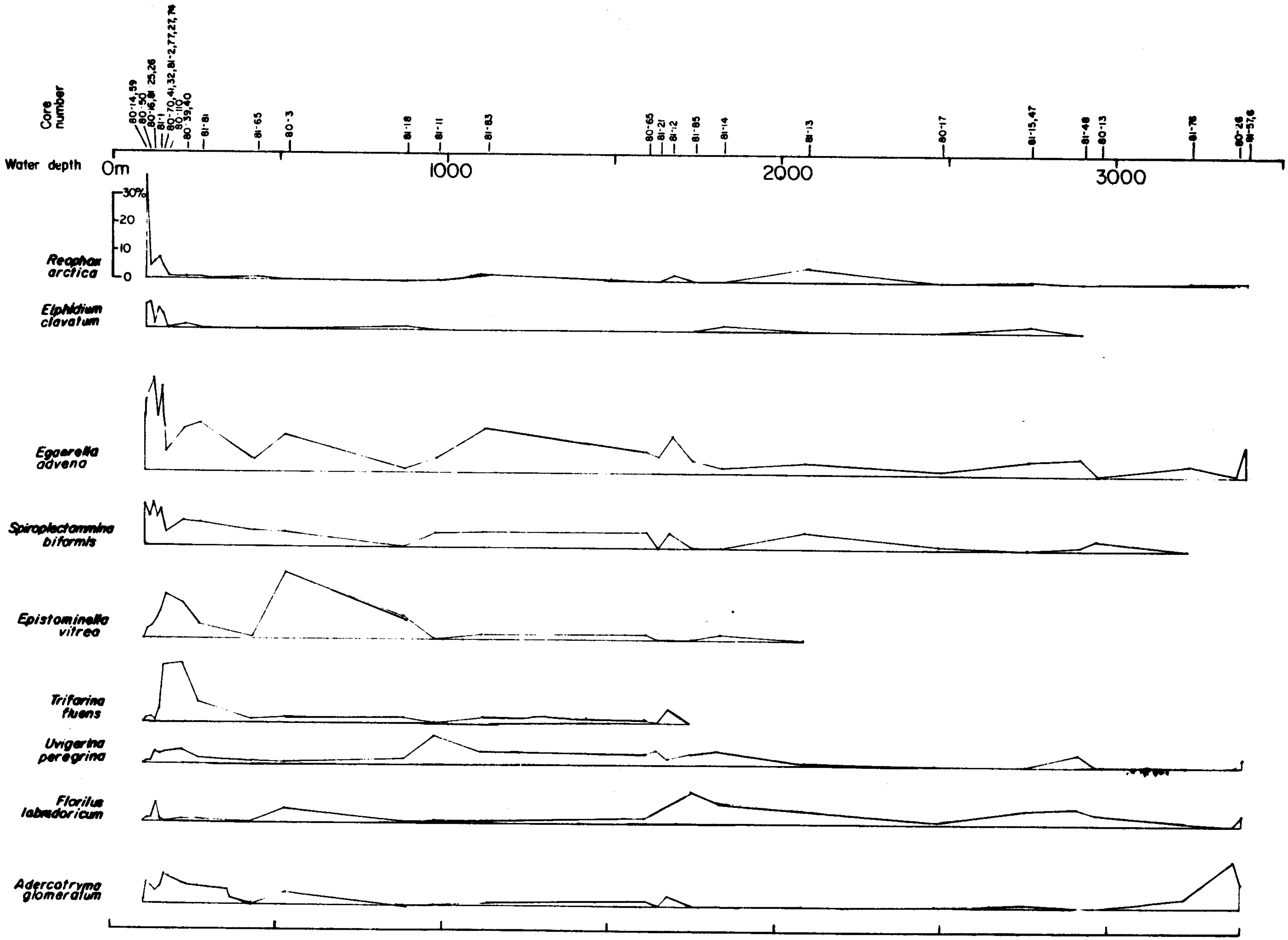

Figure 44. Relative frequency percentages of the most abundant species in surface samples plotted against increasing water depth.

in his Central Shelf fauna (48-100 m) with very low percentages in deeper water. Knebel and others (1974) report the maximum abundance for this species in the Bering Sea between 35-105 m.

Percentages of *Elphidium clavatum* are low throughout my samples with the peak abundance of 15% occurring at 99 m. This species is absent at most stations having water depths greater than 150 m (Fig. 44). This agrees with previous studies which show that *E. clavatum* is typical of shelf environments (Knebel and others, 1974; Anderson, 1963; Matoba, 1976).

Peak abundances of *Eggerella advena* and *Spiroplectammina biformis* occur in water depths shallower than 150 m; there is a general decrease in abundance with increasing water depth (Fig. 44). Anderson (1963) reports the maximum abundance of *E. advena* on the Inner Shelf (22-48 m) but finds it present in lesser numbers in the Central and Outer Shelf faunas (48-200 m).

Epistominella vitrea and *Trifarina fluens* reach maxima between approximately 150 m and 900 m water depth and disappear below 1,800 m (Fig. 44).

Fursenkoina spp., *Reophax* spp., *Textularia torquata*, *Bolivina pacifica*, and *Elphidium batialis* are most abundant below 900 m (Fig. 44).

Several species of *Fursenkoina* were grouped together as *Fursenkoina* spp., because the tests are extremely small and fragile and are difficult to separate into species. Further subdividing into species might show more clearly-defined depth trends.

Elphidium is usually considered a shelf species with highest abundance in water less than 200 m deep. However, there have been reports of a deep-water species, *Elphidium batialis* (Saidova, 1961; Matoba, 1976). This large, robust species has a sharp periphery and makes up more than 6% of the fauna at 9 stations with water depths greater than 1,100 m in the Navarin Basin province (Fig. 44). With one exception, (80-110) it is absent in water shallower than 975 m (Table 9).

The depth trends noted above may be dependent on one or more environmental factors (such as salinity, dissolved oxygen, temperature, and sediment type); however, detailed measurements of these parameters are not available at this time. Furthermore, the distribution of some tests has been affected by bottom currents, storm waves, and downslope transport.

DOWN-CORE STUDIES

Relative frequency percentages for benthic foraminiferal species which are present at various intervals in core 81-12 are listed in Table 11, and graphs showing down-core distribution of species are presented in Fig. 45.

Gravity core 81-12 is 262 cm in length and was collected from the floor of Navarinsky Canyon in 1683 m of water. A pronounced faunal and lithologic break exists between 130 cm and 140 cm within the core (Fig. 45). Visual inspection of the greater than 62 micron portion of sediment from 5 samples above 130 cm shows it to be fine sand. The eleven samples below 130 cm are

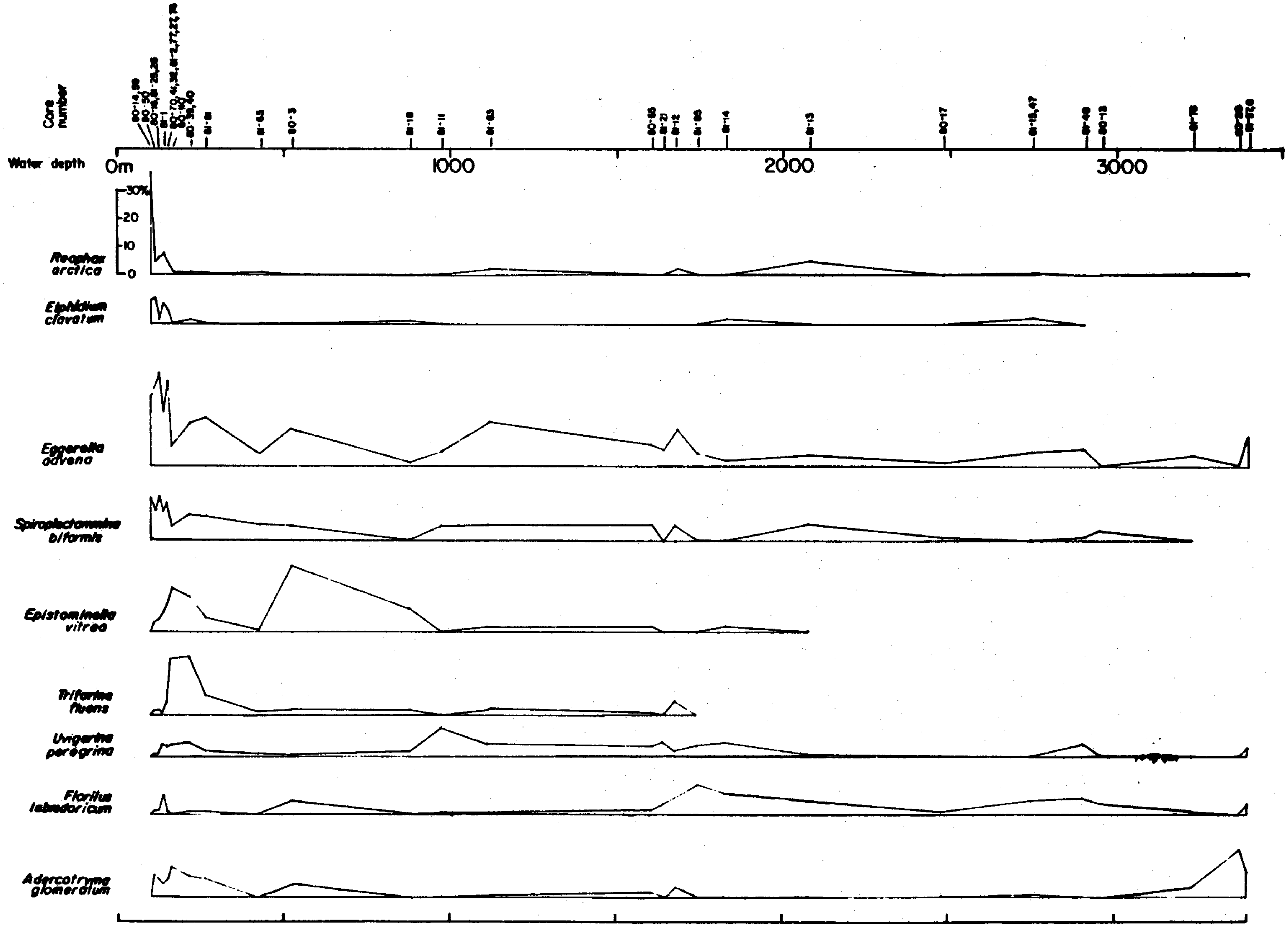

Figure 44. Relative frequency percentages of the most abundant species in surface samples plotted against increasing water depth.

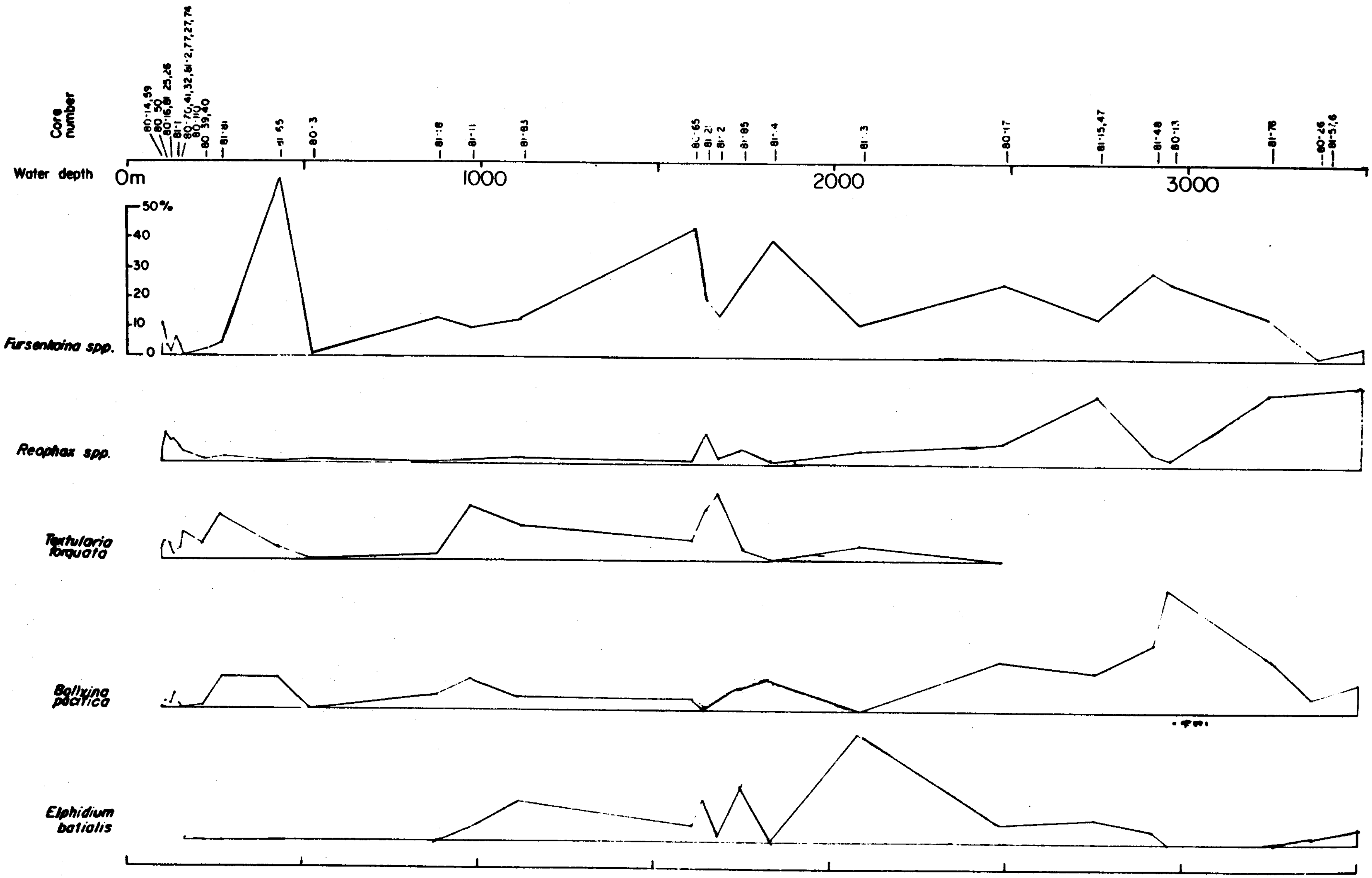

Figure 44 (continued).

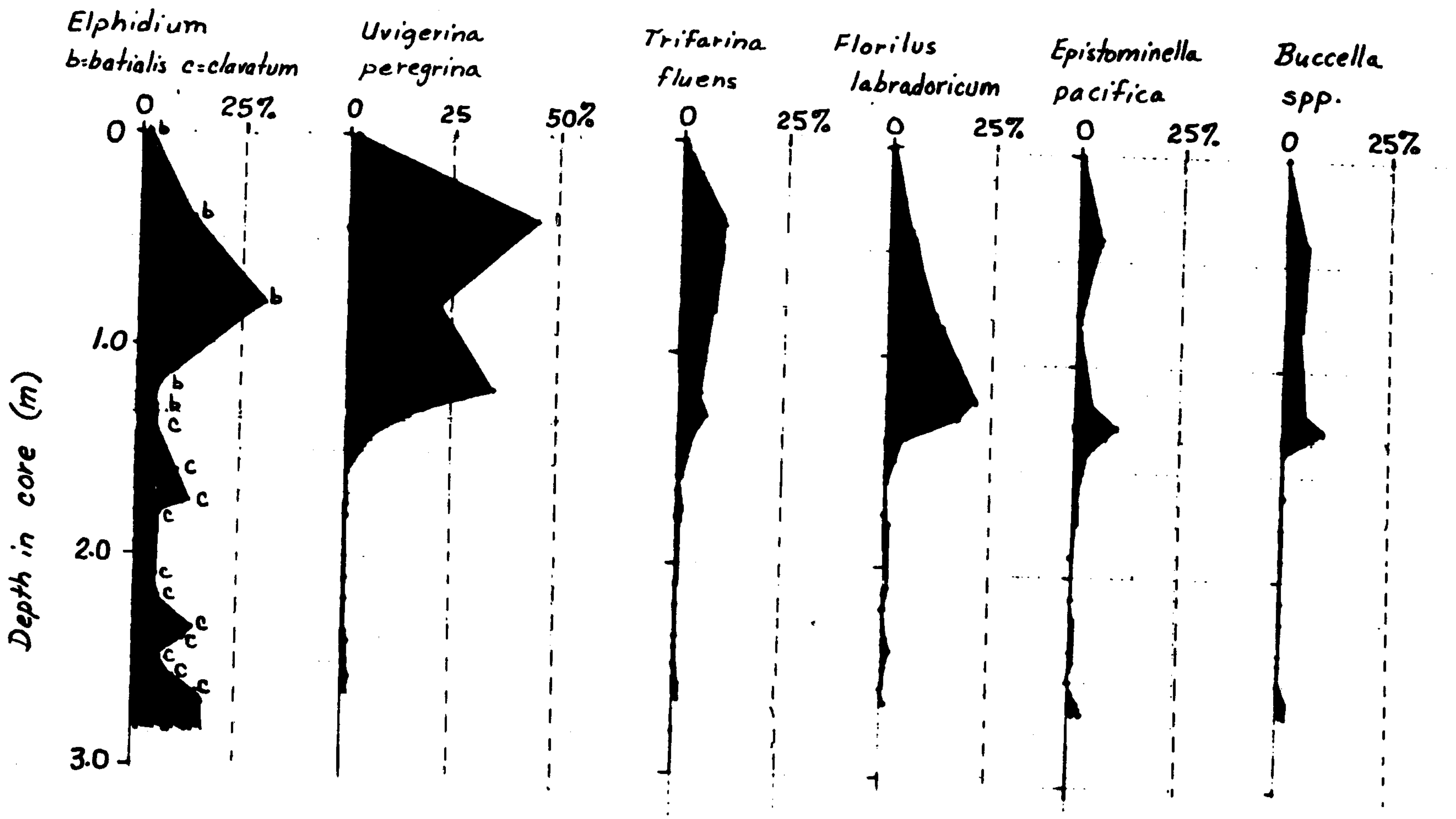

Figure 45. Relative frequency percentages of the most abundant benthic foraminiferal species plotted against depth in core 81-12.

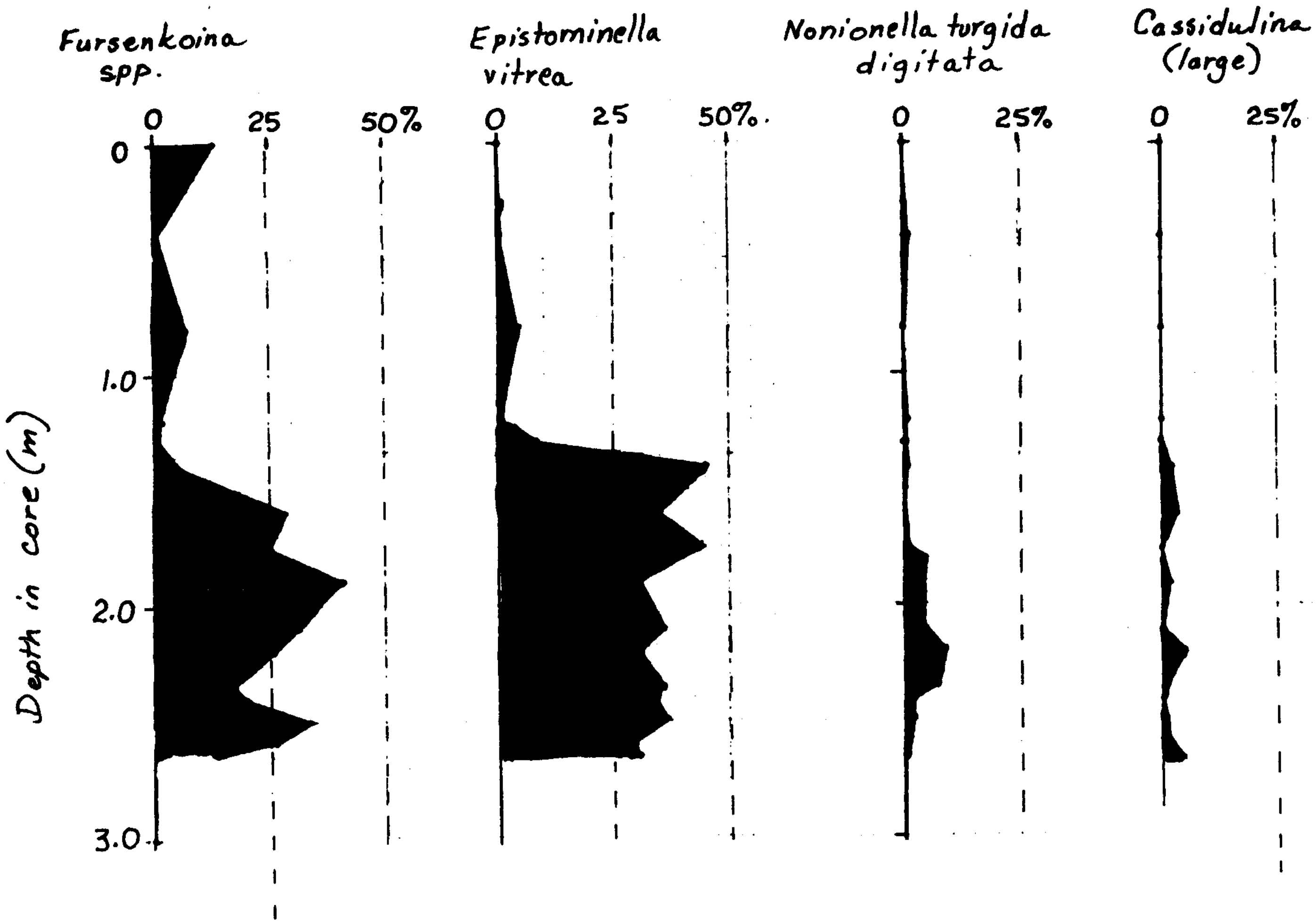

Figure 45 (continued).

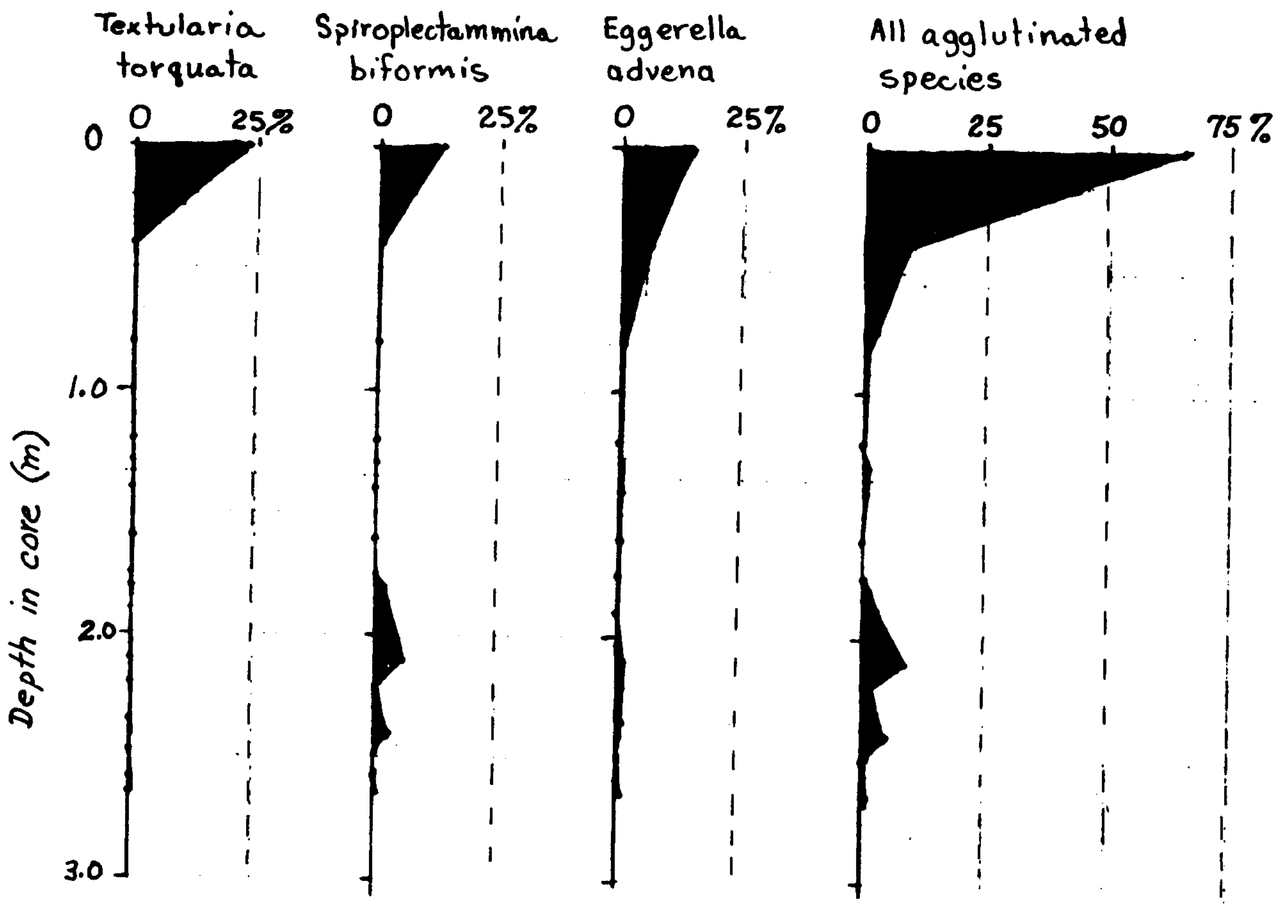

Figure 45 (continued).

generally coarser (most contain pebbles or pebble-sized silt aggregates), and contain glauconite and/or iron-stained grains. The sample at 180 cm contains several irregularly-shaped iron-sulfide plates up to 8 mm long.

Relative frequency percentages of the deep-water species *Elphidium batialis* range from 2-30% in the 5 uppermost samples (0-130 cm) of the core. The shallow-water species *E. clavatum* is not present in these 5 samples (Fig. 45). However, *E. batialis* is absent in all eleven samples below 130 cm, whereas *E. clavatum* is present in abundances ranging from 4-15%. Based on the present-day distribution of *E. clavatum* with respect to water depth, it is unlikely that this species could live at station 81-12 (1,683 m). Even with glacially lowered sea level, the water depth would be too great. Downslope transport of *E. clavatum* tests is a possible explanation for the presence of this species in deep water.

The following species have peak abundances above 130 cm in core 81-12 and decrease markedly below: *Uvigerina peregrina*, *Epistominella pacifica*, *Buccella spp.*, *Trifarina fluens*, and *Florilus labradoricum*. The following species show the opposite trend--low abundances above 130 cm and peak abundances below: *Fursenkoina spp.*, *Epistominella vitrea*, *Nonionella turgida digitata*, and large, poorly-preserved specimens of *Cassidulina* (probably reworked) (Fig. 45).

The pronounced faunal and lithologic break between 130 and 140 cm in core 81-12 may reflect physical and chemical changes in the environment resulting from a change from glacial to interglacial conditions and may represent the Pleistocene/Holocene boundary. With lowered sea level during Pleistocene glaciation, a wide area of the continental shelf was subaerially exposed, and the submerged portion of the shelf was much narrower than at present. During these times, rivers dissected the shelf and transported sediment to the present-day outer shelf (Nelson, Hopkins, and Scholl, 1974). Turbidity currents and debris flows also contributed to down-slope transport (Vallier, Underwood, Gardner, and Barron, 1980; Carlson, Karl, and Quinterno, 1982). Under these conditions, coarser sediment and shallow-water, an organism, such as *E. clavatum*, could easily be transported into deeper water.

SPECIES \ SAMPLE	80-14 (91m)	80-59 (99m)	80-50 (110m)	80-16 (120m)	81-25 (123m)	81-26 (125m)	81-01 (135m)	80-70 (142m)	81-02 (143m)	81-77 (145m)	81-27 (145m)	80-41 (150m)	80-32 (150m)	81-74 (152m)	80-110 (164m)	80-39 (220m)	80-40 (220m)	81-81 (269m)	81-09 (290m)	81-65 (436m)	80-03 (524m)	81-18 (884m)	81-11 (975m)	81-83 (1120m)
ADRGLO	1	3	80	10	90	100	50	60	40	90	40	70	90	70	110	30	120	70	0	4	40	0	0	10
ALVSPP	0	0	3	0	10	0	0	0	0	0	20	0	20	30	10	0	60	0	0	3	0	0	0	0
AMOBAC	0	0	0	0	0	0	0	0	0	0	2	0	0	0	0	0	0	0	0	0	0	0	0	0
AMDSPP	0	0	0	0	0	0	0	0	0	0	0	0	0	0	0	0	0	0	0	0	0	0	0	0
AMSSPP	0	0	0	0	0	0	0	0	0	0	0	0	0	0	0	0	0	0	0	0	0	0	0	0
AMTCAS	4	0	10	0	40	20	10	3	0	2	10	8	6	0	0	0	0	0	0	0	0	0	0	0
ASTSPP	0	0	0	0	0	0	0	0	0	1	0	0	0	3	3	0	2	3	0	0	0	0	0	0
BTYSIP	0	0	0	0	0	0	0	0	0	0	0	0	0	0	0	0	0	0	0	0	0	0	0	0
BOLDEC	0	0	0	0	0	0	0	0	0	0	0	0	1	0	0	10	0	0	0	0	70	0	0	4
BOLPAC	0	1	20	0	20	10	50	30	0	10	40	20	20	3	0	0	20	120	0	110	2	50	120	40
BOLPSE	0	0	0	0	0	0	0	0	0	0	0	0	0	0	0	0	0	0	0	0	0	50	0	0
BOLSEM	0	0	0	0	0	0	0	0	0	0	0	0	0	0	0	0	0	0	0	0	0	70	0	0
BOLSPI	0	0	0	0	0	0	0	0	0	0	0	0	0	0	0	0	0	0	0	0	0	0	10	0
BOLSPP	0	0	0	0	0	0	0	0	0	0	0	0	0	0	0	0	0	0	0	0	0	0	0	0
BUCSPP	0	10	20	1	10	20	10	10	10	20	30	10	40	30	30	30	5	5	0	10	10	2	10	30
BULELE	0	0	0	0	0	0	0	0	0	0	0	0	0	0	0	0	0	0	0	0	1	0	0	0
BULTEN	0	0	0	0	0	0	0	0	0	0	0	0	0	0	0	0	0	0	0	0	0	290	0	0
CALSP1	0	0	0	0	0	0	0	0	0	0	0	0	0	0	0	0	0	0	0	0	0	0	0	0
CASCAL	0	0	0	0	0	0	0	0	0	0	0	0	0	0	10	3	0	0	0	0	0	0	0	0
CASDEL	0	0	0	0	0	0	0	0	0	0	0	0	0	0	0	0	0	0	0	0	0	70	110	0
CASLIM	0	0	0	0	0	0	0	0	0	0	0	0	0	0	0	0	0	0	0	0	0	0	0	0
CASLRG	0	0	0	0	0	0	0	0	0	0	0	0	0	0	0	0	0	0	0	0	0	0	0	0
CASMIN	0	40	20	0	0	3	30	10	0	10	20	20	40	10	40	40	10	2	0	20	0	0	30	40
CASSPP	0	0	0	1	3	0	0	0	0	0	0	0	0	0	0	0	0	0	0	0	10	3	0	2
CSDSPP	0	0	0	0	0	0	0	0	0	0	0	0	0	0	0	0	0	0	0	0	0	5	0	0
CHISPP	0	0	0	0	0	0	0	0	0	0	0	0	0	0	0	0	0	0	0	0	0	0	10	10
CHNFIM	0	0	0	0	0	0	0	0	0	0	0	0	0	0	0	0	0	0	0	0	0	20	5	4
CIBLOB	0	0	0	0	0	0	0	0	0	0	0	0	0	0	0	0	0	0	0	0	0	0	0	0
CIBSPP	0	0	0	0	0	0	0	0	10	0	0	0	0	0	0	0	0	0	0	0	10	0	0	0
CRBSPP	40	0	0	4	0	0	0	0	0	0	0	0	0	0	0	0	0	0	0	0	0	0	0	0

Table 9. Relative frequency percentages of benthic foraminifers in surface samples.

SPECIES \ SAMPLE	80-14 (91m)	80-59 (99m)	80-50 (110m)	80-16 (120m)	81-25 (123m)	81-26 (125m)	81-01 (135m)	80-70 (142m)	81-02 (143m)	81-77 (145m)	81-27 (145m)	80-41 (150m)	80-32 (150m)	81-74 (152m)	80110 (164m)	80-39 (220m)	80-40 (220m)	81-81 (269m)	81-09 (290m)	81-65 (436m)	80-03 (524m)	81-18 (884m)	81-11 (975m)	81-83 (1120m)
CYCSPP	0	0	0	0	0	0	0	0	0	0	0	0	0	0	0	0	0	3	0	0	0	0	5	0
DENSPP	0	0	0	0	0	0	0	0	0	0	0	0	0	0	0	3	0	0	0	0	0	0	0	0
EGGADV	350	20	260	730	200	250	180	230	650	360	230	240	130	190	70	150	170	170	0	30	130	10	50	160
EGGSCR	0	0	10	0	0	20	0	10	0	0	40	30	30	30	10	0	30	40	0	10	0	0	10	20
EGGSUB	0	0	0	0	0	0	0	0	0	0	0	0	0	0	0	0	0	0	0	0	0	20	0	2
ELPBAT	0	0	0	0	0	0	0	0	0	0	0	0	0	0	10	0	0	0	0	0	0	0	40	130
ELPCLA	0	150	90	5	20	10	70	30	0	20	80	100	74	10	0	3	0	0	0	0	0	10	0	0
ELPSPP	0	4	0	4	0	0	0	0	0	0	0	3	0	0	10	0	2	1	0	4	10	2	0	0
EPIPAC	0	0	0	0	0	0	0	0	0	0	0	0	0	0	0	0	0	0	0	0	210	0	0	10
EPIVIT	0	0	30	30	50	30	70	50	0	120	70	100	100	130	160	170	70	50	0	10	240	80	0	20
EPOLEV	0	0	0	0	0	0	0	0	0	4	0	0	0	0	20	10	10	4	0	0	10	10	40	4
EPOSPP	0	0	0	1	3	0	0	0	0	0	0	0	0	0	0	0	0	0	0	0	0	0	0	0
FISSPP	0	1	0	0	0	0	0	0	0	1	0	0	0	0	6	0	0	0	0	0	1	0	0	0
FLOLAB	0	2	10	0	10	20	70	20	0	10	20	10	20	20	3	0	20	10	0	3	40	2	10	10
FURSPP	0	220	30	0	10	30	60	20	0	20	20	30	30	6	0	3	45	40	0	600	10	127	90	122
GLOSPP	0	0	10	2	0	10	10	20	0	14	20	0	10	6	0	0	0	0	0	3	2	10	30	20
GYRSPP	0	0	0	0	0	0	0	0	0	0	0	0	0	0	0	0	0	0	0	0	0	0	0	0
HAPBRA	0	0	0	0	0	0	0	0	0	1	0	0	4	0	10	0	10	30	170	1	5	0	20	0
HAPCOL	0	0	0	0	0	0	0	0	0	0	0	0	0	0	2	0	0	0	0	0	1	5	0	0
HAPSPP	0	0	3	2	0	0	3	0	0	0	0	0	0	3	0	0	2	0	170	0	0	0	0	0
HYPSPP	0	0	0	0	0	0	0	0	0	0	0	0	0	0	0	0	0	0	0	0	0	0	0	0
ISTRNR	0	0	20	4	10	0	20	10	20	20	30	40	20	40	5	20	10	0	0	0	0	0	0	0
KARBAC	0	0	0	0	0	0	0	0	0	0	0	0	0	0	0	0	0	0	0	0	0	0	0	0
LAGSPP	0	0	3	2	0	0	10	0	0	1	0	5	1	3	0	3	2	1	0	3	2	2	10	0
MAROBS	0	0	0	0	0	0	0	0	0	0	0	0	0	0	0	0	0	0	0	0	0	0	0	0
MARSPP	0	0	0	0	0	0	0	0	0	0	0	0	0	0	0	0	0	0	0	0	0	0	0	0
MELPOM	0	0	0	0	0	0	0	0	0	0	0	0	0	0	0	0	0	0	0	0	0	0	0	0
NONPUL	0	0	0	0	0	0	0	0	0	0	0	0	0	0	0	0	0	0	0	0	70	0	0	0
NONTGD	0	0	0	0	0	0	20	0	0	2	10	0	0	20	0	0	20	5	0	10	0	40	0	30
NONSPP	0	0	0	1	0	0	0	0	0	0	0	0	0	0	0	0	0	0	0	0	0	0	0	0

Table 9 (continued).

SPECIES \ SAMPLE	80-14 (91m)	80-59 (99m)	80-50 (110m)	80-16 (120m)	81-25 (123m)	81-26 (125m)	81-01 (135m)	80-70 (142m)	81-02 (143m)	81-77 (145m)	81-27 (145m)	80-41 (150m)	80-32 (150m)	81-74 (152m)	80110 (164m)	80-39 (220m)	80-40 (220m)	81-81 (269m)	81-09 (290m)	81-65 (436m)	80-03 (524m)	81-18 (884m)	81-11 (975m)	81-83 (1120m)
OOLSPP	0	0	0	0	0	0	0	0	0	0	0	0	0	0	0	0	0	0	0	0	0	0	0	0
PATCOR	0	0	0	0	0	0	0	0	0	0	0	0	0	0	0	0	0	0	0	0	0	0	0	0
PELVAR	0	0	0	0	0	0	0	0	0	0	0	0	0	0	0	0	0	0	0	0	0	0	0	0
PRTORB	0	0	0	0	0	0	0	0	2	0	0	0	0	0	0	0	2	0	0	0	0	0	0	0
PSENON	0	0	0	0	0	0	10	10	0	10	40	0	0	3	10	20	20	50	0	20	2	0	10	0
PULSPP	0	0	0	0	0	0	0	0	0	0	0	0	0	0	2	0	2	0	0	0	0	0	0	0
PYRSPP	0	0	0	0	0	0	0	0	0	0	0	0	0	0	0	0	0	0	0	0	0	0	0	0
QNQSPP	0	0	0	0	0	0	0	0	0	0	0	0	0	0	0	0	0	0	0	0	4	0	0	0
RECSPP	0	30	20	0	10	20	10	0	0	1	30	3	20	3	10	10	3	3	0	0	5	0	0	0
REOARC	350	370	40	20	90	80	70	140	2	30	10	40	20	10	10	0	2	10	0	10	0	0	0	20
REOCUR	3	0	20	2	0	20	0	3	20	0	0	20	20	10	0	0	10	20	0	0	0	2	5	0
REODIF	0	0	0	0	110	50	0	0	0	20	50	20	30	0	0	0	0	0	0	0	0	0	0	10
REOFUS	0	0	70	0	0	0	70	90	0	3	0	0	0	30	0	0	0	3	0	4	0	0	0	0
REOSCO	0	1	0	0	0	0	0	0	0	5	0	0	0	0	30	10	0	0	0	0	0	0	5	2
REOSPP	0	2	0	2	0	0	3	0	0	2	0	0	0	0	0	0	0	0	0	0	6	0	0	10
RHBSPP	0	0	0	0	0	0	0	0	0	0	0	0	0	0	0	0	0	0	0	0	0	0	0	0
SACSPH	0	0	0	0	0	0	0	0	0	0	0	0	0	0	5	0	0	0	0	0	0	0	5	2
SPRBIF	220	70	110	80	230	160	100	180	90	100	110	140	130	130	50	30	130	70	0	60	50	0	50	60
SPRSPP	0	0	0	0	0	0	0	0	0	0	0	0	0	0	0	0	0	13	0	23	0	20	0	0
TEXTOR	20	50	60	20	60	80	20	20	20	30	20	20	60	50	80	20	80	150	0	40	0	20	180	120
TEXSPP	0	0	0	0	0	0	0	0	0	0	0	0	0	0	0	0	0	0	0	0	10	0	0	10
TRIFLU	0	0	20	40	10	3	10	10	70	70	20	20	30	90	200	320	100	70	330	10	20	20	3	20
TRLTRI	0	0	0	0	0	0	0	0	0	0	0	0	0	0	0	0	0	0	0	0	0	0	0	4
TROGLO	0	0	0	0	0	0	0	0	0	0	0	0	0	0	0	0	0	0	0	0	0	0	0	0
TRONIT	0	0	0	0	0	0	0	0	0	0	0	10	0	0	0	0	0	0	0	0	0	0	0	0
TROPAC	0	0	0	0	3	0	0	0	0	0	0	0	0	0	0	0	0	0	0	0	0	10	5	0
TROSPP	0	0	0	0	3	0	0	0	10	0	0	0	3	6	20	0	0	10	170	0	10	0	3	0
UVGPRG	0	0	10	20	0	20	50	40	40	10	40	20	10	50	50	90	10	20	0	10	10	20	100	40
UVGSEN	0	0	0	0	0	0	0	0	0	0	0	0	0	0	0	0	0	0	0	0	0	0	0	0
UVGSPP	0	0	0	0	3	0	0	0	0	0	0	0	0	0	0	0	0	0	0	0	0	0	0	0

Table 9 (continued).

SPECIES \ SAMPLE	80-14 (91m)	80-59 (99m)	80-50 (110m)	80-16 (120m)	81-25 (123m)	81-26 (125m)	81-01 (135m)	80-70 (142m)	81-02 (143m)	81-77 (145m)	81-27 (145m)	80-41 (150m)	80-32 (150m)	81-74 (152m)	80110 (164m)	80-39 (220m)	80-40 (220m)	81-81 (269m)	81-09 (290m)	81-65 (436m)	80-03 (524m)	81-18 (884m)	81-11 (975m)	81-83 (1120m)
VALCON	0	0	0	0	0	0	0	0	0	0	0	0	0	0	3	0	0	1	0	0	0	0	0	0
VALGLA	0	0	0	0	0	0	0	0	0	0	0	0	0	0	0	0	0	0	0	0	0	20	0	0
VIRSPP	0	0	0	0	0	0	0	0	0	0	0	0	0	0	0	0	0	0	0	0	0	0	0	0
OTHAGG	0	0	0	0	6	20	0	26	0	0	10	10	6	0	10	0	5	0	170	3	11	0	3	2
OTHCAL	0	0	3	0	3	10	0	0	5	2	0	10	0	0	0	0	0	5	0	0	0	0	5	34
OTHMIL	0	1	0	0	0	10	3	0	0	5	0	0	1	0	0	3	3	1	0	0	0	0	0	0

Tabe 9 (continued).

SPECIES \ SAMPLE	80-65 (1609m)	81-21 (1640m)	81-12 (1683m)	81-85 (1745m)	81-14 (1826m)	81-13 (2080m)	80-17 (2481m)	81-46 (2530m)	81-15 (2750m)	81-47 (2760m)	80-22 (2842m)	81-48 (2910m)	80-13 (2962m)	80-04 (3222m)	81-76 (3230m)	80-26 (3373m)	81-57 (3395m)	81-06 (3395m)
ADRGLO	2	0	30	0	0	0	3	0	0	10	0	0	0	0	30	170	50	120
ALVSPP	4	20	0	20	0	6	3	0	0	0	0	0	0	0	0	10	0	0
AMOBAC	0	0	0	0	0	0	0	0	0	0	0	0	0	0	0	0	0	0
AMDSPP	0	0	0	0	0	0	0	0	0	0	0	0	0	0	0	0	0	0
AMSSPP	0	0	0	0	0	0	0	0	0	0	0	0	0	0	0	0	0	0
AMTCAS	0	0	0	0	0	0	0	0	0	0	0	0	0	0	0	0	0	0
ASTSPP	2	0	0	0	0	0	0	0	0	0	0	0	0	0	0	0	0	0
BTYSIP	0	0	0	0	0	0	0	0	0	0	0	0	0	0	0	0	0	0
BOLDEC	0	0	0	0	0	0	0	0	0	0	0	4	0	0	0	0	0	0
BOLPAC	30	0	30	70	100	3	170	0	80	170	420	230	420	420	180	50	130	50
BOLPSE	0	0	0	0	0	0	0	0	0	0	0	0	0	0	0	0	10	0
BOLSEM	0	0	0	0	0	0	0	0	0	0	0	0	30	0	0	0	20	0
BOLSPI	0	0	0	0	0	0	0	0	0	0	0	0	0	0	0	0	20	0
BOLSPP	2	0	0	0	0	0	0	0	0	0	0	0	0	0	0	0	0	0
BUCSPP	2	0	6	2	3	0	0	0	0	0	0	4	0	0	0	0	3	0
BULELE	0	0	0	0	4	0	0	0	0	0	0	4	0	0	0	0	0	0
BULTEN	0	0	0	0	140	0	3	0	0	0	0	0	0	0	0	0	50	0
CALSP1	0	0	0	0	0	0	0	0	0	0	0	0	0	0	0	0	0	0
CASCAL	0	0	0	0	0	0	0	0	0	0	0	0	0	0	0	0	0	0
CASDEL	0	0	0	0	0	0	0	0	0	0	0	0	0	0	0	0	0	0
CASLIM	0	0	0	0	0	0	0	0	0	0	0	0	0	0	0	0	0	0
CASLRG	0	0	0	0	0	0	0	0	0	0	0	0	0	0	0	0	0	0
CASMIN	60	60	20	60	10	40	20	0	10	20	0	20	0	0	30	10	3	10
CASSPP	2	0	0	0	0	0	0	0	0	4	0	0	0	0	0	0	0	0
CSDSPP	0	10	0	0	10	0	0	0	0	0	0	0	0	0	0	0	10	0
CHISPP	10	0	0	2	10	0	3	0	0	0	0	0	0	0	0	0	0	0
CHNFIM	10	0	3	4	70	10	0	0	0	10	40	0	30	0	0	0	20	2
CIBLOB	0	0	0	0	0	0	10	0	0	0	0	0	0	0	0	0	0	0
CIBSPP	2	0	0	0	0	0	3	0	0	0	0	0	0	0	0	20	3	0
CRBSPP	0	10	0	0	0	0	0	0	0	0	0	0	0	0	0	0	0	0

Table 9 (continued).

SPECIES \ SAMPLE	80-65 (1609m)	81-21 (1640m)	81-12 (1683m)	81-85 (1745m)	81-14 (1826m)	81-13 (2080m)	80-17 (2481m)	81-46 (2530m)	81-15 (2750m)	81-47 (2760m)	80-22 (2842m)	81-48 (2910m)	80-13 (2962m)	80-04 (3222m)	81-76 (3230m)	80-26 (3373m)	81-57 (3395m)	81-06 (3395m)
CYCSPP	0	3	0	0	0	3	0	0	0	0	0	0	0	0	0	0	0	0
DENSPP	0	0	0	0	0	0	0	0	0	0	0	0	0	0	0	0	0	0
EGGADV	70	60	130	40	2	30	10	80	30	50	0	60	0	20	30	0	10	10
EGGSCR	20	10	10	4	0	0	0	0	0	0	0	0	0	0	0	0	0	0
EGGSUB	0	0	0	0	0	0	0	0	0	0	0	0	0	0	0	0	0	0
ELPBAT	60	140	20	190	0	370	60	0	140	20	10	40	0	150	0	20	100	10
ELPCLA	0	0	0	0	20	0	0	0	50	0	0	0	0	0	0	0	0	0
ELPSPP	0	0	0	0	2	0	0	0	0	0	0	0	0	0	20	0	0	0
EPIPAC	0	0	0	0	2	0	0	0	0	0	0	0	0	0	0	0	10	0
EPIVIT	20	3	0	0	20	3	0	0	0	0	0	4	0	0	0	0	0	0
EPOLEV	4	0	0	0	0	0	70	0	20	90	190	10	0	0	10	90	10	30
EPOSPP	0	0	0	0	0	0	0	0	0	0	0	0	0	20	0	0	0	0
FISSPP	0	3	0	0	0	0	0	0	10	14	20	4	0	0	20	0	3	3
FLOLAB	20	30	3	100	70	40	10	0	10	70	0	50	30	50	10	0	50	20
FURSPP	430	190	130	250	391	110	250	0	124	130	110	290	260	20	130	10	60	15
GLOSPP	24	10	8	70	40	10	10	0	4	40	0	10	50	50	0	0	43	12
GYRSPP	0	0	0	0	0	0	10	0	0	0	0	0	0	0	0	0	0	0
HAPBRA	0	3	0	0	0	0	0	0	4	10	0	10	0	0	0	0	0	10
HAPCOL	0	0	0	0	0	0	0	0	0	0	0	0	0	0	0	0	0	0
HAPSPP	0	10	0	0	1	0	0	0	0	0	0	0	0	0	0	0	0	0
HYPSPP	0	0	0	0	0	0	0	0	0	0	0	0	0	0	0	0	0	0
ISTRNR	0	0	0	2	1	40	0	0	20	10	0	0	0	0	0	0	3	0
KARBAC	0	0	0	0	0	0	0	50	0	4	0	0	0	0	0	0	0	2
LAGSPP	2	0	3	0	4	3	3	0	10	0	0	0	0	0	0	0	0	2
MAROBS	0	0	0	0	0	0	0	0	0	0	0	0	0	0	0	10	0	0
MARSPP	0	0	0	0	0	0	0	0	0	0	0	0	0	0	0	0	0	0
MELPOM	0	0	0	0	0	0	3	0	0	10	0	4	0	0	0	0	0	0
NONPUL	0	0	0	0	0	0	0	0	0	0	0	0	0	0	0	0	0	0
NONTGD	40	20	0	40	40	20	120	0	10	40	50	80	0	0	60	0	40	10
NONSPP	0	0	70	0	0	0	0	0	0	0	0	0	0	0	0	0	0	0

Table 9 (continued).

SPECIES \ SAMPLE	80-65 (1609m)	81-21 (1640m)	81-12 (1683m)	81-85 (1745m)	81-14 (1826m)	81-13 (2080m)	80-17 (2481m)	81-46 (2530m)	81-15 (2750m)	81-47 (2760m)	80-22 (2842m)	81-48 (2910m)	80-13 (2962m)	80-04 (3222m)	81-76 (3230m)	80-26 (3373m)	81-57 (3395m)	81-06 (3395m)
OOLSPP	0	0	0	0	0	0	0	0	0	0	0	0	0	0	0	0	0	0
PATCOR	0	0	0	0	0	0	0	0	0	0	0	0	0	0	0	0	0	0
PELVAR	0	0	0	0	0	0	0	0	0	0	0	0	0	0	0	0	0	0
PRTORB	0	0	0	0	0	0	0	0	0	0	0	0	0	0	0	0	0	0
PSENON	0	0	40	0	0	0	0	0	0	0	0	0	30	0	10	10	10	2
PULSPP	0	0	0	0	0	0	0	0	0	4	0	0	0	0	0	0	0	0
PYRSPP	0	0	0	0	0	0	0	0	0	0	0	0	0	0	0	10	0	2
QNQSPP	0	0	0	0	0	0	0	0	0	0	0	0	0	0	0	10	10	0
RECSPP	0	0	0	0	0	0	0	0	10	0	0	10	0	0	0	0	0	0
REOARC	0	0	20	0	0	50	0	0	20	0	0	0	0	0	10	10	10	0
REOCUR	2	80	10	30	10	20	0	490	0	0	0	0	0	0	0	0	0	0
REODIF	4	0	0	0	0	0	50	30	100	160	50	40	0	0	140	230	120	210
REOFUS	0	0	0	20	0	0	20	0	30	0	0	0	0	0	100	50	10	20
REOSCO	0	0	0	0	0	10	0	0	40	0	0	0	0	0	0	20	30	20
REOSPP	0	20	13	0	0	10	0	110	88	34	0	0	20	80	0	60	30	90
RHBSPP	0	0	0	0	0	0	0	0	0	0	0	0	0	0	0	0	0	0
SACSPH	0	0	0	0	0	0	3	0	0	10	0	0	0	0	10	0	0	30
SPRBIF	60	0	50	0	0	60	10	0	0	0	0	10	30	0	0	0	0	0
SPRSPP	0	30	80	10	0	0	0	190	0	10	0	0	30	0	0	20	10	20
TEXTOR	70	170	230	30	3	50	0	30	0	10	0	0	0	0	0	0	0	2
TEXSPP	10	0	0	0	0	0	20	0	0	0	40	0	0	80	0	0	0	0
TRIFLU	10	0	5	0	0	0	0	0	0	0	0	0	0	0	0	0	0	0
TRLTRI	0	0	0	0	3	0	0	0	0	0	0	0	30	0	0	0	0	0
TROGLO	0	0	0	0	0	0	3	0	3	0	0	0	0	0	0	10	0	0
TRONIT	0	0	0	2	0	0	0	0	50	0	0	0	0	0	50	0	0	40
TROPAC	0	0	50	0	0	30	0	0	60	40	0	20	0	0	50	100	40	120
TROSPP	2	23	0	0	4	0	13	0	0	0	30	10	0	20	10	0	0	10
UVGPRG	30	50	20	30	40	10	0	0	0	0	0	4	0	0	0	0	50	0
UVGSEN	0	10	0	0	0	0	0	0	0	10	10	0	0	50	0	10	0	0
UVGSPP	0	0	0	0	0	0	0	0	0	0	0	0	0	0	0	0	0	5

Table 9 (continued).

SPECIES \ SAMPLE	80-65 (1609m)	81-21 (1640m)	81-12 (1683m)	81-85 (1745m)	81-14 (1826m)	81-13 (2080m)	80-17 (2481m)	81-46 (2530m)	81-15 (2750m)	81-47 (2760m)	80-22 (2842m)	81-48 (2910m)	80-13 (2962m)	80-04 (3222m)	81-76 (3230m)	80-26 (3373m)	81-57 (3395m)	81-06 (3395m)
VALCON	0	0	0	0	0	0	0	0	0	0	0	0	0	0	0	0	0	0
VALGLA	0	0	0	0	2	0	3	0	0	4	0	0	0	0	0	0	3	2
VIRSPP	0	0	0	10	0	0	0	0	0	14	0	10	0	0	0	0	0	0
OTHAGG	4	0	30	0	0	20	0	0	60	20	0	0	0	0	0	0	30	5
OTHCAL	4	10	0	20	1	3	93	0	10	10	10	74	50	20	70	40	13	72
OTHMIL	0	3	0	2	0	0	0	0	0	0	0	4	0	0	10	0	0	30

Table 9 (continued).

Table 10. List of Benthic Foraminiferal Species.

ADRGLO	*Adercotryma glomeratum*
ALVSPP	*Alveolophragmium spp.*
AMOBAC	*Ammobaculites*
AMDSPP	*Ammodiscus spp.*
AMSSPP	*Ammoscalaria spp.*
AMTCAS	*Ammotium cassis*
ASTSPP	*Astrononion spp.*
BTYSIP	*Bathysiphon*
BOLDEC	*Bolivina decussata*
BOLPAC	*Bolivina pacifica*
BOLPSE	*Bolivina pseudobeyrichi*
BOLSEM	*Bolivina seminuda and B. seminuda var. foraminata*
BOLSPI	*Bolivina spissa*
BOLSPP	*Bolivina spp.*
BUCSPP	*Buccella spp.*
BULELE	*Buliminella elegantissima*
BULTEN	*Buliminella tenuata*
CALSP1	small, transparent calcareous foram
CASCAL	*Cassidulina californica*
CASDEL	*Cassidulina delicata*
CASLIM	*Cassidulina limbata*
CASLRG	*Cassidulina lomitensis and C. l. elegantula*
CASMIN	*Cassidulina minuta*
CASSPP	*Cassidulina spp.*
CSDSPP	*Cassidulinoides spp.*
CHISPP	*Chilostomella spp.*
CHNFIM	*Chilostomellina fimbriata*
CIBLOB	*Cibicides lobatulus*
CIBSPP	*Cibicides spp.*
CRBSPP	*Cribrostomoides spp.*
CYCSPP	*Cyclammina spp.*
DENSPP	*Dentalina spp.*
EGGADV	*Eggerella advena*
EGGSCR	*Eggerella scrippsi*
EGGSUB	*Eggerella subadvena*
ELPBAT	*Elphidium batialis*
ELPCLA	*Elphidium clavatum*
ELPSPP	*Elphidium spp.*
EPIPAC	*Epistominella pacifica*
EPIVIT	*Epistominella vitrea*
EPOLEV	*Eponides leviculus*
EPOSPP	*Eponides spp.*
FISSPP	*Fissurina spp.*
FLOLAB	*Florilus labradoricum*

FURSPP	*Fursenkoina spp.*
GLOSPP	*Globobulimina spp.*
GYRSPP	*Gyroidina spp.*
HAPBRA	*Haplophragmoides bradyi*
HAPCOL	*Haplophragmoides columbiense*
HAPSPP	*Haplophragmoides spp.*
HYPSPP	*Hyperammina spp.*
ISTRNR	*Islandiella teretis/norcrossi*
KARBAC	*Karreriella baccata*
LAGSPP	*Lagena spp.*
MAROBS	*Marginulina obesa*
MARSPP	*Martinottiella spp.*
MELPOM	*Melonis pompiliodes*
NONPUL	*Nonionella pulchella*
NONTGD	*Nonionella turgida digitata*
NONSPP	*Nonionella spp.*
OOLSPP	*Oolina spp.*
PATCOR	*Patellina corrugata*
PELVAR	*Pelosina variabilis*
PRTORB	*Protelphidium orbiculare*
PSENON	*Pseudononion spp.*
PULSPP	*Pullenia spp.*
PYRSPP	*Pyrgo spp.*
QNQSPP	*Quinqueloculina spp.*
RECSPP	*Recurvoides spp.*
REOARC	*Reophax arctica*
REOCUR	*Reophax curtus*
REODIF	*Reophax difflugiformis*
REOFUS	*Reophax fusiformis*
REOSCO	*Reophax scorpiurus*
REOSPP	*Reophax spp.*
RHBSPP	*Rhabdammina spp.*
SACSPH	*Saccammina sphaerica*
SPRBIF	*Spiroplectammina biformis*
SPRSPP	*Spiroplectammina spp.*
TEXTOR	*Textularia torquata*
TEXSPP	*Textularia spp.*
TRIFLU	*Trifarina fluens*
TRLTRI	*Triloculina spp.*
TROGLO	*Trochammina globigerinaformis*
TRONIT	*Trochammina nitida*
TROPAC	*Trochammina pacifica*
TROSPP	*Trochammina spp.*
UVGPRG	*Uvigerina peregrina*
UVGSEN	*Uvigerina senticosa*
UVGSPP	*Uvigerina spp.*
VALCON	*Valvulina conica*
VALGLA	*Valvulineria glabra*
VIRSPP	*Virgulina spp.*
OTHAGG	Other agglutinated species
OTHCAL	Other calcareous species
OTHMIL	*Miliollids*

SPECIES \ Sample number and depth interval within core	81-12 TOP (~2cm)	40-42cm	80-82cm	120-122cm	129-132cm	140-142cm	160-162cm	175-177cm	180-183cm	210-212cm	220-222cm	235-237cm	240-242cm	248cm	257-260cm	core catcher
ADRGLO	30	0	0	0	0	0	0	0	0	0	0	0	0	0	1	0
ALVSPP	0	0	0	0	0	0	0	0	0	0	0	0	0	0	0	0
AMOBAC	0	0	0	0	0	0	0	0	0	0	0	0	0	0	0	0
AMDSPP	0	0	0	0	0	0	0	0	0	0	0	0	0	0	0	0
AMSSPP	0	0	0	0	0	0	0	0	0	0	0	0	0	0	0	0
AMTCAS	0	0	0	0	0	0	0	0	0	0	0	0	0	0	0	0
ASTSPP	0	0	0	2	0	0	3	0	1	0	0	0	1	0	2	0
BTYSIP	0	0	0	0	0	0	0	0	0	0	0	0	0	0	0	0
BOLDEC	0	0	20	0	6	10	10	10	4	3	5	0	10	20	20	20
BOLPAC	30	20	10	20	20	40	60	30	20	40	30	20	40	50	40	30
BOLPSE	0	0	0	2	6	3	0	2	0	0	0	0	1	0	0	0
BOLSEM	0	0	0	0	3	0	0	0	2	0	0	0	0	0	1	0
BOLSPI	0	0	0	0	0	3	0	0	0	0	0	0	0	0	0	0
BOLSPP	0	0	0	0	0	0	0	0	0	0	0	0	0	0	0	0
BUCSPP	6	50	30	50	90	10	10	4	1	6	10	10	10	0	20	20
BULELE	0	0	0	10	3	3	1	0	0	10	0	10	1	0	0	10
BULTEN	0	3	0	10	6	40	4	4	10	10	10	10	20	10	20	20
CALSP1	0	0	0	0	0	0	0	0	0	0	0	0	0	0	0	0
CASCAL	0	0	0	0	0	20	30	0	0	0	0	0	0	0	0	0
CASDEL	0	0	0	2	0	0	0	0	0	0	0	0	0	0	2	0
CASLIM	0	0	0	0	0	0	0	0	0	0	0	0	0	0	0	0
CASLRG	0	0	0	0	0	0	0	4	20	3	50	10	4	0	20	40
CASMIN	20	30	90	20	70	30	0	30	30	40	60	50	60	30	50	70
CASSPP	0	0	0	0	0	0	0	0	0	0	0	0	0	10	0	0
CSDSPP	0	0	0	50	30	0	0	2	1	0	0	0	0	0	0	0
CHISPP	0	0	0	0	0	0	0	0	0	0	0	0	0	0	0	0
CHNFIM	3	0	0	10	10	10	4	10	10	0	20	30	10	5	20	10
CIBLOB	0	0	0	0	0	0	10	0	0	0	5	0	0	10	10	20
CIBSPP	0	0	3	10	0	10	1	0	2	3	0	0	10	0	1	0
CRBSPP	0	0	0	0	0	0	0	0	0	0	0	0	0	0	0	0

Table 11. Relative frequency percentages of benthic foraminiferal species in core 81-12.

SPECIES / Sample number and depth interval within core	81-12 TOP(~2cm)	40-42cm	80-82cm	120-122cm	129-132cm	140-142cm	160-162cm	175-177cm	180-183cm	210-212cm	220-222cm	235-237cm	240-242cm	248cm	257-260cm	core catcher
CYCSPP	0	0	0	0	0	0	0	0	0	0	0	0	0	0	0	0
DENSPP	0	0	0	0	0	0	0	0	0	0	0	0	0	0	0	0
EGGADV	130	60	5	0	3	10	0	0	2	10	10	10	10	2	2	10
EGGSCR	10	0	0	0	0	0	0	0	0	0	0	0	0	0	0	3
EGGSUB	0	0	0	0	0	0	0	0	0	0	0	0	0	0	0	0
ELPBAT	20	130	300	50	40	0	0	0	0	0	0	0	0	0	0	0
ELPCLA	0	0	0	0	6	50	100	120	60	40	60	140	110	60	90	150
ELPSPP	0	0	0	0	6	0	3	10	2	6	3	0	10	0	20	20
EPIPAC	0	50	5	40	100	30	10	10	0	3	10	3	10	4	20	30
EPIVIT	0	10	40	10	80	450	350	440	310	360	310	360	340	370	290	310
EPOLEV	0	0	10	0	3	3	0	10	1	0	0	0	0	0	1	0
EPOSPP	0	0	0	0	0	0	0	0	0	0	0	0	0	0	0	0
FISSPP	0	0	0	2	3	0	2	2	2	3	4	0	1	10	5	0
FLOLAB	3	50	100	210	170	30	2	0	10	10	5	10	20	2	2	10
FURSPP	130	10	70	30	20	63	280	250	412	323	260	170	202	330	261	140
GLOSPP	8	10	10	30	20	40	20	10	10	3	10	3	20	10	10	30
GYRSPP	0	0	0	0	0	0	0	0	0	0	0	0	0	0	0	0
HAPBRA	0	0	0	0	0	0	0	0	0	3	0	0	0	0	0	0
HAPCOL	0	0	0	0	0	0	0	0	0	0	0	0	0	0	0	0
HAPSPP	0	0	0	0	0	0	0	0	0	0	0	0	0	0	0	0
HYPSPP	0	0	0	0	0	0	0	0	0	0	0	0	0	0	0	0
ISTRNR	0	0	0	5	10	3	4	4	2	10	10	10	10	4	10	20
KARBAC	0	0	0	0	0	0	0	0	0	0	0	0	0	0	0	0
LAGSPP	3	6	3	5	15	0	4	2	0	0	0	0	0	2	1	0
MAROBS	0	0	0	0	0	0	0	0	0	0	0	0	0	0	0	0
MARSPP	0	0	0	0	0	0	0	0	0	0	0	0	0	0	0	0
MELPOM	0	0	0	0	0	0	0	0	0	0	0	0	0	0	0	0
NONPUL	0	0	0	0	0	0	0	0	0	0	0	0	0	0	0	0
NONTGD	0	10	0	10	0	10	0	10	40	40	80	70	20	20	0	3
NONSPP	70	0	0	0	0	0	10	0	0	0	0	0	0	10	0	0

Table 11 (continued).

SPECIES / Sample number and depth interval within core	81-12 TOP (~2cm)	40-42cm	80-82cm	120-122cm	129-132cm	140-142cm	160-162cm	175-177cm	180-183cm	210-212cm	220-222cm	235-237cm	240-242cm	248cm	257-260cm	Core catcher
OOLSPP	0	0	0	0	0	0	0	0	0	0	0	0	0	0	0	0
PATCOR	0	0	0	0	0	3	0	0	0	0	0	3	0	0	0	0
PELVAR	0	0	0	0	0	0	0	0	0	0	0	0	0	0	0	0
PRTORB	0	0	0	0	0	0	0	0	0	0	0	0	0	0	0	0
PSENON	10	0	0	0	20	0	0	0	10	0	10	10	0	0	10	10
PULSPP	0	0	0	2	0	3	0	0	0	0	0	0	0	0	0	0
PYRSPP	0	0	0	0	0	0	0	0	0	0	0	0	0	0	0	0
QNQSPP	0	0	0	0	0	0	0	0	0	0	0	0	0	0	0	0
RECSPP	0	0	0	0	0	0	0	0	1	0	0	0	0	0	0	0
REOARC	20	0	0	0	0	0	0	0	5	6	0	0	3	2	1	0
REOCUR	10	3	0	0	0	0	0	0	0	0	0	0	0	0	0	0
REODIF	0	0	0	0	0	0	0	0	0	0	0	0	0	0	0	0
REOFUS	0	0	0	0	0	0	0	0	0	0	0	0	0	0	0	0
REOSCO	0	0	0	0	0	0	0	0	0	0	0	0	0	0	0	0
REOSPP	13	0	0	0	0	0	0	0	0	0	0	0	0	0	0	0
RHBSPP	0	0	0	0	0	0	0	0	0	0	0	0	0	0	0	0
SACSPH	0	0	0	0	0	0	0	0	0	0	0	0	0	0	0	0
SPRBIF	50	10	0	0	0	0	0	0	20	60	10	20	30	4	0	3
SPRSPP	80	0	0	0	0	0	0	0	1	0	0	0	0	0	0	0
TEXTOR	230	0	0	0	0	0	0	0	1	0	0	0	4	0	0	0
TEXSPP	0	0	0	0	0	0	0	0	0	0	0	0	0	0	0	0
TRIFLU	5	100	80	50	60	30	10	10	2	0	0	0	3	0	10	10
TRLTRI	0	0	0	0	0	0	0	0	0	0	0	0	0	0	0	0
TROGLO	0	0	0	0	0	0	0	0	0	0	0	0	0	0	0	0
TRONIT	0	0	0	0	0	0	0	0	0	0	0	0	0	0	0	0
TROPAC	50	0	0	0	0	0	0	0	0	0	0	0	0	0	0	0
TROSPP	0	3	3	0	3	0	0	0	0	0	0	0	0	0	0	0
UVGPRG	20	450	210	350	180	70	10	4	10	6	10	10	0	10	20	20
UVGSEN	0	0	0	0	0	0	0	0	0	0	0	0	0	0	0	0
UVGSPP	0	0	0	0	0	0	0	0	0	0	0	0	20	0	0	0

Table 11 (continued).

SPECIES \ Sample number and depth interval within core	81-12 TOP (~2cm)	40-42cm	80-82cm	120-122cm	129-132cm	140-142cm	160-162cm	175-177cm	180-183cm	210-212cm	220-222cm	235-237cm	240-242cm	248cm	257-260cm	core catcher
VALCON	0	0	0	0	0	0	0	0	0	0	0	0	0	0	0	0
VALGLA	0	0	0	2	0	0	0	0	0	0	0	0	0	0	2	0
VIRSPP	0	0	0	0	0	0	0	0	0	0	0	0	0	0	0	0
OTHAGG	0	0	0	0	0	0	0	0	0	0	0	3	0	0	1	0
OTHCAL	0	0	7	0	30	10	4	0	4	6	[illegible]	12	10	0	10	3
OTHMIL	0	0	0	0	0	0	1	2	0	0	0	0	3	0	0	0

Table 11 (continued)

REFERENCES

Anderson, G. J., 1963, Distribution patterns of Recent foraminifera of the Bering Sea: Micropaleontology, v. 9, no. 3, p. 305-317.

Carlson, P. R., Karl, H. A., and Quinterno, Paula, 1982, Sedimentologic processes in world's largest submarine canyons, Bering Sea, Alaska: Geological Society of America Abstracts with Programs, v. 14, no. 7, p. 459-460.

Knebel, H. J., Creager, J. S., and Echols, R. J., 1974, Holocene sedimentary framework, east-central Bering Sea continental shelf, in Herman, Y. (ed.), Marine Geology and Oceanography of the Arctic Seas: New York, Springer-Verlag, p. 157-172.

Lisitsyn, A. P., 1966, Recent sedimentation in the Bering Sea (in Russian): Inst. Okeanol. Akad. Nauk, USSR, (translated by Israel Program Sci. Transl., Jerusalem), Washington, D.C., U.S. Department of Commerce: National Science Foundation, 614 p.

Matoba, Yasumochi, 1976, Recent foraminiferal assemblages off Sendai, Northeast Japan, in Schafer, C. T. and Pelletier, B. R., First International Symposium on Benthonic Foraminifera of Continental Margins: Maritime Sediments, Special Publication no. 1, p. 205-220.

Nelson, C. H., Hopkins, D. M., and Scholl, D. W., 1972, Cenozoic sedimentary and tectonic history of the Bering Sea, in Hood, D. W. and Kelley, E. J. (eds.), Oceanography of the Bering Sea: Occasional Publication no. 2, Institute of Marine Science, University of Alaska, Fairbanks, p. 485-516.

Quinterno, P. J., 1981, Preliminary report on benthic foraminifers from Navarin Basin province, Bering Sea, Alaska, in Carlson, P. R. and Karl, H. A. (eds.), Seafloor geologic hazards, sedimentology and bathymetry: Navarin Basin Province, northwestern Bering Sea: U.S. Geological Survey Open-File Report 81-1217, p. 135-149.

Saidova, Kh. M., 1961, Ekologiia foraminifer paleogeografiia dal'nevostochnykh morei (in Russian): Moscow, Academy of Sciences of the Soviet Union, 232 p., 31 plates.

_____ 1967, Depth changes in Bering Sea during the Upper Quaternary, as indicated by benthonic foraminifera, in Hopkins, D. (ed.), The Bering Land Bridge: Stanford University Press, p. 364-368.

Vallier, T. L., Underwood, M. B., Gardner, J. V., and Barron, J. A., 1980, Neogene sedimentation on the outer continental margin, southern Bering Sea: Marine Geology, v. 269-287.

CHAPTER 10: DIATOM ANALYSIS OF SURFACE SAMPLES RECOVERED FROM PERVENETS CANYON

by

Jack G. Baldauf

INTRODUCTION

The Navarin Basin province within the Bering Sea (Fig. 46) is geographically divided into a shallow shelf, steep slope, and a deep marginal basin. Five major submarine canyons (Zhemchug, Pervenets, St. Matthew, Middle, and Navarinsky) occur within this region (Fisher and others, 1982).

Previously, Baldauf (1982) analyzed thirty surface samples from this region and documented the existence of two distinct diatom assemblages separated from each other by the shelf-slope break. The basin-slope assemblage is characterized by the species *Denticulopsis seminae* which typically comprises 20-40 percent of the entire assemblage. Other species within this group include; *Coscinodiscus marginatus*, *Coscinodiscus oculus-iridis*, *Rhizosolenia hebatata* forma *hebatata*, and *Thalassiorsira oestrupii*. Most basin-slope species, although most abundant in the deeper waters, are present on the shelf. For example, *Denticulopsis seminae* composes less than 10 percent of the overall assemblage on the continental shelf compared to 20-40 percent in the basin-slope region.

The shallow water assemblage is dominated by *Nitzschia grunowii* (previously referred to as *Nitzschia oceanica* in Baldauf (1981, 1982)) which composes greater than 20 percent of the shelf assemblage. Additional species in this assemblage include: *Nitzschia cylindrus*, *Thalassiorsira nordenskioldii*, and an increase in abundance of both benthonic and brackish water species.

The presence of these two assemblages within the surface sediment may be useful in determining the effect that secondary processes such as sediment transport or winnowing have on surface sediment within the canyon and slope regions of the Navarin basin province. The very abundant occurrence of shelf species within the surface samples examined from the canyon regions would suggest the erosion and transportation of sediment from the shelf and deposition of these sediments in the canyon.

To examine the usefulness of diatoms for interpreting the effect of sedimentary processes, thirty-three surface samples were examined within the region of Pervenets Canyon (Fig. 47). Pervenets Canyon was selected for this preliminary study due to its relatively small size in comparison to the dimensions of Zhemchug and Navarinsky Canyons. An additional motive for selecting Pervenets Canyon, was the occurrence of *Rhizosolenia curvirostris* and *Thalassiosira nidulus* in sample G-80-66 recovered from within this canyon. The presence of these species suggests that sample G-80-66 has an age greater than 0.26 Ma, the age cited by Donahue (1970) and Schrader (1976) for the last occurrence of *Rhizosolenia curvirostris*.

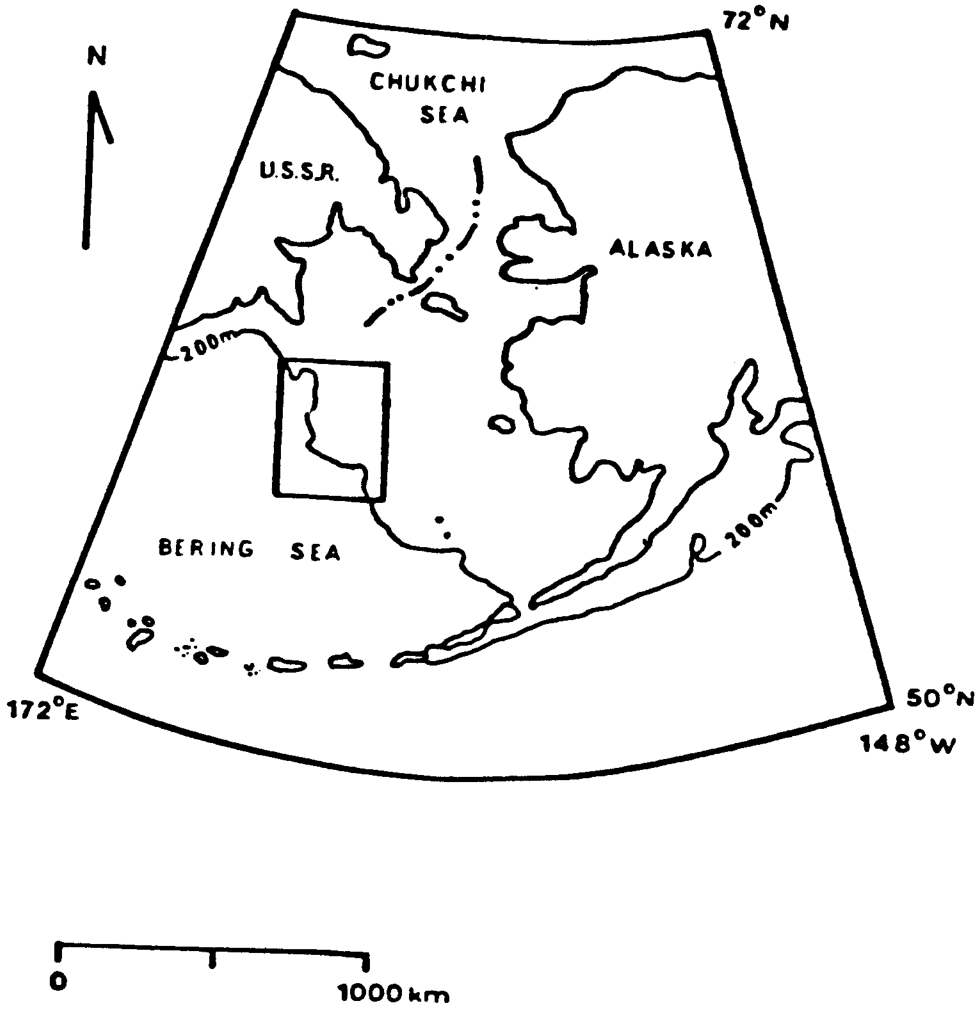

Figure 46. Index map of the Navarin Basin Province, Bering Sea.

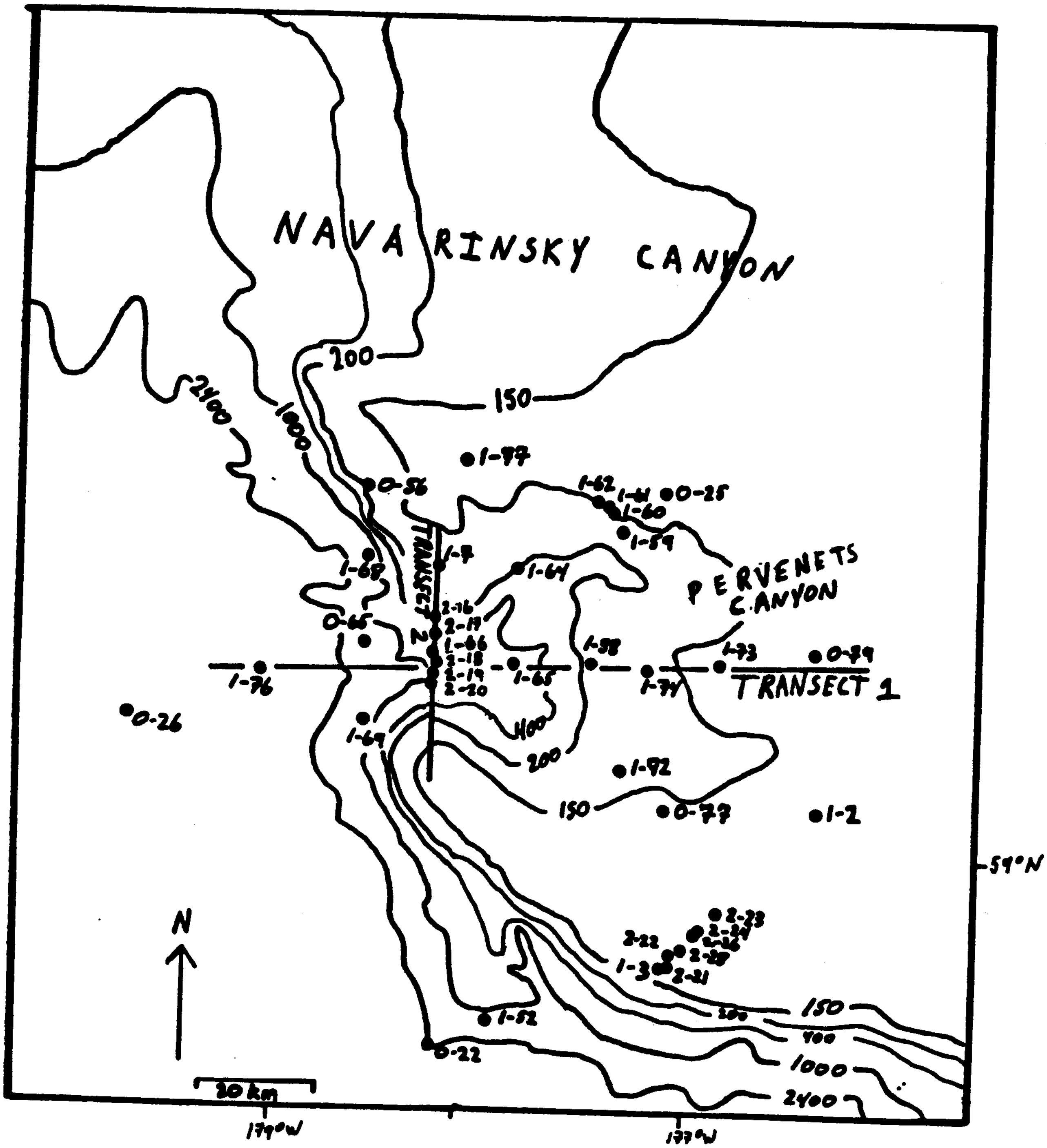

Figure 47. Location of surface samples collecte.i from Pervenets Canyon (0 = 1980; 1 = 81; 2 = 82).

Pervenets Canyon, located within the central portion of the Navarin Basin province, is approximately 125 kilometers long and heads in a water depth of approximately 150 meters. The mouth of this canyon occurs at an approximate water depth of 3000 meters. Pervenets Canyon is approximately 30 kilometers wide at the shelf break, which is narrow when compared to both Zhemchug and Navarinsky Canyons which have an approximate width of 100 kilometers. Two main tributaries which form a right angle at the head of Pervenets Canyon are 80-90 kilometers long and have an approximate gradient of 0.30 degrees.

METHODS AND PROCEDURES

In addition to samples previously examined (Baldauf 1981, 1982), thirty-three surface samples were obtained from cores collected in and around Pervenets Canyon by the NOAA research vessel DISCOVERER during the summers of 1980, 1981, and from the U.S. Geological Survey vessel S.P. LEE during the summer of 1982. Strewn slides of unprocessed sediment were prepared for each sample and examined at 500x for age diagnostic species. Samples of Quaternary age were further examined at 1250x with the first 300 specimens tabulated to determine the abundance of individual species within each sample.

The preservational quality of each sample is based on the presence and absence of delicate forms such as *Thalassiosira hyalina*, *Pseudopodosira elegans*, and *Asteromphalus robustus* and heavily silicified forms such as *Coscinodiscus marginatus*, *Rhizosolenia hebatata* forma *hebatata*, *Stephanopyxis turris*, *Bacteriosira fragilis*, and *Thalassiosira gravida*. The occurrence of both robust and delicate species suggests well preserved samples whereas the presence of only robust forms indicated poorly preserved samples.

RESULTS

With the exception of samples G-82-18, G-82-20 and G-81-66 all samples examined are latest Quaternary in age. Samples G-82-18 and G-82-20 are equivalent in age with previously examined sample G-81-66, based on the presence of *Rhizosolenia curvirostris* and *Thalassiosira nidulus*. The occurrence of these two species suggests that these samples are older than 0.26 Ma. Samples G-81-66, G-82-18, and G-82-20 are located in Pervenets Canyon at a water depth of 580, 625, and 739 meters, respectively (Fig. 47).

Sample G-82-19, which is located between samples G-82-18 and G-82-20 (Fig. 47) at a water depth of 852 meters, is latest Quaternary in age, as it lacks both *Rhizosolenia curvirostris* and *Thalassiosira nidulus*. This suggests that material is swept clean of the canyon walls and deposited on the canyon floor. However, the sediment associated with core G-82-19 also could be derived from the adjacent continental shelf.

A seismic profile perpendicular to the canyon's axis (Figs. 47 and 48) shows surface exposures of stratigraphically older seismic reflectors within the upper canyon walls. A portion of these reflectors occur in proximity of samples G-81-66, G-82-18, and G-82-20 which suggests an age greater than 0.26 Ma for these reflectors. Although exact correlation between these samples and specific seismic reflectors is uncertain, the water depth of each sample

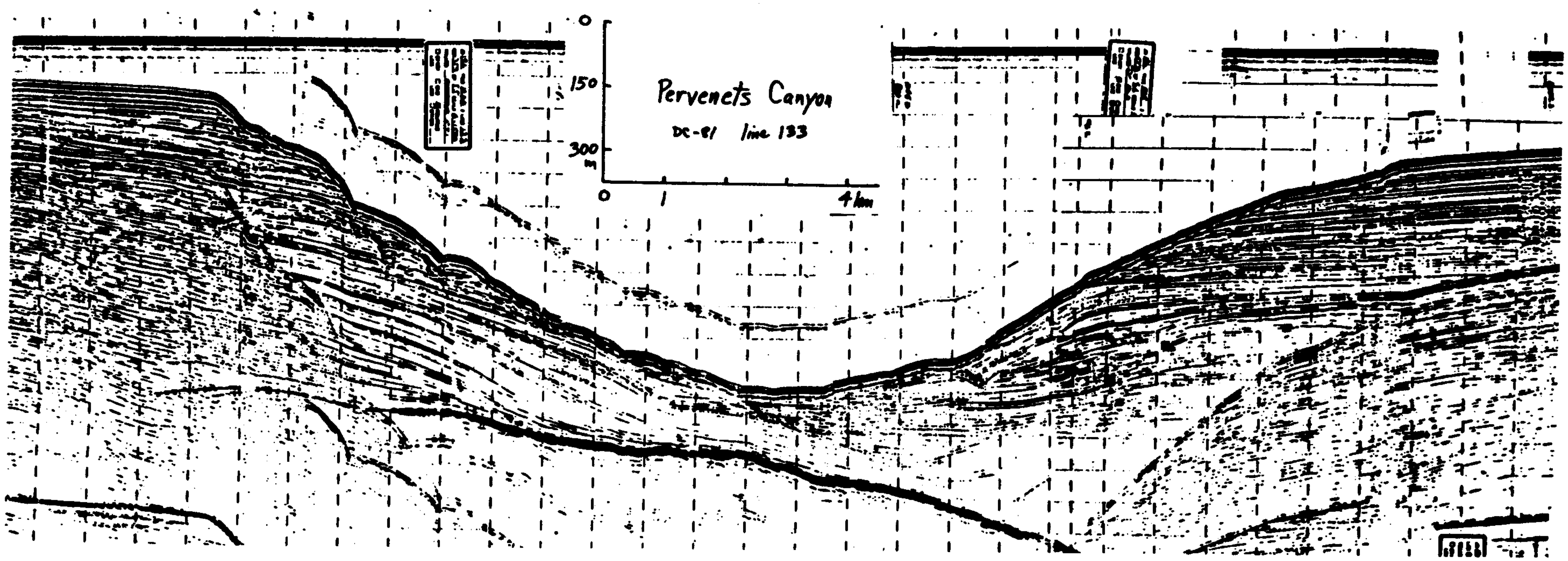

Figure 48. Seismic reflection profile across Pervenets Canyon showing surface exposures of stratigraphically older reflectors. Line 33, DC4-81-BS/NB. See Fig. 47, transect 2 for profile location.

allows approximate correlation and suggests that the reflectors of interest are exposed surficially between the depths of 580-739 meters.

Table 12 shows the occurrence of species encountered during the examination of the latest Quaternary age surface sediment from Pervenets Canyon. The over-all species distribution agrees well with the previous conclusions of Baldauf (1982) in which two assemblages separated by the shelf-slope break were observed. The deeper water assemblage is dominated by Denticulopsis seminae from the shelf, to mid-slope, to lower slope and basin Nitzschia grunowii.

The latest Quaternary samples from the Pervenets Canyon area (Fig. 47) range in water depth from 145 meters to 3230 meters. One major transect from the shelf (sample G-80-79, 128 meters) to the basin (sample G-81-76, 3230 meters; Fig. 47 transect 1) shows an increase in the abundance of Denticulopsis seminae from the shelf, to mid slope, to lower slope and basin (Fig. 49). In sample G-80-65, water depth 1609 meters, D. seminae composes approximately 33 percent of the assemblage. This unusally high concentration of D. seminae is the probable result of either high productivity within a very restricted microenvironment or sediment transport. The abundance of other species within this sample is equivalent to their abundance within nearby samples.

The abundance of Denticulopsis seminae in samples from transect 2 (Figs. 47 and 48) perpendicular to the canyon axis (samples G-82-16,17,19, and G-81-67; Fig. 49) is similar to the above results. D. seminae composes approximately 15-17 percent of the assemblage at a depth between 100-500 meters, and increases in abundance to 23-26 percent of the assemblage at a water depth greater than 500 meters. Although samples G-80-76,77 are exceptions to this trend for presently unknown reasons, the conformity of all other samples to this trend suggest that depth either directly or as a secondary factor is responsible for the distribution of D. seminae within the Navarin Basin province.

To determine the abundance of shelf species in the surface sediments of Pervenets Canyon, the same samples used in the transects for determining the distribution of Denticulopsis seminae, were also used to compare the abundance of the shelf species Nitzschia grunowii.

The abundance of Nitzschia grunowii within surface samples from Pervenets Canyon (Fig. 50) shows more irregularities than that observed in the distribution pattern of Denticulopsis seminae. As a general trend, Nitzschia grunowii increases in abundance as one proceeds from the slope region to the inner shelf (see Baldauf, 1982).

The abundance of Nitzschia grunowii within Pervenets Canyon, however, disagrees with this pattern. N. grunowii in most samples within the canyon between the depths of 150-2400 meters constitutes approximately 10-17 percent of the entire assemblage. No trend in abundance vs. depth is observed. Furthermore, in sample G-80-26, Nitzschia grunowii composes 19 percent of the assemblage which is equivalent elsewhere in the Navarin Basin to its abundance within water depths of less than 125 meters.

Table 12. Abundance (in percent) of species encountered during the examination of surface sediments from the Pervenets Canyon region

SPECIES \ SAMPLE	80-04	80-12	80-13	80-22	80-25	80-26	80-28	80-30	80-35	80-36	80-50	80-51	80-52	80-56	80-65	80-77	80-79	80-81	80-83	80-84	80-89
Actinocyclus curvatulus	-	-	0.3	-	0.6	-	-	-	-	-	-	-	0.6	1.0	-	-	-	-	-	0.6	0.3
A. divisus	0.6	0.6	0.3	0.3	1.6	0.3	2.6	0.3	1.0	0.6	1.0	1.0	0.3	1.6	-	0.6	0.6	2.0	2.3	2.3	1.0
A. ochotensis	-	-	-	1.0	-	-	-	0.6	0.6	-	-	-	1.0	1.6	-	-	-	-	-	1.0	1.0
Actinoptychus undulatus	-	-	-	-	0.6	-	0.3	-	-	-	0.6	-	-	-	0.3	-	0.3	0.3	0.6	-	-
A. vulgaris	-	0.3	-	-	-	-	-	-	-	0.3	-	-	-	-	-	-	-	-	-	-	-
Asteromphalus robustus	-	0.6	-	-	-	-	-	-	0.6	-	-	-	-	-	-	-	-	-	-	-	-
Bacteriosira fragilis	6.0	6.6	2.6	3.0	4.3	4.3	7.3	7.3	3.3	6.0	9.3	9.0	10.6	7.0	3.0	7.6	7.0	7.3	6.0	5.3	3.0
Biddulphia aurita	3.0	1.6	2.6	1.0	1.0	2.0	1.0	1.6	2.3	1.3	2.0	1.3	1.6	1.3	0.3	1.3	0.6	1.0	1.6	2.3	2.3
Coscinodiscus lacustris	-	-	-	0.3	-	-	-	0.3	-	-	0.6	-	-	-	-	-	0.3	0.3	-	-	-
C. marginatus	0.6	2.0	0.3	0.6	-	1.6	1.0	0.3	1.3	0.3	-	0.3	1.6	1.3	2.3	0.3	2.0	1.0	1.3	1.3	1.6
C. oculis-iridis	1.0	1.3	1.3	0.3	-	1.3	0.6	0.3	1.3	1.3	0.6	1.6	0.6	0.3	2.6	-	0.6	0.6	0.3	1.6	2.0
C. radiatus	-	-	-	-	-	-	-	-	-	-	-	-	-	-	-	-	-	-	-	-	-
C. stelaris	-	-	-	-	-	-	-	-	-	-	-	-	-	-	-	-	-	-	-	0.3	0.3
C. tabularis	0.3	0.3	-	-	-	0.6	-	-	0.3	-	0.3	0.6	0.3	-	-	-	-	-	-	-	0.6
Denticulopsis seminae	28.0	27.0	31.3	38.3	4.0	26.0	7.3	3.0	17.0	29.0	7.0	6.3	6.0	14.3	33.0	27.6	10.0	10.6	13.0	11,3	37.0
Melosira "GROUP"	1.0	1.0	0.6	1.0	9.3	1.0	2.6	5.3	4.0	2.6	3.6	5.3	4.0	4.6	1.6	2.3	5.3	11.6	-	9.0	2.3
Navicula sp. 1.	0.3	0.3	-	0.3	2.0	0.6	5.0	4.3	1.6	0.6	3.3	2.6	2.3	0.3	1.0	0.3	1.6	2.3	0.3	1.3	0.3
Navicula sp. 2.	-	0.3	0.3	0.3	1.0	-	0.6	-	1.3	1.6	0.6	1.3	0.6	0.6	0.6	-	0.6	-	0.3	1.0	0.6
Navicula sp. 3.	0.3	0.3	-	-	-	-	-	-	0.6	0.3	0.3	0.3	1.0	0.3	-	-	0.3	1.0	1.0	-	0.3
Nitzschia cylindrus	4.0	3.0	3.6	3.1	9.0	5.6	10.6	13.6	10.0	7.0	9.0	10.3	10.6	8.3	7.3	6.6	9.3	6.0	6.6	7.6	1.0
N. grunowii	16.3	10.6	9.6	11.0	26.3	19.0	19.3	36.0	18.6	15.0	25.6	24.3	20.6	20.3	11.3	16.6	16.6	17.6	15.3	9.0	5.6
Pleurosigma sp.	-	-	-	0.3	-	-	0.6	-	-	0.3	-	0.3	-	-	-	-	0.6	-	0.3	-	-
Porosira glacialis	1.0	2.0	1.3	1.6	2.3	3.0	4.6	2.6	3.6	3.6	2.0	1.3	6.0	3.3	4.0	1.3	3.3	1.3	3.3	4.0	2.6
Pseudopodosira elegans	1.3	3.0	-	1.3	1.3	0.6	0.6	-	0.6	-	-	1.0	-	2.6	-	2.0	1.0	0.6	0.3	1.0	-
Rhaphoneis sachalinensis	-	-	-	0.3	0.6	-	-	-	1.0	0.3	-	0.3	-	-	0.3	0.3	1.3	0.3	0.6	-	-
R. surirella	-	0.3	-	-	1.3	-	-	1.3	2.3	-	0.6	-	0.3	-	0.3	-	-	-	-	2.0	-
Rhizosolenia hebatata	2.6	3.0	4.6	3.0	1.6	3.3	1.6	0.3	2.0	1.6	0.3	1.6	2.6	2.3	2.3	2.3	3.0	2.0	0.3	1.3	2.3
R. styliformis	1.3	2.3	-	1.0	0.3	-	-	0.6	0.3	0.3	0.3	1.3	1.6	0.6	2.6	1.6	1.3	0.3	1.3	2.3	2.0
Stephanopyxis turris	-	-	-	-	-	0.6	-	-	0.3	-	-	-	-	-	0.3	-	-	-	-	-	-
Thalassionema nitzschoides	-	-	1.6	1.0	3.6	0.3	2.0	2.6	2.6	1.0	1.3	0.6	3.0	2.6	2.0	0.6	1.6	-	2.6	4.6	4.0
Thalassiosira decipiens	2.3	3.3	2.0	2.0	1.3	2.6	2.6	1.6	2.6	1.0	3.3	2.3	2.6	3.3	2.0	3.3	4.3	2.3	3.3	3.6	1.6
T. eccentrica	-	-	-	-	-	-	-	-	-	-	-	-	-	-	-	-	-	-	-	-	-
T. gravida	7.3	6.6	2.3	3.0	3.6	2.3	4.6	8.6	1.6	4.3	10.0	12.3	3.0	2.6	2.6	5.6	6.3	10.0	7.0	1.0	2.3
T. hyalina	10.0	8.0	11.0	5.6	5.6	7.6	8.6	0.6	6.6	5.0	7.0	5.0	5.0	6.0	5.3	3.0	5.3	5.0	3.6	4.0	6.3
T. leptopus	1.0	-	0.3	-	0.6	-	0.3	0.3	0.3	-	0.3	1.0	0.6	0.3	-	-	-	0.3	-	0.3	-
T. nordenskioldii	3.0	-	6.0	5.6	3.6	4.6	8.0	4.6	1.6	6.3	4.0	3.6	5.3	4.3	4.0	6.0	4.6	4.6	1.6	5.3	4.0
T. oestrupii	-	1.3	2.0	2.0	-	1.3	2.0	-	2.6	2.6	-	1.0	-	2.6	0.3	2.0	2.0	1.3	2.3	2.6	1.0
T. trifulta	6.6	8.3	10.0	7.3	4.6	10.3	3.3	2.0	5.3	6.0	3.3	2.3	3.0	3.3	5.3	7.3	6.6	5.6	6.0	8.3	10.3
T. undulosa	-	1.6	1.0	1.6	0.6	1.6	-	-	0.6	1.3	0.6	0.6	1.0	1.6	1.3	0.6	1.3	0.3	-	0.6	0.3
Thalassiothrix longissima	1.0	0.6	3.0	1.6	1.0	1.6	1.0	0.6	1.6	0.3	0.3	-	0.6	1.0	0.3	-	-	-	1.0	0.6	1.3
Xathiopyxis ovalis	0.6	0.3	0.3	0.6	-	0.3	-	-	-	0.3	-	-	-	-	0.6	0.6	-	-	-	-	0.6
FRESH WATER SPECIES	-	-	-	-	-	-	-	-	-	-	-	-	-	-	-	-	-	-	0.3	-	-

Table 12. cont'd

SAMPLE / SPECIES	80-94	80-96	80-98	80100	80101	80105	80-10	80110	80112	81-3	81-2	81-7	81-51	81-58	81-59	81-60	81-61	81-62	81-64	81-65	81-68	81-69
Actinocyclus curvatulus	-	1.0	0.3	-	0.6	0.6	-	-	-	-	-	-	0.3	-	-	-	-	-	-	-	-	-
A. divisus	0.6	0.6	-	1.0	1.0	1.0	3.0	2.0	2.3	-	-	-	0.6	-	0.3	0.6	-	-	-	-	0.3	-
A. ochotensis	0.6	2.0	0.3	-	1.0	1.0	-	0.6	0.6	0.6	-	0.6	-	-	0.3	1.3	-	0.3	-	-	0.6	-
Actinoptychus undulatus	0.6	1.0	-	-	-	0.3	-	-	-	-	-	-	-	-	-	-	-	-	-	-	-	-
A. vulgaris	-	-	-	-	-	-	-	-	-	-	-	-	0.3	-	-	0.3	-	-	0.3	0.3	-	-
Asteromphalus robustus	-	-	-	0.6	-	-	-	-	-	0.3	-	-	-	0.3	-	-	-	-	-	-	-	0.3
Bacteriosira fragilis	7.0	6.0	4.3	4.3	3.6	4.6	4.3	6.6	5.6	4.3	8.0	6.6	1.3	5.0	6.0	5.0	4.6	7.3	5.6	2.3	3.6	5.0
Biddulphia aurita	1.3	1.3	1.0	0.3	2.3	2.0	1.6	3.3	0.6	2.0	2.3	0.6	1.6	2.3	2.0	1.0	1.6	0.3	2.3	3.3	1.0	0.6
Coscinodiscus lacustris	-	-	-	-	-	0.3	-	-	0.3	-	0.3	0.3	-	-	0.6	0.3	0.6	-	-	1.0	-	-
C. marginatus	0.3	0.6	1.3	1.6	0.6	0.6	1.6	-	1.0	2.0	0.3	1.3	0.3	-	0.3	2.6	1.0	-	1.3	0.3	2.3	1.3
C. oculus-iridis	1.0	1.0	1.0	0.6	1.3	1.3	1.3	0.6	0.6	1.0	-	1.0	-	1.3	-	0.6	-	-	0.3	2.6	2.0	-
C. radiatus	-	-	-	-	-	-	-	-	-	-	0.6	-	-	-	-	1.0	-	-	-	-	-	-
C. stellaris	-	-	-	-	-	-	-	-	-	-	-	-	-	0.3	0.3	-	-	-	-	-	-	0.3
C. tabularis	-	-	0.3	1.3	-	1.0	-	-	0.3	-	-	-	0.3	0.6	-	-	-	0.3	1.0	-	-	1.3
Denticulopsis seminae	9.6	10.3	17.6	28.0	24.0	22.3	33.3	15.0	14.6	11.3	17.6	17.6	40.6	15.7	6.6	14.0	9.6	9.6	14.0	16.3	24.3	24.0
Melosira GROUP	12.0	6.0	4.6	2.0	2.6	7.0	1.0	4.0	10.3	2.3	5.3	2.0	0.3	5.5	4.0	3.3	3.6	3.6	3.6	1.0	1.3	2.0
Navicula sp. 1.	1.0	3.0	1.6	1.0	0.3	2.0	-	-	-	4.3	0.3	1.3	0.6	-	1.3	1.0	0.3	2.0	1.3	2.0	1.0	0.3
Navicula sp. 2.	0.3	-	1.3	-	-	-	-	-	-	0.6	-	-	-	1.3	-	-	1.0	0.3	-	0.3	0.3	-
Navicula sp. 3.	-	0.3	0.3	-	-	0.3	-	-	-	0.3	0.3	0.6	-	0.3	-	0.6	0.3	-	1.3	-	0.3	0.6
Nitzschia cylindrus	8.0	9.6	9.3	3.0	3.0	6.6	4.6	5.6	4.3	5.6	4.3	9.0	1.3	6.0	9.3	4.3	9.6	8.0	6.0	9.0	6.6	4.0
N. grunowii	21.0	15.6	17.6	13.0	11.0	13.0	7.0	21.0	21.6	8.2	12.0	12.3	6.6	11.0	17.3	16.0	16.6	14.6	16.3	16.6	8.6	13.6
Pleurosigma sp.	-	-	-	0.3	-	-	-	-	-	0.6	-	-	-	-	-	-	-	0.6	-	-	-	-
Podosira glacialis	4.0	3.3	3.6	2.0	2.6	1.6	4.0	1.6	2.0	2.0	5.0	1.6	2.6	1.3	1.3	3.3	1.7	1.0	1.0	1.6	1.0	-
Pseudopodosira elegans	2.6	-	-	1.0	1.6	0.6	0.6	1.0	0.6	1.6	1.0	1.0	1.0	0.3	1.0	0.6	0.3	2.0	0.6	0.6	0.6	0.6
Rhaphoneis sachalinensis	0.3	0.3	-	-	-	-	-	-	-	0.3	-	0.6	-	0.3	1.3	0.3	-	1.3	-	-	0.3	1.0
Rh. surirella	2.0	1.3	2.0	-	0.3	0.6	-	-	1.6	-	0.3	-	-	-	-	0.6	-	-	-	-	-	-
Rhizosolenia hebatata	2.3	0.6	2.3	2.6	5.3	1.3	3.0	1.3	2.3	4.6	3.6	1.6	7.3	1.6	1.0	5.0	1.3	3.6	2.3	1.0	2.0	2.0
R. styliformis	1.6	0.6	2.0	3.3	1.6	2.0	0.6	0.6	0.3	-	0.6	-	0.3	0.3	-	0.3	-	-	-	-	-	-
Stephanopyxis turris	-	-	-	-	0.3	-	-	-	-	-	-	-	-	-	-	-	-	-	-	-	-	-
Thalassionema nitzschoides	2.3	4.0	3.0	0.6	3.0	3.3	1.6	0.6	4.0	8.3	2.6	7.3	4.3	6.6	10.0	4.6	7.6	8.3	7.6	10.3	7.6	6.0
Thalassiosira decipiens	1.3	2.6	3.0	3.0	1.0	2.3	1.2	2.3	2.3	1.0	0.6	-	-	1.6	3.3	0.3	2.3	0.6	1.0	1.0	0.6	-
T. eccentrica	-	-	-	-	-	-	-	-	-	3.0	2.6	0.6	1.0	1.6	3.0	-	1.0	3.0	1.6	0.6	1.6	4.3
T. gravida	3.6	4.3	1.3	2.6	4.0	3.3	4.3	5.3	3.0	3.0	12.0	11.6	5.6	8.2	3.0	12.6	8.0	7.6	5.6	3.6	7.3	6.6
T. hyalina	2.6	4.0	7.6	7.6	5.3	7.0	7.3	4.6	6.0	9.0	3.0	4.6	4.3	5.3	9.6	4.0	6.6	5.0	5.0	6.0	9.3	5.3
T. leptopus	0.3	-	0.3	0.3	-	0.6	0.6	-	-	0.3	1.0	0.6	0.3	-	0.3	-	-	0.6	0.3	-	0.3	-
T. nordenskioldii	3.0	5.6	1.6	6.6	6.0	4.3	3.6	3.3	5.6	9.4	6.6	2.3	2.6	6.3	8.0	6.0	6.3	5.0	6.6	8.0	5.0	5.3
T. oestrupii	1.0	1.6	0.6	1.0	0.3	1.3	2.6	0.6	0.6	-	-	0.3	0.3	0.6	-	0.6	-	1.0	1.0	0.3	0.6	1.3
T. trifulta	5.0	6.0	6.0	7.3	17.0	6.3	8.3	2.6	4.3	3.3	4.3	5.0	5.0	7.3	2.3	3.3	2.3	5.0	3.6	4.0	6.6	4.0
T. undulosa	0.6	1.3	0.6	0.6	0.3	1.6	1.6	0.6	1.3	2.3	-	2.3	-	3.0	1.0	3.0	2.3	1.3	-	2.3	2.3	3.3
Thalassiothrix longissima	1.0	1.0	0.6	1.6	0.6	1.3	1.0	0.3	0.6	1.0	0.6	1.0	-	2.0	1.3	1.3	2.3	2.0	2.3	0.3	1.6	-
Xanthiopyxis ovalis	-	-	-	0.3	0.6	0.3	1.0	0.3	0.3	-	-	-	0.3	0.3	-	0.3	-	-	0.3	0.6	-	0.3
FRESH WATER SPECIES	-	-	-	-	-	-	-	-	-	0.6	0.3	-	-	-	0.3	-	0.3	-	0.3	-	-	-

535

Table 12. cont'd

SAMPLE / SPECIES	81-72	81-73	81-74	81-76	81-77	82-16	82-19	82-21	82-22	82-23	82-24	82-26	82-28
Actinocyclus curvatulus	-	-	-	-	-	-	-	-	-	-	-	-	-
A. divisus	0.3	-	-	-	-	0.3	-	0.6	-	1.0	1.0	1.3	0.6
A. octanerus	-	-	0.3	-	-	-	-	-	0.3	-	0.3	-	-
Actinoptychus undulatus	-	-	-	-	-	0.6	-	0.3	-	-	-	0.3	0.3
A. vulgaris	-	-	-	-	-	0.3	0.3	-	-	-	0.3	-	0.3
Asteromphalus robustus	-	-	-	-	0.6	0.3	0.3	0.3	-	0.3	0.6	-	-
Bacteriosira fragilis	5.0	9.6	5.0	6.0	5.0	2.3	2.0	2.6	4.3	7.3	5.0	5.3	4.6
Biddulphia aurita	1.3	1.3	2.0	0.6	1.0	3.0	1.0	1.6	3.0	1.6	0.6	2.3	1.0
Coscinodiscus lacustris	-	-	-	-	-	0.3	1.0	0.3	0.3	0.3	-	--	0.6
C. marginatus	0.6	1.0	2.3	-	1.3	2.6	2.3	2.0	2.3	2.3	2.6	1.0	2.0
C. oculus-iridis	0.3	0.3	1.0	-	-	1.0	--	1.6	1.3	0.3	2.0	0.6	1.0
C. radiatus	0.6	-	-	-	-	0.6	-	1.6	0.3	0.6	-	0.3	-
C. stellaris	-	-	0.3	0.3	0.3	-	-	-	-	-	-	-	0.3
C. tabularis	-	-	-	-	0.3	-	0.3	0.3	0.3	-	0.3	-	0.3
Denticulopsis seminae	9.3	12.4	14.3	22.3	14.0	23.3	26.3	18.6	20.6	13.3	18.3	23.3	20.3
Melosira "GROUP"	2.0	3.6	1.6	1.3	3.3	2.0	2.6	2.3	2.6	2.3	3.6	3.0	2.3
Navicula sp. 1.	0.3	1.3	2.3	0.6	0.6	1.3	1.0	-	-	1.6	0.3	0.6	-
Navicula sp. 2.	-	-	0.3	1.0	0.3	0.6	0.6	-	-	-	-	-	0.3
Navicula sp. 3.	-	0.3	0.6	-	0.3	1.0	-	0.3	-	-	-	-	0.3
Nitzschia cylindrus	5.0	8.3	5.0	5.6	6.3	2.3	3.0	4.0	5.0	3.6	7.6	4.3	3.6
N. grunowii	6.3	17.3	14.0	15.6	17.0	10.3	10.0	16.6	16.6	10.6	18.0	15.6	15.3
Pleurosigma sp.	0.3	-	-	-	-	0.6	-	-	-	-	-	-	-
Podosira glacialis	3.0	0.6	1.3	-	1.3	1.6	2.0	2.6	1.3	3.0	2.6	1.0	1.3
Pseudopodosira elegans	-	0.6	0.6	0.3	1.3	1.3	2.6	-	-	-	0.3	0.3	1.0
Rhaphoneis sachalinensis	-	0.3	0.3	0.3	0.6	0.3	1.0	1.3	1.0	0.3	-	-	-
R. surirella	0.3	0.6	0.6	-	-	0.6	1.3	-	0.3	0.3	-	0.3	0.3
Rhizosolenia hebatata	-	2.6	2.3	1.3	1.3	1.6	3.3	4.3	4.6	3.6	2.3	5.3	3.0
R. styliformis	1.3	-	-	-	0.3	-	-	-	0.3	-	-	-	0.3
Stephanopyxis turris	-	-	-	-	-	-	-	0.3	-	-	-	-	-
Thalassionema nitzschoides	2.6	5.6	8.0	10.6	13.0	3.0	5.0	4.3	4.0	4.3	4.0	5.3	6.0
Thalassiosira decipians	1.0	0.6	0.3	1.0	0.3	0.6	1.6	-	1.0	0.6	1.3	0.3	1.3
T. eccentrica	-	0.3	2.0	0.6	1.3	3.3	3.0	1.0	-	1.0	0.3	1.6	2.6
T. gravida	9.6	7.0	9.3	2.6	6.0	7.6	6.0	9.6	8.6	10.0	5.6	7.3	9.0
T. hyalina	5.0	3.6	5.3	6.0	2.6	5.6	4.0	4.0	3.6	4.6	5.0	3.3	7.6
T. leptopus	0.3	-	-	1.0	-	0.6	0.3	0.3	-	0.6	-	0.3	0.6
T. nordenskioldii	7.0	6.6	6.0	6.6	5.6	4.3	6.0	5.0	4.0	4.6	3.6	3.0	3.3
T. oestrupii	1.0	0.6	0.3	0.3	0.6	0.6	1.3	1.0	0.6	0.6	0.3	1.0	0.6
T. trifulta	5.0	6.3	6.0	4.0	4.6	7.6	6.6	4.6	6.6	7.3	4.0	4.3	3.0
T. undulosa	2.0	3.8	2.0	0.6	2.3	2.3	1.6	3.0	3.3	5.0	3.0	1.6	2.6
Thalassiothrix longissima	1.0	1.0	1.0	1.6	1.3	1.3	2.0	0.6	1.0	1.3	1.0	1.3	0.6
Xanthiopyxis ovalis	0.6	-	0.3	-	-	-	-	0.6	-	-	-	-	0.3
FRESH WATER SPECIES	0.3	1.0	-	-	-	-	-	-	-	-	-	-	-

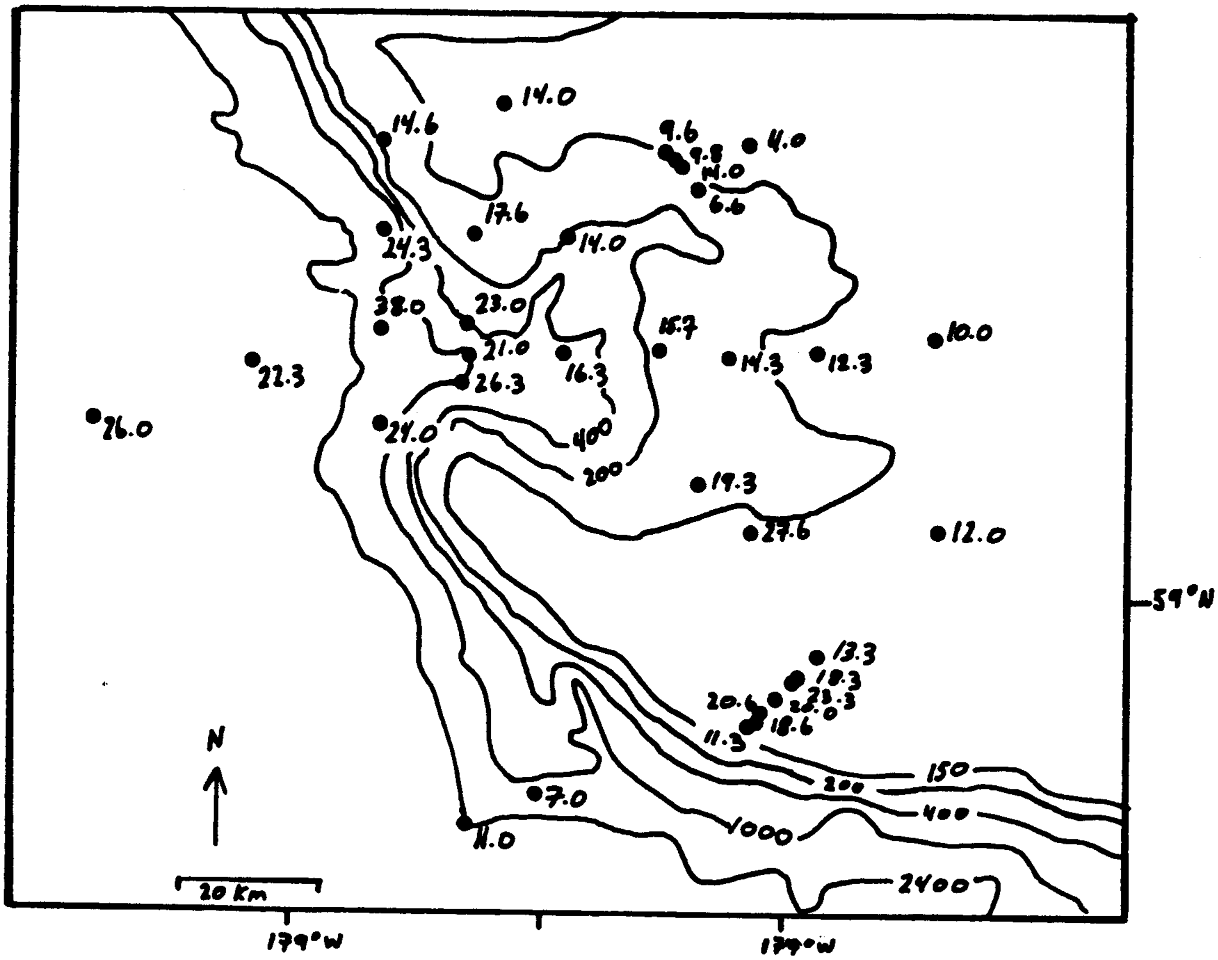

Figure 49. Distribution of Denticulopsis seminae in the surface sediments (values are in percent).

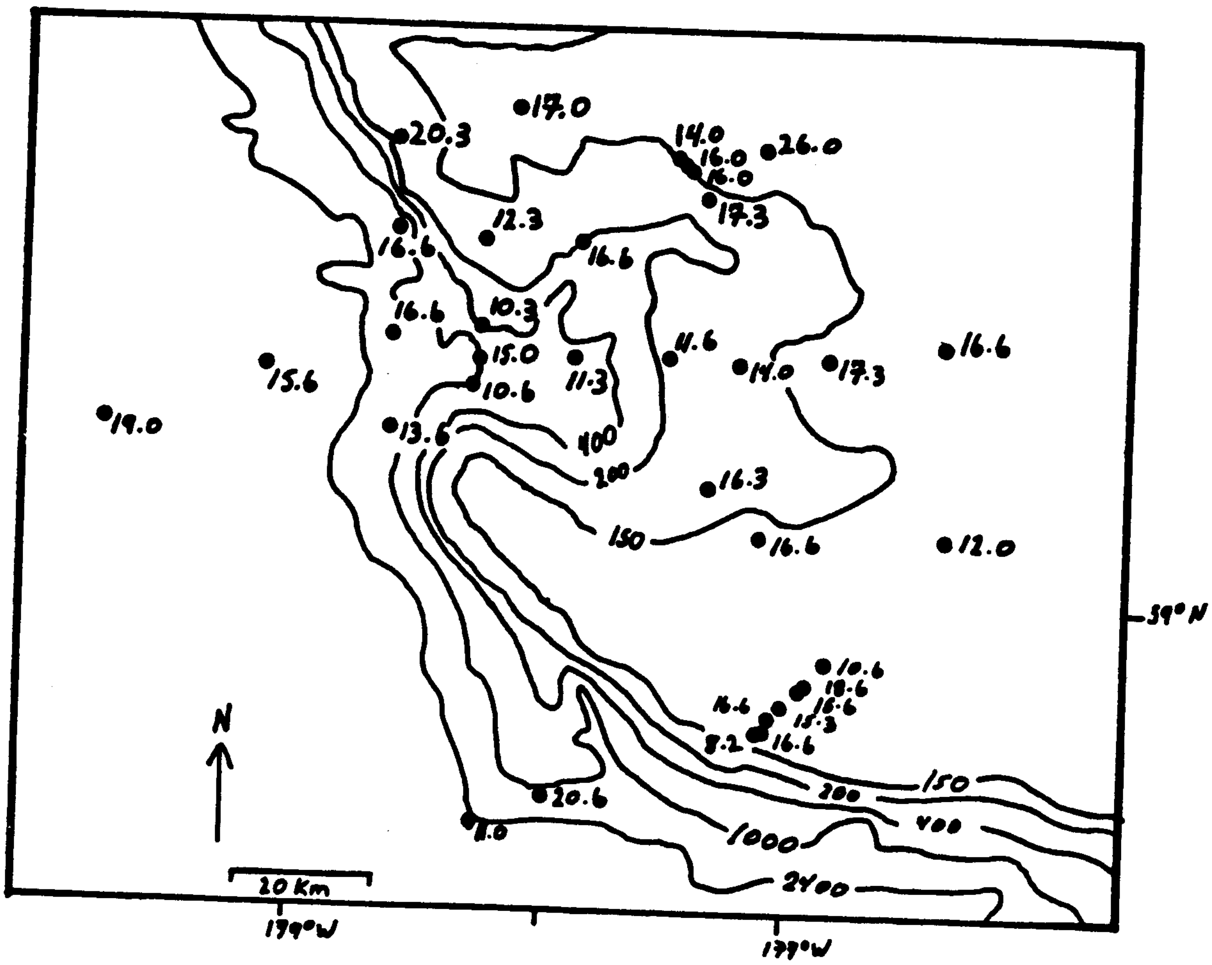

Figure 50. Distribution of Nitzschia grunowii in the surface sediment (values are in percent).

The difference in abundance patterns of N. grunowii between samples within Pervenets Canyon and elsewhere within the Navarin Basin (see Baldauf, 1982) suggests that sediments within the canyon may be under the influence of post depositional processes of which sediment transport of shelf sediments in to the canyon may be a primary factor.

However, further studies are required to determine all factors which influence this process as well as to examine in detail additional distribution patterns of species not only restricted to shelf environments but also to the slope and basin regions as well.

REFERENCES

Baldauf, J. G., 1981, Diatom analysis of late Quaternary sediments from the Navarin Basin Province, Bering Sea. In Carlson, P. R. and Karl, H. A. (eds.), Seafloor geologic hazards, Sedimentology, and Bathymetry: Navarin Basin Province, Northwestern Bering Sea. U.S. Geological Survey Open-File Report 82-1217, p. 100-113.

Baldauf, J. G., 1982, Identification of the Holocene-Pleistocene Boundary in the Bering Sea by diatoms. Boreas, volume 11, p. 113-118.

Donahue, J. G., 1970, Pleistocene diatoms as climatic indicators in North Pacific sediments. Geological Society of America Memoir 126, p. 121-138.

Fischer, J. M., Carlson, P. R., and Karl, H. A., 1982, Bathymetric map of Navarin Basin province, northern Bering Sea; U.S. Geological Survey Open-File Report 82-1038, 11 p., 1 map, scale 1:1,000,000.

Schrader, H. J., 1973, Cenozoic diatoms from the Northeastern Pacific, Leg 18. In Kulm, D., von Huene, R., et al., Initial Reports of the Deep Sea Drilling Project, Volume 18, Washington (U.S. Government Printing Office), p. 673-797.

CHAPTER 11: ASPARTIC ACID GEOCHRONOLOGY OF MOLLUSKS

by

David J. Blunt and Keith A. Kvenvolden
U.S. Geological Survey, Menlo Park, CA 94025

This report considers relative and absolute ages of fossil mollusks from the Navarin Basin Province, Bering Sea, as estimated by the method of amino-acid geochronology. Blunt and Kvenvolden (1981) first reported leucine geochronology of fossil mollusks from the Navarin Basin province (Fig. 51). In the present study, aspartic acid is used for the purpose of establishing the age of fossil mollusks.

THEORY

Individual amino acids that are no longer being biologically reproduced in the protein of shell matrix undergo a stereochemical change from the L-enantiomeric to a mixture of the L- and D-enantiomeric configurations during natural hydrolysis. The process of interconversion of enantiomers is called racemization and takes place over geologic time. The kinetics of racemization can be expressed as a reversible first-order reaction:

$$\text{L-aspartic acid} \underset{k_D}{\overset{k_L}{\rightleftharpoons}} \text{D-aspartic acid}$$

where k_L and k_D are the respective reaction rate constants for the L- and D-aspartic acid enantiomers. The integrated rate expression for the racemization reaction as derived by Bada and Schroeder (1972) is:

$$\ln\left(\frac{1 + D/L}{1 - D/L}\right) - \ln\left(\frac{1 + D/L}{1 - D/L}\right)_{t\,=\,o} = 2\,kt \quad (1)$$

where k is the racemization rate constant, D/L is the ratio of D- and L-aspartic acid enantiomers, and t is time. The logarithmic term at t = o is evaluated by measuring the D/L value obtained from modern specimens. Aspartic acid has a D/L value of about 0.06 in modern mollusks (Kvenvolden and others, 1980; Blunt, unpublished data).

RESULTS

Fossil mollusks recovered from the Bering Sea have been analyzed for aspartic acid D/L values by the method of Kvenvolden and others (1979). Further characterization of the amino acid content in some of the molluscs is reported by Blunt and Kvenvolden (1981). Twenty-four specimens from ten genera of Mollusca (nine pelecypods and one gastropod, Neptunea) are reported in Table 13. These specimens occur within the top two meters of the sedimentary column. The aspartic acid values range from 0.06 in Panomya (DC-5-80, G-71) to 0.43 in Neptunea (DC-5-80, G-98). Radiocarbon analyses of organic

Table 13.--Summary of aspartic acid D/L values in mollusks from the Navarin Basin province

Specimen[1]	Cruise[2]	Station	Core No.[3]	Depth (cm)	D/L	Age	14C	Comment[5]
Macoma sp.	DC-4-80	3	G-6	10	0.07			
Macoma sp.	DC-3-81	58	G-62	18	0.07			
Macoma sp.	DC-5-80	47	G-59	13-14	0.08			
Macoma calcarea	DC-3-81	95	G-105	100	0.14		8,385 ± 310	160-190 cm
Macoma sp.	DC-2-81	28	G-31	38-39	0.14		8,815 ± 355	160-190 cm
Macoma brota	DC-5-80	49	G-62	214-220	0.21			
Macoma cf. M. obliqua	DC-5-80	34	G-44	203	0.23		14,980 ± 110	125-145 cm
Nuculana fossa	DC-2-81	22	G-24	205	0.23			
Nuculana radiata	DC-5-80	39	G-50	219-230	0.23			
Nuculana fossa	DC-5-80	34	G-44	125	0.24	*	14,980 ± 110	125-145 cm
Nuculana fossa	DC-5-80	32	G-42	170	0.30	*	13,650 ± 100	170-183 cm
Nuculana radiata	DC-5-80	20	G-26	223-230	0.30	22,000	10,880 ± 80 to	188-222 cm
							33,900 ± 610	235-260 cm
Neptunea sp.	DC-3-81	76	G-80	164	0.26	21,000		
Neptunea neptunea	S-4-76	-	G-116	90-98	0.33	*	29,197 ± 320	90-98 cm on shell[6]
Neptunea sp.	DC-5-80	79	G-98	140	0.43	41,000		
Yoldia myalis	DC-3-81	71	V.V.-75	0-2	0.07			
Yoldia myalis	DC-5-80	20	G-26	223-230	0.23 ± .01	14,000	10,880 ± 80 to	188-222 cm
							33,990 ± 610	235-260 cm
Yoldia myalis	DC-5-80	53	G-66	60	0.30	*	19,370 ± 160	65-84 cm
Clinocarium sp.	DC-2-81	29	G-32	220	0.20	*	7,500 ± 305	160-190 cm
Clinocardium nuttallii	DC-5-80	32	G-42	97	0.21	8,000	13,650 ± 100	170-103 cm
Cyclocardia crebricostata	DC-5-80	21	G-28	8	0.10			
Mya truncata	DC-5-80	19	G-25	173	0.21			
Serripes groenlandicus	DC-2-81	36	BC-41	0-2	0.08			
Panomya sp.	DC-5-80	60	G-71	1-6	0.06			

[1] **Fossil mollusks are identified by L. Marincovich, USGS, Menlo Park**

[2] DC, NOAA Research Vessel DISCOVERER; S, USGS Research Vessel SEA SOUNDER

[3] G, gravity core; V V., Van Veen sampler; B.C., box core

[4] ASP, D-aspartic acid/L-aspartic acid

[5] **Depths of radiocarbon analysis differs from depths of mollusk occurrence**

[6] Sample from southern Bering Sea, radiocarbon analysis on shell carbonate (Jim Gardner, personal communication)

* Sample used for determination of calibrated rate constant for amino acid dating

carbon in the bulk sediments range from 7,500 to 33,990 years.

DISCUSSION

Relative Age

Relative ages for the same genera of mollusks are inferred by the order of extent of aspartic acid racemization (column 6, Table 13). Older fossils have progressively larger D/L values. For example, *Macoma* of DC-4-80 G-6 has an aspartic acid D/L value of 0.07 at 10 cm depth, whereas, *Macoma* of DC-5-80 G-44 has an aspartic acid D/L value of 0.23 at 203 cm depth. *Yoldia* from DC-3-81 V.V.-75 and DC-5-80 G-66 has aspartic acid D/L values that range from 0.07 at 0.2 cm to 0.30 at 60 cm, respectively.

In several instances, however, samples with similar D/L values occur at quite different sediment-depths. For example, *Macoma* specimens from DC-3-81 G-105 and DC-2-81 G-31 have aspartic acid D/L values of 0.14 and sample depths of 100 cm and 38-39 cm, respectively. Specimens of *Yoldia* from DC-5-80 G-26 and DC-5-80 G-66 have D/L values and depth relationships of 0.23 ± .01 at 223-230 cm and 0.30 at 60 cm, respectively. Possible explanations for samples having relatively high D/L values and shallow sample depths are: 1) specimens may have been reworked; 2) sediment accumulation rates may be different at the sites.

Absolute Ages

Absolute ages of specimens are determined with equation 1, the expression of linear first-order racemization kinetics. Samples which have radiocarbon ages measured immediately next to them are used for the calculation of a calibrated rate constant (Bada and Protoch, 1973). The measured aspartic acid D/L value, radiocarbon age and correction at t = o are inserted into equation (1), and the equation is solved for k, the calibrated rate constant. The calibrated rate constant represents the integrated temperature history of the mollusk over the radiocarbon span of time. A calibrated rate constant cannot be calculated for *Macoma*, because radiocarbon ages are not available adjacent to these specimens. Calibrated rate constants for four general of mollusks are:

Nuculana	$k_{asp} = 1.53 \pm 0.30 \times 10^{-5}\ yr^{-1}$
Neptunea	$k_{asp} = 9.69 \times 10^{-6}\ yr^{-1}$
Yoldia	$k_{asp} = 1.29 \times 10^{-5}\ yr^{-1}$
Clinocardium	$k_{asp} = 1.90 \times 10^{-5}\ yr^{-1}$

These rate constants permit age estimations to be made for other specimens of the same genera that lack radiocarbon age control (Table 13). The age of *Nuculana* in G-26 from DC-5-80 is calculated to be 22,000 years by this method. This value is in agreement with the range of 10,880 to 33,990 years based on radiocarbon dates that bracket an erosional surface close to where the *Nuculana* was recovered. *Yoldia* from the same interval in G-26 gives an age of 14,000 years which also is in agreement with the radiocarbon range of

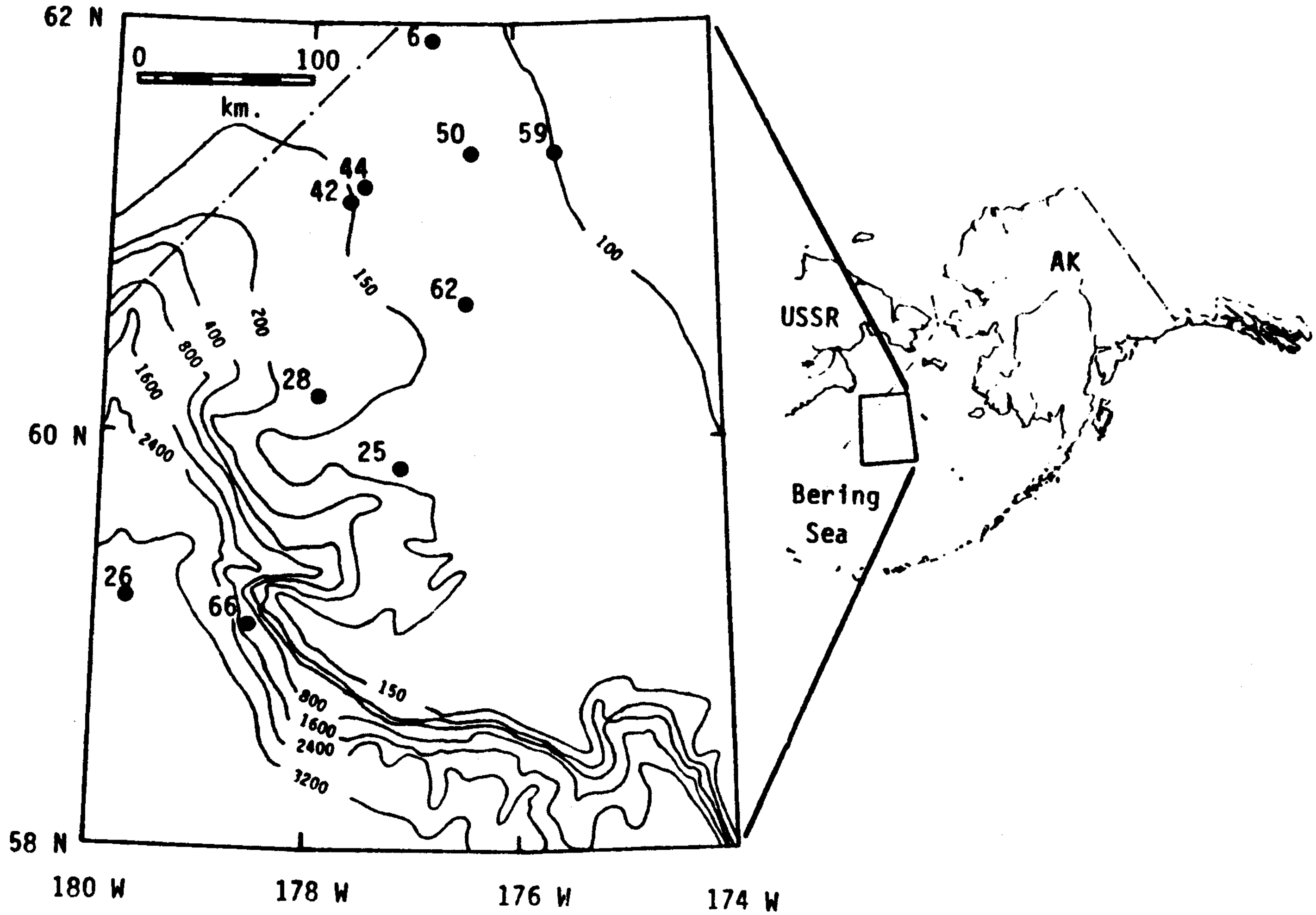

Figure 51. Location of gravity cores in the northern Navarin Basin province where fossil mollusks were studied. Bathymetry is in meters.

10,880 to 33,990 years. In core G-42 from DC-5-80 Clinocardium at 97 cm has an age of 8,000 years which is in general agreement with the radiocarbon date of 13,650 at 170-183 cm depth. Neptunea from DC-3-81 G-80 has a calibrated age of 21,000 years. The Neptunea from DC-5-80 G-98 has an age of 41,000 years at a depth of 140 cm. This is the oldest sample measured in this investigation.

Summary

Aspartic acid enantiomeric ratios were used to establish the age of five molluscan samples collected from sediment cores from the Navarin Basin province. These samples range in age from 8,000 to 41,000 years old. In general, the ages given by the amino acid method agree with radiocarbon dates.

References

Bada, J. L. and Protsch, R., 1973, Racemization reaction of aspartic acid and its use in dating fossil bones: Proceedings of the National Academy of Science, v. 70, p. 1331-1334.

Bada, J. L. and Schroeder, R. A., 1972, Racemization of isolencine in calcareous marine sediments: kinetics and mechanism: Earth and Planetary Science Letters, v. 15, p. 223-231.

Blunt, D. J. and Kvenvolden, K. A., 1981, A preliminary report on amino acid diagenesis in fossil mollusks recovered from the Navarin Basin Province, Bering Sea: in Carlson, P. R. and Karl, H. A. (eds) Seafloor Geologic Hazards, Sedimentology, and Bathymetry: U.S. Geological Survey Open-File Report 81-1217, p. 138-149.

Kvenvolden, K. A., Blunt, D. J., and H. E. Clifton, 1979, Amino acid racemization in Quaternary shell deposits at Willapa Bay, Washington: Geochimica Cosmochima, Acta, v. 43, p. 1505-1520.

Kvenvolden, K. A., Blunt, D. J., McMenamin, M. A., and Strahan, S. E., 1980, Geochemistry of amino acids in shells of the clam Saxidomus; in Douglas, A. G., and Maxwell, J. R. (eds), Advances in Organic Geochemistry 1979: Pergamon Press, Oxford, p. 321-332.

CHAPTER 12: APPENDED REPORTS

A. Carlson, P. R. and Karl, H. A., 1981, High-resolution seismic reflection profiles: Navarin Basin province, northern Bering Sea, 1980: U.S. Geological Survey Open-File Report 81-1221, 4 p., 1 map, scale 1:1,000,000.

B. Carlson, P. R. and Karl, H. A., 1982, High-resolution seismic reflection profiles: Navarin Basin province, northern Bering Sea, 1981: U.S. Geological Survey Open-File Report 82-786, 5 p., 1 map, scale 1:1,000,000.

C. Karl, H. A. and Carlson, P. R., 1982, Location and description of sediment samples: Navarin Basin province, Bering Sea, 1980-81: U.S. Geological Survey Open-File Report 82-958, 5 p., 2 maps, scale 1:1,000,000.

D. Fischer, J. M., Carlson, P. R., and Karl, H. A., 1982, Bathymetric map of Navarin Basin province, northern Bering Sea: U.S. Geological Survey Open-File Report 82-1038, 11 p., 1 map, scale 1:1,000,000.

E. Carlson, P. R., Fischer, J. M., and Karl, H. A., 1983, Two newly discovered submarine canyons on Alaskan continental margin of Bering Sea: U.S. Geological Survey Open-File Report 83-24, 36 p., 1 map, scale 1:250,000.

F. Carlson, P. R., Karl, H. A., Fischer, J. M., and Edwards, B. D., 1982, Geologic hazards in Navarin Basin province, northern Bering Sea: 14th Offshore Technology Conference, Houston, Texas, Proceedings, v. 1, 73-87.

G. Carlson, P. R., Karl, H. A., and Edwards, B. D., Puzzling features in the head of the Navarinsky Canyon, Bering Sea: submitted to Geo-Marine Letters, 13 ms. p., (1983).

H. Karl, H. A. and Carlson, P. R., Large sand waves in submarine canyon heads, Bering Sea: preliminary hypothesis of their depositional history: submitted to Geo-Marine Letters, 15 ms. p., (1983).

APPENDIX A:

HIGH-RESOLUTION SEISMIC REFLECTION PROFILES: NAVARIN BASIN PROVINCE, NORTHERN BERING SEA, 1980

by

Paul R. Carlson and Herman A. Karl

U.S. Geological Survey

INTRODUCTION

In June and July 1980, the U.S. Geological Survey conducted a high resolution geophysical and seafloor sampling cruise (DC 4/5-80 BS/NB) in the northern Bering Sea to obtain data on seafloor hazards pertinent to OCS oil and gas lease sale activity. This report contains a list of the seismic reflection records that are publicly available and includes a trackline map of the Navarin Basin province. Microfilm copies of the seismic reflection records are available for viewing:

(1) U.S. Geological Survey
Pacific-Arctic Branch of Marine Geology, Room B171
Menlo Park, CA 94025

or for purchase:

(2) National Geophysical and Solar
Terrestrial Data Center
EDS/NOAA
Boulder, CO 80302

DATA COLLECTION

DISCOVERER cruise DC 4/5-80 BS/NB left Kodiak July 2, 1980, for work in OCS lease sale are 83 (Navarin Basin). The first leg, which was 75 percent geophysics and 25 percent sampling, ended at Adak July 24, 1980. The second leg of the cruise which began July 28, 1980, consisted of 60 percent sampling and 40 percent geophysics, and ended at Kodiak August 17, 1980.

Navigation positions were determined by satellite and Loran C. Position accuracies are probably on the order of 0.5 km.

Three separate seismic reflection systems were operated simultaneously, throughout much of the study area, providing high and intermediate frequency acoustic records. The systems were: 3.5 kHz transducer (12,842 km), 400-800 Joule minisparker (4624 km), and two 40 in^3 airguns (6757 km). The 3.5 kHz system was operated continuously throughout the cruise, including transit lines to and from the study area and to and from St. Paul Island for three medivacs. The airguns were deployed along all except transit and sampling lines. The minisparker system was operated in shelf and upperslope water depths (to about 800 m). (See Table A1 and Figure A1 for line numbers along which the various systems were operational).

ACKNOWLEDGMENTS

We appreciate the assistance provided by the scientific personnel on the cruise (Brian Edwards, Jeff Fischer, George Ford, Sarah Griscom, Ken Johnson, Beth Lamb, Grant Lichtman, Paula Quinterno, Jeff Rupert, John Saladin, Rick Vail, Tim Vogel, Pat Wiberg, Bob Wilson, and Mark Yeats), the ship's captain and crew, and the marine logistics group.

The cruise was supported jointly by the U.S. Geological Survey and by the Bureau of Land Management through interagency agreement with the National Oceanic and Atmospheric Administration, under which a multi-year environmental hazards study of the Alaskan continental shelf is managed by the OCSEAP office.

Table A1. Track lines along which seismic systems were operational.

	3.5 only*			
	Transit	Study Area	Minisparker	Airguns
Leg 1 (DC-4-80)	T-1, 1, 26, 27, 32, 33, 38	None	1-3, 4-14, 18, 22-25, 28-29 31, 34-37	1-25, 28-31 34-37
Leg 2 (DC-5-80)	30, 98, 99	48-51 53-62 72-74 81-86 93-95 100 105-108 114-115 121-123	40-43, 45-47, 63-67, 69, 76-79, 87-91 97, 102-103 110, 117, 125-126	40-47, 52 63-71, 75-80, 87-92, 96-97, 101-104, 109-113, 116-120, 124-127

*3.5 kHz system was operated continuously during both legs of cruise.

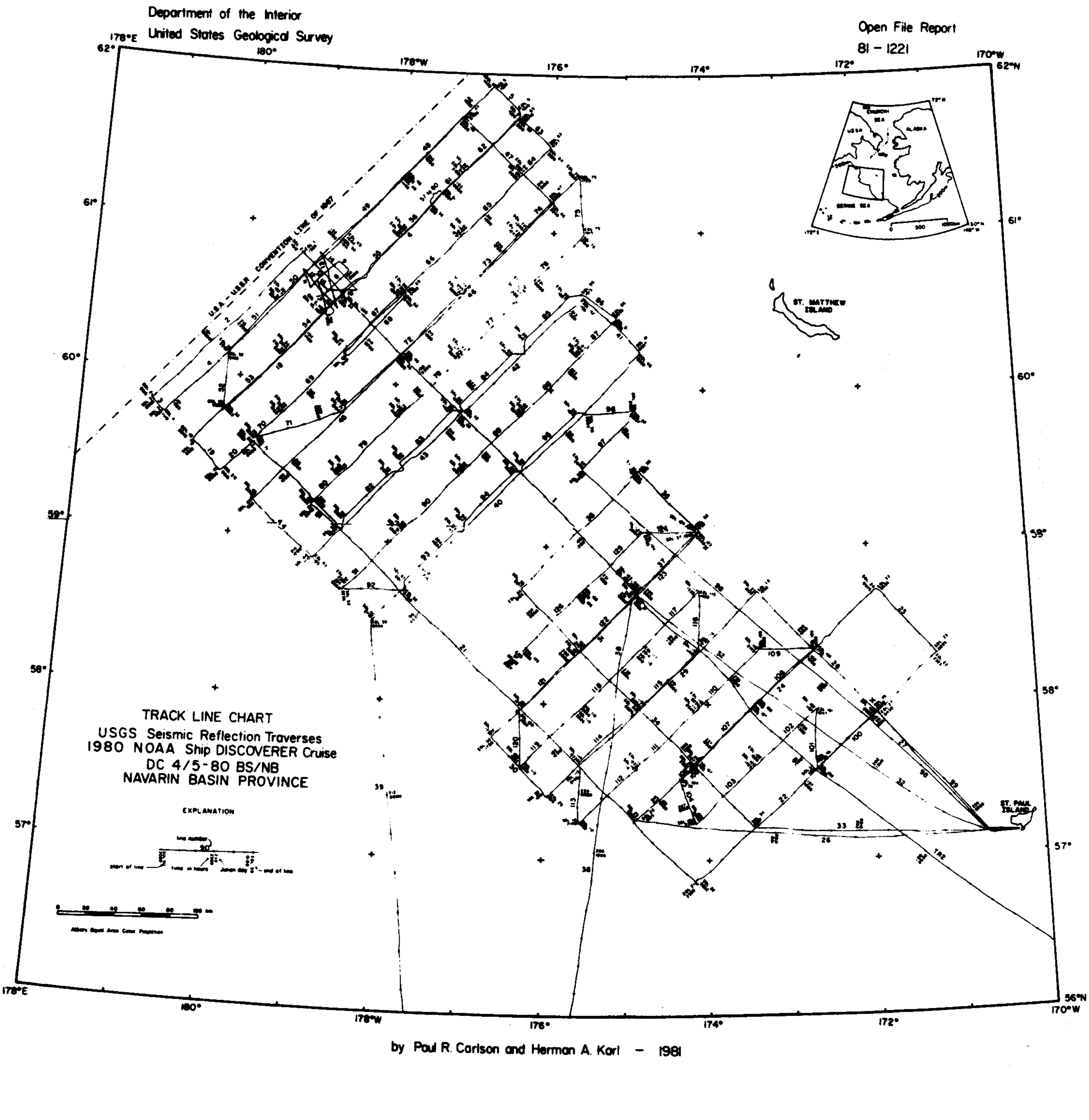

Figure A1. Track line chart for 1980 DISCOVERER Cruise DC 4/5-80 BS/NB.

APPENDIX B:

HIGH-RESOLUTION SEISMIC REFLECTION PROFILES:

NAVARIN BASIN PROVINCE, NORTHERN BERING SEA, 1981

by

Paul R. Carlson and Herman A. Karl

U.S. Geological Survey

INTRODUCTION

In June and July 1981, the U.S. Geological Survey conducted a high resolution geophysical and seafloor sampling cruise (DC 2/3-82 BS/NB) in the northern Bering Sea to obtain data on seafloor hazards pertinent to OCS oil and gas lease sale activity. This report contains a list of the seismic reflection records that are publicly available and includes a trackline map of the Navarin Basin province. Microfilm copies of the seismic reflection records are available for reviewing:

(1) U.S. Geological Survey
Pacific-Arctic Branch of Marine Geology, Room B164
Deer Creek Facility
Menlo Park, CA 94025

or for purchase:

(2) National Geophysical and Solar
Terrestrial Data Center
EDS/NOAA
Boulder, CO 80302

DATA COLLECTION

DISCOVERER cruise DC2/3-81 BS/NB left Kodiak June 8, 1981, for work in OCS lease sale area 83 (Navarin Basin). The first leg, which was 65 percent geophysics and 35 percent sampling, ended at Adak July 2, 1981. The second leg of the cruise which began July 6, 1981, consisted of 55 percent geophysics and 45 percent sampling, and ended at Dutch Harbor July 29, 1981.

Navigation positions were determined by satellite and Loran C. Position accuracies are probably on the order of 0.5 km.

Three separate seismic reflection systems were operated simultaneously throughout much of the study area, providing high and intermediate frequency acoustic records. The systems were: 3.5 kHz transducer (10,143 km), 400-800 Joule minisparker (5247 km), and two 40 in^3 airguns (8050 km). The 3.5 kHz systems as operated continuously throughout the cruise, including transit lines to the study area and part of the way to and from St. Paul Island for two medivacs. The airguns were deployed along all except transit and sampling lines. The minisparker system was operated in shelf and upper-slope water depths (to about 800 m). (See Table B1 and Figure A-2 for line numbers along which the various systems were operational.)

ACKNOWLEDGMENTS

We appreciate the assistance provided by the scientific personnel on the cruise (Jack Baldauf, Neal Barnes, Mike Bennett, Dave Blunt, Drew Comer, Merid Dates, Jon Erickson, Jeff Fischer, Dan Hurlbert, Ken Johnson, Jim Joyce, Larry Kooker, Beth Lamb, Larry Lawer, Sue McGeary, Jim Nicholson, Robert Patrick, Paula Quinterno, Robin Ross, Jeff Rupert, John Saladin, Dennis Thurston, Tim

Vogel, Hal Williams, and Mark Yeats) the ship's captain and crew, and the marine logistics group.

The cruise was supported jointly by the U.S. Geological Survey and by the Bureau of Land Management through interagency agreement with the National Oceanic and Atmospheric Administration, under which a multi-year environmental hazards study of the Alaskan continental shelf is managed by the OCSEAP office.

Table B1. Track lines along which seismic systems were operational.

	3.5 only*		Minisparker	Airguns
	Transit	Study Area		
Leg 1 (DC-2-81)	T1-T4	48,49,63,70	T2,T4,1-5, 8-20,24-28 31-47, 50-60 62, 64-68 73-82	1-47, 50-62 64-69, 71-92
Leg 2 (DC-3-81)	None	111, 119-122	106-110, 112-118, 123-137, 141-153, 159-188	95-110, 112-118, 123-188

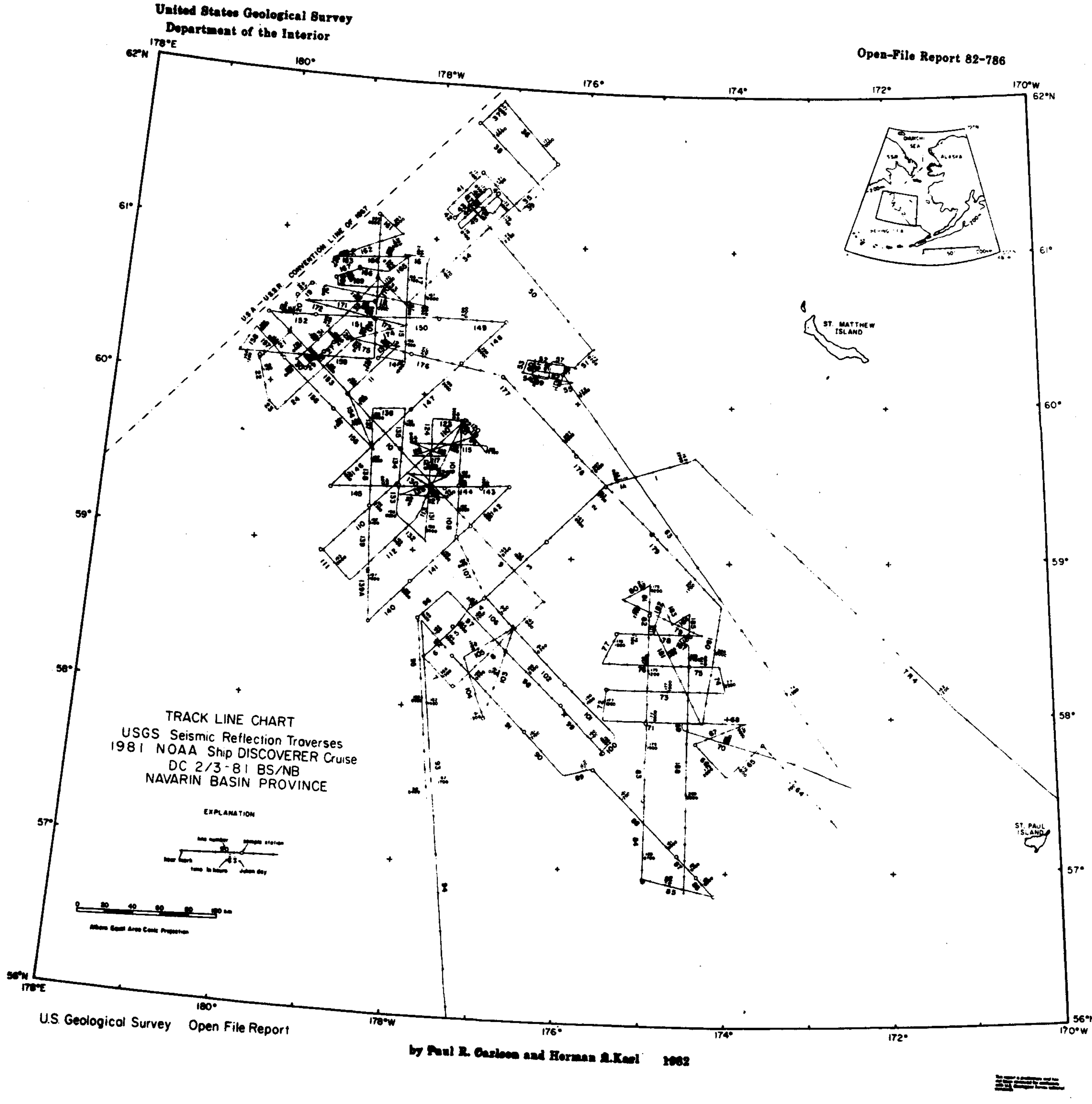

Figure B1. Track line chart for 1981 DISCOVERER Cruise DC 2/3-81 BS/NB.

APPENDIX C:

LOCATION AND DESCRIPTION OF SEDIMENT SAMPLES: NAVARIN BASIN PROVINCE, BERING SEA, 1980-1981

by

Herman A. Karl and Paul R. Carlson

U.S. Geological Survey

INTRODUCTION

Three cruises have been conducted in the Navarin Basin province (lease sale area 83) in the northern Bering Sea to obtain data on seafloor hazards pertinent to OCS oil and gas lease sale activity. This report summarizes the information that is presently available regarding sediment samples collected during those cruises. Included in this report are a station location map (Figure C1) and a map of sediment types (Figure C2) derived from qualitative visual descriptions of surface samples. Microfilm copies of the visual core description logs are available for viewing:

(1) U.S. Geological Survey
Pacific-Arctic Branch of Marine Geology, Room B 171
Menlo Park, CA 94025

or for purchase:

(2) National Geophysical and Solar Terrestrial Data Center
EDS/NOAA
Boulder, CO 80302

DATA COLLECTION

USCG Ice breaker POLAR STAR followed the ice in spring (May 2-29) 1980 and 22 gravity cores and 33 grab samples were collected during this cruise designated PST-80-BS; 104 gravity cores, 10 grab samples and 1 dredge sample were collected in summer (July 2 - August 17) 1980 during NOAA ship DISCOVERER cruise DC 4/5-80-BS/NB; and 88 gravity cores, 10 grab samples, 6 box cores, and 5 vibracores were collected in summer (June 8 - July 29) 1981 during DISCOVERER cruise DC2/3-81-BS/NB.

Cores collected on USCG POLAR STAR during cruise PST-80-BS cores were stored at Adak, Alaska from late May to late July and then transferred to NOAA ship DISCOVERER for study. PST-80-BS, DC4/5-80-BS/NB, and DC2/3-81-BS/NB cores were split and described and subsamples were collected for grain-size, geochemical, faunal, clay mineral, carbon, and geotechnical analyses at onshore laboratories. The split cores were placed in D-tubes and kept with subsamples in cold storage and are archived at the U.S. Geological Survey refrigerated core locker in Menlo Park.

Navigation was by Loran C and satellite; position accuracies are probably on the order of 0.5 km.

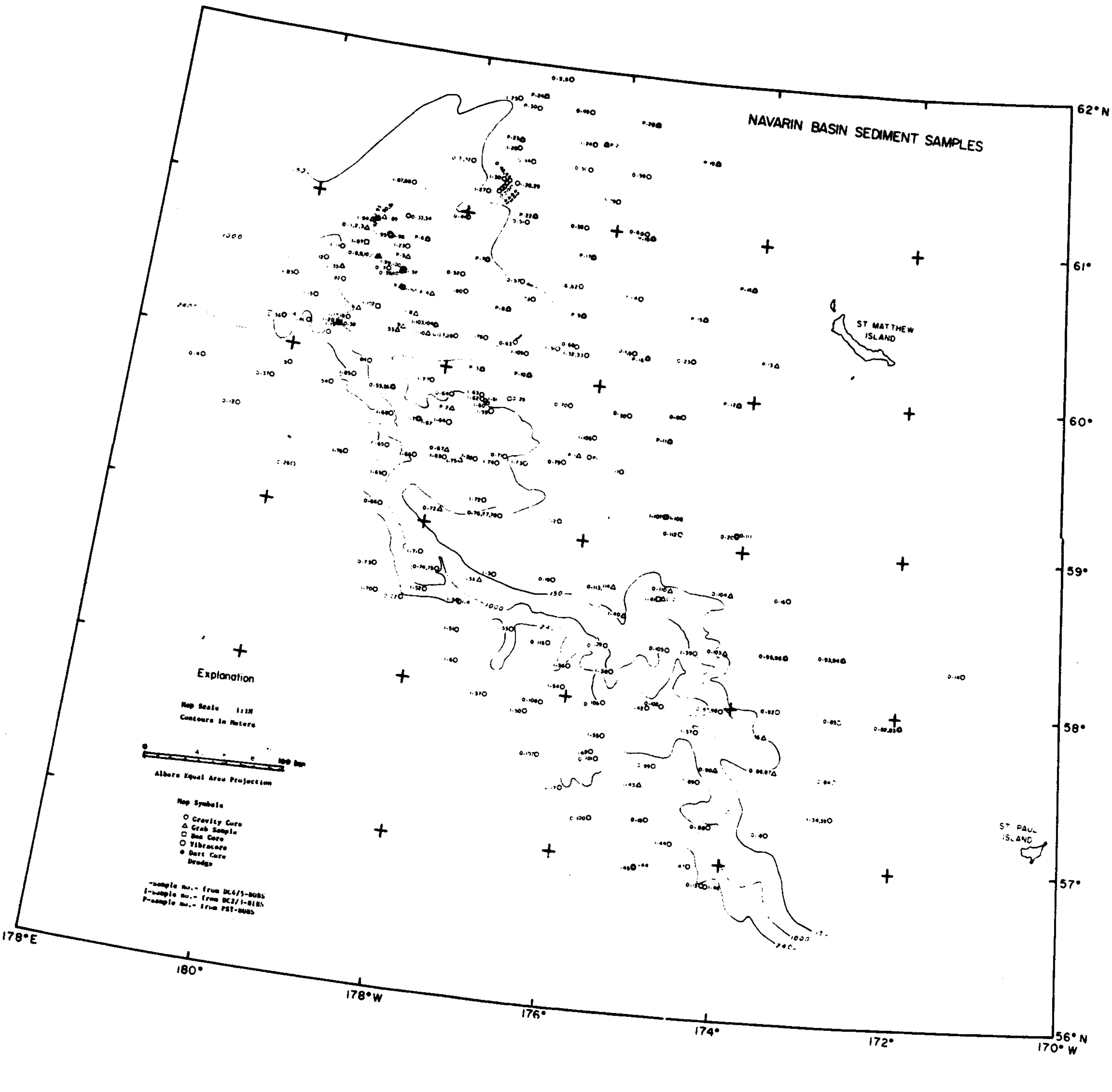

Figure C1. Station location map.

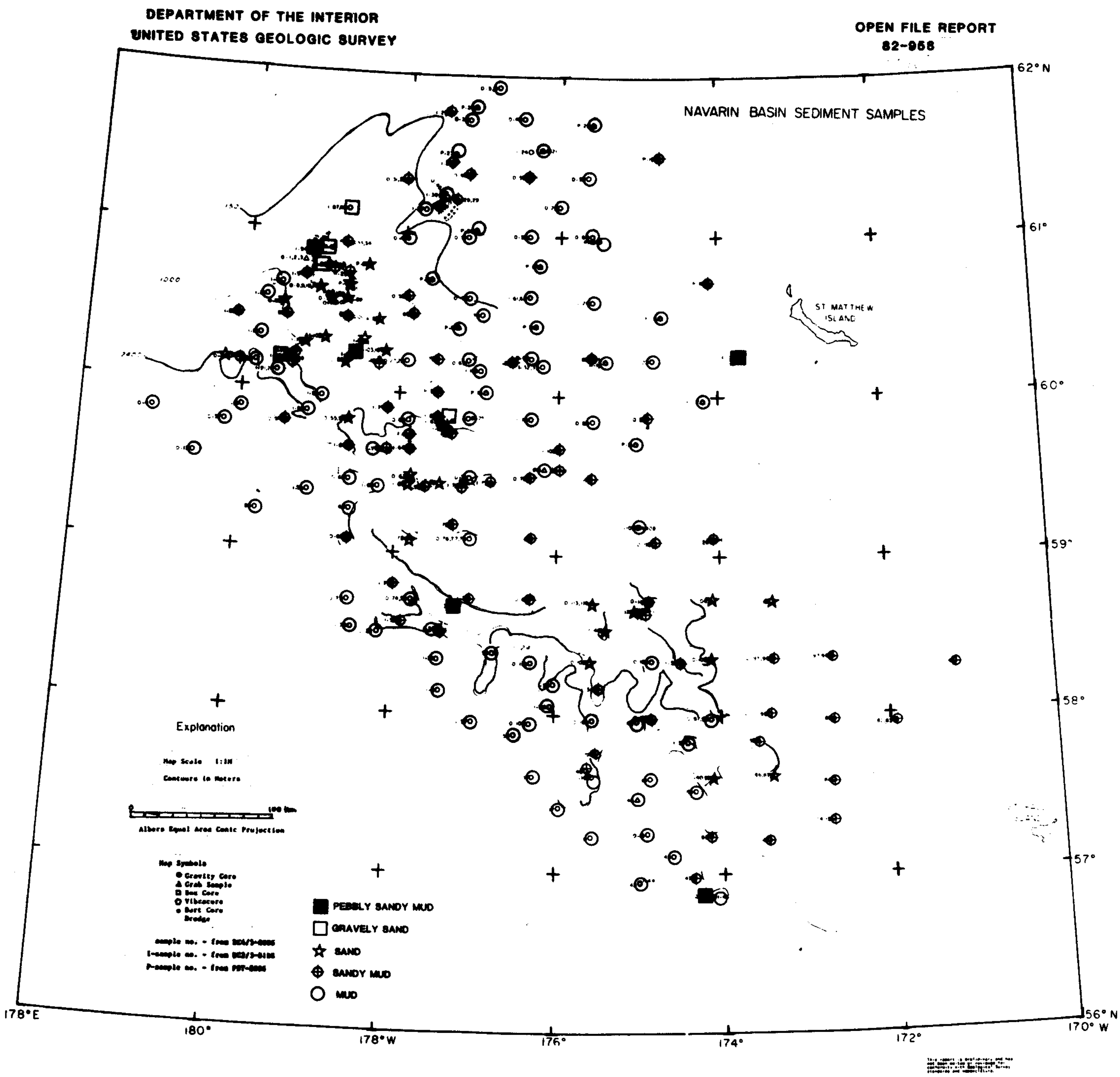

Figure C2. Map of sediment types.

OBSERVATIONS

Sediment sampling stations are plotted in Figure C1. Figure C2 shows the distribution of sediment types derived from qualitative visual descriptions of surface samples, defined as bulk subsamples from grab samples and discrete subsamples from the upper 35 cm of gravity cores. Silts generally characterize the shelf and slope, but there are zones of coarser sediments at the shelf break, on the upper slope, and in the heads of submarine canyons. Surficial sediment on the shelf tends to be coarser in the southeastern part of the area than elsewhere.

ACKNOWLEDGMENTS

We appreciate the assistance provided by the scientific personnel on each of the cruises (Jack Baldauf, Neal Barnes, Mike Bennett, Dave Blunt, Drew Comer, Merid Dates, Brian Edwards, Jon Erickson, Jeff Fischer, George Ford, Sarah Griscom, Rick Herrera, Dan Hurlbert, Ken Johnson, Jim Joyce, Larry Kooker, Beth Lamb, Larry Lawer, Grant Lichtman, Sue McGeary, Jim Nicholson, Robert Patrick, Paula Quinterno, Robin Ross, Jeff Rupert, John Saladin, Dennis Thurston, Rick Vail, Tim Vogel, Pat Wiberg, Hal Williams, Bob Wilson, and Mark Yeats) and by the ship's captains and crew and the marine logistics group.

The cruises were supported jointly by the U.S. Geological Survey and by the Bureau of Land Management through interagency agreement with the National Oceanic and Atmospheric Administration, under which a multi-year environmental hazards study of the Alaskan continental shelf is managed by the OCSEAP office.

APPENDIX D:

BATHYMETRIC MAP OF NAVARIN BASIN PROVINCE, NORTHERN BERING SEA

by

Jeffrey M. Fischer, Paul R. Carlson, and Herman A. Karl

U.S. Geological Survey

INTRODUCTION

This bathymetric map of the Navarin basin province is part of the ongoing research in preparation for OCS Lease Sale 83 which is scheduled for the spring of 1984. The intended use of this map, in addition to showing the morphology of the Navarin continental margin, is for the plotting of geologic and geophysical data. It is not intended for use in navigation. Names used herein for seafloor features are from historical and general usage and have not been formally approved.

Navarin Basin province includes an area of over 150,000 km^2 and contains the large, deep, sediment-filled Navarin Basin named by Marlow and others (1976). The study area is located in the northern Bering Sea (see index map) and extends to within 100 km of St. Matthew Island on the northeast and to within 100 km of St. Paul Island on the southeast. To the southwest, the boundary of the study area is the 3600 m isobath, and to the northwest, the U.S.-Russia Convention Line of 1867; however, the basin itself continues to within 150 km of the Siberian Coast (Marlow, Cooper, Parker, and Childs, 1981).

Previous studies of the Bering Sea have concentrated on the Siberian and Alaskan coasts, in addition to the Aleutian Arc and portions of the southeastern Bering continental margin. Within the Navarin Basin province, few studies were conducted previous to the 1960's. Maps by Baranov and others (1967), Pratt and Walton (1974), Scholl and others (1974), and Schumacher (1976) improved coverage, but the Navarin basin area has received little detailed attention, and consequently inaccuracies abounded, especially northwest of Zhemchug Canyon. The present study improves coverage up to the U.S.-Russia Convention Line of 1867 and makes significant changes in the published bathymetry, especially in the Navarinsky Canyon area.

DATA COLLECTION

The data base for the map consists of over 23,000 kms of 3.5 kHz tracklines obtained on U.S. Geological Survey cruises from 1976 to 1982 (see Fig. D1 and Table D1). Navigation was based on Loran C, updated with satellite fixes. On the continental shelf the trackline grid spacing averages about 30 km. Digitized depths along each trackline were spaced 2 km apart on the continental shelf and rise and depths were spaced 0.2 km or less apart on the continental slope. We assumed a water velocity of 1500 meters/sec with no correction for tides, temperature, or salinity. Tides in the Bering Sea, although poorly understood, are generally less than a meter (Lisitsyn, 1966) and waves during the survey periods were negligible. The depth data and navigation data were computer merged, contoured by hand, and compared with a computer contoured map as a final check. Contour intervals range from 200 m for depths below 200 m, to 25 m between 150 to 200 m, to 10 m from 0 to 150 m water depths. Contours shallower than 100 m are taken from Pratt and Walton (1974).

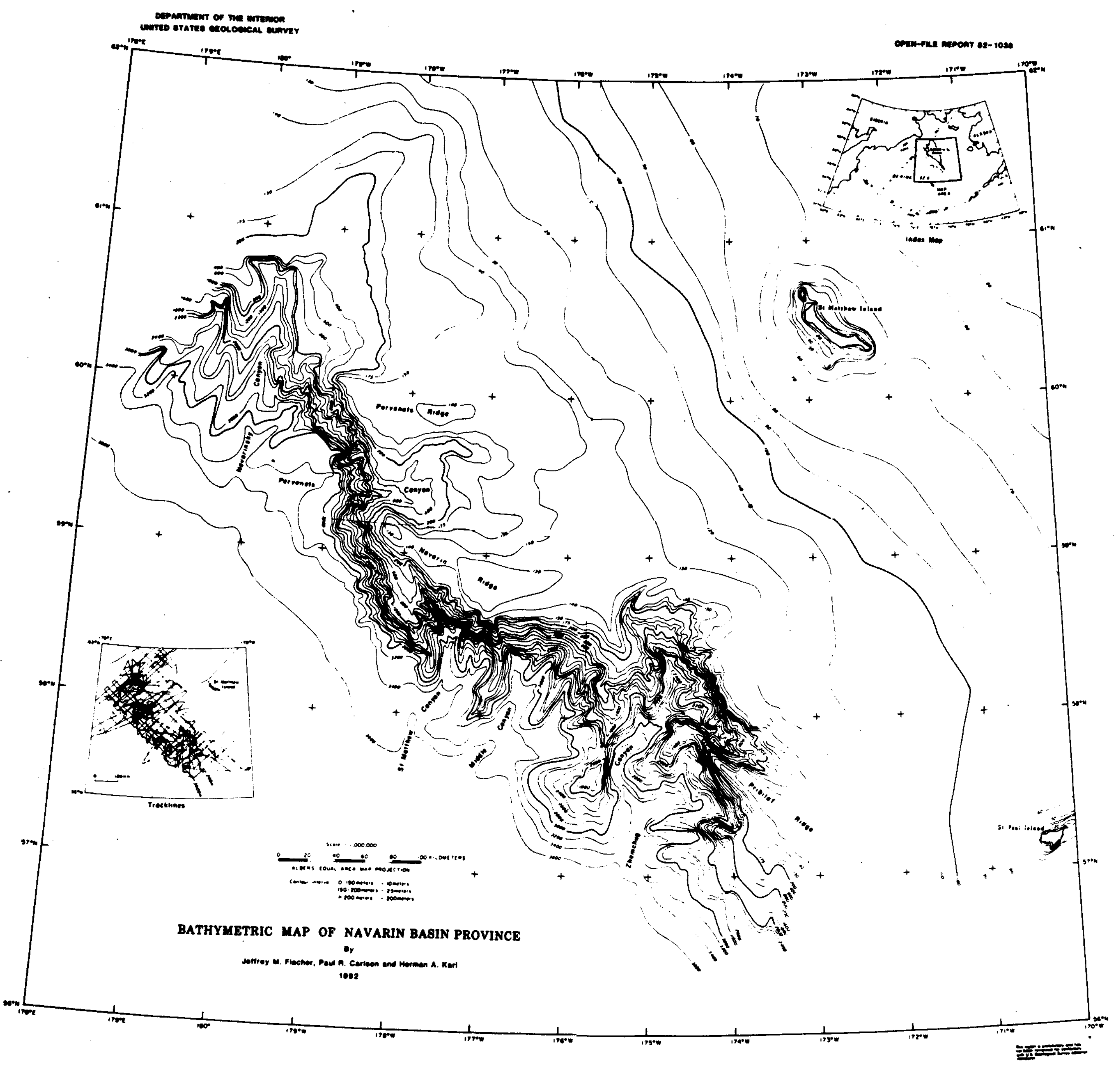

Figure D1. Bathymetric map of Navarin Basin province and inset showing tracklines.

Table D1. Sources of bathymetric data

Cruise*	km of tracklines
L-5-76	800
S-3-77	700
L-5-77	1,000
L-8-77	2,300
DC-4/5-80	6,800
DC-2/3-81	10,100
L-10-82	1,600

*Cruise identifier includes ship (L=S.P. Lee, S=Sea Sounder, DC=Discoverer), consecutive cruise number and year.

GEOLOGY

A tectonic model of the Bering shelf margin proposed by Scholl and others (1975) suggests that during the Mesozoic era the ocean plate boundary was a subduction zone of small convergence angle which ran along the present Bering shelf margin. As a result of subduction, fore-arc-eugeosynclinal rocks were uplifted and an inner magmatic arc formed (Marlow and others, 1976). Remnants of these fore-arc-magmatic-arc facies can be traced southeast from Siberia through St. Matthew and St. Lawrence Islands, where they change trend to the northeast and extend into Alaska (Patton and others, 1976). Sometime in Cretaceous or earliest Tertiary time, the subduction zone either jumped or migrated to its present position at the Aleutian Trench (Scholl and others, 1975; Patton and others, 1976). With the cessation of subduction, both fore-arc and magmatic-arc rocks were uplifted and eroded. About the same time, the compressional deformation ceased and changed to extensional rifting (Marlow and others, 1976). Extension, erosion, and subsequent subsidence have continued during much of the Cenozoic, creating the Navarin basin, among others, and influencing much of the present bathymetry. Navarin basin contains as much as 12 km of fill in places beneath the continental shelf (Marlow, Cooper, Parker, and Childs, 1981; Marlow, Carlson, Cooper, Karl, McLean, McMullin, and Lynch, 1981). The sedimentary fill consists of semi-consolidated to unconsolidated, generally flat-lying, relatively undeformed, hemipelagic deposits of Cenozoic age (Scholl and others, 1968; Marlow and others, 1979; Karl and Carlson, 1982).

GEOMORPHOLOGY

The Navarin basin province is an area of great contrasts, including the very flat continental shelf with its subtle structures, to the steep continental slope with its spectacular precipices and large canyons, and the gentle continental rise crossed by turbidity current channels and buried deep-sea fan channels. These morphologic features are influenced by, if not directly related to, the tectonic history of the region.

The continental shelf within the Navarin Basin province is extremely flat and encompasses an area of 100,000 km^2 between the 100 m and 150 m isobaths. The width of the shelf in the province varies from 100 km to 250 km and gradients range from 0.04° to 0.01°. Compared to Shepard's (1963) worldwide average shelf gradient of 0.12°, the Bering shelf appears to be one of the flattest in the world. The most prominent features are large canyons incised into the shelf and large submarine ridges oriented parallel to and located next to the shelf break. Two large submarine ridges, Navarin and Pribilof (Marlow and others, 1976), are each outlined by the 130 m isobath and are south of Pervenets and Zhemchug Canyons respectively. These ridges appear to be surface expressions of structural highs where acoustic basement rises to within less than one kilometer of the seafloor (Cooper and others, 1981). A few protrusions of probable acoustic basement crop out along these ridges, but are too small to show at this scale. Three such protruding knobs crop out on Navarin Ridge just north of Middle Canyon. Another knob, just south of Zhemchug Canyon, on Pribilof Ridge, rises to within 100 meters of the surface. The third and smallest ridge north of Pervenets Canyon, herein called Pervenets Ridge, is somewhat anomalous since shallow acoustic basement is not discernible on the seismic records.

The shelf break in Navarin Basin province occurs between the 150-175 m isobaths. Around the canyons, the break varies somewhat; Navarinsky Canyon has no distinct shelf break, in Pervenets the break is very gentle, and in Zhemchug the break is very abrupt. In general, from northwest to southeast, the depth of the break decreases until at Zhemchug Canyon the shelf break occurs at about 150 m.

The continental slope, an area of 40,000 km^2, begins at about the 150 m isobath and extends to the 2800 m isobath. The slope is dissected by five large submarine canyon systems which from north to south are Navarinsky, Pervenets, St. Matthew, Middle, and Zhemchug Canyons. It should be noted that all the above are large canyon systems, composed of numerous tributary canyons many of which are too small to resolve at our present grid spacing and map scale. The slope within the Navarin Basin province has a length of 600 km and varies in width from 200 km near Navarinsky Canyon to 15 km near St. Matthew Canyon. The Navarin continental slope ranges in gradient from 3° to 10°, compared to a world-wide average of 4.3° (Shepard, 1963).

Navarinsky Canyon has a width of 150 km at the shelf break, an axial length of 200 km, and an approximate volume of 4900 km^3. The Navarinsky system consists of two main branches, the western which is oriented roughly north-south and the eastern which trends northeast-southwest. Above the 400 m isobath, these branches form large, broad, gently sloping shelf valleys that have axial gradients of less than 0.2°. Between 400 m and 3600 m, where these two branches merge into a single deep-sea fan channel, the gradients are about 1.2°. The gradient of the fan channel between 3200 and 3600 m is approximately 0.3°. Still, both of these gradients are gentle compared to the other Navarin margin canyons.

The next major canyon to the southeast, Pervenets, is incised perpendicular to the slope and trends east to west. Pervenets Canyon has a width of 70 km at the shelf break, a downslope length of 120 km, and a volume of 1200 km^3; the major portion of this volume is above the 1000 m isobath. Above 1000 m the canyon bifurcates into two branches which can be traced to the 150 m isobath. Each of these main branches has an axial gradient of 0.4°. The larger northern branch located just south of Pervenets Ridge is well-defined, whereas the smaller southern branch of Pervenets Canyon is poorly developed and has little expression above 600 meters. Below 1000 meters the canyon system is less well-developed than any of the Navarin margin canyons. Between 1000 m and 3000 m the canyon thalweg attains a gradient of 3.8°.

The St. Matthew Canyon system, the smallest of the five canyons, contains some of the steepest relief in the Navarin basin area and is located south of the Navarin Ridge. St. Matthew Canyon consists of at least two main branches and several tributaries, the west branch with a gradient of 2.5° being the longer and the east the shorter and steeper with a gradient of 5° (Carlson and others, in press). The upper part of St. Matthew Canyon is parallel to Navarin Ridge and bounded to the southwest by the steep continental slope that reaches declivities of greater than 15°. Adjacent to St. Matthew Canyon is a large broad ridge about 30 km long and 20 km wide in water depths between 400 m and 1000 m. Another large linear ridge over 80 km long extends along the 177° W meridian and separates St. Matthew and Middle Canyons.

Directly to the east of St. Matthew Canyon lies the Middle Canyon system which is very similar to the St. Matthew system, but twice as large (Carlson and others, in press). The east and west branches of Middle Canyon are roughly equal in size and each branch has two large and several smaller tributaries. The west branch is the steeper attaining a thalweg gradient of 4.1° compared to a gradient of 3.2° for the east branch.

Neither the St. Matthew or Middle Canyon systems are incised into the shelf, perhaps due to the moderately well-consolidated nature of the sedimentary rocks and the apparent young age of both canyon systems.

Zhemchug Canyon, located in the southeast corner of the Navarin Basin province, is perhaps the most spectacular of all the Navarin margin canyons. With a length of 160 km and a width of 40 km, this canyon has a volume of over 6300 km^3. The upper half of the Zhemchug Canyon system is incised deeply into the continental shelf between Navarin Ridge and Pribilof Ridge. The main thalweg of this giant canyon cuts deeply through the structural high formed at the shelf break by Pribilof Ridge and debouches onto the continental rise at a depth of about 2600 m. The axial gradient of this canyon is about 2° and the gradient of the fan channel is 1°. Numerous small tributaries run into the main canyon and numerous small slumps occur on its sides. A long ridge, total length of 130 km separates Zhemchug and Middle canyons. This ridge has a maximum relief of about 1200 m (1800-3200 m), and extends from the shelf edge across the slope and intersects the rise.

The continental rise begins at the 2800 m isobath at the base of the slope and continues beyond the 3600 m isobath, the limit of our bathymetric data. The rise varies in width from 25 km to 100 km and gradient from 0.5° to 1.8°. Many deep-sea channels dissect the rise and all five of the previously mentioned canyon systems have well developed channels that extend across the continental rise. Cores taken in and near these channels contain sand lenses and graded sand beds suggesting turbidity current deposition (Carlson and others, 1981b).

REFERENCES CITED

Baranov, A. N., and others, eds., 1967, The World Atlas: Chief Administration of Geodesy and Cartography, under the Council of Ministers of the U.S.S.R., 2nd ed., Moscow, 250 p. (English edition).

Carlson, P. R., Karl, H. A., Johnson, K. A., and Fischer, J. M., 1981, Submarine canyons flanking Navarin Basin, Bering Sea, in U. S. Geological Survey in Alaska: Accomplishments during 1980: U. S. Geological Survey Circular 844, p. 139-141.

Carlson, P. R., Fischer, J. M., and Karl, H. A., in press, Two newly discovered submarine canyons on the Alaskan Continental Margin of the Bering Sea: U. S. Geological Survey Open-File Report 82-

Cooper, A. K., Marlow, M. S., Parker, A. W., and Childs, J. R., 1981, Structure contour map on acoustic basement in the Bering Sea: U. S. Geological Survey Miscellaneous Field Studies Map MF-1165.

Karl, H. A. and Carlson, P. R., 1982, Location and description of sediment samples: Navarin Basin province, Bering Sea, 1980-81: U. S. Geological Survey Open-File Report 82-958, 5 p., 2 map sheets scale 1:1,000,000.

Lisitsyn, A. P., 1966, Recent sedimentation in the Bering Sea: Akad. Nauk SSR Inst. Okeal., Moskva, (Israel Program for Sci. Translations, 1969; U. S. Dept. of Commerce, Clearinghouse for Federal Sci. Tech. Info., Springfield, VA, 614 p.).

Marlow, M. S., Scholl, D. W., Cooper, A. K., and Buffington, E. C., 1976, Structure and evolution of Bering Sea shelf south of St. Lawrence Island: American Association Petroleum Geologist Bull., v. 60, p. 161-183.

Marlow, M. S., Cooper, A. K., Scholl, D. W., Vallier, T. L., and McLean, H., 1979, Description of dredge samples from the Bering Sea continental margin: U. S. Geological Survey Open-File Report 79-1139, 5 p.

Marlow, M. S., Carlson, P. R., Cooper, A. K., Karl, H. A., McLean, H., McMullin, R., and Lynch, M. B., 1981, Resource Report for proposed OCS sale number 83 Navarin Basin, Alaska: U. S. Geological Survey Open-File Report 81-152, 82 p.

Marlow, M. S., Cooper A. K., Parker, A. W., and Childs, J. R., 1981, Isopach map of strata above acoustic basement in the Bering Sea: U. S. Geological Survey Miscellaneous Field Studies Map MF-1164.

Patton, W. W., Lanphere, M. A., Miller, T. P., and Scott, R. A., 1976, Age and tectonic significance of volcanic rocks on St. Matthew Island, Bering Sea, Alaska: U. S. Geological Survey, Journal of Research, v. 4, p. 67-73.

Pratt, R., and Walton, F., 1974, Bathymetric Map of the Bering Shelf: Geological Society of America, Inc., Boulder, Colo.

Shepard, F. P., 1963, Submarine geology, 2nd ed.: Harper and Row, New York, 557 p.

Scholl, D. W., Buffington, E. C. and Hopkins, D. M., 1968, Geologic history of the continental margin of North America in the Bering Sea: Marine Geology, v. 6, p. 297-330.

Scholl, D. W., Alpha, T. R., Marlow, M. S., and Buffington, E. C., 1974, Base map of the Aleutian-Bering Sea region: U. S. Geological Survey Miscellaneous Investigation Series Map I-879, scale 1:2,500,000.

Scholl, D. W., Buffington, E. C., and Marlow, M. S., 1975, Plate tectonics and the structural evolution of the Aleutian Bering Sea region, in Forbes, R. B., ed., Contributions to the geology of the Bering Sea Basin and adjacent regions: Geological Society of America Special Paper 151, p. 1-32.

Schumacher, G. M., 1976, Bathymetric map of the Aleutian Trench and Bering Sea: U. S. Geological Survey Open-File Map 76-821, scale 1:2,500,000.

APPENDIX E:

TWO NEWLY DISCOVERED SUBMARINE CANYONS ON ALASKAN CONTINENTAL MARGIN OF BERING SEA

by

Paul R. Carlson, Jeffrey M. Fischer, and Herman A. Karl

U.S. Geological Survey

Two Newly Discovered Submarine Canyons, on Alaskan Continental Margin of Bering Sea

by

Paul R. Carlson, Jeffrey M. Fischer, and Herman A. Karl

INTRODUCTION

The search for new energy resources by the U. S. Geological Survey has focused increasing attention on the Alaskan continental margin in the Bering Sea, sometimes called the Beringian margin. Although there has been emphasis on the Aleutian Islands and the Bering Strait, partly due to their strategic locations, there has been limited oceanographic and geologic coverage of the Beringian margin until the last decade. The bathymetric and geophysical track line coverage across the northern part of the margin was, until 1980, very sparse. However, regional studies by Marlow and others (1976; in press) and Scholl and others (1976), resulted in the discovery of large basins filled with thick sequences of sedimentary material of Cenozoic and perhaps Mesozoic age. These thick sedimentary sequences have become the targets of several petroleum lease sales planned for the next few years. In preparation for the scheduled sales, we collected the first publicly available, detailed, bathymetric and high-resolution geophysical data over the northern Beringian margin in the summer of 1980 (Carlson and Karl, 1981). From these data, we developed a better understanding of the margin, and in particular the three large submarine canyons, Navarinsky, Pervenets, and Zhemchug Canyons (Plate 1 and Carlson and others, 1981). The data collected in 1980 also suggested the presence of another moderate-size canyon between Pervenets and Zhemchug Canyons. A second cruise, conducted in 1981 (Carlson and Karl, 1982) provided additional data on the northern Beringian margin that showed two canyon systems to be present between Pervenets and Zhemchug Canyons (Fischer and others, 1982).

The purpose of this paper is to describe, delineate and compare these newly-discovered submarine canyons. Included in the report are a detailed bathymetric map of the two canyon systems and sketches of seismic profiles showing the canyons and the subbottom units into which they were carved. We also speculate briefly on the mode and time of formation of these canyons.

Data Collection

Data used to develop "smooth sheets" are taken primarily from 3.5 kHz transducer records complimented by simultaneously collected airgun seismic profiles collected in 1980 and 1981 (Carlson and Karl, 1981, 1982). These data are supplemented by depth data from several other cruises (Marlow and Cooper, 1979, 1980; Scholl, Buffington, and Marlow, 1976; Scholl and Marlow, 1970). Navigational control was obtained from Loran C updated with satellite positions. Water depths for the Navarin study area were digitized assuming 1500 km/sec for speed of sound in water. Records were corrected for the hull-depth of transponder systems but no other corrections were made of the depth data.

MORPHOLOGY OF THE BERINGIAN CONTINENTAL MARGIN

Three physiographic provinces make up the Beringian continental margin. These are the flat, wide, continental shelf, the steep, rugged continental slope, and the gently sloping continental rise that extends from the base of the slope to the 3600-m isobath. Large submarine canyons deeply dissect the outer shelf and slope. Coalescing fans at the mouths of these canyons form part of the wedge of sediment of the continental rise. The continental shelf, one of the widest and flattest in the world, is about 450 km wide and has a gradient of 0.02° seaward of the Yukon River delta. By comparison, Shepard (1963) reported a world-wide average continental-shelf gradient of 0.12°. The continental slope begins at about the 150-m isobath and extends to a depth of about 2800 m. The width of the continental slope is about 50 km. The gradients of the Navarin slope range from 3° to 8° and even steeper gradients exist locally (Fischer and others, 1982). These slopes compare fairly well with the world-wide average gradient for continental slopes of about 4.3° (Shepard, 1963). The continental rise begins at the base of the slope at a depth of about 2800 m and extends to the 3600-m isobath that appears to mark the beginning of the abyssal plain. The average width of the rise is about 75 km and the gradients across the rise range from 0.5° to 1.8° (Fischer and others, 1982). Deep-sea channels cross the rise in the area of the canyon mouths and apparently are connected to the submarine canyons.

Descriptions of Newly Discovered Canyons

The Beringian continental slope between the Aleutian Island chain to the southeast and Cape Navarin, U.S.S.R. to the northwest, is dissected by seven large submarine canyon systems. They are from north to south Navarinsky, Pervenets, St. Matthew, Middle, Zhemchug, Pribilof and Bering Canyons Five of these canyons have been known for at least 17 years (Kotenev, 1965). The names of St. Matthew and Middle canyons are proposed for the two canyons that have just been discovered.

The name St. Matthew Canyon is taken from St. Matthew Island located about 300 km northeast of the canyon head. Middle Canyon is the name proposed for the other canyon system for two reasons: (1) it is the middle-most canyon of the seven large slope canyons and (2) it is located at a midway point on the continental slope between the Aleutian Islands to the southeast and the U.S.S.R., to the northwest.

A. St. Matthew Canyon system

This complex dendritic canyon system, consisting of two main branches, heads near the shelf break in about 140 m of water (Plate 1). The west thalweg trends southeast obliquely across the continental slope for about 65 km where it bends to the south and continues another 12 km where the canyon debouches onto a deep-sea fan at a depth of 3200 m. St. Matthew Canyon west has an average thalweg gradient of 2.5° and reaches a gradient of 3.3° over the steepest part of the canyon (Fig. E1; Table E1). Below 3200 m, as the canyon morphology changes to that of a deep-sea fan channel, the gradient changes to 0.4° and the channel extends at least another 55 km across the fan. Selected cross-canyon profiles show a V-shaped canyon that has maximum

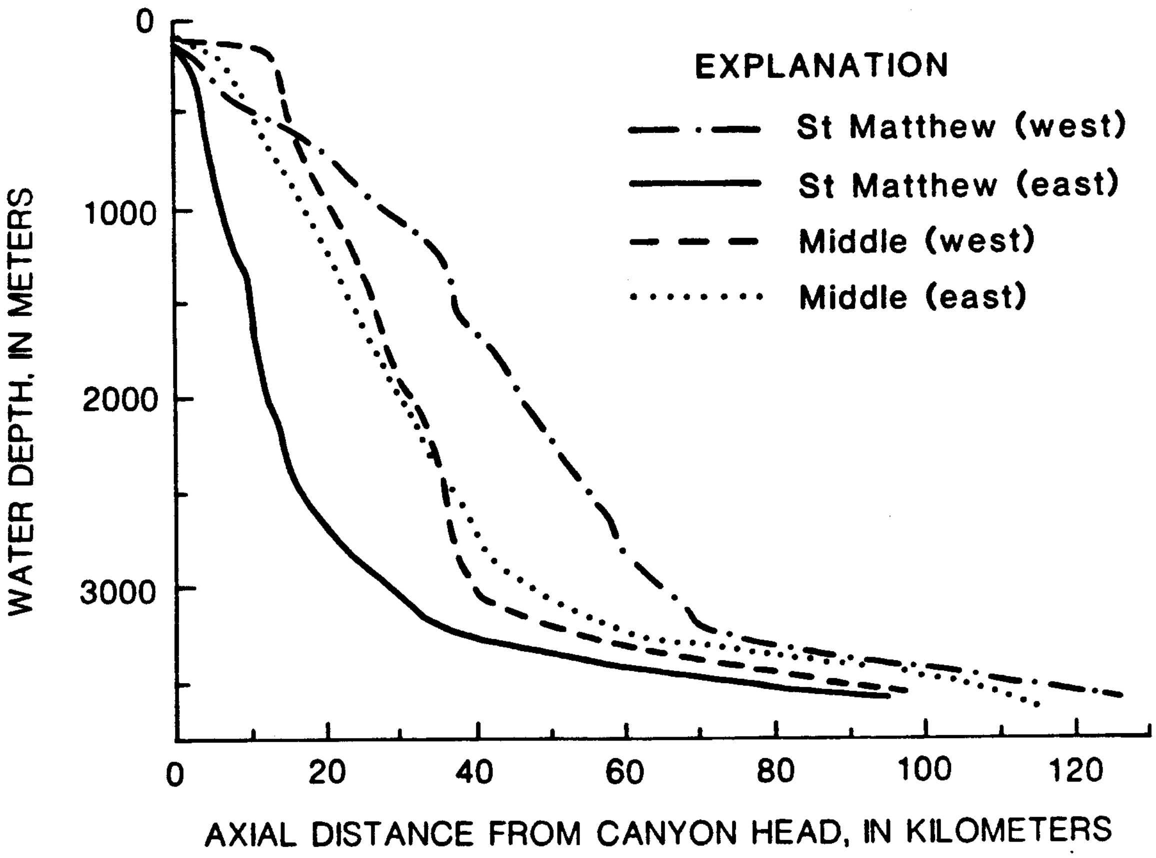

Figure E1. Thalweg profiles of main branches of St. Matthew and Middle Canyons.

Table E1. Principal Canyons and Fan Channels of the St. Matthew and Middle Systems

Canyon	Length(km)	Head(m)	Mouth(m)	Gradient	Steepest Gradient
St. Matthew					
West Branch	70	150	3000	2.5°	3.3°
East Branch	34	150	3000	5.1°	7.6°
Middle					
West Branch	40	130	3000	4.1°	6.4°
East Branch	60	140	3200	2.9°	4.3°
Fan Channel					
St. Matthew					
West Branch	55	3200	3600*	0.4°	
East Branch	64	3200	3600*	0.4°	
Middle					
West Branch	67	3000	3600*	0.5°	
East Branch	60	3200	3600*	0.4°	

* Marks extent of deepest contour; channel extends further onto fan. See Figure E3 for location of canyon systems.

relief of 2200 m on the northeast wall and 1250 m on the southwest wall (Fig. E2). The walls of the canyon have average declivities of 8.1°, ranging from as steep as 16° (profile G-H, northeast wall) to as gentle as 2° (profile O-P, east wall; Table E2a). The western branch of St. Matthew Canyon has at least nine tributaries (Fig. E3) that average 23 km in length and 5.2° in gradient, ranging in length from 6 to 42 km and in gradient from 8.5° to 2.9° (Table E3a).

The eastern branch of the St. Matthew Canyon system begins at a water depth of about 150 m and trends south-southwest for a distance of about 34 km where the canyon discharges onto a deep-sea fan at 3000 m (Plate 1). The average axial gradient of the eastern branch is about 5° and reaches a gradient of 7.6° over the steepest part of the canyon (Fig. E1; Table E1). The deep-sea channel that extends from the east branch canyon about 64 km across the fan to the 3600 m isobath, has a gradient of 0.4°. The eastern and western branches of the St. Matthew Canyon system merge on the fan at a depth of about 3600 m.

Selected cross-canyon profiles of the eastern branch of St. Matthew Canyon are much less V-shaped than those of the west branch and show maximum wall relief of 1100 m (Fig. E2b; Table E2b). The walls have average declivities of 8.2°, ranging from as steep as 16.7° (profile C-D, west wall) to as gentle as 1.1° (profile I-J, west wall). The east branch of St. Matthew Canyon has three good-sized tributaries that range in length from 26.5 to 30 km and in axial gradient from 2.3 to 4.8° (Table E3b).

B. Middle Canyon system

This complex canyon system consisting of two main branches and numerous tributaries (Plate 1), has a dendritic pattern similar to the St. Matthew system, but has approximately twice the areal extent. (St. Matthew = 3290 km^2 and Middle Canyon = 6620 km^2). The west branch of Middle Canyon, has cut a shallow valley about 20 km into the shelf. The west branch heads in 130 m of water and trends southerly across the slope about 40 km where it debouches onto a deep-sea fan at a water depth of 3000 m. The average thalweg gradient of the west branch of Middle Canyon is 4.1° and this thalweg attains a gradient of 6.4° over the steepest part of the canyon (Fig. E1; Table E1). The contiguous deep-sea fan channel extends at least 67 km across the fan at a gradient of 0.5°. Selected cross-canyon profiles are V-shaped on the slope and open up dramatically to broad channels (12-20 km wide) on the deep-sea fan (Fig. E4a). The canyon has a maximum relief of 1100 m on the west wall and 650 m on the east wall (Table E4a). The walls of the west branch canyon attain an apparent maximum steepness of 20.6° (east wall, profile C-D, Fig. E4a; Table E4a) and as low a gradient as 1.6° on the fan channel east wall (profile K-L). The walls have an average slope of 9.3°. The west branch of Middle Canyon has seven tributaries that join the canyon above a depth of 3200 m and four that merge with the fan channel between 3200 and 3600 m (Fig. E3). The longest of these eleven valleys measures 79 km (32 km above 3000 m) and the shortest is about 6 km in length (Table E5a). The gradients range from 11.3° for a slope tributary to 0.8° for a fan valley.

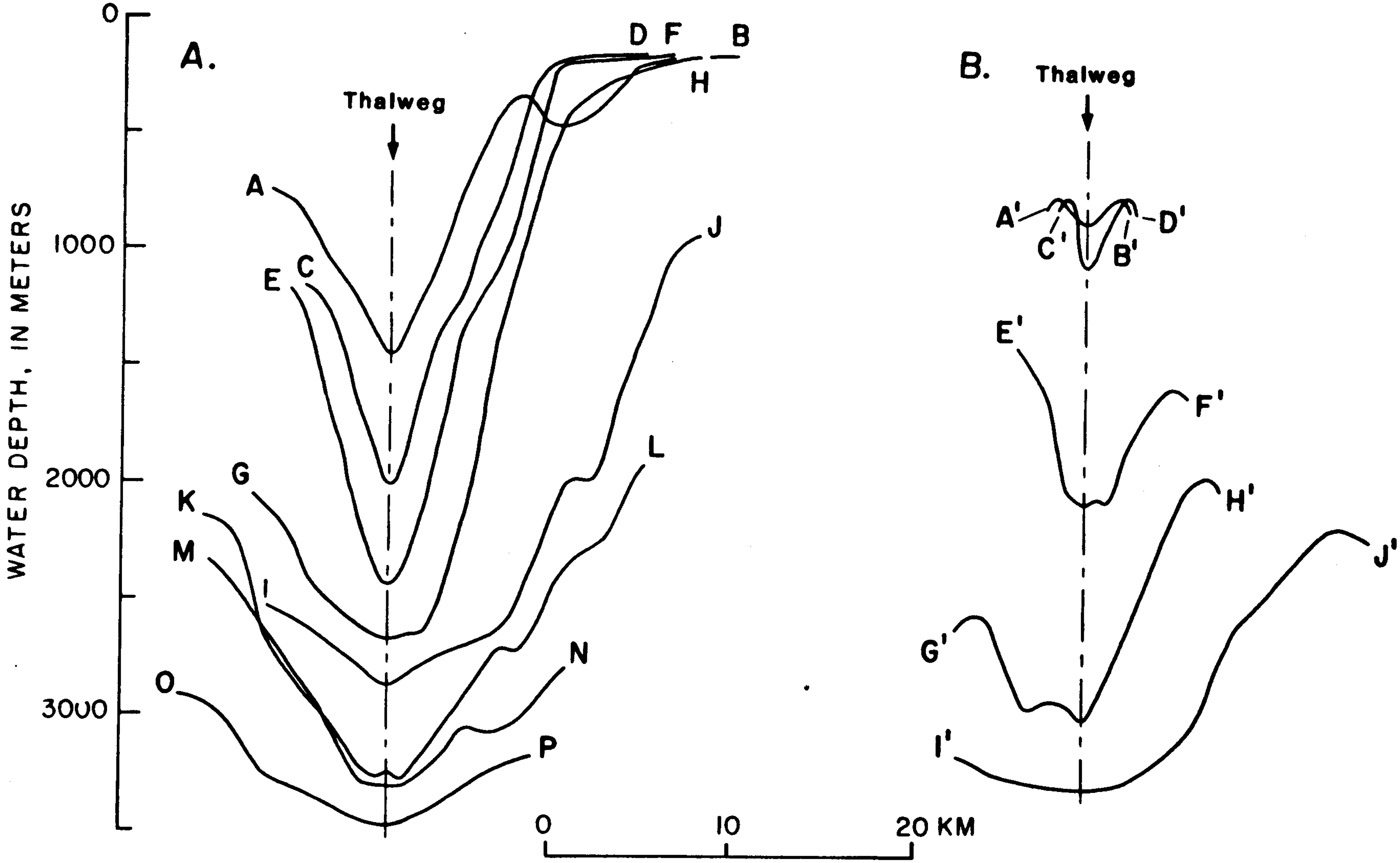

Figure E2. Transverse profiles of west (a) and east (b) branches of St. Matthew Canyon (see Fig. E3 for traverse locations).

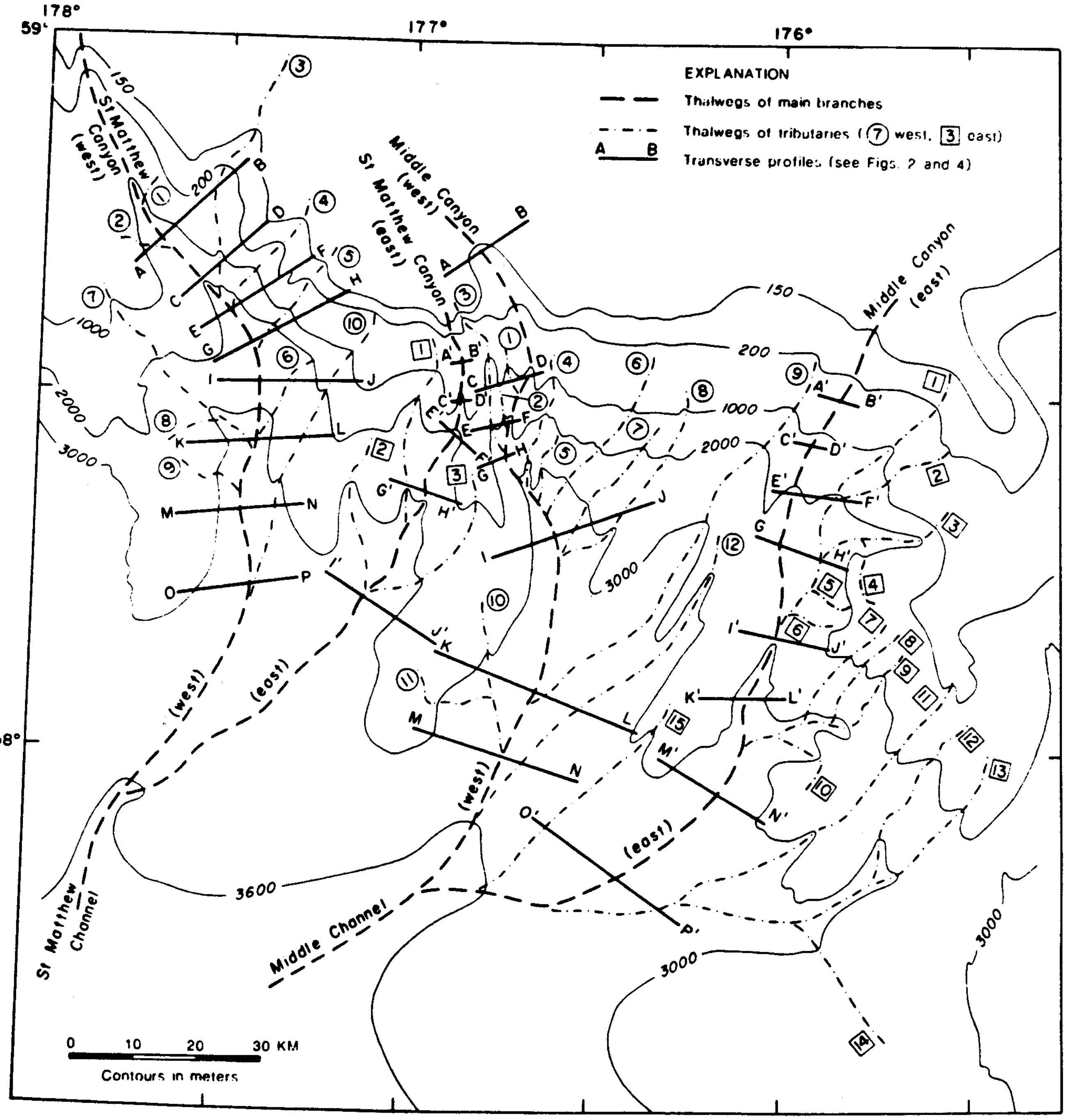

Figure E3. Map of St. Matthew and Middle Canyon systems, showing thalwegs of main branches and tributaries and locations of transverse profiles illustrated in Figures E2 and E4.

Table E2a. West Branch, St. Matthew Canyon wall gradients

Section*	Length(km)	Relief(m)	Gradient
A	5.1	650	7.3°
B	6.0	1050	10.0°
C	4.0	800	11.3°
D	8.2	1800	12.4°
E	5.0	1250	14.1°
F	8.3	2200	14.8°
G	7.6	400	3.0°
H	7.6	2200	16.1°
I	6.7	340	2.9°
J	9.5	1600	9.6°
K	7.0	1025	8.3°
L	12.3	1300	6.0°
M	8.0	800	5.7°
N	9.5	550	3.3°
O	9.0	450	2.9°
P	8.0	300	2.2°

Table E2b. East Branch, St. Matthew Canyon wall gradients

Section*	Length(km)	Relief(m)	Gradient
A'	1.5	100	3.8°
B'	1.5	100	3.8°
C'	1	300	16.7°
D'	2	300	8.5°
E'	3	650	12.2°
F'	3	500	9.5°
G'	2	400	11.3°
H'	5.5	1000	10.3°
I'	6.5	125	1.1°
J'	12	1100	5.2°

*Side of transverse profile from top of wall to thalweg of canyon. (See Fig. E3 for profile locations).

Table E3a. Tributaries of the west branch of St. Matthew Canyon system

West branch Tributaries	Length(km)	Head(m)	Mouth(m)	Gradient
1	6	200	1100	8.5°
2	8	800	1500	5.0°
3	42	140	2300	2.9°
4	22	140	2500	6.1°
5	20	140	2700	7.3°
6	16	2000	3200	4.3°
7	34	750	3200	4.1°
8	13	2200	3300	4.8°
9	14	2200	3350	4.7°
10	48	200	3500	3.9°
avg.	23.2			5.2°

Fan Channel	Length(km)	Head(m)	Mouth(m)	Gradient
8	3	3200	3300	1.9°
9	8	3200	3500	2.1°

Table E3b. Tributaries of the east branch of St. Matthew Canyon system

East branch Tributaries*	Length(km)	Head(m)	Mouth(m)	Gradient
1	29	600	3050	4.8°
2	26.5	2200	3250	2.3°
3	30	1600	3250	3.2°
avg.	28.5			3.4°

*See Figure E3 for locations of tributaries.

Table E4a. Wall gradients of the west branch of Middle Canyon

Section*	Length(km)	Relief(m)	Gradient
A	2	500	14.0°
B	2	500	14.0°
C	3	500	9.5°
D	1.2	450	20.6°
E	4	1100	15.4°
F	2	500	14.0°
G	6	850	8.1°
H	14	650	2.7°
I	8	1050	7.5°
J	16	450	1.6°
K	13	650	2.9°
L	10	300	1.7°
M	14.5	725	2.9°
N	12	350	1.7°

Table E4b. Wall gradients of the east branch of Middle Canyon

A'	3	125	2.4°
B'	5	125	2.0°
C'	2.5	125	2.9°
D'	3.5	125	2.0°
E'	3.5	150	2.5°
F'	3	125	2.4°
G'	3	450	8.5°
H'	2	725	19.9°
I'	4.5	450	5.7°
J'	7	850	6.9°
K'	5.5	700	7.3°
L'	6	450	4.3°
M'	10	500	2.9°
N'	7.5	300	2.3°
O'	3.5	125	2.0°
P'	6.0	125	1.2°

* Side of transverse profile from top of wall to thalweg of canyon. (See Fig. E3 for profile locations).

Table E5a. Tributaries of the west branch of Middle Canyon.

West branch Tributaries*	Length (Length to 300 m)	Head(m)	Mouth(m)	Gradient
1	6	800	1700	8.5°
2	6	1100	2300	11.3°
3	26	140	2650	5.5°
4	22	600	3025	6.3°
5	12	2200	3100	4.3 (7.6°)
6	33 (26)	200	3100	5.0 (6.2°)
7	26 (16)	1400	3200	4.0 (5.7°)
8	36 (26)	600	3200	4.1 (5.3°)
9	79 (32)	200	3425	2.3 (5.0°)
10	26 (9)	2200	3450	2.8 (5.1°)
11	17 (8)	2400	3400	3.4 (4.3°)
12	58 (4)	2800	3575	0.8 (2.9°)
avg.	29			4.9°

Fan Channels*	Length(km)	Head(m)	Mouth(m)	Gradient
5	6	3000	3100	1.0°
6	7	3000	3100	0.8°
7	10	3000	3200	1.1°
8	10	3000	3200	1.1°
9	47	3000	3425	0.5°
10	17	3000	3450	1.5°
11	9	3000	3400	2.5°
12	54	3000	3575	0.6°
avg.	15.1			1.2°

Table E5b. Tributaries of the east branch of Middle Canyon

Tributaries*	Length (length km to 3000 m)	Head(m)	Mouth(m)	Gradient
1	52	150	2900	3.2°
2	22	200	2100	4.9°
3	24	600	2700	5.0°
4	11	1400	2300	4.7°
5	8	2000	2850	6.1°
6	7	2400	2900	4.1°
7	23	1200	3050	4.6°
8	19	1200	3025	5.5°
9	32 (28)	1400	3225	3.3° (3.7°)
10	12.5	2700	3200	2.3°
11	77 (37)	1000	3450	2.5° (3.4°)
12	31	1200	3200	3.7°
13	84 (30)	1200	3475	1.6° (3.8°)
14	23 (19)	2000	3225	3.1° (3.6°)
15	40 (17)	2800	3600	1.2° (1.4°)
ave.	31			3.7°

Fan Channels	Length(km)	Head(m)	Mouth(m)	Gradient
9	4	3200	3225	0.4°
11	40	3200	3450	0.4°
13	54	3200	3475	0.3°
14	4	3200	3225	0.4°
15	23	3200	3600	1.0°
avg.	25			0.5°

* See Figure E3 for location of tributaries and fan channels.

The east branch of the Middle Canyon system is about the same size as the west branch and also has a complex dendritic "drainage" (Plate 1). The east branch begins at a water depth of 140 m and winds across the slope in a south-southeasterly direction for 60 km where it debouches onto a deep-sea fan at a depth of 3200 m. The east branch of Middle Canyon has an average axial gradient of 2.9° and reaches a gradient of at least 4.3° in the steepest part of the canyon (Fig. E1; Table E1). At 3200 m the axial gradient becomes greatly reduced resulting in an average gradient of 0.4° for the 60 km of channel to a depth of 3600 m. The east branch merges with the west branch of Middle Canyon at a depth of about 3600 m.

Transverse profiles of the east branch of Middle Canyon are less V-shaped than those of the west branch, coming closer in profile to the east branch of the St. Matthew Canyon system (compare Figs. E2b and E4b). The walls of the east branch of Middle Canyon show maximum relief of 850 m and range in steepness from 19.9° (profile C-D, east wall) to 1.2° (profile I-J, southeast wall of fan channel). The walls have an average slope of 6.5° (Table E4b). The east branch of Middle Canyon has six tributaries that join the main thalweg at about 3000 m and nine that join the east branch deep-sea channel between 3200 and 3600 m (Fig. E3). These tributaries have an average length of about 30 km and an average gradient of 3.7° (Table E5b). The six canyon tributaries range in length from 7 to 35 km and in gradient from 4.1° to 6.1°. The nine tributaries, that join the east branch of Middle Canyon below 3200 m, range in length from 12.5 to 84 km and in gradient from 1.2° to 5.5° (Table E5b). The gradients of these tributary valleys across the upper part of the deep-sea fan vary from 0.3° to 1.0°.

GEOPHYSICAL PROFILES AND SEAFLOOR SAMPLES

Several seismic reflection profiles (sound source: 2 - 40 in^3 airguns) were shot across the newly-discovered canyon systems (Carlson and Karl, 1981, 1982). Rocks were dredged from the walls of the two canyons (Jones and others, 1981; Marlow, pers. commun., 1982) and a total of 17 gravity cores (8.0 cm diameter) were collected from the two canyons and adjacent fans, six from the St. Matthew Canyon system and eleven from the Middle Canyon system (Karl and Carlson, 1982). Locations of these airgun profiles, dredges and gravity cores are shown in Figure #5.

Seismic-reflection profiles across both the St. Matthew and Middle Canyon systems show V-shaped gorges cut in layered sedimentary rocks. The reflectors that characterize the layered sedimentary sequences are sharply truncated at the canyon walls (Fig. #6). Hummocky, broken reflectors are present on some of the canyon walls and in some parts of the floor (Fig. 7).

A diapir-like feature has been found near the shelf-break adjacent to the southwest wall of St. Matthew Canyon (Fig. E8). A magnetometer record collected across this feature shows a 100 m gal anomally, suggesting that the feature could be related to some type of igneous intrusive. The effect of this diapir-like mass on the overlying 200+ meters of sedimentary material is a slight amount of doming of the strata. This diapiric feature does not appear to have had a noticeable effect on the west branch of St. Matthew Canyon.

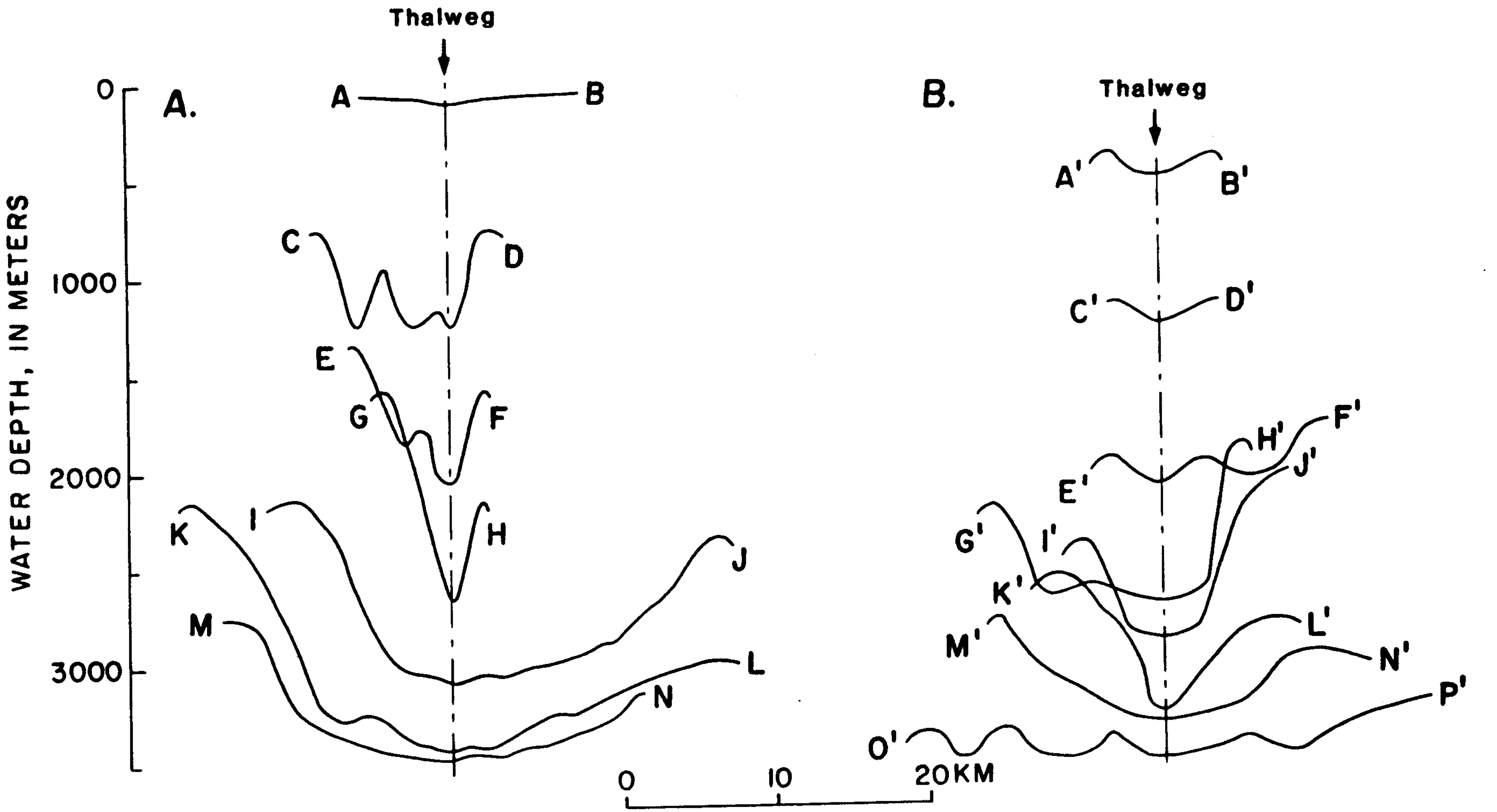

Figure E4. Transverse profiles of west (a) and east (b) branches of Middle Canyon (see Fig. E3 for transverse profiles).

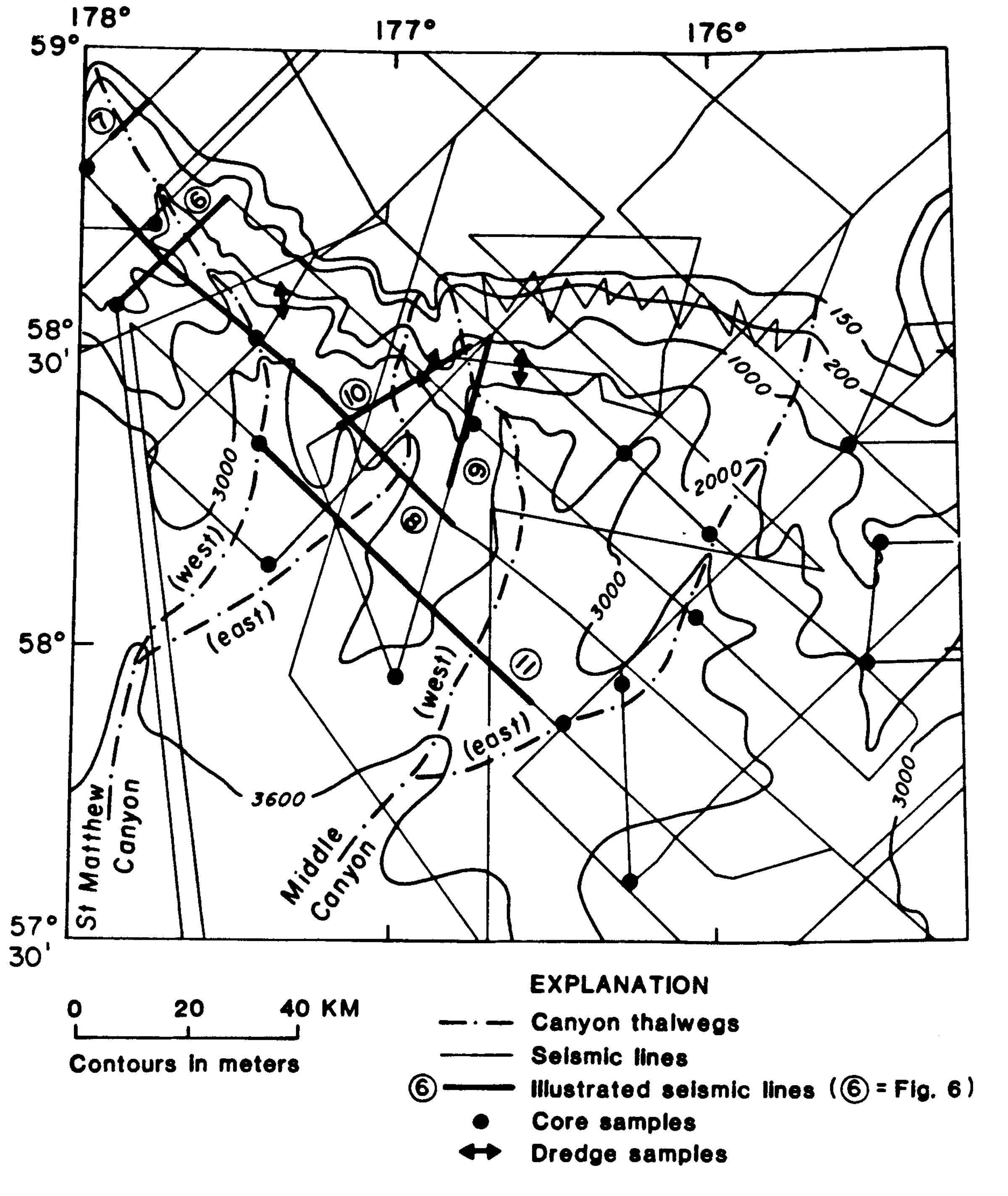

Figure E5. Map showing locations of core and dredge samples and seismic profiles, including illustrated line drawings.

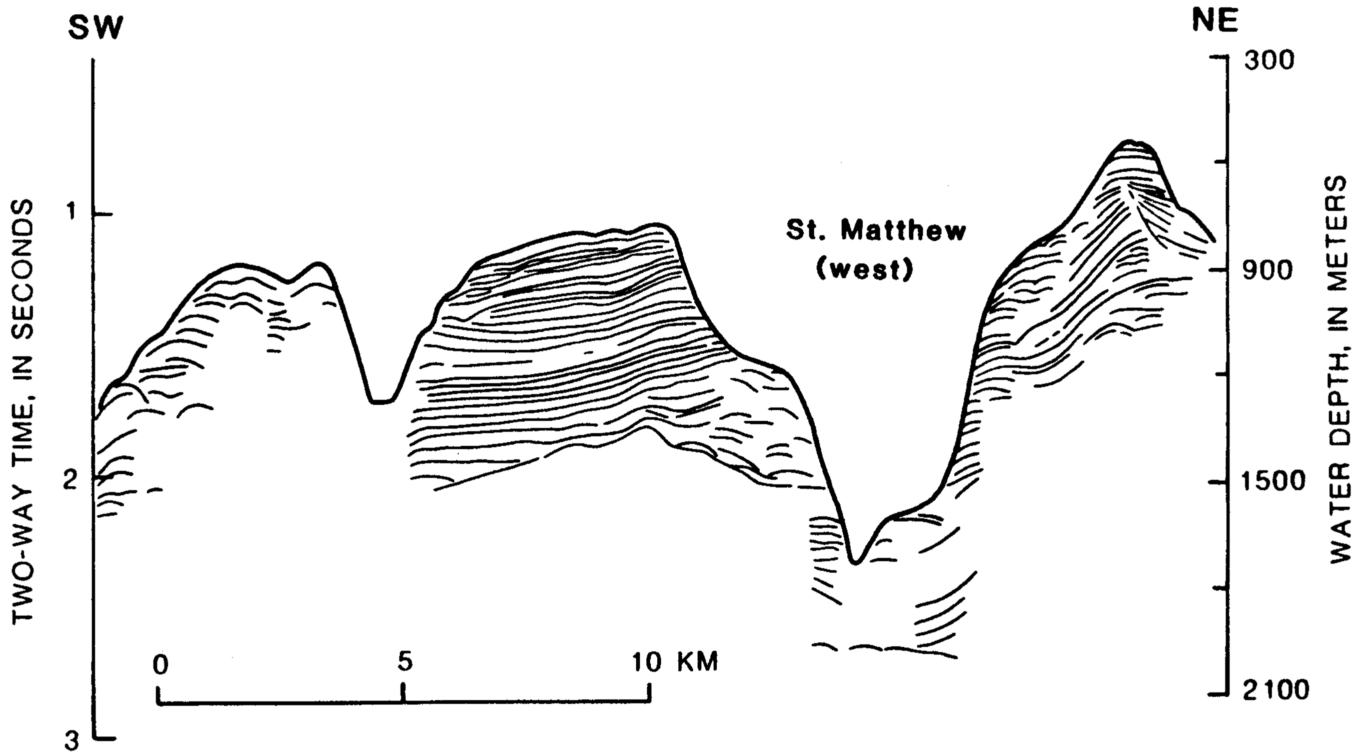

Figure E6. Interpretive line drawing of air-gun profile across west branch of St. Matthew Canyon (see Fig. E5 for location); Vertical exaggeration (V.E.) ~x7.

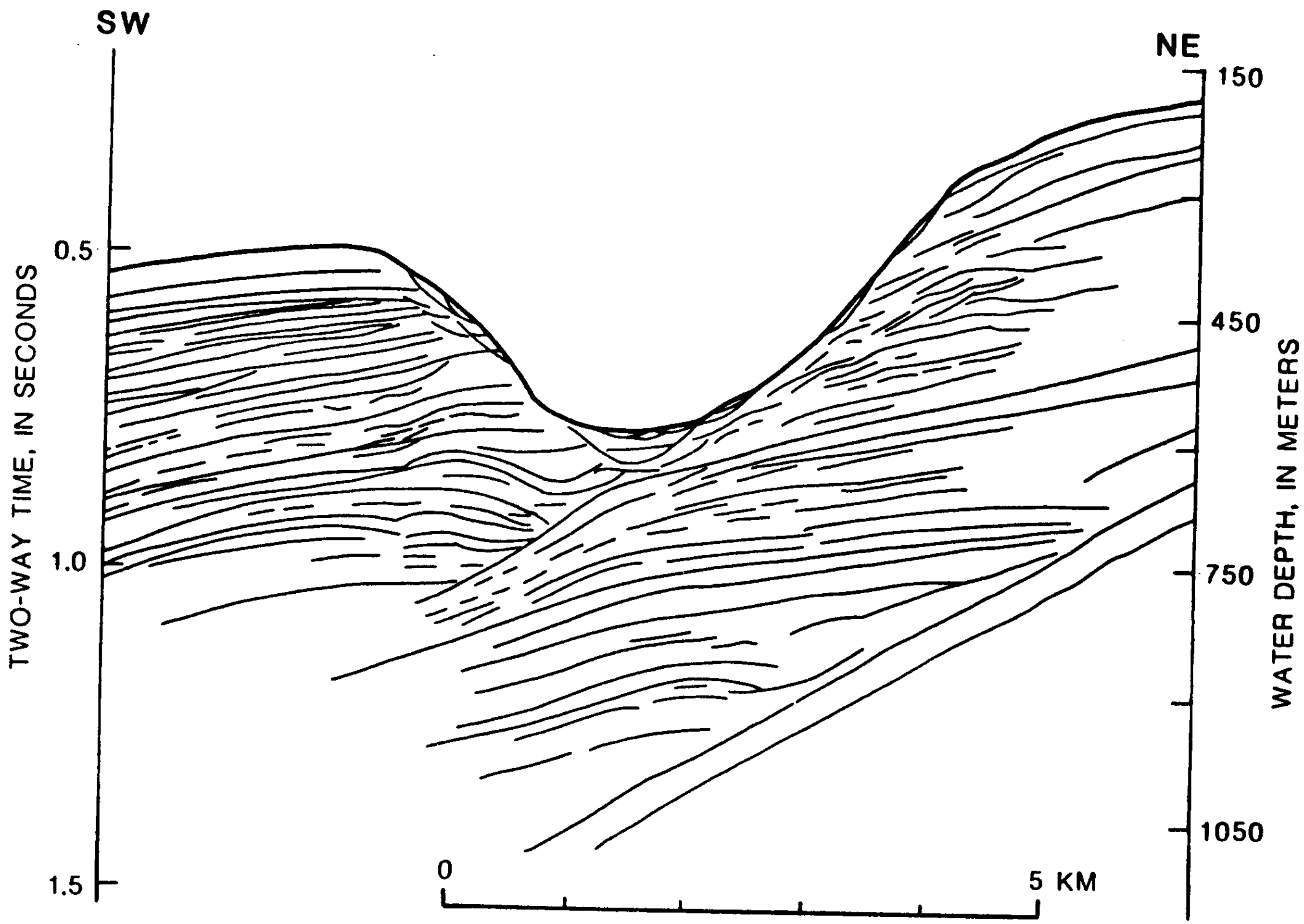

Figure E7. Interpretive line drawing of air-gun profile across west branch of St. Matthew Canyon (see Fig. E5 for location) (V.E. ~x7).

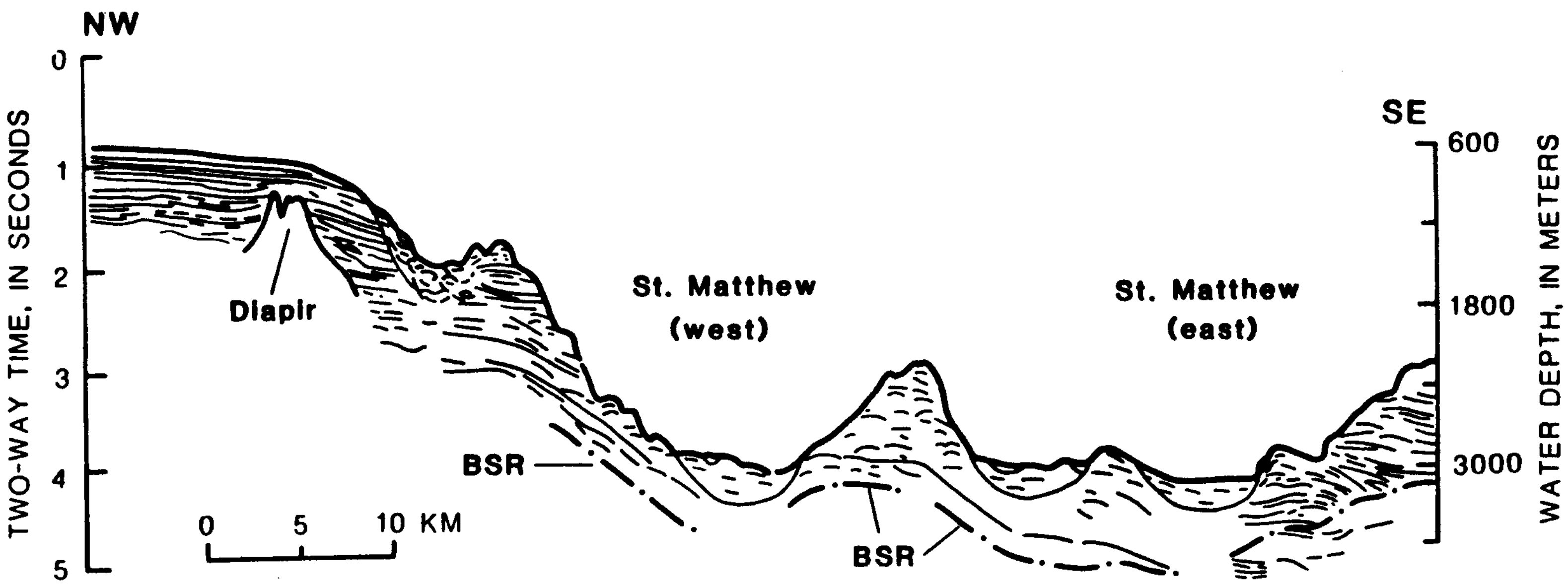

Figure E8. Interpretive line drawing of air-gun profile across west branch of St. Matthew Canyon (see Fig. E5 for location) (V.E. ~x7).

Several of the airgun profiles that were shot across the east and west branches of St. Matthew and the west branch of Middle Canyon (Fig. E9) show walls devoid of reflectors. In Middle Canyon, the opposite wall shows well-developed reflectors truncated by the canyon (Fig. #9). A dredge haul from the reflectorless wall of the east branch of St. Matthew Canyon (Fig. 10) yielded several pieces of basalt, one of which was dated by K-Ar methods to be at least as old as Eocene (Jones and others, 1981). A recent cruise of the R/V S.P. LEE (L-9-82) produced a dredge haul from the northeastern wall of the west branch of St. Matthew Canyon that yielded several igneous rocks ranging in type from basalt to dacite (M. Marlow, pers. commun., 1982). Other basalts and some tuffs were dredged from other areas on the Beringian margin (Jones and others, 1981).

Burrowed, moderately indurated mudstones dredged from the wall of the west branch of Middle Canyon, that contains well-bedded reflectors, were dated as Eocene using silicoflagellates and foraminifers (Jones and others, 1981). Other sedimentary rocks, principally burrowed mudstones and a few sandstones, dredged from the Beringian margin have ranged in age from Jurassic to Quaternary (Jones and others, 1981).

Gravity cores collected on the walls of the two canyon systems contain sediment that is primarily clayey silt and ranges in age from Pliocene to Holocene (Baldauf, 1981). This sediment is in many places draped over the older Tertiary mudstones.

Air-gun profiles across the fan channels show broad (10-15 km wide), flat valleys at the present seafloor underlain by buried channels that contain as much as 400 m of sedimentary fill (Fig. E11). Some of the deep-sea fan channel walls contain flat-lying reflectors and in other places the walls are characterized by jumbled and broken reflectors and hummocky morphology. Gravity cores (3-5 m length) collected from the floor of St. Matthew and other Navarin margin canyons and channels contain occasional thin sand or silt layers interlayered with the diatom-rich, clayey silt that pervades the Navarin margin (Baldauf, 1981). Some of these coarse layers are graded and many contain benthic foraminifers that are typically thought to be diagnostic of much shallower water (Quinterno, 1981; Carlson and others, 1982). Some of the canyon cores also contain sections of pebbly, sandy, mud and disrupted, contorted sediment that is primarily Quaternary in age (Baldauf, 1981).

DISCUSSION

Similarities in the two canyon systems

St. Matthew and Middle Canyon systems, although smaller than the five large canyons of the Beringian margin, are comparable in size to most of the submarine canyons that cut into the continental margin of the east coast of the United States, and are considerably larger than the canyons off southern California (Table E6).

The large Beringian margin canyons are cut back further into the shelf than are the St. Matthew and Middle Canyons and as a result have considerably lower axial gradients (Table E6). The very steep gradient of the east branch

Table E6. Comparison of canyons of the Beringian continental margin with canyons of the east and west coasts of the U.S. (Data for east and west coast canyons from Shepard and Dill, 1966)

East Coast Canyons	length (km)	gradient
Corsair	26	3.4°
Lydonia	30	2.3°
Gilbert	37	3.4°
Oceanographer	32	3.6°
Welker	50	2.1°
Hydrographer	50	2.1°
Hudson	92	1.3°
Wilmington	43	2.7°
Baltimore	52	1.9°
Washington	52	2.1°
Norfolk	70	2.0°
West Coast Canyons		
Astoria	115	1.0°
Eel	50	2.9°
Monterey	111	1.5°
Mugu	15	2.8°
Dume	5.6	5.5°
Redondo	15	2.2°
Scripps	2.7	5.5°
La Jolla	14	2.3°
Coronado	15	3.3°
Beringian Margin Canyons		
Navarinsky	270	0.5°
Pervenets	160	1.3°
St. Matthew	70	2.5°
Middle	40	4.1°
Zhemchug	125	0.8°
Pribilof	90	1.2°
Bering	875	0.2°

of St. Matthew Canyon, 5.1^{o} (Table E1), is steeper than most of the submarine canyons reported by Shepard and Dill (1966) and even steeper than the world wide average gradient of continental slopes (4.3°, Shepard, 1963). The east branch is cut into a slope that has an average gradient of about 6°. The west branch of Middle Canyon (thalweg gradient 4.1°) is also steeper than most of the world's submarine canyons. There are other similarities between St. Matthew and Middle Canyons in addition to their size and steepness. The west branch of each canyon makes an oblique traverse across the slope and the west branch of each is more V-shaped than the east branch. The two canyon systems apparently contribute to the build-up of one deep-sea fan; the fan channels appear to merge on the fan beyond the 3600 m isobath (Plate 1).

Both canyons are cut into Tertiary strata that ranges in age from Eocene to Pliocene. The principal rock type is a burrowed, moderately indurated mudstone. In many places throughout the Navarin province, this Tertiary mudstone is covered, probably disconformably, by several tens of meters of Pleistocene-Holocene unconsolidated sediment.

Sediment from the floor of both St. Matthew and Middle Canyon-fan-channel systems contains fine sand and silt layers interbedded with the normal diatom-rich mud. Many of these coarse layers are graded and many contain benthic foraminifers that are more typical of shallow water environments, suggesting emplacement by turbidity currents. The young ages of the sediment suggest that some turbidity current activity occurs from time to time even today. Several of the gravity cores also contain pebbly, sandy mud layers and some contain highly contorted, disrupted layers that indicate this material has slumped or slid to its present locality. The submarine sliding that is indicated by these coarse and contorted sediments very likely generates the turbidity currents. Both sliding and turbidity current activity can also be inferred from the seismic-reflection profiles we have obtained from these canyon-fan systems.

Differences between the two canyon systems

There are also several differences between the two canyons. Middle Canyon has the larger "drainage" area, has more tributaries, and has longer fan channels, whereas St. Matthew Canyon has the longest and shortest principal canyons.

Stratigraphically, the biggest difference between the canyons is the presence of an outcrop of Eocene basalt that forms part of the east wall of the east branch of St. Matthew Canyon. Basalt also has been dredged from the west branch of St. Matthew Canyon. In comparison, only sedimentary rocks have been dredged from the walls of Middle Canyon; however, additional dredging may show that the reflectorless wall of Middle Canyon (Figure E9) also contains basalt outcrops.

Genesis of the canyon systems

We subscribe to the hypothesis of Scholl and others (1976), that the large canyons of the Beringian margin were cut when lowered sea level exposed the Bering shelf to a depth of about 150 m and allowed large rivers such as

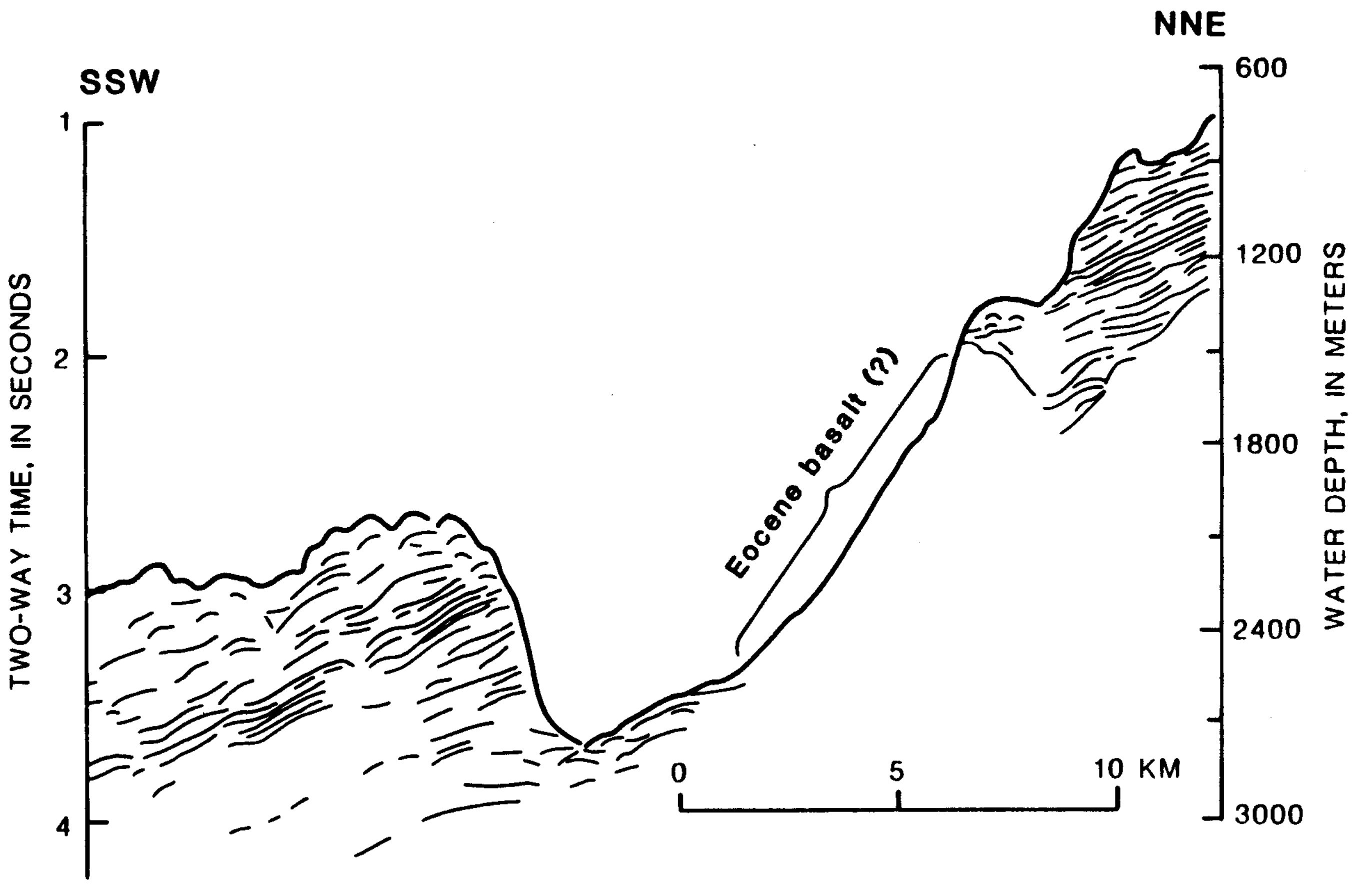

Figure E9. Interpretive line drawing of air-gun profile across west branch of St. Matthew Canyon (see Fig. E5 for location) (V.E. ~x7).

the Yukon and Anadyr to carry large amounts of sediment to the shelf edge. The most likely canyon-cutting agents were slumps and resulting turbidity currents supplemented by bioturbation of canyon walls and by erosional effects of canyon-focused waves and currents (Carlson and others, 1982).

We have deduced from seismic-reflection profiles and sediment-samples that similar processes appear to have been responsible for the carving of the St. Matthew and Middle Canyon systems. At question, however, is the reason for the much larger size of Navarinsky, Pervenets, and Zhemchug Canyons compared to St. Matthew and Middle Canyons. Perhaps the position of the canyons with respect to the major rivers (Anadyr and Yukon) that meandered across the flat Bering Shelf during Pleistocene and earlier low-stands of sea level was a key factor. If we look at a map of the Bering shelf (Plate 1 inset), we see that St. Matthew Island lies directly in line between the Yukon Delta and the heads of the St. Matthew and Middle Canyon systems. According to Patton and others (1976), St. Matthew Island is made up of some 500 m of subaerial volcanic rocks intruded by an early Tertiary age granodiorite. They suggest that the island is a southeastward extension of the Cretaceous-Early Tertiary volcanic arc that borders the Siberian Pacific margin. Perhaps this resistant island platform served as a deflector of the Yukon River as it meandered seaward across the broad shelf, thus inhibiting initiation of St. Matthew and Middle Canyons perhaps until the Pleistocene. Also the western edge of the large Navarin Basin, beneath the outer shelf and upper slope, is bordered by a northwestward trending basement high buried by 0.5 - 1.0 km of Cenozoic sediment (Marlow and others, 1976). This basement ridge would also result in restricted access of the large rivers to much of the area of the present continental slope until the basin was nearly full of sediment. Just as with any ridge system, the water gap is determined not only by low spots in the ridge but also by the presence of less-resistant or more faulted and fractured segments of the barrier. Compounding the problem, is the presence of basalt on the walls of at least St. Matthew Canyon and perhaps Middle Canyon. If this igneous rock is present as an elongate ridge parallel to the shelf-break, the cutting of these two-smaller canyons would indeed be retarded. However, igneous rocks also have been dredged from the walls of Zhemchug and Pervenets Canyons (Jones and others, 1981). Without further dredging we cannot assess the relative importance of the igneous rocks as to their influence on the rates of canyon cutting in any of the four canyons.

Our model of canyon development suggests that the large canyons began forming much earlier than did the St. Matthew and Middle Canyon systems. During low stands of sea level perhaps in the late Tertiary, the ancestral Yukon and Anadyr Rivers contributed to the development of the three large canyons. Geographically the Anadyr River seems most likely to have contributed to the formation of Navarinsky Canyon and the Yukon to Zhemchug Canyon. Pervenets Canyon could have been influenced by distributaries from either of the two major rivers. Proximity would suggest that distributaries of the Yukon River would be the most likely contributors to the St. Matthew and Middle Canyon systems.

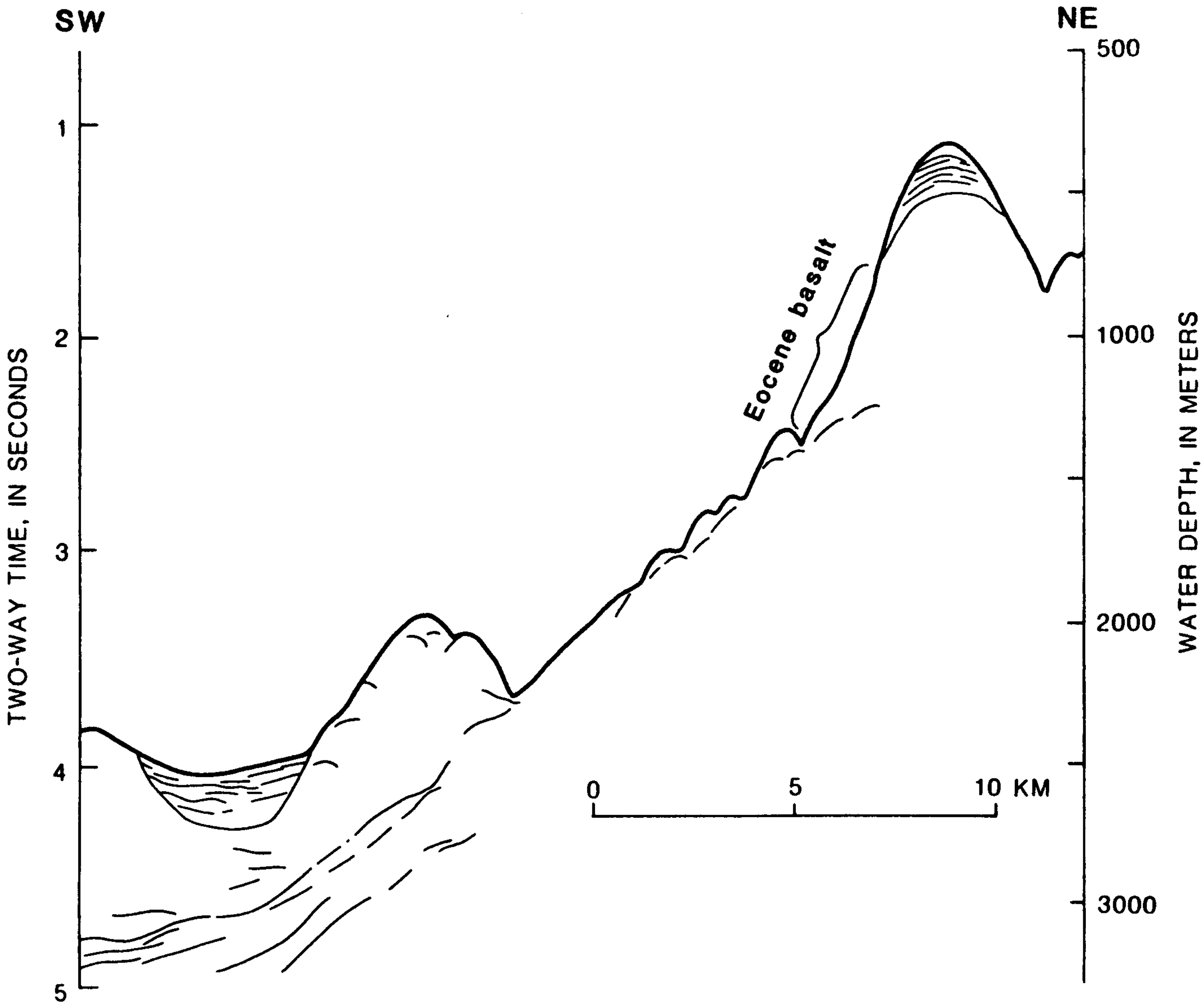

Figure E10. Interpretive line drawing of air-gun profile across west branch of St. Matthew Canyon (see Fig. E5 for location) (V.E. ~x7).

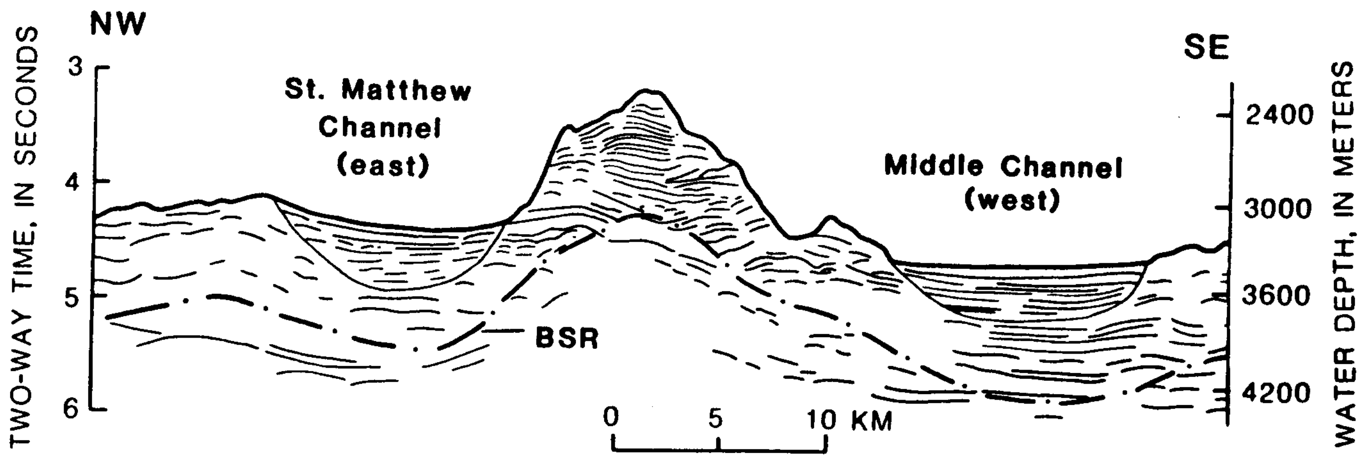

Figure E11. Interpretive line drawing of air-gun profile across west branch of St. Matthew Canyon (see Fig. E5 for location) (V.E. ~x7). (BSR = Bottom simulating reflector).

ACKNOWLEDGMENTS

We appreciate the assistance provided by the scientific personnel, the ship's captains and crew, and the marine logistics group. We thank Michael Marlow for a constructive review of the manuscript.

The cruises were supported jointly by the U.S. Geological Survey and by the Bureau of Land Management through interagency agreement with the National Oceanic and Atmospheric Administration, under which a multi-year environmental hazards study of the Alaskan continental shelf is managed by the OCSEAP office.

REFERENCES CITED

Baldauf, J. G., 1981, Diatom analysis of late Quaternary sediments from Navarin Basin province, Bering Sea, Alaska, in Carlson, P. R. and Karl, H. A., eds., Seafloor geologic hazards, sedimentology, and bathymetry: Navarin Basin province, northern Bering Sea: U.S. Geological Survey vey Open-File Report 81-1217, p. 100-113.

Carlson, P. R. and Karl, H. A., 1982, High-resolution seismic reflection profiles collected in 1981 in Navarin Basin province, Bering Sea: U.S. Geological Survey Open-File Report 82-786, 5 p., 1 map, scale 1:1,000,000.

Carlson, P. R., Karl, H. A., Johnson, K. A., and Fischer, J. M., 1981, Submarine canyons flanking Navarin Basin, Bering Sea, in: U.S. Geological Survey Circular 844, p. 139-141.

Carlson, P. R. and Karl, H. A., 1982, High-resolution seismic reflection profiles collected in 1981 in Navarin Basin province, Bering Sea: U. S. Geological Survey Open-File Report 82-786, 5 p., 1 map, scale 1:1,000,000.

Carlson, P. R., Karl, H. A., and Quinterno, P., 1982, Sedimentologic processes in world's largest submarine canyons, Bering Sea, Alaska: Geological Society of America, Abstracts with Programs, v. 15, p. 459-460.

Fischer, J. M., Carlson, P. R., and Karl, H. A., 1982, Bathymetric map of Navarin basin province, northern Bering Sea: U. S. Geological Survey Open-File Report 82-1038, 11 p., 1 map, scale 1:1,000,000.

Jones, D. M., Kingston, M. J., Marlow, M. S., Cooper, A. K., Barron, J. A., Wingate, F. H., and Arnal, R. E., 1981, Age, mineralogy, physical properties, and geochemistry of dredge samples from the Bering Sea continental margin: U. S. Geological Survey Open-File Report 81-1297, 68 p.

Karl, H. A. and Carlson, P. R., 1982, Location and description of sediment samples: Navarin Basin province, Bering Sea, 1980-81: U. S. Geological Survey Open-File Report 82-958, 5 p., 2 map sheets, scale 1:1,000,000.

Kotenev, B. N., 1965, Submarine valleys in the zone of the continental slope in the Bering Sea: All-Union Research Inst. of Marine Fisheries and Oceanography. Transactions, v. 58, p. 35-44. (U. S. Navy Electronics Lab., San Diego, CA., NEL Translation 112).

Marlow, M. S. and Cooper, A. K., 1979, Multichannel seismic reflection profiles collected in 1977 in the southern Bering Sea shelf: U.S. Geological Survey Open-File Report 79-1147.

Marlow, M. S. and Cooper, A. K., 1980, Multichannel seismic reflection profiles collected in 1976 in the southern Bering Sea shelf: U.S. Geological Survey Open-File Report 80-389.

Marlow, M. S., Cooper, A. K., and Childs, J. R., in press, Tectonic evolution of the Gulf of Anadyr and formation of Anadyr and Navarin basins: Bulletin of the American Association of Petroleum Geologists.

Marlow, M. S., Scholl, D. W., Cooper, A. K., and Buffington, E. C., 1976, Structure and evolution of Bering Sea shelf south of St. Lawrence Island: Bulletin of the American Association of Petroleum Geologists, v. 60, no. 1, p. 161-183.

Patton, W. W., Lanphere, M. A., Miller, T. P., and Scott, R. A., 1976, Age and tectonic significance of volcanic rocks on St. Matthew Island, Bering Sea, Alaska: U. S. Geological Survey J. of Research, v. 4, p. 67-73.

Quinterno, P. J., 1981, Preliminary report on benthic foraminifers from Navarin Basin province, Bering Sea, Alaska, in Carlson, P. R. and Karl, H. A. eds., Seafloor geologic hazards, sedimentology, and bathymetry: Navarin Basin province, northwestern Bering Sea: U. S. Geological Survey Open-File Report 81-1217, p. 114-129.

Scholl, D. W. and Marlow, M. S., 1970, Bering Sea region seismic reflection profiles, 1969: U. S. Geological Survey Open-File Report.

Scholl, D. W., Buffington, E. C., and Marlow, M. S., 1976, Aleutian-Bering Sea regional seismic reflection profiles: U. S. Geological Survey Open-File Report 76-748.

Shepard, F. P., 1963, Submarine geology, 2nd ed.: Harper and Row, New York, 557 p.

Shepard, F. P. and Dill, R. F., 1966, Submarine Canyons and other sea valleys: Rand McNally and Co., Chicago, 381 p.

APPENDIX F:

GEOLOGIC HAZARDS IN NAVARIN BASIN PROVINCE,
NORTH BERING SEA

by

Paul R. Carlson, Herman A. Karl,
Jeffrey M. Fischer, and Brian D. Edwards

U.S. Geological Survey

OTC 4172

Geologic Hazards in Navarin Basin Province, Northern Bering Sea

by Paul R. Carlson, Herman A. Karl, Jeffrey M. Fischer, and Brian D. Edwards, *U.S. Geological Survey*

ABSTRACT

Navarin Basin, scheduled for leasing in 1984 (OCS sale 83), may contain vast accumulations of oil and gas. Several geologic and oceanographic processes that may be active in and around Navarin Basin province could be hazardous to commercial development. These potential hazards include submarine slides; sea-floor instability resulting from disturbance of gas-charged sediment; sediment transport and erosion caused by storm waves, tsunamis, internal waves, or bottom currents; pack ice; and active faults and ground motion.

INTRODUCTION

The quest for energy independence by the United States includes exploration of new segments of the outer continental shelf. The Navarin Basin lease sale (OCS sale 83) is scheduled for the spring of 1984. The study area, hereafter referred to as the "Navarin Basin province," is located on the outer continental shelf and upper slope in the northern Bering Sea (Fig. F1). The area is bounded on the northwest by the U.S.-U.S.S.R. convention line of 1867 and on the southwest by the base of the continental slope; it extends to within 100 km of St. Matthew Island to the northeast and of St. Paul Island to the southeast. This region potentially contains commercially exploitable accumulations of oil and gas, and it is likely to be the subject of intensive exploration. The purpose of this paper is to delineate, describe, and assess potential geologic hazards on the sea floor in the Navarin Basin province that must be considered in the design of offshore facilities.

Data Collection

The principal sources of data for this study have been seismic-reflection profiles and sediment samples collected in 1980 and 1981 on the R/V Discoverer (Carlson and Karl, 1981). The seismic-reflection systems used included two 40-in^3 airguns, an 800-J minisparker, and a 3.5-kHz transducer as acoustic sources. Spacing between geophysical tracklines over this immense area averages about 15 km; sea-floor geological samples were taken at intersections of track lines and at selected geologically significant sites. Navigational control was LORAN C updated with satellite positioning.

Shear-strength measurements were made on selected cores by means of a motorized Wykeham-Farrance* miniature-vane shear device. Tests were made at 20-cm intervals on core segments that had been split longitudinally. Immediately following strength testing, water-content and bulk-density subsamples were obtained at the locations of the vane tests. Consolidation analyses were performed on selected cores.

Additional data collected in 1980 from the USCG Polar Star and the R/V S.P. LEE were incorporated into our data base as were seismic-reflection records collected over the past 15 years by the U.S.Geological Survey for resource evaluation (Marlow and others, 1981). Other sources of data include studies by scientists from the Universities of Washington and Alaska, and from Russia, and Japan (e.g. Knebel, 1972; Sharma, 1979; Lisitsyn, 1966; Takenouti and Ohtani, 1974).

MORPHOLOGY OF NAVARIN BASIN PROVINCE

Three physiographic provinces comprise the Navarin study area. These are the flat, wide, continental shelf; the steep, rugged continental slope, and the continental rise that extends from the base of the slope to the 3600-m isobath. Three large submarine canyons deeply dissect the outer shelf and slope (Fig. F2). Coalescing fans at the mouths of these canyons form part of the wedge of sediment of the continental rise.

Shelf

The Bering Sea continental shelf, one of the widest and flattest in the world, is about 700 km wide and has a gradient of 0.02° seaward of the Yukon River delta. By comparison, Shepard (1963) reported a world wide average continental-shelf gradient of 0.12°. The part of the Bering shelf that includes the Navarin Basin province lies between the 100-m and 150-m isobaths and ranges in width from about 120 km in the

*Use of trade names is for descriptive purposes only and does not constitute endorsement by the U.S. Geological Survey.

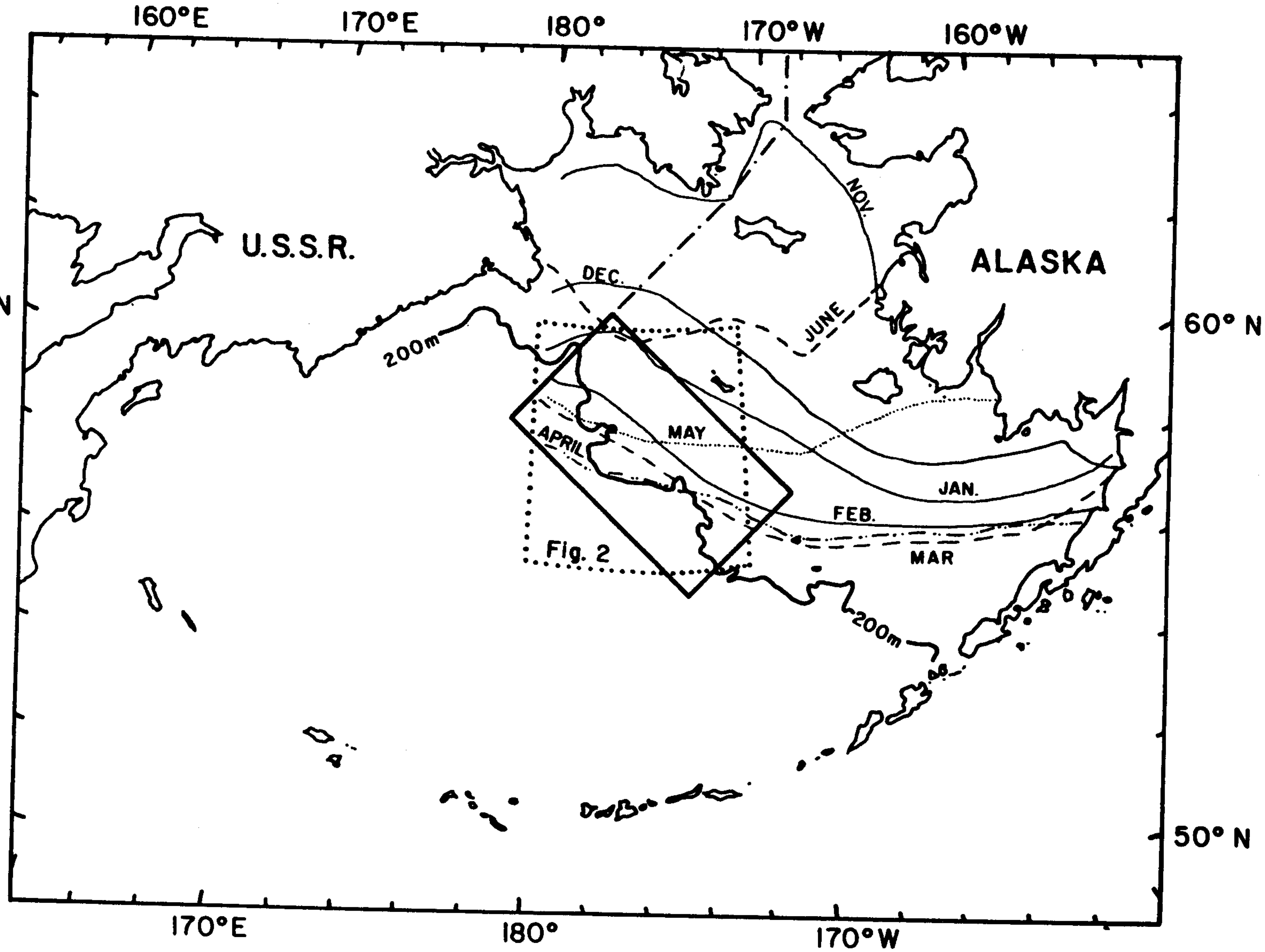

Fig. F1 — Location of Navarin Basin province (outlined) and lines of average monthly ice-front positions (after Webster, 1979); ice positions for the 15th of month

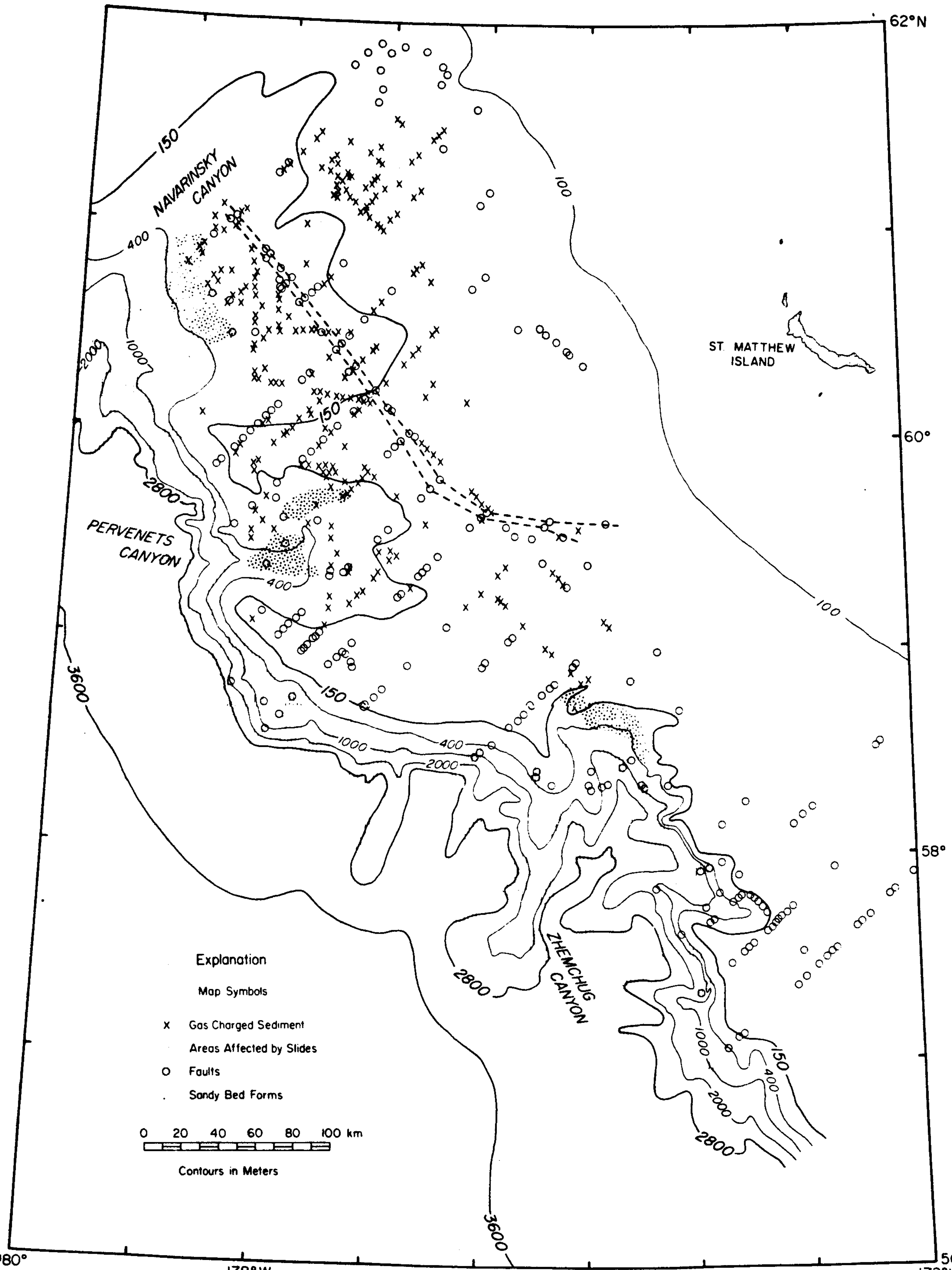

Fig. F2 — Preliminary map of sea-floor geologic hazards in Navarin Basin province northern and southern parts of the study area to a maximum of about 235 km in the central part (Fig. F2). These boundaries define an area of about 100,000 km^2. Although the outer continental shelf is cut by three massive submarine canyons, there are no apparent morphologic expressions of these canyons landward of the 125-m isobath.

Slope

The continental slope that forms the southeastern boundary of the Navarin Basin province begins at the 150-m isobath and extends to a depth of 2800 m (Fig. F2). The width of the continental slope ranges from 47 km in the middle of the province to 19 km south of Zhemchug Canyon. The slope includes an area of about 47,000 km^2. The gradients of the Navarin slope range from 3° to 8° with even steeper gradients locally. This compares with the world wide average gradient for continental slopes of about 4.3° (Shepard, 1963).

Submarine Canyons

The three major submarine canyons that cut deeply into the Bering continental margin head in water depths less than 140 m (Fig. F2). Extensive deep-sea fans have developed at the mouths of the canyons in water depths of about 3000 m. Navarinsky is the longest canyon (340 km), Pervenets the shortest (125 km), and Zhemchug is intermediate in length (240 km). Both Navarinsky and Zhemchug Canyons are about 100 km wide at the shelf break, but the smaller Pervenets Canyon is only 30 km wide there. Local wall relief of the three canyons at the shelf break ranges from 700 m in Navarin and 800 m in Pervenets, to a spectacular 2600 m in Zhemchug. Each of the three canyons consists of two main branches or tributaries on the landward side of the shelf break. The two tributaries of Zhemchug Canyon trend 180° away from each other, forming a large trough-shaped basin. All three canyons are incised into Neogene and older, more lithified Paleogene rocks, principally mudstones, that are thought to make up much of Navarin Basin (Marlow and others, 1976). The shapes of the canyons, especially of Zhemchug, are apparently controlled by structures as old as Paleogene (Scholl and others, 1975). The major cutting of the canyons probably occurred when glacio-eustatically lowered sea levels exposed most of the Bering shelf.

Rise

The continental rise begins at the base of the slope at a depth of about 2800 m and extends to the 3600-m isobath that marks the beginning of the abyssal plain (Fig. F2). The average width of the rise is about 75 km, ranging from 25 km northwest of Zhemchug Canyon to more than 100 km adjacent to the mouths of the three large canyons. The rise encompasses an area of 40,000 km^2. The gradients across the rise range from 0.5° to 1.8°. Deep-sea channels cross the rise in the area of the canyon mouths and apparently are connected to the submarine canyons. Gravity cores collected near the mouths of the canyons and on the adjacent rise contain sand lenses that suggest their deposition by turbidity currents.

SEA-FLOOR GEOLOGIC HAZARDS

Potential geologic hazards in the Navarin Basin province include sea-floor instability marked by submarine slides, sediment transport and erosion, and subsidence or blowouts resulting from the disturbance of gas-charged sediment; ice; and faulting with attendant ground shaking (Fig. F2).

SEAFLOOR INSTABILITY

Within the broad category of sea-floor instability, we have included discussions of three major types: submarine sliding, sediment transport and erosion, and gas-charged sediment. Liquefaction of saturated sands is another possible cause of sediment instability (Seed and Lee, 1966), but at this time we have insufficient data to assess the liquefaction potential of Navarin shelf sediment.

Submarine Sediment Slides

Submarine slide is used as an all-inclusive term for a variety of slope movements. The preliminary nature of our study makes it impractical at this time to attempt to classify each of the areas according to type of movement and type of material. Many of the submarine slides have been found in association with the large submarine canyons that are cut into the continental margin (Fig. F2).

Because of the wide spacing between tracklines, we can not correlate slide masses from line to line. None of the slides begin in water shallower than 150 m, several head below 400 m, and one appears to originate at a depth of greater than 1200 m. Some of the zones affected by down-slope movement are 50 km in length and some appear to be 25 km wide. Composite slides may affect the upper 200-300 m of the sediment column (Fig. F3). Gravity cores (2-5m in length) were collected from a few of the slide masses. These cores recovered a variety of sediment types, from pebbly mud to sandy mud to very soft mud. Preliminary evaluation of the morphology and internal reflectors observed on seismic profiles that cross the outer continental shelf and slope suggest that the slides include slumps, debris-flow deposits, and mud-flow deposits according to the classification used by Nardin and others, (1979). The causes of these failures are unknown, but likely are related to seismic ground accelerations. The build-up of pore-water pressures with attendant decrease in shear strength that results from seismic shaking and the reduction of shear strength that accompanies build-up of bubble-phase gas can both contribute to sediment instability (Hampton and others, 1978). Considering the sedimentation rates in the area (1-25 cm/10^3 yr; Askren, 1972; Blunt and Kvenvolden, 1981), the coefficients of consolidation, and the overconsolidation ratios (Table F1) and using Gibson's equations (1958), it appears unlikely that the sediment is significantly underconsolidated. However, if the observed failures are Pleistocene in age and sedimentation rates were significantly higher at that time, underconsolidation may be a relatively more important factor. Instability due to the strength reduction caused by the cyclic loading that is associated with storm waves, internal waves, or tsunamis is minimal at the water depths (200 to 1200 m) in which the slide deposits are observed (see Seed and Rahman, 1978).

Sediment Transport and Erosion

Large Bedforms

Large sediment waves have been found at the heads of Zhemchug, Pervenets, and Navarinsky Submarine

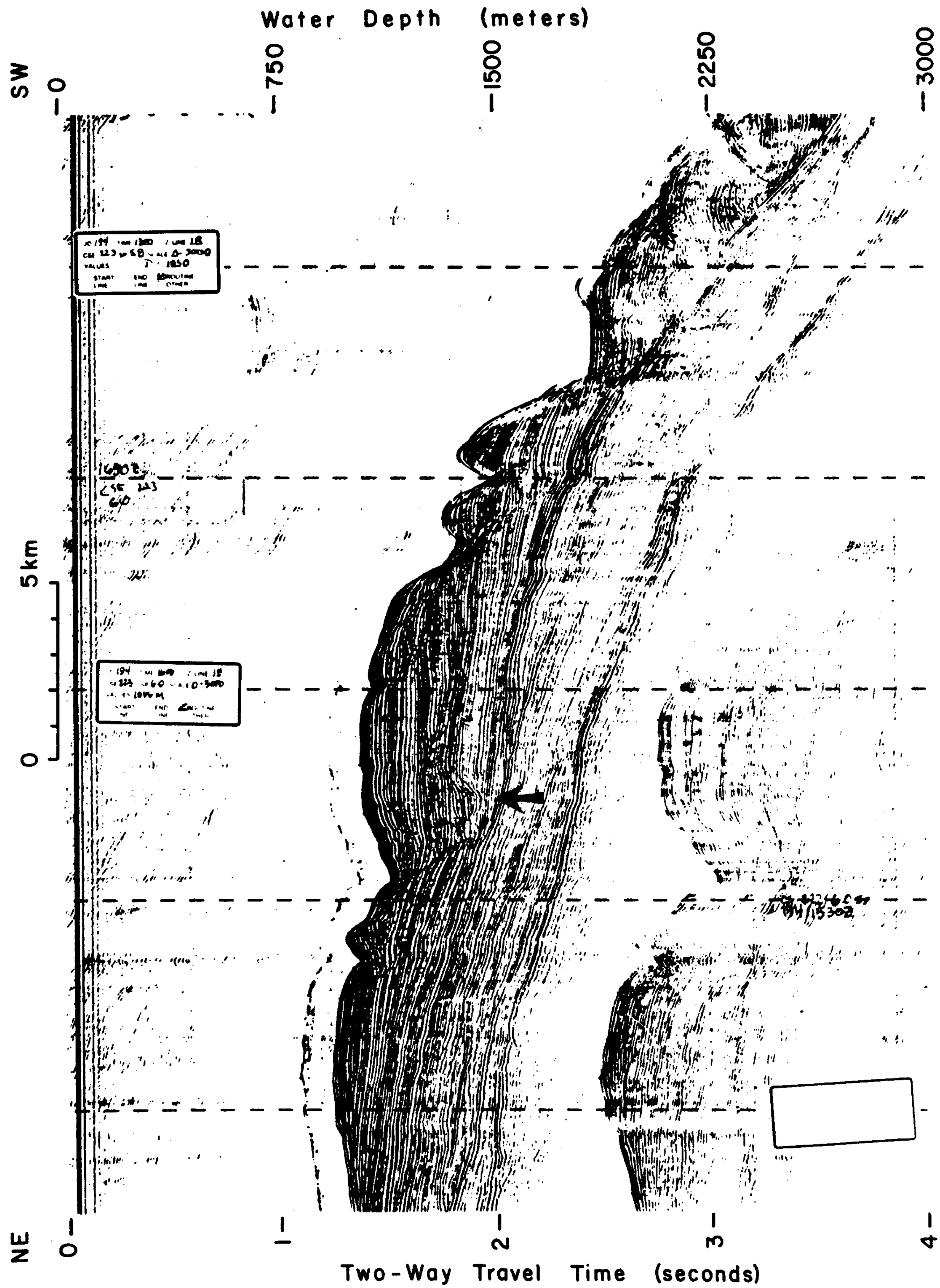

Fig. F3 — Air-gun profile showing slides in Navarinsky Canyon. Note buried channel (arrow) and associated cut-and-fill structures (V.E. ~x10).

Canyons (Fig. F2). The sediment waves in these areas are alike. Those at the head of Navarinsky Canyon have been studied in the greatest detail. These large bedforms occur on a substrate of silty, very fine sand within a 600 to 700 km^2 area between the 215- and 450-m isobaths. Crests of these bedforms trend approximately north-south; the waves have an average length of about 600 m, an average height of about 8 m, and a maximum height of 15 m (Fig. F4). Both symmetrical (the more common) and asymmetrical waves have been observed. The bedforms not only are expressed at the surface, but also are remarkably well defined in the subsurface. The stratigraphic unit containing the sediment waves developed over a flat-lying reflector, and it attains a maximum thickness of about 120 m in the sediment wave field. In a few places, the bedforms are covered by a thin layer of apparently younger sediment. One such locality occurs at the head of Pervenets Canyon, where the buried sediment waves are part of an intricate stratigraphic complex that lies below a unit of parallel-bedded reflectors (Fig. F5). The parallel-bedded unit is generally about 20 m thick, but it ranges in thickness from less than 5 m to about 110 m. If the sea-floor features are active, they, as well as the processes responsible for them, could represent hazards.

Surface Waves

Currents generated by surface waves probably are a more significant factor in the transport of silt and larger size particles on the open slope and shelf of Navarin Basin than, for example, tidal currents or the mean circulation. Bottom currents have not been measured in the study area, nor have there been good observations of surface waves. However, some surface-wave data have been compiled in areas adjacent to and including a part of the eastern boundary of the lease sale area (Brower and others, 1977).

Storms, and consequently storm-generated waves, are strongest and most frequent during the fall and winter (Litsitsyn, 1966; Brower and others, 1977). Waves as high as 15 m and with possible periods of 9 to 11 s have been observed east of the lease area (Brower and others, 1977). Waves with these heights and periods do not generate bottom currents of a strength sufficient to erode sediments over a large part of the shelf. For example, assuming a threshold value of 10 cm/s for transporting fine sand (Komar and others, 1972), an 11-s, 15-m-high wave generates currents strong enough to erode fine sand and smaller grains only in water shallower than about 135 m. A lower, but longer period wave, for example a wave 10 m high with a 15-s period, produces near-bottom currents greater than 10 cm/s in water as deep as 208 m. Extreme waves, empirically estimated to be as large as 42.5 m high, occur on the average once every 100 years in the Navarin area (Brower and others, 1977).

Gas-charged sediment

Gas-charged sediment can have a lower shear strength and bearing capacity than does equivalent gas-free sediment (Nelson and others, 1978; Whelan and others, 1976). An increase in the concentration of free or bubble-phase gas results in an increase of pore pressure and a concomitant decrease in shear strength until failure can occur. Such increases in bubble-phase gas can result from drilling into gas-charged sediment or disruption of the sediment by cyclic loading, and they may lead to the failure of pipelines or platforms (U.S. Geological Survey, 1977).

The numerous areas of gas-charged sediment mapped in Navarin Basin (Fig. F2) are identifiable on the high-resolution seismic-reflection profiles by acoustic anomalies such as displaced reflectors and "wipe out" zones (Fig. F6). These anomalies are prevalent in the upper 50 to 100 m of sediment. Commonly these shallow anomalies coincide closely with well-developed "bright spots" that appear to occur deeper in the section on multi-channel or medium-resolution single-channel profiles.

Gravity cores collected throughout the basin province were analyzed for hydrocarbons (methane through butanes) (Vogel and Kvenvolden, 1981). All of the cores sampled contained hydrocarbon gases, but none showed significant amounts of thermogenic hydrocarbons. Most of the hydrocarbon ratios can be attributed to microbial activity. Three cores, two from the shelf and one from the slope, contained concentrations of methane (5 to 9 times) and ethane (10 to 20 times) higher than background values (Vogel and others, 1981). These cores also contained ratios of ethane to ethene and of methane to ethane and propane that marginally suggest the presence of some thermogenic hydrocarbons. Possible explanations for the low concentrations of hydrocarbons include the short length of the cores (i.e., <6 m; most of the cores collected on the shelf were <2 m long) and the exceedingly spotty areal concentrations of the hydrocarbons.

Geotechnical properties of Navarin Basin sediment

Cores from 68 stations were tested to define geotechnical variables useful in describing regional changes in Navarin Basin sediment properties. Shelf sediment (<150 m water depth) typically has a peak shear strength (S_v) that ranges between 10 and 15 kPa at 1 m subbottom (1 psi = 6.9 kPa) (Fig. F7). An elongate zone of weaker sediment (shear strength <10 kPa) extends into the central part of the study area from the north and reflects the presence of a tongue of fine-grained, high-water-content sediment (Karl and others, 1981). A zone of stronger sediment (shear strength > 15 kPa) exists to the southeast, although the stations there are too sparse to allow definition. Shear strengths in the region of the shelf break (Fig. F7, lined area) are not shown because high sand content allows pore-water drainage during testing which in turn compromises measured S_v values, or because insufficient sample was recovered to warrant testing. Typically, peak shear strength decreases downslope, ranging from 11 kPa near the shelf break to 3 kPa on the abyssal floor. However, anomalously strong sediment was encountered at two stations, both at about 58°30'N, 178°30'W, in 3000 m of water. Here, the shear strengths are between 19 and 39 kPa.

Sediment at a 1-m-subbottom depth on the shelf has a water content that ranges from 40 to 110% by dry weight (Fig. F8). An elongate zone having water contents greater than 100% is seen in the north-central part of the shelf. This zone coincides with the area of anomalously low peak undrained shear strength. The water content of shelf sediment is lowest toward the southeast, except for two stations that have water contents greater than 50%. Sediment from the shelf edge and uppermost slope typically has a low water content (<50%), a value which correlates with increased sand percentage. Water content increases downslope and reaches a maximum (>300%) to the southeast, in the

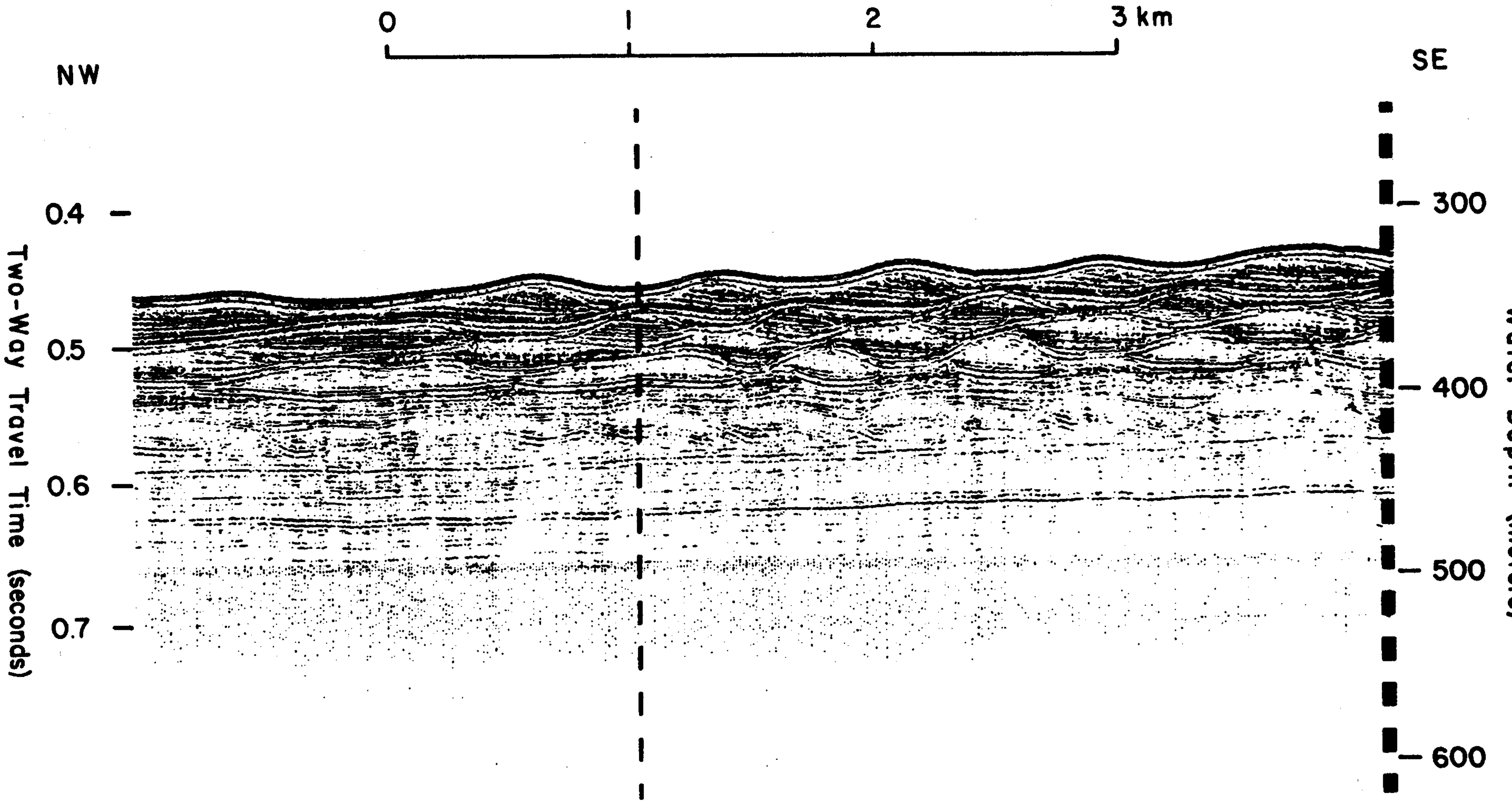

Fig. F4 — Minisparker profile showing sediment waves at head of Navarinsky Canyon (V.E. ~x7.5).

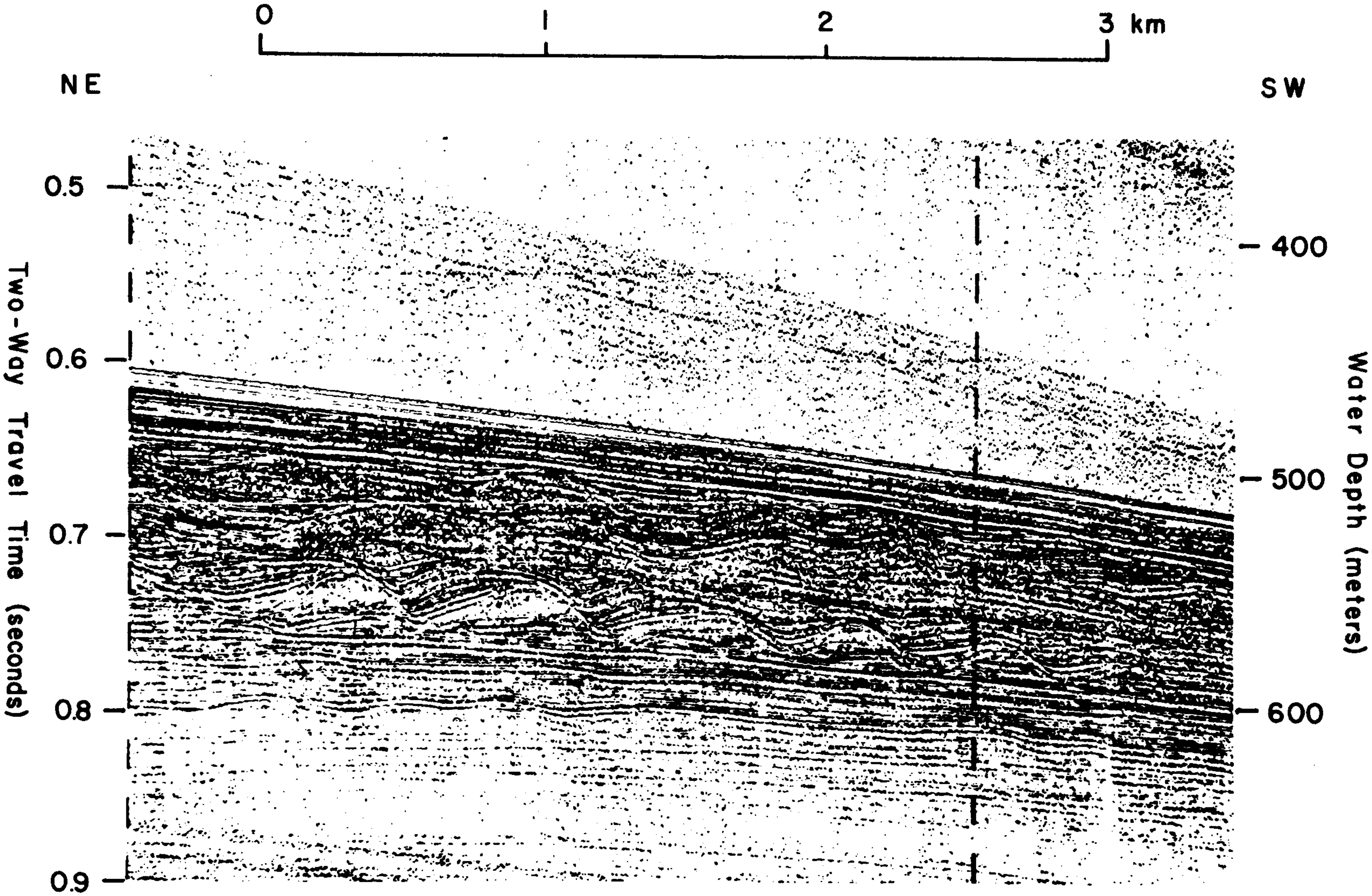

Fig. F5 — Minisparker profile showing sediment waves covered by about 20 m of parallel-bedded sediment at head of Pervenets Canyon (V.E. ~x 8.5).

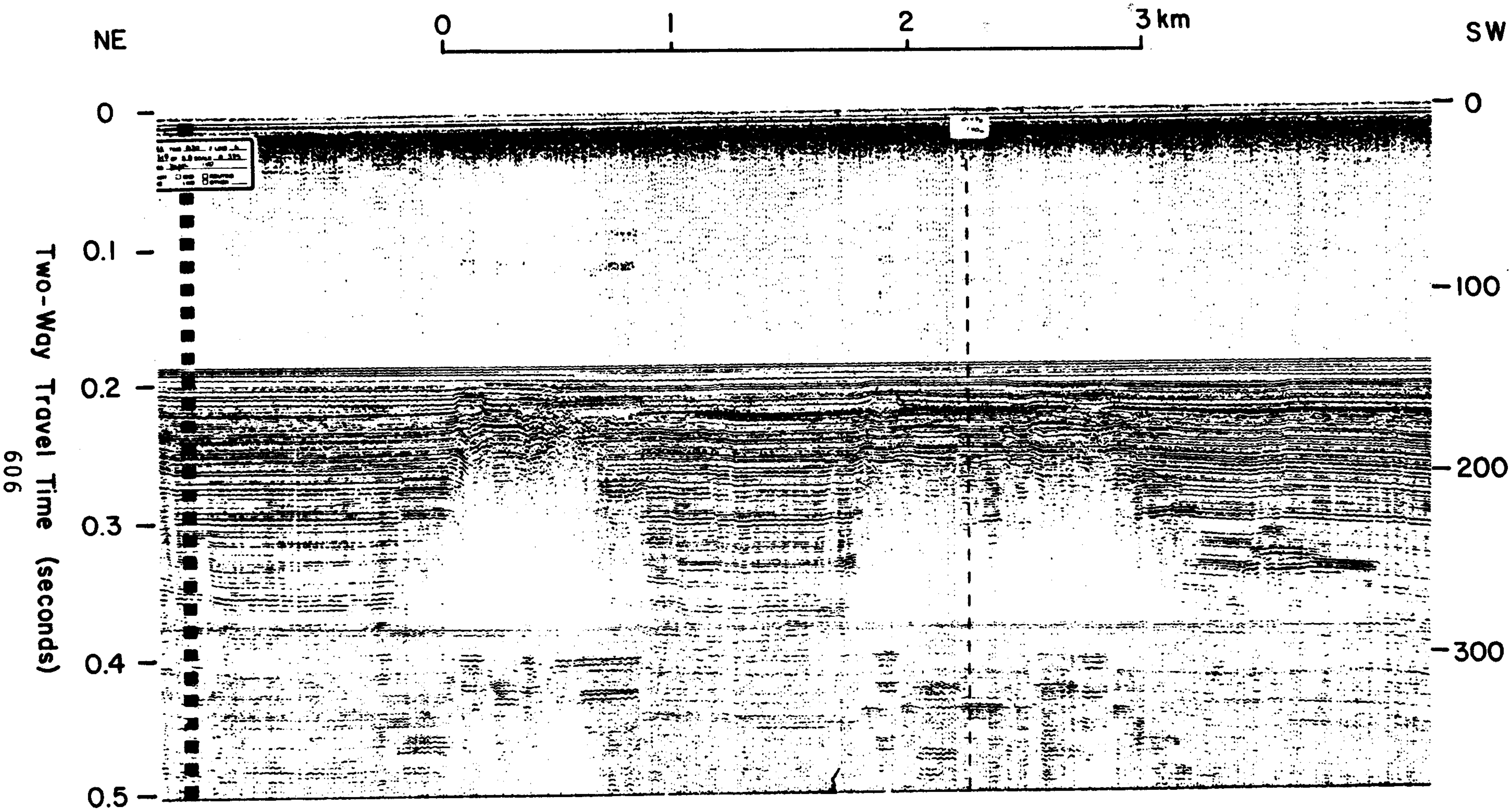

Fig. F6 — Minisparker profile from northern part of Navarin Basin province showing acoustic anomalies interpreted to be caused by gas-charged sediment (V.E. ~x7.5).

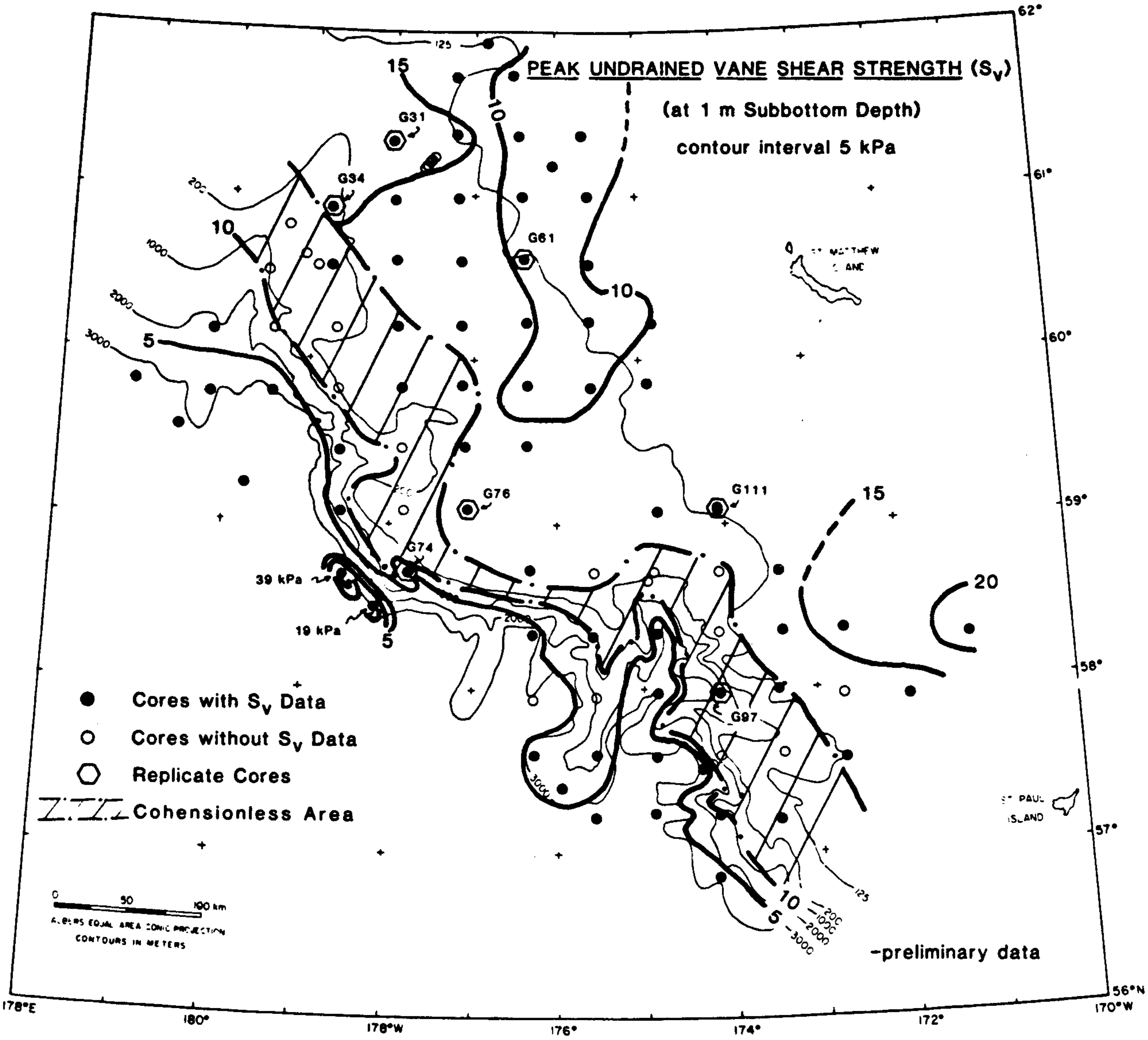

Fig. F7 — Area 1 distribution of peak undrained vane shear strength (S_v) at 1-m subbottom depth

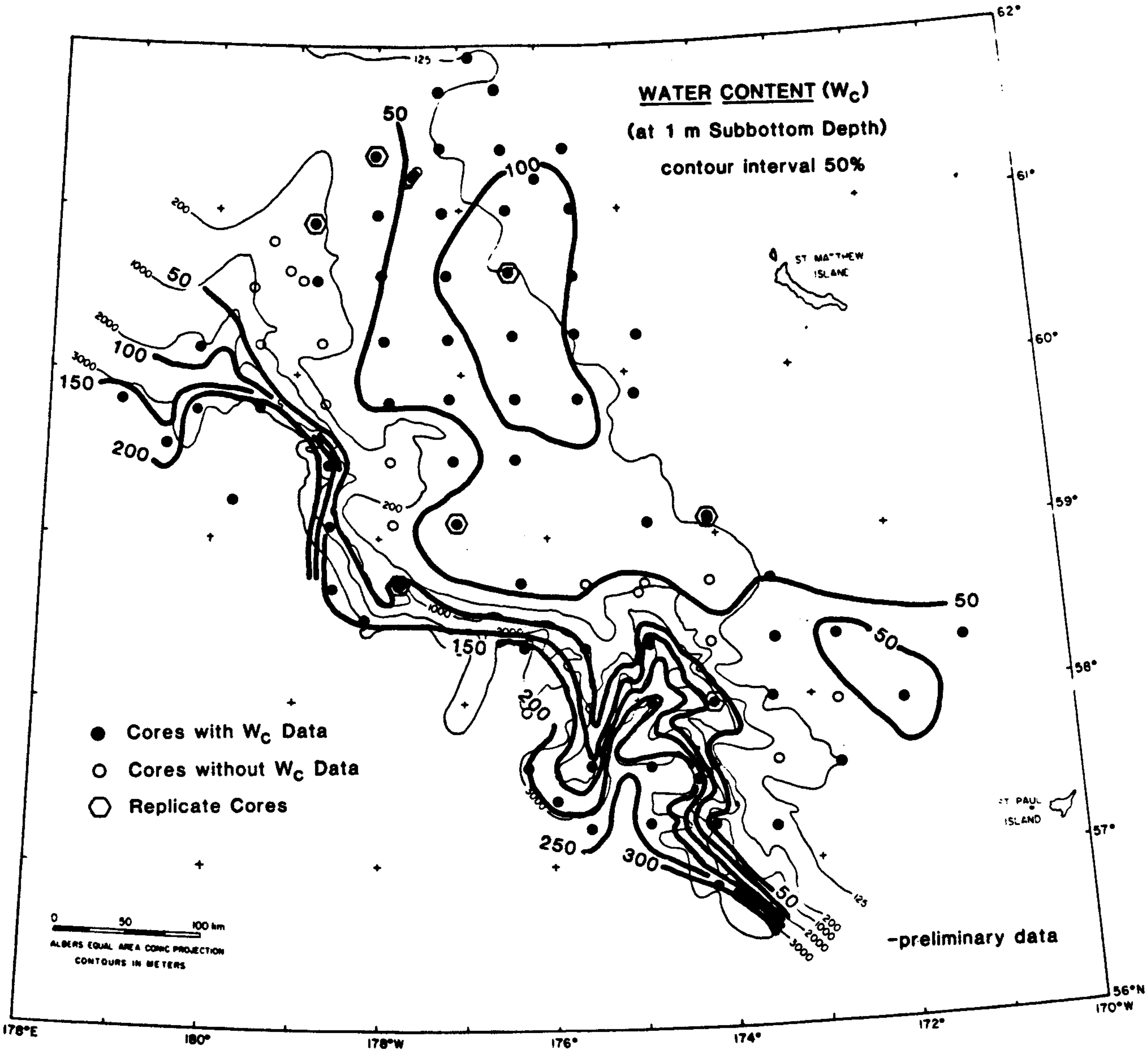

Fig. F8 — Area 1 distribution of salt-corrected water content at a 1-m subbottom depth vicinity of Zhemchug Canyon.

Near-surface sediment from Navarin Basin is lightly to moderately overconsolidated (overconsolidation ratio, or OCR: 3 - 4) except on the shelf where OCR's as high as 22 are observed (Table F1). The cause of the observed overconsolidation is not known. Sediment on the shelf is subjected to a number of loads that might be capable of inducing this state of overconsolidation (e.g., erosion of overlying material, cyclic loading, ice, and subaerial exposure at low sea-level stands). At present, our data are insufficient to evaluate these mechanisms.

ICE

We have estimated ice conditions in Navarin Basin province by synthesizing data reported by Lisitsyn (1966), McRoy and Goering (1974), and Brower and others (1977). The proposed lease area is ice free from June through October. Migratory pack ice begins to encroach upon the northern part of the lease area in November. The pack ice is fully developed by March or April, at which time the extreme southern limit of the ice edge extends over most of the lease area (Fig. F1). Ice concentrations begin to decrease in April, and the ice edge continues to retreat northward through May. First-year ice in the southern portion of the Bering Sea ranges in thickness from 30 to 71 cm, whereas ice farther north can attain a thickness of 1-2 m in unstressed floes (Lisitsyn, 1966). The southern limit and the concentration of the pack ice vary from year to year depending upon weather conditions--in some years migratory pack ice may not affect the lease area, but in other years concentrations of ice may completely cover it. In addition to the hazards that pack ice creates for man-made structures and for ships, Ivanhoe (1981) points out the significant problem of severe superstructure icing that ships will undergo while operating in the Bering Sea during the winter.

FAULTING AND SEISMICITY

The limited seismic-reflection coverage of the Navarin Basin province restricts interpretation of the length, orientation, and age of the faults. The distribution of the faults is shown in figure 2; however, because the spacing between the tracklines is as much as 30 km, correlation from line to line is uncertain. The only extensive correlation that we have attempted is to connect those points that represent the bounding faults on a graben that is oriented in a northwest-southeast direction (Fig. F2). This graben is about 5 km wide, and it has been mapped over a distance of nearly 240 km. The maximum apparent relief of this structure (Fig. F9) is about 50 m, the result of a series of offsets on each side of the down-thrown block. The throw of the individual faults varies from about 10 to 20 m. The graben is buried beneath 130 m of sediment over the depressed block and about 80 m of sediment over the adjacent flat-lying strata. The faults detected on lines oriented perpendicular to the long axis of Navarin basin greatly outnumber those on lines that parallel the basin; this pattern suggests that the faults have a northwest-southeast trend. This trend is parallel to the basin and to the shelf break. The majority of these faults occur on the continental slope and the outermost shelf.

Many of the faults shown on Figure F2 are mapped from high-resolution seismic-reflection records that have resolution of 1-3 meters; however, none of the faults mapped to date show any offset of the Holocene sea floor. Although the ages of the faults are unknown, ^{14}C dates of sediment in the southern part of the area indicate the maximum accumulation rates of the upper 6 m of sediment to be about 25 cm/10^3 yr (Askren, 1972). Therefore, faults that reach to within 3 m of the seafloor may cut sediment as young as Holocene and are considered to be active.

According to Scholl and others (1975), Cooper and others (1976), Marlow and others (1976), subduction of the Kula plate beneath the Bering Sea margin apparently ceased in late Mesozoic or early Tertiary time, and subduction of the Pacific plate shifted to the Aleutian Trench. This transfer tectonically deactivated the Bering Sea margin. The absence of modern seismicity is readily seen on the maps of Alaska earthquake epicenters published by Meyers (1976). Only six earthquakes have been reported from the Navarin Basin province for the time period prior to 1974, and all were less than magnitude six. These data, however, may be somewhat misleading because of the wide spacing and limited number of seismograph stations in western Alaska.

CONCLUSIONS

Several seafloor geologic processes of a potentially hazardous nature are identifiable in the Navarin Basin province (OCS lease-sale 83); they include sea-floor instability due to submarine slides, sediment transport and erosion, and subsidence or blowouts resulting from disturbance of gas-charged sediment; ice; and faulting with attendant ground shaking. These processes must be carefully delineated and well understood before drilling and other sea-floor operations pertinent to exploration and production, such as pipeline siting, can be accomplished with a good degree of safety.

Submarine slides are prevalent on the continental slope throughout the area, especially in association with the submarine canyons. Large bedforms are found at the heads of each of the three canyons. However, gas-charged sediment apparently is the primary concern as a possible geologic hazard on the continental shelf, because it is particularly common in the northern two-thirds of the study area. The gas is primarily biogenic methane; however, a few cores contained higher hydrocarbon homologs, the ratios of which suggest possible thermogenic origin.

An inverse correlation exists between the peak undrained shear strength (S_v) and the water content of Navarin Basin sediment. At a 1-m-subbottom depth, a tongue of relatively weak (<10 kPa), high water content (>100%), fine-grained sediment extends onto the central shelf from the north. To the southeast, near the head of Zhemchug Canyon, shear strengths are anomalously high (>15 kPa). Strength of the fine-grained, high-water-content sediment on the slope decreases with water depth from a typical value of 11 kPa near the shelf break to a low of 3 kPa at the base of the slope. Preliminary consolidation data indicate that the shelf sediment is lightly to heavily overconsolidated (OCR's range from 3 to 22 at a subbottom depth of 1 m). It is apparent that the central shelf is more heavily overconsolidated than are the adjacent areas.

Migratory pack ice will be a problem during most years in the Navarin Basin lease area. This ice can

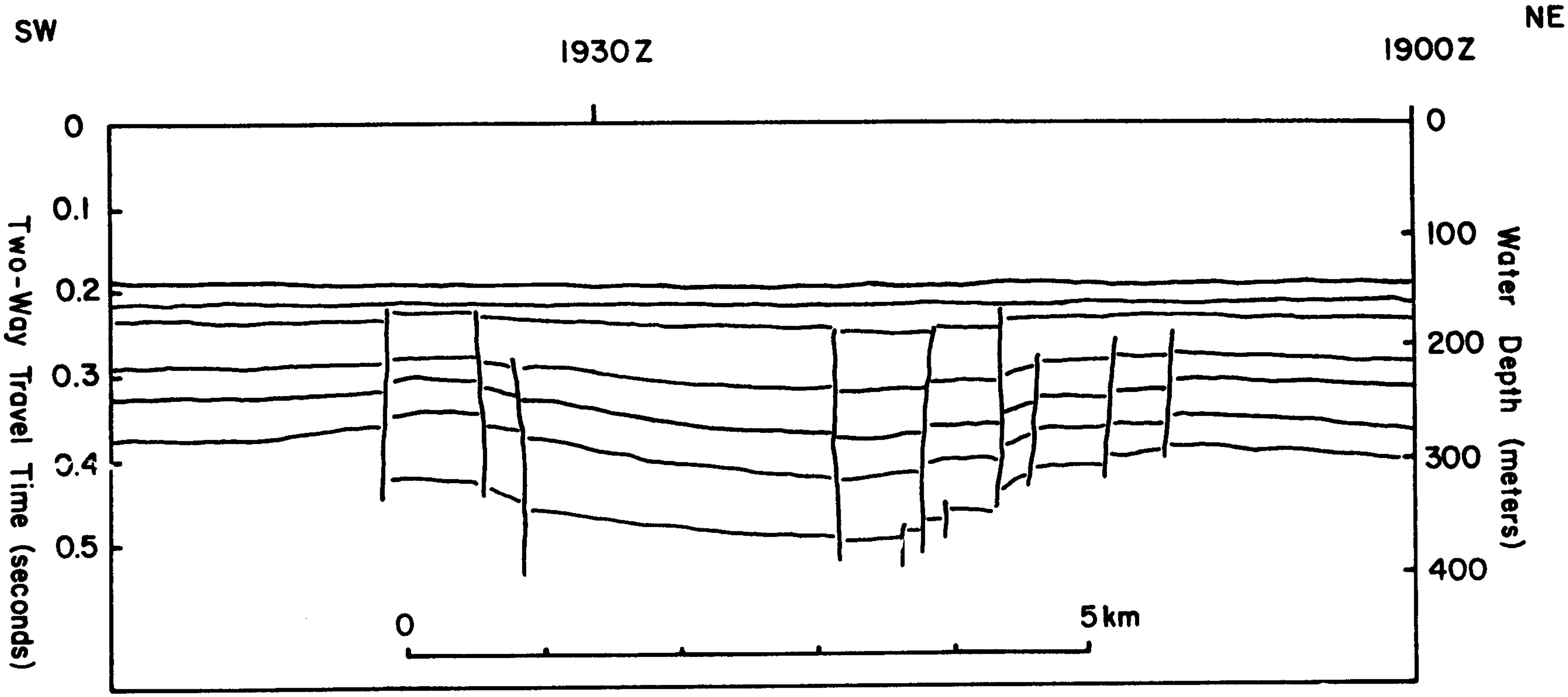

Fig. F9 — Interpretive line drawing of air-gun profile across graben in Navarin Basin province (see Fig. F2) (V.E. ~x8.5).

attain thicknesses of 1-2 m in the northern part of the area.

Earthquakes appear to be rare in the Navarin area; however, some shallow faults may cut Holocene sediment and reach to within 3 m of the sea floor. These faults must be considered to be active and that activity should be accounted for in design plans for sea-floor structures.

ACKNOWLEDGMENTS

We acknowledge the assistance provided by the officers, crew, and scientific parties of the NOAA ship Discoverer, the USCG Polar Star and the USGS R/V S.P. Lee. This paper has benefitted from discussion with Homa J. Lee and from constructive reviews by Monty A. Hampton and William R. Normark. We thank La Vernne Hutchison for typing the manuscript.

This study was funded jointly by the U.S. Geological Survey and by the Bureau of Land Management through interagency agreement with the National Oceanic and Atmospheric Administration, as part of the Outer Continental Shelf Environmental Assessment Program.

REFERENCES CITED

Askren, D. R., 1972, Holocene stratigraphic framework, southern Bering Sea continental shelf: MS thesis, Univ. of Washington, 104 p.

Blunt, D. J. and Kvenvolden, K. A., 1981, A preliminary report on amino acid diagenesis in fossil mollusks recovered from the Navarin Basin province, Bering Sea, in Carlson, P. R. and Karl, H. A., eds., Seafloor geologic hazards, sedimentology, and bathymetry: Navarin Basin province, northwestern Bering Sea: U.S. Geological Survey Open-File Report 81-1217, 149 p.

Brower, W. A., Jr., Searby, H. W., Wise, J. L., Diaz, H. F., and Prechtel, A. S., 1977, Climatic atlas of the outer continental shelf waters and coastal regions of Alaska, vol. II, Bering Sea, NOAA OCSEAP Final Report-RU 347, 443 pp.

Carlson, P. R. and Karl, H. A., 1981, High-resolution seismic reflection profiles: Navarin Basin province, Northern Bering Sea, 1980: U.S. Geological Suvey Open-File Report 81-1221, 4 p., 1 map, scale 1:1,000,000.

Cooper, A. K., Scholl, D. W., and Marlow, M. S., 1976, Plate tectonic model for the evolution of the Bering Sea basin: Geological Society of America Bulletin, v. 87, p. 1119-1126.

Gibson, R. E. 1958, The progress of consolidation in a clay layer increasing in thickness with time: Geotechnique, v. 8, p. 171-182.

Hampton, M. A., Bouma, A. H., Sangrey, D. A., Carlson, P. R., Molnia, B. F., and Clukey, E. C., 1978, Quantitative study of slope instability in the Gulf of Alaska: Proceedings of the 1978 Offshore Technology Conference, p. 2307-2318.

Ivanhoe, L. F., 1981, Sea ice will increase operating costs in Alaska's Bering Sea waters: Oil and Gas Journal, October 26, 1981, p. 267-268.

Karl, H. A., Carlson, P. R., Fischer, J., Johnson, K., and Lamb, B., 1981, Textural variations and composition of bottom sediment, in Carlson, P. R. and Karl, H. A., eds., Seafloor geologic hazards, sedimentology, and bathymetry: Navarin Basin province, northwestern Bering Sea: U. S. Geological Survey Open-File Report 81-1217, 149 p.

Knebel, H. J., 1972, Holocene sedimentary framework of the east-central Bering Sea continental shelf: Ph.D. thesis, Univ. Washington, Seattle, 186 p.

Komar, P. A., Neudeck, R. H., and Kulm, L. D., 1972, Observation and significance of deep-water oscillatory ripple marks on the Oregon continental shelf, in Swift, D. J. P., Duane, D. B., and Pilkey, O. H., eds., Shelf sediment transport: process and pattern: Dowden, Hutchinson and Ross, Inc., Stroudsburg, Pa., p. 601-619.

Lisitsyn, A. P., 1966, Recent sedimentation in the Bering Sea (in Russian): Inst. Okeanol. Ahoc. Nauk USSR, (translated by Israel Program for Scientific Translation, available from U. S. Dept. Commerce, Clearinghouse for Fed. Sci. and Tech. Info., 1969, 614 pp.).

Marlow, M. S., Carlson, P. R., Cooper, A. K., Karl, H. A., McLean, H., McMullin, R., and Lynch, M. B., 1981, Resource report for proposed OCS sale number 83 Navarin Basin, Alaska: U. S. Geological Survey Open-File Report 81-252, 82 p.

Marlow, M. S., Scholl, D. W., Cooper, A. K., and Buffington, E. C., 1976, Structure and evolution of Bering Sea shelf south of St. Lawrence Island: American Association of Petroleum Geologists Bulletin, v. 60, p. 161-183.

McRoy, C. P. and Goering, J. J., 1974, The influence of ice on the primary productivity of the Bering Sea, in Hood, D.W. and Kelley, E. J., eds., Oceanography of the Bering Sea with Emphasis on Renewable Resources: Univ. of Alaska, Fairbanks, Alaska, p. 403-419.

Meyers, H., 1976, A historical summary of earthquake epicenters in and near Alaska: N.O.A.A. Tech. Memorandum EDS NGSDC-1, 80 p.

Nardin, T. R., Hein, F. J., Gorsline, D. S., and Edwards, B. D., 1979, A review of mass movement processes, sediment and acoustic characteristics, and contrasts in slope and base-of-slope systems versus canyon-fan-basin floor systems, in Doyle, L. J. and Pilkey, O. H., eds., Geology of Continental Slopes: Society of Economic Paleontologists and Mineralogists, Special Publication No. 27, p. 61-73.

Nelson, Hans, Kvenvolden, K. A., and Clukey, E. C., 1978, Thermogenic gases in near-surface sediments of Norton Sound, Alaska: Proceedings of the 1978 Offshore Technology Conference, p. 2623-2633

Scholl, D. W., Buffington, E. C., and Marlow, M. S., 1975, Plate tectonics and the structural evolution of the Aleutian-Bering Sea region, in Forbes, R. B., ed., Contributions to the geology of the Bering Sea basin and adjacent regions: Geological Society of America Special Paper 151, p. 1-32.

Seed, H. B. and Lee, K. L., 1966, Liquefaction of saturated sands during cyclic loading: American Soc. Civil Engineers Proc., Journal of Soil Mechanics and Foundation Division v. 92, no. SM6, p. 105-134.

Seed, H. B. and Rahman, M. S., 1978, Wave-induced pore pressure in relation to ocean floor stability of cohesionless soils: Marine Geotechnology, v. 3, p. 123-150.

Sharma, G. D., 1979, The Alaska shelf, hydrographic, sedimentary, and geochemical environment: Springer-Verlag, New York, 498 p.

Shepard, F. P., 1963, Submarine geology: 2nd. ed. New York, Harper, 557 p.

Takenouti, A. Y. and Ohtani, K., 1974, Currents and water masses in the Bering Sea: a review of Japanese work, in Hood, D. W. and Kelley, E. J., eds., Oceanography of the Bering Sea: Univ. Alaska, Inst. Marine Science, Occas. Publ. 2, p.39-57.

U. S. Geological Survey, 1977, An investigation of Pennzoil's blow-out and loss of platform: U. S. Geological Survey Unpublished Administrative Report, 22 p.

Vogel, T. M. and Kvenvolden, K. A., 1981, Hydrocarbon gases in Navarin Basin province sediments, in Carlson, P. R. and Karl, H. A., eds., Seafloor geologic hazards, sedimentology, and bathymetry: Navarin Basin province, northwestern Bering Sea: U.S. Geological Survey Open-File Report 81-1217, 149 p.

Vogel, T. M., Kvenvolden, K. A., Carlson, P. R., and Karl, H. A., 1981, Geochemical prospecting for hydrocarbons in the Navarin Basin province: American Association of Petroleum Geologists Bulletin, v. 64, no.4.

Webster,B. D., 1979, Ice edge probabilities for the eastern Bering Sea: N.O.A.A. Technical Memorandum NWS AR-26, 20 p.

Whelan, T., Coleman, J. M., Roberts, H. H., and Suhayda, J. N., 1976, The occurrence of methane in recent deltaic sediments and its effect on soil stability: Bulletin of the International Association of Engineering Geology, No. 14, p. 55-64.

TABLE F1. Summary consolidation data of near-surface* sediment

Core	σ'_{vm} (kPa)	σ'_v (kPa)	c_v ($cm^2/sec \times 10^3$)	OCR	Physiographic Province
G31	20	6.8	1.5 (120)	3	Shelf
G34	28	7.0	--	4	Canyon
G61	27	4.5	0.5 (120)	6	Shelf
G74	25	9.2	3.5 (165)	3	Slope
G78	95(58)	4.3(58)	--	22	Shelf
G97	30	5.0	0.5 (190)	6	Canyon
G111	60	6.5	1.0	9	Shelf

*values at 100 cm subbottom depth except where shown in parentheses (e.g., (58) = 58 cm subbottom).

σ'_{vm} = maximum past pressure

σ'_v = effective overburden stress

c_v = coefficient of consolidation

OCR = overconsolidation ratio

APPENDIX G:

PUZZLING FEATURES IN THE HEAD OF NAVARINSKY CANYON, BERING SEA

by

Paul R. Carlson, Herman A. Karl, and Brian D. Edwards

U.S. Geological Survey

Puzzling Features in the Head of Navarinsky Canyon, Bering Sea

by

Paul R. Carlson, Herman A. Karl, and Brian D. Edwards
U.S. Geological Survey
Menlo Park, California 94025

ABSTRACT

Two types of morphologic features mapped in the head of Navarinsky Canyon are attributed to mass movement of the near-surface sediment. A series of pull-aparts(?) is located downslope of a field of large sand waves. These pull-aparts(?), possibly induced by liquefaction, affect the upper 5-10 m of sandy sediment in water depths of 350-600 m on a 1° slope. A hummocky elongate mound of muddy sand in water depths of 550-800 m that contains chaotic, disrupted internal reflectors to a subbottom depth of 30-40 m is believed to be the product of a shallow slide. We speculate that Holocene seismicity is the likely triggering mechanism.

INTRODUCTION

Mass movement has been an important process in the evolution of the world's continental margins [1-3]. As coverage of frontier areas is increased, so is knowledge of the various forms of mass movement that are continually at work modifying the continental slopes.

The purpose of this report is to illustrate and discuss two puzzling types of mass-movement features discovered in the head of Navarinsky Canyon, one of the largest (4,900-km^3 volume) of the large canyons incised into the continental margin of the Bering Sea [4,5] (Fig. G1).

The study area is a part of the navarin Basin province, a potential petroleum province that is scheduled for leasing in 1984. The Navarin Basin contains as much as 12 km of Tertiary and Cretaceous sedimentary strata [6], and thus has stimulated the interest of the petroleum industry. Understanding of the mass movement processes on the upper slope will be vital to the safe siting of sea-floor structures in water depths of > 150 m.

Data Collection

Seismic-reflection profiles and sediment samples (Fig. G1) discussed in this report were collected in 3 successive years of reconnaissance geohazards studies in the Navarin Basin area [7, 8]. Seismic systems included 20-80-in airguns, a 500-1000-J minisparker, a hull-mounted Uniboom*, and 3.5 kHz, and 12 kHz sound sources. Seafloor-sediment samples were collected primarily

*Any use of trade names in this publication is for descriptive purposes only and does not constitute endorsement by the U.S. Geological Survey.

with a gravity corer (8-cm-diameter barrel); supplementary samples were obtained with box corer and vibra-corer and a Van Veen* grab sampler.

MORPHOLOGY OF CANYON HEAD

Navarinsky Canyon is the northernmost of the large canyons that dissect the Bering continental margin (Fig. G1). The U.S.-U.S.S.R. 1867 convention line nearly bisects this canyon, which heads in 150 m of water; the canyon extends 270 km across the slope at an average axial gradient of 0.5°, where it debouches onto the continental rise at a depth of ~3,200 m [9]. Navarinsky Canyon is cut into the extremely flat Bering shelf, which has a gradient of 0.04°-0.1° [9]. The head of the canyon is a broad shallow amphitheater-shaped depression that covers an area of 16,600 km^2. The study area is in the head of the canyon between the two main thalwegs, both of which have axial gradients of ~0.2° to a depth of 400 m and steepen to ~1° between 400- and 1,000-m depth [9].

Within the head of Navarinsky Canyon, we mapped a field of large bedforms (1,000- km^2 area) that is bounded by the 200-400-m isobaths and has a seafloor gradient of 0.6° (Fig. G2). These bedforms have wavelengths of ~600 m, heights of 5-15 m, and appear on seismic-reflection records as a stack of climbing dunes that extend to a subbottom depth of 75-100 m (Fig. G3b). Grab samples, box cores, and vibracores collected in the bedform field all recovered moderately well-sorted very fine to fine sand. We speculate that the sand in these large bedforms was transported to its present site near the shelf break during Pleistocene low stands of sea level. At that time, the shoreline was near the present 130-140-m isobath and large rivers meandered across the broad flat subaerial reaches of the Bering shelf [10]. Calculations that take into account the bathymetry, sea-floor gradient, present water depth, sediment type, and oceanographic conditions suggest that these large sand waves are possible products of internal waves [11].

TYPES OF MASS MOVEMENT

Seismic-reflection records from the head of Navarinsky Canyon show two kinds of seafloor irregularities that we interpret to be the result of mass movement. These mass-movement phenomena include: (1) depression or pull-apart-like features that adjoin and overlap the field of large bedforms, and (2) a mound or ridge-shaped mass of slide debris. Figures G2 and G3 show the areal relations of all three features -- bedforms, pull-aparts, and slide mass.

Pull-aparts?

High-resolution seismic-reflection profiles show some unusual breaks in the surface sediment downslope from the bedform field (Figs. G2, G3a, G3c). These features are irregularly spaced depressions or notches in the seafloor, ~0.1 - 2.0 km apart; they average ~50 m wide, have a relief of 3-5 m, and appear to affect only the upper 5-10 m of sediment (Fig. G3c). Absence of side-scan-sonar coverage prevents determination of the true shape of these features; however, the notches are more abundant on lines perpendicular rather than parallel to the isobaths, and thus the notches appear to be

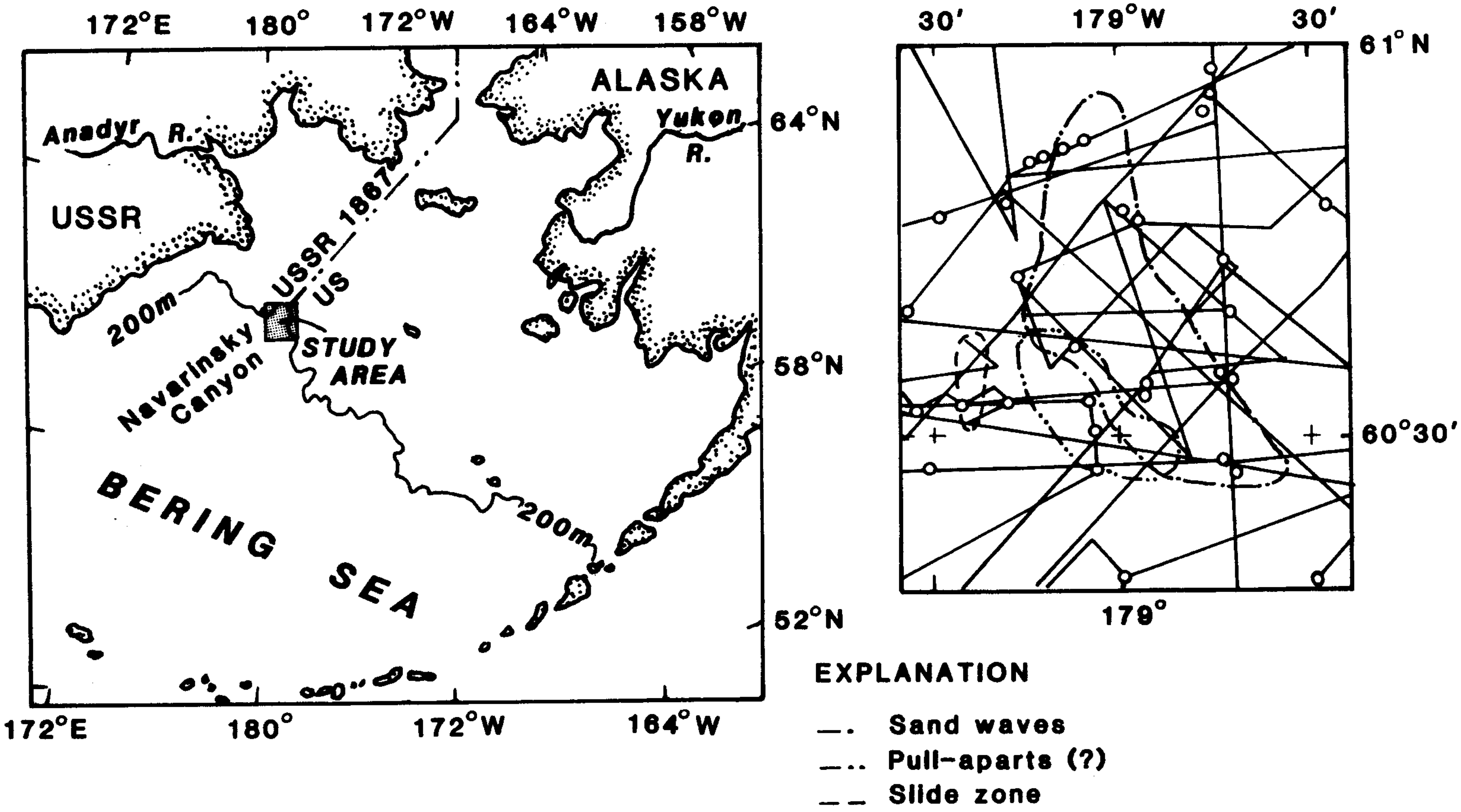

Figure G1. Sketch map of study area in northern Bering Sea, showing locations of high-resolution seismic-reflection lines, sample stations, and areas of seafloor features.

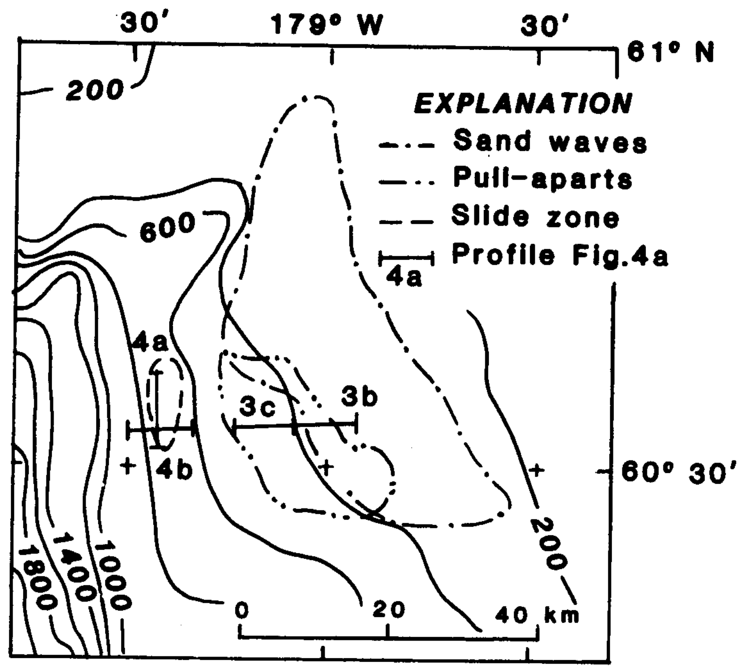

Figure G2. Seafloor morphologic features in head of Navarinsky Canyon, showing locations of illustrated profiles. Bathymetry after Fischer and others, 1982. Contour interval, 200 m.

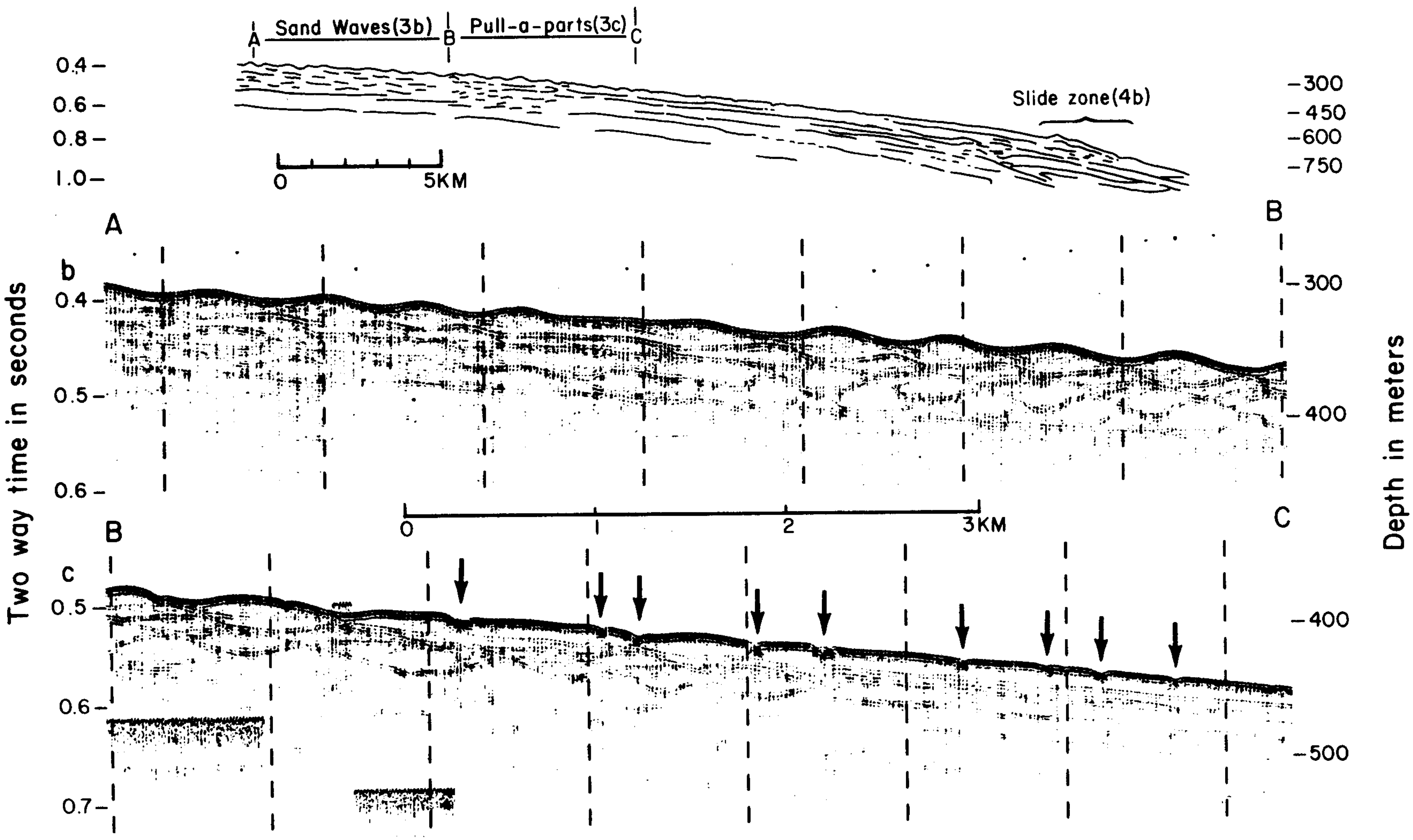

Figure G3. Seismic-reflection profiles in head of Navarinsky Canyon. (a) Line drawing of seismic-reflection profiles (20-40-in^3 airguns), showing relative positions of profiles in Figures G3b, G3c, and G4a. (b) Minisparker profile (1,000 J), showing sand waves. (c) Minisparker profile (1,000 J), showing pull-aparts (arrows). Vertical exaggeration (V.E.) ~7.5x. See Figure G2 for locations.

oriented parallel to the isobaths. The notches, which are situated between the 350- and 600-m isobaths on a slope of ~1°, have been mapped over an area of 300 km^2 (Fig. G2). The sediment in this part of the canyon is moderately well-sorted muddy to fine sand containing some pebbles and granules.

The zone of depressions, notches, or breaks in the surface sediment downslope from the field of large bedforms has the appearance and apparent orientation of pull-aparts or tensional breaks that may result from downslope flow. Another possibility is that these features are shallow craters, pockmarks, or sand boils formed by expulsion of "liquefied" sediment. The zone of pull-aparts or depressions overlaps the downslope side of the bedform field and thus has developed after the formation of the bedforms and may be continuing to develop at the present time.

Slide Zone

An elongate mound-shaped mass of sediment of hummocky surface morphology that occupies an area of ~50 km^2 is situated 4-5 km downslope from the area of surface breaks (Figs. G2, G3a). The hummocky mound of muddy sand has the characteristics commonly associated with a submarine slide mass. This elongate mound is ~3 by 14 km, and its long axis is oriented obliquely to the 550-800-m isobaths. The mound has a relief of 10-15 m, contains chaotic internal reflectors, affects the upper 30-40 m of sediment, and has formed where the slope gradient of the canyon changes from 1.1° to 2.6° (Fig. G4). Although some seismic-reflection profiles show jumbled and broken reflectors within the mound of sediment, all the profiles show well-developed relatively continuous reflectors beneath the mound, starting at a subbottom depth of ~40 m (Fig. G4). Both upslope and downslope from the mound the internal reflectors are also continuous at all levels beneath the seafloor.

The hummocky mound of muddy sand that is apparently a product of a shallow slide (Figs. G3a, G4) may have been caused by liquefaction, as postulated for the formation of the pull-aparts, or else these features may have formed totally independently.

TRIGGERING MECHANISM

To generate the types of mass movement that have occurred in the head of Navarinsky Canyon, both a supply of sediment and a mechanism to trigger the mass movement are necessary. The present rate of sediment accumulation on the outer Navarin shelf is relatively low (<20 cm/1,000 yrs on the basis of ^{14}C ages; see ref. [12]) because of the great distance (>400 km) to the nearest river mouth. The rate of sediment accumulation must have been high during low stands of sea level, however, when large rivers, such as the ancestral Anadyr and Yukon, crossed the subaerially exposed shelf. When the rate of sediment accumulation is rapid, high pore-water pressures can develop and cause sediment instability [13, 14]. Although underconsolidation may be responsible for some of the sediment instability along parts of the Navarin margin, underconsolidation is unlikely in the head of Navarinsky Canyon because the sediment there is primarily noncohesive and pore-water drainage and pressure equalization are presumably rapid.

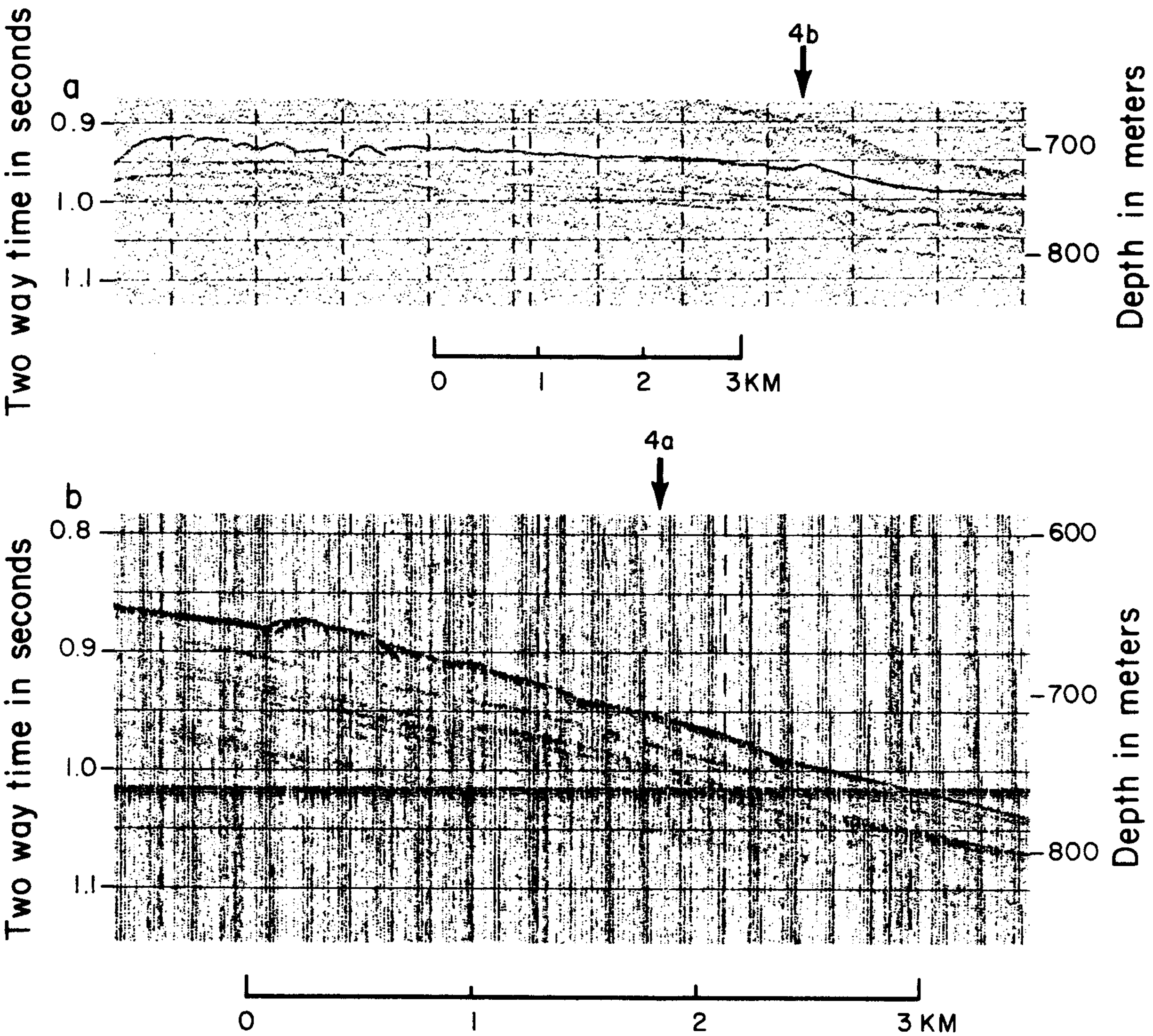

Figure G4. High-resolution profiles, showing slide zone in Navarinsky Canyon. (a) 3.5 kHz profile; V.E. ~10x. (b) Uniboom profile (1200 J); V.E. ~7.5x. See Figure G2 for locations.

The Bering Sea is a region of severe storms in which winds commonly exceed 100 km/h (62 mi/h) and, at times, exceed 165 km/h (103 mi/h); waves generated by storms of this magnitude may be as high as 15-20 m [15]. In the head of Navarinsky Canyon, the cohesionless sediment in the area of the pull-aparts and in the slide zone is presently in water depths of 350 m and probably was at >200-m depth during Pleistocene low stands of sea level. On the basis of wave-theory calculations according to the procedures of Seed and Rahman (1978), the cohesionless sediment in these areas would not appear to be vulnerable to cyclic loading from large storm waves. Thus, storm waves, either at present or during Pleistocene low stands of sea level, are an unlikely triggering mechanism for the observed failures.

Karl, and others [11] have shown that internal tides and higher frequency internal waves possibly formed the large bedforms in the head of Navarinsky Canyon. Whereas Karl and others [11] determined that energy from 4- and 12-h period internal waves is amplified in the sand-wave field and just downslope from this field, the cohesionless nature of the sediment and the small density contrasts across the pycnocline make internal waves an unlikely triggering mechanism for the mass-movement phenomena farther downslope.

Although the Aleutian Island arc is seismically active [17], the great distance (1,000 km) between the Aleutians and Navarinsky Canyon minimizes the effect of horizontal accelerations associated with ground shaking because accelerations drop off rapidly with distance from the epicenter [18]. Even a great (M>8) earthquake occurring along the Aleutian Island arc would likely cause low accelerations in the Navarinsky Canyon. Additional, Sereda (1980) located the epicenters for two small (M<4) earthquakes at Cape Navarin, U.S.S.R. Even these events, however, were >200 km from the head of Navarinsky Canyon and thus would have had little effect on the canyon sediment. Seismicity in the northern Bering Sea has been minimal over the past 85 years. Only eight earthquakes have had epicenters within a radius of 200 km of the study area, all of which were of M<5.8 [17]. On the basis of empirical evidence, for events of this magnitude to cause sediment flow or liquefaction on the Navarinsky slope the epicenter must be within ~30 km [20]. Even though we find little evidence in the modern seismologic record to support earthquakes as a triggering mechanism, a few traces of shallow faults have been mapped in the head of Navarinsky Canyon [21]. Although none of these faults shows offset of the seafloor, all appear to cut sediment as young as Holocene and therefore are considered to be active.

We conclude that earthquakes are the most likely triggering mechanism. In spite of the sparsity of local seismic events in the historical record, we note that our data base covers less than 100 years, and the features under discussion could have formed anytime in the past several thousand years. Thus, the odds of an M> 6.0 event occurring in the proximity of Navarinsky Canyon and possibly causing liquefaction of the cohesionless sediment are greatly improved.

ACKNOWLEDGMENTS

We thank Monty Hampton, David Keefer, and Homa Lee for their constructive reviews of the manuscript. This study was supported by the U.S. Geological Survey and the U.S. Bureau of Land Management through interagency agreement with the U.S. National Oceanic and Atmospheric Administration.

REFERENCES

[1.] Moore, D. G., 1977. Submarine slides. In B. Voight, (ed.), Rockslides and Avalanches, vol. 1, Natural Phenomena. Amsterdam, Elsevier: p. 563-604.

[2.] Nardin, T. J., Hein, F. J., Gorsline, D. S., and Edwards, B. D., 1979. A review of mass movement processes, sediment and acoustic characteristics, and contrasts in slope and base-of-slope systems versus canyon-fan-basin floor systems. In L. J. Doyle and O. H. Pilkey, (eds.), Geology of Continental Slopes. Society of Economic Paleontologists and Mineralogists Special Publication 27, p. 61-73.

[3.] Cook, H. E., Field, M. E., and Gardner, J. V., 1982. Characteristics of sediments on modern and ancient continental slopes. In P. A. Scholle, and D. Spearing, (eds.), Sandstone Depositional Environments: American Association of Petroleum Geologists Memoir 31 p. 329-364.

[4.] Scholl, D. W., Buffington, E. C., Hopkins, D. M., and Alpha, T. R., 1970. The structure and origin of the large submarine canyons of the Bering Sea. Marine Geology, v. 8, p. 187-210.

[5.] Carlson, P. R., Karl, H. A., and Quinterno, Paula, 1982. Sedimentologic processes in world's largest submarine canyons, Bering Sea, Alaska. Geological Society of America, Abstracts with Programs, v. 14, no. 7, p. 459-460.

[6.] Marlow, M. S., Scholl, D. W., Cooper, A. K., and Buffington, E. C., 1976. Structure and evolution of Bering Sea shelf south of St. Lawrence Island. American Association of Petroleum Geologists Bulletin, v. 60, p. 161-183.

[7.] Carlson, P. R. and Karl, H. A., 1981. Seafloor geologic hazards, sedimentology, and bathymetry; Navarin Basin province, northern Bering Sea. U.S. Geological Survey Open-File Report 81-1217, 149 p.

[8.] Karl, H. A. and Carlson, P. R., 1983. Seafloor Hazards and Related Surficial Geology, Navarin Basin Province, Northern Bering Sea. U.S. Geological Survey Open-File Report 83-   , in press.

[9.] Fischer, J. M., Carlson, P. R., and Karl, H. A., 1982. Bathymetric map of Navarin continental margin, Bering Sea. U.S. Geological Survey Open-File Report 82-1038, 11 p., 1 map sheet 1:1,000,000.

[10.] Karl, H. A., Carlson, P. R., and Lamb, B., 1982. Sediment waves in the head of Navarinsky, Pervenets, and Zhemchug submarine canyons, northwestern Bering Sea. U.S. Geological Survey Circular (Accomplishments in Alaska) 844, p. 141-143.

[11.] Karl, H. A., Cacchione, D. A., and Carlson, P. R., 1982. Large sand waves in canyon heads, Bering Sea: Products of internal waves or density currents?. International Association of Sedimentologists, 11th International Congress on Sedimentology, Hamilton, Ontario, Canada, p. 73.

[12.] Carlson, P. R. and Karl, H. A., 1983. Rates of sediment accumulation in Navarin Basin province, Bering Sea. In: H. A. Karl and P. R. Carlson, (eds.), Seafloor Hazards and Related Surficial Geology, Navarin Basin Province, Northern Bering Sea. U.S. Geological Survey Open-File Report 83- in press.

[13.] Morgenstern, N., 1967. Submarine slumping and the initiation of turbidity currents. In A. F. Richards, (ed.), Marine Geotechnique. Urbana, Ill., University of Illinois Press, p. 189-220.

[14.] Hampton, M. A., Bouma, A. H., Carlson, P. R., Molnia, B. F., Clukey, E. C., and Sangrey, D. A., 1978. Quantitative study of slope instability in the Gulf of Alaska. 10th Offshore Technology Conference, Houston, Texas, Proceedings, v. 4, p. 2307-2318.

[15.] Brower, W. A., Jr., Searby, H. W., Wise, J. L., Diaz, H. F., and Prechtel, A. S., 1977. Climatic atlas of the outer continental shelf waters and coastal regions of Alaska, v. II, Bering Sea. NOAA OCSEAP Final Report RU 347, Arctic Environmental Information and Data Center, Anchorage, Alaska, Publication B-77, 443 p.

[16.] Seed, H. B., and Rahman, M. S., 1978. Wave-induced pore pressure in relation to ocean floor stability of cohesionless soils. Marine Geotechnology, v. 3, p. 123-150.

[17.] Meyers, H., 1976. A historical summary of earthquake epicenters in and near Alaska. National Oceanographic and Atmospheric Agency Technical Memorandum EDS NGSDC-1, 80 p.

[18.] Joyner, W. B., and Boore, D. M., 1981. Peak horizontal acceleration and velocity from strong-motion records including records from the 1979 Imperial Valley, California, earthquake. Bulletin Seismological Society of America, v. 71, p. 2011-2038.

[19.] Sereda, L. I., 1980. Systems of deep-seated faults in the northeast U.S.S.R. Geotectonics, v. 14, p. 151-160.

[20.] Keefer, D. K. 1983. Landslides caused by earthquakes. Bulletin Geological Society of America, in press.

[21.] Carlson, P. R., Karl, H. A., Fischer, J. M., and Edwards, B. D., 1982. Geologic hazards in Navarin Basin province, northern Bering Sea. 14th Offshore Techology Conference, Houston, Tex., Proceedings, v. 1, p. 73-87.

APPENDIX H:

LARGE SAND WAVES IN SUBMARINE CANYON HEADS, BERING SEA: PRELIMINARY HYPOTHESIS OF THEIR DEPOSITIONAL HISTORY

by

Herman A. Karl and Paul R. Carlson

U.S. Geological Survey

ABSTRACT

Sand waves occur in the heads of large submarine canyons in the northwestern Bering Sea. These sand waves vary in height between ~5 to 15 m, and have wavelengths of 600 m. They are not only expressed on the seafloor, but are also well defined in the subsurface and resemble enormous climbing bed forms. We conjecture that the sand waves originated during lower stands of sea level in the Pleistocene. Although we cannot explain the mechanics of formation of the sand waves, internal-wave generated currents are among four types of current that could account for the sand waves.

INTRODUCTION

We observed large bed forms in the heads of three enormous submarine canyons that incise the continental margin of the northern Bering Sea (Fig. H1). Although similar in size and sediment composition to many of the large bed forms described by others, the depositional setting, internal stratification, and stratigraphic thickness of these bed forms combine to make these features unique among the bed forms heretofore reported in the literature [1,2,3,4,5]. The purpose of this paper is to describe these bed forms and to frame hypotheses about their depositional history and mode of formation.

Regional Setting.

We investigated an 80,000-km^2 area of the Bering Sea continental margin that lies about 100 km west of St. Matthew Island (Fig. H1). The 150-m isobath delineates the northwest-trending shelf break that separates the broad, flat (average gradient of 0.02°) continental shelf from the rugged, steep (gradients range from 3° to 8°) continental slope. Three large canyons dissect the slope and outer shelf [6]. Navarinsky and Zhemchug Canyons are each about 100 km wide at the shelf break. Pervenets Canyon is about 30 km wide there. The canyons appear to be controlled by structures at least of Paleocene age [7], but we presume that the major canyon erosion occurred during lowered sea levels in the Pleistocene.

The closest point sources of sediment, the Anadyr River to the north in the U.S.S.R. and the Yukon River to the east in Alaska, are over 400 km from the study area. Surface sediments on the shelf and slope generally consist of silts and silty sands; however, there are zones of fine sand at the shelf break, on the upper slope, and in the heads of the submarine canyons [6].

Oceanographic data for this area of the Bering Sea is meager. The Bering Slope Current flows from southeast to northwest, paralleling the continental slope [8]. Circulation on the shelf is poorly understood. Investigation of the outer continental shelf of the southern Bering Sea indicates predominantly east-west tidal currents with little net flow [9]. Storms can generate waves large enough to affect sediment as deep as 200 m [6].

Methods.

We collected seismic reflection profiles and sediment samples in the study area in the summers of 1980 and 1981 (Fig. H1). Reconnaissance track

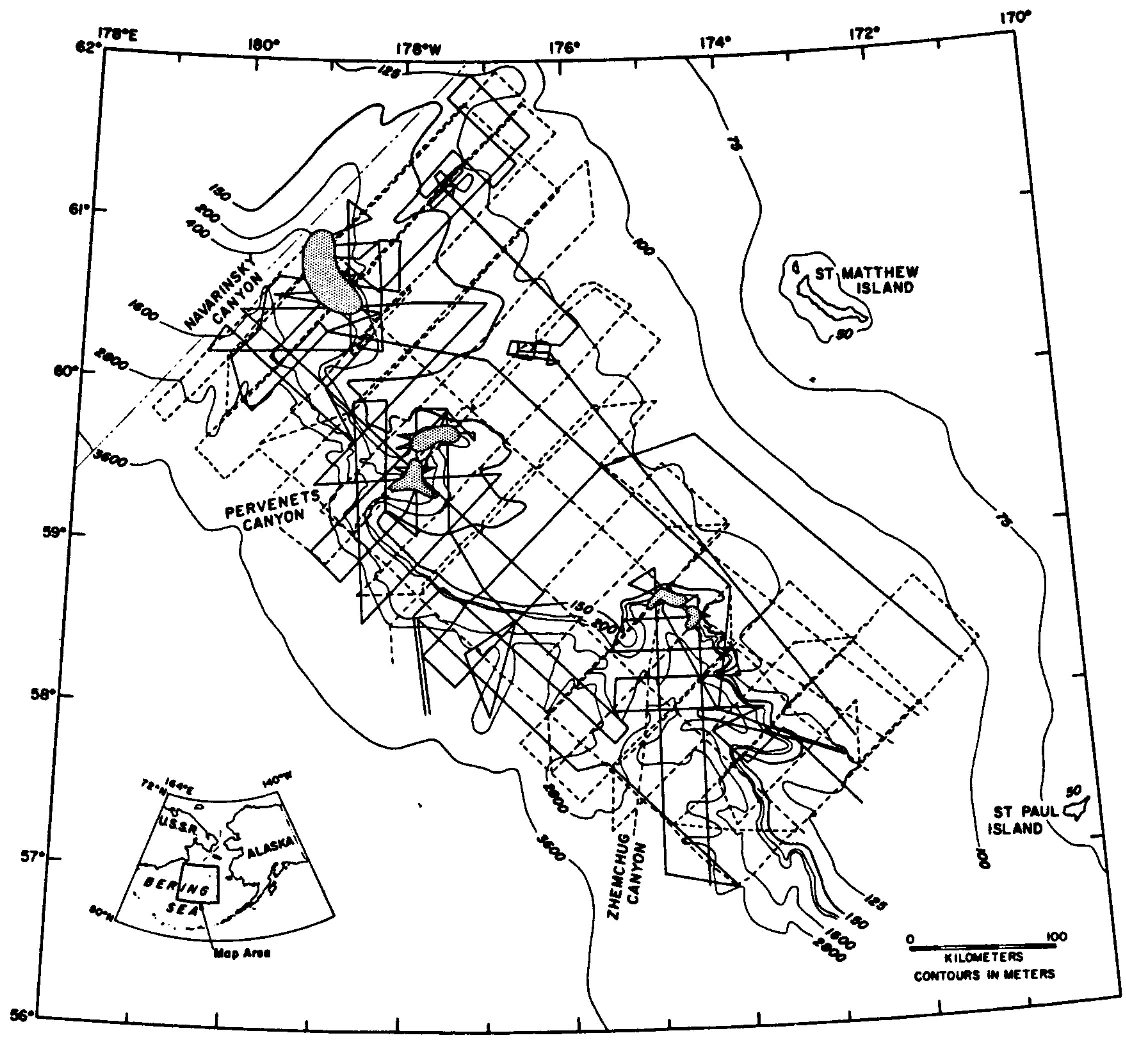

Figure H-1. Map of study area showing seismic survey tracklines and distribution of sand waves (stippled areas). Dashed lines are 1980 tracklines and solid lines are 1981 tracklines; 1981 data were collected during preparation of this manuscript; for clarity tracklines have not been shown within sand wave fields. The deeper sand wave area in Pervenets Canyon was defined almost entirely by buried bed forms.

lines were spaced 30 km apart in a rectilinear pattern; some areas were surveyed in greater detail. Sediment samples were taken at many alternate grid intersections and at sites chosen from seismic reflection profiles. Navigation was by Loran C updated by satellite.

OBSERVATIONS OF SAND WAVES

The surface sediment in the bed form area in the head of each of the submarine canyons (Fig. H1) is fine and very fine sand. Vibracores in the Navarinsky and Pervenets areas showed that sand comprised at least the upper 1.5 m of sediment. A box core collected in the Navarinsky area preserved the sediment at the water-sediment interface and revealed a thin ($\sim$1-2 cm) layer of mud covering the sand.

A detailed survey of the sand waves in the head of Navarinsky Canyon disclosed that sand waves are confined within about a 1400 km^2 area between the 215- and 450-m isobaths. The area of the Pervenets sand wave fields is approximately 800 km^2 and that of the Zhemchug fields is about 400 km^2. By measuring the apparent wavelengths of sand waves on three seismic lines that pass through the Navarinsky field at different azimuths and that nearly intersect in the southeastern corner of the sand wave field, we determined that the crests of the sand waves strike approximately north-south (N5°E), that the true wavelength is nominally 600 m, and that the heights vary from about 5 to 15 m. The sand waves are not only expressed on the seafloor, but also are remarkably well defined in the subsurface (Fig. H2). The stratigraphic unit containing the sand waves attains an aggregate thickness of 100-120 m and overlies flat, parallel reflectors. The cross-bedded unit thins to 10-15 m toward the northwestern boundary of the field, thins to about 70-90 m toward the southeastern margin, and appears to wedge out at the extreme southeastern corner of the field. The best developed sand waves occur in water depths of about 300-350 m. In shallower water the sand waves decrease progressively in amplitude, and in deeper water the bedforms often deteriorate into a "hummocky" morphology [10]. At least seven sets can be recognized in the thickest part of the section (Fig. H2). Individual cross-bedded pods within sets are as much as 20 m thick. The number of sets decreases as the unit thins. Both symmetric and asymmetric forms have been observed on the sea floor and in the subsurface. The steep faces of asymmetric waves and the internal stratification in this field have an apparent easterly dip.

DISCUSSION

The following discussion and conclusion pertain to the Navarinsky field sand waves, because we have investigated this field most thoroughly. We are convinced that the surface and buried Navarinsky field sand waves are current-generated bed forms; there is no evidence to justify the interpretation of these bed forms and cross-bedded sequences as foresets of prograding deltas or as slumps.

Mode of Formation.

Large sand waves and dunes on the continental shelf of about the same size as the Navarinsky sand waves have been attributed to unidirectional currents and to very strong tidal currents [1,11,12]. In general, though,

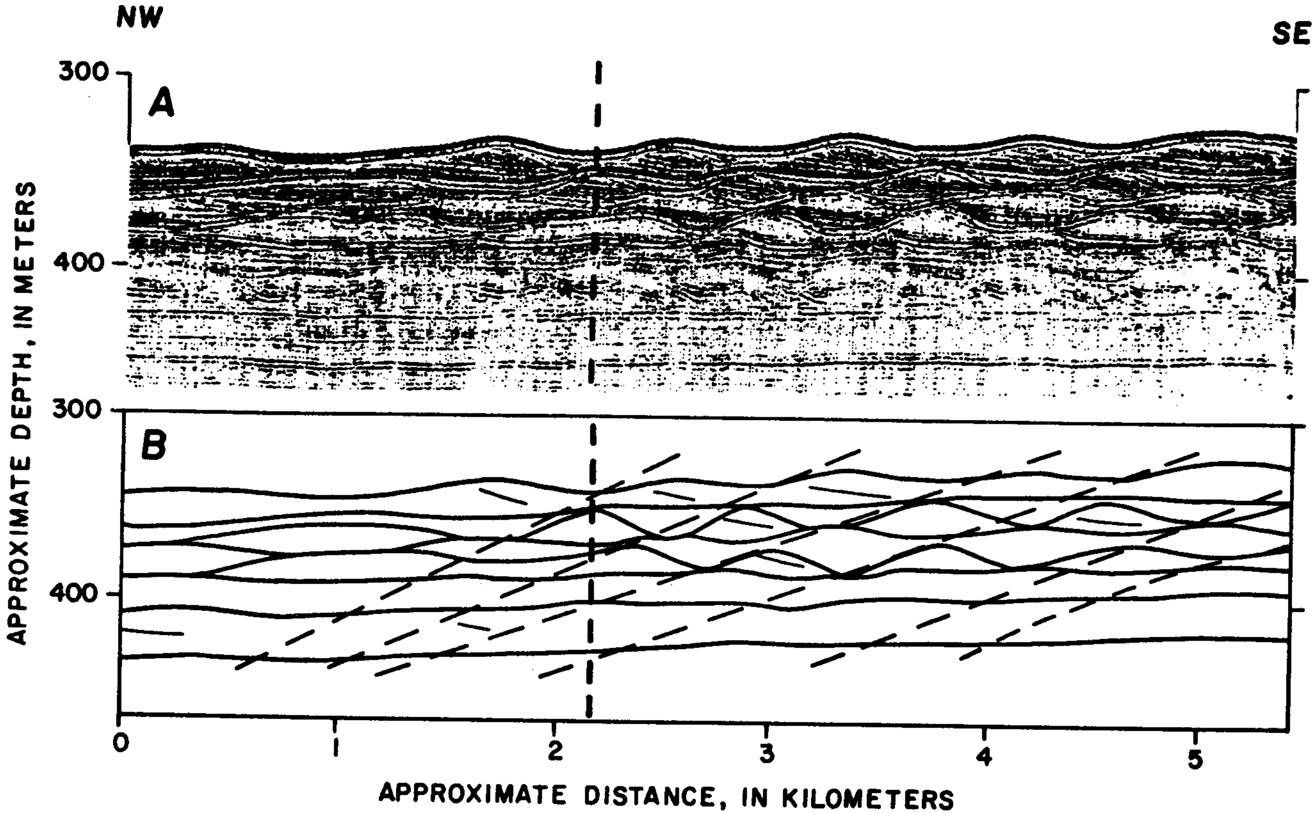

Figure H-2. Example of Navarinsky Canyon field sand waves; A, Mini-sparker record. B, Interpretive drawing; solid lines define sets of sand waves; dashed lines define angle of climb; heavy vertical dashed line is a recorder time mark.

these sand waves are more closely spaced and much more asymmetric than the Navarinsky field sand waves. Because of their sinusoidal form and low height-to-length ratio, the Navarinsky field sand waves are more closely analogous in form to those abyssal sediment waves that have been interpreted as antidunes formed by density currents -- that is to say, turbidity currents and strongly stratified flows [2,3]. However, the sand waves known to us that are most similar in shape and size to the Navarinsky field sand waves occur near the edge of the continental shelf off France in water depths of 150-160 m (La Chapelle bank); these sand waves range in height from about 8 to 12 m and are spaced about 850 m apart, and are thought to be caused by internal waves [4].

We do not know which (if any) of the four types of currents mentioned above - unidirectional, reversing unidirectional, density, and internal wave generated - is responsible for the Navarinsky field sand waves. Whichever mechanism or combination of mechanisms is responsible for the sand waves we observed, the mechanism must also explain four aspects of the sand wave fields: (1) distribution, (2) stratigraphic sequence, (3) lithology, and (4) size.

Given the uniformity of our seismic coverage of the study area, it is probably not by chance that we observed sand waves only in the heads of the submarine canyons; we think that the sand waves are causally associated with the submarine canyons. This suggests that there are processes that operate in submarine canyons that do not affect, at least as intensely, the nonincised outer shelf and upper slope. In order to deduce the mode of formation of the sand waves, it is necessary not only to identify these canyon-related processes, but also to determine whether the sand waves are active or relict features.

Using seismic reflection profiles, we have isopached the youngest stratigraphic unit in the study area [13]. The reflector defining the base of this unit is at least as old as 30×10^3 yr [14]. We have been able to trace this reflector into the upper 10-20 m of the Navarinsky sand wave sequence; however, we cannot follow the reflector through the sand wave field (Carlson and Karl, unpublished data). The sets below this reflector are certainly relict and we speculate that those above are also older than Holocene.

Two lines of evidence support the interpretation that the uppermost set of sand waves is not active. First, no available oceanographic data indicate any strong or unusual currents that could generate the sand waves. Published oceanographic reports are based on summertime measurements, so we do not know the winter currents and circulation patterns; it is conceivable that conditions intensify sufficiently during the winter to activate the bed forms. However, we are not even sure that strong currents are required to generate the sand waves. Second, the thin layer of mud covering the sand waves and the absence of any evidence of small current ripples or other bedload grain movement suggest that the bed forms were not active at the time we observed them.

The thick stratigraphic sequence of bed forms in the Navarinsky Canyon field suggests that the processes responsible for the bed forms have operated over a long period of time and that a large amount of sand was delivered to the area during this period. The sequence of seven sets of cross-beds resembles a greatly scaled-up sequence of climbing ripples (Fig. H2b). This analogy suggests continuously high rates of sedimentation during the formation of the 100-m-thick section. On the other hand, the seven sets appear to be stacked one on top of the other being separated by either non-depositional surfaces or strata draped over the sand wave surface (Fig. H2b); if this is the case, each set of sand waves was formed during a discrete period of activity that was followed by an interval of inactivity.

The sand waves on the surface, if inactive, remain unburied for at least two reasons. Only very small amounts of silt and clay are being deposited over the sand waves because the area is so great a distance from a significant sediment source; or currents in the area are sufficiently strong to inhibit deposition or to periodically remove the fine sediment that is currently being deposited; or both.

The fine and very fine sand in the canyon heads could result from the winnowing out of finer sediment by currents peculiar to the canyons. Clean sand and silty sand, however, composes the entire length of cores so long as 1.5 m, and it is not likely that this material was concentrated solely by winnowing. Major sources of sand lie hundreds of kilometers from the canyon heads. This sand could have been deposited at the canyon heads during lower stands of sea level in the Pleistocene, when numerous streams presumably flowed over the exposed shelf toward the topographically depressed canyon heads.

Conceptual Model of Depositional Environment.

Most workers estimate that the maximum eustatic lowering of sea level during the Pleistocene was 130 m [15]. A vast expanse of the Bering Sea continental shelf would have been exposed when the sea level was 130 m below the present mean sea level (Fig. H3) [16]. Pratt and Dill [17] have suggested sealevel stands as low as 240 m in the Bering Sea, but their interpretation is highly speculative. Hopkins [18] has synthesized the sealevel history of the Bering Sea during the last 250,000 years; one deduces that the paleogeography of the area is not reconstructed by simply lowering the sea level 130 m, because local tectonic and isostatic events complicate any reconstruction. Parts of the Bering Sea shelf may not have been tectonically stable during the Pleistocene (M. S. Marlow, U.S. Geological Survey, pers. comm., 1981). Moreover, it is possible that the outer shelf could have rebounded isostatically after the removal of 130 m of water; in which case, the Pleistocene shoreline during the lowest stand of sea level would have been seaward of the present-day 130-m isobath. We cannot accurately determine the position of the Pleistocene shoreline, because the amount and rate of isostatic adjustment and the tectonic effects are unknown factors. Simply as a basis for discussion, then, let us take local sea level in our study area during the Pleistocene to have been 150 m below present sea level.

If local sea level in the Bering Sea was 150 m below the present mean sea level, much of the area of the canyon heads would have been large shallow embayments along the Pleistocene coastline (Fig. H3; note caption). We use the names of the three canyons to designate these embayments. Streams draining the lowlands adjacent to these canyons would have discharged large quantities of sediment into the three embayments. Owing to the low gradients of the

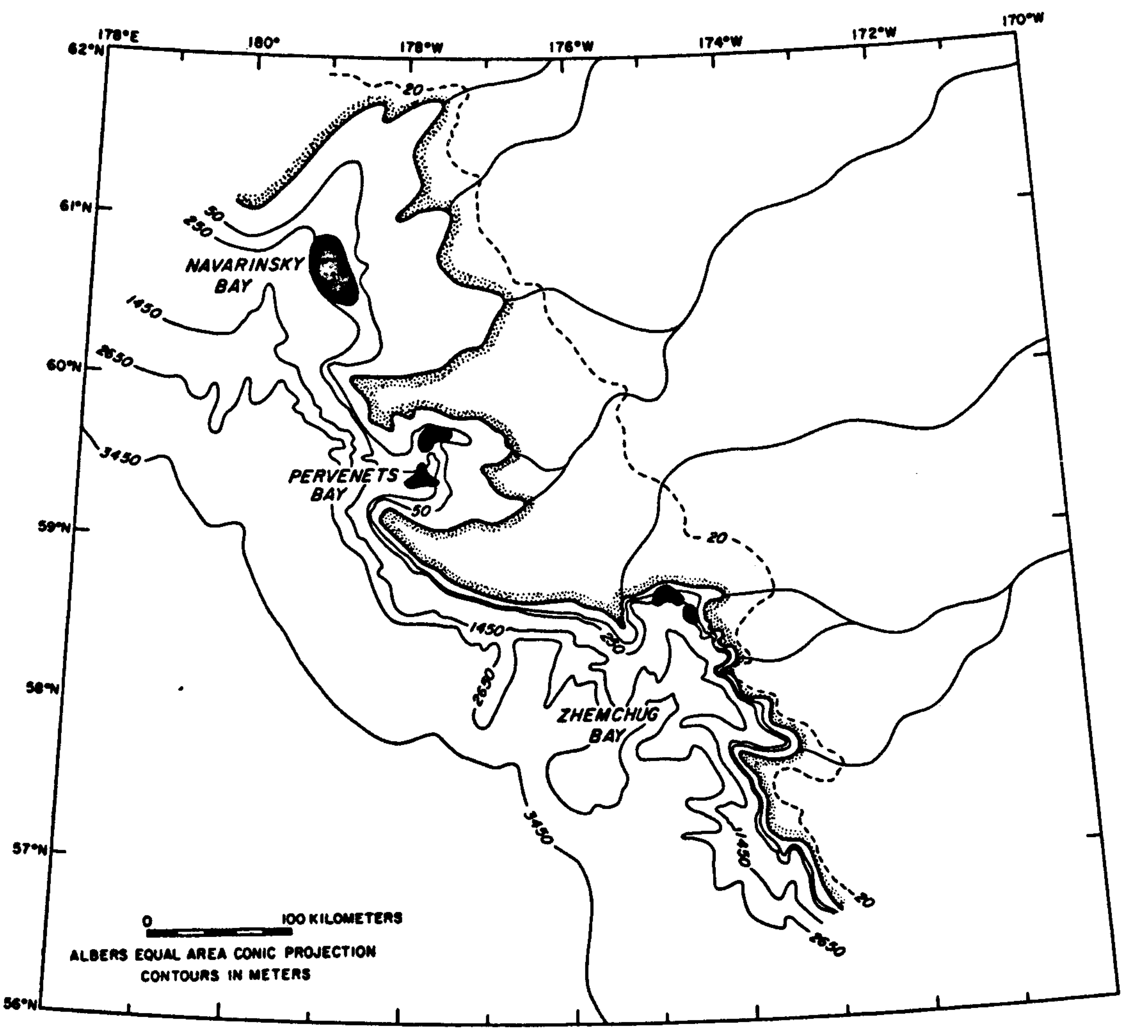

Figure H-3. Paleogeographic reconstruction of the depositional setting of the sand waves (stippled areas). Heavy solid line follows the present shelf edge and indicates the position of the Pleistocene shoreline assuming an arbitrary amount of tectonic and isostatic influence that caused local sea level to be 150 m below present sea level. Dashed line follows the present 130 m isobath. The area between these lines is that part of the shelf that would be submerged under 20 m of water assuming no local complications and only that sea level was lower eustatically by 130 m. Presence of streams is speculative.

exposed shelf, the streams would not have been competent to carry coarse material, and most of the sediment entering the embayments would have been fine sand, silt and clay. Sand would have accumulated near shore and in shallow areas of the embayments and in the heads of the submarine canyons. Most of the silt and clay in suspension would have settled out farther from shore; waves and other strong currents would have winnowed out those silts and clays that had been deposited in shallow water. The fine-grained material could have been supplied in quantities sufficient to provide the concentrations necessary to produce a low-velocity density flow; the material settling out of this flow could form antidunes.

The canyons would have dominated the submarine physiography of the embayments. Submarine canyons influence coastal and shelf sediment dynamics in several important ways. Canyons that head close to shore trap sediment moving down current in the littoral drift [19]. Internal tides and other internal waves of higher frequency are funnelled along the axes of submarine canyons and are generated at the shelf break around canyon heads [20,21]. Thus, internal wave energy can be amplified in the canyons and can be concentrated on the adjacent shelf [22]. Southard and Caccione (1972) have shown in laboratory experiments that breaking internal waves can produce bedforms. Several studies present geologic evidence that suggests that currents and water circulation patterns modified by canyons do affect the movement of sediment on the shelf [5,24]. The physiographic configuration of the embayments and canyons also may amplify such water motions as the diurnal and semidiurnal tides [25]. Low-frequency reversing water motions generated by surface or internal tides could produce symmetric sand waves or breaking internal waves of higher frequency could generate the sand waves.

The topography of the embayments could have induced vorticity in an ancestral Bering Slope Current causing a secondary circulation system in each embayment [12,26]. The asymmetry of some of the sand waves and the apparent easterly dip of internal strata indicate a net migration toward the east which is toward shore and oblique to isobaths and opposite to the northwesterly flow the present-day Bering Slope Current. Anticyclonic eddies within Navarinsky Bay shed by an ancestral Bering Slope Current could account for this direction of migration.

CONCLUSIONS

We hypothesize that the sand waves in the heads of Navarinsky, Pervenets, and Zhemchug submarine canyons originated in shallow embayments during lower stands of sea level in the Pleistocene. Obviously, sufficient data are not available to prove this conclusions, and we do not intend, by focusing on this preliminary working hypothesis, to discount or refute alternative hypotheses, as for example that the sand waves developed only after the Holocene transgression.

The working hypothesis described herein is satisfying for several reasons: (1) It accounts for the fact that sand waves have only been observed in the heads of the canyons and not on the upper slope and outer shelf between canyons; (2) It helps explain the size of each sand wave field in that the area of each field correlates with the physiography of the embayments. For example, Navarinsky Bay had the largest expanse of shallow water (shoal area) and the Navarinsky sand wave field, is the most extensive. (3) Fluctuating sea levels help explain the stratigraphy of the bed forms in the Navarinsky field if the sand waves are individual sets stacked one on the other; alternatively, the interpretation of this sequence as climbing bed forms is plausible if large amounts of sediment were supplied to the embayments during a continuous rise of sea level. The oceanic processes responsible for the sand waves became operative, and sediment was supplied to the sand wave sites, at times of lower sea level. This dynamic system was shut off or diminished in intensity during higher sea level stands. Small changes of sea level would rapidly affect large areas of the Bering Sea shelf.

ACKNOWLEDGMENTS

We thank J. B. Southard and D. M. Rubin for reviewing the manuscript. This investigation was supported by the U.S. Geological Survey and by the Bureau of Land Management through an interagency agreement with the National Oceanic and Atmospheric Administration, under which a multiyear program responding to the needs of petroleum development of the Alaskan continental shelf is managed by the Outer Continental Shelf Environmental Assessment Program Office.

REFERENCES

[1] Swift, D.J.P. and Ludwick, J. C., 1976. Substrate response to hydrodynamic processes: grain-size frequency distributions and bedforms. D. J. Stanley and D.J.P. Swift, (eds.), Marine sediment transport and environmental management: New York, John Wiley, p. 255-310.

[2] Damuth, J. E., 1980. Use of high-frequency (3.5 - 12 kHz) echograms in the study of near-bottom sedimentation processes in the deep-sea: a review. Marine Geology, v. 38, p. 51-75.

[3] Normark, W. R., Hess, G. R., Stow, D.A.V., and Bowen, A. J., 1980. Sediment waves on the Monterey Fan levee: a preliminary physical interpretation. Marine Geology, v. 37, p. 1-18.

[4] Stride, A. H. and Tucker, M. J., 1960. Internal waves and waves of sand. Nature, v. 188, p. 933.

[5] Knebel, H. J. and Folger, D. W., 1976. Large sand waves on the Atlantic outer continental shelf around Wilmington Canyon, off eastern United States. Marine Geology, v. 22, p. M7-M15.

[6] Carlson, P. R. and Karl, H. A., 1981. Geologic hazards in Navarin basin province, northwestern Bering Sea. U.S. Geol. Survey Open-File Report 81-1217, 149 p.

[7] Scholl, D. W., Buffington, E. C., and Marlow, M. S., 1975. Plate tectonics and the structural evolution of the Aleutian-Bering Sea region. In: R. B. Forbes (ed.), Contributions to the Geology of the Bering Sea Basin and Adjacent Regions, Geol. Soc. America Spec. Paper 151, p. 1-32.

[8] Kinder, T. H., Coachman, L. K., and Galt, J. A., 1975. The Bering Slope Current System. Journal of Physical Oceanography, v. 5, p. 231-244.

[9] Schumacher, J. D. and others, 1979. Structural fronts over the continental shelf of the eastern Bering Sea. Journal of Physical Oceanography, v. 9, p. 79-87.

[10] Carlson, P. R., Karl, H. A., and Edwards, B. D., in review, Puzzling features in the head of Navarinsky Canyon, Bering Sea. Geo-Marine Letters, 12 ms.p.

[11] Bouma, A. H., Hampton, M. A., and Orlando, R. C., 1978. Sand waves and other bedforms in lower Cook Inlet, Alaska. Marine Geotechnology, v. 2, p. 291-308.

[12] Fleming, B. W., 1981. Factors controlling shelf sediment dispersal along the southeast African continental margin. In: C. A. Nittrouer (ed.), Sedimentary dynamics of continental shelves, developments in sedimentology, v. 32: Amsterdam, Elsevier Scientific Publishing Company, p. 259-277.

[13] Carlson, P. R., Fischer, J. M., Karl, H. A., and Larkin, C., 1983. Isopach map of Unit A, youngest sedimentary sequence in Navarin basin, Bering Sea. In: H. A. Karl and P. R. Carlson (eds.), Geologic hazards in Navarin basin province, northwestern Bering Sea, Final report R.U. #588. Alaska continental shelf, Principal Investigators reports. NOAA, OCSEAP, Boulder, CO.

[14] Carlson, P. R., and Karl, H. A., 1983. Rates of sediment accumulation in Navarin Basin province, Bering Sea. In: H. A. Karl and P. R. Carlson (eds.), Geologic hazards in Navarin Basin province, northwestern Bering Sea, Final report R.U. #588. Alaska continental shelf, Principal Investigators.reports. NOAA, OCSEAP, Boulder, CO.

[15] Bloom, A. L., 1971. Glacial-eustatic and isostatic controls of sea level since the last glaciation. In: K. K. Turekian, (ed.), Late Cenozoic glacial ages, New Haven, Yale University Press, p. 355-379.

[16] Gardner, J. V., Dean, W. E., and Vallier, T. L., 1979. Sedimentology and geochemistry of surface sediments, outer continental shelf, southern Bering Sea. Marine Geology, v. 35, p. 299-329.

[17] Pratt, R. M. and Dill, R. F., 1974. Deep eustatic terrace levels: further speculations. Geology, v. 2, p. 155-159.

[18] Hopkins, D. M., 1973. Sea level history in Beringia during the past 250,000 years. Quaternary Research, v. 3, p. 520-540.

[19] Inman, D. L., Nordstrom, C. E., and Flick, R. E., 1976. Currents in submarine canyons: an air-sea-land interaction. Annual Review Fluid Mechanics, v. 8, p. 275-310.

[20] Apel, J. R., Byrne, H. M., Prone, J. R., and Charnell, R. L., 1975. Observations of oceanic internal and surface waves from the Earth Resources Technology satellite. Journal of Geophysical Research, v. 80, p. 865-881.

[21] Shepard, F. P., Marshall, N. F., McLaughlin, P. A., and Sullivan, G. G., 1979. Currents in submarine canyons and other sea valleys. American Association Petroleum Geologists, Studies in Geology, no. 8, p. 865-881.

[22] Karl, H. A., Cacchione, D. A., and Carlson, P. R., 1982. Large sand waves in canyon heads, Bering Sea: products of internal waves or density currents? (abs.). International Association of Sedimentologists Abstracts of papers, 11th International Congress on Sedimentology, p. 73.

[23] Shepard, F. P., Sullivan, G. G., and Wood, F. J., 1979. Perigean spring tides and unusual currents in La Jolla submarine canyons (abs.). Geological Society of America Abstracts with Programs, v. 11, no. 7, p. 515.

[24] Karl, H. A., 1980. Influence of San Gabriel submarine canyon on narrow-shelf sediment dynamics, southern California. Marine Geology, v. 34, p. 61-78.

[25] Southard, J. B. and Cacchione, D. A., 1972. Experiments on bottom sediment movement by breaking internal waves. In: D.J.P. Swift, D. Duane, and O. Pilkey, (eds.), Shelf sediment transport: process and pattern: Stroudsburg, Pa., Dowden, Hutchinson and Ross, Inc., p. 83-97.

[26] Janowitz, G. S. and Pietrafera, L. J., in press. Topographically induced upwelling in the regions of the Charleston Bump, The Carolina capes and the eastern Florida shelf. Journal of Physical Oceanography.

GEOTECHNICAL FRAMEWORK STUDY OF SHELIKOF STRAIT, ALASKA

by

Monty A. Hampton

U.S. Geological Survey

Final Report
Outer Continental Shelf Environmental Assessment Program
Research Unit 589

1983

TABLE OF CONTENTS

LIST OF FIGURES

LIST OF TABLES

INTRODUCTION

Studies have been conducted by the U.S. Geological Survey to identify geologic conditions that might impose constraints on offshore industrial activities in Shelikof Strait, Alaska, an area designated for petroleum leasing (Fig. 1; Hampton and others, 1981; Hampton and Winters, 1981). As part of these studies sediment cores were collected throughout the strait (Fig. 2), and physical properties of sediment samples were measured by laboratory geotechnical testing methods. The geotechnical data are presented in this report and are evaluated from a regional perspective to infer the deformational reponse of the sedimentary deposits to static and dynamic loads.

Application of the test data to a regional analysis is restricted by the degree to which core samples are representative of the sedimentary deposits. Interpretive geologic studies indicate that the cores used for geologic testing cover the range of surficial sediment types in the Shelikof Strait lease area, but analysis of seismic-reflection profiles reveals the existence of buried stratigraphic units that were not sampled because they lie beneath the maximum core length of 3 m (Hampton and others, 1981; Hampton and Winters, 1981). Therefore, the conclusions reached in this report apply directly to the uppermost deposits in the stratigraphic section, only. Extrapolation beyond the depths of sampling is limited by the vertical uniformity of sediment type.

GEOLOGIC SETTING

Shelikof Strait is a nearly parallel-sided marine channel situated between the Kodiak Island group and the Alaska Peninsula (Fig. 1). The strait marks the location of a northeast-trending inner forearc basin that is located

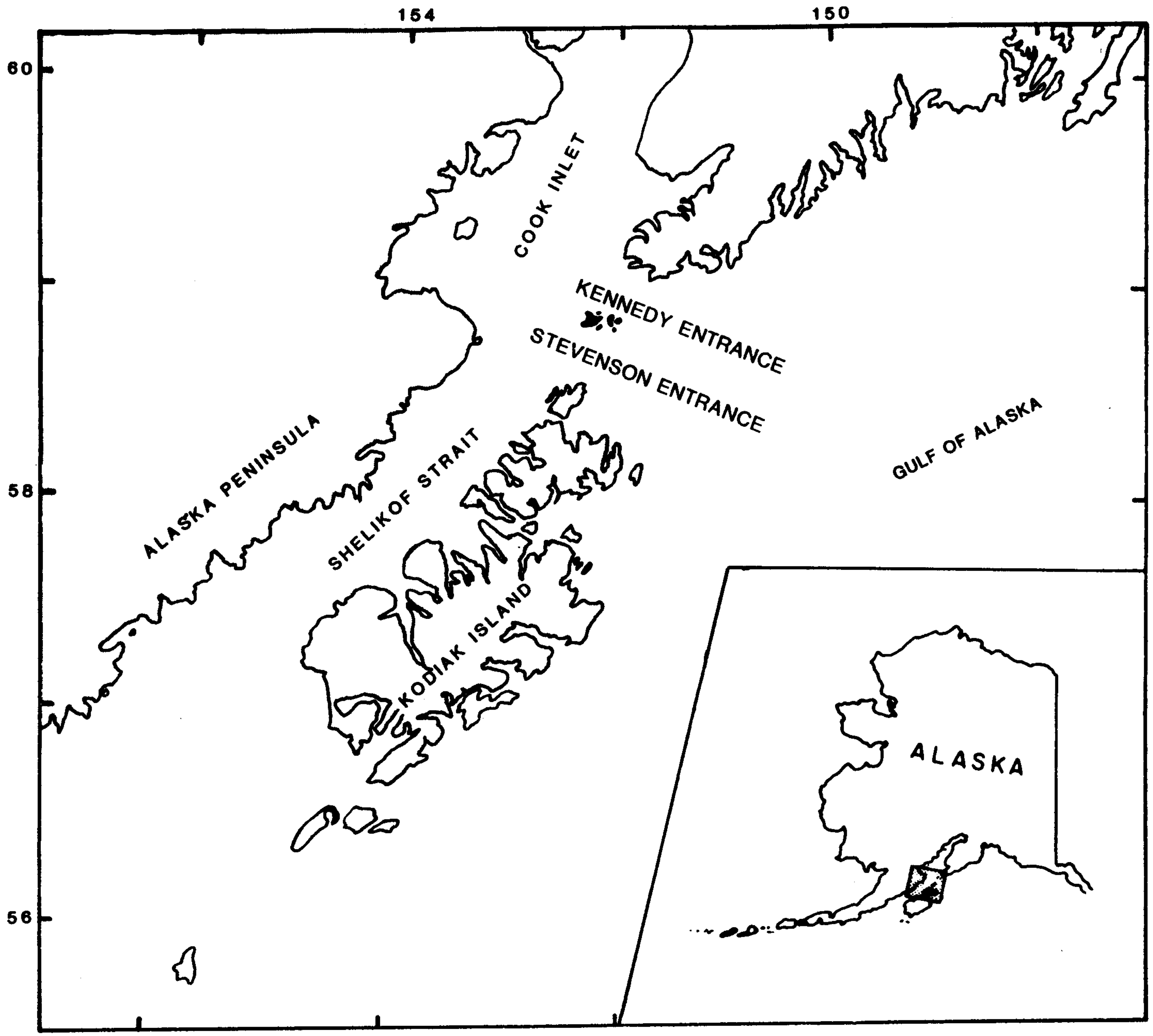

Figure 1. Location map of the study area in Shelikof Strait.

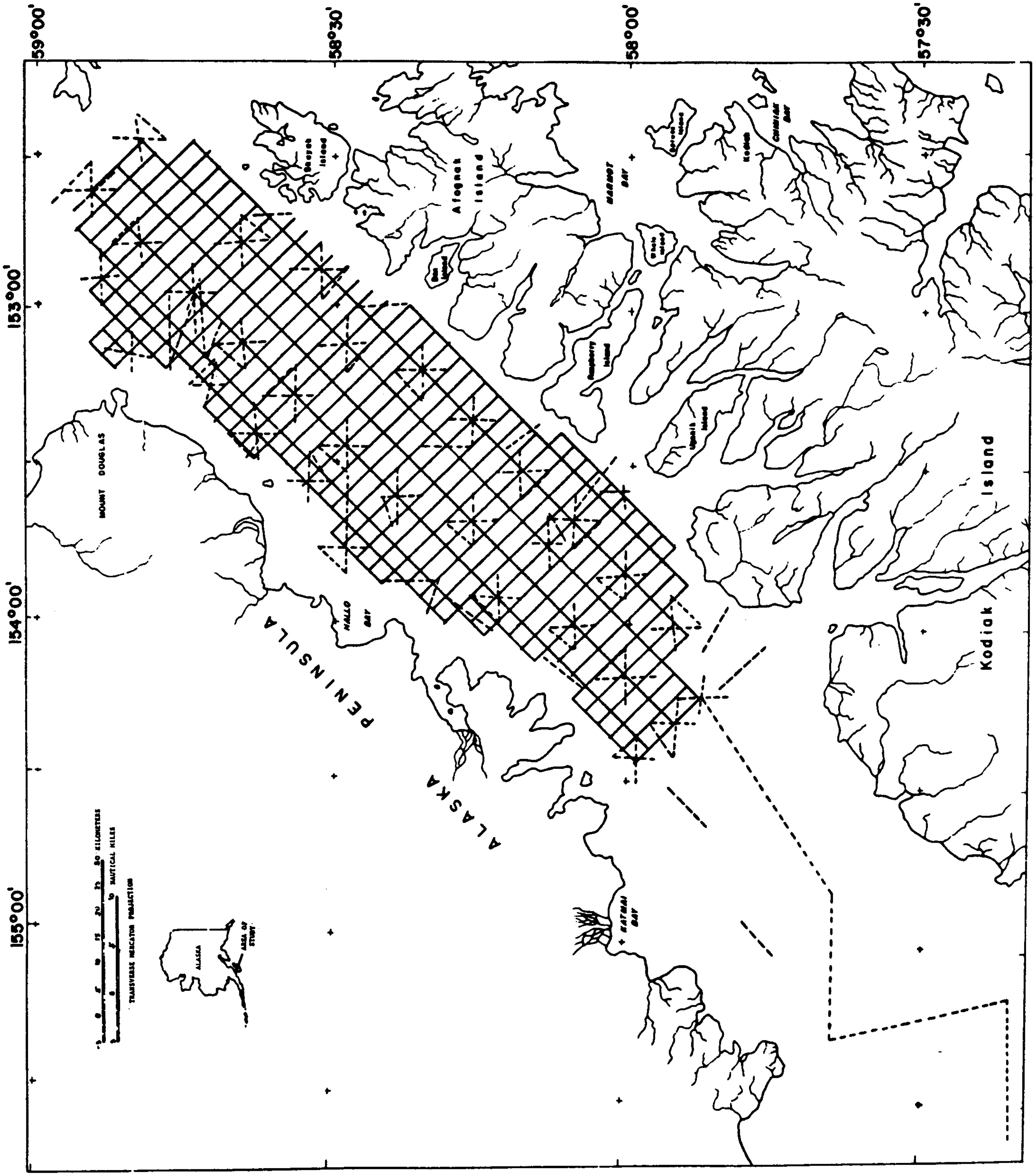

Figure 2-A. Tracklines of continuous seismic-reflection profiles. Solid lines represent a regional survey contracted by the Conservation Division, and dashed lines represent site surveys on cruises of the R/V S.P. LEE (1980) and NOAA ship DISCOVERER (1981).

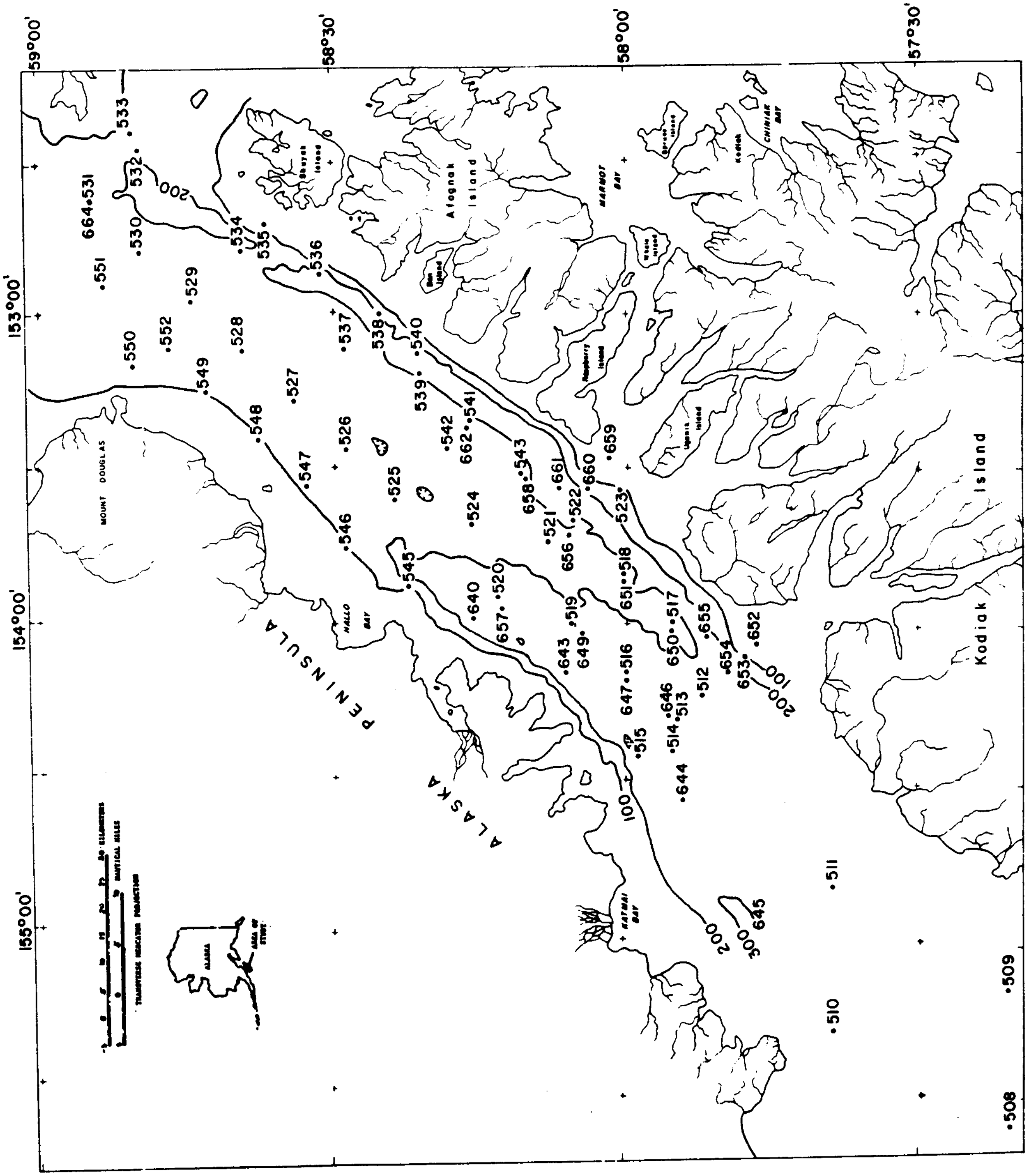

Fig. 2B

Figure 2-B. Locations of sediment-sampling stations.

near the convergent margin of the North America plate where it is being underthrust by the Pacific plate (von Huene, 1979). Large earthquakes are common to the region; at least 95 potentially destructive events (magnitude >6) have occurred since recording began in 1902. Twelve volcanoes have erupted within the last 10,000 years along the Alaska Peninsula adjacent to the strait.

The seafloor of Shelikof Strait consists of a gently southwest-sloping central platform bordered by narrow marginal channels parallel to the Kodiak islands and the Alaska Peninsula (Fig. 3). Shallow shelves trend along the adjacent landmasses, and they are connected to the marginal channels by steeply sloping seafloor. Water depth in the northeast part of the strait is generally less than 200 m, whereas in the southwest it generally exceeds 200 m and is as much as 300 m. Superimposed on the platform are some local highs and lows that have as much as 100 m relief. Along the axes of the marginal channels are several closed depressions on the order of 30 m relief.

Sedimentary deposits of presumed Pleistocene and Holocene age overlie an irregular unconformity above Tertiary and older bedrock. Thickness of the sediment above bedrock, measured from seismic-reflection profiles, is about 80 to 100 m in the northeast half of the strait and increases abruptly to more than 800 m in the southwest (Fig. 4). The thickening reflects a deepening of the unconformity.

Four seismic-stratigraphic units can be distinguished above bedrock (Fig. 5). The lowest unit (unit 1 in Fig. 5) fills the bedrock depression and reaches a thickness of 800 m. This unit is interpreted as being of glacial and glaciomarine origin (Whitney and others, 1980 a, b). The next highest unit (unit 2 in Fig. 5) is relatively thin (<60 m) and occurs mainly in the

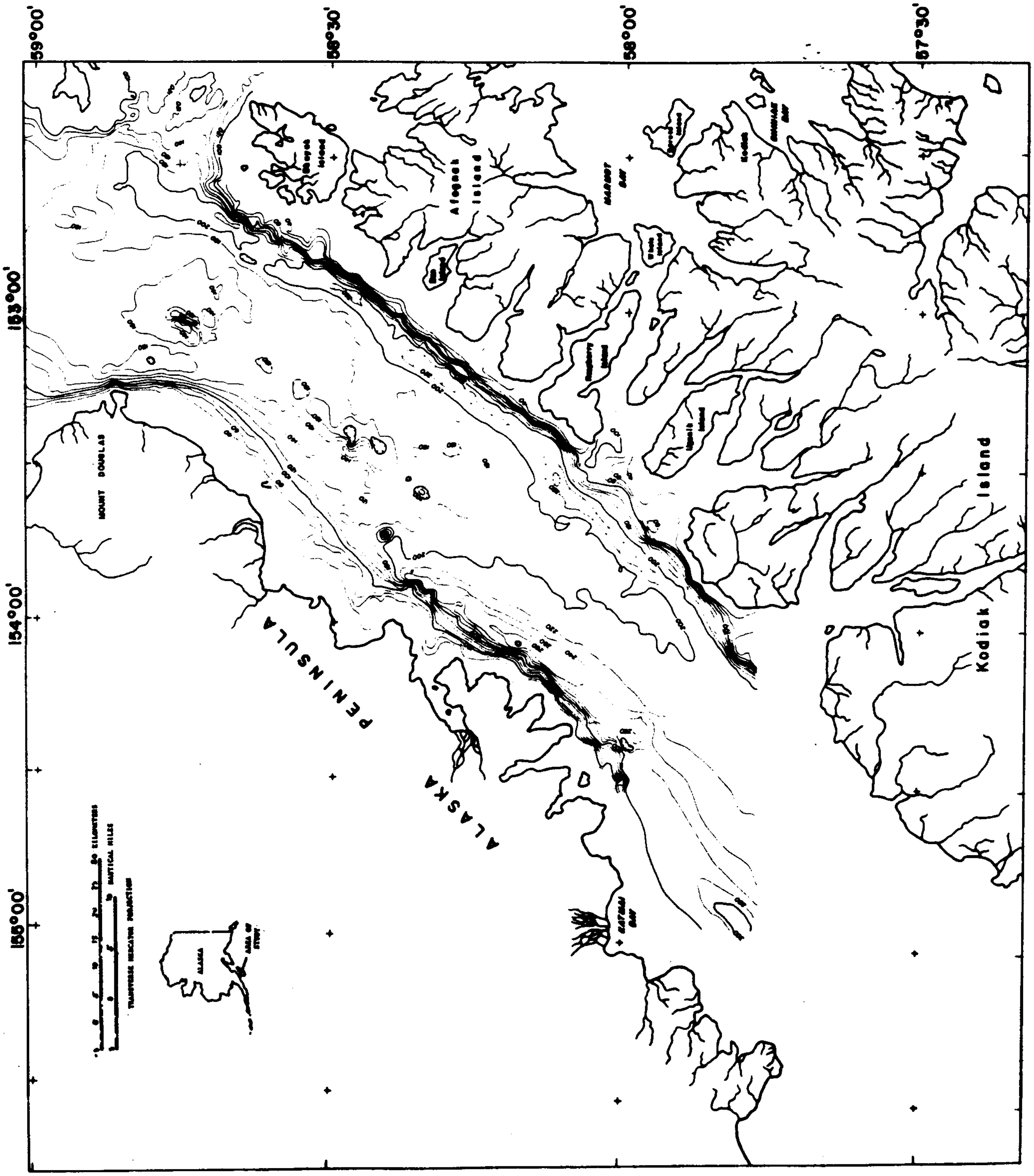

Figure 3. Bathymetry of Shelikof Strait, 20-m contour interval. Depths corrected to mean lower low water.

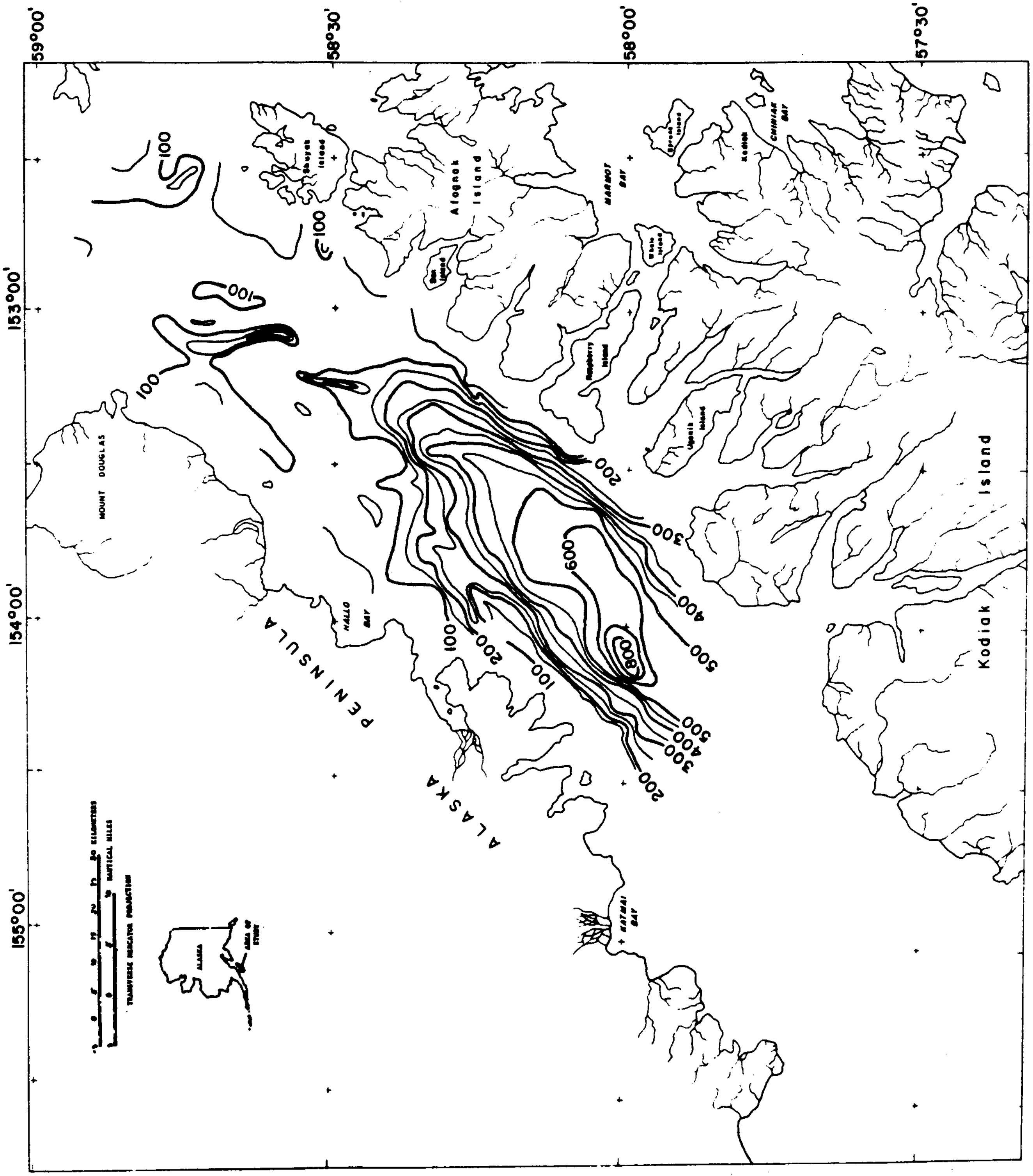

Figure 4. Thickness of sedimentary units of probably Pleistocene and younger age. Contour interval: 50 meters except for thickness greater than 500 m where contour interval is 100 m.

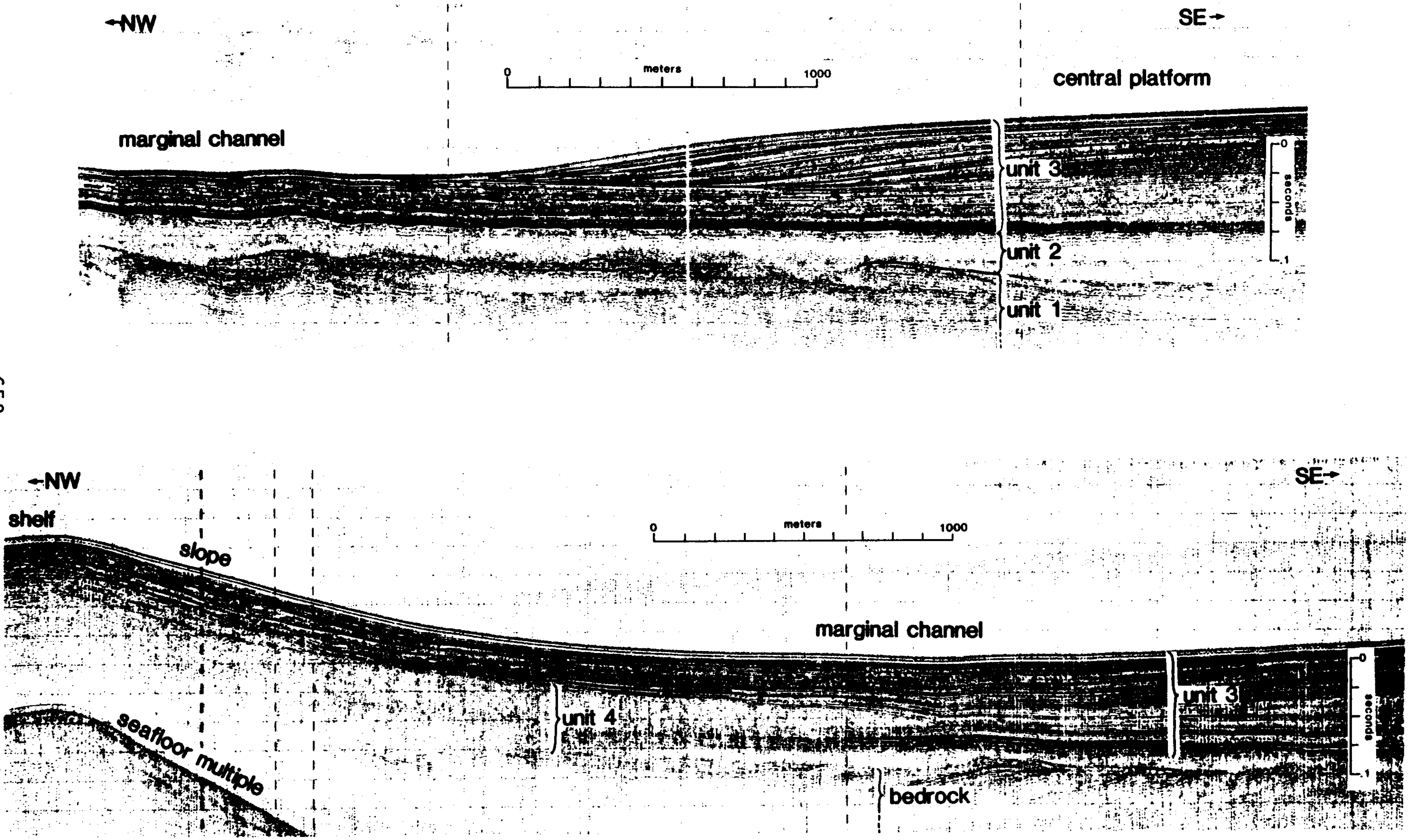

Figure 5. Representative seismic-reflection profiles showing seismic-stratigraphic units.

central part of the strait. Sediment of this unit was deposited within low areas on the upper surface of bedrock and the glacial unit, and it apparently was emplaced by marine processes during the Holocene sea-level rise. The third unit (unit 3 in Fig. 5), which covers essentially all of the seafloor in the central part of the strait (platform and marginal channels), is up to 180 m thick (Fig. 6) and was deposited by the modern-day oceanic current regime of southwesterly baroclinic flow from Cook Inlet and the eastern Gulf of Alaska (Muench and Schumacher, 1980). Unit 4 in Figure 5 underlies the shallow shelves and interfingers seaward with unit 3. It is composed of sediment eroded from the adjacent landmasses. The cores subjected to geotechnical testing and discussed in this paper were taken from unit 3.

METHODS

Sediment cores were collected at 65 stations on two cruises in Shelikof Strait, in June 1980 aboard the USGS R/V S.P. LEE and in July and August 1981 aboard the NOAA ship DISCOVERER (Fig. 2). A gravity coring system with 8.5-cm diameter plastic liners in steel core barrels was used on the 1980 cruise, whereas a vibracoring system with a 10-cm square cross-section plastic liner in thin-wall stainless steel barrel was employed on the 1981 cruise. Some grab samples were taken at locations of coarse sediment where the coring devices were ineffective.

Two cores were taken at most stations. One was designated mainly for geological analysis. It was cut into 1-m or 1.5-m-long sections, then split lengthwise for geological description and vane-shear strength testing. Subsamples were taken for index property determinations.

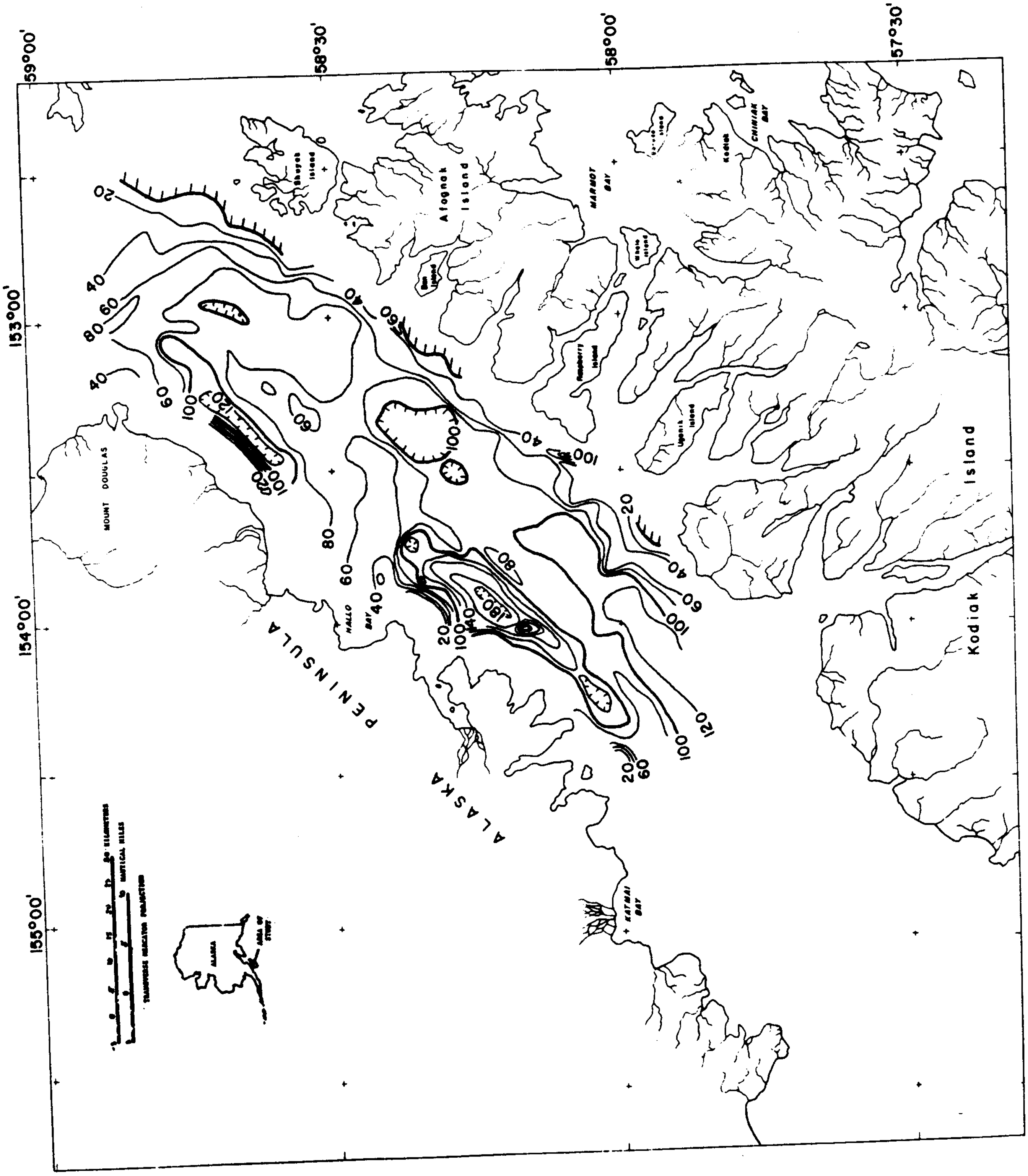

Figure 6. Thickness of highest seismic-stratigraphic unit that covers most of the seafloor of Shelikof Strait. Contour interval: 20 m.

The second core was taken expressly for geotechnical testing. It was cut into 1-m-long sections, wrapped in cheesecloth, covered with microcrystalline wax, and stored upright in a refrigerator. These cores were later subjected to a suite of geotechnical tests in laboratories at the USGS and at a commercial testing company.

Several index properties were determined for subsamples of the sediment cores. Grain size was measured by sieving and pipetting into four size classes: gravel (>2 mm), sand (2-0.062 mm), silt (0.062-0.004 mm), and clay (<0.004 mm). Water content, as a percentage of dry sediment weight, was determined from the weight of sediment samples before and after even drying at 105°C. A correction for salt content of sea water (3.5%) was made to the weighings. Atterberg limits were determined according to standard procedures (American Society for Testing and Materials, 1976), except that samples were not sieved prior to testing. Carbon content was measured with a LECO carbon determinator with induction furnace and acid digestion. Vane shear determinations of undrained shear strength were made on split core halves with a motorized device at a vane rotation rate of 90°/min. The vane is 1/2 inch diameter by 1/2 inch high and was inserted into the sediment to a depth twice the height of the vane.

Consolidation tests were run on subsamples from geotechnical cores to determine sub-failure deformational properties. Most tests were run on an oedometer in a stress-controlled mode (Lambe, 1951). Others were run in a triaxial loading cell under constant rate of strain conditions (Wissa and others, 1971). The consolidation tests measure change in volume with change in applied load. The results are normally plotted as void ratio (e = volume of voids/volume of solids) versus the logarithm of effective (buoyant) vertical stress (p'). Two useful parameters are derived from these curves: the compression index and the maximum past pressure. The compression index (C_c) is the slope of the straight-line portion of the e-log p' curve and indicates the amount of compression produced by a particular load increment. The maximum past pressure (σ'_{vm}) is the greatest effective overburden stress to which the sediment has ever been exposed and is determined from the e-log p' curve by a simple graphical construction (Casagrande, 1936). The ratio of σ'_{vm} to the effective overburden stress at the time of sampling (σ'_{vo}) is the overconsolidation ratio (OCR), which is a measure of unloading that the sediment may have experienced, by erosion for example. A third parameter, the coefficient of consolidation (c_v), is determined for each load increment of the one-dimensional consolidation test and is related to the rate of consolidation.

Static traxial tests were run on cylindrical samples 3.6-cm diameter and 7.6-cm long in order to determine strength properties of the sediment. Tests were run under undrained conditions with pore pressure measurements (Bishop and Henkel, 1964). Most samples were consolidated isotropically prior to testing, but some were consolidated anisotropically.

Dynamically loaded triaxial tests were also run, with the axial stress on samples varied sinusoidally at 0.1 Hz. Both compression and tension were applied at a predetermined percentage of the static strength. These tests can be used to evaluate the failure conditions of sediment under repeated loading, such as by earthquakes.

A first set of triaxial tests was run on sediment samples that were consolidated to somewhat arbitrary stress levels. However, the later testing program followed the normalized stress parameter (NSP) approach (Ladd and

Foott, 1974), whereby consolidation stresses are chosen on the basis of maximum past pressure (σ'_{vm}), as determined from consolidation tests. Typically, the triaxial test specimen was consolidated to four times σ'_{vm}, which eliminates some of the disturbance effects associated with coring. Overconsolidation was artificially induced in some tests by rebounding the specimen to lower stress levels before applying the triaxial load. Measured values of undrained shear strength (S_u) are normalized with respect to effective overburden stress (σ'_v). A premise of the NSP method is that the ratio S_u/σ'_v is constant for a particular value of OCR. Moreover, a relation exists between S_u/σ'_v and OCR that allows prediction of sediment strength at depths below the level of sampling (Mayne, 1980).

RESULTS

<u>Sediment description, index properties:</u> Sediment samples could only be collected to shallow depths (<3 m) beneath the seafloor. Therefore, most are from the highest stratigraphic unit (unit 3, Fig. 5). However, judging from seismic-reflection profiles over sampling stations, a few outcrops of other units were also sampled. Seismic-reflection profiles also show that unit 3 has a typical thickness of about 80 to 100 m (Fig. 6). The appearance of acoustic reflectors within this unit indicates some lithologic variability with depth, but there is no reason to suspect radical changes in sediment type, except for possible thin beds of volcanic ash. The physical properties for the cores should therefore be representative of the terrigenous component of the unit as a whole, but drill-hole samples would be necessary to confirm this.

The texture of surficial sediment on the central platform and in the adjacent marginal channels grades from gravelly and sandy material in the northeast part of the strait to mud in the southwest (Figs. 7 and 8; Appendix). A general fining trend from northwest to southeast across the platform also exists.

The two grab samples of coarse sediment recovered from Stevenson Entrance appear to have been taken from outcrops of unit 1. Most of the coarse clasts, which range to boulder size, are angular to subangular, and some are faceted. This supports the hypothesis that unit 1 was deposited by glacial processes.

A few grab samples of coarse material were also recovered from the shallow shelves and from the adjacent slopes. They probably are from unit 4. Coarse clasts have similar morphology to those from unit 1, perhaps reflecting glacial transport at some point in their history.

Sediment cores from the platform and marginal channels in the central portion of the strait have a fairly uniform stratigraphy with depth. Sandy sediment in the northeast end of the strait is predominantly greenish-gray, with variations from black to yellowish brown. Sand-filled burrows, pebble clasts, and whole or broken shells are common. In progressively finer-grained cores to the southwest, color remains greenish-gray but is less varied, and shells and clasts are rare.

A layer of volcanic ash occurs in many cores. Maximum thickness of the layer is nearly 20 cm. It is size-graded, with the coarsest basal fragments a few millimeters diameter. The color is from tan to white with a pink cast. The refractive index of the ash is 1.485 $\pm$ 0.002, which in this region is unique to the outfall from the 1912 Katmai eruption (Nayudu, 1964; Pratt and others, 1973). Depth of the ash beneath the seafloor was used to calculate

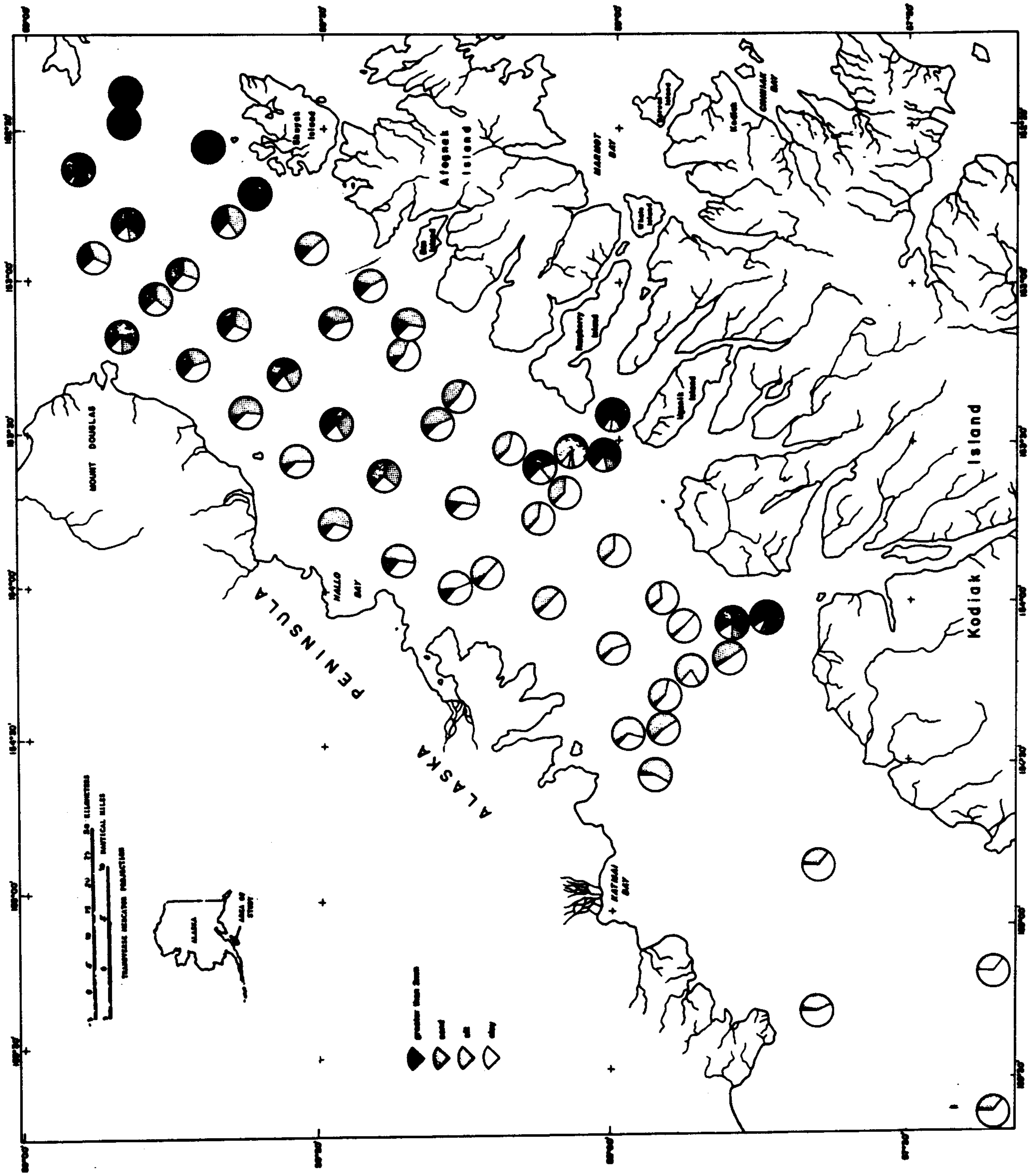

Figure 7. Pie-diagrams showing relative abundances of textural classes in seafloor sediment samples.

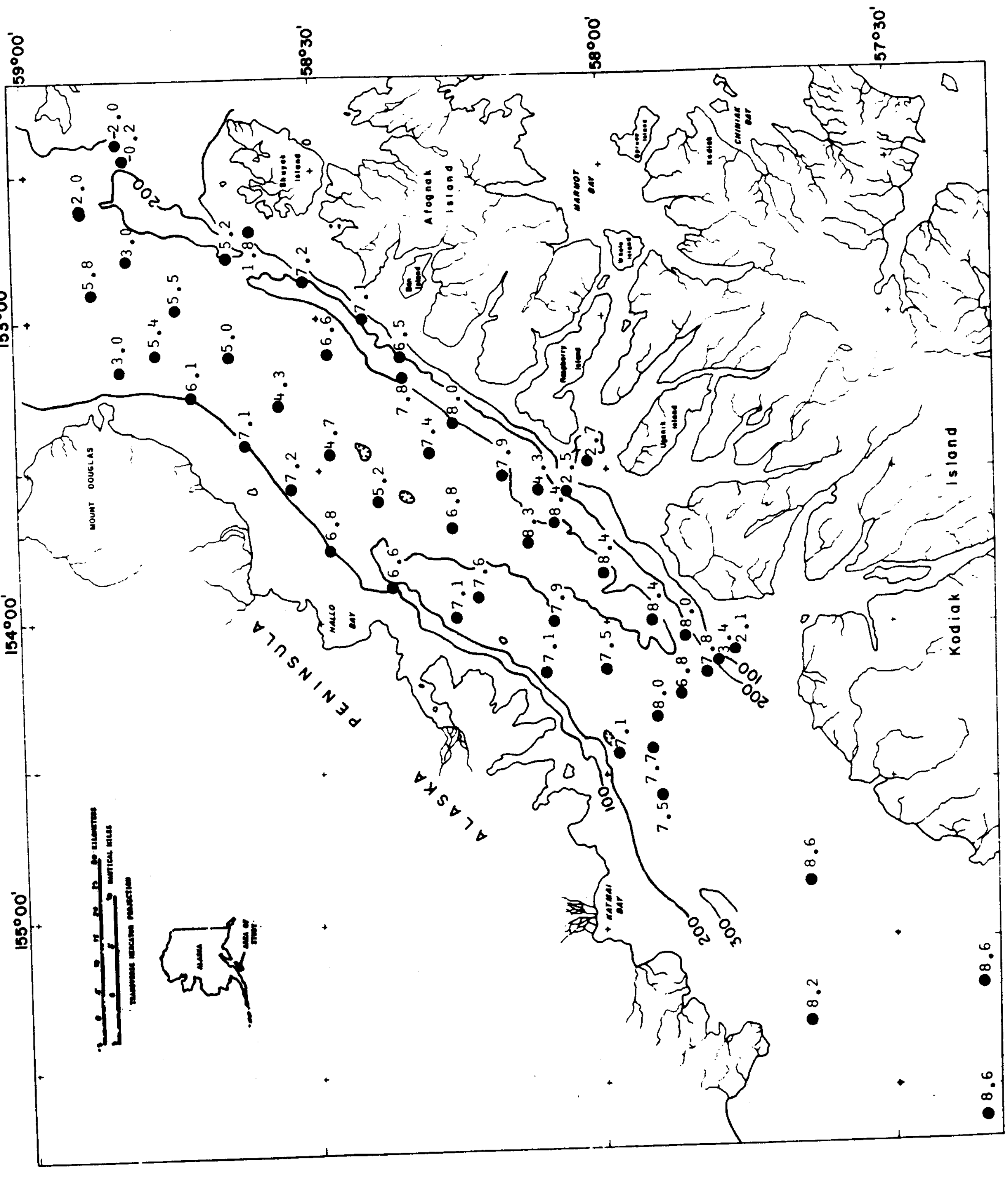

Figure 8. Mean grain size of seafloor sediment, in phi-units.

values of post-1912 sediment accumulation rate (Fig. 9). Accumulation rate varies significantly throughout the strait. It is greatest near the Alaska Peninsula at the southwest end of the strait, whereas it is near zero at places in the marginal channel along the Kodiak island group.

Water content of sediment is shown in Figure 10 as interpolated values at 1-m depth in cores. It is calculated as a percentage of dry sediment weight, and therefore, values in excess of 100% are possible if the weight of water exceeds the weight of sediment grains. Water content generally decreases to the northeast, inversely correlating with grain size. Moreover, water content increases across the strait, from the Alaska peninsula to Kodiak Island. Bulk sediment density at 1-m depth, which is calculated from water content and grain specific gravity, correspondingly decreases down and across the strait (Fig. 11). Average grain specific gravity itself shows no discernible trend (Fig. 12).

Atterberg limits describe the plasticity of sediment, in terms of the liquid limit (water content that separates plastic and liquid behavior) and the plastic limit (water content that separates semi-solid and plastic behavior). Useful derivatives are the plasticity index (difference between the liquid and plastic limits), and the liquidity index (position of the natural water content relative to the liquid and plastic limits). Certain trends in plasticity are evident in Shelikof Strait. Average liquid limit, plastic limit, and plasticity index increase down the strait toward the southwest, and also generally across the strait, toward the southeast (Figs. 13, 14, and 15; Appendix). These properties also generally increase with decrease in mean grain size (Figs. 16, 17, and 18), although the data for plastic limit are quite scattered. Plastic limit is less variable than liquid limit, which is typically the case (Mitchell, 1976; Richards, 1962).

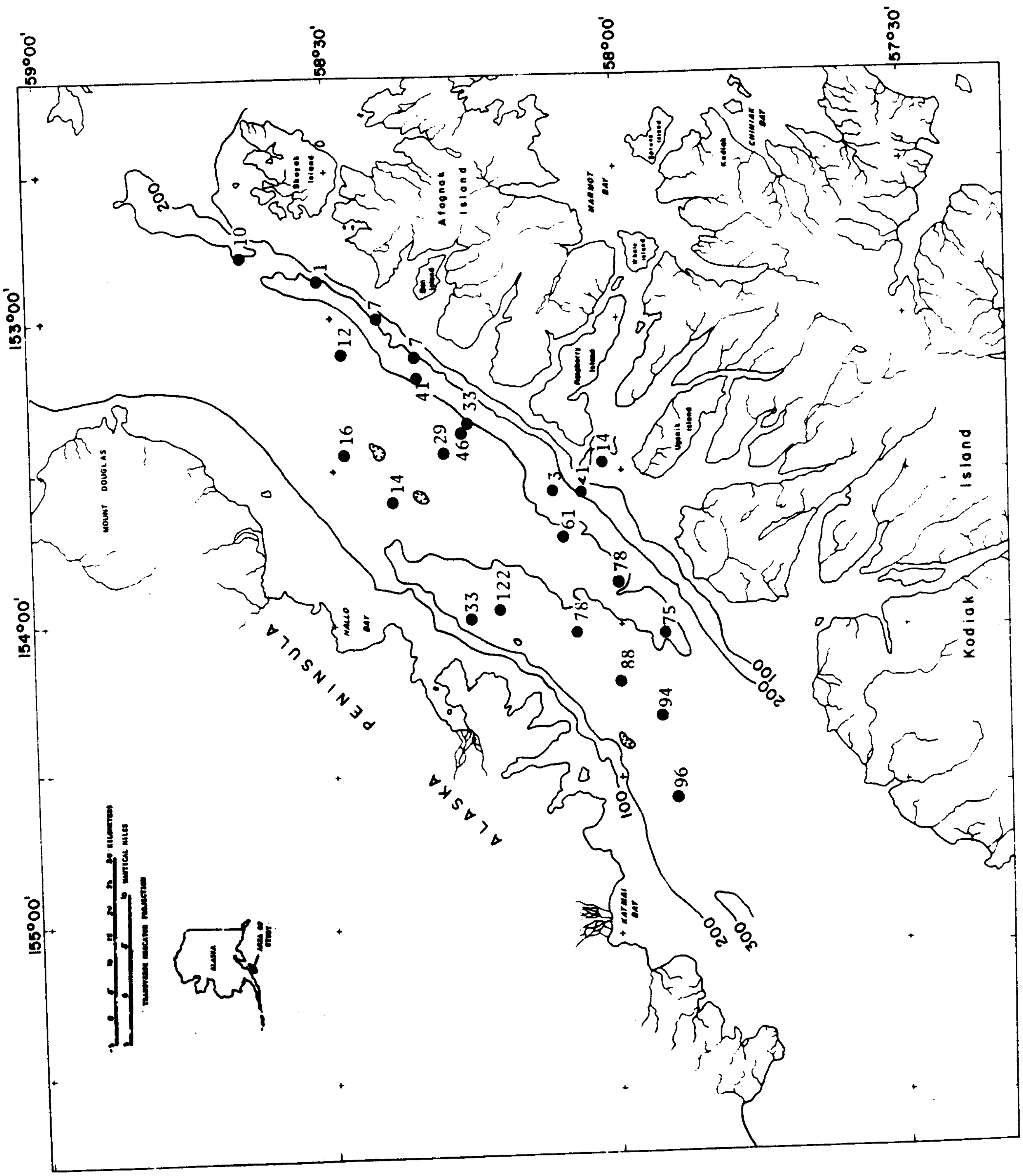

Figure 9. Sediment accumulation rates, in cm/100 yr.

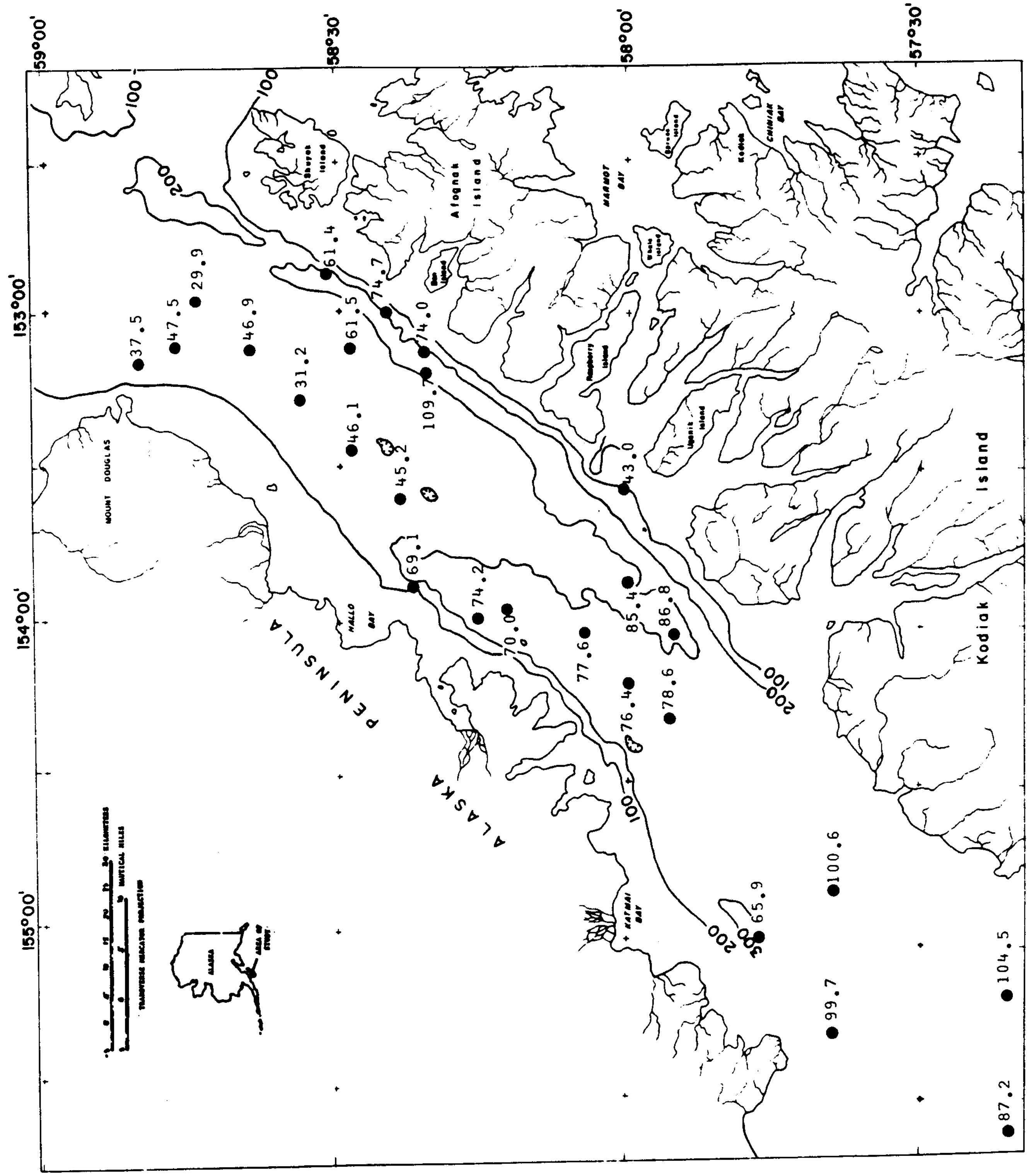

Figure 10. Water content (percent dry weight) at 1-m depth in sediment cores.

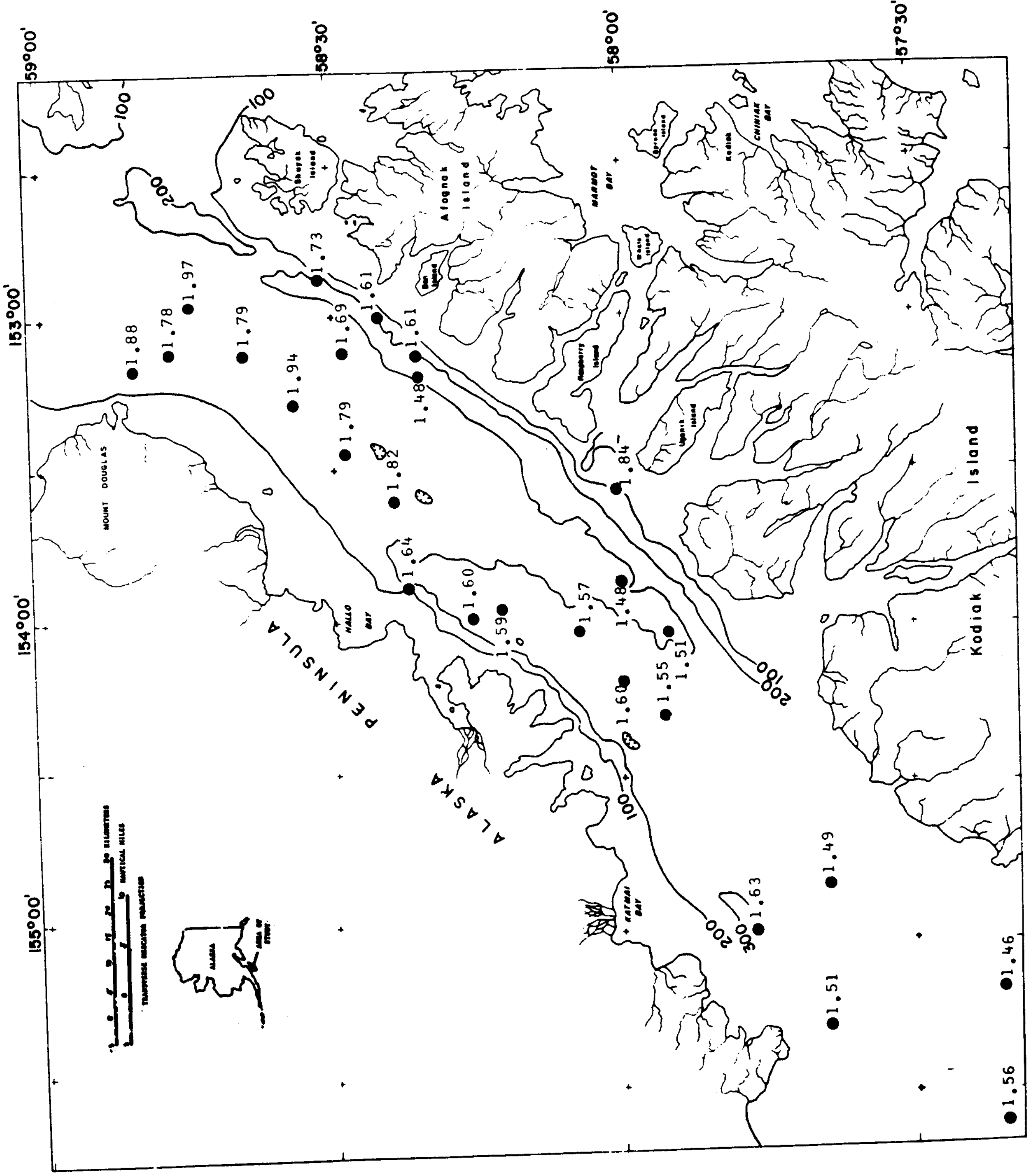

Figure 11. Bulk sediment density (gm/cm^3) at 1-m depth in sediment cores.

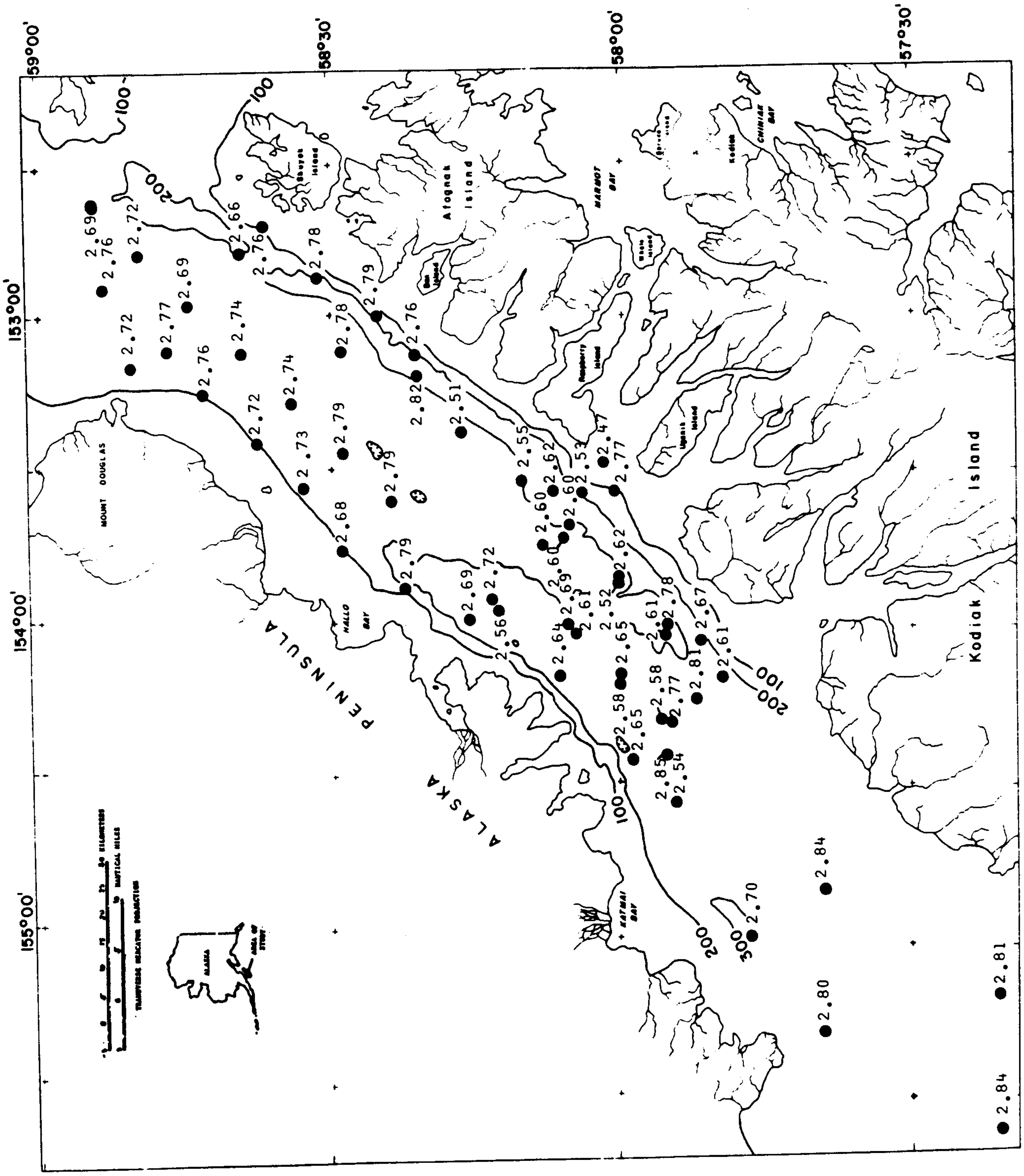

Figure 12. Average grain-specific gravity in sediment cores.

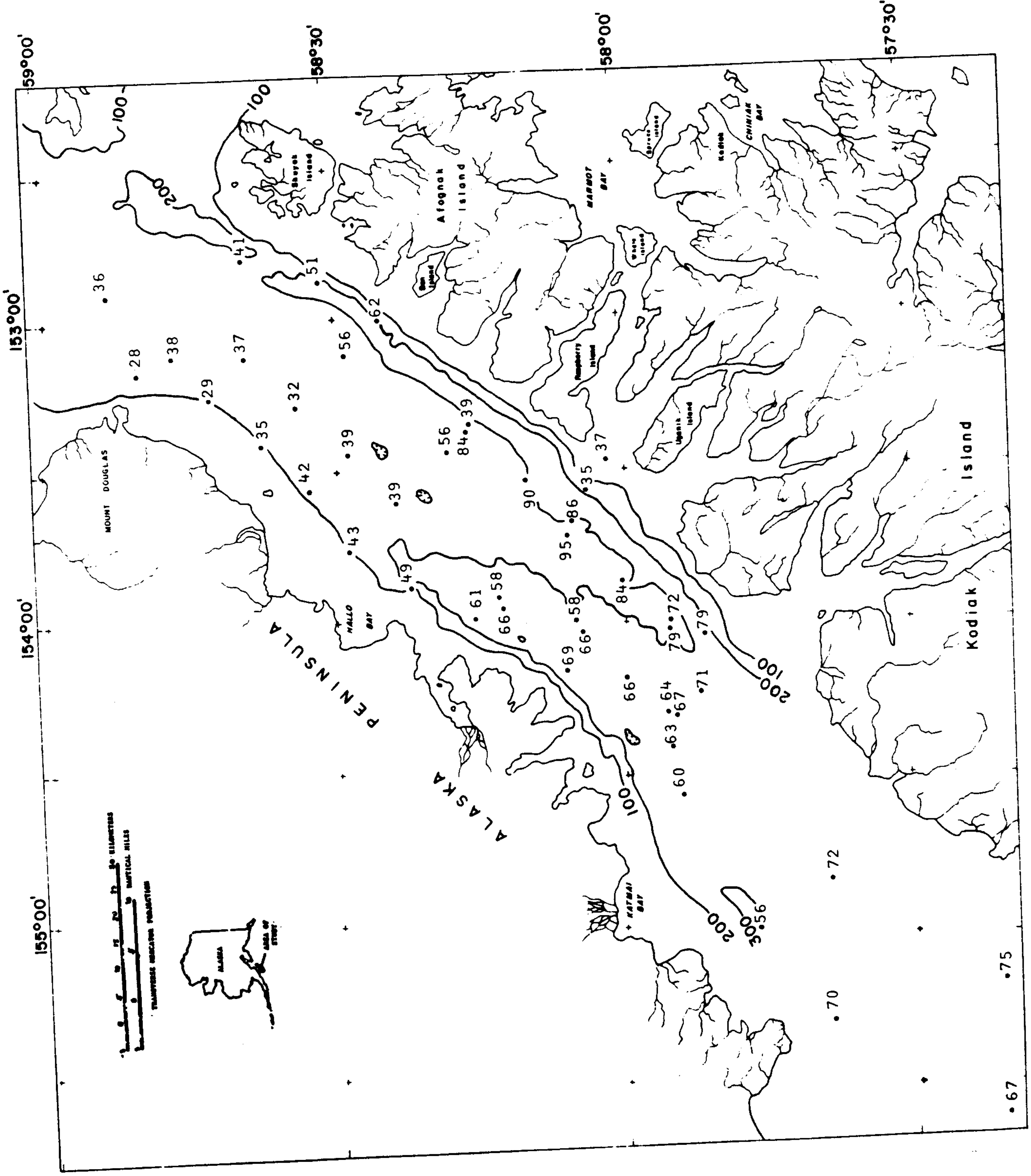

Figure 13. Average liquid limit (percent dry weight) in sediment cores.

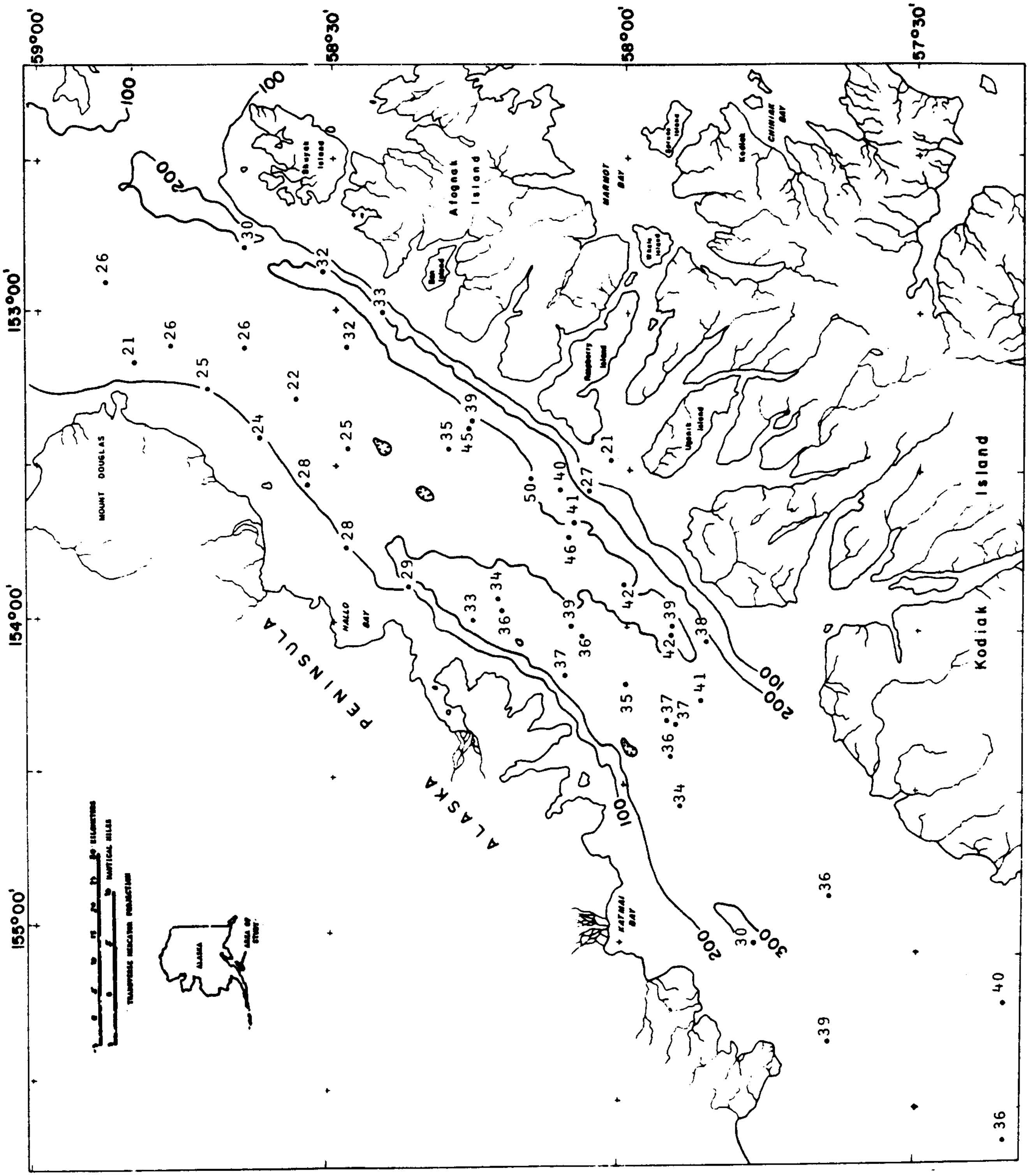

Figure 14. Average plastic limit (percent dry weight) in sediment cores.

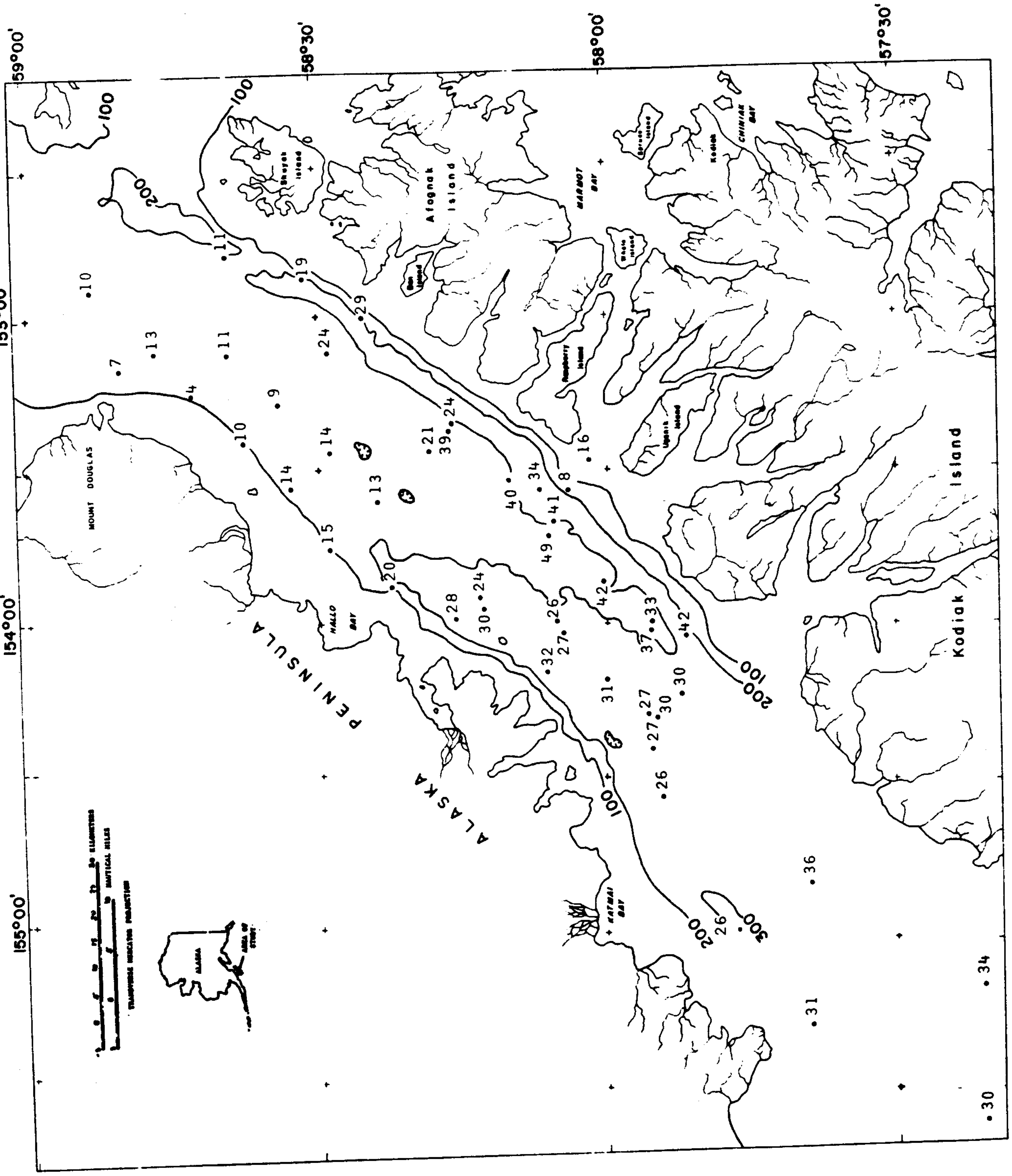

Figure 15. Average plasticity index in sediment cores.

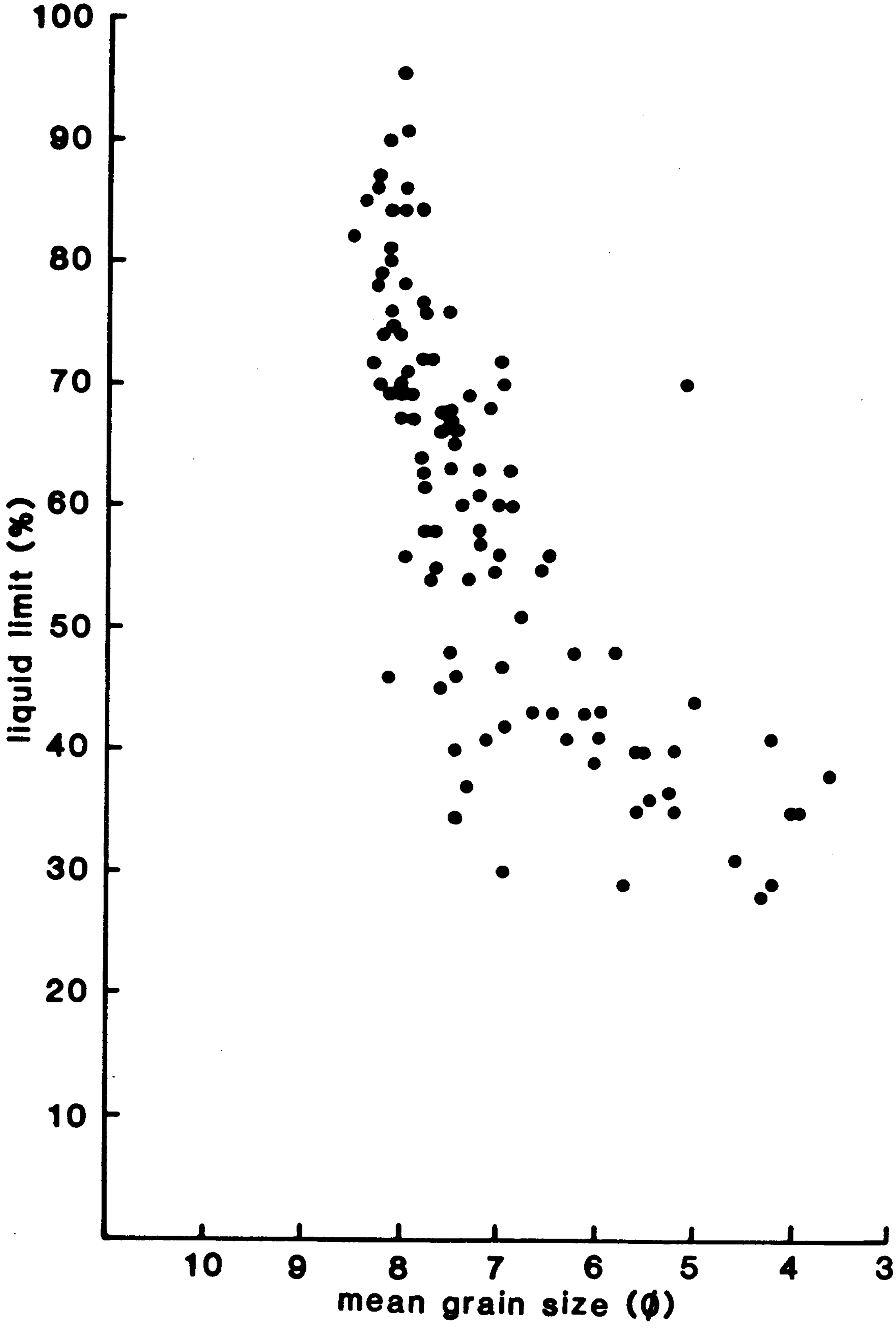

Figure 16. Liquid limit versus grain size.

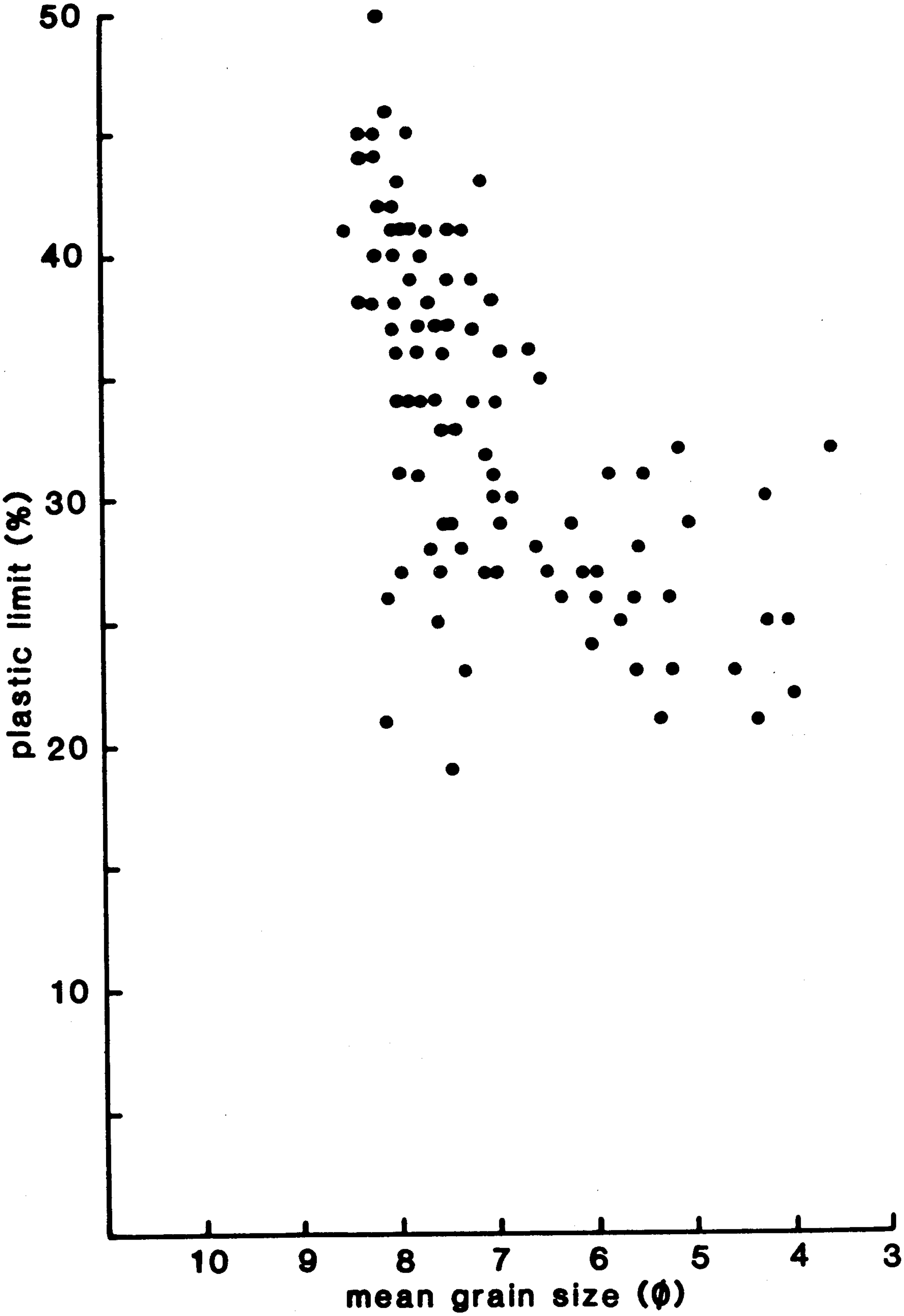

Figure 17. Plastic limit versus grain size.

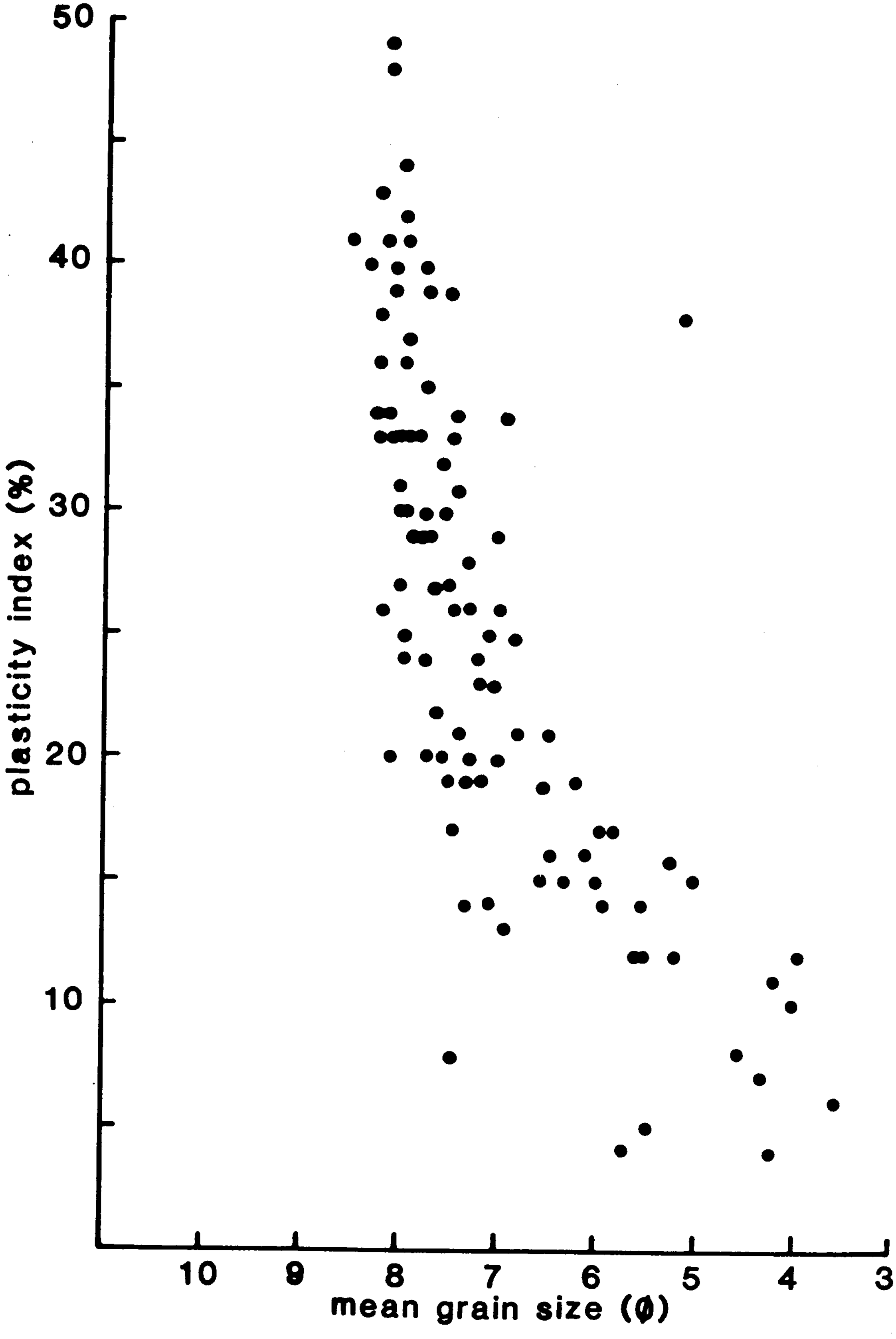

Figure 18. Plasticity index versus grain size.

Correlations have been made between liquid limit and compressibility (Herrmann and others, 1972; Skempton, 1944). The majority of Shelikof Strait samples fall within the medium (30 < liquid limit < 50) and high (liquid limit >50) compressibility ranges.

Nearly all measured liquidity indices in Shelikof Strait are greater than 1 (Appendix), which is usual for near-seafloor marine sediment. Sediment with a liquidity index greater than one behaves as a liquid when remolded.

A plot of liquidity index versus plasticity index - termed a plasticity chart (Casagrande, 1948) - shows a trend parallel to the A-line that divides basic soil types (Fig. 19). Most sediment samples from Shelikof Strait plot below the A-line, which is typical of inorganic silt and silty clay of high compressibility. The linear trend of data points is expected for samples taken throughout the same sedimentary deposit (Terzaghi, 1955; Richards, 1962).

Undrained shear strength of sediment samples (S_u), as measured with a laboratory miniature vane shear device, generally decreases toward the southwest end of the strait, and thus correlates with the water content trend, although there is much scatter (Figs. 20 and 21; Appendix). The consistency of most of the near-seafloor sediment can be classified as very soft ($S_u < 12$ kilopascals), but some is soft (12 kPa $< S_u <$ 24 kPa) to medium (24 kPa $< S_u <$ 48 kPa) (Terzaghi and Peck, 1948). Hampton and others (1981) showed that shear strength is anisotropic in Shelikof Strait sediment cores. Values of shear strength measured with the axis of vane rotation perpendicular to the axis of core samples exceed the values of strength measured with the axis of vane rotation parallel to the core axis. The magnitude of sediment strength thereby depends on the orientation of the applied stress.

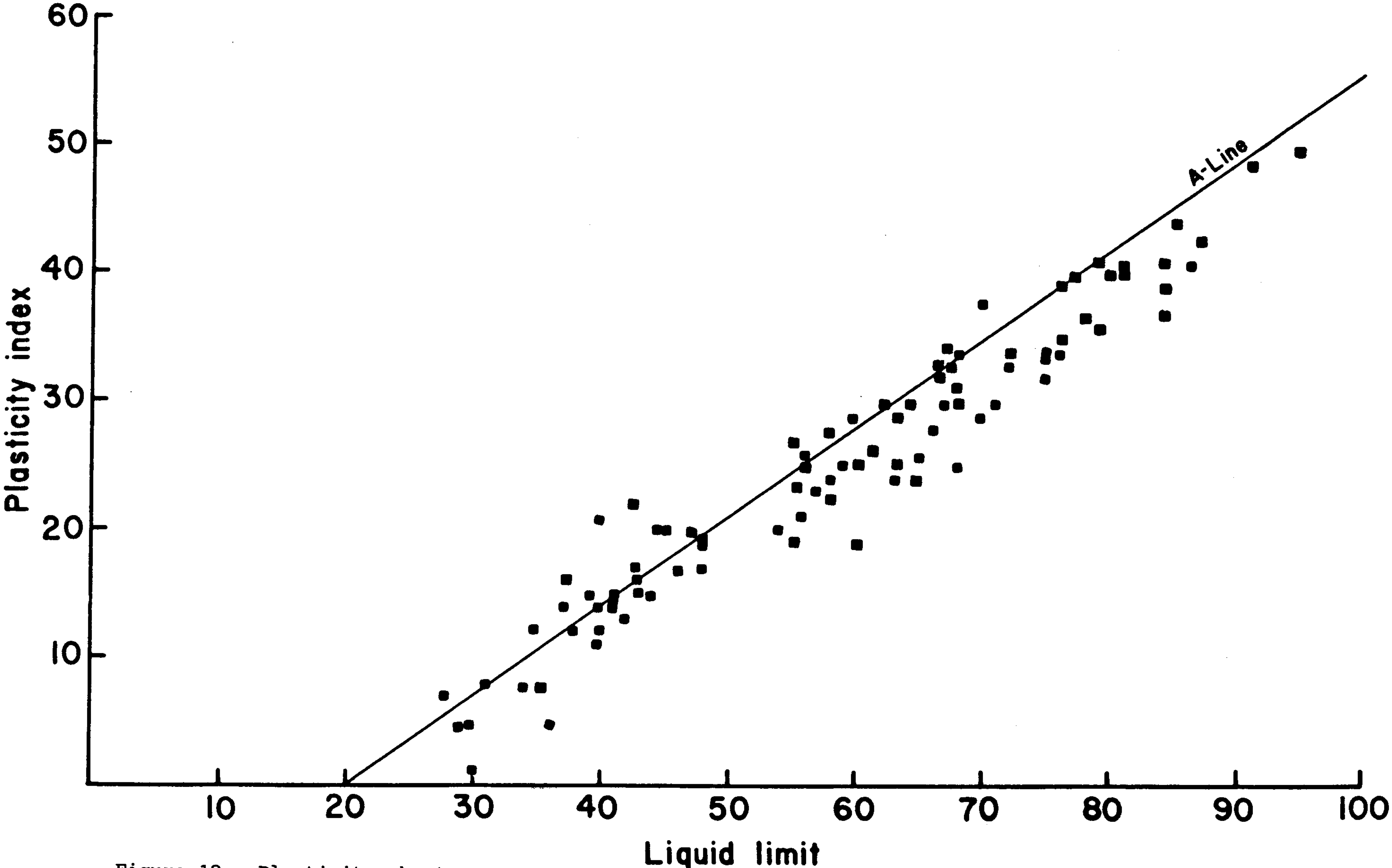

Figure 19. Plasticity chart.

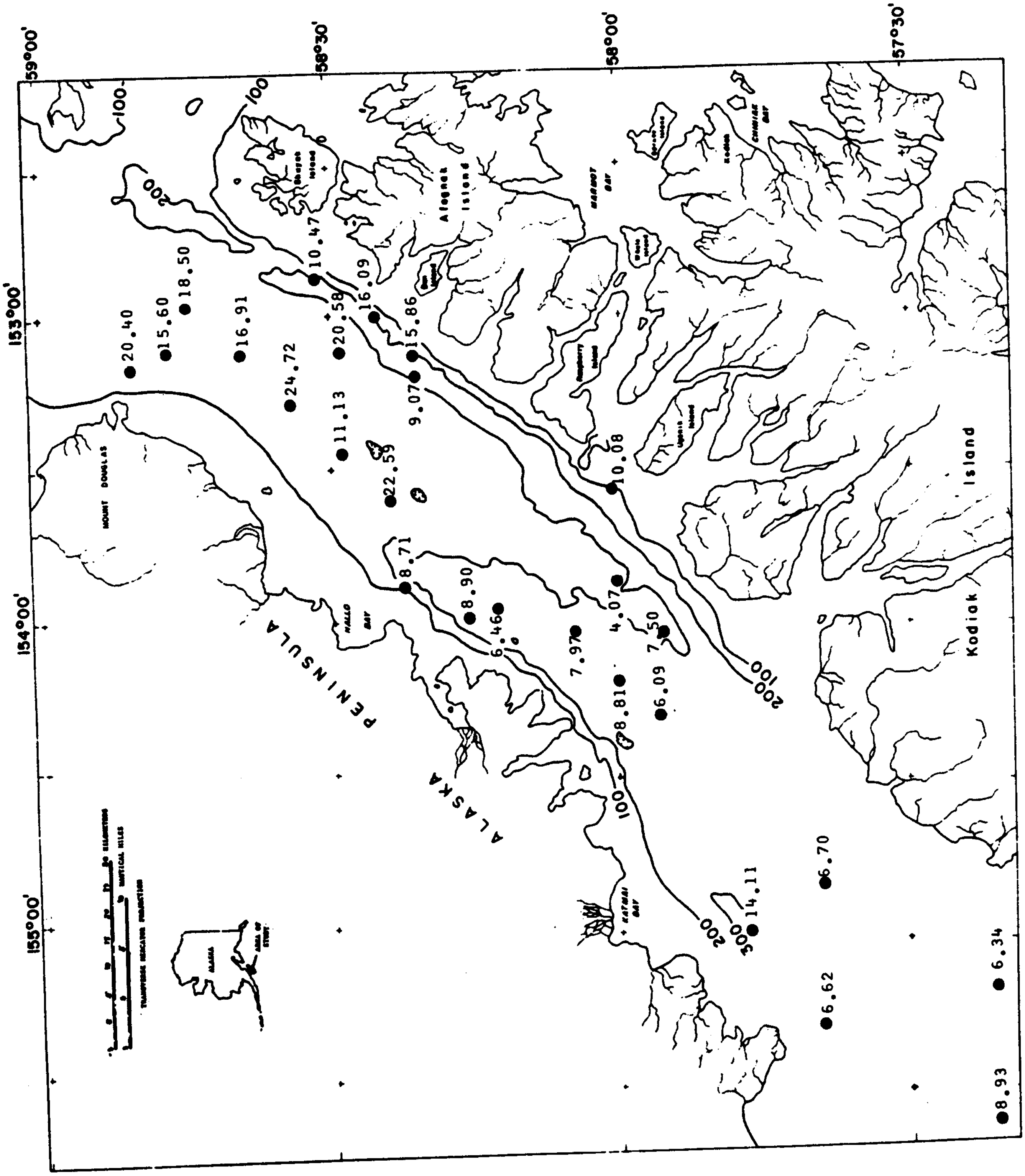

Figure 20. Vane shear strength (kPa) at 1m depth in sediment cores.

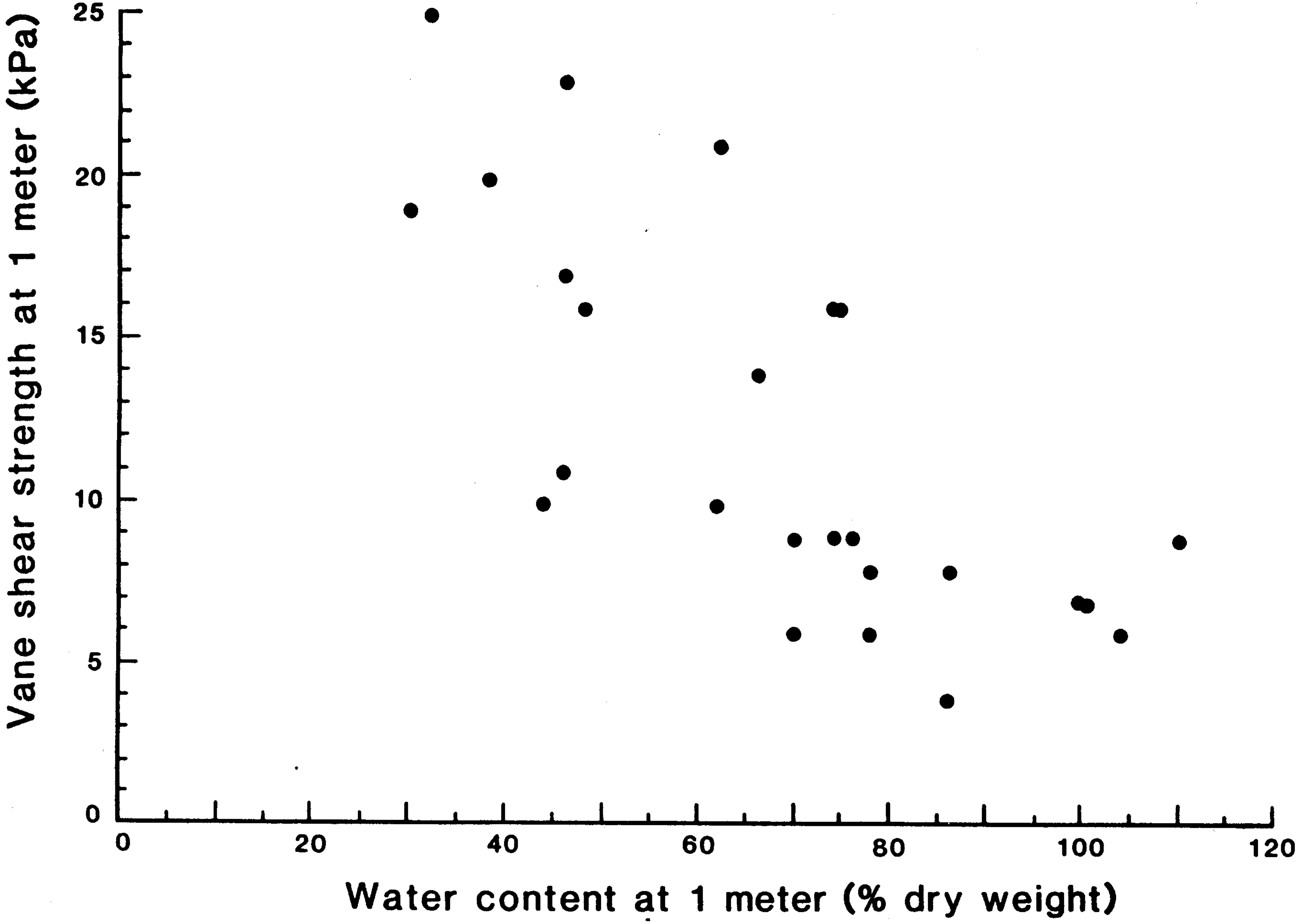

Figure 21. Vane shear strength versus water content.

Sediment samples from Shelikof Strait are characterized by low to intermediate content of organic carbon, compared to other marine areas (Bordovskiy, 1965, 1969; Gardner and others, 1980; Lisitzin, 1972; Rashid and Brown, 1975). Most values are between 0.40% and 1.50%. Organic carbon generally increases down the strait toward the southwest, as well as across the strait toward the southeast (Fig. 22; Appendix A). Correlations with other physical properties were shown by Hampton and others (1981). Organic carbon content correlates positively with water content and plasticity index, whereas an inverse correlation is found with grain size and vane shear strength. Correlations similar to those described above have been reported by others for low organic-carbon content sediment (Bordovskiy, 1965, 1969; Bush and Keller, 1981; Keller and others, 1979; Lisitzin, 1972; Mitchell, 1976; Odell and others, 1960).

Percent calcium carbonate is typically low in Shelikof Strait sediment (Fig. 23; Appendix). Most values are less than 3.50%. Two locations with anomalously high values, off Shuyak Island and in Stevenson Entrance, are near the boundary of the strait.

Consolidation properties: Consolidation properties as determined from laboratory tests are listed in Table 1. All tests indicate a maximum past pressure (σ'_{vm}) greater than the present overburden pressure (σ'_{vo}). The ratio $\sigma'_{vm}/\sigma'_{vo}$ is the overconsolidation ratio (OCR) and is greater than 1.0 for all tests. The usual implication is that the sediment has experienced unloading as a consequence of erosion. However, there is no geological evidence for erosion; in fact, sediment is accumulating at high rates throughout most of the strait (Fig. 9). The high values of OCR probably

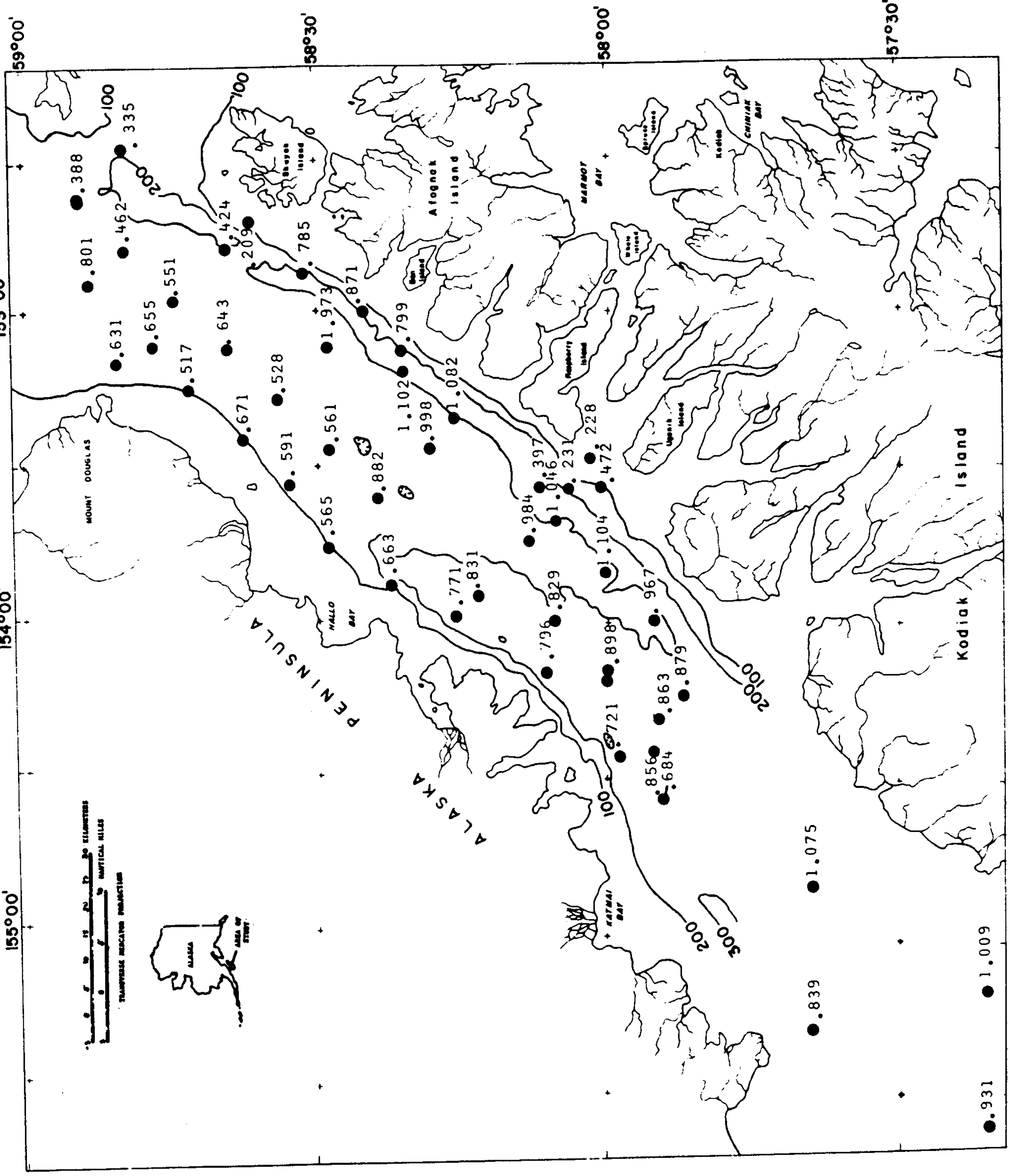

Figure 22. Average organic carbon content in sediment cores.

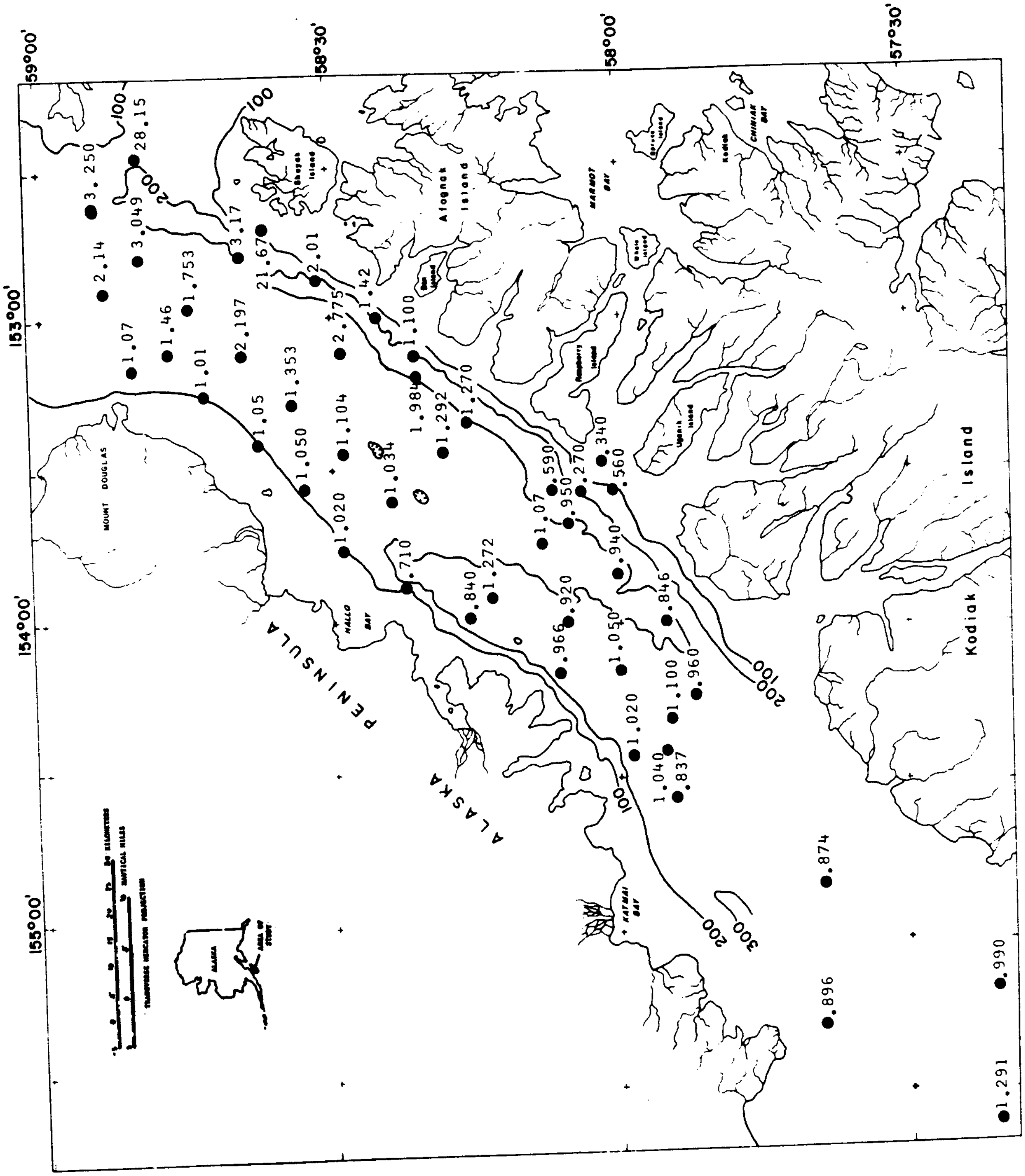

Figure 23. Average calcium carbonate content in sediment cores.

Table 1. Consolidation test results.

Station number	Depth in core (cm)	σ'_{vo} (kPa)	σ'_{vm} (kPa)	C_c	$c_v \times 10^{-2}$ (cm^2/sec) from	to	OCR
507	39	1.1	6.0	0.94	0.17	1.10	5
	171	5.0	32.0	0.76	0.22	1.13	6
509	89	3.7	20.0	0.86	0.27	2.67	5
	94	3.7	23.0	0.88	0.12	0.81	6
511	64	2.8	15.0	0.52	0.05	2.17	5
	111	4.6	9.0	0.66	0.09	1.10	2
	191	9.8	12.0	0.45	0.18	1.38	1
649	41	2.0	56.0	0.33	0.04	1.30	28
	116	6.1	30.0	0.54	0.12	0.97	5
	167	8.9	29.0	0.60	0.08	1.40	3
525	45	3.3	26.0	0.30	0.30	1.52	8
	96	6.9	28.0	0.26	0.35	1.68	4
	165	13.8	64.0	0.26	0.54	2.23	5
528	64	4.7	43.0	0.28	0.18	1.57	9
	144	10.4	45.0	0.29	0.31	3.59	4
540	47	2.8	20.0	0.50	0.11	0.50	7
	131	6.1	48.0	0.54	0.20	0.67	8
	201	11.6	65.0	0.37	0.16	0.98	6

represent initial cementation of sediment particles or grain interlocking and are not indicative of overconsolidation in the strict sense of the term.

Compression index (C_c) is a measure of the amount of consolidation that occurs for a given increment in load. The coarse sediment at the northeast end of the strait is less compressible than the progressively finer sediment to the southwest, as indicated by a southwest trend of increasing C_c (Table 1). Richards (1962) reported a range of 0.20 to 0.87 for C_c measured on samples of marine sediment from many areas, and most values from Shelikof Strait fall within this range.

Compression index commonly shows a linear relation to liquid limit (LL). The data from Shelikof Strait, when plotted in this manner, exhibit a general trend, but with much scatter (Fig. 24). Skempton (1944) found that the relation can be expressed as

$$C_c = 0.009\ (LL - 10),$$

and the regression equation for Shelikof Strait sediment is similar:

$$C_c = 0.006\ (LL + 5.7).$$

The rate at which consolidation occurs in response to loading determines the coefficient of consolidation (c_v). It is directly related to permeability of a sediment and inversely related to the compressibility. The coefficient is calculated for each load increment during a laboratory consolidation test from plots of deformation versus time. As shown in Table 1, c_v commonly varies through one to two orders of magnitude for a single test. No general trend in the data is evident, although the high expected permeability and low compressibility of coarse-grained sediment would suggest a decrease of c_v to the southwest. Measurements of c_v for clay sediment from various marine locations by Richards and Hamilton (1967) are in the range 3.2 - 6.0 x 10^{-4} cm^2/sec, which are lower than typical values in Shelikof Strait.

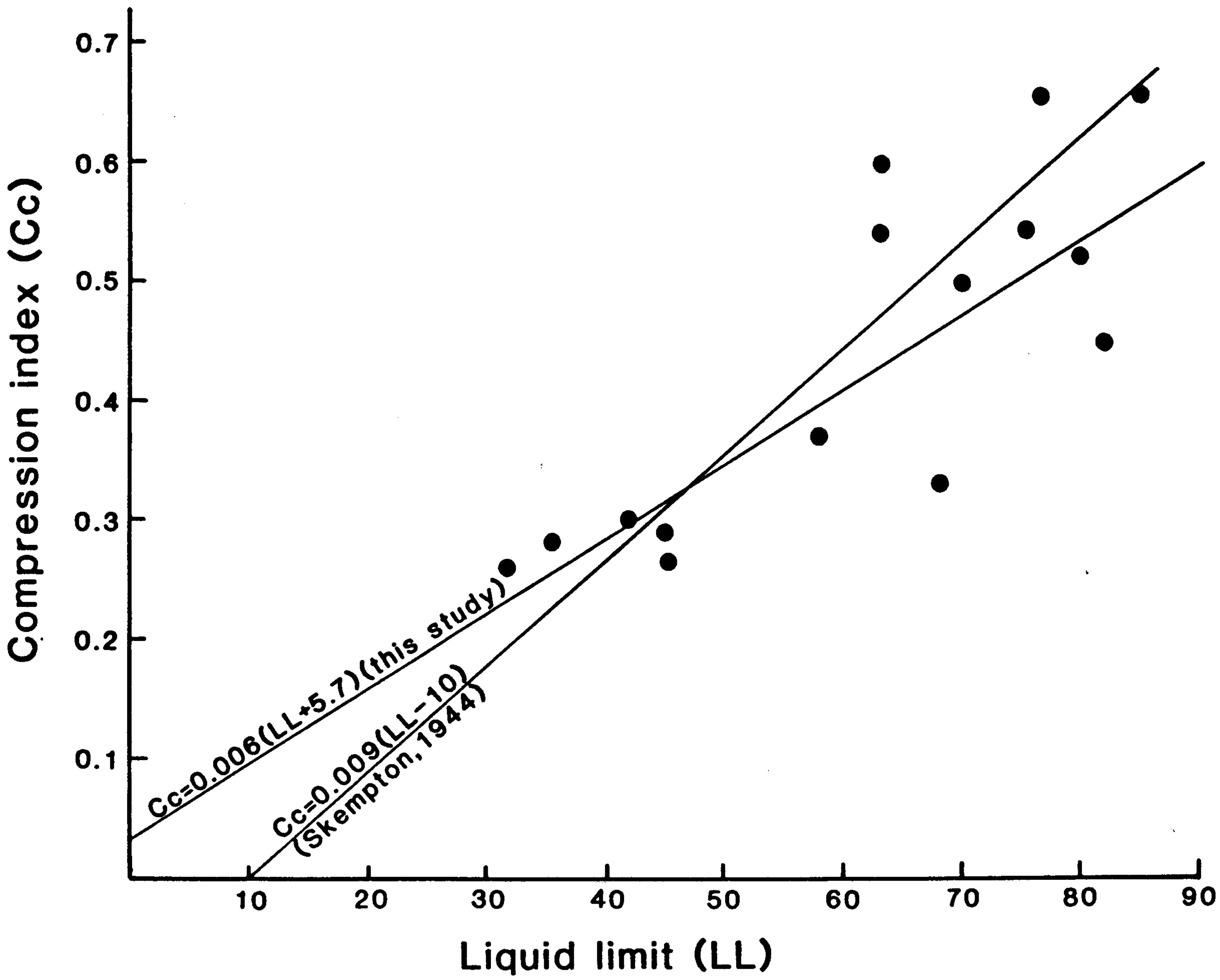

Figure 24. Graph of compression index versus liquid limit.

Static strength properties: Sediment properties derived from static triaxial strength tests are listed in Table 2. The primary measured property is the undrained shear strength (S_u). It is the maximum sustainable shear stress within a sample subjected to a particular consolidation stress (σ_c'). S_u acts along a plane inclined at 45^o to the axial load. The arisen of S_u divided by the effective normal stress across this plane is the effective angle of internal friction (ϕ'), whose magnitude is an indication of the strength behavior of the sediment under slow (drained) loading conditions. In comparison, the ratio S_u/σ_c' gives an indication of the strength behavior during rapid (undrained) loading conditions. The difference in drained and undrained strength behavior depends on the pore water pressure generated in response to the tendency for volume change when the sediment is axially loaded. If a sediment has a high tendency for volume change, the difference in strength between rapid and slow loading can be substantial.

The effective angle of internal friction for the normally consolidated sediment samples (OCR = 1) in this study is relatively high (35° - 46°). Compare with values given by Lambe and Whitman (1969, p. 149 and 306). The higher values (> 40°) are in the finer sediment cores from the southwest half of the strait (Table 2). Therefore, sediment from Shelikof Strait appears to be atypically strong under conditions of drained loading, with the finer sediment exhibiting higher strength. Samples tested at OCR > 1 tend to have ϕ' comparable to that of normally consolidated samples, except for station 649 where some overconsolidated samples have significantly higher values. The data indicate similar drained behavior of normally consolidated and overconsolidated sediment in the strait.

Table 2. Static triaxial strength test results.

Station number	Depth in core (cm)	σ_c' (kPa)	Induced OCR	S_u (kPa)	S_u/σ_c'	ϕ (degrees)
507	30	53.9	1	18.8	0.3	39
	130	140.0	1	73.5	0.5	46
509	120	172.4	1	73.4	0.4	40
	170	47.0	4.1	68.9	1.5	<42
511	17	20.7	3	25.4	1.2	39
	28	2.8	-	8.8	3.1	64
	44	1.4	-	9.6	6.3	64
	180	48.2	1	27.0	0.6	43
121	8.3	5.8	18.6	3.2	41	
649	86	24.0	5.9	57.6	2.4	<40
	86	46.7	3	52.3	1.1	<54
	109	0.3	-	13.0	43.3	<57
	109	142.3/70.7	1	58.3	0.4	39
	127	4.4	8	12.3	2.8	<69
	132	160.5	1	76.5	0.5	41
525	8	1.4	-	18.5	13.2	48
	73	19.3	6	47.5	2.5	34
	85	6.9	-	25.2	3.6	45
	152	282.5	1	121.6	0.4	37
528	37	1.4	-	18.6	12.8	50
	80	179.2	1	79.8	0.4	35
	94	6.9	-	19.0	2.8	43
	122	30.3	3.6	77.4	2.5	38
	139	178.8/89.6	1	66.7	0.3	41
540	29	15.2	6	24.2	1.6	40
	69	1.4	-	15.4	11.0	60
	120	10.3	-	16.7	1.6	47
	140	199.8	1	79.9	0.4	35
	159	114.0	1.8	82.8	0.7	40

Lambe and Whitman (1969, p. 307, Figs. 21-24) detected a relation between ϕ' and plasticity index for normally consolidated soil. Triaxial data for which there are plasticity index values in Shelikof Strait plot within the range of Lambe and Whitman's data, except for the core at station 511, which is abnormally strong for sediment with such high plasticity (Fig. 25).

Evaluation of undrained strength, in terms of S_u/σ_c', requires some judgment in order to detect trends. In particular, the tests run at low consolidation stress (σ_c') seem to give erratic values of S_u/σ_c'. This was also shown to be the case for triaxial data from nearby Kodiak Shelf (Hampton, in press). Tests run at high values of consolidation stress (which corrects some of the effects of disturbance) and OCR = 1 have values of S_u/σ_c' between 0.3 and 0.6, with no areal trend (Table 2). The value of S_u/σ_c' increases with OCR for each core tested.

The static triaxial test data are plotted according to the NSP approach in Figure 26. The slope (Λ) of the line for each core is a measure of the change in undrained strength with OCR. Most cores have Λ values between 0.79 and 0.97. Mayne (1980) compiled the results of many triaxial tests and found a mean value of $\Lambda = 0.64$ with a standard deviation of 0.18. The sediment in Shelikof Strait, with its relatively high values of Λ, would tend to retain more of its strength after unloading compared to most sediment examined by Mayne (1980). The $\Lambda = 1.43$ calculated for the sediment of station 528 is greater than the theoretical limit of $\Lambda = 1.0$, and further testing is required to resolve this conflict.

Dynamic strength properties: The data from triaxial strength tests are given in Table 3. The quantity τ_{cyc}/S_u is the cyclic stress level, the average

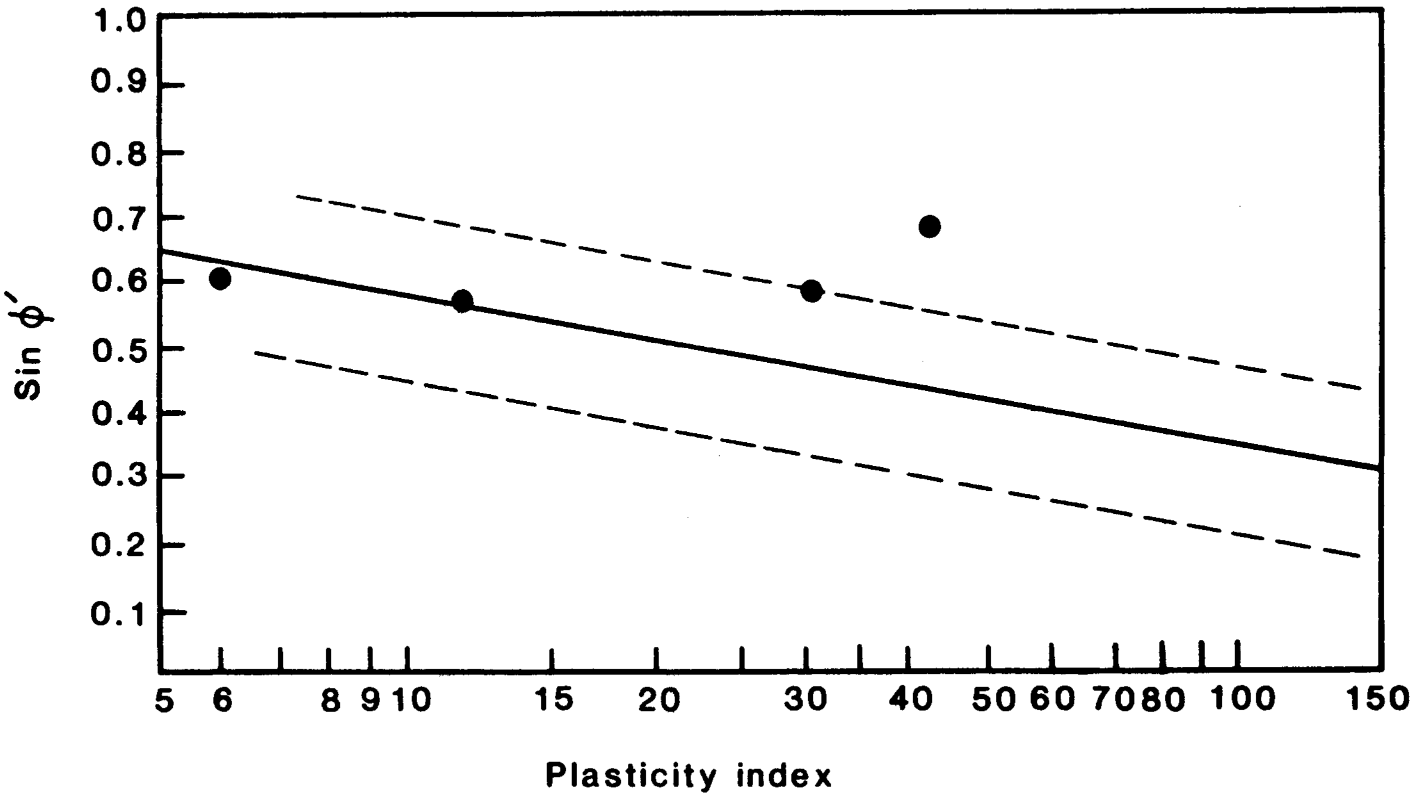

Figure 25. Graph of effective angle of internal friction versus plasticity index. Solid line shows empirical relation derived by Lambe and Whitman (1969); dashed line indicates limits of their data.

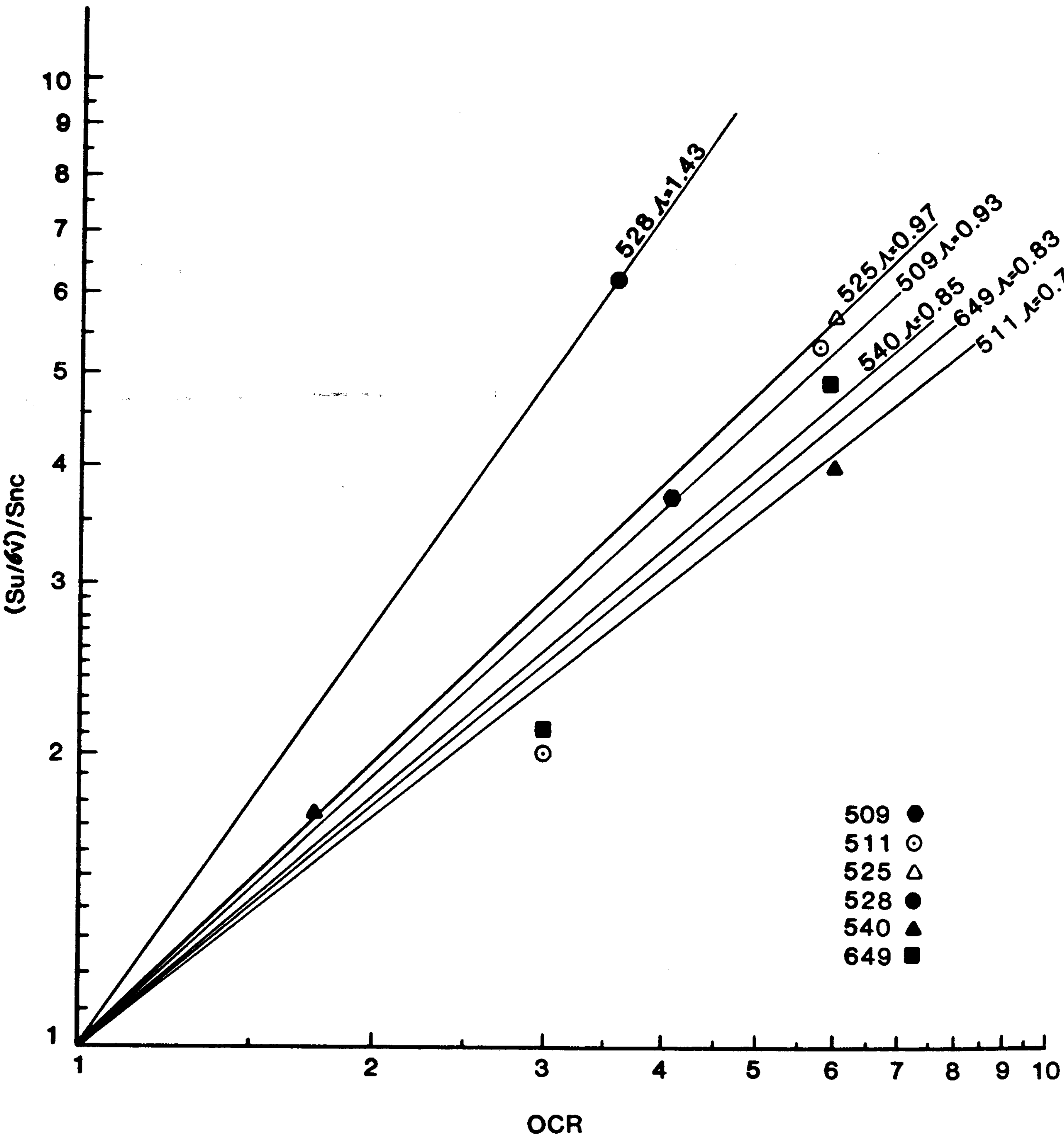

Figure 26. Graph of normalized undrained shear strength versus overconsolidation ratio.

Table 3. Dynamic triaxial strength test results.

Station number	Depth in core (cm)	σ_c' (kPa)	Induced OCR	τ_{cyc}/S_u (%)	Cycles to failure
509	137	173.6	1	49	145
	137	175.0	1	66	64
511	152	46.9	1	70	10
	167	46.9	1	47	48
649	96	153.1	1	70	22
	96	146.0	1	56	450
	140	30.2	4.4	79	17
	140	139.8	1	72	39
525	135	282.4	1	47	30
	117	282.4	1	70	7
528	23	27.5	4	32	51
	178	179.1	1	70	13
	193	179.1	1	46	110
540	152	199.8	1	71	12
	227	199.8	1	43	900+
	238	299.8	1	56	28

value of shear stress (τ_{cyc}) applied sinusoidally with full stress reversal at 0.1 Hz, expressed as a percentage of the static undrained shear strength (S_u). Pore water pressure and strain accumulate with repeated application of τ_{cyc}. At some point, the pore water pressure approaches the confining stress, strain increases abruptly, and the sediment fails. In our tests, failure was chosen when 20% strain was reached.

Samples typically fail in fewer cycles at progressively higher stress levels. Figure 27 shows the number of cycles to failure versus stress level for Shelikof Strait samples. Although there is some scatter, the data fall within the range of test results on terrigenous sediment from other areas (Lee and others, 1981; Anderson and others, 1980; Hampton, in press). Moderate cyclic strength degredation is indicated; that is, after 10 cycles of loading (as might be imparted by an earthquake, for example), the samples fail at stress levels between 60% and 80% of their static strength.

DISCUSSION

The primary geotechnical concerns in Shelikof Strait include settlement of structures, bearing capacity under static and cyclic loading lateral load capacity, and anchor breakout resistance. Natural slope failures are not a serious problem because only one small sediment slide has been documented (Hampton and others, 1981). There is some evidence for gas-charged sediment, but the problem of low strength that might exist in sediment of this type was not addressed in the present study.

Quaternary sediment in Shelikof Strait covers bedrock to a thickness of from 20 m to more than 800 m (Fig. 4). The sequence consists of Pleistocene glacial and glaciomarine sediment at the base, overlain by Holocene marine

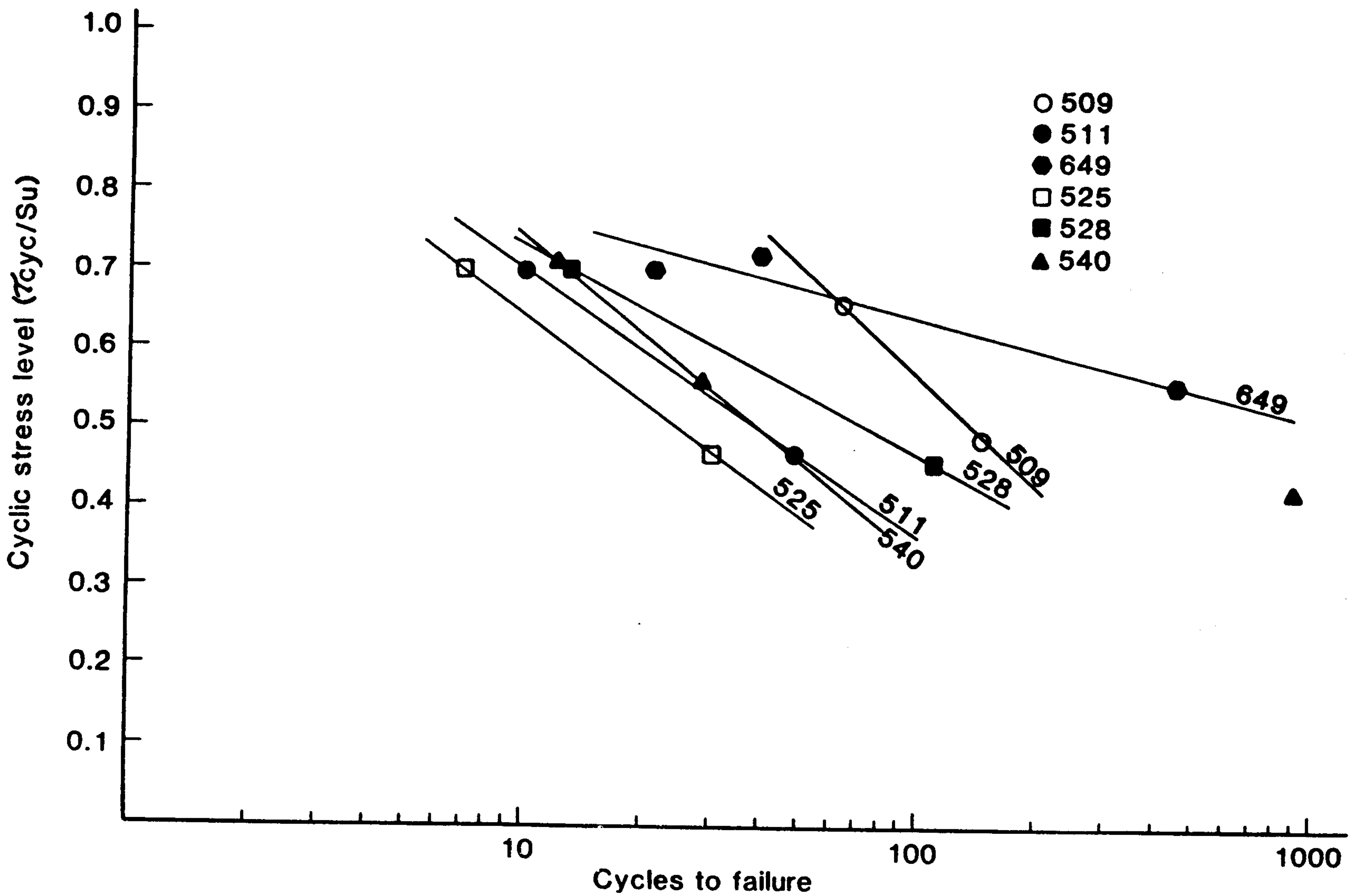

Figure 27. Graph of cyclic stress level versus number of cycles to failure.

deposits. The highest stratigraphic unit, deposited by oceanic currents as exist today, has accumulated to a thickness of 80-100 m over most of the strait; the total range is about 20 m to 180 m. Geotechnical testing was performed only on samples from this uppermost unit. A geotechnical analysis based on these data probably addresses most situations of engineering concern. Deeper stratigraphic units appear from interpretive geologic studies to be relatively coarse-grained (Hampton and Winters, 1981; Whitney, Holden, and Lybeck, 1980; Whitney, Hoose, Smith, and Lybeck, 1980), and they probably are stable, but deep drill-core samples would have to be obtained in order to confirm this by geotechnical testing.

The pattern of grain-size variation (Figs. 7 and 8) evidently reflects progressive sorting by the southwesterly flowing barotropic current that dominates circulation in the strait. The present study and the previous report by Hampton and others (1981) show that some index properties vary in relation to grain size. Properties that show a direct correlation and therefore increase to the southwest down the strait and to the southeast across the strait include water content, liquid limit, plastic limit, plasticity index, and organic carbon content (Figs. 10, 13, 14, 15, and 22). Properties that correlate inversely with grain size include bulk sediment density and undrained (vane) shear strength (Figs. 11 and 20).

Consolidation tests indicate that sediment samples are overconsolidated, but this probably is a near-seafloor diagenetic or fabric phenonenon rather than a result of erosion, because net sediment accumulation is presently occurring throughout the strait (Table 1, Fig. 9). The fine-grained sediment to the southwest has high values of compression index (C_c), which indicates that it is more compressible than the coarser material to the northeast. The rate of consolidation, as shown by the coefficient of consolidation (c_v), is highly variable for each consolidation test and does not show an areal trend (Table 1). Intuitively, a higher value of c_v would be expected for the coarser-grained sediment because of its normally higher permeability and lower compressibility, but apparently this is not the case.

Another unexpected result is that the static drained strength, in terms of the effective angle of internal friction (ϕ), is higher for the fine-grained sediment than it is for to the coarser-grained samp-es (Table 2). Drained strength does not vary appreciably with OCR. Undrained static strength behavior does not exhibit significant areal variation. Values of S_u/σ_c' for tests run at OCR = 1 are between 0.3 and 0.6. This parameter increases with OCR for each core that was tested. The NSP pore-pressure parameter ($\dot{\Lambda}$) varies from 0.79 to 0.97, which indicates significant static strength increase with OCR (Fig. 26). Again, no areal trend is apparent. But, because few data points were used to plot the lines in Figure 26 and because large scatter of data exists for some individual cores, additional strength testing at more levels of OCR would add precision to the plots and perhaps reveal some systematic variation.

Test data for most cores define similar response to cyclic loading over a broad range of number of cycles required to cause failure (e.g., cores 511, 525, 528, and 540 in Fig. 27). Dynamic strength degredation varies over a limited range at low number of cycles; for instance, it is between about 60% and 80% for 10 cycles.

Geotechnical properties of Shelikof Strait sediment can be compared with data from other studies to determine if the sediment has normal deformational behavior. However, few data exist for some properties, which makes the evaluations tentative.

Most values of compression index fall within the range of 0.20 to 0.87 reported by Richards and Hamilton (1967) for silty clay to highly colloidal clay; one test on the core from station 507 has a high value of 0.94 (Table 1). Skempton's (1944) classification of compressibility based on liquid limit indicates that Shelikof Strait samples are moderately to highly compressible (Appendix). Substitution of the class-boundary values of liquid limit (moderate compressibility: 30 < LL < 50; high compressibility: LL > 50) into the regression equation for Shelikof Strait data (Fig. 24),

$$C_c = 0.006\ (LL + 5.7),$$

indicates that the range of moderate compressibility is $0.21 < C_c < 0.33$ and the high range is $C_c < 0.33$, which is consistent with classifying the sediment as moderately to highly compressible (Table 1).

Effective friction angle (ϕ') for sediment in Shelikof Strait is high (35° - 46°) compared to the range (20° - 40°) reported by Lambe and Whitman (1969, p. 149 and 306) for normally consolidated sediment. Apparently, no compilations of ϕ' exclusively for terrigenous marine sediment have been made. Hampton (in press) reports ϕ' mostly in the 30° - 40° range for terrigenous samples from the Kodiak Shelf. Shelikof Strait terrigenous sediment is relatively strong under drained loading conditions.

Lambe and Whitman (1969, p. 452, Fig. 29.19) present data on the undrained strength of normally consolidated marine clay, and values of S_u/σ_c' are between about 0.2 and 0.4. The range for normally consolidated Shelikof Strait samples is 0.3 to 0.6, so they are relatively strong under conditions of undrained loading. S_u/σ_c' for normally consolidated terrigenous sediment from the Kodiak Shelf are also high, from 0.4 to 1.0 (Hampton, in press).

Values of the NSP factor Λ are high (0.79 - 0.97) compared to the average value of 0.64 (standard deviation = 0.18) in the extensive compilation by Mayne (1980). The implication is that the increase of strength with overconsolidation is higher than normal.

The low to moderate cyclic strength degredation of Shelikof Strait samples is similar to the behavior of clay sediment reported in other studies (Lee and others, 1981; Anderson and others, 1980; Hampton, in press). Sediment failure in response to large earthquakes certainly is a possibility, but the potential is not as great as has been predicted for some deposits of silt in the northeast Gulf of Alaska (cyclic strength at 10 cycles as low as 40% of the static strength; Lee and Schwab, in press) and volcanic ash on the Kodiak Shelf (cyclic strength at 10 cycles is 12% of the static strength; Hampton, in press). The deposit of Katmai ash in Shelikof Strait was not subjected to geotechnical testing. However, its in situ density is so great that normal gravity coring devices could not penetrate the layer. The relative density appears to be high and therefore the liquefaction potential is low. The possibility that more deeply buried ash layers are present and might be highly susceptible to liquefaction cannot be evaluated with the information presently available.

REFERENCES

American Society for Testing and Materials, 1976, Annual Book of ASTM Standards. Philadelphia, ASTM, 485 p.

Anderson, K.H., Pool, J.H., Brown, S.F., and Rosenbrand, W.F., 1980, Cyclic and static laboratory tests on Drammen clay. Journal of the Geotechnical Engineering Division, ASCE, v. 106, p. 499-529.

Bishop, A.W., and Henkel, D.J., 1964, The Measurement of Soil Properties in the Triaxial Test. London, Edward Arnold Ltd., 228 p.

Bordovskiy, O.K., 1965, Accumulation of organic matter in bottom sediments. Marine Geology, v. 3, p. 33-82.

Bordovskiy, O.K., 1969, Organic matter of recent sediments of the Caspian Sea. Oceanology, v. 9, p. 799-807.

Busch, W.H., and Keller, G.H., 1981, The physical properties of Peru-Chile continental margin sediments - the influence of coastal upwelling on sediment physical properties. Jour. Sedimentary Petrology, v. 51, p. 705-719.

Cassagrande, A., 1948, Classification and identification of soils. Transactions, American Soc. Civil Engineers, v. 113, p. 901-991.

Gardner, J.V., Dean, W.E., and Vallier, T.L., 1980, Sedimentology and geochemistry of surface sediments, outer continental shelf, southern Bering Sea. Marine Geology, v. 35, p. 299-329.

Hampton, M.A., in press, Geotechnical framework study of the Kodiak Shelf, Alaska. U.S. Geological Survey Open-File Report.

Hampton, M.A., and Winters, W.J., 1981, Environmental geology of Shelikof Strait, OCS sale area 60, Alaska. Proceedings 13th Offshore Technology Conference, p. 19-34.

Hampton, M.A., Johnson, K.H., Torresan, M.E., and Winters, W.J., 1981, Description of seafloor sediment and preliminary geo-environmental report, Shelikof Strait, Alaska. U.S. Geological Survey Open-File Report 81-1133, 86 p.

Herrmann, H. G., Rocker, K., and Babineau, P.H., 1972, LOBSTER and FMS: Devices for monitoring long-term seafloor foundation behavior. Naval Civil Engineering Laboratory, Technical Report R-775, 63 p.

Keller, G.H., Lambert, D.N., and Bennett, R.H., 1979, Geotechnical properties of continental slope deposits - Cape Hatteras to Hydrographer Canyon. Soc. Economic Paleontologists and Mineralogists Special Publication 27, p. 131-151.

Ladd, C.C., and Foott, R., 1974, New design procedure for stability of soft clays. Journal of the Geotechnical Engineering Division, ASCE, v. 100, p. 763-786.

Lambe, T.W., 1951, Soil Testing for Engineers. New York, John Wiley and sons, 165 p.

Lambe, T.W., and Whitman, R.V., 1969, Soil Mechanics. New York, John Wiley and sons, 553 p.

Lee, H.J., Edwards, B.D., and Field, M.E., 1981, Geotechnical analysis of a submarine slump, Eureka, California. Proceedings 13th Offshore Technology Conference, p. 53-65.

Lee, H.J., and Schwab, W.C., in press, Geotechnical framework, northeast Gulf of Alaska. U.S. Geological Survey Open-File Report.

Lisitzin, A.P., 1972, Sedimentation in the World Ocean. Soc. Economic Paleontologists and Mineralogists Special Publication 17, 218 p.

Mayne, P.W., 1980, Cam-clay predictions of undrained strength. Journal of the Geotechnical Engineering Division, ASCE, v. 106, p. 1219-1242.

Mitchell, J.K., 1976, Fundamentals of Soil Behavior. New York, John Wiley and Sons, Inc., 422 p.

Muench, R.D., and Schumacher, J.D., 1980, Physical oceanographic and meteorological conditions in the northwest Gulf of Alaska. NOAA Technical Memorandum ERL PMEL-22, 147 p.

Nayudu, Y.R., 1964, Volcanic ash deposits in the Gulf of Alaska and problems of correlation of deep-sea ash deposits. Marine Geology, v.1, p. 194-212.

Odell, R.T., Thornburn, T.H., and McKenzie, L.T., 1960, Relationships of Atterberg limits to some other properties of Illinois soils. Proceedings of the Soils Society of America, v. 24, p. 297-300.

Pratt, R.M., Scheidegger, K.F., and Kulm, L.D., 1973, Volcanic ash from DSDP site 178, Gulf of Alaska. Initial Reports of Deep Sea Drilling Project, v. XVIII, p. 833-834.

Rashid, M.A., and Brown, J.P., 1975, Influence of marine organic compounds on engineering properties of remolded sediment. Engineering Geology, v. 9, p. 141-154.

Richards, A.F., 1962, Investigation of deep-sea sediment cores, II. Mass physical properties. U.S. Navy Hydrographic Office Tech. Rept. 106, 146 p.

Richards, A.F., and Hamilton, E.L., 1967, Investigations of deep-sea sediment cores, III. Consolidation. <u>In:</u> Richards, A.F. (ed.), Marine Geotechnique, Urbana, University of Illinois Press, p. 93-117.

Skempton, A.W., 1944, Notes on the compressibility of clays. Geological Society of London, Quarterly Journal, v. 100, p. 119- 35.

Terzaghi, K., 1955, Influence of geological factors on the engineering properties of sediments. Economic Geology, 50th Anniversary Volume 1905-1955, p. 557-618.

Terzaghi, K., and Peck, R.B., 1948, Soil Mechanics in Engineering Practice. New York, John Wiley and Sons.

von Huene, R., 1979, Structure of the outer convergent margin off Kodiak Island, Alaska, from multichannel seismic records. In: Watkins, J.S., Montadert, L., and Dickerson, P.W., (eds.), Geological and Geophysical Investigations of Continental Margins, AAPG Memoir 29, Tulsa, American Association of Petroleum Geologists, p. 261-272.

Whitney, J., Holden, K.D., and Lybeck, L., 1980, Isopach map of Quaternary glacial-marine sediments, outer continental shelf, Shelikof Strait, Alaska. U.S. Geological Survey Open-File Report 80-2036, 1 p.

Whitney, J., Hoose, P.J., Smith, L.M., and Lybeck, L., 1980, Geologic cross sections of the outer continental shelf, Shelikof Strait, Alaska. U.S. Geological Survey Open-File Report 80-2036, 1 p.

Wissa, A.E., Christian, J.T., Davis, E.H., and Heiberg, S., 1971, Consolidation at constant rate of strain. Journal of the Soil Mechanics and Foundation Division, ASCE, v. 97, p. 1393-1410.

APPENDIX:

INDEX PROPERTY CHARTS FOR SEDIMENT CORES

FROM SHELIKOF STRAIT

Station 508 **Location** 57°21.01'N 155°36.41'W **Water depth** 270m

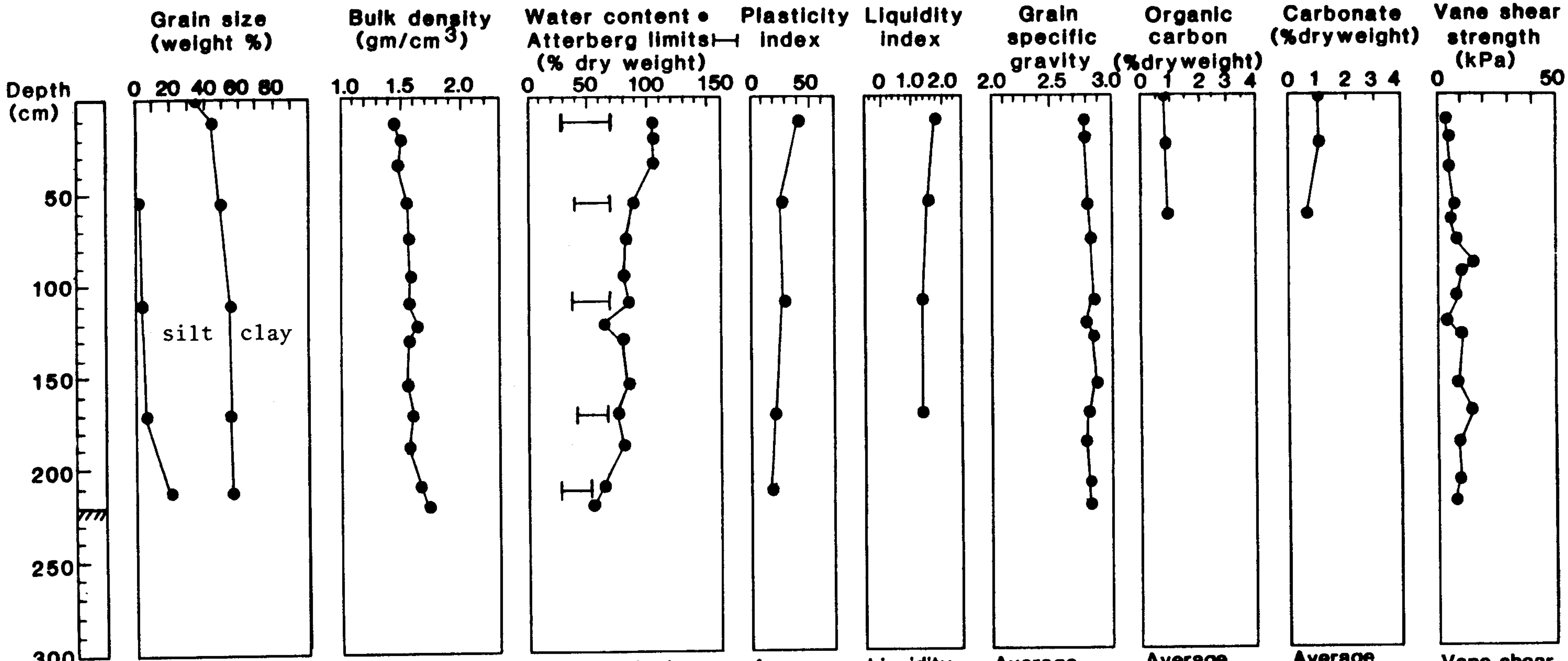

Bulk density at 1m.: 1.56

Water content at 1m.: 87.2
Average plastic limit: 36
Average liquid limit: 65

Average plasticity index: 30

Liquidity index at 1m.: 1.58

Average grain specific gravity: 2.84

Average organic carbon: 0.931

Average carbonate: 1.291

Vane shear strength at 1m.: 1.58

Station 509 **Location** 57°21.29'N 155°08.66'W **Water depth** 225m

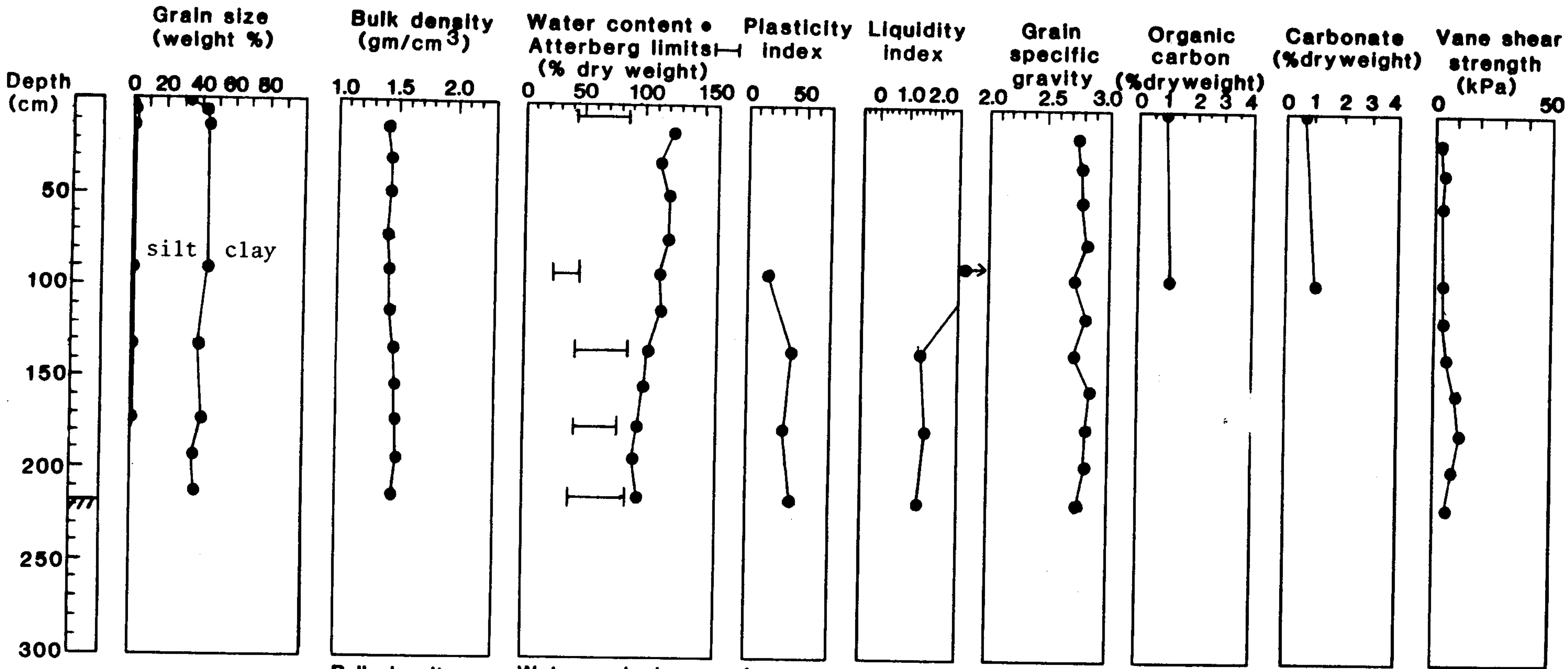

Bulk density at 1m.: 1.46

Water content at 1m.: 104.5

Average plastic limit: 40

Average liquid limit: 75

Average plasticity index: 34

Liquidity index at 1m.: 3.56

Average grain specific gravity: 2.81

Average organic carbon: 1.009

Average carbonate: 0.990

Vane shear strength at 1m.: 6.34

Station 510 Location 57°39.22'N 155°17.18'W Water depth 305m

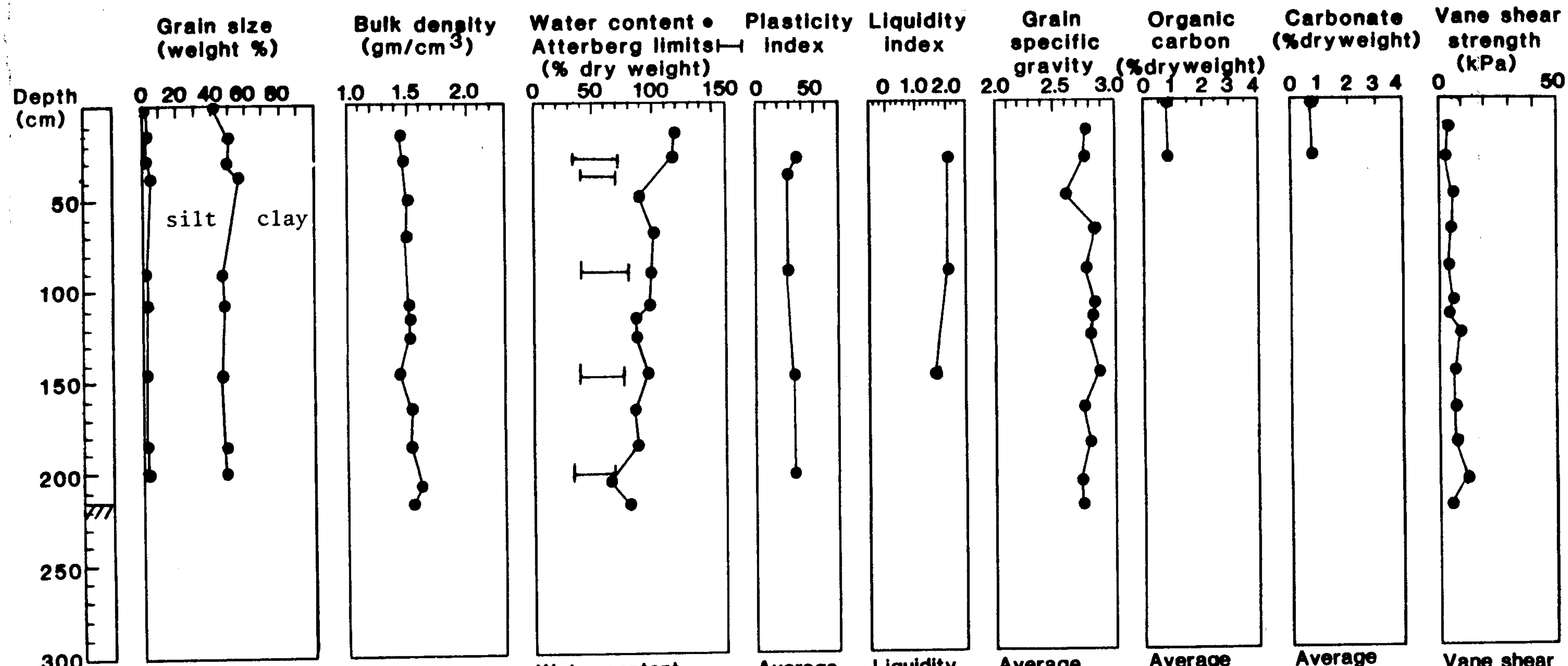

Bulk density at 1m.: 1.51

Water content at 1m.: 99.7

Average plastic limit: 39

Average liquid limit: 70

Average plasticity index: 31

Liquidity index at 1m.: 1.87

Average grain specific gravity: 2.80

Average organic carbon: 0.839

Average carbonate: 0.896

Vane shear strength at 1m.: 6.62

Station 511 **Location** 57°39.08'N 154°50.14'W **Water depth** 214m

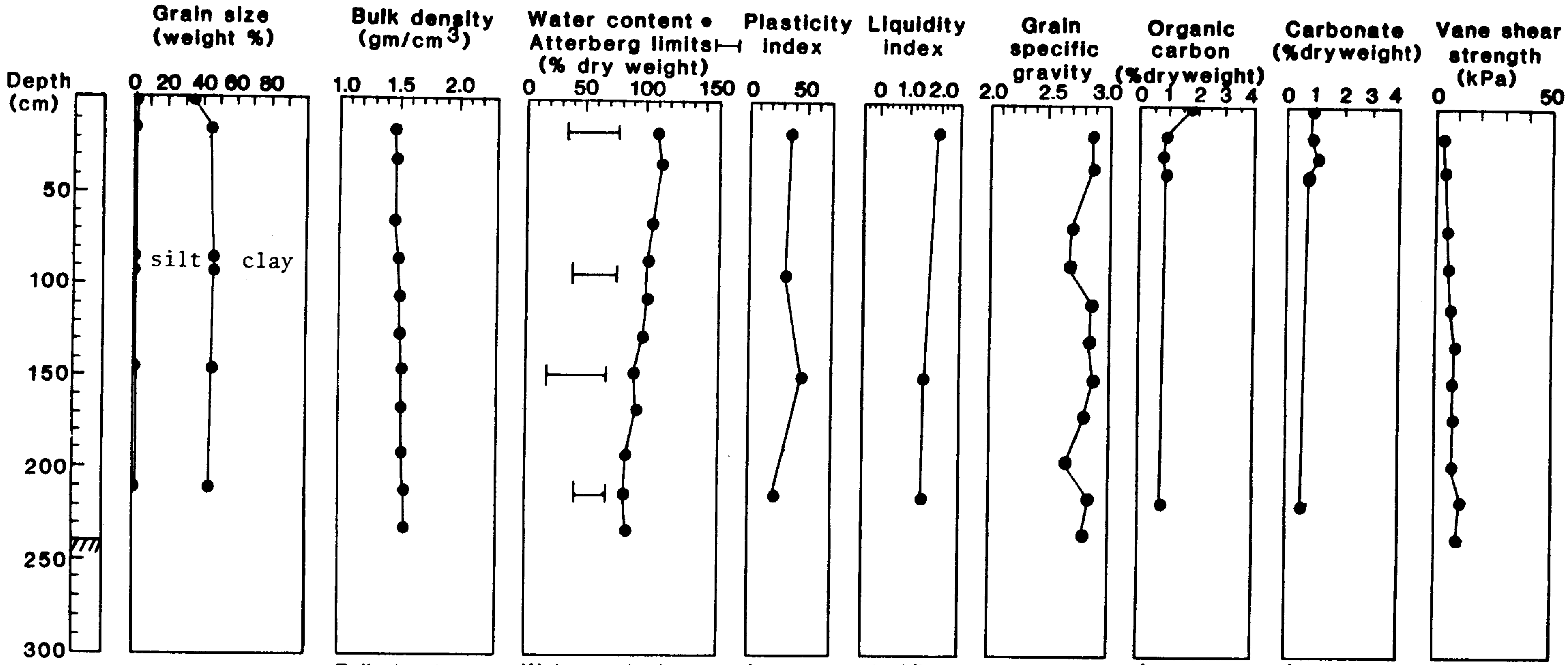

Bulk density at 1m.: 1.49

Water content at 1m.: 100.6

Average plastic limit: 36

Average liquid limit: 72

Average plasticity index: 36

Liquidity index at 1m.: 1.74

Average grain specific gravity: 2.84

Average organic carbon: 1.075

Average carbonate: 0.874

Vane shear strength at 1m.: 6.70

Station 512 **Location** 57°52.5'N 154°14.9'W **Water depth** 195m

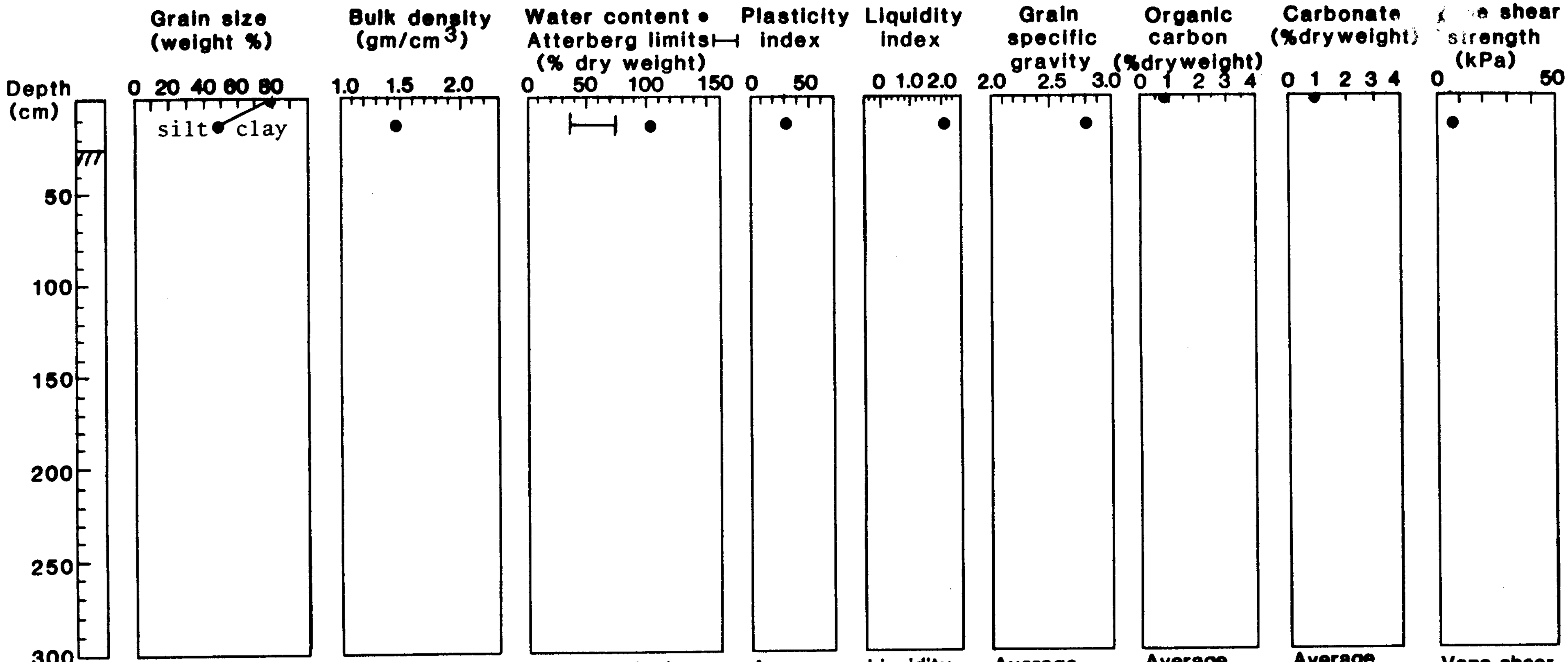

Bulk density at 1m.: ______

Water content at 1m.: ______

Average plastic limit: 41

Average liquid limit: 71

Average plasticity index: 30

Liquidity index at 1m.: ______

Average grain specific gravity: 2.81

Average organic carbon: 0.879

Average carbonate: 0.960

Vane shear strength at 1m.: ______

Station 513 **Location** 57°54.8'N 154°19.8'W **Water depth** 205m

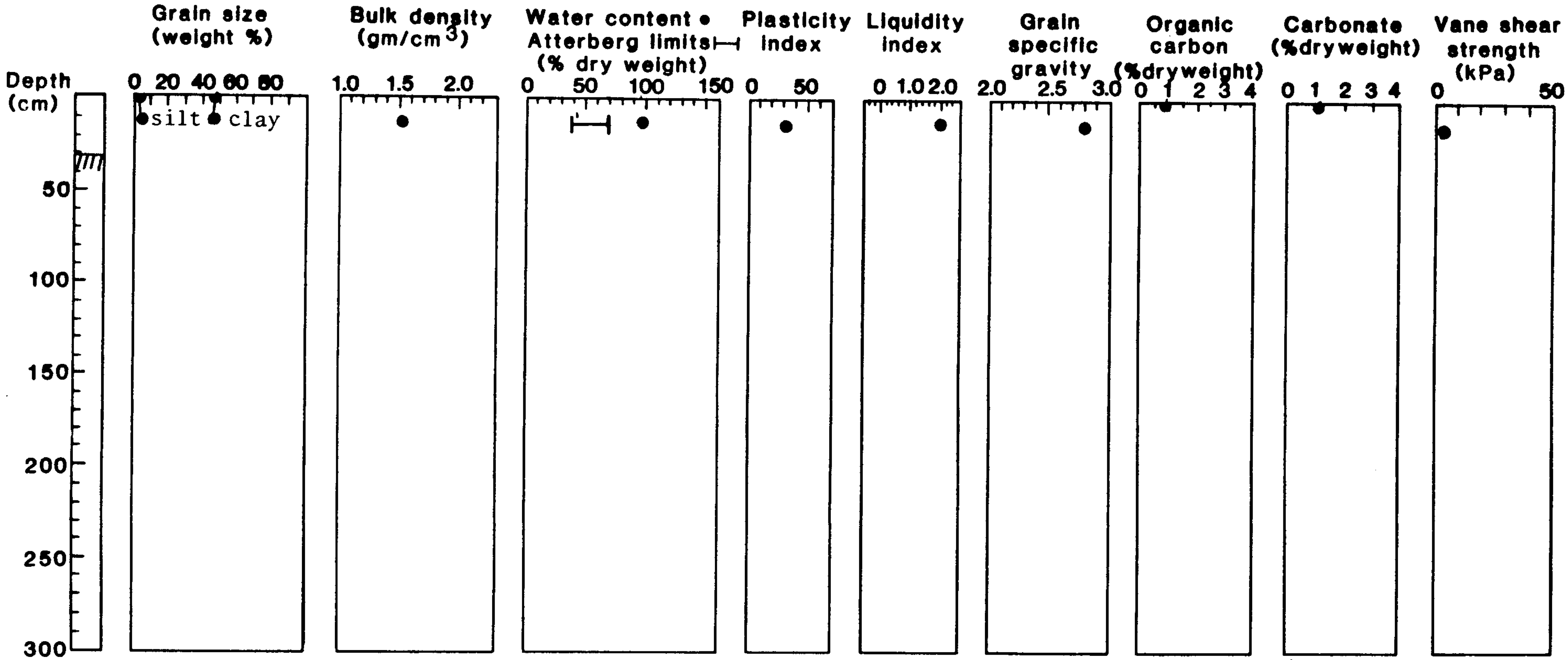

Bulk density at 1m.: ______

Water content at 1m.: ______

Average plastic limit: 37

Average liquid limit: 67

Average plasticity index: 30

Liquidity index at 1m.: ______

Average grain specific gravity: 2.77

Average organic carbon: 0.863

Average carbonate: 1.10

Vane shear strength at 1m.: ______

Station 514 **Location** 57°55.3'N 154°25.0'W **Water depth** 222m

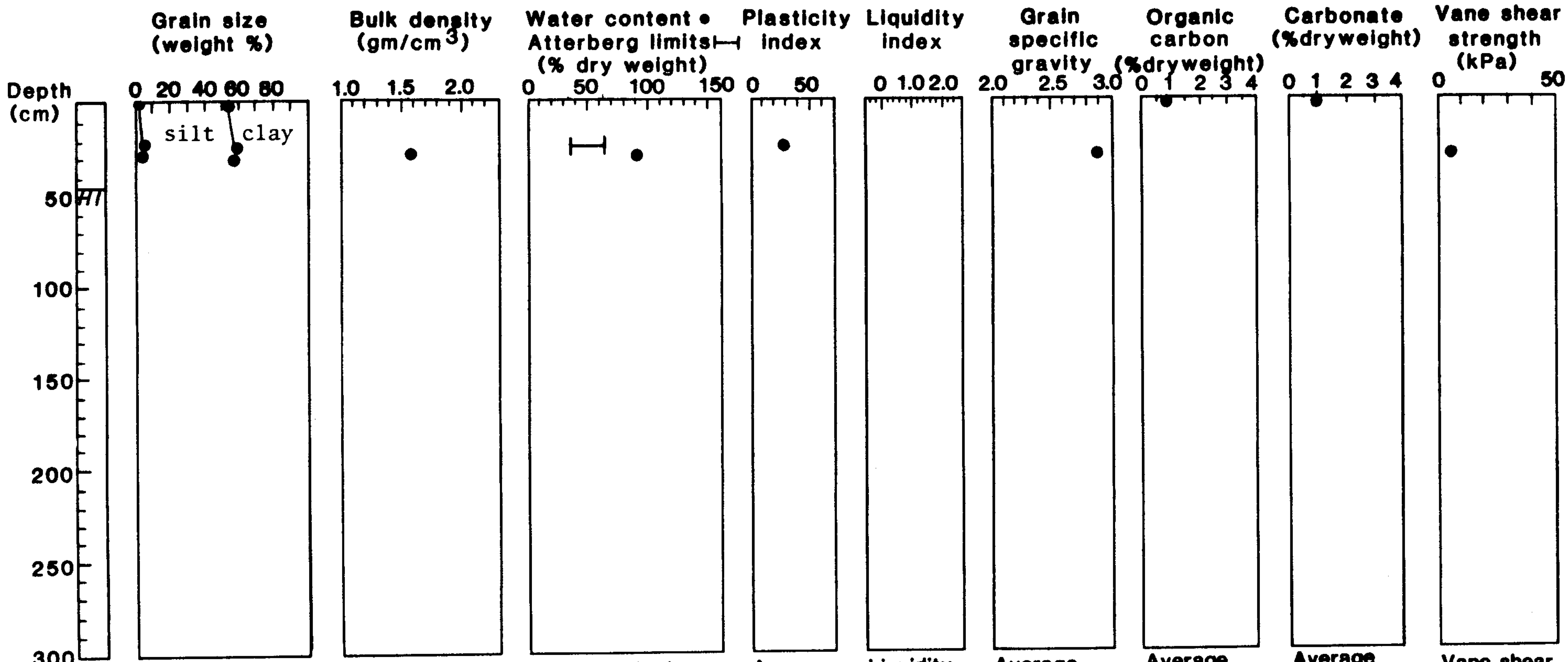

Bulk density at 1m.: _____

Water content at 1m.: _____

Average plastic limit: 36

Average liquid limit: 63

Average plasticity index: 27

Liquidity index at 1m.: _____

Average grain specific gravity: 2.85

Average organic carbon: 0.856

Average carbonate: 1.04

Vane shear strength at 1m.: _____

Station 515 Location 57°59.0'N 154°27.3'W Water depth 238m

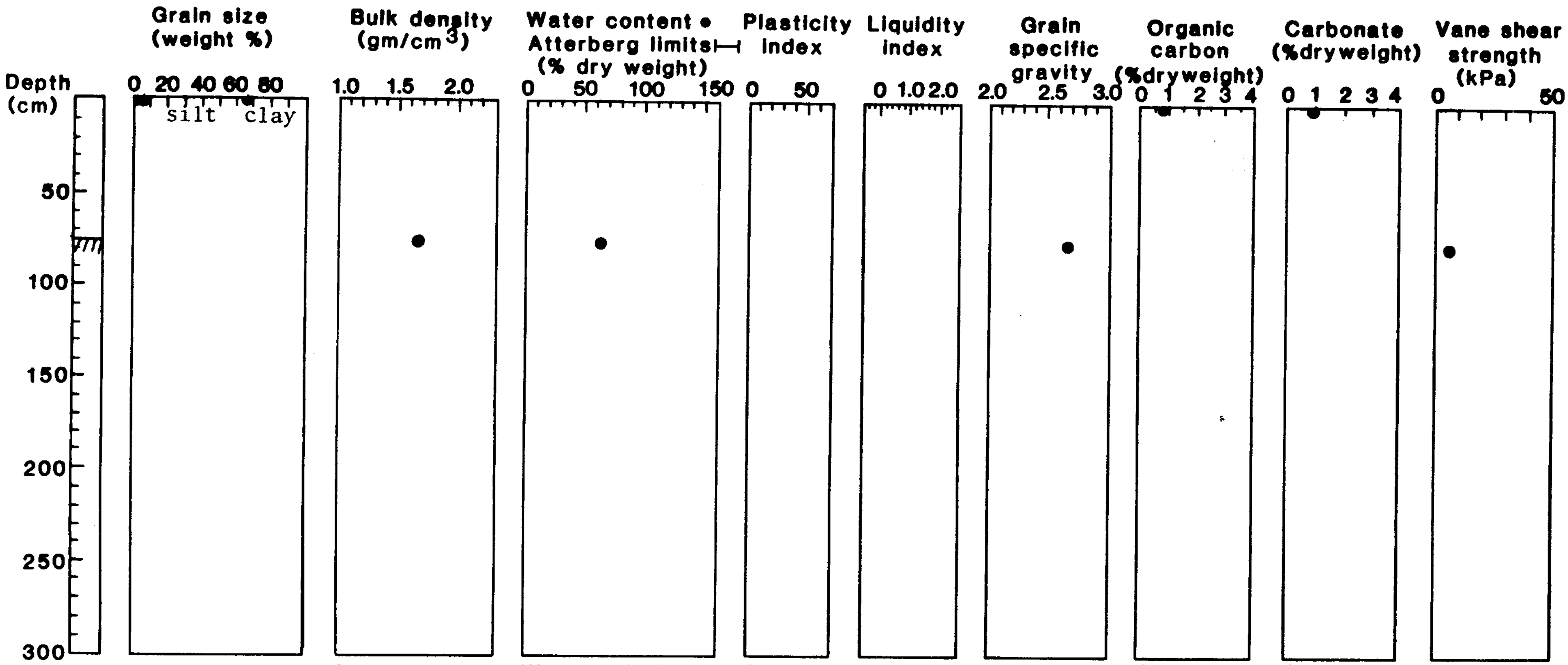

Bulk density at 1m.: ______

Water content at 1m.: ______
Average plastic limit: ______
Average liquid limit: ______

Average plasticity index: ______

Liquidity index at 1m.: ______

Average grain specific gravity: 2.65

Average organic carbon: 0.721

Average carbonate: 1.02

Vane shear strength at 1m.: ______

705

Station 516 **Location** 58°00.3'N 154°10.6'W **Water depth** 205

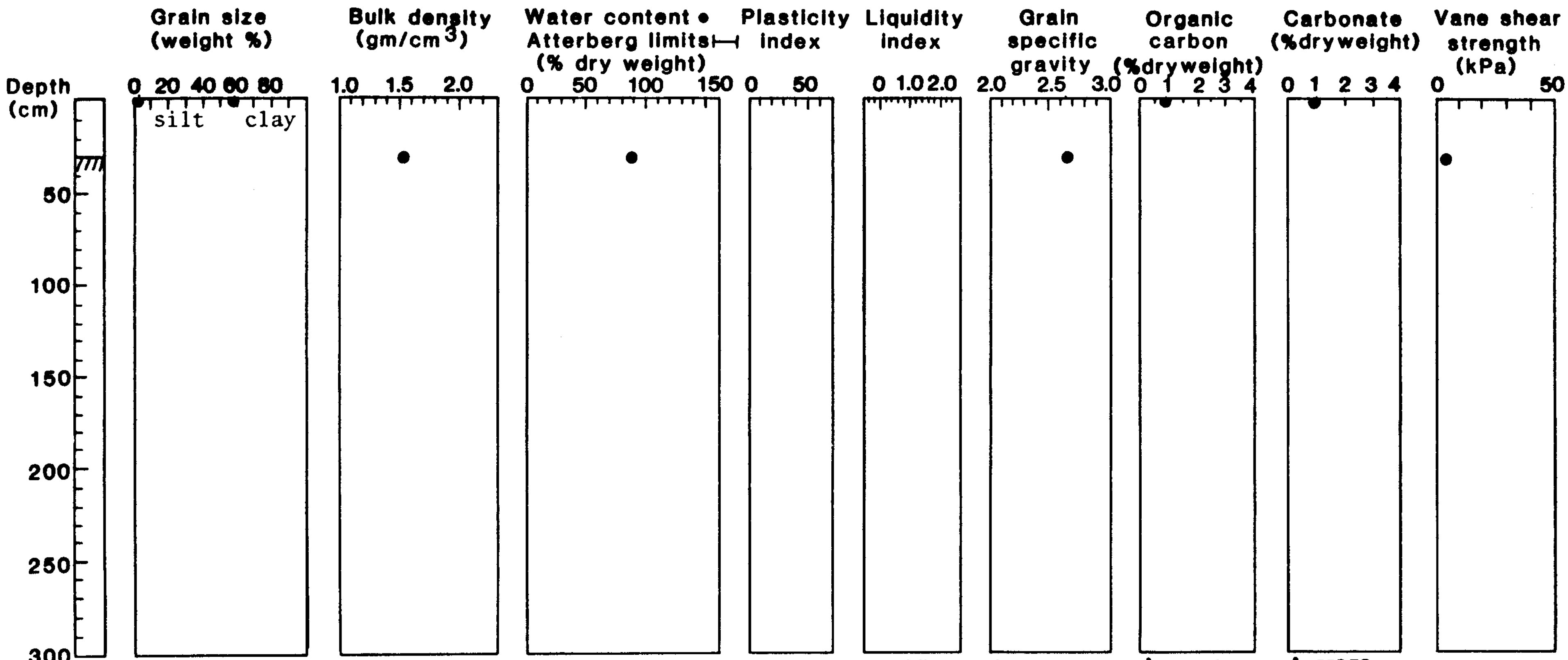

Bulk density at 1m.: ______

Water content at 1m.: ______
Average plastic limit: ______
Average liquid limit: ______

Average plasticity index: ______

Liquidity index at 1m.: ______

Average grain specific gravity: 2.65

Average organic carbon: 0.898

Average carbonate: 1.05

Vane shear strength at 1m.: ______

Station 517 **Location** 57°55.3'N 154°00.9'W **Water depth** 180m

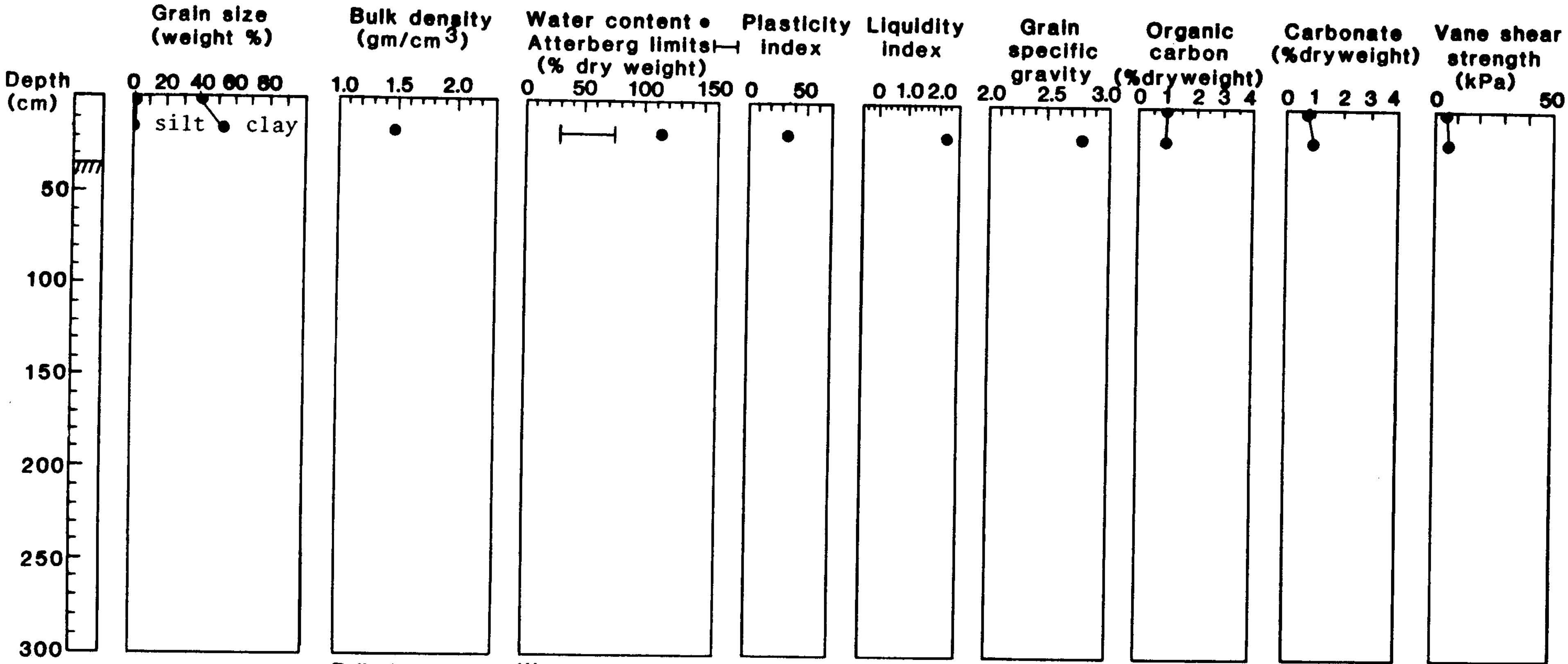

Bulk density at 1m.: ______

Water content at 1m.: ______

Average plastic limit: 39

Average liquid limit: 72

Average plasticity index: 33

Liquidity index at 1m.: ______

Average grain specific gravity: 2.78

Average organic carbon: 0.967

Average carbonate: 0.846

Vane shear strength at 1m.: ______

Station 518 Location 58°00.3'N 153°51.6'W Water depth 180m

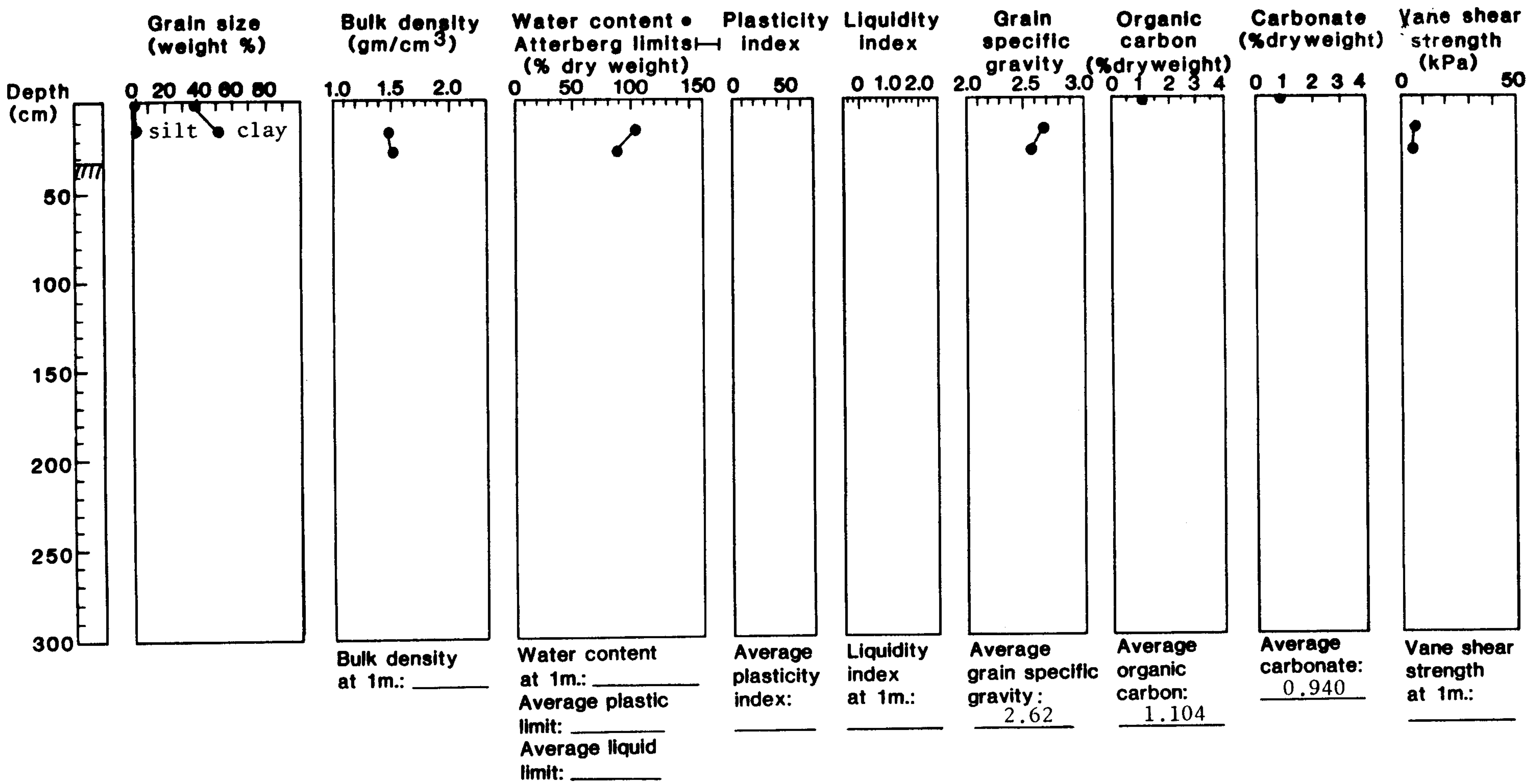

Station 519 Location 58°05.5'N 154°01.3'W Water depth 200m

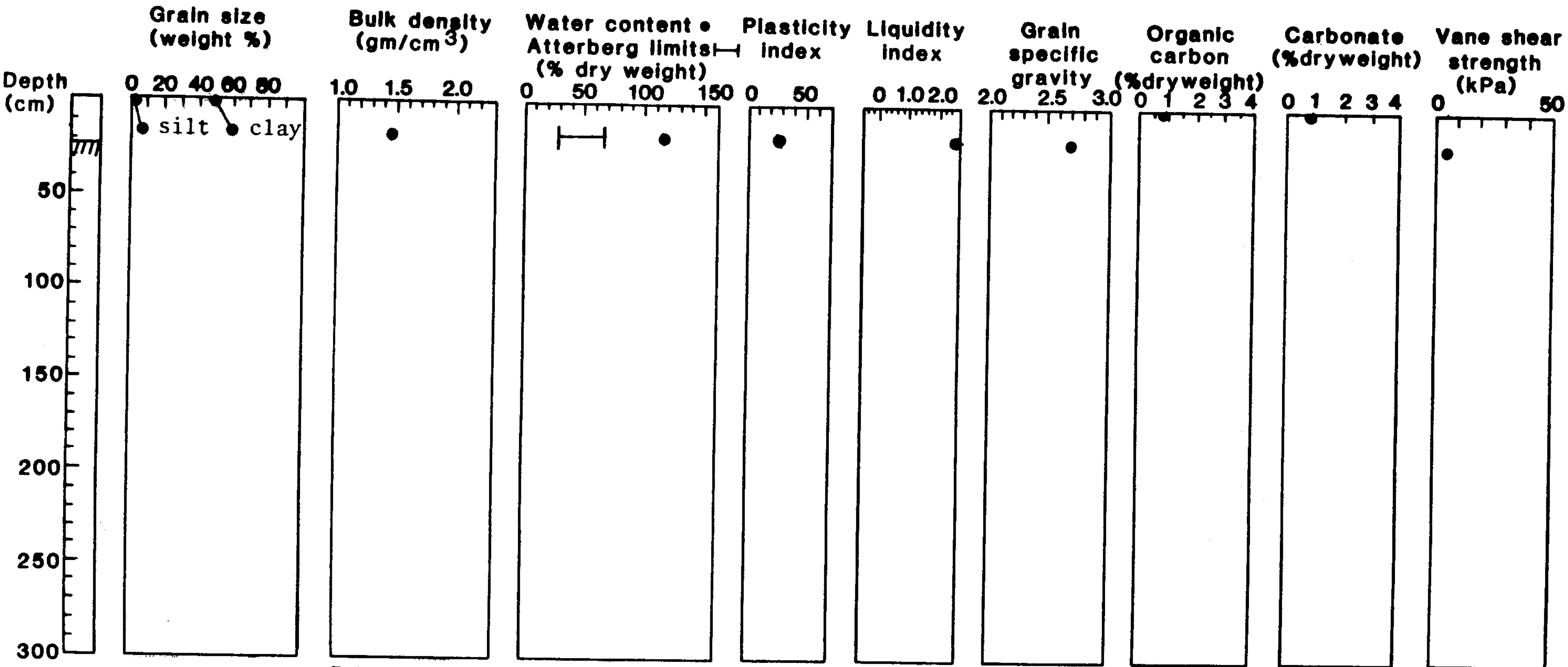

Bulk density at 1m.: ______

Water content at 1m.: ______

Average plastic limit: 39

Average liquid limit: 65

Average plasticity index: 24

Liquidity index at 1m.: ______

Average grain specific gravity: 2.70

Average organic carbon: 0.829

Average carbonate: 0.920

Vane shear strength at 1m.: ______

Station 520 Location 58°13.2'N 153°56.2'W Water depth 213m

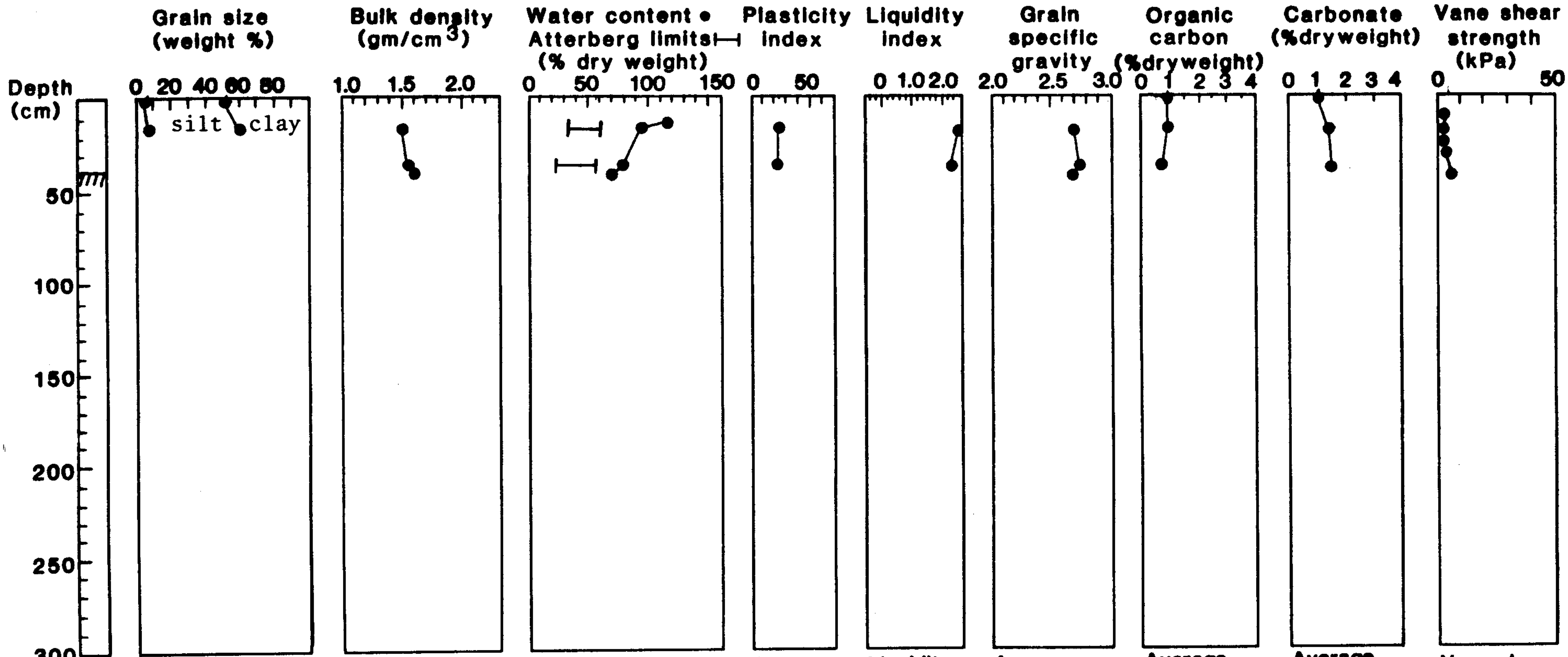

Bulk density at 1m.: ______

Water content at 1m.: ______

Average plastic limit: 34

Average liquid limit: 58

Average plasticity index: 24

Liquidity index at 1m.: ______

Average grain specific gravity: 2.72

Average organic carbon: 0.704

Average carbonate: 1.458

Vane shear strength at 1m.: ______

Station 521 Location 58°07.93'N 153°45.4'W Water depth 185m

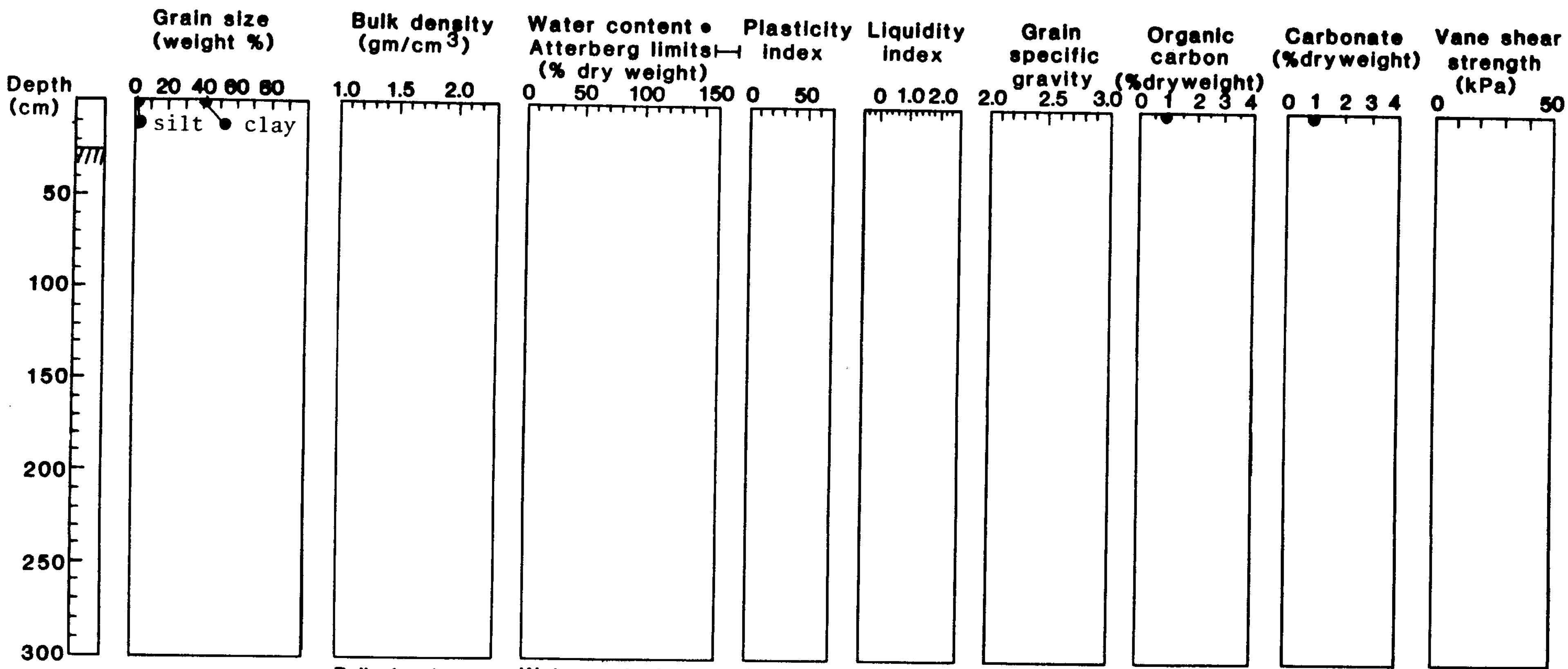

Bulk density at 1m.: ____

Water content at 1m.: ____

Average plastic limit: ____

Average liquid limit: ____

Average plasticity index: ____

Liquidity index at 1m.: ____

Average grain specific gravity: ____

Average organic carbon: 0.984

Average carbonate: 1.07

Vane shear strength at 1m.: ____

Station 522 **Location** 58°05.5'N 153°41.1'W **Water depth** 185m

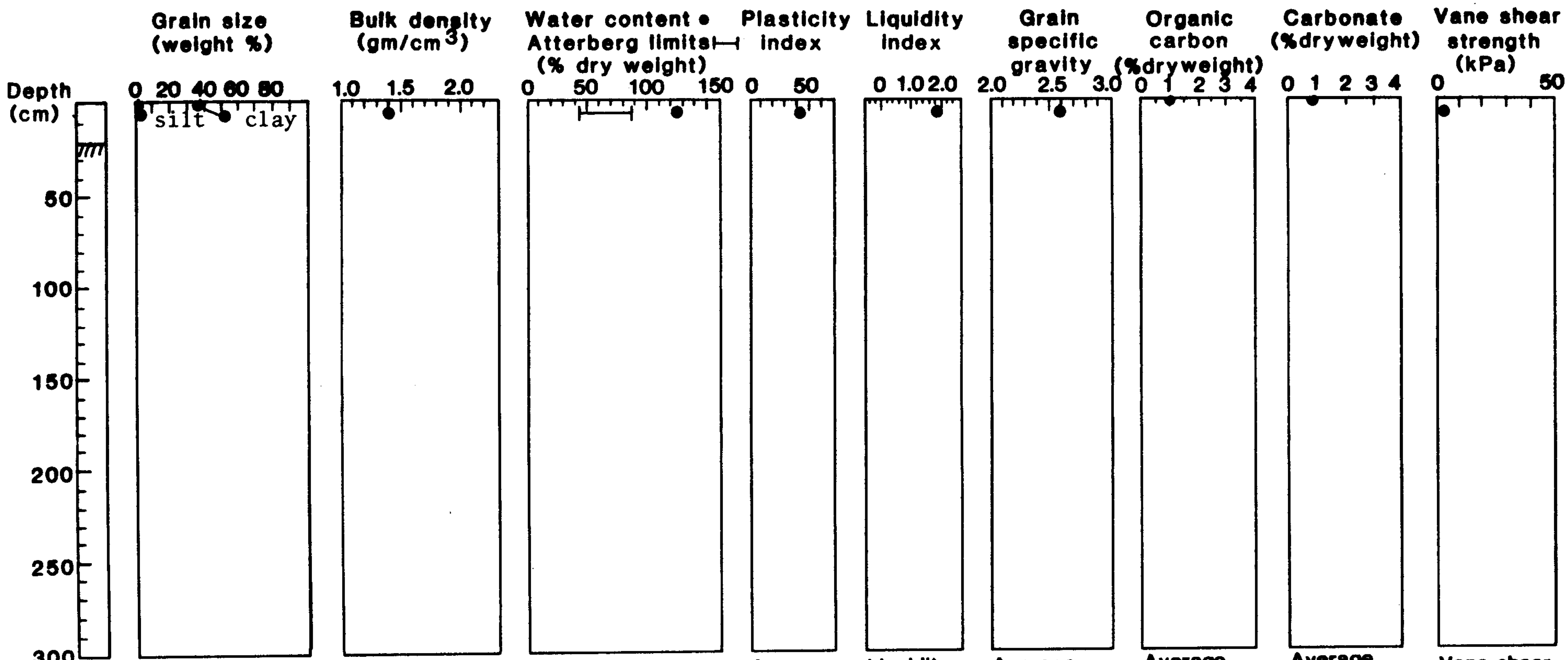

Bulk density at 1m.: ______

Water content at 1m.: ______

Average plastic limit: 45

Average liquid limit: 86

Average plasticity index: 41

Liquidity index at 1m.: ______

Average grain specific gravity: 2.60

Average organic carbon: 1.046

Average carbonate: 0.950

Vane shear strength at 1m.: ______

Station 523 Location 58°01.7'N 153°34.2'W Water depth 130m

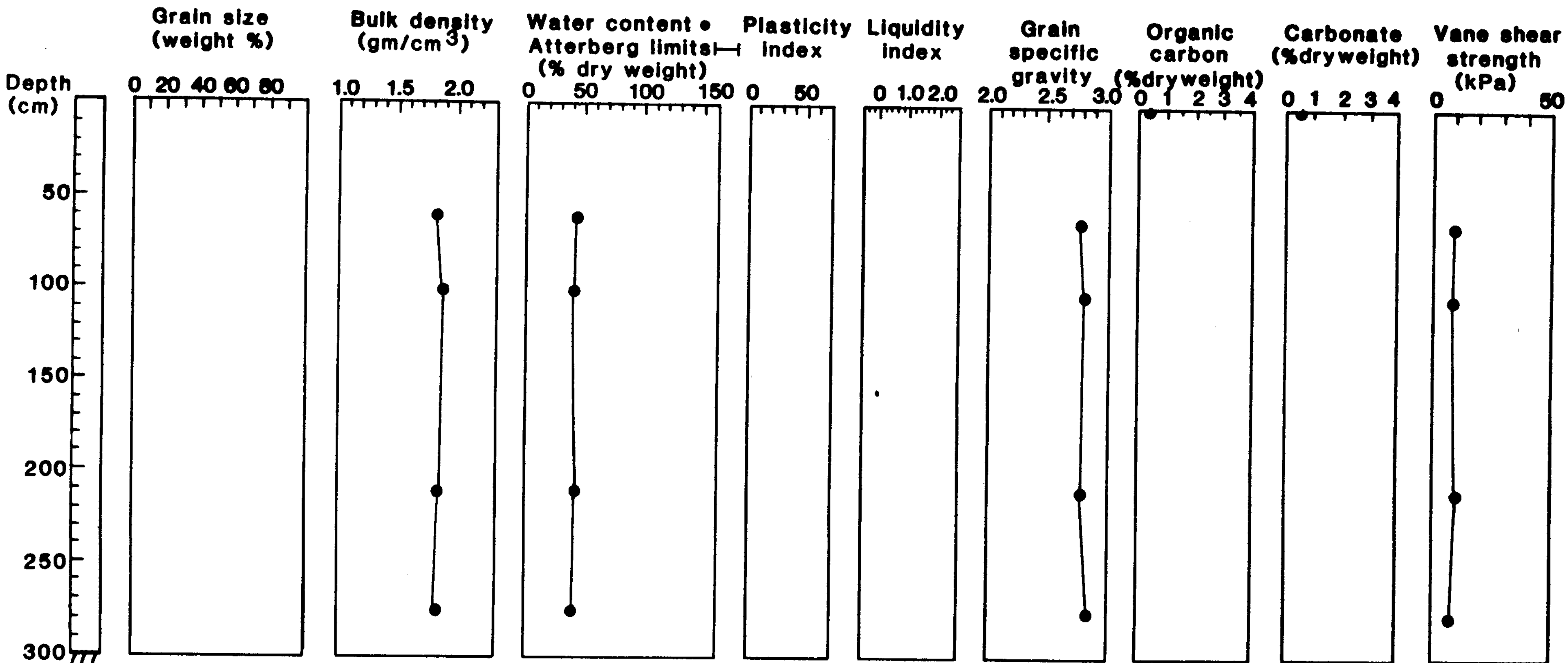

Bulk density at 1m.: 1.84

Water content at 1m.: 43.0

Average plastic limit: ______

Average liquid limit: ______

Average plasticity index: ______

Liquidity index at 1m.: ______

Average grain specific gravity: 2.77

Average organic carbon: 0.472

Average carbonate: 0.560

Vane shear strength at 1m.: 10.08

Station 524 Location 58°15.94'N 153°41.87'W Water depth 175m

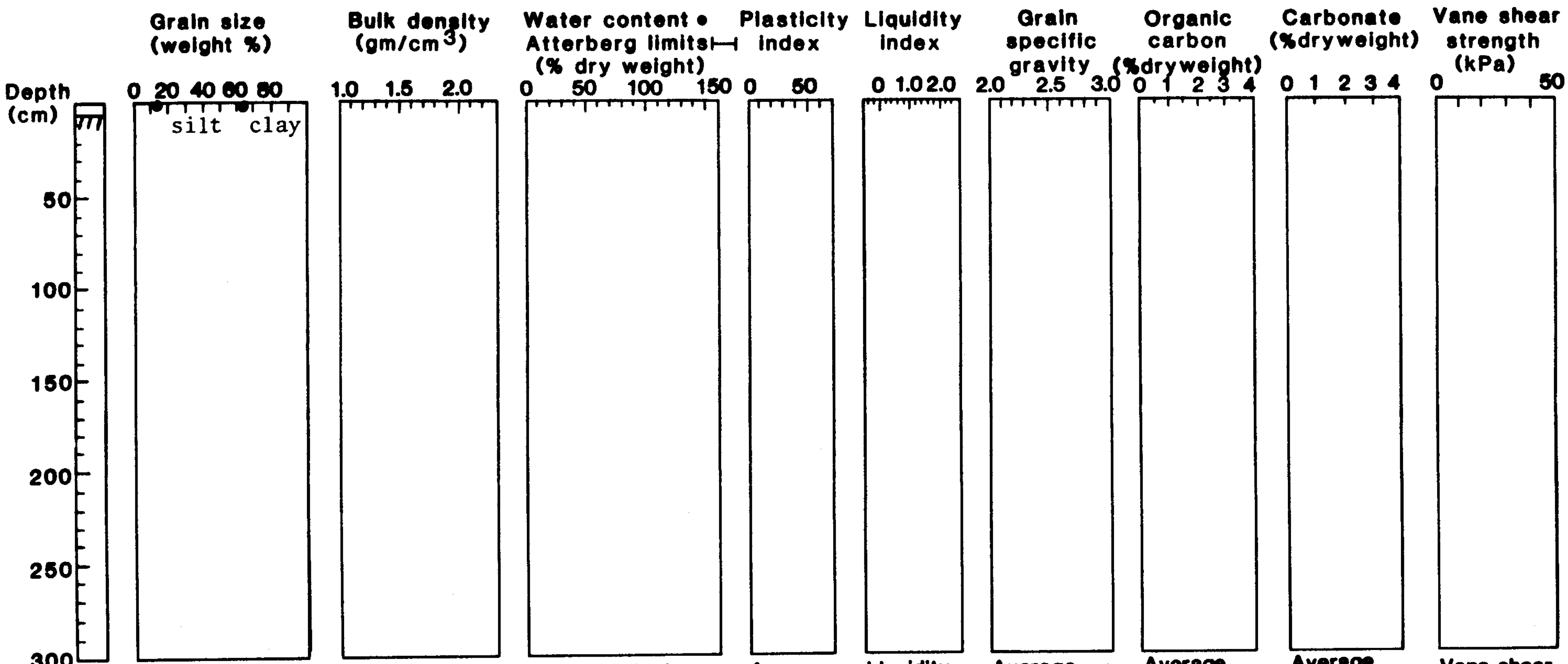

Bulk density at 1m.: ______

Water content at 1m.: ______
Average plastic limit: ______
Average liquid limit: ______

Average plasticity index: ______

Liquidity index at 1m.: ______

Average grain specific gravity: ______

Average organic carbon: ______

Average carbonate: ______

Vane shear strength at 1m.: ______

Station 525 **Location** 58°23.7'N 153°37.2'W **Water depth** 158m

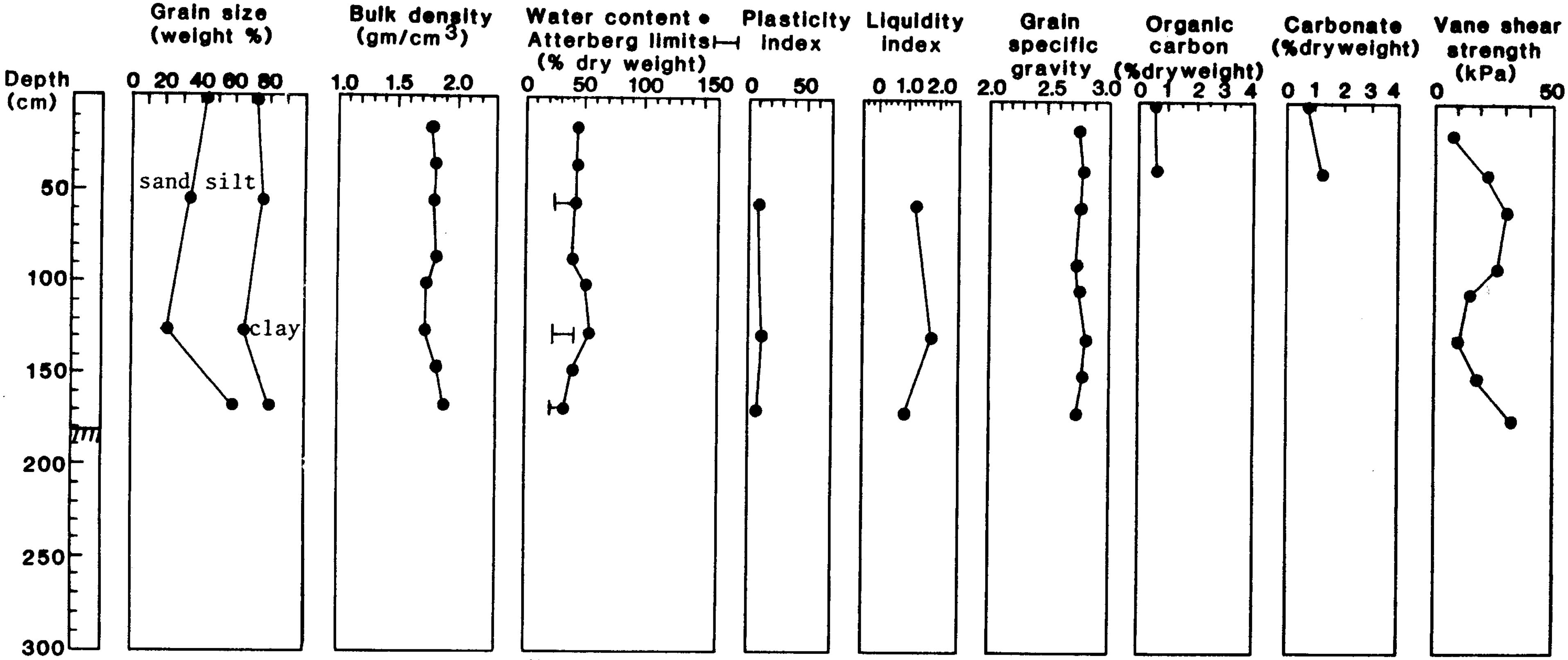

Bulk density at 1m.: 1.82

Water content at 1m.: 45.2
Average plastic limit: 27
Average liquid limit: 39

Average plasticity index: 13

Liquidity index at 1m.: 1.41

Average grain specific gravity: 2.79

Average organic carbon: 0.882

Average carbonate: 1.034

Vane shear strength at 1m.: 22.59

Station 526 **Location** 58°29.0'N 153°27.1'W **Water depth** 138m

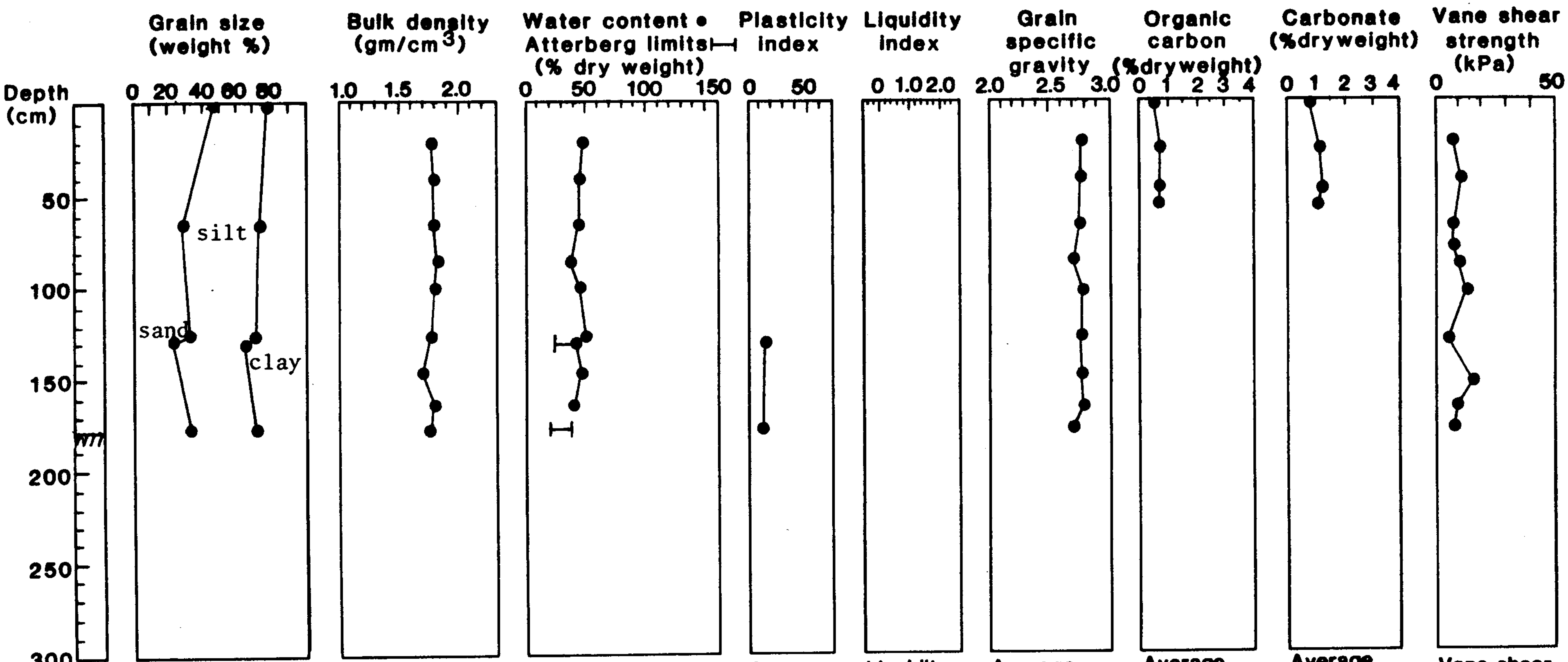

Bulk density at 1m.: 1.79

Water content at 1m.: 46.1
Average plastic limit: 25
Average liquid limit: 39

Average plasticity index: 13

Liquidity index at 1m.:

Average grain specific gravity: 2.79

Average organic carbon: 0.561

Average carbonate: 1.104

Vane shear strength at 1m.: 11.13

Station 527 **Location** 58°34.2'N 153°17.6'W **Water depth** 153m

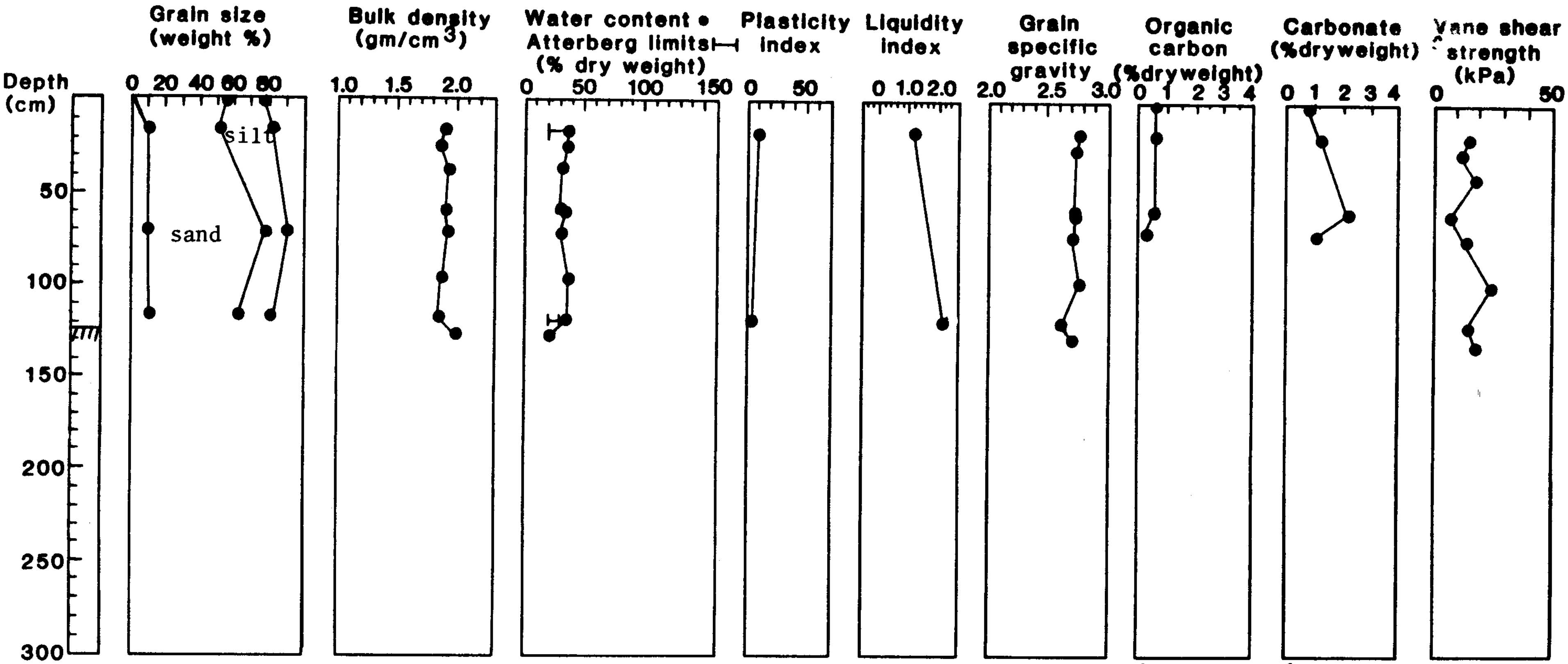

Bulk density at 1m.: 1.94

Water content at 1m.: 31.2
Average plastic limit: 22
Average liquid limit: 32

Average plasticity index: 9

Liquidity index at 1m.: 2.07

Average grain specific gravity: 2.74

Average organic carbon: 0.528

Average carbonate: 1.353

Vane shear strength at 1m.: 24.72

Station 528 **Location** 58°39.4'N 153°0.7'W **Water depth** 159m

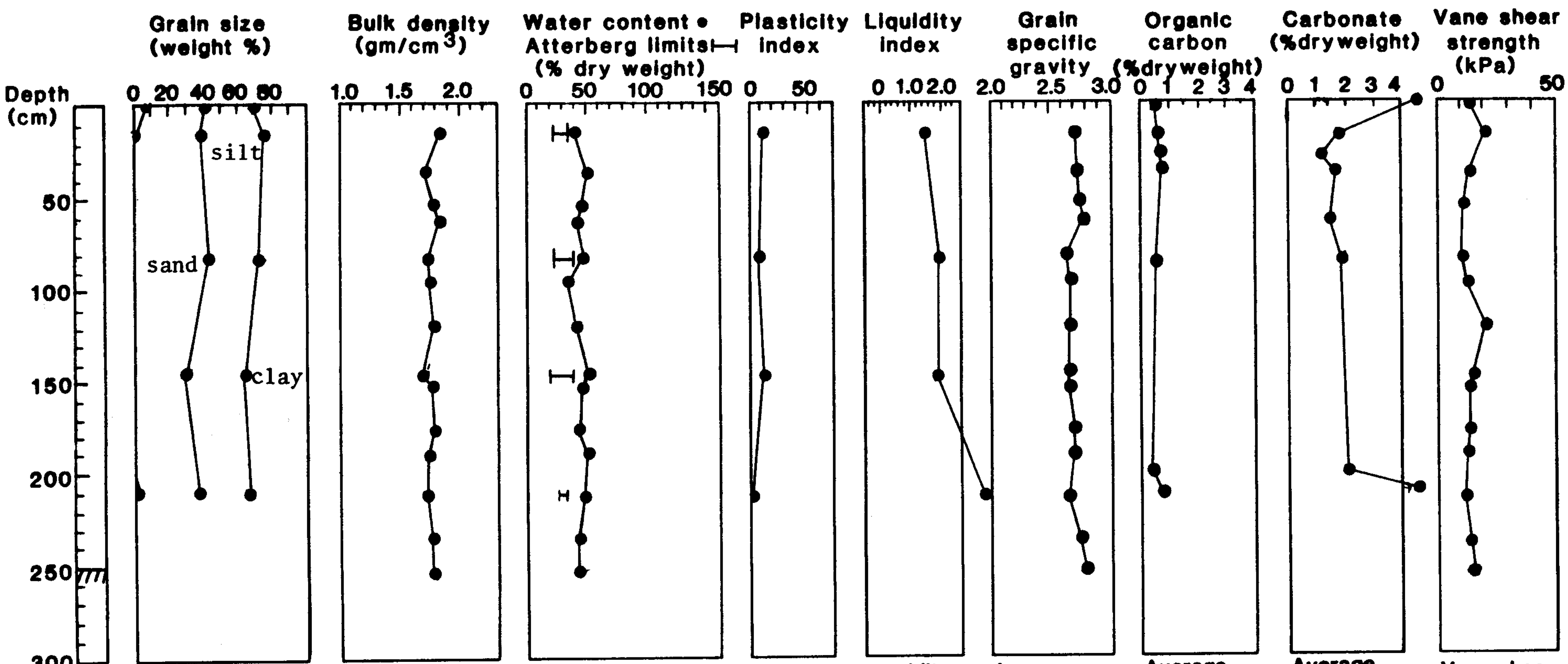

Bulk density at 1m.: 1.79

Water content at 1m.: 46.9

Average plastic limit: 26

Average liquid limit: 37

Average plasticity index: 11

Liquidity index at 1m.: 2.23

Average grain specific gravity: 2.74

Average organic carbon: 0.643

Average carbonate: 2.197

Vane shear strength at 1m.: 16.91

Station 529 **Location** 58°44.4'N 152°57.4'W **Water depth** 136m

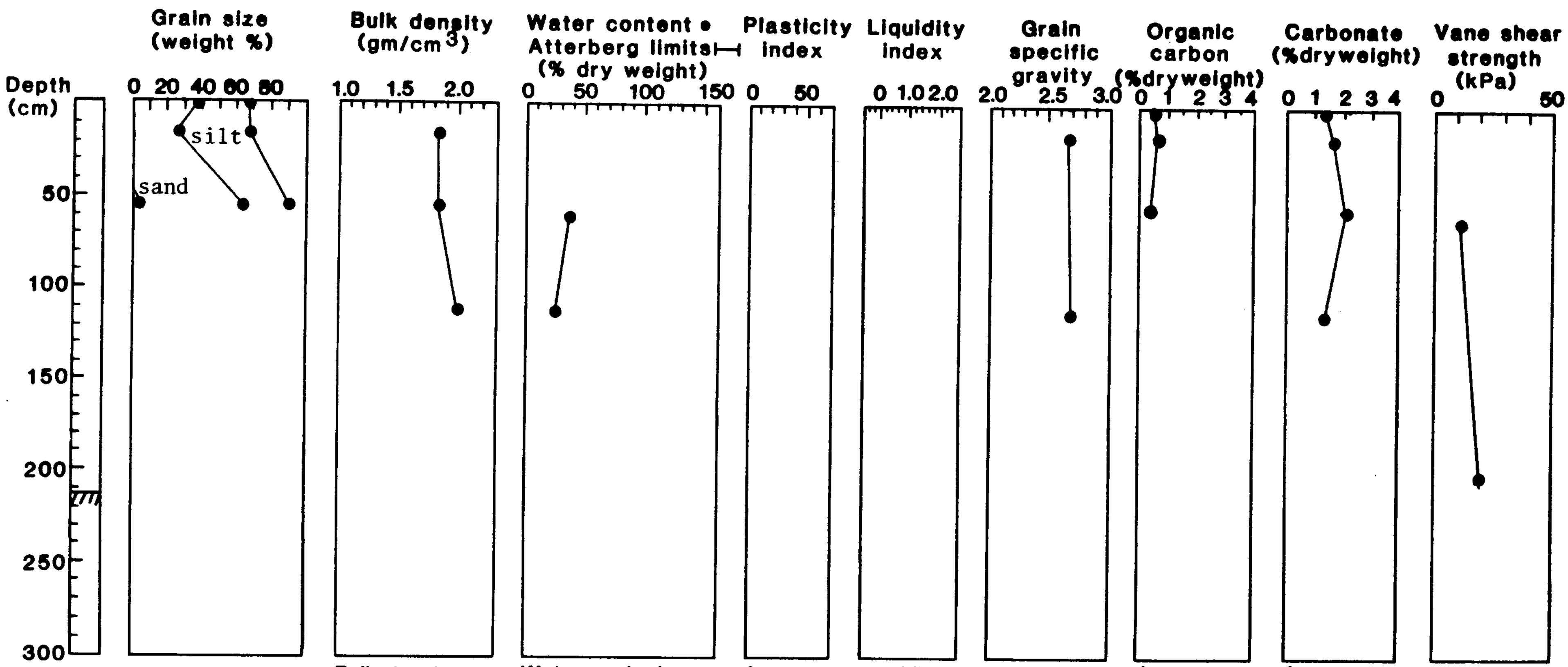

Bulk density at 1m.: 1.97

Water content at 1m.: 29.9
Average plastic limit: ____
Average liquid limit: ____

Average plasticity index: ____

Liquidity index at 1m.: ____

Average grain specific gravity: 2.69

Average organic carbon: 0.551

Average carbonate: 1.753

Vane shear strength at 1m.: 18.50

Station 530 Location 58°49.7'N 152°47.6'W Water depth 165m

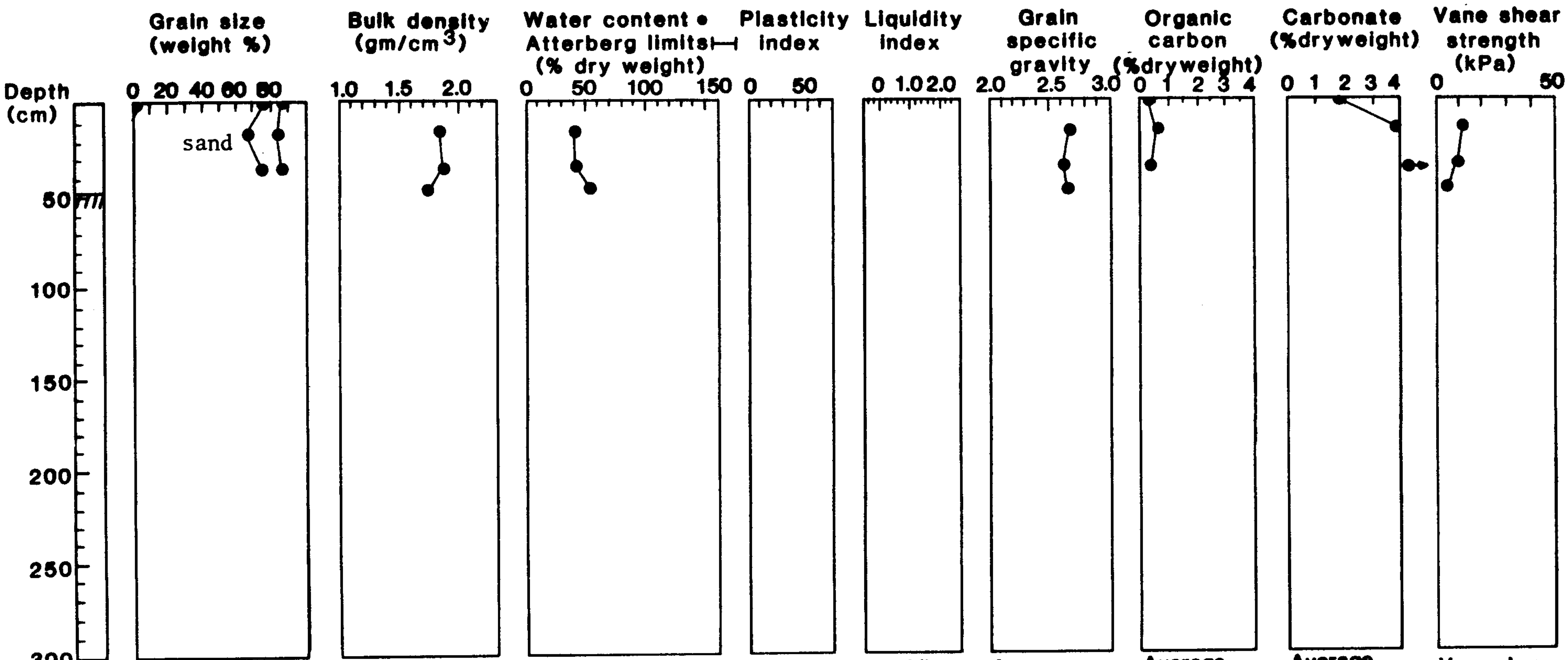

Bulk density at 1m.:

Water content at 1m.:
Average plastic limit:
Average liquid limit:

Average plasticity index:

Liquidity index at 1m.:

Average grain specific gravity: 2.72

Average organic carbon: 0.462

Average carbonate: 3.049

Vane shear strength at 1m.:

Station 531 Location 58°54.9'N 152°37.3'W Water depth 161m

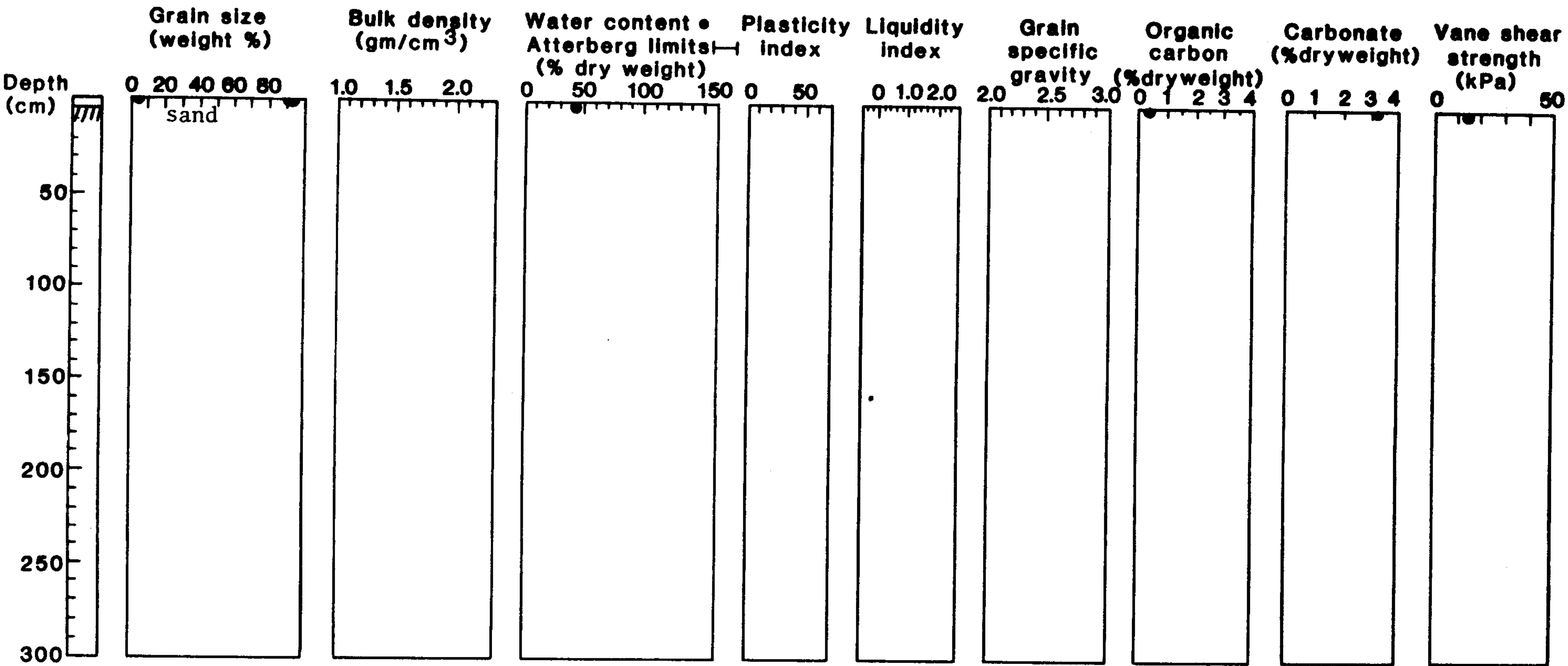

Bulk density at 1m.: ______

Water content at 1m.: ______

Average plastic limit: ______

Average liquid limit: ______

Average plasticity index: ______

Liquidity index at 1m.: ______

Average grain specific gravity: ______

Average organic carbon: 0.388

Average carbonate: 3.25

Vane shear strength at 1m.: ______

Station 532 **Location** 58°45.85'N 152°27.98'W **Water depth** 195m

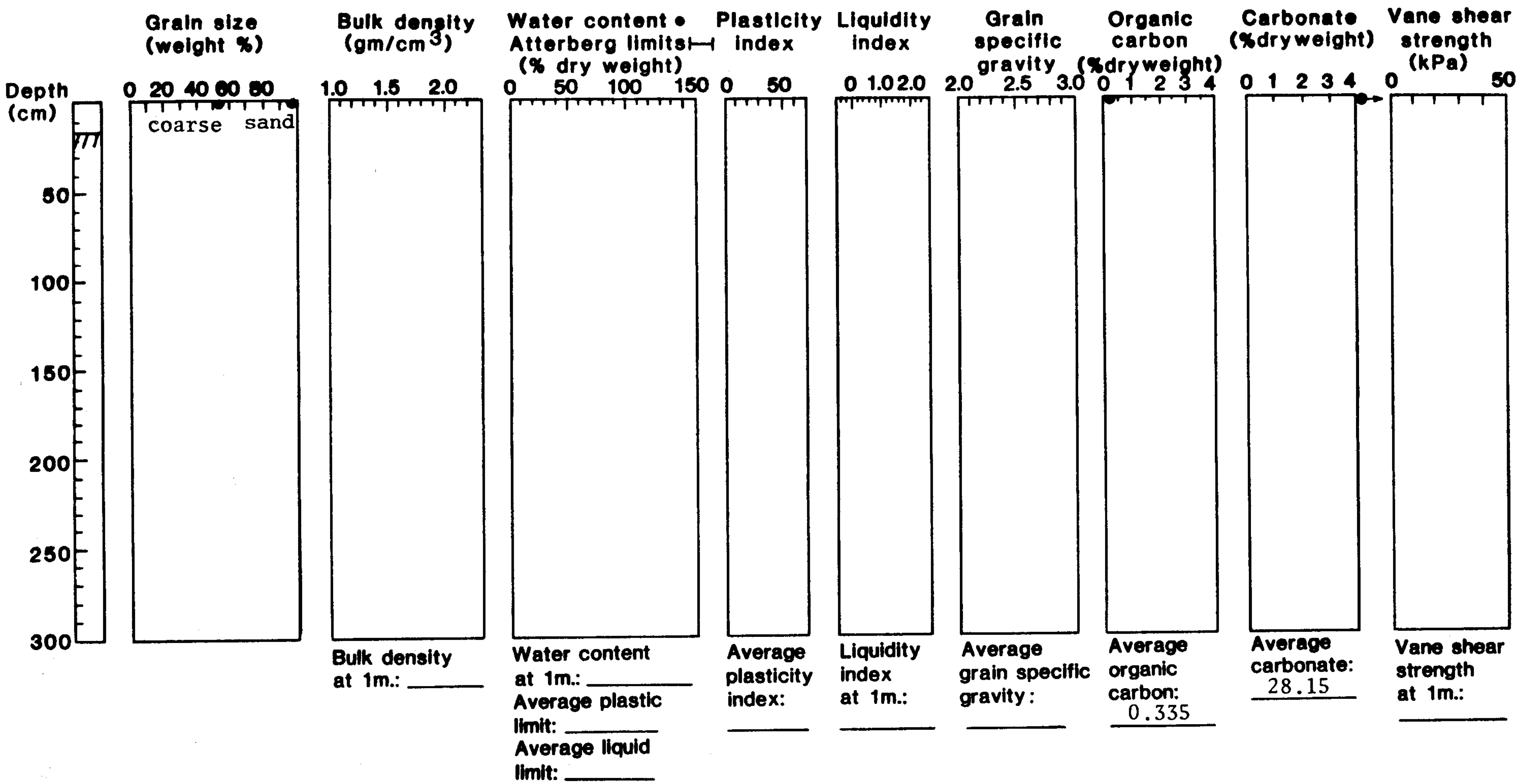

Station 533 Location 58°50.4'N 152°23.9'W Water depth 120m

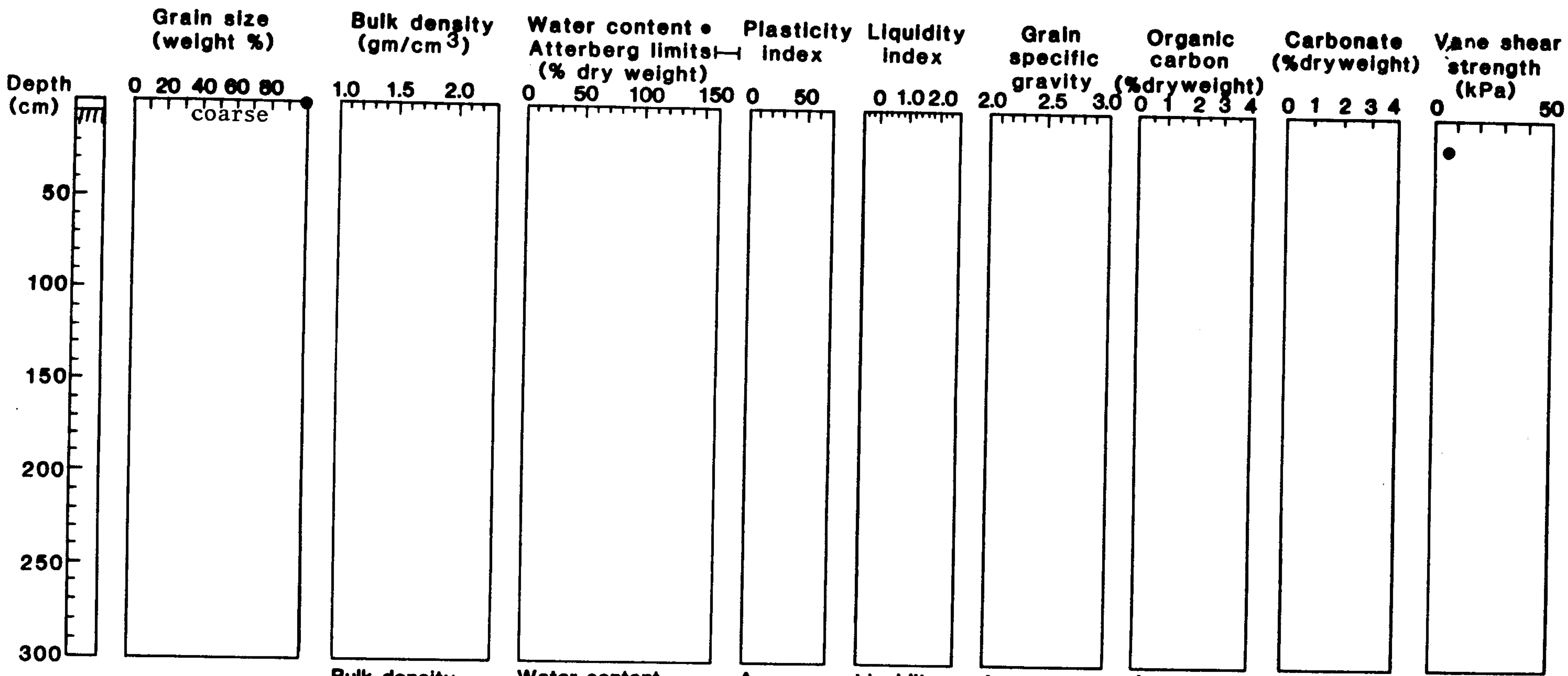

Bulk density at 1m.: ______

Water content at 1m.: ______

Average plastic limit: ______

Average liquid limit: ______

Average plasticity index: ______

Liquidity index at 1m.: ______

Average grain specific gravity: ______

Average organic carbon: ______

Average carbonate: ______

Vane shear strength at 1m.: ______

724

Station 534 **Location** 58°39.6'N 152°47.1'W **Water depth** 185m

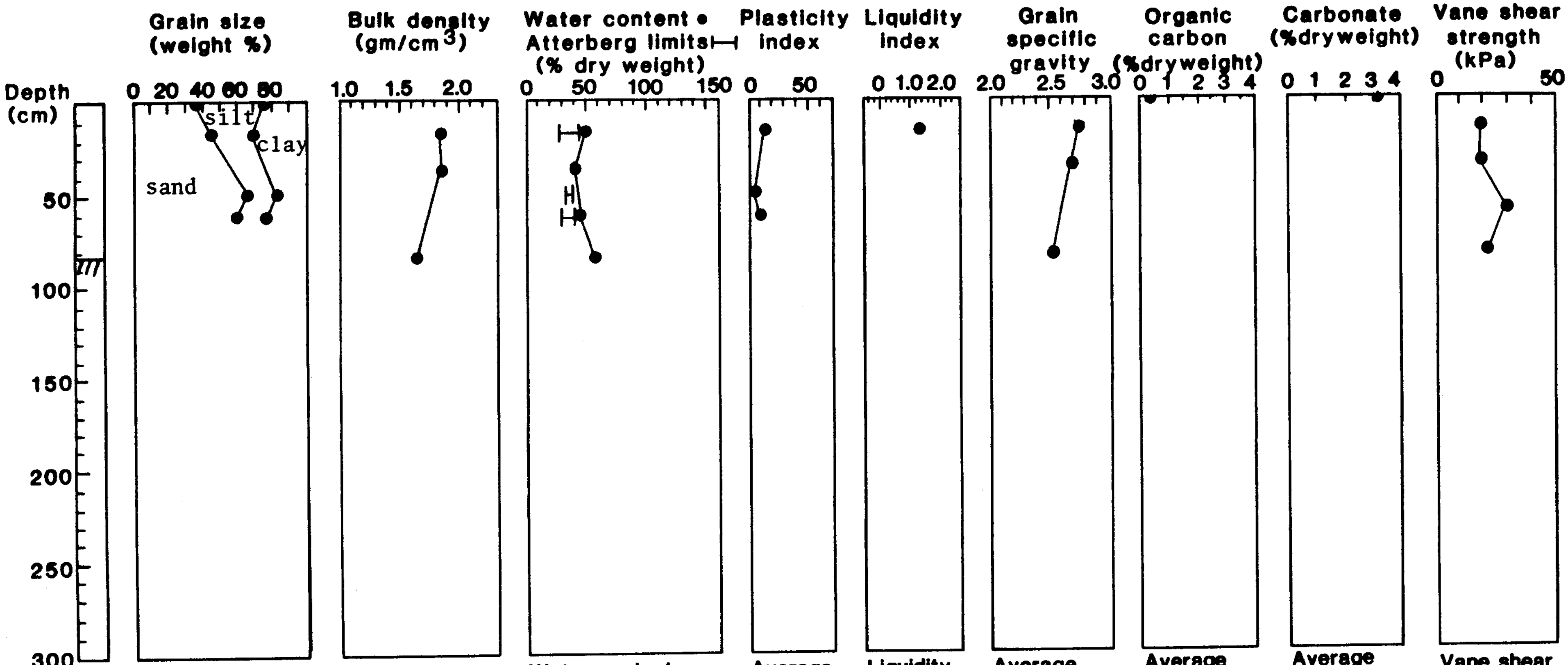

Bulk density at 1m.: ______

Water content at 1m.: ______
Average plastic limit: 30
Average liquid limit: 41

Average plasticity index: 11

Liquidity index at 1m.: ______

Average grain specific gravity: 2.66

Average organic carbon: 0.424

Average carbonate: 3.17

Vane shear strength at 1m.: ______

Station 535 Location 58°37.0'N 152°42.0'W Water depth 98m

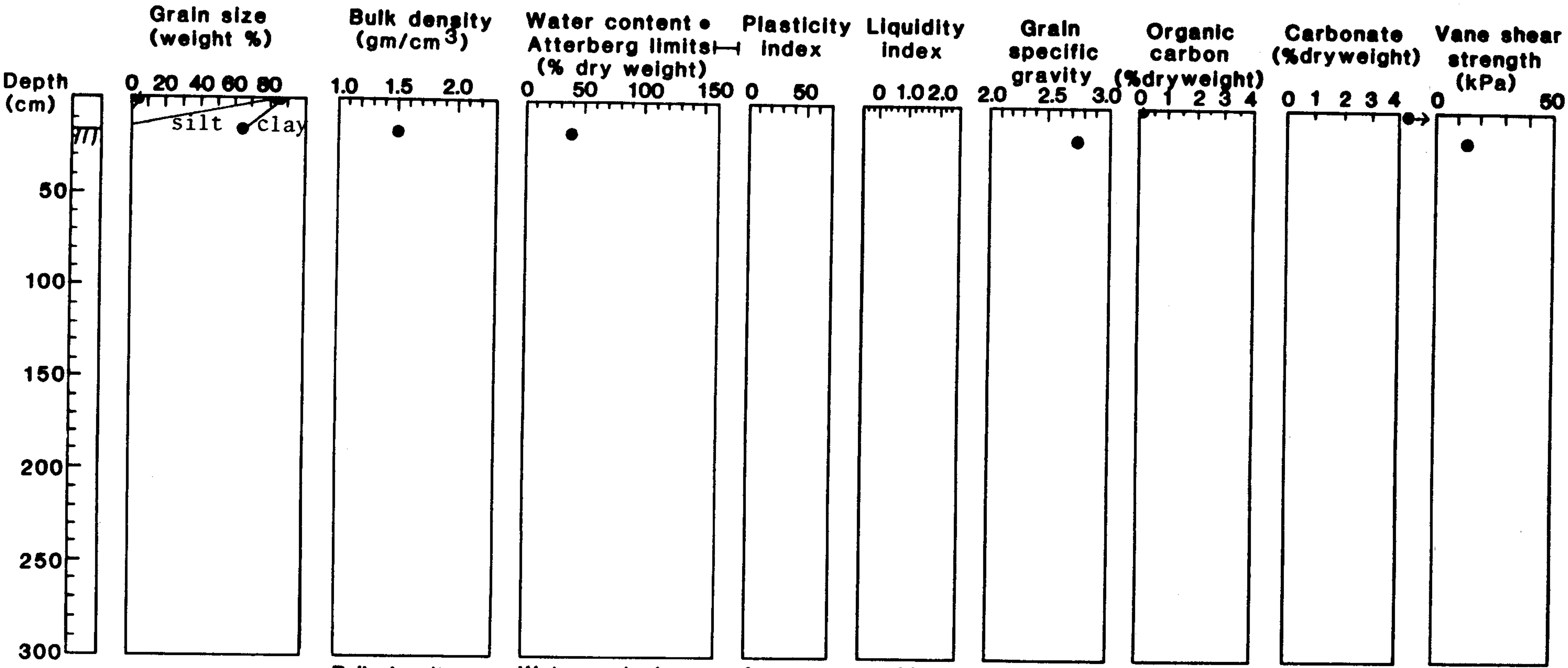

Bulk density at 1m.: ______

Water content at 1m.: ______
Average plastic limit: ______
Average liquid limit: ______

Average plasticity index: ______

Liquidity index at 1m.: ______

Average grain specific gravity: 2.76

Average organic carbon: 0.209

Average carbonate: 21.67

Vane shear strength at 1m.: ______

Station 536 **Location** 58°31.4'N 152°52.6'W **Water depth** 190m

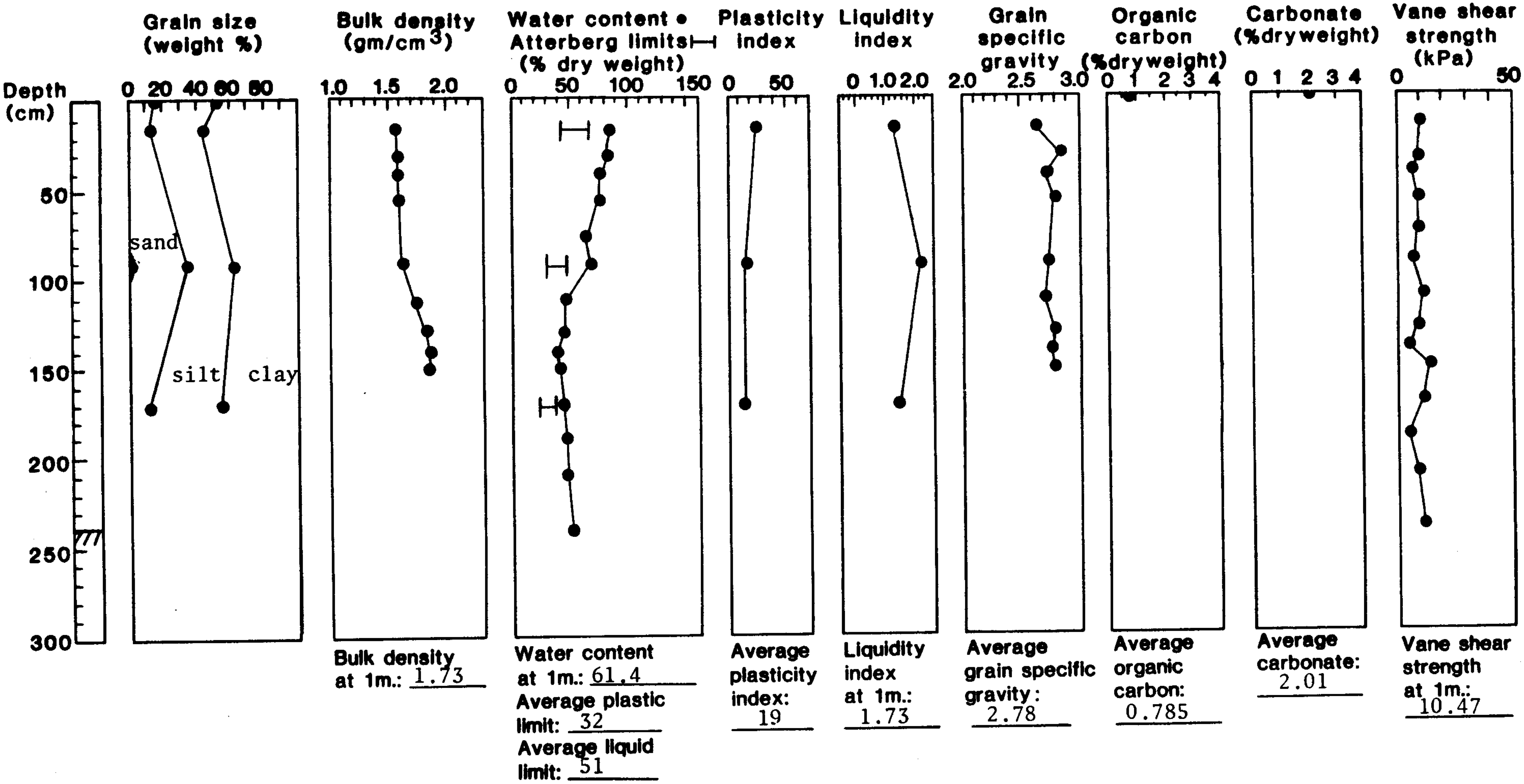

Station 537 **Location** 58°29.0'N 153°07.6'W **Water depth** 160m

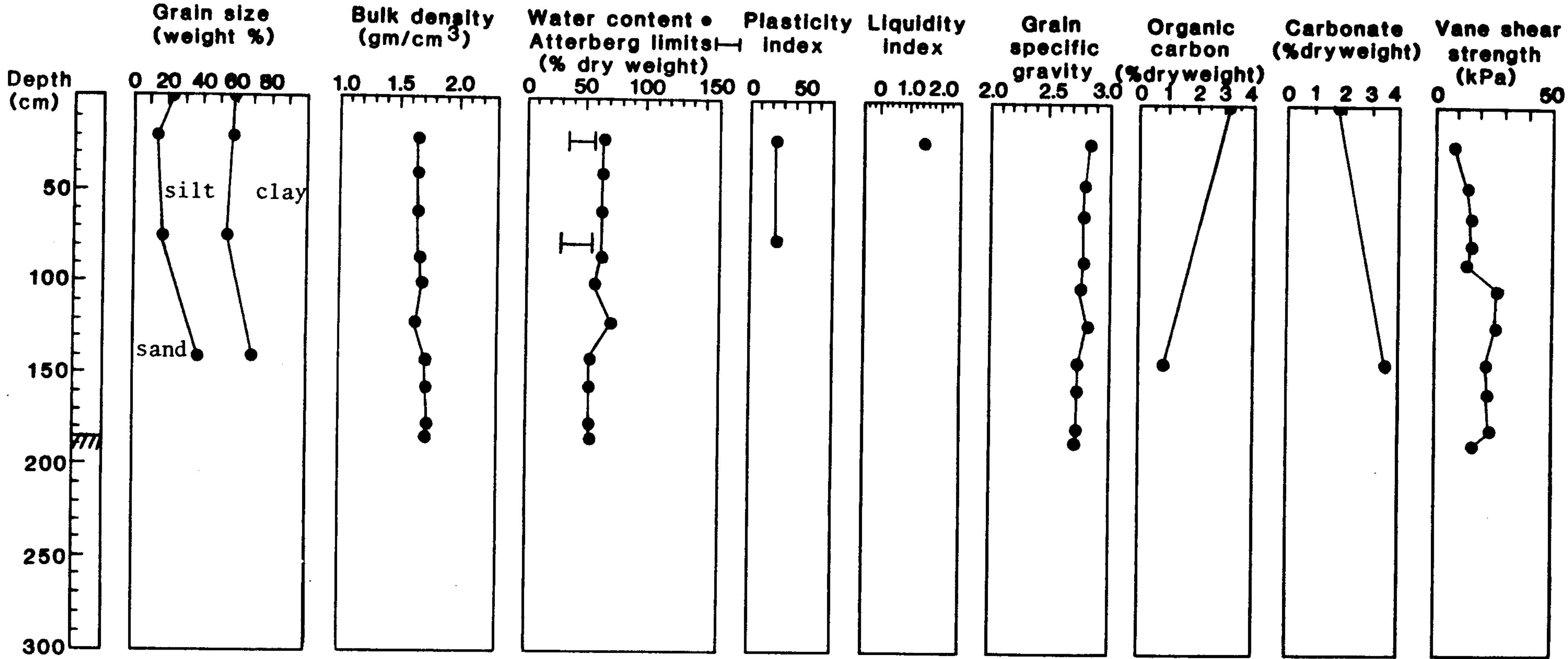

Bulk density at 1m.: 1.69

Water content at 1m.: 61.5
Average plastic limit: 32
Average liquid limit: 56

Average plasticity index: 24

Liquidity index at 1m.:

Average grain specific gravity: 2.78

Average organic carbon: 1.973

Average carbonate: 2.775

Vane shear strength at 1m.: 20.58

Station 538 **Location** 58°25.2'N 153°00.2'W **Water depth** 190m

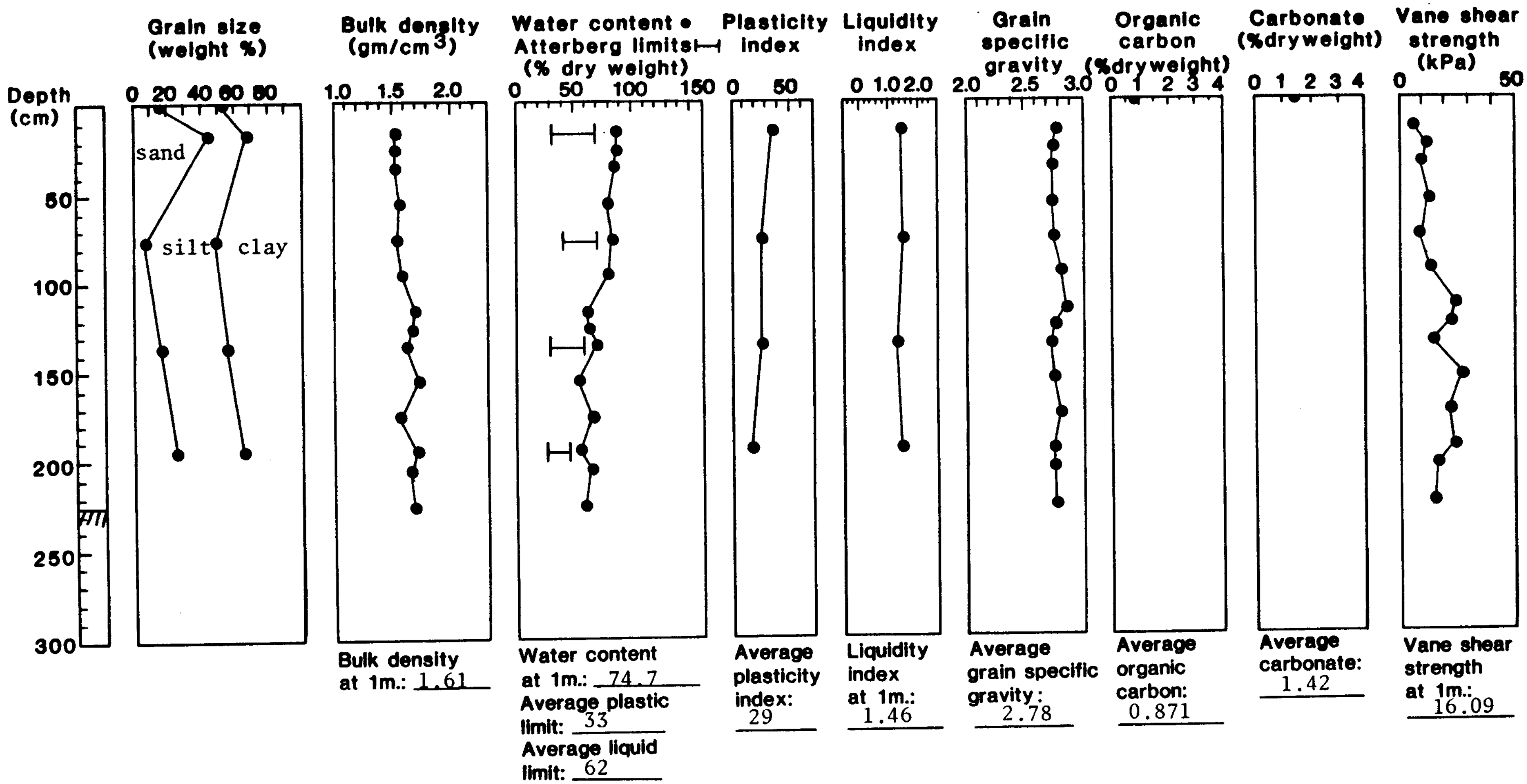

Station 539 **Location** 58°21.3'N 153°12.4'W **Water depth** 175m

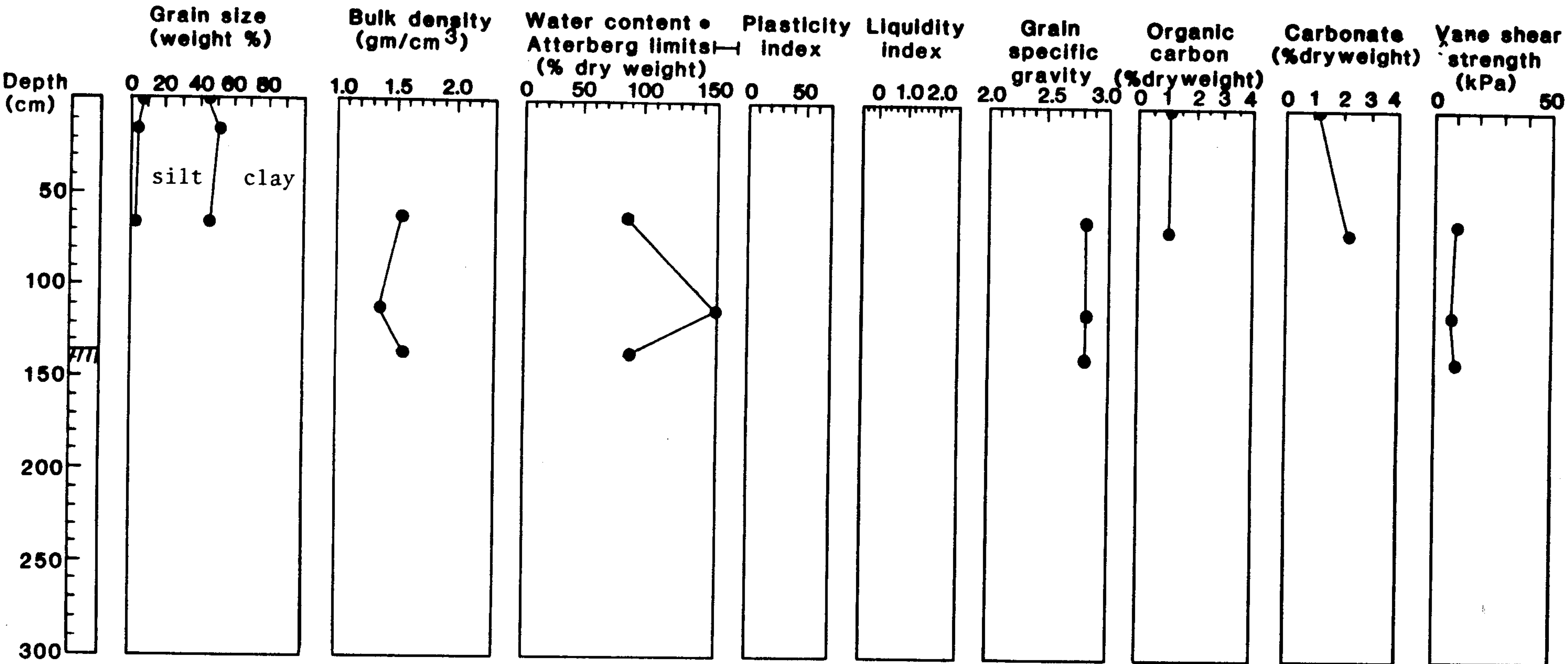

Bulk density at 1m.: 1.48

Water content at 1m.: 109.7
Average plastic limit: ______
Average liquid limit: ______

Average plasticity index: ______

Liquidity index at 1m.: ______

Average grain specific gravity: 2.82

Average organic carbon: 1.102

Average carbonate: 1.70

Vane shear strength at 1m.: 9.07

Station 540 **Location** 58°21.5'N 153°07.6'W **Water depth** 210m

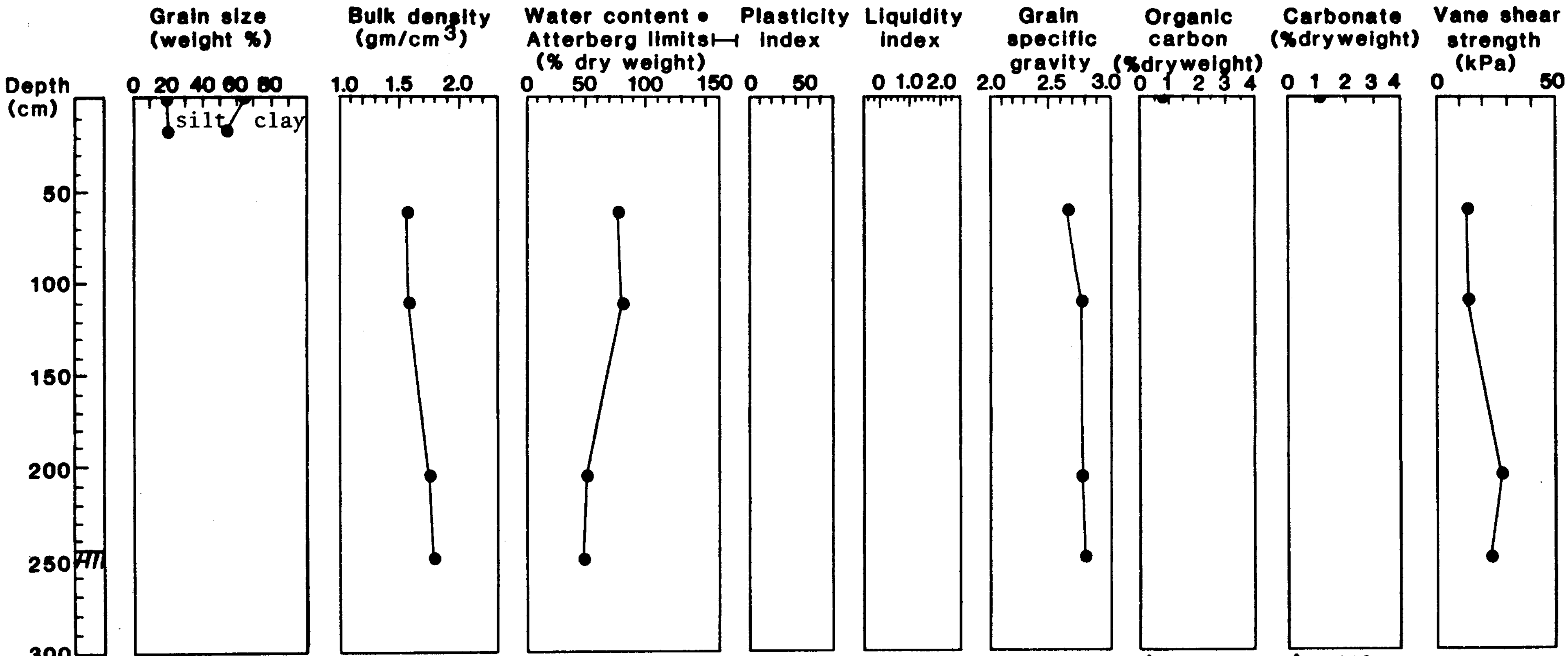

Bulk density at 1m.: 1.61

Water content at 1m.: 74.0
Average plastic limit: ______
Average liquid limit: ______

Average plasticity index: ______

Liquidity index at 1m.: ______

Average grain specific gravity: 2.76

Average organic carbon: 0.799

Average carbonate: 1.10

Vane shear strength at 1m.: 15.86

Station 541 **Location** 58°15.8'N 153°22.0'W **Water depth** 167m

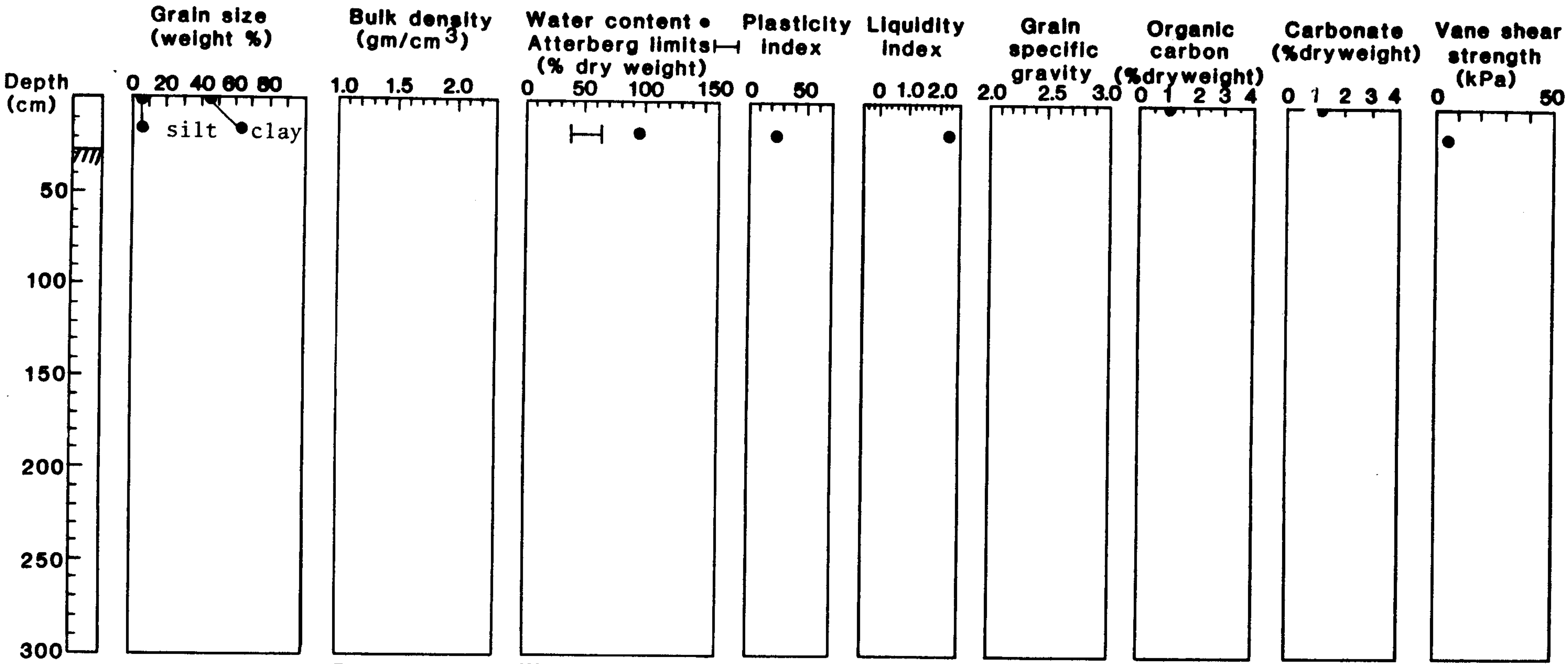

Bulk density at 1m.: ______

Water content at 1m.: ______
Average plastic limit: 39
Average liquid limit: 63

Average plasticity index: 24

Liquidity index at 1m.: ______

Average grain specific gravity: ______

Average organic carbon: 1.082

Average carbonate: 1.270

Vane shear strength at 1m.: ______

Station 542 Location 58°18.6'N 153°26.9'W Water depth 155m

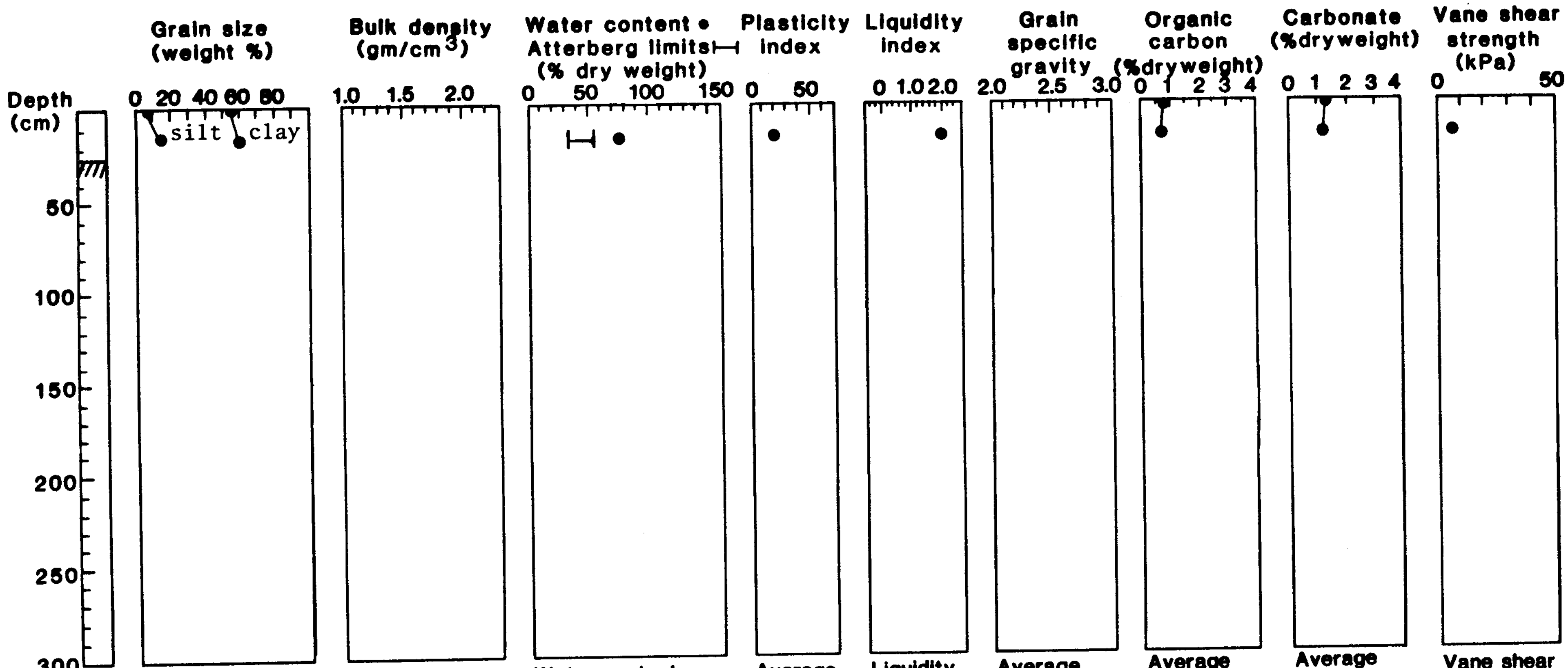

Bulk density at 1m.: ______

Water content at 1m.: ______
Average plastic limit: 35
Average liquid limit: 56

Average plasticity index: 21

Liquidity index at 1m.: ______

Average grain specific gravity: ______

Average organic carbon: 0.998

Average carbonate: 1.292

Vane shear strength at 1m.: ______

Station 543 **Location** 58°10.77'N 153°31.97'W **Water depth** 180m

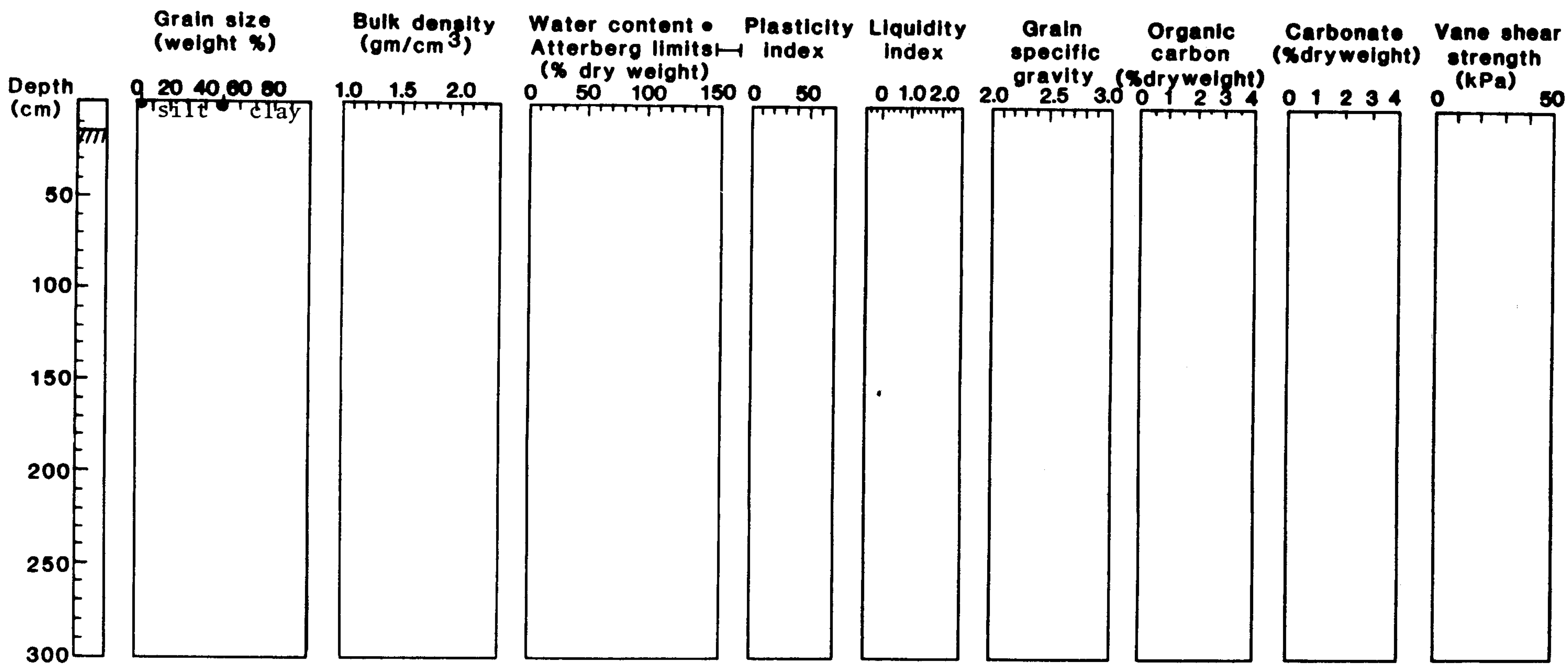

Bulk density at 1m.: ______

Water content at 1m.: ______
Average plastic limit: ______
Average liquid limit: ______

Average plasticity index: ______

Liquidity index at 1m.: ______

Average grain specific gravity: ______

Average organic carbon: ______

Average carbonate: ______

Vane shear strength at 1m.: ______

Station 545 **Location** 58°22.5'N 153°53.5'W **Water depth** 175m

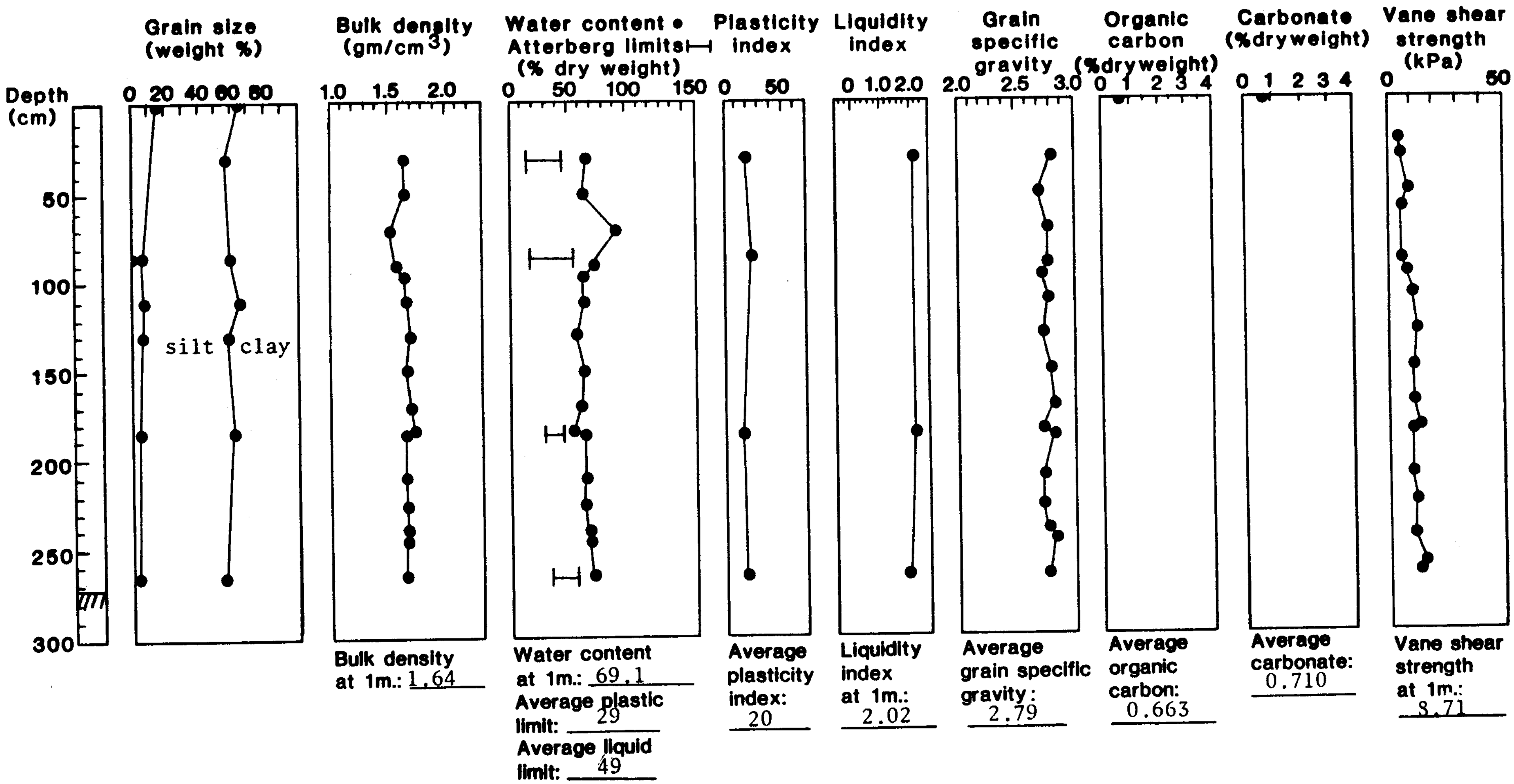

Station 546 **Location** 58°28.8'N 153°37.0'W **Water depth** 97m

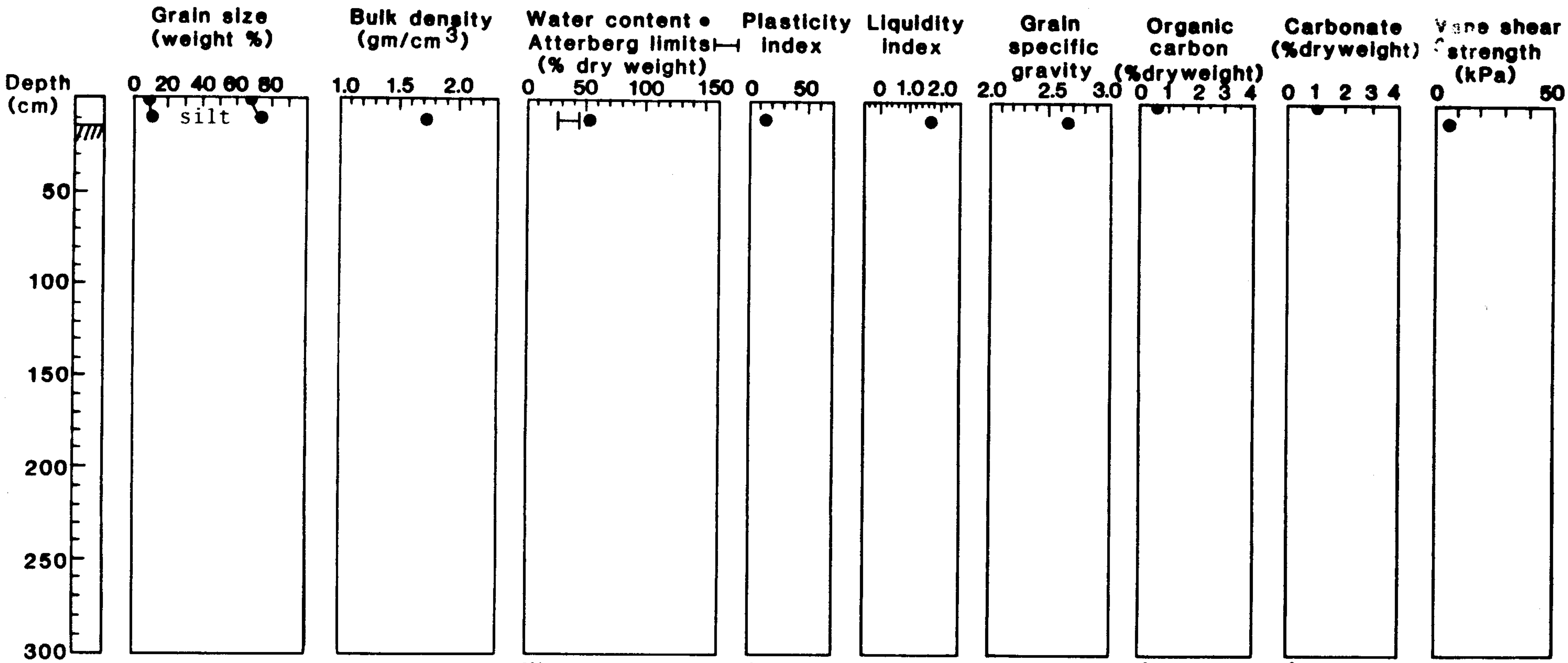

Bulk density at 1m.: ______

Water content at 1m.: ______

Average plastic limit: 28

Average liquid limit: 45

Average plasticity index: 20

Liquidity index at 1m.: ______

Average grain specific gravity: 2.68

Average organic carbon: 0.565

Average carbonate: 1.02

Vane shear strength at 1m.: ______

Station 547 Location 58°33.0'N 153°34.4'W Water depth 89m

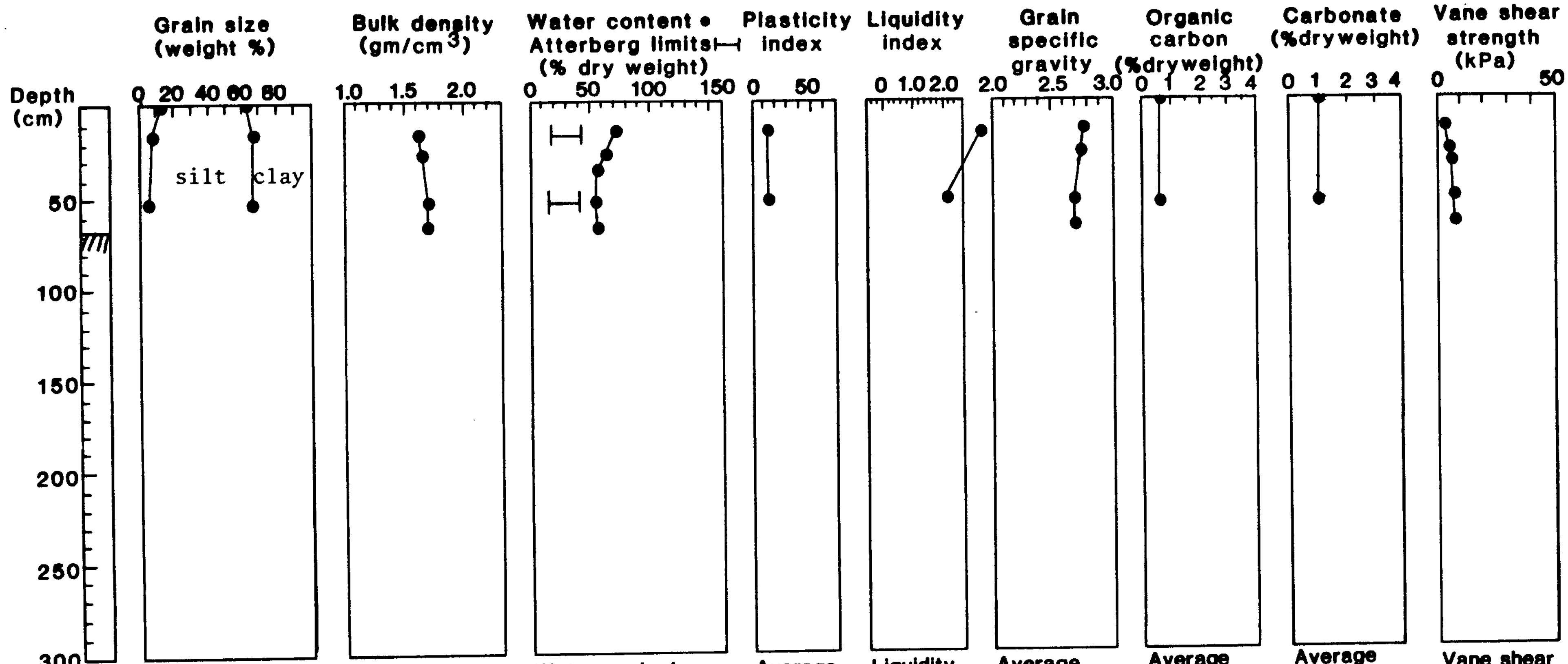

Bulk density at 1m.: ______

Water content at 1m.: ______

Average plastic limit: 28

Average liquid limit: 42

Average plasticity index: 14

Liquidity index at 1m.: ______

Average grain specific gravity: 2.79

Average organic carbon: 0.591

Average carbonate: 1.05

Vane shear strength at 1m.: ______

Station 548 Location 58°37.9'N 153°25.1'W Water depth 64m

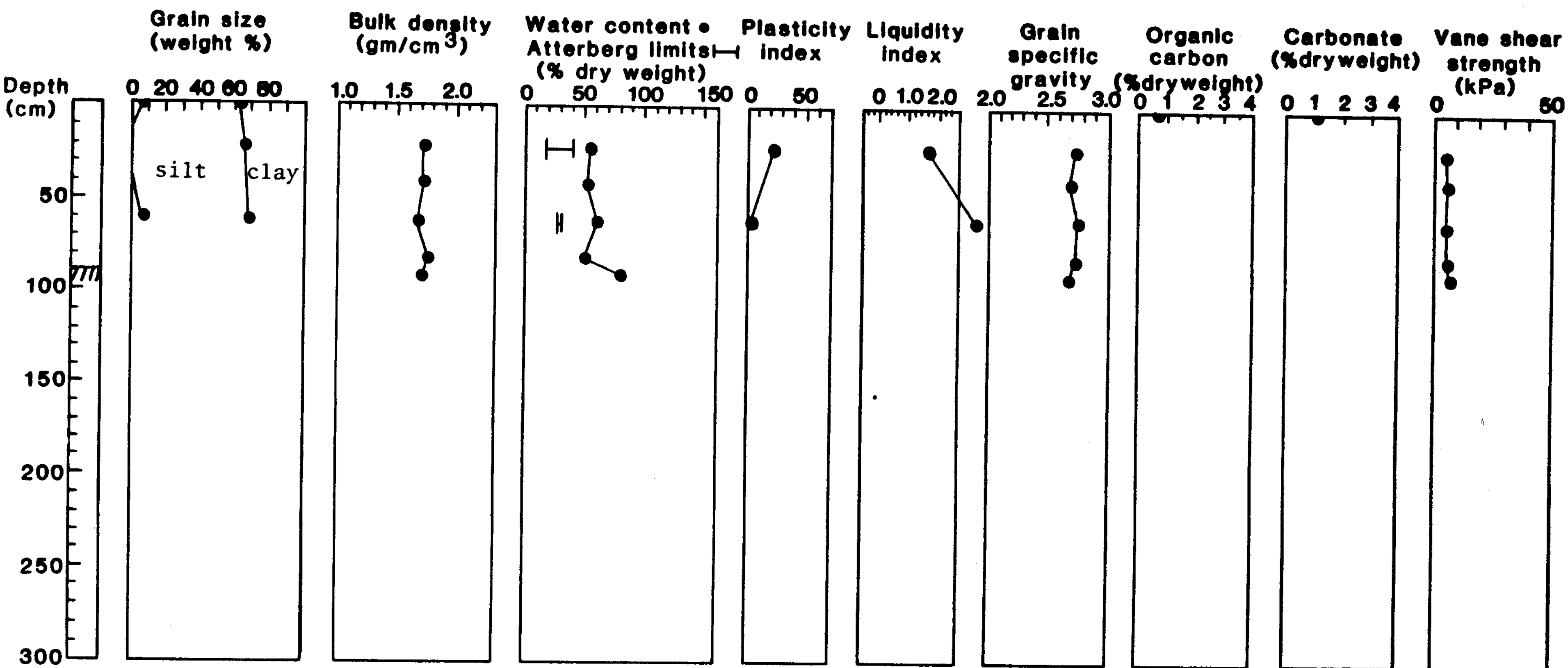

Bulk density at 1m.: ______

Water content at 1m.: ______

Average plastic limit: 24

Average liquid limit: 35

Average plasticity index: 10

Liquidity index at 1m.: ______

Average grain specific gravity: 2.72

Average organic carbon: 0.671

Average carbonate: 1.05

Vane shear strength at 1m.: ______

737

Station 549 **Location** 58°43.3'N 153°15.0'W **Water depth** 87m

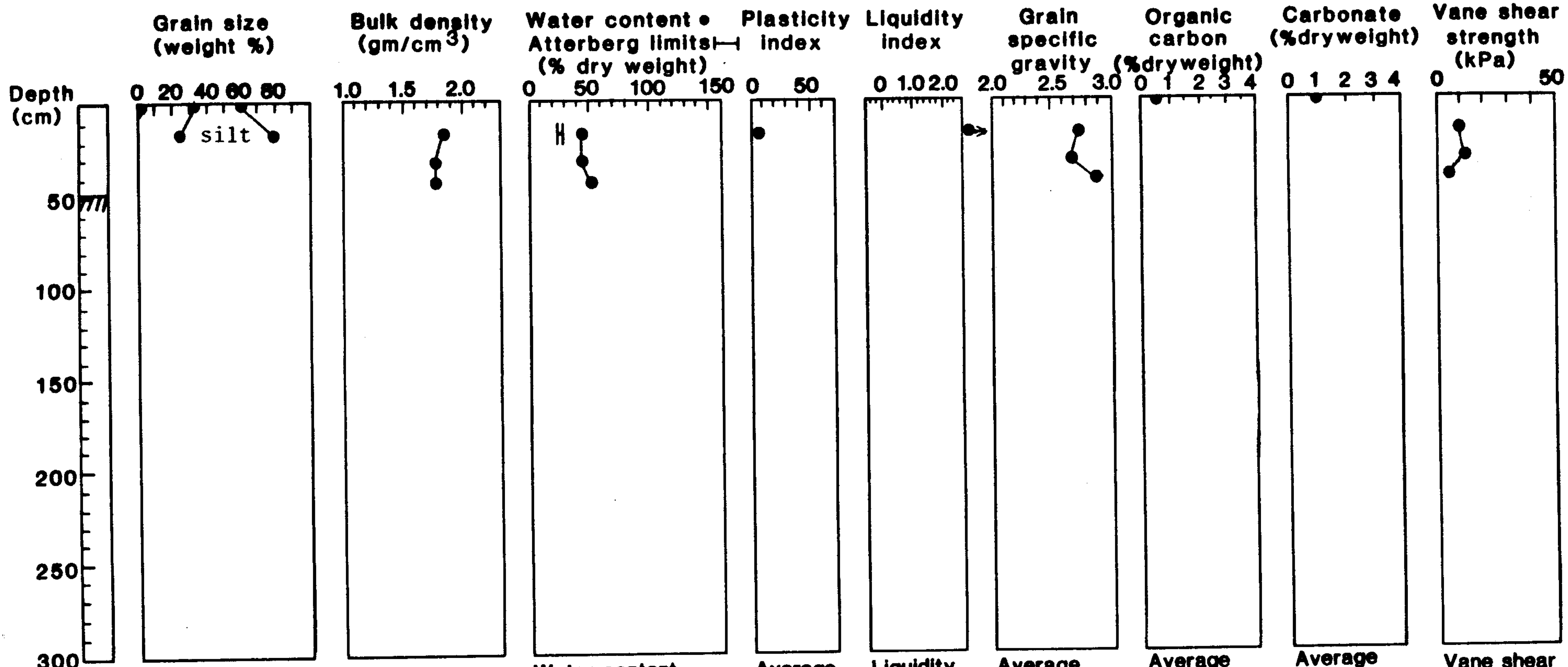

Bulk density at 1m.: ______

Water content at 1m.: ______

Average plastic limit: 25

Average liquid limit: 29

Average plasticity index: 4

Liquidity index at 1m.: ______

Average grain specific gravity: 2.76

Average organic carbon: 0.517

Average carbonate: 1.01

Vane shear strength at 1m.: ______

Station 550 **Location** 58°50.8'N 153°10.3'W **Water depth** 165m

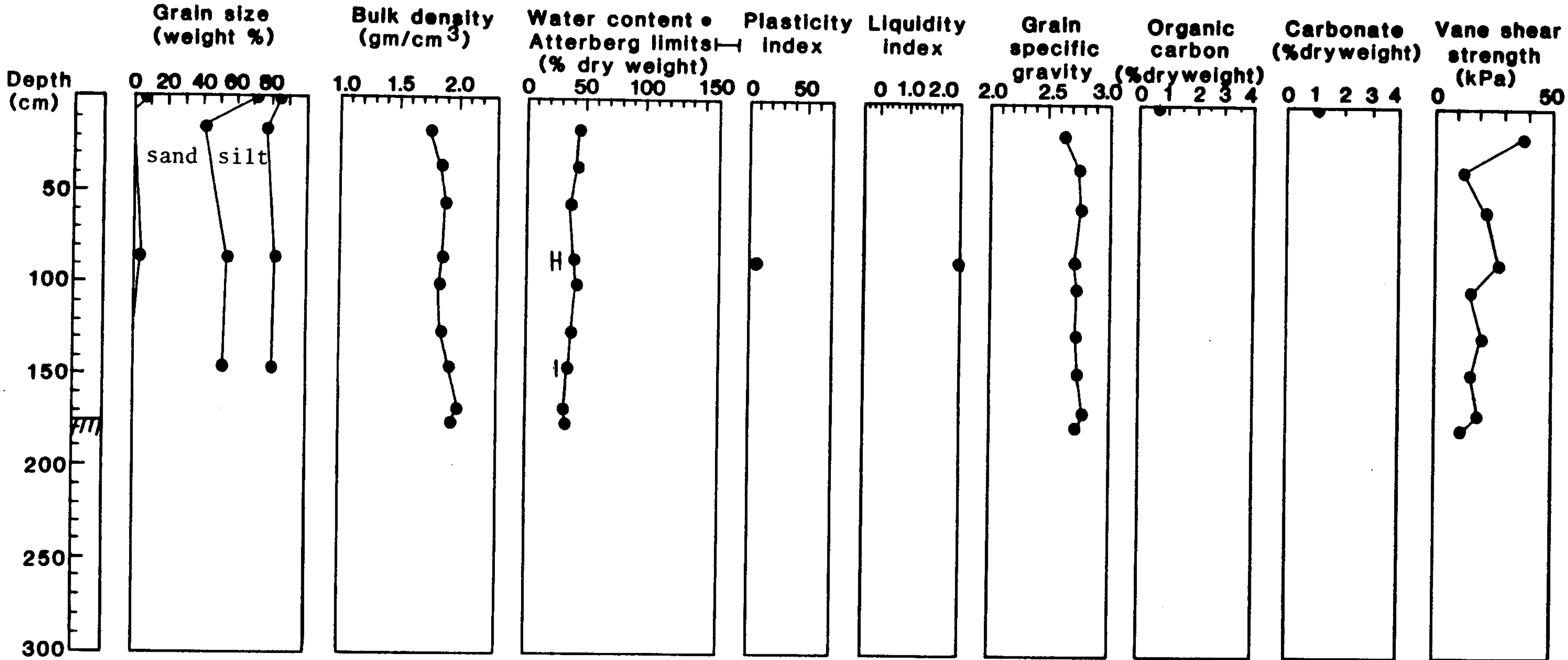

Bulk density at 1m.: 1.88

Water content at 1m.: 37.5

Average plastic limit: 21

Average liquid limit: 28

Average plasticity index: 7

Liquidity index at 1m.:

Average grain specific gravity: 2.72

Average organic carbon: 0.631

Average carbonate: 1.07

Vane shear strength at 1m.: 20.40

Station 551 **Location** 58°53.6'N 152°54.4'W **Water depth** 155m

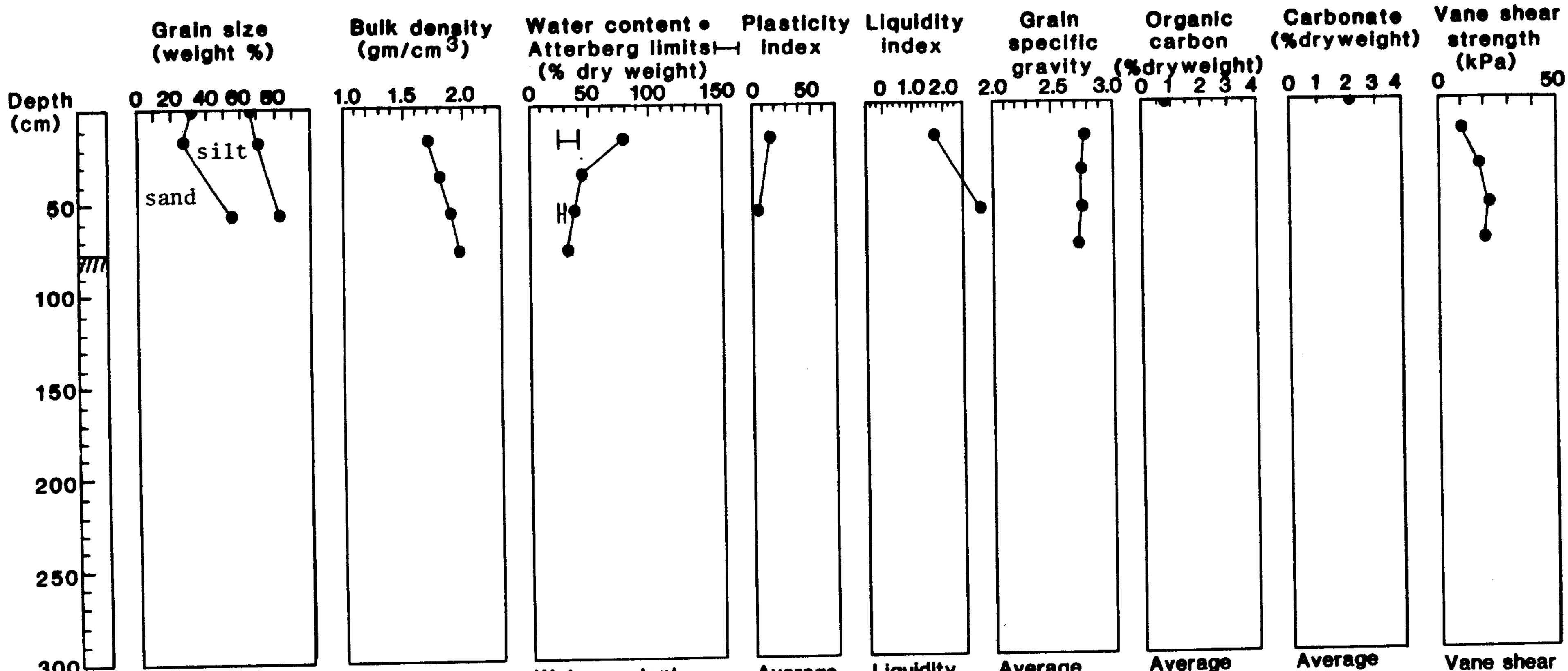

Bulk density at 1m.: ______

Water content at 1m.: ______

Average plastic limit: 26

Average liquid limit: 36

Average plasticity index: 10

Liquidity index at 1m.: ______

Average grain specific gravity: 2.76

Average organic carbon: 0.801

Average carbonate: 2.14

Vane shear strength at 1m.: ______

Station 552 **Location** 58°47.2'N 153°02.5'W **Water depth** 135m

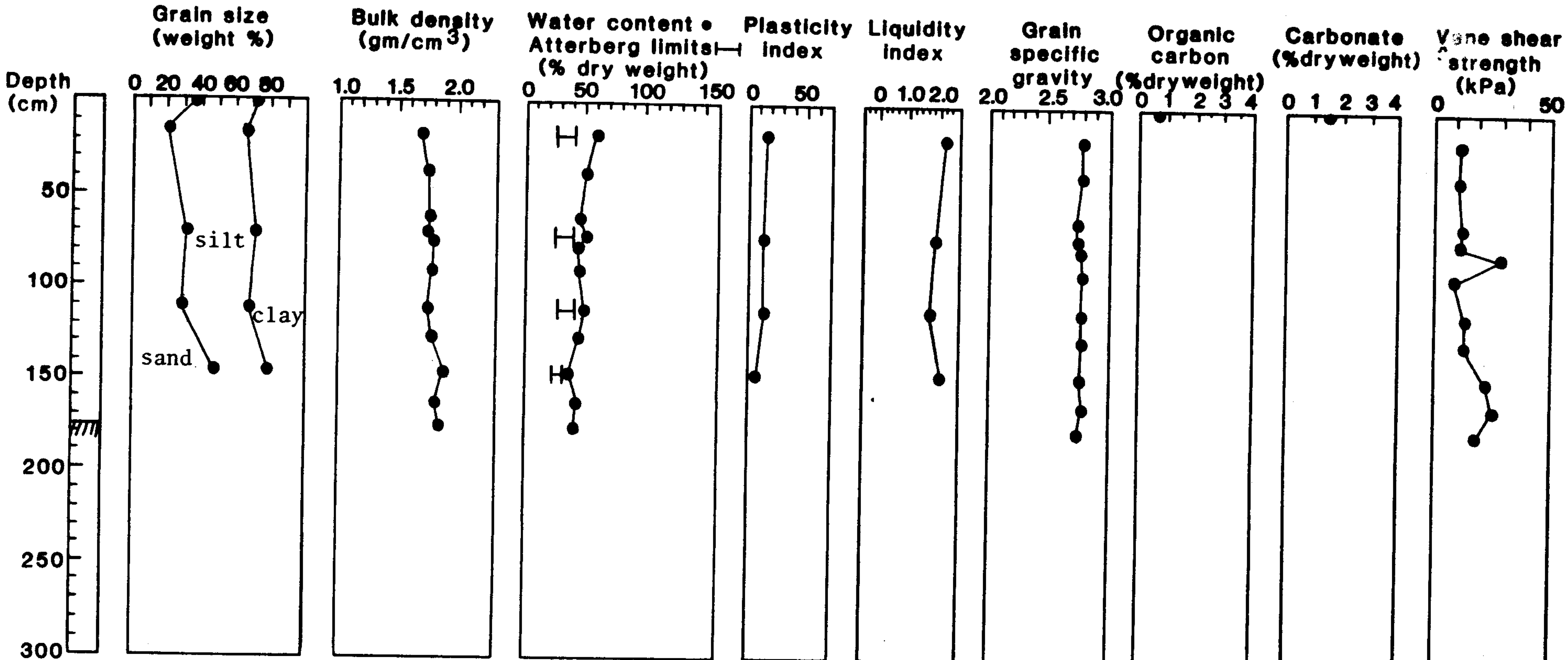

Bulk density at 1m.: 1.78

Water content at 1m.: 47.5
Average plastic limit: 26
Average liquid limit: 38

Average plasticity index: 13

Liquidity index at 1m.: 1.90

Average grain specific gravity: 2.77

Average organic carbon: 0.655

Average carbonate: 1.46

Vane shear strength at 1m.: 15.60

Station 640 **Location** 58°15.3'N 153°59.26'W **Water depth** 274m

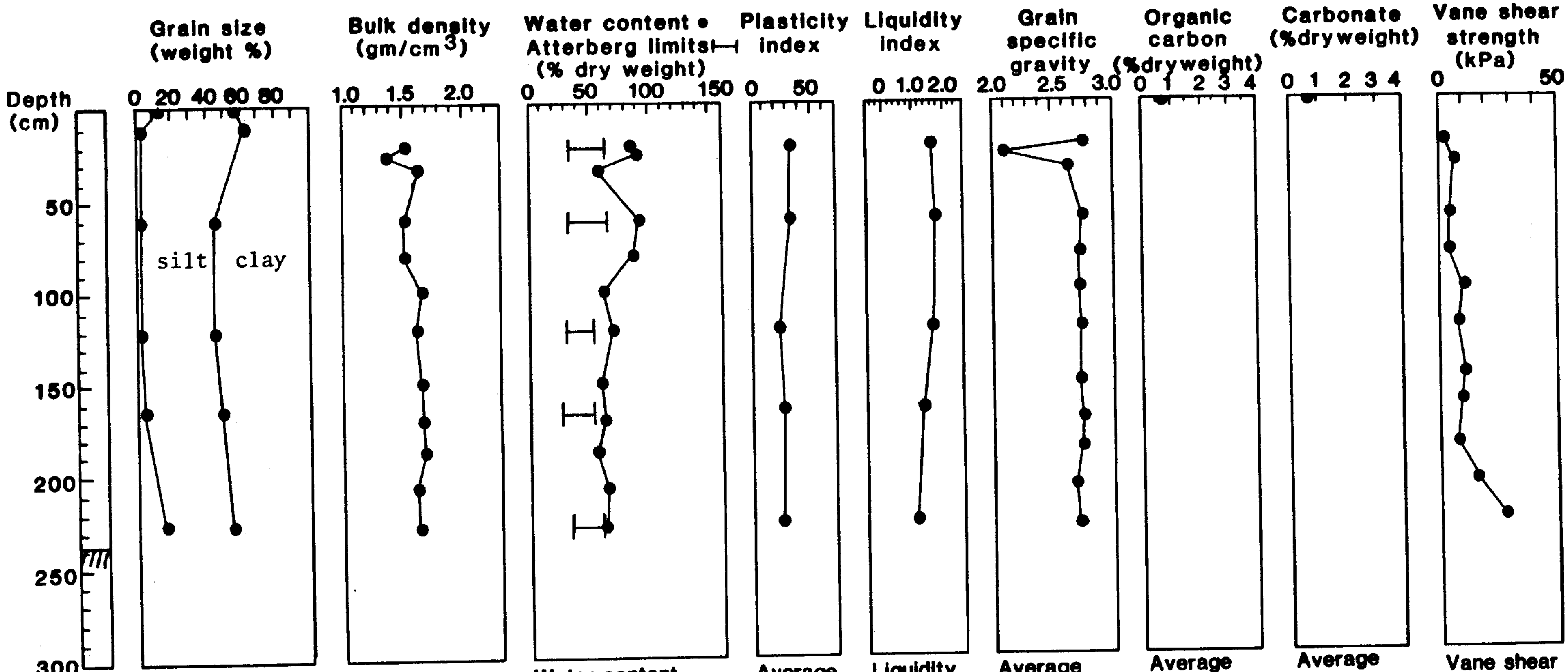

Bulk density at 1m.: 1.60

Water content at 1m.: 74.2

Average plastic limit: 33

Average liquid limit: 61

Average plasticity index: 28

Liquidity index at 1m.: 1.55

Average grain specific gravity: 2.69

Average organic carbon: 0.771

Average carbonate: 0.840

Vane shear strength at 1m.: 8.90

Station 643 **Location** 58°05.7'N 154°09.1'W **Water depth** 288m

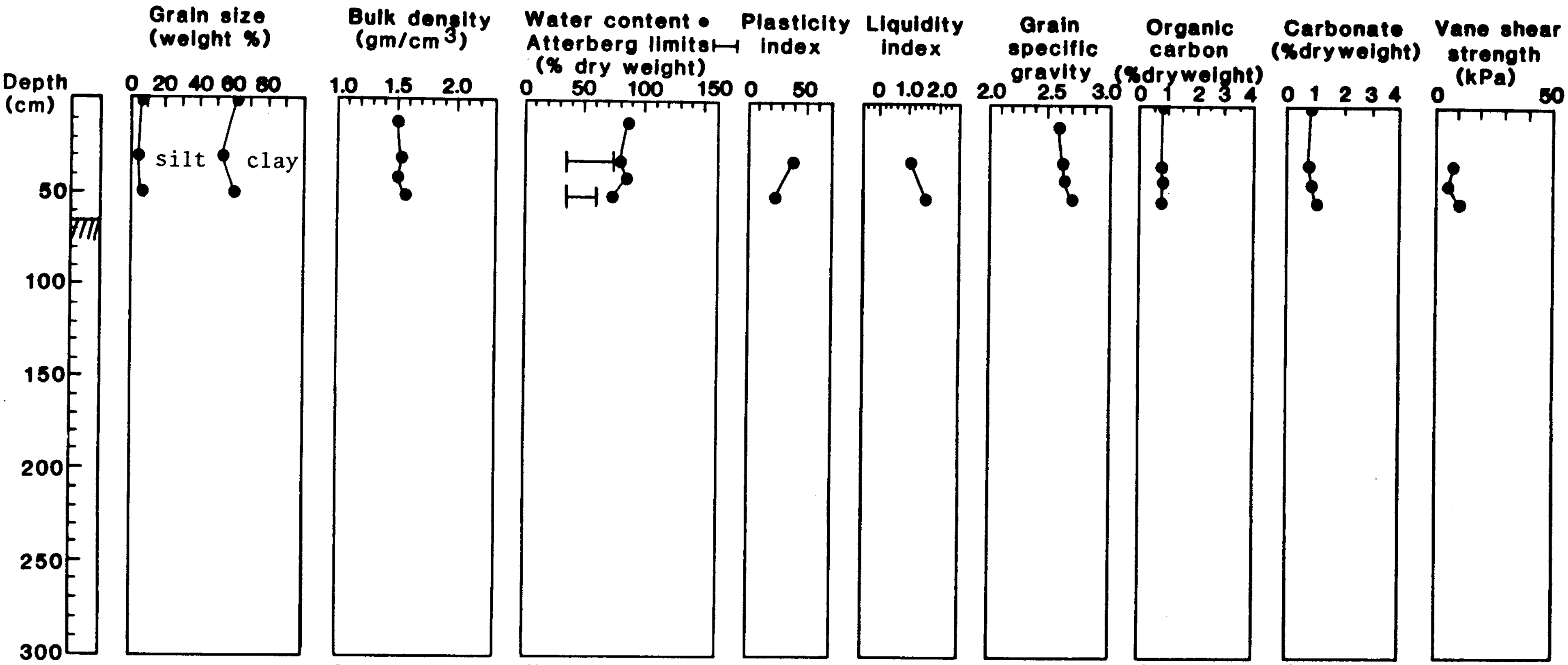

Bulk density at 1m.: ______

Water content at 1m.: ______

Average plastic limit: 37

Average liquid limit: 69

Average plasticity index: 32

Liquidity index at 1m.: ______

Average grain specific gravity: 2.64

Average organic carbon: 0.796

Average carbonate: 0.966

Vane shear strength at 1m.: ______

Station 644 **Location** 57°54.6'N 154°33.9'W **Water depth** 278m

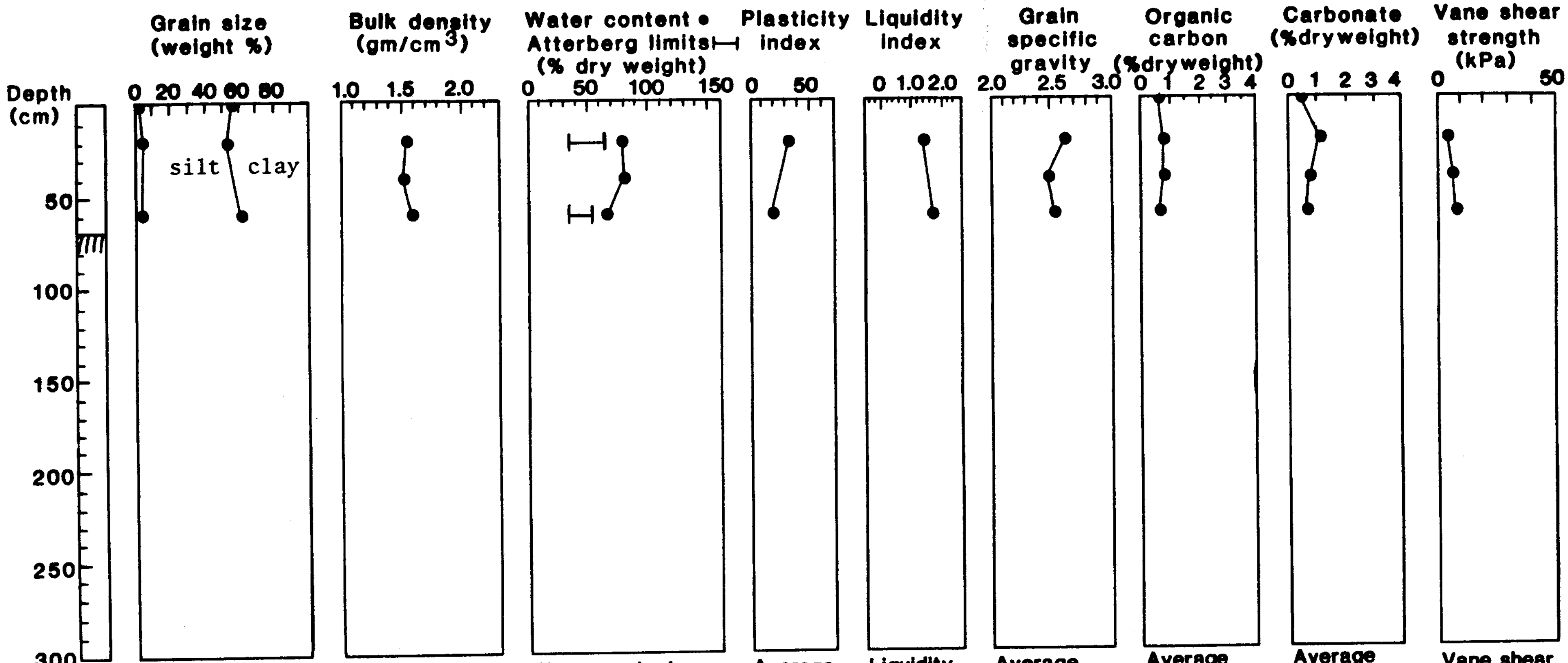

Bulk density at 1m.: ____

Water content at 1m.: ____
Average plastic limit: 34
Average liquid limit: 60

Average plasticity index: 26

Liquidity index at 1m.: ____

Average grain specific gravity: 2.54

Average organic carbon: 0.684

Average carbonate: 0.837

Vane shear strength at 1m.: ____

Station 645 **Location** 57°47.0'N 154°58.8'W **Water depth** 315m

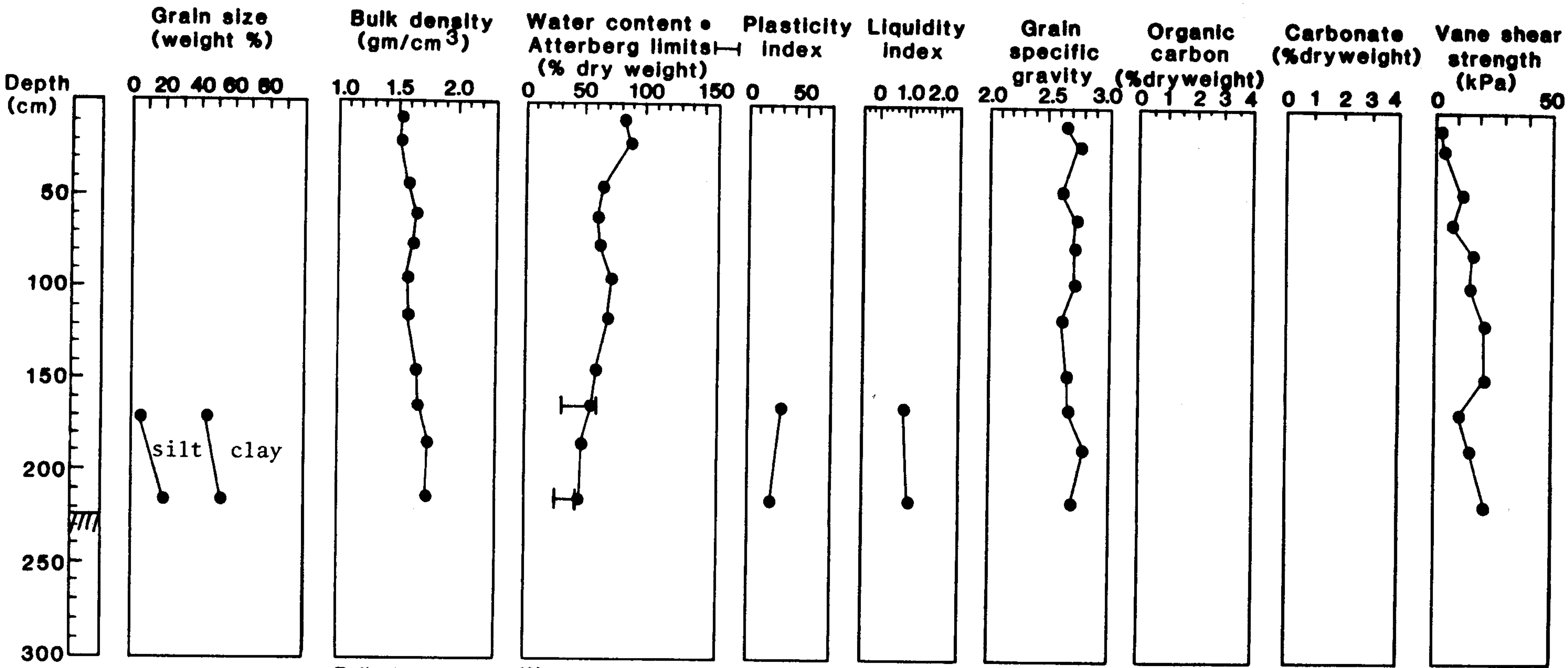

Bulk density at 1m.: 1.63

Water content at 1m.: 65.9

Average plastic limit: 30

Average liquid limit: 56

Average plasticity index: 26

Liquidity index at 1m.:

Average grain specific gravity: 2.70

Average organic carbon:

Average carbonate:

Vane shear strength at 1m.: 14.11

Station 646 **Location** 57°55.3'N 154°17.5'W **Water depth** 216m

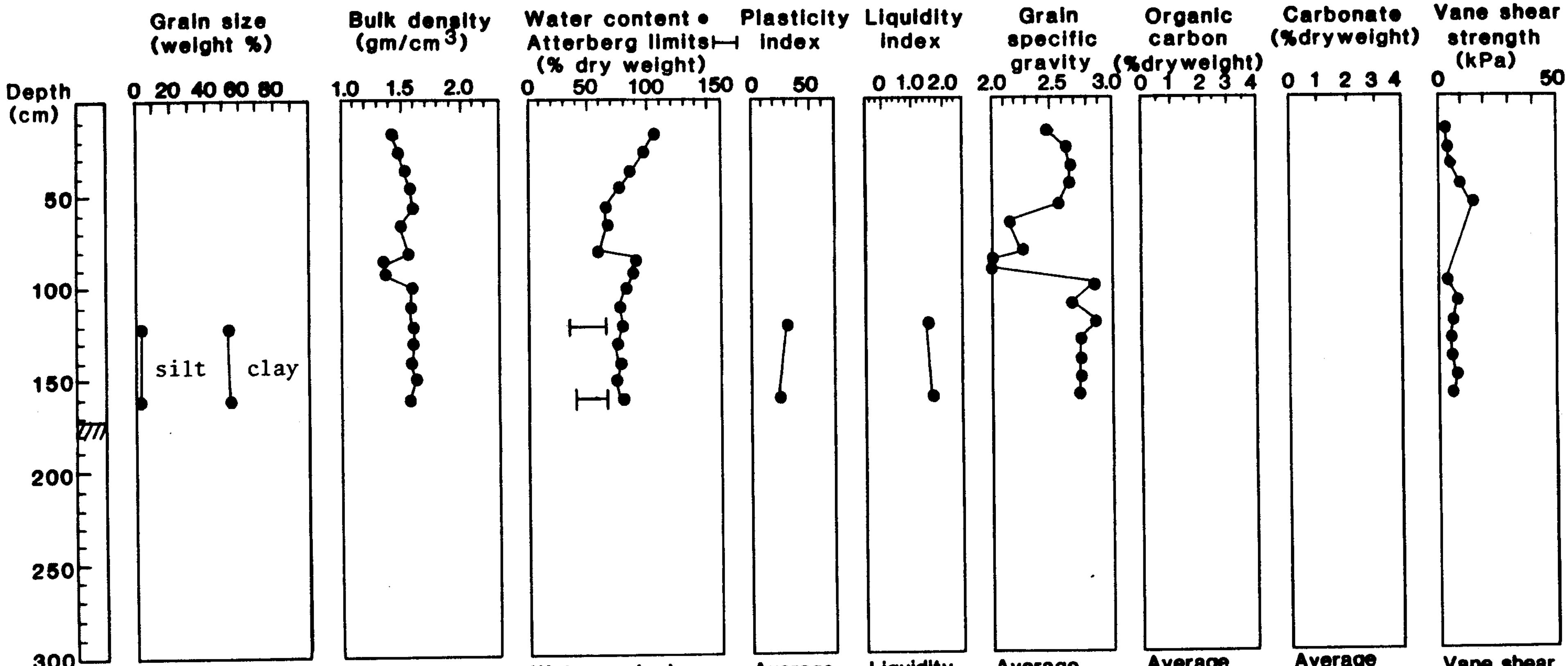

Bulk density at 1m.: 1.55

Water content at 1m.: 78.6
Average plastic limit: 37
Average liquid limit: 64

Average plasticity index: 27

Liquidity index at 1m.: ____

Average grain specific gravity: 2.58

Average organic carbon: ____

Average carbonate: ____

Vane shear strength at 1m.: 6.09

Station 647 Location 57°59.8'N 154°10.7'W Water depth 220m

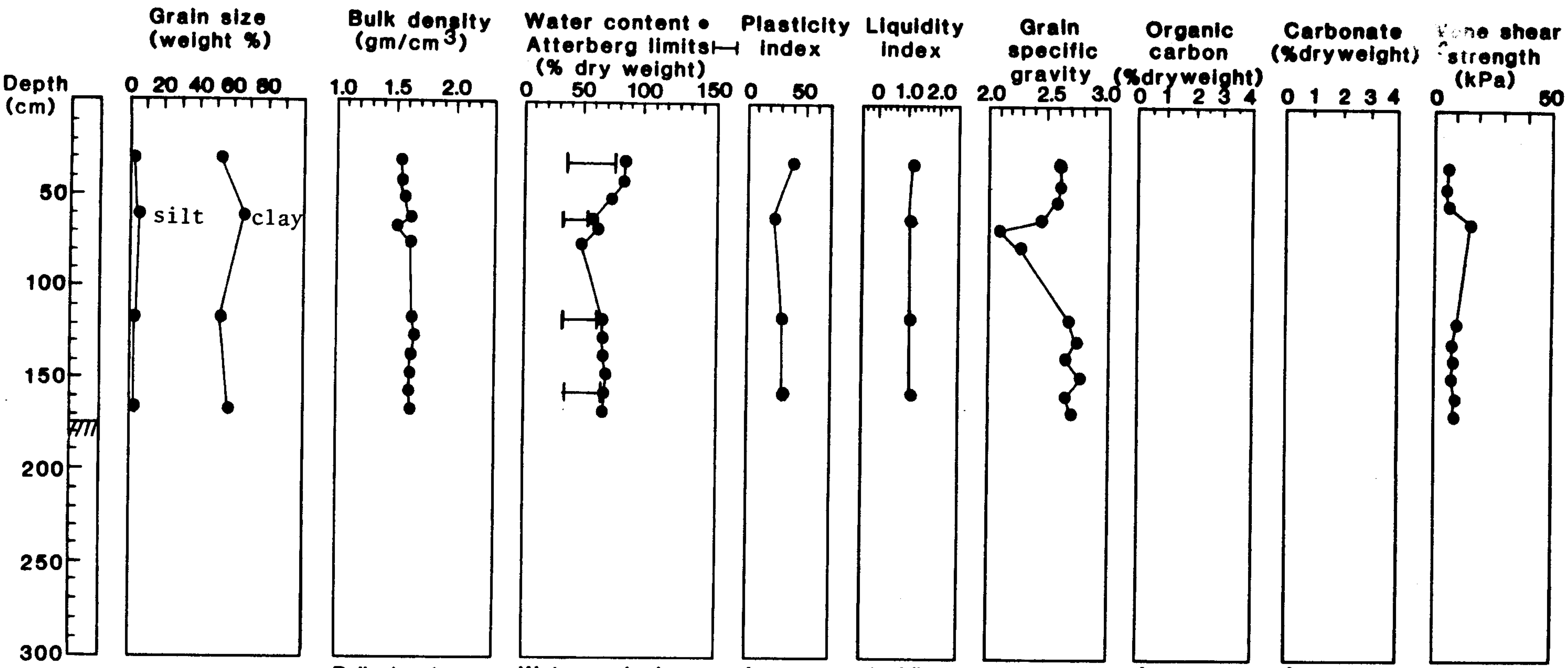

Bulk density at 1m.: 1.57

Water content at 1m.: 76.4

Average plastic limit: 35

Average liquid limit: 66

Average plasticity index: 31

Liquidity index at 1m.: 1.11

Average grain specific gravity: 2.58

Average organic carbon:

Average carbonate:

Vane shear strength at 1m.: 8.81

Station 649 **Location** 58°04.7'N 154°01.9'W **Water depth** 209m

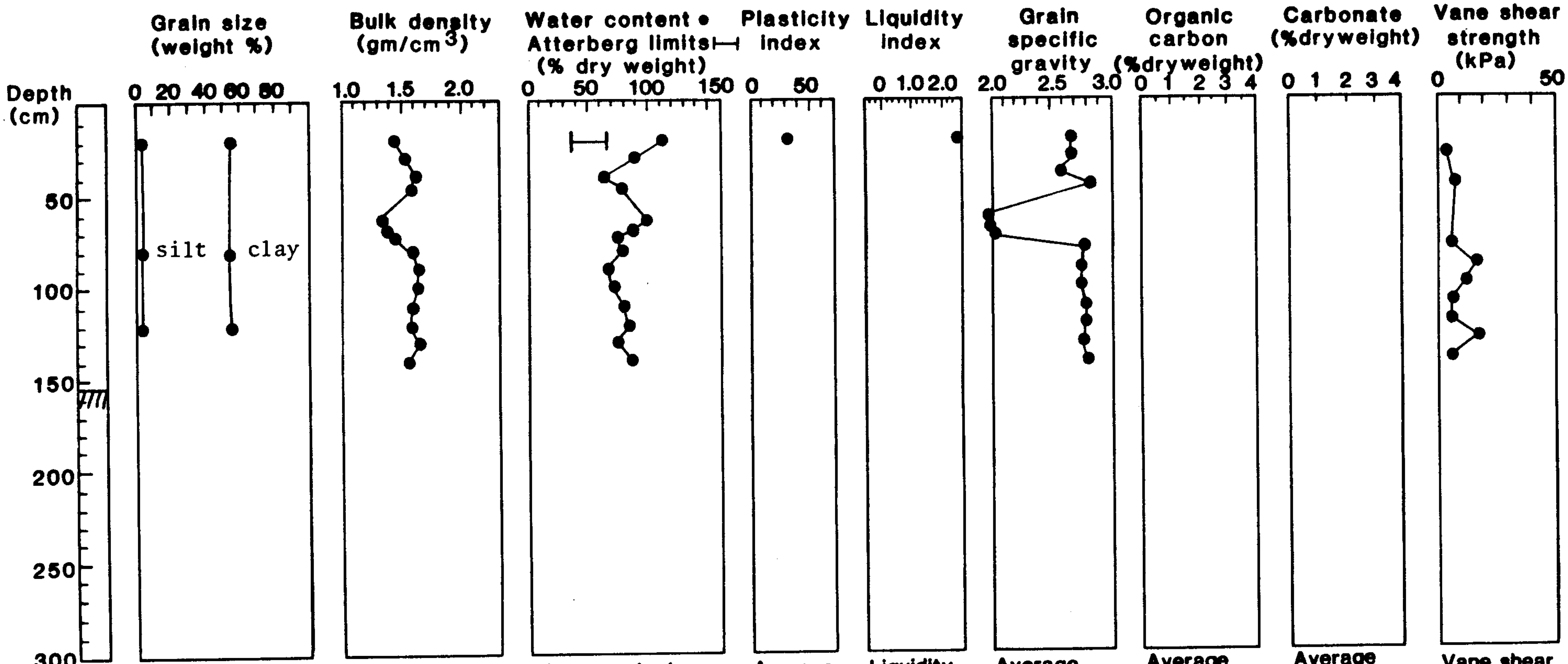

Bulk density at 1m.: 1.57

Water content at 1m.: 77.6
Average plastic limit: 36
Average liquid limit: 63

Average plasticity index: 27

Liquidity index at 1m.:

Average grain specific gravity: 2.61

Average organic carbon:

Average carbonate:

Vane shear strength at 1m.: 7.97

Station 650 Location 57°55.0'N 154°01.1'W Water depth 199m

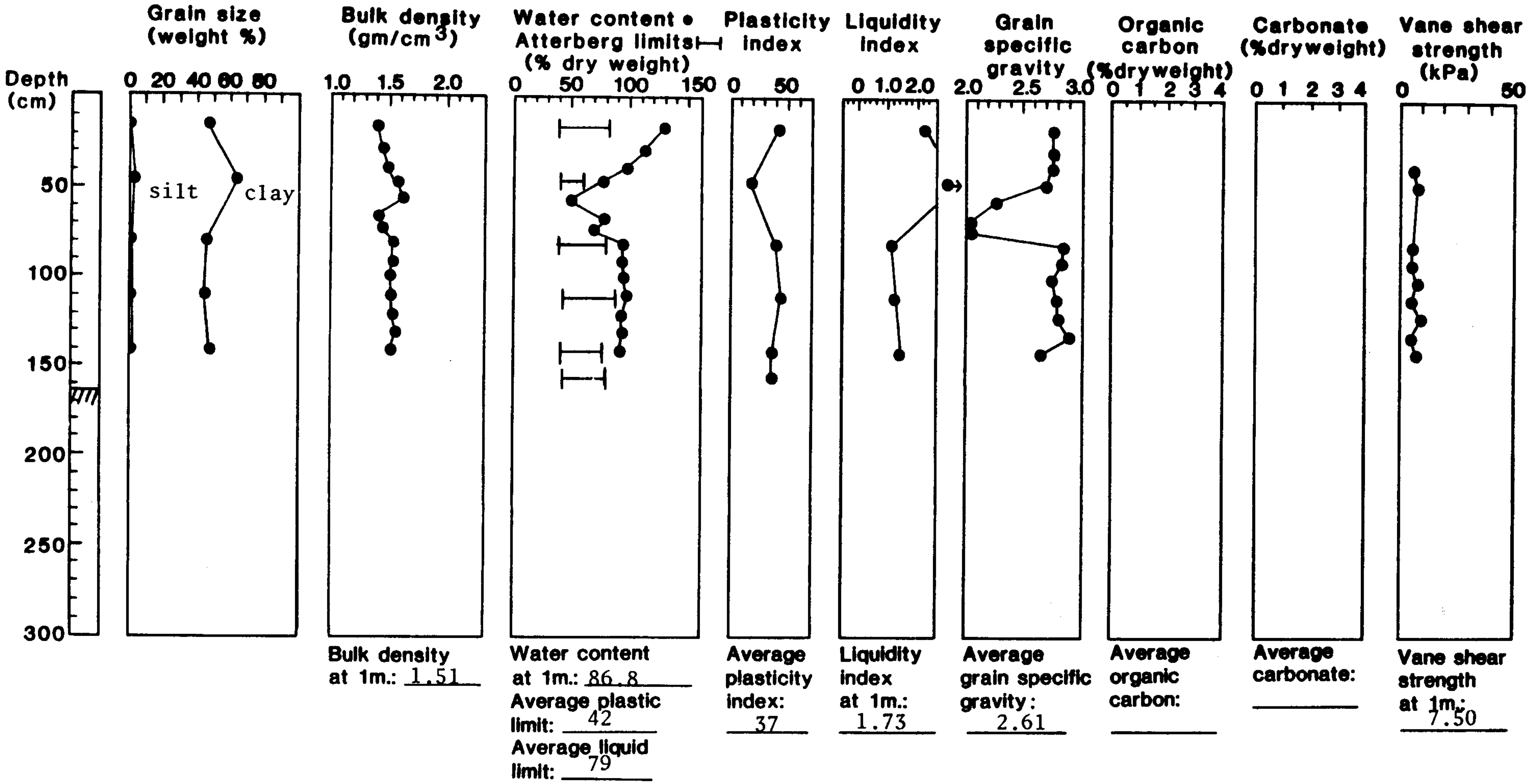

Station 651 **Location** 58°00.1'N 153°52.6'W **Water depth** 194m

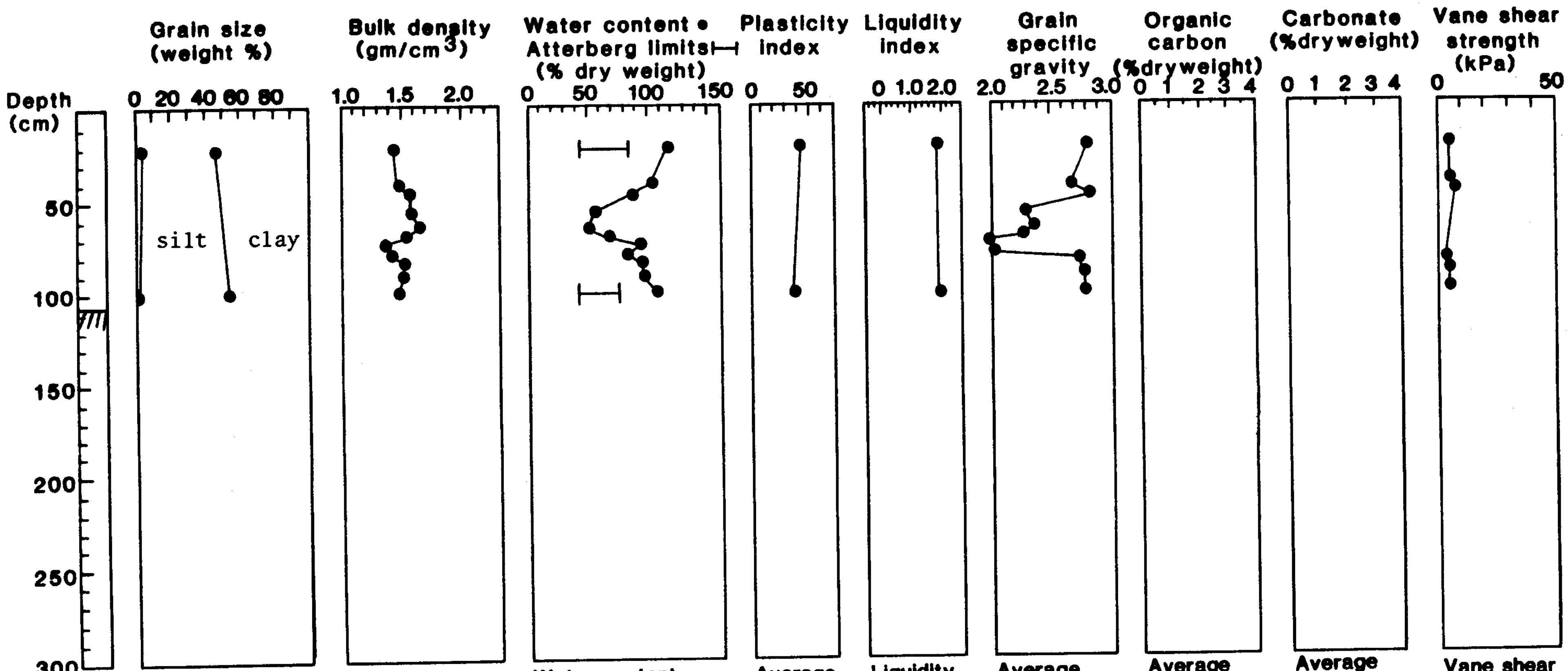

Bulk density at 1m.: 1.48

Water content at 1m.: 85.4

Average plastic limit: 42

Average liquid limit: 84

Average plasticity index: 42

Liquidity index at 1m.: 1.89

Average grain specific gravity: 2.52

Average organic carbon:

Average carbonate:

Vane shear strength at 1m.: 4.07

Station 654 **Location** 57°07.4'N 154°09.0'W **Water depth** 232m

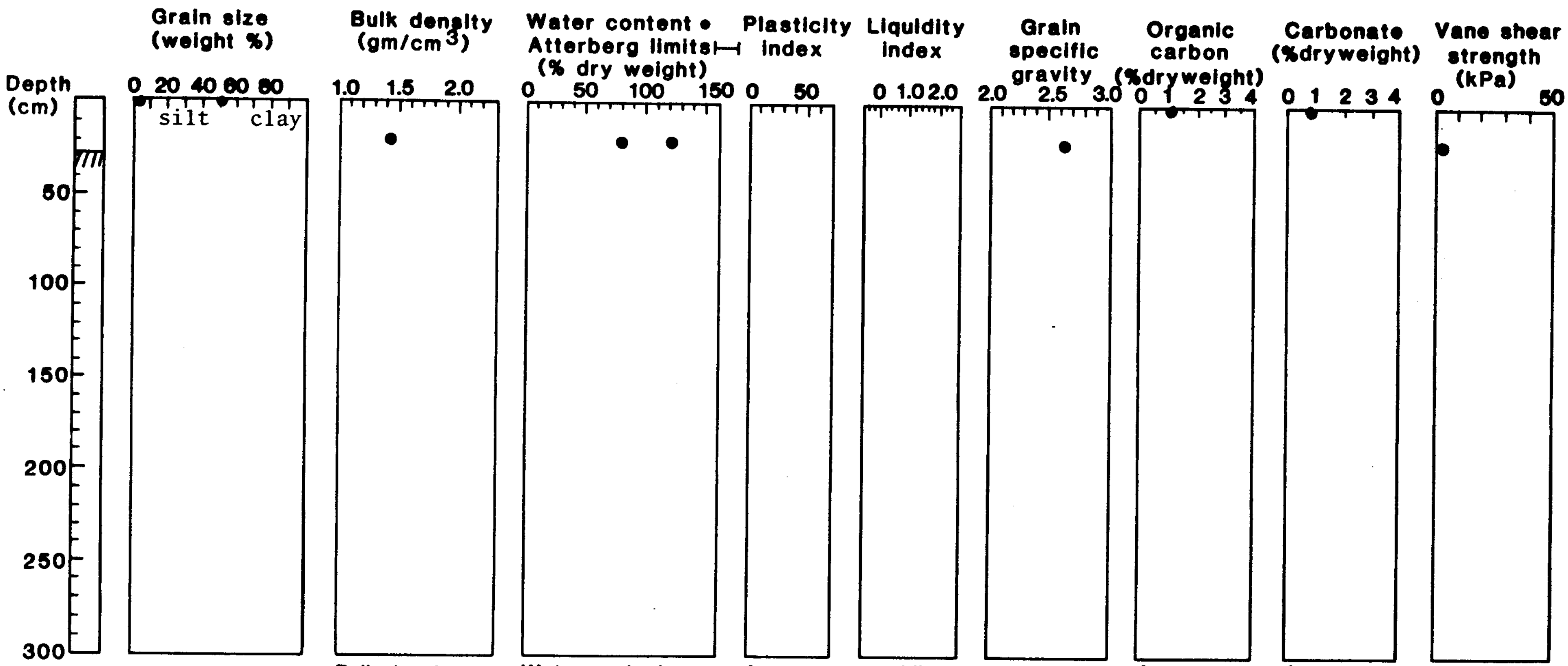

Bulk density at 1m.:	Water content at 1m.:	Average plasticity index:	Liquidity index at 1m.:	Average grain specific gravity: 2.61	Average organic carbon: 1.006	Average carbonate: 0.870	Vane shear strength at 1m.:
	Average plastic limit:						
	Average liquid limit:						

Station 655 **Location** 57°51.8'N 154°09.0'W **Water depth** 204

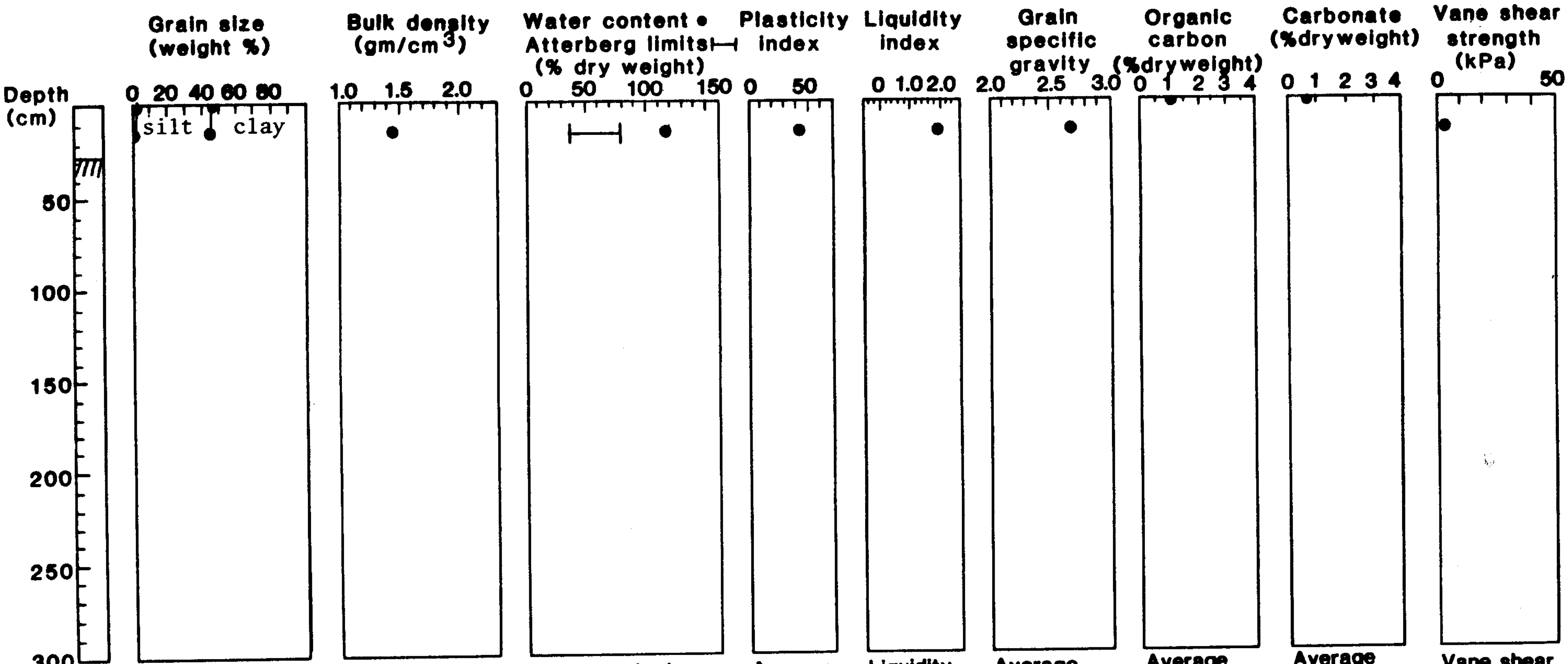

Bulk density at 1m.: ______

Water content at 1m.: ______

Average plastic limit: 38

Average liquid limit: 79

Average plasticity index: 41

Liquidity index at 1m.: ______

Average grain specific gravity: 2.67

Average organic carbon: 1.101

Average carbonate: 0.750

Vane shear strength at 1m.: ______

Station 656 Location 58°05.7'N 153°43.8'W Water depth 194m

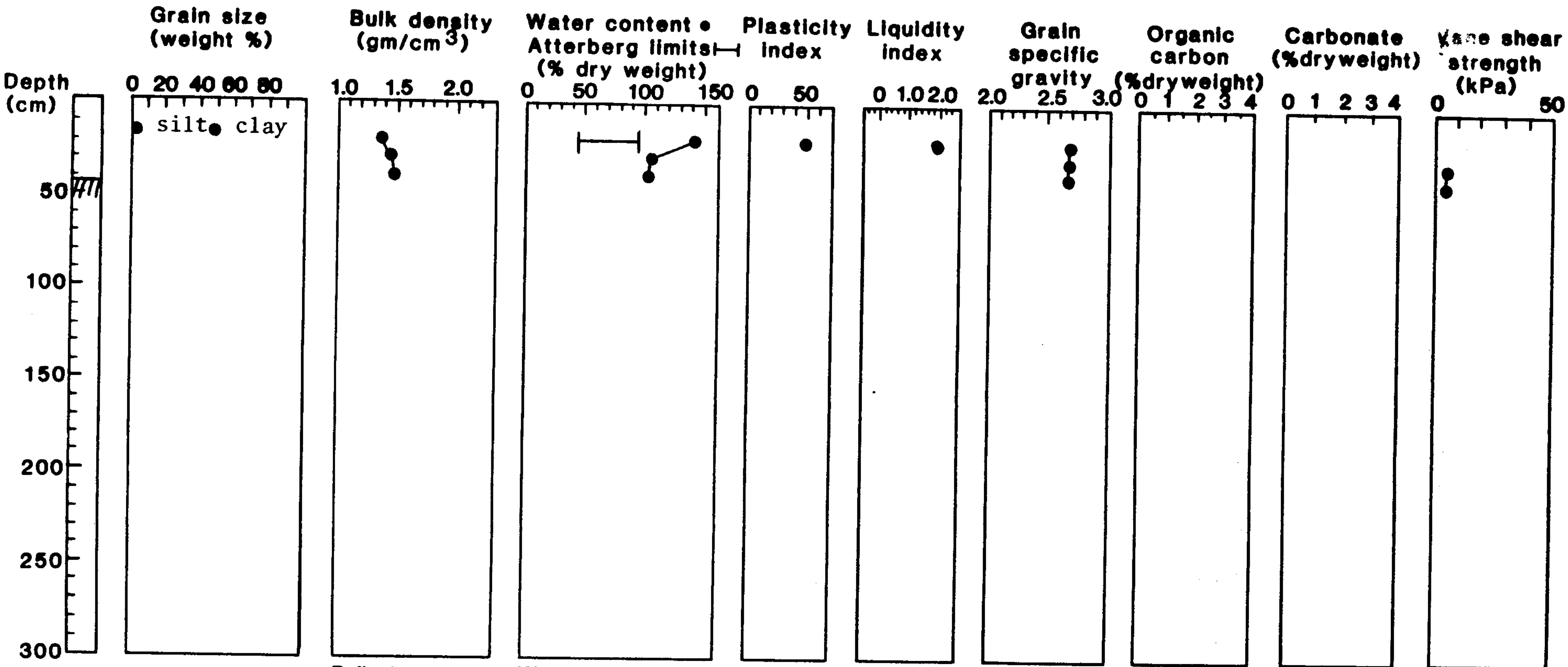

Bulk density at 1m.: ______

Water content at 1m.: ______
Average plastic limit: 46
Average liquid limit: 95

Average plasticity index: 49

Liquidity index at 1m.: ______

Average grain specific gravity: 2.69

Average organic carbon: ______

Average carbonate: ______

Vane shear strength at 1m.: ______

753

Station 657 **Location** 58°12.9'N 153°57.4'W **Water depth** 232m

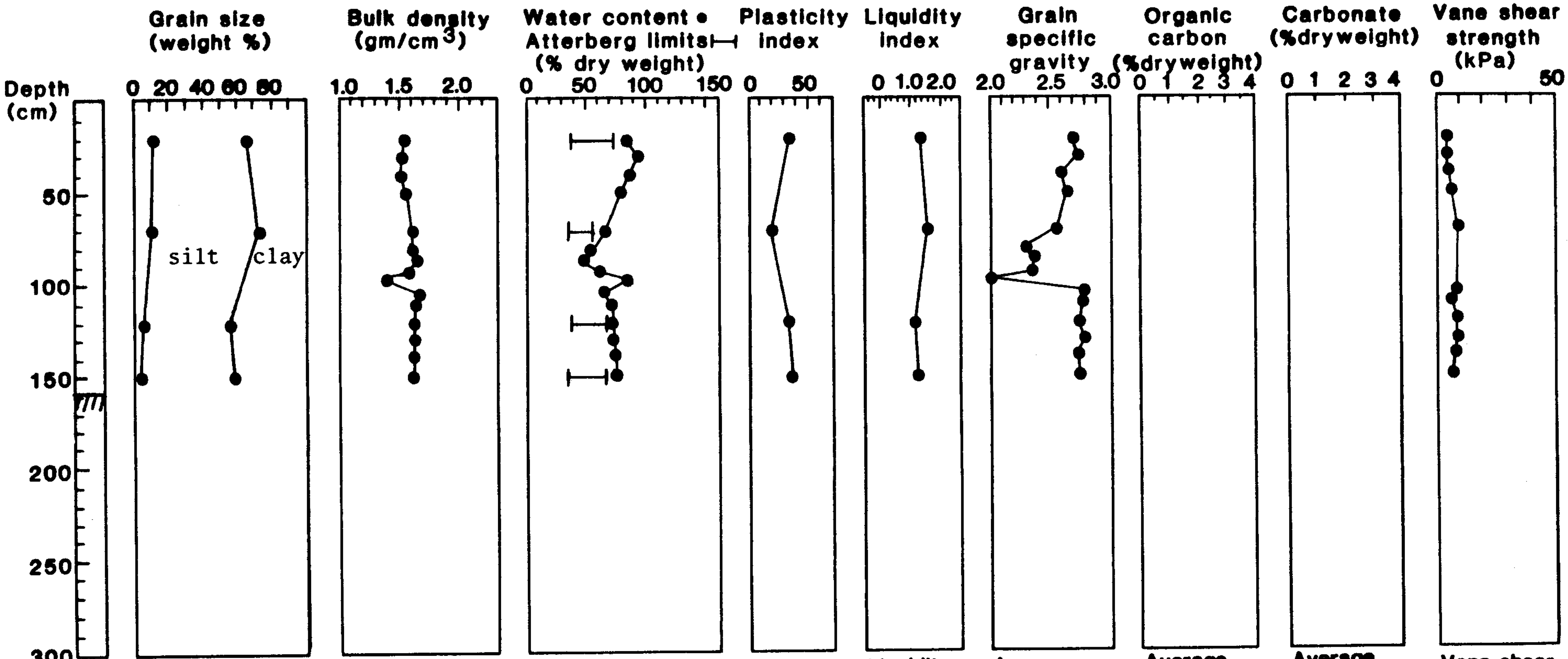

Bulk density at 1m.: 1.59

Water content at 1m.: 70.0
Average plastic limit: 36
Average liquid limit: 66

Average plasticity index: 30

Liquidity index at 1m.: 1.28

Average grain specific gravity: 2.56

Average organic carbon:

Average carbonate:

Vane shear strength at 1m.: 6.46

Station 658 **Location** 58°10.6'N 153°32.6'W **Water depth** 190m

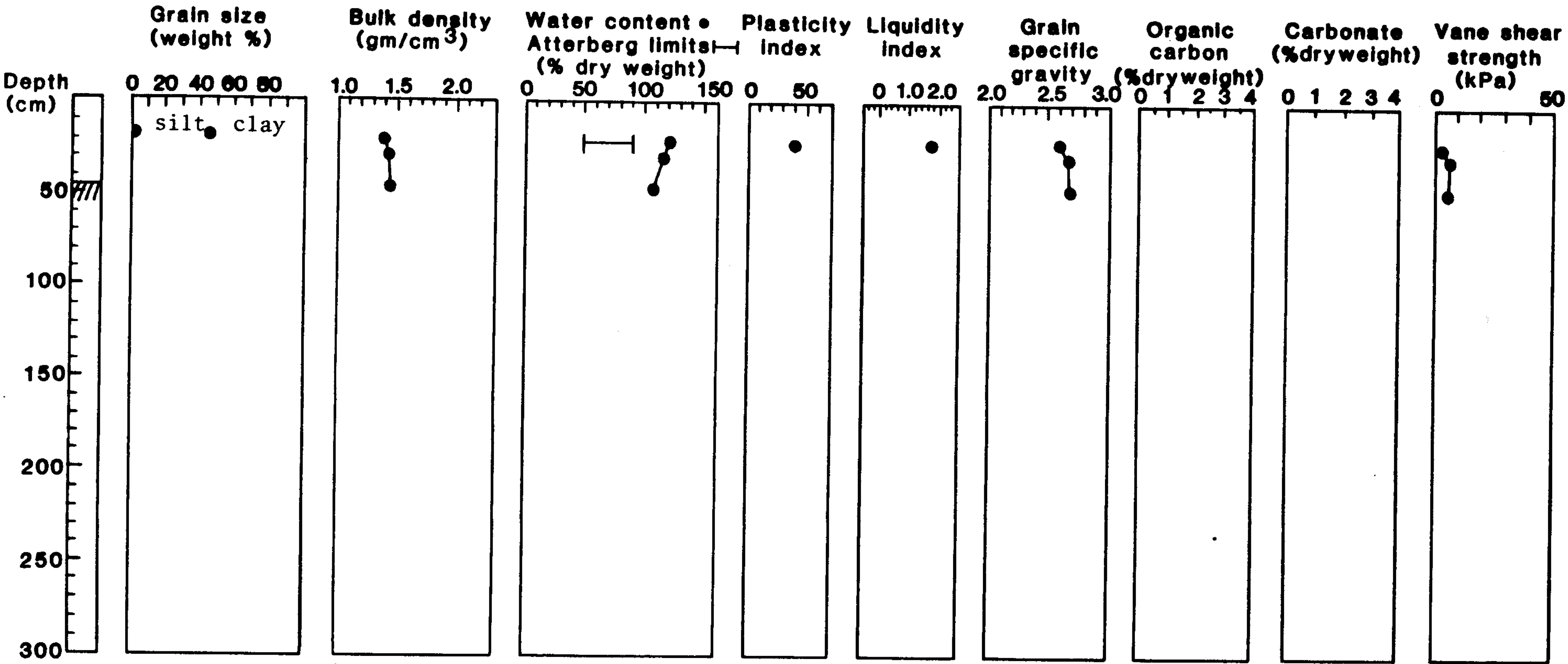

Bulk density at 1m.: ______

Water content at 1m.: ______

Average plastic limit: 50

Average liquid limit: 90

Average plasticity index: 40

Liquidity index at 1m.: ______

Average grain specific gravity: 2.55

Average organic carbon: ______

Average carbonate: ______

Vane shear strength at 1m.: ______

Station 659 **Location** 58°01.8'N 153°28.5'W **Water depth** 112m

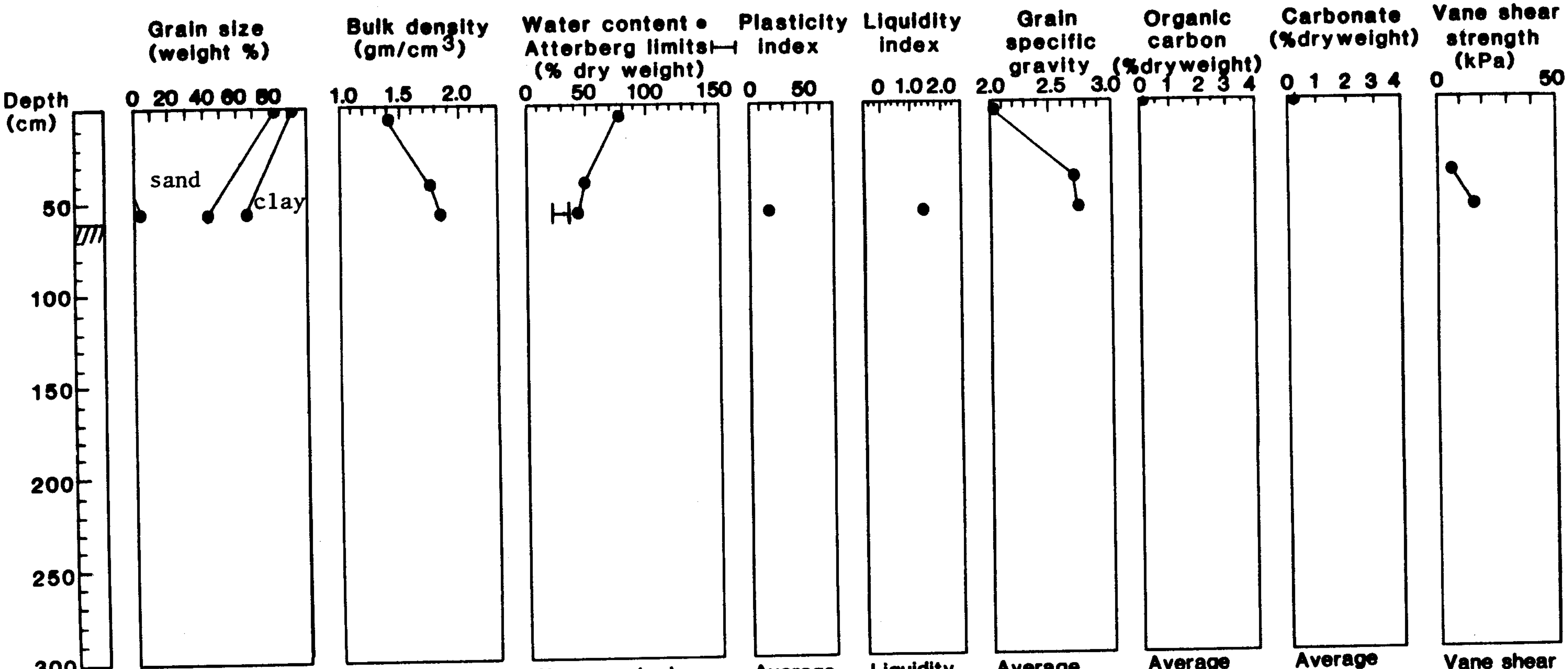

Bulk density at 1m.: ______

Water content at 1m.: ______

Average plastic limit: 21

Average liquid limit: 37

Average plasticity index: 16

Liquidity index at 1m.: ______

Average grain specific gravity: 2.47

Average organic carbon: 0.228

Average carbonate: 0.340

Vane shear strength at 1m.: ______

Station 660 **Location** 58°03.9'N 153°32.9'W **Water depth** 146m

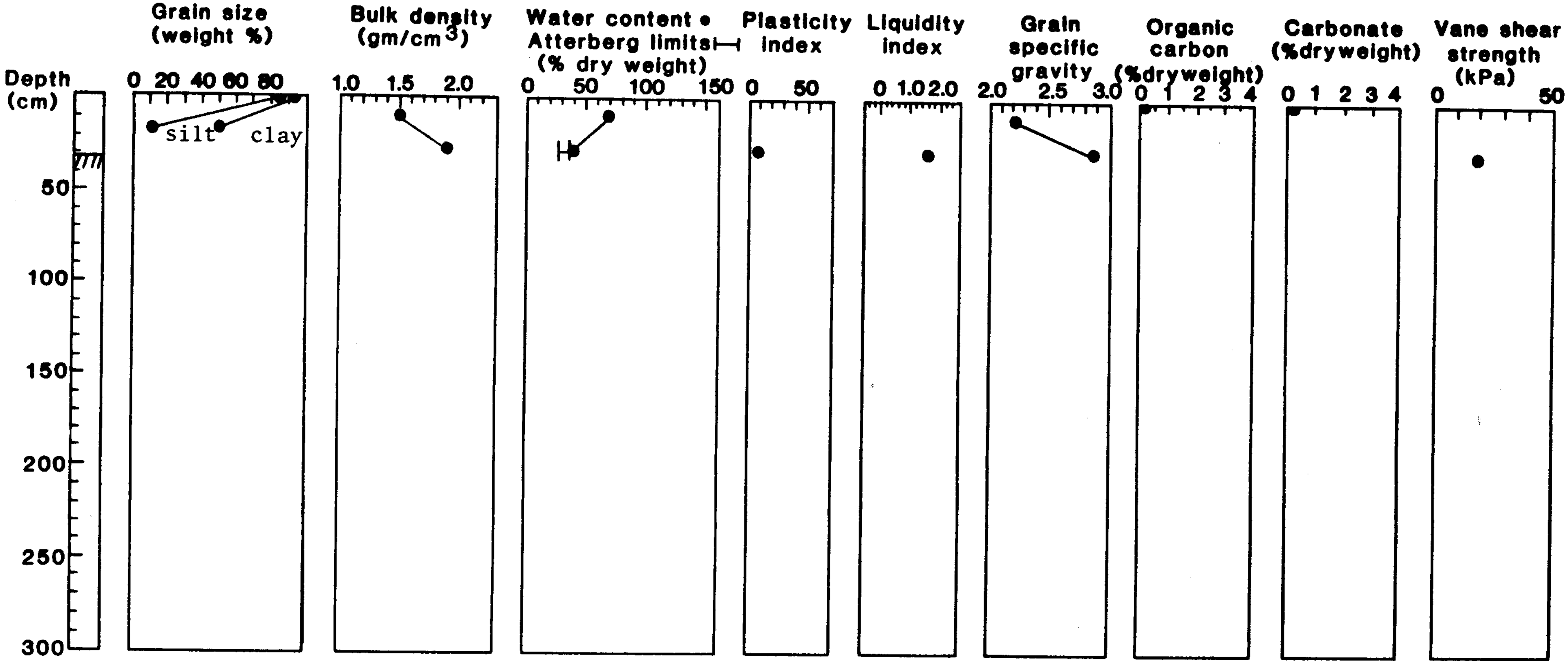

Bulk density at 1m.: ______

Water content at 1m.: ______

Average plastic limit: 27

Average liquid limit: 35

Average plasticity index: 8

Liquidity index at 1m.: ______

Average grain specific gravity: 2.53

Average organic carbon: 0.231

Average carbonate: 0.270

Vane shear strength at 1m.: ______

Station 661 **Location** 58°06.50'N 153°34.20'W **Water depth** 238m

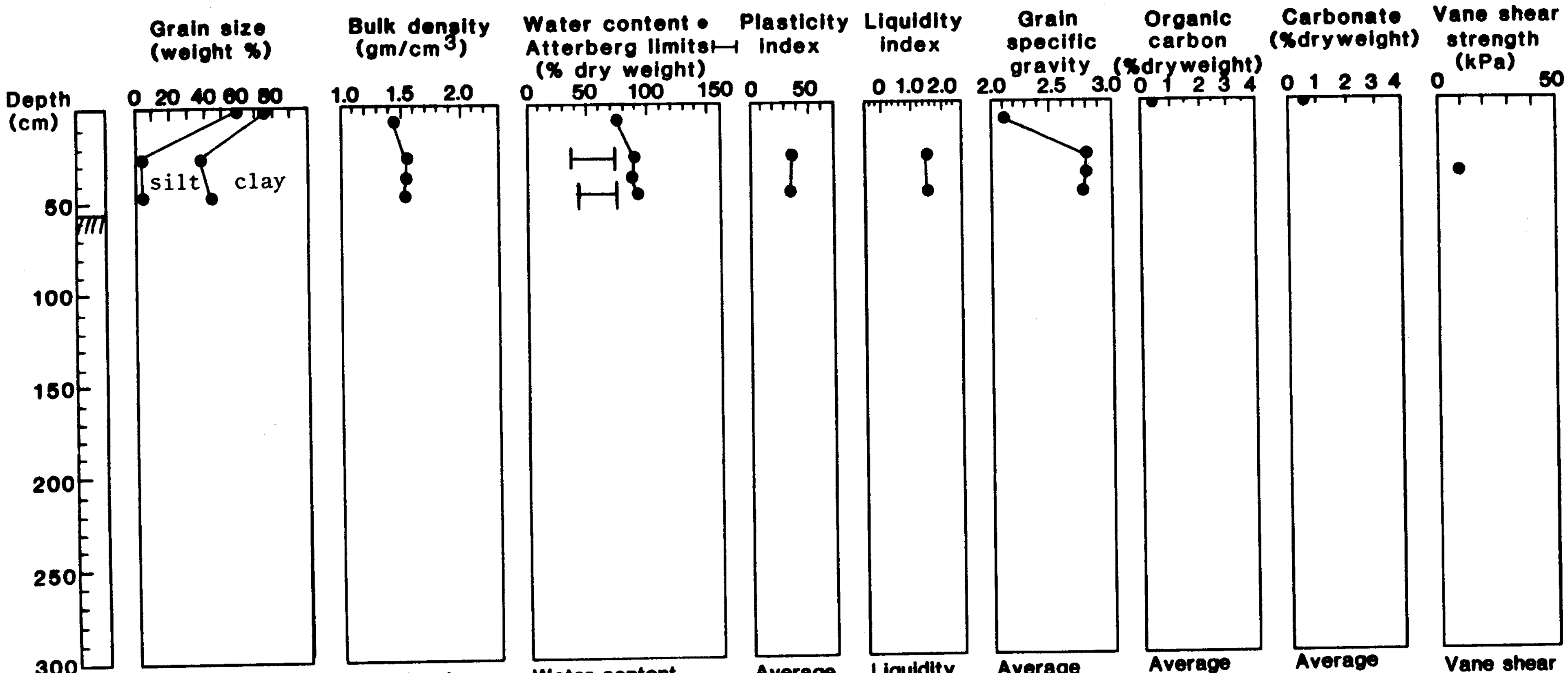

Bulk density at 1m.: ______

Water content at 1m.: ______

Average plastic limit: 40

Average liquid limit: 74

Average plasticity index: 39

Liquidity index at 1m.: ______

Average grain specific gravity: 2.62

Average organic carbon: 0.397

Average carbonate: 0.590

Vane shear strength at 1m.: ______

759

Station 662 **Location** 58°15.80'N 153°23.00'W **Water depth** 176m

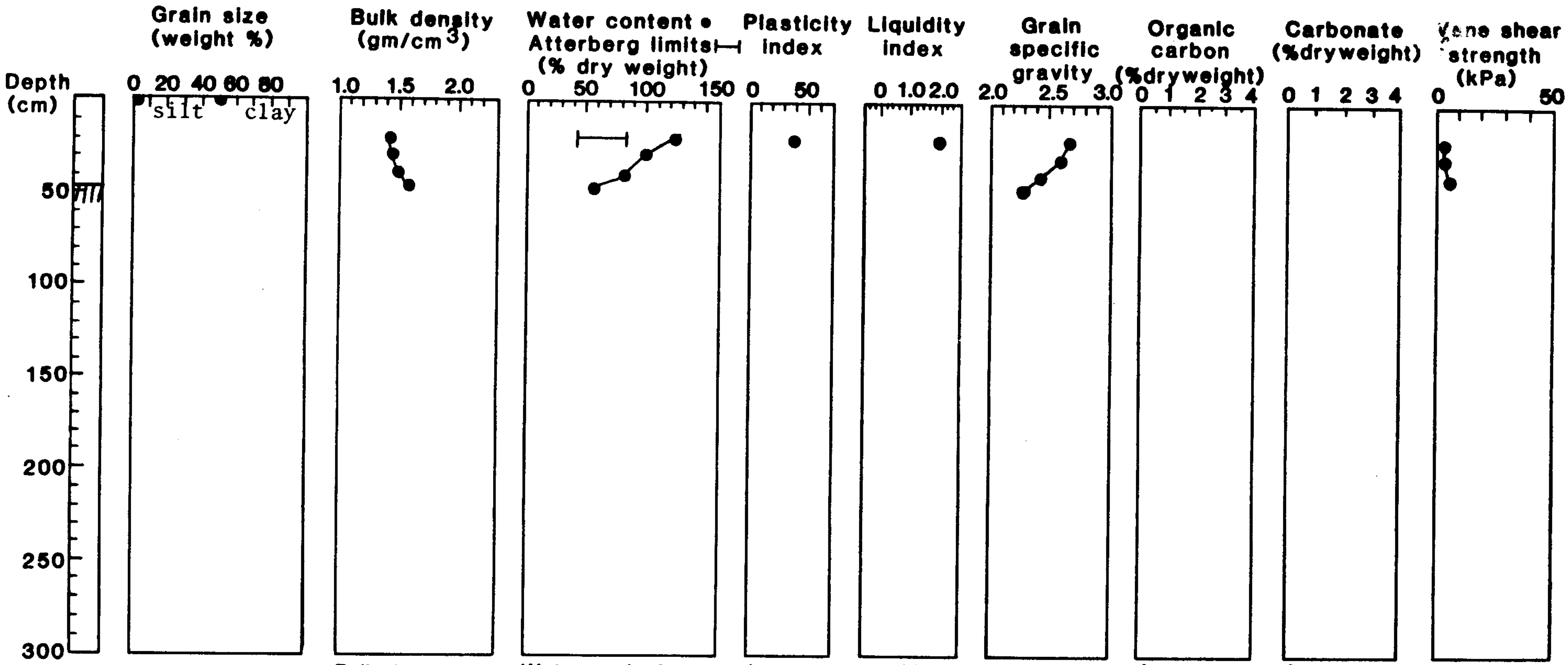

Bulk density at 1m.: ______

Water content at 1m.: ______

Average plastic limit: 45

Average liquid limit: 84

Average plasticity index: 39

Liquidity index at 1m.: ______

Average grain specific gravity: 2.51

Average organic carbon: ______

Average carbonate: ______

Vane shear strength at 1m.: ______

Station 664 **Location** 58°55.00N 153°36.90W **Water depth** 174m

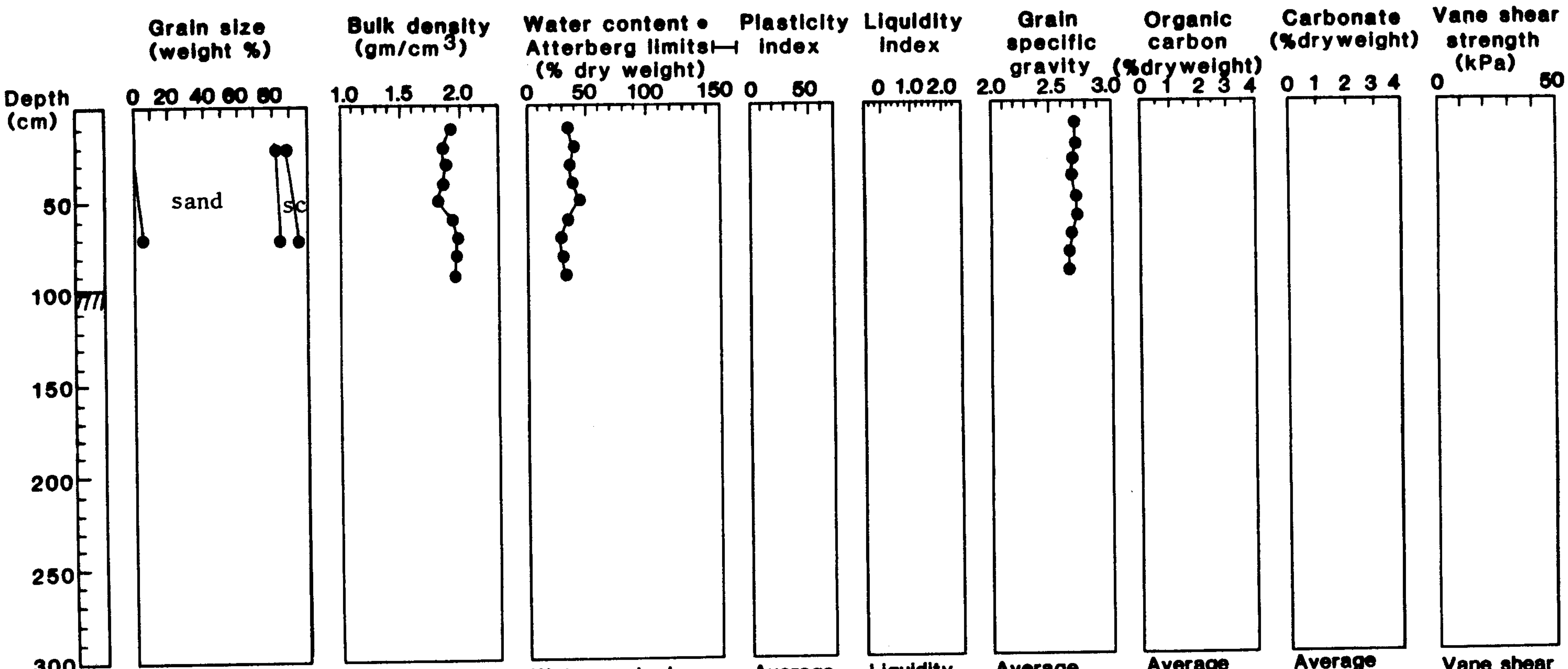

Bulk density at 1m.: ______

Water content at 1m.: ______
Average plastic limit: ______
Average liquid limit: ______

Average plasticity index: ______

Liquidity index at 1m.: ______

Average grain specific gravity: 2.69

Average organic carbon: ______

Average carbonate: ______

Vane shear strength at 1m.: ______